TRANSACTIONS

American Society for Metals

VOL. XLVIII 1956

TECHNICAL PROGRAM AND REPORTS OF OFFICERS AMERICAN SOCIETY FOR METALS—37th ANNUAL CONVENTION, PHILADELPHIA, OCTOBER 15-21, 1955

FOR the purposes of record and for the benefit of members who were not in attendance at the Thirty-Seventh Annual Convention of the Society, held in Philadelphia, October 15–21, 1955, the Programs of the Technical Papers and Educational Lectures together with the Reports of Officers for 1955 are herewith published in full.

ASM Seminar on Theory of Alloy Phases

Saturday, October 15

Crystal Ballroom, Benjamin Franklin Hotel—9:30 A.M.

Presiding Officer
E. R. Jette, Los Alamos Scientific Laboratory,
University of California, Los Alamos, New Mexico

Bonding Forces in Solids, by Fred Seitz, University of Illinois, Urbana, Illinois

Band Theory of Bonding in Metals, by J. C. Slater, Massachusetts Institute of Technology, Cambridge, Mass.

Density of States as Determined by Soft X-Ray Spectroscopy, by C. H. Shaw, Ohio State University, Columbus, Ohio

Crystal Ballroom, Benjamin Franklin Hotel—2:00 P.M.

Presiding Officer
T. Read, Jr., Bell Telephone Laboratories, Murray Hill, New Jersey

Intermediate Phases and Electronic Structure, by T. Massalski, University of Chicago, Chicago

Crystal Structure and Atomic Size, by F. Laves, Polytechnic Technical Institute, Zurich, Switzerland

Bonding Forces in Alkali Metals, by Dr. H. Brooks, Cruft Laboratory, Harvard University, Cambridge, Mass.

Crystal Ballroom, Benjamin Franklin Hotel—8:00 P.M.

Presiding Officer
C. S. Barrett, University of Chicago, Chicago, Illinois

The Electronic Structure of Metals and Alloys, by L. Pauling, California Institute of Technology, Pasadena, California

Sunday, October 16

Crystal Ballroom, Benjamin Franklin Hotel—9:30 A.M.

Presiding Officer
J. C. Fisher, General Electric Company, Research Laboratory,
Schenectady, New York

Intermediate Phases in Alloys of the Transition Elements, by Pol Duwez, California Institute of Technology, Pasadena, California

Ferromagnetism, Antiferromagnetism and Crystal Structure, by Clarence Zener, Westinghouse Research Laboratory, East Pittsburgh, Pa.

Atomic and Magnetic Ordering in Intermediate Phases, by J. S. Kasper, General Electric Company, Schenectady, New York

Crystal Ballroom, Benjamin Franklin Hotel—2:00 P.M.

Presiding Officer

R. Maddin, University of Pennsylvania, Philadelphia, Pa.

Atomic Moments of Transition Elements in Solid Solution Alloys, by C. Shull, Brookhaven National Laboratory, Long Island, New York

Solid Solutions and Ordering, by B. L. Averbach, Massachusetts Institute of Technology, Cambridge, Mass.

Alloy Phase Diagrams, by G. V. Raynor, Birmingham University, Birmingham, England

Technical Program of the American Society for Metals

Monday, October 17

Crystal Ballroom, Benjamin Franklin Hotel—9:30 A.M.

Titanium

Presiding Officers

W. L. Finlay, Rem-Cru Titanium, Inc., Midland, Pa.
P. D. Frost, Battelle Memorial Institute, Columbus, Ohio

Rate of Diffusion of Carbon in Alpha and Beta Titanium, by F. C. Wagner, E. J. Bucur and M. A. Steinberg, Horizons, Inc., Cleveland, Ohio

Hydrogen Contamination in Descaling and Acid Pickling of Titanium, by G. A. Lenning, C. M. Craighead and R. I. Jaffee, Battelle Memorial Institute, Columbus, Ohio

Mechanical Properties of Ti-Cr-Mo Alloys as Affected by Grain Size and Grain Shape, by H. R. Ogden, F. C. Holden and R. I. Jaffee, Nonferrous Physical Metallurgy Division, Battelle Memorial Institute, Columbus, Ohio

Investigation of the Heat Treatability of the 6% Aluminum-4% Vanadium-Titanium-Base Alloy, by R. G. Sherman and H. D. Kessler, Titanium Metals Corp. of America, Henderson, Nevada

Franklin Room, Benjamin Franklin Hotel—9:30 A.M.

Mechanical Properties

Presiding Officers

J. F. Libsch, Lehigh University, Bethlehem, Pa.
V. H. Patterson, Climax Molybdenum Co., New York, N. Y.

Notch Ductile High-Strength Nodular Irons, by G. A. Sandoz, H. F. Bishop and W. S. Pellini, Metal Processing Branch Metallurgy Division, Naval Research Laboratory, Washington, D. C.

Fatigue and Anistropy in Copper, by M. L. Ebner and W. A. Backofen, Metals Processing Lab., Massachusetts Institute of Technology, Cambridge, Mass.

Influence of Vibration on the Solidification of An Aluminum Alloy, by R. S. Richards, Titanium Metals Corporation, Henderson, Nevada and W. Rostoker, Supervisor, Armour Research Foundation, Metals Research, Chicago

Conference on Ductile Chromium Metal and Its High Alloys

(Jointly sponsored by Office of Ordnance Research, U.S. Army and ASM)

World Wide Research on Ductile Chromium

Betsy Ross Room, Benjamin Franklin Hotel—10:30 A.M.

Presiding Officer

J. W. Dawson, Chemical Sciences Division, Office of Ordnance Research, U.S. Army, Durham, North Carolina

Introductory Remarks, by P. N. Gillon, Office of Ordnance Research, U.S. Army, Durham, North Carolina

Research on Chromium in America, by William J. Kroll, Consulting Metallurgist, Corvallis, Oregon

Research on Chromium in Australia, by Henry L. Wain, Aeronautical Research Laboratories, Melbourne, Australia

Research on Chromium in Europe, by A. H. Sully, The British Steel Castings Research Association, Sheffield, England

Crystal Ballroom, Benjamin Franklin Hotel—2:00 P.M.

Titanium-Zirconium

Presiding Officers

G. W. Birdsall, Reynolds Metals Co., Richmond, Virginia
J. L. Wyatt, Horizons, Inc., Cleveland, Ohio

Tensile Properties of Zirconium-Chromium Alloys-Particle-Strengthening Effects, by J. H. Keeler, General Electric Co., Schenectady, N. Y.

Nature and Decomposition Kinetics of Alpha Prime in Titanium-Vanadium Alloys, by F. R. Brotzen, Rice Institute, Houston, Texas, E. L. Harmon and A. R. Troiano, Case Institute of Technology, Cleveland

Metallography of Tempering of Alpha-Prime in Titanium Alloys, by R. F. Domagala, and W. Rostoker, Armour Research Foundation, Chicago

Progress in the Development of Creep-Resistant Zirconium Alloys, by Walston Chubb, Battelle Memorial Institute, Columbus, Ohio

Conference on Ductile Chromium Metal and Its High Alloys

Betsy Ross Room, Benjamin Franklin Hotel—2:00 P.M.

Physical Metallurgy of High Chromium Alloys

Presiding Officer

J. H. Holloman, General Electric Research Laboratory, Schenectady, N. Y.

Influence of Chromium Metal Purity on the Properties of Chromium Alloys, by D. J. Maykuth and Robert I. Jaffee, Battelle Memorial Institute, Columbus, Ohio

Solubility of Nitrogen and Oxygen in Solid Chromium, by D. Caplan, M. J. Fraser, and A. A. Burr, Rensselear Polytechnic Institute, Troy, N. Y.

Chromium-Nickel-Nitrogen Ternary Diagram, by E. P. Abrahamson II and N. J. Grant, Massachusetts Institute of Technology, Cambridge, Mass.

Kinetics of the Formation of the Sigma Phase in Chromium-Iron Alloys, by Pol Duwez and Howard Martens, California Institute of Technology, Pasadena, California

Volume Change and Evolution of Gases on Heating Electrolytic Chromium, by Kenneth A. Moon and George A. Consolazio, Watertown Arsenal, Watertown, Mass.

Panel Discussion on Vacuum-Melted Metals

Crystal Ballroom, Benjamin Franklin Hotel—4:30 P.M.

The discussion started with presentation on current applications of vacuum-melted metals, particularly antifriction bearings and jet engine components. Engineering properties and workability were considered next, with discussions of statistical data on the ranges of properties obtained from a large number of consecutive heats. Other topics dealt with included comparisons of different ingot sizes, properties of bar stock versus forged components, induction compared with arc melting, control of process variables, trends in specifications for vacuum-melted metals and in the melting equipment.

Presiding Officer

W. E. Jones, General Electric Co., Detroit, Michigan

Panel Members

F. N. Darmara, Utica Drop Forge & Tool Corp., Utica, N. Y.
S. G. Demirjian, General Electric Co., West Lynn, Mass.
W. W. Dyrkacz, Allegheny Ludlum Steel Corp., Watervliet, N. Y.
G. A. Fritzlen, Haynes Stellite Company, Kokomo, Indiana

James H. Moore, Vacuum Metals Corp., Syracuse, N. Y.
James D. Nisbet, Universal-Cyclops Steel Corp., Bridgeville, Pa.
C. E. Norton, General Motors Corp., Bristol, Conn.
W. H. Sharp, Pratt & Whitney Aircraft, East Hartford, Conn.
R. G. Ulrech, Consolidated Vacuum Corp., Rochester, N. Y.

Crystal Ballroom, Benjamin Franklin Hotel—8:00 P.M.

Continuation of panel discussion.

Tuesday, October 18

Crystal Ballroom, Benjamin Franklin Hotel—9:30 A.M.

Tempering of Steel

Presiding Officers

F. T. McGuire, Deere and Co., Moline, Ill.
P. Payson, Crucible Steel Co. of America, Pittsburgh.

Some Effects of Silicon on the Mechanical Properties of High Strength Steels, by C. H. Shih, B. L. Averbach and Morris Cohen, Massachusetts Institute of Technology, Cambridge, Mass.

Some Relationships Between Endurance Limit and Torsonial Properties of Steel, by S. T. Ross, R. P. Sernka and W. E. Jominy, Chrysler Corporation, Detroit, Mich.

Influence of Molybdenum and Tungsten on Temper Embrittlement, by A. E. Powers, General Electric Co., Schenectady, N. Y.

Hardness of Tempered Martensite in Carbon and Low Alloy Steels, by R. A. Grange, Fundamental Research Laboratory, and R. W. Baughman, U. S. Steel Corp., Kearny, New Jersey

Franklin Room, Benjamin Franklin Hotel—9:30 A.M.

Deformation

Presiding Officers

N. J. Grant, Massachusetts Institute of Technology, Cambridge, Mass.
W. D. Manly, Oak Ridge National Laboratory, Oak Ridge, Tenn.

Deformation of Beryllium Single Crystals at 25 to 500°C., by H. T. Lee, University of Pennsylvania, Philadelphia and R. M. Brick, Continental Can Co., Inc., Chicago

Grain Boundary Creep in Aluminum Bicrystals, by F. N. Rhines, W. E. Bond and M. A. Kissel, Metals Research Laboratory, Carnegie Institute of Technology, Pittsburgh

Deformation of Fracture Mechanisms of Polycrystalline Magnesium at Low Temperatures, by F. E. Hauser, P. R. Landon and J. E. Dorn, University of California, Berkeley, California

Influence of Cold Work on Strength of Steel at Elevated Temperatures, by Paul Shahinian, High Temperature Alloys Branch, Metallurgy Division, Naval Research Laboratory, Washington, D. C.

Conference on Ductile Chromium Metal and Its High Alloys

Betsy Ross Room, Benjamin Franklin Hotel—9:00 A.M.

Ductile Chromium Metal

Presiding Officer

A. B. Kinzel, Union Carbide & Carbon Research Laboratory, New York, N.Y.

Properties of High Purity Iodide Chromium, by I. E. Campbell, Battelle Memorial Institute, Columbus, Ohio

First Commercial Plant for Electrowinning Chromium from Trivalent Salt Solutions, by M. C. Carosella and J. D. Mattler, Electro Metallurgical Co., Division of Union Carbide & Carbon Co., Niagara Falls, N.Y.

Melting Point of High Purity Chromium, by LeRoy L. Wyman and J. T. Sterling, National Bureau of Standards, Washington, D. C.

Mechanical Properties of Bureau of Mines Chromium, by G. Asai and E. T. Hayes, U. S. Bureau of Mines, Albany, Oregon

Effects of Impurities on the Ductility of Chromium, by W. H. Smith and A. U. Seybolt, General Electric Research Laboratory, Schenectady, N. Y.

Betsy Ross Room, Benjamin Franklin Hotel—2:00 P.M.

High Chromium Alloys

Presiding Officer

P. R. Kosting, Watertown Arsenal, Watertown, Mass.

Ductility and Toughness of High Chromium Alloys, by R. W. Fountain and J. L. Lamont, Electro Metallurgical Co., Niagara Falls, N.Y.

Mechanical Properties and Toughness of Chromium-Iron Alloys, by H. Kato and E. T. Hayes, U. S. Bureau of Mines, Albany, Oregon

Some Structures and Properties of the Chromium-Nickel-Nitrogen Ternary Alloys, by E. P. Abrahamson II and N. J. Grant, Massachusetts Institute of Technology, Cambridge, Mass.

A Forgeable Chromium-Iron-Based Alloy, by D. P. Moon, H. A. Blank and A. M. Hall, Battelle Memorial Institute, Columbus, Ohio

Metallography of Chromium, by W. D. Forgeng and G. T. Motock, Electro Metallurgical Company, Niagara Falls, N. Y.

Crystal Ballroom, Benjamin Franklin Hotel—2:00 P.M.

Steel

Presiding Officers

R. D. Chapman, Chrysler Corp., Detroit, Mich.
A. R. Troiano, Case Institute of Technology, Cleveland, Ohio

Inhibition by Nitrogen of Graphitization in Steel, by G. V. Smith, Cornell University and B. W. Royle, American Steel & Wire Div., U.S. Steel Corp., Cleveland

An Approach to the Study of the Effect of Rare-Earth Additions to Steel by Use of Radioactive Tracer Techniques, by C. S. DuMont and J. E. Gates, Battelle Memorial Institute, Columbus, Ohio, and C. N. Henderson, Mallinckrodt Chemical Works, St. Louis

Optimum Boron Content for Hardenability, by J. C. Shyne, E. R. Morgan and D. N. Frey, Ford Motor Company, Dearborn, Mich.

On Banding in Steel, by C. Jatczak, D. J. Girardi and E. S. Rowland, The Timken Roller Bearing Co., Canton, Ohio

Furnaces, Combustion Equipment and Induction Heating

Ballroom, Convention Hall—2:00 P.M.

Presented by the Industrial Heating Equipment Association
Under the Auspices of the American Society for Metals

Presiding Officer

Alfred E. Tarr, Leeds and Northrup Co., Philadelphia

Vacuum Melting By Induction and Arc, by Frank Chestnut, Ajax Electrothermic Corp., Trenton, N. J.

Batch-Type Strip Annealing Furnaces—Multiple and Single Stack, by Fred Olmstead, Lee Wilson Engineering Co., Cleveland

Combustion Systems in Steel Mills, by Fred Bloom, Bloom Engineering Co., Pittsburgh

Wednesday, October 19

Crystal Ballroom, Benjamin Franklin Hotel—9:00 A.M.

ASM Annual Meeting

Edward DeMille Campbell Memorial Lecture

Walter E. Jominy, Chrysler Corp., Detroit, Chairman

Low-Carbon Martensites, by Robert H. Aborn, Director of Fundamental Research Laboratory, U. S. Steel Corp., Kearny, N. J.

Crystal Ballroom, Benjamin Franklin Hotel—2:00 P.M.

Steel

Presiding Officers

H. S. Avery, American Brakeshoe Co., Mahwah, N. J.
J. A. Berger, University of Pittsburgh, Pittsburgh, Pa.

Some Effects of Metal Removal and Heat Treatment on the Surfaces of Hardened Steel, by Karl E. Beu, Goodyear Atomic Corp., Portsmouth, Ohio and Donald P. Koistinen, Research Laboratories Division, General Motors Corp., Detroit

Effect of Temperature on Delayed Yielding of Mild Steel for Short Loading Duration, by Joseph M. Krafft, Naval Research Laboratory, Washington, D. C.

Effect of Tempering Temperature on Stress Corrosion Cracking and Hydrogen Embrittlement of Martensitic Stainless Steels, by P. Lillys and A. E. Nehrenberg, Crucible Steel Company of America, Pittsburgh

Static Fatigue of High Strength Steel, by R. H. Raring, N.A.C.A., Washington, D. C. and J. A. Rinebolt, Republic Steel Co., Canton, Ohio

Betsy Ross Room, Benjamin Franklin Hotel—2:00 P.M.

Molybdenum-Vanadium-Tantalum

Presiding Officers

D. J. McPherson, Armour Research Foundation, Chicago
G. Timmons, Climax Molybdenum Co., Detroit

Initiation of Discontinuous Yielding in Ductile Molybdenum, by J. A. Hendrickson, D. S. Wood and D. S. Clark, California Institute of Technology, Pasadena, California

Properties of Vanadium Consolidated by Extrusion, by C. E. Lacy and C. J. Beck, Knolls Atomic Power Laboratory, General Electric Co., Schenectady, N. Y.

Mechanical Properties of Vanadium-Base Alloys, by W. Rostoker and A. S. Yamamoto, Armour Research Foundation, Chicago, Ill. and R. E. Riley, Rem-Cru Titanium Corp., Midland, Pa.

Rolling Textures in Tantalum, by J. W. Pugh and W. R. Hibbard, Jr., General Electric Co., Schenectady, N. Y.

Mechanized Heat Treating Equipment

Ballroom, Convention Hall—2:00 P.M.

Presented by the Industrial Heating Equipment Association
Under the Auspices of the American Society for Metals

Presiding Officer

Alfred E. Tarr, Leeds and Northrup Co., Philadelphia

Mechanized Molten Baths, by Leon Rosseau, Ajax Electric Co., Trenton, N. J.

Mechanized Batch-Type Furnaces, by Martin Neumeyer, Sunbeam Corp., Chicago

Mechanized Continuous-Type Furnaces, by George McCormick, Industrial Heating Equipment Co., Detroit

Metallurgical Aspects Associated With Induction Heating, by Harry Osborn, Tocco Division, Ohio Crankshaft Co., Cleveland

Thursday, October 20

Crystal Ballroom, Benjamin Franklin Hotel—9:30 A.M.

Stainless Steels

Presiding Officers

D. J. Carney, U. S. Steel Corp., Chicago, Ill.
G. A. Fritzlen, Haynes Stellite Co., Kokomo, Ind.

Influence of Alloying Elements on the Impact Transition Behavior of 12% Cr Steels Aged at 900°F., by E. J. Whittenberger and E. R. Rosenow, U. S. Steel Corp., Chicago

Creep Rupture Properties of Cold Worked Type-347 Stainless Steel, by N. J. Grant, A. G. Bucklin and Warren Rowland, Massachusetts Institute of Technology, Cambridge, Mass.

Notch Ductility of Type-410 (12% Cr) Stainless Steel, by F. A. Brandt, H. F. Bishop and W. S. Pellini, Metal Processing Branch, Metallurgy Division, Naval Research Laboratory, Washington, D. C.

Influence of Strain Rate and Temperature on the Ductility of Austenitic Stainless Steel, by G. W. Form, Ecole Polytechnique, Montreal, Canada, and W. M. Baldwin, Jr., Case Institute of Technology, Cleveland

Powder Metallurgy in Atomic Energy

(Jointly Sponsored by U.S. Atomic Energy Commission and American Society for Metals)

Betsy Ross Room, Benjamin Franklin Hotel—9:30 A.M.

Presiding Officer

Henry H. Hausner, Manager of Atomic Energy Engineering, Sylvania Electric Products, Inc., Bayside, N. Y.

General Metallurgical Problems in the Design of Nuclear Power Reactors, by Vincent P. Calkins, Aircraft Nuclear Propulsion Project, General Electric Co., Cincinnati

Preparation of Metal Powders for Nuclear Reactor Purposes, by Premo Chiotti and Harley A. Wilhelm, Institute for Atomic Research, Iowa State College, Ames, Iowa

Latest Developments in the Theory of Sintering, by Leslie L. Seigle and A. Pranatis, Fundamental Metallurgy Section, Sylvania Electric Products, Inc., Bayside, N. Y.

Powder Metallurgy of Beryllium and Zirconium, by Harold Hirsch, Knolls Atomic Power Lab., General Electric Co., Schenectady, N. Y.

Crystal Ballroom, Benjamin Franklin Hotel—2:00 P.M.

Stainless Steels

Presiding Officers

W. O. Binder, Electro Metallurgical Co., Niagara Falls, N. Y.
G. V. Smith, Cornell University, Ithaca, N. Y.

High Nitrogen Austenitic Cr-Mn Steels, by V. F. Zackay, Scientific Laboratory, Ford Motor Co., Dearborn, Mich., J. F. Carlson, Hoskins Mfg. Co., Detroit, Mich., and P. L. Jackson, Misco Precision Casting Co., Whitehall, Mich.

Effect of Composition and Structure on the Creep Rupture Properties of 18-8 Stainless Steels, by F. C. Monkman, P. E. Price and N. J. Grant, Massachusetts Institute of Technology, Cambridge, Mass.

Austenitic Fe-Cr- C-N Stainless Steels, by G. F. Tisinai, J. K. Stanley and C. H. Samans, Standard Oil Co. (Indiana), Whiting, Indiana

Effects of Chemical Composition and Heat Treatment Upon the Microstructure and Corrosion Resistance of AISI Types 309 and 310, by D. J. Carney and E. R. Rosenow, U. S. Steel Corp., Chicago

Powder Metallurgy in Atomic Energy

(Jointly Sponsored by U. S. Atomic Energy Commission and the American Society for Metals

Betsy Ross Room, Benjamin Franklin Hotel—2:00 P.M.

Alloy Formation By Powder Metallurgy, by Henry A. Saller and Frank Rough, Battelle Memorial Institute, Columbus, Ohio

New Methods of Powder Metallurgy for Nuclear Reactor Purposes, by John H. Cooks and W. D. Manly, Oak Ridge National Laboratory, Oak Ridge, Tenn.

Safe Handling of Pyrophoric and Radioactive Materials, by A. B. Shuck, L. R. Kelman, R. C. Goertz and W. D. Wilkinson, Argonne National Laboratory, Lemont, Ill.

Summary of Recently Disclosed Information on Thorium, Uranium and Special Metals for Nuclear Reactors, by Henry H. Hausner, Manager of Atomic Energy Engineering, Sylvania Electric Products, Inc., Bayside, N. Y.

ASM—LECTURE COURSE

Tuesday, October 18, 4:30 P.M.

All Sessions in Room 200, Convention Hall, Benjamin Franklin Hotel

Embrittlement Phenomena

Presiding Officer

Otto Zmeskal, University of Florida, Gainesville, Fla.

Embrittlement of Metals, by B. R. Queneau, U.S. Steel Corp., Duquesne, Pa.

Tuesday, October 18, 8:00 P.M.

Presiding Officer

C. H. Lorig, Battelle Memorial Institute, Columbus, Ohio

Temper Embrittleness, by B. R. Queneau, U.S. Steel Corp., Duquesne, Pa.

Wednesday, October 19, 4:30 P.M.

Presiding Officer

J. Harry Jackson, Battelle Memorial Institute, Columbus, Ohio

Tempered Martensite Brittleness, by B. R. Queneau, U.S. Steel Corp., Duquesne, Pa.

Wednesday, October 19, 8:00 P.M.

Presiding Officer

James J. Heger, U.S. Steel Corp., Pittsburgh

Embrittlement of Stainless Steels, by B. R. Queneau, U.S. Steel Corp., Duquesne, Pa.

ANNUAL MEETING OF AMERICAN SOCIETY FOR METALS

Crystal Ballroom, Benjamin Franklin Hotel, 9:00 A.M.

The annual meeting was called to order by President George A. Roberts. The order of business was:

1. President's address
   Printed in this volume of TRANSACTIONS, page 9.
2. Report of the Treasurer
   Printed in this volume of TRANSACTIONS, page 15.
3. Report of the Secretary
   Printed in this volume of TRANSACTIONS, page 20.
4. Report of ASM Foundation for Education and Research
   Printed in this volume of TRANSACTIONS, page 31.
5. Presentation of President's Medal and Certificate to James B. Austin.
6. Presentation of Henry Marion Howe Medal to:
   A. E. Nehrenberg and Peter Lillys for their paper entitled, "High Temperature Transformations in Ferritic Stainless Steels Containing 17 to 25% Chromium" adjudged the paper of highest merit published in the ASM TRANSACTIONS in 1954.
7. Presentation of ASM Teaching Award to:
   Kenneth E. Rose, University of Kansas
8. Election of Officers
   The report of the election of officers appears on page 35.
9. Campbell Lecture
   Printed in this volume of TRANSACTIONS, beginning on page 51.

ANNUAL ADDRESS OF THE PRESIDENT

GEORGE A. ROBERTS, *President*

Thirty-seventh Annual Meeting, Philadelphia, October 19, 1955

MOST people, upon greeting the President of a National Technical Society, and particularly of the American Society for Metals, look upon his healthy countenance with surprise and express astonishment that one could fare so well physically in the face of such an arduous task. They evidently cannot remember that which has been so often pointed out to them that this job is not a chore but a privilege, an honor, and an experience full of lasting memories. I have been particularly fortunate in serving during a year in which several special events have taken place, particularly the highly successful Western Metals Congress and the Joint Metallurgical Societies Meetings in Europe. In the course of these duties I have traveled seventy-three thousand seven hundred fifteen miles—enjoying travel to its fullest, this could not be better. I am only sorry that preparations for the Western Metals Congress and other important events prevented our National Secretary, William H. Eisenman, from being with me on some of my chapter visits. His absence was noted, not only by the Chapters but by your President.

I am sure, although I say this hopefully, that the American Society for Metals has continued to further its aims and objectives during the year. Three years ago, John Chipman pointed out that the communities in which Chapters of the American Society for Metals are located have come to regard their Chapter as the fountain head of all knowledge on the metallic subjects. Certainly there has been no lessening of this aspect, but there has been a heightening of others, including an awareness of the many responsibilities of technical and professional people in providing for proper influx of graduates into their profession. The American Society for Metals' program to encourage this influx of properly qualified people has, after many years, been firmly implanted at the local level. We can be proud of our individual Chapters for their activities in this regard.

A report of this scope should probably consider the biggest things first. One year ago, at this Meeting, there was presented a report entitled "The ASM of Tomorrow." We are now one year into this "Tomorrow" and I know that many of you are anxious to learn what action your Board of Trustees has taken with regard to the five points put forth in that program. Action on two of these points is started—indeed was started during the preceding official year. Action on a third has just been authorized, but has not been taken on the remaining two.

President Austin referred last year to the appointing of a Site Committee (Van Horn, Wilson, Austin, Roberts, Schaefer) to study

the matter of improving facilities for the National Office. During the year this Committee made a preliminary report to the Board, as a result of which additional studies were authorized. These were to include on an architectural and an engineering basis

1.) An urban site
2.) A suburban site,

both to be in the metropolitan Cleveland area. It is possible that within the next few months final reports of these groups will be available for Board consideration.

Point number two, the Metals Engineering Institute has likewise been started. Under the direction of Anton Brasunas these are the correspondence type educational courses, also designed for in-plant training and home study. That such course material will also serve local Chapters is apparent.

The Board approved, in principle, the establishment of the American Society for Metals Metallurgical Institute (called Seminars in last year's report) to cover point three of the program entitled "The ASM of Tomorrow." It is expected that this program will be formulated in detail during the coming year.

So many have asked about the establishment of an American Society for Metals Research Laboratory, and an American Society for Metals Institution for Higher Learning in Metallurgy, thinking that these were accomplished facts or at least approved in principle. It is important to note here that absolutely no formal consideration of either of these proposals has been given by the Board of Trustees. In the original program it was pointed out by the Secretary that these were, in his opinion, long range objectives, and were not to be initiated in the immediate future. There will be ample time for the proper debate regarding the feasibility and advisability of both programs. In the meantime, the Site Committee is establishing plans for space requirements, based on the currently approved portions of our plan.

During the year, the Board of Trustees held three meetings. Your President visited thirty-seven Chapters and participated in two Regional Meetings, which included an additional eight Chapters. Other Trustees visited 26 Chapters and 2 Regional Meetings, thus bringing the total to 63 Chapters and 4 Regional Meetings.

It has often been said that the strength of the American Society for Metals lies in the local Chapter, and I am sure that those of us who have been privileged to speak to so many Chapters and to discuss problems with their Officers are more firmly convinced of this than ever. Your comments are not only an inspiration but a stimulant to the work of those temporarily assigned to tasks at the national level. During the year new Charters were granted to the following Chapters:

Old South (Greenville, S. C.)
Southern Technical Institute (student group) (Macon, Ga.)
Quebec (from Montreal)
Edmonton, and
Long Island

bringing the total number to 93.

Regarding our student chapters the Board considered and approved an interpretative change so that any student in the engineering department of a school should be privileged to enroll for student membership in the ASM, if he desires.

The Treasurer's report will make it apparent that the management of your Society has kept adequate controls over the purse strings. The incidence of a record year in funds available for appropriation is not, in any sense, a source of embarrassment but a source of pride. The incidence of two expositions, Western and National, in one year, has contributed to the excellent position. You will note that a significant appropriation has been made to the Building Fund. It is hoped that within another year there will be sufficient money in this Fund to begin a Building or Purchasing Program that will result in a headquarters of which we can all be proud. In addition, you should note a substantial contribution to the American Society for Metals Foundation for Education and Research.

Following much consideration, the Board of Trustees made, on September 1, a significant reduction in its holdings of common stocks, bringing the level of these holdings, based on market value, from about 48.3 to about 41.9%. The level, based on cost or carrying value, is about 31%—a substantially conservative position.

That we are now about ready to embark upon a program of investing these funds in facilities, educational courses, etcetera, is proof of the foresight of those who have insisted upon the establishment of such funds over the years. It is further a cogent argument for the retention of exposition functions in the hands of the Technical Societies, and for the unqualified support of such technical society-managed industrial expositions on the part of industry.

The Pension Committee of the Society has been active in reviewing the present pension and insurance program for its full-time employees. A possible alteration of the program may be recommended during the coming year.

I could report to you a continuation of many of our engineering educational functions. The program of support in the junior and senior high schools; of support at the collegiate and post-graduate levels through scholarships; visiting lectureships, and support at the vocational level through our active Vocational Education Committee continues as in the past. In addition, your President is serving as Chairman of a Special Study Group to point out where the several

programs on stimulating collegiate enrollment for Engineering need to be coordinated and intensified. This group will be particularly concerned with Metallurgical Engineering, Mining Engineering, and the field of Ceramics.

During the year, it was felt important to review our entire policy with regard to the publication of papers and the programming and presentation of these papers and technical reports at our Nationally Sponsored Congresses. Accordingly, the Board of Trustees authorized the appointment of a Committee, under the direction of William E. Mahin, to review this entire matter in an effort to stimulate interest, raise quality, and provide efficiency of service to the members. A report from this Committee will be received soon.

In the Treasurer's report you may note an appropriation for a new service of literature indexing.

A committee composed of Trustee Walter Crafts, Don Hilty, Dan Girardi, Amos Shaler, Mrs. Hyslop and Ernie Thum has studied this problem throughout the past year and the Board has approved the Committee's recommendation that the American Society for Metals sponsor a pilot operation testing the feasibility and utility of the application of computing-type equipment to the indexing and correlation of metallurgical literature. The Secretary is prepared to expand on the implementation of this aim.

Your Officers and Trustees, with one exception, attended, upon invitation of the European Metallurgical Societies, the Joint Metallurgical Societies Meetings in Europe during the month of June, 1955. In the course of this stimulating, though somewhat exhaustive, event, we had an opportunity to meet with industrial leaders of England, Scotland, Wales, Germany, Belgium, France, Sweden, and Italy. Representatives from other countries, principally Spain, Switzerland, Yugoslavia, The Netherlands, and Finland were also in attendance. Approximately two hundred and fifty Americans who attended came away highly impressed with what they saw. In the course of these deliberations, Honorary Life Memberships in the American Society for Metals were presented, in your behalf, to the following:

Kenneth Headlam-Morley, Secretary,
British Iron and Steel Institute
Lt. Col. S. C. Guillan, Secretary,
British Institute of Metals
Sir Charles Bruce-Gardner, President,
British Iron and Steel Institute
Dr. Maurice Cook, President,
British Institute of Metals
Dr. Kurt Thomas, Secretary,
Verein deutscher Eisenhuttenleute

Dr. Herman Schenck, President,
Verein deutscher Eisenhuttenleute
Dr. P. Brenner, President,
Deutsche Gesellschaft fur Metallkunde
Dr. Bernard Trautmann, Secretary,
Deutsche Gesellschaft fur Metallkunde
Pierre Coheur, Director,
Centre National de Recherches Metallurgiques
Fransois Perot, President,
Centre National de Recherches Metallurgiques
Raoul de Vitry, President,
Societe Francaise de Metallurgie
Eugene DuPuy, Secretary,
Societe Francaise de Metallurgie
Dr. Aldo Dacco, President,
Associazione Italiana di Metallurgia
Dr. Sancho-Plana, President,
Spanish Iron and Steel Institute
Howard Biers,
Union Carbide and Carbon Corp.
S. Fornander,
Jernkontoret, Sweden

Your President received, in behalf of the Society, honors from the British Institute of Metals, The Verein Deutscher Eisenhuttenleute, The Societe Francaise de Metallurgie, and The Association of Engineering Alumni of the University of Liege. In addition, he was presented with a Silver Medal of the City of Paris.

Your Secretary was honored by receiving honorary membership in The British Iron and Steel Institute, The Deutsche Gesellschaft fur Metallkunde as well as by the French and Belgium groups mentioned before.

We are greatly indebted to all of the members of these host Societies who participated with us in this event.

Further on the international scene, the Board gave final authorization for the Second World Metallurgical Congress to be held in Chicago two years from now on November 2–8, 1957, at the time of the 1957 National Metals Congress and Exposition. Invitations to England, Germany, Belgium, France, Spain, and Italy have already been extended.

ACTA METALLURGICA has now completed its third year of operation and is expected to be on a nearly self-supporting basis in one more year. The net operating deficit for the coming year is expected to be only Ten Thousand Dollars. The number of subscriptions stands at 1791. The American Society for Metals is extremely disappointed in the fact that it has been the only sponsoring Society for

this International Scientific Journal. It would welcome any manifestation of greater interest in the affairs of the Journal which would be occasioned by additional sponsoring support.

It is with regret that we note the passing during the year of one of our distinguished Past Presidents. Herbert J. French, who was President of your Society in the year ending 1943, succumbed on August 17, 1955, after an illness of moderate duration. Mr. French presented the Campbell Memorial Lecture in 1933, and was the Henry Marion Howe Medalist in 1930; a truly remarkable man whom we shall all miss.

It is customary for the President's report to record the awards and outstanding events of the previous National Metals Congress. In Chicago in 1954, the President's Medal was presented to Ralph L. Wilson. The ASM Medal for the Advancement of Research was awarded to William E. Unstattd, President of Timken Roller Bearing Company, and the Albert Sauveur Award was given to Dr. Alexander L. Feild, Associate Director, Research Division, Armco Steel Corporation. The Gold Medal of the Society was not awarded in 1954. The Henry Marion Howe Medal was awarded to F. L. Ver Snyder and H. J. Beattie, Jr. of the General Electric Company. The Campbell Memorial Lecture was presented by Kent R. Van Horn, Director of Research, Aluminum Research Laboratories, Aluminum Company of America and Past President of the American Society for Metals. ASM Teaching Awards were presented to Joseph F. Libsch, Lehigh University, Maurice J. Sinnott, University of Michigan, and Ele E. Stansbury of the University of Tennessee.

On behalf of the American Society for Metals, I wish to express our thanks to those Societies which have joined us in this National Metals Congress for their fine cooperation. The programs of the Institute of Metals Division of the American Institute of Mining and Metallurgical Engineers of the American Welding Society, of the Society for Non-Destructive Testing, and of the Industrial Heating Equipment Association, Special Libraries Association, Atomic Energy Commission and United States Army Ordnance Department have made a significant contribution to the success of this unique gathering.

I wish to also express my appreciation for the wholehearted support that I have received from Chapter Officers and my colleagues on the Board of Trustees. Particularly, should the support and cooperation shown throughout the past few years by our retiring members of the Board of Trustees not go unnoticed; to Past President and retiring Trustee James B. Austin for his specific encouragement and for his extreme contribution to the success of the European Meeting this Summer; to our retiring Treasurer William A. Pennington, whose good humor and sound judgment have been

stimulating; to retiring Trustee Robert J. Raudebaugh and G. M. Young. And in the same breath, may I welcome the new Officers to be elected this morning.

No President's report would be complete without a repetition of the heartfelt sentiment and gratitude that he carries out of office with him for the genius of and creative assistance given by Bill Eisenman. His staff, performing their tasks in exemplary and efficient manner, are likewise a tribute to his skill as a Manager for your Society's affairs. Without this support no President could even begin to do some of the things assigned to his office.

TREASURER'S REPORT

WILLIAM A. PENNINGTON, *Treasurer*

ON August 31, 1955, as the year closed, the net assets of the American Society for Metals were $3,003,772.75, a gain of $247,473.85, for the year. The ninety-three chapters have kept pace by increasing their net worth by some $22,000 to an approximate value of $302,000.

The carrying value of all securities was $2,044,631.48. The estimated market value was $2,660,254.17, an increase of $629,402.62 (in market value) for the year. Part of this increase resulted from new investments made in the special accounts set up for the building site and building; the rest of the increase came from the rise in the market.

Dividends and interest amounted to $85,806.47, which is 4.20% of the carrying value of the total securities; last year it was 4.35%.

The general cash account contained $110,268.92; the cash in the fund for building site and building was $132,553.92.

At the last meeting of the Board of Trustees a complete review of the investment situation was made. As of August 8, 1955,—52.4% of the Society's funds (market value) were invested in stocks, 48.3% being in common stocks; 41.0% in bonds; 4.4% in cash; and 2.2% in land trust certificates. The entire cost of stocks was $550,735, but the value on August 8, was $1,150,072. It was decided to reduce the percentage of common stock to be in line with the 40-60 policy previously set by the Board. As a result, approximately $150,000 (market value) worth of stock was sold bringing the percentage of common stock in the portfolio at that time down to 41.9%.

Total income and expenses are shown in Table I.

Table I
Income and Expenses—Fiscal Year Ended August 31, 1955

Income	$1,946,621.31
Expenses	1,495,552.96
Net Income	$451,068.35

Appropriations:		
Educational Purposes	$ 100,578.35	
Building Site and Building	350,490.01	
Total appropriations		$451,068.35
Unappropriated net income		$000,000.00

The relative income and expense for various items are shown in Table II where the values are expressed in percentage of total income. Like last year, about 75% of the income came from Metal

Table II
ASM Income and Its Disposition—Fiscal Year Ended August 31, 1955

	Income (%)	*Outgo* (%)
Metal Progress	41.7	31.5
Metal Expositions	34.2	18.7
Membership (Net)	8.4	3.2
Books	5.6	4.7
Dividends and Interest	4.4	—
Metals Handbook	3.1	2.2
Metals Review	1.2	3.3
Transactions	0.6	2.7
General and Administrative	—	10.0
Other	0.8	0.5
	100.0	76.8
Appropriations	—	23.2
	100.0	100.0

Progress and the Metal Expositions. The net dues from membership amounted to about 8.5%. Metal Progress and the Metal Expositions also accounted for the greater part of the out-go, amounting to approximately 65% of the total expenses. The net income was 23.2% of the total income; the entire amount was appropriated for educational purposes and for the building site and building.

Appropriations for 1955 are shown in Table III, and a history

Table III
Appropriations for 1955

No.		*Amount*
1.	Acta Metallurgica	$ 10,000.00
2.	Teaching Awards	2,500.00
3.	Chapter Educational Activities	1,891.77
4.	World Metallurgical Congress	25,000.00
5.	Program with National Science Teachers Association	11,662.53
6.	Visiting Lectureships	4,524.04
7.	New Headquarters' Site	0.00
8.	New Building	350,490.01
9.	Metals Handbook Revision	0.00
10.	Cooperative Activities with Defense Activities	0.00
11.	Grant to American Society for Metals Foundation for Education and Research	25,000.00
12.	Mechanical Literature Searching	15,000.00
13.	Building Site Committee	5,000.00
	TOTAL	$451,068.35

of the appropriations, over the past five years, is shown in Table IV. In the latter table, the identification by Item Number is the same as that in the preceding table.

Table IV
History of Appropriations (1951–55 Incl.)

No.	*Appropriated*	*Expended*	*Balance (8-31-55)*
1.	$ 80,521.50	$ 65,521.50	$ 15,000.00
2.	25,000.00	19,732.93	5,267.00
3.	46,891.77	36,891.77	10,000.00
4.	115,000.00	65,760.79	49,239.21 (See No. 10)
5.	51,662.53	36,662.53	15,000.00
6.	22,524.04	12.524.04	10,000.00
7.	150,000.00	0.00	150,000.00*
8.	608,706.35	0.00	608,706.35*
9.	30,000.00	0.00	30,000.00
10.	10,000.00	3,207.28	6,792.72**
11.	***	***	***
12.	15,000.00	0.00	15,000.00
13.	5,000.00	0.00	5,000.00
	$1,160,306.19	$240,300.84	$920,005.35

*Does not include earned interest or dividends. Special funds have been set up with the Cleveland Trust Company for investment; the interest earned to date is $14,155.16, making a total in both funds of $772,861.51.

**Transferred to the appropriations for The World Metallurgical Congress making the total in the Congress item—$56,031.93.

***See Foundations separate report.

Again it is a pleasure to face the fact that the Society has had a good year financially. As a matter of fact, it is our best year to date. Last year our good Secretary, W. H. Eisenman, said, "We must go forward;" we are on our way—we did just that during the year. It is with more than satisfaction that your Treasurer acknowledges his leadership in the management of the Society. We wish to call attention to the cooperation of and the hard work performed by the Assistant Treasurer, A. A. Hess.

We, the Officers and Members of the Board of Trustees, wish to express our appreciation of the advice and guidance of the Trust Officers, Messrs. W. W. Horner and A. W. Marten of the Cleveland Trust Company.

FINANCIAL STATEMENT

Board of Trustees,
American Society for Metals,
Cleveland, Ohio

We have examined the balance sheet of American Society for Metals as of August 31, 1955, and the related statements of income and expenses and surplus for the year then ended. Our examination was made in accordance with generally accepted auditing standards, and accordingly included such tests of the accounting records and such other auditing procedures as we considered necessary in the circumstances.

In our opinion, the accompanying balance sheet and statement of income and expenses present fairly the financial position of American Society for Metals at August 31, 1955, and the results of its operations for the year then ended, in conformity with generally accepted accounting principles applied on a basis consistent with that of the preceding year.

ERNST & ERNST
Certified Public Accountants

Cleveland, Ohio
September 24, 1955

BALANCE SHEET

AMERICAN SOCIETY FOR METALS

August 31, 1955

ASSETS

CASH			$ 110,268.10
SECURITIES (approximate market or redemption prices aggregate $2,083,832.96)			
Bonds, stocks, and land trust certificates—at cost		$1,458,576.79	
Accrued interest		6,842.58	1,465,419.37
CASH SURRENDER VALUE OF LIFE INSURANCE			83,581.60
ACCOUNTS RECEIVABLE			
Advertising accounts	$81,730.15		
National Metal Exposition—Philadelphia—October, 1955	55,835.00		
Miscellaneous	24,322.25	$ 161,887.40	
Less allowance for doubtful accounts		2,000.00	159,887.40
INVENTORIES—at cost or lower			
Bound and unbound publications, books, etc.		$ 203,453.75	
Less allowance for obsolescence		6,000.00	197,453.75
OTHER ASSETS			
Officers, employees, and sundry accounts and deposits			27,469.17
FUND FOR BUILDING SITE AND BUILDING			
Principal cash		$ 132,553.92	
Bonds—at cost (approximate redemption prices $576,421.21)		586,054.69	
Accrued interest		3,762.89	722,371.50
REAL ESTATE (at cost less allowances for depreciation)			44,250.00
OFFICE FURNITURE, FIXTURES, AND EQUIPMENT (at cost less allowances for depreciation)			95,320.62
DEFERRED CHARGES			
Prepaid exposition expenses:			
National Metal Exposition—Philadelphia—October, 1955		$ 57,271.85	
Prepaid sundry expenses		33,127.54	
Prepaid insurance		7,351.85	97,751.24
			$3,003,772.75

LIABILITIES, RESERVES, AND SURPLUS

LIABILITIES			
Accounts payable:			
For purchases, expenses, etc.		$ 96,035.49	
Payroll taxes and taxes withheld from employees		4,614.01	
For apportionment of dues to local chapters		4,477.68	$ 105,127.18
INCOME APPROPRIATED FOR EDUCATIONAL PURPOSES			186,299.00
INCOME APPROPRIATED FOR BUILDING SITE AND BUILDING			50,490.01
RESERVES			
For METALS HANDBOOK		$ 85,786.34	
For conventions		60,000.00	
For dues paid in advance		50,000.00	
Campbell Memorial lecture fund		15,000.00	
H. M. Howe medal fund		5,000.00	
Sauveur Achievement award		5,000.00	220,786.34
FUND FOR BUILDING SITE AND BUILDING			
Reserve			722,371.50
DEFERRED INCOME			
National Metal Exposition—Philadelphia—October, 1955		$412,382.75	
Advance receipts on publications		3,707.40	416,090.15
SURPLUS			
Balance at September 1, 1954, and August 31, 1955 (no change during the year)			1,302,608.57
			$3,003,772.75

STATEMENT OF INCOME AND EXPENSES

AMERICAN SOCIETY FOR METALS — **Year Ended August 31, 1955**

INCOME		
METAL PROGRESS—monthly publication		$ 886,710.72
Metal expositions		667,401.78
Memberships		164,856.14
Book sales		90,868.46
Dividends and interest earned		85,806.47
METAL PROGRESS—special issue		58,524.65
METALS HANDBOOK sales		39,425.50
THE METALS REVIEW—monthly publication		24,991.72
METALS HANDBOOK SUPPLEMENT		21,102.32
Review of Metal Literature		18,379.36
TRANSACTIONS sales		11,277.41
General reprints		6,742.89
Sundry sales, etc.		3,539.00
Increment in cash value and dividends on life insurance		2,643.23
Discount earned		1,577.84
Sale of purchased books		334.67
TOTAL INCOME		$2,084,182.16
EXPENSES		
METAL PROGRESS—monthly publication	$ 683,774.43	
National Metal Exposition—Chicago—November, 1954	251,806.25	
Western Metal Show—Los Angeles—March, 1955	114,799.10	
General expenses	83,429.13	
Books published	77,585.46	
THE METALS REVIEW—monthly publication	70,030.32	
Memberships	63,792.55	
METAL PROGRESS—special issue	62,515.97	
TRANSACTIONS	52,738.70	
METALS HANDBOOK	34,047.39	
Secretary's office	33,791.48	
Accounting department	26,156.63	
Headquarters	16,379.50	
Warehouse	12,989.00	
Review of Metal Literature	12,255.31	
Transfer of net income to fund for building site and building	10,440.14	
National committees	7,849.03	
METALS HANDBOOK SUPPLEMENT	7,109.05	
President's office	4,143.28	
Trustees	2,530.54	
Medals, awards, and lectures	2,242.67	
Technical books	1,208.68	
Miscellaneous merchandise	611.53	
Special committees	492.49	
Library	395.18	
TOTAL EXPENSES		1,633,113.81
NET INCOME—Note A		$ 451,068.35
Income appropriated as authorized by the Board of Trustees:		
For educational purposes	$100,578.34	
For building site and building	350,490.01	$ 451,068.35
UNAPPROPRIATED NET INCOME		$ —0—

Note A—In addition to expenses shown above, expenditures in the amount of $74,346.30 were made during the year from prior years' appropriations (see accompanying statement).

STATEMENT OF APPROPRIATED INCOME

INCOME APPROPRIATED FOR BUILDING SITE AND BUILDING		
Balance September 1, 1954		$258,216.34
Add amount appropriated during year		350,490.01
		$608,706.35
Less amount transferred to fund for building site and building		558,216.34
BALANCE AUGUST 31, 1955		$ 50,490.01
INCOME APPROPRIATED FOR EDUCATIONAL PURPOSES		
Balance September 1, 1954		$160,066.96
Less expenditures during year:		
World Metallurgical Congress	$29,689.65	
Science award program	12,181.77	
Acta Metallurgica	10,000.00	
Chapter educational courses	7,928.65	
Teaching awards	6,201.30	
Visiting lectureships	4,622.92	
A. S. M. Foundation for Education and Research	3,500.00	
Metallurgical Advisory Board	222.01	74,346.30
		$ 85,720.66
Add amount appropriated during year		100,578.34
BALANCE AUGUST 31, 1955		$186,299.00

ANNUAL REPORT OF THE SECRETARY

WILLIAM H. EISENMAN, *Secretary*

THE ASM OF TOMORROW

AS A reminder to those who were present at the Annual Meeting a year ago and for the benefit of those who were not present, I wish your indulgence while I restate, briefly, the five points I proposed in my plan for THE ASM OF TOMORROW.

NO. 1—(APPROVED)
A NEW, ADEQUATE, IMPOSING ASM HEADQUARTERS BUILDING

Leadership is the sum total of many things, not the least of which is looking the part! The present ASM headquarters lack the sufficient space, are susceptible to fire, burglary and are located in a down-trend area. To correct this, it has been approved that a new headquarters site be selected and a new concept of ASM'S present and future needs be incorporated in today's planning of the building.

NO. 2—(APPROVED)
THE ASM METALS ENGINEERING INSTITUTE

This vital and aggressive idea was born of an urgent national need . . . that of developing on-the-job and home-study courses to produce a vast and extremely useful number of skilled technicians in industry. With fewer than 9,000,000 skilled men in our current labor force of some 62,000,000 . . . this nation needs millions more men in the metals industries who will know not only what is happening to the metals they work with . . . but why . . . and how.

To create these on-the-job and home-study courses, the best talent in the country has been selected and men of real achievements in metallurgy, in metals engineering, production and development were assigned to write clear . . . easily understandable . . . nontechnical courses on the subjects in which they excel. Some of these courses have been completed and they offer a quick, concise and workable method of turning millions of skilled men into the skilled and knowing technicians! There will be forty such courses available . . . for ASM Chapter Educational Courses . . . for on-the-job training . . . for home-study by individuals.

NO. 3—(APPROVED)
THE ASM METALLURGICAL SEMINARS

Top metals scientists and metals specialists will head intensive one-week and two-week seminars on current phases of metallurgy and metals engineering. Scheduled throughout the year, these ASM Metallurgical Seminars would fill a great need . . . will provide working metals engineers with quick, effective and profitable refresher

courses . . . or highly informative and helpful introduction to new metals, methods and processes.

No. 4—(To be Considered at a Later Date)
The ASM Metals Research Laboratory

In line with the dynamic expansion plans so far approved, the Metals Research Laboratory, properly organized and directed, would fill an area now unoccupied and perform important functions now neglected, yet of great importance to America's metallurgical advances. At present, laboratories in and for the metals industry may be roughly subdivided as follows: (1) laboratories in the individual plant or in a central location of a single corporation . . . (2) Government laboratories, essentially in the same categories as those mentioned above . . . (3) Commercial testing laboratories, many of which are doing development work. However, in metallurgy these are largely confined to inspection and representation . . . (4) University and endowed (or self-supporting) research institutes, whose work is principally an extension of that listed in subdivisions 1 and 2 upon well-defined problems beyond the manpower or instrumentation available in the sponsor's own laboratory . . . (5) Laboratories for fundamental research, of which there are but a few.

With only one of the above listed laboratory groups working at the advanced frontiers of knowledge, it may be readily seen that there is a very wide—and fruitful—field open to the ASM Metals Research Laboratory . . . the whole area of industrial problems in metals of widest generality, useful to the whole metals industry, or to the whole heat treating industry, or to the whole super-power industry, etc. Since—there is nothing like it in America . . . the ASM Metals Research Laboratory with the objective of solving general problems concerning the use, improvement and application of metals in industry—would not be competing with existing effort, but would, in fact, fill a great gap in American metallurgical research.

No. 5—(To be Considered at a Later Date)
The ASM Metal Science University

An intriguing and provocative idea, a natural step from the research desk to the teaching platform . . . certain to attract to it the top metal scientists, engineers and researchers. It would offer courses only in metal sciences . . . beginning with third-year students and continuing through the post-graduate studies. To such student body, the great teaching abilities of the best in America would be offered . . . and from such a group of teachers and students would, of necessity, come important achievements and trained scientists. These five points represent large plans.

I can think of no better way to enlist your support for the ASM

OF TOMORROW than to recall the supplication made last year when the original plans were presented which was "the ASM should make no LITTLE plans."

May I repeat the statement of the eminent architect, David H. Burnham, who wrote:

> "Make no little plans
> They have no magic to stir one's blood and probably themselves will not be realized.
> Make only big plans
> Aim high in hope and work
> Remembering that a noble, logical diagram once recorded
> Will never die
> But long after we are gone
> Will be a living thing
> Asserting itself with ever growing insistency."

I am sure a new life of service and usefulness is unfolding for the ASM. It has and will continue to grow in stature and prestige. You have established its leadership. These plans for the present and future have kindled for the members a brilliant vision of new progress, expansion and services.

The receipt from many members of commendations and their assurances of support and cooperation in the fulfillment of these plans has been a source of great satisfaction to all concerned. It proves that the members also aim high in hope, and are deep in the belief that no logical plan is impossible of accomplishment when united effort goes to work. The ASM has taken on new life and vigor by directing its capabilities in new and constructive channels.

If the ASM is not to grow old and stagnant and travel in the same old yearly rut, one must ask this question: "Is the ASM continually widening its interests? Is it looking to the future and planning for the great events ahead, of which it is so capable?"

I can give you the answer. With my knowledge of your wholehearted support and tremendous abilities to grasp and do new things, I can state with every assurance that the first 38 years of this Society's existence have witnessed only the beginning of its accomplishments. The years to come will sparkle with magnificent achievements that you are now constructing on today's firm foundation.

The ASM will never grow old—for a society becomes old only when it ceases to grow. "Cease to grow" could never be the motto of the ASM OF TOMORROW.

1955—Annual Report of the Secretary

The American Society for Metals on October 1, 1955 had a total membership of 25,250, a gain of 950 members since last October.

Of this number 21,690 are regular members, 1170 are student members, 2211 are sustaining members, 78 are honorary and life members and 101 are in the armed forces.

Publications Committee

Seventeen persons constitute the membership of the Publications Committee for 1955, under the chairmanship of Peter Payson, Crucible Steel Co. of America, Pittsburgh. The members of the Committee and their Chapter affiliation are: B. L. Averbach, Boston; Howard S. Avery, New Jersey; J. Alfred Berger, Pittsburgh; W. O. Binder, Buffalo; G. W. Birdsall, Louisville; D. J. Carney, Chicago; R. D. Chapman, Detroit; H. J. Elmendorf, Worcester; G. A. Fritzlen, Purdue; J. L. Gregg, Oak Ridge; Robert I. Jaffee, Columbus; Joseph F. Libsch, Los Angeles; W. D. Manly, Oak Ridge; G. V. Smith, Southern Tier; James L. Wyatt, Cleveland and Ray T. Bayless, Secretary, Cleveland.

During the year the Committee has reviewed 96 papers. Of this number 47 papers were approved for publication in Transactions, 39 of which were selected for presentation at the October National Metal Congress and 8 for publication in Transactions only. Forty-nine papers were not approved for publication and returned to authors. A few of these may be revised according to Committee suggestions and returned to the Society for re-review. Ten papers are now in the process of review.

The Publications Committee held one formal meeting on July 14 and 15, 1955, at which time the final arrangements for the technical program at this Convention were made.

Educational Committee

The Educational Committee for the year 1955 was composed of the following personnel: C. H. Lorig, Columbus, Chairman; D. J. Blickwede, Bethlehem; W. J. Buechling, Warren; J. M. Edge, Birmingham; R. S. Guinan, Rochester; W. T. Lankford, Pittsburgh; Melvin R. Meyerson, Washington, D. C.; A. U. Seybolt, Schenectady; Harold J. Smith, Louisville and Ray T. Bayless, Secretary, Cleveland.

This Committee held one formal meeting on January 20, 1955 at which time the educational lectures for this Convention were discussed and the lectures for the 1956 Convention were arranged. These lectures are:

1955

Four Lectures on "Embrittlement Phenomenon"
by B. R. Queneau, United States Steel Corporation

1956

"Residual and Trace Elements in Metals and Their Effect on Properties"

It was planned that this would be a series of 4 or 5 one-hour lecture sessions to be held Monday and Tuesday morning and afternoon. The coordinators for this symposium are A. U. Seybolt and D. J. Blickwede, but no authors were selected to take part in this series at this meeting.

Educational Films

It is interesting to know that the 3 different films produced under the guidance of the Educational Committee have had a remarkable usage by the Chapters and other educational groups.

Metal Crystals.....726 times
Iron-Carbon Alloys.....330 times
Heat Treatment of Steel.... 27 times

No plans were laid for additional or future motion pictures produced as an ASM activity under this committee.

ASM Metals Handbook Committee

The work toward the next full edition of the ASM METALS HANDBOOK continues, with the contributions of the author committees for the past year being made immediately available to the members as a Supplement. This second Supplement was again issued as a 13th issue of METAL PROGRESS, dated August 15, 1955.

Nineteen author committees submitted reports on 21 subjects selected by the Handbook Committee. These reports, which were approved for publication by the Handbook Committee, include revisions of Handbook articles as well as new subjects.

Additional committees are being formed to bring the Handbook articles up to date.

Sales of the 1948 edition were 1722.

Special Libraries Association

The Metals Division of the Special Libraries Association is again presenting its popular display of current reference sources and services at the National Metal Exposition. It is also sponsoring a three-day meeting including technical sessions and inspection trips. One session is a symposium on the indexing systems in industrial libraries, and another is on the literature of powder metallurgy. Field trips are scheduled to Bethlehem Steel Co., Franklin Institute and the American Society for Testing Materials.

At the Exposition literature specialists are in attendance at the S.L.A. booth to demonstrate library service on current problems and suggest pertinent sources for requirements in individual fields.

Mechanized Literature Searching

At the meeting of the Board of Trustees on March 29, 1955 a committee was appointed to investigate the feasibility of ASM activity in the field of literature searching by mechanical methods using computing type of equipment. This committee was under the chairmanship of D. C. Hilty, Metals Research Laboratories of the Electro Metallurgical Company. As a result of the committee's investigation and report, the Board of Trustees at its meeting on August 22 approved a pilot plant study of mechanized searching to be conducted under a contract with the Center for Documentation and Communication Research at Western Reserve University. This contract, which will be executed by J. W. Perry and Allen Kent, respectively Director and Associate Director of the Center for Documentation and Communication Research, provides for the indexing of informative abstracts in current metallurgical literature and preparation of a coding system for machine searching and correlating.

It is estimated that the pilot operation will take from 2 to 5 years and will encompass the indexing of some 23,000 documents. The contract is written on an annual basis at a cost of $15,000 per year. During the pilot operation test searches will be conducted periodically, and as soon as the system has been worked out satisfactorily and determined to be successful, it will be turned over to ASM to operate as a bibliographic service to members and the metals industry. During the pilot operation a steering committee of ASM members will provide guidance and evaluation of progress at appropriate intervals.

Assuming that the system is proved successful, services of various types will be possible—answers to specific questions, compilation of bibliographies, monthly lists of references in certain specific branches of metallurgy. Thus the ASM will not only be able to offer a greatly expanded literature service to its members and to the profession, but is also taking the lead in solving a problem that is most pressing in all scientific fields.

Transactions

Since the last National Metal Congress, Vol. 47 and Vol. 47A of the Transactions were published and distributed in May to those in our membership who requested them. Vol. 47 totals 1068 pages and contains 48 technical papers and their discussions. It contains all of the papers that were presented at the 1954 Convention held in Chicago, together with 8 interim papers. The president's, secretary's and treasurer's reports for 1954 and other current items of record were included in Vol. 47 together with a report of the 1954 Convention.

Vol. 47A contains 12 papers (238 pages) presented at the Seminar on "Impurities and Imperfections" held on Saturday and Sunday, October 30 and 31, 1954, during the National Metal Congress and Exposition in Chicago. This seminar was sponsored by the American Society for Metals, the subject being selected by a committee appointed by the Board of Trustees. The personnel of this committee was: David Turnbull, chairman; P. A. Beck, Harvey Brooks, Bruce Chalmers, R. L. Cunningham, Eric Jette, L. K. Jetter, E. S. Machlin, R. Maddin, O. T. Marzke, A. S. Nowick and Frederick Seitz. The preparation and coordination of the series of subjects and solicitation of authors was conducted by O. T. Marzke.

Preprints of Convention Papers

Thirty-nine papers were selected by the Publications Committee for presentation at this convention. These papers were preprinted and distributed to members of the Society. The total number of pages in this series of preprints is 834. A total of 46,000 preprint copies was distributed free to those members who requested them.

Metal Progress

This report concerns the 12 regular monthly issues of Metal Progress, prepared by the editorial staff. The 13th issue in mid-August will be noted in the report of the Metals Handbook Committee.

Fiscal 1955 was the most successful financial year in the history of your monthly engineering magazine. Although the total advertising volume (1911 pages) has been exceeded five times by small margins, the slightly higher rates per page and lower printing costs have resulted in a surplus of income over expenditure of nearly $203,000.00. Editorial pages in the 12-months' issues totalled 854 pages—also an all-time high. High quality of content and appearance was maintained, as indicated by the continuing reader survey conducted by the R. O. Eastman organization, and also by a most favorable critique held in New York City at the February meeting of the American Institute of Graphic Arts with Charles Tudor, Art Editor of *Life* as moderator.

The January issue of Metal Progress, which was its third international review of metallurgy, contained 14 articles from foreign experts who described progress currently being made in their respective specialties. These articles came from all over the free world —England, Australia, Sweden, Japan, Belgium, West Germany, France and Switzerland—together with one not very flattering appraisal of metallurgical conditions in Russia as gleaned from bits of escaping information. Other notable series of articles were on furnace atmospheres and atmosphere generation, on brittle failure

of steel structures, and on molybdenum metal and its alloys. The usual departments were continued, such as "Critical Points," "Atomic Age," "Book Reviews," "Biographies" and "Digests of Important Articles."

Shortly after the turn of the year, John Parina, Jr., Associate Editor, transferred to the editorial staff of METALS HANDBOOK and was replaced by John F. Tyrrell, a metallurgist who had been in the New York business office for several years. The present staff consists of E. E. Thum, Editor; John F. Tyrrell, Associate Editor; Marjorie R. Hyslop, Managing Editor; George H. Loughner, Production Manager; and Edith W. Bennington, head of the secretarial staff.

With the end of the 1955 fiscal year, METAL PROGRESS is completing the first 25 years of its life, and it is being commemorated with an anniversary issue dated September, wherein 17 interesting articles on as many branches of the metals industry describe the existing situation, tell how we got that way and venture an opinion about where we go from here. Mr. Thum and Mrs. Hyslop were present 25 years ago when METAL PROGRESS was born and are responsible for its safe upbringing to maturity. Sale of advertising space has been under the direction of A. P. Ford for almost 20 years, and from a financial standpoint the magazine has more than justified the hopes of the Board of Trustees when it was conceived. The consolidated profit-and-loss statement, 1931 to 1955 inclusive, shows a net gain of $1,294,195.75.

METALS REVIEW

During the twelve months from October 1954 through September 1955 METALS REVIEW published a total of 632 pages—359 pages, or 57%, devoted to news of chapter activities, doings of members and headquarters actions; 273 pages, or 43% devoted to the ASM Review of Metal Literature. Special features carried during the year included the annual Student Members Placement Service in the February issue, a series of special stories on the Joint Metallurgical Societies Meeting in Europe, and programs of the National Metal Congress and Western Metal Congress.

One of the noteworthy developments during the year has been an increase of more than 100% over 1954 in amount of paid advertising. Most of this is for company recruitment of personnel, which supplements the Society's free employment service to members. During the months of August and September the increase was threefold—144 column-inches (six-pages) in September 1955 as against 43 column-inches in September 1954.

The monthly Review of Metal Literature was again correlated into the 11th bound volume, which carries a total of 831 pages and 9303 annotations.

Books

During the past fiscal year 30,161 books published by the Society were sold to members of the Society and others. This figure includes 1953 ASM Metals Handbooks and 4757 Metals Handbook Supplements printed in July 1954 and 2978 Transactions.

During this period 7 titles were added to the publication list. They are:

Basic Metallurgy
Behavior of Metals Under Impulsive Loads
Transactions of ASM - Vol. 47
Impurities and Imperfections
Review of Metal Literature - Vol. XI
The Metal Beryllium - 39 Authors
Utilization of Heat Resistant Alloys - 17 Authors

Seminar on Theory of Alloy Phases

The Seminar on Theory of Alloy Phases this year was indeed an outstanding success in every respect. It was arranged into five sessions, three on Saturday and two on Sunday with the meeting room filled to capacity. This interest is a great compliment to the Committee and especially to the authors who presented their subject matter so splendidly.

The Seminar Committee on arrangements consisted of the following personnel: P. A. Beck, Chairman, Peoria; B. L. Averbach, Boston; Bruce Chalmers, Boston; R. L. Cunningham, Ottawa Valley; J. C. Fisher, Eastern New York; Eric Jette, Los Alamos; E. S. Machlin, New York; R. Maddin, Baltimore; A. S. Nowick, New Haven; Thornton Read, New Jersey; Frederick Seitz, Urbana and O. T. Marzke, Washington. The preparation and coordination of the series of subjects and solicitation of the speakers were under the direction of Paul A. Beck.

ASM Science Achievement Awards

The ASM's Fifth Annual Program of SCIENCE ACHIEVEMENT AWARDS for students in the Junior and Senior High Schools, public, parochial and private in the United States and Canada has just been announced by the National Science Teachers Association under whose auspices the program is carried out. There are 140 awards totaling $10,000 in Government bonds for projects in any field of science or mathematics.

In addition, projects at any grade level which deal with metals and metallurgy will be considered for 20 special national awards of $100 each.

The principal purpose behind these awards is to create an interest on the part of the student in science, hoping he will ultimately be prepared and will wish to enter an engineering school.

While many groups are working at the High School level to recruit students for the engineering schools, the ASM is the only society extending its activities into both the Junior and Senior grades.

After four years of operation and now at the beginning of the fifth program, we have definite evidence that the results are very encouraging indeed and is a movement forward in the right direction.

Honorary Life Memberships

Honorary life memberships in the Society were conferred on the following: Howard Biers, Union Carbide & Carbon Corp., New York, N.Y.; Paul Albert Brenner, Deutsche Gesellschaft für Metallkunde, Germany; Sir Charles Bruce-Gardner, The Iron and Steel Institute, England; Pierre Coheur, Centre National de Recherches Metallurgiques, Belgium; Dr. Maurice Cook, Institute of Metals of Great Britain; Aldo Dacco, Associazione Italiana di Metallurgia, Italy; Raoul de Vitry, Societe Francaise de Metallurgie, France; Docteur Eugene L. Dupuy, Secretary-General, Societé Francaise de Métallurgie, France; S. Fornander, Jernkontoret, Sweden; S. C. Guillan, The Institute of Metals, England; K. Headlam-Morley, The Iron and Steel Institute, England; F. Perot, Centre National de Recherches Métallurgiques, Belgium; Augustin Plana, Instituto Del Hierro y Del Acero, Spain; Dr. Hermann Schenck, Verein Deutscher Eisenhüttenleute and Deutsche Gesellschaft für Metallkunde, Germany; Kurt Thomas, Verein Deutscher Eisenhüttenleute and Deutsche Gesellschaft für Metallkunde, Germany; Dr. B. Trautmann, Deutsche Gesellschaft für Metallkunde, Germany.

National Metal Congress

The program for the Congress this year was more varied and intense than any during the previous years.

The general trend of the Convention program has been greater diversification of the subjects presented, and while this leads to a more varied technical program, nevertheless it serves the wide interests of the Metal Congress attendance and in this manner creates a greater attendance, with the resultant wider dissemination of valuable technical information.

National Metal Exposition

The National Metal Exposition now in session equals the number of exhibitors, some 450, and the amount of square feet, 150,000 net, that has characterized the expositions in the past.

It has been three years since the National Metal Congress was in the East, consequently, the new developments and the new processes being shown at the Exposition represent new ideas and profitable projects to the group of spectators who found it impossible

to follow the Show in its procession to Cleveland and Chicago and return.

This is the 6th Metal Exposition that has been held in Philadelphia, and is the 37th in number.

The first Exposition was held in Chicago in 1919, and the second was held in Philadelphia, just 35 years ago.

We are all especially appreciative of the fine displays and operating exhibits that are placed before the members and their guests. They have made the Exposition an outstanding one. Until today it is the largest annual exhibit held in America.

Young Engineers' Day

The Society again extended an invitation to all student members of all educational institutions within a radius of 100 miles to be the guests of the Society on Friday, October 21, to visit the Exposition and attend the Distinguished Service Luncheon, given by the Society in honor of the 25-year members.

Some 200 student members and faculty attended this event together with over 200 of the 25-year members.

Vocational Education Committee

The VOCATIONAL EDUCATION COMMITTEE under the capable chairmanship of William Collins of the Boston Chapter, has had as its principal field for the past three years Vocation Teacher Training in Metals Technology. This activity has the full cooperation of top state level administration. The states cooperating are—

New York	Illinois
Connecticut	Indiana
Massachusetts	Kansas
Pennsylvania	California, and
Michigan	British Columbia

The momentum inaugurated by the Committee has been such that the Teacher Training is now proceeding on its own, and the Committee is now turning its concentrated energies to work in cooperation with Technical Institute.

ASM Visiting Lectureship

These Lectureships have become increasingly popular and 12 schools made application for lecturers to conduct a two-day seminar on the campus. The reports from the schools express their thanks for the service and indicated complete satisfaction.

Those schools availing themselves of this ASM Service were—Laval University, British Columbia University, McGill University, Toronto University, Missouri School of Mines, University of Cincinnati, South Dakota School of Mines, New York University, Illinois Institute of Technology, Notre Dame University, University of Wisconsin, and Johns Hopkins University.

Metallographic Exhibit

The METALLOGRAPHIC EXHIBIT held each year during Convention Week at the Exposition Hall has assembled some of the top metallographic studies of the year. It always seemed a shame that some of those members who could not get to the Convention should fail to see them.

Consequently a traveling exhibit of the prize winners, and a few Honorable Mentions were mounted and started on a Chapter circuit. The panels were placed on display before some 19 chapters and several educational schools.

Comments from the Chapters were very flattering and the "Traveling Micrograph Galleries" will become our annual feature.

American Society for Metals Foundation for Education and Research Annual Report of the President

James B. Austin, *President*

THIS report covers the twelve months from September 1, 1954 to August 31, 1955. During this period the Trustees have continued the policy of concentrating on support for metallurgical education. As in earlier years an undergraduate scholarship of $400 was awarded to each college in the United States and Canada having a day-school degree course in metallurgy or metallurgical engineering. The list of such colleges was again carefully reviewed and a total of 49 such scholarships were granted to the following schools:

Report on Scholarships for 1954–55

The following is a listing of the 48 participating schools in U. S. and Canada with the scholarship winners:

School	Location	Dept. Head	Scholarship Winner	Address
University of Alabama	University, Ala.	E. C. Wright	Harry Duane Bradshaw	Messick, Va.
University of Arizona	Tucson, Ariz.	J. B. Cunningham	Cletis C. Land	Yuma, Ariz.
University of British Columbia	Vancouver, B. C.	F. A. Forward	Grenville Robert Mason	5619 Kerr St. Vancouver 16, B. C.
Carnegie Inst. of Tech.	Pittsburgh, Pa.	R. F. Mehl	Paul Borland (Repeat)	Aspinwall, Pa.
University of Cincinnati	Cincinnati, O.	Wm. Licht	James Myers	719 Charles St. Middletown, O.
University of California	Berkeley, Calif.	E. R. Parker	Charles Arlen Kindness	2600 Ridge Rd. Berkeley, Calif.
Case Institute of Technology	Cleveland, O.	A. R. Troiano	Kenneth Fetheroff	1282 E. 152nd St. Cleveland, O.
Colorado School of Mines	Golden, Colo.	H. Gordon Poole	Stanley G. Young	Colorado Springs, Colo.

School	Location	Dept. Head	Scholarship Winner	Address
Columbia University	New York, N. Y.	M. Gensamer	Ernst B. Weglein	New York, N. Y.
Cornell University	Ithaca, N. Y.	F. H. Rhodes	Robert Hillis Steels	903 Hamilton Ave. Latrobe, Pa.
Drexel Institute of Technology	Philadelphia, Pa.	A. W. Grosvenor	Richard Dampman	149 W. Albemarle Lansdowne, Pa.
University of Illinois	Urbana, Ill.	T. A. Read	Joseph Francis Enrietto	406 W. Devlin St., Spring Valley, Ill.
Illinois Institute of Technology	Chicago, Ill.	L. F. Mondolfo	Lawrence N. Hjelm	Bensenville, Ill.
University of Kansas	Lawrence, Kan.	K. E. Rose	Robert Wayne Reck	227 W. 11th St. Hutchinson, Kan.
University of Kentucky	Lexington, Ky.	C. S. Crouse	Geo. D. Ravencraft	2245 High St. Ashland, Ky.
Lafayette College	Easton, Pa.	L. Donovan Clark	John P. Smith	252 W. Wilkes-Barre Easton, Pa.
Universite Laval	Quebec City, Quebec	L. Letendre	Paul-Henri Doyon	Sherbrooke, P. Q.
Lehigh University	Bethlehem, Pa.	Allison Butts	John E. Brokloff	Fullerton, Pa.
Massachusetts Institute of Technology	Cambridge, Mass.	John Chipman	Ronald Stanley Kintisch	2845 S. Buchanan Arlington, Va.
McGill University	Montreal, Que.	J. U. MacEwan	Richard Arthur Winter	18 Bluebell Rd. Worcester 6, Mass.
University of Michigan	Ann Arbor	Donald L. Katz	Dwight Alan Kraai	Holland, Mich.
Michigan College of Mining and Technology	Houghton, Mich.	C. T. Eddy	Auvo I. Kemppinen	420 Lovell Rd. Houghton, Mich.
Michigan State	East Lansing, Mich.	A. J. Smith	Neal T. Saunders	3360 Polk St. Dearborn, Mich.
University of Minnesota	Minneapolis, Minn.	R. L. Dowdell	Willmar K. Boeder	5325 Bloomington, Minneapolis, Minn.
Missouri School of Mines	Rolla, Mo.	A. W. Schlechten	Warren Lieberman	3265 Bainbridge New York, N. Y.
Montana School of Mines	Butte, Mont.	F. A. Hames	Samuel A. Worcester	1115 W. Woolman Butte, Mont.
New York University	New York, N. Y.	J. P. Nielsen	Arnold Lent	114 Field Place Bronx, N. Y.
University of Notre Dame	South Bend, Ind.	E. A. Peretti	Dewey C. Antrobus	705 N. Willette Memphis, Tenn.
Nova Scotia Technical	Halifax, N. S.	A. E. Campbell	Gordon Samuel Trivett	Sydney, N. S. 37 Castle Drive

School	Location	Dept. Head	Scholarship Winner	Address
Ohio State University	Columbus, O.	M. G. Fontana	Thomas William Griffiths	Box 528 North Lima, O.
University of Pennsylvania	Philadelphia, Pa.	R. M. Brick	Robert L. Novak	1646 Maryland St. Camden, N. J.
University of Pittsburgh	Pittsburgh, Pa.	J. Alfred Berger	Harold M. Priestley	Pittsburgh, Pa.
Pennsylvania State University	State College, Pa.	Amos J. Shaler	Gerald E. Cooper	1802 McGalliard Trenton, N. J.
Polytechnic Institute of Brooklyn	Brooklyn, N. Y.	E. L. Midgette	Olev Paul	320—50th St. Brooklyn, N. Y.
Purdue University	Lafayette, Ind.	R. Schuhmann	Lee Roy Duffner	3244 S. 51st St. Milwaukee, Wisc.
Queen's University	Kingston, Ontario	T. V. Lord	Desmond Mathew Peplinski	Kingston, Ont.
Rensselaer Polytechnic Institute	Troy, N. Y.	Arthur A. Burr	Chas. O. Kunz	Delmar, N. Y.
South Dakota School of Mines	Rapid City, So. Dak.	Paul Anderson	Sherrill G. Swenson	Rapid City, So. Dak.
Stanford University	Stanford, Calif.	O. Cutler Shepard	Ray Remy Dils	522 Mayfield Ave. Stanford, Calif.
University of Tennessee	Knoxville, Tenn.	E. E. Stansbury	B. M. Hargis	Knoxville, Tenn.
Texas Western	El Paso, Tex.	J. C. Rintelen, Jr.	Robt. Boisvert	El Paso, Tex.
University of Toronto	Toronto, Ont.	L. M. Pidgeon	D. H. Jurden	Sudbury, Ontario
University of Utah	Salt Lake City, Utah	John R. Lewis	Bartholomeus Herbert	480 Third Ave. Salt Lake City, Utah
Virginia Polytechnic	Blacksburg, Va.	M. V. Nevitt	John Dorsey White	7208 W. Franklin Richmond, Va.
State College of Washington University of Washington	Pullman, Wash.	J. P. Spielman	Verl H. Kahle	Pullman, Wash.
Wayne University	Detroit, Mich.	Harold G. Donnelly	John Garfield Dodge	Clawson, Mich.
University of Wisconsin	Madison, Wisc.	E. R. Shorey	Henry G. Goehring, Jr.	Madison, Wisc.
			C. Barcley Gilpin	Madison, Wisc.
Yale University	New Haven, Conn.	Arthur Phillips	John Q. Hunsicker IV	Darien, Conn.

In addition, the Trustees established for the year 1955–56 an ASM Graduate Fellowship for advanced study in the amount of $2400 for a single person, or $3000 for a married man, with an accompanying grant of $1200 to his college for tuition and research

expenses. The recipient of this award was William Upthegrove, who has selected the University of Michigan for further graduate work.

The Foundation continued in good financial condition, as is evident from the following brief (unaudited) summary:

Endowment Principal

As of August 31, 1954	$654,343.61
Additional grant from ASM, September 1, 1954	3,500.00
Net gain on disposal of securities	207.56
Principal as of August 31, 1955	$658,051.17

Income and Expense

Income		
Balance as of August 31, 1954	$ 9,120.43	
Income from interest	29,866.40	
		$38,986.83
Expense		
Scholarships awarded	$ 19,600.00	
Other expense	2,904.43	
		$22,504.93
Excess of income over expense		$16,481.90

The Trustees of the Foundation take this opportunity to thank the American Society for Metals for permission to make this report at the Annual Meeting and to publish it in the Transactions of the Society.

J. B. Austin, President
G. A. Roberts
John Chipman
R. L. Wilson
W. E. Jominy, Treasurer

BALANCE SHEET

AMERICAN SOCIETY FOR METALS FOUNDATION FOR EDUCATION AND RESEARCH—November 30, 1955

ASSETS

CASH ON DEPOSIT		
The Cleveland Trust Company:		
Income cash	$ 20,079.40	
Principal cash	329.59	$ 20,408.99
MARKETABLE SECURITIES (approximate market prices aggregate $833,719.40)		
Bonds and stocks—Note A		682,784.77
OTHER INCOME ASSET		
Accrued bond interest		3,318.59
		$706,512.35

FUNDS

PRINCIPAL OF ENDOWMENT FUND		
Grants from American Society for Metals	$680,346.10	
Profit on disposal of securities	2,768.26	$683,114.36
UNAPPROPRIATED NET INCOME		23,397.99
		$706,512.35

Note A—Securities obtained by grant from American Society for Metals are stated at market price at July 15, 1952. Subsequent additions are at cost.

STATEMENT OF INCOME AND EXPENSES AND UNAPPROPRIATED NET INCOME

AMERICAN SOCIETY FOR METALS FOUNDATION FOR EDUCATION AND RESEARCH—Year ended November 30, 1955

INCOME		
Dividends, interest and discount earned		$ 30,370.08
EXPENSES		
Fiscal agents' fees and expenses	$ 1,516.66	
Professional services	600.00	
Stationery and supplies	203.57	
Board of Trustees	58.38	
Other travel expenses	53.26	2,431.87
NET INCOME		$ 27,938.21
Unappropriated net income at beginning of year		19,259.78
		$ 47,197.99
Scholarship awards	$ 19,600.00	
Graduate Fellowship award	4,200.00	23,800.00
UNAPPROPRIATED NET INCOME NOVEMBER 30, 1955		$ 23,397.99

Board of Trustees,
American Society for Metals Foundation
for Education and Research, Cleveland, Ohio.

We have examined the balance sheet of American Society for Metals Foundation for Education and Research as of November 30, 1955, and the related statement of income and expenses and unappropriated net income for the year then ended. Our examination was made in accordance with generally accepted auditing standards, and accordingly included such tests of the accounting records, and such other auditing procedures as we considered necessary in the circumstances.

Securities were confirmed to us by the Cleveland Trust Company, agent.

In our opinion, the accompanying balance sheet and statement of income and expenses and unappropriated net income present fairly the financial position of American Society for Metals Foundation for Education and Research at November 30, 1955, and the results of its operations for the year then ended, in conformity with generally accepted accounting principles applied on a basis consistent with that of the preceding year.

ERNST & ERNST
Certified Public Accountants

Cleveland, Ohio
December 12, 1955

ELECTION OF OFFICERS

PRESIDENT ROBERTS: We will now proceed with the election of officers. Complying with the Constitution, I appointed in March 1955 the following Nominating Committee selected from a list of candidates suggested by the eligible chapters prior to March 1, 1955.

Chairman: Max W. Lightner-Pittsburgh

William L. Badger—Boston
M. A. Hunter—Eastern New York
W. J. Nash, Jr.—Los Angeles
A. J. Schied, Jr.—Calumet
Hiram Brown—Des Moines
H. J. Huester—Jacksonville
George Perkins—Louisville
Don Sener—York

The Nominating Committee met on May 19, 1955 and made the following nominations:

FOR PRESIDENT

A. O. Schaefer, Vice President,
Midvale Company, Nicetown, Pa.—1 year

FOR VICE-PRESIDENT

D. S. Clark, Professor of Mechanical Engineering,
California Institute of Technology, Pasadena, Calif.—1 year

FOR TRUSTEES

G. E. Shubrooks, Manager of Research Lab.,
Hamilton Watch Company, Lancaster, Pa.—2 years

H. A. Wilhelm, Research Professor of Chemistry,
Iowa State College, Ames, Iowa—2 years

Complying with the Constitution, the Secretary has informed me that no additional nominations were received prior to July 15, 1955 for any of the vacancies appearing on the Board of Trustees. Consequently, the nominations were closed. I now call upon the Secretary to carry out the provisions of the Constitution with respect to the election of officers:

SECRETARY EISENMAN: Conforming to the provisions and requirements of the Constitution of the American Society for Metals, I hereby cast the unanimous vote of the members for the election of the aforenamed candidates who were nominated on May 19, 1955.

The President introduced the newly elected officers and called upon the President-elect, Adolph O. Schaefer, to say a few words.

PRESIDENT ROBERTS: Has anyone present anything to bring before the meeting for the good of the Society?—If not, then a motion to adjourn is in order.

The meeting then adjourned.

ASM ANNUAL DINNER

On Thursday evening, October 20, members and guests assembled in the Crystal Ballroom of the Benjamin Franklin Hotel for the Annual Dinner of the Society. The attendance was in excess of 400.

Those persons seated at the speakers' table were: John P. Clark, Jr., Partner, John P. Clark Co.—Chairman, Philadelphia Chapter, ASM; Geoffrey V. Raynor, University of Birmingham (England)—ASM Visiting Lecturer; Walter Crafts, Electro Metallurgical Division, Trustee, ASM; G. M. Young, Aluminum Co. of Canada, Ltd.,—Trustee, ASM; Robert J. Raudebaugh, Interna-

tional Nickel Co.,—Trustee, ASM; William A. Pennington, University of Maryland—Treasurer, ASM; Kenneth E. Rose, University of Kansas, Recipient of 1955 ASM Teaching Award; Donald S. Clark, California Institute of Technology—Vice-President-Elect, ASM; James P. Gill, Vanadium-Alloys Steel Co.—Past-President, ASM; Alfred L. Boegehold, General Motors Corp., Recipient of 1955 ASM Gold Medal; Adolph O. Schaefer, The Midvale Co., Vice-President and President-Elect, ASM; James B. Austin, United States Steel Corp., Past-President-Trustee, ASM; Rear Admiral H. G. Rickover, USN, United States Atomic Energy Commission and speaker of the evening; George A. Roberts, Vanadium-Alloys Steel Co.—President, ASM; Roger W. Straus, American Smelting & Refining Co., Recipient of the 1955 ASM Medal for the Advancement of Research; Kent R. Van Horn, Aluminum Co. of America, Past-President, ASM; William J. Kroll, Consulting Metallurgist, Recipient of Sauveur Achievement Award, 1955; Albert E. White, Consulting Metallurgical Engineer, Founder-Member and First-President, ASM; John A. Marsh, International Nickel Co., Inc., Recipient of Distinguished Service Award for International Nickel Co.; Bradley Stoughton, Consultant, Dean of Engineering, Retired, Lehigh University—Past-President, ASM; Karl L. Fetters, Asst. to Vice Pres., in Charge of Operations, Youngstown Sheet & Tube Co.—Trustee, ASM; Clarence H. Lorig, Battelle Memorial Institute—Treasurer-Elect, ASM; H. A. Wilhelm, Atomic Energy Commission and Iowa State College—Trustee-Elect ASM; Peter Lillys, Crucible Steel Co. of America—Recipient of Henry Marion Howe Medal, 1955; A. E. Nehrenberg, Crucible Steel Co. of America—Recipient of Henry Marion Howe Medal, 1955; Harry N. Ghenn, American Viscose Corp.—Secretary, Philadelphia Chapter, ASM; William H. Eisenman, Founder-Member and Secretary, ASM.

Award for Distinguished Service

In 1955 the Board of Trustees of the American Society for Metals established the Award for Distinguished Service which was presented to John A. Marsh, Vice President and General Manager of the Operating Department of the International Nickel Company, Inc. In presenting Mr. Marsh, President George A. Roberts read the citation of International Nickel Company's accomplishments. The citation is:

> The Award is made on the 50th anniversary of the first production of Monel Nickel-Copper Alloy direct from the Sudbury ore. This alloy, by virtue of its strength and corrosion resistance, pioneered engineering applications of nonferrous metals in great number. From its basic composition has been developed several important modifications having increased strength,

workability, stability at high temperature, and resistance to especially corrosive surroundings. . . . For pioneering achievement, for continuous research, for far-sighted development of production facilities for an essential metal, the International Nickel Company, Inc. has performed unusually meritorious services to the Free World. . . . Therefore, by unanimous vote of the Board of Trustees of American Society for Metals this Award for Distinguished Service has been engrossed and presented on October 20, 1955.

Honorary Membership

Honorary membership in the Society was conferred on Paul D. Merica, Director of the International Nickel Co. In conferring this membership, Past-President Bradley Stoughton read the following citation:

Honorary membership in the American Society for Metals is awarded to men of outstanding achievement in the field of metallurgy who have contributed to the success of the ASM.

Dr. Merica pre-eminently merits this honor. He is a distinguished metallurgist, is generally credited with the precipitation theory of hardening. Three universities have honored him with a Doctor of Science degree.

Dr. Merica has been prominent in business. He was President of the International Nickel Company of Canada and of the International Nickel Company, Incorporated, until 1954. He is a Director of both Corporations as well as The American Metal Company, Babcock & Wilcox Company and Whitehead Metal Products Company.

He has been active in the ASM since the earliest days, being Chairman of the New York Chapter in 1922. His interest, support and attendance at functions of the Society have encouraged others to take active parts in the ASM activities.

MR. PRESIDENT, I present to you for HONORARY MEMBERSHIP in the American Society For Metals, DR. PAUL D. MERICA.

Albert Sauveur Achievement Award

In 1934 the Board of Trustees established an award consisting of a metal plaque and certificate in honor of Dr. Albert Sauveur, distinguished metallurgist and for many years an honorary member of the ASM. The purpose of this award is to recognize a metallurgical achievement which has stood the test of time and stimulated others along similar lines to the extent that a marked basic advance has been made in the metal arts and sciences. The 1955 candidate was William Justin Kroll, Consulting Metallurgist. In presenting Dr.

Kroll, Past-President Albert E. White read the citation of Dr. Kroll's accomplishments. President Roberts then conferred the award. The citation is:

> The Award is made in recognization of his pioneering achievements which have stimulated organized research along similar lines to such an extent that marked basic advance has been made in metallurgical knowledge.
>
> Dr. Kroll has many significant achievements to his credit; more than one of which would undoubtedly meet the requirements for the Sauveur Award. The achievement which was selected as the basis for this award was his pioneering work on malleable titanium. Against a background of much research work which resulted in no commercial process, Dr. Kroll recognized the necessity for producing an unadulterated metal. His work was started in 1937 and led to the first successful method for making satisfactory titanium in commercial quantities. The value of Dr. Kroll's work was recognized by the U. S. Bureau of Mines and then accepted by industrial companies. His success has stimulated a tremendous amount of additional work designed to improve or replace his process. Regardless of the outcome of these studies there is little question but that the ultimate position of titanium as a commercial metal will owe much to the pioneering activities of Dr. Kroll.
>
> Mr. President, on behalf of the past Presidents of this Society, it gives me great pleasure to present Dr. William Justin Kroll.

Conferring of the ASM Medal for the Advancement of Research

The 1955 ASM Medal for the Advancement of Research was awarded to Roger Williams Straus, Chairman of the Board of Directors and Chief Executive Officer of the American Smelting and Refining Company, in recognition of his consistent sponsorship, foresight and influence in financing and prosecuting metallurgical research, which have helped substantially to advance the arts and sciences relating to metals.

In presenting Mr. Straus, Past-President Kent R. Van Horn read the citation engrossed on the scroll which accompanies the medal. President Roberts then conferred the award. The citation is:

> A firm advocate of progress by new process development and orderly growth and expansion, Mr. Straus has never permitted financial limitations to harass the operations and growth of research within the company, a policy which was maintained even during the dark period of the early thirties

when the budget of the Research Department was courageously increased even in the face of vanishing profits.

During this period the debismuthizing of lead by means of calcium and magnesium was applied and work was initiated which resulted in the development of the Asarco process for the continuous casting of copper, and ultimately, its alloys, in a wide variety of shapes. A continued interest in the preparation and properties of the company's metals in highly purified form led to the first commercial production of high-purity selenium and to the laboratory production of high purity copper, lead, silver, zinc, arsenic, indium, tellurium, thallium, cadmium and bismuth. While the production of high purity metals was initiated to permit the measurement of basic properties of the company's metals, the realization of these has led to numerous improvements in the company's processes which have resulted in commercial products of higher purity and quality as the need for them was demonstrated.

While the above, and other activities of the Central Research Laboratories of the American Smelting and Refining Company are reasonably well known to many of this audience, the broader policy of applying funds for research within production units of the company is less well known but of no less credit to Mr. Straus' administration. These have resulted in fewer plants and furnaces producing a greater tonnage of metal at costs which have not increased in proportion to the inflation of world currencies.

A well-rounded research policy involving breadth of planning and initiative in fields not narrowly limited to production metallurgy are illustrated by the internationally known Department of Agricultural Research and the newer Department of Hygiene.

Perhaps the most obvious, but by no means most important, demonstration of Mr. Straus' support of industrial research is shown in the recently completed Central Research Laboratories at South Plainfield, New Jersey, and in the Western Research Section Laboratory being erected at El Paso, Texas.

Conferring of Gold Medal of ASM

The Gold Medal of the ASM, established in 1943, recognizes the recipient for outstanding metallurgical knowledge and great versatility in the application of science to the metal industry, as well as exceptional ability in the diagnosis and solution of diversified metallurgical problems. The 1955 ASM Gold Medal was awarded to Alfred L. Boegehold of General Motors Research Laboratory. In

presenting Mr. Boegehold, Past-President James P. Gill read the citation engrossed on the scroll which accompanies the medal. President Roberts then conferred the award. The citation is:

> Mr. Boegehold's technical education began with mechanical engineering but he chose metallurgical research as a career. The result was a successful combination of two philosophies which produced many ideas and inventions for new products and improved methods of processing and fabricating metals.
>
> More than thirty years ago, as a pioneer in the field of powder metallurgy, he was studying the technology of oil-less porous bushings for use as bearings. Eventually, a means was provided for the control of porosity without sacrificing mechanical strength. This had an important influence on advancing oil-less bearings to a commercial stage of production. A continuing interest led to many subsequent patents for the manufacture of the powdered iron, the binding of low carbon particles with high carbon particles, and the application of controlled atmospheres.
>
> Major contributions were made to the technology of malleable iron, which included a shortening of the malleable cycle by suitable control of chemistry and heat treatment and the addition of specific elements that permitted the size of castings to be increased. This work has resulted in reduced costs without sacrificing properties.
>
> An example of the versatility of his efforts are the improved coatings for the protection of ferrous metals operating at high temperatures. He suggested the aluminum dip, followed by a controlled heat treatment, which produces a protective oxide layer. This coating permitted substantial savings in critical materials in gas turbines and improved the life of furnace parts exposed to high temperature.
>
> His application of end-quench hardenability data on a sound engineering basis was an important stimulus in the proper utilization of steels through control of cooling rates to obtain uniform mechanical properties.

Address of the Evening

President Roberts then presented Rear Admiral H. G. Rickover, USN, Chief, Naval Reactors Branch, Division of Reactor Development, U. S. Atomic Energy Commission, who was the principal speaker of the evening. The address is printed in full herewith:

Chairman Strauss of the Atomic Energy Commission was to have spoken to you tonight. He has asked me to express his regrets that he is not able to be here. Also, he has asked me to tell you

that he recognizes the important role your organization plays in supporting and extending our country's atomic energy program.

I cannot give you the broad view of our program that Mr. Strauss would have presented. But I do appreciate this opportunity to speak to you because we have major problems in the use of metals in the application of atomic energy to the propulsion of ships and I am sure you can help solve them.

The successful operation of the NAUTILUS assures the application of nuclear power to many other naval vessels. Such application must be based on sure knowledge of all aspects of nuclear power plants, including materials performance.

Although I will discuss primarily the problems associated with naval plants, I am sure you will recognize that what I say applies with equal force to nuclear power plants for central stations, such as the one we are building at Shippingport, Pennsylvania.

The problems which face us are of two kinds. First are those unique to atomic energy—such as the fuel elements and other reactor components that use uranium, zirconium or beryllium and which must withstand the impact of the nuclear fission process. Second are the ones we have with conventional materials and components—such as carbon steels and stainless steels which are used in valves and heat exchangers; these are just as important as the special materials.

It is a common belief that atomic power development is primarily the province of the nuclear physicist. Nothing could be further from the truth. What actually faces us is how to determine, by calculation and by experiment, the best way to remove heat from a reactor, and then to design and build all of the components of the reactor system so that they will operate safely and reliably under the most rigorous conditions.

The problems include the familiar ones of using materials at high temperature and pressure. They also include the ability to withstand corrosion to a very high degree. The new problems raised by atomic power are caused by the fact that in nuclear fission heat is generated inside a fuel element and proceeds outward, whereas in the chemical combustion process the heat is applied from the outside and proceeds inward. In chemical combustion we are normally limited to a maximum of about 3000°F, but in nuclear fission we can achieve temperatures of millions of degrees. Moreover, we are faced with radioactivity and its tendency to distort and to weaken materials. The fact that many materials capture neutrons and thus tend to stop the chain reaction severely restricts us in their choice.

First of all, the development of suitable reactor fuel elements is the greatest problem we face. The fuel elements are those parts of the reactor core that contain the fissionable material which pro-

duces the heat, and hence must withstand high temperatures and the radiation impact of the fission process. Changes in form and substance in fuel elements are inherent in the operation of a reactor. And yet these changes must not be allowed to destroy the over-all integrity of the fuel element nor interfere with the functioning of a complex reactor with its close tolerances. The service demands on fuel elements are greater than those I know of in any other application. Work on fuel elements is a challenging new field which is receiving wide attention, and in which millions of dollars are being spent. But much creative and fundamental work still remains to be done.

The problems in fuel elements involve new materials such as uranium, zirconium, and beryllium. These are well known to you. Your society has held technical sessions on both zirconium and beryllium, and we have worked together publishing a book on zirconium and one on beryllium.

A challenging problem in the design of the NAUTILUS reactor was the development of zirconium. It was selected in 1949 because it had a low cross section for the capture of neutrons and because it was also supposed to be corrosion resistant. I vividly recall my concern when I learned that this material which we considered extremely desirable was not in production on a commercial scale and that its engineering properties were, for all practical purposes, unknown. To be sure, enough was known to indicate that it could be a suitable material, but you all know the vast gap between meager laboratory data and the full information which is needed for practical design.

We were faced with the problem of continuing with zirconium or of employing the "green pasture" approach—that is, changing to another metal. The "green pasture" concept is a very seductive one. You know the faults of what you are working with, but the new metal always appears to be much more attractive because you have not yet discovered its faults and difficulties.

Fortunately we stuck with zirconium. The naval program would have suffered substantially had we abandoned zirconium at that time. We decided to tackle the difficulties and we set up a very tight schedule for solving them. A number of the organizations represented here tonight participated with us in the crash program which led to the investigation of its engineering properties and to its production in commercial quantities.

While the production problem was being solved we learned that zirconium had corrosion qualities unsuitable for our purpose. Again an integrated crash program between industry and government got underway and was successful in providing corrosion resistant metal in time.

A "task force" consisting of a representative from each organiza-

tion doing work on zirconium was established to develop and select a more corrosion-resistant alloy. Each representative had access to his management so that the necessary changes in the program would be effected without delay. The result was development of Zircaloy-2 in time for its successful use in the NAUTILUS. Without this urgent need and the concentrated attack it probably would have taken many years before zirconium reached its present state of development.

Another example where management is helping the development of new materials is in the use of aluminum for cladding fuel elements. As you know, aluminum is much cheaper than zirconium and has as good nuclear characteristics. The problem is that for power reactors, the temperatures are so high that they result in excessive corrosion of presently available aluminum alloys. One large aluminum producer is spending its own money in cooperation with AEC laboratories to find alloys which will be satisfactory. More companies should analyze future needs and push such developments.

The development of uranium, which is essential to nuclear reactors, has been marked from the outset by insufficient knowledge of its properties. This has made it extremely difficult to develop processes for its production. For instance, as late as 1942 the tables gave the melting point of uranium at 1800°C. It is now known to be 1133°C. And yet uranium has been known since 1789 and was in use for many years prior to 1942. The actual melting point only became known during early casting operations carried out for the atomic bomb project.

So far, the metallurgical problems that have arisen in the development of nuclear power have had to be solved by empirical means since there is a scarcity of knowledge of the fundamental principles involved. Thus our metallurgical advancements have required the use of extensive manpower and the expenditures of large sums of money. Until the fundamental processes involved are understood additional large-scale use of manpower and money will be required to solve each slightly different problem as it arises. This empirical approach has just about reached its limit. The methods we are using are rapidly becoming unsuitable for solving our problems.

The empirical approach has also resulted in unexpected and unexplainable flaws and failures. These continue to plague us and cause considerable delay.

Let me illustrate what happens when there is a lack of basic understanding of metallurgy. About a year ago we decided to do basic research in uranium in the attempt to develop an alloy resistant to corrosion in water at high temperature. A number of the most experienced metallurgists and solid state physicists agreed to help

in this problem. I asked them this question: "Using the phase diagrams and other characteristics of uranium alloy presently known, what particular region would you recommend as one which offers possible promise?" They replied that they didn't even know where to start. As a result an extensive and costly empirical program has had to be undertaken.

Now I would like to review some of the specific metallurgical problems we are facing. But some may say: "It is easy to list problems, but difficult to solve them." To this I would reply: "In achievement I expect to fail, but let me never recoil from endeavor."

A major problem we face in the application of nuclear power is that of corrosion. We like to use thin sections of protecting metal as a jacket between the radioactive fuel and the coolant which conducts the heat. Thick sections of metal require the use of additional nuclear material. This tends to make the reactor larger, reduces the neutron economy, and results in increased cost. But the use of thin jacket sections of metal makes it more possible for radioactive fission products to escape into the coolant stream if undue corrosion should occur.

The undesirable effects of corrosion are not, to be sure, unique for nuclear power, but their effects can be more serious. The special coolants and operating conditions in nuclear power plants present corrosion problems quite different from the problems previously faced by industry. Most of our corrosion work has had to be done by testing a large number of slightly different materials under a wide variety of conditions before a satisfactory one could be found. Even a partial understanding of the mechanism of corrosion would permit a drastic reduction in the number of tests.

It has been estimated that corrosion of metals entails a waste of about four billion dollars per year. This points up the importance of launching a large-scale program to learn the mechanism of corrosion.

In addition to the problems of fuel elements and corrosion resistance of materials, a third area of concern is the application of conventional materials to nuclear reactors. Here also the lack of knowledge of fundamentals is holding us back.

In a large number of instances where conventional materials were specified for nuclear power plants on the basis that these materials had been used effectively and for a long time by industry we found that the basic knowledge of the reasons it had been possible to use the materials effectively was extremely meager.

In order to apply these materials to nuclear power plants with some degree of assurance that they would work satisfactorily it became necessary to make a large number of tests since there was no hope that an understanding of the fundamentals involved would

be reached within any reasonable length of time. Of these conventional materials, stainless steel has been our biggest problem. This steel has many fine properties and will continue to be important in nuclear work. However, we are demanding a great deal from it. In addition to its use for structural members, applications include use for many parts with close tolerances which are lubricated by hot water.

The state of knowledge in the welding of stainless steel is far from satisfactory. It has been necessary to devote an extreme amount of attention to its fabrication and welding, to assure that the end product is satisfactory. More effective methods and techniques are urgently needed.

Some difficulties we have had on the NAUTILUS and the SEAWOLF will indicate what I have in mind. The NAUTILUS heat exchangers have tube sheets several feet in diameter and about one foot thick; they are made from stainless steel forgings. In order to obtain four satisfactory tube sheets, eight had to be made; the first four forgings had to be rejected because of poor quality.

The pressure vessel for the NAUTILUS consists of a cylindrical shell and a hemispherical head. The shell and the head are each separately heat treated. The reactor core is then inserted, and the head is placed in position and welded to the shell. Because the core might be damaged in the process, the complete pressure vessel assembly could not be heat treated as required by code practice. As a result the weld was backed up with large bolts capable of taking the entire pressure load. This added complexity, weight, cost, and delay to the job.

We had no evidence that the weld alone was not adequate. It was simply the case that no technical information existed to tell us whether it was or was not. Since we could not take a chance and there was not time to find out, we designed the pressure vessel to use bolts in addition to the weld. In other words, an expensive complication had to be introduced because adequate knowledge was not available.

The SEAWOLF has also had its problems with stainless steel forgings for heat exchanger tube sheets. Carbon steel nuts and bolts were found embedded in the stainless steel forgings. These inclusions were discovered after machining of the tube sheets had commenced. Apparently they remained unmelted in the original ingot and were not detected during the forging operation. This certainly indicates that quality control can be improved.

Currently we are experiencing a series of difficulties with conventional materials. Unbonded areas have been found in stainless steel roll-bonded to carbon steel. In another case, a large carbon steel forging for a pressure vessel exhibited internal cracks; these

were detected after considerable work had been done on the forging and were found to be caused by shrinkage voids.

Many stainless steel castings for valve bodies have been porous —in fact, it is very difficult to obtain sound castings consistently. We have become reconciled to having extra parts made in order to be certain of obtaining sufficient good ones. And we still have not learned *why* the difficulties arise and *how* sound parts can be assured.

One of the tools we use for quality control is "ultrasonics." This is a potentially useful method for nondestructive testing. However, we do not feel that we can safely rely on it because there is still no accepted standard to tell us what ultrasonic indications actually mean.

Now, let me give you an example of what can happen when material is not properly identified. Shortly before the completion of the NAUTILUS we discovered that some welded pipe had been installed in the steam plant instead of seamless pipe which had been specified. Removal and replacement of the wrong piping caused months of delay in the completion of the ship and considerable extra cost. A storekeeper had issued the wrong kind of pipe. The specifications had permitted the pipe to be marked inadequately. As a result of this an opportunity existed for a mix up in the pipe racks, and a mix up eventually occurred.

The responsibility for this failure must partly be borne by the producers of the pipe and by those who wrote the specifications. Analysis of the specifications showed that they were difficult to interpret. Investigation showed that similar instances had occurred in other naval vessels, and it is possible that this has also occurred ashore. As a result of this instance the Government stepped in and issued an additional military specification which requires all ferrous pipe purchased by the Department of Defense to be plainly and continuously marked. Also, the Atomic Energy Commission has adopted this military specification.

You may say that the Government was responsible in not having insisted on proper marking. I will agree. But after all there was in existence a society for the testing of materials and we had depended on them. Perhaps there should be more active consumer representation on the society's committees.

But what of nonferrous piping and of plates and shapes? The advances in technology in recent years have forced the use of material at levels of temperature, pressure, tensile strength and corrosion resistance much nearer their upper limits than has heretofore been the case. And this trend is continuing. It may interest you to know that the Atomic Energy Commission and the Department of Defense are presently working to obtain a specification for continuous markings of nonferrous piping and of plates, shapes and bars,

both ferrous and nonferrous. I am sure that you will cooperate in every way so we can eliminate this source of difficulty and danger both for military and industrial uses.

We in government are very hesitant to enter into fields of this type. We believe it is properly the function of industry to take care of its own products. I hope that from now on you will take the initiative in matters of this sort, so that the products on which you have expended so much care during manufacture are not improperly used.

I am sure that by this time some of you will have recalled the story of the farmer who hired a mule tamer to tame his mules. The farmer was aghast when the mule tamer began by taking a full swing with a sledge hammer on the mule's head.

"I hired you to tame the mules, not to kill them," said the farmer.

"Sure," said the mule tamer, "but you have to attract their attention first."

Our attention must be attracted first to facts. After we have corralled them we can try to tame them with scientific and engineering effort.

I have presented some of the stubborn facts which hinder the development of atomic energy. Permit me to make some observations on how the situation may be improved.

Metallurgy has reached a crossroads in its history. It needs to convert itself from an art into a science. The problems presented by nuclear energy merely serve to focus attention on the urgency of this need.

Dr. Cyril Smith, Director of the Institute for the Study of Metals, at the University of Chicago is a leader in the program for transforming metallurgy into a science. He has expressed his thesis in an article which was published in the January 1952 issue of METAL PROGRESS.

I will quote briefly from Dr. Smith's article.

> "The metallurgist from the earliest days when he first produced the bronze and the iron tools whose importance was sufficient to name whole eras of civilization, has been purely practical. The justification of his work has lain solely in its material products, and not in what he thought about them. . . . The very basis of his success lay in his disregard of theory and his willingness to try empirical experiments. But there is a limit to what a man can do in a lifetime, and empirical knowledge . . . cannot easily be transmitted to grow from generation to generation in the manner of a body of organized knowledge tied to a conceptual framework. . . . The empirical stages of knowledge are generally developed by people with short-range

> motivation and . . . uncultural curiosity who collect data in isolated fields without regard to their connection with others. . . . The scientist, however, seeks underlying laws applicable to all physical phenomena, and eventually it will be he who, by showing the relations of any given observation with all others, makes previously complex relations simple. . . . In this century for the first time in history it is possible to attempt a description of the properties and behavior of metals in terms of the same concepts that apply to all other matter. . . . The more fundamental the research . . . the more certain it is to be of eventual use somewhere, but the less obvious its immediate utility. . . . In the long run fundamental scientific research will discover important new principles which directly open up profitable technological areas. . . . It is currently impossible to predict with certainty what kind of alloy will result on alloying any two or more metallic elements, but the search for the principles is progressing rapidly and in a few decades it will probably be possible to design an alloy with the certainty that one now designs a machine for a given purpose. . . . The dollar value for such knowledge will be enormous."

Dr. Smith's clear statement of the case can hardly be improved upon.

As I have stated, nuclear energy has brought into sharp focus the necessity for building metallurgy on a scientific basis. But it has also provided powerful tools which can help to achieve this objective. One example is radioactive tracers. Another is radiation damage studies which may also become a means for understanding the physical metallurgy of metals. For example, a problem of long standing is the phenomenon of the brittle transition temperature. Below this temperature fractures are brittle; above this temperature they are ductile. It has been found that exposure to nuclear irradiation raises the brittle transition temperature. This may furnish a valuable tool for solving what is presently a mystery.

Today, metallurgists need no longer work alone. They can become part of a closely knit team which embraces many disciplines. Physicists and chemists especially are helping to get a better understanding of metallurgy because the problems are now partly in their realm. It may be that nuclear energy will be the catalyst for wiping out the fading boundary between metallurgy, chemistry and physics. After all, atoms do not obey different laws for metallurgists than they do for chemists or for physicists.

It should be obvious from what I have said that many difficult problems lie before you. Metallurgy holds the key not only for the rapid development of atomic power but for many other fields as well.

But with this tremendous task in sight, it is discouraging to note that according to figures prepared by the Advisory Committee on Metallurgical Education of your Society, the number of engineering graduates in the United States and Canada with Bachelor's degrees in your field dropped from 476 in 1950 to 204 in 1953. By 1955 the number had increased to 486. However from 1950 to 1955 the total enrollment of undergraduates and graduates steadily dropped from 3887 to 3050.

The satisfactory resolution of this situation will require a sustained and coordinated industry-wide attack over a period of many years. It may require the establishment of special schools by your industry, and a permanent system of recruitment and support of students. It may also require a very liberal policy of university instruction for your present employees, both at undergraduate and at graduate levels.

With the existing shortage of scientists and engineers in the United States, and the rapid development of all technology, it is certain that for many years to come the shortage of trained personnel will not be satisfied.

An essential function of management and leadership, both in government and in industry, is to plan for the future. What we do today was largely determined for us by the vision and action of those who preceded us. Likewise, tomorrow's events will depend on what we plan and do today—on the wisdom we use in planning for the future.

You are faced with the tremendous problem of converting metallurgy from an art to a science. To do so will require the efforts of a very large number of skilled scientists and engineers. The major problem which you face is the recruitment and training of these people. In my opinion those organizations which take heroic steps to solve this problem will be tomorrow's leaders.

More than two millenniums ago Archimedes said, "Give me a fulcrum and I can move the world." If he were alive today he might say, "Give me a suitable metal and I can contain temperatures as high as those of the sun."

LOW CARBON MARTENSITES
(1955 Edward DeMille Campbell Memorial Lecture)

By R. H. Aborn

Introduction

MR. Chairman, Members and Guests of the American Society for Metals! We have convened this morning for the Thirtieth Annual Lecture honoring Edward DeMille Campbell. Let us pause in the presence of the spirit of this great teacher and creative scientist as we view his portrait.

In these days, when Americans are so conscious of their heritage of freedoms, we in the field of metals recognize how rich is our heritage from such an indomitable pioneer as Professor Campbell, who gave to the world the results of some seventy-five researches all but three of which were done after complete loss of his eyesight. Truly many can look for one who can see, but thousands can see for one who can understand and create.

Professor Campbell, working with Dr. William L. Fink in the year this Lecture was established, made the notable experimental discovery of the tetragonality of martensite (1).[1] Thus it is particularly appropriate on this occasion to take a new look at martensite, this time in the low carbon area of martensitic steels.

Acknowledgments

Realizing, in these times of science team work, that this honor is essentially a recognition of the work of the Fundamental Research Laboratory of the United States Steel Corporation at Kearny, New Jersey, I humbly accept it on behalf of all of my colleagues, and gratefully acknowledge the special contributions of O. Borch, R. F. Campbell, L. S. Darken, E. T. Gioia, F. Garofalo, Q. Henderson, A. S. Keh, H. E. Knechtel, R. Koumaras, S. Lentz, E. K. Lynn, D. S. Miller, J. P. Nizolak, R. L. Rickett, C. Rossi, W. B. Seens, J. R. Vilella and L. Zwell. The counsel and support of Dr. J. B. Austin have been a constant encouragement. Most of all I am indebted to R. A. Grange and R. M. Fisher for their expert handling of the programs and interpretation of results.

We are also indebted to P. R. Wray and J. M. Hodge of United States Steel Corporation for helpful discussions of the problems and

[1]The figures appearing in parentheses pertain to the references appended to this lecture.

This is the Thirtieth Edward DeMille Campbell Memorial Lecture, presented by R. H. Aborn, director of Fundamental Research Laboratory, United States Steel Corporation, Kearny, N. J. The lecture was presented October 19, 1955, during the Thirty-seventh Annual Convention of the Society, held in Philadelphia.

for arranging to obtain the steels used. We are grateful to W. L. Grube and D. P. Koistinen of General Motors Research Laboratories for measurements of retained austenite by their high precision technique (2).

The detailed results of the researches have been omitted in order to emphasize the "forest" rather than the "trees."

Importance of Martensite

Martensite is considered to be a supersaturated solution of carbon in iron, having a body-centered tetragonal lattice; it is formed by the diffusionless transformation of austenite on cooling below a temperature denoted as Ms, which is controlled by austenite composition, except for the intervention of plastic deformation.

It seems unnecessary, on this occasion, to describe at any length the great importance of martensite in ferrous metallurgy. It will suffice to point out that it is unique in at least two practical aspects. It provides the hardest matrix obtainable in steel, and, when suitably tempered, it offers the highest shock toughness and resistance to crack propagation.

But martensite itself, in the raw, untempered state, has long been regarded as so brittle and crack prone as to be beyond consideration, and even anathema to engineers. This concern for the potential dangers of martensite led to the long standing reluctance of design engineers to permit the use of quenching in the manufacture of pressure vessels.

More recently, with increasing need of higher working stress levels, metallurgists have had another look at martensite and found that the medium carbon variety, with low temper, can have considerable toughness with ultra high strength.

Defining Low Carbon Martensites

Lowering the carbon further to a maximum of 0.2% has led to the development of a new class of quenched and tempered martensitic steels with enhanced engineering properties, combining strength, toughness, formability and weldability. The remarkable toughness of such steels has led very recently to the first limited use of quenched and tempered steel in pressure vessels. To this class of steels the term *low carbon martensites* is given. This lecture will survey some of the basic properties of these steels, in relation to their inner structure, and demonstrate that low carbon martensite is not raw and untempered as is its high carbon brother, but has, in a sense, been automatically conditioned to set the stage for a favorable combination of maximum advantages with minimum disadvantages.

Low Carbon Martensites for Basic Study

For the basic study, a 0.13% carbon steel, Type 1013, was adopted, and will be referred to by that number. A 0.15% carbon, low alloy steel, Type 4315, was added to provide ample martensitic hardenability* for mechanical test specimens of ASTM standard size. The composition and treatment of these steels are given in Table I.

Mechanical Properties

Hardenability tests demonstrated that, even with large austenite grain size, 1013 steel is limited in rectangular sections to about 0.1-inch thickness for complete martensitic hardening when quenched in ice-brine. Obviously then, if the mechanical properties of the two steels are to be compared as martensite, special means must be found to test specimens of very small thickness.

To compare notch toughness, it was necessary to austenitize both steels to the same large grain size, No. 3 on ASTM Scale, and to test them as quarter-width Charpy specimens, with the V-notch one-quarter of its ASTM standard length; the specimen, however, was standard in all other respects. All such specimens were heat treated slightly oversize and ground and notched afterward. The heat treatment was standardized to give a reproducible microstructure, with no more than a trace of nonmartensitic transformation product.

The problem of measuring sharply reduced energy levels, resulting from the 75% reduction in volume of metal under the notch, was met by the use of a special impact test machine with full scale deflection for 24 foot-pounds of fracture energy. No detectible twisting or buckling occurred during the testing of these relatively thin specimens, and the reproducibility of observed energy values compared favorably with that for corresponding standard Charpy V-notch specimens, with which they were calibrated using 4315 martensite for both sizes.

Three conditions of martensite were studied: as quenched from austenite; *low tempered* for 1 hour at 400°F, corresponding to the final conditioning treatment of the core of many case-carburized parts; and *high tempered* to a nominal hardness level of Rockwell C 29, corresponding to about 100,000 psi yield strength—a level of increasing interest to design engineers for readily welded, high strength structures.

Notch Toughness of Large Grain 1013—A typical set of results—those for quarter-size, V-notch, Charpy specimens of quenched 1013 martensite—is shown in Fig. 1. Here, as in later charts, comparison is facilitated by using smoothed curves based on the average of several observations at each temperature. The change of fracture

*Reference 3.

Table I
Origin and Composition of Steels*

Type of Steel	Manufacturing Practice	Rolled Section Size	C	Mn	P	S	Si	Cu	Ni	Cr	Mo	V	B	Ti	Acid Soluble Al
1013	Commercial—Open-Hearth	0.62 in. Diam.	0.13	0.67	0.010	0.027	0.15	0.07	0.03	0.03	0.004	Trace	None	Trace	0.038
4315	Laboratory—Induction	0.75 in. Diam.	0.15	0.73	0.008	0.005	0.29	0.01	1.76	0.45	0.28	None	None	Trace	0.012
4320	Commercial—Open-Hearth	1.12 in. Diam.	0.19	0.68	0.017	0.022	0.30	0.06	1.81	0.65	0.23	None	None	None	0.049
4330	Laboratory—Induction	0.62 in. Square	0.31	0.76	0.014	0.015	0.16	0.06	2.04	1.00	0.33	None	None	None	0.036
4340	Commercial—Electric-Arc	1.06 in. Diam.	0.42	0.74	0.010	0.013	0.30	0.11	1.89	0.76	0.28	None	None	None	0.038
"4360"	Commercial—Open-Hearth	1.25 in. Diam.	0.57	0.82	0.016	0.019	0.30	0.04	1.16	1.07	0.26	None	None	None	0.036
43BV12	Commercial—Electric-Arc	0.75 in. Diam.	0.13	0.83	0.006	0.012	0.35	0.09	1.76	0.54	0.27	.06	.0029	.038	0.050

*Spectrographic analysis indicated no significant percentage of any minor element detectable by this method.

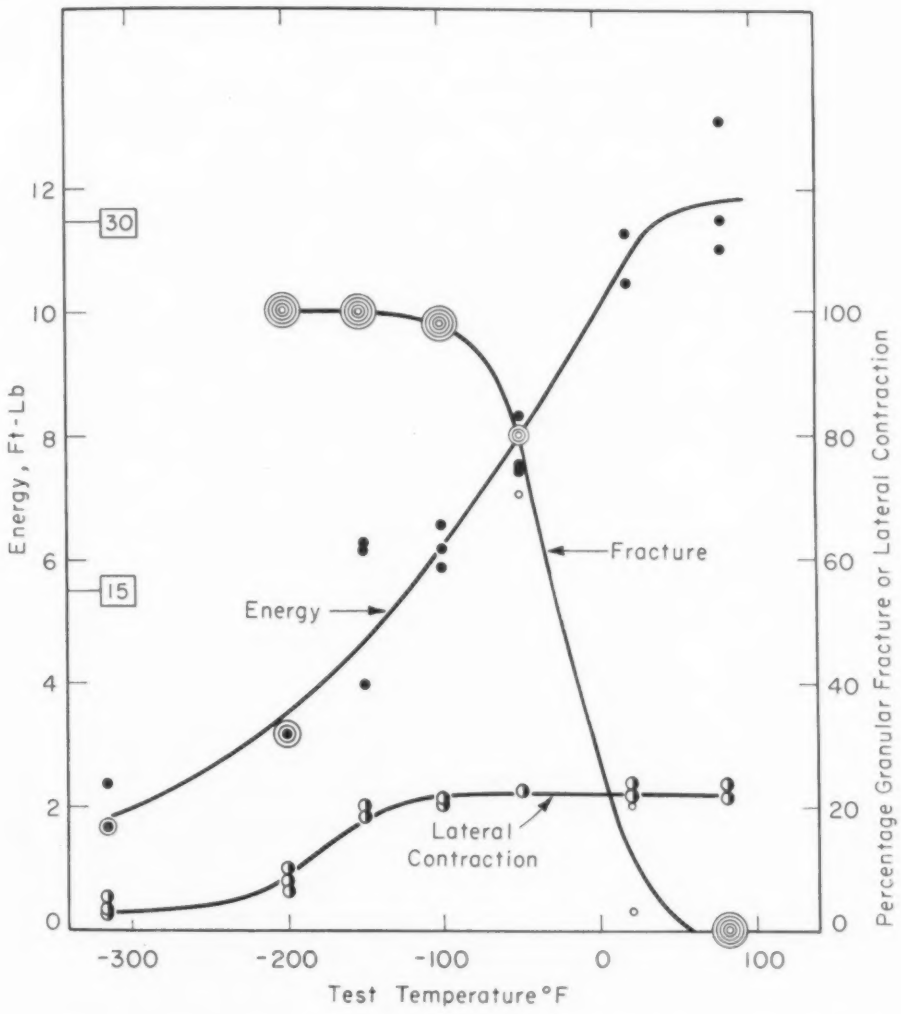


Fig. 1—Notch Toughness of Quenched Martensitic 1013 Steel. Quarter-Size, V-Notch, Charpy Specimens Quenched in Ice-Brine From 2200°F; Not Tempered. 400 DPH.

texture, from fibrous to granular with decreasing temperature, correlates with the change of energy with temperature. On the other hand, lateral contraction, measured with a comparator microscope at the base of the notch as an indication of relative ductility, remains at a high level with decreasing temperature until the fracture has become almost entirely granular.[2] The two boxed numbers on the energy scale show the equivalent 30 and 15 foot-pound levels for standard-size Charpy V-notch specimens. These energy levels have been suggested, in a recent Naval Research Laboratory Report (29), as suitable criteria for comparing high tempered and low tempered martensitic steels, respectively.

[2]The so-called granular fracture includes both cleavage and intergranular types.

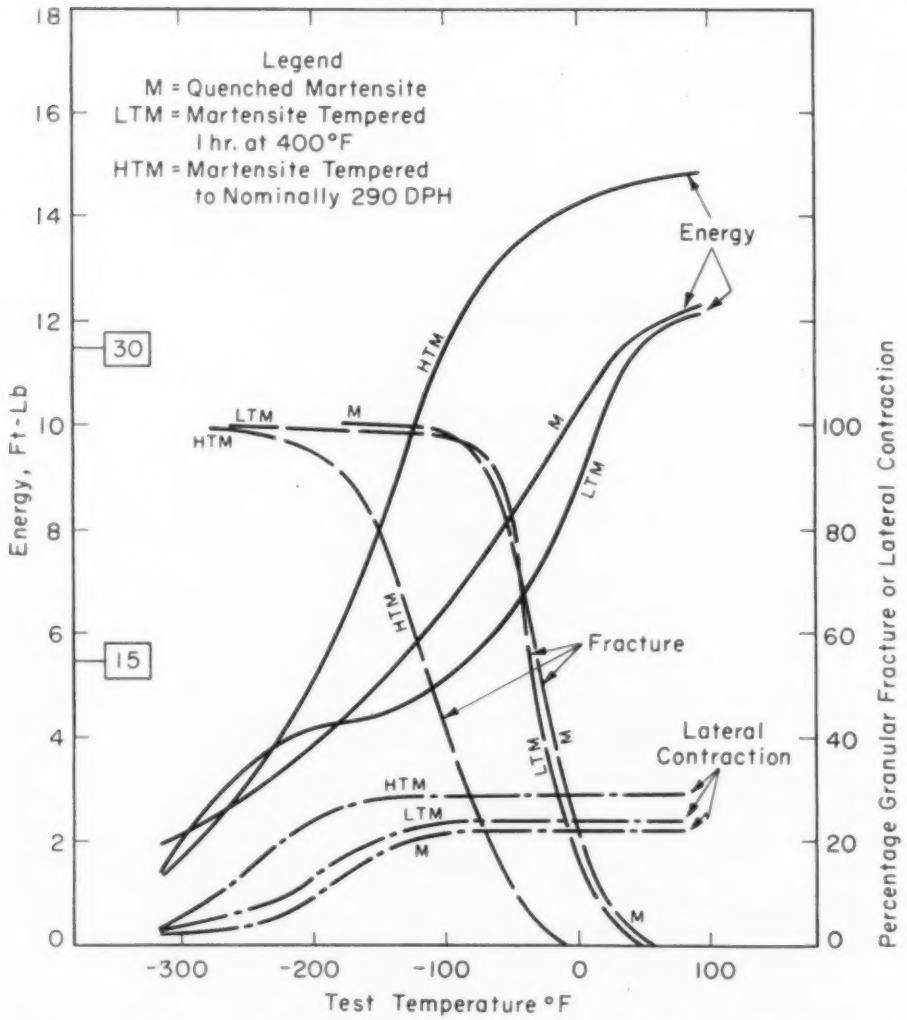


Fig. 2—Influence of Tempering on the Notch Toughness of Martensitic 1013 Steel. Quarter-Size, V-Notch, Charpy Specimens Quenched in Ice-Brine From 2200°F; Austenite Grain Size No. 3 ASTM.

The influence of tempering on the notch toughness of 1013 martensite is shown in Fig. 2. The upper trio of curves compare energy for the three conditions of martensite, the middle trio compare fracture type, and the lower trio compare lateral contraction. The energy curves show that this quenched martensite is somewhat tougher than the same martensite after a low temper. Actually, plain low carbon quenched martensite, even though born of large grain austenite, has an equivalent 15 foot-pound transition temperature at −140°F. Furthermore, as would be expected, the high tempered martensite has the highest notch toughness, with an equivalent 30 foot-pound level at −100°F.

Notch Toughness of Large Grain 4315 (Quarter-Size Specimens)

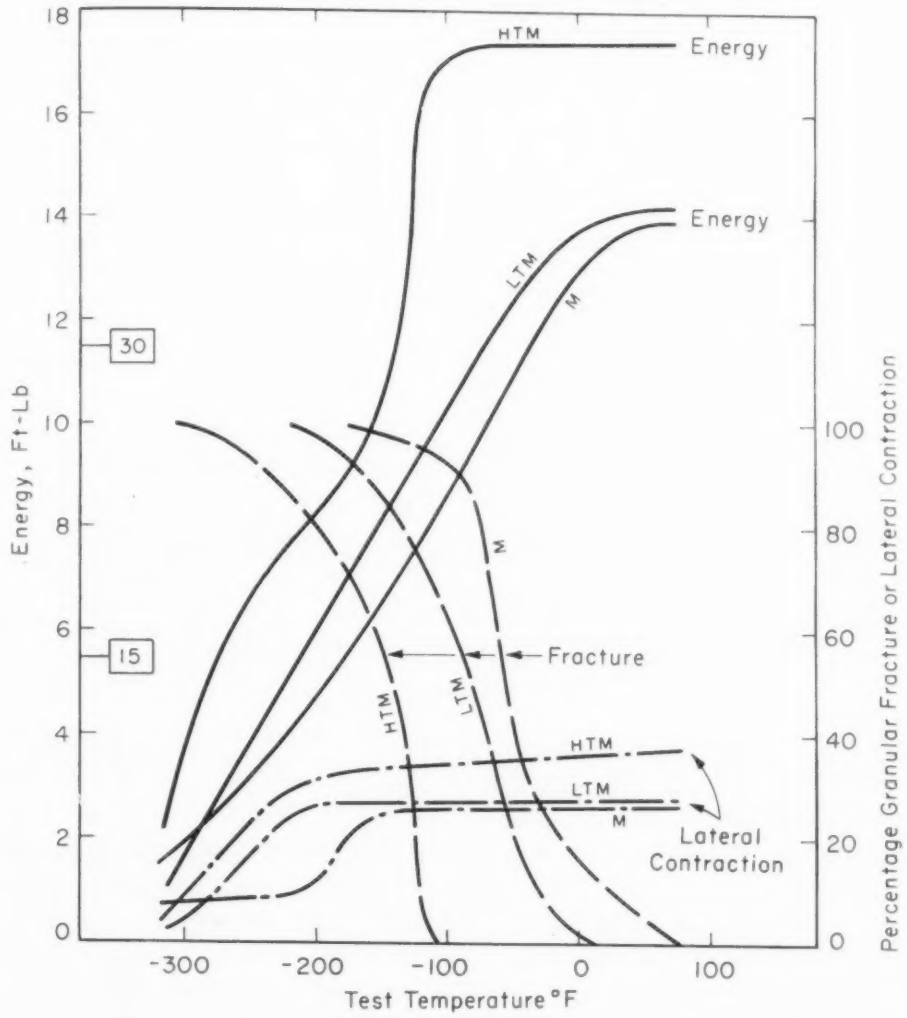


Fig. 3—Influence of Tempering on the Notch Toughness of Martensitic 4315 Steel. Quarter-Size, V-Notch, Charpy Specimens Quenched in Ice-Brine From 2000°F; Austenite Grain Size No. 3 ASTM. (See Fig. 2 for Meaning of HTM, LTM & M).

—Turning now to the large grain 4315 steel, a similar study of quarter-size specimens led to the results shown in Fig. 3. In this steel and specimen size, quenched martensite is less notch-tough than either of the tempered martensites; however, even it displayed as much as 3% lateral contraction at −315°F, demonstrating a remarkable degree of ductility in this low carbon martensite at a strength level approaching 200,000 psi.

Comparison of Notch Toughness of 1013 and 4315—Comparison of the notch toughness of these two martensitic steels shows that this 4315 steel is consistently tougher than the 1013 heat for each treatment. This comparison is illustrated graphically in Fig. 4 for the quenched and high tempered conditions. Reviewing the differences in the two steels that may contribute to the superior notch

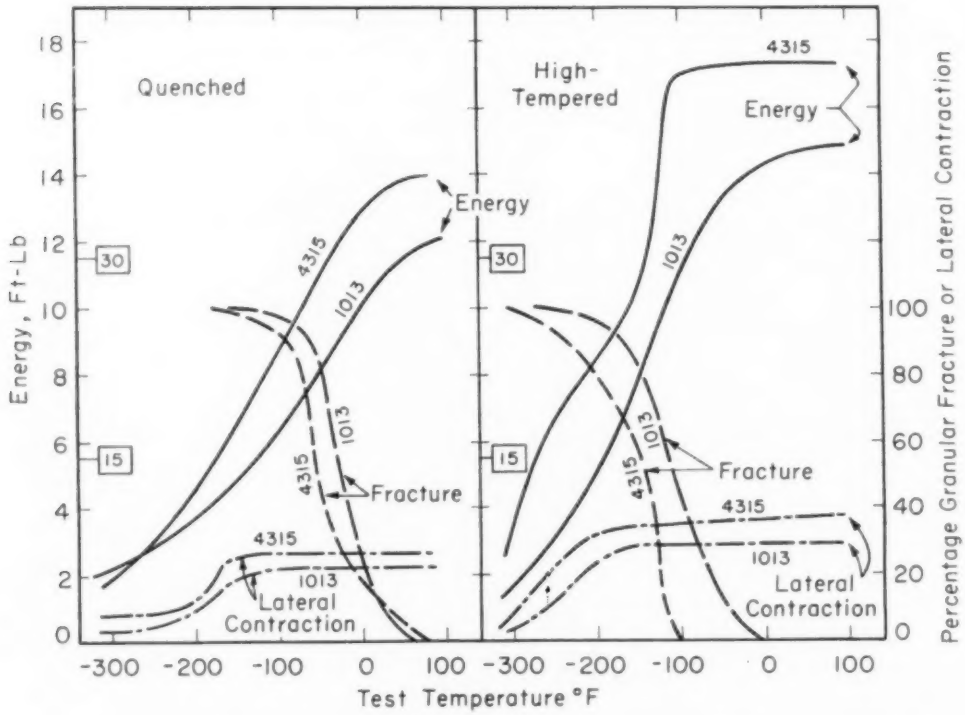


Fig. 4—Comparison of Notch Toughness of 1013 and 4315 Steel. Left: Quenched Martensite; Right: Martensite Tempered to 290 DPH. Quarter-Size, V-Notch, Charpy Specimens.

toughness of this 4315 heat, it is clear that grain size is not a factor, because both steels were heat treated to the same austenite grain size. Carbon content cannot be regarded as a favorable factor for 4315, for it is two points higher than in 1013, and, as will be shown later, increasing carbon reduces the toughness of martensite in the 4300 series of steels. The alloy additions, particularly the nickel content in 4315, may have a favorable influence, though published data on normalized steels suggest considerably less improvement than observed in this low alloy martensite. Extensive chemical and spectroscopic analyses of both heats disclosed no other significant differences known to correlate with notch toughness. Another difference is in steel-making practice; the 1013 was a commercial, open-hearth heat, whereas the 4315 was a laboratory, electric induction heat. Kinzel, in the 1947 Campbell Lecture (6), commented on the unexplained superior toughness of laboratory heats compared to commercial heats. A final difference is in the martensitic structure itself, and to that we will return later.

Influence of Austenite Grain Size on Notch Toughness of 4315—Returning now to standard Charpy V-notch specimens, Fig. 5 compares the energy-temperature curves for 4315 martensite from small-grain austenite (No. 8 ASTM Scale) and large grain austenite (No. 3

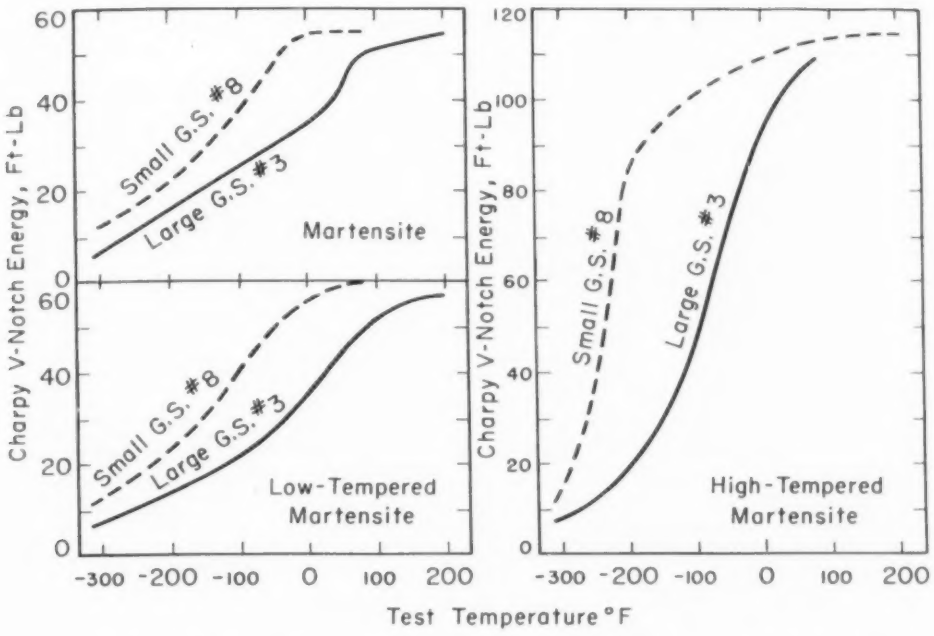


Fig. 5—Influence of Austenite Grain Size on Notch Toughness of 4315 Steel As-Quenched to Martensite and with Two Degrees of Tempering. Standard-Size, V-Notch, Charpy Specimens.

ASTM Scale). For each condition of martensite, from quenched to high temper, the finer textured martensite or temper products resulting from the smaller austenite grain size have distinctly greater notch toughness at any given test temperature.

With higher energy absorbed at any given temperature, one would expect the small grain series to show greater maximum lateral contraction than shown by the large grain series. This was confirmed at all cold temperatures.

Influence of Carbon Content on Mechanical Properties of Martensite—To understand better the value of low carbon martensite, the next step was to compare the effect of increasing carbon content, in the same base steel, on some of the mechanical properties. Again, to provide ample hardenability to insure a fully martensitic structure in standard size specimens, a 4300 steel series was chosen for this study. This series comprised steels of nominal types, 43BV12, 4315, 4320, 4330, 4340 and "4360," whose compositions are given in Table I. Standard Charpy and ¼-inch diameter tensile specimens of each steel[3] were austenitized to dissolve all carbide and yet maintain small austenite grain size (7-9 ASTM Scale), and brine-quenched. For the Charpy series, three conditions of martensite were explored: as-quenched, low tempered 1 hour at 400°F, and high tempered to 290 DPH or about 130,000 psi tensile strength.

[3]The tensile series omitted 4330 steel owing to insufficient material.

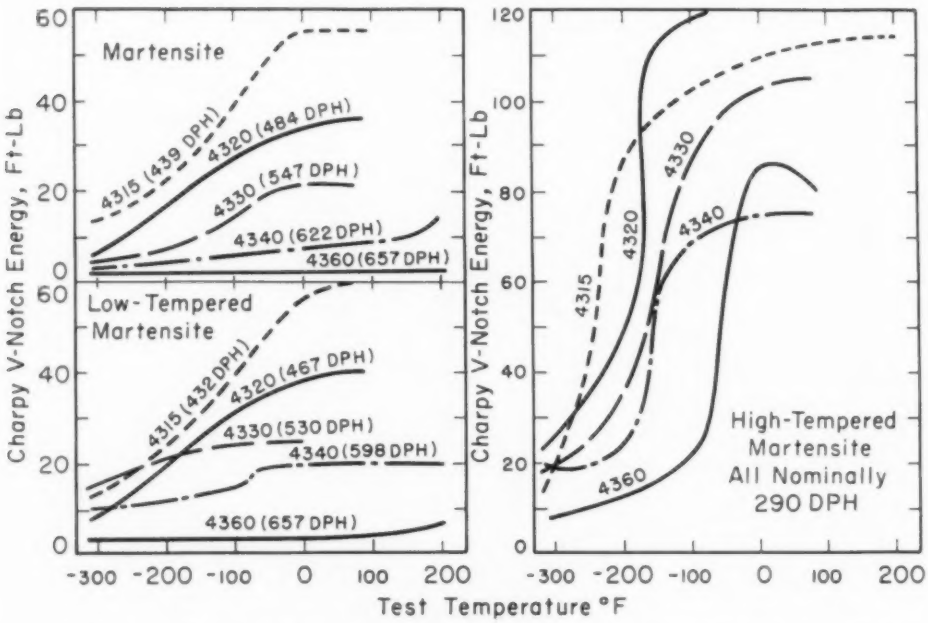


Fig. 6—Influence of Carbon Content on Notch Toughness of Small Grain 4300 Type Steels As-Quenched to Martensite and with Two Degrees of Tempering.

The tensile series included as-quenched 43BV12 and all of the steels tempered 1 hour at 400°F and also to three common hardness levels: Rockwell C44, C36 and C29. All of the tempering treatments were devised to minimize temper embrittlement, and therefore included quenching from the tempering temperature. All specimens were heat treated slightly oversize and ground to final dimensions afterward, including the Charpy notches.

Notch Toughness in Relation to Carbon Content—The notch toughness results, shown in Fig. 6, demonstrate the controlling influence of carbon content. The energy-temperature curves are displaced toward reduced toughness with each increment of carbon. Austenite grain size is not a significant factor, because 4340 with slightly smaller and 4360 with slightly larger grain size than the others show consistently the lowest notch toughness of the series. Similarly, hardness does not consistently correlate with notch toughness, as the curves for high tempered martensite represent essentially the same hardness.

The outstanding notch toughness of low carbon martensites is evident in all three treatments. The higher carbon martensites, 4330 and 4340, are markedly toughened by the low temper, and the 4320 martensite is slightly improved, whereas the 4315 martensite is substantially unchanged, for reasons which will unfold shortly.

It is evident that carbon content of the martensite is the outstanding factor. This is carried further in Fig. 7, which correlates

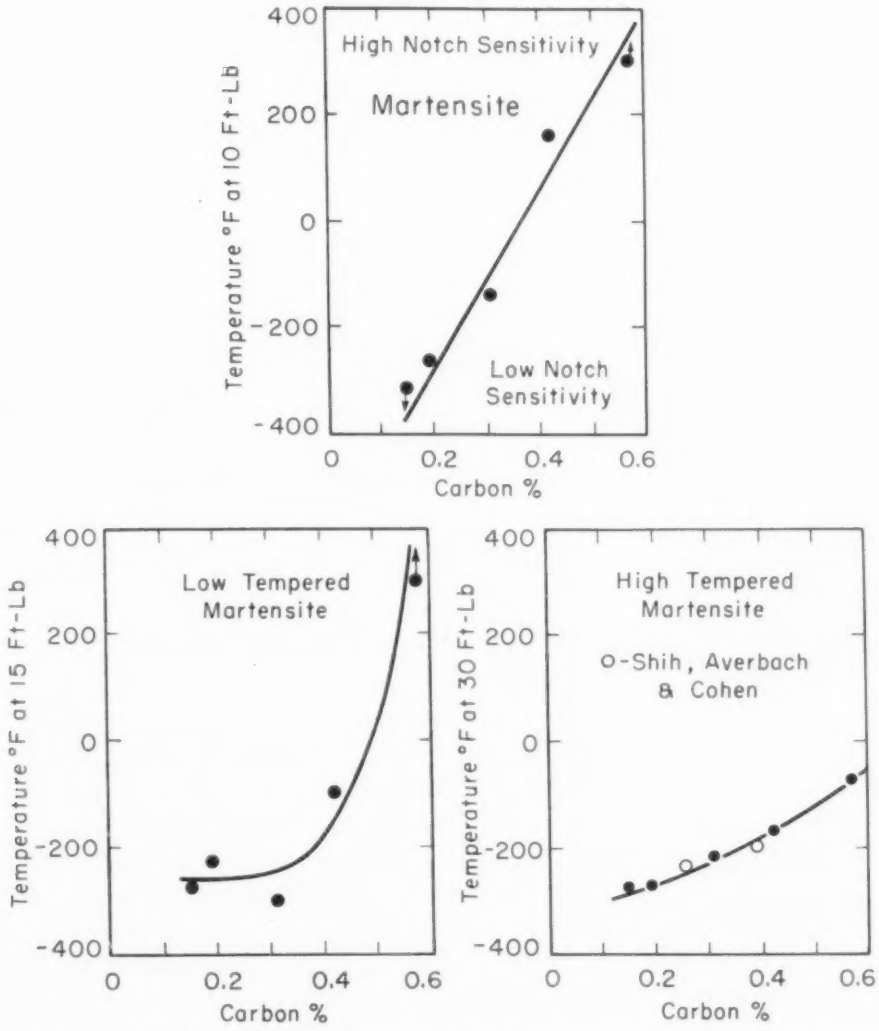


Fig. 7—Correlation of Carbon Content of Small Grain 4300 Type Martensitic Steels with Lowest Temperature for Indicated Level of Charpy V-Notch Impact Energy. Data from Fig. 6.

carbon level with the lowest temperature for a specific fracture energy level. The only comparable energy level for as-quenched martensite over the entire series is 10 foot-pounds, and on this basis there is a consistent linear relation from below −300°F at 0.15% carbon to above +300°F at 0.57% carbon. Comparison of the curve for as-quenched martensite with the corresponding curve for low tempered martensite at the 15 foot-pound energy level indicates that low tempering has greatly improved the medium carbon 4330 and 4340 martensites, but has had little effect on the two low carbon members because they were relatively tough before tempering. For high tempered martensite, at the 30 foot-pound level, the effect of carbon in decreasing notch toughness is remarkably consistent at

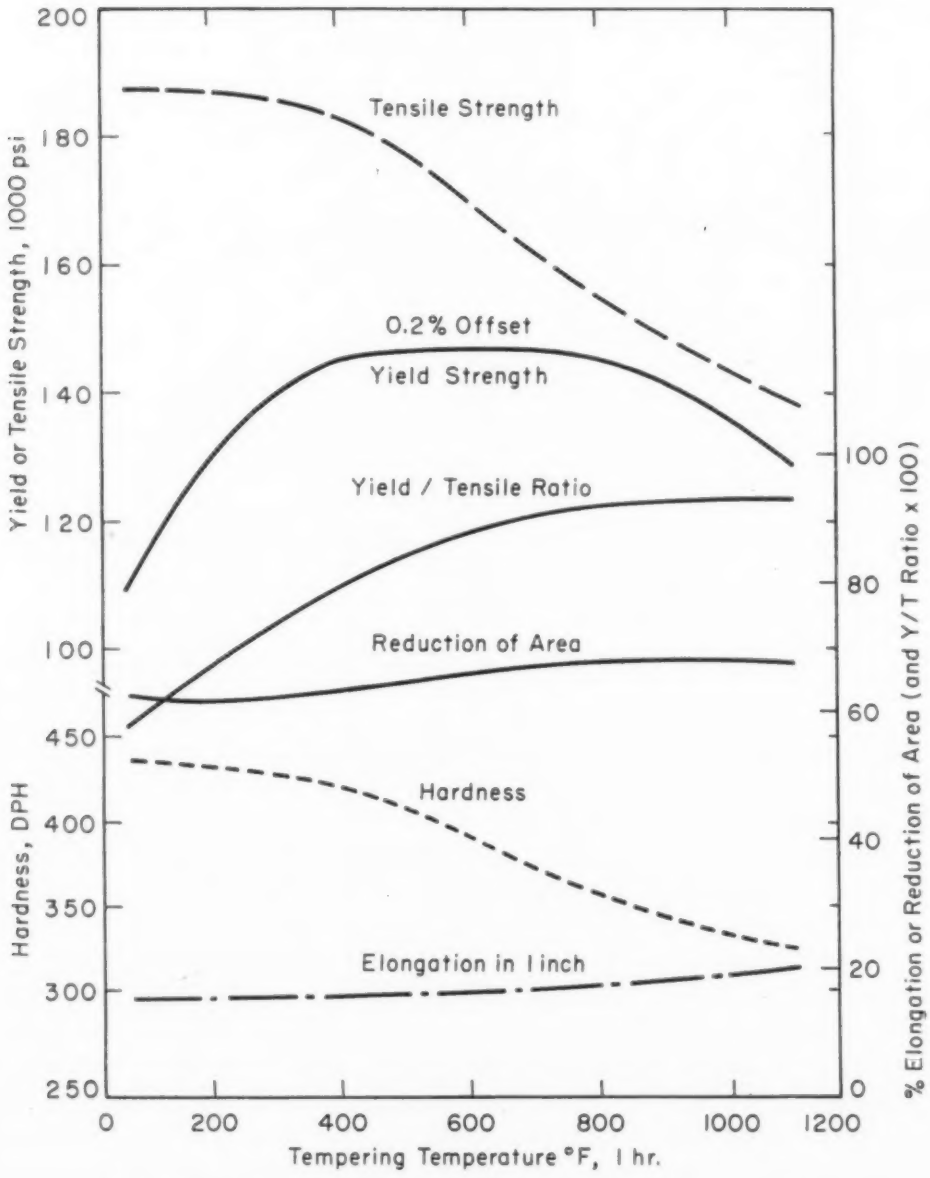


Fig. 8—Tensile Properties of Quenched Martensitic and Tempered Martensitic Small Grain 43BV12 Steel. 0.252-inch Diameter Specimens.

this ultimate strength level of about 130,000 psi, with a hardness variation of only one Rc unit from the mean over the entire five steels. The two additional points for 4325 and 4340 steels on the curve for high tempered martensite are taken from the current paper by Shih, Averbach and Cohen (7), and provide further confirmation of the adverse influence of carbon.

Influence of Carbon on Tensile Properties—The tensile properties of a typical low carbon, low alloy martensite (Type 43BV12 steel) as-quenched and after tempering at various temperatures are

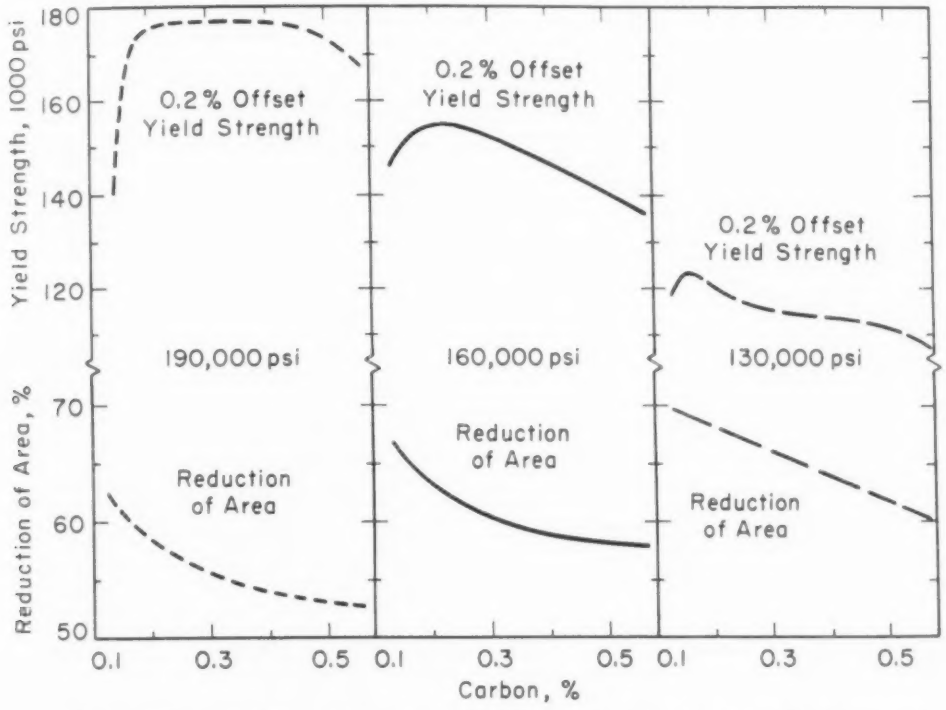


Fig. 9—Effect of Carbon Content of Small Grain 4300 Type Steels on Yield Strength and Reduction of Area of Martensite Tempered to Each of Three Tensile Strength Levels.

depicted in Fig. 8. This quenched martensite with a tensile strength of 187,000 psi has remarkable ductility, as evidenced by the 63% reduction of area. The notable effect of tempering at 400°F is to greatly increase the yield strength with a slight lowering of tensile strength and very little change in ductility. A corresponding improvement in yield strength on low tempering of low carbon martensite has been reported by Busby, Hawkes and Paxton (8) and by Nehrenberg (9). Further tempering improves the yield/tensile ratio with minor improvement in ductility. The optimum tempering temperature to confer both high yield strength and high ductility for a 1 hour treatment is about 700°F.

The influence of carbon content on yield strength and reduction of area of tempered martensite in Type 4300 steels is compared at each of three tensile strength levels in Fig. 9. These curves again demonstrate the controlling influence of carbon modified by the conditions of tempering. Bearing in mind that these data are limited to one heat of each grade, the optimum carbon level to confer the highest combination of ductility and flow resistance (measured by yield strength) is 0.19% in the 4320 steel. This steel, tempered 1 hour at 660°F to an ultimate strength level of 196,000 psi, developed a yield strength of 175,000 psi with 63% reduction of area. When yield strength alone is the criterion there is an optimum carbon

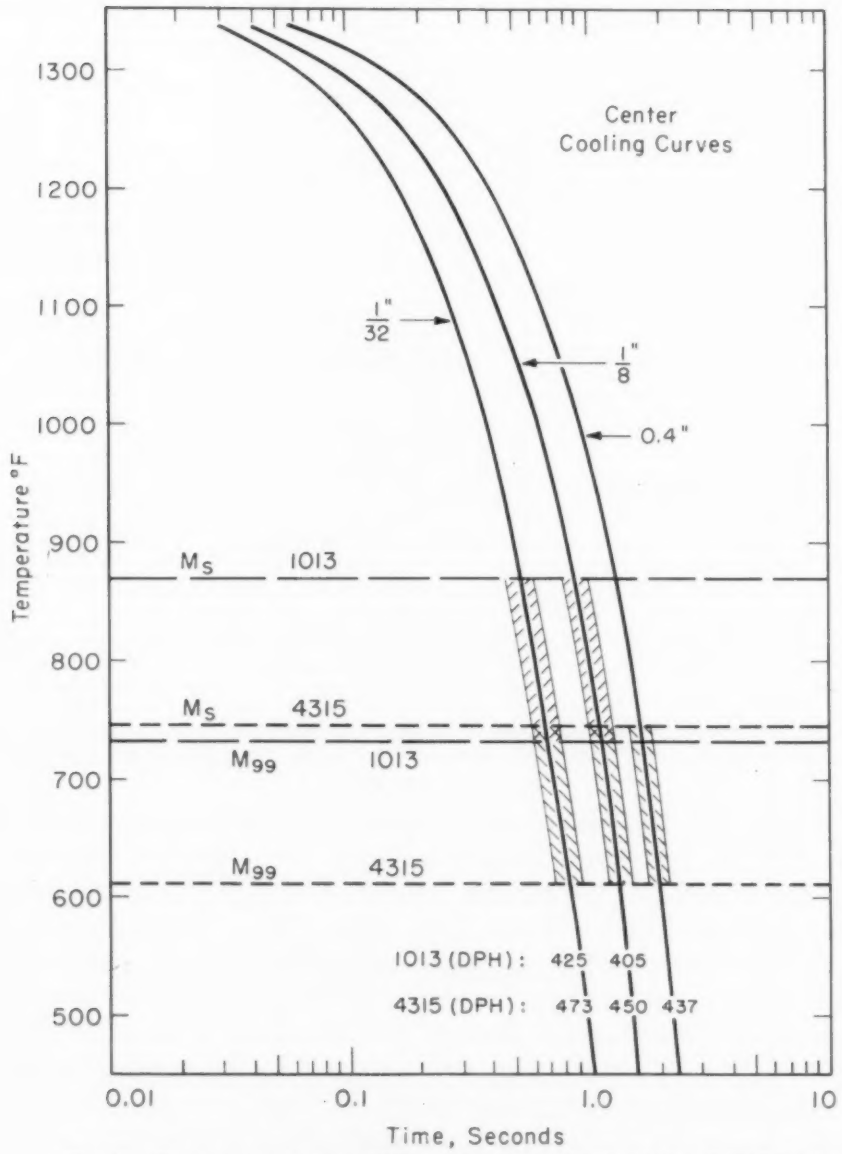


Fig. 10—Temperature Range of Martensite Formation in 1013 and 4315 Steels and Idealized Cooling Curves for Each of Three Specimen Thicknesses Quenched in Ice-Brine.

level which rises with tensile strength, as shown by the peak yield strengths.

Nature of Low Carbon Martensites

This survey has demonstrated some of the unique combinations of useful engineering properties of low carbon martensites such as high notch toughness at high strength levels and high flow resistance, as measured by yield strength, with relatively high ductility. This has led us to look into the nature of low carbon martensite to account for such mechanical behavior beyond normal expectation.

Martensite Transformation—The temperature range in which austenite transforms to martensite during quenching is more dependent upon carbon content than upon any other solute element. This is evident in the formula for Ms, the temperature at which martensite begins to form on cooling, in that the factor for carbon is about ten times larger than that of any other solute (10). As carbon diminishes, the temperature range of formation rises steeply and narrows somewhat, as shown by Grange and Stewart (11). Fig. 10 compares this range for 1013 and 4315 steels. Martensite formation begins in 1013 steel at about 870°F and is essentially completed at 735°F just below the starting temperature in 4315. However, even in 4315 steel, martensite formation is essentially completed at 610°F—a temperature above that at which it begins to form in most medium carbon, low alloy steels. Most significant of all is the position of this temperature span, namely, 900–600°F.

The idealized cooling curves* shown in Fig. 10 for the center zone of $\frac{1}{32}$ and $\frac{1}{8}$-inch thick slice specimens and 0.4-inch square-section specimens demonstrate that the first-formed martensite in 1013 steel may be exposed to temperatures above 600°F for periods ranging from about $\frac{1}{3}$ of a second for the $\frac{1}{32}$-inch, to one-half second for the $\frac{1}{8}$-inch section. The corresponding time intervals for martensite in 4315 steel range from about $\frac{1}{6}$ of a second for the thinnest to $\frac{1}{3}$ second for the thickest (0.4-inch) section.

Although martensite is the only transformation product formed in any of these specimens on quenching, it is important to note that the hardness values, shown at the base of the cooling curves in Fig. 10, reveal definite softening with increasing section thickness in both steels, amounting to nearly 40 DPH units in 4315 with the greater thickness range. This hardness was measured at mid-thickness on surfaces prepared for metallographic examination as described below; the load was 5 kg. for the $\frac{1}{32}$-inch series, and 10 kg. for all thicker specimens. The hardness of the thinnest section of the 1013 steel agrees well with the published maximum for that carbon level (12,13). The thinnest 4315 sample is somewhat harder than the corresponding published maximum.

In contrast to higher carbon steels, untransformed or retained austenite is an insignificant feature in these quench-hardened, low carbon steels. Repeated checks using X-ray methods showed that the amount of retained austenite present in these low carbon martensites was never more than 0.5%.

Microstructures of these steels in both quenched and tempered conditions were examined extensively, using both light and electron metallographic techniques. All specimens were mounted either in metal clamps or in cold-setting plastic and were wet ground to mid-

*References 4 and 5.

thickness on lead laps to avoid tempering during preparation. Light micrographs, made under identical picral-etching and photographic conditions at a magnification of ×2000, insured true comparisons within the entire series. The actual magnification of all micrographs as reproduced may be determined from the unit (μ) scale adjoining each group in Figs. 11,12,13,14,16,17 and 20; 1 μ represents 1 micron or 40 millionths of an inch.

Two different replica methods were used in preparing electron micrographs. Those designated "shadow" in Fig. 11,14,16 and 17 were taken of conventional uranium-shadowcast plastic impressions of surface relief on the specimen, resulting from differential etching in "super-picral".[4] The other electron micrographs, marked "extraction" in Figs. 11,12,13,14,16 and 17, were prepared by a relatively new method (14), in which fine precipitate particles are stripped from the specimen with the replica, and examined directly in the electron microscope. The release of the particles from the matrix is accomplished by etching through the plastic replica, in this instance with "super-picral." Since the actual particles, rather than mere replicas of them, are examined, it is possible to identify the precipitate by electron diffraction analysis of selected areas.

Nature of Martensite in 1013 Steel—Light, shadow and extraction micrographs of $\frac{1}{32}$-inch and $\frac{1}{8}$-inch slice specimens of 1013 martensite, compared in Fig. 11, reveal that the effect of thickness, and thus of cooling rate, on hardness, is associated with differences in microstructure. In the light micrographs, some martensite plates in the thicker sample appear slightly darker than the matrix. The shadow micrographs show more difference, with an indication of some precipitation in occasional martensite plates in the $\frac{1}{8}$-inch specimen. However, the extraction micrographs show that precipitation of extremely fine particles actually has occurred in some martensite plates in both samples. Plates containing such fine particles are considerably more common in the thicker sample, which contains larger and more numerous particles. No precipitate was found near the more rapidly cooled surface of the thinner specimen.

The individual particles within the broad diagonal bands across the extraction micrographs of Fig. 11 may not be apparent, because even the largest is only a few millionths of an inch in length. These particles, similar in shape to thin paper matches, are termed "straws" from their jumbled jackstraw appearance in the extraction micrographs. They have been identified as *cementite* by electron diffraction in these and many similar specimens. It should also be noted that the remainder of the martensitic matrix gives a *mottled* pattern.

[4] 2 cc. of a 12.8% solution of "Zephiran Chloride" (Winthrop Chemical Co.) added to each 100 cc. of standard picral (Metals Handbook, page 394, 1948).

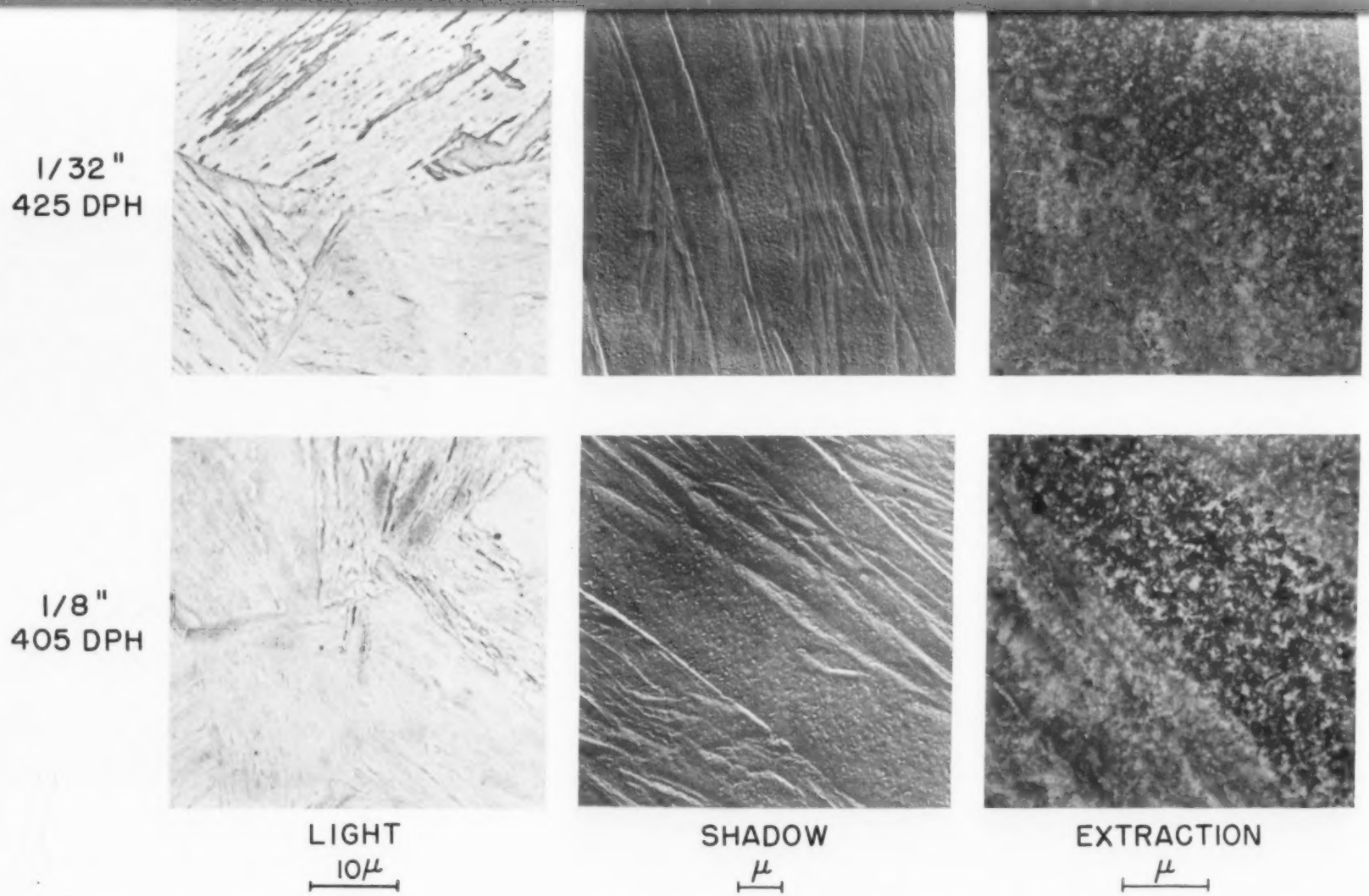


Fig. 11—Microstructure of Quenched Martensitic 1013 Steel at the Center of $\frac{1}{32}$-inch and $\frac{1}{8}$-inch Specimens Quenched in Ice-Brine From 2200°F. Picral Etch.

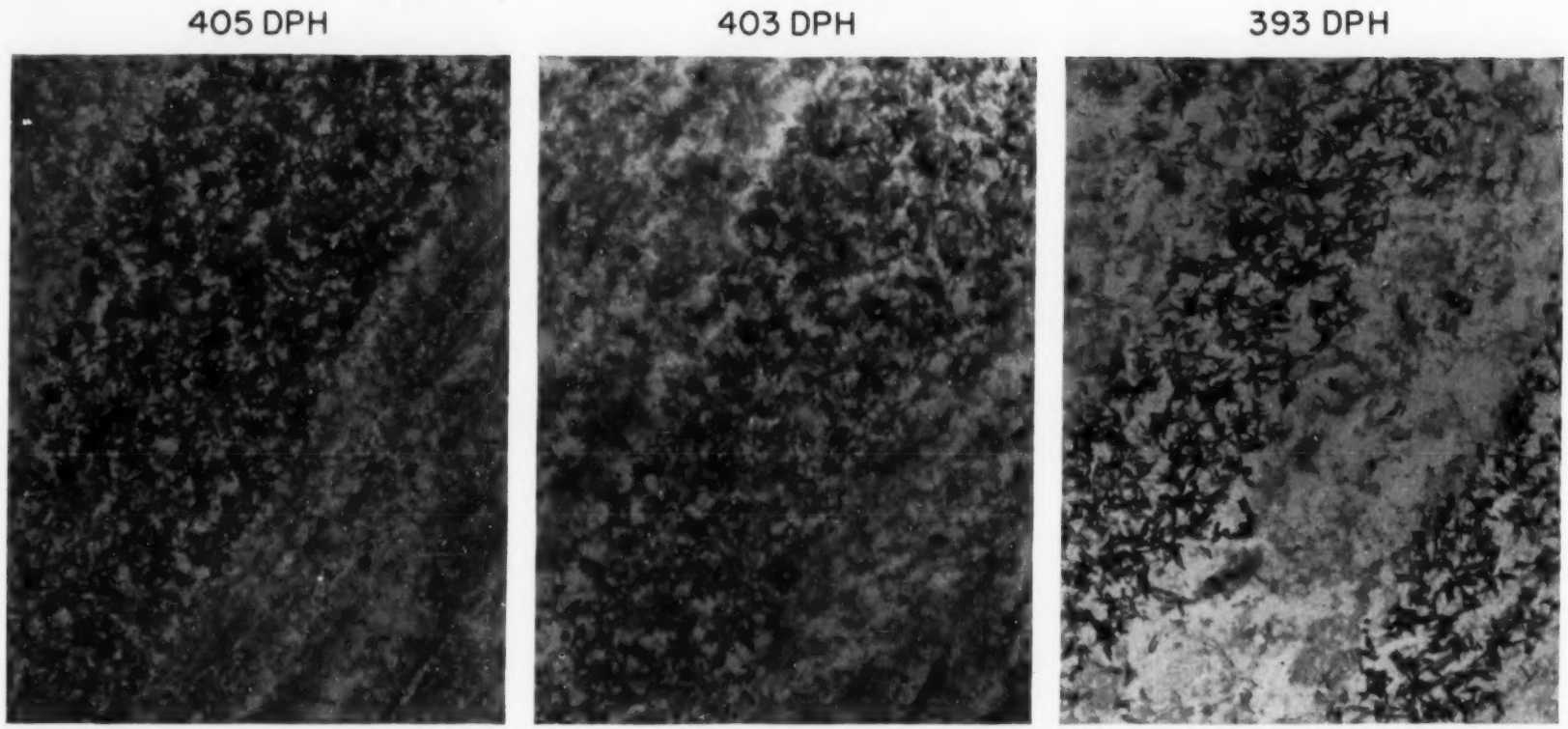


Fig. 12—Duplication of Quenched Microstructure in 1013 Steel by Tempering ½-inch Specimens. Extraction Micrographs. Picral Etch.

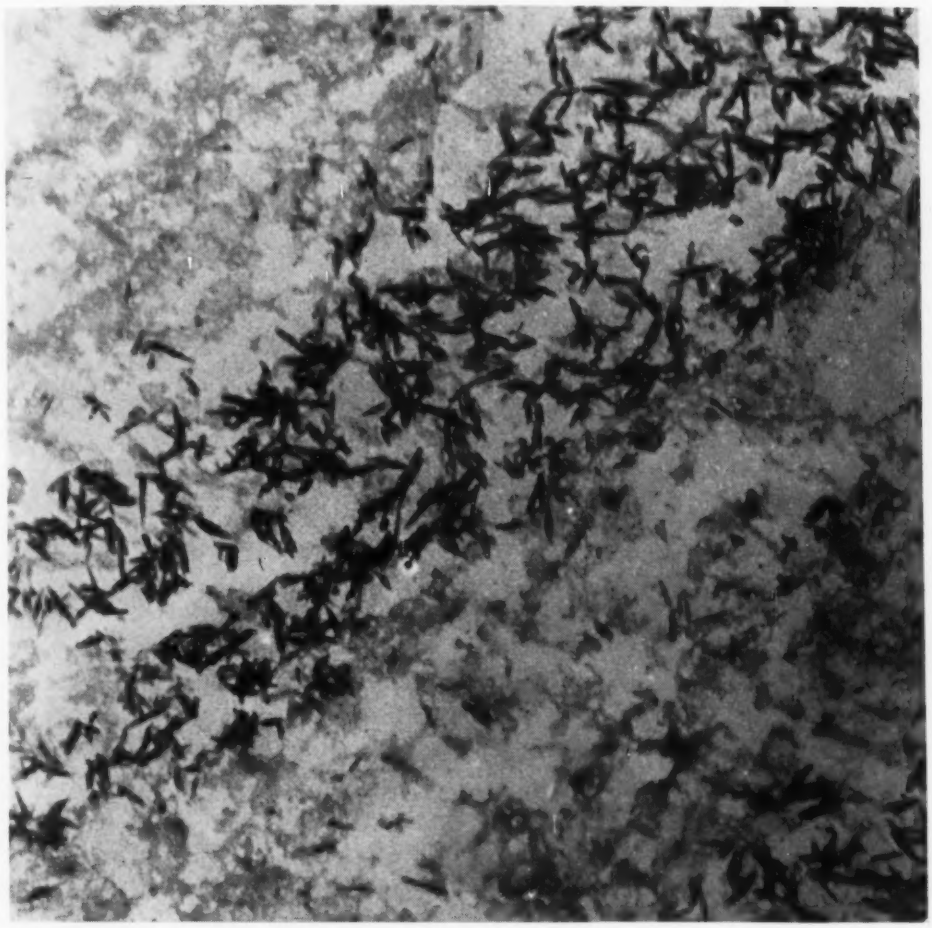


Fig. 13—Enlargement of Extraction Replica Electron Micrograph Showing Cementite "Straws" Formed on Q-Tempering of Martensitic 1013 Steel.

The microstructure and the hardness of the thicker (1/8-inch) specimen of 1013 martensite can be nearly duplicated by a very brief (2 second) tempering at 600°F of a thinner (1/32-inch) quenched section as shown in Fig. 12. The same brief time at 650°F results in larger and more numerous particles with a much lighter mottled background.

Thus it is evident that decreasing hardness and increasing alteration of the structure of low carbon martensites with increasing thickness are due to an unavoidable tempering during quenching. In subsequent discussion this form of tempering is termed *quench tempering*, or, more briefly, *Q-tempering*, since it occurs during the same quenching operation in which low carbon martensite forms. It produces a mottling of the martensitic matrix and a fine precipitate of minute ce-

mentite "straws" in certain plates, as shown clearly in the enlarged extraction micrograph in Fig. 13.

The *extent* to which Q-tempering can occur depends both on the temperature at which martensite forms, and its subsequent cooling rate. By retarding the cooling rate during quenching of certain low carbon, low alloy steels, the extent of Q-tempered "straw" zones in the martensite has been increased to as much as 50% of the entire microstructure. Slower cooling rates of larger sections resulted in transformation products other than martensite.

The straw-laden zones are believed to represent the first-formed martensite plates which Q-tempered to cementite platelets in supersaturated ferrite. The mottled material from the surrounding martensitic matrix gives no crystalline diffraction pattern, so it might be regarded as carbon soot formed during etching. However, its characteristic micrographic pattern, and because it has not been found on etched retained austenite or high carbon martensite, suggest that it may represent aggregates of pre-precipitation clusters of carbon, which form in the low carbon martensite during quenching and are caught on the extraction replica. It is not possible to resolve the individual clusters with present techniques.

Nature of Martensite in 4315 Steel—Lowering the temperature range of martensite formation by addition of alloying elements reduces the extent of Q-tempering for a given cooling rate; thus, for the same thickness, the extent of Q-tempering is less in 4315 than in 1013 martensite, as illustrated in Fig. 14. There is no evidence of Q-temper "straws" in the strongly mottled extraction micrograph of the $\frac{1}{32}$-inch slice sample. However, the slower cooled 0.4-inch square section shows evidence of Q-tempering in all three micrographs. The light micrograph shows scarcely resolvable dots in occasional dusky plates, whose microhardness is distinctly less than that of the light-etching plates. The shadow micrograph shows slightly elongated particles, whereas the extraction micrograph reveals the largest straws found in any Q-tempered specimen. It was further observed that the structure of this 0.4-inch section is about equivalent to adding a 2-second tempering at 650°F to the faster cooled, Q-tempered $\frac{1}{32}$-inch section.

This Q-tempering reaction has been observed in other low carbon alloy steels, and it now seems certain that, except for extremely thin sections or high alloy content, low carbon martensites are probably never observed as wholly fresh, untempered martensite, but always with some Q-tempering. The degree of Q-tempering depends on the composition, thickness and quenching procedure, and it conditions the microstructure and the properties of low carbon martensites. However, before discussing the dependence of some mechanical properties on Q-tempering, it will be helpful to examine

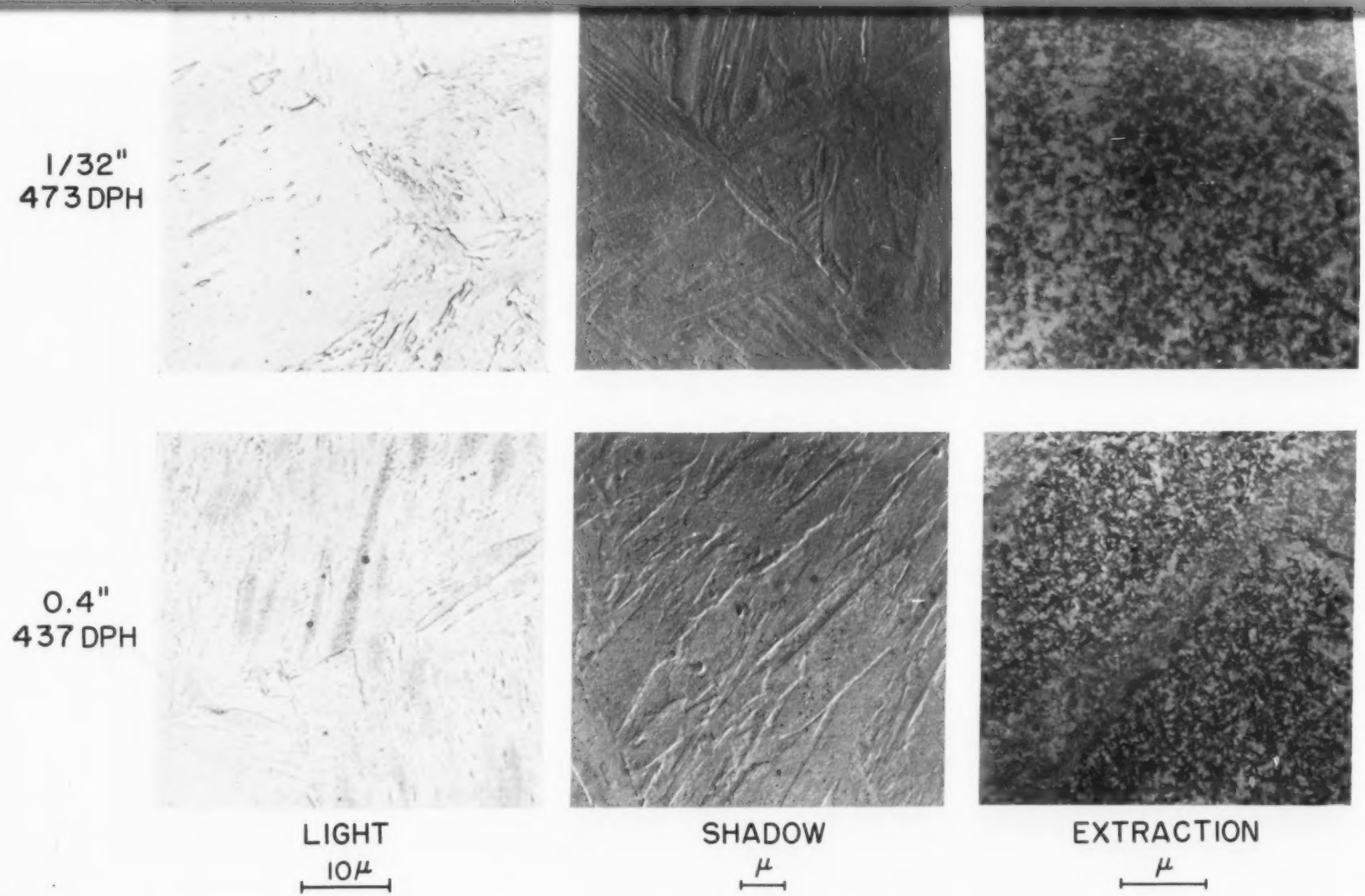


Fig. 14—Microstructure of Quenched Martensitic 4315 Steel at the Center of $\frac{1}{32}$-inch and 0.4-inch Specimens Quenched in Ice-Brine From 2000°F. Picral Etch

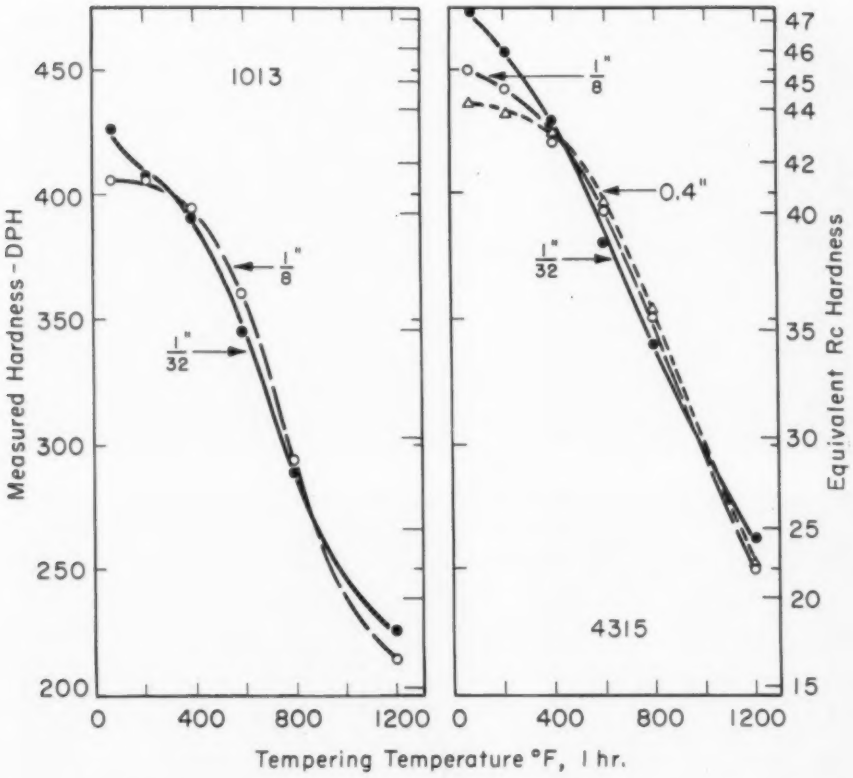


Fig. 15—Quench-Temper and Applied Temper Softening of 1013 and 4315 Martensites in Relation to Specimen Size.

the effects of deliberate or applied tempering by reheating these Q-tempered, low carbon martensites. As before, the martensites were made from large grain austenite, quenched in ice-brine and tempered 1 hour at intervals over the range from 212 to 1200°F, and again quenched.

Tempering of Low Carbon Martensites

The effect of applied tempering on the hardness of Q-tempered 1013 and 4315 martensites is shown in Fig. 15. First, it may be noted that the initial Q-tempered hardness is progressively lower as the specimen thickness increases, although martensite is the only transformation product. This hardness trend is in agreement with the degree of Q-tempering observed in the electron micrographs of Figs. 11 and 14. The higher initial levels for the 4315 steel are readily explained by the higher carbon and lower temperature range of martensite formation. Second, it is evident that, as the sections thicken, the extent of softening diminishes on applied tempering below 400°F. Above 400°F the usual features occur, but it may be noted that softening of the thicker sections appears to be slightly retarded.

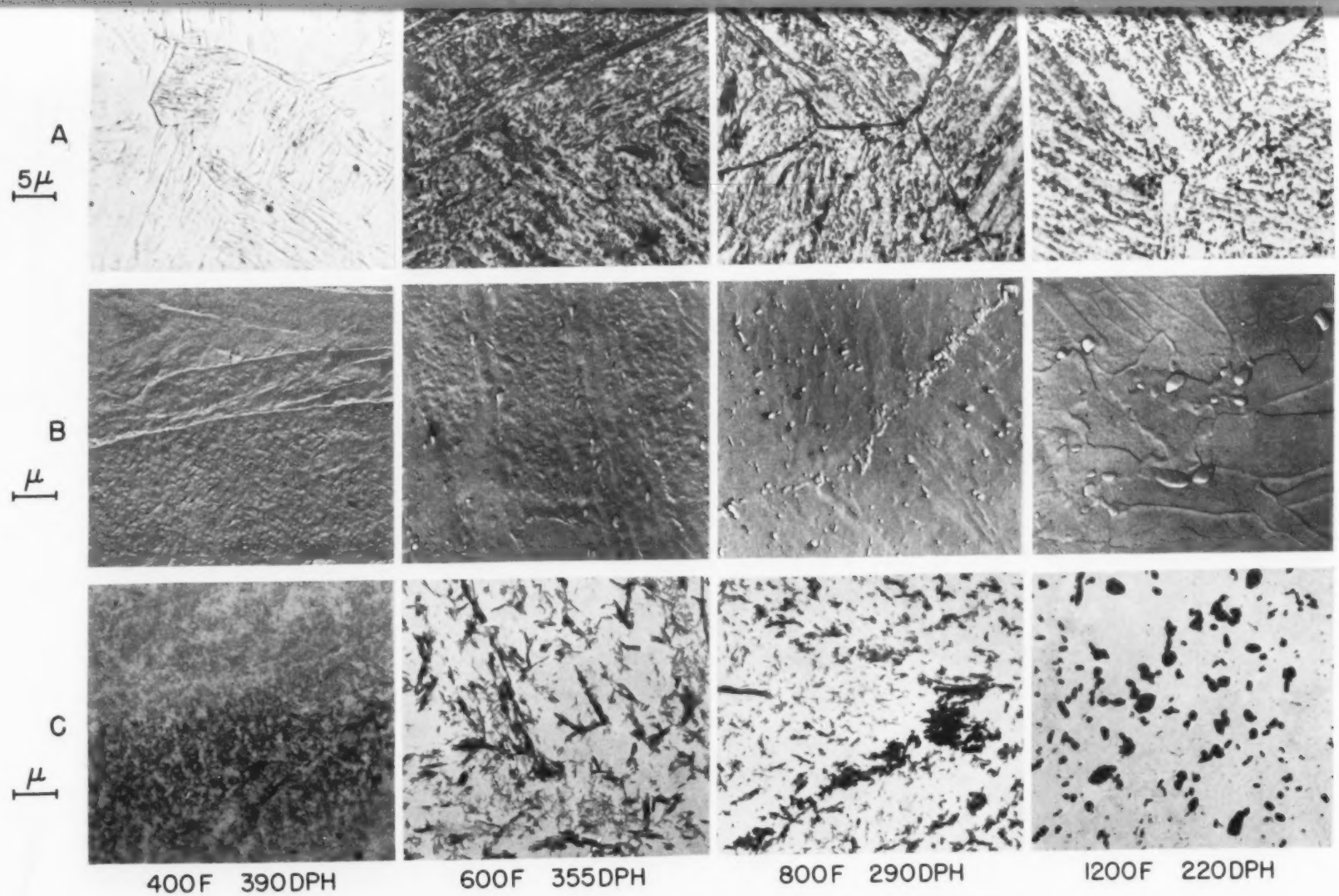


Fig. 16—Microstructure of Martensitic 1013 Steel Tempered for 1 Hour at Each Indicated Temperature. Row A: Light Micrographs; Row B: Shadow Micrographs; Row C: Extraction Replica Micrographs. Specimens $\frac{1}{32}$ inch Thick. Picral Etch.

Tempered Structures in 1013 Steel—The main structural changes observed on tempering 1013 martensite formed in slice specimens of $\frac{1}{32}$-inch thickness are illustrated in Fig. 16, which compares light micrographs, shadow micrographs and extraction micrographs, each representing the center zone of specimens tempered 1 hour at 400, 600, 800 and 1200°F. No appreciable change was found in the Q-tempered structure after a 1 hour temper at 212°F, and 1 hour at 300°F caused only slight growth of straw particles. However, there was considerable growth of "straws" and extent of the straw zones during 1 hour treatment at 400°F. Although the mottled matrix did not change its general appearance, a detailed study of these areas revealed the presence of an occasional stubby particle.

After tempering at 450°F, the mottled regions contained numerous particles, which were slightly broader and less match-like than the "straws." This change was found to be more pronounced after tempering at 500°F, and after tempering 1 hour at 600°F the mottled structure was wholly replaced by an aggregate of clustered stubby particles. *Like the "straw" particles, all of the stubby particles were found to be cementite.*[5] The incomplete diffraction pattern obtained from both types was similar to the usual pattern of cementite formed at intermediate temperatures in higher carbon steels. It is considered to result from extreme thinness of the particles along certain crystallographic directions, and such particles have been termed platelet or predominantly two-dimensional cementite. *No evidence has been found for the formation of epsilon carbide during tempering of any of the low carbon martensites investigated*, in agreement with the mechanism of the tempering of martensite as it is now understood (15,30).

A dark-etching network, representing a concentration of cementite particles in the prior austenite grain boundaries, developed during tempering at 800°F. The relatively narrow, carbide-rich network in the light and shadow micrographs is revealed as a broader band of clustered cementite platelets in the extraction micrograph, because this procedure reveals the particles of a precipitated phase in depth or volume instead of their cross section. The shadow replica micrographs are well adapted to reveal grain outlines and the location of larger precipitates. The selective etching effects, shown by the shadow micrographs in the matrix of specimens tempered at 400, 600 and 800°F, suggest either clusters of tiny martensite plates (about one-tenth of a micron or four-millionths of an inch in width) along the massive martensite plates which formed earlier, or that there are sub-grains in the martensite as proposed by Lement (15).

[5]Lement (15) stated that the carbide particles formed on applied tempering of a purified iron-carbon martensite containing 0.15% C were believed to be cementite, but he did not identify them.

The 1200°F shadow micrograph reveals sharply not only the ferrite grain size—about No. 14 on the ASTM Scale—but also some veining in these grains. Although a similar minute ferrite grain size has been found in low alloy, high tempered martensites (16,17), its persistence does not appear to depend on any special addition or impurity, as Lement, Averbach and Cohen recently observed it in highly purified iron-carbon alloys (30).

Tempered Structures in 4315 Steel—The corresponding structural changes on tempering 4315 martensite of $\frac{1}{32}$-inch section are illustrated in Fig. 17. The slowest cooled, 0.4-inch section of Q-tempered 4315 martensite revealed in the light microscope certain more rapidly etched plates with faintly resolvable dots, as shown in Fig. 14; this distinction, illustrated in the dusky areas of the corresponding micrograph in Fig. 17, increased on tempering up to 400°F. The extent of these areas agreed well with the extent of the straw-laden zones in the corresponding extraction micrographs.

Below about 800°F, the sequence of structural changes described for 1013 steel appear to be essentially the same as for 4315. The dark-etching network which formed in 1013 steel at 800°F did not appear until 1000°F in 4315 steel, but was considerably more pronounced. Some grains in the specimens tempered at 1000 and 1200°F appear to contain only extremely fine particles. This difference in carbide size between adjacent regions in the sample, more obvious in the 1000 and 1200°F extraction micrographs, suggests alloy carbide formation, but electron diffraction showed only cementite. Probably this dual size is associated with different alloy content of the cementite in the two areas. The numerous fine particles permit a closer approach to equilibrium distribution of chromium, molybdenum and manganese between cementite and ferrite, leading to higher alloy cementite. Higher alloy content would of course greatly hinder coalescence, and thus account for this observed phenomenon.

Cementite Straws and Softening—Extensive measurements of the size of cementite "straws" in Q-tempered specimens and their subsequent growth on applied tempering revealed a wide range of size. The smallest observed "straws" measurable on the extraction micrographs were found in Q-tempered, $\frac{1}{32}$-inch 1013 specimens, and measured 3.5×10^{-3} microns (0.14-millionths of an inch) in average width and 50×10^{-3} microns (2-millionths of an inch) in average length. The thickness of these "straws" was found to be below the resolving power of the microscope. When these specimens were further tempered by reheating at 400°F for 1 hour, the "straws" grew to an average width of 16×10^{-3} microns (0.64 millionths of an inch) with an average length of 270×10^{-3} microns (10.8 millionths of an inch) and thickness about one-third of the width.

Fig. 17—Microstructure of Martensitic 4335 Steel Tempered for 1 Hour at Each Indicated Temperature. Row A: Light Microscopy; Row B: Shadow Microscopy; Row C: Extraction Replica Microscopy. Nital Etch. Third Page.

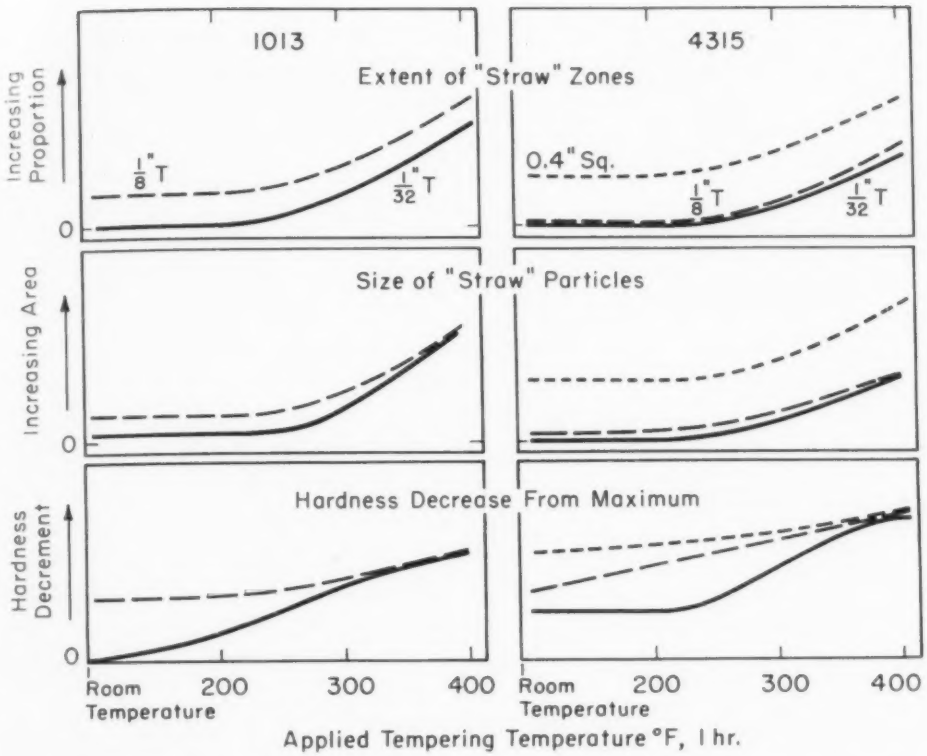


Fig. 18—Correlation of Softening During Tempering with Relative Extent of "Straw" Zones and Size of "Straw" Particles.

These measurements and similar measurements of the extent of straw-laden zones in the structure are compared in Fig. 18 with the extent of softening during tempering up to 400°F. Softening is plotted in the lower chart as the difference between the maximum hardness observed before applied tempering and the hardness after such tempering. This comparison shows that the increasing extent of the straw-laden zones and the increasing size of the "straw" particles correlate qualitatively with softening. This correlation suggests a pattern of precipitation of a new crystalline phase—cementite—and its growth, with corresponding depletion of the matrix as described by Geisler in his classic review (21). The lack of complete correlation with softening emphasizes that other factors, such as stress relief and undetected changes in the mottled matrix, may influence loss of hardness on tempering in this temperature range.

Low versus High Carbon Martensites—Comparison of the sequence and mechanism of tempering low carbon and high carbon martensites in carbon steels in Fig. 19 illustrates the basic differences. On quenching high carbon eutectoid austenite, martensite forms in the relatively low temperature range of 400 to 200°F. When this high carbon martensite is reheated to successively higher temperatures, it decomposes in the first stage of tempering into

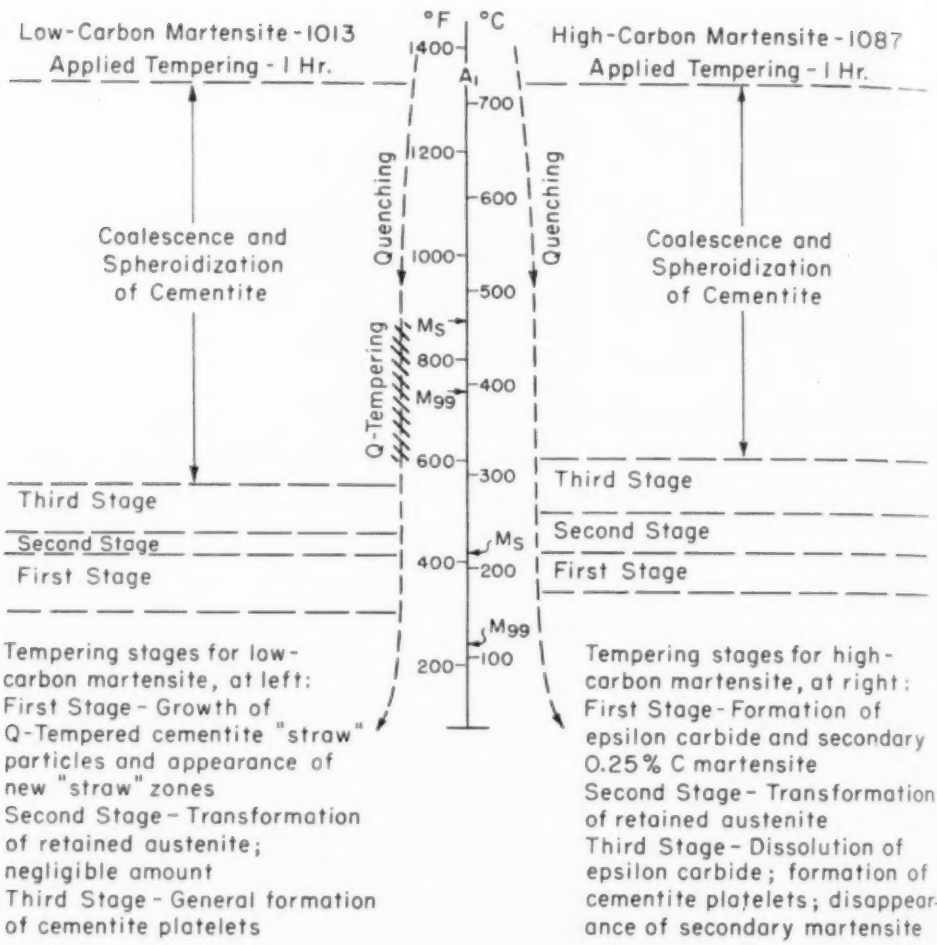


Fig. 19—Comparison of Mechanism of Tempering Low Carbon and High Carbon Martensites.

epsilon carbide and secondary martensite containing about 0.25% carbon. In the second stage, retained austenite transforms to bainite. In the third stage, epsilon carbide dissolves and cementite forms as the secondary martensite gradually becomes ferrite. The temperature range of each of the several stages is, of course, time-dependent as illustrated recently by Fisher (33), and here it is based on 1 hour at the tempering temperature. Also the stages actually are not sharply separated as indicated for simplified presentation, but overlap each other.

When low carbon 1013 austenite is quenched, martensite forms both above and below 800°F and is automatically Q-tempered. This Q-tempering occurring in low carbon martensites during quenching appears to have a profound influence on the course of applied tempering up to about 600°F. Q-tempering has nucleated cementite and *no* epsilon carbide is formed. In the first stage of applied tempering, the Q-tempered cementite "straws" grow and

the straw-laden zones increase in extent. The amount of retained austenite is negligible, so the second stage can be neglected. In the third stage cementite platelets are formed throughout the Q-tempered mottled matrix.

When carbide-forming alloying elements are added, indirect evidence suggests that the Q-tempered "straw" zones may be the sites of cementite particles enriched in alloy, which remain relatively small even during prolonged tempering near A_1 temperature. This characteristic may well account, at least in part, for the observed easy weldability of such quench-hardened and tempered low carbon, low alloy steels, for these more stable carbide particles dissolve less rapidly during the extremely brief weld heating.

If Q-tempering of low carbon martensites nucleates and forms cementite because it is the stable carbide phase at the relative high temperatures at which Q-tempering occurs, it may be that the minute amount of Q-tempering which can occur, if at all, only at relatively low temperatures following the formation of high carbon martensites, sets the stage for the nucleation of epsilon carbide, stable only at the same relatively low temperatures.

Correlation of Mechanical Properties with Microstructure

This interpretation of the microstructure of low carbon martensites suggests a correlation of those features with some salient characteristics of the mechanical properties: first, with respect to softening during Q-tempering and applied tempering. During Q-tempering, the extent of formation of ferritic zones containing cementite "straws" and their growth in the first stage of applied tempering closely parallels the softening curve. The thicker sections have a greater degree of Q-temper softening and less impetus for additional softening on applied tempering up to 400°F. The disappearance of mottling during third-stage tempering at 450–550°F corresponds to the rapid softening of all sections.

The high notch toughness of low carbon martensites is believed to be a consequence of Q-tempering of the martensitic matrix, evident in the mottled structure. On this basis, the relative changes of notch toughness on applied tempering up to 400°F are associated with still invisible changes in the mottled matrix.

Above 400°F the story changes. As the incipient stage of general cementite formation has been associated with diminished notch toughness in higher carbon martensites (15,18), so it appears to be in these low carbon martensites, for Payson (19) has confirmed the existence of a similar drop in toughness of low carbon martensites tempered at about 500–600°F. In low carbon martensites reheated in this 500–600°F zone, changes associated with the third stage of tempering—namely, formation of cementite platelets becomes de-

tectible throughout the matrix, and mottling of the matrix disappears. These two circumstances may well set the stage for decreased resistance to plastic flow and increased susceptibility to crack formation and propagation.

One more set of unusual characteristics in mechanical properties remains for correlation. The very marked rise in yield strength or flow resistance observed in low carbon martensites, without significant change in tensile strength on tempering at 400°F, has commonly been associated with relief of internal stresses. However, as Cottrell points out (20), the yield stress is very structure-sensitive; that is, its value is greatly affected by the presence of foreign atoms, precipitates, and grain boundaries because these obstruct the movement of imperfections or dislocations through each grain under applied load.

If the mottling of the Q-tempered martensitic matrix represents a very early stage of precipitation in which aggregates of atom clusters are beginning to form, a low applied tempering, as in the first stage zone, may promote this aggregation to obstruct slip more effectively. When such a structure is subjected to increasing applied load, to use Cottrell's picture, the free movement of dislocations along favored slip planes in the lattice is obstructed successively by these atom cluster aggregates, so the yield stress is raised, and no sudden yielding occurs. This does not entail any significant change in ductility or tensile strength, each of which is measured after severe plastic deformation.

With further tempering as in the third-stage zone, coalescence of the clustered aggregates leading to the general formation of detectible cementite platelets throughout the matrix will increase the mean free path (21,22) for unobstructed dislocation movements so much that flow resistance will begin to diminish.

Klingler (18), Averbach (23) and Muir (24) have cited similar rises in flow resistance on low tempering of medium carbon martensites. However, in contrast to this general behavior in low and medium carbon martensites, it appears from the data of Read (25) that, in high carbon martensite, flow resistance is a maximum in the untempered state and diminishes progressively on tempering. It may be that the high state of supersaturation and the low formation temperature of high carbon martensite develop such a high degree of strain energy in the lattice that flow resistance with low tempering is influenced primarily by the reduction in strain energy with increasing growth of atom cluster aggregates and subsequent carbide platelet formation.

Other Examples of Low Carbon Alloy Martensites

Although 1013 and 4315 martensites have been emphasized, this survey would be like a presidential poll confined to Maine if it did

not include brief mention of a few of the many other low carbon martensites which are much more prominent.

Constructional Alloy Steels—Several low carbon steels with multiple alloying elements totaling under 3% have recently been developed for use in the tempered martensitic condition with yield strengths approximating 100,000 psi and characterized by ready formability and weldability, and by high notch toughness at any ambient temperature. Boodberg and Parker (26) reported outstanding toughness in one of these steels tested as a restrained weldment at low temperature. Full-scale tests of pressure vessels made of another of these steels have recently led to limited approval by the ASME Boiler and Pressure Vessel Committee of the use of such quenched and tempered steels in pressure vessel construction (31).

Type 4815 nickel-molybdenum steel is one of the most widely used carburizing steels in heavy duty applications requiring a low carbon, low-tempered, fully martensitic core. A steel containing about 9% nickel and 0.1% carbon can be made entirely martensitic in considerable thickness and, when suitably tempered, has a rather high notch toughness at temperatures as low as −315°F.

Stainless Steels—Turning finally to stainless steels, the grade containing about 12% chromium and 0.1% carbon, known as Type 403, is widely used in the tempered martensitic condition as turbine blading in the steam power industry.

Precipitation-hardened stainless steels probably stand at the highest commercial alloy end of low carbon martensites. Many of these involve three-stage treatments: an austenite conditioning treatment, transformation to martensite and additional hardening of the martensite by precipitation of another phase. Several such steels are based on modifications of the basic Type 301, containing nominally 17% chromium and 7% nickel with 0.1% carbon.

Type 301 itself is very widely used as a high strength constructional steel in the lightweight transportation industry. When cooled from high temperature it is normally austenitic at room temperature. It is, however, so unstable that it very readily transforms when plastically deformed and, as this transformation occurs by the martensitic mechanism, the product is really low carbon martensite though commonly termed ferrite.

Demonstration of Formation of Low Carbon Martensite During Cold Work—A phenomenon observed at Kearny and reported twenty-five years ago (27)—namely, that the slip bands of cold-worked unstable austenite appear much thicker than the slip bands of stable austenite and are believed to represent zones of transformation—suggested recently that the high-speed motion picture camera might show the successive stages of the process. Further encouragement came from Machlin's report (28) that a speed of about 3000 frames per second should be sufficient to record the progressive formation

of slip band projections on the polished surface. A few weeks ago, with the aid of a special device which stretches a polished strip of Type 301 steel across the stage of a microscope, the Laboratory succeeded in obtaining a brief motion picture of the onset and progress of plastic deformation and associated transformation. Within a large grain stretched 7% during 1 second at 75°F. the exposures were made at a maximum speed of 3000 frames per second.

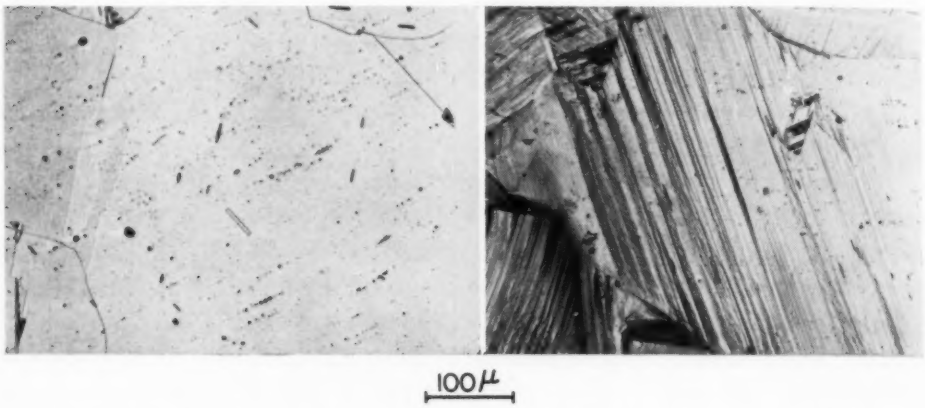


Fig. 20—Micrographs of Type 301 Steel Before (Left) and After Stretching 7% (Right). Both Etched 2 Minutes in Hydrochloric-Picric Acid Reagent[32] Before Stretching.

Unfortunately, it is not feasible to publish this motion picture shown during the oral presentation of this Lecture. However, micrographs of initial and final structure are reproduced in Fig. 20. The left micrograph shows a typical field of this unstable austenite solution-treated and quenched from 2300°F to establish a grain size of minus 1 ASTM Scale, with all carbon dissolved. The right micrograph shows the actual field viewed in the motion picture photographed at the conclusion of the picture. The principal grain in this field was favorably oriented to the horizontal axis of stretching to reveal the formation, lengthening and thickening of slip bands by surface contour changes. The few black "arrow-heads" in the upper part of the grain are typical of minor transformation during polishing even though electrolytic, because this particular austenite was so unstable that the most careful mechanical polishing transformed most of the surface layer.

By slow motion analysis, it was found that the projection or trace of the first visible slip band crossed the entire grain in 1/10 of a second; progressing probably by short, high speed jumps; so what was observed was a discontinuous advance, with an apparent average rate of advance of about 2 mm. per second, and when viewed at 16 frames per second the band crossed the grain in about three sec-

onds. New slip bands started before the first one reached the opposite edge of the grain. The next obvious stage in the motion picture was the selective thickening or widening of certain bands approaching the widths in the right micrograph of Fig. 20. The microhardness of these broad slip bands was found to be twice that of adjoining layers free of slip, a change far greater than the strain hardening of stable austenite stretched to this extent. Further stretching near the end of the motion picture produced slip bands in adjoining grains less favorably oriented for easy slip. Portions of these grains appear at the left and top sides of the right micrograph in Fig. 20. Although much of the grain after stretching 7% was still free of slip bands, the correspondence of these bands to transformed regions was confirmed by their high microhardness and by X-ray diffraction, showing approximately 25% transformation in the stretched zone of the specimen.

Summary

In summarizing this survey of low carbon martensites, three unique characteristics are paramount:

1. The high temperature range of formation of martensite, leading to Q-tempering, less residual stress, less distortion because the change of volume at transformation is less, and very little retained austenite, thereby virtually avoiding delayed hardening stresses.

2. Cementite, which begins to form during Q-tempering, is the first and, at present knowledge, the only carbide formed on tempering except for alloy carbide in higher alloy steels.

3. Avoidance of the more complex sequence involving the decomposition of high carbon martensite to low carbon martensite and epsilon carbide minimizes detrimental structural disturbances.

These characteristics are believed to account for the remarkable properties of low carbon, martensitic steels.

Low carbon martensites combine high strength up to 200,000 psi with high toughness and favorable combination of flow resistance and ductility. These properties, when adjusted to suitable formability and weldability, and enhanced in some stainless steels by exceptional corrosion resistance, make low carbon martensites among the most versatile of structural materials.

In conclusion, paraphrasing Georg Masing's remarks some years ago in concluding an Institute of Metals Lecture, we know we do not fully understand the fundamental inner behavior of low carbon martensites, but we do believe we are beginning to get acquainted with it, and it's a lot of fun!

References

1. W. L. Fink and E. D. Campbell, "Influence of Heat Treatment and Carbon Content on the Structure of Pure Iron-Carbon Alloys," *Transactions*, American Society for Steel Treating, Vol. 9, 1926, p. 717.

2. W. L. Grube, Report to American Society for Testing Materials Committee on Electron Microstructure of Metals, June 1955.
3. *Atlas of Isothermal Transformation Diagrams*, Second Edition, 1951, published by U. S. Steel Corporation.
4. D. J. Carney, "Another Look at Quenchants, Cooling Rates and Hardenability," TRANSACTIONS, American Society for Metals, Vol. 46, 1954, p. 882.
5. A. L. Boegehold and E. W. Weinman, "Cooling Rates of Plates and Rounds," METAL PROGRESS, American Society for Metals, Vol. 51, January 1947, p. 96B.
6. A. B. Kinzel, "Ductility of Steels for Welded Structures," TRANSACTIONS, American Society for Metals, Vol. 40, 1948, p. 27.
7. C. H. Shih, B. L. Averbach and M. Cohen, "Some Effects of Silicon on the Mechanical Properties of High Strength Steels," TRANSACTIONS, American Society for Metals, Vol. 48, 1956.
8. C. C. Busby, M. F. Hawkes and H. W. Paxton, "Tensile and Impact Properties of Low Carbon Martensites," TRANSACTIONS, American Society for Metals, Vol. 47, 1955, p. 135.
9. A. E. Nehrenberg, Discussion of article by C. C. Busby, M. F. Hawkes and H. W. Paxton, "Tensile and Impact Properties of Low Carbon Martensites," TRANSACTIONS, American Society for Metals, Vol. 47, 1955, p. 153.
10. ASM METALS HANDBOOK, 1948 Edition, p. 611, published by American Society for Metals.
11. R. A. Grange and H. M. Stewart, "The Temperature Range of Martensite Formation," *Transactions*, American Institute of Mining and Metallurgical Engineers, Vol. 167, 1946, p. 467.
12. E. C. Bain, ALLOYING ELEMENTS IN STEEL, 1939, p. 36, published by The American Society for Metals, Cleveland.
13. J. L. Burns, T. L. Moore and R. S. Archer, "Quantitative Hardenability," TRANSACTIONS, American Society for Metals, Vol. 26, 1938, p. 1.
14. R. M. Fisher, American Society for Testing Materials, Special Publication No. 155, 1953, p. 49.
15. B. S. Lement, B. L. Averbach and M. Cohen, "Microstructural Changes on Tempering Iron-Carbon Alloys," TRANSACTIONS, American Society for Metals, Vol. 46, 1954, p. 851.
16. M. Baeyertz, W. F. Craig, Jr. and E. S. Bumps, "Effect of Ferrite Grain Structure upon Impact Properties of 0.80% Carbon Spheroidite," *Transactions*, American Institute of Mining and Metallurgical Engineers, Vol. 188, 1950, p. 1464.
17. R. M. Fisher and J. F. Boyce, Discussion of Reference 16, *Transactions*, American Institute of Mining and Metallurgical Engineers, Vol. 191, 1951, p. 1064.
18. L. J. Klingler, W. J. Barnett, R. P. Frohmberg and A. R. Troiano, "The Embrittlement of Alloy Steel at High Strength Levels," TRANSACTIONS, American Society for Metals, Vol. 46, 1954, p. 1557.
19. Peter Payson, *Transactions*, American Institute of Mining and Metallurgical Engineers, Vol. 200, 1954, p. 1242.
20. A. H. Cottrell, *Theoretical Structural Metallurgy*, Second Edition, 1955, p. 241, published by St. Martin's Press.
21. A. H. Geisler, *Phase Transformation in Solids*, 1951, p. 387, published by John Wiley & Sons, Inc., New York.
22. M. Gensamer, "Strength and Ductility," TRANSACTIONS, American Society for Metals, Vol. 36, 1946, p. 30.
23. B. L. Averbach, S. G. Lorris and M. Cohen, "Stress-Induced Transformation of Retained Austenite in Hardened Steel," TRANSACTIONS, American Society for Metals, Vol. 44, 1952, p. 746.
24. H. Muir, B. L. Averbach and M. Cohen, "The Elastic Limit and Yield Behavior of Hardened Steels," TRANSACTIONS, American Society for Metals, Vol. 47, 1955, p. 380.
25. T. A. Read, H. Marcus and J. M. McCaughey, FRACTURE OF METALS, 1948, p. 228, published by American Society for Metals, Cleveland.

26. A. Boodberg and E. R. Parker, "Transition Temperatures of Structural Steels. Effects of Geometry and Welding on High Yield Strength Steels," *Welding Journal*, Vol. 28, April 1949, p. 167S.
27. E. C. Bain, *AISI Yearbook*, 1930, p. 271.
28. E. S. Machlin, "Deformation by Transformation Makes Alloys Tougher," *Iron Age*, Vol. 171, January 22, 1953, p. 106.
29. P. P. Puzak and W. S. Pellini, Naval Research Laboratory Report 4545, June 22, 1955.
30. B. S. Lement, B. L. Averbach and M. Cohen, "Further Study of Microstructural Changes on Tempering Iron-Carbon Alloys," TRANSACTIONS, American Society for Metals, Vol. 47, 1955, p. 291.
31. ASME Boiler and Pressure Vessel Code, Case Interpretation No. 1204-1, Mechanical Engineering, Vol. 78, 1956, p. 101, 185.
32. ASM METALS HANDBOOK, 1948 Edition, Reagent 3, p. 395.
33. R. M. Fisher, American Society for Testing Materials Committee E-4 XI Meeting, June 1955. To be published in *Proceedings*, American Society for Testing Materials, 1956.

SOME EFFECTS OF SILICON ON THE MECHANICAL PROPERTIES OF HIGH STRENGTH STEELS

By C. H. Shih, B. L. Averbach and Morris Cohen

Abstract

The effects of increasing the silicon content in 4340 and 4325 steels to 1.5% have been observed as a function of tempering temperature. The softening on tempering is retarded by silicon, and it appears possible to obtain somewhat higher strengths in the silicon steels without a corresponding loss in ductility or in Charpy impact strength. At high strength levels the elastic limit is approximately one-half of the engineering yield strength; silicon additions have no influence on the maximum elastic limit. Although the introduction of silicon has several beneficial effects at high strength levels, undesirable impact properties may be introduced by tempering at high temperatures (temper embrittlement). Retained austenite data are presented as a function of cooling rate from the hardening temperature, and it is shown that substantial amounts of retained austenite may be developed on retarded cooling. There is also some indication that the endurance limits and the elastic limits may be related. (ASM-SLA Classification: Q general, AY)

Introduction

THE addition of silicon to hardenable steels has been shown to retard the softening which occurs on tempering (1,2,3)[1]. Steels with high silicon content have been employed in springs for many years, and recently a series of such steels has also been used for high strength structural purposes. In this paper the effects of an increased silicon content in AISI 4340 and 4325 are described.

These studies indicate that increasing the silicon to 1.5% reduces the softening which occurs on tempering. The increased silicon content also results in a higher tensile strength with no attendant decrease in ductility. The Charpy impact values of the higher silicon steels are equivalent to those of the normal steels at high hardness. At lower hardness levels, however, the silicon steels have less favorable impact properties.

[1]The figures appearing in parentheses pertain to the references appended to this paper.

This work was performed under the sponsorship of the Wright Air Development Center under Contract No. AF 33(616)-2012.

A paper presented before the Thirty-Seventh Annual Convention of the Society, held in Philadelphia, October 17–21, 1955. The authors, C. H. Shih, B. L. Averbach and Morris Cohen, are associated with the Department of Metallurgy, Massachusetts Institute of Technology, Cambridge. Manuscript received April 11, 1955.

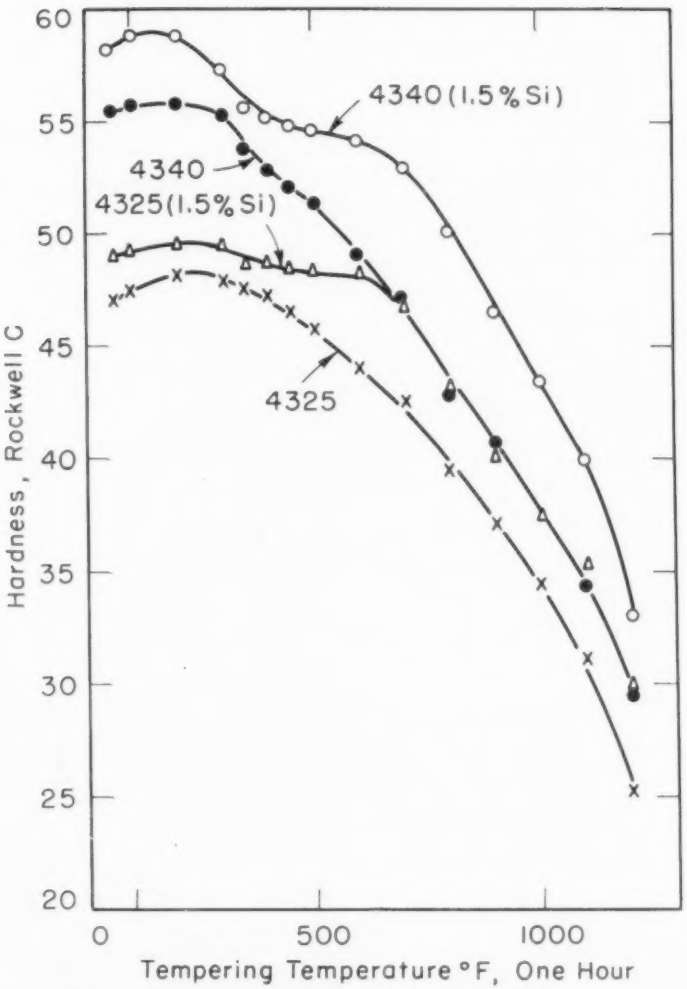


Fig. 1—Effect of Tempering on Hardness of Four High Strength Steels.

An extensive investigation on the tempering kinetics of these steels is now under way, including a study of the microstructural changes and of the retained austenite behavior. It appears that the presence of silicon retards almost all of the tempering phenomena. A detailed study of the kinetics will be presented elsewhere.

Materials

Four alloy steels were used in this investigation: AISI 4340, 4340 (1.5% silicon), AISI 4325, 4325 (1.5% silicon). The chemical compositions are shown in Table I. The 4340 steel was taken from a commercial heat and the others were induction furnace laboratory heats.[2] The ingots were forged to ½ inch and ¾ inch rounds, and then annealed.

[2]The authors are indebted to M. W. Lightner of the U. S. Steel Corporation for his cooperation in procuring these materials. An induction furnace heat of 4340 was tested sufficiently to show that comparable results could be obtained in commercial and laboratory heats.

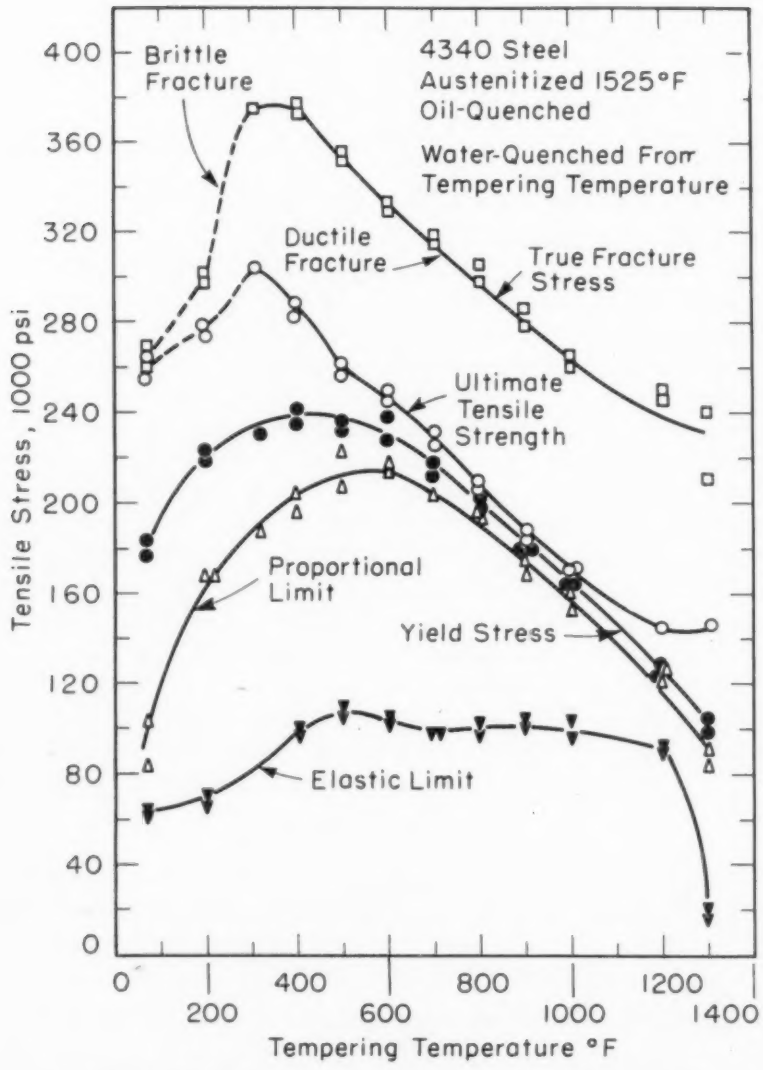


Fig. 2—Effect of Tempering on Tensile Properties of 4340 Steel.

Table I
Chemical Composition of Steels

	Weight Percent							
	C	Mn	P	S	Si	Ni	Cr	Mo
4340*	0.39	0.75	0.007	0.012	0.31	1.66	0.75	0.24
4340(1.5% Si)	0.37	0.76	0.010	0.019	1.45	1.95	0.84	0.24
4325	0.26	0.63	0.010	0.020	0.23	1.91	0.77	0.26
4325(1.5% Si)	0.26	0.76	0.009	0.018	1.42	1.95	0.60	0.25

*Commercial heat. The remaining are laboratory induction heats.

Experimental Methods

All of the materials were normalized at 1600°F prior to machining. The tensile properties were measured on 0.252 inch diameter

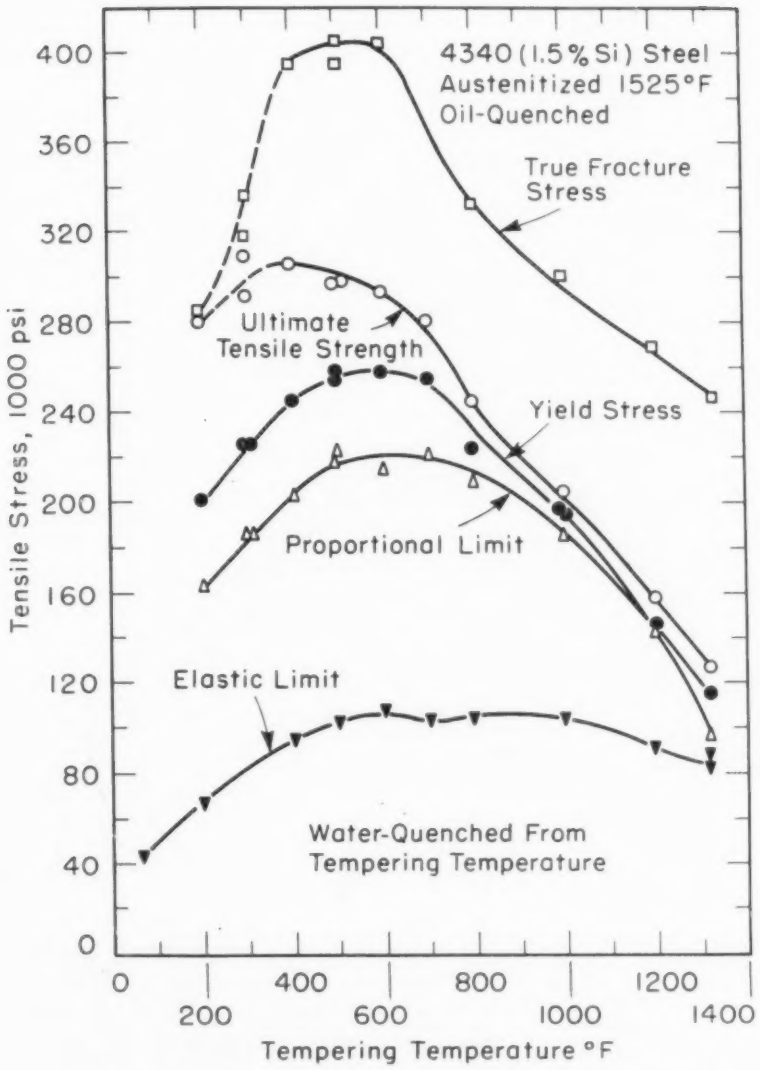


Fig. 3—Effect of Tempering on Tensile Properties of 4340 (1.5% Si) Steel.

test bars (5), and impact properties were evaluated by means of standard V-notch Charpy specimens. In order to minimize the effects of surface condition on the impact properties, the specimens were rough machined to 0.020 inch above the final size and then finish machined after heat treatment.

The 4340 steels were austenitized for 30 minutes in a lead pot at 1525°F and the 4325 steels at 1550°F. All specimens were quenched into oil at 75 ± 5°F. Tempering was performed in oil, salt or lead pots, depending on the temperature.

Elastic limits were determined on the tensile specimens using the method developed by Muir, Averbach and Cohen (5). In this

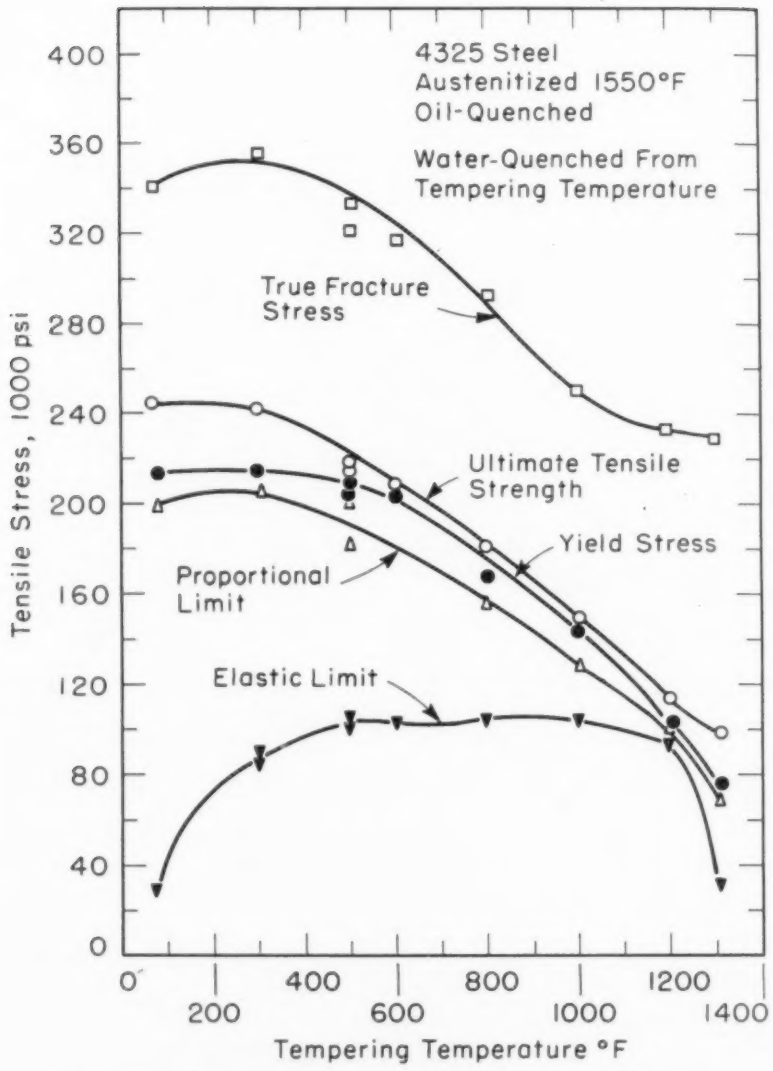


Fig. 4—Effect of Tempering on Tensile Properties of 4325 Steel.

technique successively higher stresses are applied and the residual strain on unloading is determined by means of electrical resistance strain gages. The elastic limit is defined as a stress above which the residual strain becomes progressively larger on repeated loading, and is probably accurate within 2000 psi. Other tensile properties were obtained by means of conventional stress-strain recording apparatus.

Experimental Results

Mechanical Properties

The hardness and tensile properties of these steels are summarized in Figs. 1–5 as a function of the tempering temperature.

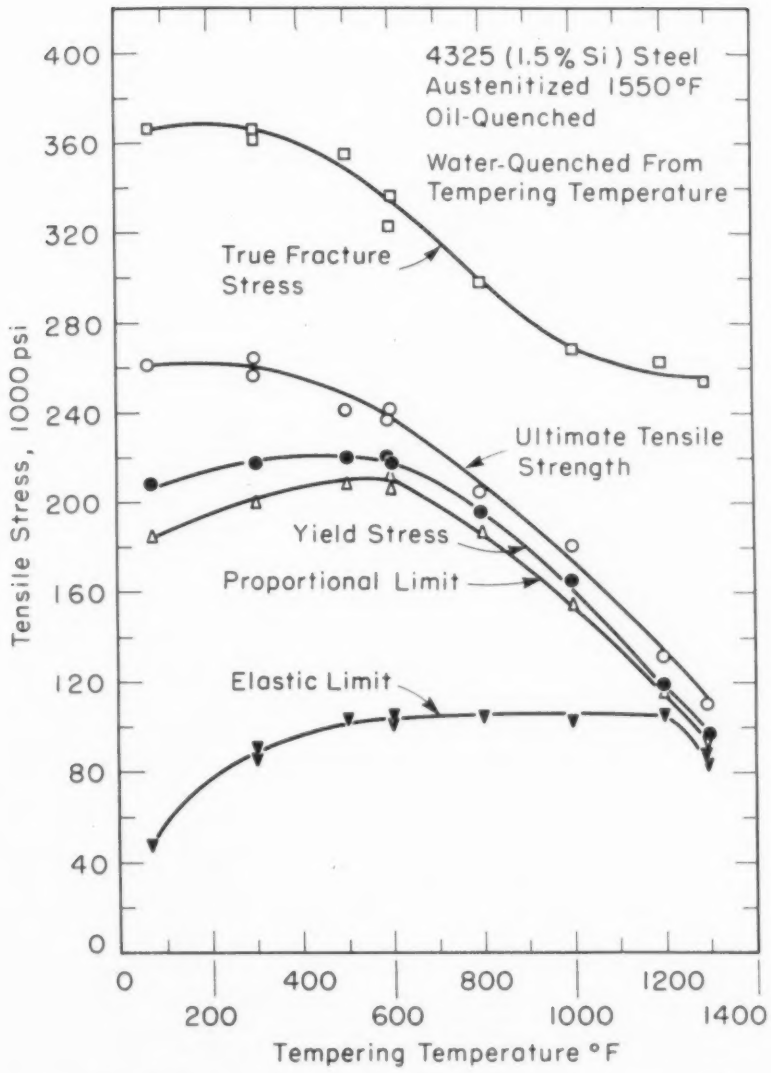


Fig. 5—Effect of Tempering on Tensile Properties of 4325 (1.5% Si) Steel.

Each specimen was tempered for 1 hour at the temperature indicated. The effectiveness of silicon in retarding the softening on tempering is shown in Fig. 1; for example, on tempering above 600°F, the hardness of 4325 (1.5% silicon) is as high as that of 4340.

Each of these steels has a similar variation of tensile properties with tempering temperature. The ultimate tensile strength and fracture stress increase as the tempering temperature is decreased, being terminated by brittle fracture in the higher carbon steels. The yield stress and proportional limits, however, seem to reach a maximum on tempering in the neighborhood of 300–600°F, and a decrease in these properties is observed as the tempering temperature is lowered further. The elastic limit is considerably below the

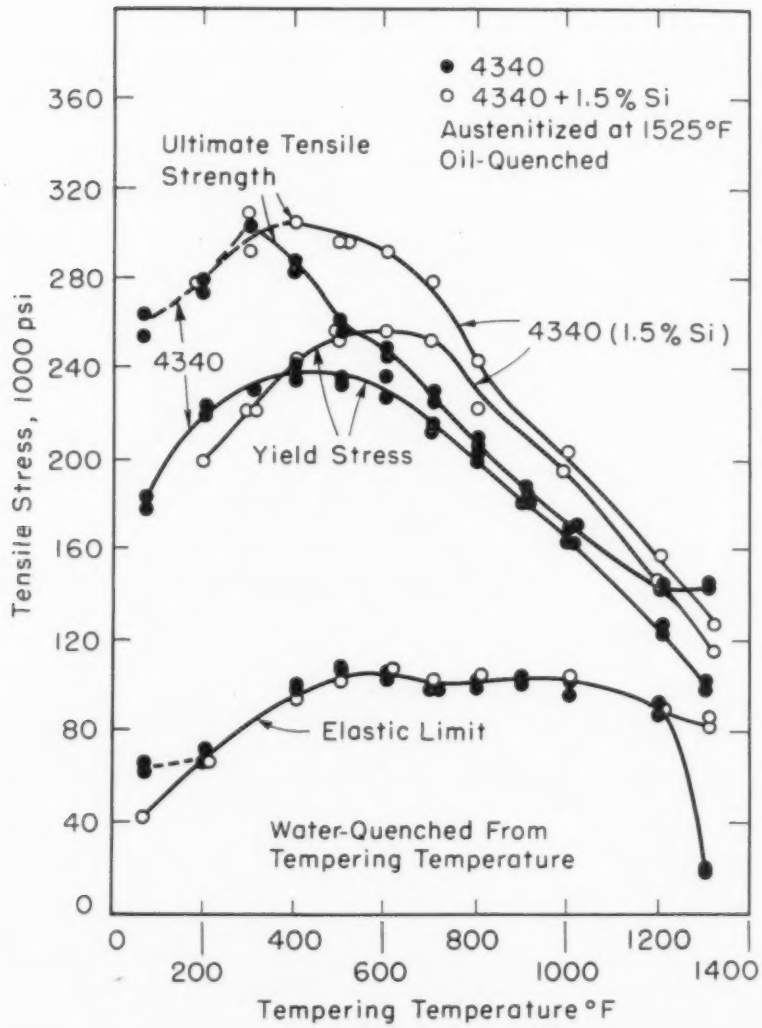


Fig. 6—Effect of Silicon Addition to 4340 on Tensile Properties.

proportional limit and, at high strength levels, it is only about 50% of the engineering yield stress. The elastic limit also decreases on tempering below about 400°F.

Fig. 6 indicates the effects of silicon on the tensile properties of 4340. It is evident that the tensile and yield strengths are both raised by the silicon addition, but the elastic limit is unaffected. At high strength levels, i.e., at low tempering temperatures, the increase in tensile strength can be as high as 40,000 psi. Similar comparisons may be made for the 4325 and 4325 (1.5% silicon) steels.

The elastic limits of 4340 steel are compared with those of plain carbon steels containing 0.29, 0.41 and 0.82% carbon (5) in Fig. 7. It is evident that the elastic limit follows approximately the same trend for each steel as a function of tempering temperature. The

4340 steel has about the same maximum elastic limit as that obtained for the plain carbon steels. However, the elastic limit of the plain carbon steels drops off more rapidly on tempering at higher tempering temperatures than does the 4340 steel.

Figs. 8 and 9 illustrate the effects of silicon on ductility. Reduction in area, total elongation, and the relative elongation before necking are shown as functions of tempering temperature. The ductility properties seem to be unaffected by the addition of silicon

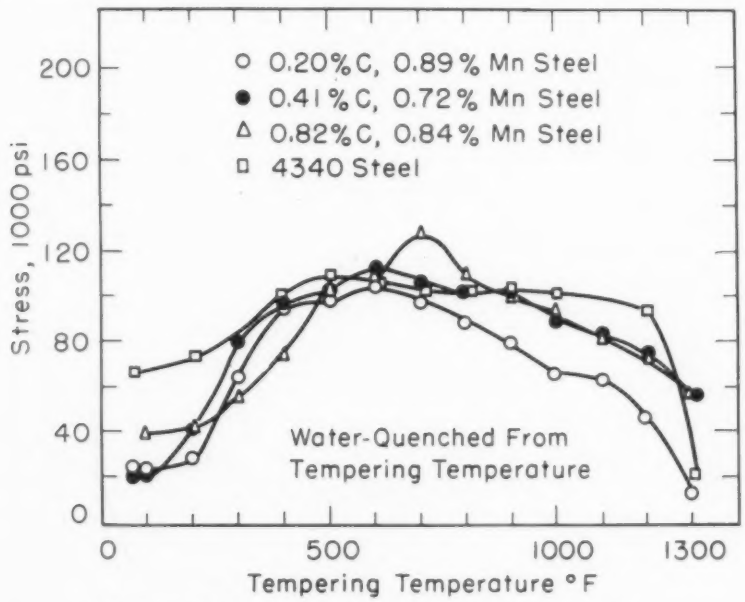


Fig. 7—Elastic Limit of Plain Carbon and 4340 Steels.

even though higher tensile strength and hardness values are observed in the silicon steels at the lower tempering temperatures.

Fig. 10 shows the influence of silicon on the yield-tensile ratio as a function of the tensile strength. The yield-tensile ratio at the high strength levels appears to be increased by the addition of silicon in the 0.40% carbon steel, although a similar effect is not observed in the 0.25% carbon steel.

The influence of cooling rate from the tempering temperature on the elastic limit is indicated in Fig. 11 which compares results obtained on air cooling and water quenching from each tempering temperature. A difference becomes noticeable only on tempering above 500°F in that the elastic limit of the water-quenched sample then falls consistently below that of the air-cooled sample. A particularly large decrease in elastic limit is observed after water quenching from 1300°F. Inasmuch as similar effects are found in plain carbon steels (5), this behavior is presumed to arise from the introduction of residual stresses on rapid cooling from the tempering temperature.

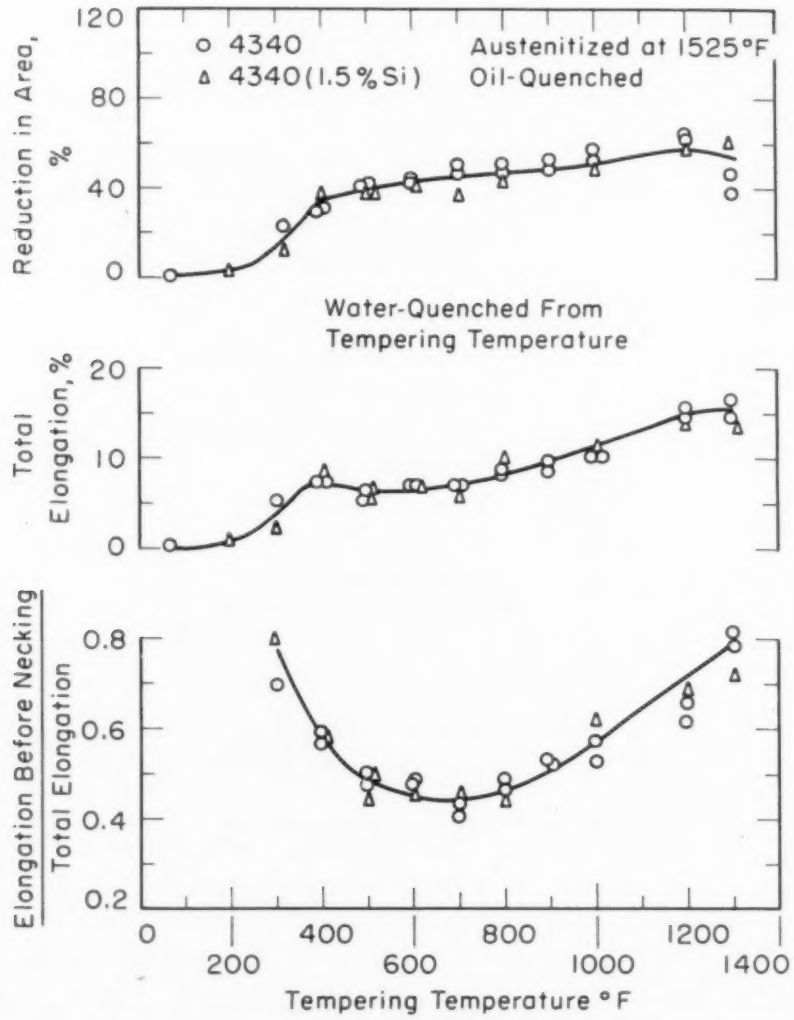


Fig. 8—Effect of Tempering on the Tensile Ductility of 4340 and 4340 (1.5% Si).

Fig. 11 also presents the elastic limits measured on a few specimens which were refrigerated in liquid nitrogen (−320°F) after hardening but prior to tempering. The elastic limits of these specimens were identical with those of unrefrigerated samples. However, the retained austenite content in each case was low (3% without refrigeration, 1.5% after refrigeration) and hence these data probably do not reflect the influence of retained austenite in commercial practice.

From the relationship between hardness and tensile strength in Fig. 12, it is evident that the steels follow a consistent relationship in this respect. Figs. 13–16 show the strength and ductility properties as a function of hardness. It is interesting to note that the elastic limit maintains its maximum value at a higher hardness (and tensile

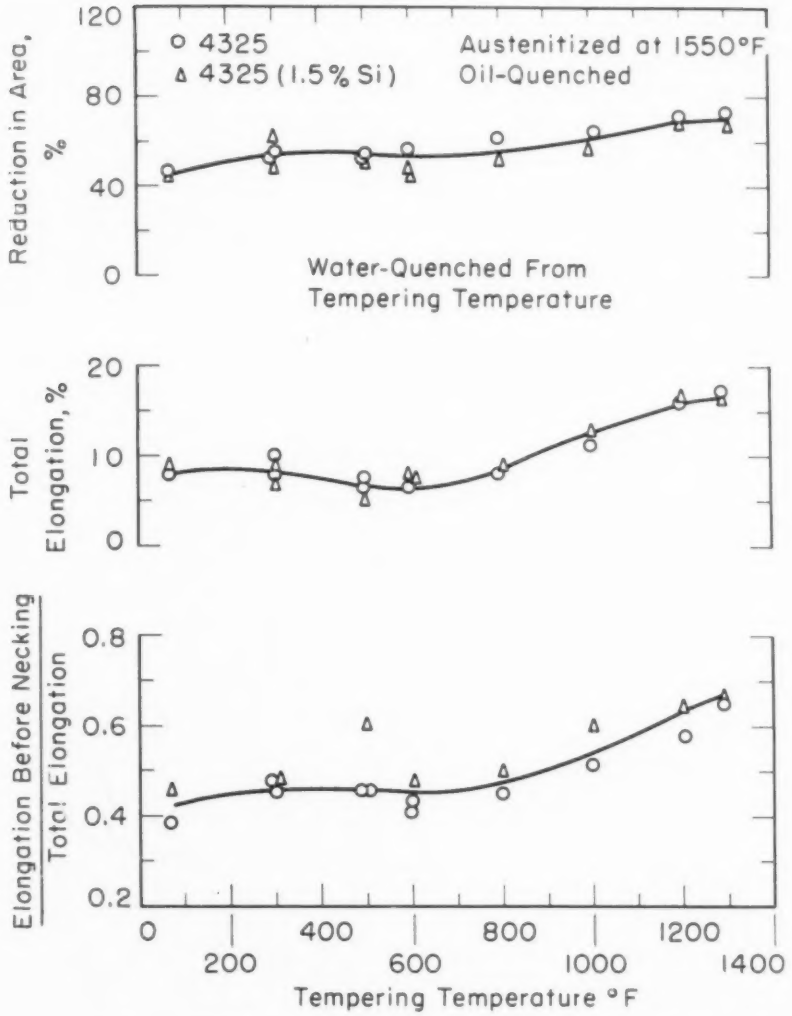


Fig. 9—Effect of Tempering on the Tensile Ductility of 4325 and 4325 (1.5% Si).

strength) in the 4340 steel than in the 4325 material; moreover, the addition of silicon increases the useful hardness to some extent in each case. The proportional limit and the yield stress increase almost linearly with hardness except at the highest hardness levels.

The impact properties of these steels at room temperature as a function of tempering temperature and hardness are plotted in Figs. 17–20. The importance of brittle failure in high strength steels has been recently investigated (6,7,8) although the minimum impact level for a given structural member is somewhat uncertain (4). Figs. 17–18 indicate that the impact properties at high strength levels are slightly improved by the addition of silicon. However, as the tempering temperature is increased above 700°F the impact properties of regular 4340 and 4325 are superior to those of the high

silicon steels. The slight minimum or plateau in the impact strength of 4340 and 4325 in the vicinity of 600°F is shifted to higher temperatures in the corresponding silicon steels. Figs. 19 and 20 show the impact properties as a function of hardness and tensile strength. Below a tensile strength of about 250,000 psi (Rockwell C-50) in the 0.40% carbon steels, silicon is detrimental to the impact strength, but becomes advantageous when the strength is higher than 250,000

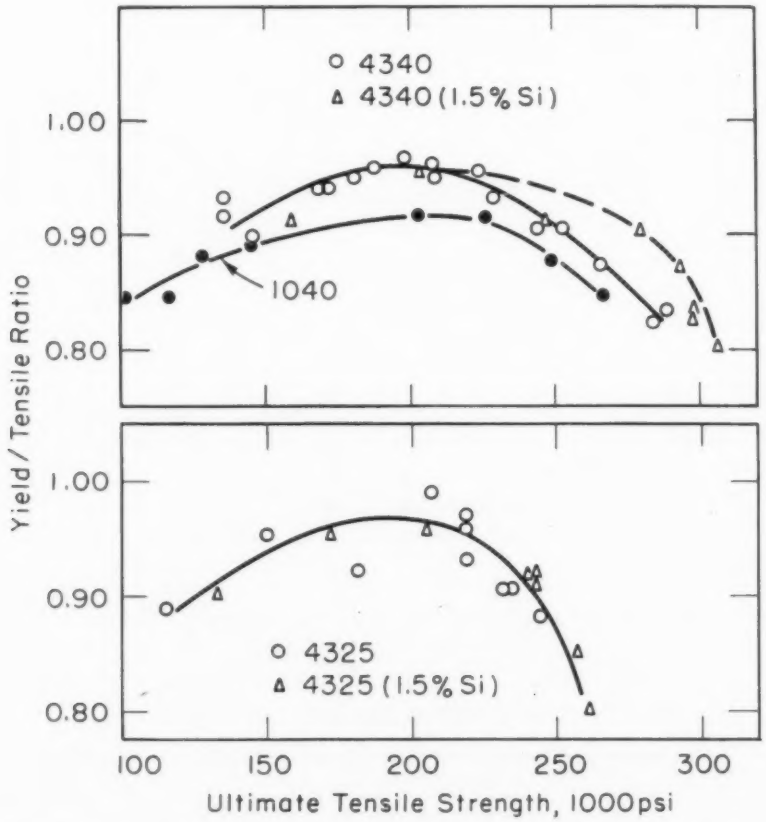


Fig. 10—Effect of Silicon on Yield/Tensile Ratio in 4340 and 4325.

psi. A similar trend is found in the 0.25% carbon steels, but the cross-over point is 180,000 psi (Rockwell C-40).

It should be noted that the impact properties of the 4325 steels are higher than those of the 4340 steels after low tempering treatments. It is possible to obtain a tensile strength in the neighborhood of 250,000 psi, with about 8% elongation and with a Charpy impact of 25 ft-lbs in 4325 (1.5% silicon) on tempering at 400°F. This combination of high strength, ductility, and notch toughness may be desirable for many structural purposes.

Temper embrittlement may become significant at lower hardness levels because of the tempering temperatures employed. Impact

properties were obtained as a function of testing temperature for steels treated to various strength values. The data are summarized in Figs. 21–24. On tempering at 500°F, Fig. 21 shows that the addition of silicon has little influence on the transition behavior. If anything, the effect of silicon is beneficial in this respect. However, on tempering back to Rockwell C-30, it is evident from Figs. 22 and

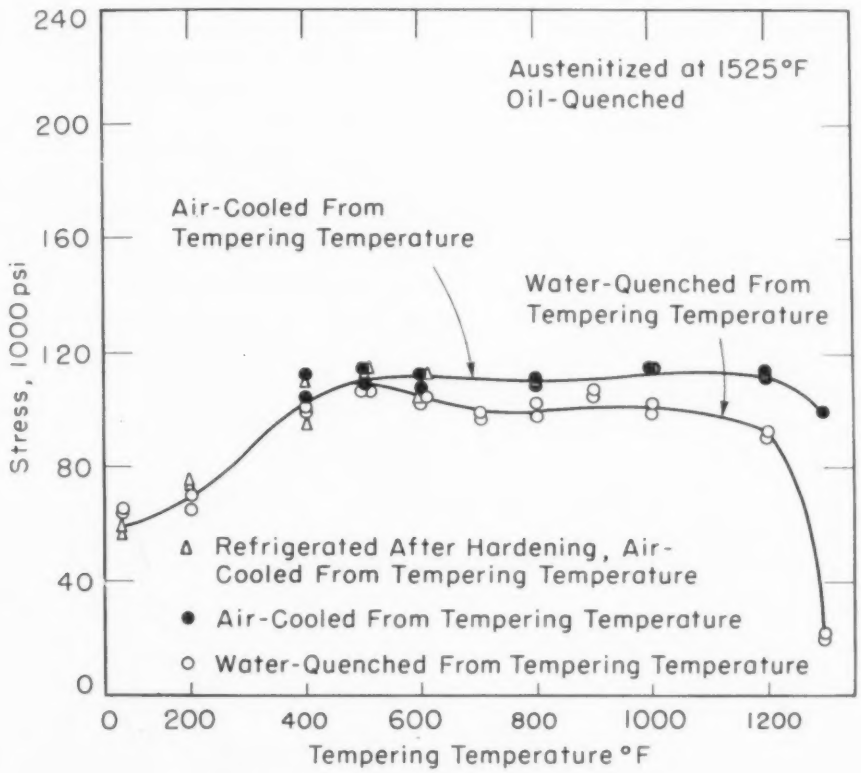


Fig. 11—Elastic Limit Values of 4340 Steel.

23 that the transition temperature is raised considerably by the addition of silicon, both after water quenching and after furnace cooling from the tempering treatment. The regular and high silicon steels are both subject to temper embrittlement, but silicon seems to intensify the effect (compare the water-quenched and furnace cooled impact values for each steel).

The important influence of quenching stresses on the elastic limit is indicated in Fig. 11 by the large decrease in elastic limit caused by water quenching from high tempering temperatures. The changes in length associated with different cooling rates from 1200°F for 4″ × 3/8″ diameter specimens of 4340 and 4325 are summarized in Table II. A specimen of each steel was first tempered for 300 hours at 1200°F in order to eliminate changes in length associated with subsequent tempering and then furnace cooled to establish a

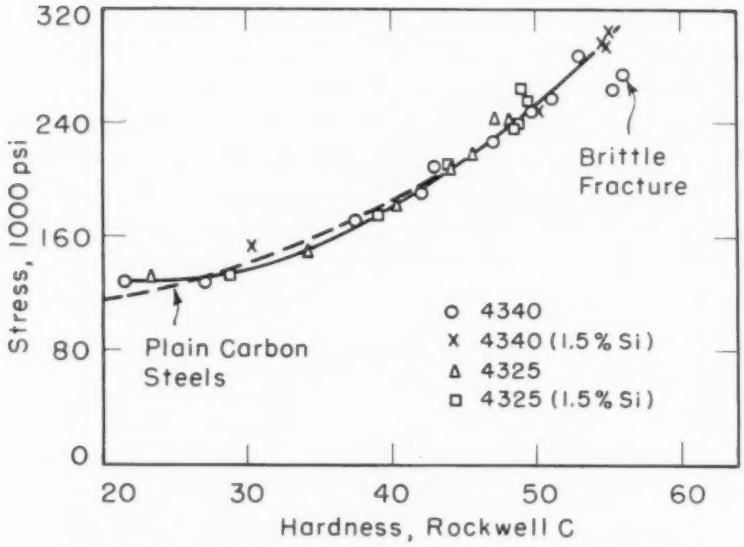


Fig. 12—Hardness vs. Ultimate Tensile Strength of the Four High Strength Steels.

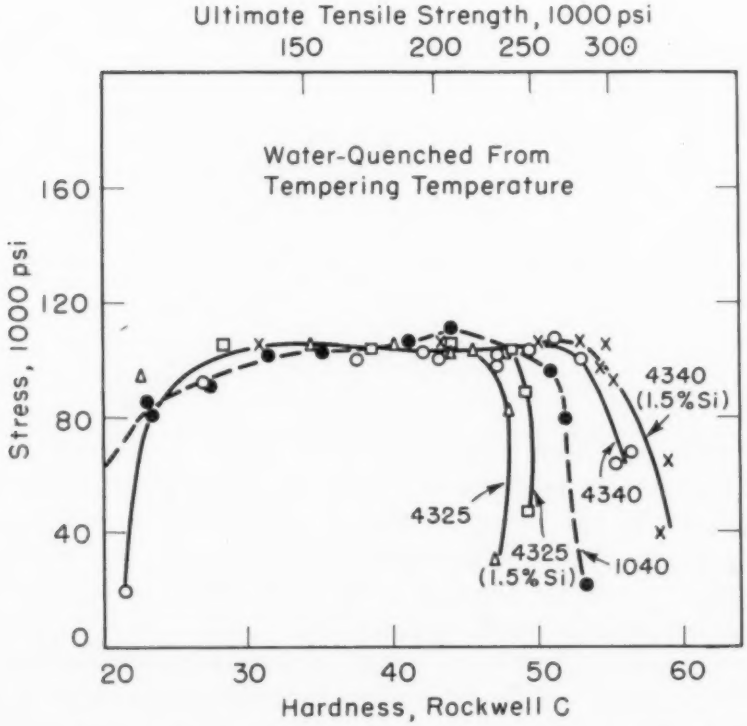


Fig. 13—Elastic Limit as a Function of Hardness and Tensile Strength.

relatively stress-free reference length. Each specimen was reheated to 1200°F in an evacuated Vycor tube and air-cooled, after which the resultant relative change in length was measured in an optical

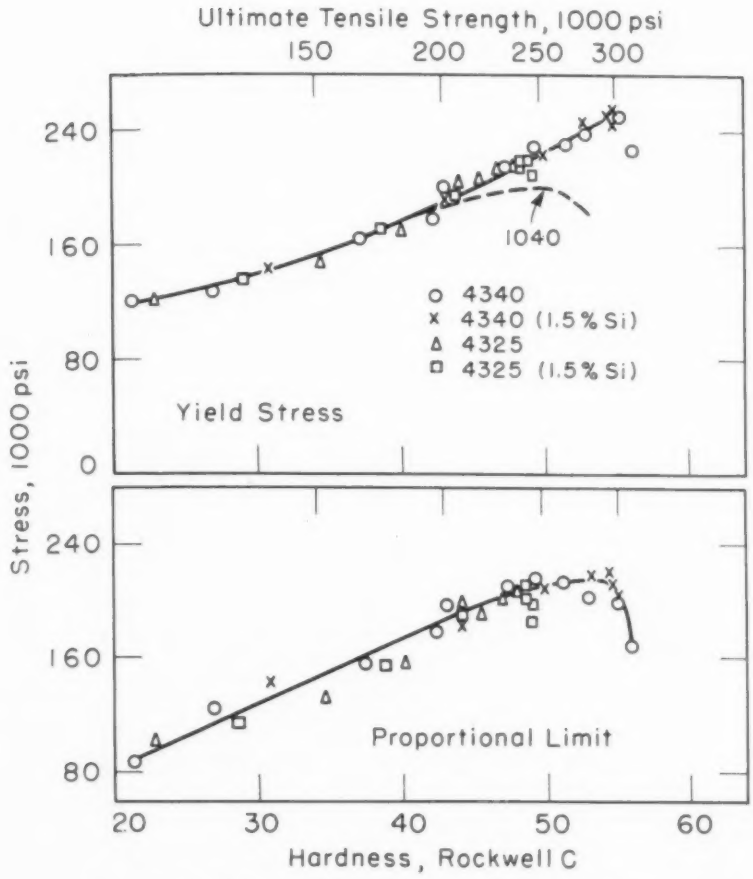


Fig. 14—Yield Stress and Proportional Limit as a Function of Hardness and Tensile Strength.

comparator. The specimens were then reheated and water-quenched, and finally reheated and quenched into iced-brine. The elongation increased with increasing severity of quench, reflecting the higher residual stresses produced by the more drastic quenching.

The effect of retempering on the quenching stresses is shown qualitatively in Fig. 24A. Specimens which had been brine-quenched from 1200°F were first heated for 1 hour at 200°F, air-cooled to

Table II
Length Changes Associated with Quenching Stresses

Austenitized and oil-quenched; Tempered 1200°F, 300 hours; Specimens 4" long ⅜" diameter.

Cooling rate from tempering temperature	$\Delta L/L(10^{-6})$ 4340	4325
Furnace-cooled	0*	0*
Air-cooled	+12	+16
Water-quenched	+40	+35
Iced-brine quenched	+94	+96

*Reference length

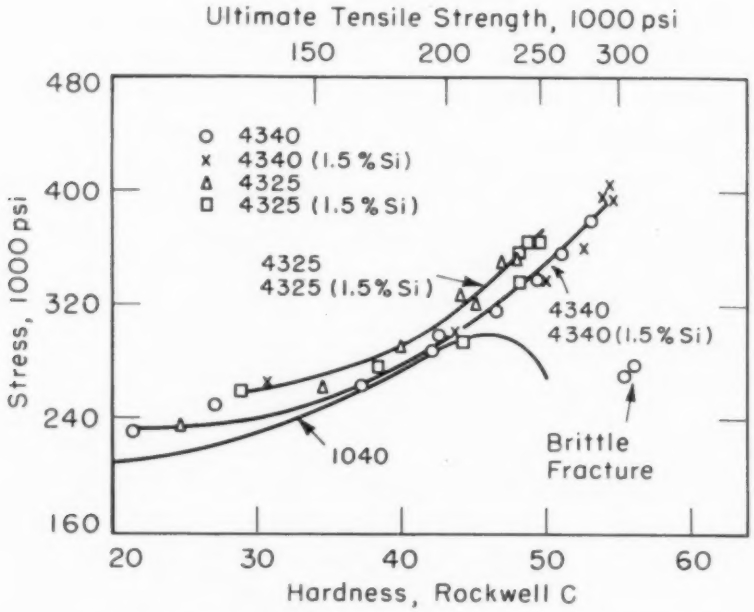


Fig. 15—True Fracture Stress as a Function of Hardness and Tensile Strength.

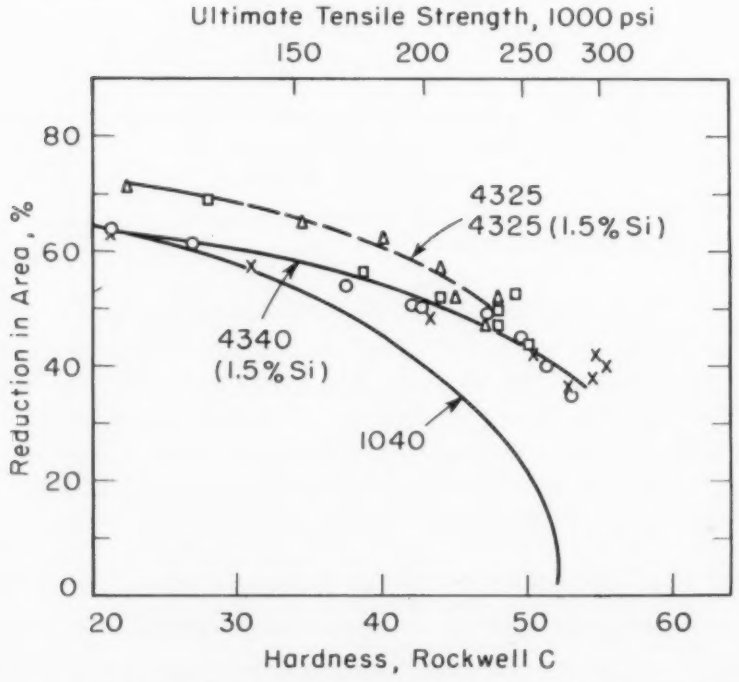


Fig. 16—Reduction in Area as a Function of Hardness and Tensile Strength.

room temperature, and then measured. The same samples were reheated at 400 and 600°F, and the accumulated residual length changes are plotted in Fig. 24A. It is seen that considerable stress relief can be accomplished by heating at 600°F. It is unlikely that

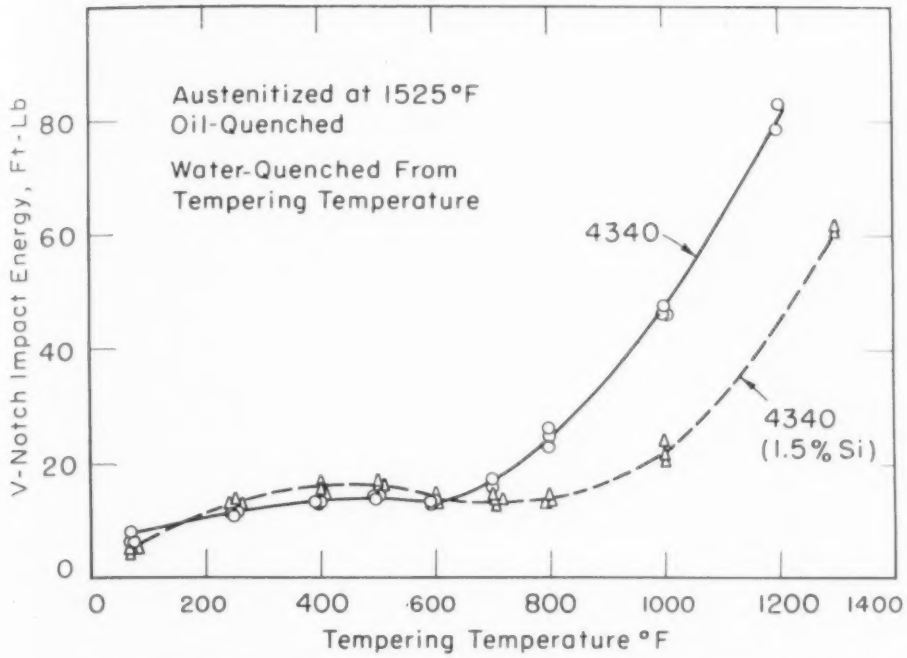


Fig. 17—Effect of Tempering Temperature (One Hour) on Charpy Impact Properties of 4340 and 4340 (1.5% Si) Steels.

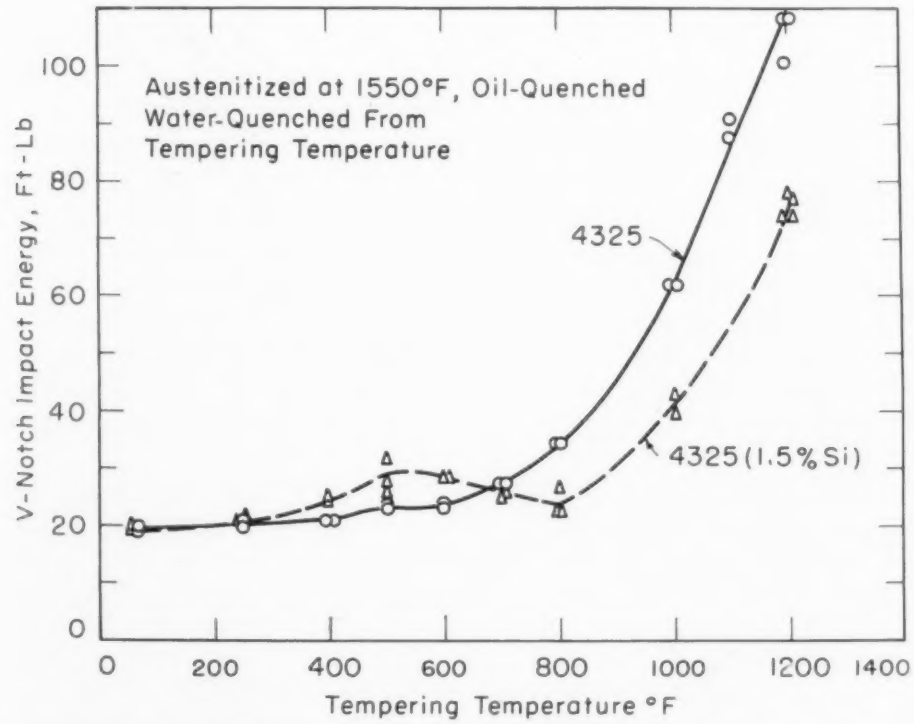


Fig. 18—Effect of Tempering Temperature (One Hour) on Charpy Impact Properties of 4325 and 4325 (1.5% Si) Steels. Tested at 72°F.

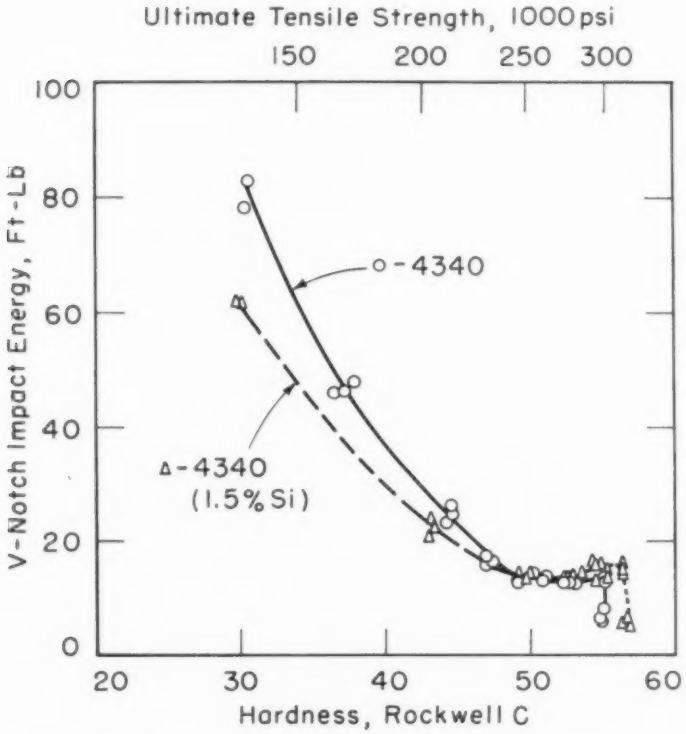


Fig. 19—Charpy Impact Properties as a Function of Hardness and Tensile Strength of 4340 and 4340 (1.5% Si) Steels.

these length changes are attributed to a quench aging process (9) since the hardness was not changed by the difference in cooling rates or by aging at various temperatures after quenching.

The effect of stress relief on the elastic limit was demonstrated in another series of experiments. A group of specimens of 4340 was hardened, tempered at 1300°F for 1 hour, and then water-quenched from the tempering temperature. A pair of specimens was then retempered at a series of temperatures up to 1200°F, with air cooling from each retempering treatment, and the elastic limits measured. The results are summarized in Fig. 24B and it is evident the very low elastic limit on water quenching from 1300°F, (20,000 psi) can be raised to the level of 100,000 psi by a stress relieving treatment at 600°F.

The effect of stress relief on the impact transition temperature is demonstrated in Fig. 25. The stress-relieving treatment appears to lower the transition temperature and there is also some indication that the maximum impact strength for the stress-relieved samples is higher.

Hardenability and Retained Austenite

End quench hardenability measurements were made using specimens $^{23}/_{32}$ inch diameter and $4\frac{1}{2}$ inches long. This sub-standard

size was adopted because ¾ inch diameter rod was the largest available. The hardenability curves so obtained are not directly comparable to those derived from standard (one inch) specimens, but they provide a good measure of the relative hardenability for the four steels investigated here. The data are summarized in Fig.

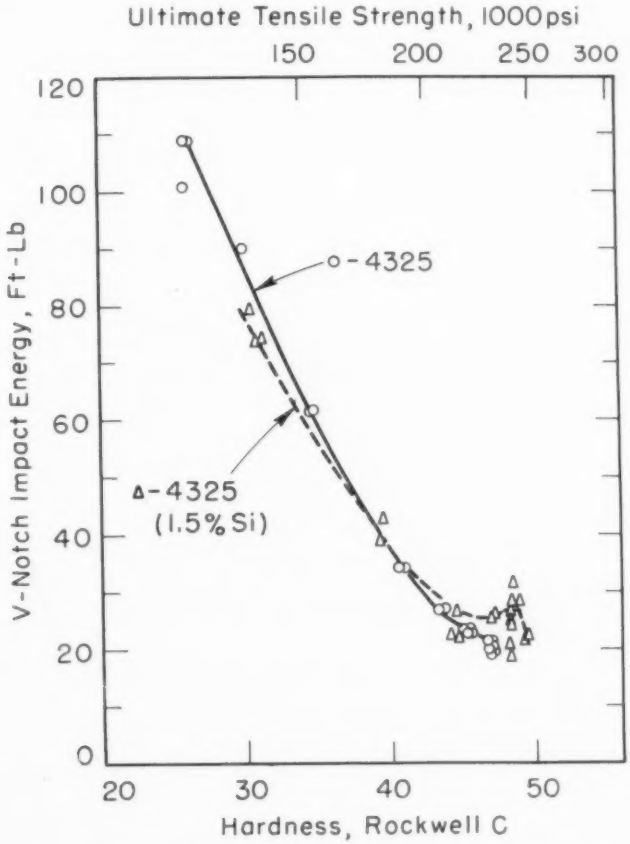


Fig. 20—Impact Properties as a Function of Hardness and Strength of 4325 and 4325 (1.5% Si) Steels.

26. The 4340 is probably at the low end of the hardenability band for such steels, but it is evident that the addition of silicon has markedly increased the hardenability of this steel as well as the 4325.

In order to determine whether the mechanical properties determined here were influenced by variations in hardenability, hardness measurements were made on sections of ¾ inch diameter bars of each steel after oil quenching from the hardening temperature. The hardness was uniform across the section in each case. Since the test specimens were always considerably smaller than ¾ inch diameter, it appears that the differences in mechanical properties reported in the foregoing section reflect differences in the properties of the (tempered) martensite and are not attributable to the presence of other transformation products.

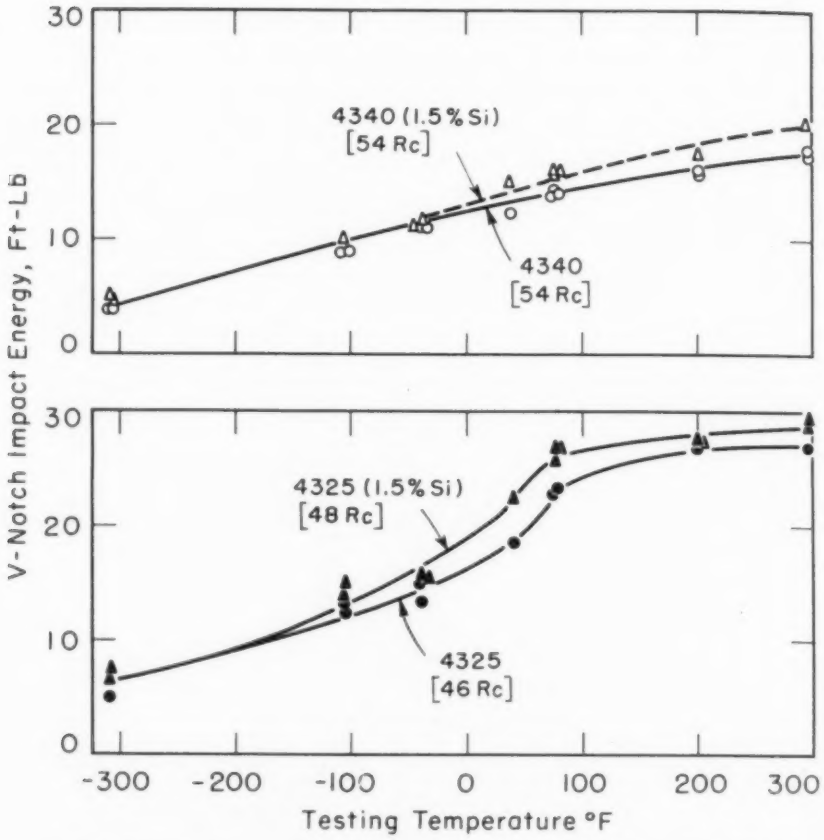


Fig. 21—Charpy Transition Curves for 4325, 4325 (1.5% Si), 4340 and 4340 (1.5% Si) Steels. (Tempered at 500°F for 1 Hour)

Retained austenite measurements were made at various positions along the end quench bars by means of an X-ray method (10). Care was taken to etch away the worked surface due to sectioning; each austenite content given is the average of four determinations. The probable error in the X-ray measurements is of the order of $\pm 0.3\%$.

Figs. 27–30 show the retained austenite as a function of distance from the quenched end. The retained austenite can reach approximately 12% on retarded cooling in contrast to the value of under 3% obtained on rapid quenching. As much as 20% retained austenite was produced by holding at 700°F for 2 hours during the cooling from the austenitizing treatment. Silicon does not have much effect on the retained austenite contents of rapidly quenched steels, but it does play a more important role on slack quenching, perhaps by influencing the amount of nonmartensitic products that form.

The decrease in hardness with increasing distance from the quenched end should not be associated with the corresponding increase in retained austenite. According to previous experience, 12%

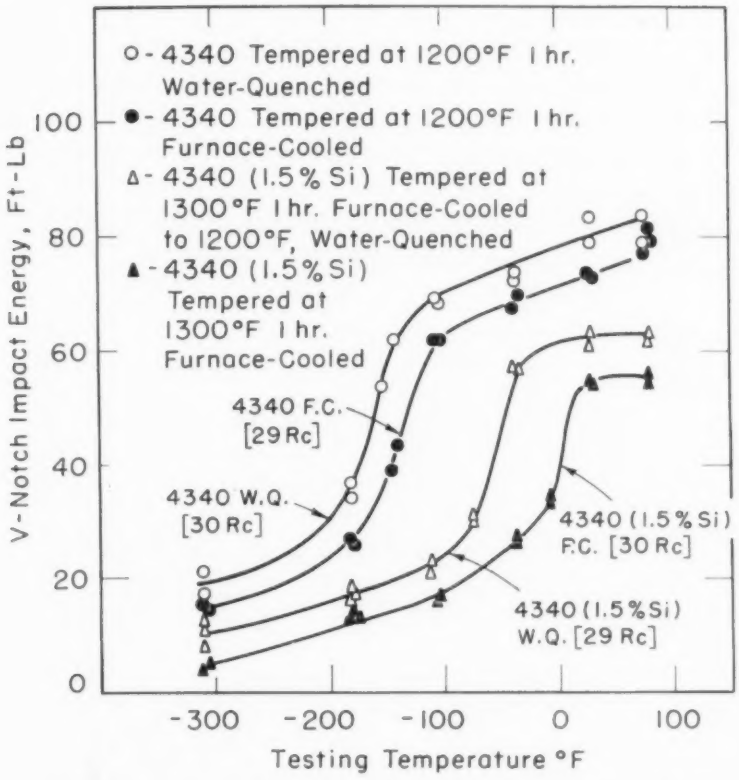


Fig. 22—Charpy Transition Curves for 4340 and 4340 (1.5% Si) Steels.

retained austenite would decrease the hardness only slightly (about 1 Rockwell C). Microscopic examination shows that the decrease in hardness is caused by the separation of bainite or ferrite during slow cooling. Figs. 31A, B, C and D were taken at sections one inch from the quenched end, and Figs. 31E, F, G, H were taken at sections three inches from the quenched end. At the 1-inch position it is seen that bainite is starting to form in the 4340 and 4340 (1.5% silicon) steels, and a ferritic constituent in the 4325 and 4325 (1.5% silicon) steels. At the 3-inch position, appreciable quantities of ferrite have formed in the steels of lower hardenability, 4340, 4325, 4325 (1.5% silicon), whereas in the 4340 (1.5% silicon) steel, martensite and bainite are the main constituents. Thus the mechanical properties associated with the presence of slack quench products is an important engineering problem and may well be a decisive factor in the choice of steels used for heavy sections.

Elastic Limit and Endurance Limit

Figs. 32 and 33 suggest that there may be a significant correlation between the elastic limits measured by the repeated load method (5) and the endurance limit obtained from rotating beam

tests (11,12). The elastic and endurance limits are given in Fig. 32 for several 0.40% carbon steels as a function of tempering temperature. A similar relationship is seen in Fig. 33, wherein the endurance and elastic limits are plotted as a function of hardness. According to these criteria, the maximum useful hardness for the 0.40% carbon steels appears to lie in the range 45–51 Rockwell C; attempts to use these materials at higher hardness values could lead simultaneously to microyielding and inferior fatigue life.

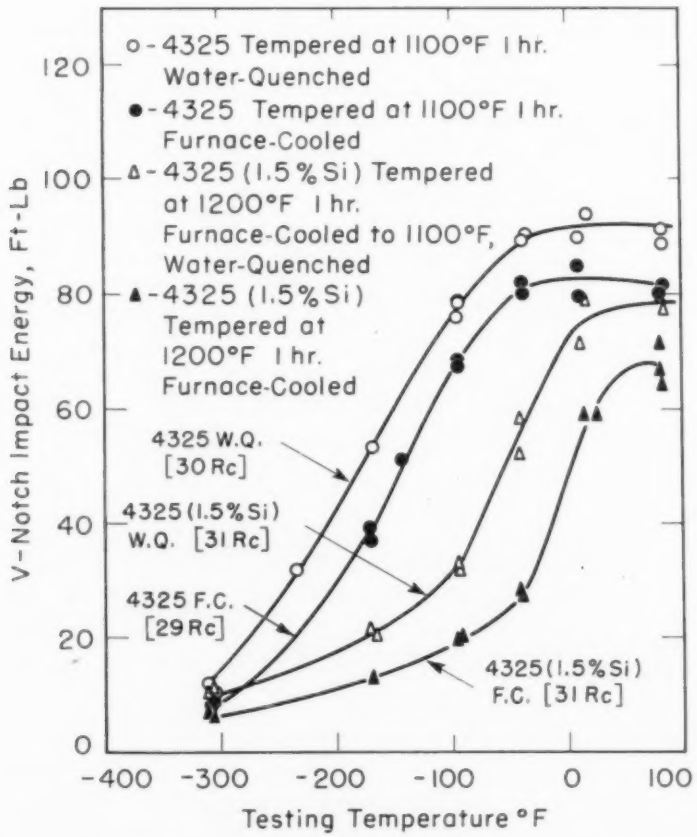


Fig. 23—Charpy Transition Curves for 4325 and 4325 (1.5% Si) Steels.

In establishing the method for determining the elastic limit (5), it was shown that repeated applications of load above the elastic limit produce small increments of plastic strain, whereas repeated loading below the elastic limit results in no plastic strain. If we assume that the fatigue damage is incurred when minute plastic deformation takes place, it would appear that the rotating beam endurance limits and the elastic limits could be related. However, it should be recognized that if the endurance limits were measured under repeated tension (with zero minimum stress) to simulate the

loading cycles used for the elastic limit determinations, the endurance limits would then be appreciably higher than the rotating beam values plotted in Figs. 32 and 33. Thus, the emphasis should be placed on the similar variation of the endurance and elastic limits as a function of hardness, and not on the fact that the numer-

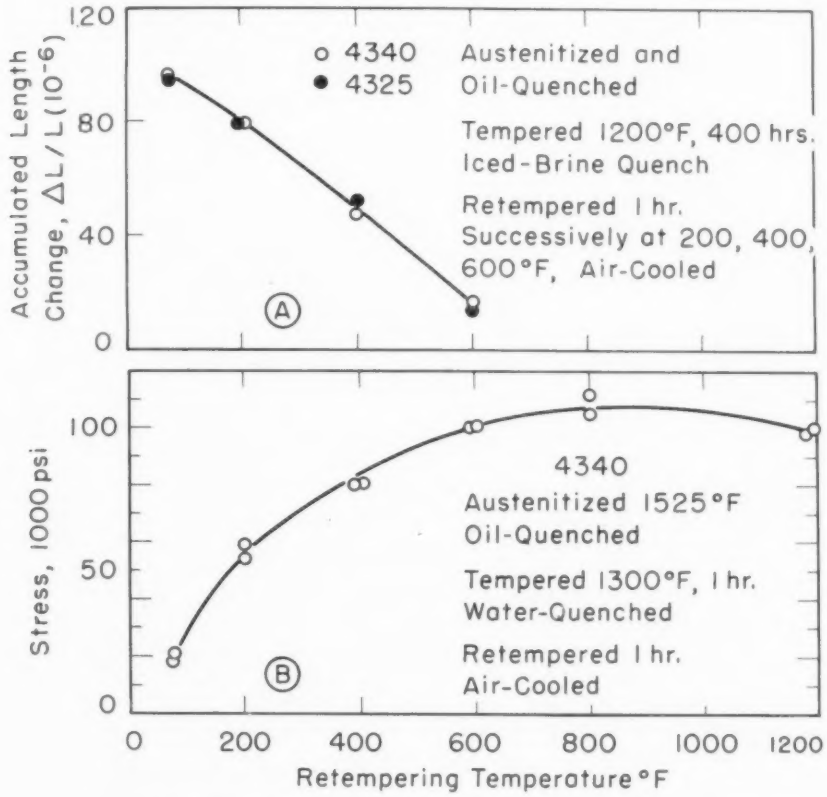


Fig. 24(A)—Decrease in Length of Severely Quenched Specimen on Retempering.

Fig. 24(B)—Effect of Retempering on the Elastic Limit of Severely Quenched Tensile Specimens.

ical values of the two properties happen to be equal. Considerably more testing is required to ascertain the real correlation between the processes involved. For the present, the potential relationship is intriguing since it may point toward a better understanding of fatigue damage.

Summary

An improvement in high strength mechanical properties may be obtained in 4340 and 4325 steels by increasing the silicon content to 1.5%. Tables III and IV summarize the properties of these steels on being treated at the same tempering temperature and on being treated to the same strength level respectively. The maximum

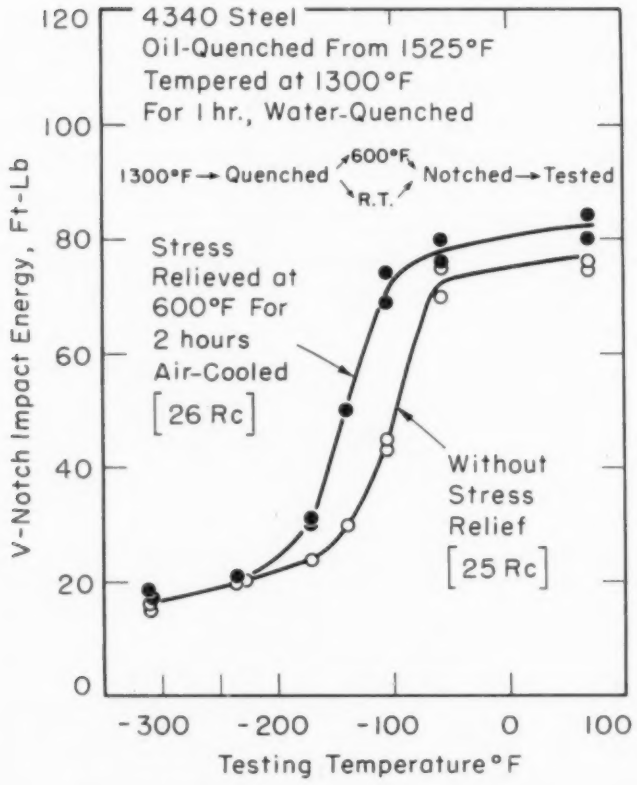


Fig. 25—Effect of Stress Relief on Charpy Impact Strength of 4340.

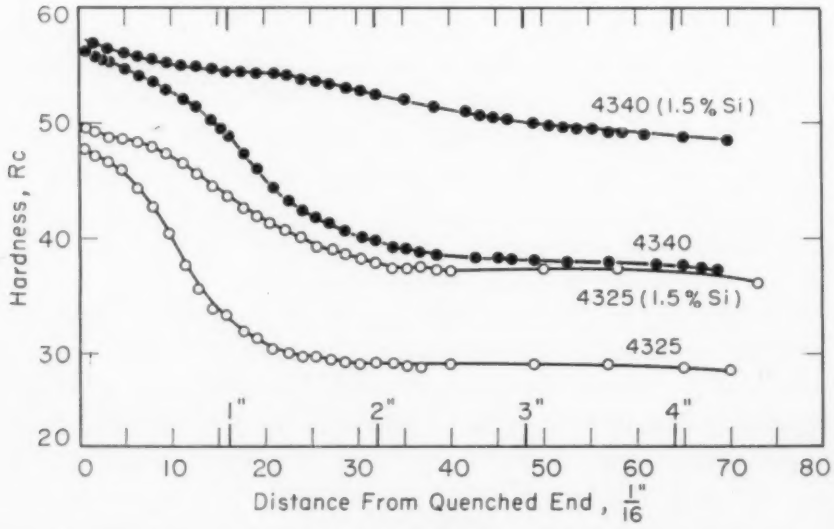


Fig. 26—Comparative Hardenability of Steels. ($^{33}/_{32}$ Inch Diam. Specimens)

strength is increased by the addition of silicon at each carbon content. Tensile strengths of 280,000–300,000 psi are attainable in the 4340 (1.5% silicon) steel, with about 6.5–8% elongation and about

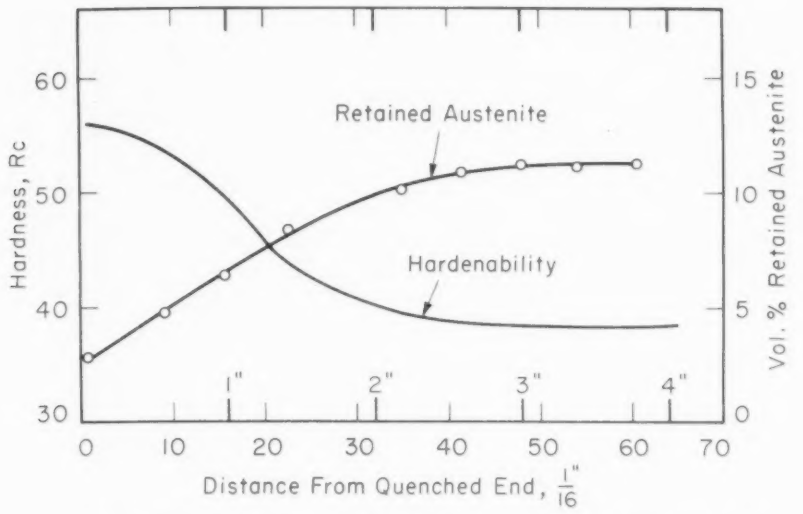


Fig. 27—Hardenability and Retained Austenite for 4340 (23/32 Inch Diam. Specimens).

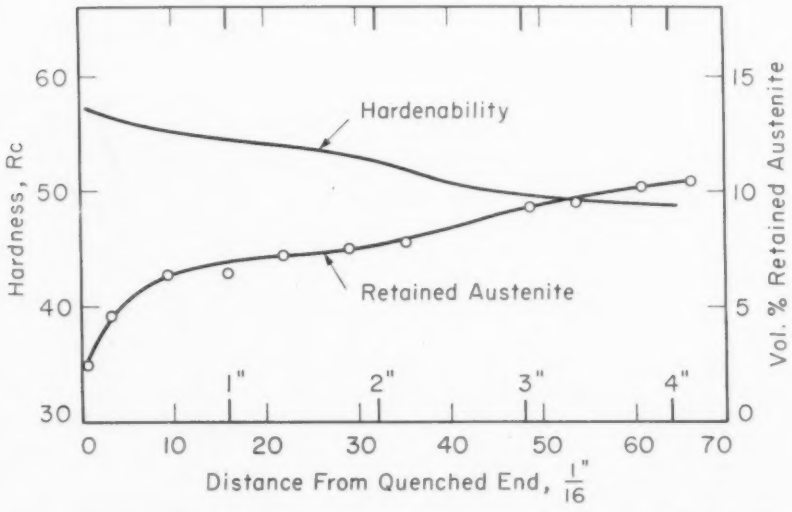


Fig. 28—Hardenability and Retained Austenite for 4340 (1.5% Si) (23/32 Inch Diam. Specimens).

14 ft-lbs in V-notch impact toughness at room temperature. However, at a strength level of 250,000 psi, the 4325 (1.5% silicon) steel has substantially higher notch toughness than the 4340 steels.

The introduction of silicon has several beneficial effects at high strength levels, but at low strength levels less favorable impact properties are encountered.

There is also some indication that the endurance limits and the elastic limits may be related.

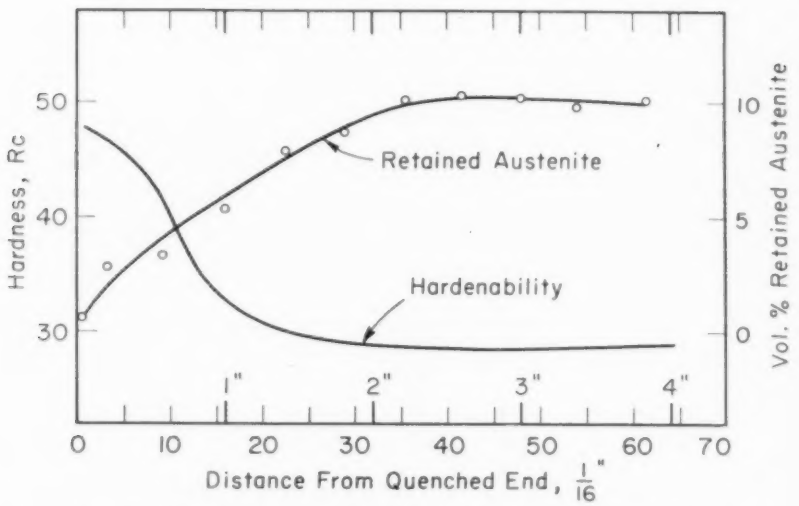


Fig. 29—Hardenability and Retained Austenite for 4325 ($^{23}/_{32}$ Inch Diam. Specimens).

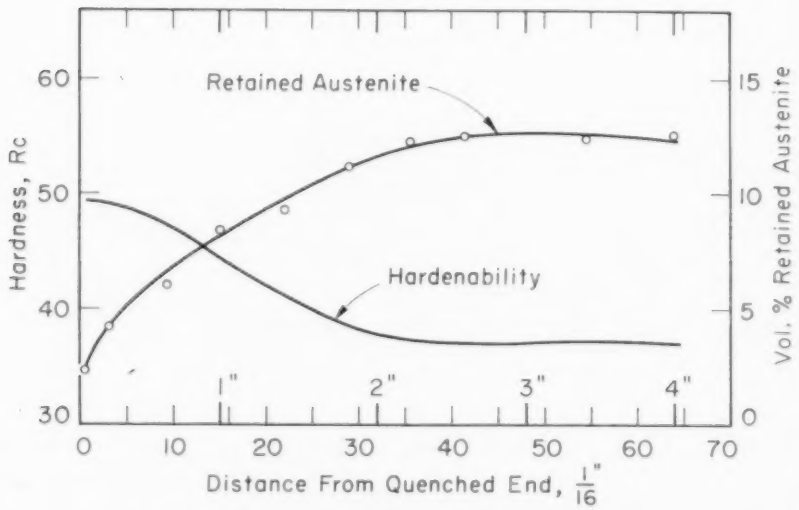


Fig. 30—Hardenability Test and Retained Austenite for 4325 (1.5% Si) ($^{23}/_{32}$ Inch Diam. Specimens).

Table III
Mechanical Properties of 4340, 4340 (1.5 Si), 4325 and 4325 (1.5 Si) Steels Hardened and Tempered at 500°F for 1 Hour

	4340	4340 (1.5 Si)	4325	4325 (1.5 Si)
Hardness (Rc)	51	54.5	45.4	48.2
Tensile Strength (psi)	260,000	300,000	218,000	241,000
True Fracture Stress (psi)	337,000	400,000	319,000	356,000
Yield Stress (psi)	230,000	256,000	206,000	220,000
Proportional Limit (psi)	220,000	220,000	190,000	208,000
Elastic Limit (psi)	107,000	102,000	104,000	104,000
Elongation (percent)	6.7	6.3	7.6	6.5
Reduction in Area (percent)	40	40	54	50
Room Temperature Charpy Impact Strength, V-notch (ft-lb)	14.3	15.9	23.2	26.5

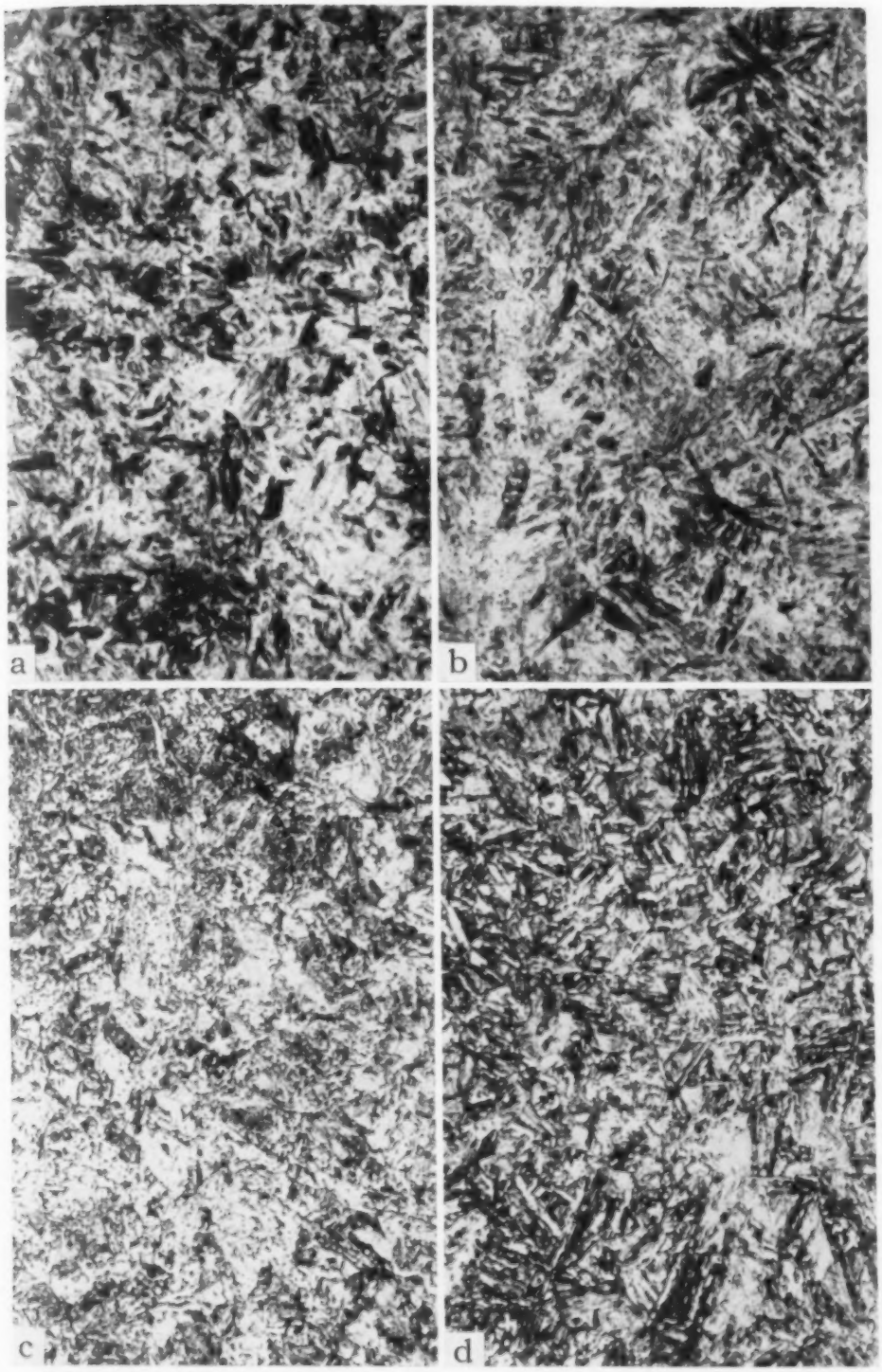


Fig. 31—Microstructures at a Distance of One and Three Inches from Quenched End. One Inch Position
a. 4340
b. 4340 (1.5% Si)
c. 4325
d. 4325 (1.5% Si)

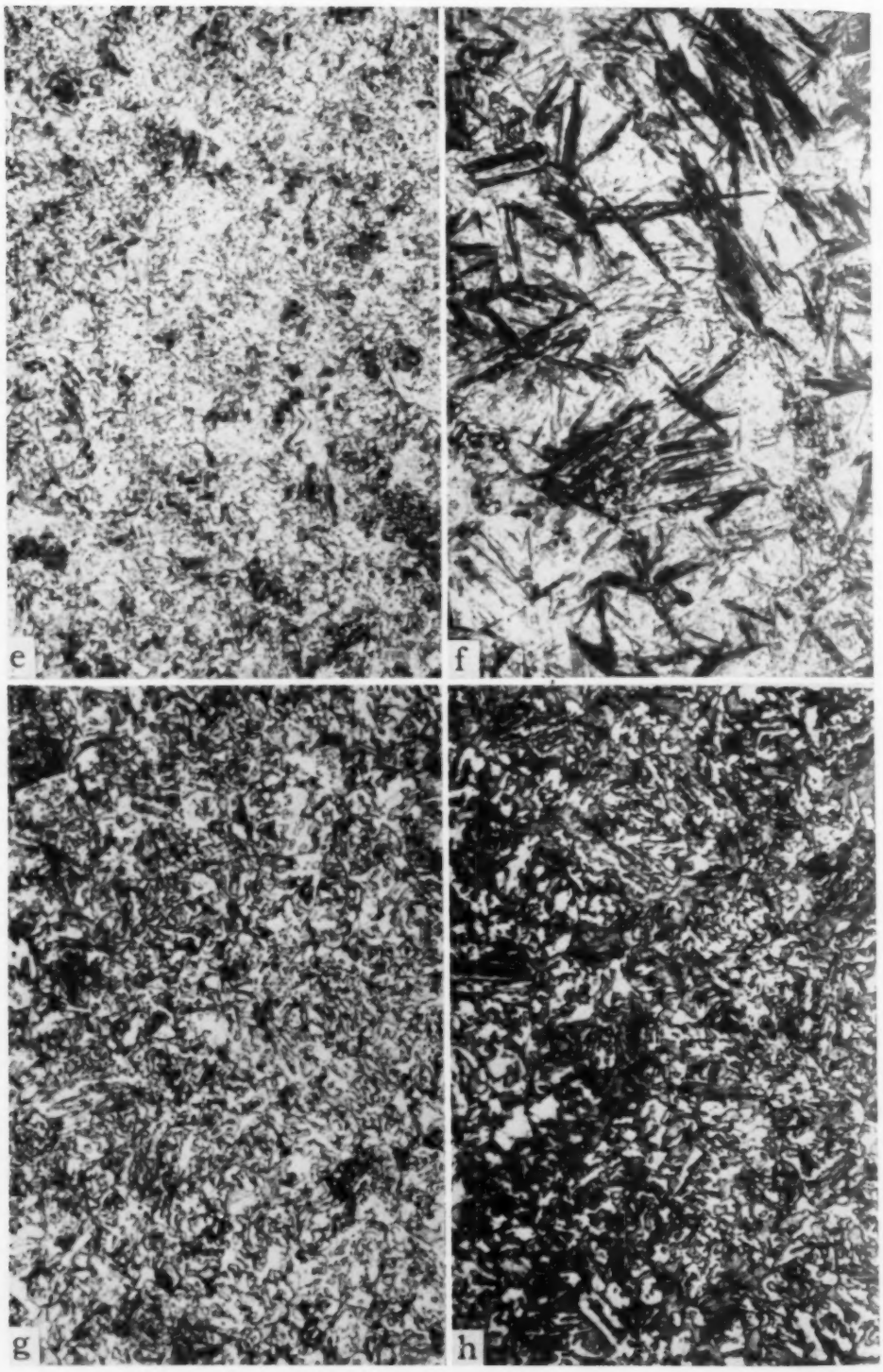


Fig. 31—Microstructures at a Distance of One and Three Inches from Quenched End.
Three Inch Position
e. 4340
f. 4340 (1.5% Si)
g. 4325
h. 4325 (1.5% Si)
Nital Etch 500 X

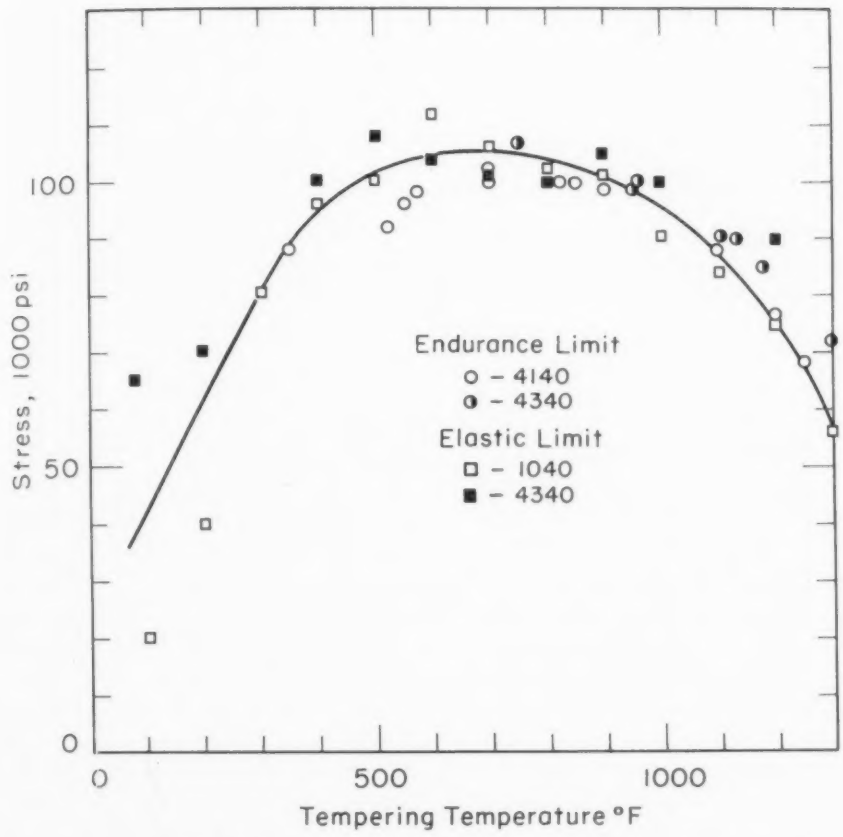


Fig. 32—Effect of Tempering Temperature on Endurance and Elastic Limits of 0.4% C Steels.

Table IV
Comparison of Some Mechanical Properties of 4340 and 4340 (1.5 Si) at a Strength Level of 280,000 psi

	4340	4340 (1.5 Si)
Tensile Strength (psi)	280,000	280,000
Hardness (Rc)	53	53
True Fracture Stress (psi)	370,000	368,000
Yield Strength (psi)	240,000	245,000
Proportional Limit (psi)	206,000	220,000
Elastic Limit (psi)	102,000	106,000
Reduction in Area (percent)	36	40
Elongation (in 2") (percent)	7.5	8
Room Temperature Charpy Impact Strength, V-notch (ft-lb)	13.7	13.9
Tempering Temperature (°F)	400	700

Acknowledgments

The authors would like to acknowledge the sponsorship of this work by the Wright Air Development Center. They also appreciate the assistance of Mr. Edward Sudenfield and Mr. Carl Cann in the experimental phases of the program.

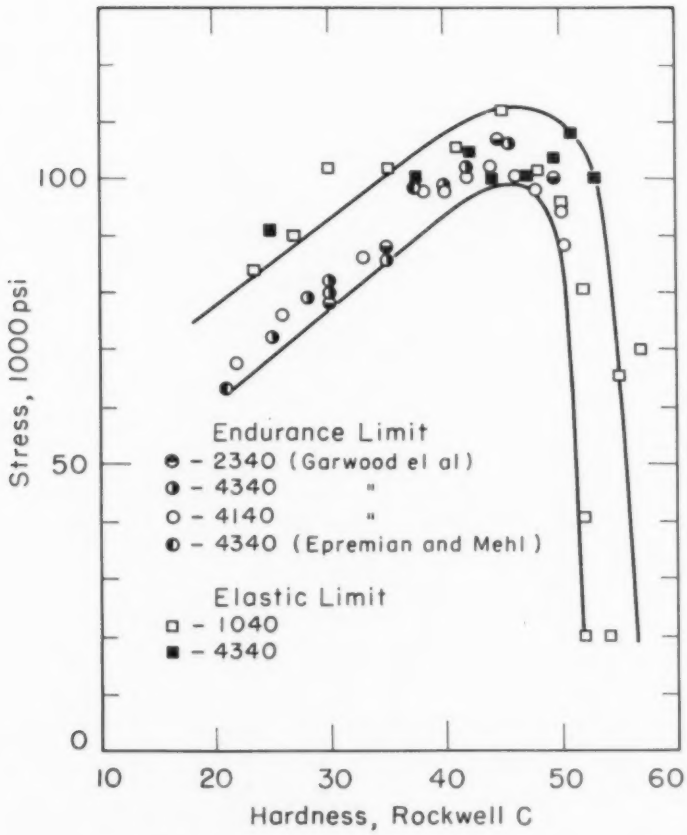


Fig. 33—Variation of Endurance and Elastic Limits of 0.4% C Steels with Hardness.

References

1. A. G. Allten and P. Payson, "The Effect of Silicon on the Tempering of Martensite," TRANSACTIONS, American Society for Metals, Vol. 45, 1953, p. 498.
2. W. S. Owen, "The Effect of Silicon on the Kinetics of Tempering," TRANSACTIONS, American Society for Metals, Vol. 46, 1954, p. 812.
3. P. Payson and A. E. Nehrenberg, "New Steel Features High Strength and High Toughness," *Iron Age*, Vol. 162, 1948, October 21, p. 64; October 28, p. 74.
4. M. A. Melcon, "Ultra High Strength for Aircraft Structures," *Product Engineering*, Vol. 24, October 1953, p. 129.
5. H. Muir, B. L. Averbach and M. Cohen, "The Elastic Limit and Yield Behavior of Hardened Steels," TRANSACTIONS, American Society for Metals, Vol. 47, 1955, p. 380.
6. L. J. Klingler, W. J. Barnett, R. P. Frohmberg and A. R. Troiano, "The Embrittlement of Alloy Steel at High Strength Levels," TRANSACTIONS, American Society for Metals, Vol. 46, 1954, p. 1557.
7. H. B. Knowlton, Discussion to "The Embrittlement of Alloy Steel at High Strength Levels" by L. J. Klingler, W. J. Barnett, R. P. Frohmberg and A. R. Troiano, TRANSACTIONS, American Society for Metals, Vol. 46, 1954, p. 1594.
8. George Sachs, "Survey of Low Alloy Aircraft Steels Heat-Treated to High Strength Levels," Part III—Failure Cases. Wright Air Development Center, February 1954.

9. N. J. Petch, "The Fracture of Metals," *Progress in Metal Physics*, Vol. 5, 1954, edited by Chalmers and King, Pergamon Press Ltd., London 1.
10. B. L. Averbach, "Retained Austenite Determinations by X-ray Methods," *Journal of Metals*, American Institute of Mining and Metallurgical Engineers, Vol. 5, 1953, p. 87.
11. M. F. Garwood, H. H. Zurburg and M. A. Erickson, "Correlation of Laboratory Tests and Service Performance," INTERPRETATION OF TESTS AND CORRELATION WITH SERVICE, published by American Society for Metals, 1952, p. 1.
12. E. Epremian and R. F. Mehl, "The Statistical Behavior of Fatigue Properties and the Influence of Metallurgical Factors," *Symposium on Fatigue with Emphasis on Statistical Approach—II*, American Society for Testing Materials, 1952, p. 25.

DISCUSSION

Written Discussion: By John Vajda, John J. Hauser and Cyril Wells, Metals Research Laboratory, Carnegie Institute of Technology, Pittsburgh.

This paper is of special interest to us inasmuch as a similar study of the effect of silicon on mechanical properties is also being made at the Carnegie Institute of Technology. The authors of the paper have restricted their investigation to longitudinal properties and we have restricted ours largely to transverse mechanical properties so that many of their results and ours are complementary.

The authors state "... it appears possible to obtain somewhat higher strengths in the silicon steels without a corresponding loss in ductility or in Charpy impact strength"; ductility and Charpy impact strength referred to here are, of course, longitudinal ductility and Charpy impact strength for longitudinal specimens. That transverse ductility may be lowered quite drastically by silicon is apparent from results given in Table V; each value is an average of two.

Table V
Effect of Silicon on Longitudinal (RAL) and Transverse (RAT) Reduction of Area

Steel	Tensile Strength psi	RAL %	RAT %	Estimates of RAL and RAT at 200,000 psi* RAL	RAT
AISI 8740	190,000	50.0		48.0	
AISI 8740	194,000		18.5		16.7
AISI 8740+Si	210,000	45.0		47.0	
	205,000		4.5		6.0

*Relations (a) between tensile strength and RAL, (b) between tensile strength and RAT given in publication by Wells and Mehl.[3]

[3]Cyril Wells and Robert F. Mehl, "Transverse Mechanical Properties in Heat Treated Wrought Steel Products," TRANSACTIONS, American Society for Metals, Vol. 41, 1949, p. 715.

It is our opinion that (a) this lowering of transverse ductility was caused by high silicon content type nonmetallic inclusions and that (b) the detrimental effect of 1.5% or so of silicon on transverse ductility in steels sufficiently free from these damaging inclusions may be so small, if it exists, as to be unimportant from an engineering point of view. Results given in Table V for longitudinal tensile specimens show that the addition of silicon did not significantly affect longitudinal ductility; in this respect our results and those of the present authors are in agreement.

That silicon had little effect on the amount of retained austenite in a fully quenched AISI 4340+1.5% silicon steel but markedly increased the amount of

retained austenite in the slack quenched steel is apparent from results in Fig. 34.[4] These results support the authors' point of view that "Silicon does not have much effect on the retained austenite contents of rapidly quenched steels, but it does play a more important role on slack quenching by influencing the amount of non-martensitic products that form."

The data presented in Fig. 34 were obtained on end-quenched 7 inch×7 inch rounds; the quenching technique used was developed by Vajda and Busby and is described in a recent publication.[5] Rockwell "C" hardness traverses for the two steels referred to in Fig. 34 are given in Table VI as a function of distance from the quenched end.

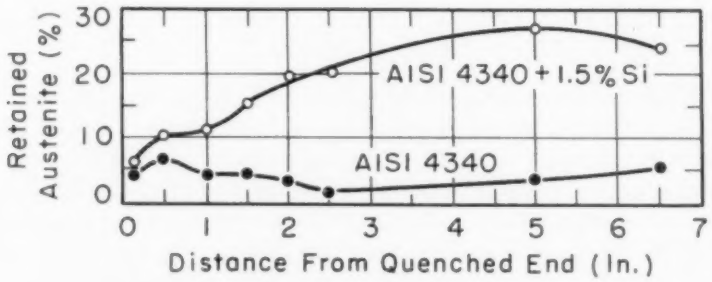


Fig. 34—Effect of Adding 1.5% Silicon to a 4340 Steel on the Retained Austenite Content in End-Quenched 7-Inch Rounds.

The conclusion ". . . it appears possible to obtain somewhat higher strengths in the silicon steels without a corresponding loss in ductility or in Charpy impact strength" applies not only to the effect of silicon in 4340 but probably to the effect of silicon in other composition steels too. Data given by Payson and Nehrenberg[6] tend to show that Hy-Tuf at a tensile strength of about 240,000 psi had better longitudinal ductility (possibly due to the lower carbon content of the Hy-Tuf) and better toughness than AISI 8645, 3145, 3250, 2345, 4640, or 4340. In one of the Symposium papers on Ultra High Strength Steels in Aircraft Applications presented in March, 1953,[7] a comparison is shown between a modified AISI 4330 steel and Hy-Tuf. Compositions of these steels are listed in Table VIII.

Table VI
Rockwell "C" Hardness Traverses on End-Quenched 7-Inch Rounds Of a 4340 and 4340+1.5% Si Steel

	Distance from Quenched End (In.)											
Steel	1/16	¼	½	¾	1	1½	2	2½	3	4	5	6
AISI 4340	57.0	56.0	54.0	51.0	45.5	39.0	37.0	36.0	35.0	34.0	34.0	35.0
AISI 4340 +1.5% Si	57.5	57.5	57.0	56.0	54.5	50.5	48.0	47.0	46.0	44.5	43.5	42.5

[4]Information given in Fig. 34 and Tables I and II was obtained on Air Force Contract No. AF33(616)-2286, sponsored by the Wright Air Development Center, Wright-Patterson Air Force Base, Ohio.

[5]John Vajda and Paul E. Busby, "Transverse Mechanical Properties of Slack-Quenched and Tempered Wrought Steel," TRANSACTIONS, American Society for Metals, Vol. 46, 1954, p. 1331.

[6]Peter Payson and A. E. Nehrenberg, "New Steel Features High Strength and High Toughness," *The Iron Age*, Vol. 162, 1948, (October 21 and October 28).

[7]Cyril Wells, "Composition and Heat Treatment of High Strength Steels," published in *Symposium-Ultra High Strength Steels in Aircraft Applications*, ASM-SAE Seminar, March 1953. Published by Society of Automotive Engineers, Inc.

Table VIII
Compositions of Hy-Tuf, Modified AISI 4330, and 4325

Steel	C	Mn	Si	Ni	Cr	Mo	V
			Per Cent of Element				
Modified 4325	0.24	0.80	0.28	2.35	1.09	0.48	0.10
Modified 4330	0.31	0.87	0.30	1.82	0.74	0.43	0.10
Hy-Tuf	0.26	1.38	1.30	1.78	—	0.39	—

In this case at a tensile strength level of about 235,000 psi, longitudinal ductility is about equal in both steels while toughness (measured at 70°F) is slightly higher in Hy-Tuf. At higher tempering temperatures, that is, at lower tensile strengths, Hy-Tuf had the lower toughness; possibly at the higher tempering temperature, the Hy-Tuf was slightly more temper brittle than the modified 4330. Of course, the comparisons shown in the paper are more direct than those made in this discussion. However, fortunately, there appears to be in general an overall consistency which we think increases the justification for accepting the conclusions drawn as applying not only to the effect of silicon on the mechanical properties of 4340 but also to the effect of silicon on mechanical properties in certain steels of other compositions.

In the summary the statement is made "at a strength level of 250,000 psi, the 4325 (1.5 Si) steel has substantially higher notch toughness than the 4340 steels." Do you think that your 4325 (1.5 Si) steel tempered to a tensile strength of 250,000 psi would have higher notch toughness than your 4325 steel tempered, say, at 200°F to give a tensile strength of 250,000 psi? One of our steels, a modified 4325 (Table VIII), tempered at 212°F for 24 hours to give a tensile strength of 250,000 psi gave Charpy impact values of about 24 ft-lbs (average 24.2); values close to 26.5 ft-lbs were reported by the authors for their 4325 (1.5 Si) steel, tempered to a tensile strength of 241,000 psi.

Authors' Reply

We are pleased to have this pertinent report by Messrs. Vajda, Hauser and Wells concerning the related work being conducted at the Carnegie Institute of Technology.

The comparisons between the longitudinal and transverse properties are most

Table IX
Mechanical Properties at Room Temperature
4340, 4340 (1.5 Si), 4325, 4325 (1.5 Si)

Tensile Strength Level	300,000 psi	280,000 psi		260,000 psi			240,000 psi			
Steel	4340 1.5 Si	4340	4340 1.5 Si	4340	4340 1.5 Si	4325 1.5 Si	4340	4340 1.5 Si	4325	4325 1.5 Si
Tensile Strength (10^3 psi)	306	280	281	258	262	262	239	240	241	241
Yield Stress (10^3 psi)	245	240	245	231	244	220	226	228	216	220
Elastic Limit (10^3 psi)	94	102	107	108	104	90	101	106	82	104
Reduction in Area (%)	40	36	38	40	42	44	45	43	51	50
% Elongation (in 2")	8	7	6.5	7	7.5	7.5	7	10	8.5	7
V-Notch Impact (ft-lb)	14.5	13.5	14	14.5	14.5	22	15	15	21	27
Tempering Temperature (°F-1 hr.)	400°	450°	700°	500°	750°	300°	650°	820°	300°	500°

significant. It appears that silicon, as such, in the amounts studied here is not detrimental to the longitudinal and transverse ductility. However, an adverse effect on transverse ductility will accompany these comparatively high silicon additions if nonmetallic inclusions are thereby produced.

The increase in retained austenite in 4340 plus 1.5% silicon steel due to slack quenching is noteworthy. It has been pointed out by Dr. D. J. Blickwede of the Bethlehem Steel Company that relatively little ferrite or upper bainite is formed in the process of slack quenching. Hence, the excess retained austenite may be attributable to a real stabilizing effect, rather than to carbon build-up in the austenite due to the formation of high-temperature transformation products.

The discussors have asked about the notch toughness of 4325 and 4325 plus 1.5% silicon steels when each is tempered to a tensile strength level of 250,000 psi. Such comparisons are given in the accompanying table for strength levels ranging from 240,000 to 300,000 psi and including the 0.40 as well as the 0.25% carbon steels. At a tensile strength of about 240,000 psi, the 4325 plus 1.5% silicon steel has a higher notch toughness, a higher elastic limit, and about the same ductility as the 4325 steel, presumably due to the fact that the latter cannot be tempered above 300°F for this strength requirement, while the former can be tempered at 500°F.

SOME RELATIONSHIPS BETWEEN ENDURANCE LIMIT AND TORSIONAL PROPERTIES OF STEEL

By S. T. Ross, R. P. Sernka, and W. E. Jominy

Abstract

Comparison of fatigue and torsion test results shows that the maximum endurance limit of tempered low alloy steels can be approximated from torsional yield strength-hardness data. The torsion yield strength-hardness relation is linear until a region of high hardness is reached where this relation ceases and a condition of instability occurs. In this region, electron micrographs showed the presence of many fine percarbide particles in the tempered martensite as well as films of percarbides outlining tempered martensite needles.

Torsion tests resulted in three types of failure: shear fractures on planes perpendicular to specimen axes; tensile fractures on helical planes at 45 degrees to specimen axes; and combination shear and tensile fractures containing some shear surfaces parallel to specimen axes, accompanied by shattering. (ASM-SLA Classification: Q7, Q1, AY)

RESEARCH by Garwood, Zurburg and Erickson (1)[1] has indicated that the endurance limit of several commercial steels is a function of hardness resulting from quenching and tempering. This function is a straight line up to certain hardness values, above which it deviates from first order relation with much data scatter. Olleman, Wessel and Hull (2) have shown that the same type of relation exists between torsional yield strength and tempered hardness of tool steel alloys. In a private communication, Scott (3) drew attention to possible relation between torsional yield strength and endurance limit. Consideration of these reports indicates that endurance limit values might be approximated from torsion test results. The purpose of this investigation was to determine the feasibility of substituting torsion test data for those of the fatigue test with saving of expense and testing time.

Specimen Preparation

Twenty-one torsion test specimens were prepared from each of six medium carbon steels (SAE 2340, 4052, 4063, 4140, 4340, and

[1]The figures appearing in parentheses pertain to the references appended to this paper.

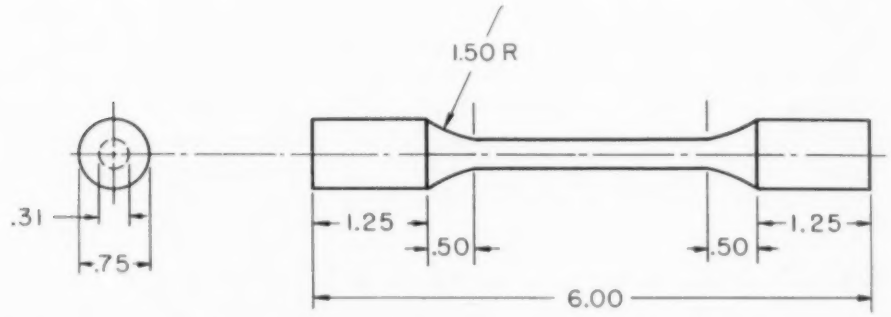
A paper presented before the Thirty-Seventh Annual Convention of the Society, held in Philadelphia, October 17–21, 1955. Of the authors, S. T. Ross is project engineer, R. P. Sernka is research metallurgist, and W. E. Jominy is chief metallurgist, Metallurgical Research, Chrysler Corp., Detroit. Manuscript received April 11, 1955.

5150). Chemical analyses of these steels are given in Table I. The extent of preliminary machining from 7/8-inch round bars is indicated by Fig. 1a. To prevent decarburization, 0.0005-inch copper was plated on the bars prior to heat treatment.

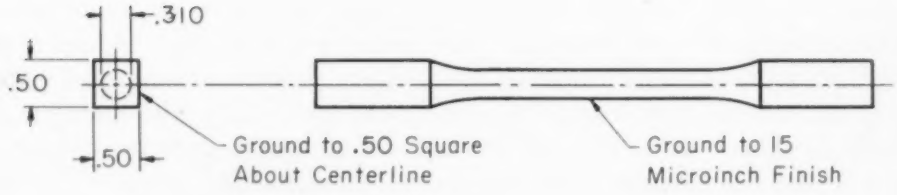
Specimens were heat treated as shown in Table II. Three speci-

Table I
Chemical Analyses of Torsion Test Steels

Steel	C	Mn	P	S	Si	Cr	Ni	Mo
SAE 2340	0.40	0.83	0.015	0.030	0.25	0.05	3.50	
SAE 4052	0.50	0.79	0.015	0.020	0.25	0.05	—	0.25
SAE 4063	0.65	0.86	0.015	0.018	0.25	—	—	0.24
SAE 4140	0.42	0.92	0.020	0.026	0.26	0.98	—	0.19
SAE 4340	0.40	0.73	0.010	0.020	0.35	0.88	1.68	0.25
SAE 5150	0.51	0.77	0.015	0.020	0.20	0.78	—	0.20



a - Torsion Specimen As Machined From .875 Round
Plated With .0005 Copper Prior to Heat Treatment



b - Torsion Specimen Ground After Heat Treatment

Fig. 1—Torsion Specimen Ground After Heat Treatment.

mens were given each treatment. Austenitizing was done in a muffle furnace provided with a cracked-gas atmosphere. The air:gas ratio was held at 3:1 at the cracker so that as nearly neutral a furnace atmosphere as possible was obtained. All specimens were austenitized for one hour and quenched in agitated oil. Tempering was done in a pot-type circulating air furnace, and the bars were air-cooled upon removal. Hardness values for the as-quenched conditions shown in Table II indicate that only very small amounts, if any, of retained

Table II
Specimen Heat Treatment

Steel	Sample No.	Austenitizing Temperature, °F	Tempering Temperature, °F	Tempering Time, Hr.	Ave. Rc
SAE 2340	106–108	1450	950	1	38.0
SAE 2340	109–111	1450	825	1	41.0
SAE 2340	112–114	1450	720	1	43.0
SAE 2340	115–117	1450	600	1	48.0
SAE 2340	118–120	1450	400	1	54.0
SAE 2340	121–123	1450	200	1½	60.0
SAE 2340	124–126	1450	As-Quenched	—	62.0
SAE 4052	22–24	1500	1040	1	36.5
SAE 4052	25–27	1500	915	1	41.0
SAE 4052	28–30	1500	765	1	47.0
SAE 4052	31–33	1500	620	1	52.0
SAE 4052	34–36	1500	450	1	56.0
SAE 4052	37–39	1500	200	1½	63.0
SAE 4052	40–42	1500	As-Quenched	—	64.5
SAE 4063	13–15	1450	1080	1½	36.0
SAE 4063	10–12	1450	970	1½	40.5
SAE 4063	7–9	1450	830	1½	45.0
SAE 4063	4–6	1450	560	2	52.5
SAE 4063	1–3	1450	440	2	57.5
SAE 4063	16–18	1450	350	1	61.0
SAE 4063	19–21	1450	As-Quenched	—	65.0
SAE 4140	64–66	1550	1075	1	35.5
SAE 4140	67–69	1550	950	1	40.5
SAE 4140	70–72	1550	800	1	46.0
SAE 4140	73–75	1550	600	1	50.0
SAE 4140	76–78	1550	450	1	53.0
SAE 4140	79–81	1550	250	1½	60.0
SAE 4140	82–84	1550	As-Quenched	—	61.0
SAE 4340	85–87	1550	1075	1	36.0
SAE 4340	88–90	1550	950	1	40.5
SAE 4340	91–93	1550	800	1	44.5
SAE 4340	94–96	1550	600	1	49.0
SAE 4340	97–99	1550	450	1	52.0
SAE 4340	100–102	1550	250	1½	58.0
SAE 4340	103–105	1550	As-Quenched	—	59.0
SAE 5150	43–45	1500	1175	1	29.0
SAE 5150	46–48	1500	1060	1	33.0
SAE 5150	49–51	1500	925	1	39.0
SAE 5150	52–54	1500	720	1	47.5
SAE 5150	55–57	1500	500	1	53.0
SAE 5150	58–60	1500	300	1½	60.5
SAE 5150	61–63	1500	As-Quenched	—	61.0

austenite were present in the heat treated torsion bars. This was later confirmed by metallographic examination.

After heat treatment, the specimens were finished by grinding. Each shank was ground to a ½-inch square, and its surfaces were made true and parallel. All were then ground to the test diameter of the smallest bar as shown in Fig. 1b.

Torsion Tests

Specimens were tested in a 2000-pound capacity Tinius Olsen torsion machine, using the specially designed grips illustrated in Fig. 2. Yield strengths at 0.5-degree twist were obtained with a testing speed of 0.1 rpm. Some of the specimens heat treated to high hardnesses failed without measurable yielding. It has been assumed for the purposes of this study that ultimate strengths and yield strengths

Table III
Torsion Test Data

Steel	Ave. Rc	Ave. Yield Pt., 2° Offset, In-Lb.	Fracture Type
SAE 2340	38.0	375	A
SAE 2340	41.0	450	A
SAE 2340	43.0	510	A
SAE 2340	48.0	580	A
SAE 2340	54.0	605	A
SAE 2340	60.0	580	A
SAE 2340	62.0	570	C
SAE 4052	36.5	410	A
SAE 4052	41.0	490	A
SAE 4052	47.0	565	A
SAE 4052	52.0	670	A
SAE 4052	56.0	750	B
SAE 4052	63.0	700	B
SAE 4052	64.5	680	C
SAE 4063	36.0	480	A
SAE 4063	40.5	570	A
SAE 4063	45.0	675	A
SAE 4063	52.5	870	B
SAE 4063	57.5	930	B
SAE 4063	61.0	875	C
SAE 4063	65.0	375	C
SAE 4140	35.5	435	A
SAE 4140	40.5	490	A
SAE 4140	46.0	570	A
SAE 4140	50.0	640	A
SAE 4140	53.0	655	A
SAE 4140	60.0	690	A
SAE 4140	61.0	600	C
SAE 4340	36.0	420	A
SAE 4340	40.5	485	A
SAE 4340	44.5	550	A
SAE 4340	49.0	600	A
SAE 4340	52.0	590	A
SAE 4340	58.0	630	A
SAE 4340	59.0	580	C
SAE 5150	29.0	330	A
SAE 5150	33.0	380	A
SAE 5150	39.0	460	A
SAE 5150	47.5	590	A
SAE 5150	53.0	665	A
SAE 5150	60.5	710	A
SAE 5150	61.0	645	C

are identical for these brittle specimens. Table III lists the average yield strength and Rockwell C hardness obtained for each group of three heat treated samples.

Twisting was carried to fracture after the yield strengths were obtained. Three characteristic fracture types were noted: Type A fracture resulted when the specimens sheared cleanly into two pieces on a plane perpendicular to the axes. Fracture surfaces were bright. Type B fracture resulted when the specimens shattered into many pieces along irregular fracture surfaces having dull appearance. However, these fractures contained some bright surfaces in shear planes either perpendicular to or parallel with specimen axes. Type C fractures were found along helical planes at 45 degrees to specimen axes. The specimens broke into two pieces and displayed the same dull appearance as those of Type B, but contained no bright shear

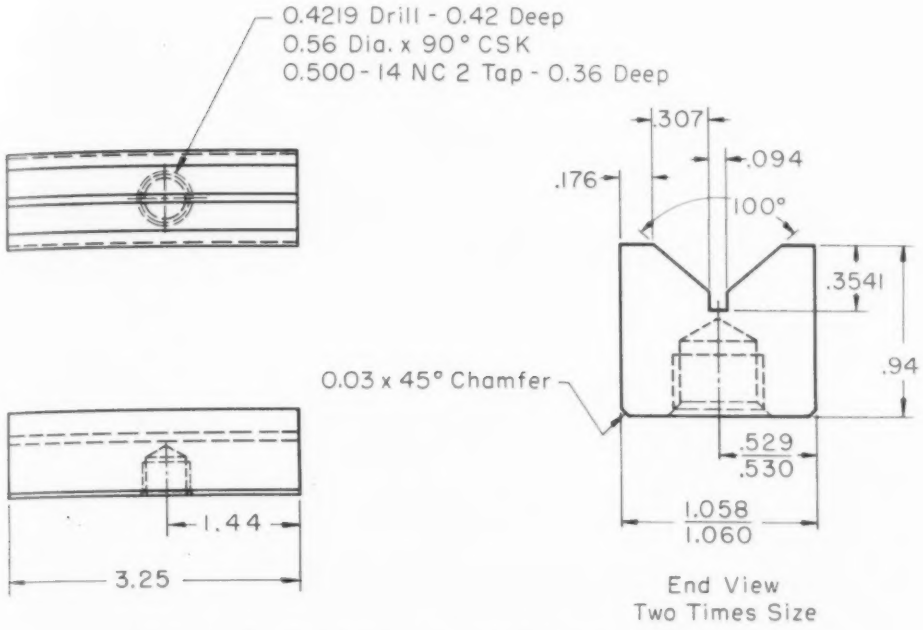


Fig. 2—Torsion Test Grips—Oil Hardening Tool Steel 58-62 (RC).

surfaces. Fig. 3 through Fig. 5 are representative photographs of the fracture types. Table III lists these fracture types obtained from continuation of the torsion tests to failure.

Fatigue Tests

Garwood, Zurburg and Erickson (1) have established endurance limits for each steel included in this investigation. Their work was

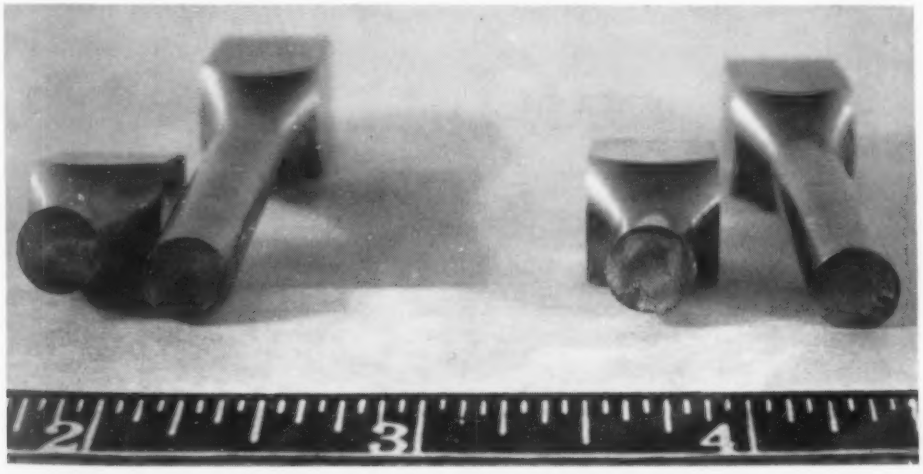


Fig. 3—Fracture Type A: Torsion Test Bars No. 11 and 14 Have Sheared Into Two Pieces on Planes Perpendicular to Their Axes.



Fig. 4—Fracture Type B: Torsion Test Bars No. 2 and 4 Have Shattered Along Irregular Surfaces. Some bright shear surfaces are noted on planes parallel to the original specimen axes.

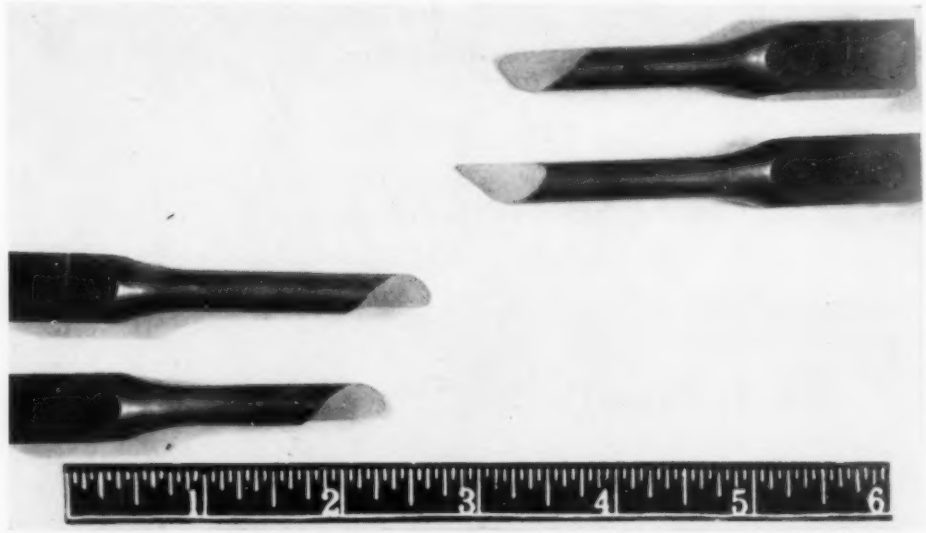


Fig. 5—Fracture Type C: Torsion Test Bars No. 19 and 20 Have Failed Along Helical Planes at 45 Degree Angles to Specimen Axes.

performed on R. R. Moore machines which stressed specimens in alternating flexure. Table IV lists chemical analyses and results of the fatigue tests performed by Garwood, et. al. The data were obtained at room temperature and are for smooth bars of standard dimensions.

Table IV
Fatigue Data of Garwood, Zurburg and Erickson

Steel	Endurance Limit, psi.	Ave. Rc	Chemical Analysis C	Mn	P	S	Si	Cr	Ni	Mo
SAE 2340	79,000	30	0.39	0.80	0.015	0.030	0.30	0.06	3.47	—
SAE 2340	88,000	40				(Heat 120175)				
SAE 2340	107,000	46								
SAE 2340	100,000	50								
SAE 4052	83,500	33.5	0.52	0.76	0.015	0.021	0.25	0.06	0.13	0.22
SAE 4052	96,000	39.0				(No Heat Designation)				
SAE 4052	112,000	45.0								
SAE 4052	108,000	49.0								
SAE 4052	102,000	55.0								
SAE 4063	60,000	20.0	0.64	0.78	0.015	0.019	0.24	—	—	0.23
SAE 4063	77,500	28.0				(Heat 709369)				
SAE 4063	100,000	38.0	0.66	0.85	0.015	0.037	0.28	0.11	0.09	0.22
SAE 4063	115,000	45.0				(Heat CY)				
SAE 4063	124,000	53.0								
SAE 4063	130,000	56.0								
SAE 4063	125,000	60.0								
SAE 4063	122,000	61.0								
SAE 4063	123,000	61.5								
SAE 4063	127,000	61.5								
SAE 4063	112,000	65.0								
SAE 4140	69,000	22.0	0.41	0.75	0.010	0.025	0.37	0.87	—	0.19
SAE 4140	76,000	27.0				(Heat 15324)				
SAE 4140	86,000	33.5	0.39	0.75	0.012	0.023	0.35	0.92	—	0.15
SAE 4140	97,000	38.0				(Heat E-1268)				
SAE 4140	97,000	40.5	0.39	0.80	0.010	0.020	0.37	0.90	—	0.22
SAE 4140	100,000	42.5				(Heat 130379)				
SAE 4140	100,000	43.5								
SAE 4140	100,000	46.5								
SAE 4140	98,000	48.5								
SAE 4140	88,000	50.5								
SAE 4140	93,500	51.0								
SAE 4340	72,000	25.0	0.42	0.72	0.025	0.020	0.36	0.85	1.78	0.27
SAE 4340	80,000	30.0				(Heat 30947)				
SAE 4340	82,000	30.0	0.41	0.76	0.015	0.020	0.27	0.72	1.78	0.22
SAE 4340	86,500	34.5				(Heat Z)				
SAE 4340	99,500	40.0	0.38	0.80	0.011	0.007	0.23	0.80	1.92	0.24
SAE 4340	102,000	41.0				(Heat 4x2873)				
SAE 4340	107,000	47.5								
SAE 5150	87,500	36.0	0.52	0.76	0.015	0.021	0.25	0.86	0.13	0.22
SAE 5150	99,000	39.0				(No Heat Designation)				
SAE 5150	106,500	44.0								
SAE 5150	118,000	48.0								
SAE 5150	119,000	50.0								
SAE 5150	113,500	52.0								

Comparison of Fatigue and Torsion Data

Fig. 6 through Fig. 11 are plots of that fatigue data and the torsion test results obtained during this investigation. Both sets of data display straight-line relationships up to certain hardness values and considerable scatter, with marked deviation from linearity, above these values. It is significant to note that, in each case, the endurance limit becomes nonlinear in its relation to hardness at a lower value than does the torsional yield strength. The estimated highest hardness values for the linear portion of each relationship are indicated in Table V. These values show relation to carbon content in that they are highest for SAE 5150 and 4063 steels. Differences be-

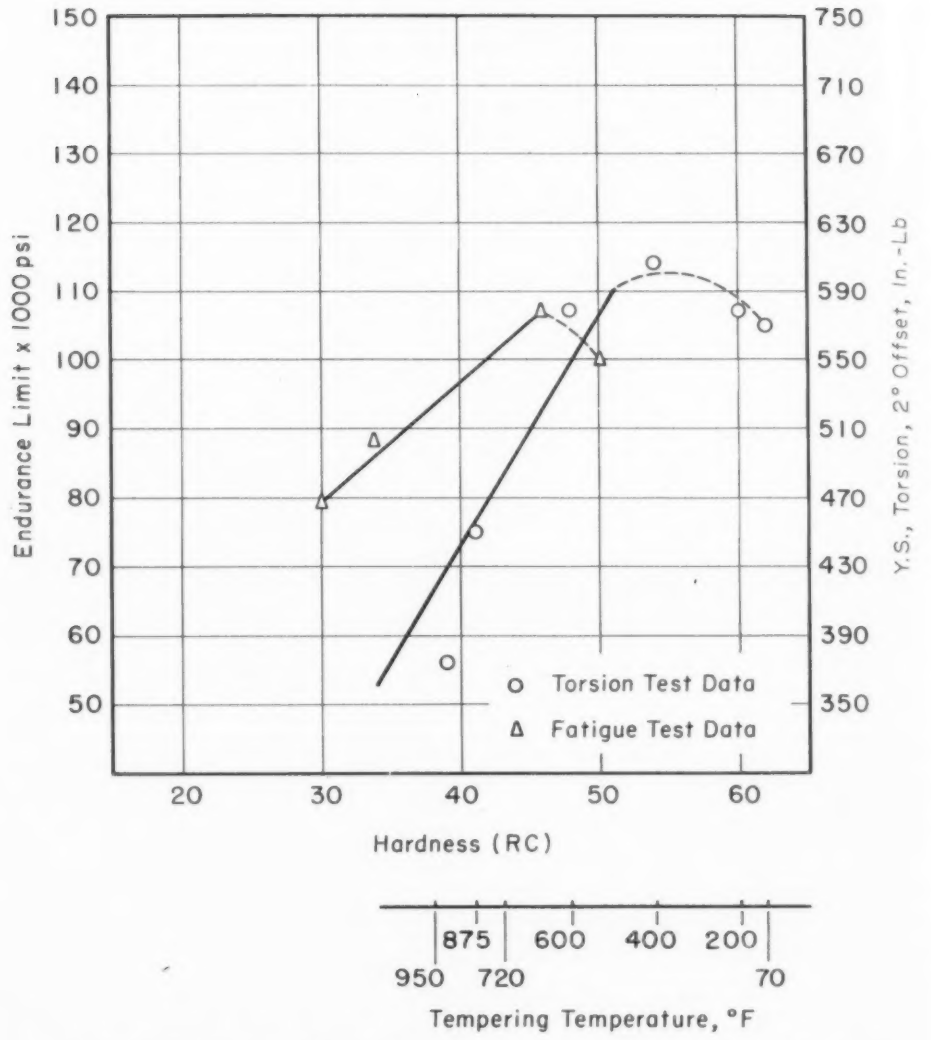


Fig. 6—Comparison of Torsion Test and Fatigue Test Data, SAE 2340 Steel.

tween these hardness values are also listed. They range from 5.5 to 7.5 points Rockwell C.

Interpretation of Electron Micrographs

After torsion testing, three specimens of each steel were selected for electron micrographic investigation. One of the three represented a point plotted on the linear portions of torsion test curves. The others represented points in regions of instability.

Examination was made of cross-sections cut from cylindrical areas between the shanks of the torsion bars. The bars were submerged in coolant while cutting was performed by an abrasive wheel. To prevent further structural change, those bars tempered in the 200-350°F range were not mounted in bakelite, but were clamped

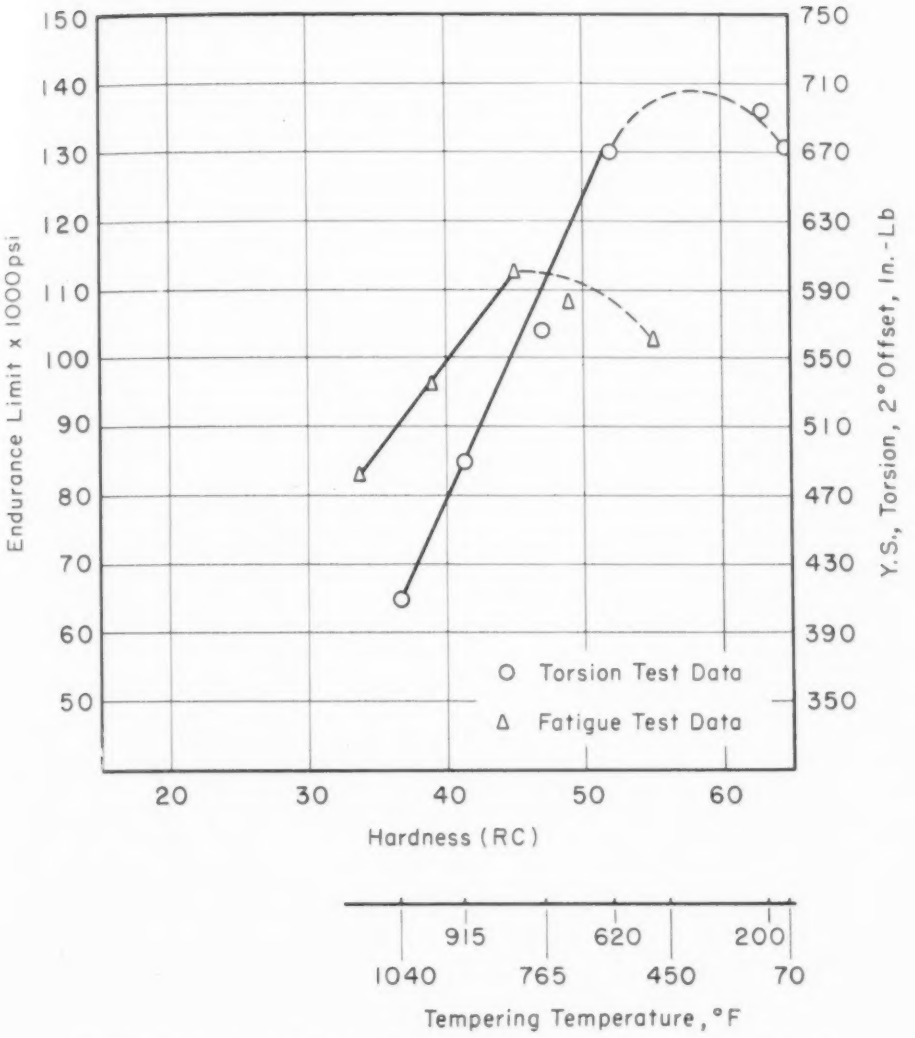


Fig. 7—Comparison of Torsion Test and Fatigue Test Data, SAE 4052 Steel.

Table V
Comparison of Fatigue and Torsion Test Data

Steel	Highest Rc Value in Linear Portion		Rc Difference
	Yield Str., Torsion	Endurance Limit	
SAE 2340	52.5	46.0	6.5
SAE 4052	52.5	45.0	7.5
SAE 4063	57.5	52.0	5.5
SAE 4140	50.0	42.5	7.5
SAE 4340	50.0	42.5	7.5
SAE 5150	55.0	48.0	7.0

mechanically. Likewise, polishing of those samples was done with care, using coolants to prevent surface temperatures from rising above original tempering temperatures.

Formvar replicas were taken after polished surfaces had been etched with 4% picral containing 0.1% zephiran chloride. The repli-

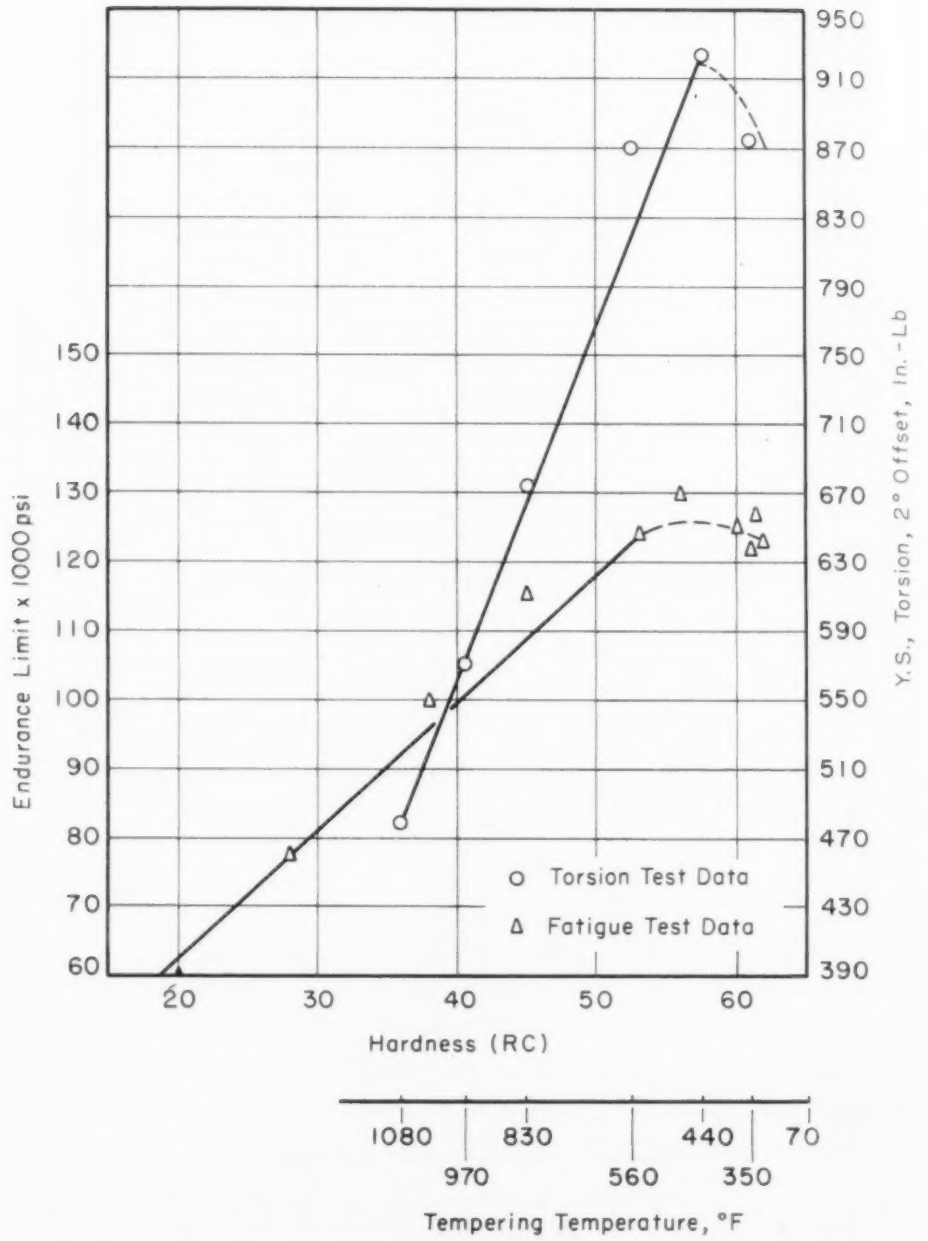


Fig. 8—Comparison of Torsion Test and Fatigue Test Data, SAE 4063 Steel.

cas were shadowed with chromium at an angle of approximately 45 degrees. Figs. 12 through 24 are electron micrographs of these specimens at magnifications of 30,000 diameters.

Structures representative of those torsion bars tempered at 200-350°F are illustrated in Figs. 12 through 15. The tempered martensite needles contain many fine carbide particles and are outlined by films. The nature of these particles has been indicated by the work of Jack (4), Hagg (5), Austin and Schwartz (6) and others. There ap-

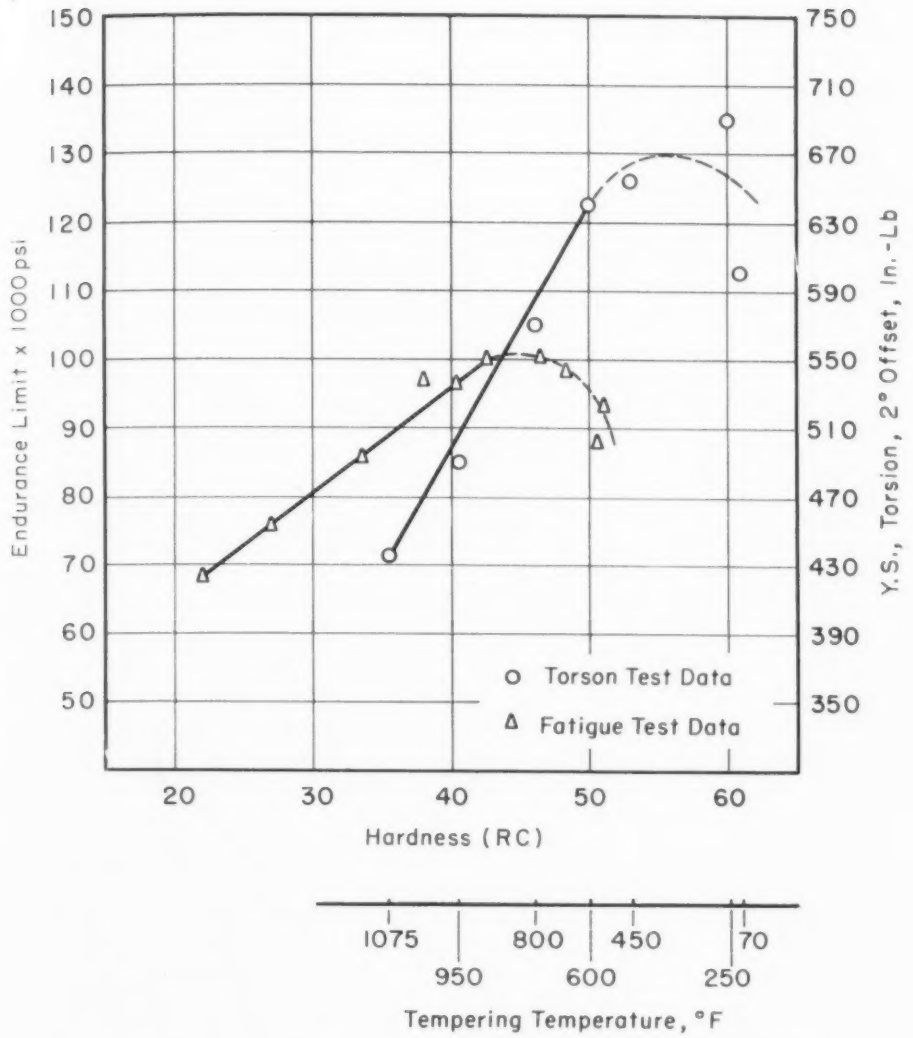


Fig. 9—Comparison of Torsion Test and Fatigue Test Data, SAE 4140 Steel.

pears doubt as to their exact composition, or if more than one form is found during tempering. Therefore, in this paper, the generic term, percarbides, has been used. Lighter etching areas around the percarbides are regarded as regions of lower carbon solid solution as suggested by Kurdjumov and Lyssak (7). Films around the needles are also considered to be composed of percarbides, since, according to data tabulated by Lement, Averbach and Cohen (8), cementite is not present in steels tempered at such low temperatures. Needles partially outlined by percarbide films are most clearly seen in Figs. 12 and 14. The matrix material is considered to be ferrite supersaturated with carbon as indicated by Kurdjumov and Lyssak (9). No indications of retained austenite were found in any of the torsion bars examined.

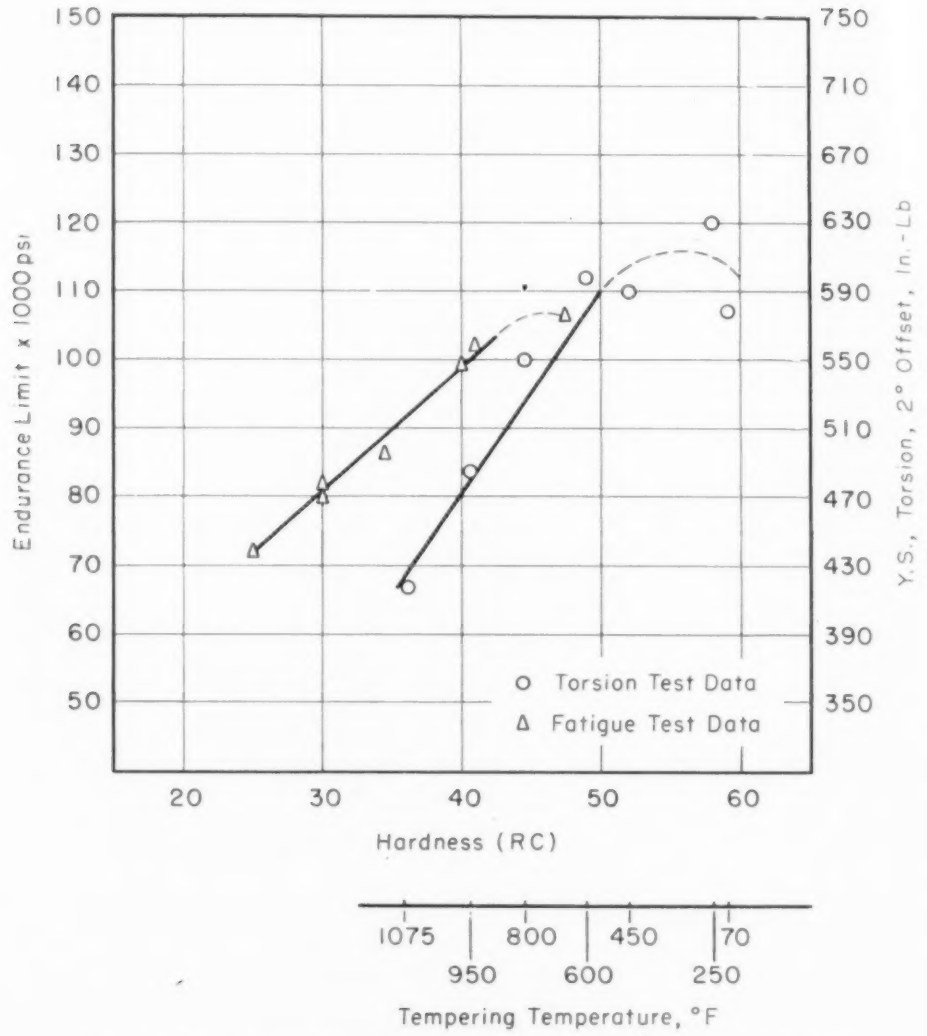


Fig. 10—Comparison of Torsion Test and Fatigue Test Data, SAE 4340 Steel.

Fig. 16 is an electron micrograph of SAE 5150 steel tempered at 300°F and purposely over-etched before replication. Comparison with Fig. 15 of the same test bar, properly etched, indicates a striking difference in structure. It will be noted that when the sample was etched too deeply, fine percarbides no longer appeared as discrete particles. Instead, an artefact network was produced.

Typical electron micrographs of those torsion bars tempered in the 400-500°F range are found in Figs. 17 through 20. Examination indicates that all contain two sizes of carbide particles. The fine percarbides appear to have been partially supplanted by coarser particles of cementite. Also, percarbide films which outlined the martensite needles at lower temperatures of tempering have partially changed to large, elongated, noncontinuous cementite particles.

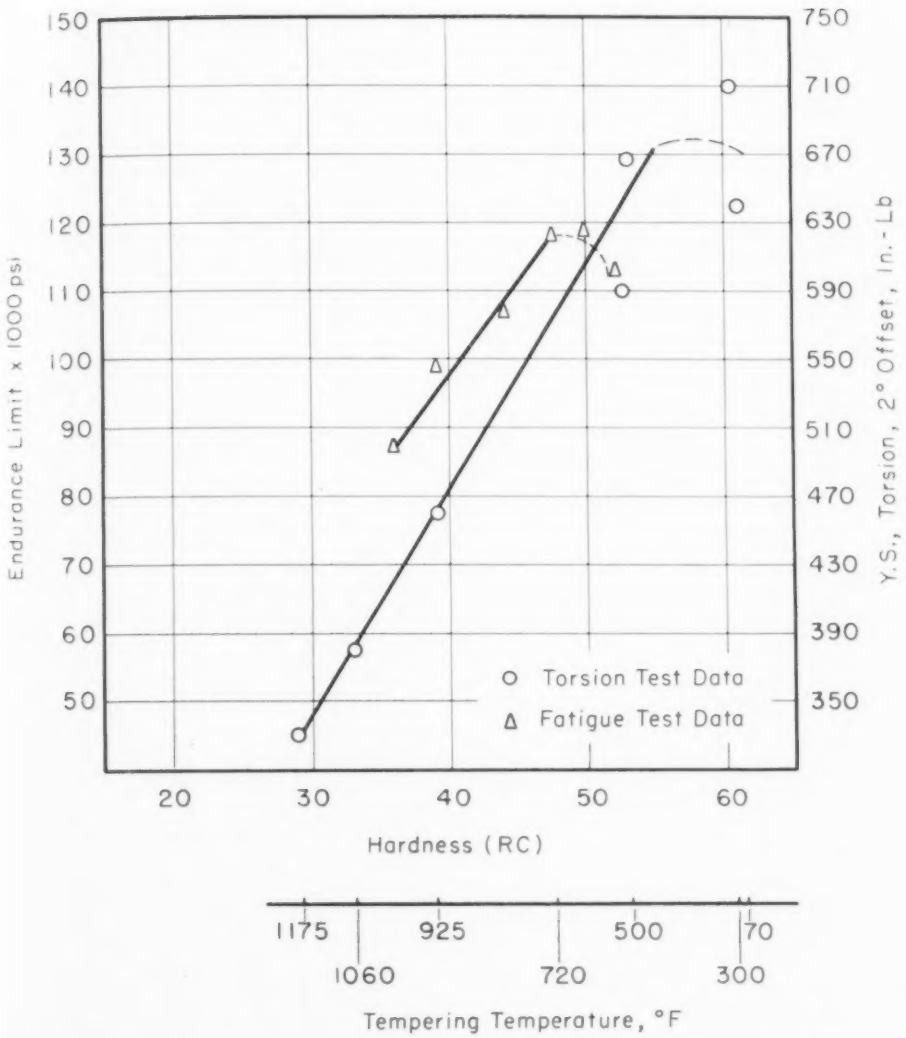


Fig. 11—Comparison of Torsion Test and Fatigue Test Data, SAE 5150 Steel.

Figs. 21 through 24 are electron micrographs of test bars representing points on linear portions of the torsion test curves. Cementite particles are seen in a matrix of smooth ferrite. Very few percarbide particles were noted. No significant differences were detected among structures of the various steels tempered under the same conditions of time and temperature.

Discussion

Mechanical Test Data

Graphical presentation (Figs. 6-11) of torsion test data indicates a straight-line relation between torsional yield strength and hardness up to a limiting Rockwell C value for each steel. Similar presentation

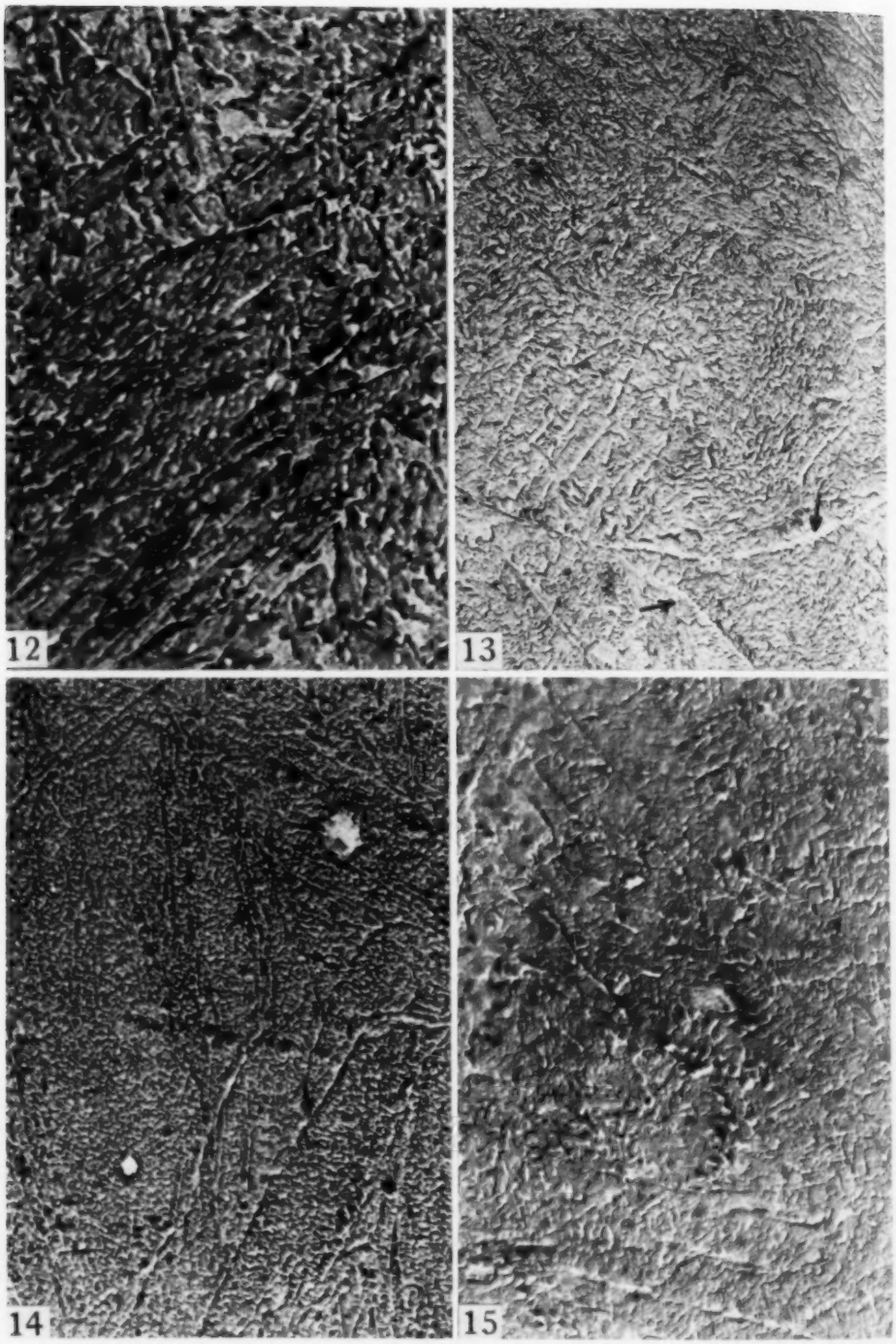
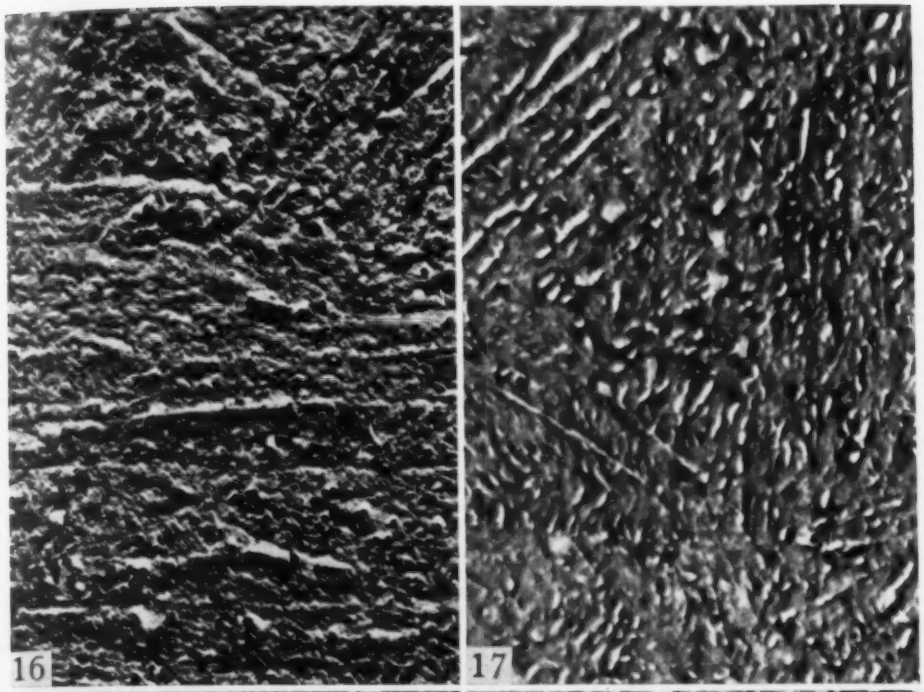


Fig. 12—SAE 2340 Steel, Tempered at 200°F for 90 Minutes. Fine percarbide particles in a matrix of supersaturated ferrite. Arrows denote percarbide films enveloping tempered martensite needles. Lighter-etching areas in matrix around percarbides are lower carbon solid solution. × 30,000, reduced ¼.

Fig. 13—SAE 4063 Steel, Tempered at 350°F for 60 Minutes. Fine percarbide particles in a matrix of supersaturated ferrite, etched more deeply than Fig. 12. Arrows point to boundaries retained from the prior austenite. × 30,000, reduced ¼.

Fig. 14—SAE 4140 Steel, Tempered at 250°F for 90 Minutes. Fine percarbide dispersion in supersaturated ferrite matrix. Apparent pits are artefacts. Arrows point to percarbide films. Lighter-etching areas of lower carbon solid solution tend to broaden and lengthen particles. × 30,000, reduced ¼.

Fig. 15—SAE 5150 Steel, Tempered at 300°F for 90 Minutes. Fine percarbides in a matrix of supersaturated ferrite. Some percarbide films are evident. × 30,000, reduced ¼.



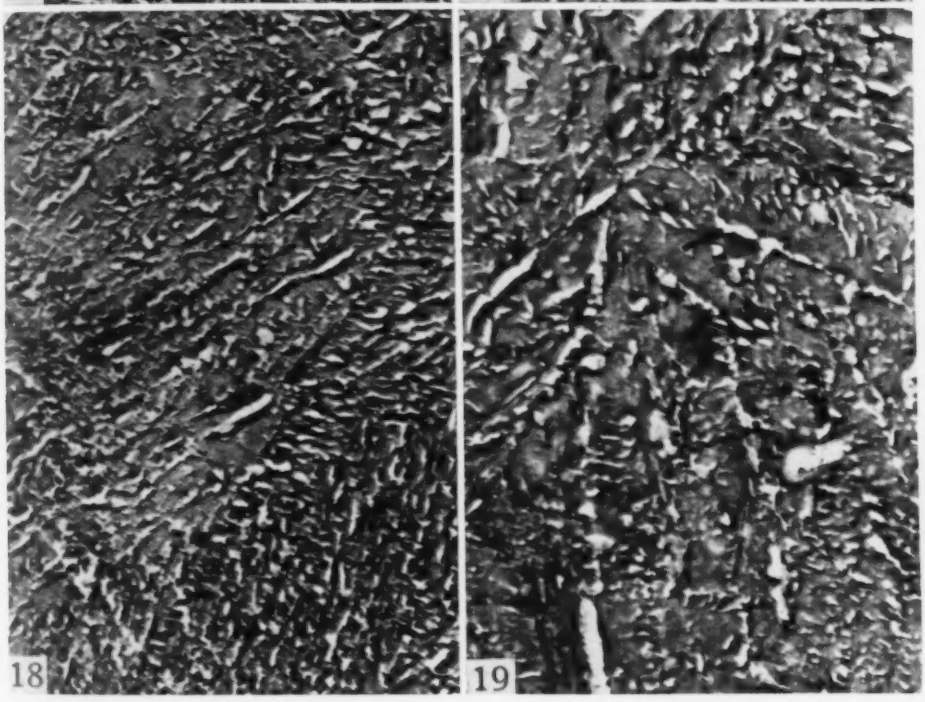


Fig. 16—SAE 5150 Steel, Tempered at 300°F for 90 Minutes. Heavy etch causes percarbides to appear larger and as a network within martensite needles. × 30,000, reduced ⅓.

Fig. 17—SAE 4052 Steel, Tempered at 450°F for 60 Minutes. Duplex structure of Coarse cementite and fine percarbides in a matrix of supersaturated ferrite. × 30,000, reduced ⅓.

Fig. 18—SAE 4063 Steel, Tempered at 440°F for 120 Minutes. Coarse cementite and fine percarbide particles in supersaturated ferrite. 30,000 ×, reduced ⅓.

Fig. 19—SAE 4140 Steel, Tempered at 450° for 60 Minutes. Arrows point to coarse, elongated cementite particles at former martensite needle boundaries. Duplex carbide structure is evident. × 30,000, reduced ⅓.

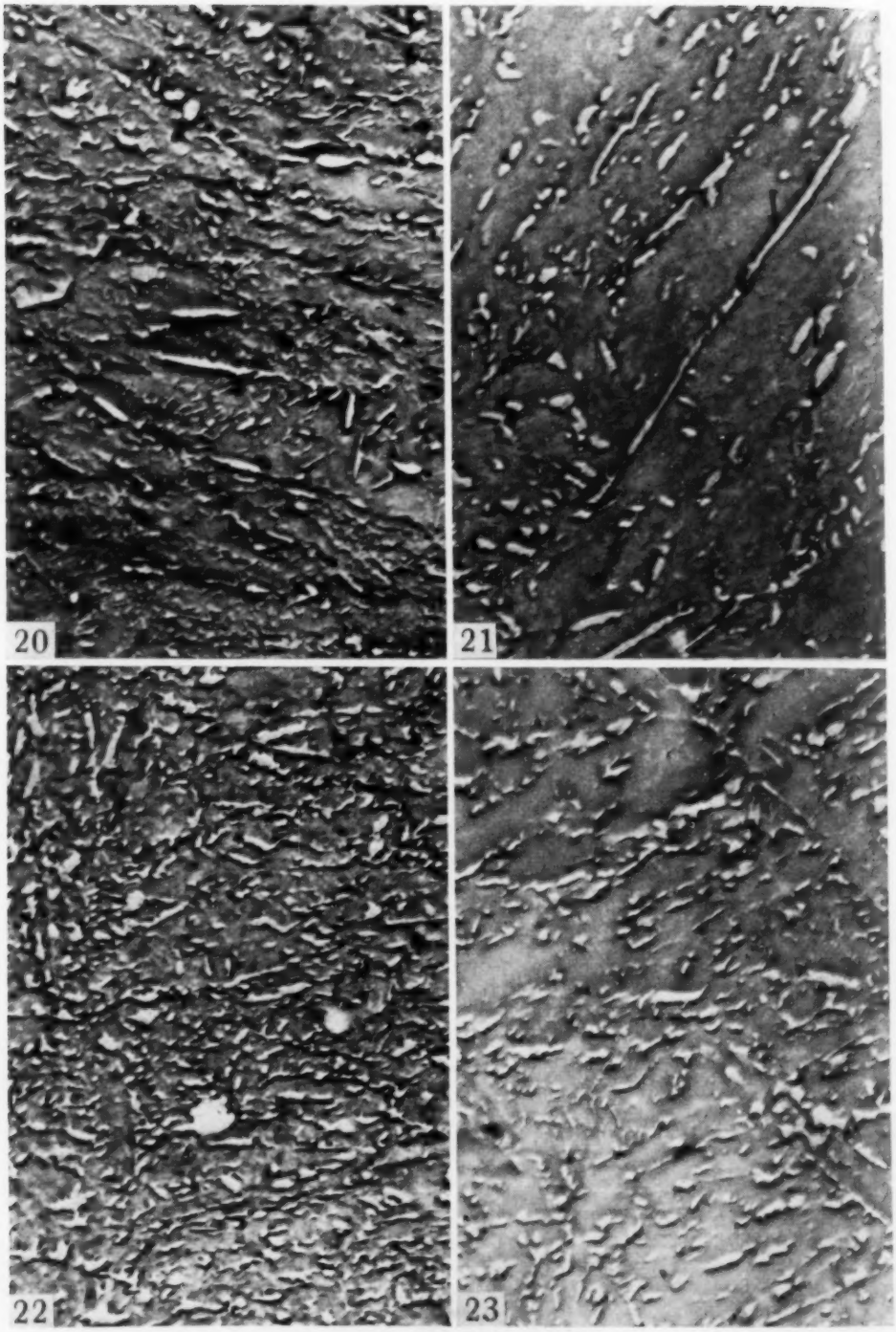


Fig. 20—SAE 4340 Steel, Tempered at 450°F for 60 Minutes. Duplex carbide structure and coarse, elongated cementite particles are evident. × 30,000, reduced ⅓.

Fig. 21—SAE 2340 Steel, Tempered at 600°F for 60 Minutes. Cementite particles in a matrix of smooth ferrite. Arrow points to elongated cementite particle at former martensite boundary. × 30,000, reduced ⅓.

Fig. 22—SAE 4052 Steel, Tempered at 620°F for 60 Minutes. Cementite particles in ferrite matrix. × 30,000, reduced ⅓.

Fig. 23—SAE 4063 Steel, Tempered at 830°F for 90 Minutes. Cementite particles in ferrite. × 30,000, reduced ⅓.

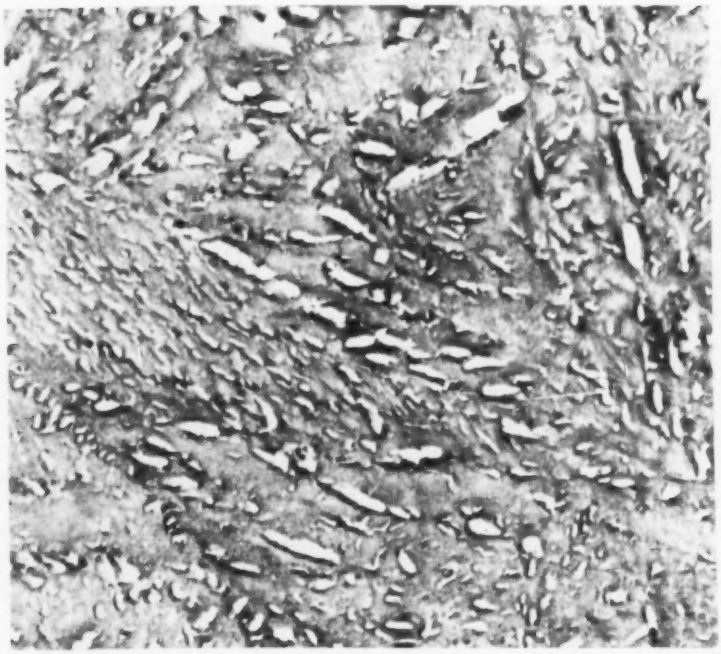


Fig. 24—SAE 5150 Steel, Tempered at 500°F for 60 Minutes. Traces of percarbide particles remain. Majority of carbides are cementite in a ferrite matrix. × 30,000, reduced ⅓.

of the fatigue data of Garwood, et. al. indicates a direct relation between endurance limit and hardness also up to a limiting Rockwell C value for each steel. At greater hardnesses, both fatigue and torsion data reflect a great amount of scatter as well as nonlinearity.

It is noted that, for each steel, first order relationship ceases at a higher Rockwell C value for the torsional yield strength-hardness relation than for the endurance limit-hardness relation. When the difference between these limiting values is obtained (Table V), it is found to range between 5.5 and 7.5 Rockwell C for all steels investigated. This difference can be considered constant, since ± 1.0 Rockwell C is within the limits of hardness testing error and the fatigue and torsion samples were not taken from the same heats of each steel.

However, this does not necessarily indicate that the mechanism of fatigue failure differs from that of torsional yielding. Nor does it indicate that the cause of instability (scatter and nonlinearity) is different for each relation. It does indicate that these instabilities are related to certain ranges of Rockwell C hardness. In this investigation, Rockwell C hardness of quenched test bars was altered by change of the tempering temperature, only. Thus, the structural changes occurring during tempering are assignable causes of data instability. Cycle-dependance of fatigue failure appears to increase sensitivity to structural change so that instability of endurance data occurs over a wider range of hardness.

Torsional Fracture Characteristics

Fracture Type A has been defined as that which resulted when torsion specimens sheared cleanly into two pieces on planes perpendicular to their axes. The fracture surfaces were bright. Olleman, et al have characterized these as pure shear failures. The plotted torsion test data, when correlated with fracture type indicate that all points on linear portions of the torsional yield strength-hardness curves were obtained from bars which failed with Type A fracture.

Type B fracture resulted in shattering of torsion specimens into several pieces along irregular fracture surfaces. The pieces had a generally dull appearance except for bright surfaces originally on planes parallel with specimen axes. Closer study of these fractures indicates that failure was initiated on the bright surfaces. They are defined as planes of shear by Nadai (10). Type B fractures did not occur in all steels. The Type B fractures that occurred are all represented by points plotted in the nonlinear portions of the data curves. In no case was Type B fracture noted in bars of the highest hardness of the material being tested.

Failure along helical planes at 45 degrees to the specimen axes are defined as Type C fractures. Type C surfaces were dull, containing no bright areas. Fig. 5 indicates that no shattering accompanied failure. Under conditions of the torsion test, 45-degree planes are the location of maximum tensile stresses. Thus, Type C fractures represent tensile failures. For all steels, Type C fractures were noted on bars of maximum hardness, representing points on the nonlinear portions of the torsional yield strength-hardness curves.

Both Type B and Type C fractures are considered effects of microstructural changes causing instability of the linear relation of test data. Residual stresses may also be a contributing factor in producing the region of instability. However, measuring them was outside the scope of this investigation. Type B represents transition from shear to tensile failure with increasing hardness.

Electron Micrographs

Muir (11) noted that instability in elastic limit-hardness data coincided with the formation of cementite films in the 450–500°F tempering range as reported by Lement (8). However, he regarded improvement in the data for samples tempered above 500°F as a function of the relief of quenching and transformation stresses. Nevertheless, correlation of electron micrographs (Figs. 12 to 24) with mechanical properties data (Figs. 6 to 11) indicates that the endurance limit and the torsional yield strength are extremely structure-sensitive. Instabilities in test data coincide with occurrence of fine percarbide particles dispersed throughout the matrix of ferrite supersaturated with carbon and of percarbide films outlining tempered martensite needles.

This investigation has shown that cementite films are not formed during the tempering process. It is indicated by Figs. 12 to 15 that percarbide films are present at tempering temperatures as low as 200°F. Figs. 17 to 20 show that these films are gradually supplanted by large, elongated and discontinuous cementite particles at temperatures above 450°F, after one hour or more of tempering. Identification of the films outlining martensite needles at low tempering temperatures agrees with the view of Kurdjumov and Lyssak (7), that formation of percarbides can begin at martensite boundaries in the 200–300°F tempering range.

It has been pointed out by Ross (12) that the concept of three distinct stages in tempering has been based on temperature only. When both temperature and time dependance are considered, the limits dividing tempering into stages must be very broad, if existant at all. The authors agree with the concept that percarbides and supersaturated ferrite are intermediate products in the transformation of martensite to ferrite and cementite during the tempering process. However, Figs. 12 through 15 indicate that percarbides do not form a subgrain network in martensite. This is not in agreement with the consideration by Lement, et. al. that the appearance and subsequent dissolution of such a network is a factor in the kinetics of tempering.

In a previous paper (13), the authors have referred to fine carbides in martensite associated with bainite in end-quench bars as being indicative of a subgrain structure. Refinements in metallographic techniques have resulted in electron micrographs which indicate that subgrains do not exist in tempered 100% martensite nor in partially transformed areas of hardenability bars. Effects caused by improper surface preparation and regions of lower carbon solid solution have led to identification of an artificially produced network and its incorrect representation as a martensite subgrain structure.

The importance of sample preparation in electron metallography cannot be emphasized too highly. Fineness of tempered martensite structures will not be revealed properly unless extreme care is taken that every trace of disturbed metal is removed by etching. Further, the etch must be only of sufficient depth to delineate the particles. As reported by the ASTM Sub-Committee on Electron Metallography (14) and indicated by Figs. 15 and 16, shadowing effects will mask the true structure if over-etching has occurred.

It is also of significance that the steels studied in this investigation when tempered at the same temperature and for the same length of time display the same electron microstructure. It appears that, while the amount of carbide particles in tempered martensite is determined by chemistry, their size and distribution is a function of the time and temperature of tempering.

Conclusions

Consideration of the results of this investigation have led to the following conclusions:

1. For each of the alloys investigated (SAE 2340, 4052, 4063, 4140, 4340, and 5150), there is a straight-line relationship between yield strength in torsion and hardness up to a limiting Rockwell C value. This is similar to that previously reported to exist between endurance limit and hardness for the same alloys.

2. The beginning of instability in the endurance limit-hardness relation occurs at 5.5–7.5 points Rockwell C lower than that in the torsion yield strength-hardness relation.

3. Electron micrographs indicate that finely divided percarbides are present in tempered martensite over the range of instability of the hardness-torsional yield strength relationship.

4. Electron micrographs show that percarbide films outline martensite needles tempered for an hour or more in the 200–350°F range. Above 450°F, these films are supplanted by elongated and discontinuous cementite particles.

5. No martensite subgrain network was found in electron micrographs of the torsion bars.

6. No microstructural differences were detected in electron micrographs of various steels tempered under the same conditions of time and temperature.

7. Three types of fracture were noted when torsion tests were carried to failure: shear fracture on planes normal to specimen axes; combination shear and tensile fracture containing some shear surfaces along planes parallel to specimen axes; and tensile fracture on helical planes at 45 degrees to specimen axes.

8. Specimens on straight-line portions of the hardness-torsional yield strength curves failed with normal shear fractures. For each steel, those specimens heat treated to highest hardness fractured at 45 degrees along the helical plane of maximum tensile stress.

References

1. M. F. Garwood, H. H. Zurburg and M. A. Erickson, "Correlation of Laboratory Tests and Service Performance," Interpretation of Tests and Correlation with Service, 1951, p. 1, published by American Society for Metals.
2. R. D. Olleman, R. T. Wessel and F. C. Hull, "A Study of Factors Controlling Strength in the Torsion Test," Transactions, American Society for Metals, Vol. 46, 1954, p. 87.
3. H. Scott, Westinghouse Electric Corp., private communication, January 29, 1953.
4. K. H. Jack, "Structural Transformations in the Tempering of High Carbon Steels," *Journal*, Iron and Steel Institute, Vol. 169, 1951, p. 26.
5. G. Hagg, *Zeitschrift Kristallographie*, Vol. 89, 1934, p. 92.
6. A. E. Austin and C. M. Schwartz, "Electron-Diffraction Study of Iron Carbides in Bainite and Tempered Martensite," American Society for Testing Materials, Preprint No. 165, 1952.

7. G. Kurdjumov and L. Lyssak, "Kinetics of the First Stage of Martensite Decomposition," *Zhurnal Teckhnicheskoi Fiziki* (Journal of Technical Physics), USSR, Vol. 19, 1949, p. 525. (Brutcher Trans. 3041).
8. B. S. Lement, B. L. Averbach and M. Cohen, "Microstructural Changes on Tempering Iron-Carbon Alloys," TRANSACTIONS, American Society for Metals, Vol. 46, 1954, p. 851.
9. G. Kurdjumov, L. Lyssak, "The Application of Single Crystals to the Study of Tempered Martensite," *Journal*, Iron and Steel Institute, Vol. 156, 1947, p. 29.
10. A. Nadai, *Plasticity*, 1931, published by McGraw-Hill.
11. H. Muir, B. L. Averbach and M. Cohen, "The Elastic Limit and Yield Behavior of Hardened Steels, TRANSACTIONS, American Society for Metals, Vol. 47, 1955, p. 380.
12. S. T. Ross, discussion on article by B. S. Lement, B. L. Averbach and M. Cohen, "Further Study of Microstructural Changes on Tempering Iron-Carbon Alloys," TRANSACTIONS, American Society for Metals, Vol. 47, 1955, p. 291.
13. S. T. Ross, R. P. Sernka and W. E. Jominy, "An Electron Metallographic Study of the Dependence of Microstructure on Hardenability," TRANSACTIONS, American Society for Metals, Vol. 47, 1955, p. 727.
14. "Techniques for Ferrous Electron Metallography—Part II, Etchants and Etch Depths," *Proceedings*, American Society for Testing Materials, Vol. 53, 1953, p. 515.
15. F. E. Werner, "Tempering of Iron-Carbon Single Crystals", M.I.T., Department of Metallurgy Sc. D. Thesis, (Sept. 1955).
16. C. S. Roberts, B. L. Averbach, and Morris Cohen, "The Mechanism and Kinetics of the First Stage of Tempering", TRANSACTIONS, American Society for Metals, Vol. 45, 576–604, (1953).

DISCUSSION

Written Discussion: By Martin A. Erickson, section supervisor, Laboratory Test Section, Tractor and Implement Div., Ford Motor Co., Birmingham, Michigan.

The authors are to be complimented for their contributions in arriving at a simplified method for approximating the endurance limit of polished steel.

They point out that linearity exists in both the static torsion data and the fatigue data up to certain ranges of Rockwell C hardness after which scatter occurs. The implication is that because of this relationship in linearity, the magnitude of the torsional stress at 2 degrees offset and of the endurance value for the same hardness should be comparable. Fig. 25 shows that linearity also exists in the case of tension. Using the same reasoning as implied we would anticipate correlation between tensile strength data and endurance data at the same level.

The writer has attempted to make a quantitative analysis of the available data which was collected from the paper, from the authors' unpublished tests and from the report by Garwood, Zurburg, and Erickson. By plotting ratios as shown in Fig. 26, it was observed for example, that the torsional yield at 2 degrees offset agreed more closely with the endurance limit than did the torsional strength data. It was also observed that when 50% of the tensile strength was used, which is generally the value taken for rule of thumb evaluations of the endurance limit that agreement was somewhat closer. See Fig. 27. The data published by Garwood et al shows the endurance limit to vary from 0.46 to 0.77 of the tensile strength for the steels tested. It would appear that for estimating the endurance limit of a smooth bar of the size used that the tensile strength gives equal if not somewhat better data and is in most cases easier to obtain.

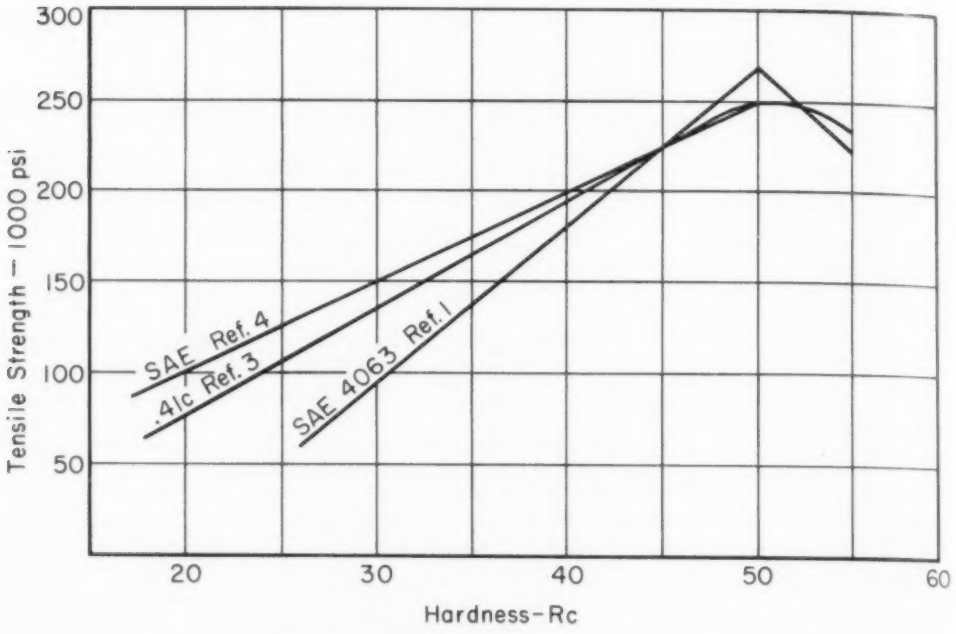


Fig. 25—Showing that Linearity Also Exists in the Case of Tension.

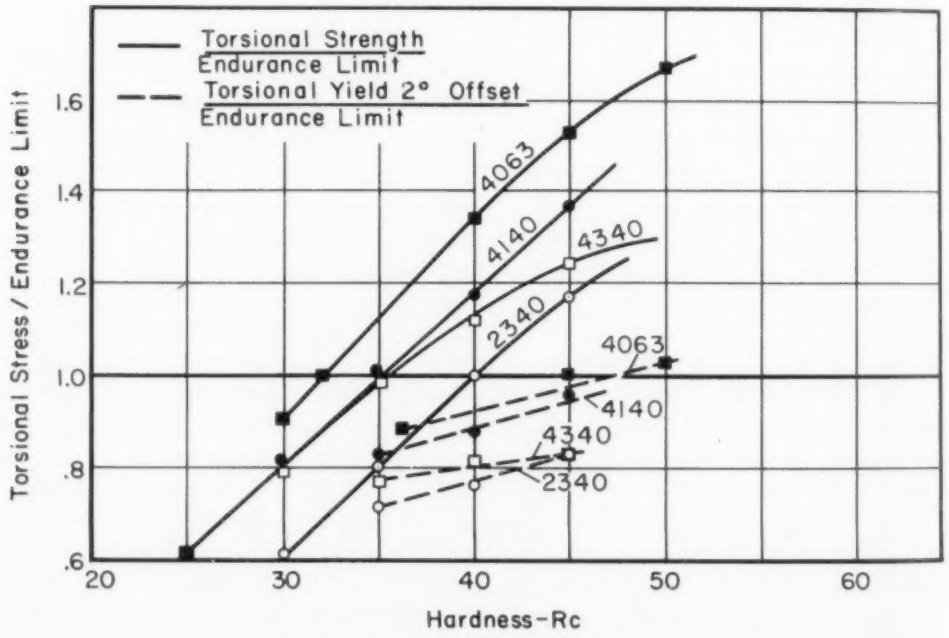


Fig. 26—Torsional Strength and Torsional Yield at 2 Degrees Offset.

In seeking a practical use for the data presented by the authors one must keep in mind that the results apply only to polished or superfinished specimens. Linearity between endurance limit and tensile strength or hardness disappears as the surface finish becomes more irregular, such as when notches or scale are present in the surface under strain. This is clearly shown by Lipson, Noll and Clock in Fig. 28. It is also known that the simple torsion or static test values would

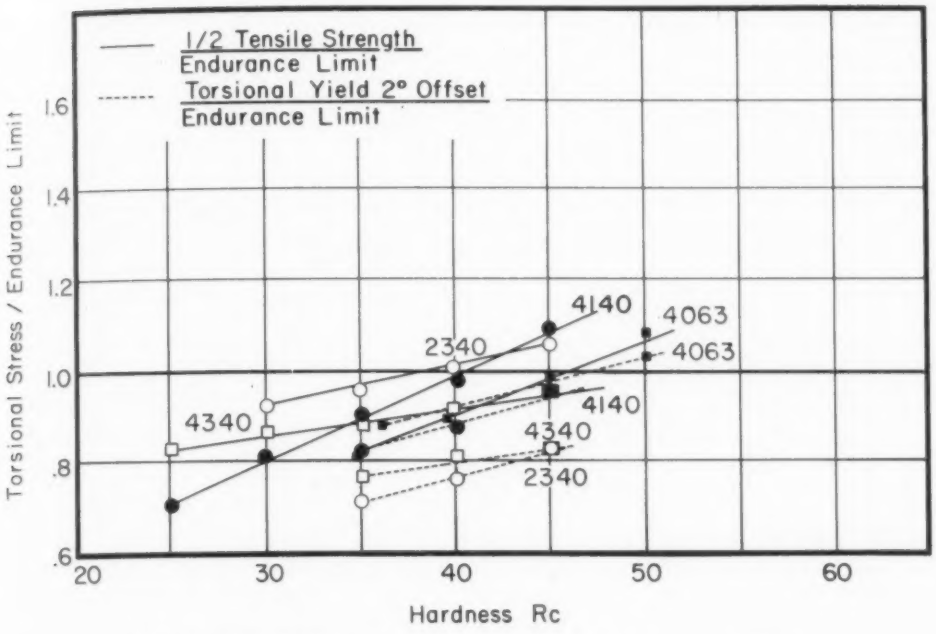


Fig. 27—Tensile Strength and Torsional Yield at 2 Degrees Offset.

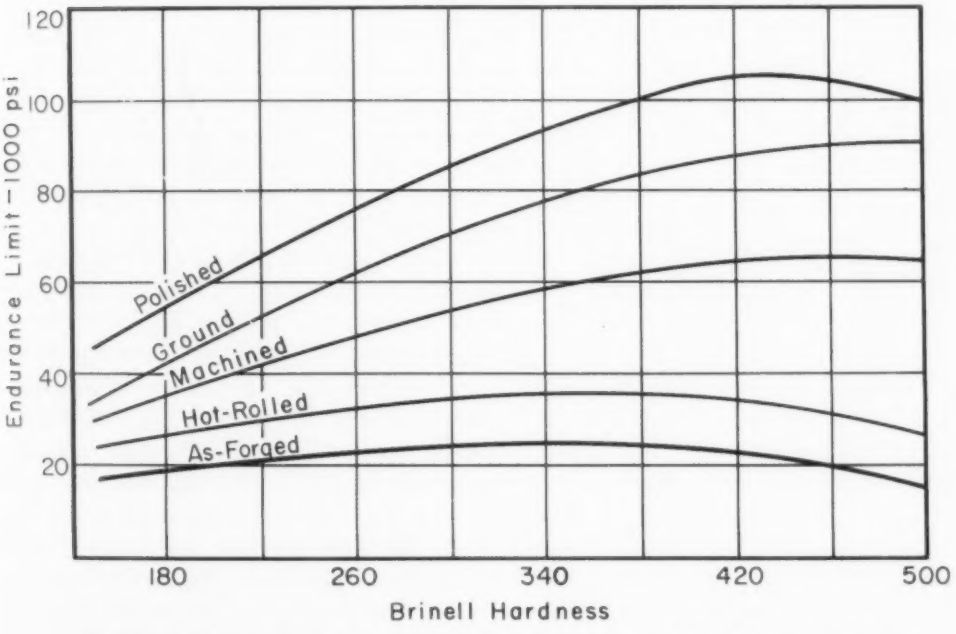


Fig. 28—Endurance Limit Versus Hardness Curves for Steels Under Various Manufactured Surface Conditions.

remain linear with hardness up to Rockwell C-40–45 in spite of the surface condition since stress concentrations are not sensitive to static loads. These differences in the static and dynamic tests are significant and would suggest that the two are very much unrelated and thus difficulty of correlation would be expected.

Above Rockwell C-40–45 hardness instability occurs in tensile values as well as endurance and torsion values as shown by the authors. This instability is

caused by the residual stress distribution set up by the heat treatment. If a plain low carbon steel is made to maximum hardness it must be quenched drastically in a salt solution followed by little or no tempering. This steel may have a surface hardness of Rockwell C-40–45 but will exhibit brittle properties due to the inherent residual stresses. On the other hand a high carbon alloy steel moderately quenched in oil and tempered at a relatively high temperature 900–1000°F or so would exhibit ductile properties at Rockwell C-40–45 due mainly to low residual stress magnitudes. Thus it would be anticipated that the higher carbon steels would show linear stress-hardness characteristics to a higher value of hardness than the low carbon series due to the stress relief obtained by higher tempering temperatures.

It will also be found that steels free of biaxial and triaxial residual stress distribution obtained by stress relieving will exhibit ductile failures below Rockwell C-45 similar to those shown by the authors. When these residual stresses are present the material will exhibit brittle properties and fracture will be due to maximum tensile stress rather than shear. In between these two extremities a combination of ductile and brittle failure will occur similar to those shown in Fig. 4.

Written Discussion: By B. S. Lement, research staff, Division of Industrial Cooperation, Department of Metallurgy, Massachusetts Institute of Technology, Cambridge, Mass.

On the basis of their electron microscopic examination of low alloy steels, the authors have presented a somewhat different description of the microstructural changes during tempering than that advanced by the discussor in a previous study of high purity, iron-carbon alloys (8). Although the alloy contents of the steels used in the present investigation might conceivably affect the kinetics of the tempering stages and the etching response as compared to high purity, iron-carbon alloys, one would expect the main features of the tempering changes to be similar. However, it is difficult to reach agreement as to what these features actually are because of differences in techniques, interpretation and terminology.

The authors conclude that during the first stage of tempering "percarbides" form both as fine discrete particles within martensitic plates and as films at martensitic boundaries. Based on Figs. 12 to 15, it seems difficult for one to decide whether discrete particles rather than films at sub-boundaries are really present within the martensitic plates. This difficulty could arise from irregularities or discontinuities in a sub-boundary film, assuming it to be present. In the previous study (8), variations in thickness and apparent discontinuities in the sub-boundary film were observed; however, the term "network" was used to take into account the possibility of local coalescence as well as unresolvable portions of the film. The distinction between an irregular or discontinuous "film" and "discrete particles" might be considered academic. Nevertheless, the term "film" does have significance if it is used to indicate the presence of a carbide in essentially 2-dimensional form along some type of interfacial surface. From considerations of interfacial energy, one would logically expect the fine carbides observed to be located at sub-boundaries within the martensitic plates. The main question seems to be whether subgrains actually exist in martensite. Since overetching is usually necessary to bring out subgrains, Fig. 16 might be interpreted as revealing the presence of subgrains in 5150 steels which are the same size (of the order of 1000Å) as reported for the high purity, iron-carbon alloys (8). The existence of subgrains in martensite about 200 Å in size has recently been deduced from analysis of the broadening of X-ray diffraction lines (15).

The authors reach the conclusion that the "percarbide films" at martensitic boundaries are supplanted by "elongated and discontinuous cementite particles" on further tempering. The question arises as to why the authors made a distinction between "films" and "particles" in this connection. Both types of carbides occur at martensitic boundaries, both are elongated, and both appear discontinuous in the electron micrographs shown. In the previous paper (8), the discussor used the term "elongated films" to describe the cementite that formed at martensitic boundaries without intending to imply that these films were continuous. "Elongated particles" would be a more appropriate term if, for example, the cementite were considered to be rod-shaped rather than essentially 2-dimensional.

The formation of what the authors call "percarbide films" at martensitic boundaries is an interesting observation. In the high purity, iron-carbon alloys of the previous investigation (8), virtually no evidence was found of increased film formation at martensitic boundaries during the first stage of tempering. In fact, it was only after tempering high enough to induce precipitation of cementite, that the martensitic boundaries became sufficiently delineated to be recognized as such under the electron microscope. This apparent difference in behavior between high purity, iron-carbon alloys and low alloy steels is difficult to rationalize unless one assumes that the initial films at the martensitic boundaries observed in the low alloy steels are actually cementite. The occurrence of cementite could be due to inadvertent tempering on passing through the Ms range during the quenching operation. This phenomenon has been termed Q-tempering by Dr. Aborn in his Campbell lecture and is a factor if the Ms is relatively high and/or cooling through the Ms range is relatively slow. Considering the fact that the 4140 steel has a calculated Ms of about 575°F[2] and that the metallographic specimens were taken from torsion bars (0.31-inch gage diameter) hardened by oil quenching, it seems possible that a significant amount of Q-tempering could occur. From the previous investigation (8) in which ice-brine quenched specimens (⅛ inch thick) of high purity, iron-carbon alloys with low Ms points were studied, it appears that on regular tempering cementite forms at martensitic boundaries even before it forms within the martensitic plates. It therefore seems likely that cementite would form preferentially along martensitic boundaries on Q-tempering of the low alloy steels and thus be present in the as-quenched condition. Did the authors consider this possibility?

Finally, it should be made clear that what the authors refer to as "supersaturated ferrite" matrix coexisting with "percarbides" at low tempering temperatures (200–350°F) is actually b.c.t. martensite. It has been shown on the basis of X-ray diffraction measurements of tetragonality (9,15,16), that the matrix at the end of the first stage tempering is b.c.t. martensite containing about 0.3% carbon and that it is necessary to temper for 1 hour at about 500°F in order to reduce the tetragonality and result in b.c.c. ferrite. Although Kurdjumov (9) uses the term "supersaturated ferrite" as synonymous with b.c.t. martensite, this is ambiguous since it seems probable that the b.c.c. ferrite that eventually forms is supersaturated with respect to carbon. According to Kurdjumov, there may be about 0.1% carbon present in the newly formed b.c.c. ferrite although this remains to be proven.

Written Discussion: By Henry E. Frankel, National Bureau of Standards, Washington, D. C.

The authors are to be complimented on the fine electron metallographic

[2]The actual Ms is probably higher because of incomplete carbide solution.

results obtained. There is, however, one question that I would like to have clarified.

It can be assumed that in almost every instance the basic structure, after austenitizing and quenching was martensite. After this treatment, the stock was tempered at various times and temperatures, thus permitting any retained austenite to transform as well as obtaining varying degrees of martensitic decomposition products. The micrographs illustrate these points very well. It, therefore, seems that, what was really tested were specimens with different metallographic structures: the hardness level merely being one manifestation of this. I wonder if the authors observed an optimum structure which would correspond to a maximum fatigue limit. Such an optimum structure has been inferred by Hodge and Lankford.[3]

Written Discussion: By Howard Scott, Westinghouse Electric Corp., Pittsburgh.

This paper is another major contribution to the basic metallurgical problem of identifying factors controlling or limiting the strength of hardened steels. The authors have taken advantage of the wide range of hardness values available in quenched steels simply by varying the drawing temperature, to study the accompanying highly significant changes in mechanical properties. It is of interest to contrast their results with previous related work on static mechanical properties.

As early as 1931, Emmons[4] showed that a maximum occurs in the static torsional strength of a bearing steel as hardness is so varied. We have found a similar maximum in the simple tensile test and in the notched bar tensile test of an air hardening steel though at lower hardness values than for torsion loading. It might be expected then that a maximum would be found also in the fatigue strength of steels tested at sufficiently high hardness values. The present authors, giving in detail the earlier result of Garwood, Zurburg and Erickson,[5] have covered a sufficient hardness range to establish clearly the existence of such maxima in fatigue strength, apparently for the first time.

These maxima in strength are obviously of great importance in the selection of steels and treatments for specific applications. They represent, however, sharp limits to the gain in strength possible by conventional treatment. To attain still higher values, we need to know what causes them.

The cause of the maximum in static torsional strength is obvious enough if one examines the fracture surfaces in great detail. Olleman, Wessel and Hull[6] have done so and find that maximum shear stress determines fracture on the softer side of the maximum, maximum tension stress on the hard side. Evidently shear fracture strength increases with hardness while the brittle or tension fracture strength is falling. Since the shear and tension stresses on their respective planes of maximum value are equal in the torsion test, a maximum in torsional strength occurs at the hardness level where the shear and tension fracture strengths are equal.

The interpretation of fractures obtained in the tension test is not so straightforward because of the cup-cone type of fracture commonly found. The work of

---

[3]J. M. Hodge and W. T. Lankford, "Influence of Non-martensitic Transformation Products on Mechanical Properties of Tempered Martensite," NACA TN 2862, December, 1952.

[4]J. V. Emmons, "Some Physical Properties of Hardened Tool Steel," *Proceedings*, American Society for Testing Materials, Vol. 31, 1931, Part II, p. 47.

[5]Garwood, Zurburg and Erickson, "Correlation of Laboratory Tests and Service Performance," 1951, published by the American Society for Metals.

[6]Olleman, Wessel and Hull, "A Study of Factors Controlling Strength in the Torsion Test," TRANSACTIONS, American Society for Metals, Vol. 46, 1954, p. 87.

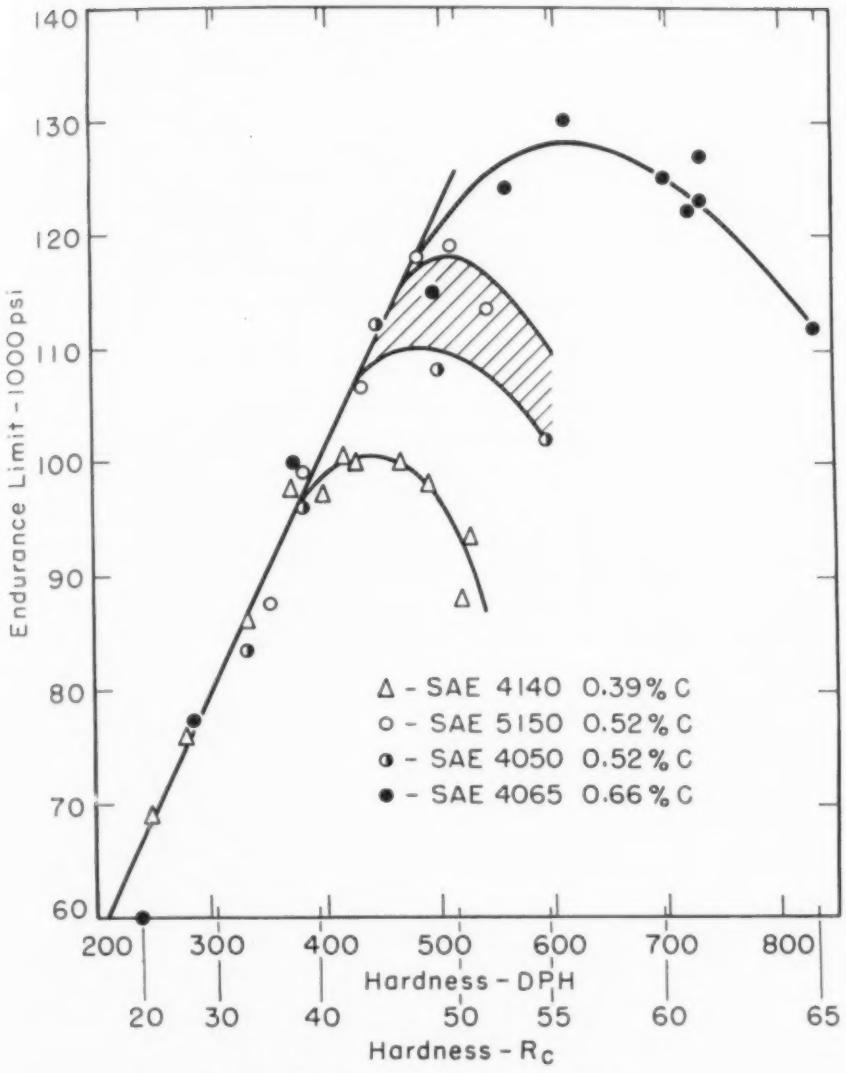


Fig. 29—Fatigue Strength of Several Steels.

Parker, Davis and Flanigan,[7] however, shows clearly that the same factors control in the tension test as in the torsion test, the essential difference being in the ratio of shear to normal stress at the origin of fracture.

These observations are cited because of their possible relation to the maximum in fatigue strength. An analysis of the tensile and torsion data suggests strongly that austenite content reduces tension fracture strength and therefore displaces the strength maximum to a lower hardness level. The authors' data, however, are quite positive in showing that maximum fatigue strength is reached at hardness levels where austenite is completely transformed and, therefore, is not a controlling factor. Carbon content, on the other hand, is clearly a dominant variable determining the maximum attainable endurance limit, Fig. 29. Evidently the

[7]Parker, Davis and Flanigan, "A Study of the Tension Test," *Proceedings*, American Society for Testing Materials, Vol. 46, 1946, p. 1159.

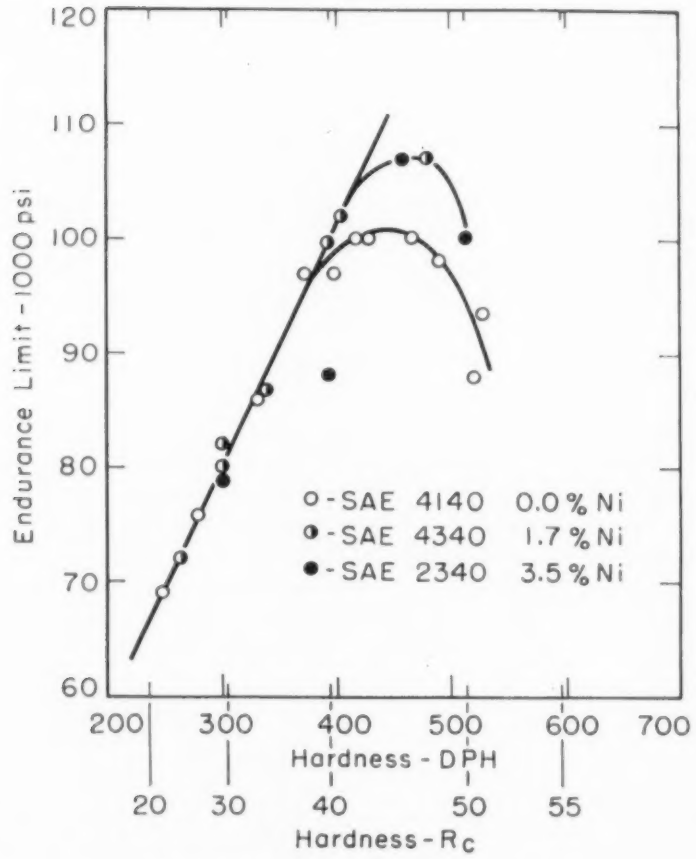


Fig. 30—Fatigue Strength of Several Steels.

linear relation of endurance limit to hardness is terminated at a higher hardness, the higher the carbon content. Though one might expect some austenite in the 0.66% carbon steel drawn at about 500°F to a hardness of Rockwell C-56, this composition and treatment produced maximum fatigue strength.

Nickel also is an austenite stabilizer but the two steels having an appreciable nickel content at 0.40% carbon fail to show a lower fatigue value at their respective maxima, Fig. 30. Accordingly, one needs to consider other basic variables than austenite content for an explanation of the maxima in fatigue strength.

Grain size might be suspected as a factor influencing fatigue strength as indeed it is in single phase alloys. Sinclair and Dolan,[8] however, show that it has no appreciable effect in quenched and tempered steel of 110,000 psi ultimate strength. Furthermore, the variation in austenitic grain size among the steels and treatments used by the authors is probably too small to be significant so one must seek some other cause for the displacement of the peak endurance limit to higher hardness with increased carbon content.

There is certainly no immediately obvious reason for the displacement but one might suspect residual stress as a factor. The opportunity for carbon concentration gradients to remain after austenitizing is greater in the lower carbon steels

[8]G. M. Sinclair and T. J. Dolan, "Some Effects of Austenitic Grain Size and Metallurgical Structure on the Mechanical Properties of Steel," American Society for Testing Materials, Preprint 15, 1950.

than in the higher carbon ones which are close to the eutectoid ratio. Because of the large increase in specific volume of martensite with carbon content, large microstresses can develop from small gradients.

Heterogeneity in carbon distribution might arise also from the presence of oxygen, the content of which is normally lower the higher the carbon content. If this is the case, vacuum melting should raise the maximum in fatigue strength and displace it towards higher hardness values. A larger effect would then be expected at the lower end of the carbon range considered than at the higher end. Obviously this is a fertile field for further experimental work with good prospects for the eventual evaluation of the metallurgical factors controlling the fatigue strength of tempered steels.

Authors' Reply

The authors wish to thank the various discussors for their contributions to this paper. Mr. Erickson suggests that we have attempted to determine endurance limit values from our study of torsional yield strength data and electron micrographs of corresponding tempered structures. Actually, we have established that there is a virtually constant difference in the hardness at which optimum endurance limit is obtained and that at which optimum torsional yield strength is obtained in the tempered steels investigated. While it may be true that actual values of the endurance limit can be estimated from tensile data as well as from torsional data, this consideration was beyond the scope of our paper. We have shown that relatively inexpensive torsion tests can indicate the hardness to which medium carbon, low alloy steels should be tempered to attain maximum fatigue properties.

We agree with Mr. Erickson that surface finish is an important factor in both torsion and fatigue testing. Our torsion specimens were ground to a high degree of surface finish to avoid occurrence of surface stress raisers. We believe that this is consistent with good testing practice.

We agree with both Messrs. Erickson and Scott that residual stresses also play a part in the phenomena we have investigated. We have shown the existence of microstructural variations which we have described as assignable causes for instability of properties. We have not seen quantitative measurements which give residual stresses the same importance. We do not deny that they may also be causes of instability.

We appreciate the correlation of our work by Mr. Scott with data obtained previously on related static mechanical properties. We agree that similar investigation of vacuum-melted alloys might indicate that higher maximum values are possible with improved matrix strength. However, we feel that displacement of maxima to higher hardness values is not likely, since vacuum melting would probably have little effect on the carbide size, type, and distribution in the steels under consideration.

In answer to Frankel, we believe that our results indicate that there is a tempered structure which promotes maximum endurance behavior in steels. It is that which is obtained when the tempering temperature and time are just sufficient to result in microstructures free of films and finely-divided particles of percarbide. Our samples were quenched in such a way as to obtain 100% martensite before tempering. The relative importance of percarbide particles and percarbide films in this connection is the subject of research now in progress at the Chrysler Corporation Research Laboratories.

Mr. Lement has referred to a first stage of tempering in discussing our results. We have indicated previously (12) that his assignment of definite stages to the tempering process requires the restriction of tempering time to one hour. We have shown that tempering phenomena are time-dependant as well as temperature-dependant. Our removal of the time restriction leads to the conclusion that temperature limits dividing tempering into definite stages based on microstructure are very broad, if they exist at all.

Mr. Lement uses the term network which presumes continuity of the percarbide particles. Our electron micrographs show them as discrete particles. We have also found that a percarbide network is an artefact which appears in electron micrographs of over-etched specimen surfaces. Thus, the precipitation of these particles does not delineate a subgrain structure in martensite. We are not familiar with Mr. Werner's deductions from X-ray line broadening, although this technique has been used by several others, previously. However, we do not believe that over-etching can reveal subgrains in martensite of tempered medium carbon steels, even though they may exist. The large number of percarbide particles present in such a degree of relief effectively mask any suggestion of subgrains in the matrix of the tempered steels under consideration.

This technique might, however, reveal a subgrain structure in very low carbon alloys. We would like to emphasize our differentiation between the terms percarbide film and elongated cementite particle. We have shown that, in addition to existing as fine particles, percarbides exist as films around prior martensite needles at low tempering temperatures or after short tempering times. Above temperatures at which percarbides become unstable with time, these percarbide films are shown to be supplanted by elongated, discrete cementite particles. In previous work (8) Mr. Lement has referred to such cementite particles as cementite films and failed to note the existence of percarbide films at lower tempering temperatures. Study of our electron micrographs indicates that percarbide films exist in all our samples at low tempering temperatures.

Mr. Lement has suggested that percarbide films might have been present in our specimens as a result of tempering below the M_s during quenching. He cites the work of Dr. Aborn[9] in this connection. However, Dr. Aborn's work was concerned with steels of less than 0.20% carbon content and of much higher M_s temperatures. We do not believe that the phenomenon of Q-tempering is occurring to a sufficient extent to be observable in our specimens. We examined them before tempering and found no evidences of percarbide films in the as-quenched condition.

We have used the term supersaturated ferrite to denote the incompletely tempered matrix which coexists with percarbides to differentiate it from the as-quenched structure, martensite. Mr. Lement indicates that he would prefer to call this structure low-carbon martensite based on diffraction data which indicate a slight degree of matrix tetragonality. We prefer to retain the term supersaturated ferrite since it implies neither a cubic structure nor a specific degree of tetragonality. Rather, it is a general term for the transition matrix structure between martensite and bcc ferrite obtained during low-temperature tempering.

[9]R. H. Aborn, "Low-Carbon Martensites," TRANSACTIONS, American Society for Metals, (Campbell Memorial Lecture) Vol. 48, 1955.

THE INFLUENCE OF MOLYBDENUM AND TUNGSTEN ON TEMPER EMBRITTLEMENT

By A. E. Powers

Abstract

The influence of molybdenum and tungsten up to 2% on the susceptibility of a 1% chromium, 1% manganese steel has been studied. The steels were aged for 1000 hours at various temperatures within the temper embrittling region and the susceptibility to embrittlement was measured from the rise in the transition temperatures. (ASM-SLA Classification: Q23, Ay)

TEMPER brittleness is a familiar ailment of steel to almost any engineer, for it has been a continual problem since the turn of the century when the Krupp organization sought its alleviation in armor plate by quenching after the tempering operation. Since then, our understanding of the characteristics and nature of the embrittlement has naturally progressed; but today it remains a most intriguing phenomenon, because after several decades of research, much more remains to be learned of the factors affecting its development, and a precise description of its mechanism is yet to be established. Before discussing the experimental work of this paper, it should be well to review briefly our knowledge of temper brittleness for the purpose of an easier understanding of the principles and factors involved. (More complete reviews are found in References 1 and 2.)[1]

Measurement of Temper Brittleness

Temper brittleness appears to be an intergranular embrittlement developing most rapidly upon aging in the proximity of 900°F or upon slow cooling through this temperature region. It is evidenced by a decrease in resistance of the steel to brittle fracture. This is interpreted as a lowering of the cohesion strength of the undeformed metal. Such embrittlement is most conveniently measured by fracturing notched-bar specimens at lower and lower temperatures until a brittle type of fracturing appears. The higher this temperature of transition between the ductile and brittle-type fracture, the more brittle the steel. Utilizing a steel free from embrittlement as a base,

[1]The figures appearing in parentheses pertain to the references appended to this paper.

A paper presented before the Thirty-Seventh Annual Convention of the Society, held in Philadelphia, October 17–21, 1955. The author, A. E. Powers is metallurgical engineer, Materials and Processes Laboratory, Large Steam Turbine-Generator Department, General Electric Company, Schenectady. Manuscript received April 4, 1955.

the degree of temper brittleness is judged as being proportional to the rise in the transition temperature above the base transition temperature for any standardized testing method.

In the past, lack of consideration of the embrittlement-free standard has promoted difficulties. First of all, the embrittlement as measured by the increase in fracture-transition temperature is a function of the transformation microstructure of the steel; i.e., pearlite microstructures appear to be less susceptible than martensitic, although there appears to be little difference in behavior between martensitic and bainitic structures (3,4,5). All data dealing with this matter have involved appreciable differences in hardness among the various tempered microstructures. Since it is established that a hard steel is more susceptible than a soft steel (4,6), it is probable that the differences in susceptibility among the various structures are more a result of differences of hardness after tempering than of primary structure, per se.

Furthermore, a coarse-grained steel is more susceptible than a fine-grained steel (4,7,18). If one is to compare the susceptibility of several steels, therefore, all of the steels should be at least acicular in microstructure, but most important, they should be of the same hardness and possess equal austenitic grain size.

Time-Temperature Relationship

The kinetics of the embrittling process can be illustrated by plotting fracture-transition temperatures as a function of both aging temperature and time. Such a diagram, originating from the Watertown Arsenal and one of the most detailed and precise diagrams available, is reproduced in Fig. 1 (8). This diagram alone reveals much about the characteristics of temper brittleness. For example, if the steel is aged at 1000°F, embrittlement develops rapidly but soon reaches an equilibrium state in about 5 hours. On the other hand, if aging takes place at 800°F, embrittlement will develop much more slowly but will proceed continuously for 10,000 hours or more and to more severe values than is possible at higher aging temperatures. The embrittlement can be dissipated in a few minutes by reheating to temperatures above 1050°F and may be redeveloped as many times as desired.

Suggested Mechanism

Numerous theories have been put forth to describe the mechanism of temper brittleness. Most of these theories have dealt with a precipitation; however, no precipitation has ever been identified—only a uniform etching of the grain boundaries is seen. Actually, recent work on copper alloys containing small amounts of antimony has illustrated that a mere intergranular segregation of solute atoms,

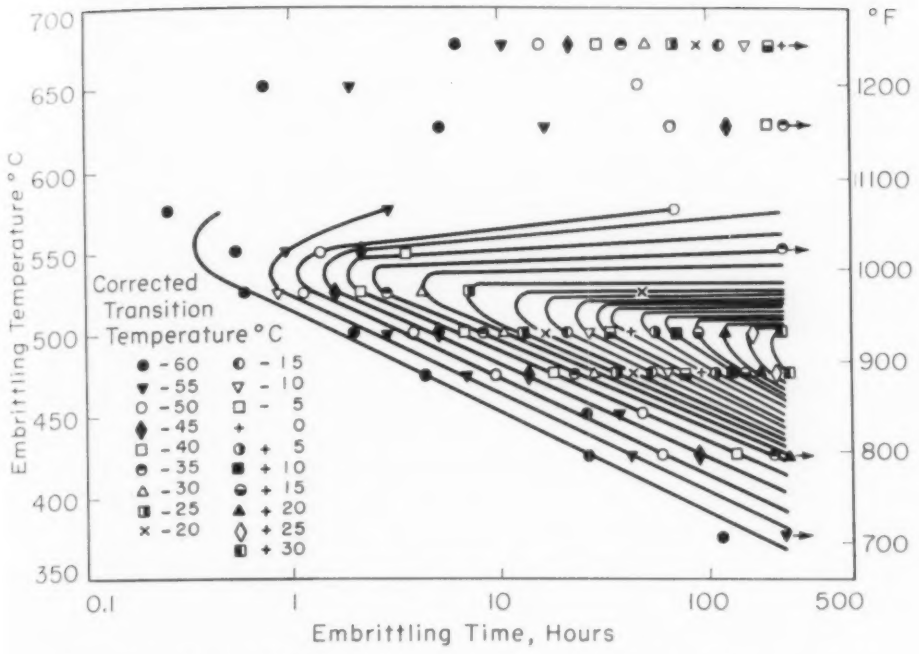


Fig. 1—Isothermal Embrittlement Diagram for SAE 3140 Steel. From Carr, Goldman, Jaffe, and Buffum (8).

rather than a precipitation of a second phase, can bring about considerable intergranular embrittlement (9). This viewpoint could easily be applied to temper brittleness. In essence, by a lowering of interfacial free energy, alloying elements tend to segregate to the major lattice discontinuities particularly the former austenitic grain boundaries. However, reheating to above 1050°F can rapidly disperse the solid-solution segregation (10). A balance is reached between the forces of segregation and thermal dispersion, limiting the intensity of segregation when aging takes place in the vicinity of 1000°F or just above the temperature for maximum embrittlement as is illustrated in Fig. 1.

Influence of Composition

Susceptibility to temper brittleness appears to be almost a sole function of the alloy content of the steel, or more precisely, of the alloying elements dissolved in the ferrite. Some of the more potent elements are phosphorus, manganese, chromium, and, to a lesser extent, nickel.

Peculiarly, however, molybdenum and tungsten—in moderate amounts at least—strongly inhibit the development of embrittlement (11–18). To add perplexity to the phenomenon, there are several indications in the literature that molybdenum in quantities greater than ¾% is no longer effective (13,18,19). A systematic investigation of this matter has never been made. Tungsten seems to

Table I
Composition and Hardness of Steel

Heat No.	COMPOSITION C	Si	Mn	Cr	Mo	W	Brinell Hardness Before Aging
2967	0.24	0.49	0.98	0.95			248,262
2968	0.26	0.44	1.02	0.95	0.50		262,262
2969	0.25	0.30	0.97	0.98	1.01		248,255
2970	0.24	0.41	0.99	1.03	1.51		262,269
2971	0.27	0.40	1.04	0.94	2.00		241,248
2972	0.22	0.40	0.98	0.98		0.50	248,255
2973	0.23	0.20	1.00	0.98		0.97	255,262
2974	0.20	0.28	0.95	0.95		1.47	241,255
2978	0.27	0.28	1.00	0.96		1.90	241,255

behave similarly. Over 20 years ago, Houdremont and Schrader found by observing room-temperature, notched-bar impact tests, that ¾ and 1.0% tungsten were approximately as effective as an equal atomic percentage (0.4 weight %) of molybdenum in suppressing temper embrittlement (20).

Furthermore, Vidal observed that a large amount of tungsten (3.8%) did not have a suppressing effect (19).

In the following paper, a systematic investigation of the effect of molybdenum and tungsten on temper brittleness has been attempted. The results should be of interest not only to academic-minded, but also to those design engineers who are concerned with high temperature, ferritic steels for operation in the vicinity of 700 to 1100°F for thousands of hours as in steam boilers, turbines, heat treating furnaces, chemical-processing equipment, etc. Not only do the steels for such applications invariably contain ½ and higher per cent molybdenum, but as the demand for more creep-resistant steels continues, molybdenum contents tend to increase. Tungsten has been very little used in high temperature ferritic steels because of its high cost; nevertheless, its potentialities should not be ignored.

Materials and Procedure

The steels used for this investigation had a base composition of 1% manganese and 1% chromium with additions of molybdenum and tungsten in amounts of ½, 1, 1½, and 2%. The compositions are listed in Table I.

These nine steels were cast as 55-pound ingots from an induction furnace, using 0.1% aluminum deoxidation. Slabs, ½ inch thick×6 inches wide×5 feet long, were forged from the ingots and subsequently normalized from 1700°F. The slabs were sliced into ½×6×2½ inch plates, from which V-notched charpy specimens were eventually machined after heat treating and aging.

Since susceptibility to temper embrittlement is affected by hardness and austenitic grain size, an attempt was made to keep these properties uniform in all steels. Hardening was done by oil quenching after ½ hour at 2100°F. Austenitic grain sizes ranged

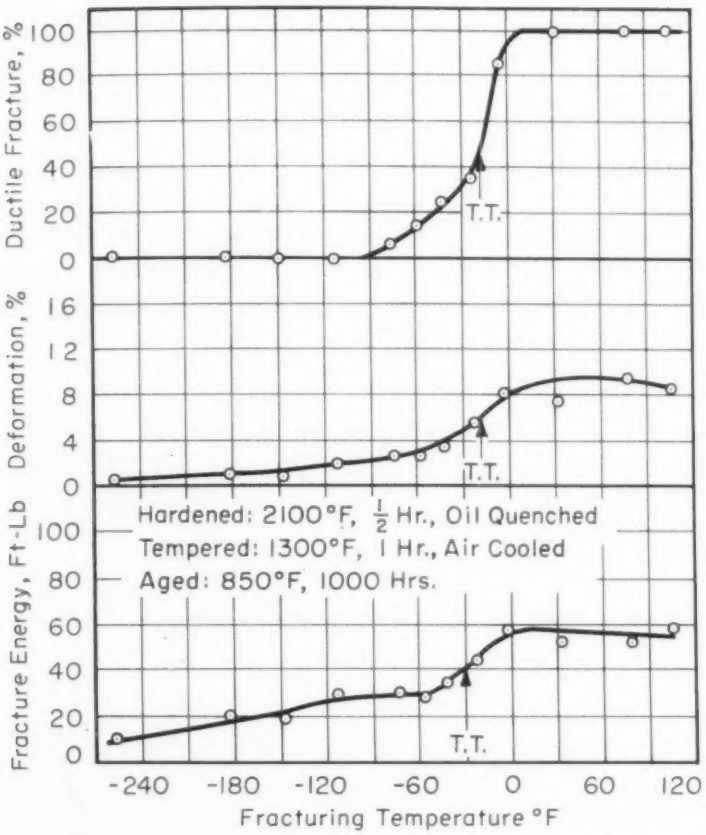


Fig. 2—Results of Fracturing V-notched Charpy Impact Specimens of Steel 2969 (1% Mo).

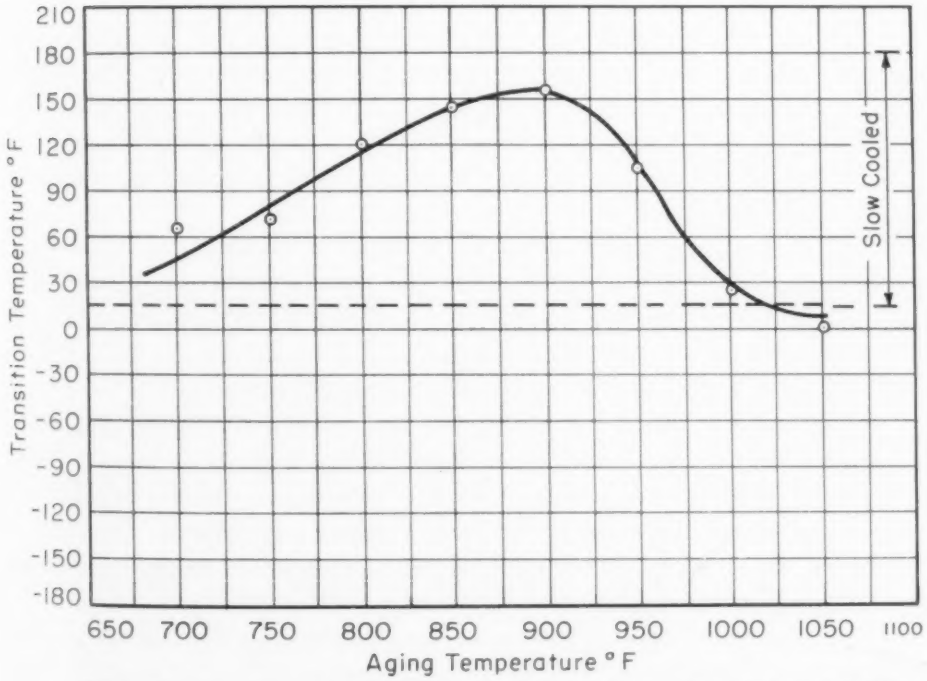


Fig. 3—Fracture Transition Temperatures for Steel 2967 (no Mo or W) After Aging for 1000 Hours at Various Temperatures.

from ASTM No. 3 to 4 except in the ½% tungsten steel which had a grain size of about ASTM No. 1. Each steel was tempered individually to attain approximately 250 Brinell hardness. Table I lists the resulting hardness readings.

Embrittling was done by aging for 1000 hours at temperatures ranging from 700 to 1050°F in 50°F intervals in order to obtain a cross section of the isothermal embrittlement diagram at 1000 hours (see Fig. 1). When transition temperatures are plotted as a function of aging temperature, one would expect the transition temperatures to show a peak at the 900°F aging temperature. One plate, of course, was retained in the unaged condition.

In addition to the isothermal embrittling, each steel was given a slow cooling treatment consisting of heating to 1100°F, cooling to 1075°F, holding for 24 hours, cooling to 1050°F, holding for 24 hours, and so on, until a temperature of 700°F is reached 16 days later.

From each plate was machined twelve V-notch Charpy specimens. The specimens were fractured over a range of temperatures suitable for the construction of transition temperature curves.

Results

Impact Tests on Molybdenum and Tungsten Steels

A sample of the transition temperature curves is given in Fig. 2. The quantities measured on each specimen were energy of fracture, percentage expansion on the compression side of the fracture, and the proportion of the fracture area that was of the shear or ductile type. After examination of all of the curves, the most suitable criteria for transition temperatures were considered to be the 40 ft-lb level on the energy curve, the 6% expansion level on the deformation curve, and the 50% ductile-fracture level on the fracture-appearance curve. The values of these transition temperatures are recorded in Table II of the Appendix.

For correlation purposes, only the transition temperatures derived from the 50% ductile-fracture area were used. The transition temperatures derived from the other two types of measurements—fracture energy and fracture deformation—were used as verifying checks on the fracture-appearance curve.

Figs. 3,4,5,6, and 7 present the transition temperatures after aging for 1000 hours at the various aging temperatures. On the right-hand side of each figure is an indication of the transition temperatures resulting from the slow-cooling operation. The dashed horizontal line represents an estimate of the most probable transition temperatures in the unembrittled condition.

The transition temperatures produced by the slow cooling treatment are on an average a little higher than the maximum

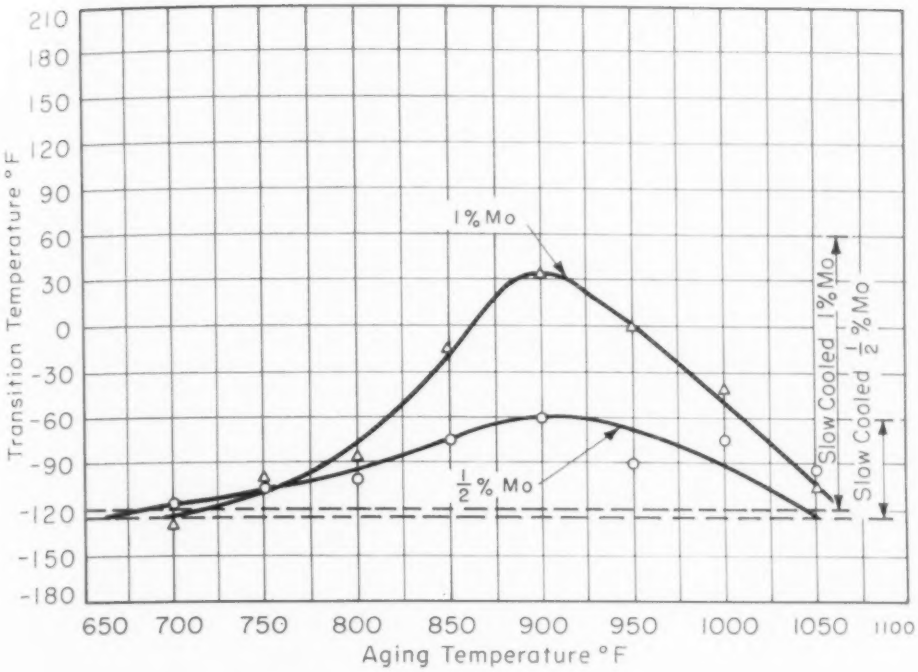


Fig. 4—Fracture Transition Temperatures for Steels 296 (½% Mo) and 2969 (1% Mo) After Aging for 1000 Hours at Various Temperatures.

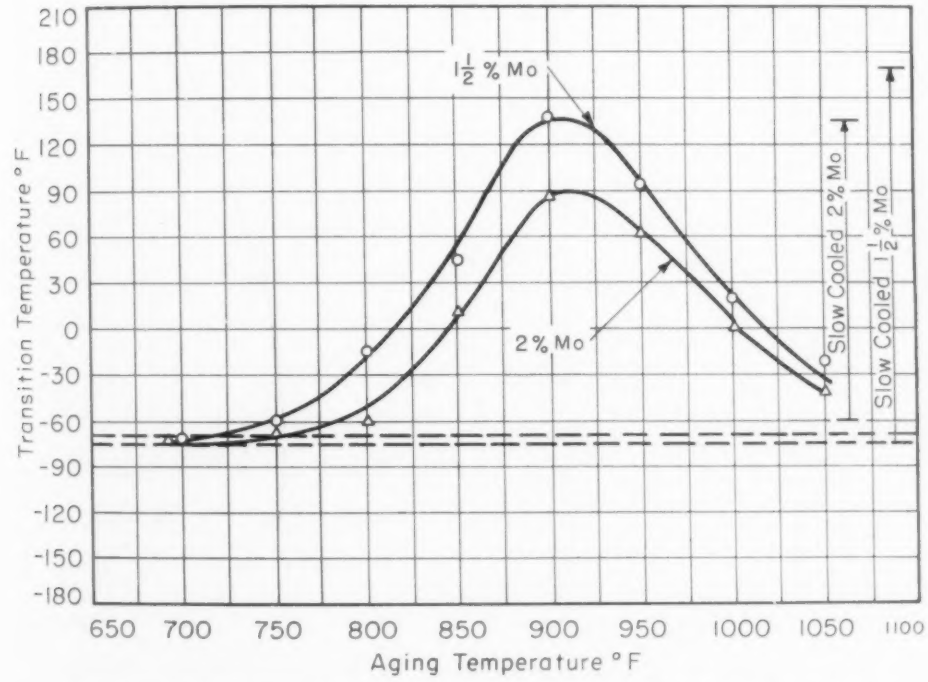


Fig. 5—Fracture Transition Temperatures for Steels 2970 (1½% Mo) and 2971 (2% Mo) After Aging for 1000 Hours at Various Temperatures.

transition temperatures produced by isothermal aging, which, in all cases, was at a temperature around 900°F. Slightly more embrittle-

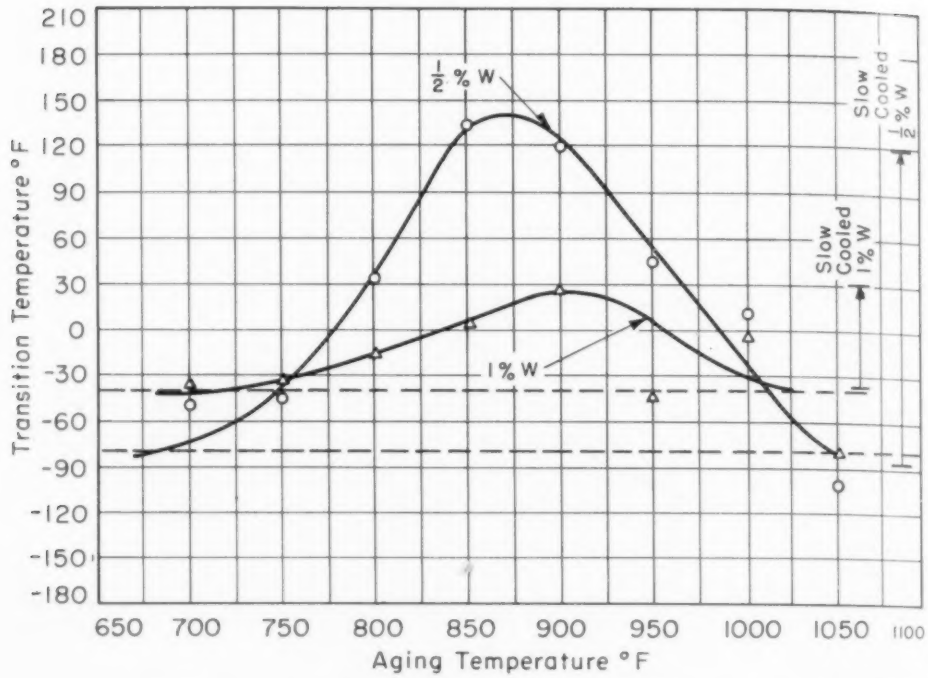


Fig. 6—Fracture Transition Temperatures for Steels 2972 (½% W) and 2973 (1% W) After Aging for 1000 Hours at Various Temperatures.

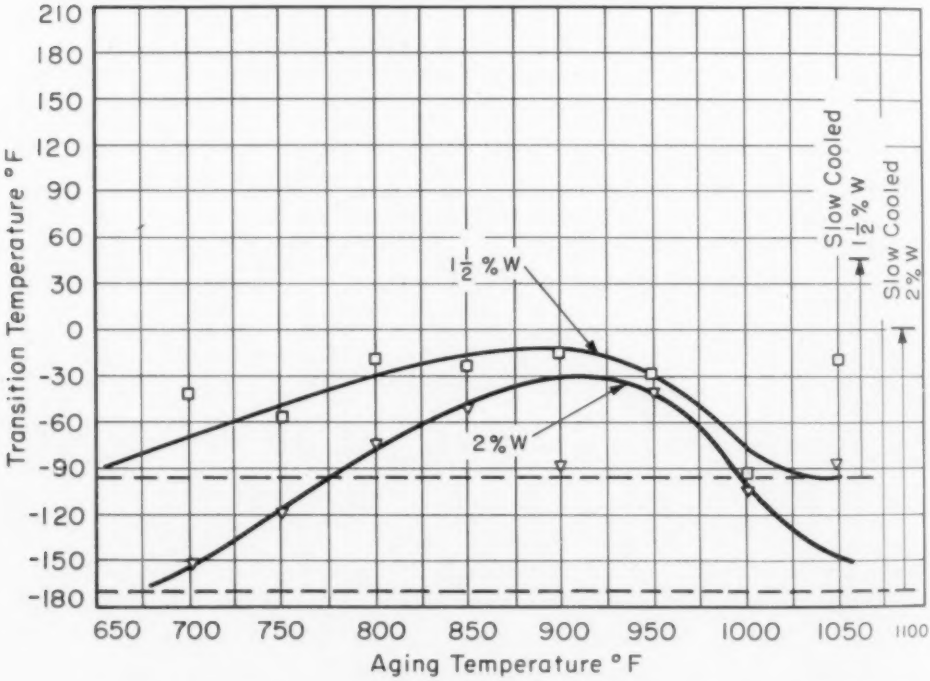


Fig. 7—Fracture Transition Temperatures for Steels 2974 (1½% W) and 2978 (2% W) After Aging for 1000 Hours at Various Temperatures.

ment occurred, in other words, during slow cooling within a period of 2 weeks than was possible during isothermal aging for six weeks.

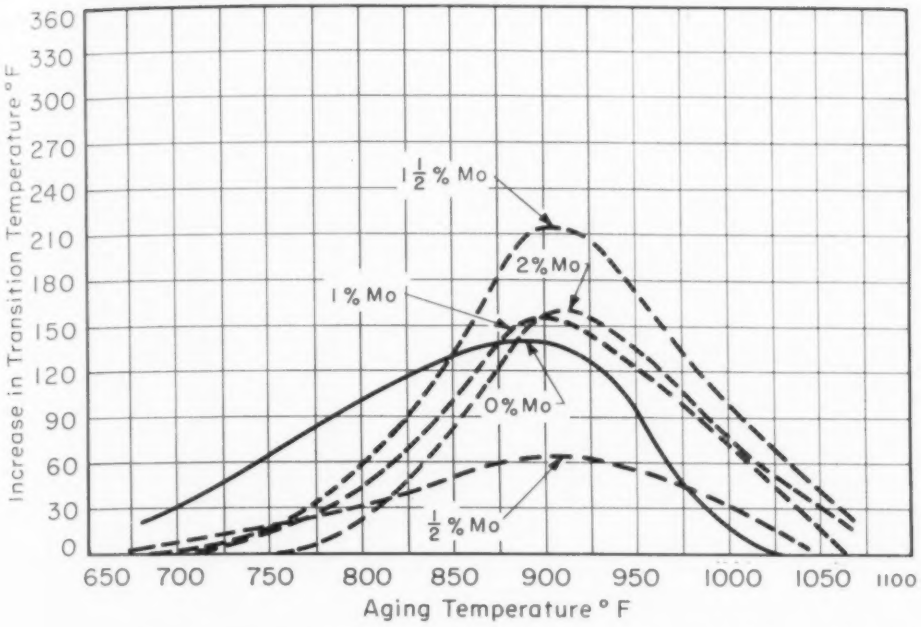


Fig. 8—Development of Temper Embrittlement by the Molybdenum Steels Upon Aging for 1000 Hours at Various Temperatures.

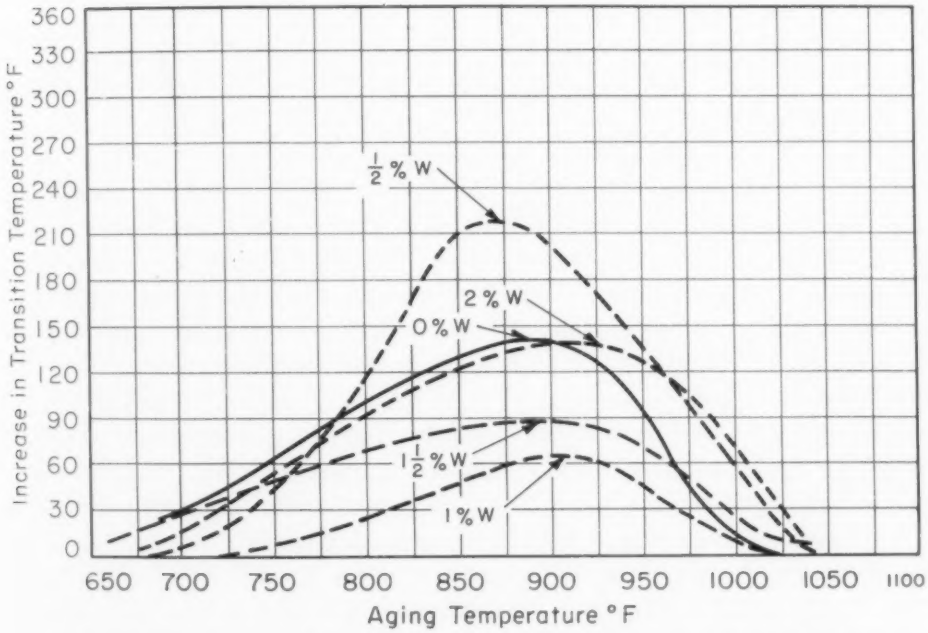


Fig. 9—Development of Temper Embrittlement by the Tungsten Steels Upon Aging for 1000 Hours at Various Temperatures.

One can visualize how this can come about by re-examining Fig. 1. During slow cooling, embrittlement develops rapidly in the upper regions of the embrittling range, but is restricted early by the attainment of equilibrium. As cooling progresses, embrittlement can proceed further; thus during slow cooling, there is an initial time

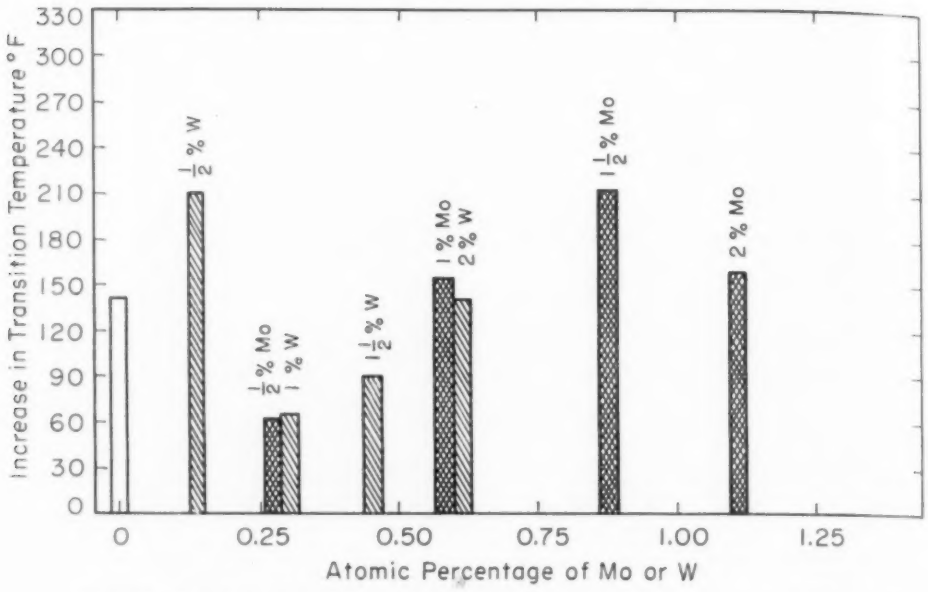


Fig. 10—Development of Temper Embrittlement by Molybdenum and Tungsten-Containing Steels Upon Aging for 1000 Hours at 900°F.

advantage not possessed by an isothermal aging treatment at 900°F.

When attempting to compare the embrittlement curves of Figs. 3,4,5,6, and 7, a difficulty arises in that the transition temperatures for the unembrittled condition vary among the steels. Can the rise in transition temperature upon temper embrittlement of a steel with an initially high transition temperature be directly compared with the increase in transition temperature of a tougher steel? There is no information to the contrary for acicular structures and, until there is, it is judged proper to compare the actual increases in transition temperature upon embrittlement without applying correction factors that are governed by the unembrittled transition temperatures.

Figs. 8 and 9 present direct compilations of the previous embrittlement curves. Maximum embrittlement is least for ½% molybdenum and 1% tungsten. One, 1½, and 2% molybdenum and also 2% tungsten do not appear effective in suppressing the susceptibility exhibited by the chromium-manganese base composition. This suggests that tungsten behaves in a manner similar to molybdenum in its effect upon temper brittleness when considered on an atomic-percentage basis. Fig. 10, a plot of the embrittlement for 1000 hours at 900°F as a function of atomic percentage of molybdenum and tungsten, is a clear illustration of the behaviors of these two elements and of the equivalence of tungsten. The anomalously high degree of embrittlement exhibited by the ½% tungsten steel may possibly be a result of the unusually large austenitic grain size of this steel. A

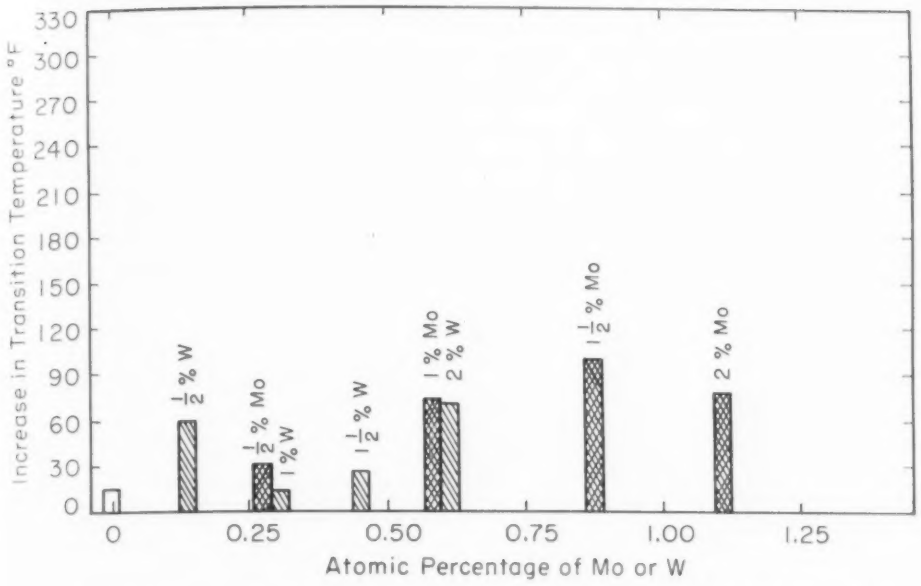


Fig. 11—Development of Temper Embrittlement by Molybdenum and Tungsten-Containing Steels Upon Aging for 1000 Hours at 1000°F.

spectrographic analysis of the total aluminum content of this steel and of a few others indicated that perhaps the ½% steel did not receive sufficient aluminum deoxidation to inhibit rapid grain growth at 2100°F. The aluminum contents are as follows:

½% Mo, 2968—0.102% Al—ASTM #4
½% W, 2972—0.072% Al—ASTM #1
1 % W, 2973—0.093% Al—ASTM #4
1½% W, 2974—0.081% Al—ASTM #3

Maximum embrittlement occurs at or near 900°F for all steels; although there appears to be a slight upward shift in optimum embrittling temperature as molybdenum and tungsten increase.

When considering embrittlement at a high temperature of 1000°F all of the molybdenum and tungsten steels showed equal or greater susceptibility than the chromium-manganese base composition as illustrated specifically in Fig. 11. On the other hand, at relatively low aging temperatures, all of the molybdenum and tungsten steels (with the exception of the "out-of-order" ½% tungsten steel) show less susceptibility than the base composition. This is shown for 800°F aging in Fig. 12. In fact, the 2% molybdenum steel shows the lowest susceptibility of all the steels at aging temperatures below 825°F. Thus when considering the optimum molybdenum or tungsten content for minimum susceptibility one must consider the operating or aging temperature. For slow cooling operations, however, ½% molybdenum or 1% tungsten are optimum and equivalent.

In the past there has often been speculation as to whether

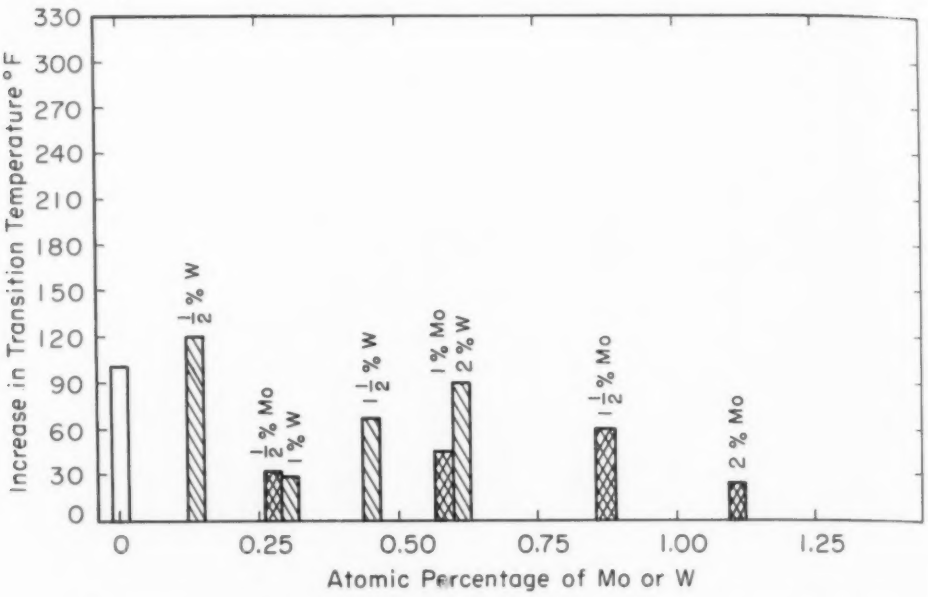


Fig. 12—Development of Temper Embrittlement by Molybdenum and Tungsten-Containing Steels Upon Aging for 1000 Hours at 800°F.

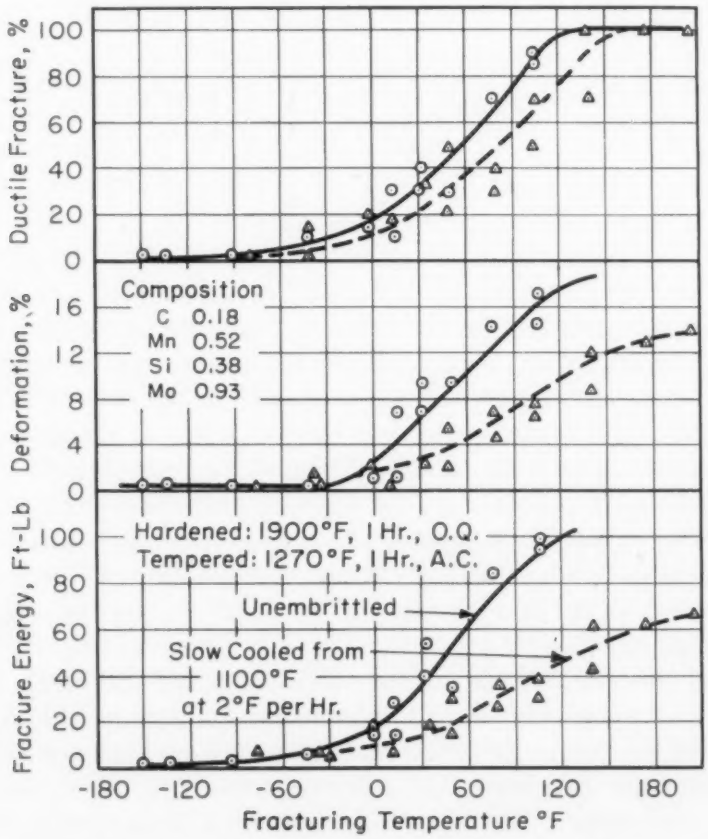


Fig. 13—Results of Fracturing V-Notched Charpy Specimens of a Molybdenum Steel in the Unembrittled and Embrittled Condition.

molybdenum reduces susceptibility by reducing the total amount of embrittlement that can occur or by reducing the rate of embrittlement (1, 12, 16). Examination of Fig. 8 shows that a reduction of the rate of embrittlement definitely occurs at temperatures of 800°F and below, and at 750°F the reduction unhaltingly continues with increasing molybdenum content up to 2%. The action of tungsten is similar but not as definite. At temperatures above 900°F however, a converse behavior by molybdenum and tungsten is encountered; the equilibrium degree of embrittlement is advanced to higher intensities as the elements are added. Even ½% molybdenum, which strongly inhibits temper embrittlement at lower temperatures, increases the equilibrium degree of embrittlement at 1000°F. Doubtlessly, this augmentation of equilibrium embrittlement plays a part in the high susceptibility of the steels containing large amounts of molybdenum and tungsten. Nevertheless, a reversal in the rate of embrittlement must still occur at temperatures above 850°F, for as Fig. 8 shows, the 1, 1½ and 2% molybdenum steels embrittle more rapidly at 900°F than the molybdenum-free steel. An augmentation of the equilibrium embrittlement for aging treatments above 900°F cannot fully account for the high rate of embrittlement of the high-molybdenum and tungsten steels at 900°F.

Tests on a Carbon-Molybdenum Steel

The steels discussed so far were composed of a base composition possessing considerable susceptibility to temper brittleness. In order to investigate briefly the effect of molybdenum on a steel of low susceptibility, a steel of the following composition was made:

C	Mn	Si	Mo
0.18	0.52	0.38	0.93

The steel, after forging and heat treating, was embrittled by the 16-day stepped-cooling process described previously. The V-notched Charpy impact data for the embrittled and unembrittled specimens are given in Fig. 13. The increase in transition temperature upon embrittling is slight and is what would be expected from a ½% manganese steel. One-per cent molybdenum apparently does not contribute any susceptibility—neither does it suppress embrittlement.

Conclusions

Molybdenum and tungsten have been found to have a complex influence on the temper brittleness of a 1% chromium, 1% manganese steel. When aging at a temperature to promote maximum rate of embrittlement (900°F for 1000 hours) ½% molybdenum or 1% tungsten strongly inhibited temper brittleness. The effectiveness of both elements diminished at high percentages with the result

that the 1, 1½, and 2% molybdenum steels and the 2% tungsten steels possessed susceptibilities at least equal to that of the chromium-manganese base composition.

At sufficiently higher temperatures, such as at 1000°F, the equilibrium degree of embrittlement was increased by all molybdenum and tungsten contents up to 2%. On the other hand, at relatively low aging temperatures of 800°F and lower, the rate of embrittlement was diminished by all molybdenum and tungsten contents up to 2%. In all cases, the influence of tungsten is similar to that of molybdenum for equal atomic percentages and can be equally as effective in inhibiting the embrittlement. For slow cooling operations, the ½% molybdenum and 1-per cent tungsten compositions are optimum for minimum embrittlement.

Slow cooling from the tempering temperature over a period of 2 weeks will produce a degree of embrittlement at least equal to that resulting from isothermal aging for 6 weeks at the optimum embrittling temperature.

ACKNOWLEDGMENT

Credit is given to the assistance of C. J. Giedroc in performing the numerous impact tests. Appreciation is expressed to the Large Steam Turbine-Generator Department of the General Electric Company for making this investigation possible.

References

1. J. H. Hollomon, "Temper Brittleness," TRANSACTIONS, American Society for Metals, Vol. 36, 1946, p. 473.
2. B. C. Woodfine, "Temper Brittleness: A Critical Review of the Literature," *Journal*, Iron and Steel Institute, Vol. 173, Part 3, 1953, p. 229.
3. W. S. Pellini and B. R. Queneau, "Development of Temper Brittleness in Alloy Steels," TRANSACTIONS, American Society for Metals, Vol. 39, 1947, p. 139.
4. B. C. Woodfine, "Some Aspects of Temper Brittleness," *Journal*, Iron and Steel Institute, Vol. 173, Part 3, 1953, p. 240.
5. D. C. Buffum and L. D. Jaffe, "Some Effects of Microstructure Upon Temper Brittleness," *Journal of Metals*, Vol. 5, 1953, No. 10, p. 1373.
6. G. W. Austin, A. R. Entwisle and G. C. Smith, "Effect of Arsenic and Antimony on Temper Brittleness," *Journal*, Iron and Steel Institute, Vol. 173, Part 4, 1953, p. 376.
7. A. Hurlich, Written discussion to paper by S. A. Herres and C. H. Lorig, "Influence of Metallurgical Factors on the Mechanical Properties of Steel," TRANSACTIONS, American Society for Metals, Vol. 40, 1948, p. 805.
8. F. L. Carr, M. Goldman, L. D. Jaffe, and D. C. Buffum, "Isothermal Temper Embrittlement of SAE 3140 Steel," *Journal of Metals*, Vol. 5, 1953, p. 998.
9. D. McLean, "The Embrittlement of Copper-Antimony Alloys at Low Temperatures," *Journal*, Institute of Metals, Vol. 20, 1952, p. 121.
10. A. E. Powers, Written discussion to paper by J. W. Spretnak and R. Speiser, "A Hypothesis for the Boron Hardenability Mechanism," TRANSACTIONS, American Society for Metals, Vol. 46, 1954, p. 1123.
11. R. H. Greaves and J. J. A. Jones, "Temper Brittleness of Steel," *Journal*, Iron and Steel Institute, Vol. 111, No. 1, 1925, p. 231.
12. F. C. Lea and R. N. Arnold, "The Embrittlement of Alloy Steels," *Proceedings*, Institute of Mechanical Engineers, London, Vol. 131, 1935, p. 539.

Appendix

Table II
Transition Temperatures

Embrittling Treatment	Transition Temperature, Degrees F: 40 Ft-Lbs Energy	6% Deformation	50% Ductile Fracture
Heat 2967			
None	0	0	+ 15
Slow cooled	+180	+140	+180
700°F—1000 hours	+ 70	+ 70	+ 70
750	+ 70	+ 65	+ 70
800	+135	+120	+120
850	+155	+140	+145
900	+150	+150	+155
950	+112	+105	+105
1000	+ 20	+ 10	+ 25
1050	− 15	− 25	0
Heat 2968—½ Mo			
None	−120	−110	−125
Slow cooled	− 50	− 60	− 60
700°F—1000 Hrs.	−115	−100	−115
750	−105	−105	−105
800	−130	−120	−100
850	− 75	− 60	− 75
900	− 75	− 80	− 60
950	− 70	− 70	− 90
1000	− 75	− 75	− 75
1050	− 85	− 90	− 95
Heat 2969—1 Mo			
None	−135	−120	−120
Slow cooled	+ 60	+ 60	+ 60
700°F—1000 hrs.	−135	−120	−130
750	−115	−105	−100
800	−105	− 90	− 85
850	− 30	− 25	− 15
900	+ 30	+ 30	+ 35
950	+ 10	0	0
1000	− 40	− 35	− 40
1050	−105	−100	−105
Heat 2970—1½ Mo			
None	− 75	− 75	− 85
Slow cooled	+220	+200	+170
700°F—1000 hrs.	− 60	− 60	− 70
750	− 55	− 45	− 60
800	− 10	− 10	− 15
850	+ 45	+ 45	+ 45
900	+150	+150	+140
950	+120	+120	+ 95
1000	+ 20	+ 20	+ 20
1050	− 10	0	− 20
Heat 2971—2 Mo			
None	− 75	− 65	− 60
Slow cooled	+140	+130	+135
700°F—1000 hrs.	− 60	− 65	− 70
750	− 75	− 60	− 65
800	− 45	− 60	− 60
850	0	+ 10	+ 10
900	+100	+100	+ 75
950	+ 60	+ 60	+ 60
1000	+ 10	0	0
1050	− 35	− 35	− 40

13. E. Maurer, O. H. Wilms and H. Kiessler, "Brittleness in Alloy Steels," *Stahl and Eisen*, Vol. 62, 1942, p. 81 and 115.
14. H. Jolivet and G. Vidal, "Value of the Resilience Test for the Study of Temper Brittleness," *Revue De Metallurgie*, Vol. 41, 1944, p. 378 and 403.
15. A. P. Taber, J. F. Thorlin and J. F. Wallace, "Influence of Composition on Temper Brittleness in Alloy Steels," TRANSACTIONS, American Society for Metals, Vol. 42, 1950, p. 1033.

Table II Cont'd

Embrittling Treatment	Transition Temperature, degrees F 40 Ft-Lbs Energy	6% Deformation	50% Ductile Fracture
Heat 2972—½ W			
None	− 90	− 85	− 85
Slow cooled	+130	+110	+120
700°F—1000 hrs.	− 65	− 65	− 50
750	− 65	− 60	− 45
800	+ 40	+ 30	+ 35
850	+130	+120	+135
900	+120	+120	+120
950	+ 30	+ 25	+ 45
1000	+ 10	+ 5	+ 20
1050	−100	−100	−100
Heat 2973—1 W			
None	− 35	− 25	− 35
Slow cooled	+ 10	+ 5	+ 30
700°F—1000 hrs.	− 40	− 40	− 40
750	− 45	− 45	− 35
800	− 35	− 45	− 15
850	− 10	− 20	+ 5
900	+ 5	+ 5	+ 25
950	− 55	− 55	− 45
1000	− 5	− 15	+ 5
1050	−120	−105	− 80
Heat 2974—1½ W			
None	−130	−105	− 95
Slow cooled	+ 40	+ 35	+ 45
700°F—1000 hrs.	− 45	− 60	− 40
750	− 75	− 60	− 55
800	− 30	− 25	− 20
850	− 45	− 50	− 25
900	− 25	− 25	− 15
950	− 45	− 45	− 30
1000	−100	− 90	− 95
1050	− 40	− 40	− 20
Heat 2978—2 W			
None	−170	−160	−170
Slow cooled	0	− 15	0
700°F—1000 hrs.	−160	−145	−150
750	−130	−115	−120
800	− 90	− 90	− 75
850	− 65	− 60	− 50
900	− 85	− 85	− 90
950	− 45	− 55	− 40
1000	−105	−100	−105
1050	− 90	− 95	− 85

16. A. Preece and R. D. Carter, "Temper Brittleness in High-Purity Iron-Base Alloys," *Journal*, Iron and Steel Institute, Vol. 173, Part 4, 1953, p. 387.
17. G. Bhat and J. F. Libsch, "Isothermal Embrittlement in Chromium and Molybdenum Alloy Steels During Tempering," *Journal of Metals*, February 1955, p. 330.
18. R. Hultgren and J. C. Chang, "Investigation of the Temper Brittleness of Steel—Effect of Chemical Composition," Final Report, University of California, February 15, 1951.
19. G. Vidal, "Temper Brittleness in Chromium, Molybdenum, and Tungsten Steels," *Revue de Metallurgie*, Vol. 42, 1945, p. 149.
20. E. Houdremont and H. Schrader, "The Problem of Temper Brittleness," *Archiv fur das Eisenhuttenwesen*, Vol. 7, 1933, p. 49.

HARDNESS OF TEMPERED MARTENSITE IN CARBON AND LOW ALLOY STEELS

By R. A. Grange and R. W. Baughman

Abstract

The hardness of martensite in a number of plain carbon and alloy steels after tempering for various combinations of temperature and time is presented and data compared to reveal the effect of carbon and alloying elements. An empirical method for estimating, within limits, from chemical composition the hardness of tempered martensite was developed from these data. (ASM-SLA Classification: Q29, ST)

Introduction

STEELS containing more than about 0.2% carbon are too brittle for use in the quenched condition and are softened to some desired degree by tempering prior to use. The tempering operation is thus a very common one and the tempering cycle is usually selected by trial and error. Because it is conveniently measured, hardness is often used as the criterion of the other mechanical properties developed by a tempering cycle. The degree of softening resulting from a particular tempering cycle is dependent upon composition of the steel and its prior structure. For a prior martensitic structure, the effect of difference in composition has been extensively studied(1),[1] but because both time and temperature of tempering are interrelated variables affecting the result, quantitative evaluation of the effect of carbon and alloying elements on resistance to softening during tempering has been difficult. By combining the effect of temperature and time of tempering into a single functional variable, or parameter, Hollomon and Jaffe (2) have provided a much-needed simplification and have put it to use in developing a broad rationalization of time-temperature effects in the tempering of steel. (ASM-SLA Classification: Q29, ST).

A considerable number of measurements revealing the hardness of martensite in a variety of steels after tempering for various times and temperatures have been accumulated at our Laboratory. It occurred to us that these data should be analyzed by the method developed by Hollomon and Jaffe, especially because the latters' own analysis was handicapped by lack of a sufficient quantity of carefully measured data. When this was attempted, it developed that,

[1]The figures appearing in parentheses pertain to the references appended to this paper.

A paper presented before the Thirty-Seventh Annual Convention of the Society, held in Philadelphia, October 17–21, 1955. The authors, R. A. Grange and R. W. Baughman, are associated with the Fundamental Research Laboratory, United States Steel Corp., Kearny, N.J. Manuscript received April 8, 1955.

although the Hollomon and Jaffe tempering parameter was a most useful concept, it was desirable to use a somewhat different approach than that adopted by these authors to the problem of relating the hardness of tempered martensite to steel composition.

Experimental Procedure

The composition of each steel whose tempering behavior is considered in this paper is given in Table I. All these steels were commercial heats and were rolled or forged to a size smaller than 2 inches in diameter.

Specimens were always sufficiently small to insure quenching entirely to martensite except for a small percentage of retained austenite present in such steels quenched to room temperature. Steels containing less than 0.45% carbon were quenched in brine, others in oil. Austenitizing temperatures were within the range recommended for each corresponding grade of steel (3). Prior to quenching, carbides were essentially all dissolved in austenite with the exception of the 6145 steel which, due to the presence of vanadium, contained a few small undissolved carbides.

Lead alloy baths were used for tempering, during which temperature was maintained within 5°F of that specified. After temper-

Table I
Composition of Steels

AISI-SAE Type	Composition—%									
	C	Mn	P	S	Si	Ni	Cr	Mo	V	Other
1026	0.25	0.79	0.012	0.026	0.11					
1030	0.31	0.57	0.008	0.025	0.09	0.02	0.02			
1035	0.36	0.74	0.019	0.030	0.24	0.02	0.02	0.01		
1040	0.40	0.60	0.010	0.013	0.27	0.02	0.07	0.01		
1042	0.44	0.79	0.020	0.030	0.24	0.02	0.02	0.01		
1045	0.45	0.73	0.017	0.030	0.17	0.01	0.02	0.01		
1038	0.39	0.75	0.048	0.043	0.18					
1049	0.48	0.76	0.046	0.048	0.14					
1050	0.50	0.91	0.046	0.041	0.13					
1065	0.63	0.87	0.023	0.018	0.17	0.02	0.04	0.00		
1065	0.65	0.87	0.040	0.042	0.19					
1080	0.82	0.75	0.054	0.055	0.30					
4027	0.26	0.87	0.015	0.030	0.29	0.03	0.06	0.26		
4037	0.35	0.80	0.022	0.028	0.24	0.06	0.06	0.25		
4047	0.48	0.94	0.015	0.030	0.16	0.04	0.03	0.25		
4068	0.68	0.87	0.024	0.029	0.26	0.01	0.03	0.24		
1335	0.35	1.85	0.020	0.026	0.19	0.01	0.03	0.00		
2340	0.37	0.68	0.014	0.021	0.21	3.41	0.05	0.00		
3140	0.38	0.72	0.019	0.033	0.21	1.32	0.49	0.00		
4140	0.37	0.77	0.019	0.026	0.15	0.04	0.98	0.21		
4340	0.42	0.78	0.018	0.027	0.24	1.79	0.80	0.33		
4640	0.36	0.63	0.018	0.021	0.19	1.84	0.06	0.23		
5140	0.42	0.68	0.026	0.032	0.16	0.07	0.93	0.00		
6145	0.43	0.74	0.019	0.024	0.23	0.06	0.92		0.16	
9264	0.55	0.78	0.012	0.022	1.62	0.00	0.77	0.01		
Nitriding Steel	0.41	0.57	0.017	0.005	0.24	0.17	1.57	0.36		Al–1.26

Table II
Tempering Data for Plain Carbon Steels SAE-AISI 10XX Series

Time (Hours)	Temp. °F	Diamond Pyramid Hardness 1026	1030	1035	1040	1042	1045	Rockwell "C" Hardness 1038	1049	1050	1065	1065	1080
0.167	400	523	547	550	564	598	631	—	—	57.1	—	—	62.7
(10	500	490	502	520	543	571	594	—	—	—	—	—	—
mins.)	600	432	439	470	499	514	533	—	—	51.3	—	—	57.6
	700	396	393	439	446	467	487	—	—	—	—	—	—
	800	364	366	377	391	413	427	—	—	45.8	—	—	50
	900	311	305	329	344	357	371	—	—	—	—	—	—
	1000	275	272	290	307	318	329	—	—	36	—	—	42
	1100	255	249	270	285	290	295	—	—	—	—	—	—
	1200	223	214	242	261	258	262	—	—	—	—	—	—
	1300	197	203	212	237	226	229	—	—	—	—	—	—
	400	499	505	537	554	586	618	51.5	55	56	58.3	59.2	61.3
	500	459	459	499	520	543	564	49	52	54	55.9	56.5	59.5
	600	418	415	465	481	499	517	46	49	50	52.4	53.5	56.7
	700	383	385	409	422	444	459	41.5	44	46.5	49.5	50	51
	800	329	334	353	370	387	398	37	40	41	44.8	45	47
	900	291	294	307	326	336	348	32.5	35.5	37.7	39.7	41.5	43.2
	1000	252	251	274	289	298	305	28	30.5	32.6	34.5	36.5	38.8
	1100	—	—	244	264	265	269	22.2	24.5	27.2	29.7	31.2	32.5
	1200	201	197	219	242	233	239	18.2	19	18.5	23.4	25.8	27
	1300	185	191	200	218	205	208	—	—	—	16.7	—	—
4	400	481	490	515	530	564	586	—	—	—	—	—	—
	500	444	446	490	508	523	554	—	—	—	—	—	—
	600	400	400	446	467	487	502	—	—	—	—	—	—
	700	362	364	383	404	422	439	—	—	—	—	—	—
	800	314	312	333	346	364	375	—	—	—	—	—	—
	900	275	271	293	309	320	328	—	—	—	—	—	—
	1000	241	242	260	277	277	286	—	—	—	—	—	—
	1100	212	194	231	254	249	251	—	—	—	—	—	—
	1200	188	185	203	223	216	224	—	—	—	—	—	—
	1300	179	180	185	201	189	194	—	—	—	—	—	—
24	400	454	470	502	523	547	575	—	—	53.6	—	—	60
	500	429	434	473	493	511	533	—	—	—	—	—	—
	600	398	400	432	446	462	478	—	—	48.7	—	—	53.5
	700	337	346	360	375	396	409	—	—	—	—	—	—
	800	290	286	311	326	339	353	—	—	39.5	—	—	43.8
	900	258	256	266	286	290	299	—	—	—	—	—	—
	1000	230	217	241	261	256	262	—	—	26.5	—	—	32
	1100	194	177	211	230	222	229	—	—	—	—	—	—
	1200	164	159	187	207	196	200	—	—	—	—	—	—
	1300	166	163	172	192	181	190	—	—	—	—	—	—

ing, specimens were carefully ground and, in many instances, polished as though for metallographic examination. Hardness was measured with the Rockwell tester and often with the Vickers tester as well. Hardness impressions were located midway between surface and center of the cross-section to minimize any possible effect of segregation. Each hardness value listed in Table II for carbon steels and Tables III and IV for alloy steels is the average of ten measurements per specimen.

Method of Graphically Summarizing Tempering Data

Typical of the results are those listed in Table III for a 1335 steel. A range of tempering temperatures from 400 to 1200°F, and a range of time from 40 seconds to 32 hours is covered. They may be plotted, as in Fig. 1, with hardness as a function of time and each temperature individually represented by a curve; an alternative method would involve plotting hardness as a function of tempera-

Table III
Tempering Data for SAE Alloy Steels

Time Hours	Temperature°F	Diamond Pyramid Hardness 1335	2340	3140	4140	4340	4640	5140	6140
0.011	800	446	432	444	482	500	450	489	502
(40 secs.)	1000	371	361	378	421	435	383	416	409
	1100	340	331	344	385	400	358	388	392
	1200	309	307	315	343	377	330	346	381
0.033	800	426	408	438	472	481	427	479	489
(2 mins.)	1000	353	340	366	406	434	381	395	399
	1100	326	320	331	371	414	350	377	380
	1200	299	283	302	335	365	325	341	373
0.083	800	419	391	424	464	472	418	466	481
(5 mins.)	1000	341	324	350	394	431	376	384	393
	1100	324	303	313	355	391	336	356	373
	1200	288	277	292	332	348	307	317	361
0.25	800	390	384	411	451	451	416	453	461
(15 mins.)	1000	330	314	335	384	405	362	373	382
	1100	300	284	303	339	388	333	336	354
	1200	270	262	276	314	338	293	309	350
1	400	539	543	547	585	593	546	596	593
	500	495	510	507	531	545	513	541	544
	600	470	473	482	496	506	476	509	517
	700	440	421	446	486	496	439	491	493
	800	382	366	398	448	456	398	437	450
	900	337	331	350	403	423	365	386	403
	1000	305	303	313	373	389	331	344	373
	1100	281	271	286	346	365	311	313	354
	1200	247	240	265	311	322	266	285	304
2	400	532	546	545	581	586	542	584	583
	600	465	461	468	490	510	466	509	515
	800	370	359	379	436	448	388	424	436
	1000	293	284	301	355	383	326	327	360
	1200	229	227	249	286	269	246	296	280
4	400	527	540	537	568	576	535	575	570
	600	464	454	472	499	505	463	504	511
	800	365	349	376	433	443	386	417	431
	1000	285	274	290	352	376	323	318	351
	1200	220	222	241	275	258	242	290	270
8	400	522	544	522	559	572	535	570	568
	600	466	450	463	503	509	456	503	507
	800	364	348	366	430	439	380	407	422
	1000	278	266	283	345	376	319	314	352
	1200	211	217	230	265	248	231	276	259
16	400	525	540	521	561	566	531	568	568
	600	469	446	466	507	508	459	502	510
	800	359	346	363	420	437	378	403	423
	1000	270	261	276	340	370	314	303	348
	1200	203	212	217	256	234	222	262	244
32	400	519	534	525	555	564	524	558	560
	600	467	440	464	501	505	452	500	505
	800	356	338	355	420	440	377	399	418
	1000	262	254	268	335	358	309	296	344
	1200	200	206	210	244	225	216	254	235

ture with each time represented by a curve. Either type of chart adequately describes the softening of martensite on tempering; however, such plots are tedious to construct, require many measurements, and reliable interpolation is relatively difficult.

The tempering parameter proposed by Hollomon and Jaffe (2) is $T(c+\log t)$, where T is the absolute temperature equal to °F+460, t the time, and c a so-called constant for a particular steel. The value

Table IV
Hardness of Tempered Martensite in SAE-AISI 40XX Steels, 9264 and Nitriding Steel

Hours	Temp. °F	Rockwell "C" Hardness 4027	4037	4047	4068	9264	Nitriding Steel
0.167 (10 Mins.)	400	50.3	52.6	57.5	61.5	61	55.3
	500	46.4	51	53.9	58.5	59.3	53.4
	600	43	47.6	50.7	55	58.8	52.7
	700	40.7	45	48	52	57.5	51.0
	800	38	42	45	49	54.8	49.8
	900	34.8	38.5	41.6	44.9	49.8	46.2
	1000	31.5	35.6	39	41.6	45.2	43.2
	1100	28.6	32.7	34.6	37.5	41.3	41.0
	1200	25	28.5	29.5	33.5	39.2	35.5
	1300	20.5	23	25	28	34.7	31.6
1	400	49	51.6	55.5	59.5	59.9	54.2
	500	45.5	49	51.5	57	58.9	53.0
	600	42.5	47	49.5	53.5	58.3	52.6
	700	39.7	43.9	46.5	50.5	56.7	50.7
	800	35.9	40.5	43.2	47	51.9	47.9
	900	32.5	37	40	43.5	47.0	45.0
	1000	29.7	34	36.5	39.5	42.1	42.5
	1100	27	31	33	35.2	38.8	37.7
	1200	22	25	26.2	29.5	34.2	33.3
	1300	15.5	18	19.5	21.2	29.0	27.5
4	400	47.5	51.5	55	58.7	59.1	53.5
	500	45	48.1	50.9	56	58.6	52.6
	600	41.5	45.7	48	52.7	58.1	51.7
	700	38.7	42.9	46	49.5	55.5	50.3
	800	35	39.5	42.5	45.7	50.0	46.6
	900	32	36.1	39	42	45.0	44.7
	1000	29.1	32.5	35.5	37.5	40.8	42.1
	1100	25	29.5	31	32.5	36.7	35.9
	1200	19	22.2	22.5	25	30.5	31.3
	1300	12	13.5	14	17	25.5	23.5
24 (22 hrs. for Nitriding Steel)	400	46	50.7	53.5	58.5	58.9	53.2
	500	44.2	47.7	50.2	55.5	58.5	52.5
	600	40.7	45.2	47.5	52	57.7	50.8
	700	37.5	41.5	44.5	47.5	53.5	49.0
	800	34.1	38.5	41.5	44.5	48.3	45.6
	900	31	35	38	40.5	42.9	43.6
	1000	28.1	31.5	34.4	36.5	38.5	38.8
	1100	23	26	27.5	27.7	32.2	33.9
	1200	15.5	17.2	16.5	19	26.3	27.7
	1300	6	9.5	7	12	20.5	17.0

of "c" was found by these authors to vary with carbon content, although the exact value selected for "c" in a particular steel was not extremely critical; for time in hours, "c" ranged from 15 to 20 depending on the carbon content. This parameter was subsequently applied to high alloy tool steels (4,5) and stainless steel (6,7) and found to facilitate presentation and interpretation of tempering data.

Application of this parameter to our data demonstrated that, in any particular steel, "c" varied at different hardness levels, the variation being especially great in an alloy steel where "c" sometimes varied by a factor of four or more. Because "c" varied so widely in each steel, an average value meant very little, and so different arbitrary values were tried to determine by trial and error which gave the least scatter in the plotted data. As a result, it became apparent that a single value of "c" of the order of 18 was reasonably satisfac-

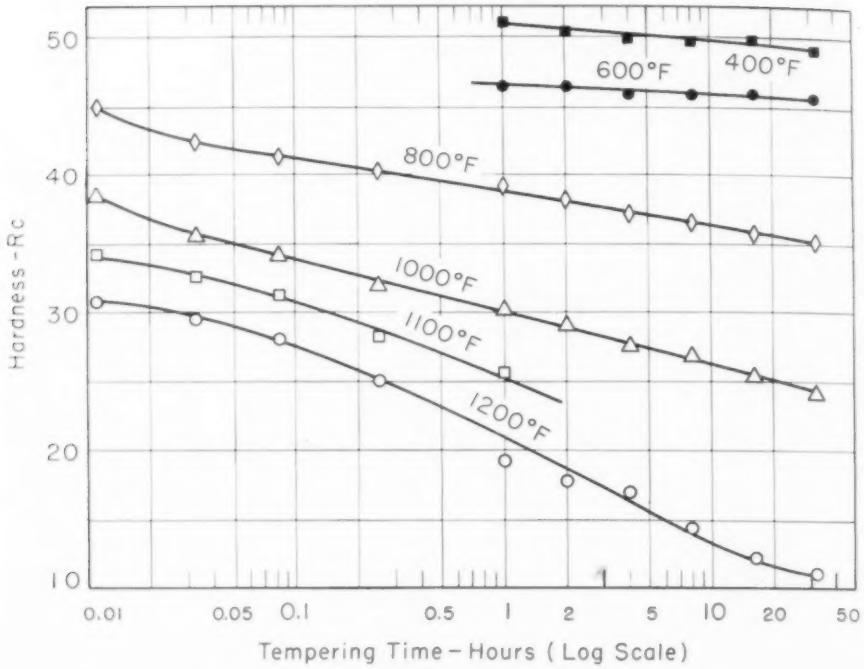


Fig. 1—A Common Method of Graphically Summarizing Tempering Data.

tory for all of our steels. The exact value of "c" was not critical, and a value of 16 or 20 was almost as satisfactory as 18, the value chosen. In selecting this value for "c", principal emphasis was placed upon the relative scattering of data between tempering temperatures of 700 to 1100°F. Plotting data for all the steels to exactly the same parameter offers the great advantage that all resulting curves, each representing a different steel, are directly comparable.

In Fig. 2a, the measured hardness of the 1335 steel is plotted against this parameter; in Fig. 2a, the measured hardness is Rockwell "C" and in Fig. 2b, it is DPH.[2] Although there is some scattering of the points, the single curve as drawn fits the data reasonably well in either chart, and thus for 1335 steel the hardness of martensite tempered for any combination of temperature and time can be determined from a single curve. The use of DPH, as in Fig. 2b, instead of Rockwell "C" results in a more satisfactory curve, inasmuch as it more nearly approximates a straight line.[3] DPH numbers, which are proportional to the area of the indentation made by a square-base diamond indenter, provide a more fundamental basic scale than Rockwell "C" numbers, which represent an increment in depth produced by adding a major load to a previously applied minor load on a conical diamond indenter. Accordingly, DPH was selected as the basic scale in subsequent plots of the tempering data.

[2]Diamond Pyramid Hardness was measured with a Vickers hardness tester using a 30 Kg or a 50 Kg. load.

[3]The dash-line curve in Fig. 2b will be referred to later.

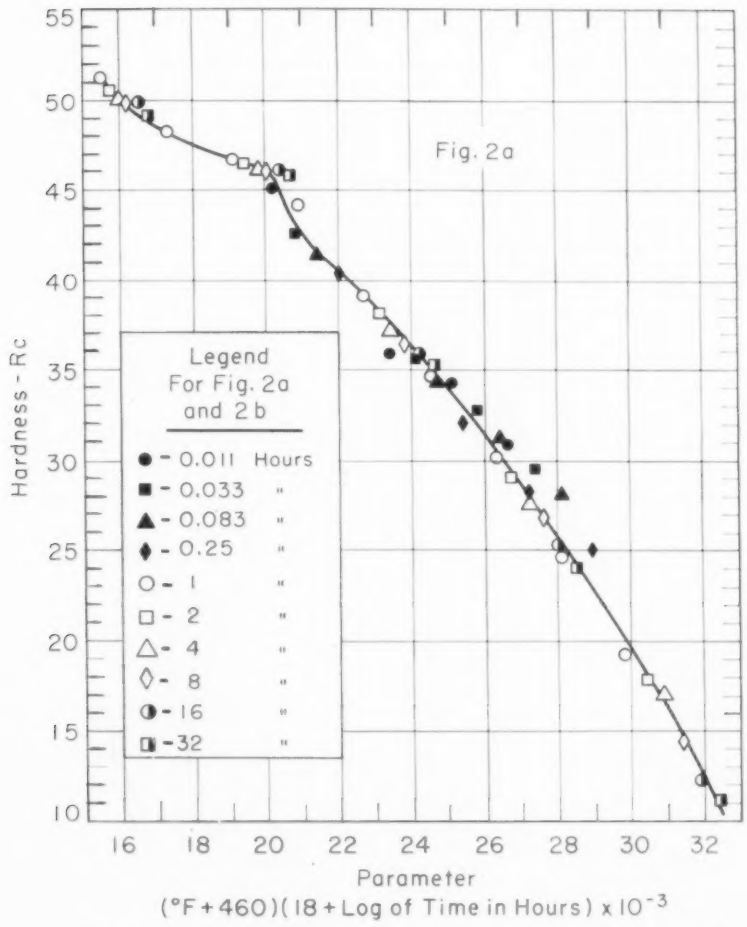


Fig. 2a—Hardness of Tempered Martensite in a 1335 Steel Plotted Against a Parameter Which Combines the Effect of Temperature and Time. In Fig. 2a, The hardness scale is Rockwell "C".

Hardness is more commonly measured and expressed as Rockwell "C", but this is of little consequence because any value on either scale can be readily converted to the other by means of a published table (8).

The significance of various values of the parameter in terms of temperature and time is shown in Fig. 3. This chart avoids the necessity of calculating the parameter for each tempering cycle and is convenient in interpreting subsequent tempering curves plotted on the parameter type of chart.

Effect of Carbon on the Hardness of Tempered Martensite

A tempering curve for each of the twelve carbon steels for which data are given in Table II was plotted on the parameter type of chart. Fig. 4 shows such curves for three representative steels. Regardless of the carbon content, points for each steel fall upon a single smooth curve, which demonstrates that the parameter with "c"

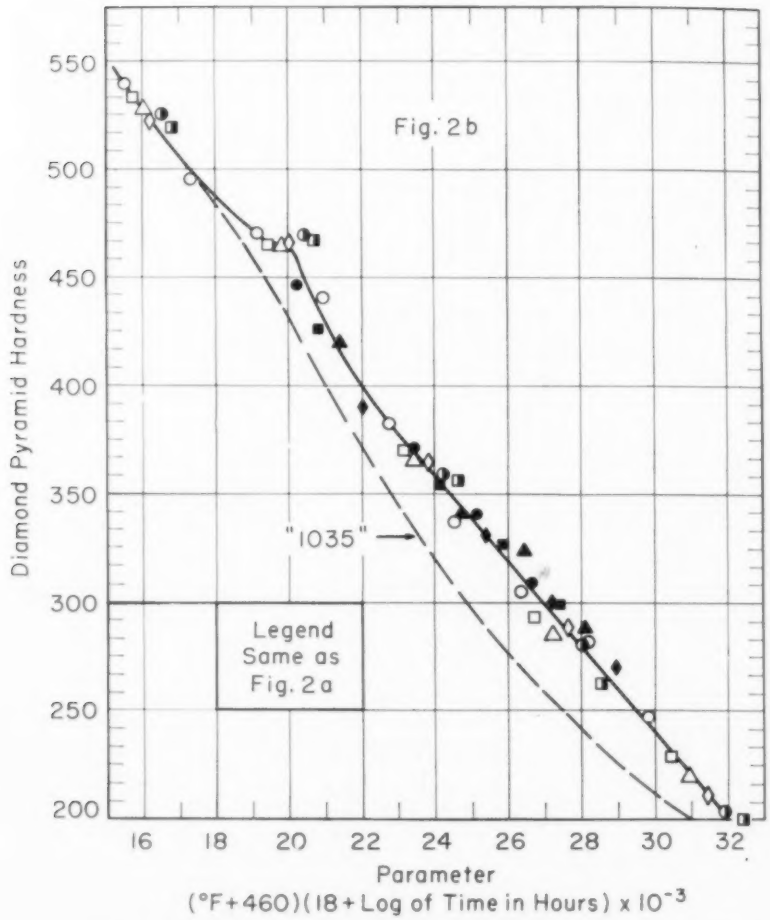


Fig. 2b—Hardness of Tempered Martensite in a 1335 Steel Plotted Against a Parameter Which Combines the Effect of Temperature and Time. The hardness scale is Diamond Pyramid Hardness.

equal to 18 is reasonably satisfactory. The complete series of curves for all twelve carbon steels reveals the large effect of carbon upon the hardness of tempered martensite. However, interpolation for carbon contents not specifically represented among the steels investigated is facilitated and minor inconsistencies in the over-all trends are eliminated by the method of plotting points taken from these curves shown in Fig. 5. In constructing this chart, the parameter value for each 50 DPH increment from 200 to 650 DPH, wherever possible, was determined from the tempering curve for each carbon steel and plotted against each respective carbon content. Smooth curves, each representing one hardness level, were fitted to each set of points. The points exhibit some scatter which is probably due principally to variation in the composition of these steels apart from their carbon content. In particular, there was some variation in residual elements which, although present individually in small percentages, may have had an appreciable effect on hardness as measured. The curves of Fig.

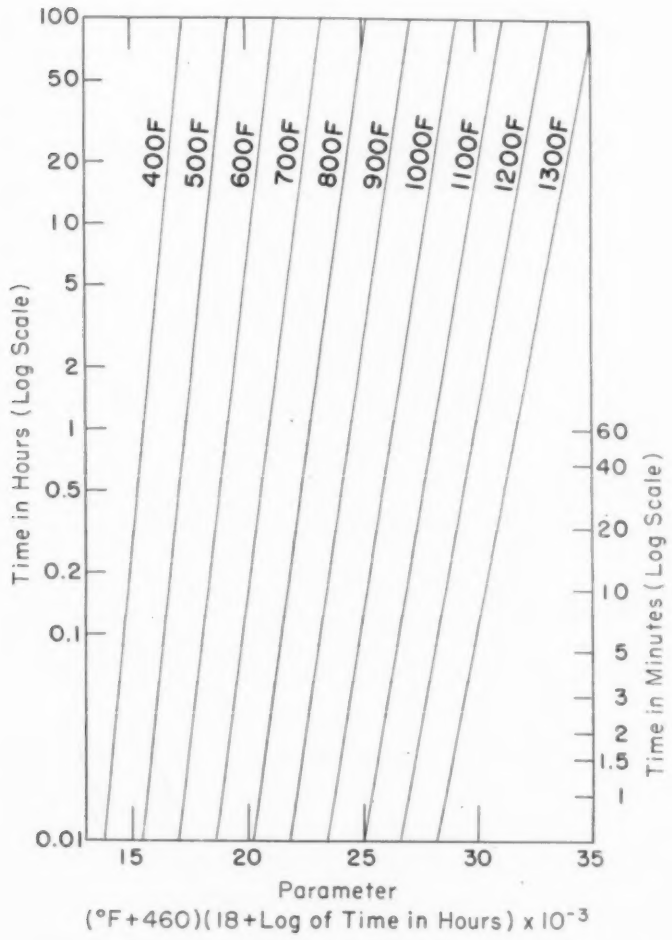


Fig. 3—Chart Showing Relationship of the Parameter With "C" =18 to Temperature and Time.

5 are believed to represent parameter-hardness values as a function of carbon content in typical commercial carbon steels and, as such, may be used to construct the tempering curve for any carbon steel between 0.2 and 0.85% carbon. Such curves tend to "average out" the effect of variation of manganese in the range 0.6/0.9% and of other elements, including residuals, within the usual range encountered in commercial carbon steels. The 0.2/0.85% range in carbon comprises that of principal interest. With less than 0.2% carbon, it is not possible to quench carbon steel to all martensite except in very small sections; above 0.85% carbon, quenched steel ordinarily contains undissolved carbides and its hardness after tempering involves additional variables associated with the austenitizing temperature and prior structure.

Tempering curves for a graded series of carbon contents constructed by drawing smooth lines through points taken from Fig. 5 and plotted on the parameter chart are shown in Fig. 6. The effect of

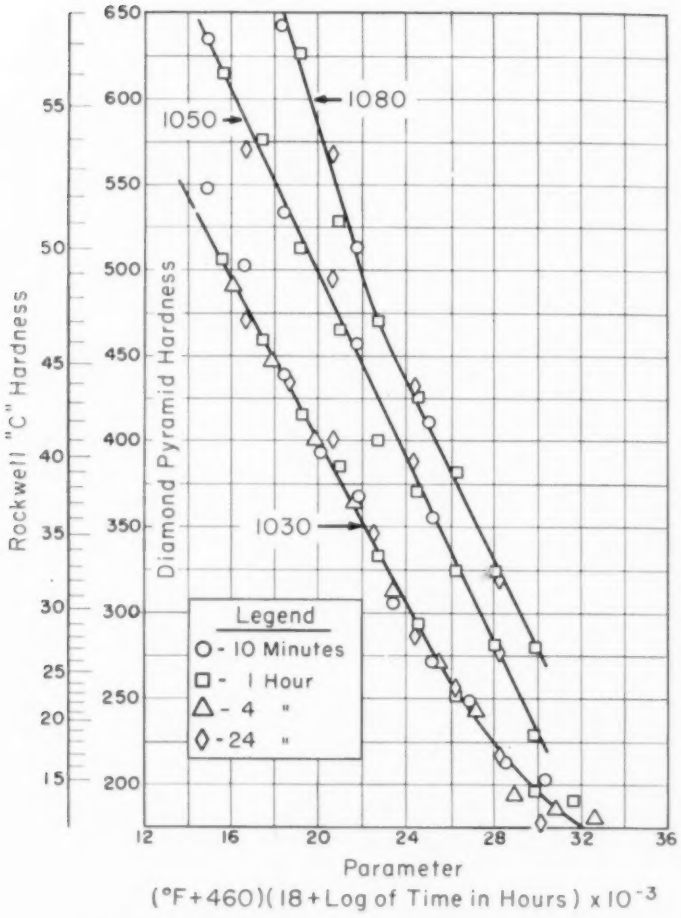


Fig. 4—Tempering Curves for the 1030, 1050 and 1080 Steels.

carbon is to markedly increase the hardness of tempered martensite, as would be expected, but a particular increment in carbon has a much greater effect at high than at low hardness; hence, the curves are not parallel but tend to merge at very low hardness as a structure of very few large carbides is developed and hardness approaches that of the ferrite. In these carbon steels, the curves are relatively simple in shape, but none are straight lines.

Tempering Curves for Low Alloy Steels

The tempering curve for each of eleven low alloy steels is shown in Fig. 2b and Figs. 7 to 16, inclusive. On each chart, the curve of the plain carbon steel of corresponding carbon content constructed from Fig. 5 is shown as a dash-line. The difference in the two curves on each chart is due to the resistance to softening on tempering conveyed by the alloying element or combination of alloying elements in the alloy steel.

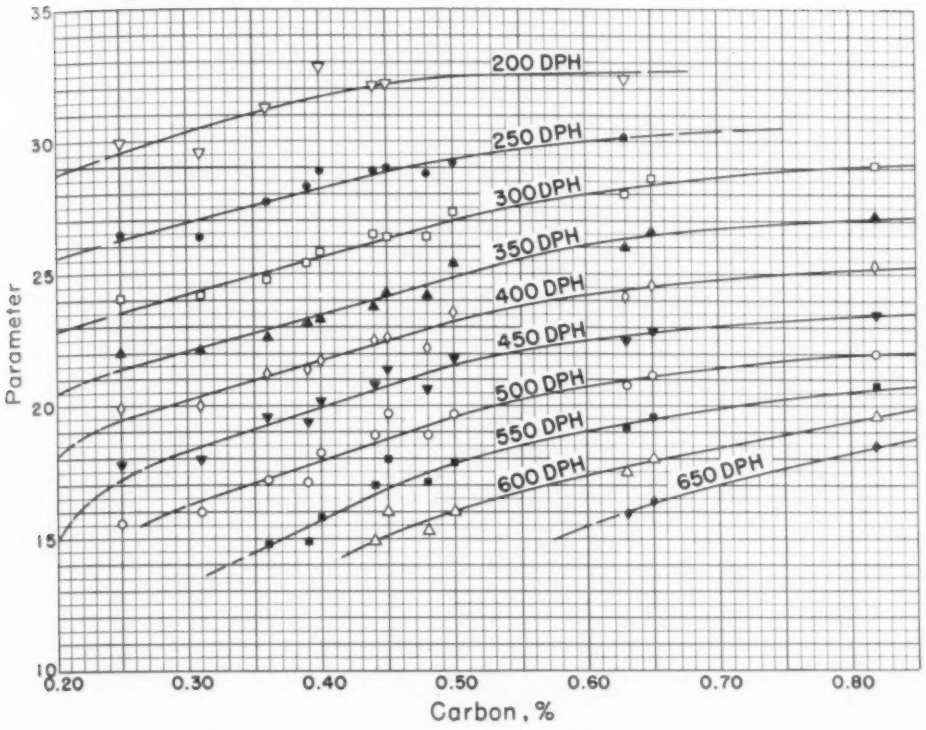


Fig. 5—Variation in Parameter Value With Carbon Content at Each Indicated Hardness Level.

Several of the tempering curves for alloy steel have an "arrest" in the vicinity of a parameter value of 20*, corresponding to tempering for 1 hour at 650°F. This results from the fact that the steel did not soften appreciably with longer tempering times in the vicinity of this temperature. There are two principal reasons for attributing this phenomenon to the transformation of austenite which was retained on quenching to room temperature. First, retained austenite is known to transform in the time-temperature range at which the arrest occurs; and, second, the arrest is usually more pronounced when the composition of the steel favors larger percentages of retained austenite. When relatively soft retained austenite transforms in the 600–700°F range to harder bainite, the over-all softening due to coalescence of carbides is presumably temporarily arrested. When tempered below this range, the presence of retained austenite would lower hardness somewhat, but there would be virtually no effect due to retained austenite above parameter of about 20.

Effect of Alloying Elements on Resistance to Softening on Tempering

Alloying elements convey a resistance to softening on tempering so that the tempering curve of an alloy steel is above that of the car-

*Actually 20,000 but it is convenient to divide by 1000 in referring to parameter values in accordance with the numerical scale on the charts.

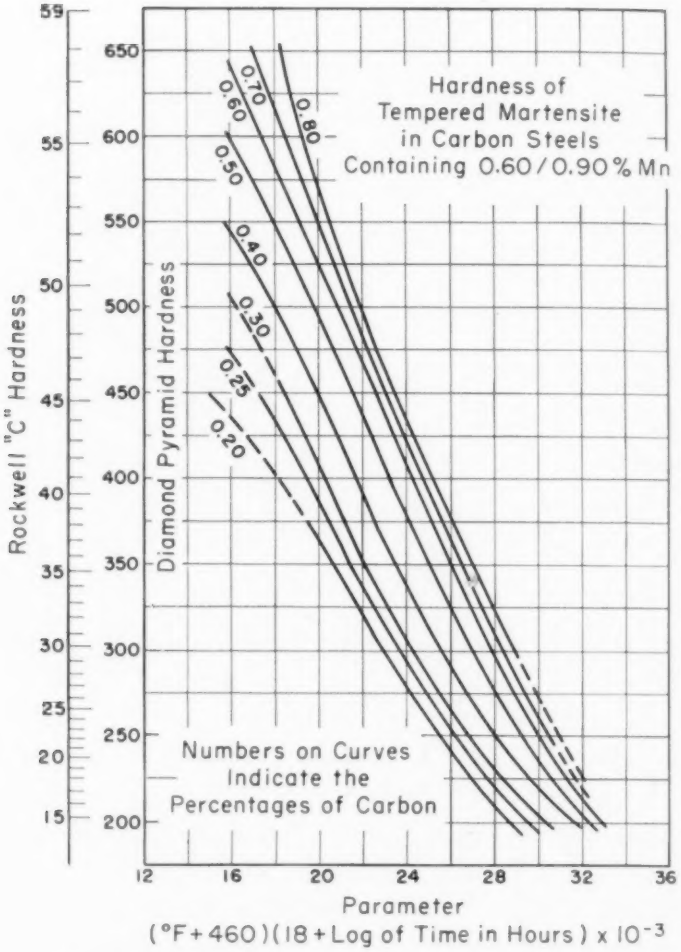


Fig. 6—Tempering Curves for Plain Carbon Steels.

bon steel of corresponding carbide content. The two curves are rarely parallel, however, because the effect of an alloying element varies with the parameter. For example, in Fig. 9 the effect of 0.25% molybdenum is greatest at a parameter value of 28 and diminishes both above and below this value. This is shown to better advantage in Fig. 17 in which the hardness difference or increment, between the 4047 and "1048" curves is plotted against the corresponding parameter value. Although the tempering curves for the 4027, 4037 and 4068 steels are not reproduced in the paper, points taken from these curves are also shown in Fig. 17. The curve, which was judged by eye to best fit all the points, shows the quantitative effect of 0.25% molybdenum in retarding softening on tempering martensite.

The quantitative effect of manganese as revealed by Fig. 2b is similarly presented in Fig. 17. In this case, the carbon steel basic curve labelled "1035" is for a steel containing 0.6–0.9% manganese and the 1335 steel curve thus represents the effect of nominally an

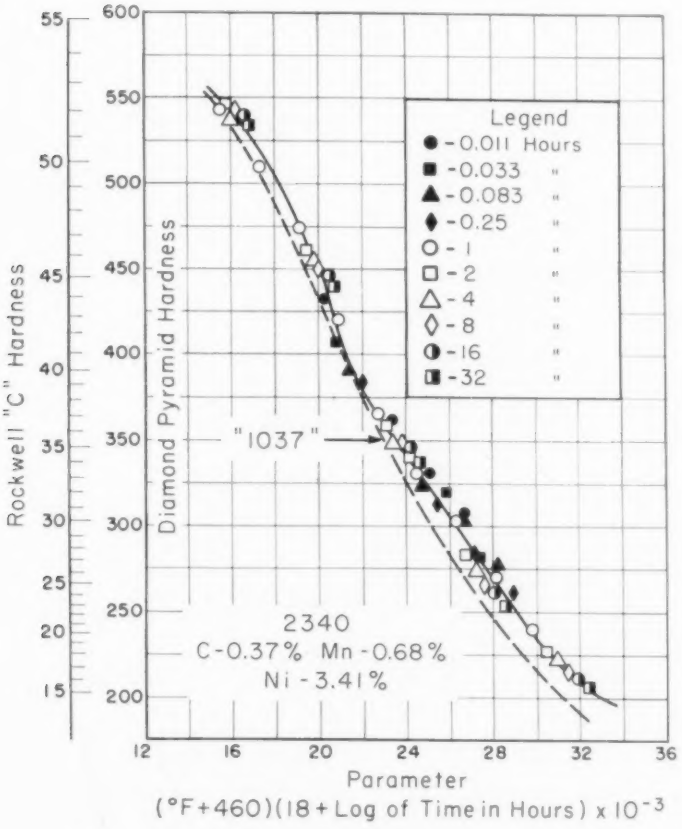


Fig. 7—Hardness of Tempered Martensite in a 2340 Steel.

additional 1% manganese. The effect of 3.4% nickel and of 1% chromium, according to Figs. 7 and 13, respectively, is also shown in Fig. 17. None of the steels investigated contained only vanadium as the alloying element, but by correcting for the effect of chromium by adding to the basic "1043" curve the previously determined effect of 1% chromium, the difference between the resulting "5143" curve and that for 6145 steel (Fig. 14) is assumed to represent the effect of vanadium as shown in Fig. 17. Finally, the effect of silicon was determined by adding to a "1055" curve the effect of 0.77% chromium on a proportional basis from the previously determined effect of 1% chromium. The difference between the hypothetical "1055+ 0.77% Cr" curve thus estimated and the curve for 9264 (Fig. 15) is assumed to represent the effect of 1.6% silicon corrected for the nominally 0.3% silicon present in the "1055" base curve. In agreement with the observations of others (9,10) silicon was found to convey a marked resistance to softening at a low parameter range where other common alloying elements are ineffective.

The tempering curves of 4140, 4340, 4640 and nitriding steel in comparison with each respective basic carbon steel curve reveals the

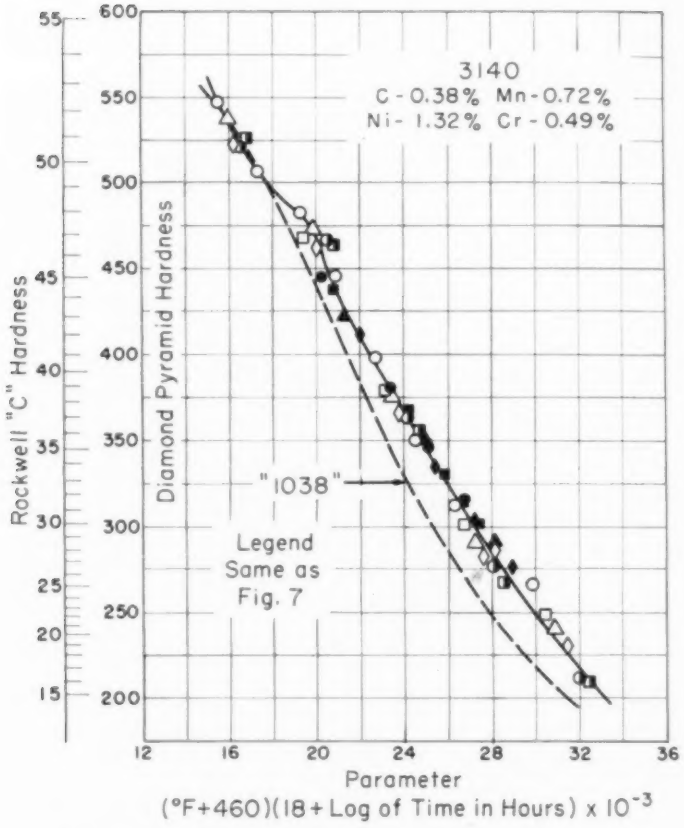


Fig. 8—Hardness of Tempered Martensite in a 3140 Steel.

effect of a combination of two or more alloying elements. That of nitriding steel is especially interesting because it indicates that an appreciable percentage of aluminum, like silicon, conveys a resistance to softening at low parameters; this observation agrees with that of Allten (11).

Estimation of the Hardness of Tempered Martensite from Chemical Composition

Assuming that the resistance to softening on tempering conveyed by each alloying element, expressed as DPH increments to be added to a basic carbon steel curve, is directly proportional to the percentage present and independent of the carbon content within the 0.2 to 0.85% carbon range, the effect of alloying elements on the hardness of tempered martensite can be expressed as a "factor" by which the percentage present is to be multiplied. Such factors, based upon Fig. 17, are given for each of several parameter values in Table V. Because alloying elements generally have more effect at certain tempering temperatures than at others, the factor for each particular element is often different at different parameters. Using

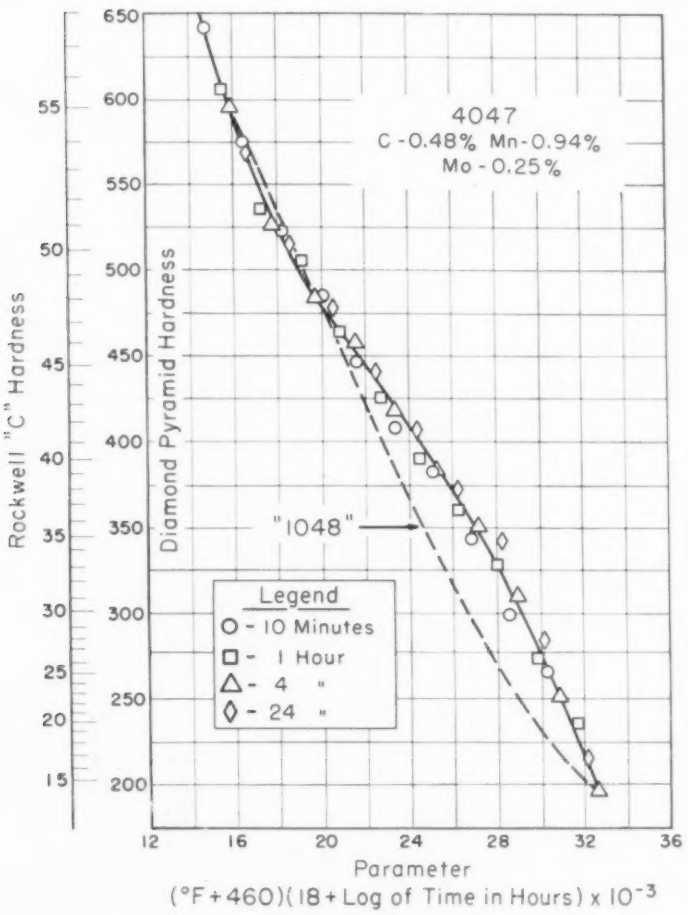


Fig. 9—Hardness of Tempered Martensite in a 4047 Steel.

Table V
Factors for Predicting the Hardness of Tempered Martensite

Element	Range	Factor at Indicated Parameter Value 20	22	24	26	28	30
Manganese	0.85/2.1%	35	25	30	30	30	25
Silicon	0.3/2.2%	65	60	30	30	30	30
Nickel	Up to 4%	5	3	6	8	8	6
Chromium	Up to 1.2%	50	55	55	55	55	55
Molybdenum	Up to 0.35%	40	90	160	220	240	210
		(20)*	(45)*	(80)*	(110)*	(120)*	(105)*
Vanadium**	Up to 0.2%	0	30	85	150	210	150

*If 0.5/1.2% Cr is also present, use this factor.
**For SAE-AISI chromium-vanadium steels; may not apply when vanadium is the only carbide former present.
Note: Boron factor is 0.

these factors in conjunction with "basic" curves for plain carbon steel constructed from Fig. 5 to estimate tempering curves for various alloy steels, it became apparent that certain limitations must be imposed in order to insure estimation of sufficient accuracy to be useful.

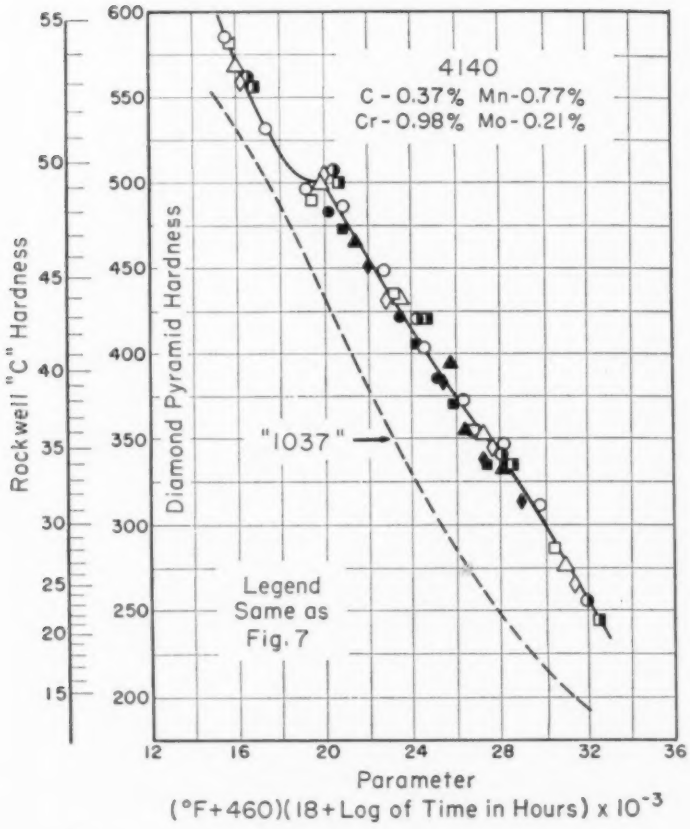


Fig. 10—Hardness of Tempered Martensite in a 4140 Steel.

First, the effect of an alloying element, particularly one which forms a carbide, was obviously not directly proportional to the percentage present. Rather, the effect appears to decrease with successive increments, at least beyond a certain percentage, so that when a relatively large amount of an alloying element is present in a steel the factors given in Table V indicate too high hardness. Nevertheless, the factors may be sufficiently adequate for useful estimations provided a limit is placed upon the percentage of each element. In Table V, therefore, a range for each element within which the factors apply is given. This includes a minimum limit in the case of manganese and silicon in accordance with the nominal percentage of these elements always present in commercial plain carbon steels.

The second limitation found necessary concerns the additivity of the effect of each individual alloying element when two or more are present in a particular steel. When both chromium and molybdenum were present in appreciable percentages, as in 41XX and 43XX steels, direct application of the factors resulted in too high an estimated hardness. These elements tend to compete with one

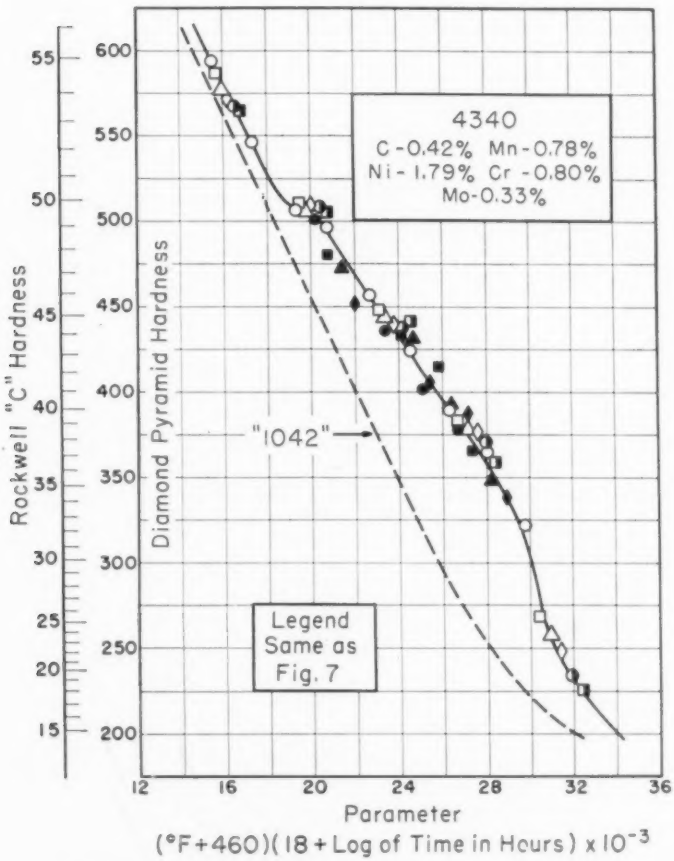


Fig. 11—Hardness of Tempered Martensite in a 4340 Steel.

nother for carbon in order to form their respective alloy carbide, nus reducing the effectiveness of each over that which results when nly one of the elements is present. This difficulty was empirically esolved by halving the molybdenum factor for each parameter hen estimating the effect of molybdenum in a steel containing lso 0.5/1.2% chromium, as specified in Table V. The same dif- culty would likely have been encountered with vanadium, another trong carbide-former, had its effect been evaluated in an alloy steel ontaining only vanadium. However, vanadium factors in Table V ere based upon data for a chromium-vanadium steel (6145), and nasmuch as 61XX steels are the only SAE-AISI standard steels ontaining vanadium, no modification in vanadium factors is re- uired. The factors given for vanadium may not apply to straight anadium steels nor to steels containing vanadium in combination ith elements which are not strong carbide-formers.

A third limitation involves the range in parameter values (tem- ering temperatures) within which reasonably reliable estimation is robable. At tempering temperatures lower than about 650°F (para-

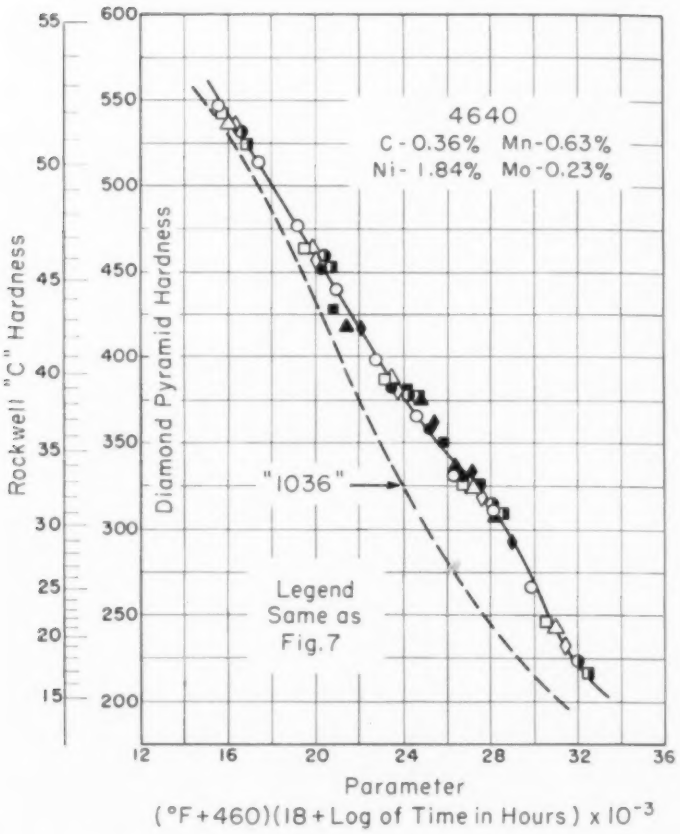


Fig. 12—Hardness of Tempered Martensite in a 4640 Steel.

meter on the order of 20), the hardness of tempered martensite as ordinarily measured is influenced by the rate of cooling during the prior quench, which is affected by specimen size and shape and the severity of quench. The effect of these factors on the hardness of tempered martensite is due, in part, to difference in the amount of austenite retained on reaching room temperature, which, as has been discussed, causes somewhat lower hardness at low tempering temperatures and an austenite-transformation "arrest" to an increasing degree as more austenite is retained in a given steel. In many instances, especially when the steel contains carbon on the low side of the 0.2/0.85% range, slower cooling through the temperature range of martensite formation (M_s-M_f) results in lower hardness as quenched and as tempered at temperatures nearly as high as M_s. This is because martensite is to some extent "tempered" as it forms during cooling. The relative degree of such "quench-tempering" is greater the higher the M_s-M_f range (lower the carbon and, to a lesser extent the amount of alloy) and the slower the cooling through the M_s-M_f region. For a particular steel, due to "quench-tempering", the tempering curve at low parameter values is likely,

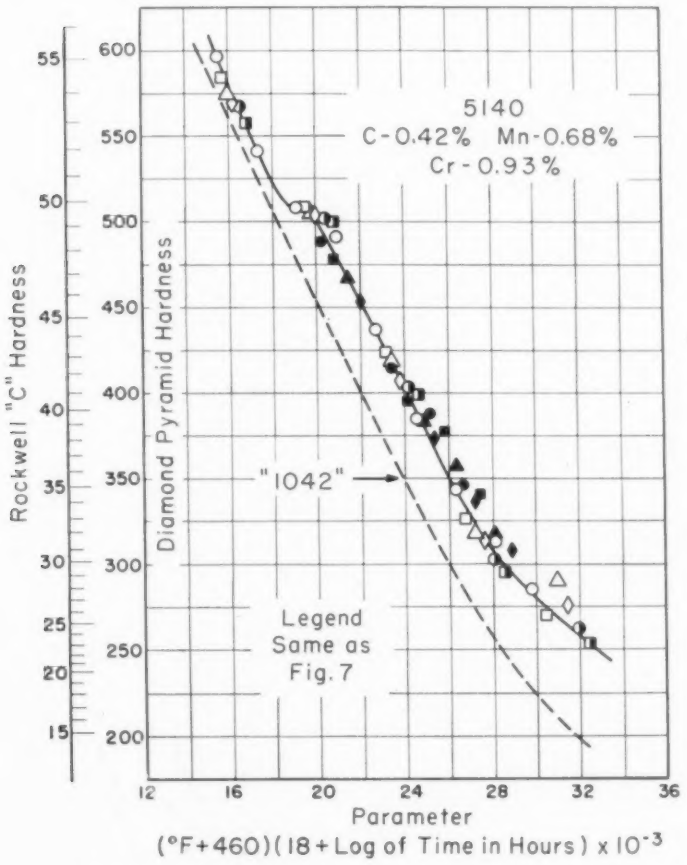


Fig. 13—Hardness of Tempered Martensite in a 5140 Steel.

herefore, to be somewhat lower as the specimen is larger, even hough not too large to "quench out", and if quenched in oil rather han water or brine. Because of these circumstances, estimation of he hardness of tempered martensite at parameter values below bout 20, which corresponds to tempering 1 hour at 650°F, is often ikely to be unreliable, and in Table V alloy factors are not listed or parameters below 20.

There are also several reasons for not including in Table V lloy factors at a parameter of 32. This parameter represents a empering treatment of 1 hour at slightly over 1300°F, which is bove the Ac_1 for steel containing several per cent of nickel. Moreover, measured hardness values were relatively more erratic for high empering temperatures and the difference between an estimated nd measured value in any given specimen could consequently sometimes be considerable. At high tempering temperatures, neglect of he effect of variation from steel to steel in the percentage of minor lements such as nitrogen, which seemingly contribute very little o resistance to softening at lower temperature, may become im-

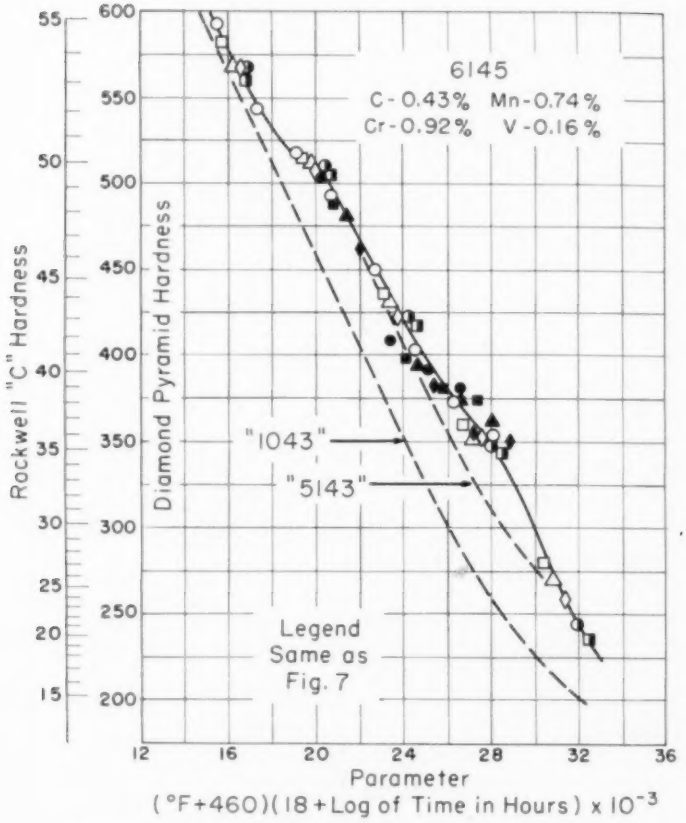


Fig. 14—Hardness of Tempered Martensite in a 6145 Steel.

portant and probably cannot be neglected in a reliable estimation. Significant precipitation hardening is also possible if the steel is cooled rapidly after tempering at high temperature. In order to avoid these difficulties, it is therefore advisable to forego any attempt to estimate the hardness of martensite tempered in the vicinity of 1300°F, and alloy factors are accordingly not listed for a parameter above 30 in Table V.

Application of the Method Proposed for Estimating the Hardness of Tempered Martensite

Based upon measurements on specimens from twelve carbon steels and six alloy steels, a comparatively simple method for estimating the hardness of tempered martensite in any SAE-AISI standard steel containing 0.2 to 0.85% carbon has been proposed. It remains to demonstrate that the method permits estimates of sufficient accuracy and reliability to be useful.

Measured data for a 4340 steel have been listed in Table III and plotted on the parameter chart in Fig. 11. This steel contains three principal alloying elements, nickel, chromium and molyb-

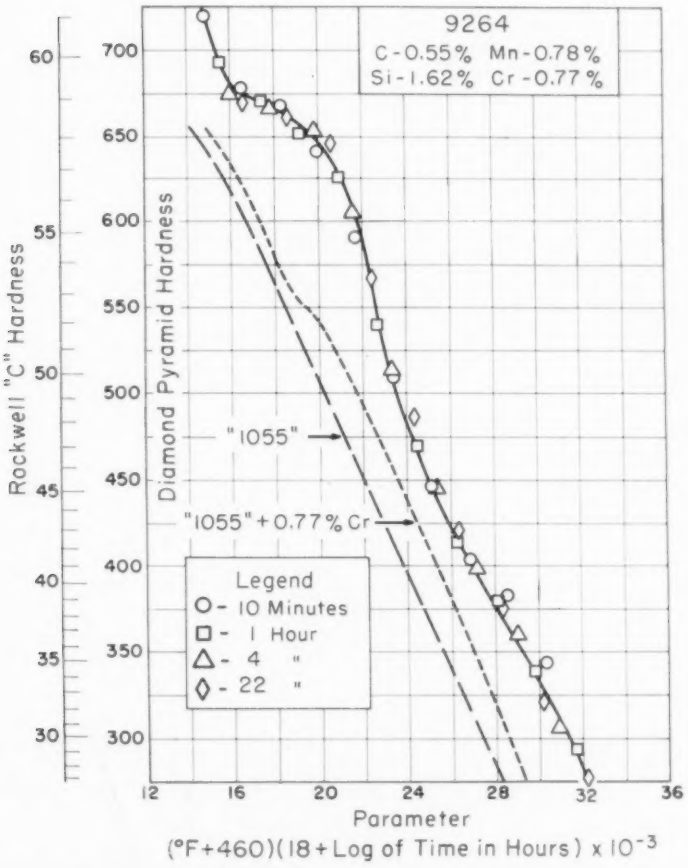


Fig. 15—Hardness of Tempered Martensite in a 9264 Steel.

lenum, which makes it especially suitable for demonstrating the application of the method of estimation. The procedure involved in constructing the estimated hardness curve of this 4340 steel is described in some detail as an aid for those who may wish to apply the method to some steel of interest to them. The carbon content of this particular 4340 steel is 0.42%; hence, the first step consists of referring to Fig. 5 and noting the parameter value where each isohardness curve intersects a vertical line at 0.42% on the abscissa. A point representing each parameter-hardness combination thus determined is then plotted on a parameter chart, such as that shown in Fig. 18. These points are shown in Fig. 18 as open circles and the smooth curve drawn through them and labelled "1042" is the tempering curve of a plain carbon steel containing 0.42% carbon. Neglecting possible minor composition differences, the 4340 steel differs from "1042" in containing 1.79% nickel, 0.80% chromium and 0.33% molybdenum. The effect of these elements is next calculated for each parameter listed in Table V. For example, at a parameter of 20, the factor for nickel is 5, for chromium 50, and for molybdenum

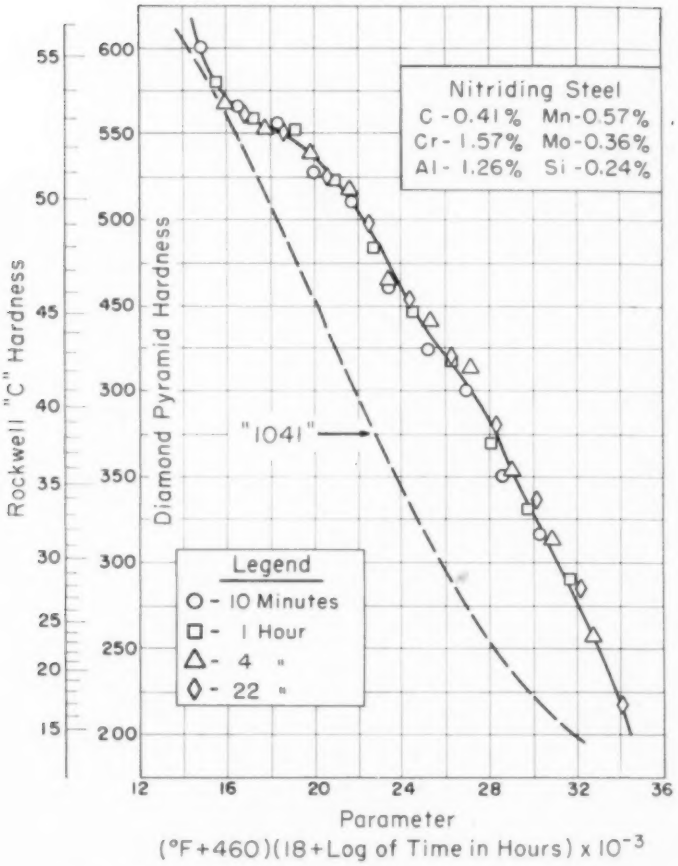


Fig. 16—Hardness of Tempered Martensite in a Nitriding Steel.

20. Multiplying these factors by the respective percentage of each element present and adding: $5\times\%$ Ni$+50\times\%$ Cr$+20\times\%$ Mo$=5\times1.79+50\times0.80+20\times0.33=55$. The value 55 is the hardness increment to be added to the "1042" curve at a parameter of 20; doing this gives the point represented by the uppermost filled circle in Fig. 18. Other hardness increments are similarly calculated for parameters of 22, 24, 26, 28 and 30 and plotted on Fig. 18. The smooth curve drawn through these points, labelled "4340 estimated" indicates the estimated hardness of tempered martensite in this steel. This curve agrees very well with the dash-line curve, labelled "4340 measured" which was transferred from Fig. 11.

If, for example, it is desired to know the hardness resulting from tempering a specimen of the fully hardened 4340 steel for 5 hours at 1000°F, the parameter for this tempering treatment is 27.3 (see Fig. 3) and, according to the estimated curve, the hardness would be Rockwell C-37.5 (or 368 DPH). The measured curve indicates a hardness of Rockwell C-38 (or 372 DPH). Thus, in this instance, the method of estimation proved to be satisfactory, espe-

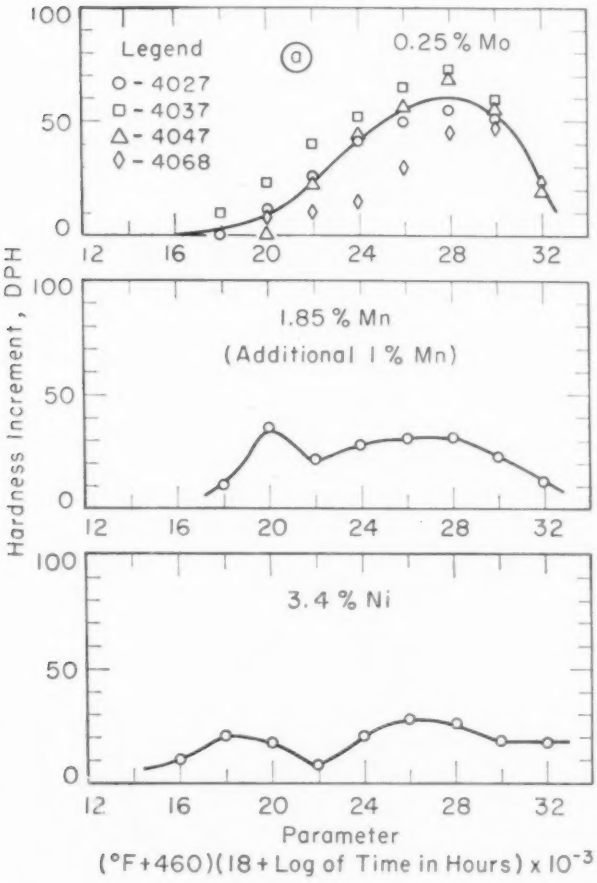


Fig. 17a—Effect of Specified Amount of Each of Common Alloying Elements Upon Resistance of Martensite to Softening on Tempering.

cially since Rockwell C-0.5 or 4 DPH is within the limit of experimental error in hardness testing. Estimated tempering curves for the 3140, 4140, and 4640 steels were similarly constructed and compared with the corresponding measured curves; in each instance, there was reasonably satisfactory agreement between the estimated and measured hardness of tempered martensite.

Tempering data for a considerable number of alloy steels are listed in Table VI. These data may be used to compare estimated and measured hardness values for tempered martensite in a representative group of alloy steels. For each of twenty-one different grades of alloy steel, after one or more tempering treatments, the hardness of tempered martensite was estimated by the method described above. Table VI lists the steels, tempering treatments, and the measured and estimated hardness. Although the estimated value occasionally differs from the corresponding measured hardness by as much as 2 or even more Rockwell C points, the agreement in the majority of cases is quite satisfactory. In Fig. 19, estimated hardness

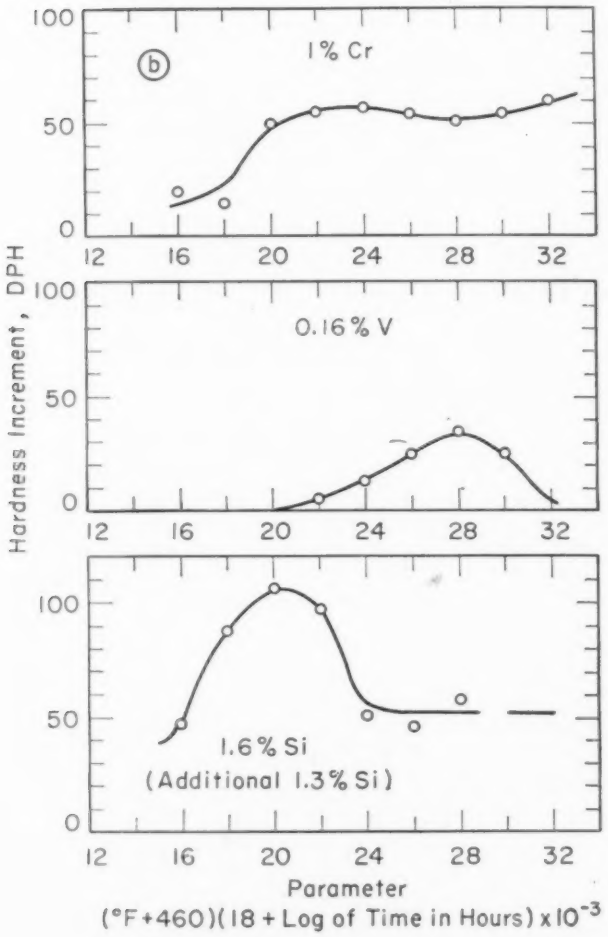


Fig. 17b—Effect of Specified Amount of Each of Common Alloying Elements Upon Resistance of Martensite to Softening on Tempering.

is plotted against measured hardness to summarize the correlation. Most points lie within 1 Rockwell C of the line of perfect correlation; those which do not are located about equally above and below this line. This indicates that the method could not be improved by simple adjustment of carbon and alloy factors, although a more complicated method might reduce the scatter. However, the method proposed for estimating the hardness of tempered martensite from chemical composition of steel appears to be sufficiently accurate and reliable to be of value as a preliminary to, or even a substitute for, exploratory tests to determine the tempering treatment required to develop a desired hardness in SAE-AISI standard steels or others whose composition does not exceed the limits specified in Table V.

The fact that it is seemingly possible to estimate the hardness of tempered martensite for carbon and low alloy steels within a considerable range in tempering treatments and composition demon-

Table VI
Comparison of Estimated and Measured Hardness of Tempered Martensite in Miscellaneous Alloy Steels (all tempered for 1 hour)

SAE-AISI Number	Tempering Temp. °F	Hardness Rc Measured	Hardness Rc Estimated	SAE-AISI Number	Tempering Temp. °F	Hardness Rc Measured	Hardness Rc Estimated
2320	750	34.5	33.5	3140	800	42	43
	950	27.5	27.5		950	37	36.5
	1150	19	17.5		1150	29	28.5
4620	750	37.5	35.5	2340	750	40.5	41.5
	950	31.5	31.5		800	39	39
	1150	24.5	25		950	32.5	33
					1150	23.5	24
4320	750	35	37.5				
	950	29.5	32	4140	800	46	46
	1150	21.5	25.5				
				6150	800	47.5	48
8620	750	38.5	39		950	42	42.5
	950	31.5	31		1150	35	35
	1150	24	24				
				4063	800	47	47.5
1330	800	38	38		950	41.5	43
	950	32.5	31		1150	31.5	34
	1150	23	23				
				51B60	700	52.5	52
8630	700	42	41.5		800	47.5	48.5
	950	33	32.5		900	43.5	45
	1150	26	25.5		1000	39.5	40.5
					1100	35.5	35
9430	800	38.5	37.5		1200	31.5	30
2330	700	41	38.5	8660	700	51.5	51.5
	950	31.5	28.5		800	48	48.5
	1150	24.5	25		900	45.5	45
					1000	42.5	42.5
4130	700	44.5	45		1100	38.5	36.5
	950	37	36.5		1200	33.5	31
	1150	28.5	29.5				
				9262	700	58	58
1340	800	41.5	41.5		800	51.5	52
	950	35	34.5		900	47.5	47.5
	1150	25	25		1000	43.5	43.5
					1100	39.5	39
8440	800	41	40.5		1200	34.5	34
	950	35	35				
	1150	26	27				
8640	750	45	44				
	800	44	42				
	950	38.5	36				
	1150	31	29				
9440	800	39.5	40.5				
	950	34.5	34.5				
	1150	26	27.5				

strates that resistance of martensite to softening on tempering is due to the combined effect of the carbon and alloying elements present in a steel. Tempering data can thus be rationalized and simply interpreted on this basis.

Summary and Conclusions

The parameter proposed by Hollomon and Jaffe (2) is satisfactory for combining the effect of temperature and time during the

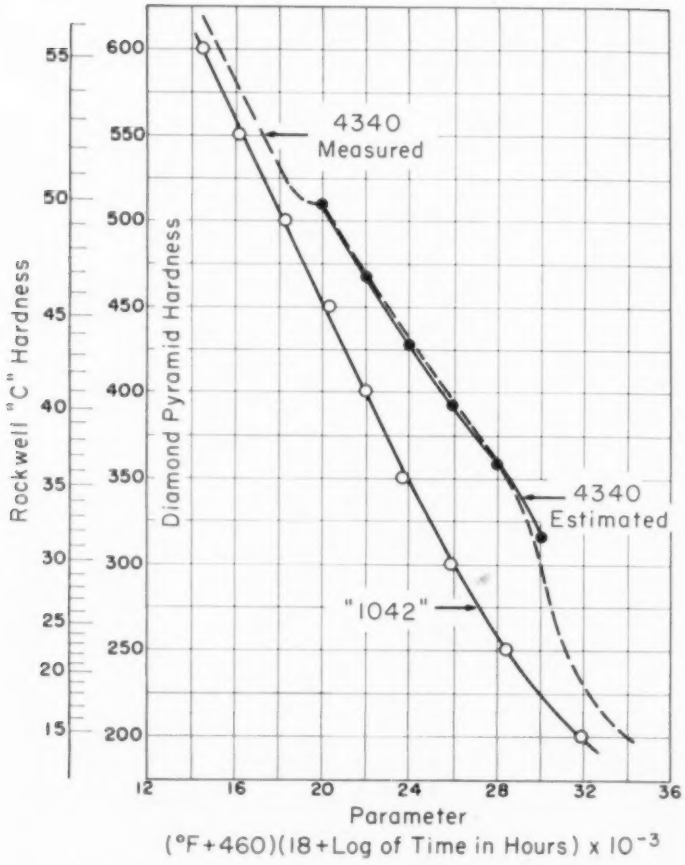


Fig. 18—Comparison of Estimated and Measured Hardness of Tempered Martensite of a 4340 Steel.

tempering of martensite in SAE-AISI carbon and alloy steels with less than 5% total alloy. It suffices to use for all these steels a value of 18 as the constant in this parameter, thus making such tempering curves directly comparable.

Tempering curves for a series of plain carbon steels plotted against this parameter quantitatively reveal the effect of carbon on the hardness of tempered martensite. By interpolation, the curve for any carbon content in the range 0.2 to 0.85% can be estimated.

Comparing the tempering curve of an alloy steel with the curve for a plain carbon steel of identical carbon content reveals the resistance to softening or tempering conferred by alloying elements. This can be quantitatively expressed as a hardness increment. Because the effect of an alloying element is usually greater at certain tempering temperatures, or parameter values, evaluation of its over-all effect involves determination of the hardness increment at each of a series of parameter values.

If restricted to a tempering temperature range of 650–1200°F and to a limited range in composition, it is seemingly possible by an

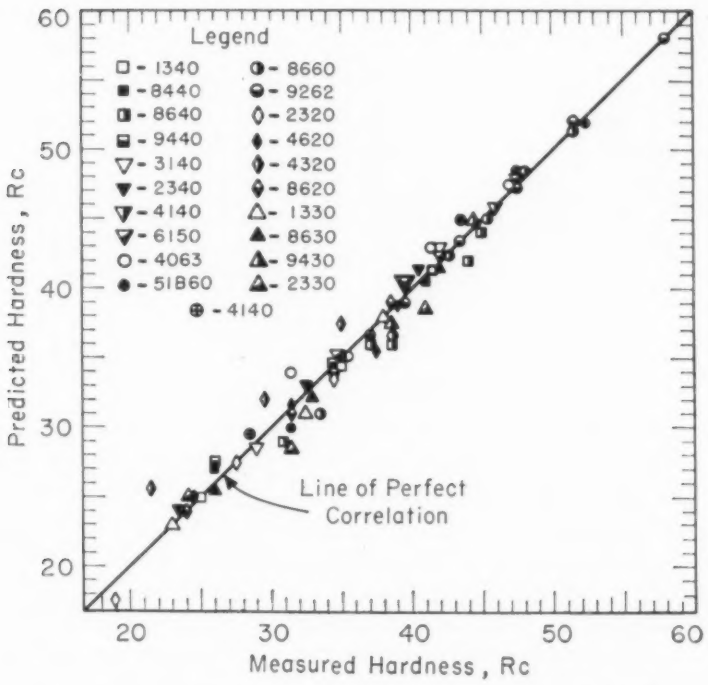


Fig. 19—Correlation of Measured and Predicted Hardness of Tempered Martensite in Various Alloy Steels.

empirical method developed from the data to estimate from chemical composition the hardness of martensite after tempering for any combination of temperature and time. The composition range within which reasonably reliable estimation is possible on this basis includes the AISI-SAE carbon and alloy steels containing 0.2 to 0.85% carbon and less than 5% total alloy.

Acknowledgments

Many of the tempering data were measured by associates of the authors at the United States Steel Corporation Fundamental Research Laboratory.

References

1. E. C. Bain, Functions of Alloying Elements in Steel, 1939, p. 228, published by the American Society for Metals, Cleveland, Ohio.
2. J. H. Hollomon and L. D. Jaffe, "Time-Tempering Relations in Tempering Steels," *Transactions*, American Institute of Mining and Metallurgical Engineers, Vol. 162, 1945, p. 223.
3. Society for Automotive Engineers *Handbook*, 1954 Edition, p. 102.
4. G. A. Roberts, A. H. Grobe and C. F. Moersh, Jr., "The Tempering of High-Alloy Tool Steels," Transactions, American Society for Metals, Vol. 39, 1947, p. 521.
5. A. H. Grobe and G. A. Roberts, "Effect of Carbon Content on 18-4-1 High Speed Steel," Transactions, American Society for Metals, Vol. 45, 1953, p. 475.
6. A. E. Nehrenberg, "Master Curves Simplify Stainless Tempering," *Steel*, Vol. 127, October 23, 1950, p. 475.

7. R. L. Rickett, W. F. White, C. S. Walton, and J. C. Butler, "Isothermal Transformation, Hardening and Tempering of 12% Chromium Steel," TRANSACTIONS, American Society for Metals, Vol. 44, 1952, p. 138.
8. METALS HANDBOOK, American Society for Metals, 1948 Edition, p. 99.
9. A. G. Allten and P. Payson, "The Effect of Silicon on the Tempering of Martensite," TRANSACTIONS, American Society for Metals, Vol. 45, 1953, p. 498.
10. W. S. Owen, "The Effect of Silicon on the Kinetics of Tempering," TRANSACTIONS, American Society for Metals, Vol. 46, 1954, p. 812.
11. A. G. Allten, (Discussion) of article by Walter S. Owen "The Effect of Silicon on The Kinetics of Tempering," TRANSACTIONS, American Society for Metals, Vol. 46, 1954, p. 828.

DISCUSSION

Written Discussion: By Walter Crafts and J. L. Lamont, Metals Research Laboratories, Electro Metallurgical Company, Niagara Falls, New York.

The authors are to be congratulated for providing a relatively simple calculation for estimating tempered hardness in hardened and tempered low alloy steels. However, there is always a temptation to extend such a useful calculation to conditions beyond those limitations that have been rigorously defined by the authors. It is, therefore, felt that caution should be exercised if the calculation is applied to a steel that is incompletely hardened or to a composition beyond the indicated range.

In an earlier paper[5] empirical factors governing the tempering of wholly and incompletely hardened steel were described for low alloy steel with an accuracy of about plus or minus 4 Rockwell C. However, the factors assigned to the hardness increment due to alloys were assumed to be constant, except in the case of nickel, above a certain critical temperature at which the maximum effect was achieved, namely, at 600°F for silicon, 800°F for manganese and chromium, and 1000°F for molybdenum. It was subsequently found in a later study,[6] as confirmed by Grange and Baughman, that the increments of hardness due to alloys passed through a maximum at an intermediate temperature. In that paper, which covered a range up to over 1% carbon, 12% chromium, 5% molybdenum, 5% vanadium, and 18% tungsten, with tempering from 600 to 1300°F over periods of up to 1000 hours, it was also reported that interference between carbide-forming elements could be related rationally to their carbide-forming tendencies. For this reason, it is anticipated that the compromise factors for chromium and molybdenum suggested by Grange and Baughman for chromium-molybdenum steels may require some adjustment in relation to the carbon content at the extreme ends of the range. For the same reason, it is believed that special factors may be needed for steels containing chromium or molybdenum higher than in the common low alloy steels.

In our study, 85% of the hardness values calculated for steels over a broad range of composition were within 3 Rockwell C of the actual hardness, but the accuracy left much to be desired. The method of calculation also might be rationalized more effectively and made less cumbersome. Since much remains to be done in this field, it is hoped that the authors will be interested in continuing their study.

[5] Walter Crafts and John L. Lamont, "Effect of Alloys in Steel on Resistance to Tempering," *Transactions*, American Institute of Mining and Metallurgical Engineers, Vol. 172, 1947, p. 222.
[6] Walter Crafts and John L. Lamont, "Secondary Hardening of Tempered Martensitic Alloy Steel," *Transactions*, American Institute of Mining and Metallurgical Engineers, Vol. 180, 1949, p. 471.

Written Discussion: By R. D. Chapman, Chrysler Corporation, Detroit.

The authors are to be congratulated for an erudite paper on tempering. This phase in heat treating is often neglected for studies of quenching and, as pointed out, is an important phase. Some of the work done at Chrysler on the tempering phenomenon correlates very well with the data presented by the authors. Our findings, however, do not show as great an effect on the resistance to tempering of the element molybdenum. In our studies end quench hardenability bars of the

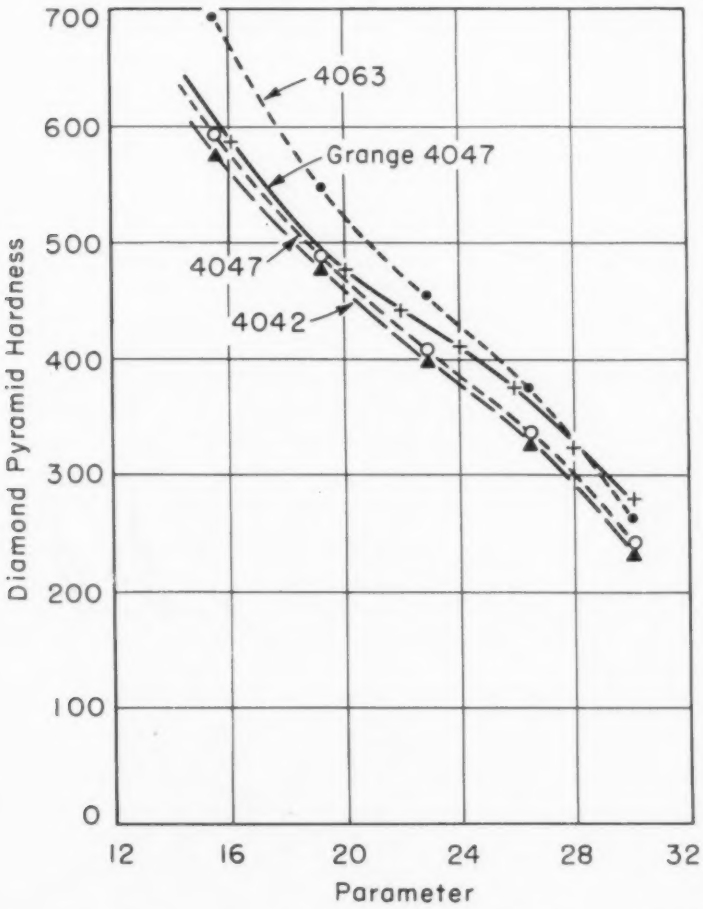


Fig. 20—Hardness of Tempered Martensite of Grange 4047 Compared with Chapman 4042, 4047 and 4063.

SAE 4000 series were carefully tempered at various temperatures for periods of 1 hour. Some of these results were published in Metal Progress in April, 1950.

Using the 1/16 position on the end-quenched bar and superimposing our data on Fig. 9 of the authors, it can be seen in Fig. 20 that with a parameter value of 24 to 28 none of the three steels show as much resistance to tempering as shown by Grange. Plotting this difference as the authors have for molybdenum, in Fig. 17 they show a maximum hardness increment over plain carbon steel of 60 D.P.H. at a parameter of 28. When our data is plotted in a comparable manner, this increment reaches a maximum of only 35 D.P.H. with a parameter of 27. The authors curve and ours are very similar in shape but ours is displaced to lower hardness values than that of the authors. However, the authors actual determinations cor-

respond more closely to our data than to their calculations. If we compare his values indicated in Table VI with our values, we find better agreement than with his calculations, as shown in Table VII.

Table VII

Temperature (°F)	Chrysler Data (Rc)	GRANGE Estimated (Rc)	GRANGE Data (Rc)
800	46	47.5	47
900	41	43	41.5
1150	31.5	34	31.5

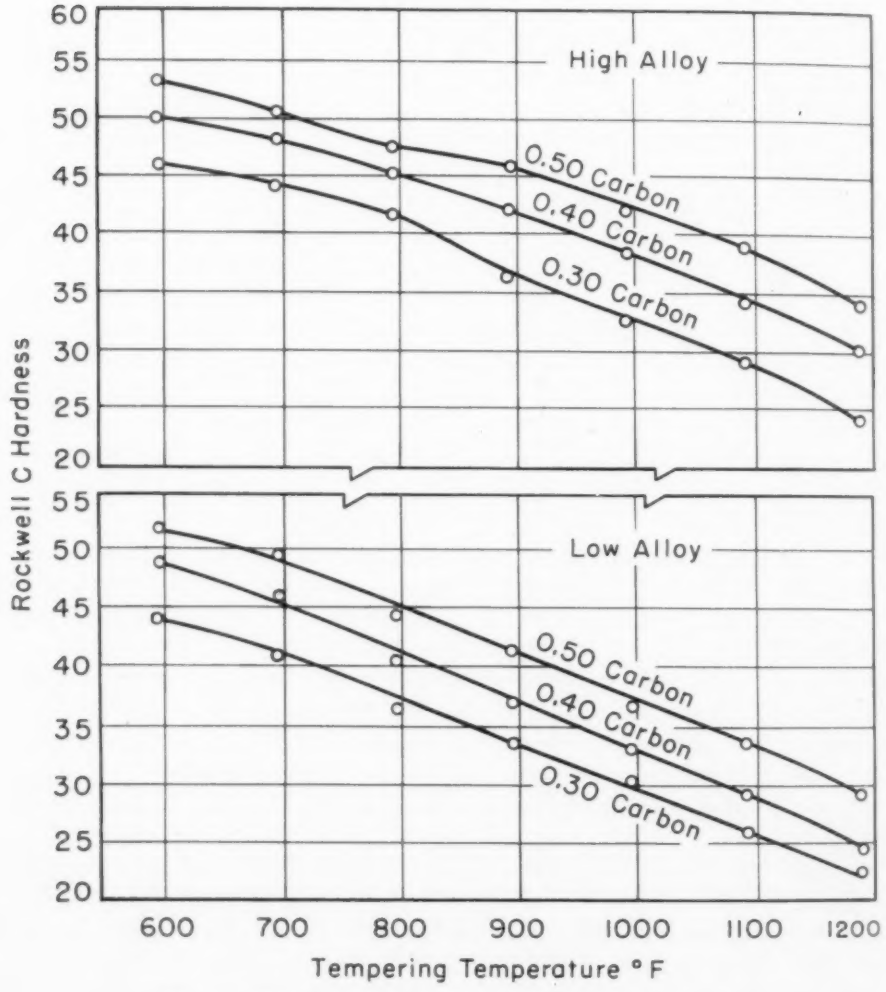


Fig. 21—Effect of Hardenability on Tempering Hardness.

We have attempted to relate tempered hardnesses and hardenability on several of the grades of the steels reported in Table VI by the authors. The common SAE constructural steels seem to classify themselves into three groups, namely: plain carbon steel, the low alloy steels, and those possessing high hardenability.

Our data were obtained from published sources which presented both composition and tempered hardnesses. It is limited to as-quenched microstructures containing an excess of 95% of martensite. From this investigation, the alloy steels seem to classify themselves into two groups with the division as follows:

30 carbon at an ideal critical diameter of 3 inches; 40 carbon, 4 inches; and 50 carbon, 5 inches.

Any steel whose ideal critical diameter was below the above values was classified as low alloy steel; anything above was considered high alloy steel. Results of these plots after averaging all the values are shown in Fig. 21.

Although the authors did not publish the composition of the steels presented in their Table VI an attempt was made to correlate their data with those in Fig. 21. In the majority of cases, predicted hardness from Fig. 21 was satisfactory. Here the hardness prediction is approximately the same as that made by the authors. In comparing values for the SAE 2340 a greater discrepancy exists between our predicted value and the measured values of Grange, where there is as much as three points of Rockwell C difference. Since we did not know the actual carbon content this could, in effect, account for part of this discrepancy. However, in comparing the SAE 2330 it will be noted that the authors' prediction was also three points of Rockwell from the measured hardness. Our values for this steel were approximately one point of Rockwell from the measured value.

The authors are certainly to be congratulated for their work and for developing a formula to predict tempered hardness with accuracy.

Written Discussion: By C. W. Spicer, chief control met., Duquesne Works, U. S. Steel Corp., Duquesne, Pa.

In the commercial heat treatment of carbon and low alloy steel bars, the estimation of hardness after tempering is of significant economic importance, inas-

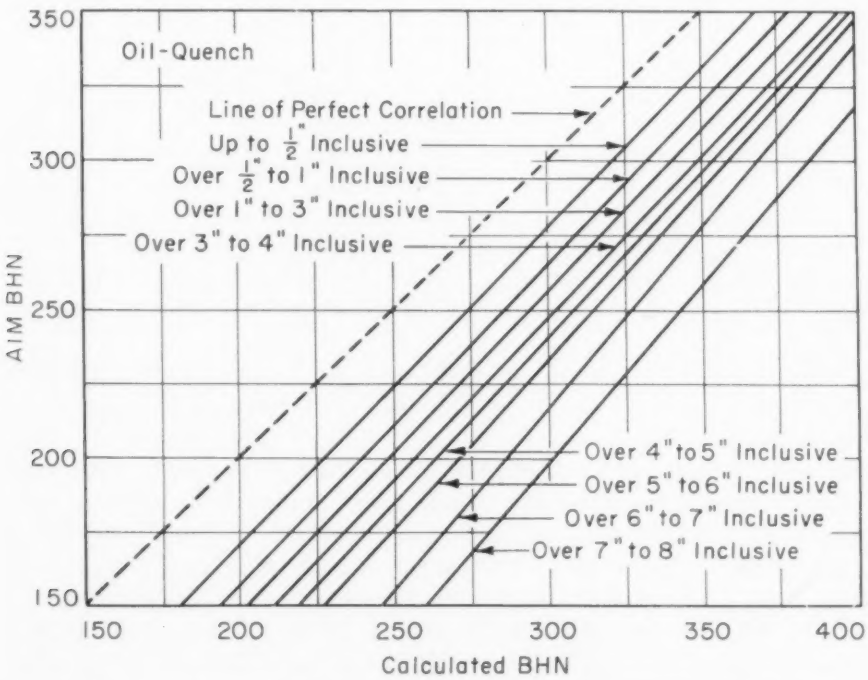


Fig.—22 Effect of Size on the Deviation from Estimated Hardness. Oil-Quenched.

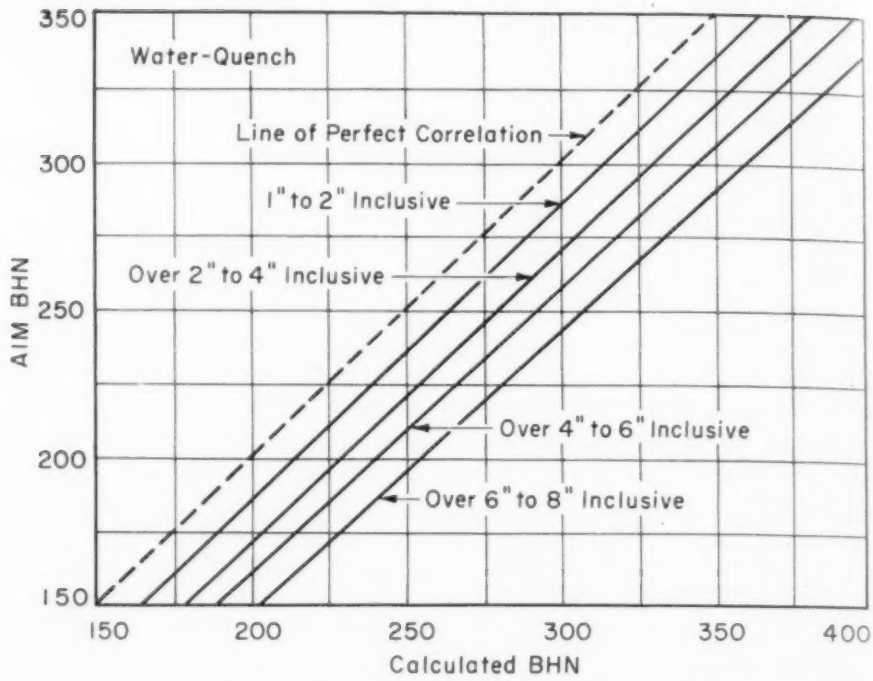


Fig. 23—Effect of Size on the Deviation from Estimated Hardness. Water-Quenched.

much as the incidence of retreatment is largely determined by the accuracy by which the tempering temperature is selected. By modifying the method proposed by the authors to suit commercial conditions, successful estimation of tempering temperatures has been carried out in the heat treatment of bars up to 8 inches in diameter of compositions ranging from plain carbon steels to AISI 4340 at Duquesne Works of United States Steel Corporation.

Since 100% martensitic structures are not always obtained in commercial heat treating operations, and since tempering conditions for large masses are considerably different from those of the laboratory, the hardness after tempering, calculated as proposed, was found to be higher than that obtained in Duquesne's heat treating plant. This variation was dependent upon the type of quenching medium and the section being treated. The series of curves plotted in Fig. 22, for oil-quenched material, show the effect of size on the deviation from the estimated hardness. Similarly, the curves in Fig. 23 show the effect for water-quenched material.

This correlation between actual and calculated hardness makes it possible to estimate tempering temperatures by applying the factors for hardness as shown by the authors in Table V.

Knowing the desired hardness, the calculated hardness to be used in determining the tempering temperature can be found from the appropriate curve in Fig. 22 for oil-quenched material or Fig. 23 for water-quenched material. After constructing the hardness curve for the particular composition involved by calculating the hardness increments at various parameter values, the parameter corresponding to the particular calculated hardness can be determined. Since the time of tempering has been established for each size being treated, the tempering temperature can be estimated directly from Fig. 3 which correlates tempering temperature, parameter value and time.

This means of establishing tempering temperatures has been used for several months at Duquesne, with a resultant decrease in retreatments due to selection of an improper tempering temperature.

Authors' Reply

We are pleased to have received discussions from those who have given much thought to the problem of relating the hardness of tempered martensite to steel composition and appreciate their valuable contributions to this subject.

Although our limited data permitted a seemingly useful method for estimating the hardness of tempered martensite, we agree with Messrs. Crafts and Lamont that additional work is desirable in order to determine more precisely the quantitative effect of each alloying element over an appreciable range of composition. The fact that data obtained previously by Messrs. Chapman and Jominy indicated that molybdenum conveyed considerably less resistance to softening than we found further emphasizes the desirability for additional study of the effect of molybdenum.

Fig. 2 of Chapman and Jominy's discussion permits a very convenient estimate of the hardness of tempered low alloy steels. However, it implies that all heats of the same grade have the same temperability. Actually, hardness after tempering for any particular combination of temperature and time varies from heat to heat of the same grade in accordance with the appreciable range in composition permitted by the SAE-AISI specification. Selecting the 4340 grade as an example and comparing a heat with all elements on the extreme low side with another heat having all elements on the extreme high side of the composition range, there would be a difference of about 5 Rockwell C if both were tempered for 1 hour at 1000°F. In order for both to have a common hardness of 38 Rockwell C, the low chemistry heat would have to be tempered at 945°F and the high chemistry heat at 1060°F—a difference of over 100°F in tempering temperature for a common tempering time of 1 hour. Thus, probably the greatest usefulness of any method for estimating the hardness of tempered martensite lies in its ability to predict the necessary adjustment in the tempering cycle for each individual heat from a determined result for a heat previously successfully tempered.

Mr. Spicer's discussion describes an adaptation of the method proposed in the paper to large scale heat treating operations. Failure to quench-out as well as less time actually at temperature, particularly in the center of large sections, made it necessary to work out correlation charts to suit his particular conditions. That he was able to do this successfully demonstrates the practical usefulness of being able to estimate hardness after tempering on the basis of steel composition.

STATIC FATIGUE OF HIGH STRENGTH STEEL

By R. H. Raring and J. A. Rinebolt

Abstract

The susceptibility to static fatigue of air-melted, vacuum-melted and argon-melted AISI 4340 steel at the 230,000 psi and 280,000 psi strength levels was determined by applying sustained loads to notched tensile specimens. At the 230,000 psi strength-level, susceptibility was negligible; at 280,000 psi strength-level, static fatigue fractures at stresses as low as 83% of the breaking strength in the short-time test were obtained. The melting practice had no significant effect.

Cadmium plated specimens at the 230,000 psi strength-level failed in static fatigue at stresses as low as 48% of the short-time breaking strength. Baking at 350°F for 1½ hrs. after plating did not significantly improve the resistance to static fatigue.

The breaking strength in the short-time test is shown to be decreased by static fatigue stressing specimens for times which approach the fracture limit. This damage is attributed to cracks which grow slowly during the static fatigue test. (ASM-SLA Classification: Q7, Ay)

Introduction

THE brittle fracture of high strength steel after long periods of time under static load has been a subject of theoretical interest and increasing engineering concern. The increased concern in the practical aspect of the problem is a consequence of recent failures of structures fabricated from steels heat treated to strength levels well above the traditional maximum of about 180,000 psi tensile strength. These failures were developed in structural components of aircraft and were characterized by nominal stresses well below the yield strength of the steel, by stress cycles much less than is generally associated with cyclic fatigue failures, and by the absence of surface markings characteristic of cyclic fatigue. For these reasons, this phenomenon is frequently and aptly called static fatigue.

Sachs (1)[1] recently compiled an analysis of static-fatigue failures of high strength steel in which it is noted that in many instances the failed part had been electroplated; this suggests hydrogen embrittlement as a cause of failure. In addition to electroplating, hydrogen

[1]The figures appearing in parentheses pertain to the references appended to this paper.

A paper presented before the Thirty-Seventh Annual Convention of the Society, held in Philadelphia, October 17–21, 1955. Of the authors, R. H. Raring is associated with the National Advisory Committee for Aeronautics, Washington, D. C. and J. A. Rinebolt is associated with the Republic Steel Company, Canton. The authors were formerly associated with the Naval Research Laboratory, Washington, D.C. Manuscript received March 30, 1955.

may be introduced into steel during other operations, such as melting, heating, pickling and electrolytic cleaning; therefore, it is possible that hydrogen-induced susceptibility to static fatigue is not peculiar to electroplated parts. Bucknall, Nicholls, and Toft (2) produced delayed fractures in conical washers of high strength steel which did not contain deliberately-introduced hydrogen. The stress levels, however, were very close to the ultimate tensile strength.

The work reported herein represents certain phases of an investigation being conducted at the Naval Research Laboratory under the sponsorship of the Wright Air Development Center, and deals with various factors which are known to influence hydrogen content. Melting in vacuum or in argon is known to result in a lower gas content, including hydrogen, than is obtained in air melting. To determine the possible benefit that might be realized by such melting practices, vacuum-melted, argon-melted and air-melted heats were compared with respect to their resistance to static fatigue. The effects of cadmium plating, which is known to introduce hydrogen, and of baking after cadmium plating to expel hydrogen, on the resistance to static fatigue, were also investigated.

Materials and Methods

The steels, within the composition limits specified by AISI for 4340, were melted in a laboratory induction furnace. The vacuum heats were melted under a pressure of about 20 microns and held under this pressure for 35 minutes after melt-down. It was found necessary to introduce a pressure of about 50mm of argon to the chamber before the addition of the alloying elements because of the violent boil which would otherwise occur. The vacuum heats were poured and allowed to solidify in this same atmosphere. After solidification, the furnace was evacuated and the vacuum was maintained until the ingot reached room temperature. The argon heats were melted, poured and allowed to freeze in an atmosphere of 760mm of argon. The average hydrogen content of the ingots were: air-melted, 0.5–1.3 ppm; argon-melted, 0.3–0.6 ppm; and vacuum-melted, 0.2–0.6 ppm. The analytical method used in the determination of hydrogen is reproducible to within ± 0.1 ppm.

The ingots, which weighed about 30 pounds, were cut into billets, homogenized at 2200°F for 1 hour, and forged into $\frac{5}{8}$″ square bars. The bars were saw-cut to specimen-blank size, normalized at 1650°F, and machined to 0.020 inch oversize specimens. These specimens were then austenitized at 1550°F, oil-quenched and tempered, after which final machining was performed.

Specimens which were to be tested in the plated condition were degreased, anodically cleaned, pickled, and then cadmium plated in a cyanide bath containing a brightener. The thickness of the cad-

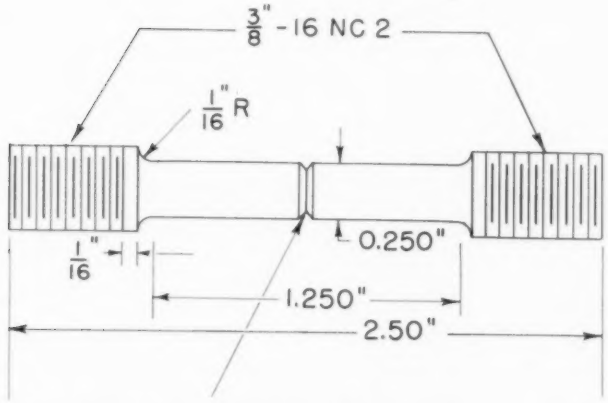


Fig. 1—Static Fatigue Specimen.

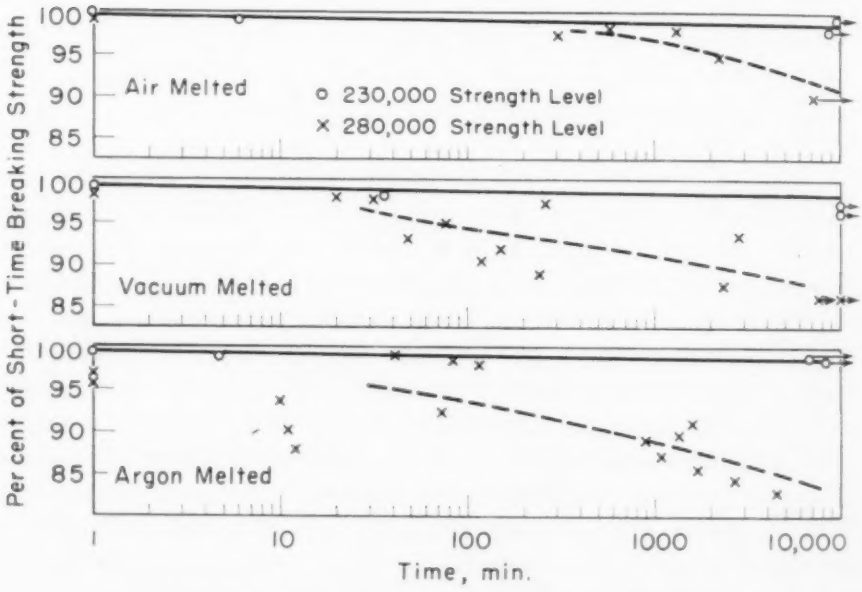


Fig. 2—Static Fatigue Curves of Unplated 4340 Steel.

mium plate was 0.0005 inches. The baking treatment consisted of placing the plated specimens in a muffle furnace at 350°F for 1½ hours; the specimens reached 350°F in approximately 15 minutes. The plate thickness and baking conditions are typical of commercial practice.

Fig. 1 illustrates the static-fatigue test specimen. A dead-weight lever-arm type of machine, patterned after the conventional stress-rupture machines used in the testing of high temperature alloys, was used for loading. The time to fracture was determined by a device which opened the circuit of an electric timer when fracture occurred.

Effects of Melting Practice and Strength Level

The effects of melting practice on hardenability, tensile properties, and Charpy V-notch impact properties, at high strength levels had been determined previously and reported in reference (3). There was no significant effect of melting practice on these properties.

Fig. 2 shows results of static fatigue tests of air-melted, vacuum-melted and argon-melted 4340 at two strength levels, 230,000 psi and 280,000 psi. The stress ordinate is plotted as percent of the breaking strength of the notch specimen in a short-time tensile test (cross-head speed of 0.1 inches per minute). The breaking strength in the short-time test varied from heat to heat, within the limits of $\pm 3\%$ of the plotted values. The average breaking strengths in the short-time notch-tensile tests, and the tensile strength as determined by tests of 0.357 inch diameter unnotched specimens, are listed below:

Tensile Strength psi	Melting Practice	Notch Tensile Strength in Short-Time Test
235,000	Air	322,500 psi
231,000	Vacuum	318,000 psi
231,000	Argon	315,000 psi
287,000	Air	368,500 psi
280,000	Vacuum	355,000 psi
282,000	Argon	374,000 psi

A few breaks occurred at times less than a minute after the full load was applied. Such breaks are plotted on the one-minute ordinate. It is evident from Fig. 2 that the susceptibility to static fatigue of the steels at the 230,000 psi strength level is very slight, at least for times up to about 170 hours. The lowest stress at which a static fatigue failure occurred in steel of this strength level is within 3% of the short-time breaking strength. It may be concluded that at the 230,000 psi strength level a static fatigue phenomenon which could be likened to delayed fractures observed in service was not produced in these tests.

At the 280,000 psi strength level, delayed breaks were obtained at stresses as low as 83% of the strength in the short-time test; the data suggest that if the test-time had been extended, even lower values might result. It is evident that at the 280,000 psi strength level, static fatigue is a factor which must be reckoned with even for steels which are not exposed to hydrogen-generating operations such as electroplating. It is evident also that no significant benefit resulted from either vacuum-melting or melting in an argon atmosphere.

Effects of Cadmium Plating

Specimens of the air-melted steel of 230,000 psi strength level were tested in static fatigue within ½ hour after cadmium plating,

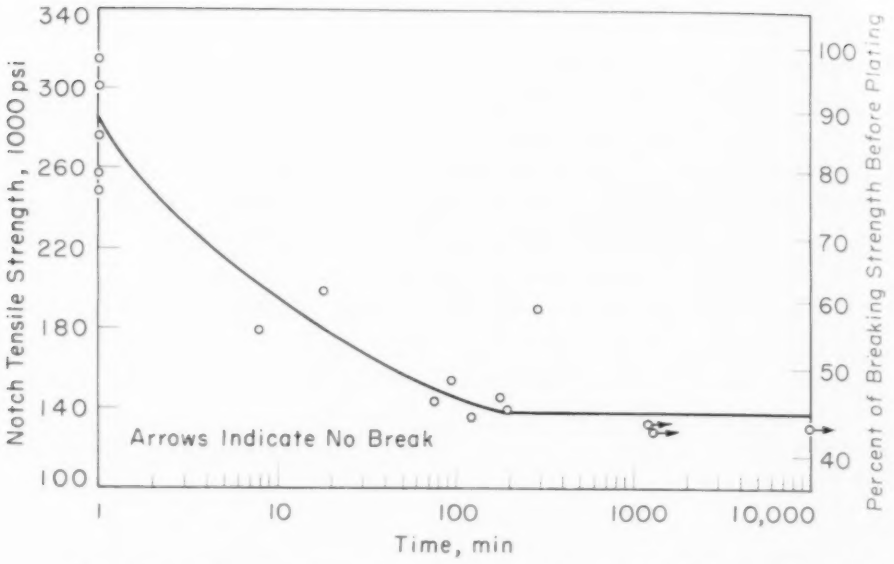


Fig. 3—Static Fatigue Curve of 4340 Steel of 230,000 psi Tensile Strength; Cadmium Plated, Not Baked.

with the results shown in Fig. 3. The results of five short-time tests represented on the one-minute ordinate, indicate that electroplating lowered the breaking strength. The average breaking strength of this steel in short-time tests before plating was 322,500 psi, whereas after plating, it varied from 248,000 psi to 315,000 psi, with an average of 281,000 psi.

The effect of plating on the susceptibility to static fatigue was much greater than its effect on the short-time breaking strength, as may be observed by comparison of Figs. 2 and 3. The data from the static fatigue tests show a stress vs. log-time relationship not unlike the well-known S-N curves characteristic of cyclic fatigue tests. Fig. 3 suggests the existence of a static fatigue limit, for this particular steel and treatment, of about 130,000 psi.

Effects of Baking

Static fatigue data for a vacuum melted steel of 230,000 psi strength level after cadmium plating and baking (350°F for 1½ hours) and of the same steel before cadmium plating, are shown in Fig. 4. This steel represented a different heat from that of Fig. 2. The susceptibility to static fatigue of the unplated steel is again indicated to be very slight at the 230,000 psi strength level. Although the baking operation reduced the scatter in the breaking strength in the short-time test and restored the strength nearly to that of the unplated specimens, the susceptibility to static fatigue was not changed appreciably. The inadequacy of the baking treatment (350°F, 1½ hours) is evident from these results. It is interesting to note that the

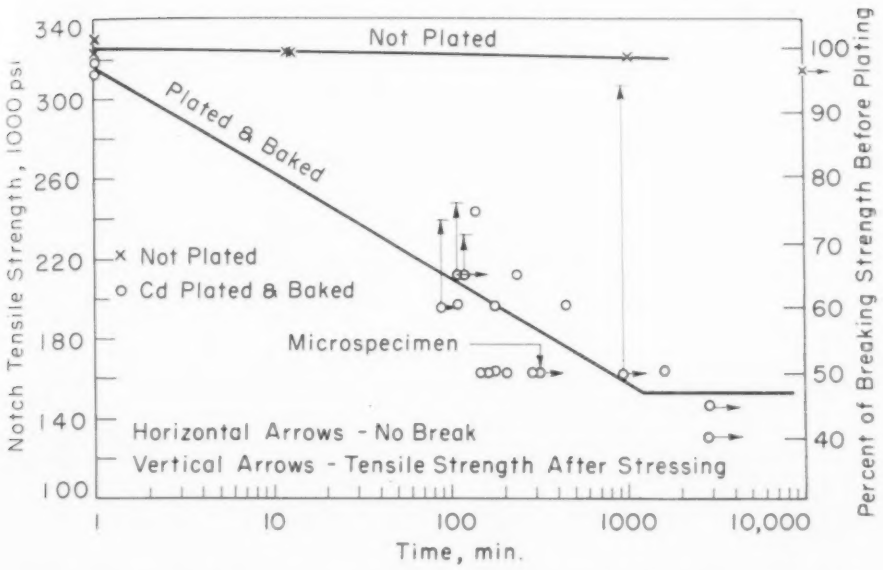


Fig. 4—Static Fatigue Curve of 4340 Steel of 230,00 psi Tensile Strength; Cadmium Plated and Baked.

ASTM standards (4) require a baking time of at least ½ hour and recommend a maximum of 400°F for cadmium plated parts; the requirement of Federal Specifications (5) is 350–400°F for 3 hours. The hydrogen content before baking was 0.7 to 1.1 ppm; after baking it was 0.6 to 0.7 ppm.

Tests were also made to compare tensile properties as determined by unnotched tensile specimens before plating and after plating and baking. The unnotched tensile specimens were the same as the notched static-fatigue specimens, except for the notch. Results of these tests were as follows:

	Before Plating	After Plating & Baking (350°F, 1½ hrs.)
Tensile Strength psi	234,000	230,000
Yield Strength psi	208,000	208,000
% Elongation in 1"	15.0%	15.0%
% Reduction of Area	57.0%	52.5%

It is apparent that full recovery may be indicated by the conventional tensile tests whereas the notched static fatigue tests indicate essentially no recovery due to the baking operation.

Mechanism of Damage

Certain tests were made to determine if a stress, which is known to be high enough to lead ultimately to a static fatigue fracture but applied for a time insufficient to cause a break, would effect any permanent and irreversible change in the properties of the steel. Such an effect would be similar to the well-known "damage"

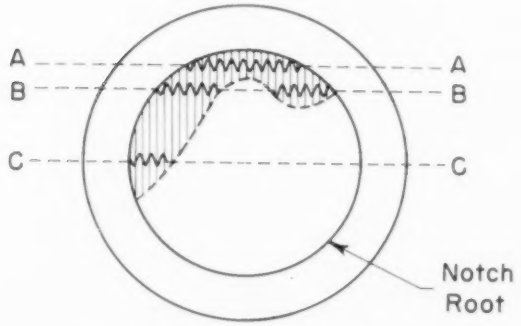


Fig. 5—Transverse Section at Notch Root Showing Longitudinal Sections of Figure 6. Serrated Lines Indicate Cracks.

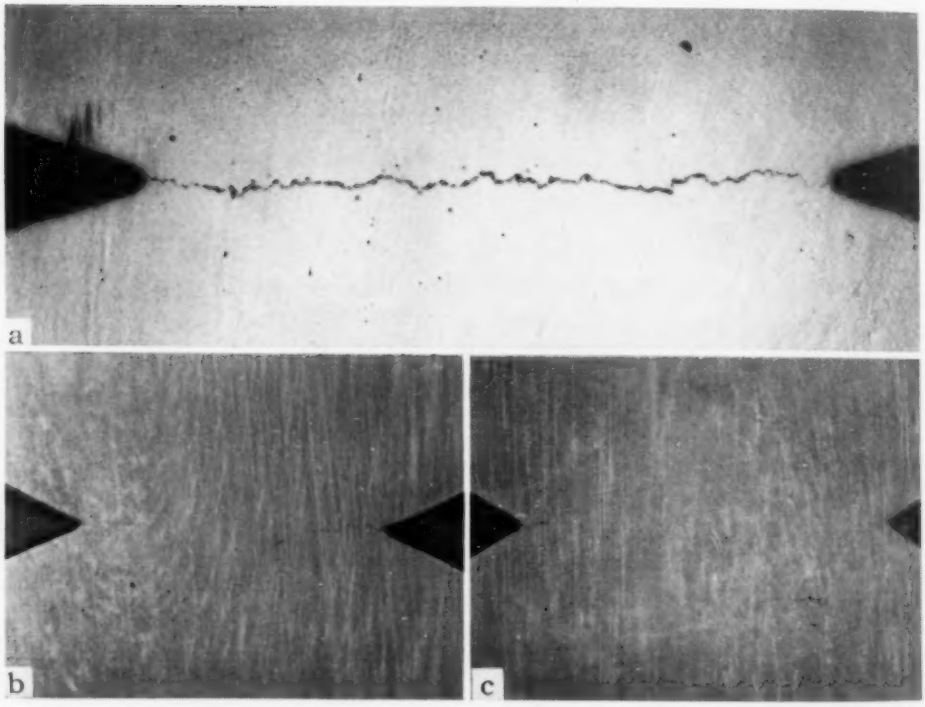


Fig. 6—Macrophotographs of Longitudinal Sections Indicated in Fig. 5. (a) Section AA, ×50; (b) Section BB, ×12; (c) Section CC, ×11. Reduced 20% in reproduction.

effect in cyclic fatigue. To answer this question, specimens were removed from the static-fatigue machine prior to fracture and then broken in a tensile test. Microexamination of notch tips was also performed to determine if cracks were developed during the holding period.

These specimens are represented on Fig. 4 by points with horizontal arrows, indicating no break, and vertical arrows which terminate at the stress level at which the specimen broke in the subsequent short-time test. Three of the specimens revealed damage which reduced the short-time breaking strength by 21 to 28%; the

third suffered a reduction of only 2½%. It is noteworthy that the latter specimen was stressed at a level near to the lower limit for delayed breaks for times up to 50 hours.

Specimens which were removed from the static fatigue test before fracture were carefully examined at the notch root with a binocular microscope for evidence of cracks. No cracks could be detected by this method. One specimen, identified on Fig. 4, was sectioned longitudinally at various depths and examined metallographically. The first, rather shallow cut revealed a transverse crack at the

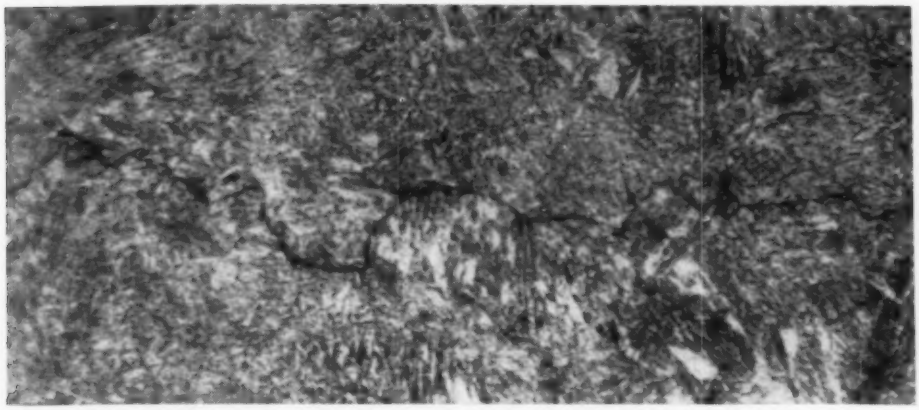


Fig. 7—Photomicrograph of Damaged Crack. ×1000. Reduced 20% in reproduction.

notch root. Further grinding to greater depths showed that the crack had grown both circumferentially and radially, as indicated in Fig. 5. Macrographs of the longitudinal sections are shown in Fig. 6, which illustrates the general shape and size of the crack at positions A, B and C of Fig. 5. The appearance of the crack in a microsection at high magnification is shown in Fig. 7. The marked tendency for the crack to delineate areas of like orientation of martensite indicates that it follows the boundaries of prior austenite grains.

Petch and Stables (6) recently proposed a mechanism to explain the effect of hydrogen on delayed fracture under static load. Their explanation is based on the Griffith mechanism. The delay of fracture in steel containing hydrogen is explained by assuming that at stresses above a certain minimum, the growth of Griffith microcrack is arrested as soon as it begins to grow because the new crack surface developed is clean and therefore of high surface energy. Dissolved hydrogen is assumed to migrate to the surface of the new crack causing a decrease in the surface energy. As the result of the decreased surface energy the crack will then grow slightly again, and the sequence of events is repeated until the crack is large enough to cause sudden fracture.

It is interesting to note that the Petch and Stables mechanism may be extended to predict a static fatigue limit; while the Petch and Stables mechanism provides a plausible explanation it cannot be said that it is proved by these observations. The mechanism also predicts that hydrogen level and diffusion rates of hydrogen at various temperatures would influence the development of static-fatigue failures.

Discussion

The results of this investigation show that properties of steels at high strength-levels, as determined by conventional short-time tests, are not necessarily a reliable indication of their behavior in service. The development of a static-fatigue phenomenon in such steels must be recognized in the selection and treatment of high strength steels for engineering structures.

Susceptibility to static fatigue apparently increases as strength level increases; the quantitative relationships, however, are not established by data available to date. The fact that delayed fractures in service have been encountered only for steels of very high strength levels, and the marked difference in resistance to static fatigue between 230,000 psi shown herein, and 280,000 psi steels indicate a dependency on strength level. The development of a static fatigue phenomenon for unplated steels of 280,000 psi strength level indicates that the problem is not entirely one of processing operations, such as electroplating, which introduces hydrogen. Moreover, the use of special melting practices aimed at lowering the hydrogen content of the steel had no significant effect on resistance to static fatigue.

Baking as a means of restoring resistance to static fatigue of cadmium plated specimens was ineffectual in these tests. Although somewhat higher baking temperatures and longer baking times may be of benefit and should be investigated, the baking conditions used in these tests are representative of industrial treatments. It should be noted also that while the short-time tests of plated and baked specimens, both notched and unnotched, indicated essentially complete restoration of strength and ductility, the resistance to static fatigue was not restored by baking. These results suggest that sole reliance on short-time tests to evaluate the efficacy of baking may lead to misleading conclusions.

Summary

The effects of melting in vacuum or argon atmospheres on the susceptibility to static fatigue of AISI 4340 heat treated to high strength levels, and of baking treatments to effect recovery of plated steels, was investigated in relation to the problem of static fatigue

failures. Resistance to static fatigue failure was determined by applying loads to notched tensile specimens for extended periods of time. The following conclusions were indicated:

1. Melting in vacuum or in an argon atmosphere has no significant effect on resistance to static fatigue.

2. Susceptibility to static fatigue of unplated 4340 steel at the 230,000 psi strength level was negligible. At the 280,000 psi strength level, static fatigue failures at loads as low as 83% of the breaking strength in the short-time tests occurred.

3. Cadmium plating lowered the breaking strength and greatly increased the susceptibility to static fatigue.

4. Baking at 350°F for 1½ hours restored the breaking strength in the short-time test to within 2% of the breaking strength of unplated specimens, but had very little effect on resistance to static fatigue. Static fatigue fractures at loads as low as 50% of the breaking loads in the short-time test occurred after baking.

5. Specimens stressed at loads lower than the breaking strength in the short-time test, and subsequently broken by short-time tests, were found to have suffered a reduction as great as 27% in breaking strength. Metallographic examination disclosed that the loss in strength resulted from the slow growth of cracks which is the initiating mechanism of static fatigue failures.

Acknowledgment

The work reported herein represents several phases of an investigation being conducted at the Naval Research Laboratory and supported by the Aeronautical Research Laboratory of the Wright Air Development Center, U. S. Air Force, under Order No. 53-203 WADL-N. Permission to publish these results is gratefully acknowledged. The interest and counsel of Mr. W. S. Pellini, Superintendent of the Metallurgy Division, Naval Research Laboratory, and the assistance of Mr. Frank Bird, are acknowledged with thanks.

References

1. G. Sachs, "Survey of Low-Alloy Aircraft Steels Heat Treated to High Strength Levels," Part 3—Failure Cases, WADC Technical Report 53-254, Part 3, February 1954.
2. F. H. Bucknall, W. Nicholls and L. H. Toft, "Delayed Cracking in Hardened Alloy Steel Plates," *Symposium on Internal Stresses in Metals and Alloys*, Institute of Metals, London, 1948, p. 351.
3. J. A. Rinebolt, "NRL Memorandum Report No. 345, Progress Report on the Effect of Gases on Steel," March 1953–July 1954.
4. "Preparation of High-Carbon Steel for Electroplating," American Society for Testing Materials Designation B242-53.
5. Federal Specification QQ-P-416.
6. N. J. Petch and P. Stables, "Delayed Fracture of Metals Under Static Load," *Nature*, Vol. 169, No. 4307, May 17, 1952, p. 842.

DISCUSSION

Written Discussion: By K. Winterton, assistant director, Ontario Research Foundation, Toronto, Canada.

The authors are to be congratulated on their approach to this interesting problem. They do not always explicitly ascribe the cause of low static fatigue strength to the presence of hydrogen. I would, therefore, like to emphasize that hydrogen, even in very small quantities, can have a pronounced effect on alloy steels in the quenched condition. Fig. 8 shows the dead-load rupture strength (or static fatigue strength) for a carbon-manganese steel as a function of cooling rate.

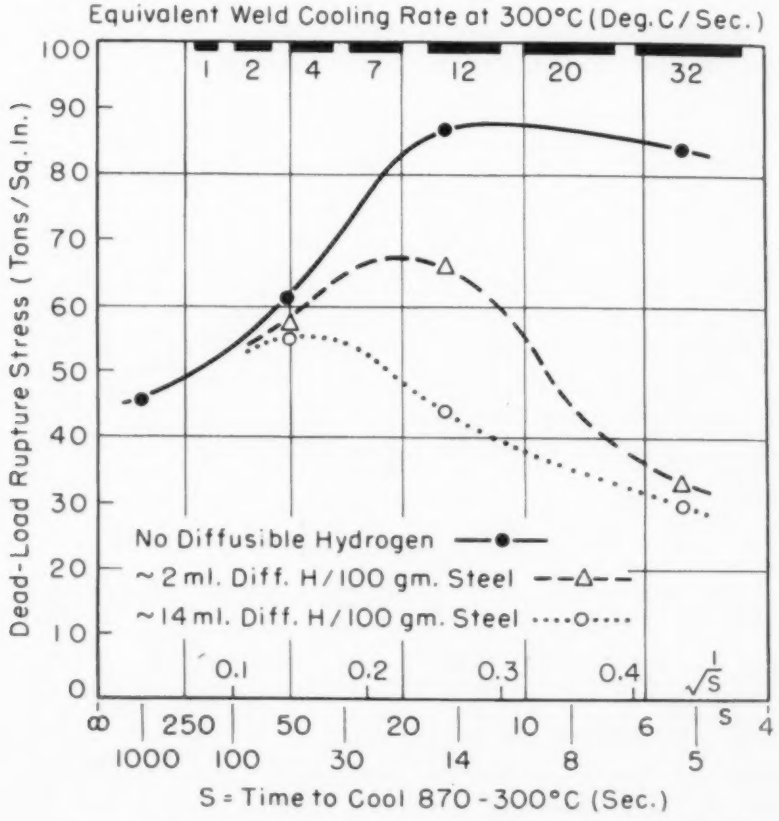


Fig. 8—Effect of Hydrogen Content and Cooling Rate on Dead-Load Rupture Stress of a C-Mn Steel (Notched Specimens, Peak Temperature 1300°C Approximate).

The upper curve represents the values obtained for untreated specimens. The two lower curves were obtained after introducing by electrolysis 2 cc. and 14 cc. per 100 grams of hydrogen respectively. There is quite a marked drop in rupture strength, particularly at high cooling rates, even with only 2 cc. per 100 grams of hydrogen present. It may be noted that 1 cc. per 100 grams is approximately equivalent to 1 ppm. Fig. 9 illustrates the same sort of result for a more highly alloyed steel, this being a 3½%-nickel: chromium: molybdenum: vanadium steel. In the as-received condition this steel contained 0.35 cc. per 100 grams of hydrogen. After de-gassing, which was done in vacuo at 750°C (1380°F) there was a marked improvement in rupture strength. In both cases illustrated, the results were obtained on notched, hollow, cylindrical specimens which were subjected to a ther-

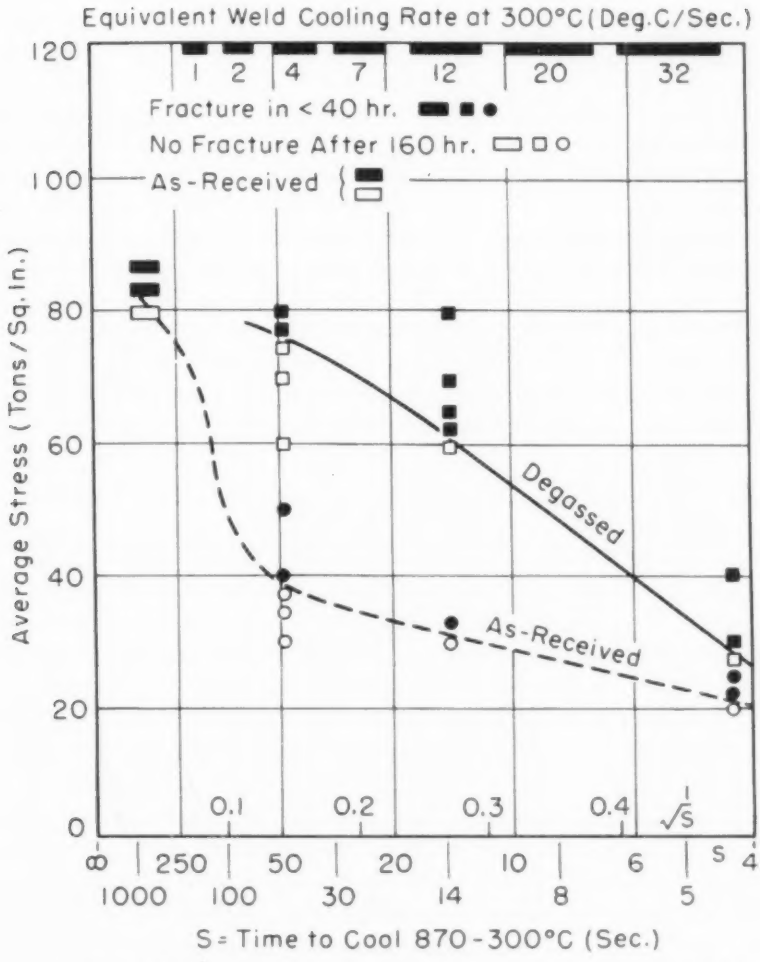


Fig. 9—Effect of Hydrogen Content and Cooling Time on the Dead-Load Rupture Stress of a 3½% Ni-Cr-Mo Steel.

mal cycle, imitating that received in the hardened zone of a metal arc weld, prior to static tensile testing. The work quoted was done at the British Welding Research Association.[2]

Finally, I think that we should be careful in thinking about hydrogen content in ppm in this connection. This is quite satisfactory for solid solution or for a separate solid phase, but if there is any chance of the gas coming out of solution I think that we should recall that 1 ppm is equivalent to 8% by volume. To illustrate this, imagine a block of steel about the size of a grapefruit, this containing a single pore about the size of a large pin's head with hydrogen present in the pore at a pressure of 100,000 atmospheres. The system represents a hydrogen content of 1 ppm.

Written Discussion: By E. P. Klier, B. B. Muvdi, V. Weiss and G. Sachs, Syracuse University Research Institute, Metallurgical Research Laboratories, Syracuse, New York.

[2]C. L. M. Cottrell, "Hydrogen—Barrier to Welding Progress," (published in part) Welding Journal, Vol. 1, No. 4, April, 1954, p. 167.

The authors in their very interesting paper advance the concept that sustained load failures in ultra high strength steels result from "static fatigue." Since the indicated reduction in notch strength is greater than 15% for failures within a loading period of 100 hours at the 280,000 psi strength level, it may be concluded from these data that strength levels much above 230,000 psi are of very limited practical value. Additional data bearing on this conclusion are, therefore, desirable.

The potential reduction in the sustained-load strength of high strength steels has been the subject of extensive and continuing studies at the Syracuse Univer-

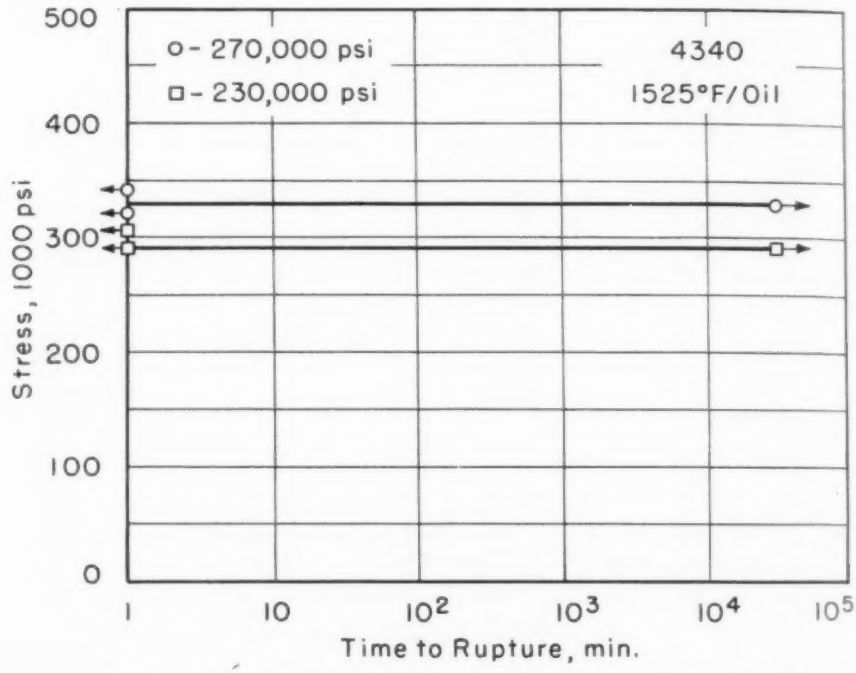


Fig. 10—Stress-Rupture Diagram for Notched (K-5) 4340 Steel Specimens at Two Strength Levels (3).

sity Research Institute. Among the factors pertinent to this phenomenon, which have been studied for 4340 steel are:

1. Strength level,
2. Loading pattern,
   - —sustained,
   - —variable loading rate,
   - —oscillatory-fatigue.
3. Stress concentration,
4. Nonembrittled condition,
5. Hydrogen embrittled,
   - —cathodically embrittled,
   - —plated.

The results of these tests indicate that sustained-load failures are probably due to the presence of hydrogen in the metal, and are thus not uniquely the result of a surface phenomenon as is proposed for static fatigue in glass-like materials. Thus, as is indicated in Fig. 10, sustained-load failures were found to be absent in

our tests on commercial 4340 steel, at a strength level of 270,000 psi and the respective data fall within the expected scatter range.[3]

The examination of notch roots for evidence of cracking after removal of the load is difficult for cadmium-plated specimens. On the other hand, the growth of the crack at the base of sharply-notched, copper-plated specimens is readily detectable if the specimens are examined with the aid of a low power lens while the load is applied.[4] This crack growth, however, applies only to sharply notched specimens; mildly-notched specimens, on the other hand, have been observed to fail without any indication of a slowly progressing crack and, therefore, probably from the development of internal cracks.

In the course of the tests at Syracuse University, the circumferential development of the crack in the sharply-notched specimens was examined and it was usually found to be rather uniform all around the periphery. Where the crack developed asymmetrically, this could be attributed to nonaxial loading conditions.[5]

Authors' Reply

The authors agree with Dr. Winterton's observation that there is evidence that hydrogen, even in relatively small quantities, can have a pronounced effect on the susceptibility of high strength steel to static fatigue. Fig. 8 clearly shows that electrolytic charging reduced the dead-load rupture stress of steel, and that the degree of reduction increased with the hardness.

The hydrogen content of steel has been reported in the literature in terms of several different units. The authors preferred to report it in parts per million because the results come out in numbers that can be read quickly and remembered easily, and because chemists conventionally used these units for reporting elements in very low concentrations. But, as Dr. Winterton points out, expressing the hydrogen content in terms of cc/100g (or perhaps even better as Vol H/ Vol steel) certainly has a merit of being a more graphic method for those who like to envisage an internal pressure generated by hydrogen in voids in the steel.

It is gratifying to learn that Dr. Klier and his associates also have observed cracks growing slowly from the notch root of electroplated tensile specimens of 4340 steel at high strength levels, and the authors look forward with interest to the publication of these results in the paper they have submitted to American Institute of Mining and Metallurgical Engineers. It is implicit in their discussion that the term "static fatigue" should be reserved for the surface phenomenon associated with the slow development of surface cracks in glasses. The authors were aware of this prior use of the term, but still prefer it to the less descriptive or more awkward terms "delayed fracture under static load," "stress-rupture," or "sustained load failure," which have been used in the recent past. Among other considerations, several points of similarity between characteristics of these fractures and those of cyclic fatigue in metals suggest that "static fatigue" is the most apt and nicest terminology. This is a question of nomenclature, of course, and it is hoped that in the near future common usage will be established.

---

[3] E. P. Klier, V. Weiss and G. Sachs: Discussion to E. M. Lape and J. D. Lubahn, "On the Relations Between Various Laboratory Fracture Tests," Paper No. 55-SA-70, 1955 ASME Diamond Jubilee Semi-Annual Meeting.

[4] E. P. Klier, B. B. Muvdi and G. Sachs, "Effects of Hydrogen Embrittlement on High-Strength Steels," (Static Properties), WADC TR 55-18 Pt. 1. (Submitted for publication to AIME)

[5] G. Sachs, B. B. Muvdi and E. P. Klier, "Effects of a Number of Variables on the Mechanical Properties of Aircraft High-Strength Steels," WADC TR 55-103.

The conclusion of Klier et al. that "strength levels much above 230,000 psi are of very limited practical value" is considered to be somewhat premature or unduly pessimistic. The very fact that their results indicated no susceptibility to static fatigue at strength levels as high as 270,000 psi suggests that susceptibility is not necessarily associated with high strength levels. Work on steels at these strength levels is still in an early stage. Eventually, the factors at the root of the phenomena might be understood and brought under control. It should be mentioned, however, that many tests subsequent to those reported in the paper not only confirm the reality of static fatigue in high strength steels that had not been subjected to embrittling treatments but showed static fatigue failures as low as 82% of the short time breaking strength.

The suggestion that the asymetrical development of the crack was the result of nonaxial loading is reasonable. Tests made subsequent to those reported in the paper resulted in cracks of uniform depth around the periphery. This was attributed to improved alignment of the load and the test specimen.

SOME EFFECTS OF METAL REMOVAL AND HEAT TREATMENT ON THE SURFACES OF HARDENED STEELS

By Karl E. Beu and Donald P. Koistinen

Abstract

Some effects of metal removal and heat treatment on the surfaces of hardened steel were studied using retained austenite and residual stress measurements as criteria. Both austenite and stress measurements were made using X-ray diffraction techniques. It was found that metal removal using a standard metallographic polishing sequence (a) affected the austenite content significantly to measurable depths below the final polished and etched surfaces and (b) left large compressive stresses in these surfaces. It was also found that metal removal using a belt sander (a) increased the austenite content of the surface if the metal was removed rapidly and (b) decreased the austenite content of the surface if the metal was removed slowly. In either case, large compressive stresses were left in the surface. After any of the above procedures, the compressive stresses could be reduced essentially to zero by removing about 0.005 inch metal electrolytically. Decarburization was studied by means of austenite content, austenite and martensite lattice parameter, and chemical carbon measurements with depth. The effectiveness of copper plate in protecting the surfaces from decarburization is discussed. (ASM-SLA Classification: N8, L10, J general, ST)

Introduction

THE effects of metal removal and heat treatment on and near the surfaces of hardened steel parts are of practical interest because of the possible relationship of these effects on the engineering performance of such parts. These effects are difficult to evaluate since they cannot generally be completely controlled. For example, it is accepted practice to grind off several thousandths of an inch to remove the decarburized layer on a hardened steel part; however, grinding in itself may introduce additional surface effects. Thus, a finished hardened part may have nonuniform phase or stress distributions near the surface as a result of heat treatment, finishing opera-

A paper presented before the Thirty-Seventh Annual Convention of the Society, held in Philadelphia, October 17–21, 1955. Of the authors, Karl E. Beu is supervisor, Physical Measurements Department, Goodyear Atomic Corp., Portsmouth, Ohio, and Donald P. Koistinen is research physicist, General Motors Corp., Research Laboratories Division, Detroit. Manuscript received March 21, 1955.

tions, or both. These nonuniformities may, in turn, have a profound effect on the physical properties of hardened steel parts.

The effects of heat treatment and metal removal have been previously studied by measuring surface[1] gradients of (a) microhardness (1)[2], (b) chemical carbon, (c) residual stress (2,3,4), and (d) retained austenite (5) in hardened steels. It has also been pointed out that grinding induces phase changes (1,6), that retained austenite can be decomposed in the vicinity of the fracture surface of a tensile or impact test bar (7,8,9), and that the surface of an alpha iron single crystal can be partially transformed to gamma iron by very slight abrasion (10). These experiments indicate that the physical characteristics of the sample material near the surface of hardened steel parts (or even pure iron) can be readily affected by relatively minor mechanical or chemical disturbances of the surface. In fact, it has been pointed out that the decomposition of retained austenite with mechanical stressing "illustrates the possibility of using retained austenite as an internal strain gage" in tensile test bars even before necking occurs (8). Other than this, however, relatively little has been reported on the relationship of surface retained austenite and residual stress variations to metal removal and heat treatment problems.

These problems of surface austenite variations have generally been side-stepped by carefully removing the original heat treated surface using a combination of careful sanding or grinding techniques with chemical or electrolytic etching. The austenite content of this newly formed surface is then said to be representative of the sample. This has been found to be true in some, but not all, instances and it is a purpose of this paper to indicate some of the limitations of such an interpretation. In addition it is hoped that some of the experiments to be described may indicate ways for establishing a relationship of heat treatment and final finishing operations to the quality of the finished hardened steel product in terms of some physical surface characteristics such as retained austenite and residual stress distributions.

Some Effects of Mechanical Metallographic Polishing on Hardened Steel Surfaces

Mechanical metallographic polishing has been considered for studying surface effects in metal removal since it is as gentle a mechanical removal method as is ordinarily available. If metallographic polishing causes measurable surface changes in hardened steel it is likely that any other more drastic metal removal technique would

[1]Unless otherwise stated, the word "surface" shall imply both the immediate surface and depths below the surface to about 0.050".

[2]The figures appearing in parentheses pertain to the references appended to this paper.

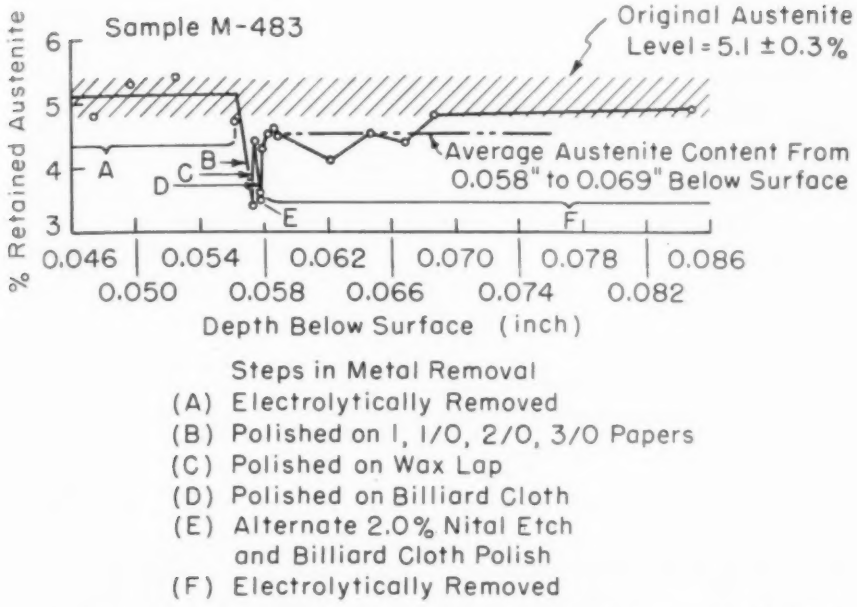


Fig. 1—The Effect of Metallographic Polishing on Retained Austenite Content at the 5% Austenite Level.

also cause changes in surface characteristics. If it causes no changes, then it may be used as a standard for comparison with other metal removal methods. As a secondary consideration, the physical properties of metals are often related to a microscopic examination of polished sections, assuming that the polished section is representative of the sample. If this is not so, then errors in interpretation may arise.

A study has been made on a series of hardened plain carbon steels with retained austenite contents in the range of 5 to 30% to determine (a) the utility of metallographic polishing as a metal removal standard and (b) the validity of mechanically polished and etched surfaces as being representative of these samples. Results of this study on three samples are summarized in Figs. 1 and 2. Each sample was prepared as follows prior to mechanical polishing and etching:

Sample No.	Steel	Heat Treatment
M-483	SAE 1070	Austenitized 1900°F 1 hr., brine-quenched, tempered 300°F ½ hr.
M-554	SAE 1095	Austenitized 1600°F 1 hr., brine-quenched, tempered 300°F ½ hr.
M-472	SAE 1.31% carbon	Austenitized 1700°F 1 hr., brine-quenched, tempered 300°F ½ hr.

Each sample was cut from bar stock finished as a disk ⅞ inch diameter by 3/16 inch thick, and plated with 0.002 inch copper before heat treatment. It has been found that this preparation procedure is

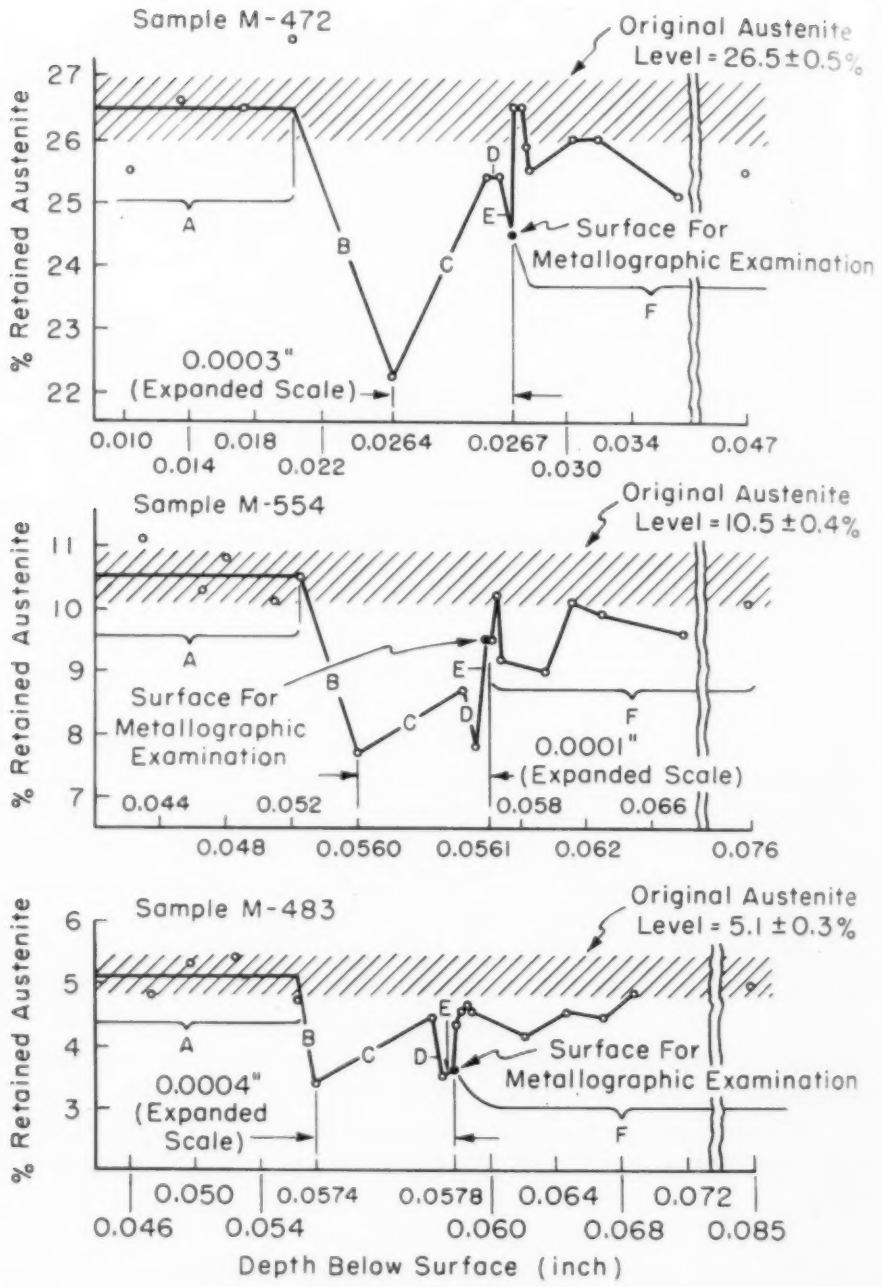


Fig. 2—The Effect of Metallographic Polishing on Retained Austenite Content at the 5, 10, and 25% Austenite Levels.

effective in providing a sample of uniform austenite content from the surface to the interior for plain carbon and low alloy steels. After heat treatment the copper plate was stripped chemically and austenite measurements made in increments to depths of at least 0.020 inch, metal being removed electrolytically after each step. It has been found that electrolytic metal removal does not affect the austenite content of this type of sample even when as much as 0.100 inch is removed in this manner.

The uniformity of austenite content for each of these three samples is indicated in step A in Figs. 1 and 2. Referring to Fig. 1, the austenite level of Sample M-483 was established at $5.1 \pm 0.3\%$ by averaging the austenite measurements over a depth of about 0.010 inch prior to removing metal in the metallographic polishing sequence. The X-ray method used for measuring retained austenite concentrations has been previously described (11–14). The standard deviation of the austenite measurements (15) ($\pm 0.3\%$ for this sample) is indicated by the shaded band labelled "original austenite level" and, as can be seen, nearly all the experimental points in step A fall within this shaded band. This indicates that the austenite content of this sample is essentially uniform within the experimental error of measurement. After having established austenite level and uniformity, the sample was then prepared for metallographic examination using the following sequence:

B) Rough polishing with 1, 1/0, 2/0, and 3/0 papers on a rotary lap using oleum spirits as a lubricant.
C) Polishing on a wax lap using Linde A abrasive.
D) Polishing on billiard cloth using Linde B abrasive.
E) Alternate billiard cloth polishing and 2.0% nital etch.

Austenite measurements were made after each step in the above sequence. Since so little metal was removed in these steps, the variations in austenite percentages are difficult to see because the experimental points fall so closely together in Fig. 1. In order to present these data more clearly, the abscissa in the region of steps B through E has been expanded as shown in Fig. 2. Since the same type of data was obtained on samples M-554 and M-472, the results on these samples are also included in Fig. 2.

It can be seen from sample M-483 that the austenite content dropped from a level of 5.1 to 3.4% in step B (rough polishing on papers). The significance of this 1.7% drop in austenite with rough polishing will be discussed in detail below. Step C (polishing on a wax lap) resulted in a small but significant[3] increase in austenite toward the original level. Step D (polishing on billiard cloth) re-

[3]By significant is meant a change in austenite percentage larger than ± sigma (standard deviation). This reproducibility error (15) should be kept in mind for all austenite percentages reported since it will not be indicated explicitly for each percentage.

sulted in a slight decrease in austenite with essentially no change after step E (alternate polishing and etching).

The surface after step E is that which would be examined metallographically. The austenite content of this surface is not representative of this sample since X-ray measurements indicate 3.6% austenite at this surface as compared to an austenite level of 5.1 ± 0.3%. Quantitative measurements on this surface using lineal analysis techniques (16), for example, would be in error even more seriously than X-ray measurements if it is considered that the X-ray austenite measurements represent an average over a depth of about 0.0003 of an inch (17). (This problem is in addition to that of being able to detect and measure small amounts of austenite microscopically). Since the austenite content of this sample increases rapidly below the surface after step E, the austenite content of the immediate surface accessible to metallographic examination would be less than 3.6%. This statement of the averaging effect of the X-ray austenite measurement can be generalized to include the idea that, whenever austenite concentrations are changing rapidly with depth, the X-ray measurement smooths out the change so that the true maximum or minimum is not observed by this method.

Metal was next removed electrolytically in small increments for the first part of step F to see how rapidly the austenite level would recover to its original value. Although the austenite content increased from 3.6 to 4.3% in 0.0002 inch, it did not return to its original level until about 0.010 inch had been removed electrolytically. A final measurement was made on this sample by removing an additional 0.015 inch electrolytically in step F. The austenite content at this depth was 4.9% indicating that it had essentially returned to its original level and that this sample was homogeneous in austenite content over the depth of about 0.085 inch used in this experiment.

The average austenite level in the first 0.010 inch of step F was 4.5% (see Fig. 1). This is significantly lower than the original 5.1% austenite level and may be due to slight tempering of the sample in step B, the tempering temperature being sufficiently high (above 400°F) to decompose some of the retained austenite. Steps C, D, and E probably do not contribute to the tempering effect since the austenite content after these steps remains within the upper value of 5.1% of the original austenite level and the lower value of 3.4% after step B. This illustrates two points, namely: (a) that a polishing sequence such as was followed in steps B through D may affect the austenite content to a depth of several thousandths of an inch, most of the effect probably being due to the rough polishing on papers and (b) that the gentle removal of metal in steps C and D, together with an alternate polish and etch, is insufficient to remove the tempering effects due to rough polishing.

It should be pointed out that the effects of polishing in steps B, C, and D, have not been examined separately since the primary purpose of this experiment was to ascertain the effects of a standard metallographic polishing procedure as a metal removal technique on the physical characteristics of the final surface. By electrolytically removing metal before and after each of steps B, C, and D, their separate effects may be determined. It may also be worthwhile to compare the effects of hand lapping with those of the rotary lap used in step B.

Returning to Fig. 2, sample M-554 and M-472 with austenite levels of $10.5 \pm 0.4\%$ and $26.5 \pm 0.5\%$ respectively showed many of the same characteristics as sample M-483 although there are some interesting differences. The austenite level dropped from 10.5 to 7.7% after step B for sample M-554, with a slight rise after step C, and a slight fall after step D. After step E the austenite percentage increased almost to the original austenite level indicating that the surface to be examined metallographically was essentially representative of the sample in terms of austenite content.

Subsequent electrolytic removal of 0.0005 inch in step F resulted in a slight further increase to 10.2% austenite followed by a drop to about 9.0% over a depth of about 0.003 inch and a subsequent rise approximately to the original level of $10.5 \pm 0.4\%$. This particular cycling in step F may seem to be fortuitous since it is not much greater than the reproducibility error of measurement at this austenite level; however, it should be pointed out that this same type of cycling seems to occur for samples M-483 and M-472. Even if a smooth curve is drawn through the points of step F, the austenite level would be significantly lower over the first 0.005 inch in this step. This effect may be due to a slight tempering effect over a depth of several thousandths of an inch as was suggested previously for sample M-483.

If the cycling effect in the first part of step F is real, it may be interpreted as a re-austenitizing and tempering cycle such as that described by Littman in his grinding experiments (1). Littman showed that a ground surface (20 microinches in depth) may be heated sufficiently to re-austenitize and reharden it while a layer immediately below the rehardened surface is depleted in retained austenite in the region where the temperature gradient falls below the critical temperature. A reason for speculating on this analogy is to suggest that it may be possible for very high surface temperatures (above 1500°F) to be generated to measurable depths when using a standard metallographic polishing procedure.

Sample M-472 apparently does not have the austenite uniformity in step A that the other two samples do since two experimental points fall somewhat outside of the standard deviation band. Nevertheless, the austenite variations in steps B through F follow essen-

tially the same pattern that they did for the other two samples.

Some residual stress measurements were made on the body-centered phases (martensite+ferrite) in sample M-554 after each of steps A through E using the X-ray method described by Christenson and Rowland (18). These results are recorded in Table I.

Table I
Residual Stress Measurements Before and After Various Steps in a Standard Metallographic Polishing Sequence on Sample M-554

Step	Description	Residual Stress Parallel to Surface, thousands of psi *
A	Electrolytic removal	+ 9
B	Rough polishing on papers	−159
C	Polishing on wax lap	− 73
D	Polishing on billiard cloth	− 77
E	Billiard cloth polish and nital etch	− 73
F	Electrolytic removal	− 14

*Estimated reproducibility of measurement is ±5000 psi
Estimated accuracy is ±10,000 psi
Measurement averaged over depth of about 0.0003 inches (17)
Positive stress is tensile; negative stress is compressive

As can be seen, the surface stress was essentially zero (+9000 psi) after electrolytically removing about 0.050 inch. Rough polishing on 1 through 3/0 papers left a compressive stress of about 160,000 psi parallel to the surface. The stresses normal to the surface during the metal removal operation in this step were probably tensile and would account for the decrease in austenite content in the surface. These stresses normal to the surface, however, cannot be measured by X-rays and can be inferred only from the "strain-gage" properties of austenite referred to earlier in this paper (8).

Subsequent polishing on a wax lap and billiard cloth with alternate polishing and etching reduced the compressive stress to about 75,000 psi, but was insufficient to eliminate the stresses induced in the rough polishing step. Final electrolytic removal of about 0.005 inch, however, was sufficient to eliminate essentially all stresses parallel to the surface.

Experiments similar to those just described were carried out on two other samples, one on hardened SAE 52100 steel and the other on an 18% Cr, 8% Ni austenitic valve steel. The SAE 52100 steel gave results very similar to those of sample M-554 (SAE 1095) of Fig. 1, while the austenitic valve steel showed the presence of 8.1% ferrite after polishing and etching. Subsequent electrolytic metal removal on this sample resulted in the disappearance of the ferrite diffraction lines.

Some Effects of Belt Sanding on a Hardened Steel Surface

As a more drastic method of metal removal, preliminary experiments were carried out on a belt sander. A sample of hardened

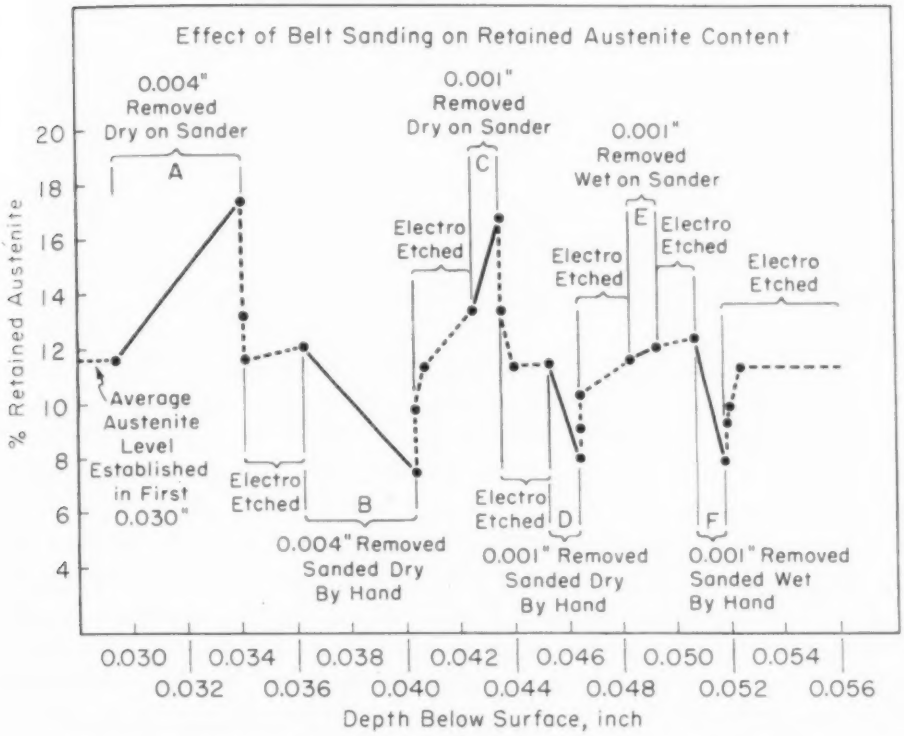


Fig. 3—The Effect of Belt Sanding on the Retained Austenite Content of Hardened SAE 1095 Steel.

SAE 1095 was prepared identically to that of sample M-554 in Fig. 1 and metal was removed using several different conditions including fast, slow, dry, and wet sanding, as well as electrolytic removal techniques. The use of a grinder would probably have been preferable to that of a belt sander to permit comparison with grinding practice. The sander was chosen, however, because it was possible to maintain uniform hand pressure of the sample on the sanding belt from one experiment to the next thereby minimizing the effect of this variable on these experiments.

The austenite level in the hardened SAE 1095 sample was established in the first 0.030 inch at $11.6 \pm 0.4\%$ (see Fig. 3). Metal was then removed using a belt sander with 80 grit paper running at about 15 lineal feet per second. The first step (A) involved holding the sample lightly against the moving paper until 0.004 inch had been removed. An austenite measurement at this point indicated 17.4% on the sanded surface, an increase of 5.8% over the original austenite level. Subsequent chemical and electrolytic removal of 0.0001 inch brought the austenite percent back to the original level of 11.6%. Further electrolytic removal of 0.002 inch showed no change in austenite percent, indicating that the original austenite level had been regained in about 0.0001 inch after the sanding operation, taking

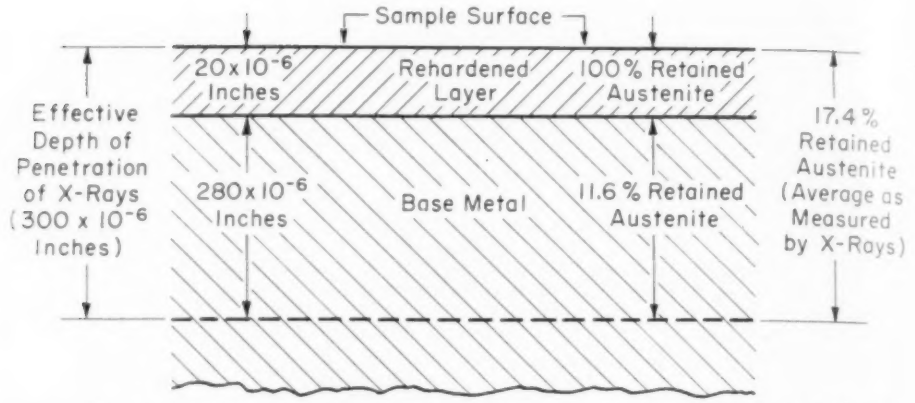


Fig. 4—Estimate of the Retained Austenite Concentration of the Surface Layer Rehardened by Dry Sanding Hardened SAE 1095 Steel.

into account the averaging effect due to the penetration of X-rays into the sample (17).

It has been pointed out that a rehardened layer is formed when the surface temperature exceeds 1550°F (1); however, no indication of the phase composition of this rehardened layer is given other than to point out that it consists of a mixture of retained austenite and untempered martensite. The relative proportions of the phases in the rehardened layer can be estimated from the austenite measurements in step A of Fig. 2 using Littman's estimate of the thickness of the rehardened layer (about 20 microinches) (1) and Schaal's estimate of the effective penetration of X-rays into the sample surface (17). The effective penetration of iron K alpha X-rays into iron cannot be determined directly from Schaal's data; however, a reasonable estimate for these purposes would be about 300 microinches. Using this information, the retained austenite content of the rehardened layer is estimated to be 100% (see Fig. 4).

It should be pointed out that this estimate of the austenite content of the rehardened layer is a reasonable one, since the effect of tempering below the rehardened layer was ignored to simplify the illustration of Fig. 4. The depth of the tempered layer (in which most of the retained austenite is decomposed) has been estimated to be about 50 microinches (1). Even if the rehardened layer were 100 microinches thick instead of 20, the retained austenite content of this layer would be about 30%. There is good evidence that this layer is not more than 100 microinches thick since the austenite level after sanding in step A of Fig. 3 recovered its original value in about 100 microinches.[4]

[4]The rehardening process was also studied on a sample of SAE 1095 steel austenitized at 1600°F for 1 hour, brine-quenched, and tempered at 700°F for ½ hour so that all of the retained austenite was decomposed. This sample was sanded as in step A of Fig. 3 and 1.6% austenite was measured at the surface. Using Littman's (1) and Schaal's (17) data as described above, the austenite content of a rehardened layer 20 micro-inches thick was estimated to be about 25%. This indicates that substantial amounts of austenite can be retained in the surface of a sample consisting primarily of ferrite and cementite when it is sanded lightly. These observations are similar to those previously reported for an electron diffraction study on an abraded ferrite single crystal (10).

The reason for the recovery of the austenite level in about 100 microinches for step A is not entirely clear especially when it is considered that the much gentler polishing in step B (Fig. 2) did not result in a recovery of the austenite level for several thousandths of an inch. The rapid recovery in step A (Fig. 3), however, has been observed several times on various samples of hardened SAE 1095 and 52100 steels and is not believed to be accidental.

It is realized that the estimate of 100% austenite content for the rehardened layer may be contrary to currently accepted ideas. Nevertheless, it is difficult to interpret the data otherwise if the estimates of the thickness of the rehardened layer and the effective depth of penetration of X-rays are accepted. Further study on this aspect of the problem is recommended to help clear up the apparent anomaly.

Returning to Fig. 3, the second step (B) involved removing 0.004 inch dry on the belt sander using the same 80 grit paper as for the previous step. This time, however, the metal was removed slowly by hand, the sanding belt remaining stationary. The austenite percentage dropped to 7.3% after this step. This can be explained in at least two ways, either or both of which may be effective here: (a) because of the slow rate of metal removal, the surface temperature did not exceed 1550°F with the result that the surface was tempered only rather than being re-austenitized, and (b) the tensile component of stress resulting from tearing out pieces of metal from the surface may result in austenite decomposition (7,8). Subsequent electrolytic removal brought the austenite level approximately to its original level of 11.6%.

The next two steps (C and D) were identical with steps A and B respectively except that only 0.001 inch was removed on the sander in each case. The results are directly comparable with steps A and B indicating that the rate of metal removal has a more pronounced effect on austenite content than the actual amount of metal removed.

The last two steps (E and F) were identical with C and D respectively except that metal was removed using oleum spirits as a lubricant. In step E the austenite content did not change significantly. This can be interpreted as a balancing of the increase in austenite by rehardening against the decrease in austenite due to tempering and stressing. Step F resulted in an austenite decrease comparable to those of steps B and D indicating that the decomposition of austenite due to tempering and stressing is the predominant factor in slow metal removal whether it is done wet or dry.

Residual stress measurements (18) were made before and after several of the metal removal steps of Fig. 3 and are tabulated thus:

Table II
Residual Stress Measurements After Various Steps of Metal Removal on Hardened SAE 1095 Steel Using a Belt Sander and 80 Grit Paper

Step	Description	Residual Stress, Parallel to Surface, thousands of psi		
		Non-directional*	Parallel to sanding scratches	Perpendicular to sanding scratches
—	0.030 inch electrolytic removal	+12	—	—
C	0.001 inch removed dry with sander running	—	− 93	−122
—	0.006 inch electrolytic removal	− 7	—	—
D	0.001 inch removed dry by hand	—	−111	−168
—	0.004 inch electrolytic removal	− 5	—	—
E	0.001 inch removed wet with sander running	—	− 54	—
—	0.005 inch electrolytic removal	+ 7	—	—
F	0.001 inch removed wet by hand	—	−150	—
—	0.003 inch electrolytic removal	− 3	—	—

*These stresses are probably due to quenching and are essentially uniform (± 10,000 psi) in any direction parallel to the surface.

It can be seen that, whether the metal is removed fast, slow, wet, or dry on a belt sander, the stresses parallel to the surface are compressive with the stress component perpendicular to the sanding direction always greater in magnitude than the parallel component as pointed out by Letner (4). Electrolytic removal of 0.003 to 0.006 inch always brought the stresses essentially back to zero.

Some Effects of Heat Treatment on Hardened Steel Surfaces

In order to study the effects of metal removal on austenite content it is desirable to prepare hardened steel samples which have uniform austenite contents from the immediate surface to the interior. To prepare such samples it is necessary either to austenitize them in a completely neutral atmosphere or to protect their surfaces from the atmosphere while austenitizing. Except for an argon atmosphere furnace or a gas furnace with automatic carbon potential control, it has been found difficult to obtain hardened samples which do not show evidences of reaction with the atmosphere for austenitizing times of two hours or less. On the other hand, samples protected with about 0.002 inch of copper plate showed no effect on austenite content in either gas or "neutral" salt furnaces even though unprotected samples heat treated simultaneously usually showed marked effects.

Substantially thinner or thicker[5] copper plate than 0.002 inch, was found to provide ineffective protection against the atmosphere. Hence, 0.002 inch copper plate was used whenever it was desired to prepare hardened samples which were completely homogeneous in austenite content. On the other hand, it seemed desirable to study the effects of furnace atmosphere on austenite content as part of the

[5]Thin plate tends to be slightly porous while thick plate tends to develop minute cracks. In either case, the atmosphere would penetrate the plate and react with the underlying steel surface.

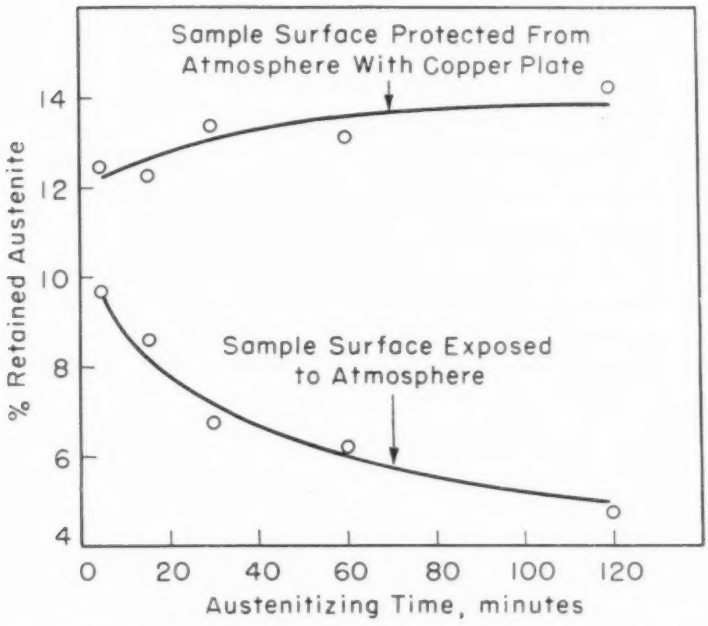


Fig. 5—Variations in Surface Austenite Content with Austenitizing Time at 1600°F Using SAE 1095 Steel.

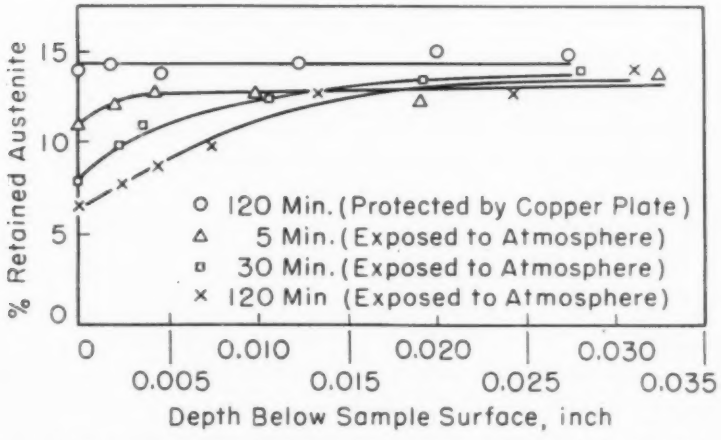


Fig. 6—Variations in Austenite Content with Depth for Several Austenitizing Times at 1600°F.

overall program relating surface physical variations with fatigue properties of hardened steel parts.

The conditions chosen for these experiments included copper plating one side of 7/8 inch diameter, 3/16 inch thick disks of SAE 1095 steel leaving the second side bare.[6] Samples prepared in this way were austenitized in a slightly decarburizing atmosphere at 1600°F for times up to 2 hours, brine-quenched, and tempered at 300°F for 1/2 hour. The copper plate was then chemically stripped thus providing a single sample with a reference surface and a surface

[6]Chemical carbon analyses on the original bar stocks from which the disks were cut indicated variations not greater than 0.05% from the surface to the interior or along the length of the bars.

for studying depth variations of austenite due to heat treatment conditions.

The variations in austenite content with austenitizing time on the bare and protected surfaces of a set of samples are given in Fig. 5. The slight increase in austenite for the protected surfaces up to about 30 minutes austenitizing time indicates the time required to put the cementite completely into solution at 1600°F. The decrease in austenite content with time for the bare sample surfaces follows approximately an exponential decay curve. It is interesting to note that the austenite content begins to decrease almost immediately from zero austenitizing time. The depth to which the austenite content is affected for various austenizing times is shown in Fig. 6. As can be seen, the austenite content for a copper plated surface is not affected even after austenitizing for two hours, while the austenite content is affected to a depth of about 0.003 inch on a bare surface after only 5 minutes at 1600°F.

This variation in austenite content with depth in hardened SAE 1095 steel is due to decarburization, as has been suggested by Gardner, Cohen, and Antia (5) for 5% nickel steels and is illustrated in Fig. 7.[7] These decarburization effects may be demonstrated in several ways. The carbon content of the austenite can be measured using (a) the relationship of per cent retained austenite to carbon content for a given austenitizing temperature and (b) the relationship of austenite lattice parameter to carbon content (19). The carbon content of the martensite can be measured using martensite lattice parameters (19) and total carbon can, of course, be measured chemically. Residual quenching stresses were measured with depth on the bare and protected surfaces of the same sample to permit an estimate of the effect these stresses would have on the parameter measurements.

As can be seen in the left hand column of Fig. 7, the austenite content (6.5%) is substantially lower at the sample surface exposed to the atmosphere (surface A) than it is in the interior of the sample (14.0%). This variation in austenite content can be related to a variation in carbon content of the austenite (19). By measuring the retained austenite contents of plain carbon steels with carbon concentrations ranging from zero to 1.27% and austenitizing temperatures ranging from 1400 to 1800°F, this relationship has been extended to include a family of curves as shown in Fig. 8.[8] Using the

[7]Austenite variations in hardened SAE 52100 (1.0% carbon, 1.5% chromium) steel were also observed which were nearly identical with those reported for hardened SAE 1095 steel.

[8]These curves were obtained for samples processed identically and heat treated the same day. Slight variations in procedure, however, may result in variations in per cent retained austenite. For example, SAE 1095 austenitized at 1600°F for various times over a period of years has been found to contain austenite in the range of 11 to 18% with most samples in the range of 12 to 14%. These variations are not believed to be due to departures from chemical specifications, decarburization, or carburization because of the care taken in eliminating these factors in sample selection and heat treatment.

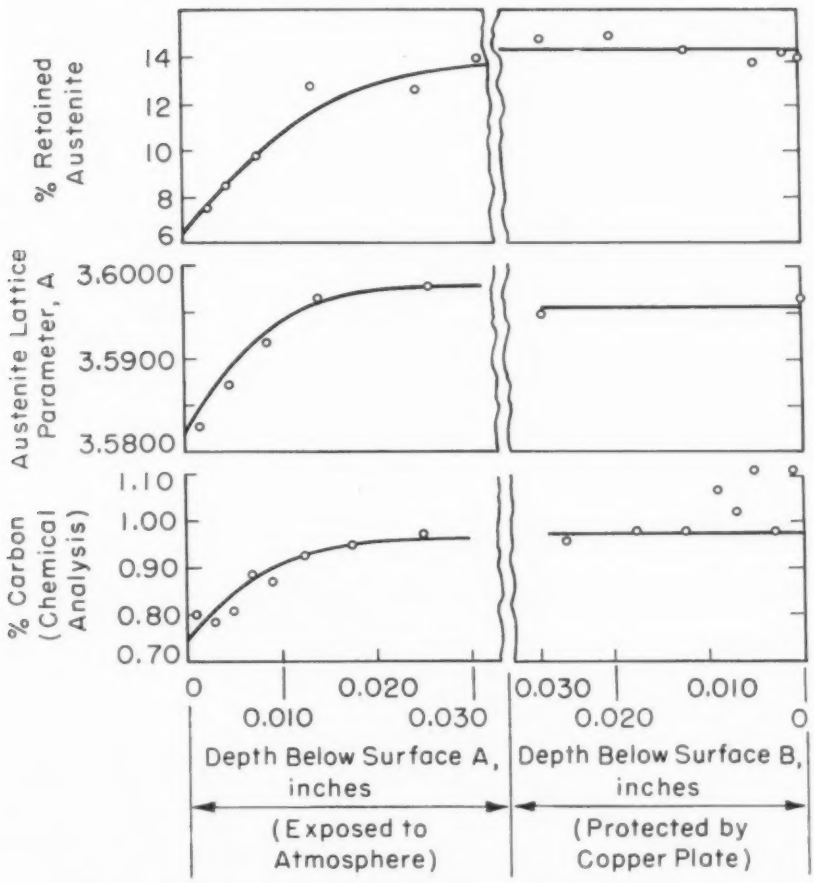


Fig. 7—Variations in Austenite Content, Austenite Lattice Parameter, Chemical Carbon, with Depth in $\frac{3}{16}$ inch Thick Samples Austenitized Two Hours at 1600°F.

1600°F curve in this figure, it can be seen that the carbon content of the retained austenite varies from 0.67% (6.5% retained austenite at surface A in Fig. 7 to 0.99%) (14.0% retained austenite in the interior of the sample) thus indicating the extent of decarburization from the surface to the interior for this sample.

The variation of austenite lattice parameter with carbon content has been studied extensively (19), the larger the lattice parameter, the greater the carbon content of the austenite. Thus, the curve of austenite lattice parameter with depth in the left hand column of Fig. 7 indicates decarburization of austenite at the surface with respect to the interior. A few martensite lattice parameter measurements were made on untempered samples as spot checks. The carbon content of the martensite thus measured agreed substantially with austenite lattice parameter measurements at the same surface in each case. Finally, chemical carbon measurements with depth indicate decarburization of the total sample from the surface A side. On the other hand, the variations in per cent retained

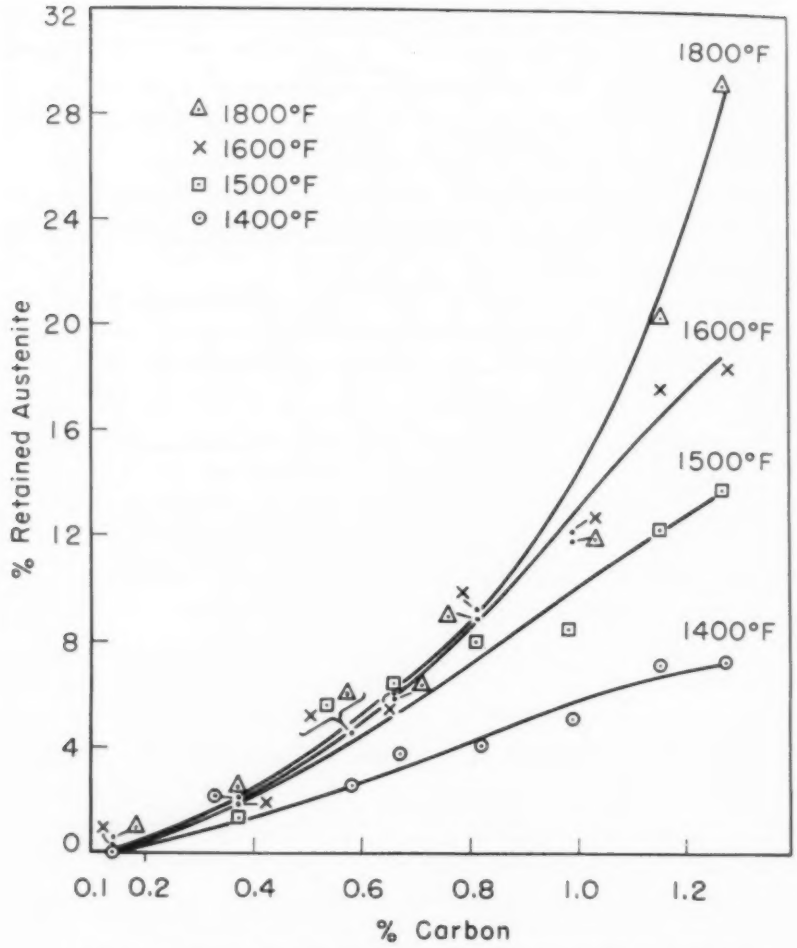


Fig. 8—Percent Retained Austenite vs. Percent Carbon in Plain Carbon Steels for Austenitizing Temperatures from 1400 to 1800°F.

austenite, austenite lattice parameter, and chemical carbon with depth from the surface protected by copper plate (surface B in Fig. 7) are negligible. The slightly higher and erratic values of chemical carbon in the first 0.010 inch below the protected surface may be ascribed to the small sample size (less than 100 mg) chosen for the first five layers removed from this sample.

Variations of residual quenching stresses with depth were also measured. Quenching stresses as well as carbon content can be expected to affect the austenite lattice parameter measurements. The magnitude of the stress change, however, is small enough that its effect on the carbon content calculation from austenite lattice parameter measurements is almost negligible. For example the maximum quenching stress change with depth was found to be about 50,000 psi. This corresponds to a change in austenite lattice parameter of 0.0012 Å using engineering values for Young's modulus

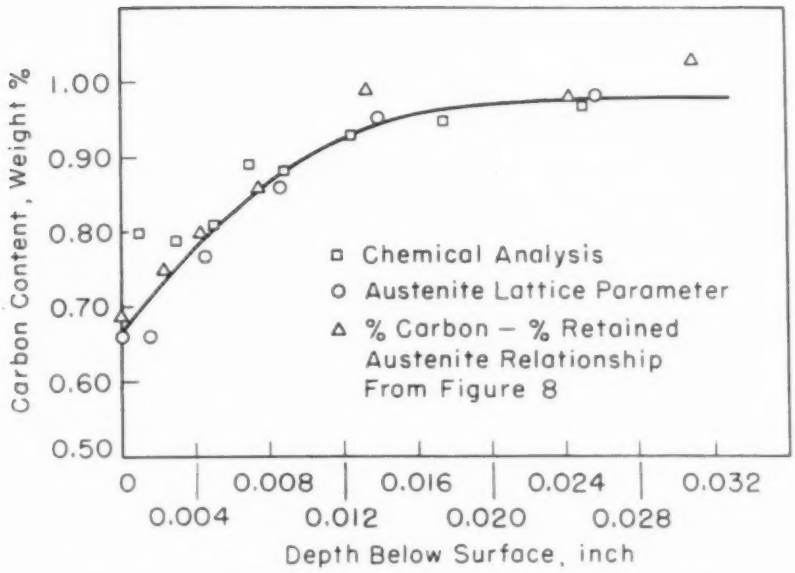


Fig. 9—Percent Carbon (by chemical analysis, austenite lattice parameter, and austenite-carbon-temperature relationship) with Depth in Hardened SAE 1095 Steel Austenitized 2 Hours at 1600°F.

and Poisson's ratio for steel. This change in austenite lattice parameter, in turn would correspond to a change in carbon content of 0.03% if lattice parameter changes were interpreted entirely as carbon content variations.

The variations in carbon content with depth from the surface exposed to the austenitizing atmosphere using (a) the relationship of per cent retained austenite with per cent carbon in Fig. 8, (b) austenite lattice parameter, and (c) chemical carbon measurements[9] are summarized in Fig. 9. As can be seen the carbon measurements with depth agree well among themselves, verifying the effect of decarburization, not only in the sample as a whole, but also in the individual crystalline components, retained austenite and martensite, by two independent X-ray methods.

Acknowledgments

The authors are grateful to Harry Sturner who carried out the many austenite calculations and sample preparations required, and to Grace Huff who made the stress measurements.

References

1. W. E. Littman, "The Influence of the Grinding Process on the Structure of Hardened Steel," Transactions, American Society for Metals, Vol. 47, 1955, p. 692.
2. H. J. Snyder, "The Effect of Quenching and Tempering on Residual Stresses in Manganese Oil Hardening Tool Steel," Transactions, American Society for Metals, Vol. 45, 1953, p. 605.

[9]The chemical carbon measurements for the first 0.010 inch (in increments of 0.002 inch) were high compared to the austenite lattice parameter measurements, for example. These high values are ascribed to the small samples used (about 100 mg) similar to the high values for the small sample carbon analyses on the first 0.010 inch on the protected sample sides.

3. H. R. Letner and H. J. Snyder, "Grinding and Lapping Stresses in Manganese Oil-Hardening Tool Steel," *Transactions*, American Society of Mechanical Engineers, Vol. 75, 1953, p. 873.
4. H. R. Letner, "Residual Stresses in Hardened Steel," *Transactions*, American Society of Mechanical Engineers (to be published).
5. F. S. Gardner, M. Cohen and D. P. Antia, "Quantitative Determination of Retained Austenite by X-Rays," *Transactions*, American Institute of Mining and Metallurgical Engineers, Vol. 154, 1943, p. 306.
6. P. Spear, I. R. Robinson and K. J. B. Wolfe, Properties of Metallic Surfaces, published by the Institute of Metals, London, 1953, p. 91.
7. B. L. Averbach, S. G. Lorris and M. Cohen, "Stress-Induced Transformation of Retained Austenite in Hardened Steel," TRANSACTIONS, American Society for Metals, Vol. 44, 1952, p. 746.
8. L. S. Castleman, B. L. Averbach and M. Cohen, "Effect of Retained Austenite Upon Mechanical Properties," TRANSACTIONS, American Society for Metals, Vol. 44, 1952, p. 240.
9. L. W. Pateman and H. S. Peiser, "An X-Ray Diffraction Study of the Transformation of Retained Austenite by Fracture," *Nature*, Vol. 171, 1953, p. 696.
10. R. P. Agarwala and H. Wilman, "The Transformation of Alpha-Iron to Gamma-Iron During Abrasion," *Proceedings*, Royal Society, Vol. 223A, 1953, p. 167.
11. B. L. Averbach and M. Cohen, "X-Ray Determination of Retained Austenite by Integrated Intensities," *Transactions*, American Institute of Mining and Metallurgical Engineers, Vol. 176, 1948, p. 401.
12. B. L. Averbach, L. S. Castleman and M. Cohen, "Measurement of Retained Austenite in Carbon Steels," TRANSACTIONS, American Society for Metals, Vol. 42, 1950, p. 112.
13. K. E. Beu, "Modifications of an X-ray Method for the Measurement of Retained Austenite Concentrations in Hardened Steels," *Transactions*, American Institute of Mining and Metallurgical Engineers, Vol. 194, 1952, p. 1327.
14. K. E. Beu, "Notes on the Determination of Retained Austenite by X-Ray Methods," *Transactions*, American Institute of Mining and Metallurgical Engineers, Vol. 197, 1953, p. 1539.
15. K. E. Beu, "The Sensitivity, Reproducibility and Accuracy of X-Ray Diffraction Measurements of Retained Austenite" (to be published).
16. A. L. Ellis and F. K. Iverson, "Quantitative Metallography with the Electron Microscope," ASTM Bulletin, No. 183, 1952, p. 66.
17. A. Schaal, "Experimental Determination of Effective Depth of Penetration in Radiographic Stress Determinations," *Zeitschrift fur Metallkunde*, Vol. 41, 1950, p. 293.
18. A. L. Christenson and E. S. Rowland, "X-Ray Measurement of Residual Stress in Hardened High Carbon Steel," TRANSACTIONS, American Society for Metals, Vol. 45, 1953, p. 638.
19. C. S. Roberts, "Effect of Carbon on the Volume Fractions and Lattice Parameters of Retained Austenite and Martensite," *Transactions*, American Institute of Mining and Metallurgical Engineers, Vol. 197, 1953, p. 203.

DISCUSSION

Written Discussion: By L. P. Tarasov, Research and Development Department, Norton Company, Worcester, Massachusetts.

This is a very interesting paper on a subject which has been thoroughly ignored in the past on the optimistic assumption that good mechanical metallographic polishing of hardenable steels does not disturb the microstructure except for a cold-worked layer which can be removed by etching and repolishing. The authors have clearly shown that the amount of retained austenite can fluctuate

appreciably as a result of such polishing, but there are certain other points that call for detailed comment.

It is claimed that belt sanding produced a rehardened surface layer containing 100% retained austenite. This can be disputed on the grounds that rehardening implies an appreciable breakdown of austenite, so that the amount retained must of necessity be correspondingly less than 100%. The method of arriving at the conclusion that this surface contained 100% retained austenite is based on the totally unjustified assumption that the depth of the rehardened layer obtained by Mr. Littmann can be considered representative. There is no representative value for the depth of such metallurgical changes any more than there is a representative hardenability value for steels in general.

When hardened steel is ground very carefully, there may be only the slightest trace of tempering (which would show up as a slight darkening after suitable etching) even at the highest optical magnification combined with taper sectioning.[11] Under these circumstances, it can safely be assumed that no austenitization could have occurred except perhaps in the outermost atomic layers. At the other extreme, the depth of rehardening associated with abusive grinding may easily be several thousandths of an inch, and the depth of softening may be ten times as great. Thus it would be purely fortuitous if the 20 microinch and 50 microinch values mentioned by the authors for the depths of the rehardened and tempered layers, respectively, were applicable to their specimens, which were prepared by belt sanding and not by grinding with a wheel.

Another point to keep in mind is that taper section microhardness studies[12] of surfaces rehardened to appreciable depths by abusive grinding have shown the hardness of the transformed, white-etching surface layer to be around Rockwell C-63 for two different tool steels. The white layer had the same metallographic appearance throughout its thickness and there was no evidence that the outermost portion of this layer, where useful microhardness indentations could not be placed, was in any way different from the rest of the layer, which consisted of white martensite and some retained austenite. On the basis of this metallographic and microhardness study, it would appear much more probable that the authors' transformed surface layer was a rehardened one containing appreciable retained austenite. This would be in line with their alternative suggestion that the layer contained only 30% retained austenite on the assumption that it was 100 microinches thick.

Some unpublished experiments conducted by the writer on 52100 steel specimens austenitized at various temperatures showed that even though the retained austenite after tempering at 300°F varied between 8 and 26% as determined by X-ray diffraction, the specimens all had the same hardness of Rockwell C-63/64. Even 26% retained austenite did not cause any lowering of the hardness, presumably because the finely dispersed austenite was constrained by the martensitic matrix. Thus if the authors had some 30% retained austenite in their surface layer, it would probably not cause any observable drop in microhardness. With 100% retained austenite, however, a much lower hardness would be expected.

The authors point out that whereas in belt sanding the original austenite content was restored in about 100 microinches, the austenite in the metallo-

[11]Assuming that 10 microinches can be resolved at high magnification, a layer only 0.1 microinch in thickness can be detected when further magnified mechanically by means of a 100:1 taper section. The latter thickness corresponds to about 10 unit cells of iron.

[12]L. P. Tarasov and C. O. Lundberg, "Nature and Detection of Grinding Burn in Steel," TRANSACTIONS, American Society for Metals, Vol. 41, 1949, p. 893.

graphically polished specimen was not restored until several thousandths of an inch were removed. It should not be overlooked, however, that belt sanding reaustenitized the surface and increased the austenite content considerably while metallographic polishing decreased the amount of retained austenite, so that different mechanisms were involved. The first was a thermal effect (reaustenitization), while the second was perhaps partly thermal (tempering) and partly mechanical (cold working). Concurrent metallographic and microhardness studies would probably have clarified the apparent anomaly by establishing more definitely the nature and depth of the layers created by the two types of operation.

Written Discussion: By H. R. Letner and L. E. Alexander, Mellon Institute, Pittsburgh.

X-ray diffraction is a tool which can furnish a great deal of information concerning the nature of ground and polished surfaces. Its application to the measurement of retained austenite to supplement, and perhaps evaluate, methods depending upon metallographic preparation is highly commendable. The authors' data point quite clearly to the possibility that the latter methods may frequently furnish misleading results.

If the authors' interpretation of their data in Fig. 2 is correct, the operation in step B is perhaps more severe than they had anticipated. By way of comparison, surface grinding of a ball bearing steel similar to SAE 52100, oil-quenched and tempered 2 hours at 400°F to Rockwell C-59, causes plastic deformation of the surface to depths ranging from less than 0.001 to 0.008 inch, depending upon the grinding severity.[13] Surface grinding of SAE 4340, heat treated to Rockwell C-55, results in plastic flow over approximately the same range.[14] Messrs. Littmann and Wulff have demonstrated that surface grinding of SAE 52100, heat treated to Rockwell C-64, causes tempering of layers up to 0.015 inch thick, again depending upon the severity of the operation.[15] The authors conclude that step B of their metallographic polishing sequence causes transformation of retained austenite by plastic strain and elevated temperature to a depth of 0.010 inch or more. If this is the case, step B is comparable to the more severe surface grinding operations in its effect upon the steel. Although such an occurrence is by no means outside the realm of possibility, an alternative interpretation of the data in Fig. 2 seems worth suggesting.

An examination of the experimental points in Fig. 2 raises a question concerning the justification for indicating the original austenite contents by straight, horizontal bands. Is it possible that the original level for sample M-472 is drawn too high, and that the initial austenite content in all three specimens was not strictly constant, but decreased slightly with depth so that the shaded bands should slope downward toward the right? If so, the austenite contents of all three samples may have completely recovered their initial values within a few ten-thousandths of an inch in step F. This behavior is consistent with an intuitive feeling that step B of the metallographic polishing sequence is less severe than step A of the belt sanding sequence (Fig. 3), from which the authors show that the initial austenite level is completely recovered within 0.0001 inch. In the absence of other information, it seems that the experimental points in steps A and F of

[13]H. R. Letner, "Residual Grinding Stresses in Hardened Steel," *Transactions*, American Society of Mechanical Engineers, Vol. 77, 1955, p. 1089.

[14]L. V. Colwell, M. J. Samnott and J. C. Tobin, "The Determination of Residual Stresses in Hardened, Ground Steel," *Transactions*, American Society of Mechanical Engineers, Vol. 77, 1955, p. 1099.

[15]Authors' reference (1).

Fig. 2 may establish an initial austenite gradient in the specimens which is more accurate than the constant level extrapolation of the values in step A alone.

Estimating the "effective depth of penetration" of Fe$K\alpha$ X-rays into iron to be 300 microinches, the authors arrive at an austenite concentration of 100% in the rehardened layer. It is, however, a straightforward proposition to compute the austenite concentration on the more realistic basis of an exponential decrease in the contribution of successively deeper layers to the total intensity of an austenite diffraction line. If the austenite concentrations of the rehardened layer of thickness t and interior of the specimen are respectively a and b, and if the analyzed concentration is c, it can be shown that

$$c = a\ (1\text{-}e^{-k\mu t}) + be^{-k\mu t}.$$

It is acceptable to regard μ as being uniform and equal to about 560 cm.$^{-1}$ for the several iron-carbon phases that may be present, while k is related to the X-ray path length in the sample and may be assigned a typical value of 2.4. Then

$$0.174 = a\ (1\text{-}e^{-1340t}) + 0.116e^{-1340t}.$$

This equation permits the concentration in the rehardened layer, a, to be computed as a function of the assumed layer thickness, t. If t is arbitrarily assigned Messrs. Littmann and Wulff's value of 20 microinches (0.00005 cm.), we find $a = 1.01$, or 101%. For $t = 100$ microinches (0.00025 cm.) $a = 0.32$, or 32%. These results agree very well with those derived by the authors on the basis of the simple picture that the X-rays penetrate to an "effective depth" of 300 microinches.

Thus it is seen that a more exact analysis of the X-ray diffraction process in no way contradicts the authors' finding of a high austenite content in the rehardened layer. It does, however, lead to the conclusion that the thickness of this layer cannot be less than 20 microinches and that it is probably considerably greater.

Authors' Reply

The authors wish to thank Mr. Tarasov and Drs. Letner and Alexander for their interest in this paper. Mr. Tarasov points out that Littmann's estimate of the thickness of a rehardened layer formed on ground surfaces does not necessarily apply in the case of belt sanding. Considering the inherent differences between the two methods, this is probably true. A concurrent metallographic examination should help to establish the true thickness of the rehardened layer so that a closer estimate of the retained austenite content can be made.

The calculation of the depth of penetration of Fe Kα X-rays into the steel was actually made by a method fundamentally the same as that outlined by Dr. Letner and Dr. Alexander. The "effective depth" model was used only to simplify the illustration.

Dr. Letner and Dr. Alexander also suggest that the original austenite level of the samples used in the study on the effects of metallographic polishing may have decreased slightly with depth and hence the affected layer under step F may be only a few ten-thousandths of an inch thick. In various experiments we have had occasion to examine plain carbon hardened steel samples of this size (3/16 of an inch thick) with depth and have never observed such a gradient in the austenite content. An example is shown in Fig. 7 where the austenite content is plotted as a function of the depth below a copper plated surface (surface B) and no gradient is discernible up to 0.030 inch. Therefore, the interpretation that the rough polishing affects the steel to a depth of several thousandths of an inch is probably more valid.

THE INFLUENCE OF TENSILE STRESS ON THE ISOTHERMAL DECOMPOSITION OF AUSTENITE TO FERRITE AND PEARLITE

By George L. Kehl and Subrata Bhattacharyya

Abstract

The influence of externally applied tensile stress on the isothermal decomposition of austenite to pearlite in AISI 1085 steel at 1273°F, and to ferrite and pearlite in AISI 10B45 steel at 1253°F, has been investigated.

It was found that applied stress markedly affected both the beginning and ending times of transformation, and accelerated the rate of transformation.

The rate of nucleation of pearlite in the eutectoid steel was increased by a factor of about 55 arising from application of stress. The rate of growth, however, was virtually unaffected.

In the hypoeutectoid steel, an applied stress increased the rate of nucleation of proeutectoid ferrite by a factor of about 2, and possibly the rate of nucleation of the pearlite subsequently formed. The rate of growth of ferrite was increased by a factor of about 2.5 attending the application of 13,000 psi stress whereas the rate of growth of pearlite was unaffected in the early stages of formation, but was increased markedly later in the process.

Critical observations of the fully transformed structures indicated no significant alterations arising from stress, except the interlamellar spacing of pearlite in the eutectoid steel was slightly smaller compared to that formed under no stress.
(ASM-SLA Classification: N8, CN)

WHEN austenite is allowed to transform isothermally at temperatures above the knee of its appropriate C curve, the resulting structure is principally dependent upon carbon content, and will consist of either pearlite, or of pearlite and a proeutectoid phase. In solid state reactions of this kind, involving nucleation and growth processes, it may be expected that stress and attending deformation of the austenite may affect and alter the course of the transformation. As demonstrated by Bhattacharyya and Kehl (5)[1], the decomposition of austenite to bainite was markedly affected by this circumstance. As a logical outgrowth of this investigation (5), the present paper constitutes a report on the kinetics of the pearlite

[1] The figures appearing in parentheses pertain to references appended to this paper.

The authors, George L. Kehl and Subrata Bhattacharyya, are associated respectively with the Division of Metallurgy, School of Mines, Columbia University, New York, and Hindustan Steel Ltd., Rourkela, India. Manuscript received August 17, 1955.

and proeutectoid ferrite reactions as influenced by the application of tensile stress to the transforming austenite.

Several authors have investigated the effect of externally applied stress on the austenite to pearlite transformation reaction. Guarnieri and Kanter (1) observed that above the knee of the C curve of a 0.26% carbon, 5% chromium, 0.5% molybdenum cast steel, stress had little accelerating effect on the formation of pearlite. This circumstance was attributed to the transformation temperatures being sufficiently high to render the more rapid diffusion rates relatively insensitive to the strain factor.

Jepson and Thompson (3), investigating the formation of pearlite and upper bainite under stress in a eutectoid carbon steel, concluded that deformation of the transforming austenite resulted in a greater abundance of alpha-iron nuclei compared to transformation under no stress. Schnitzel and Bhattacharyya (4) observed that applied stress had a pronounced effect on the decomposition of austenite to pearlite in a plain carbon eutectoid steel. Within a certain stress range, the amount of pearlite formed increased sharply. This latter circumstance has been found also in the transformation of austenite to bainite (5).

In the investigation to be described, particular attention has been given to the effect of externally applied tensile stress on the acceleration of austenite decomposition, on the rates of nucleation and growth of ferrite and pearlite wherever possible, and on the alteration in microstructure of the partially and fully transformed structures. The investigation was confined to a hypoeutectoid steel (AISI 10B45) and to a eutectoid steel (AISI 1085), isothermally transformed at temperatures of 1253 and 1273°F, respectively.

Experimental Procedure

The chemical compositions of the two steels employed in this investigation are given in Table I. The procedure of fabrication of the bar stock into wire-type specimens is identical to that reported previously (5). Similarly, the transformation apparatus (See Fig. 1) and the experimental procedures are identical, excepting a lead-bismuth transformation bath was used instead of salt, and helium was employed as a quenching medium instead of air. It was necessary to invoke these changes owing to excessive attack of the speci-

Table I
Check Chemical Analysis of Steels Investigated

Steel	Percent By Weight							
	C	Mn	P	S	Si	Ni	Cr	B
AISI 1085	0.89	0.29	0.013	0.013	0.19	—	0.08	—
AISI 10B45	0.48	0.85	0.015	0.030	0.25	0.05	0.05	0.003

men cable system by heat treating salts at the temperatures employed, and the inability of an air-blast quench to transform instantaneously the remaining austenite to martensite.

The range of transformation times, applied stress, and other pertinent data are summarized in Table II.

The progress of austenite decomposition in the eutectoid steel

Table II
Range of Transformation Times and Applied Stresses

Steel	Austenitizing Treatment: Temperature, °F	Austenitizing Treatment: Time, min.	Isothermal Transformation Temperature, °F	Range of Isothermal Transformation Time, sec[1]	Range of Applied Stress, psi	Austenite Grain Size, A.S.T.M.
AISI 1085	1650	7	1273	3—200	0—13,000[2]	5—6
AISI 10B45	1630	7	1253	2—150	0—13,000[2]	7—8

[1] Prior to measuring the time of transformation, five seconds were allowed for the specimen to attain the temperature of the transformation bath.
[2] Maximum stress feasible to avoid local necking of the specimens.

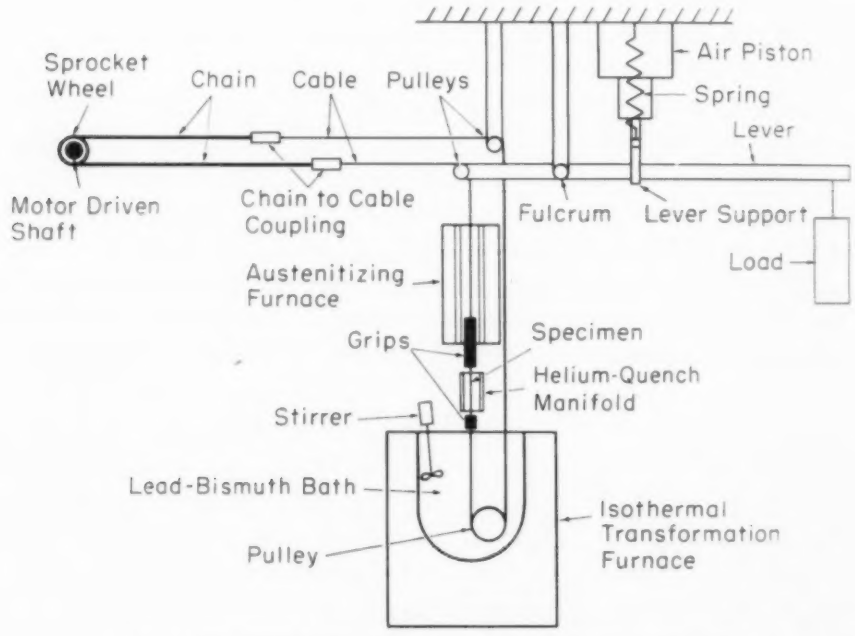


Fig. 1—Schematic Diagram of the Transformation Apparatus.

was determined metallographically by using both chart comparison and lineal analysis methods. In the case of the hypoeutectoid steel, lineal analysis was the sole method employed, wherein the total transformation (ferrite and pearlite) was determined. The amount of pearlite was separately measured subsequently and by difference between the amounts of total transformation and pearlite, the quantity of ferrite in the structure was determined.

Methods for Determining the Rate of Growth and Rate of Nucleation of Pearlite and Ferrite

(a) Eutectoid Carbon Steel—Methods for calculating the rate of growth and rate of nucleation of pearlite in eutectoid carbon steel have been described in the literature and a detailed analysis has been given by Hull, Colton, and Mehl (6). Briefly, the rate of growth is determined by measuring the radius of the largest nodule found in each of a series of specimens transformed for increasing periods of time. A plot of these radii as a function of time provides a curve of which the slope is the rate of growth G, given in units of mm/sec. This curve is characteristically a straight line which indicates the rate of growth G to be constant.

The pearlite reaction at 1273°F is known as "group-nodule transformation," and the reaction may be expressed mathematically as (6):

$$f(t) = 1 - \exp\left\{-\frac{\pi N\ G^3 t^4}{3}\right\} \qquad \text{Equation 1}$$

where, $f(t)$ = The fraction of austenite transformed as a function of time t
G = rate of growth of pearlite nodule in terms of increase in nodule radius with time, mm/sec
N_v = rate of nucleation, i.e., the number of nuclei forming per unit time per unit volume of untransformed austenite, number/mm^3/sec
t = time of transformation, sec.

Although N_v varies during the progress of transformation, the calculations may be simplified without the introduction of appreciable error by assuming N_v to be constant. Under this circumstance, N_v may be calculated from the following equation, provided G and the time for 50% transformation are known,

$$N_v = \left(\frac{0.9}{t_{0.5}}\right)^4 \cdot \frac{1}{G^3} \qquad \text{Equation 2}$$

where N_v and G are the same quantities as in Equation 1
$t_{0.5}$ = time for 50% transformation, sec.

(b) *Hypoeutectoid Steel*—In hypoeutectoid steel, the pearlite reaction is preceded by rejection of proeutectoid ferrite. Proeutectoid ferrite nucleates almost exclusively at the austenite grain boundaries, and grows with time isothermally along the boundary and thickens simultaneously. Mehl and Dubé (7) have shown that the lengthwise growth rate is high compared to the rate of thickening. The rate of growth along the grain boundary is at first rapid and constant, and eventually decreases with further increase in transformation time. The perpendicular growth rate (thickening of the ferrite grains) appears to be parabolic.

When the number of ferrite grains nucleated at the austenitic grain boundaries increases with time, forming an envelope around the austenitic grains, platelets of ferrite grow inwardly to produce a Widmanstätten structure. The ferrite protuberances from the grain-

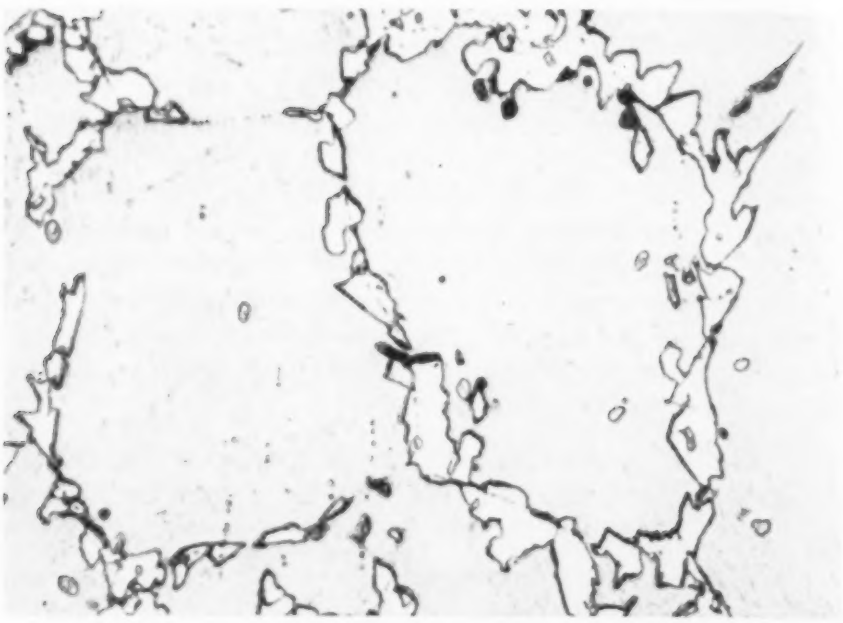


Fig. 2—Grain Boundary Ferrite in AISI 10B45 Steel Isothermally Transformed at 1253°F for 20 sec. Under 13,000 psi. ×1000. Etchant—2% Nital.

boundary ferrite appear to have an interplate spacing characteristic of the transformation temperature. The spacing increases at the higher temperatures, and if the prior austenitic grain size is small, the spacing may exceed the austenitic grain diameter and, in consequence, the Widmanstätten pattern will not be manifested.

In analyzing the growth rate of proeutectoid ferrite, the formation of any Widmanstätten ferrite must be accounted for in the analysis. Unfortunately, however, the derivation of a reaction equation in terms of rates of nucleation and growth that accounts for the presence of ferrite protuberances is extraordinarily complex. In consequence, and because the prior austenitic grain size of the hypoeutectoid steel investigated is relatively small and would lessen the manifestation of Widmanstätten ferrite, the growth rate in the first approximation has been determined experimentally by measuring the length of grain boundary ferrite grains as a function of transformation time. Typical grain boundary ferrite, as formed in the steel investigated, is illustrated in Fig. 2.

Theoretical derivation of the rate of growth of pearlite in hypoeutectoid steel is complicated by the presence of proeutectoid ferrite. It is well established that ferrite-austenite interfaces serve as preferred sites for nucleation of pearlite. Owing to the pearlite nucleus and eventual nodule being in contact with ferrite, the nodule is prevented from growing freely in all directions into the remaining austenite. With this restriction in ideality, the relationship between maximum pearlite radius and transformation time will give a rea-

sonably accurate approximation to the rate of growth, provided the measured radius is made on a growing nodule that does not impinge upon proeutectoid ferrite other than the ferrite patch to which it is attached.

Experimental Results

Effect of Stress on the Beginning and the Ending Times of Transformation

The amount of austenite isothermally transformed under no stress and 13,000 psi is plotted versus log-time and is shown in Figs. 3 and 4, for AISI 1085 and 10B45 steels, respectively. It is evident from these data that under stress both the beginning and ending

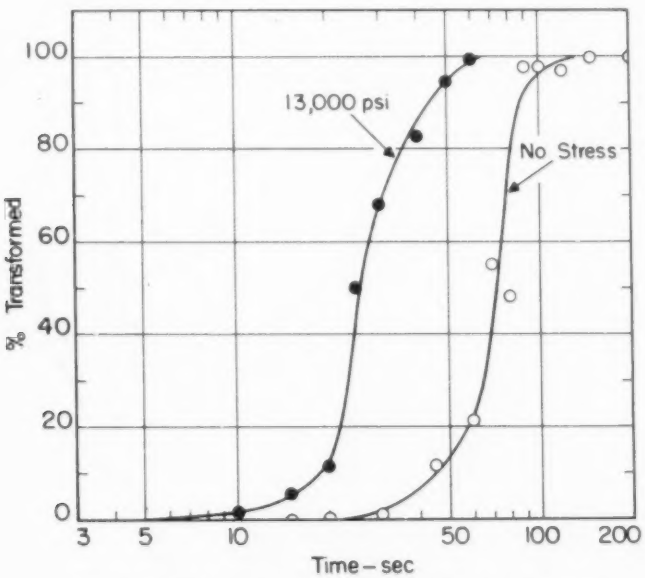


Fig. 3—Reaction Curves of AISI 1085 Steel Isothermally Transformed at 1273°F.

times[2] of transformation are shortened; the beginning times, however, are shortened to a greater extent than are the ending times. Typical progress of transformation in AISI 1085 steel, as influenced by stress, is illustrated in Fig. 5.

In Fig. 4 the austenite decomposition product consists of both proeutectoid ferrite and pearlite. By means of lineal analysis, and as shown in Fig. 6a and 6b, it is possible to discriminate between the beginning and ending times of transformation of ferrite and pearlite respectively. It is evident from this analysis that the beginning and ending times for both the proeutectoid ferrite and pearlite reactions are shortened by the application of stress.

[2]The criteria of the beginning and ending of transformation are taken at 1% and 99% decomposition of austenite, respectively.

Effect of Stress on Overlapping of the Ferrite and Pearlite Reactions in Hypoeutectoid Steel

The lineal analysis data from which Fig. 6 was derived, are plotted in Figs. 7a and 7b in such manner that overlapping of the pearlite and proeutectoid ferrite reactions can be noted. Overlapping refers to the onset of the pearlite reaction with respect to the fraction of the total ferrite that will eventually form, and to the fraction of total pearlite present when the ferrite reaction has ceased. It is evident from Figs. 7a and 7b, that stress has a moderate effect on

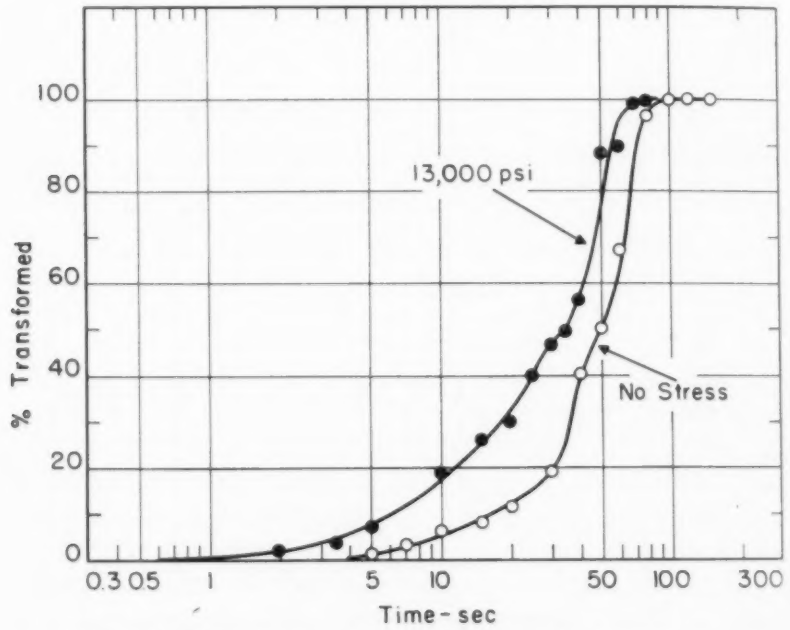


Fig 4—Reaction Curves of AISI 10B45 Steel Isothermally Transformed at 1253°F.

overlapping of the two reactions. The effect is one of increasing the percentage of total pearlite for the same percentage of total ferrite present when formed under stress compared to that of pearlite formed under no stress.

Effect of Stress on the Rate of Decomposition of Austenite

From the data of Figs. 3 and 4, the true rate of austenite decomposition cannot be determined readily since the amount of austenite remaining untransformed continuously decreases as transformation proceeds. Inasmuch as the true rate of austenite decomposition must be related to a unit volume of untransformed austenite, it becomes necessary to determine the true rate by plotting $\log_e [1-f(t)]$ versus transformation time, where $f(t)$ is the fractional amount of austenite isothermally transformed in a given time. The

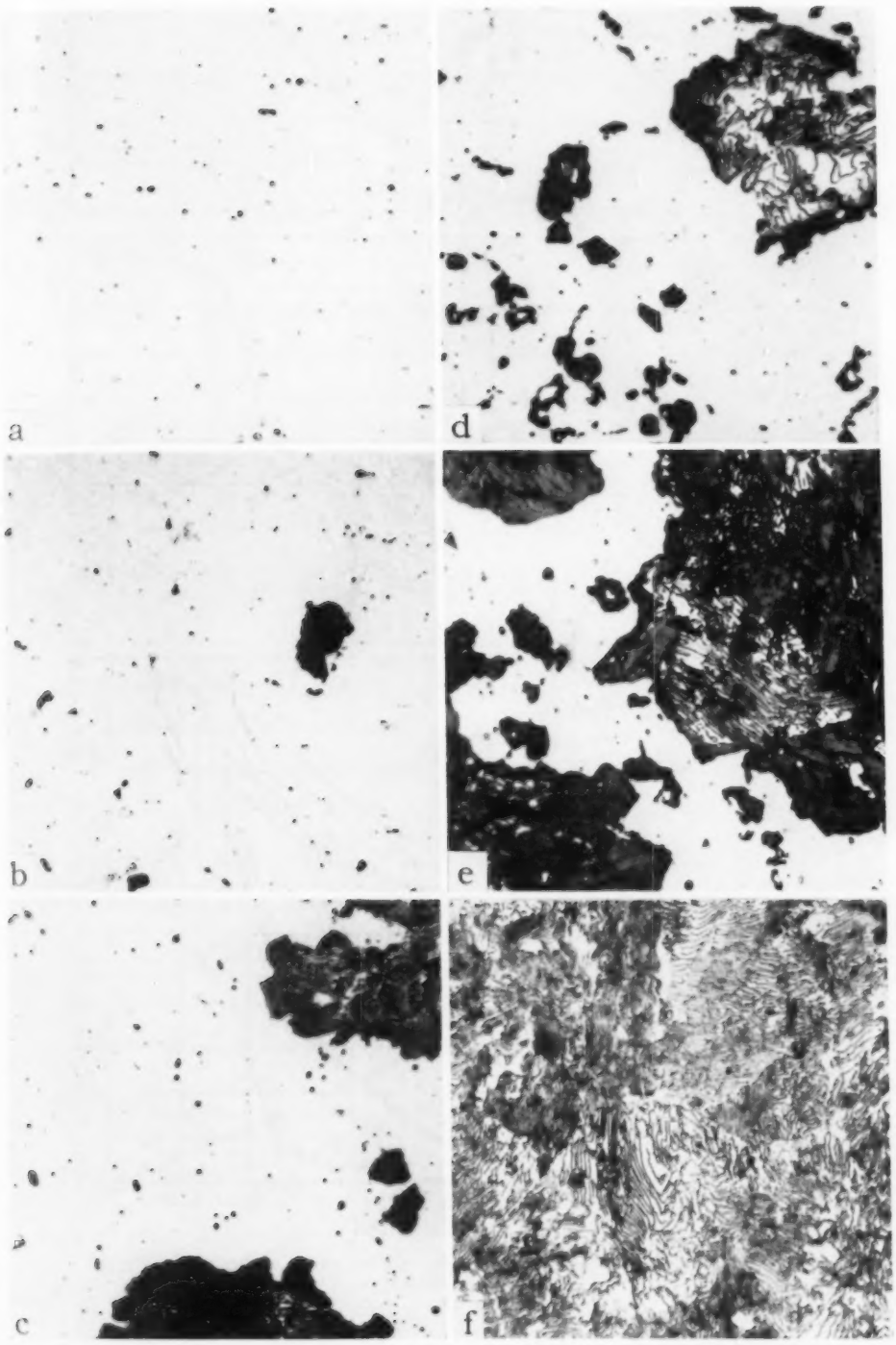


Fig. 5—Illustrating the Effect of Stress and No Stress on the Amount of Pearlite Isothermally Formed at 1273°F in AISI 1085 Steel; (a—c) No Stress, (d—f) 13,000 psi. Times of transformation a and d, 10 sec; b and e, 20 sec; c and f, 60 sec. ×500. Etchant—Saturated Picral.

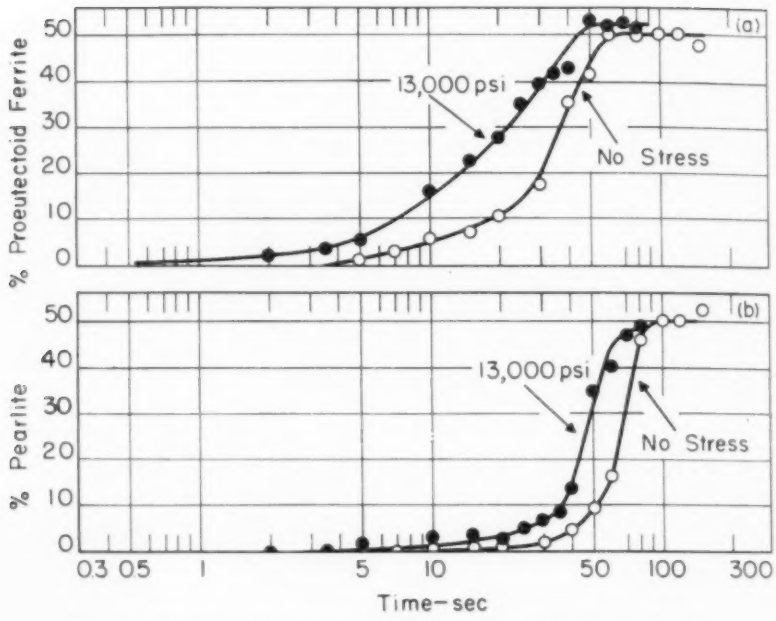


Fig. 6—Reaction Curves of AISI 10B45 Steel Isothermally Transformed at 1253°F. (a) Proeutectoid Ferrite; (b) Pearlite.

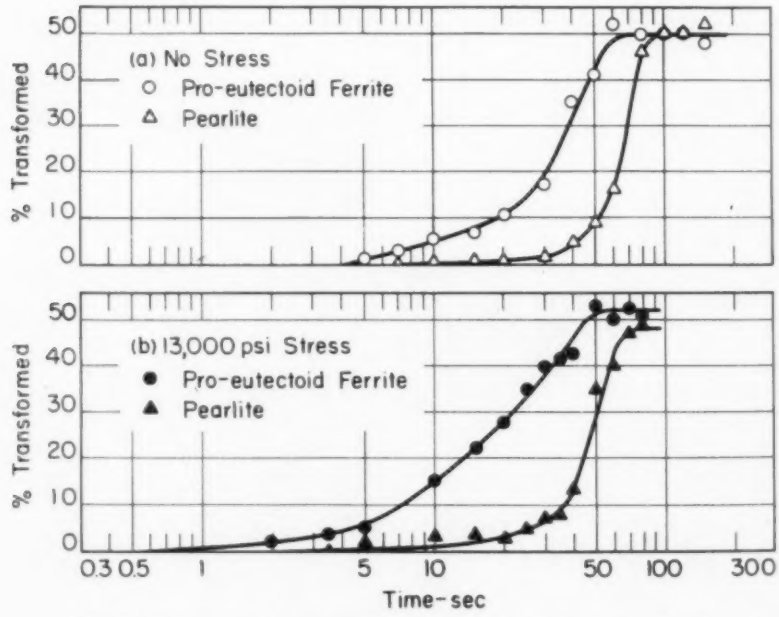


Fig. 7—Reaction Curves of AISI 10B45 Steel Isothermally Transformed at 1253°F. (a) No Stress; (b) 13,000 psi.

slopes of the curves represent the true rates of decomposition of residual austenite per unit volume of untransformed austenite, and may be expressed,

$$\frac{d}{dt}\left\{\log_e[1-f(t)]\right\} = -\frac{1}{1-f(t)}\cdot\frac{df(t)}{dt} \qquad \text{Equation 3}$$

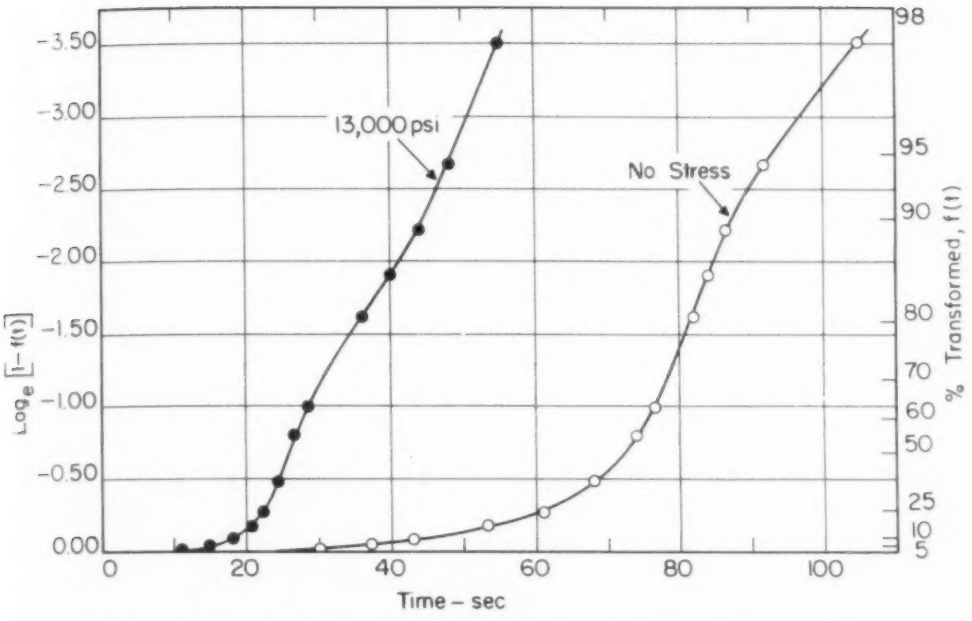


Fig. 8—Relationship Between the Amount of Untransformed Austenite and Transformation Time at 1273°F in AISI 1085 Steel for No Stress and 13,000 psi.

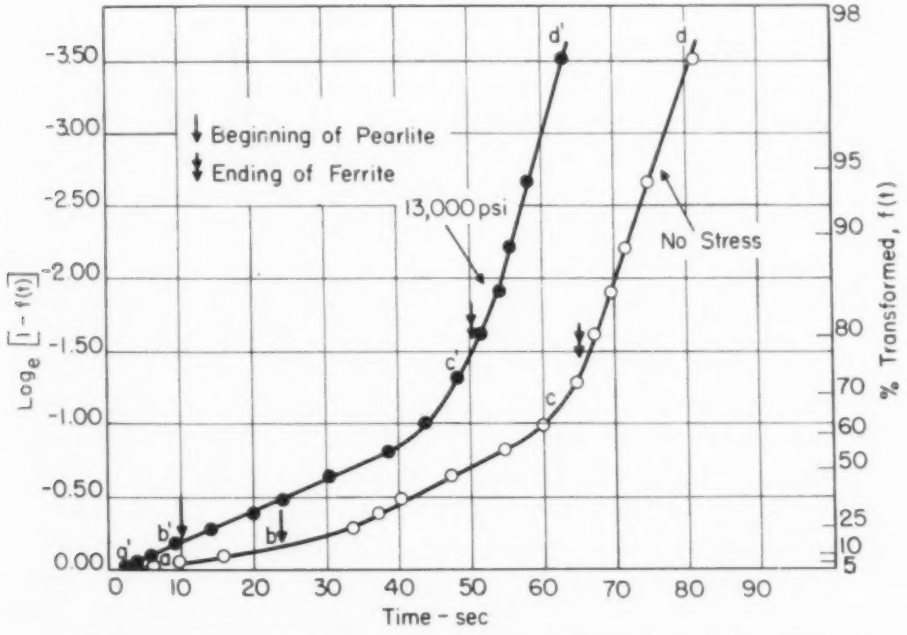


Fig. 9—Relationship Between the Amount of Untransformed Austenite and Transformation Time at 1253°F in AISI 10B45 Steel for No Stress and 13,000 psi.

where $\frac{df(t)}{dt}$ is the rate of transformation, $[1-f(t)]$ is the fractional amount of austenite remaining after a transformation time, t.

Determinations as described above are plotted in Figs. 8 and 9 for 1085 and 10B45 steels, respectively. By noting the change in slope of the no stress curve in Fig. 8, it is evident that the rate of

transformation increases gradually and reaches a maximum; it then remains constant, and finally decreases. In the case of transformation under a stress of 13,000 psi, the rate after decreasing begins to increase slightly. This circumstance may be more apparent than real, because in the region of the curve where this increase occurs any slight error in drawing the time-transformation curve (Fig. 3) will introduce considerable deviation in the value of $\log_e [1-f(t)]$. It appears from the slopes of the two curves that the maximum rate of transformation under stress is not appreciably higher than that under no stress, although the maximum rate is attained earlier during transformation under stress.

Fig. 9 shows that the rate of austenite decomposition in 10B45 steel, as indicated by the slopes of the two curves, increases gradually and eventually becomes constant. The decomposition product of the austenite consists of two structural constituents, ferrite and pearlite, and this causes some difficulty in interpretation of the rate of reaction owing to the overlapping of austenite-ferrite and austenite-pearlite reactions. However, since during the early part of the transformation only one phase, namely ferrite, is present, the rate of reaction during this period indicates the rate of austenite decomposition to ferrite. Similarly, at a later time when all the ferrite has formed, the slope of the curve reflects the true rate of decomposition of austenite to pearlite. The ferrite reaction rates are obtained from those parts of the curves marked a-b, and a′-b′, and the rate of pearlite formation from parts c-d and c′-d′, for no stress and 13,000 psi stress, respectively. It is evident from the slopes of the curves between a-b, a′-b′, c-d, and c′-d′, respectively, that the rates of formation of both ferrite and pearlite are increased under stress; the ferrite rate being affected relatively more than the pearlite rate.

Effect of Stress on the Rate of Growth of Pearlite

In Figs. 10 and 11 are plotted the maximum pearlite nodule radii vs. transformation times for AISI 1085 and 10B45 steels under no stress and 13,000 psi, respectively. The curves in Fig. 10 and the data in Table III indicate that the rate of growth of pearlite is constant and is virtually unaffected by stress.

In the case of the hypoeutectoid steel, and under restrictions of measuring pearlite nodule radii as mentioned heretofore, the curves of Fig. 11 indicate that the growth rate of pearlite is constant during the early stages of transformation and then gradually decreases with time. This constant growth rate is practically unaffected by applied stress. The effect of stress on rate of growth is most noticeable at the longer times of transformation; the rate under stress being about 8 times greater than that under no stress.

The proeutectoid ferrite existing in the prior austenitic grain boundaries was measured metallographically (in a direction along

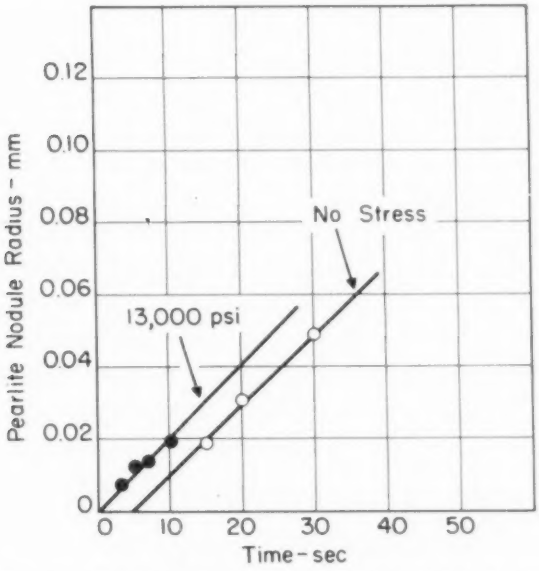


Fig. 10—Relationship Between Pearlite Nodule Radii and Transformation Time in AISI 1085 Steel Isothermally Transformed at 1273°F Under No Stress and 13,000 psi.

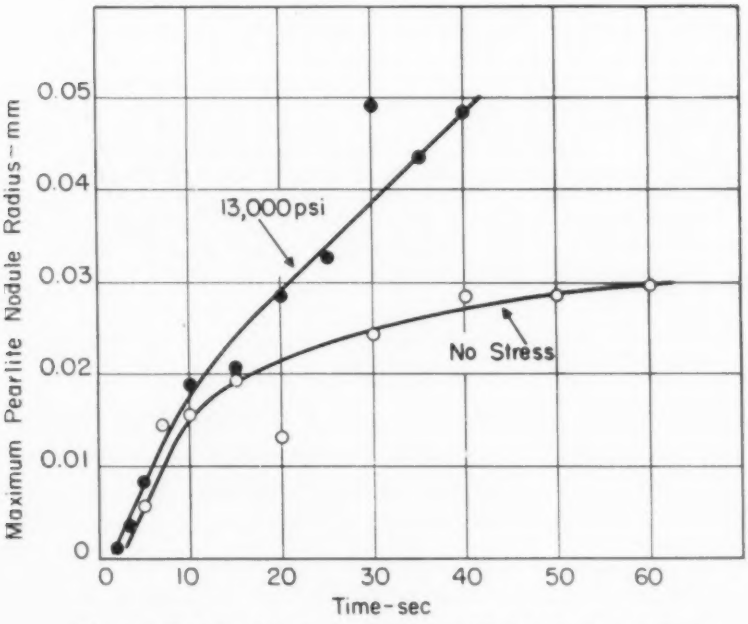


Fig. 11—Relationship Between Pearlite Nodule Radii and Transformation Time in AISI 10B45 Steel Isothermally Transformed at 1253°F Under No Stress and 13,000 psi.

the grain boundary) as a function of transformation time. These data, expressed in terms of half length of ferrite, are shown in Fig. 12. The curves indicate that during the early stages of transformation the rate of growth of proeutectoid ferrite is high and remains fairly constant, after which the rate gradually decreases with time. The initial rate of growth is increased by a factor of about 2.4 owing to a stress of 13,000 psi. (See Table III).

Table III
Effect of Tensile Stress On the Rates of Growth of Ferrite and Pearlite

Steel	Transformation Temperature, °F	Rate of Growth, mm/sec: No Stress	Rate of Growth, mm/sec: 13,000 psi	Remarks
AISI 1085	1273	1.9×10^{-3}	2.0×10^{-3}	Pearlite only.
AISI 10B45	1253	3.4×10^{-3}	8.0×10^{-3}	Initial constant rate of ferrite growth along austenite grain boundaries (lengthwise growth)
		1.6×10^{-3}	1.75×10^{-3}	Average ferrite growth rate during first 20 sec of transformation*
		2.1×10^{-3}	2.1×10^{-3}	Initial constant rate of pearlite growth

*Up to 20 sec transformation time about 1% pearlite present. The rate is therefore essentially that of ferrite formation.

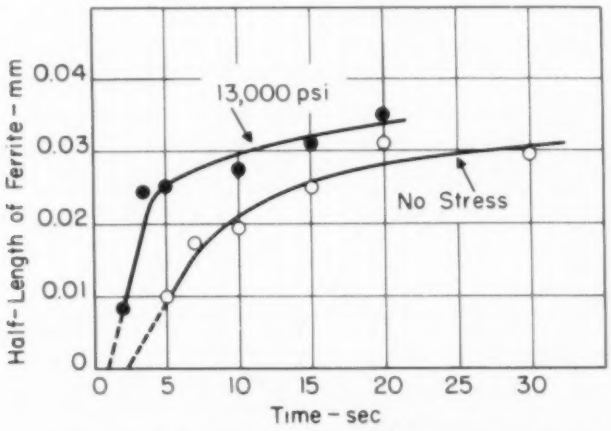


Fig. 12—Relationship Between Ferrite Half-Length and Transformation Time in AISI 10B45 Steel Isothermally Transformed at 1253°F Under No Stress and 13,000 psi.

Effect of Stress on the Rate of Nucleation of Pearlite in AISI 1085 Steel

Using the rate of growth values tabulated in Table III, the rate of nucleation N_v was calculated by appropriate substitution in Equation 2 and determination of $t_{0.5}$ from Fig. 3.

Such calculations indicated the rate of nucleation under a stress of 13,000 psi and at a transformation temperature of 1273°F to be 1.87×10^2 nuclei/mm^3/sec. as compared to 3.37 under no stress. The influence of stress was therefore to increase the rate of nucleation by a factor of about 55.

Effect of Stress on The Rates of Nucleation of Ferrite and Pearlite in AISI 10B45 Steel

No quantitative data on the rates of nucleation of proeutectoid ferrite and of pearlite are possible from the experimental data owing to the complexities in deriving adequate mathematical equations to define these quantities. However, on a comparative and qualitative

basis, the experimental data suggest that the application of stress during the formation of proeutectoid ferrite increases the rate of nucleation to a greater degree than it does the rate of growth. As evident from the slope of the curves in Fig. 9, in the regions a-b and a′-b′, the reaction rate of ferrite formation is increased by a factor of 2.75 through application of stress during formation. The *average* growth rate of proeutectoid ferrite, as deduced from the slope of the curves in Fig. 12,[3] is increased only by a factor of about 1.1 through application of the same stress. Inasmuch as the overall reaction rate is dependent upon the rates of nucleation and growth, it therefore appears that stress application during transformation has the more pronounced effect on the rate of nucleation.

Metallographic Observations

a. *Pearlite in AISI 1085 Steel*

To determine whether or not the application of stress significantly altered the character of the pearlite in fully transformed specimens, critical observations were made metallographically. In both stressed and unstressed specimens, unresolved pearlite patches were present at a magnification of 2000, and it is believed that such areas were present in somewhat greater abundance in the stressed specimens.

Electron photomicrographs were secured of several fully transformed structures formed under no stress and 13,000 psi, and subjected to critical measurement regarding the interlamellar spacing. The imposition of stress during transformation decreased the spacing distance by about 10% on the average.

b. *Ferrite and Pearlite in AISI 10B45 Steel*

Critical metallographic observations of a variety of fully transformed structures formed under no stress and 13,000 psi indicated no significant differences in the proeutectoid phase or in the pearlite constituent.

Conclusions

The isothermal transformation of austenite at temperatures above the knee of the appropriate C curve, is accelerated in AISI 10B45 and 1085 steels by applied stress. Both the beginning and ending times are shortened; the beginning time being more affected by stress than the ending times.

In AISI 10B45 steel, the amount of ferrite in the fully transformed structure is probably increased slightly due to stress. The

[3]Slope determined over the time interval from the onset of transformation to the time where about 1% pearlite is formed.

overlapping of the ferrite and pearlite reactions are also found to be extended. The rate of nucleation of proeutectoid ferrite is probably more than doubled by a stress of 13,000 psi; the rate of growth is increased by an amount considered insignificant. The rate of growth of pearlite is unaffected by stress in the early stages of transformation, but increases greatly later in the process.

In AISI 1085 steel, the application of stress increases profoundly the nucleation rate of pearlite; the growth rate, however, is virtually unaffected.

No significant changes were observed in the microstructures of the two steels investigated that could be attributed to stress application during transformation, except a slight decrease in the interlamellar spacing of the pearlite in the eutectoid steel.

Acknowledgment

Conduction of this research was made possible through support of the Office of Naval Research.

The assistance of Messrs. Jack S. Brett and Paul Rothstein with the experimental work, and the contribution of selected steels by Mr. Raymond A. Grange of the U. S. Steel Corporation Research Laboratory, Kearny, N.J. are gratefully acknowledged.

References

1. G. J. Guarnieri and J. J. Kanter, "Some Characteristics of the Metastable Austenite of 4 to 6% Chromium plus ½% Molybdenum Cast Steel," TRANSACTIONS, American Society for Metals, Vol. 40, 1948.
2. P. A. Dixon, Jr., "The Effect of Stress on the Transformation Rate of Austenite," M.S. Thesis, Columbia University, 1949 (Unpublished).
3. M. D. Jepson and F. C. Thompson, "The Acceleration of the Rate of Isothermal Transformation of Austenite," *Journal*, Iron and Steel Institute, Vol. 162, 1949.
4. R. Schnitzel and S. Bhattacharyya, "The Effect of Externally Applied Tensile Stress on the Isothermal Transformation Rate of Austenite," M.S. Thesis, Columbia University, 1950 (Unpublished).
5. S. Bhattacharyya and G. L. Kehl, "The Isothermal Transformation of Austenite Under Externally Applied Tensile Stress," TRANSACTIONS, American Society for Metals, Vol. 47, 1955.
6. F. C. Hull, R. A. Colton, and R. F. Mehl, "Rate of Nucleation and Rate of Growth of Pearlite," *Transactions*, American Institute of Mining and Metallurgical Engineers, Vol. 150, 1942.
7. R. F. Mehl and A. Dubé, *Phase Transformations in Solids*, 1951, John Wiley and Sons, Inc., New York.

EFFECT OF TEMPERATURE ON DELAYED YIELDING OF MILD STEEL FOR SHORT LOADING DURATION

By Joseph M. Krafft

Abstract

A bar loading technique has been developed for applying uniform compressive stress for a duration of 100 microseconds and for allowing measurement of time delay before plastic yielding within this duration. With the apparatus, the relationship between loading stress and delay time was measured for a mild steel at five temperatures in the temperature range 100 to −196°C (210 to −319°F). The results show that the loading stress increases linearly with decreasing logarithm of the delay time. The rate of increase is, however, much greater than would be anticipated from extrapolation of the similar relationships measured by Clark and Wood for loading times greater than 100 microseconds. Agreement is found between such extrapolation and the stress supported after yielding, or flow stress. At −196°C (−319°F) a waiting time before yielding could not be detected. At the next lowest temperature, −75°C (−103°F), delay time was found but always shorter than about 25 microseconds. Activation energy for delayed yield evaluated at a series of stress levels decreases with increasing stress level. (ASM-SLA Classification: Q23, CN)

Introduction

INVESTIGATIONS of enhanced strength of iron when stressed for very short time intervals were made by J. Hopkinson during the period beginning about 1875 (1,2).[1] Recent studies of this anomaly have been strongly influenced by the Clark and Wood measurements begun in the mid 1940's, which disclosed a waiting time before onset of rapid yielding of diminishing duration for larger loading stress (3). Increased interest in the topic has occurred both because of increased interest in shock loading of mild steel structures and because of the currently improved opportunity to obtain measurements having theoretical significance. Clark, Wood and their associates have published extensive data for mild steel showing the effect of temperature ranging from 121 to −196°C (250 to −320°F) on the duration of loading before yielding through the range of 10^{-4} sec. to 10^{3} seconds (4,5,6). While the existing information is sugges-

[1]The figures appearing in parentheses pertain to the references appended to this paper.

A paper presented before the Thirty-Seventh Annual Convention of the Society, held in Philadelphia, October 17–21, 1955. The author, Joseph M. Krafft, is associated with the Mechanics Division, Naval Research Laboratory, Washington, D.C. Manuscript received April 11, 1955.

tive with respect to the theoretical and practical answers sought, much remains to be found out about this eighty year old mystery (7).

Although the measurement of delayed yield is a comparatively recent development, the associated phenomena of yield point elevation with increased straining speed has been studied for some time (8,9,10). Both types of experiment give a measure of enhanced strength for short time. The measures will differ, however, because of differences in the treatment of the variables—load and time. In the delayed yield experiment, load is applied very suddenly, then held essentially constant until the specimen yields. The interval between application of the load and the occurrence of gross plastic yielding is called the time delay and is measured as a function of loading stress. Here the independent variable is stress; the dependent variable, time. On the other hand, in the elevation of yield point studies, load is applied less rapidly and at a controlled rate. The stress at which yielding occurs is then measured as a function of loading rate. The variables are now reversed; the independent variable is time (or loading rate); the dependent variable, stress. For the present studies measurement of delay time was chosen in hopes that the essential simplicity inherent in maintaining the stress and the strain rate constant would be advantageous in understanding experimental results in terms of fundamental characteristics of material.

The present experiments extend the range of delay measurement to much shorter time intervals—from the 10^{-4} seconds of the Clark and Wood compression experiments to 10^{-6} seconds. Investigation of shorter time intervals appeared to offer the best opportunity for discovery of phenomenon which could enhance a fundamental understanding of delayed yield. The use of refined bar loading techniques and high speed oscillographic equipment has made such an extension feasible. To allow direct comparison, the specimen temperature in these experiments was varied over a range comparable to that used by Clark and Wood.

Experimental Technique

In this experiment, compressive loading is produced by the longitudinal impact of bars of equal diameter and conveyed to the specimen by the propagation of an elastic wave. It is to be distinguished from the more usual impact loading with a massive hammer in which the load is sustained for a time equivalent to wave traverse many times the length of the hammer and thus of sufficient duration to average through initial wave propagation effects in the specimen. Bar impact methods are well suited for maintaining constant load during a time less than 10^{-4} seconds. The nine-inch steel

bar used in these tests, for example, applied an approximately uniform stress for about ninety microseconds. If plastic yielding occurs within this loading interval, the waiting or delay after onset of load was measured from the effect of yielding on the propagation of the loading wave.

The apparatus (Fig. 1) has been described by the author and his associates in previous publications (11,12); modification to per-

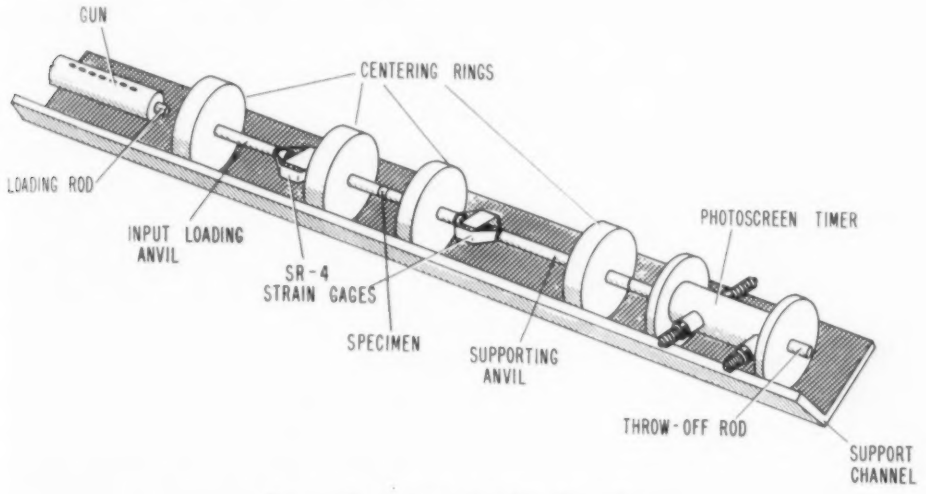


Fig. 1—Bar Impact Loading Apparatus

mit the present delay-time measurements has been more with respect to technique than to physical specification. The loading bar system is comprised essentially of four axially aligned bars of hardened steel and a gun which accelerates one of the bars. In operation the sequence of events begins with the firing of the gun (at left in Fig. 1). A loading rod, ½-inch O.D., 9-inch long, is accelerated in the gun until its base end uncovers pressure ventilating holes near the muzzle. Still guided by the remainder of the gun tube, the bar emerges and strikes the input loading anvil—the first of two stationary bars which adjoin the specimen. As a result of the impact, a rectangular strain wave of "uniform" compression is propagated forward through the input loading anvil; it is measured as it passes the midsection of the bar with wire resistance strain gages (SR4, C-10, 1000 Ω, G. F. 3.3) and oscillographic recording apparatus (Dumont 294-A and camera). The length of the input anvil bar (20 inch) is slightly greater than two times the loading bar length (18 inch) in order to permit all of the loading wave to be recorded at the gage site before the reflected wave can return to the gages from the bar end. The specimen (½ inch O.D., ½ inch long) is positioned adjacent to the bar end, and is backed up by another anvil bar identical in dimension and instrumentation to the impact anvil bar.

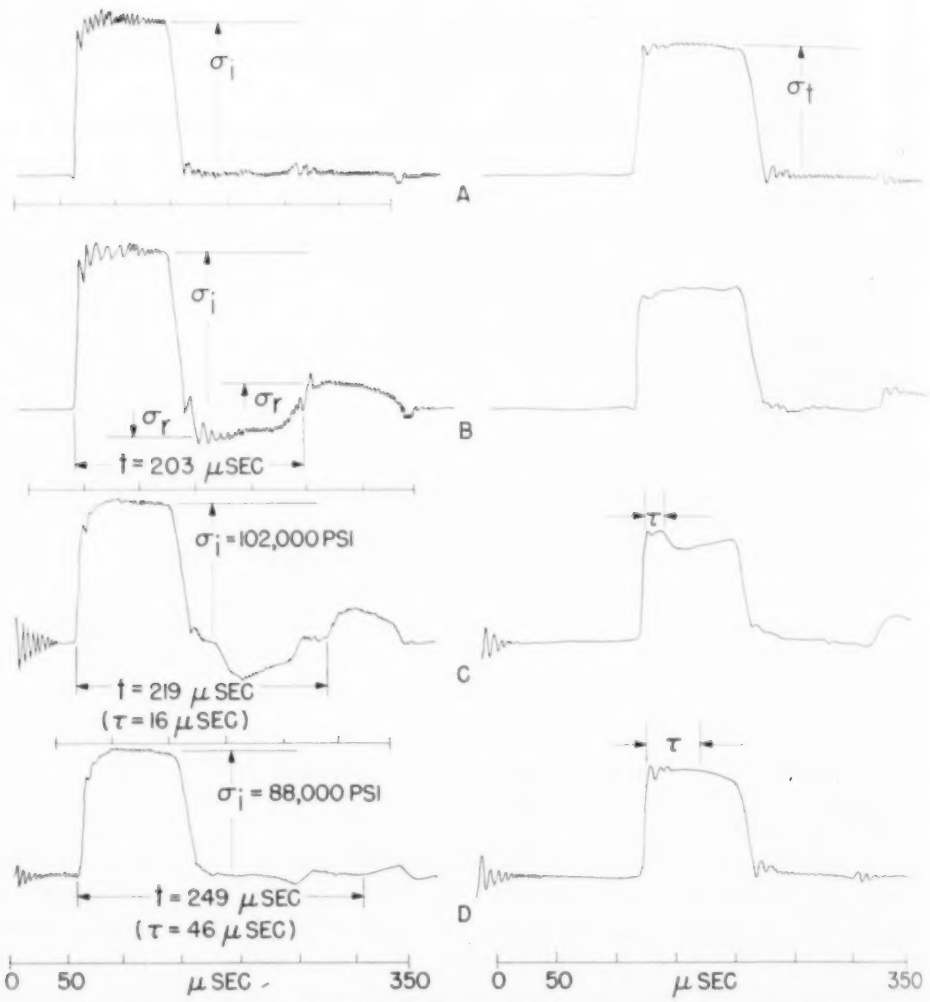


Fig. 2—Typical Strain-Time Oscillograms: Left from Input Loading Anvil; Right from Supporting Anvil illustrating A) No Yielding of specimen, B) Yielding without Delay, C) Yielding with 16 Micro-second Delay, D) Yielding with 46 Micro-second Delay. These Tests at +25°C (77°F)

The remainder of the loading wave which passes through the input anvil bar, the specimen, and the supporting anvil is trapped in a throw-off bar, ½ inch O.D., 10 inch long. As the tensile reflection of the wave from its free end cannot reenter the anvil bar system, the throw-off bar acquires a velocity proportional to the area under the strain-time pattern as recorded in the supporting anvil bar. Measurement of the throw-off bar velocity thus provides direct calibration of the strain measuring apparatus.

Method of Delay Time Measurement

Typical examples of strain measurements recorded simultaneously at the mid-section of input and backup anvil bars (traced for Fig. 2) illustrate the technique of delay measurement.

A) If a loading stress is introduced which is not sufficient to cause yielding of the specimen, the stress σ_i recorded in the input anvil bar is supported by the specimen and transmitted σ_t essentially without change to the support anvil bar (Fig. 2A). No reflection returns to the gage site in the input anvil.

B) If the loading stress is increased sufficient to cause yielding and the specimen yields immediately (i.e., without delay), the loss of stiffness in the specimen will cause a tensile reflection σ_r to return to the loading anvil gages (Fig. 2B). The transmitted stress σ_t is reduced in amplitude and becomes essentially the difference between σ_i and σ_r, neglecting effects of plastic wave propagation in the specimen (and differences in gain and linearity of the oscillograph in the supporting anvil circuit).

C) If the loading stress is such that, for a time, the specimen behaves as though elastic after which it yields and becomes plastic, the first part of the resulting strain patterns should correspond to the elastic case (Fig. 2A) and the remainder to the plastic case (Fig. 2B). The waiting time before yielding can then be measured from the time at which transition from elastic to plastic behavior occurs on the records. Thus it is seen that until the specimen yields, no reflected signal σ_r will be returned to the gages in the input anvil bar. By measuring the actual time of arrival of the reflected signal (after delayed yielding) and comparing this with its time of arrival when yielding occurs without delay (Fig. 2B) the waiting time is directly determined as a simple difference. The shape of the transmitted wave σ_t can be used to corroborate measurement from the relative displacement of the reflected signal σ_r. In actual practice, the position of the second reflection σ_r (compression) returning from the impact end of the bar is used to determine the delay, as its position with respect to the loading wave is independent of gage position along the bar and further is less affected by residual strain in the wake of the loading wave σ_i. Fig. 2D shows an example of delayed yield after a somewhat longer delay (46 microsec.) than that illustrated in Fig. 2C (16 microsec.).

The measurements have shown that the present technique by which delay time is measured from the effect of yielding on the wave propagation in loading bars appears to be of comparable sensitivity to methods based on actual strain measurement on the specimen. As a matter of convenience, it greatly facilitates procedure as wire gages need be applied only once to the anvil bars to serve for tests of an indefinite number of specimens.

Calibration

Calibration is afforded by comparison of the velocity, and thus the linear momentum with which the throw-off bar is ejected with

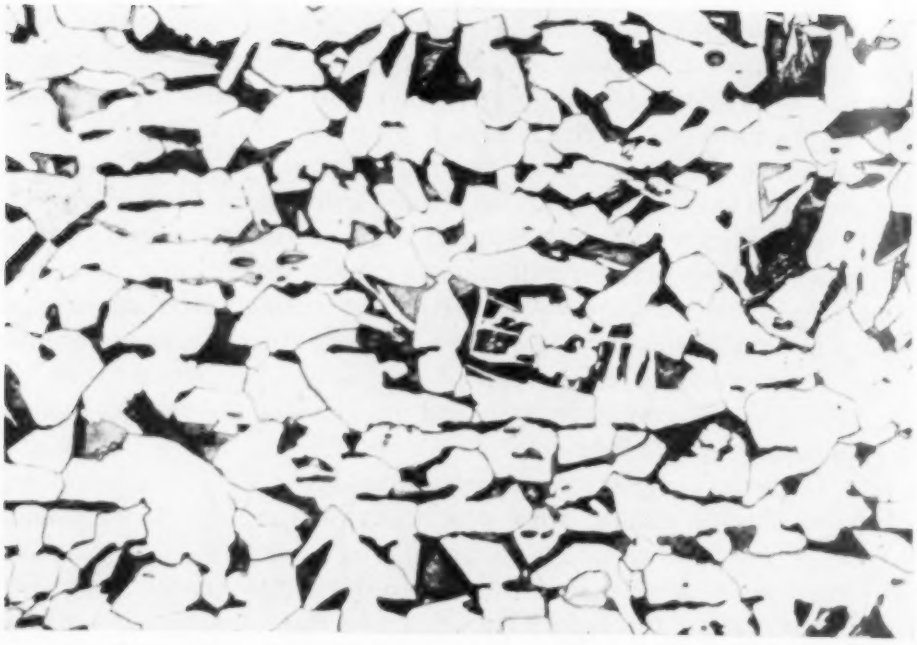


Fig. 3—Photomicrograph of Cross-section of Specimen, Nital Etch, ×200

the area under the transmitted stress (σ_t) curve. In addition, every record is calibrated by observing the trace deflection produced by incremental steps in resistance introduced in series with the strain gages (these traces omitted from Fig. 2). The agreement between calibration by the two methods was within 3%.

Temperature Range

A temperature bath was provided to surround the specimen and about two inches along each adjoining bar. In addition to room temperature at 77°F, four testing temperatures were provided: 1) −196°C (−319°F) by immersion in liquid nitrogen; 2) −75°C (−103°F) by immersion in a dry ice and alcohol bath; 3) −25°C (−13°F) by controlled additions of dry ice to an alcohol bath; and 4) +100°C (212°F) by boiling water with an immersion-type electric heater. Temperature was measured with a Copper-Constantan thermocouple in contact with the specimen.

Specimen Material and Preparation

The mild steel used in these tests was cut from the center part of a ¾-inch thick plate of Al-killed ship plate. Its composition by chemical analysis was found to be as follows:

C	Mn	Si	P	S	Ni	Cr	Mo	Ca	Al
0.204	0.84	0.191	0.010	0.026	0.09	0.046	0.018	0.138	0.03

Specimens were cylindrical in shape, 0.5 inch O.D. and 0.5 inch

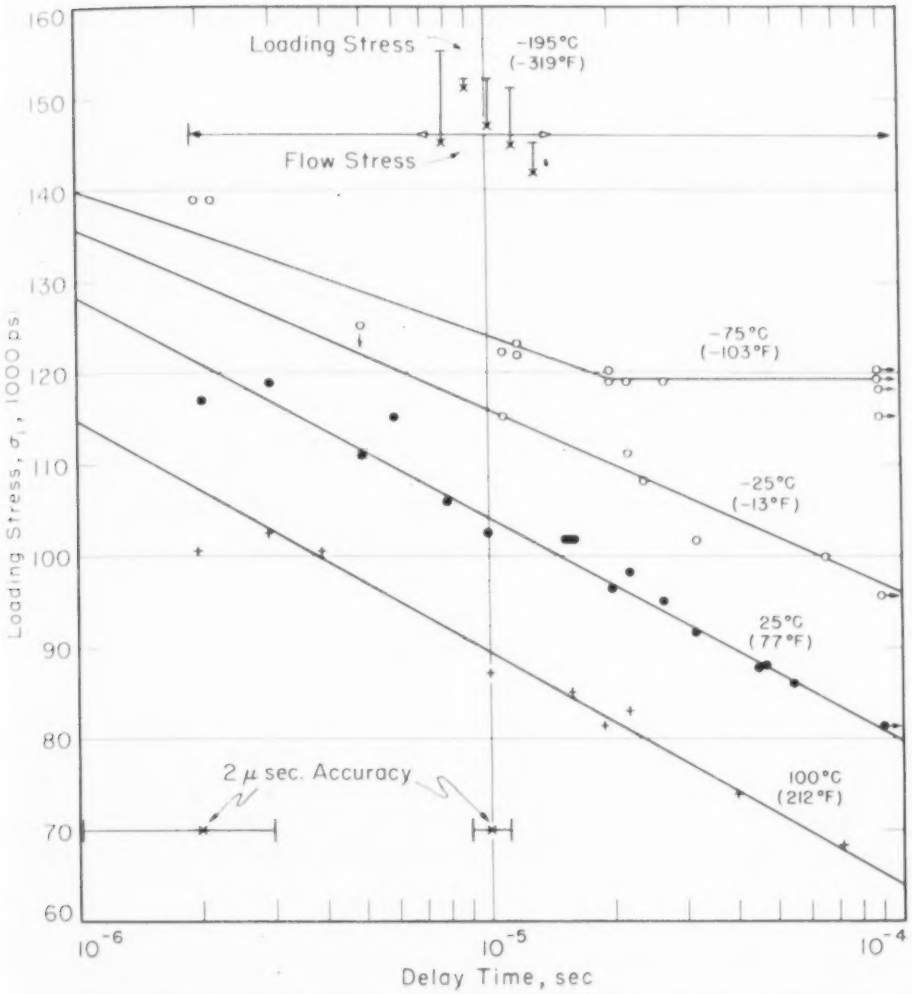


Fig. 4—Experimental Results Showing Relation between Loading Stress (1000 psi) and Time Delay before Yielding (sec) at +100°C (212°F), +25°C (77°F), −25°C (−13°F), −75°C (−103°F), −196°C (−319°F)

long, with longitudinal axis transverse to the rolling direction parallel to the original surfaces of the plate. A photomicrograph of a cross section is shown in Fig. 3. Sawed strips of the as-received material were heated to 1100°F for 1 hour and furnace cooled to relieve internal stress. Final machining removed decarburized material near the surfaces.

Some specimens were tested in the static compression using the test jig described in a previous publication (11). Average values from four tests at room temperature gave an upper yield strength of $36{,}000 \pm 1500$ psi; lower yield strength, $33{,}000 \pm 500$ psi.

Results

The data obtained in the dynamic compression tests is shown in Fig. 4 as a plot of log delay time versus loading stress. The data

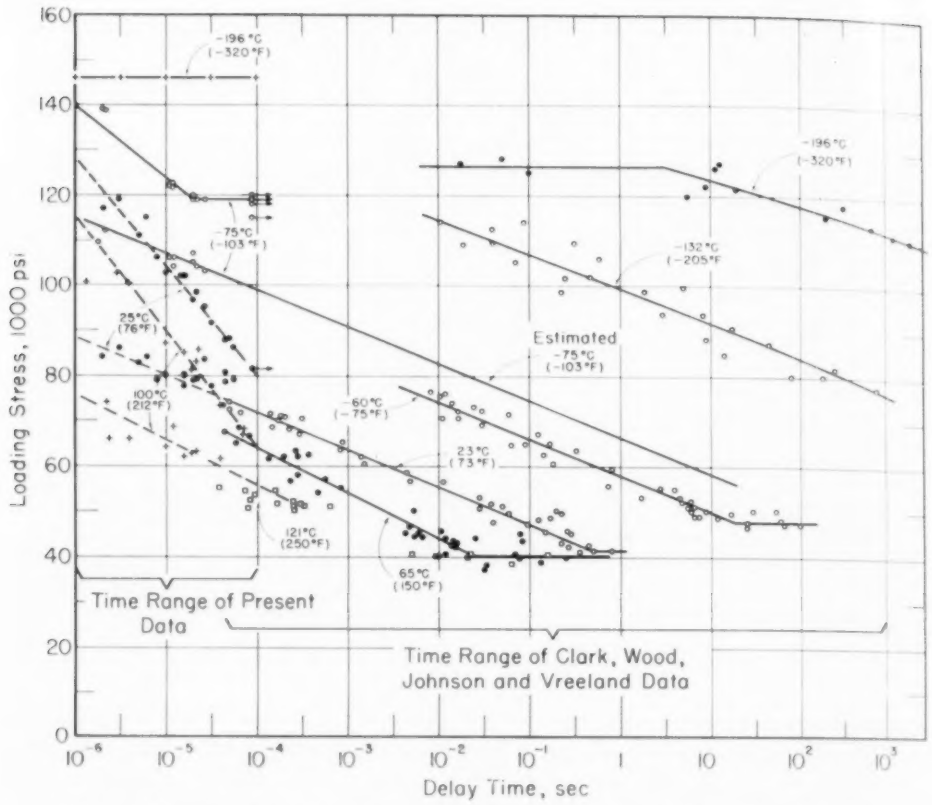


Fig. 5—Present Results showing both Loading Stress Before Yield as well as Flow Stress after Yield versus Delay Time in 10^{-6} to 10^{-4} sec. Range compared with Clark, Wood, Johnson, and Vreeland Results showing Loading Stress Before Yield versus Delay Time in 10^{-4} to 10^{3} sec. Range

points at each temperature appear to be well fitted by a straight line, agreeing in this respect with the similar functional relationship already established by others. The accuracy to which the waiting time can be measured is about two microseconds, rather independent of the magnitude of the waiting time. As a consequence, the data points toward the longer delay time side (right) of Fig. 4 more accurately define the slope and character of the delay time relationship. Another plot (Fig. 5) shows the present data (except that at −25°C) on a graph showing also the delay-time data of Clark and Wood for a mild steel at various temperatures.

At −196°C (−319°F), a critical stress (146,000 psi) extended throughout the range of time observation. Above this stress, yielding occurred without measurable delay, below, no yielding occurred. This could well be an extension of the plateau observed by Clark and Wood (5) (126,000 psi) at the same temperature for loading time shorter than about three seconds. The difference in magnitude could be a result of differences in specimen material and/or geometry. Baron has suggested that the lack of delay time at this tem-

perature could be a result of deformation by twinning (13). That twinning at this temperature is the dominant feature of the deformation is clear from earlier work by the writer and associates (11) as well as from work by Rosenthal and Woolsey (14).

In the tests at −75°C (−85°F) another critical value of stress (119,000 psi) was found below which no yielding occurred. Unlike the plateau at −196°C (−319°F) yielding at stresses above the plateau stress showed a measurable delay time. These were, however, always shorter than about 26 microseconds. The −75°C (−85°F) plateau of stress must terminate after some waiting time longer than presently observable as this stress is far above static upper yield strength values for −75°C (11,13). At this temperature the plateau is unlikely the result of strain aging which was suggested by Clark and Wood as the reason for plateaus at longer waiting times and higher temperatures. It was observed that polished longitudinal sections of specimens deformed at −75°C show plentiful formation of Neumann Lamellae. If the plateau is, as suggested for −196°C, the result of an initial deformation by twinning, one might consider the sloped delay time curve at the left a measure of delay time for deformation by twinning at −75°C. Specimens loaded at the higher temperatures showed no appreciable formation of Neumann Lamellae so that the corresponding delay-time curves would appear to define critical stress, time, temperature combinations for failure by slip.

From the relationship between temperature and waiting time (Fig. 4) it is possible to calculate an energy of activation for the yielding process. It is customary to use an Arrhenius type expression for the delayed yield as a thermally activated process such as

$$\tau = A\, e^{Q/kT} \qquad \text{Equation 1}$$

where τ is the delay time, Q, an activation energy, is a function of stress level, k is the gas constant, T is the absolute temperature and A is a constant. The constant A can be eliminated in solving Equation 1 for Q at constant stress, thus obtaining

$$Q = K \frac{(\ln t)}{1/T} \qquad \text{Equation 2}$$

From Equation 2 it is seen that slopes taken from curves of log delay time versus 1/T will give values of the activation energy. Such data are shown in Fig. 6 for stress levels from 80,000 to 130,000 psi (in 10,000 psi steps) taken from the straight lines on the log delay time vs loading stress data. The plot does appear to define a family of straight lines for points taken at +100°C, +25°C, and −25°C. However those from −75°C fall below the line passing through the

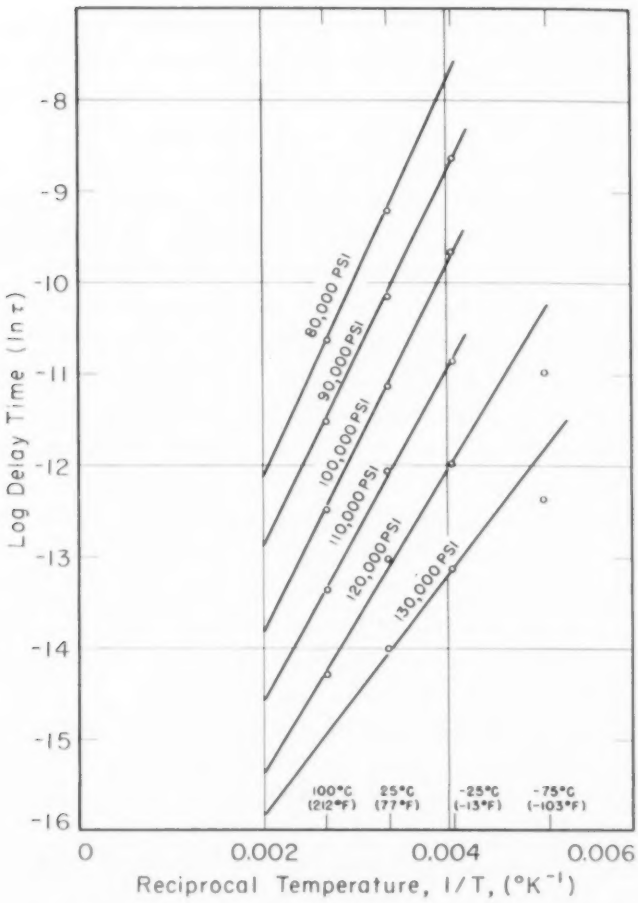


Fig. 6—Plot of Reciprocal of Absolute Temperature versus the Logarithm of the Yielding Delay-Time. Slope of Curves Gives a Measure of Activation Energy. Data was taken from Lines Drawn in Fig. 4

other points—suggestive of an activation energy lower for twinning than for slip processes.

Slopes measured from Fig. 6 are shown in Fig. 7 as a plot of activation energy Q versus stress level. The activation energy values range from 3000 to 4400 cal. per mole increasing with decreasing stress levels. Baron in a similar treatment of the Clark and Wood data finds similar values of Q (Fig. 7D). These values are somewhat lower than the curve considered most likely by Cottrell and Bilby (15) (their curve 4).

Elevated Flow Strength

The delayed yielding effects described in the foregoing are of some fundamental interest. As a practical point, however, one should be careful to note that a delay time can be observed only if stress is applied uniformly over a substantial volume of the specimen material. Stress concentration in the specimen will lead to immediate

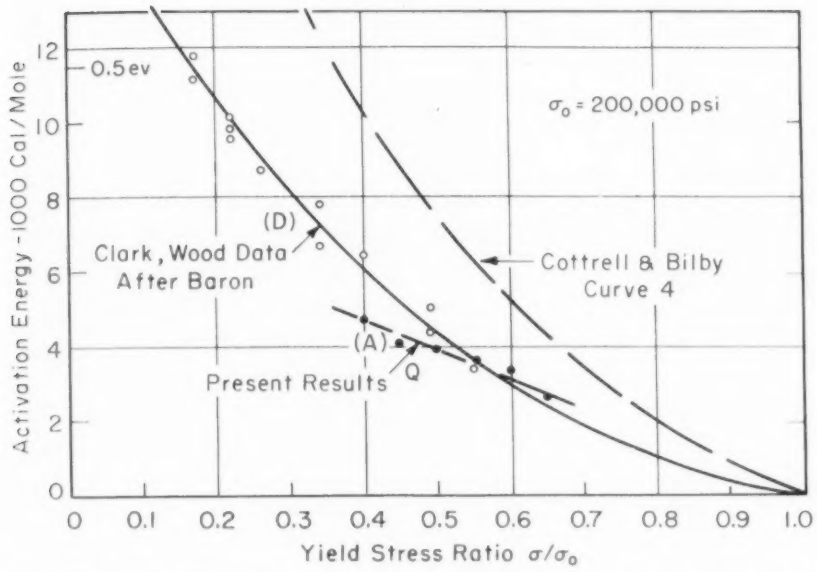


Fig. 7—Plots of Activation Energy versus Stress Level divided by 200,000 psi (σ/σ_0) A) Q for present data, D for Clark, Wood data after Baron, Cottrell and Bilby, Curve 4

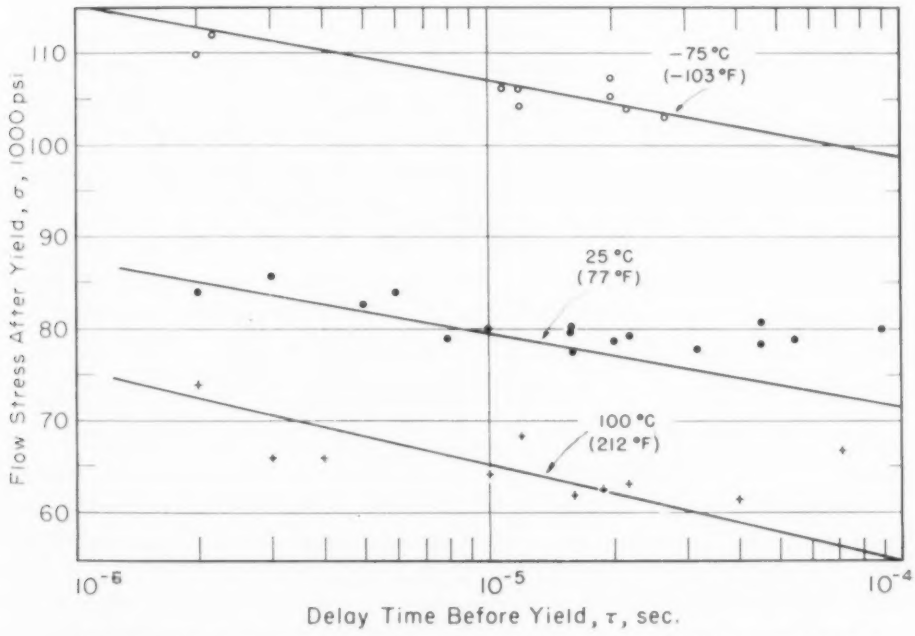


Fig. 8—Plot of Flow Stress Supported by Specimen after Yielding versus Delay Time before Yielding. Lines Represent Extensions of Clark, Wood Data as shown in Fig. 5

yielding. What should be of practical importance, however, is that after yielding substantial increases in flow strength are realized for the whole time of loading. This enhanced strength occurs very dependably even if, for some reason, delayed yielding is not in evidence. It is the increase in flow strength, rather than the "delayed yield,"

which one might expect to increase the resistance of mild steel structures to impulsive loading.

The strain-time records of the bar loading experiment give direct measure of the flow stress after plastic yielding. In the transmitted stress pattern σ_t (Fig. 2) the stress amplitude appearing is that supported by the specimen and thus applied to the face of the backup anvil bar. The flow stress can be measured directly from the transmitted stress wave σ_t after yielding or as the difference between the loading wave amplitude σ_i and the reflected wave amplitude σ_r. Curves showing the flow stress (σ_i minus σ_r) versus log delay time for three temperatures are shown in Fig. 8. The shorter delay time points correspond to greater loading stress and correspondingly increased average strain rates. A slight increase in flow stress with shorter delay times (increase in strain rate) appears in these records. The line drawn through these points are those extrapolated from the Clark-Wood delay time data at longer waiting times.

It is indeed curious that the present flow stress curves would appear to extend the Clark-Wood delay time curves (Fig. 5) while the present delay time curves do not, having a much greater slope or time sensitivity. Early results by Clark and Wood did show an upward trend in slope of stress vs delay time curves for shorter delays (2). Their recent tests, however, show a straight line relationship. A reason for this difference is not apparent at present. It is hoped that investigations of the effect of specimen geometry and size, of the rolling direction, and through a more extended time range will clarify this anomaly. The measurement of micro-yielding before gross yield in the shorter time range would also prove enlightening.

Acknowledgment

The author is indebted to G. R. Irwin, Superintendent, Mechanics Division, Naval Research Laboratory, for continued interest and encouragement in this work, and to his associate, A. M. Sullivan, for micrographs of the specimens, and to H. G. Baron for kind advice regarding an error in the original text.

References

1. J. Hopkinson, "Original Papers by the Late John Hopkinson," Vol. II, Cambridge University Press, 1901.
2. B. Hopkinson, "The Effects of Momentary Stresses in Metals," *Proceedings*, Royal Society, London, Vol. 74, 1904, p. 498.
3. D. S. Clark and D. S. Wood, "Time Delay for the Initiation of Plastic Deformation at Rapidly Applied Constant Stress," *Proceedings*, American Society for Testing Metals, Vol. 49, 1949, p. 717.
4. D. S. Wood and D. S. Clark, "The Influence of Temperature upon the Time Delay for Yielding in Annealed Mild Steel," TRANSACTIONS, American Society for Metals, Vol. 43, 1951, p. 571.

5. D. S. Wood and D. S. Clark, "Delayed Yielding in Annealed Mild Steel with Special Reference to Low Temperatures," Fourth Technical Report, Contract NConr-24418, Proj. Desig. N. R. 031-285, Office of Naval Research, 1951.
6. D. S. Clark, "Behavior of Metals under Dynamic Loading," TRANSACTIONS, American Society for Metals, Vol. 46, 1954, p. 49.
7. G. R. Irwin, *Modern Research Techniques in Physical Metallurgy*, American Society for Metals, Cleveland, 1953, p. 205.
8. C. F. Elam, "The Influence of Rate of Deformation on the Tensile Test with Special Reference to the Yield Point in Iron and Steel," *Proceedings*, Royal Society, London, Vol. 165, 1938, p. 568.
9. E. A. Davis, "The Effect of Speed of Stretching and Rate of Loading on the Yielding of Mild Steel," *Transactions*, Journal of Applied Mechanics, Vol. 60, 1938.
10. A. F. C. Brown and R. Edmonds, "The Dynamic Yield Strength of Steel at an Intermediate Rate of Loading," *Proceedings*, Institute of Mechanical Engineers, Vol. 159, 1948, p. 11.
11. J. M. Krafft, A. M. Sullivan, C. F. Tipper, "Effect of Static and Dynamic Loading and Temperature of the Yield Stress of Iron and Mild Steel in Compression," *Proceedings*, Royal Society, London, Vol. 221, 1953, p. 114.
12. J. M. Krafft, "Elimination of Transient Strain Fluctuations which Result from Longitudinal Impact of Bars," accepted for publication in Society for Experimental Stress Analysis *Transactions*, Vol. 12, 1955.
13. H. G. Baron, "Stress-Strain Curves of Some Metals and Alloys at Low Temperatures and High Rates of Strain," Ministry of Supply, Armament Research Establishment Metallurgy Report No. 22/54, London, Aug. 1954.
14. D. Rosenthal and C. C. Woolsey, Jr., "The Effect of Strain Rate on Twinning and Brittle Fracture," *Journal*, American Welding Society Research Supplement, Vol. 17, 1952, p. 475.
15. A. H. Cottrell and B. A. Bilby, "Dislocation Theory of Yielding and Strain Aging of Iron," *Proceedings*, Physical Society, Vol. 62, A, 1949, p. 49.

DISCUSSION

Written Discussion: By C. W. Curtis, professor of physics, Lehigh University, Bethlehem, Pennsylvania.

Dr. Krafft should be complimented both for the development of an ingenious application of the "pressure bar" technique and for his measurements supplementing the work of Messrs. Clark and Wood.

I will confine my remarks to two general observations concerning the technique.

First, this method of measurement is attractive since the "pressure bar" provides a means of suddenly applying a large stress to the specimen and of maintaining this stress approximately constant until the specimen yields. To the extent that the stress can be applied instantaneously and then be kept constant, the experiment is ideal. Actually, however, a short but finite time is required for the stress to reach a maximum and this is followed by periodic variations which may be as great as 20% of the final average value.[2,3,4] This behavior results from the presence of the free lateral surface of the bar and is therefore inherent in the method. Dr. Krafft noted in an earlier report[5] that the periodic variations can be reduced by decreasing the rate at which the force is applied to the "input loading

[2]R. M. Davies, *Transactions*, Royal Society, London, Serial 240A, 1948, p. 375.
[3]E. A. Ripperger, *Proceedings*, First Midwest Conference, Solid Mechanics, University of Illinois, April, 1953.
[4]C. W. Curtis, *Journal of Applied Physics*, Vol. 25, 1954, p. 928.
[5]J. M. Krafft, SESA, Vol. 12, 1955.

anvil," but this is done at the expense of increasing the time for the stress to reach a maximum. Measurements we have made indicate that, even when the total force is applied within a fraction of a microsecond to the end of a steel "input loading anvil" having the dimensions used by Dr. Krafft, approximately 5 microseconds will elapse before the stress applied to the specimen reaches a maximum and with other loading conditions the rise time will be longer. The existence of the finite rise time should not appreciably change Dr. Krafft's results, at least for the longer delay times, but it does limit the method to the observation of delay times, or other events, longer than a few microseconds.

Secondly, it is noted that SR4, type C10, iso-elastic wire gages were used in this work. Recently Dr. Meitzler observed that when gages of this type were subjected to rapidly varying stresses, they developed voltages across their terminals even when there was no gage current and when they were bonded to nonmagnetic bars.[6] This signal is proportional to rate of strain rather than to strain and with current through the gage is superimposed on the normal signal resulting from a change in gage resistance. It should not have affected the measurement of arrival times, but might have distorted the rate at which the stress appears to rise to a maximum.

Written Discussion: By D. S. Clark and D. S. Wood, California Institute of Technology, Pasadena, Calif.

The group at California Institute of Technology are very much interested in the work reported by Dr. Krafft. The author may be correct in his presumption that the change in slope of the stress versus delay time is associated with a change in the manner of deformation. It is conceivable that above a certain stress the deformation may occur or be nucleated by twinning. Further consideration and investigation will be necessary before a definite answer can be given to this behavior. The author's results are very interesting and significant.

Has the author obtained any results of tests made with the same material used by Clark and Wood[7] and Johnson, Wood, and Clark?[8] The extension of the data obtained by these authors to shorter delay time would be of considerable interest.

Author's Reply

I wish to thank Professors Clark and Wood and Professor Curtis for their interesting discussions. As the remarks of Professor Curtis pertain to the validity of the method, I will reply first to him before discussing the questions on the results of using this method. The anomolous strain rate dependent signal from wire gages was known to us during the preparation of the present data. As this signal can be measured with no applied gage current independent of the apparent strain signal with gage current, it is possible to correct for this effect. This correction was included in the numerical results although not in the oscillograms shown in Fig. 2. Since last Spring when I learned from Professor Curtis and Dr. Meitzler that this effect was attributable directly to the use of C-type SR4 gages, I have converted my apparatus to use the copper nickel wire A-type SR4 gages which do not show

[6]Forthcoming Letter to the Editor, RSI.

[7]D. S. Clark and D. S. Wood, "The Time Delay for the Initiation of Plastic Deformation at Rapidly Applied Constant Stress," *Proceedings*, American Society for Testing Materials, Vol. 49, 1949, p. 717.

[8]J. E. Johnson, D. S. Wood, and D. S. Clark, "Delayed Yielding in Annealed Low-Carbon Steel under Compression Impact," *Proceedings*, American Society for Testing Materials, Vol. 53, 1953, p. 755.

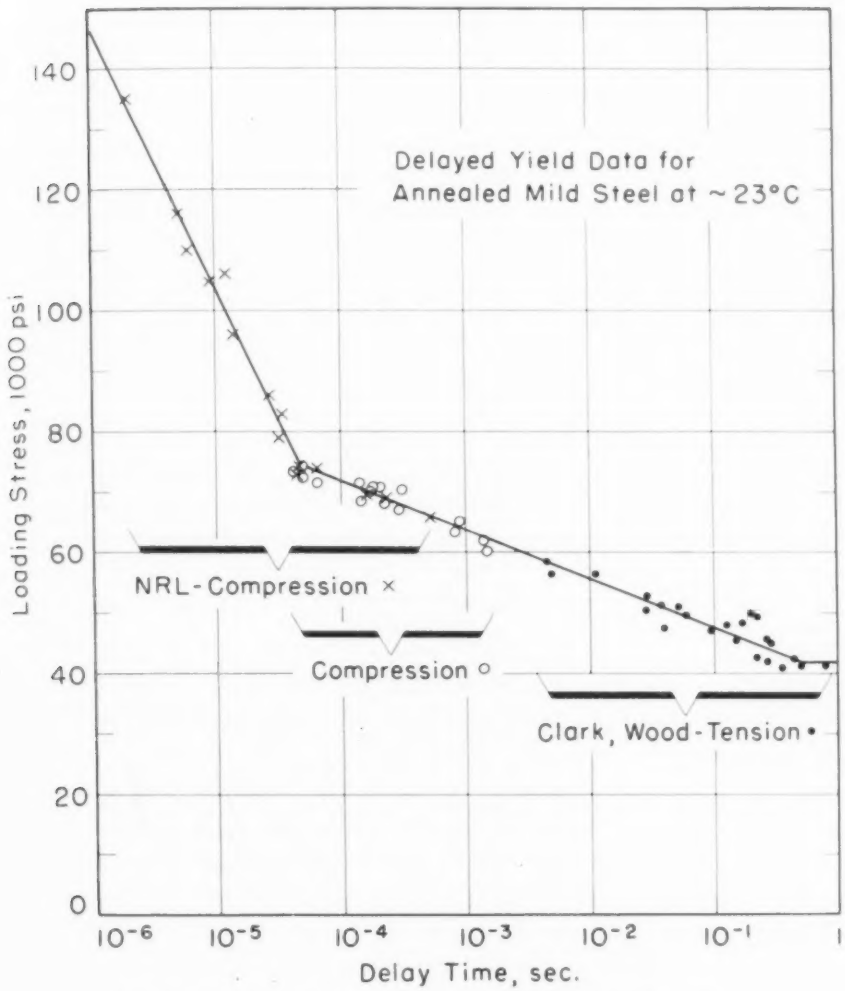


Fig. 9—Delayed Yield Data for Annealed Mild Steel at 23°C.

this effect. The resulting loading patterns are thereby much improved over those shown in this paper.

In ascribing a limit beyond which the present measurements of delay time is not meaningful, the finite rise time is a primary and inherent limitation. Times as short as two microseconds were included in the data (Fig. 4) even though the total rise time was greater than this because during a large portion of the rise time the stresses involved would cause yielding only after waiting time much greater than five microseconds. Thus it was felt that the rise time from the order of 80% of maximum load to the maximum might define an effective loading time, and this time is more the order to two rather than five or ten microseconds. In addition a similar experiment using 6/10 scale bars and specimens with a correspondingly shorter rise time indicated an identical trend of loading stress versus delay time in the short time range. Even with this qualification, however, I agree with Professor Curtis that the data at very short delay times must be regarded as questionable.

With respect to the discussion of Professors Clark and Wood, a development since the preparation of my original manuscript is of interest. Through the kind-

ness of Professor Wood I have obtained specimens from the stock used in his work on mild steel. These were machined into short compression specimens and then annealed in dry hydrogen at 1600°F. In order to obtain yield delays overlapping the room temperature data of Professors Clark and Wood, loadings at constant stress level were repeated until the specimen yielded—the delay being then measured as the cumulative time under load. The results plotted in Fig. 9 show surprisingly excellent agreement with Professors Clark and Wood results in the region of overlap. But at shorter delay times there is a distinct break in the curve with the points defining a line of much steeper slope quite similar to that for the ship plate on which the original experimental data was obtained. This break occurs in a range of waiting times in which the effect of finite rise time should not be a serious objection. That it should be so sharply defined is of considerable interest in contrast to the gradual shift predicted by Fisher.[9]

Further experimental evidence for the change in slope of the delay time relationship has been published recently by Ramberg and Irwin[10] working at the Bureau of Standards. We have also made measurements of delayed yield on this material at room temperature and find excellent agreement with their results in range up to sixty microseconds. A knee in the delay time curve is not sharply defined in the Ramberg-Irwin data but this could be attributed to experimental uncertainty in their data.

[9] J. C. Fisher, "Application of Cottrell's Theory of Yielding to Delayed Yield in Steel," TRANSACTIONS, American Society for Metals, Vol. 47, 1955, p. 451.

[10] W. Ramberg and L. K. Irwin, "Longitudinal Impact Tests of Long Bars with a Slingshot Machine," American Society for Testing Materials, Preprint 93a, 1955.

THE OPTIMUM BORON CONTENT FOR HARDENABILITY

By J. C. Shyne, E. R. Morgan and D. N. Frey

Abstract

The relationship between boron content and hardenability has been established for a series of high purity iron-carbon-boron alloys. This correlation has been made in terms of "effective" rather than the total boron content. A method for determining effective boron contents is described.

A maximum boron hardenability effect was obtained in an alloy which contained 0.00033% effective boron. This amount of boron is believed to represent the limit of boron solubility in these steels at the austenitizing temperature of 1550°F. (ASM-SLA Classification: J26, ST)

Introduction

As a hardenability agent, boron is unique in several respects. In contrast to other alloying elements, boron increases the hardenability of steel by retarding the rate of nucleation of ferrite or pearlite nucleated by ferrite, without influencing the rate of growth of these constituents (1).[1] Small additions of boron to steel cause an increase in hardenability equivalent to that produced by much larger additions of any other element. With other common alloying elements the hardenability effect is proportional to the amount added; this is not the case with boron. Several investigators have shown that there is an optimum boron content which gives a maximum hardenability effect (1,2,3). This optimum boron content has been estimated variously from 0.0001 to 0.0025%. It has been suggested that the disparity can be attributed to the presence of impurities in the steels investigated. The present paper describes an attempt to correlate the boron content and hardenability of high purity iron-carbon-boron alloys.

Experimental

All the alloys used in this work were prepared by vacuum melting to obtain minimum amounts of soluble oxygen and nitrogen without resorting to additions of such elements as aluminum or titanium. To avoid ambiguities caused by other elements the alloys were prepared from electrolytic iron (Plast Iron A 101) and spectrograph-

[1] The figures appearing in parentheses pertain to the references appended to this paper.

A paper presented before the Thirty-Seventh Annual Convention of the Society, held in Philadelphia, October 17–21, 1955. The authors, J. C. Shyne, E. R. Morgan and D. N. Frey are associated with the Metallurgy Department, Ford Motor Company, Dearborn, Michigan. Manuscript received May 31, 1955.

ically pure carbon. The carbon contents of the alloys were held within the range 0.48 to 0.51%. The only compositional variable was boron which was added as ferroboron. The vacuum cast alloys were either forged and swaged or hot rolled from 2-½ inch diameter ingots down to ⅝ inch diameter bars. Hardenability specimens and specimens for compositional analysis were machined from only the center portions of the ⅝ inch diameter bars.

The critical cooling rate, the slowest rate of cooling that avoids any transformation to pearlite and ferrite, was used as the measure of hardenability. This method rather than the Jominy hardenability test was chosen because it was a more sensitive measure of the low hardenability exhibited by the present alloys which did not contain the usual residual amounts of alloying elements found in commercial steels.

Small specimens, 0.100×0.100×0.040 inches, for critical cooling rate determinations were machined from the experimental steels and then nickel plated to prevent decarburization. The plated specimens were spot welded to chromel and alumel wires, so that each specimen acted as the bead of a thermocouple. Two-hole ceramic thermocouple spaghetti served as handles for the specimens as well as insulators for the thermocouple wires.

The specimens were austenitized at 1550°F for 10 minutes in a tube furnace constructed for the purpose. The work of Roberts and Mehl indicated that 10 minutes at 1550°F was long enough to dissolve all the carbides and to homogenize the austenite (4). This austenitizing treatment resulted in an ASTM grain size of 6 to 7 in all the alloys used. Higher austenitizing temperatures were not used because grain coarsening occurred in some of these alloys at 1600°F. Longer austenitizing times were not used because of the danger of deboronizing the small specimens to significant depths. It was not possible to avoid deboronization by any special austenitizing atmosphere or by any plating technique (5). The possible effects of deboronization were avoided by observing the microstructures only at the centers of the specimens.

After austenitizing for 10 minutes at 1550°F the specimens were plunged into a quench chamber directly below the austenitizing furnace; simultaneously, the quenchant, nitrogen gas, was released through a nozzle into the quench chamber. Cooling rates were adjusted by varying the nitrogen flow rate.

During quenching, the specimen temperatures were recorded as a function of time by a Consolidated recording galvanometer which was attached to the specimen thermocouple. The traces made by this instrument were measured to obtain the cooling rates of the specimens. The experimental cooling rates were taken as the average rate of cooling from 1300 to 900°F in every case.

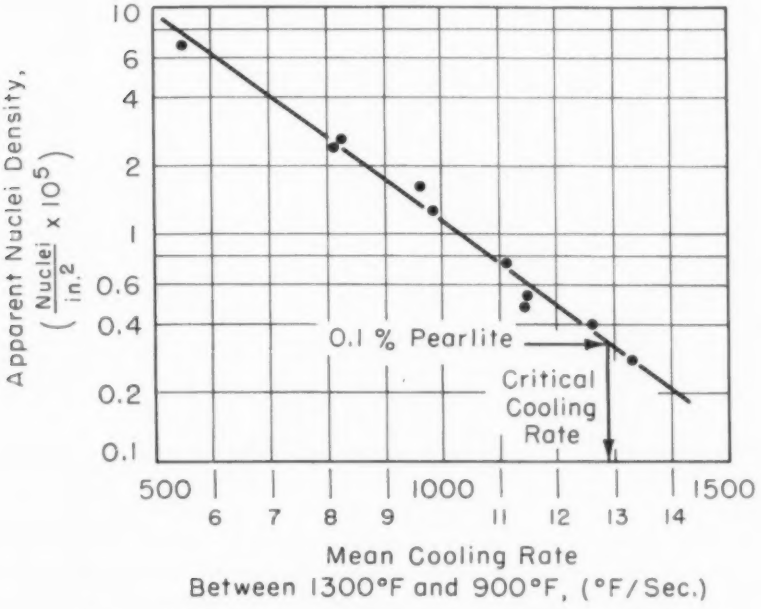


Fig. 1—Nuclei Density as a Function of Average Cooling Rate Between 1300 and 900°F. Alloy: 0.48% Carbon, 0.00054% Effective Boron, Austenitized at 1550°F.

Each quenched specimen was cut in half, polished and etched. The number of pearlite colonies per unit area of polished surface at the specimen center, the nuclei density, was counted by visual observation at high magnification. It was necessary to correct these nuclei density data by subtracting the density of inclusions which were indistinguishable from small pearlite colonies. This correction was obtained for each alloy by counting the "nuclei density" of very rapidly cooled specimens in which there was no pearlite.

For each alloy the logarithm of the corrected nuclei density was plotted against the cooling rate and the best straight line was drawn through the experimental points. Fig. 1 shows such a plot for a typical alloy. From these curves the cooling rate which corresponded to a nuclei density of 3.3×10^4 nuclei per square inch was taken as the critical cooling rate for the alloy. This nuclei density represents 0.1% pearlite. Thus, the reported critical cooling rates represent the cooling rate for each alloy which resulted in the formation of 0.1% pearlite.

In order to observe the variation in hardenability of the alloys as a function of their boron contents, special spectrographic analytical methods were required. Samples containing less than 0.0010% boron were analyzed by the improved spectrographic technique of Runge, Brooks, and Bryan (6). This method yields results which are accurate within $\pm$ 0.00005%.

It was necessary to measure the "effective" rather than the total boron contents of the alloys. The effective boron content can be defined as that boron which is free to dissolve in and diffuse through

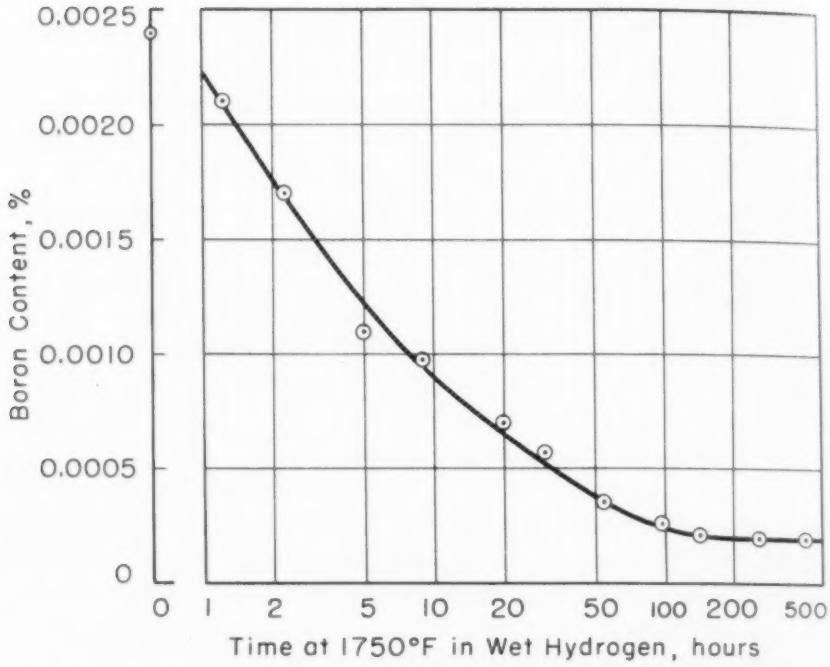


Fig. 2—Deboronization of SAE 81B40 Steel (¼ Inch Pins) in Wet Hydrogen at 1750°F.

the austenite lattice. Boron oxide and probably boron nitride are stable compounds which, when once formed in boron steels, will not be decomposed by the usual heat treatments. Boron tied up in such stable compounds cannot be effective toward increasing hardenability. In view of the low nitrogen contents which resulted from the vacuum melting process it is improbable that a significant amount of boron nitride was formed. However, even the best vacuum melting technique used left about 0.002% oxygen, some of which combined with boron.

The boron oxide or ineffective boron content was measured by the spectrographic analysis of deboronized specimens. The effective boron was free to diffuse through the lattice and could be rapidly removed by surface oxidation at elevated temperatures in much the same way that decarburization occurs. One-quarter inch diameter pins of the boron steels were heated to 1750°F in an atmosphere of wet hydrogen and held for sufficient time to complete the deboronization. After this treatment, the surfaces of the pins were machined off to a depth of one sixty-fourth of an inch to remove any boron oxide adhering to the surface. The boron oxide originally present in these pins could not dissolve and diffuse out, therefore, spectrographic analysis after the wet hydrogen deboronization treatment showed the original boron oxide content or percentage of ineffective boron in each alloy. The effective boron is the total boron content less the measured amount of ineffective boron oxide.

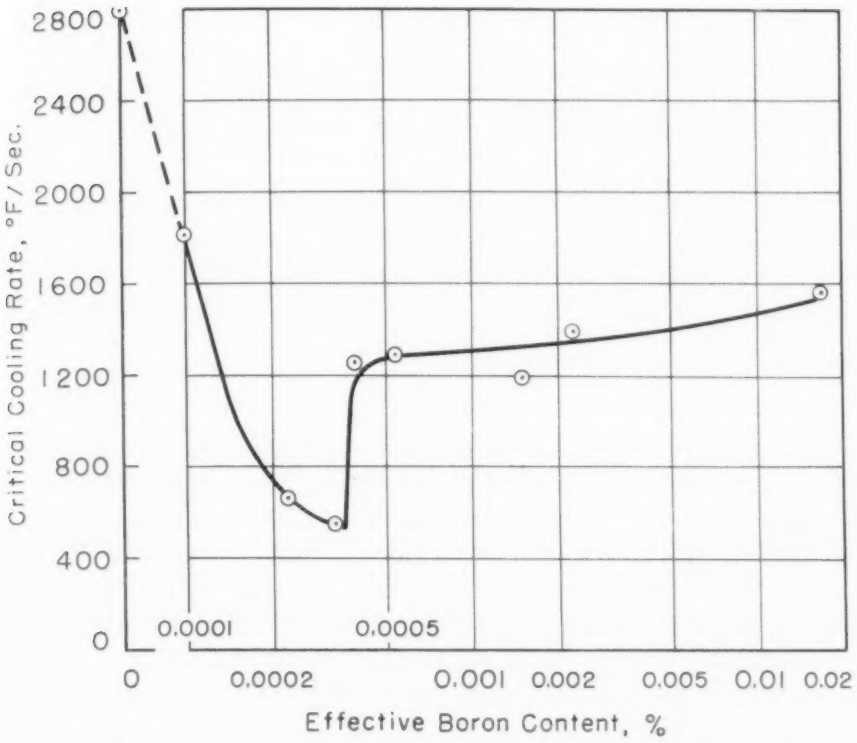


Fig. 3—Critical Cooling Rate as a Function of Effective Boron Content.

Table I
Compositions and Critical Cooling Rates of Experimental Boron Steels

Carbon Percent	Nitrogen* Percent	Oxygen* Percent	Total Boron Percent	Effective Boron Percent	Critical Cooling Rate (°F/Sec)
0.49	<0.00001	0.0029	0.00013	Nil	2790
0.49	0.0002	0.0040	0.00010	0.00010	1810
0.50	0.0006	0.0029	0.00040	0.00025	660
0.51	0.00005	0.0017	0.00058	0.00033	550
0.50	0.00025	0.0025	0.00053	0.00039	1255
0.48	0.00018	0.0024	0.00068	0.00054	1290
0.49	—	—	0.0017	0.0015	1195
0.49	0.00005	0.0029	0.0025	0.0023	1395
0.50	< .00001	0.0024	0.017	0.017	1560

All the above alloys were made with electrolytic iron containing less than 0.10% metallic impurities.

*Nitrogen and oxygen analyses by vacuum fusion.

The time required for complete removal of the effective boron depended on the rate of diffusion of boron in austenite. In order to determine the necessary time at 1750°F, samples of SAE 81B40 steel were held for various periods of time in wet hydrogen at 1750°F and then analyzed for boron. This preliminary work led to the adoption of 200 hours at 1750°F as the standard deboronization treatment for one-quarter inch round specimens.

Results

The preliminary deboronization tests on one-quarter inch rounds of SAE 81B40 steel showed that a constant boron content was obtained after 150 hours in wet hydrogen at 1750°F. These data are plotted in Fig. 2.

The critical cooling rate of the iron-carbon-boron alloys containing 0.50% carbon is shown as a function of effective boron content in Fig. 3. The hardenability increased to a maximum (indicated by a minimum critical cooling rate) at 0.00033% effective boron. The compositions of the alloys are listed in Table I.

Discussion

The rate at which deboronization occurred in the SAE 81B40 samples was slightly lower than would be predicted from the diffusivity data for boron in austenite as reported by Busby, Warga, and Wells (7). Using their diffusivity data it can be computed that at the centers of 0.25-inch rounds only 0.5 of 1.00% of the original effective boron would remain after 77 hours at 1750°F. In the present work, no observable lowering in boron content occurred after 150 hours in the case of the SAE 81B40 steel. The 200 hour treatment, which was used to obtain measurements of the boron oxide contents of the experimental steels, was considered sufficient.

Boron increases hardenability by reducing the rate of nucleation of the upper transformation products. It is generally agreed that dissolved boron in austenite must be segregated to the potential nucleation sites for ferrite and pearlite. These sites are regions of high energy such as grain boundaries, interfaces between inclusions and the austenite matrix or any other place where the regularity of the lattice is imperfect. The size of the boron atom, small for a substitutional but large for an interstitial solute, severely limits the solubility of boron in iron and favors the segregation of dissolved boron to disturbed regions such as grain boundaries. By occupying positions suitable to their size at disturbed regions the boron atoms reduce the lattice strain energy at the potential nucleation sites for ferrite and pearlite. This increases the activation energy required for the formation of stable nuclei at these regions and reduces the rate of nucleation.

The hardenability effect of most elements is proportional to the amount present in solution; in this respect boron is a typical alloying element at the lower boron contents. The experimental steels containing 0.00033% effective boron or less, exhibited increasing hardenability with increasing amounts of boron. An increase in the amount of boron in solution led to an increase in the amount of boron adsorbed at the grain boundaries and other imperfections and lowered the rate of nuclei formation.

The effective boron content of 0.00033% at which the hardenability suddenly decreased is believed to represent the solubility limit of boron in austenite at 1550°F. When the amount of effective boron exceeded the solubility limit the critical cooling rate abruptly increased because of the presence of a boron rich phase in the austenite prior to quenching. This boron rich phase (iron-boride or a borocarbide) must have been dispersed as fine particles which acted as sites for pearlite nucleation and therefore decreased the hardenability. When the boron content was further increased, a gradual increase in the critical cooling rate was observed representing a further slight reduction in hardenability. Although more boron must have created more nucleation sites this only increased the critical cooling rate slightly. Increasing the boron content could not change the nature of the interface between the boron rich particles and the saturated matrix. Therefore, in the alloys containing boron in excess of the solubility limit at the austenitizing temperature, the hardenability was relatively insensitive to variations in boron content.

The experimental results indicate that there is a maximum boron hardenability effect at an optimum boron content which corresponds to the limit of solid solubility. However, for practical purposes there is no optimum boron content. It would be quite difficult in commercial steelmaking practice to control the effective boron content to obtain the very low optimum amount. The common practice of adding 0.001 to 0.003% boron gives a dependable hardenability effect if the proper care is taken to protect the boron addition. The addition of less than 0.0005% boron probably would result in erratic hardenability.

References

1. C. R. Simcoe, A. R. Elsea, and G. K. Manning, "Study of the Effect of Boron on the Decomposition of Austenite," *Journal of Metals*, Vol. 7, January 1955, p. 193.
2. M. A. Grossmann, "Hardenability Calculated from Chemical Composition," *Transactions*, American Institute of Mining and Metallurgical Engineers, Vol. 150, 1942, p. 227.
3. W. Crafts and J. L. Lamont, "Effect of Some Elements on Hardenability," *Transactions*, American Institute of Mining and Metallurgical Engineers, Vol. 158, 1944, p. 157.
4. G. A. Roberts and R. F. Mehl, "The Mechanism and the Rate of Formation of Austenite from Ferrite-Cementite Aggregates," TRANSACTIONS, American Society for Metals, Vol. 31, 1943, p. 613.
5. J. C. Shyne and E. R. Morgan, "Deboronization of Steels," METAL PROGRESS, American Society for Metals, Vol. 65, June 1954, p. 88.
6. E. F. Runge, L. S. Brooks, and F. R. Bryan, "Spectrographic Determination of Trace Quantities of Boron in Steel," *Analytical Chemistry*, Vol. 27, October 1955, p. 1542.
7. P. E. Busby, M. E. Warga, and C. Wells, "Diffusion and Solubility of Boron in Iron and Steel," *Transactions*, American Institute of Mining and Metallurgical Engineers, Vol. 197, 1953, p. 1463.

DISCUSSION

Written Discussion: By J. W. Spretnak, associate professor of metallurgy, The Ohio State University, Columbus.

This experimental investigation on the relationship of boron content and hardenability of high purity iron-carbon-boron alloys was read with interest. The experiments are significant, but it is feared that the conclusions drawn, considerably outstrip the scope of the investigation.

The initial part of this discussion consists of a series of questions:

1. What is meant by the "nucleation of pearlite," which is an aggregate of two phases?

2. What was the analysis of the ferro-boron used in the preparation of the high purity alloys?

3. What is the response of the recording galvanometer and accessories used?

4. Did the count of the "nuclei density" on very rapidly cooled specimens amount to an inclusion count on unetched specimens? Also, what were the inclusions observed?

5. What is the theoretical basis for plotting the logarithm of the corrected nuclei density against cooling rate?

6. Why was the preliminary investigation on the rate of deboronization done on a commercial steel, whereas the experimental work was done on high purity alloys?

7. How reliable are the determinations of the critical cooling rates?

It must be kept in mind that reactions involving the decomposition of austenite occur very rapidly in high purity iron-carbon alloys. It will be noted that the composition giving the minimum rate of about 550°F per second is within the cited experimental error of the next higher composition for which a critical cooling rate of about 1250°F per second was reported. Along this line, how can it be stated that the maximum hardenability occurs at a boron content of 0.00033%, when the reported error in the analytical procedure is ±0.00005%? This error amounts to five parts in ten million, which makes a metallurgist, at least, shudder.

The second phasé of the writer's remarks is concerned with the section entitled "Discussion" and is being written in the interest of objectivity in metallurgical science. Initially, this section presents an explanation of the mechanism by which boron enhances the hardenability of heat treatable steels. Is it to be presumed that the explanation arises from the experimentation presented? If so, the writer stoutly maintains that scope of the work is too limited to attempt to formulate a theory of the boron effect. If the work and thinking of other investigators is included, why are they not cited? How can an explanation of the boron behavior neglect the contributions, to name just a few, of R. Grange and associates, L. S. Darken, T. Digges and associates, M. Nicholson, Messrs. Simcoe, Elsea, and Manning, C. Wells and associates, H. T. Chandler, and the writer's laboratory. Finally, a boron explanation cannot ignore the shear type transformation involved in the transformation of gamma iron to alpha iron predicted by Spretnak and Speiser,[2] and recently confirmed by Heidenreich,[3] employing the electron emission microscope. Heidenreich finds that austenite decomposes in general by a diffusionless transformation of austenite to supersaturated alpha, followed by a diffusion controlled precipitation of iron carbide to form pearlite, or bainite.

[2] J. W. Spretnak and R. Speiser, "A Hypothesis for the Boron Hardenability Mechanism," TRANSACTIONS, American Society for Metals, Vol. 46, 1954, p. 1089.

[3] R. D. Heidenreich, "Thermionic Emission Microscopy of Metals II Transformations in Plain Carbon Steels," *Journal of Applied Physics*, Vol. 26, No. 7, July 1955, p. 879.

In the second part of this section, the solubility of boron in austenite is deduced from hardenability data. It is evident that the decomposition of austenite is much too complicated a phenomenon to form a sound basis of determining the solubility of an element in austenite. More serious is the ignoring of the careful measurements of solubility of boron in gamma iron reported in the literature by C. Wells, M. Nicholson, and the writer.[4] These independent investigators find a solubility value which is ten-fold higher than assumed by the authors. It is very doubtful that the presence of 0.50% carbon could reconcile this discrepancy. For instance, in the writer's laboratory unpublished work on the effect of carbon on the solubility of boron in gamma iron indicates no significant effect of 0.44% carbon at 925°C (1695°F). In any event, would it not have been more sound to appraise the current method of determining the solubility of boron and to compare the results so obtained with carefully determined values published in the literature?

Written Discussion: By C. R. Simcoe, Battelle Memorial Institute, Columbus, Ohio.

The authors have shown the existence of an optimum boron content which produces a maximum hardenability. A boron hardenability mechanism was proposed recently which pointed out the possibility of an optimum boron content in this composition range.[5] Experimental work which will soon be published shows that 0.0003 to 0.0004% boron produced a maximum hardenability of 0.25, 0.35, and 0.50% carbon steels with a base composition similar to the 8600 series.

It should be pointed out that other factors not touched upon in this paper have considerable influence upon the hardenability of boron steels. For example, grain growth generally increases the hardenability of most alloy steels, but this is not usually true of a boron treated steel. Grain growth in a boron steel increases the boron concentration at the grain boundaries. If the concentration is already above the optimum amount (as it is in most commercial boron steels), the steel will show a decrease in hardenability with grain growth.

I do not agree with the authors in their statement that "for practical purposes there is no optimum boron content." The knowledge that increased hardenability and more consistent results can be obtained with a minimum of boron (that is 0.0005 to 0.001 rather than 0.002 to 0.003% boron) should be of considerable value in manufacturing boron steels. Furthermore, the present paper points out a relatively easy method for determining the amount of effective boron, although it has been our experience that all the boron added will be effective if the steel is thoroughly deoxidized.

It is gratifying to see that the boron hardenability mechanism recently proposed has been so well accepted, and that the more recent investigations have substantiated the earlier observations.

Written Discussion: By Cyril Wells, Carnegie Institute of Technology, Pittsburgh.

The authors state "a maximum boron hardenability effect was obtained in an alloy which contained 0.00033% effective boron" and that "this amount of boron is believed to represent a limit of boron solubility in these steels at the austenitizing temperature of 1550°F."

It is thought, at least from a practical point of view, that these conclusions apply not only to the high purity iron-carbon-boron alloys used by the authors

[4]C. C. McBride, J. W. Spretnak and R. Speiser, TRANSACTIONS, American Society for Metals, Vol. 46, 1954, p. 499.

[5]C. R. Simcoe, A. R. Elsea, and G. K. Manning: "Study of the Effect of Boron on the Decomposition of Austenite," *Journal of Metals*, Vol. 7, January, 1955, p. 193.

but also to certain commercial steels. One may note, for example, that a solubility value reported in the literature[6] for one commercial steel (composition of Steel 1 is given in Table II) is 0.0006% boron—temperature 817°C (1503°F); this figure is probably on the high side because it is the "total" rather than "effective" boron content figure.

Table II
Chemical Compositions of Steels
Per Cent of Element

Steel No.	C	Mn	P	S	Si	Ni	Cr	Mo	V	B
1	0.43	1.64	0.020	0.019	0.37	0.01	0.04	0.045	—	0.0038
6A	0.37	0.78	0.013	0.018	0.31	0.79	0.67	0.50	0.09	0.0009 (added)

In addition, the accuracy of the boron analysis was unlikely to be better than ±0.0002%. In view of these facts, one should not be surprised if the actual "effective boron" were 0.0003%, that is, close to the solubility, 0.00033% at 1550°F (842°C) given by the authors for their high purity alloys.

That the maximum boron hardenability effect is associated with the solubility limit at the austenitizing temperature used also seems to be a reasonable point of view and applicable to certain commercial steels as well as to the high purity alloys. In this connection one may observe from Fig. 4 that a commercial steel (Steel 6A—composition given in Table II) to which 0.0009% boron was added

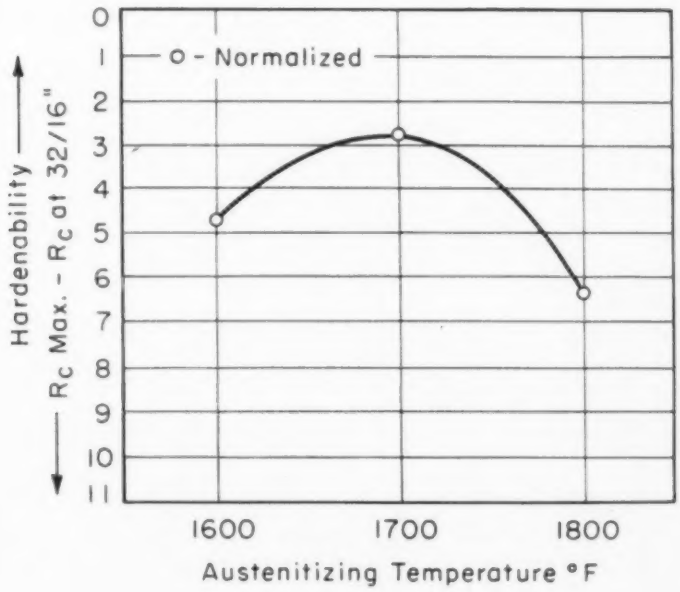


Fig. 4

[6]Paul E. Busby, Mary E. Warga, and Cyril Wells, "Diffusion and Solubility of Boron in Iron and Steel," *Transactions*, American Institute of Mining and Metallurgical Engineers, Vol. 197, 1953, p. 1463.

has a maximum hardenability at 1700°F (926°C); the boron solubility at 930°C (1706°F) reported in the literature[6] is 0.0010% boron. Steel 6A was aluminum killed and the boron added as Grainal #79 was probably for the most part "effective boron." Apparently as the austenitizing temperature increased the optimum "effective boron" content (solubility) to give maximum hardenability increased also. Attempts have been made to explain the decrease of hardenability with increasing temperature beyond that at which the maximum hardenability occurs; perhaps the true explanation is closely connected with the relation between grain boundary adsorption effect and boron content in unsaturated solution.

The method used for determining "effective boron" contents should be of interest. Here again the principle on which the method is based has other applications. For example, it has been used in the determination of hydrogen diffusion coefficients where, as in the boron case, some of the diffusing element "effective hydrogen" enters into the diffusion process and some "ineffective hydrogen," does not.[7]

Written Discussion: By Morris E. Nicholson, Institute for the Study of Metals, University of Chicago, Chicago.

The authors have demonstrated very effectively that in carefully prepared, vacuum-cast alloys the boron content for maximum hardenability occurs at 0.0003 weight % boron when austenitized at 1550°F. I think this observation may be important in leading us to a proper understanding of the influence of boron on the hardenability of steel.

In discussing the critical boron content of 0.0003%, the authors suggest that this may be the solid solubility of boron in austenite at 1550°F. This agrees approximately with the studies of solid solubility which have been made recently.[8,9] However, I question whether or not the suggestion that the critical cooling rate abruptly increases because of the presence of a boron-rich phase in the austenite prior to quenching is correct. If this were the case, theré should be a critical boron concentration for each temperature equal to the solid solubility at that temperature. I do not believe this behavior is observed.

The authors state that the decrease in hardenability is abrupt with concentration of boron above 0.00033%. This certainly is true when the data are plotted on the basis of the logarithm of the concentration. However, it is not true when the boron concentration is plotted directly in terms of weight %. Is there any physical reason for plotting the concentration logarithmically?

On the basis of Fig. 3 it would appear more reasonable that the initial decrease in hardenability was due to an excess of boron in solid solution, which at subcritical temperatures accelerates nucleation, after the hypothesis of Simcoe, Elsea and Manning (1). It would also seem that the relatively constant hardenability beyond 0.0005% B might indicate that this percentage represents the solid solubility at 1550°F.

One final observation concerns the apparent dioxidizing power of boron in the authors' alloys. Apparently the amount of "ineffective" boron in these steels was about 0.0002% boron. This is apparently only a small fraction of the amount of oxygen in the steels. Further this amount does not seem to appear to be any

[7]Cyril Wells, "Chemical Techniques and Analysis of Diffusion Data," ATOM MOVEMENTS, American Society for Metals, Cleveland, Ohio, 1951, p. 26.

[8]M. E. Nicholson, "Constitution of Iron-Boron Alloys in the Low Boron Range," *Transactions*, American Institute of Mining and Metallurgical Engineers, Vol. 200, 1954, p. 185.

[9]C. C. McBride, J. W. Spretnak and Rudolph Speiser, "A Study of the Fe-Fe_2B System," TRANSACTIONS, American Society for Metals, Vol. 46, 1954, p. 499.

simple function of the amount of oxygen present. It was my experience that in iron containing no carbon, boron combined with virtually all of the oxygen present to form B_2O_3. Do the authors believe that the oxygen in their steels might have been present in combined form rather than in solid solution in iron? Is it possible, for example, that an alumina crucible was used which might have introduced aluminum into the iron which dioxidized it during subsequent heat treatment?

Written Discussion: By Paul E. Busby, Heppenstall Company, Pittsburgh.

The authors are to be commended for their excellent research on a difficult subject. Their results demonstrate quite conclusively what many metallurgists have suspected for some time regarding the effect of boron on hardenability, namely, that like other elements, increasing the amount in solution does increase hardenability. Although the authors state that grain coarsening occurred in some of their alloys at austenitizing temperatures higher than 1550°F, it would be interesting to see data for higher austenitizing temperatures; from the iron-boron phase diagram, one would predict that the optimum boron content for hardenability should increase quite rapidly with increasing austenitizing temperature.

The authors state that "the rate at which deboronization occurred in the SAE 81B40 samples was slightly lower than would be predicted from the diffusivity data for boron in austenite as reported by Busby, Warga, and Wells (7)." They note that computations based on our published data gave a value of 77 hours for the time required to reduce the boron content at the center of their specimens to ½ of 1% of the amount of boron present whereas their experimental results showed that "no observable lowering in boron content occurred after 150 hours."

In a private communication, it was learned that the authors' computations were based on the data of Russell.[10] In the opinion of the writer, the apparent discrepancy noted above is due, in part, to the fact that the boundary conditions required by the applied form of Fick's Law were not satisfied when the calculation was made.

The solution used by the authors is similar to that of Newmann[11] and calculations similar to theirs but based on Newmann's work also gives a value of approximately 77 hours. However, when the same method is applied to the authors' experimental results, the following D values are obtained if it is assumed that the values given in Fig. 2 represent the average boron content over the cross-section of the samples:

t (hrs)	D (cm^2/sec)
1	0.4×10^{-7}
2	2.5×10^{-7}
5	4.1×10^{-7}
10	3.7×10^{-7}
20	2.9×10^{-7}
50	2.0×10^{-7}
77	1.7×10^{-7}

The relatively low D values corresponding to the extremes of time are indicative of the partial failure of the method near the beginning and end of the diffusion period. The more accurate values are associated with the median times where the so-called fractional saturation (amount of material diffusing out in time, t, divided by the amount of material which would diffuse out in infinite time) is near 0.50. These values are in excellent agreement with the D value calculated from our published diffusion data—3.6×10^{-7} cm^2/sec at 1750°F.

[10]First Report of the Alloy Steels Research Committee, Iron and Steel Institute Special Report #14, 1936, p. 149.

[11]Newmann, *Transactions*, American Institute of Chemical Engineers, Vol. 27, 1931, p. 310.

Authors' Reply

The authors wish to thank those who have offered the interesting and informative discussions to this paper.

The data presented by Professor Wells is especially interesting. It shows that in a commercial steel a maximum hardenability effect was obtained at the austenitizing temperature for which it was most probable that the boron solubility was equal to the boron content. As Professor Wells points out this evidence does support the authors' conclusion that the optimum boron content is the same as the limit of boron solubility at the austenitizing temperature.

Dr. Busby's comments demonstrate that the authors' deboronization data were in agreement with the published boron diffusivity[12] and not somewhat slower as was concluded. For the purposes of this paper, the authors were entirely interested in the practical end point of the deboronization process and therefore based their conclusions about the rate of boron diffusion on the end point. While this was a valid procedure it was certainly less accurate than the method suggested by Dr. Busby.

The boron contents in Fig. 3 were plotted on a logarithmic scale simply to magnify the scale in the low boron region. A cartesian plot of reasonable size covering the reported range of boron content severely condenses the important low boron region. It appears to the authors that the decrease in hardenability between 0.0003 and 0.0004% boron seems equally abrupt when plotted on cartesian coordinates. The authors feel that this data is entirely consistent with the hypothesis that the decrease in hardenability was caused by exceeding the solid solubility of boron at the austenitizing temperature. If the solubility data for boron in pure gamma iron[13] reported by Professor Nicholson is extrapolated down to 1550°F a solubility of 0.0003 to 0.0004% boron is indicated. This is the effective boron content for maximum hardenability observed by the authors. Admittedly such an extrapolation cannot be regarded as absolutely dependable, however, we feel that it supports the idea that a decrease in hardenability is caused by exceeding the solid solubility of boron at the austenitizing temperature.

The authors agree with Professor Nicholson that at these low boron and low oxygen levels there was no apparent correlation between oxygen content and the effective boron content. It may be as Professor Nicholson suggests, that some of the measured oxygen content came from entrained refractory oxides. The problem of the formation of B_2O_3, BN and other boron compounds in boron steels should be a rewarding area for study.

The authors agree with Dr. Simcoe that other variables not touched upon in the present paper do influence the hardenability of boron steels. Certainly variations in grain size and austenitizing temperature may cause boron steels to respond in special ways.

Professor Spretnak asks, "What is meant by the nucleation of pearlite?" This subject has been very adequately treated in a recent paper, "On the Nucleation of Pearlite," by Professor M. E. Nicholson.[14]

The lot analysis of the ferro-boron used in the preparation of the experi-

[12]P. E. Busby, M. E. Warga and C. Wells, "Diffusion and Solubility of Boron in Iron and Steel," *Transactions*, American Institute of Mining and Metallurgical Engineers, Vol. 197, 1953, p. 1463.

[13]M. E. Nicholson, "Constitution of Iron-Boron Alloys in the Low Boron Range," *Transactions*, American Institute of Mining and Metallurgical Engineers, Vol. 200, 1954, p. 185.

[14]M. E. Nicholson, "On the Nucleation of Pearlite," *Transactions*, American Institute of Mining and Metallurgical Engineers, Vol. 200, 1954, p. 1071.

mental alloys indicates 17.5% boron and as impurities, 1.22% silicon, 0.35% carbon, and 0.04% aluminum.

The cooling rates were determined by recording the output EMF of the specimen thermocouples, on a Consolidated recording galvanometer (Consolidated No. 7-215). The galvanometer had a natural frequency of 100 cps and was shunted to obtain a damping factor of 0.7. This resulted in a response time of 0.005 second over the full range of deflection. This was much faster than actually required for the experiments.

The inclusion counts on the very rapidly cooled specimens were done on etched specimens as it was the appearance of inclusions in the etched samples that was of interest. The exact nature of the inclusions is unknown. Possibly they may have been particles of refractory oxides from the crucible.

The logarithm of nuclei density was plotted against cooling rate (as in Fig. 1) to expand the scale in the region of low nuclei density in order to facilitate the determination of the critical cooling rates. The fact that the data resulted in a straight line when so plotted, was regarded as fortuitous. The authors do not imply any theoretical basis for this.

An SAE 81B40 steel was used in the preliminary deboronization work because of the limited supply of the high purity alloys.

By the "accuracy" of the spectrographic boron determination the authors meant to imply absolute accuracy which is a different thing from reproducibility or precision. The accuracy of ± 0.00005% boron takes into account the dependability of the reference standards, plate background line density and like factors. This means that the whole curve of critical cooling rate versus effective boron content may be displaced ± 0.0005% boron in the low boron range. However the reproducibility of the analytical method is believed to be better than this. Four analytical samples were used to obtain each reported value. In the range of 0.0003 to 0.0010% boron, the coefficient of variation was no more than 10%. The precision of the reported boron contents is therefore believed to be ± 0.00002 or 0.00003% boron. These boron determinations were obtained by E. F. Runge using an improved spectrographic method which is described in detail in a paper by Runge et al.[15]

As Professor Spretnak suggests the authors could have cited many more references. However as this paper was intended neither as a critical review of the subject nor as a report of an all inclusive experimental program, only papers immediately pertinent to the present work were cited.

[15]E. F. Runge, L. S. Brooks and F. R. Bryan, Analytical Chemistry, Vol. 27, 1955, p. 1543.

ON BANDING IN STEEL

By C. F. Jatczak, D. J. Girardi and E. S. Rowland

Abstract

The banding phenomenon was studied in 1340, 2340, 4140, 4340 and 5140 type steels. The banding characteristics of these steels were established by studying transformation behavior to ferrite and pearlite and to martensite on direct quenching and after a prior isothermal treatment at the upper nose of the TTT curve.

Transformation studies after homogenization treatments at 2200°F indicated that chemical heterogeneity is the primary cause of banding. Steel analyses containing primarily carbide forming elements homogenize more readily than those containing primarily solution type elements.

Comparison of physical properties between banded and homogenized (100 hours at 2200°F) 4340 steel shows that only transverse ductility is improved. However, the degree of improvement is not commercially significant. (ASM-SLA Classification: N8, M27, Ay)

Introduction

BANDED structures in steels arise from carbon segregation into preferred regions. This banding phenomenon has been the subject of numerous investigations. Although other factors have been considered, it is generally agreed that the primary cause of banding is the effect of alloy segregation on carbon location. Other factors influence the degree, type and form of banding either per se or by their influence on the degree of chemical segregation. Some of these factors are austenitizing temperature and time, diffusion rates of carbon and alloy, grain size, cooling rates, and rates of nucleation and growth of decomposition products of austenite. Much of the controversy concerning banded structures arises from the lack of sufficient information on the influence of these various factors on the degree, type and form of bands.

The type steels chosen for this investigation were 1340, 2340, 4140, 4340, and 5140. Analyses are given in Table I. These particular grades were chosen in order to include analyses having primarily carbide forming type elements, analyses having primarily solution type elements and analyses having both carbide forming and solu-

A paper presented before the Thirty-Seventh Annual Convention of the Society, held in Philadelphia, October 17–21, 1955. Of the authors, E. S. Rowland is chief metallurgical engineer, D. J. Girardi is research metallurgical engineer, and C. F. Jatczak is research metallurgist, The Timken Roller Bearing Company, Steel and Tube Division, Canton, Ohio. Manuscript received April 13, 1955.

Table I
Chemistry of Heats Investigated

Type	C	Mn	Si	Cr	Ni	Mo	As-Received Size
1340	0.39	1.70	0.27	0.16	0.29	0.03	1⅛" Round
2340	0.41	0.68	0.29	0.23	3.20	—	1¼" Round
4140	0.39	0.82	0.31	0.96	0.13	0.20	1¼" Round
4340	0.42	0.72	0.29	0.82	1.74	0.25	1¼" Round
5140	0.42	0.85	0.27	0.81	—	—	2" Round

tion type elements. This selection is based on the different effects of various alloy segregates on carbon location (1–4)[1]. Because of the more sluggish characteristics of the 4340 analysis, it was investigated more extensively.

The banding characteristics of these steels were established by studying transformation behavior to:

1. Ferrite and pearlite
2. Martensite on direct quench
3. Martensite on quenching after a prior isothermal treatment at the upper nose of the TTT curve.

Austenite transformation to ferrite and pearlite is a nucleation and growth process which is affected by chemical heterogeneity and other nonuniform nucleating conditions. Austenite transformation to martensite is essentially a nondiffusion process which is not nucleated in the ordinary sense and is affected solely by chemical heterogeneity (considering no grain size variation). A study of banding under both of these conditions of transformation is convenient as a means of separating the effects of concentration gradients from other persistent nucleating conditions. The use of an isothermal treatment prior to transformation to martensite was used to bring out specific effects that will be discussed in the body of the paper.

Procedure

As-Received Steels

Various continuous cooling and isothermal cycles were run from an austenitizing temperature of 1550°F on the as-received materials to determine the treatment most sensitive toward the development of banding in each steel. Continuous cooling treatments ranging from 10 to 100°F per hour for the 4340 steel and 10 to 20°F per hour for the other steels were run. Isothermal transformation characteristics were surveyed from 1300°F down to 600 °F for all analyses. The lower temperatures were investigated to exclude the possibility that banding would appear more pronounced in the bainite region. For the isothermal treatments, temperatures corresponding to the nose of the respective TTT curves were found to be most sensitive. These temperatures were 1100°F for 2340,

[1]The figures appearing in parentheses pertain to the references appended to this paper.

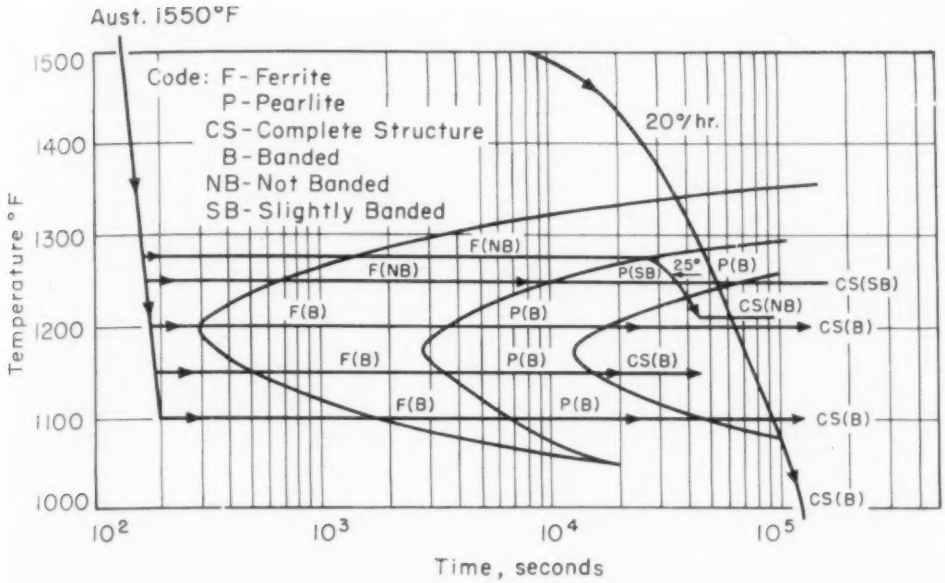


Fig. 1—Effect of Isothermal and Continuous Cooling on Banding in 4340 Steel.

1150°F for 1340 and 1200°F for 4140, 4340 and 5140. Isothermal transformation results obtained in the upper regions for the 4340 steel are shown in Fig. 1. Similar isothermal transformation results obtained on the other steels are revealed in figures and tables throughout the paper and are not reproduced in the form of Fig. 1. Comparisons between the continuous cooling and isothermal treatments show that the isothermal treatment is more sensitive for developing banded structures. Fig. 2 compares the banded condition in the 4340 steel as developed by both continuous cooling and isothermal treatments. Comparison can also be made between Fig. 3 showing the results of continuous cooling 4340 at 20°F per hour from 1550°F after various homogenization treatments at 2200°F and Fig. 7 showing results of isothermally treated 4340 with like homogenization treatments.

The banding behavior of each steel in the martensite region was assessed by the well known Ms technique of Greninger and Troiano (5). Wafer specimens 1/16 inch or less were austenitized at 1550°F and treated according to the method shown in Fig. 4. Ms temperatures of 570°F and below were investigated for the 4340 steel and 600°F, 650°F and 550°F and below for the 4140, 5140 and 2340 steels, respectively. In this treatment, the dark or tempered martensite which appears in bands (Fig. 2) is normally representative of the lowest alloyed regions in the steel.

For all treatments on as-received material, including partial homogenization, the center to center distance of the bands in each steel averaged about 0.008 inch.

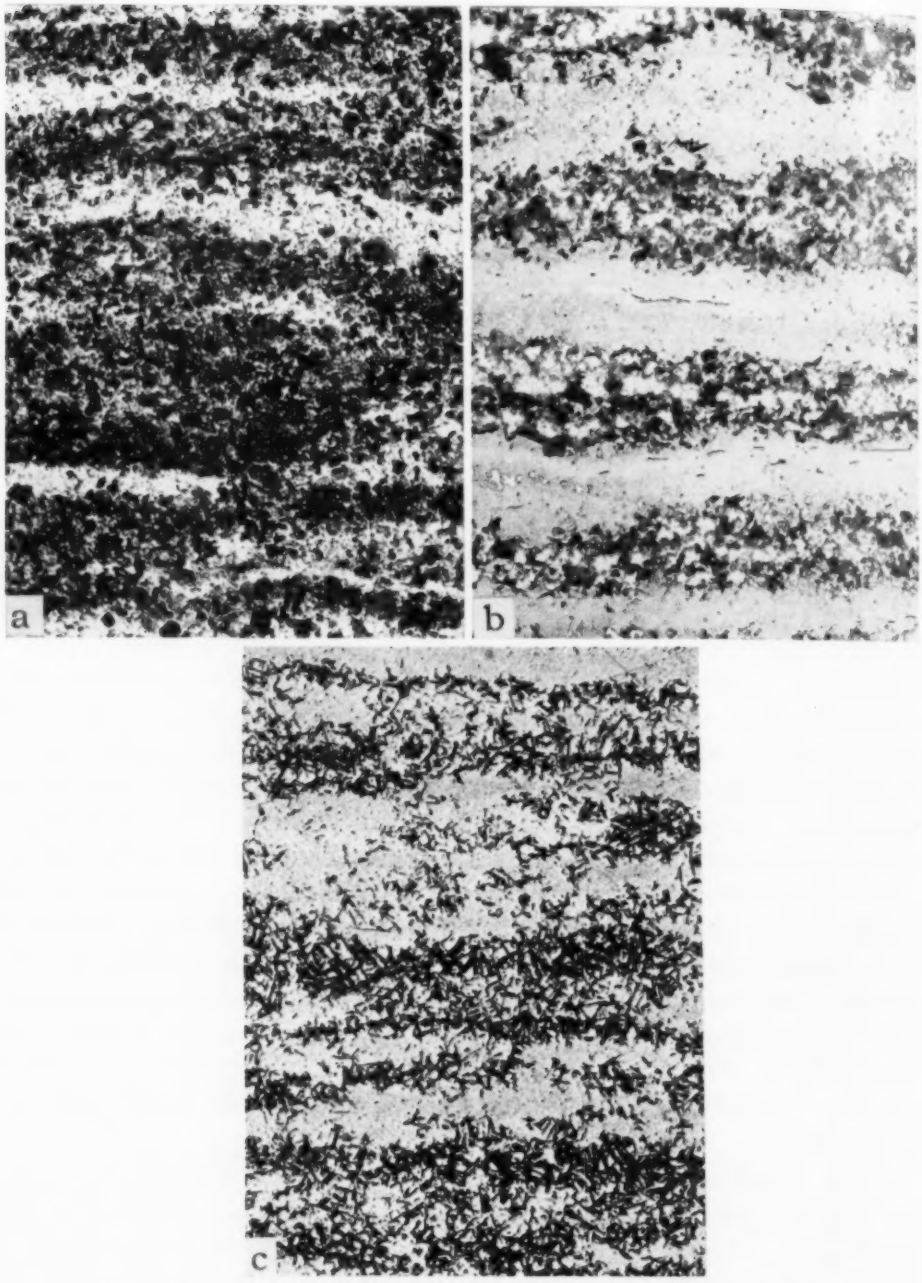


Fig. 2—Banding Condition in As-Received 4340 Material as Revealed by:
(a) Continuous Cooling Cycle of 20°F Per Hour—×100
(b) Isothermal Method—1200°F—30 Minutes—×100
(c) M_s Technique—550°F

Homogenizing Treatments

Homogenizing treatments of 25 and 100 hours at 2200°F were carried out on 1340, 2340, 4140 and 5140 and of 5, 16, 25, 50, 75, 100 and 200 hours on 4340. These cycle times were calculated from diffusion data shown in Table II. Calculations were based on a geo-

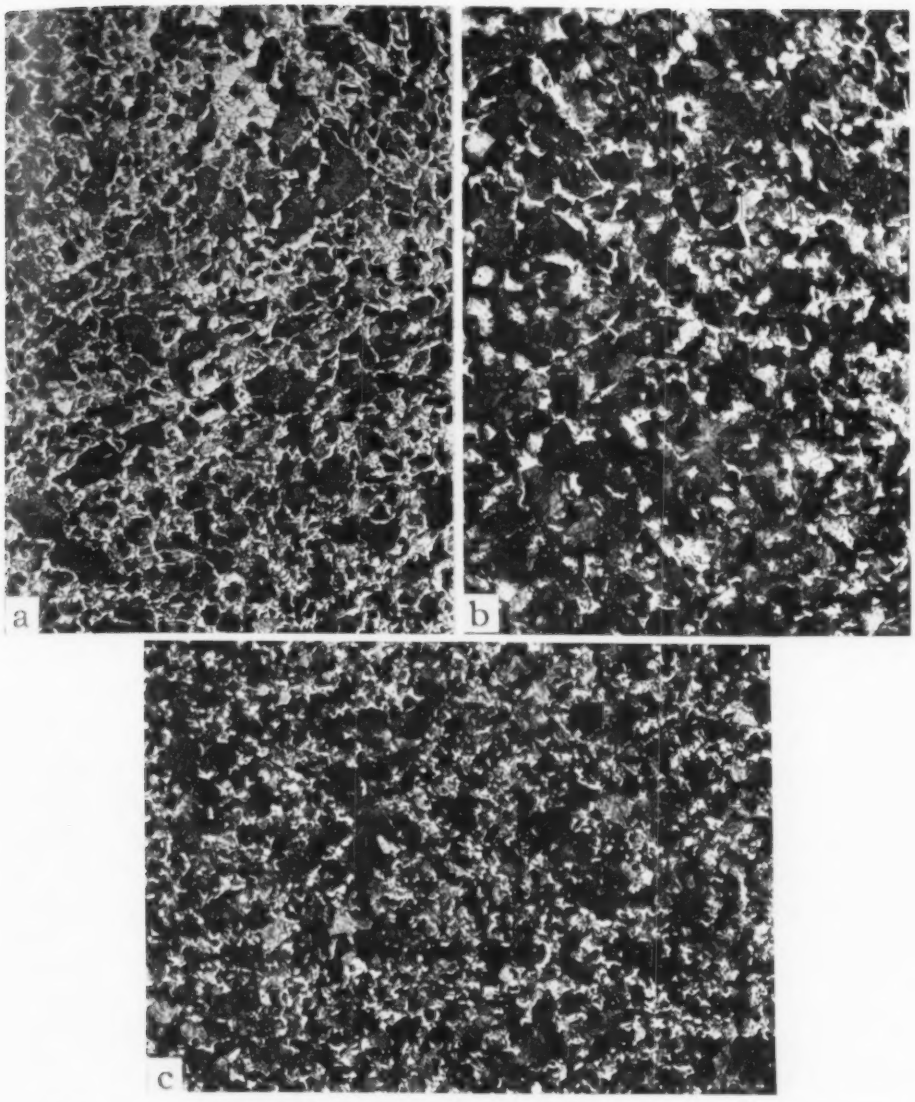


Fig. 3—Structure of 4340 Upon Continuous Cooling (20°F per Hour) from 1550°F After Several Homogenizing Treatments at 2200°F.
(a) 5 Hours; (b) 16 Hours; (c) 75 Hours (Nital ×100)

Table II
Rates of Diffusion of Various Alloying Elements at 2200°F (1225°C)

	D—cm² Per Second
Silicon (1300°C) (7)*	1.5×10^{-9}
Chromium (7)*	1.4×10^{-9}
Molybdenum (8)*	9.0×10^{-10}
Manganese (9)*	1.36×10^{-10}
Nickel (10)*	3.75×10^{-11}
Iron (Self-Diffusion) (11)*	3.56×10^{-11}

*References

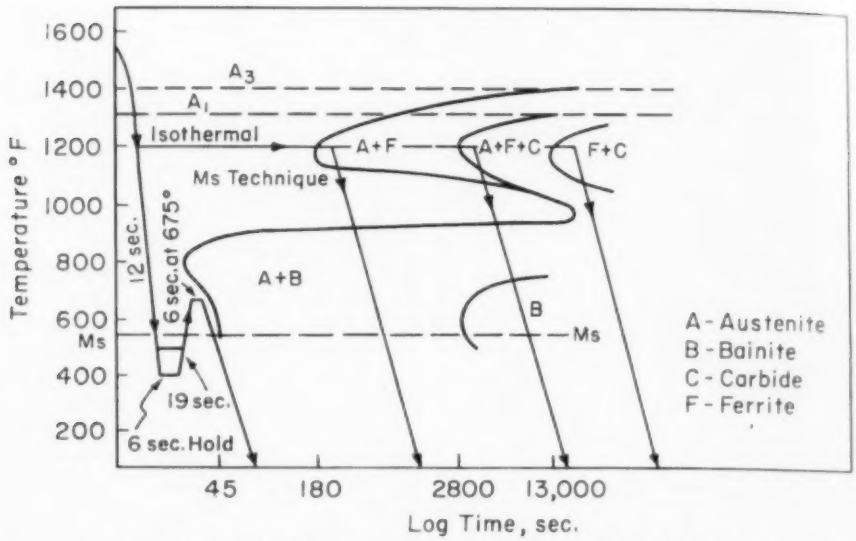


Fig. 4—Details of the Isothermal and Ms Quench Technique Employed in Study of Banded 4340 Steel.

metric arrangement of segregates as infinitely long rods distributed equi-distantly throughout the steel (Fig. 5). To preserve the original carbon and alloy content, steel samples were enclosed in a 0.40% carbon 6 inch round billet and cap welded. No difficulties with loss of carbon or alloy and with overheating were experienced. Five successive grain refining normalizes, two at 1700°F and three at 1550°F, were imposed on all material treated at 2200°F. Only grain refined specimens were used in the isothermal and martensite studies to determine the degree of band homogenization.

Analysis Of The Degree Of Homogenization

The degree of homogenization attained in the various treatments was established by analyzing quantitatively the ferrite-pearlite transformation and/or the martensite reaction in adjacent bands by lineal analysis techniques with the aid of a Hurlbut counter. Isothermal structures were studied at ×1350 and the martensitic structures at ×2900. The former were etched in 5% $FeCl_3$ and the latter in 3% nital. Traverses were made in each sample in order to gather information on three points. First, traverses were made along those bands showing the worst degree of banding. Secondly, traverses were made along numerous low and high alloy regions to measure the average transformation in each region. Thirdly, traverses were made across band layers to determine the overall average transformation.

Nonmetallic inclusions were employed as fiducial markers of high alloy regions. Inclusions are, in general, interdendritic and thus coincide with high alloy concentrations as shown in Fig. 2.

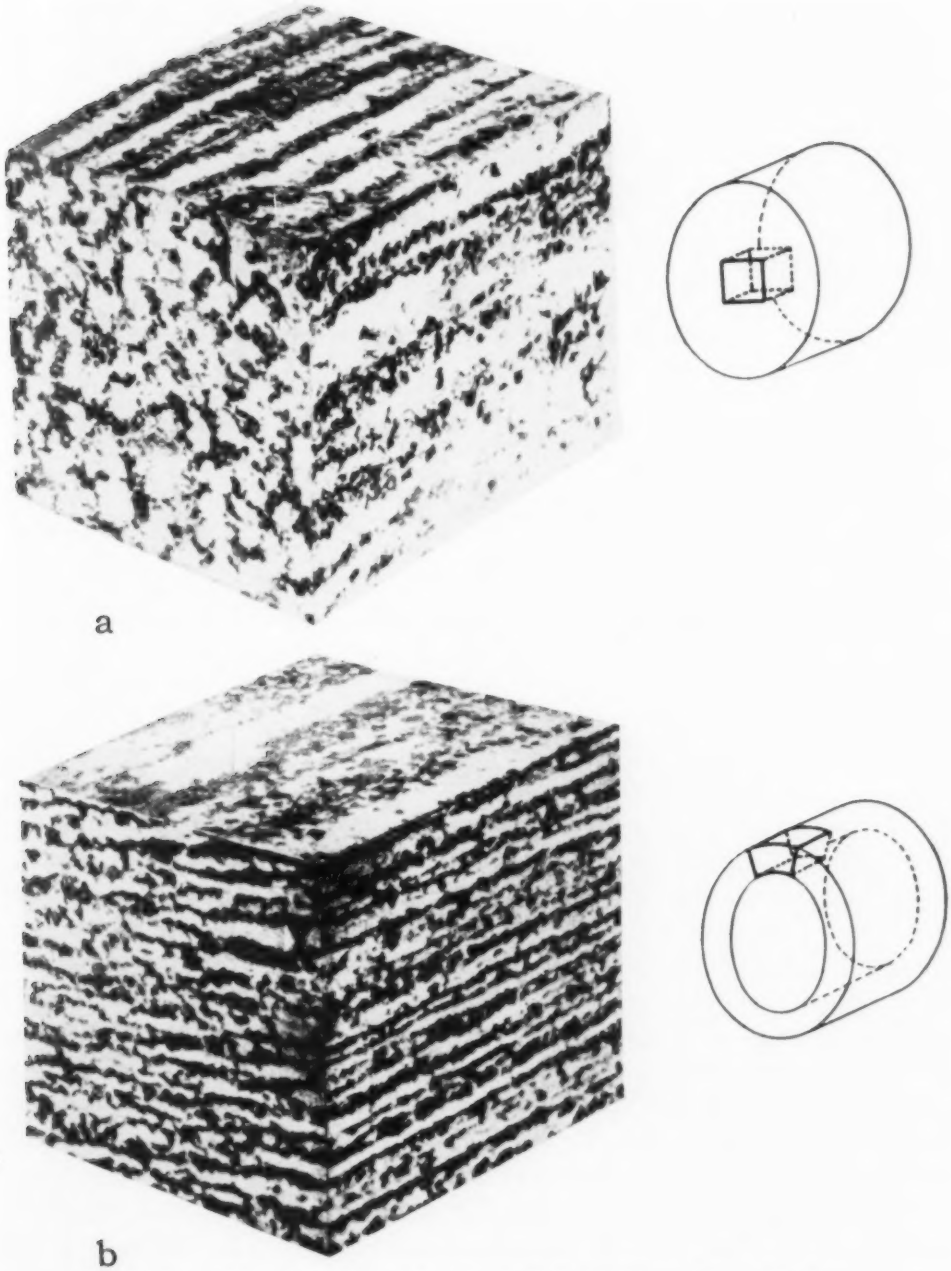


Fig. 5—Three Dimension View of Banding in Rolled Solids and Pierced Tubes.

Physical Properties Of Banded Versus Homogenized 4340

Longitudinal and transverse tensile and impact properties were determined on quarter section material taken from 6×6 inches square billets of 4340 in the as-received condition and after homogenizing for 100 hours at 2200°F. Samples were hardened from 1550°F in oil and tempered at 1175°F to about 275 Brinell.

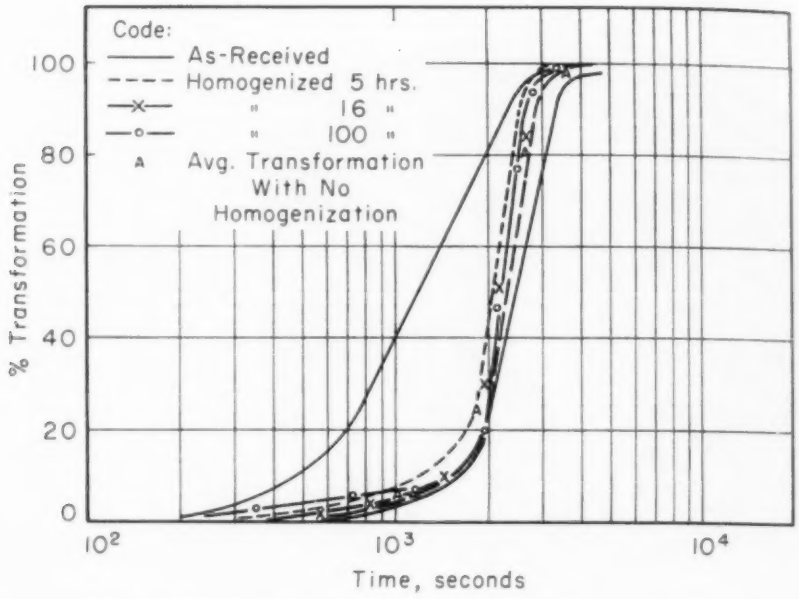


Fig. 6—Effect of Homogenization at 2200°F on Isothermal Transformation Behavior of Banded 4340 Steel at 1200°F.

Results

Homogenization Of 4340

The influence of homogenization on the isothermal transformation characteristics of the 4340 steel is shown in Fig. 6. The data shown represent average per cent transformation in various high and low alloy regions. Representative fields of the worst condition of banding which prevailed after different homogenization treatments are shown for various stages of isothermal transformation in Fig. 7. It is evident that the ferrite and the pearlite reactions respond differently. The pearlite reaction in its intermediate stages is a more sensitive indicator of banding and on this basis the 4340 steel shows banding at the 200 hour homogenization treatment. On the basis of ferrite transformation and of the completely transformed structure (ferrite formation pattern governs final structure pattern) the 4340 steel is completely randomized between 5 and 16 hours at 2200°F.

The influence of homogenization on the martensite reaction under direct quenched conditions is shown in Figs. 8 and 9. Fig. 8 shows the results obtained for the average per cent transformation in the low and high alloy regions and Fig. 9 shows representative fields of the worst condition of banding which prevailed after different homogenizing treatments. It is observed that complete randomness of the martensite reaction is achieved in about the same time required to produce random ferrite isothermally. Since the

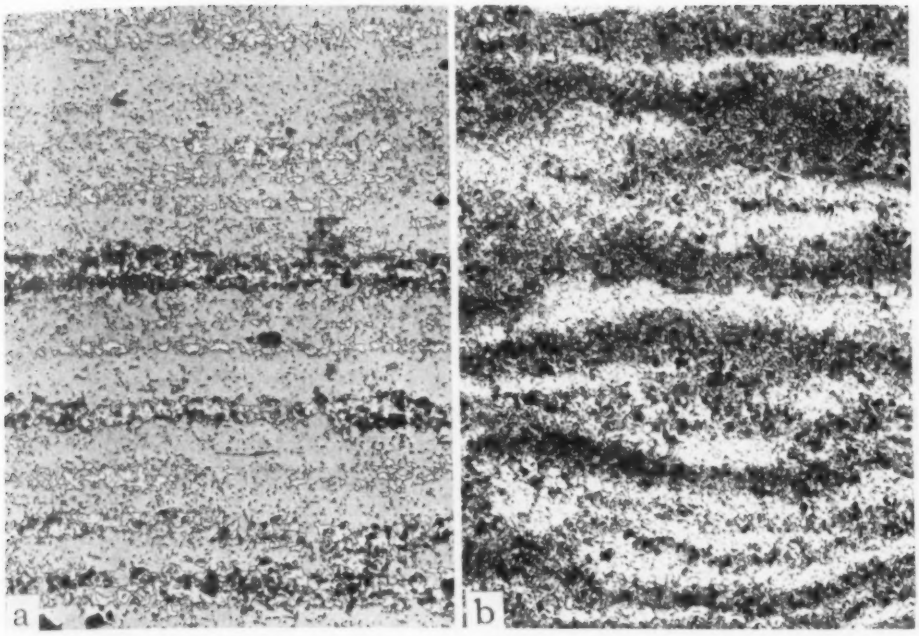


Fig. 7a-7b—Progress of Homogenization in Banded 4340 Steel After Various Treatments at 2200°F—as Depicted at Various Stages in Isothermal Study at 1200°F—×100. Fig. a, b—0 Hours.

martensite reaction is generally considered to be sensitive to chemistry (assuming no grain size variations) one would be tempted to conclude that the original chemical heterogeneity in the 4340 steel is completely homogenized in this relatively short time. However, results to be presented shortly will show that this is not necessarily true.

In the case of the martensite reaction further insight into the banding phenomenon can be attained by subjecting the homogenized steel to a prior isothermal incubation period at about the nose of the TTT curve. Such a treatment may cause an increase in the degree of segregation (primarily carbon) in the austenite because of the effects of alloy gradient, temperature and transformation. Incubation times were so chosen as to produce no transformation or some ferrite transformation or some ferrite and pearlite transformation. The effects of isothermal incubation of austenite at 1200°F on the martensite reaction for 4340 specimens homogenized 16 to 75 hours are shown in Fig. 10. Samples homogenized up to 50 hours and which previously showed random martensite on direct quenching now developed banded structures as a direct result of the incubation treatments. This banding developed regardless of whether transformation did or did not occur during the isothermal treatments. Another interesting observation of the influence of isothermal holding is that the dark martensite occurs principally (>85%) over nonmetallic inclusions as shown in Fig.

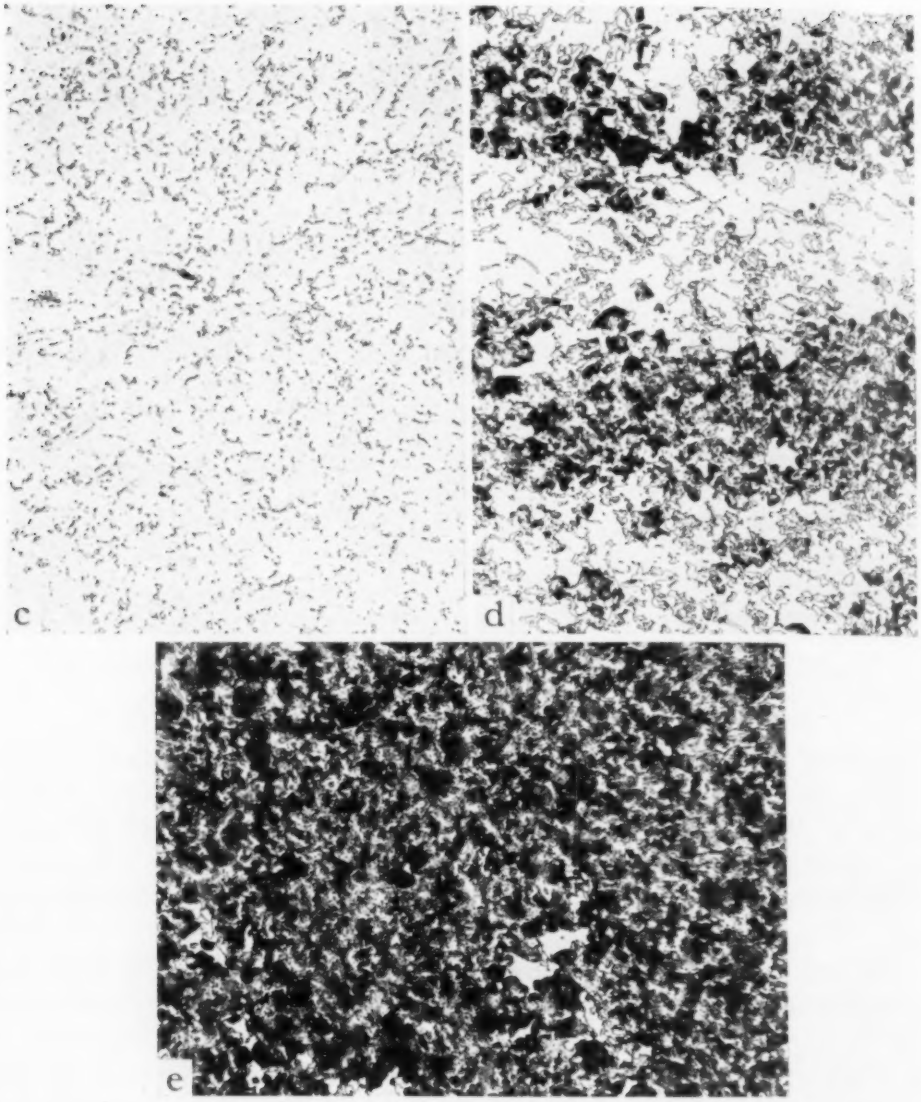


Fig. 7c-7e—Progress of Homogenization in Banded 4340 Steel After Various Treatments at 2200°F—as Depicted at Various Stages in Isothermal Study at 1200°F—×100. Fig. c, d, e—5 Hours.

11. In the direct quench treatment for both the nonhomogenized as-received 4340 and the partially homogenized but still banded 4340 the dark martensite occurred between the nonmetallic inclusions as shown in Figs. 2 and 9. Apparently during the isothermal treatment the factors which influence martensite formation have shifted one-half band width from a position between inclusions (low alloyed regions in as-received material) to coincidence with inclusion position (high alloyed regions in as-received material). The isothermal hold did not develop martensitic banding in 4340 samples homogenized for 75 or more hours at 2200°F.

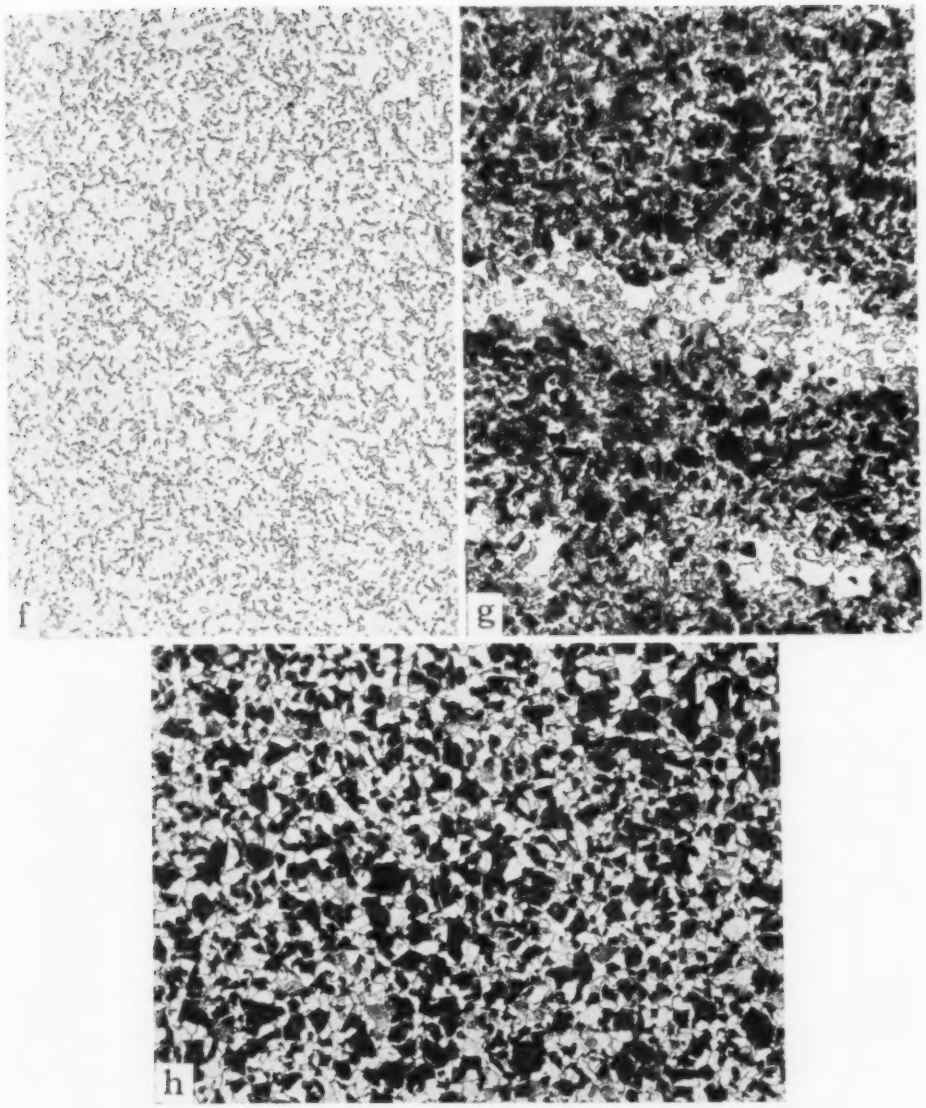


Fig. 7f-7h—Progress of Homogenization in Banded 4340 Steel After Various Treatments at 2200°F—as Depicted at Various Stages in Isothermal Study at 1200°F—×100. Fig. f, g, h—25 Hours.

Homogenization Of 1340, 2340, 4140 And 5140

The as-received banded conditions in these steels are shown in Fig. 12. The influence of homogenization treatments on isothermal ferrite-pearlite transformation is shown in Table III. Photomicrographs for these structures are not given. The 1340, 4140 and 5140 steels, when homogenized for 25 or 100 hours, showed random ferrite and pearlite for intermediate and completely transformed structures. For the 2340 steel faintly banded conditions existed for the 100 hour homogenization treatment. These results are in general agreement with diffusion data shown in Table II.

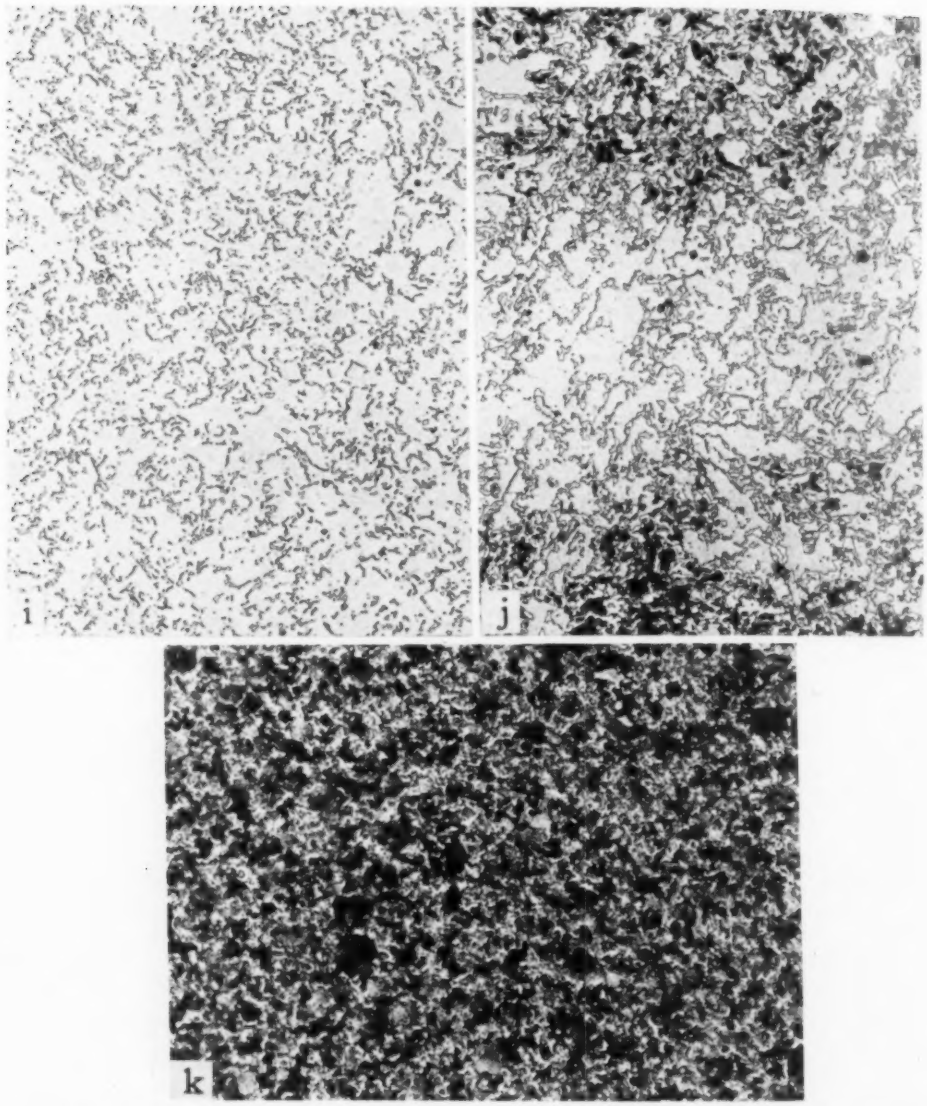


Fig. 7i-7k—Progress of Homogenization in Banded 4340 Steel After Various Treatments at 2200°F—as Depicted at Various Stages in Isothermal Study at 1200°F—×100. Fig. i, j, k—200 Hours.

When banding occurs in the 1340, 4140 and 5140 analyses the segregation of ferrite and pearlite into bands is rather marked. In the case of the 2340 analysis, the bands are more diffused. Banding is, therefore, more vivid in the 1340, 4140 and 5140 analyses even though these grades homogenize more readily than the 2340 steel.

For the 1340, 4140 and 5140 steels the non-metallics were located primarily in the heavy pearlite bands. For the 2340 analysis after the 25 and 100 hour homogenization treatments, the non-metallics were located principally in regions of first ferrite formation.

The general effect of the 100 hour homogenization treatment on the martensite reaction on direct quenching was studied for all

Table III
Effect of Homogenization at 2200°F on Banding of 1340, 2340, 4140 and 5140 Steels As Revealed by Study of Partial and Complete Isothermal Transformation

Steel Type	Isothermal Treatment And Type	Non-Homogenized	Homogenized 25 Hours	Homogenized 100 Hours
1340	1525–1150°F, 4 Minutes, Water Quenched (Partial)	Ferrite Banded Between The Non-Metallics Depicting The High Alloyed Regions	Ferrite Random	Ferrite Random
	1525–1150°F, 12 Minutes, Water Quenched (Partial)	Ferrite And Pearlite Banded—Non-Metallics In Martensite Or High Alloy Region	Ferrite Random—Pearlite Slightly Banded—Non-Metallics Between Pearlite Bands	Ferrite And Pearlite Completely Random
	1525–1150°F, 20 Minutes, Water Quenched (Complete)	Complete Structure Banded—Non-Metallics In Heavy Pearlite (High Alloy Regions)	Complete Structure Random	Complete Structure Random
2340	1525–1100°F, 4 Minutes, Water Quenched (Partial)	Ferrite Banded—Same As In 1340 Above—Non-Metallics In Martensite (High Alloy Band)	Ferrite Banded—Non-Metallics Predominantly In Ferrite Bands	Ferrite Faintly Banded Over Non-Metallics
	1525–1100°F, 35 Minutes, Water Quenched (Partial)	Ferrite And Pearlite Banded—Non-Metallics In Martensite	Ferrite And Pearlite Banded—Non-Metallics Same As Above	Ferrite And Pearlite Diffusely Banded
	1525–1100°F, 2 Hours, Water Quenched (Complete)	Complete Structure Banded—Non-Metallics In Heavy Pearlite (High Alloy Region)	Complete Structure Faintly Banded	Complete Structure Random
4140	1550–1200°F, 30 Seconds, Water Quenched (Partial)	Ferrite Banded—Non-Metallics Between Bands In Martensite	Ferrite Random	Ferrite Random
	1550–1200°F, 3 Minutes, Water Quenched (Partial)	Ferrite And Pearlite Banded—Non-Metallics Between Bands In Martensite—Same As In 1340	Ferrite Random—Pearlite Slightly Banded—Non-Metallics Between Bands	Ferrite And Pearlite Completely Random
	1550–1200°F, 30 Minutes, Water Quenched (Complete)	Complete Structure Banded—Non-Metallics In Heavy Pearlite	Complete Structure Random	Complete Structure Random
5140	1550–1200°F, 5 Seconds, Water Quenched (Partial)	Ferrite Banded, Same As In 1340	Ferrite Random	Ferrite Random
	1550–1200°F, 45 Seconds, Water Quenched (Partial)	Ferrite And Pearlite Banded—Same As In 1340	Ferrite Random—Pearlite Faintly Banded—Non-Metallics Between Bands	Ferrite And Pearlite Random
	1550–1200°F, 11 Minutes, Water Quenched (Complete)	Complete Structure Banded	Complete Structure Random	Complete Structure Random

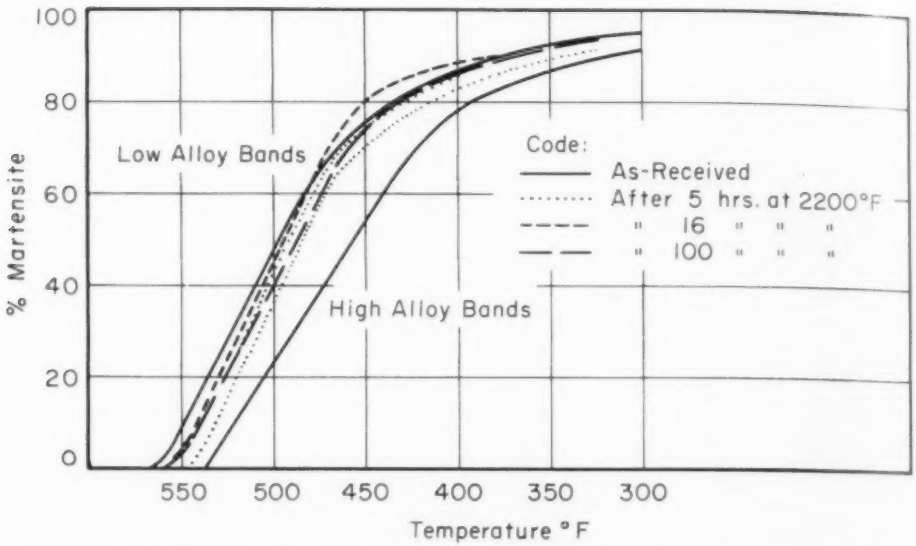


Fig. 8—Effect of Homogenization at 2200°F on Martensite Transformation in Banded 4340 Steel.

steels. However, only the results for the 1340 and 2340 steels are shown in Fig. 13. The results on the 4140 and 5140 analyses were similar to those for the 1340 steel. A significant point here is that the 2340 steel remains banded after the 100 hour treatment while the 1340, 4140 and 5140 grades are not. Also, the first forming martensite in the 2340 steel occurs in regions of inclusions (Fig. 11) while in the other steels it forms between inclusions.

The effects of isothermal treatments on the martensite reaction in the 1340, 2340, 4140 and 5140 steels are shown in Fig. 14. In contrast to the 4340 steel, isothermal treatments of 1340, 4140 and 5140 did not develop banded structures for homogenization treatments that gave random martensite on direct quench. The 2340 steel, which never attained randomness of martensite on direct quench, did not show any significant effects from the incubation treatment.

Throughout the transformation studies on as-received and homogenized materials, it was observed that the effect of nonmetallic inclusions on ferrite-pearlite transformation and the martensite reaction was almost nonexistent (5,6). At times, ferrite was observed at inclusions but in almost all instances, this condition did not arise from premature or early precipitation. Elongated and/or banded regions of inclusions per se have little influence on banding.

Physical Properties Of Banded Versus Homogenized 4340

Table IV gives the results of longitudinal and transverse tensile and impact properties of 4340 material before and after homogeniz-

Table IV
Physical Properties of Nonhomogenized and Homogenized 4340 Steel[1]

A. TENSILE PROPERTIES

Yield Strength .2% Offset P.S.I.	Ultimate Strength P.S.I.	Yield To Ultimate Ratio	Elongation %	Reduction Of Area %	Brinell Hardness
NON-HOMOGENIZED STEEL					
Longitudinal Direction					
123,750	137,750	0.90	15.5	60.7	277
123,250	137,500	0.89	17.0	61.2	277
123,750	137,000	0.90	21.0	62.6	277
123,750	138,500	0.89	21.0	60.2	285
Ave. 123,600	137,680	0.895	18.6	61.2	280
Transverse Direction					
124,250	137,500	0.90	14.0	25.8	285
123,000	137,000	0.90	12.6	24.0	277
122,500	137,500	0.89	13.5	27.5	285
122,500	137,500	0.89	11.0	19.0	285
Ave. 123,100	137,375	0.895	12.8	24.3	283
HOMOGENIZED STEEL					
Longitudinal Direction					
124,500	136,500	0.91	22.5	59.4	285
125,000	138,000	0.90	21.0	60.6	277
122,000	136,500	0.89	20.0	62.2	285
122,650	136,500	0.90	20.0	61.0	285
Ave. 123,540	136,900	0.90	20.6	60.8	283
Transverse Direction					
124,250	139,000	0.89	14.5	30.1	285
123,250	137,500	0.89	17.0	41.1	285
121,750	137,000	0.89	12.0	21.2	285
123,000	138,750	0.89	17.0	40.0	285
123,250	138,500	0.89	16.0	37.0	285
Ave. 123,100	138,150	0.89	15.3	34.0	285

B. IMPACT PROPERTIES[2]

Longitudinal Direction Charpy "V" Notch Ft. Lbs.	Brinell Hardness	Transverse Direction Charpy "V" Notch Ft. Lbs.	Brinell Hardness
Non-Homogenized Steel			
82.0	285	32.0	285
80.0	277	33.0	285
81.0	285	33.0	277
80.0	285	31.0	285
86.0	285	32.0	285
—	—	32.0	269
—	—	28.0	280
Ave. 82.0	285	31.4	281
Homogenized Steel			
78.0	285	38.0	277
86.0	277	38.0	285
96.0	277	40.0	285
81.0	285	40.0	277
87.0	285	38.0	277
—	—	38.0	277
—	—	41.0	285
Ave. 86.0	282	39.0	280

[1]Homogenized 100 hours at 2200°F, re-normalized at 1550°F five times to remove last vestiges of coarse grain. Specimens prepared from quarter section of 6" ×6" square billet, oil quenched from 1550°F, and tempered at 1175°F for 2 hours.
[2]Charpy "V" notch.

ing for 100 hours at 2200°F. Prior to homogenizing, the 4340 material was grossly banded, while after homogenizing the annealed prior to quench structure was reasonably free from banding. It is evident that longitudinal properties are little influenced by homog-

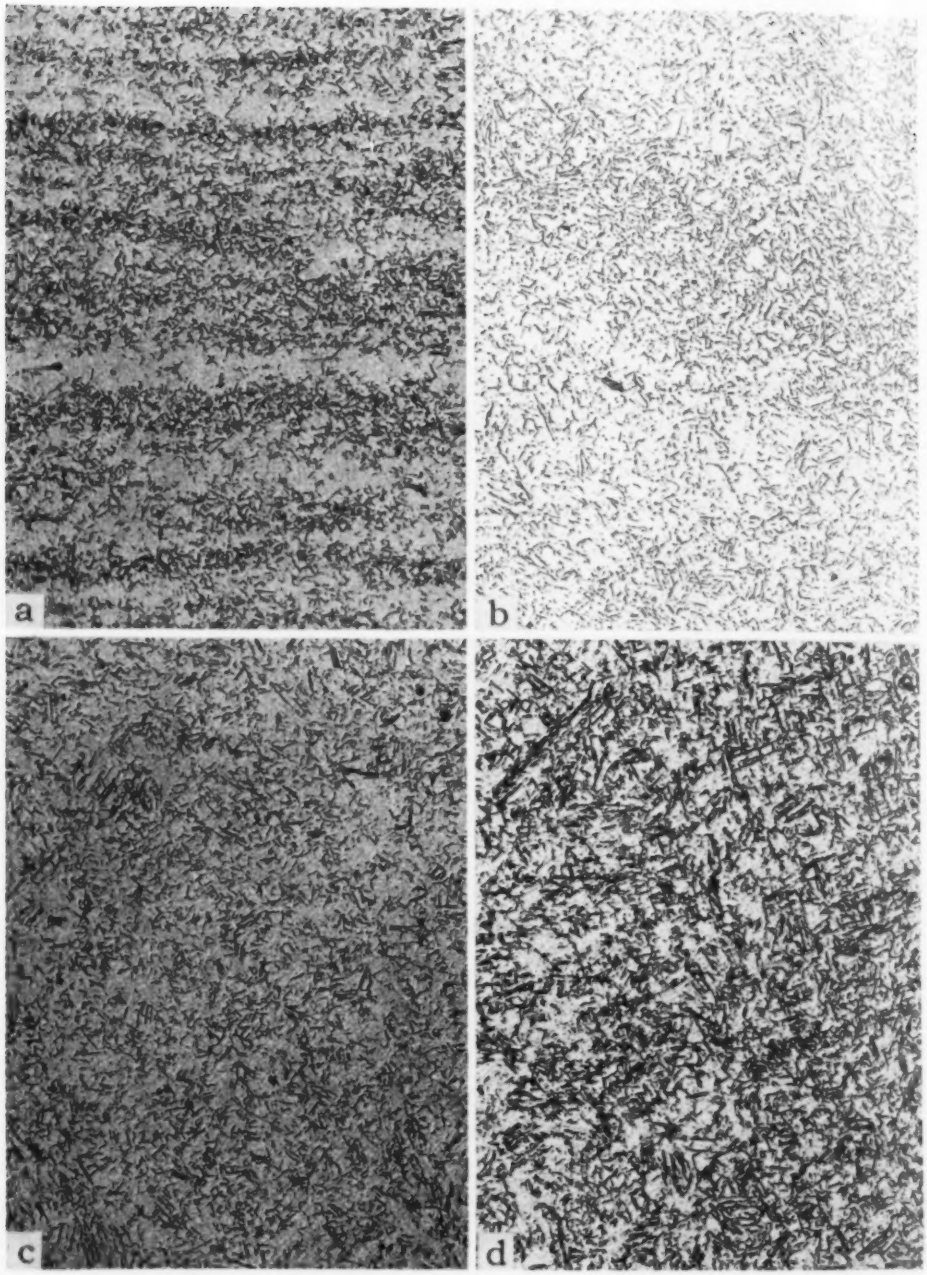


Fig. 9—Progress of Homogenization in Banded 4340 Steel After Various Treatments at 2200°F as Revealed by Ms Technique.
(a) 0 Hours; (b) 5 Hours; (c) 25 Hours; (d) 200 Hours ×100

enizing. However, transverse ductility (elongation and reduction of area) and impact are somewhat improved by homogenizing, although the degree of improvement is not of commercial significance.

Discussion

Banding in 1340, 2340, 4140, 4340 and 5140 steels is the direct

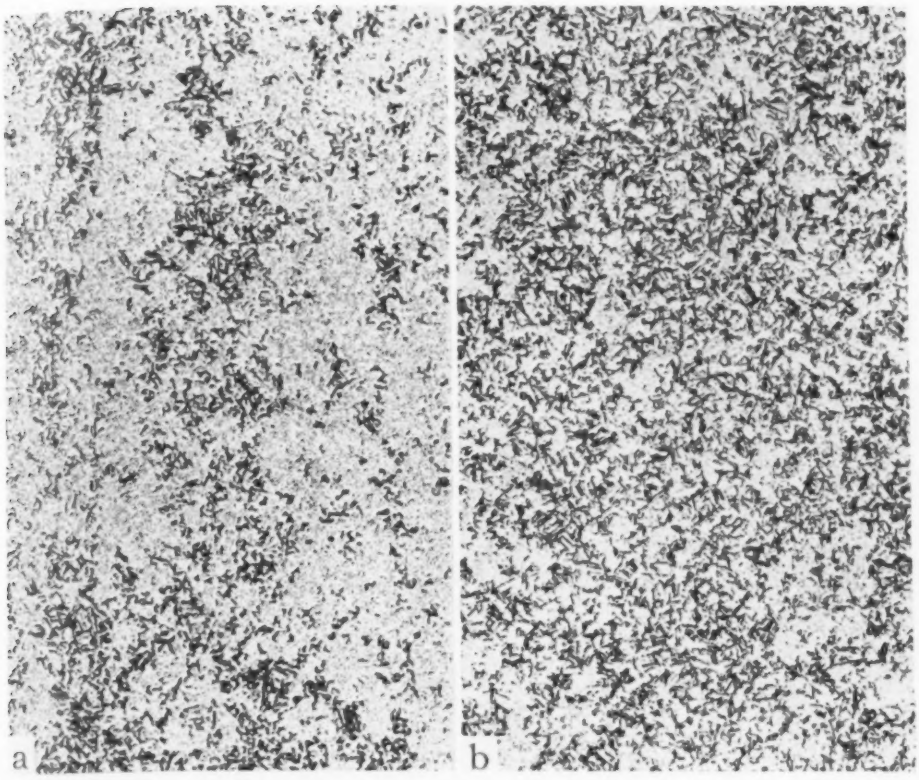


Fig. 10a-f—Effect of Austenite Incubation and Transformation at 1200°F on Characteristics of Martensite Reaction of 4340 Steel. ×100.

Fig. 10a—Austenitized 1550°F, Held 3 Minutes at 1200°F, Quenched to 540°F, Tempered Directly at 675°F, then Water-Quenched. Representative of Specimens Homogenized 16, 25, and 50 Hours at 2200°F.

Fig. 10b—Treatment same as (a) Representative of Specimens Homogenized 75 Hours and Longer at 2200°F— ×100.

result of heterogeneous austenite with respect to alloy and carbon. The results obtained with the chemistry sensitive martensite reaction bear this out. The heterogeneity of carbon in austenite is due to the presence of banded concentration levels or aggregates of alloy. The relative effect of the various alloying elements on the location of carbon is evident from the results obtained on the 2340 steel as compared to the 1340, 4140 and 5140 steels. In the case of partially homogenized 2340, the first precipitation of ferrite, pearlite and martensite occurred always in regions of relatively high nickel (inclusion region). In the as-received and partially homogenized 1340, 4140 and 5140 steels, first precipitation of these constituents occurs in the low alloy regions (between inclusions). This difference in the banding behavior of these steels is believed to be due to the opposing effects of nickel and the carbide formers on the location of carbon (and carbon activity) in austenite at austenitizing temperatures, during cooling and during transformation. In high nickel bands, the carbon concentration tends to be relatively low while in low nickel regions or bands containing relative high amounts of

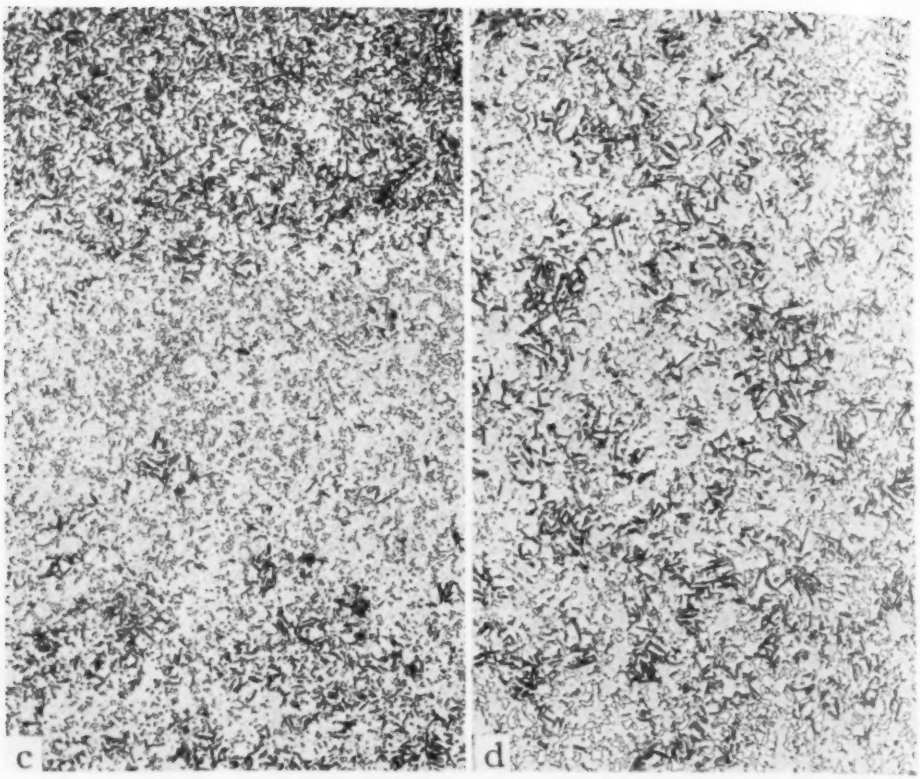


Fig. 10c—Austenitized 1550°F, Held 25 Minutes at 1200°F, Quenched to 540°F, Tempered Directly at 675°F, then Water-Quenched—Homogenized 16, 25, and 50 Hours at 2200°F.
Fig. 10d—Treatment Same as Above—Homogenized 75 Hours at 2200°F.

carbide forming type elements, the carbon concentration tends to be relatively high. The resulting effect is a higher than average Ms for the high nickel bands and a lower than average Ms for the low nickel and/or high carbide forming element bands. Similarly corresponding effects on ferrite formation and even greater effects on pearlite formation may be expected, not only because of the initial carbon and alloy segregation in the austenite but also because of the added influence of cooling conditions and transformation on carbon and alloy segregation.

It appears that the relative effect of the carbide forming elements toward increasing carbon concentration in their vicinity is greater than the influence of nickel toward decreasing carbon in its vicinity. In the case of the 2340 steel (0.91% manganese plus chromium versus 3.20% nickel) a lesser amount of total carbide forming type elements apparently had the dominating effect because the first pearlite and martensite precipitated between the inclusions. Available data on the effects of nickel (3) and manganese (4) on the activity of carbon indicate that the above effects are to be expected.

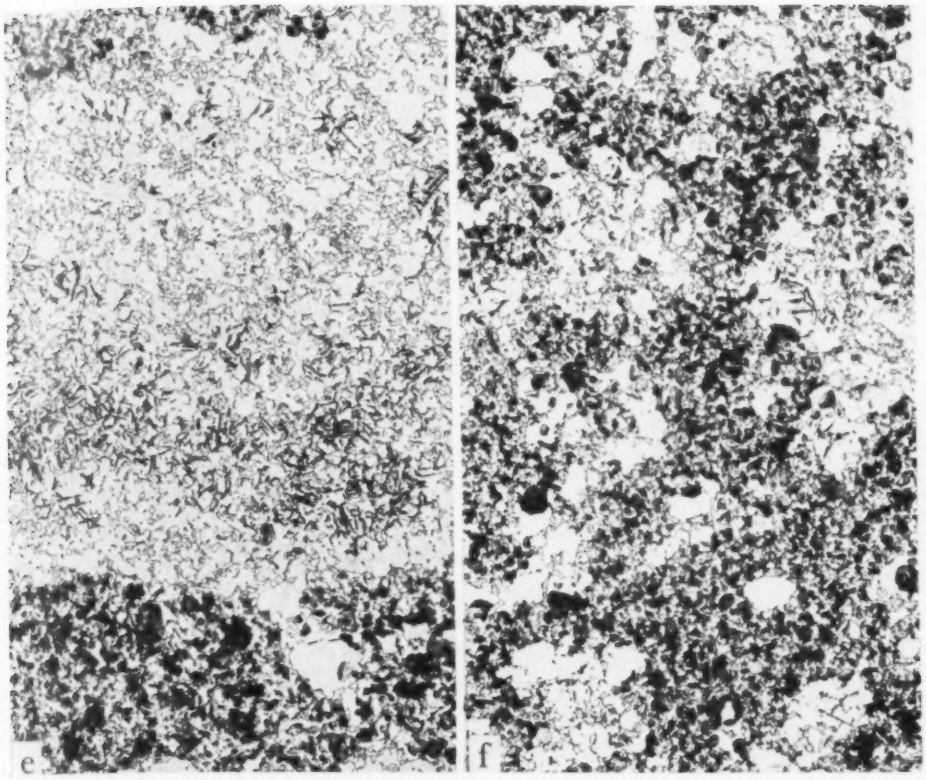


Fig. 10e—Austenitized 1550°F, Held 45 Minutes at 1200°F, Quenched to 490°F, Tempered Directly at 675°F, then Water-Quenched—Homogenized 16, 25, and 50 Hours at 2200°F.

Fig. 10f—Austenitized 1550°F, Held 45 Minutes at 1200°F, Quenched to 520°F, Tempered Directly at 675°F, then Water-Quenched—Homogenized 75 Hours at 2200°F.

The carbide forming elements present in the analyses under study diffuse more rapidly than nickel at 2200°F (Table II). Therefore, for a ternary alloy steel, assuming the diffusion rate of a given element is not greatly influenced by the presence of other alloys in the range under consideration, there comes a time during homogenization when the carbide forming type elements are relatively homogenous while nickel is still relatively segregated. Therefore, in a partially homogenized 4340 steel, the formerly high alloy regions of manganese, chromium, nickel and molybdenum are now relatively highly alloyed with respect to nickel alone. These relatively high nickel regions may become bands of lower carbon, higher Ms or early ferrite and pearlite formations. Therefore, an approximate half band width shift in the position of the initial precipitation of these constituents may occur in partially homogenized 4340 with respect to their position in the as-received material. If the time of homogenization is sufficient to remove nickel segregation then, of course, random structures will result. An actual reversal of band position between the as-received and the partially homogenized 4340

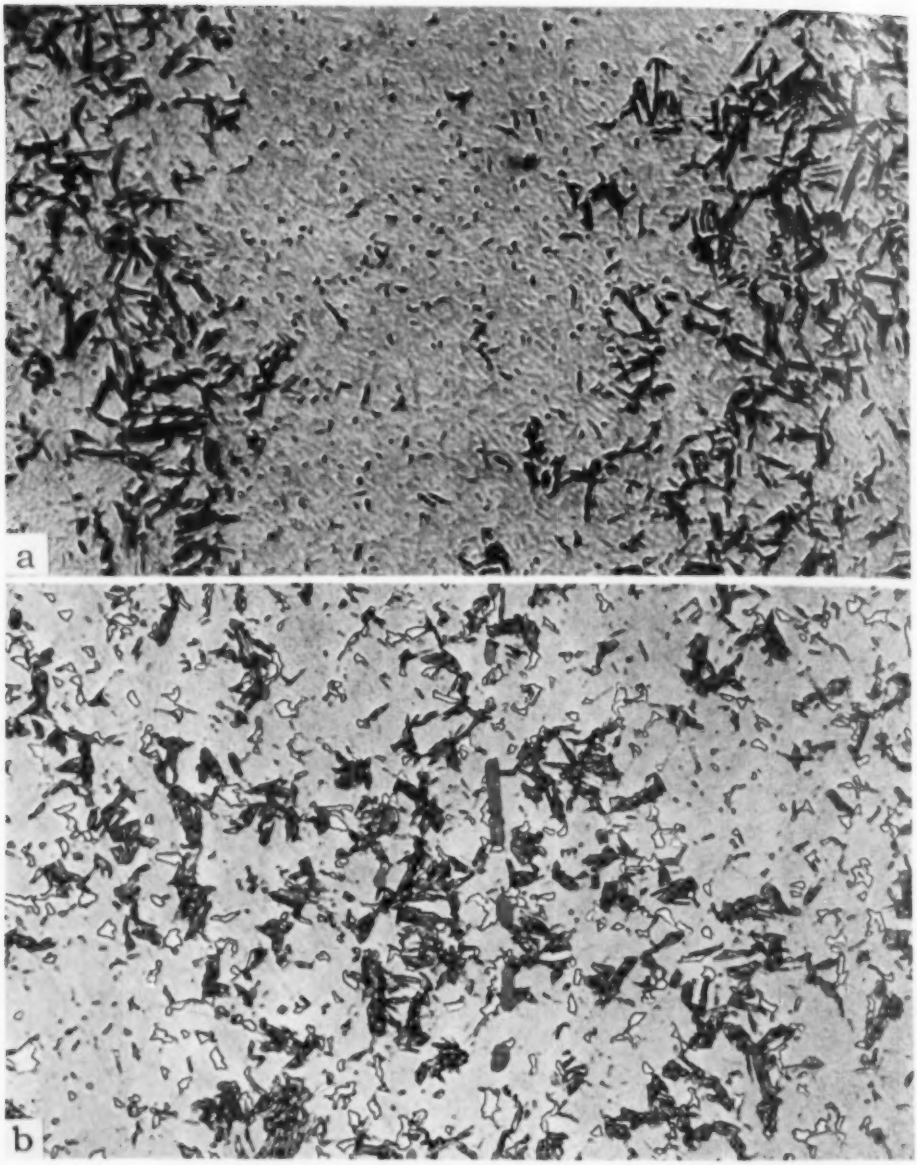


Fig. 11a-b—Shift of Initial Martensite Transformation to Position Along Inclusions as Result of Austenite Incubation.

Fig. 11a—4340 Steel Homogenized 50 Hours at 2200°F—Austenitized 1550°F—Held Temporarily at 1200°F for 3 Minutes—Quenched to Martensite Range— ×400.

Fig. 11b—2340 Steel Homogenized 100 Hours at 2200°F—Austenitized 1525°F—Held at 1100°F for 25 Minutes—Quenched to Martensite Range— ×500.

steel was noted in the case of the martensite transformation following a prior isothermal treatment at the nose of the TTT curve (Figures 10 and 11). In the case of the ferrite-pearlite reaction, the question of band reversal becomes more complicated. For low homogenization times, sufficient diffusion of alloy does not take place to give rise to band shifts. Homogenization times sufficiently long to allow alloy diffusion give rise to random ferrite patterns and,

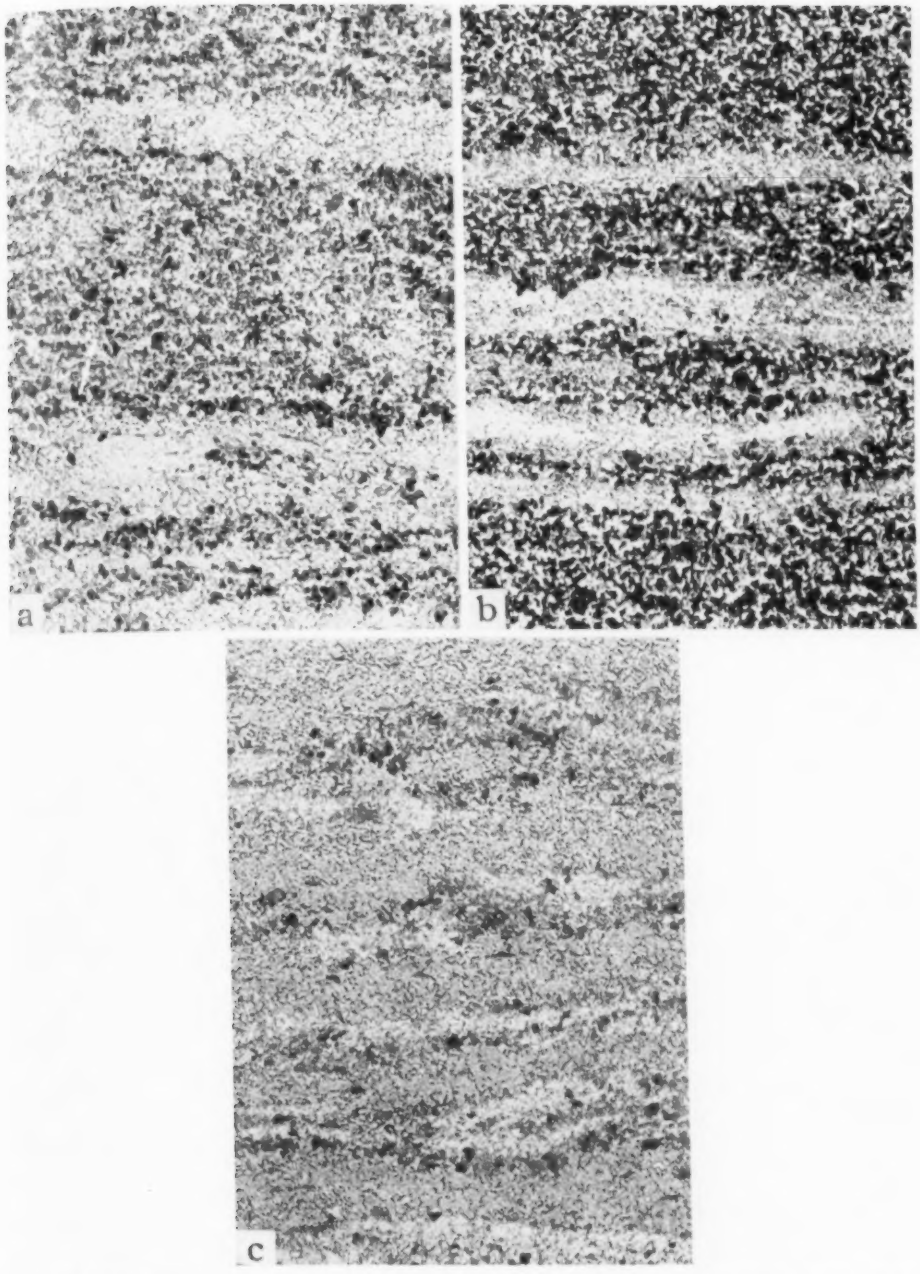


Fig. 12—Banding in As-Received (a) 1340, (c) 2340 and (b) 4140 Steels as Revealed by Isothermal Method (5140 Similar to 4140 and not Shown)—×100.

therefore, random final structures so that the band shifting phenomena must be looked for during the early stages of pearlite formation. For the latter conditions, band shift was noted during the early stages of pearlite formation.

From a practical viewpoint, the data on longitudinal and transverse properties of banded versus homogenized 4340 steel given in

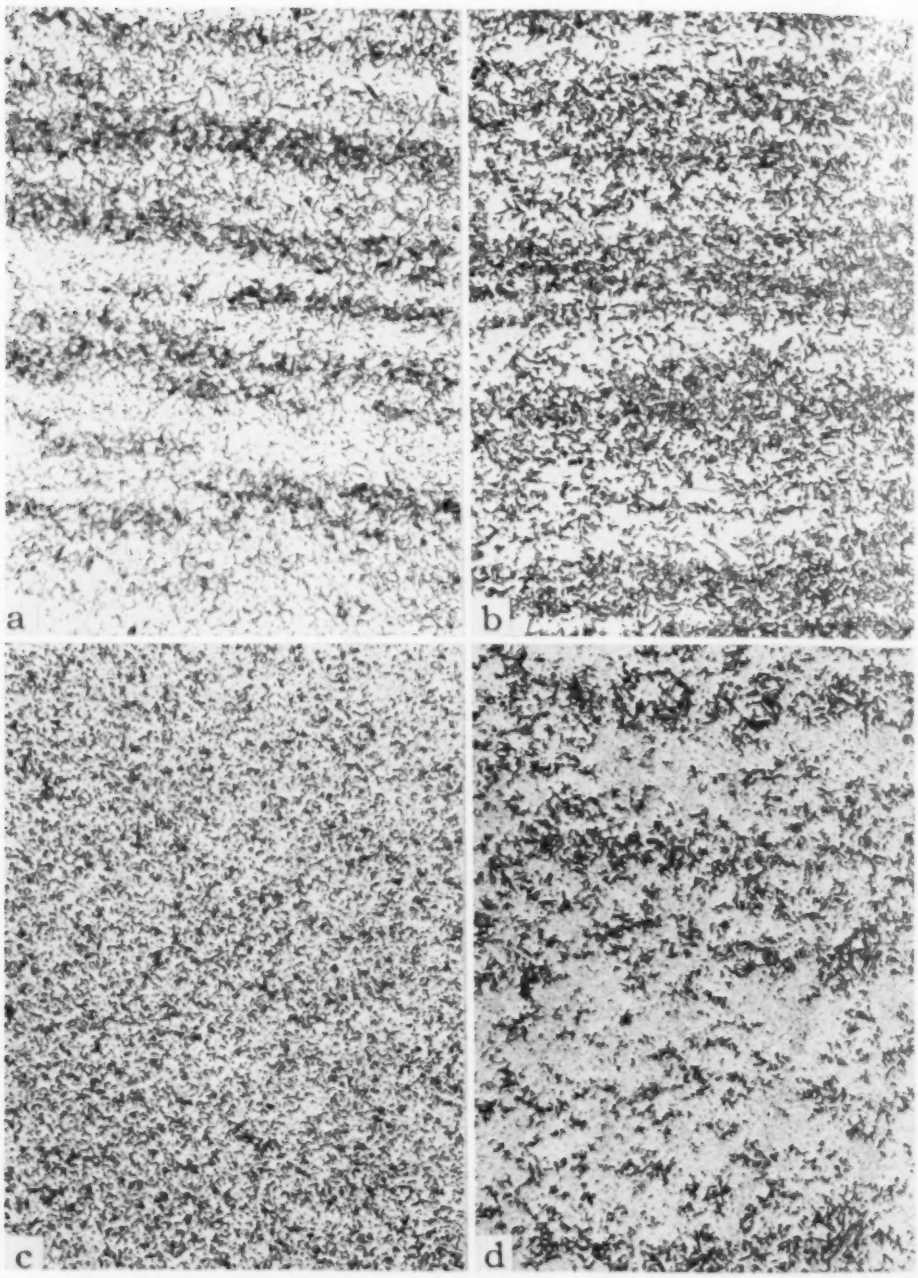


Fig. 13—Effect of Homogenization on Characteristics of Martensite Reaction in 1340, 2340, 4140 and 5140 Steel Types— ×100 (a) 1340—no Homogenization (4140 and 5140 similar); (b) 2340—no Homogenization; (c) 1340—Homogenized 100 Hours at 2200°F. (4140 and 5140 similar); (d) 2340—Homogenized 100 Hours at 2200°F.

Table IV show that banding plays only a minor role in accounting for the difference between longitudinal and transverse ductility properties of rolled steel products.

Conclusions

1. The primary cause of banding in rolled steel products is

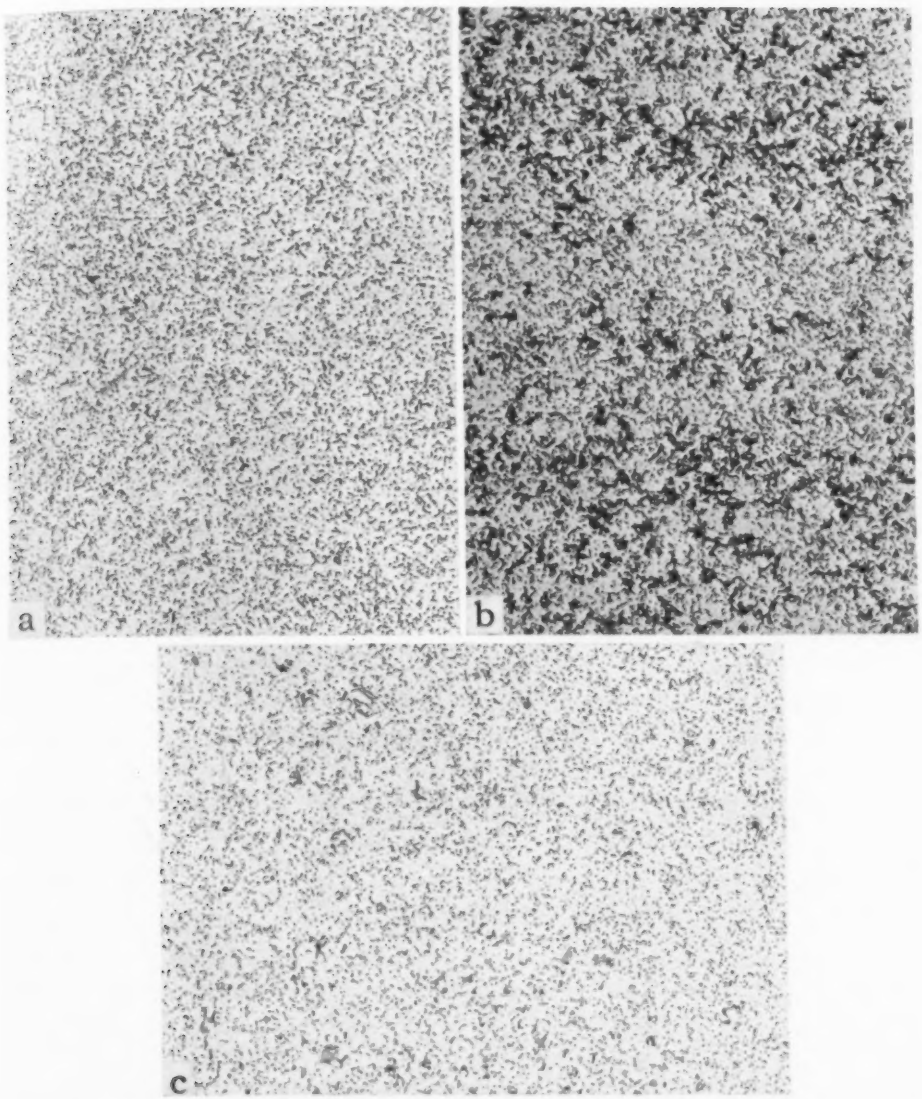


Fig. 14—Effect of Austenite Incubation on Characteristics of Martensite Reaction in (a) 1340, (b) 2340 and (c) 4140 Steels (5140 Similar to 4140)—×100.

chemical heterogeneity. The effects of other nucleating agents such as banded inclusions, etc., are either minor or nonexistent.

2. Chemical heterogeneity produces visible banding through its effect on nucleation and growth of ferrite and pearlite from austenite. The pattern of nucleating and growth of ferrite and pearlite is determined primarily by the aggregate effect of alloy heterogeneity on carbon segregation.

3. In the analyses studied, carbide forming type elements tend to increase carbon concentration in their vicinity while solution type elements (nickel) tend to decrease carbon concentration in

their vicinity. Therefore, in single alloyed steels, the degree of carbon segregation and the location of high and low carbon areas relative to a fixed marker depend solely on the amount and distribution of the one alloying element. As noted in the paper, the location of high carbon bands relative to inclusions differs for the carbide forming type elements versus nickel. In multi-alloyed steels, these visual banded conditions depend upon a balanced influence as determined by alloy types, amounts and distribution.

4. The overall effect of chemical heterogeneity on nucleation and growth of ferrite and pearlite from austenite into carbon segregated structures is further influenced by the added effects of cooling conditions from austenitizing temperatures and also transformation.

5. Isothermal transformation at the nose of the TTT curve is a very sensitive measure of banding. Continuous cooling treatments and direct quench Ms techniques were found to be less sensitive. Ms techniques were found to be very sensitive if preceded by an incubation treatment.

6. Banding in the 1340, 4140 and 5140 analyses presents a more vivid separation of ferrite and pearlite than the 2340 steel. However, the 1340, 4140 and 5140 analyses homogenize more readily than the 2340 grade.

7. Comparison of physical properties between banded and homogenized (100 hours at 2200°F) 4340 steel shows that only transverse ductility is improved. However, the degree of improvement is not commercially significant.

References

1. A. V. Prohkoroff, "Ferrite Banding in Forged and Rolled Steel," *Metallurgia*, Vol. 13, April 1936, p. 179.
2. L. S. Darken, "Diffusion of Carbon in Austenite with a Discontinuity in Composition," Metals Technology, Vol. 15, September 1948, #16, Technical Publication #2443.
3. C. H. Toensing, "Thermodynamic Studies on Austenite Solid Solution Activity of Carbon as a Function of Composition in Fe-Ni Steels," Unpublished Doctor's Thesis, Massachusetts Institute of Technology, Cambridge, Mass.
4. R. P. Smith, "Equilibrium of Fe-C-Si and Fe-C-Mn Alloys with Mixtures of CH_4 and H_2 at 1000°C," *Journal*, American Chemical Society, Vol. 70, August 1948, p. 2724.
5. A. B. Greninger and A. R. Troiano, "Kinetics of the Austenite to Martensite Transformation in Steel," TRANSACTIONS, American Society for Metals, Vol. 28, 1940, p. 537.
6. R. F. Mehl, "Structure and Rate of Formation of Pearlite," TRANSACTIONS, American Society for Metals, Vol. 29, 1941, p. 831.
7. H. L. Mead, "Diffusion of Cr and Si in Steel," Personal Conference, Unpublished Work, Massachusetts Institute of Technology, Cambridge, Mass.
8. J. L. Ham, "Rate of Diffusion of Molybdenum in Austenite and in Ferrite," TRANSACTIONS, American Society for Metals, Vol. 35, 1945, p. 331.

9. C. Wells and R. F. Mehl, "Rate of Diffusion of Manganese in Gamma Iron of Low Carbon and High Carbon Manganese Steels," *Transactions*, American Institute of Mining and Metallurgical Engineers, Vol. 145, Iron and Steel Division, 1941, p. 315.

10. C. Wells and R. F. Mehl, "Rate of Diffusion of Nickel in Gamma Iron of Low Carbon and High Carbon Nickel Steels," *Transactions*, American Institute of Mining and Metallurgical Engineers, Iron and Steel Division, Vol. 145, p. 329.

11. C. E. Birchenall and R. F. Mehl, "Self-Diffusion in Alpha and Gamma Iron," *Transactions*, American Institute of Mining and Metallurgical Engineers, Metals Branch, Vol. 188, 1950, p. 144.

DISCUSSION

Written Discussion: By Paul P. Mozley, staff metallurgist, Lockheed Aircraft Corporation, Burbank, Calif.

The authors' work on banding is of considerable interest, especially since the aircraft industry is now using 4340 steel at extreme strength levels. We have been concerned with the effects of banding in this steel but have been especially apprehensive about the effects on the fatigue life of highly loaded, complex parts such as landing gear components. The author's tests indicated little to fear as to static properties, however, the effects on dynamic properties should afford an additional field for study.

Thus far, we have been fortunate in not encountering much banding in parts to be used at extreme strength levels but have not been so fortunate in hand forged and formed billets, machined into parts to be used at more conventional strength levels.

Apparently a small amount of work during banding at 1900°F and subsequent heat treatment resulted in severe banding and isolated islands which have been called "Colonization." Either annealing or austenitizing at usual temperatures seemed to accentuate the banding. An anneal at 2000°F after banding and before austenitizing resulted in a structure free or almost free from banding and which was considered to be in a structurally sound condition. As a salvage measure several parts already in a severely banded condition were sufficiently homogenized by the 2000°F treatment to show uniform micro-hardness traverses indicating that considerable improvement had been accomplished. In some cases the severely banded material was not greatly improved by the treatment.

The above experience has led us to believe that the dispersal or segregation causing banding may be accentuated by recrystallization resulting from slight amounts of work and that this becomes an additional factor in banding phenomena. This is another item that might be worthy of future study.

All studies of banding have assumed the segregation of constitutents in bands or layers. None have explained why the dispersal of the constituents should be in layers or bands. Perhaps we are at the point where the colloid chemist is needed. Possibly we are the victims of the colloidal migration and segregation into bands known as the Liesegang phenomenon. Research on banding of steels has possibly not gone back far enough into the history of the steels studied.

I wish to congratulate the authors on their work and their excellent report and hope that my few comments may serve to stimulate them to further study of the factors causing banding in steels.

Written Discussion: By U. Wyss, chief metallurgist, Maag Gear Wheel Comp. Ltd., Zurich, Switzerland.

The authors have presented a very interesting contribution to the study of banding in steel. Some of the essential results described in the paper quite agree with my own metallographic observations on this subject. I especially wish to support the statement that chemical heterogeneity is the primary cause of banding in rolled and forged steel products (and, of course this chemical heterogeneity is due to dendritic segregation).

The authors relate the location of high carbon bands to inclusion regions. It would be interesting to learn to what kind of inclusions this statement refers. Probably sulphide inclusions are meant. This question seems to be an important one as I repeatedly observed in many metallographic examinations, that after solidification of steels distinct types of inclusions are always in the same location relative to dendrites. For example, silicate-type inclusions which are formed before the crystallization of steel have a very pronounced tendency to be accumulated at the first formed thread-like axis or branches of dendrites—probably by the effect of surface tensions—so that the last solidifying interdendritic zones remain free of this type of inclusions. Contrary to this, the eutectically formed sulphide-type inclusions always are precipitated within interdendritic zones. Hence in hot-worked steels, silicate-type inclusions generally are located in low alloy bands whilst sulphide inclusions always are to be found in high alloy bands. This fact is the reason why in former times nonmetallic inclusions were regarded as the only cause of the band-like arrangement of decomposition products of austenite.

In addition to the steels examined by the authors, it might be interesting to mention the different behavior of hypoeutectoid carbon steels: After transformation of such steels into ferrite and pearlite, the bands corresponding to interdendritic zones, which contain the sulphide inclusions, are ferritic and the bands caused by dendrites, in which most of the silicate-type inclusions are accumulated, are pearlitic. This is due to the nucleating effect of the interdendritically enriched phosphorus and is an example for a different behavior of these steels compared with the nonhomogenized steels described in the paper.

Authors' Reply

The authors wish to thank Mr. Wyss for his interest in our paper and appreciate his comments. It is gratifying to receive his support with respect to our conclusions.

The inclusions employed as fiducial markers of high carbon regions were almost wholly identified as sulphides. It was regrettable that this fact was not fully discussed in the paper. The silicate type of inclusion was found to exist primarily in the low alloy regions, as surmised by Mr. Wyss. Since not many of these inclusions are normally found in aluminum-killed steels, we were not confused by this factor. The alumina type inclusions were found to exist in juxtaposition with the sulphides or at boundaries of low and high carbon regions. Again, these types were in the minority and did not confuse the use of sulphides as markers of the higher alloyed regions.

Mr. Wyss' explanation for the existence of the various inclusion types in the particular regions on freezing agrees well with our own interpretation of the ingot freezing phenomena and also with our results.

We are cognizant of the possible differences in the banding behavior of plain carbon steels as opposed to our alloy steels. We thank Mr. Wyss for his remarks on this point. Since we do not have any data on plain carbon steel, we have nothing constructive to add. In speculating, however, it can be shown why phosphorus would cause a banding condition reversed to that shown in our alloy steels if present in large amounts. Phosphorus is known to strongly increase the activity of carbon in steel, akin to nickel and silicon. Since it deposits interdentrically, it would cause these regions to be ferritic, and the dendritic areas to be pearlitic.

AN APPROACH TO THE STUDY OF THE EFFECT OF RARE EARTH ADDITIONS TO STEEL BY USE OF RADIOACTIVE TRACER TECHNIQUES

By C. S. DuMont, J. E. Gates, and C. M. Henderson

Abstract

Additions of radioactive misch metal were made to an alloy of 25% nickel, 20% chromium, 3.5% copper, and 2.5% molybdenum to determine the distribution of residual misch metal constituents within the alloy. Compared autoradiographs and metallographic analyses showed that cerium and neodymium atoms were dispersed throughout the matrix and were also slightly concentrated in the interdendritic zones of the as-cast material. There was no evidence of any concentrations of these atoms at the grain boundaries or within the nonmetallic inclusions. Heat treatment at forging temperatures tended to homogenize the interdendritic concentrations of the two radioactive constituents of the misch metal. (ASM-SLA Classification: S19, M25, AY)

A CURRENT joint effort between Mallinckrodt Chemical Works and Battelle Memorial Institute has been devoted to a search for the causes of poor hot forgeability in steels and to an evaluation of the effects of rare earth additions as a possible cure. One natural phase of this study has been an interest in microstructure and any evidence of harmful segregation of intermetallic compounds or nonmetallic inclusions. To gain more information along these lines, the program has turned to the addition of radioactive trace elements in the hope of thus delineating the location and distribution of impurities which might not be revealed by conventional metallography. This paper describes a first study of this sort in which radioactive misch metal was added to a stainless steel.

As a further step in research on this problem, it was decided to study the distribution of rare earths in stainless steels by radioactive tracer and autoradiographic techniques.

Experimental Procedure

In radioactive tracer techniques, the alloy constituent that is

A paper presented before the Thirty-Seventh Annual Convention of the Society, held in Philadelphia, October 17-21, 1955. Of the authors, C. S. DuMont is associate consultant, Physical Metallurgy Division, and J. E. Gates is research radiochemist, Radioisotope and Radiation Division, Battelle Memorial Institute, Columbus, Ohio, and C. M. Henderson is associated with the Development Department, Mallinckrodt Chemical Works, St. Louis. Manuscript received April 26, 1955.

of interest is made radioactive. This can be done, as it was in this research, by irradiation of the constituent with neutrons in a nuclear reactor before the constituent is added to the melt. When an element is subjected to neutron irradiation, a nuclear reaction may take place. Frequently, the reaction produces another isotope of the same element which may be radioactive. An example of a nuclear reaction is:

$$58Ce^{140} + 0n^{1} \text{——} 58Ce^{141} (32 \text{ days}, \beta, \gamma),$$

in which a neutron of mass 1 and charge (atomic number) 0 reacts with the nucleus of a cerium atom having a mass of 140 and charge of 58 to form a radioactive isotope of cerium with a mass of 141 and a charge of 58. The radioactive isotope in this example emits both beta and gamma radiation as it decays with its characteristic half-life of 32 days. A radioactive isotope of an element can be used as a tracer because such an isotope emits a characteristic radiation by which it may be identified, even though it does not differ measurably from other isotopes of that element. With a few exceptions of no importance in this work, the isotopes of an element have essentially identical chemical properties. Differences in properties that depend on mass are small enough to be negligible.

The actual location of the radioactive constituent of the alloy may be determined by autoradiographic techniques since nuclear radiations will expose photographic emulsions (1)[1]. Special emulsions are available that are sensitive only to beta radiation which has very low penetrating power. One type of emulsion, termed permeable-base stripping film, can be applied directly to the polished surface of the metal containing a radioactive constituent. In the emulsion, the beta radiation produces a latent image of a thin surface layer of the metal. The depth of the surface layer, which emits beta radiation that penetrates to the emulsion, is controlled by the energy of the radiation and is, at most, a few millimeters with higher energy beta particles. After exposure, the image in the emulsion is made visible by photographic development. Since the emulsion remains attached to the metal and is optically clear, the developed silver grains and the microstructure of the metal may be examined simultaneously with the aid of a microscope. The silver grains appear as black spots superimposed on the surface of the metal. The location of the developed silver grains indicates the location of the radioactive constituent that is emitting the beta radiation. Resolutions in the range of 2 to 5 microns have been reported (2) using the strip-film method.

Another type of nuclear emulsion that is available for use in autoradiography is attached to a glass slide and is termed a track plate. The radioactive specimen is simply placed on the track plate

[1]The figures appearing in parentheses pertain to the references appended to this paper.

for the exposure time, and then the slide is developed. Only visual correlation between the macrostructure of the metal and the autoradiographic exposure is possible with this technique.

In this particular study, a specimen of Mallinckrodt Misch Metal 45C[2] weighing 2.1 grams was irradiated with neutrons in the X-10 Reactor at the Oak Ridge National Laboratories for seven

Table I
The Radioactive Isotopes Produced During the Neutron Irradiation of Misch Metal

Radioactive Isotope	Half-Life	Types [b] of Emitted Radiation	Radioactivity [a] Produced, Millicuries/Gram
Cerium-137	36 hrs.	K-capture X-ray & Gamma	14
Cerium-139	140 days	K-capture X-ray & Gamma	0.67
Cerium-141	32 days	Beta and gamma	2.16
Cerium-143	33 hrs.	Beta and gamma	1.0
Lanthanum-140	40 hrs.	Beta and gamma	147
Neodymium-147	11.6 days	Beta and gamma	3.8
Neodymium-149	1.8 hrs.	Beta and gamma	1.4
Neodymium-151	12 mins.	Beta and gamma	0.77
Praseodymium-142	19.3 hrs.	Beta and gamma	54

[a] Values calculated from $S = \frac{1.64}{A}\left(1 - e^{-0.693\frac{t}{T_{\frac{1}{2}}}}\right)$ where

S = activity of target in curies/gm (one curie = 3.7×10^{10} disentegrations/sec.
e = thermal neutron capture cross section in barns.
F = neutron flux $\times 10^{11}$.
A = atomic weight of target element.
t = time of irradiation in same units as $T_{\frac{1}{2}}$.
$T_{\frac{1}{2}}$ = half-life of the produced radioisotope.

The calculations were based on the irradiation of one gram of misch metal for seven days at a neutron flux of 5×10^{11} neutrons/cm^2/second.

[b] General Electric Chart of the Nuclides, Knolls Atomic Power Laboratory, Fourth Edition, November, 1952.

Table II
The Isotopic Composition [a] of the Elements in Misch Metal

Stable Isotope	Percentage Abundance [b]
Cerium-136	0.19
Cerium-138	0.26
Cerium-140	88.5
Cerium-142	11.1
Lathanum-139	100
Neodymium-142	25.95
Neodymium-143	13.0
Neodymium-144	22.6
Neodymium-145	9.2
Neodymium-146	16.5
Neodymium-148	6.8
Neodymium-150	5.95
Praseodymium-141	100

[a] General Electric Chart of the Nuclides, Knolls Atomic Power Laboratory, Fourth Edition, November, 1952.

[b] This is the percentage of the naturally existing isotope of the element.

days at a flux of approximately 5×10^{11} neutron-cm^{-2}-sec^{-1}. Based on calculations, the irradiation produced a total of 445 millicuries of the radioisotopes listed in Table I. Only the major constituents of the misch metal—cerium, lanthanum, praseodymium, and neodym-

[2] Composition: Cerium 44%, Lanthanum 29%, Neodymium 17%, Praseodymium 7%, Gadolinium 1%, Magnesium 2%, Iron 0.1%

ium—were considered in the calculations. The isotopes of these elements are listed in Table II. Decay rates of the longer lived, beta-emitting isotopes, based on the relative amounts of each that were produced and their known half-lives, are plotted in Fig. 9. The fraction of the total radiation that was due to a particular radioisotope at any time after the irradiation was determined from these curves. Calculations based on the energy of the beta particles of the radioisotopes, cerium-141 and neodymium-147, whose radiations produced the autoradiographs, indicated that the radiation would penetrate the emulsion from a maximum depth in the stainless steel of approximately 0.4 millimeter (3).

The results of previous laboratory work had shown that the addition of misch metal to a 25% nickel, 20% chromium, 3.5% copper, and 2.5% molybdenum alloy had consistently resulted in improved hot working properties as measured by the hot-forge cone test. It appeared advisable to continue to work with this grade of stainless steel. A 16-pound heat of the above alloy was melted in a magnesia-lined induction furnace. The melt was deoxidized with 0.05% calcium as calcium silicide. Following deoxidation of the heat, one forge test cone was poured after which a misch metal addition, equivalent to ten pounds per ton, was made to the remainder of the melt in the furnace. A second forge test cone was then poured and 2.1 grams of radioactive misch metal was added to the metal remaining in the furnace. The total misch metal addition was 0.07 pound. Subsequent analysis of this heat indicated a total rare-earth content of 0.114% which is equivalent to a recovery of 22%.

One of the primary interests in this phase of the work was to establish the distribution of the misch metal in the alloy with particular regard to whether it occurred in the grain boundaries or within the grains. Therefore, in order to obtain a maximum grain size, the melt was allowed to solidify in the furnace, as such a procedure is known to produce coarse-grain structure.

After the metal in the furnace had cooled to room temperature, it was removed, cleaned, and sectioned. The ingot was approximately 4 inches in diameter and 3 inches high. A 1-inch cube was removed from the center of the ingot and was forged to 0.25-inch thickness at a temperature of 2250°F to check the forgeability of the alloy. Two small cracks occurred along one edge during the final stage of forging.

To study the effect of soaking time on the distribution of the misch metal, a second section was removed from the ingot and was held for 24 hours at 2400°F and allowed to cool in the furnace. Additional samples were taken from the as-solidified metal for metallographic and radiographic examination.

Eastman Kodak Type NTB plate and permeable base strip-

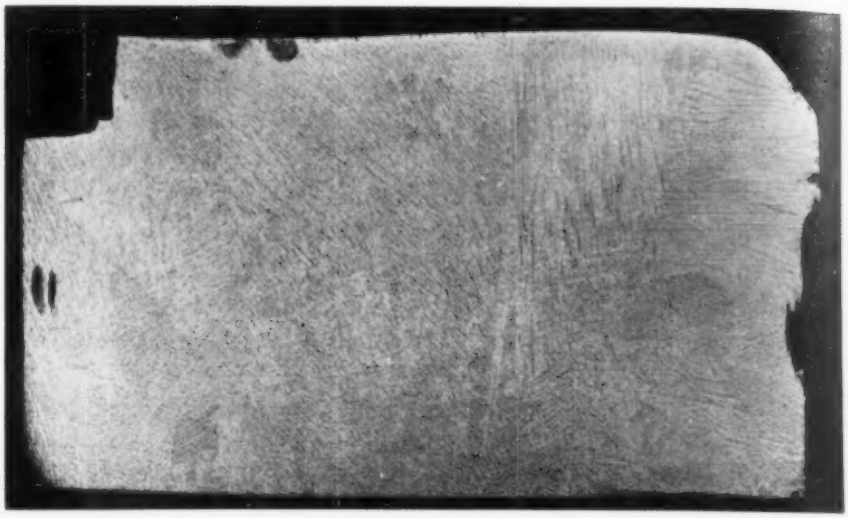


Fig. 1—Macrostructure of Specimen As-Solidified in the Melting Furnace. Right hand edge shows metal furnace lining interface. Etchant 4HC1: 1HNO. ×2.

emulsion autoradiographic films were used in the initial analytical work. The results showed that the strip emulsion was more satisfactory than the plate film. It was difficult to obtain true flat surfaces on the prepared specimens and, when the plates were pressed on top of the mounts, the uneven contact would result in a decrease in resolution of the image. The strip emulsion, however, provided intimate contact with the surface and eliminated this difficulty. The strip emulsion was developed in place with the advantage of providing absolute correlation of the autoradiographic exposure with the microstructure of the underlying etched sample. Photomicrographs were then made showing in a single exposure both the exposed areas of the strip film and the structure of the metal beneath the emulsion. The autoradiographs were produced approximately 17 days after the neutron irradiation of the misch metal. Referring to the curves shown in Fig. 9, it is indicated that 95% of the exposure in the autoradiographs was produced by the beta radiation from cerium-141 and neodymium-147.

Autoradiographs of nonradioactive stainless steel specimens were produced as controls. Inspection of these autoradiographs revealed no exposure in them. This indicated that the exposures produced in the autoradiographs of the radioactive specimens were caused by radiation from the radioactive constituents of the misch metal and not by chemical reaction between the metal specimens and the emulsion.

Results and Discussion

Fig. 1 shows a photomacrograph of a polished and etched specimen from the furnace-cooled sample of Heat B-1039. The massive

dendritic structure is plainly visible. The outside edge of the ingot is at the bottom of the photomacrograph.

Fig. 2 shows a direct print of a track plate autoradiograph of the same specimen shown in Fig. 1. The exposed sections of the autoradiograph, indicating the location of the radioactive constituents, show as light areas in the direct print. The exact location of the radioactive tracers cannot be determined from this autoradiograph, but careful examination of Fig. 2 will reveal an image of the dendritic

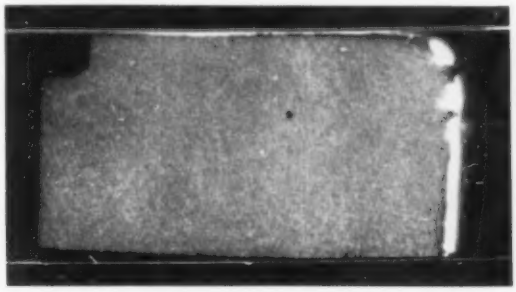


Fig. 2—Direct Print from an Autoradiographic Negative Prepared on Specimen Shown in Fig. 1. The light area along the right edge indicates a relatively high level of radioactivity. This suggests some concentration of rare earths at the metal furnace lining interface. ×1

structure shown in Fig. 1. This indicates that the distribution of the misch metal constituents cerium and neodymium was related to the dendritic structure of the metal.

The highly radioactive area at the outside edge of the specimen, shown in Fig. 2 as a white area at the right edge of the print, indicates that a large percentage of the radioactive material was either rejected from the melt or tended to concentrate at the metal-crucible interface during slow cooling, possibly due to selective oxidation. Radioactive areas in the remaining figures are shown as dark areas in the photomicrographs.

Figs. 3 and 4 show the autoradiographic image superimposed on the microstructure at 100 and 250 magnifications of a specimen in the as furnace-cooled condition. The exposed areas in the autoradiograph, produced by beta radiation from the radioactive constituents in the metal, show as dark irregular areas in Fig. 3 and as shaded areas in Fig. 4. These are indicated by arrows. Thus, the radioactive misch metal constituents cerium and neodymium appear to be concentrated in the last volumes to freeze in the dendritic structure. There was no evidence of any concentration of radioactivity at the grain boundaries or in the inclusions.

Figs. 5 and 6 show the combined structures of a specimen which was annealed for 24 hours at 2400°F. A comparison of these structures with those of Figs. 3 and 4 shows that the heat treatment

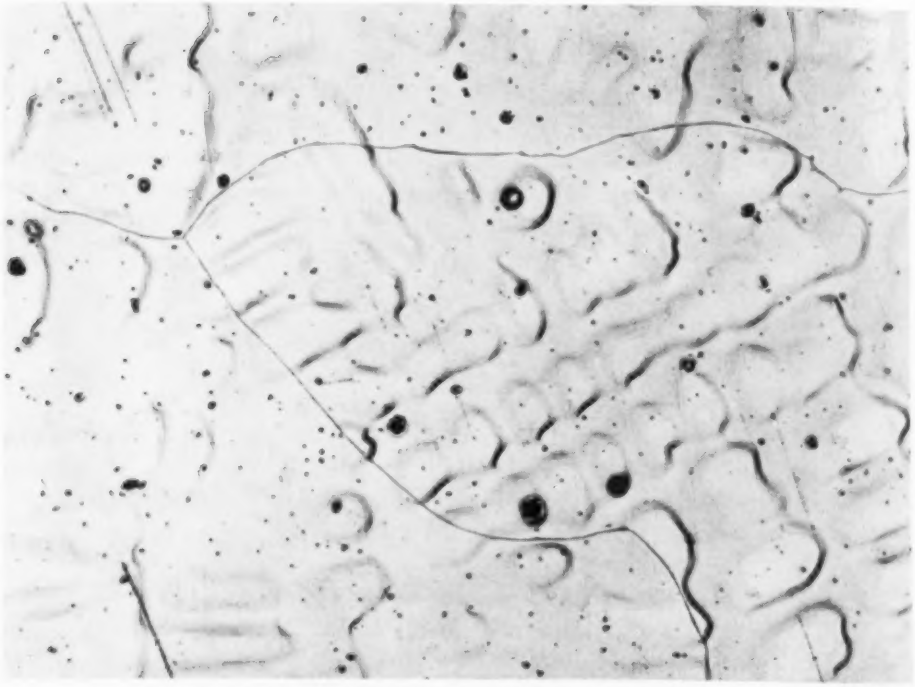


Fig. 3—Combined Micro and Autoradiographic Structure of a Polished and Etched Specimen from a Furnace-cooled Sample. In the above and following photomicrographs the concentration of radioactivity is shown as irregular dark areas. ×100.



Fig. 4—Same as Fig. 3 at a Higher Magnification. ×250.

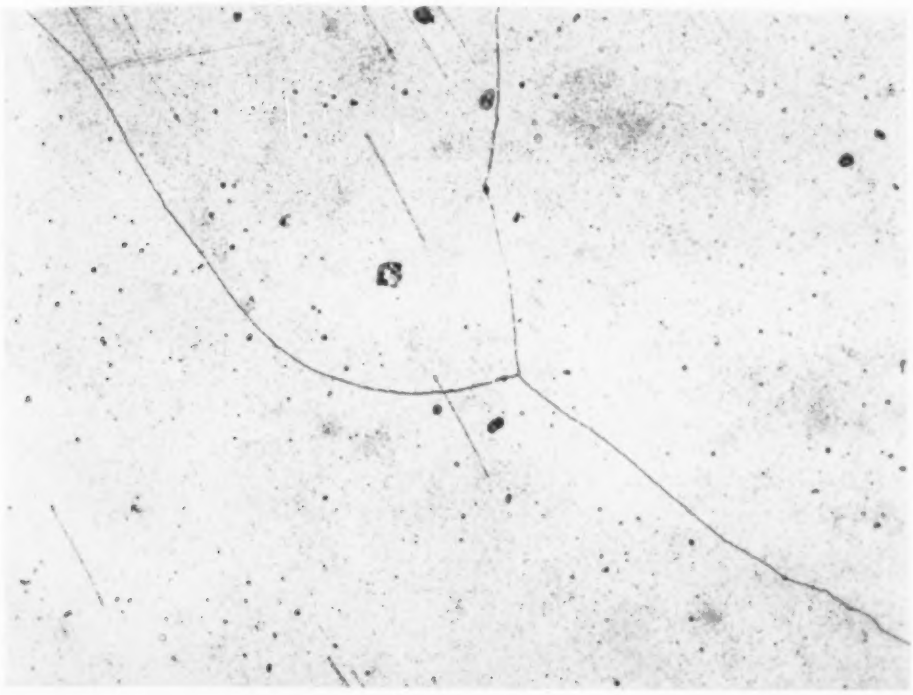


Fig. 5—Combined Micro and Autoradiographic Structure of Specimen Annealed for 24 Hours in Air at 2400°F. ×100.

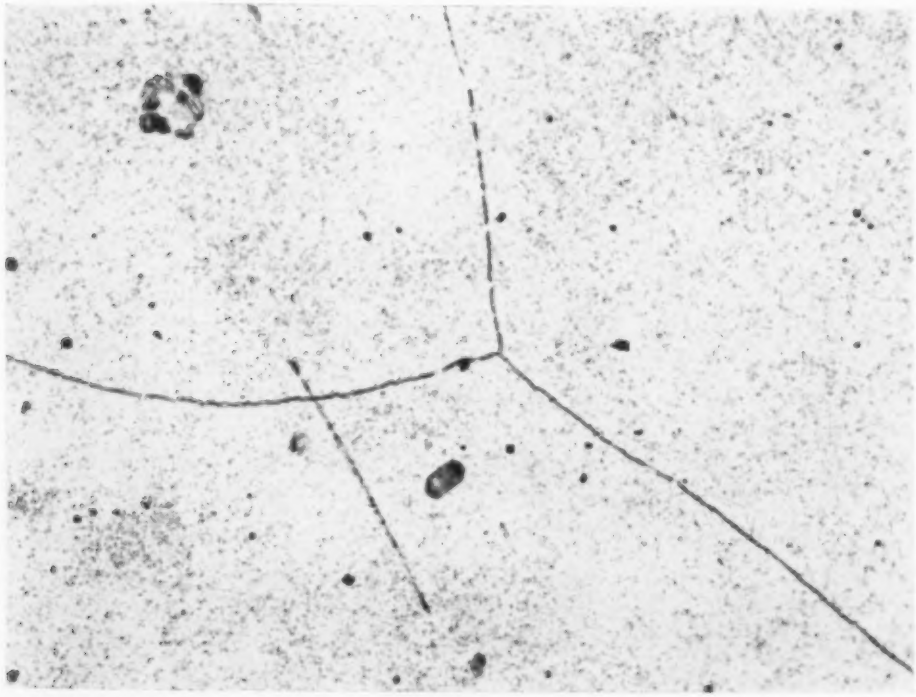


Fig. 6—Combined Micro and Autoradiographic Structure of Specimen Annealed for 24 Hours at 2400°F. ×250.

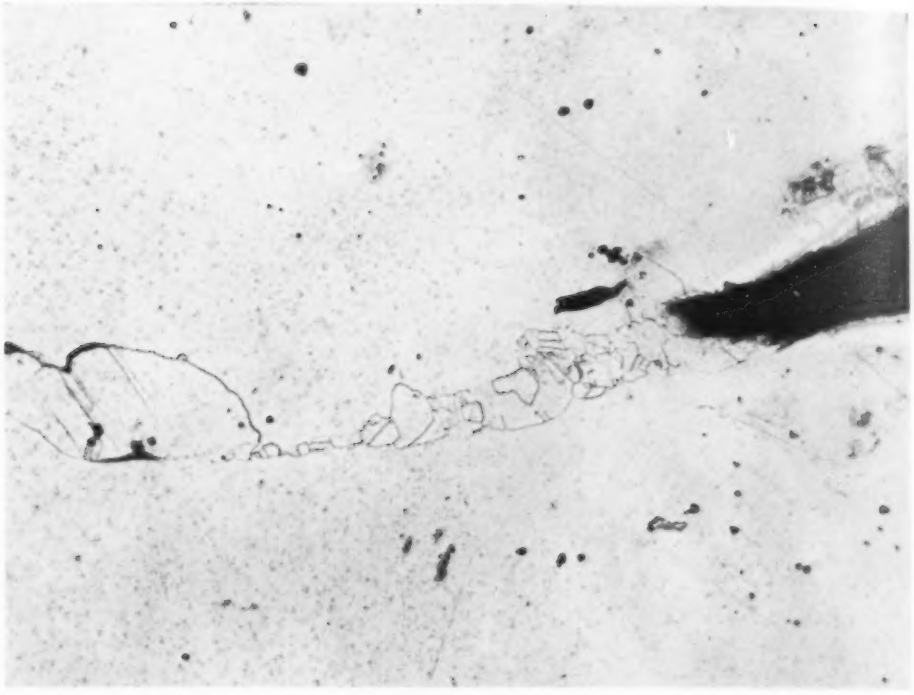


Fig. 7—Outside Area of Forged Specimen (Note Incipient Crack). ×250.

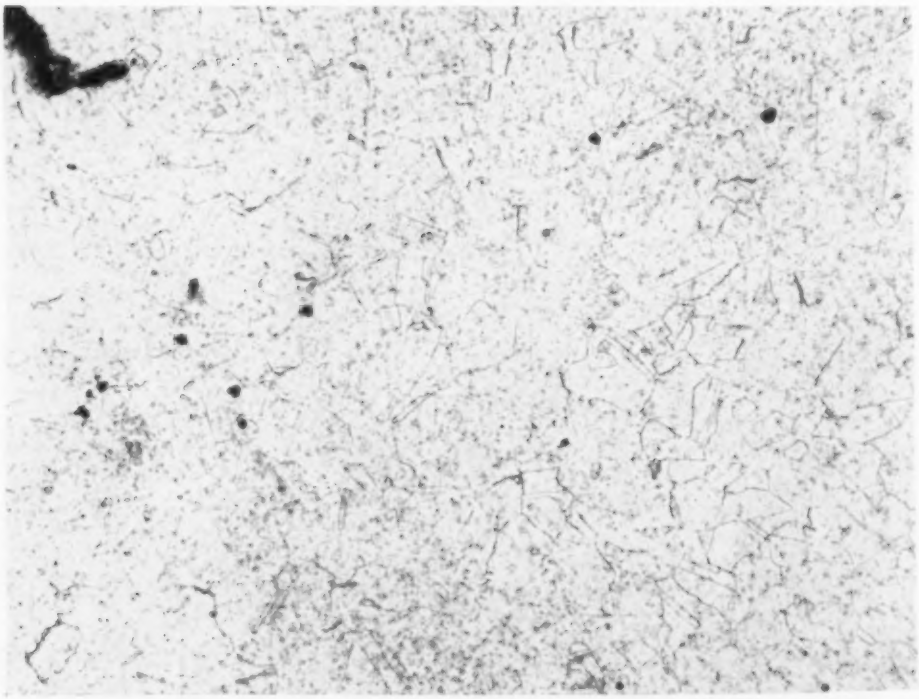


Fig. 8—Center Area of Combined Structure of Forged Specimen. ×250.

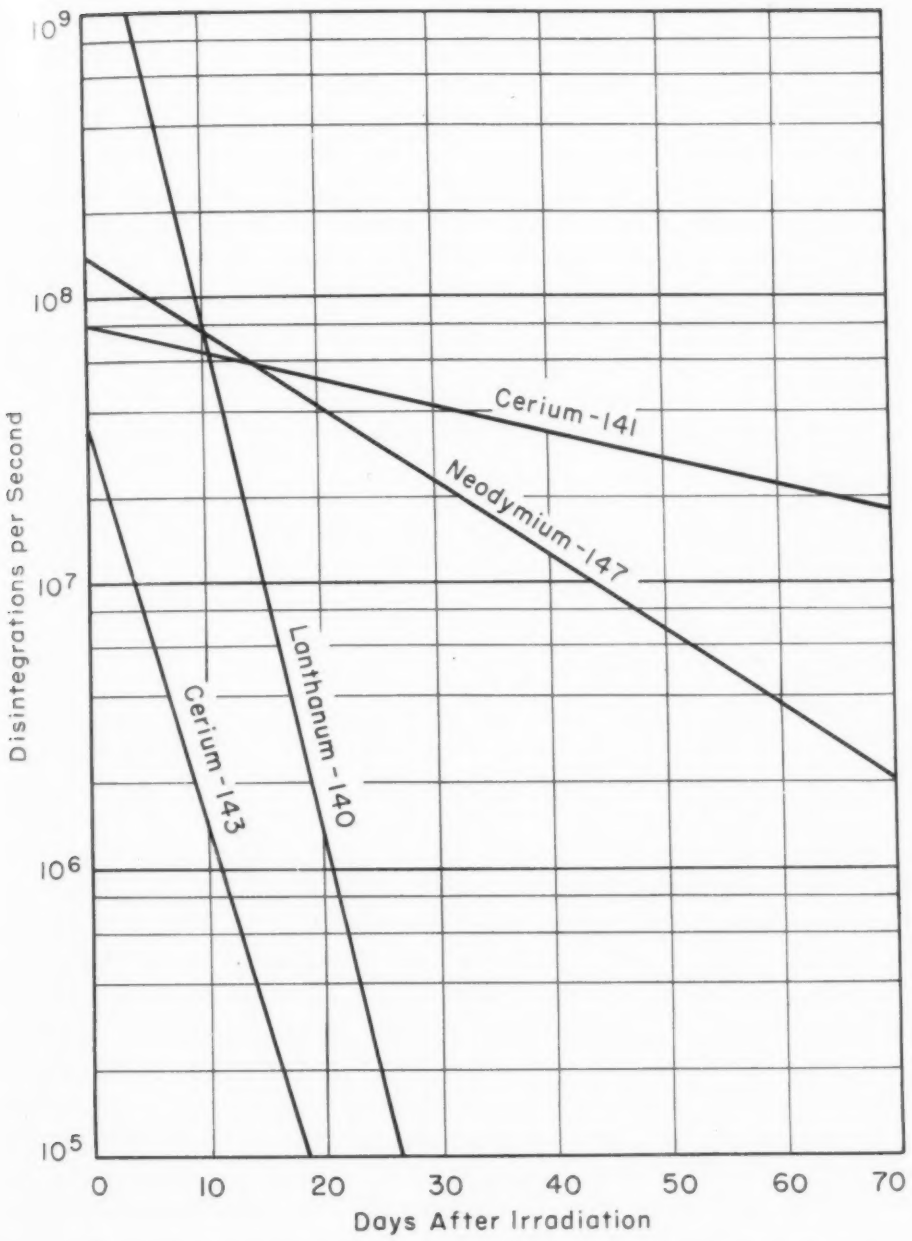


Fig. 9—Radioactive Decay Curves for the Longer Lived Beta Emitting Radioisotopes Produced During Neutron Bombardment of Misch Metal.

tended to homogenize the interdendritic concentrations of cerium-141 and neodymium-147. The dark concentration lines present in Fig. 3 are not found in Fig. 5. A slightly longer development time for the autoradiograph resulted in larger silver grains than those appearing in Figs. 3 and 4. Figs. 7 and 8 show the areas at the edge and near the center of the forged sample B which are not related to the respective edge and center areas of the as-solidified ingot. As

mentioned previously, the forged samples showed some slight cracking in the final states of reduction. Fig. 7 shows the structure surrounding a small crack at the outer edge of the forged specimen. This fracture appears to follow a grain boundary. Of more interest in the current study is the gradual transition from a light concentration of radioactivity at the outer edge of the specimen (right-hand edge of Fig. 7) to a fairly dense concentration at the center of the specimen (center of Fig. 8). The reason for this decrease in activity at the outer edge is not clear. The specimen shown in Figs. 5 and 6 was held at the forging temperature (2400°F) for 24 hours without showing any evidence of outward diffusion of the radioactive constituents. Thus, it does not appear that the change in concentration can be attributed solely to the thermal treatment of the specimen.

It is of interest to note that the inclusions shown in the microstructure of all specimens do not show any evidence of radioactivity in the autoradiographs. If there had been any segregation of radioactive cerium-141 and neodymium-147 at these inclusions, there would have been a heavily exposed area of the autoradiograph centered over them. This would be caused by the much higher concentration of radioactivity per unit volume around the inclusions. This is not contrary to the findings of other investigators (4), but indicates that neither neodymium nor cerium segregates at these inclusions.

Other considerations that may prompt questions concerning the validity of the present findings include the use of a split addition and correlation of the experimental method with industrial practice. With regard to the split addition, the possibility is recognized that the first addition of misch metal may have combined or reacted with any of the tramp elements present and, in so doing, would take up unknown locations within the matrix. Under such conditions, the later addition of radioactive misch metal could merely have proved to be an excess that went into solution in the steel. This aspect will be further explored in future work.

With regard to the correlation of the experimental methods with industrial practices, it was not the intention to reproduce production technology. The melt was allowed to solidify in the furnace as a means for producing a large grain size with the thought in mind that such a structure would afford a more direct correlation with behavior during forging than would a fine-grained structure.

The results of the work to date indicate that additions of radioactive misch metal are uniformly distributed throughout the matrix of a 25% nickel, 20% chromium melt. Examination of the various samples by means of a combined metallographic-autoradiographic technique showed some slight concentration of radioactivity in the

interdendritic zones of the as-slow-cooled sample. Further, the forged specimens showed some variation in the degree of concentration between the outer and center sections of the sample.

The future work will be directed to a further study of the effect of misch metal on the hot working properties of austenitic stainless steels. In this work, elements known to have a harmful effect on the hot working properties of the matrix will be added as radioactive isotopes. Additions of misch metal will then be made to portions of the heats to study whether such additions have any effect on the distribution and form of the impurities present.

Acknowledgments

The authors gratefully acknowledge the sponsorship of this research by the Mallinckrodt Chemical Works and wish to thank them for permission to publish the results of this work. In addition, the authors wish to express their appreciation to various divisions and personnel at Battelle Memorial Institute and the Mallinckrodt Chemical Works for their cooperation during this study. The assistance and critical comments of Mr. R. B. Fischer, Chief, Physical Metallurgy Division, and Mr. G. D. Calkins, Chief, Radioisotope and Radiation Division, of Battelle Memorial Institute, were most helpful during the course of this work.

References

1. H. Yagoda, *Radioactive Measurements With Nuclear Emulsions*, 1949.
2. H. J. Gomberg, "High Resolution Autoradiography for Study of Grain Boundaries in Metals," Engineering Research Institute, University of Michigan, No. 2029-1-F, February 1954.
3. E. Bleuler and G. J. Goldsmith, *Experimental Nucleonics*, 1952, published by Rinehart and Company, Inc.
4. R. H. Henke and R. A. Lula, "Rare Earths Counteract Hot Rolling Defects in Stainless Steel," *Journal of Metals*, Vol. 6, 1954, p. 883.

DISCUSSION

Written Discussion: By D. J. Dilworth, Jr., director of metallurgy and E. A. March, chief metallurgist, Crucible Steel Company of America, Pittsburgh.

The experimental technique used in this paper represents one which shows great promise as a means of giving assurance in the solution of problems of a complex nature both in the laboratory and in production. We are quite interested in this technique but have had no direct experience with it. We have, however, studied the effect of rare earth additions to steels.

In using misch metal one of our primary causes for concern has been the fact that there have been occasions when nonmetallic inclusions were found to an abnormal degree in the material treated. Two theories have been postulated as to the mode of formation of these inclusions.—

1. The first rare earth material added, being very reactive, forms nonmetallic compounds with the residual amount being effective through some other mechanism.

2. The second theory indicates that it is mainly the quantity of misch metal in excess of that required to improve hot workability which is entrapped in the form of nonmetallics. This work tends to confirm the first theory but does not firmly establish the facts since the inclusion shown has the appearance of those sometimes found in steels deoxidized with calcium silicon. Perhaps the authors can further describe the constitution of the inclusions found.

It seems that the irradiated portion of the rare earth addition represented somewhat less than 10% of the total addition. It would be of interest to know if the recovery of the second addition was of the same order as the total recovery. This might provide a further clue as to the action of each of the two additions.

In spite of considerable work done by many organizations, there is no universally accepted method of determining whether or not a rare earth addition to steel has been effective except to determine the effect of this addition on hot workability. Therefore, it would seem of some interest to also include in this work a comparison of the forgeability of the cone test ingots before and after the addition to insure that the normally expected reactions were actually obtained. We would also like a comment from the authors as to the cracks which developed during the forging of the 1-inch cube. Are these indicative of the hot workability having been improved or not?

We are quite interested in the future work proposed by the authors. There is a dearth of information concerning the mechanism through which rare earth additions improve hot workability. Any contribution to our knowledge on this subject would be very welcome. Now that the authors have ably demonstrated the applicability of tracer techniques to this problem, the work which they propose should be of definite value. In this connection it might be well to account for the 78% of the rare earth material not recovered. It might be possible to show that the rare earth material not recovered was as effective in accomplishing the end result as was that which was recovered.

It might also be possible through the identification of the rare earth compounds formed, to better define the action which has taken place.

Authors' Reply

The authors appreciate the comments offered by Messrs. Dilworth and March.

Throughout the course of extensive research on the effects of rare earth additions to stainless steel, we have attempted to establish the identity of the inclusions. However, except for modification of the sulphide inclusions of various types, it has not been possible to positively identify other forms of inclusions associated with or attributed to rare earth additions in the present work.

With regard to the recovery of the second addition, our experience has shown a nominal recovery of approximately 20% of the misch-metal addition. Thus, the initial addition of 0.51% could result in a residual rare earth content of about 0.12%. At the same rate of recovery, the further addition of 0.05% radioactive misch-metal would result in an increase in the residual rare earth contents of about 0.01%. To compare the difference between the rare earth contents after the first and the second additions would amount to comparing residual contents of 0.12% and 0.13% for an estimated 20% recovery of rare earths. There was some question whether the analytical procedures could accurately detect this small difference with sufficient accuracy. However, the authors

agree that it would be of interest to know what portion of the second addition was recovered.

In reply to the question regarding the effect of the initial addition on forgeability, only single forge test cones were poured before and after the misch-metal addition. While the forged cube taken from the metal which was allowed to solidify in the furnace showed two small cracks after forging, the limited number of samples did not appear sufficient to justify any conclusion regarding the effect of such additions on the forgeability of the base alloy.

INHIBITION BY NITROGEN OF GRAPHITIZATION IN STEEL

By G. V. Smith and B. W. Royle

Abstract

Graphitization, during an arbitrary heat treatment known to promote it, was inhibited in 8 heats of cold-rolled, high-carbon, steel strip, by prior heating in an atmosphere of nitrogen for 6 hours at 1900°F, which increased the nitrogen content from a level of about 0.005 to about 0.013%. Heating in hydrogen for 2 hours at 1900°F, on the other hand, reduced the nitrogen content to about 0.003% and increased graphitization. (ASM-SLA Classification: N8, CN)

PREVIOUS work(1),(2)[1] has shown that the introduction of nitrogen into bar samples of eutectoid carbon steel, by heating in an atmosphere of gaseous nitrogen, caused a surface rim in which the carbide phase was resistant to graphitization during heating of initially martensitic material for 10 days at 1200°F.

Among the possible applications of this discovery is that of preventing the graphitization that has been observed sporadically in the processing of various commercial articles from cold-rolled, high carbon steel strip. Consequently, samples of eight such steels were obtained, austenitized either in helium or nitrogen for 6 hours at 1900°F, quenched to form a martensitic microstructure (most susceptible to graphitization 1-3) and heated for 10 days at 1200°F under vacuum. As an adjunct to the investigation, samples of the steels were also austenitized for 2 hours in hydrogen, before quenching and heating at 1200°F, to test previously reported observations(4) that hydrogen inhibits graphitization.

Materials and Procedure

The chemical composition of the steels employed in the program is given in Table I. The analyses for nitrogen and aluminum (soluble in 1:1 HCl in either case) represent check determinations. The hot-rolled samples, as received, had a thickness of about 0.10

[1]The figures appearing in parentheses pertain to the references appended to this paper.

A paper presented before The Thirty-Seventh Annual Convention of the Society, held in Philadelphia, October 17–21, 1955. Of the authors, G. V. Smith is Bard professor of metallurgical engineering, Cornell University, Ithaca, New York and B. W. Royle is with the American Steel and Wire Div., U. S. Steel Corp., Cleveland. The authors were formerly associated with the Fundamental Research Laboratory, U. S. Steel Corp., Kearny, New Jersey, where the investigation was performed. Manuscript received April 6, 1955.

Table I
Identification of Test Steels

Code	Heat No.	C	Mn	Si	Cr	Al*	N*	P	S
1	27T009	1.26	0.36	0.18	0.25	0.015	0.005	0.008	0.025
2	25C660	1.23	0.35	0.18	0.27	0.014	0.004	0.015	0.022
3	21C604	1.31	0.40	0.23	0.40	0.007	0.005	0.007	0.026
4	38D530	1.24	0.43	0.26	0.28	0.012	0.005	0.015	0.027
5	22C457	1.28	0.41	0.22	0.32	0.014	0.005	0.010	0.026
6	22T565	1.19	0.42	0.20	0.32	0.022	0.006	0.008	0.028
7	21C603	1.23	0.39	0.19	0.35	0.008	0.005	0.006	0.024
8	21C606	1.22	0.43	0.24	0.29	0.008	0.005	0.008	0.024

*Acid soluble in 1:1 HCl.

inches; a variable small amount of surface metal was removed in hand grinding before heat treatment.

One lot of samples of the steels was heated in purified helium, and another lot in purified nitrogen, for 6 hours at 1900°F. Both lots were quenched in brine. Purification of the gases was effected by passage over heated copper and then through activated alumina. Another set of samples was heated in purified hydrogen for 2 hours at 1900°F and brine quenched; purification was effected in the same train used for the helium or nitrogen with the addition of passage over heated magnesium turnings. Microscopic examination showed all quenched samples to be completely martensitic, the structure known from previous experience to be most easily graphitized. The three lots of samples were then separately sealed in Vycor under vacuum, and heated for 10 days at 1200°F.

Results and Discussion

The results of the investigation are summarized in Figs. 1, 2 and 3, which show the microstructural appearances of the whole cross sections of the samples.

All of the steels heated in helium graphitized to some extent with the exception of Steel No. 5. Except for this steel, the quantity of graphite is roughly proportional to the aluminum content.

None of the steels heated in nitrogen graphitized, with the exception of Steel No. 1, which showed a trace of this phase. Samples of the steels which had been treated in nitrogen were analyzed chemically, with results, Table II, showing that the nitrogen con-

Table II
Nitrogen Content after Heating 6 Hours in Nitrogen at 1900°F

Code	% N*
1	0.014
2	0.014
3	0.014
4	0.012
5	0.014
6	0.014
7	0.013
8	0.013

*Acid soluble in 1:1 HCl.

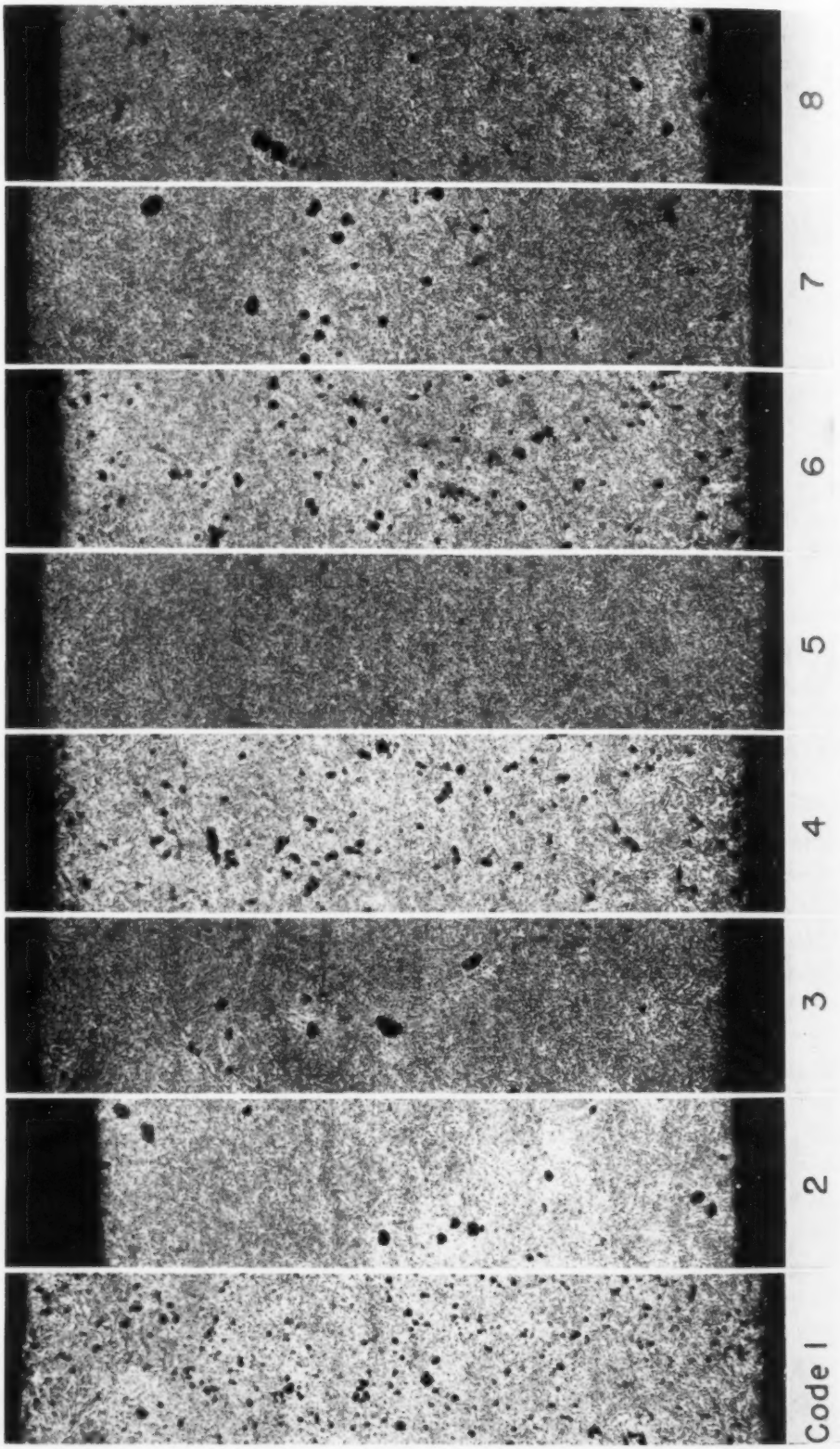


Fig. 1.—Microstructures After Austenitizing in Helium for 6 Hours at 1900°F, Quenching to Form Martensite, and Reheating 10 Days at 1200°F. Picral Etch X50.

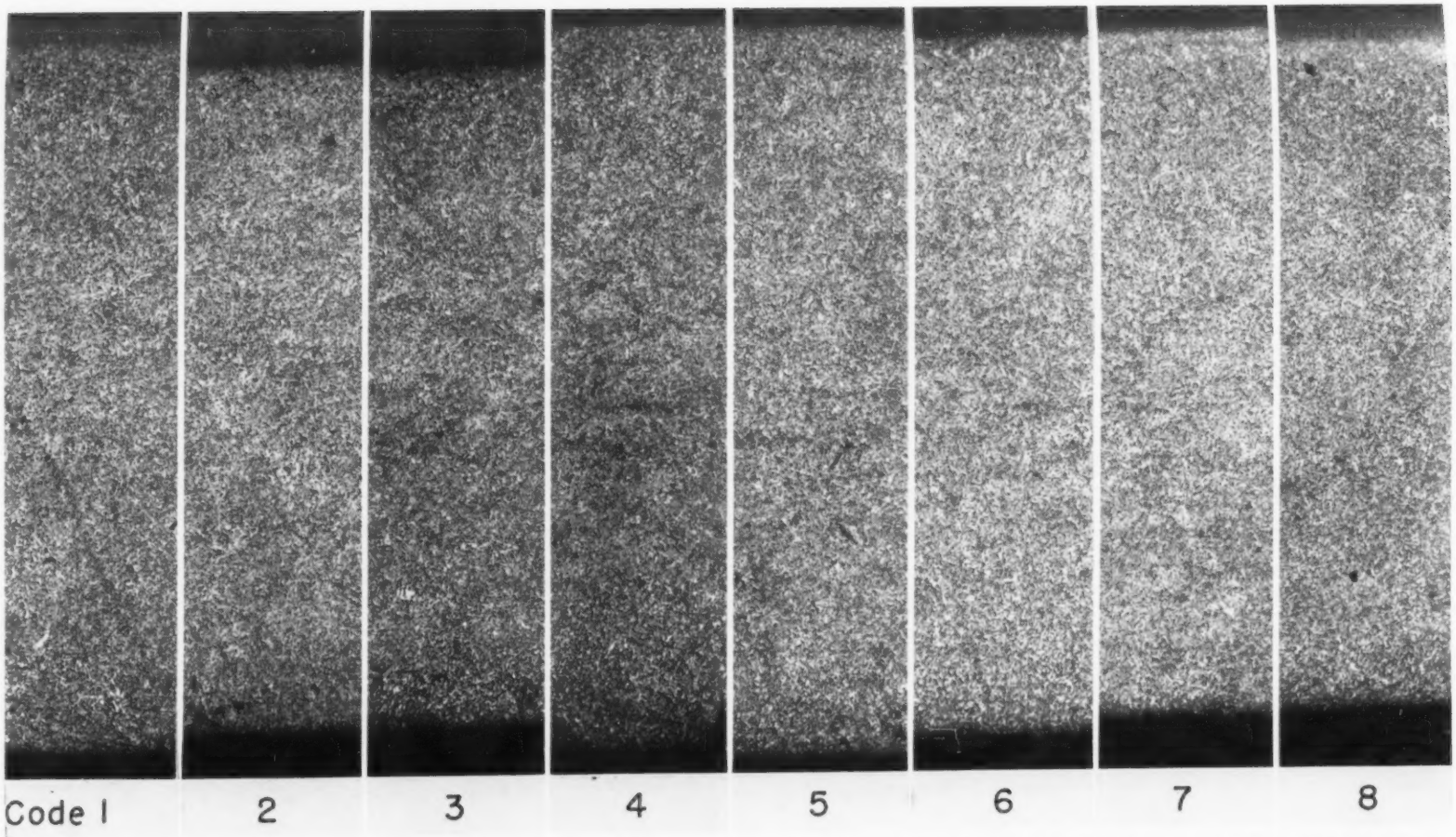


Fig. 2—Microstructures After Austenitizing in Nitrogen for 6 Hours at 1900°F, Quenching to Form Martensite, and Reheating 10 Days at 1200°F. Picral Etch X50.

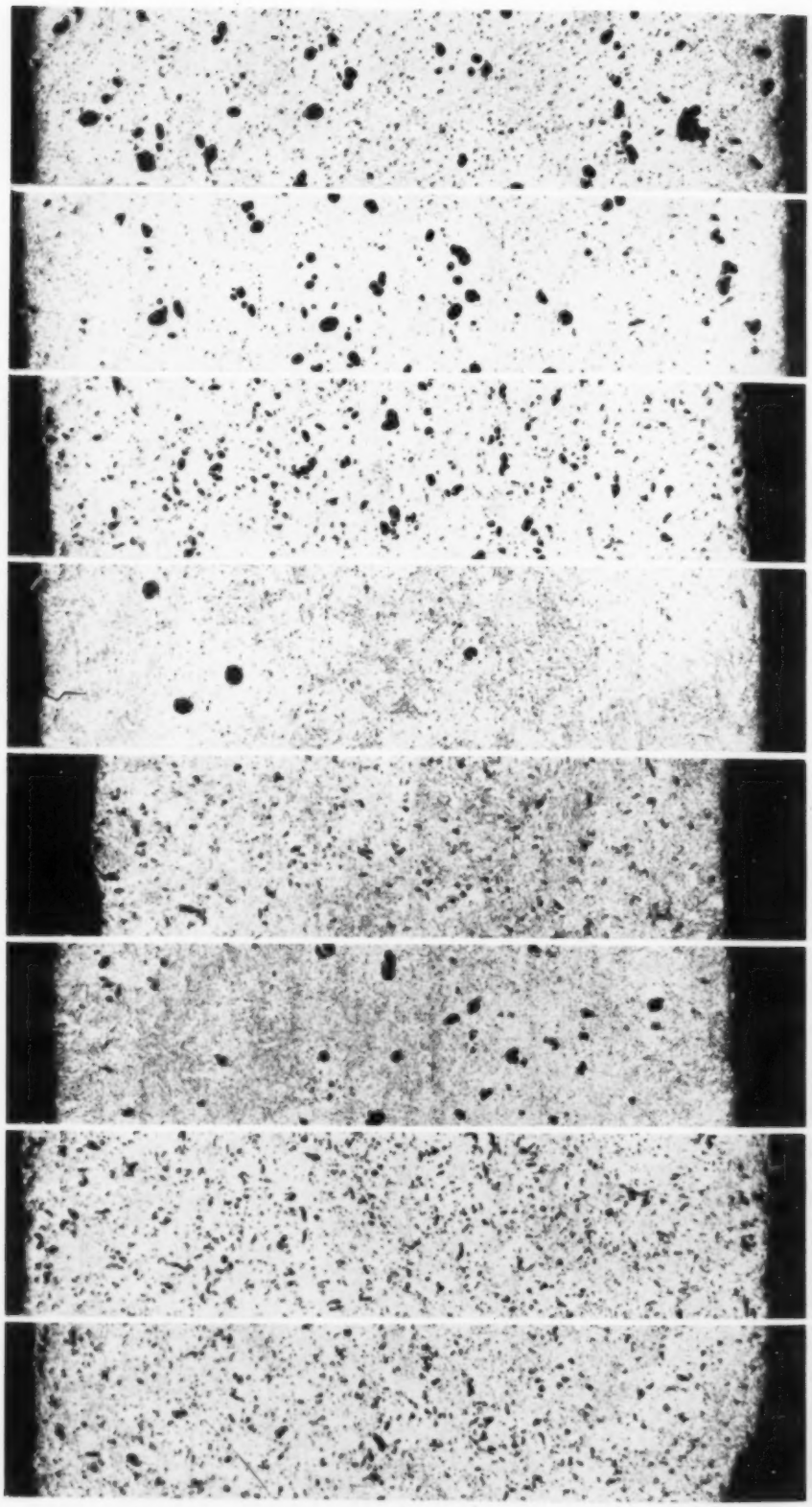


Fig. 3—Microstructures After Austenitizing in Hydrogen for 2 Hours at 1900°F, Quenching to Form Martensite, and Reheating 10 Days at 1200°F. Picral Etch X50.

tent had been increased to about 0.012-0.014% from an initial level of about 0.005%.

Whereas the graphitizing treatment employed in this study does not simulate the processing of certain commercial articles of these steels, it is the severest test that we have been able to devise (without employing plastic deformation) and it seems probable that steel resistant to graphitization in our experiments would not graphitize during commercial processing.

Heating in hydrogen for 2 hours at 1900°F resulted in appreciably more graphitization, Fig. 3, than was observed after heating in helium for 6 hours at 1900°F, when the samples were subsequently

Table III
Nitrogen Content after Heating 2 Hours in Hydrogen at 1900°F

Code	% N*
2	0.003
7	0.003
8	0.003

*Acid soluble in 1:1 HCl.

heated at 1200°F. Unless this difference can be attributed to the difference in time of austenitizing, which does not seem likely, our observations appear to contradict those that have been previously reported(4) for cast irons. Again, the quantity of graphite is roughly proportional to the aluminum content, with the exception of Steel No. 5. Chemical analysis of several of the steels, Table III, suggested that heating in hydrogen had increased susceptibility to graphitization by lowering the nitrogen content to 0.003 from about 0.005%.

Summary

All except one steel of those heated in helium developed graphite in some degree, Fig. 1, whereas graphitization was completely absent in those steels heated in nitrogen, except for one steel which showed a trace of this phase, Fig. 2. Chemical analysis showed that the nitrogen content of these resistant steels was on the order of 0.012 to 0.014%.

The results of the experiment involving heating in purified hydrogen, Fig. 3, showed that all steels graphitized, including the one that had not graphitized at all after heating in helium, and to a greater extent than after heating in helium. Thus, these results indicate that hydrogen promotes, rather than hinders, graphitization of these steels, unless, as seemed unlikely, the difference in behavior is accounted for by the difference in austenitizing times employed (2 hours in hydrogen, 6 in helium). Chemical analysis showed that heating in hydrogen had lowered nitrogen from the initial level of about 0.005 to 0.003 per cent. It seems possible, therefore,

that the increased susceptibility to graphitization that results from heating in hydrogen may be an indirect effect of the simultaneous lowering of nitrogen.

ACKNOWLEDGMENT

The samples were furnished by the American Steel and Wire Division, U. S. Steel Corporation.

References

1. G. V. Smith, J. A. MacMillan and E. J. Dulis, "Some Aspects of Graphitization in Steel," TRANSACTIONS, American Society for Metals, Vol. 43, 1951, p. 692.
2. E. J. Dulis and G. V. Smith, "Roles of Aluminum and Nitrogen in Graphitization," TRANSACTIONS, American Society for Metals, Vol. 46, 1954, p. 1318.
3. G. V. Smith, E. J. Dulis and B. W. Royle, "Effect of Pretreatment of Martensite on Subsequent Graphitization at 1200°F," Accepted for publication in Welding Journal Research Supplement.
4. F. Brown and M. F. Hawkes, "Effect of Hydrogen on Graphitization," *Transactions*, American Foundryman's Society, Vol. 60, 1952, p. 635.

DISCUSSION

Written Discussion: By Floyd Brown, head, Physical Metallurgy Branch, Metallurgy Division, Naval Research Laboratory, Washington, D. C.

In view of numerous observations that hydrogen in quantity inhibits graphitization in cast irons, some alternate explanation seems more desirable to account for the increased graphitization observed in the authors' hydrogen-treated specimens than to attribute the increase to a direct effect of hydrogen.

It was observed in reference (4) that when the atmosphere of hydrogen was replaced with helium, the inhibiting effect disappeared in a very few minutes even without vacuum treatment, and it is known also that hydrogen escapes rapidly from steel at room temperature, so that one should not be surprised to find that the hydrogen inhibition did not survive the quench and the vacuum sealing operations in the present investigation. We know that hydrogen will remove nitrogen from steel at high temperatures as HCN, and the authors find an approximately 40% reduction in nitrogen in their hydrogen-treated specimens; they also convincingly confirm the intrinsic graphitization-inhibiting effect of nitrogen.

The authors' alternative explanation therefore that the increased susceptibility to graphitization following hydrogen treatment simply reflects removal of nitrogen seems the preferred one.

Authors' Reply

We are pleased to have Dr. Brown's views, which confirm our own, regarding the reason for an increased susceptible to graphitization of the samples that we austenitized in hydrogen before graphitizing.

EFFECT OF TEMPERING TEMPERATURE ON STRESS-CORROSION CRACKING AND HYDROGEN EMBRITTLEMENT OF MARTENSITIC STAINLESS STEELS

By Peter Lillys and A. E. Nehrenberg

Abstract

Data on the susceptibility to cracking by stress corrosion and hydrogen embrittlement are reported for Types 410, 420, 422 and 436 stainless tempered at various temperatures in the range 300 to 1200° F. Beam type specimens were stressed by bending, generally well below the elastic limit, and were either exposed to 5% NaCl spray or were arranged as the cathode in a cell containing 0.1 N H_2SO_4+3 mg As/liter as the electrolyte.

The data indicate that a temper at about 500° F provides minimum susceptibility to cracking by hydrogen embrittlement for high levels of hardness. Maximum susceptibility to stress corrosion cracking and hydrogen embrittlement results from a temper at about 800 to 1000° F.

Delta ferrite minimizes the tendency for stress corrosion cracking by narrowing the range of tempering temperatures which produce susceptibility, and by interfering with crack propagation. (ASM-SLA Classification: R1, Q23, J29, SS)

Introduction

MANY metals and alloys are known to be susceptible to stress corrosion cracking, that is, cracking which is attributable to the combined action of a static tensile stress and a corroding environment. Generally, the stress involved in a stress corrosion failure is a residual stress resulting from cold forming, welding, or some other processing operation, but external tensile stresses encountered in service may also contribute to this type of failure.

Franks, Binder and Brown (1)[1] have suggested that a "limiting" or "threshold" stress must be exceeded before stress corrosion cracking will occur. The magnitude of this stress may be considerably less than the yield strength.

A variety of environments have been found to promote stress corrosion cracking (2). In general, these environments are not partic-

[1]The figures appearing in parentheses pertain to the references appended to this paper.

A paper presented before the Thirty-Seventh Annual Convention of the Society, held in Philadelphia, October 17–21, 1955. Of the authors, Peter Lillys is research metallurgist and A. E. Nehrenberg is supervisor of the Research Laboratory, Crucible Steel Company of America, Pittsburgh. Manuscript received May 31, 1955.

ularly corrosive. Stress corrosion has not been observed in environments which are severely corrosive and thus produce a rapid, over-all-attack. In the case of the austenitic stainless steels it is generally believed that environments containing chlorides are required, but some failures have been reported in media which contained no chlorides (2).

The cracking which is observed progresses in a direction which is approximately normal to that of the residual or applied tensile stress and may or may not be intergranular in character (3,4). The precipitation of a phase at grain boundaries, such as chromium carbide in the case of the austenitic stainless steels, or $CuAl_2$ in the case of aluminum-copper solid solution alloys, provides grain boundary zones which may be anodic with respect to the grains themselves in a particular environment so that localized corrosion can proceed along the grain boundaries. Such precipitation does not necessarily promote intergranular stress corrosion cracking, however. Transgranular stress corrosion cracking has been observed in spite of the presence of grain boundary precipitation (2,5,6). Conversely, in high purity lead and high purity aluminum intergranular stress corrosion cracking has been observed although there is no evidence of precipitation in the grain boundaries (7). Inasmuch as freedom from both intergranular and transgranular stress corrosion cracking can be readily obtained by employing an electric current for cathodic protection, it seems reasonable to conclude that stress corrosion cracking involves an electro-chemical mechanism (3,7,8). This mechanism seems applicable to the austenitic stainless steels and many nonferrous metals and alloys.

In the case of the hardenable stainless steels, such as the 12% Cr martensitic stainless steels, a different mechanism has been proposed to explain stress corrosion cracking. Uhlig (9) has demonstrated that failure of such a steel by cracking is accelerated, rather than prevented, by making it the cathode in an electrochemical cell. When coupled with anodic aluminum in a 3% NaCl solution, a 12.5% Cr stainless steel was observed to crack overnight, for example. Inasmuch as hydrogen is discharged at the surface of the steel when it is the cathode, Uhlig has suggested that this type of failure is more properly the consequence of "hydrogen embrittlement."

Cracking of 12% Cr martensitic stainless steels, as well as other high strength steels, has been observed when these steels are exposed to an aqueous solution of hydrogen sulphide. Under such conditions hydrogen is generated by the corrosion reaction, but there is lack of agreement concerning the role played by hydrogen. Fraser and Treseder (10) consider that failures in hydrogen sulphide solution are stress corrosion failures and that the hydrogen produces additional localized stress which accelerates the rate of crack propagation

through the metal. Others argue that the failures observed are the result of "hydrogen embrittlement" (11,12,13).

Evidently, more work is required to establish more definitely the exact nature of the mechanism responsible for the cracking of stressed martensitic stainless steels in various corroding media. Also, the effect of tempering temperature on the susceptibility of stressed 12% Cr steels to failure in mildly corroding environments appears not to have been thoroughly investigated although Badger (14) and Thielemann and his associates (15) have published some data which are pertinent. In view of the commercial importance of martensitic stainless steels, it seemed desirable to evaluate the effect of tempering temperature on the susceptibility of these steels to stress corrosion cracking or cracking by hydrogen embrittlement. It was hoped also that such an investigation would furnish data which would be useful in providing a better understanding of the mechanisms by which these steels fail by cracking when exposed in the stressed condition to a mildly corrosive medium.

Material

During the course of this investigation a considerable number of commercial heats of Types 410, 420, 422 and 436 stainless were studied. The analyses of two or three representative heats of each of these types of hardenable stainless steel are shown in Table I. All of the steels were obtained in the form of hot rolled bars of various sizes. These bars were forged to rectangular bars 5/8 inch x 1/4 inch, a convenient size for the specimens which were to be used for this investigation. The bars were annealed by a subcritical temper to soften them adequately for easy machining.

Procedure

The test procedure employed during the early stages of this investigation was the same as that described by Scheil (4). Test

Table I
Compositions of Representative Steels

Steel	Type	C	Mn	Si	Ni	Cr	V	W	Mo
A1	410	0.10	0.50	0.33	0.44	12.60	—	—	0.27
A2	410	0.08	0.47	0.38	0.36	12.26	—	—	0.28
A3	410	0.09	0.39	0.54	0.37	13.14	—	—	0.28
B1	422	0.23	0.87	0.14	0.70	13.16	0.25	1.02	1.01
B2	422	0.20	0.79	0.44	0.76	12.89	0.31	1.05	1.26
B3	422	0.19	0.83	0.28	0.73	13.13	0.34	1.11	1.03
*C1	420	0.34	0.42	0.34	—	14.82	—	—	—
C2	420	0.18	0.45	0.37	—	13.15	—	—	—
D1	436	0.16	0.41	0.39	2.10	12.67	—	3.04	0.18
D2	436	0.15	0.34	0.38	2.03	13.39	—	3.22	0.12

*Chromium content is outside standard range 12.0/14.0

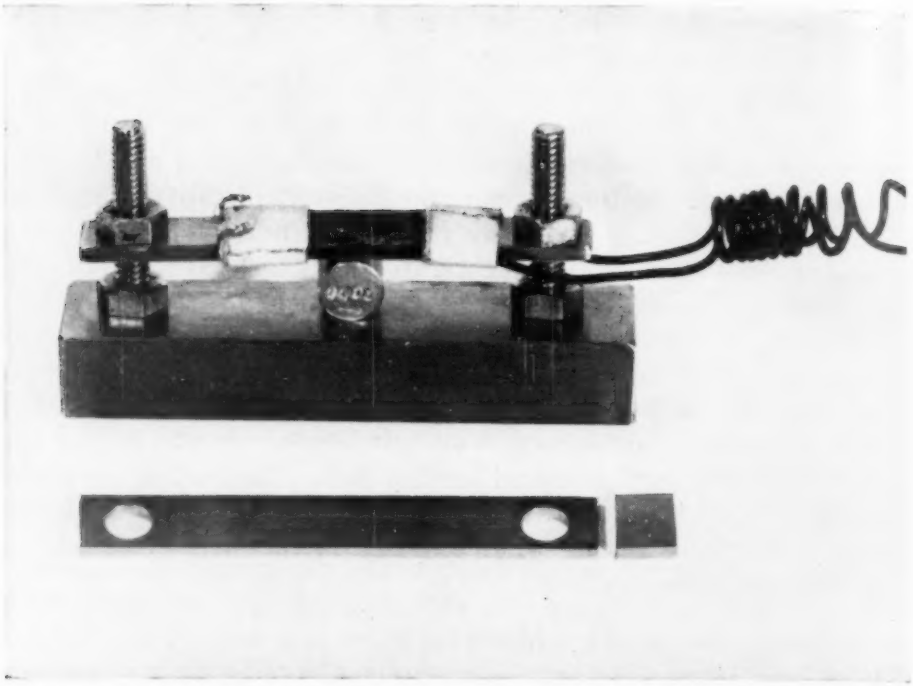


Fig. 1a—Stress Corrosion Test Assembly Showing Simple Beam with Single Point Loading. Type A-1 strain gage mounted on test specimen. Test specimen with ½ inch section cut off one end for hardness measurements. In foreground.

specimens 0.500 x 0.125 x 4 inch were stressed by bending and the magnitude of the stress produced was measured by employing Type A-1 SR-4 resistance strain gages. These strain gages have a gage length of 13/16ths of an inch. Thus, the measured stress is the average stress over this gage length. The test assembly is illustrated by Fig. 1a.

After the test specimens were bent to obtain the desired stress level the strain gages were removed, the test assembly was washed thoroughly in soap and water, dried in alcohol and degreased in carbon tetrachloride vapor. Most of the assembly was then coated with paraffin wax to minimize contact corrosion and to prevent corrosion of the specimen holder. Only the outer surface opposite the fulcrum where the fiber stress was a maximum was left exposed. The total length of this exposed surface was about 1 inch.

This test assembly was then placed in a salt spray cabinet and exposed to an atmosphere of 5% NaCl until failure occurred, or until 75 days had elapsed without failure.

A specimen was considered to have failed when visible cracking or actual fracture was observed. In the case of the specimens most susceptible to stress corrosion cracking, it was found that the rate of crack propagation was very high with the result that the times for appearance of visible cracking and for fracture were nearly the same.

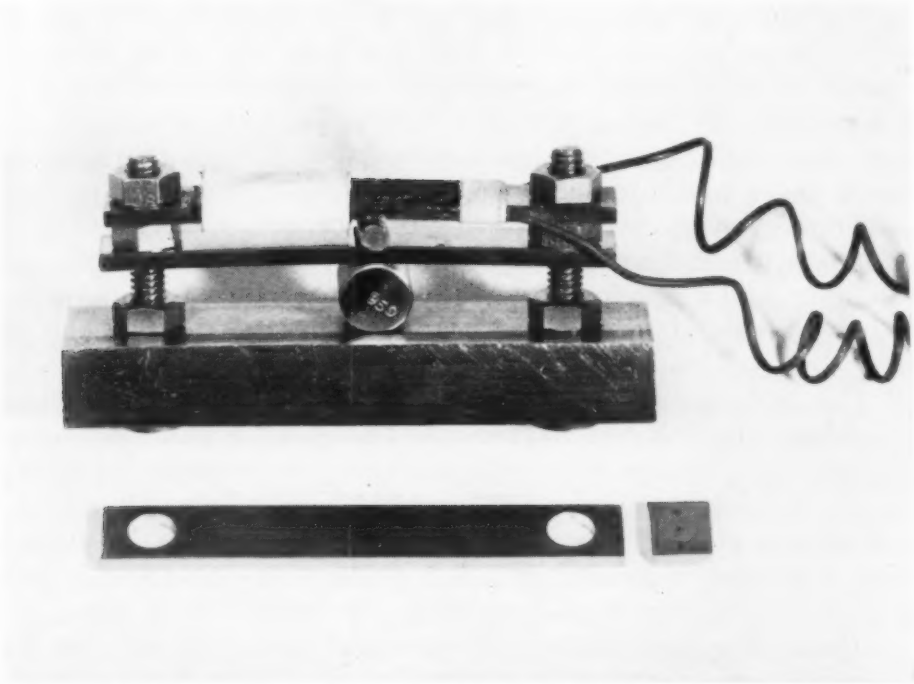


Fig. 1b—Stress Corrosion Test Assembly Illustrating Modified Procedure. Stress is determined on test specimen (bottom) by means of dummy specimen (top) on which a Type A-1 strain gage is mounted. The two nuts separating specimens are 0.200 inches thick. Fulcrum is 0.200 inch in diameter.

In the case of the specimens less susceptible to stress corrosion cracking the rate of crack propagation was much less rapid. Each specimen was examined daily for evidence of cracking except on weekends.

The mounting of strain gages on each test specimen was found to be time consuming. Inasmuch as several hundred specimens were to be tested during the course of this investigation, it seemed desirable to try to simplify this procedure. It was found that the procedure illustrated by Fig. 1b could be used to eliminate the necessity for mounting strain gages on each test specimen. This simply involves bending a dummy specimen on which a strain gage is mounted the same amount as the test specimen. Under these conditions, the stress measured in the dummy specimen is the same as that in the test specimen. This is accomplished by inserting two nuts and a fulcrum of the same thickness between the dummy and the test specimen as illustrated by Fig. 1b. Stress is applied to the test specimen as in the earlier procedure by turning the nuts in contact with it to produce bending. Then, the dummy specimen is brought tight against the two nuts separating it from the test specimen. Inasmuch as the dummy specimen and test specimen are then equidistant from each other the outer fiber stresses are the same. After the test piece is stressed in this way to the desired value, the dummy specimen is

removed and used again in stressing another specimen. This method was found to be reproducible within 2% in the range 70,000 to 100,000 psi. For stresses below 70,000 psi, the procedure described earlier was used. The fulcrum used for bending a particular test specimen was made from the same material and heat treated in the same manner as the test specimen.

The two methods of measuring the fiber stress described above and illustrated by Figs. 1a and 1b were checked occasionally against each other, and it was found that the time for failure for a particular level of stress and for a given heat treatment was essentially the same.

The test specimens employed in this investigation were machined from the annealed flats to 0.600 x 0.225 x 4 inch austenitized at appropriate temperatures, oil-quenched and tempered for 2 hours at temperatures in the range 300 to 1200°F. For Type 410 a 1 hour austenitizing at 1800°F was employed. For Type 420 the austenitizing treatment consisted of a 1 hour heating at 1850°F. Types 422 and 436 stainless were austenitized at 1900°F for 1 hour.

After being austenitized, oil-quenched and tempered, the test specimens were ground to final size, that is, 0.500 x 0.125 x 4 inch, and were abraded on dry belt grinders to obtain a #120 grit finish. Hardness measurements were made on a ½ inch length cut from each test piece as illustrated by Fig. 1. Some of the failed specimens were subjected to metallographic examination.

In order to evaluate the susceptibility of the hardenable stainless steels to hydrogen embrittlement, test specimens which were prepared and stressed as described above were immersed as the cathode in a solution of 0.1 normal sulphuric acid containing 3 mg of arsenic per liter of solution (16). The potential across the cell amounted to 3 volts and the current used was 0.6 ampere. The specimens were observed continuously while current was flowing through the cell and the time for failure by cracking was noted. When no failure was observed after 3 hours of exposure, the test specimen was removed from the assembly and immersed in a beaker of water at 200°F to produce effervescent bubbling as evidence that the specimen actually had absorbed hydrogen.

The stress levels employed for both the stress corrosion and hydrogen embrittlement studies were selected to lie in the vicinity of, or below, the elastic limit. It seemed desirable to avoid using stresses which would produce significant amounts of plastic deformation. The stress level used for the Type 410 specimens was 70,000 psi. For the higher strength steels, Types 420, 422 and 436, a stress of 100,000 psi was applied.

The amount of delta ferrite in the microstructures of some of the steels studied was evaluated quantitatively by lineal analysis (17).

Results

Effect of Tempering Temperature and Microstructure

Typical stress corrosion data for Types 410, 420, 422, and 436 stainless are summarized in Tables II, III, IV and V, respectively. The data indicate that each of these steels is most susceptible to stress corrosion cracking when it is tempered at about 900°F. Specimens in the as-quenched condition, those tempered at 700°F or less, and those tempered at temperatures of 1100°F or higher showed no evidence of failure after 75 days exposure to the salt atmosphere.

Also, the data indicate that the susceptibility to stress corrosion cracking is minimized when 5 to 10% delta ferrite is present. The data of Table II show, for example, that a heat of Type 410 stainless which contained no delta ferrite, steel A1, failed by stress corrosion cracking when it was tempered at temperatures of 800, 900, 950 and 1000°F. On the other hand, steels A2 and A3 which contained 5 and 10% delta ferrite respectively, failed only when a 900°F temper was employed. Furthermore, the time required for failure after a 900°F temper is much greater when 5 to 10% delta ferrite is present.

The data in Tables IV and V indicate that delta ferrite tends to minimize the susceptibility to stress corrosion cracking in Types 422 and 436 stainless also, but the effect of delta ferrite is not as great as was observed for Type 410.

Type 420 stainless contains no delta ferrite, and the data of Table III indicate that this steel, like Type 410, containing no delta ferrite, is susceptible to stress corrosion cracking after a temper at temperatures in the range 800 to 1000°F.

Many of the specimens which failed by stress corrosion cracking were examined metallographically to ascertain the nature of the cracking produced. It was found that the cracking was intergranular when a tempering temperature of 950 to 1100°F had been employed. Typical intergranular cracking in a steel containing no delta ferrite is illustrated by Fig. 2. Note in the upper left corner of the micrograph that there is evidence of precipitation in a prior austenite grain boundary. The minimum tempering temperature for evidence of grain boundary precipitation in the steels of this investigation was found to be 850°F. With increase in tempering temperature above 850°F precipitation at the former austenite grain boundaries became more prominent. After a 950°F temper there was an almost continuous network of grain boundary precipitation. The etching solutions employed for these examinations consisted of dilute concentrations of HCl in 5% picral. Such solutions are known to be particularly sensitive to carbide precipitation in steels of this general type (18).

When the tempering temperature is high enough, the steels become immune to stress corrosion. Specimens tempered at temperatures just below the minimum temperature for immunity to stress

Table II
Effect of Tempering on the Susceptibility of Type 410 to Stress Corrosion Cracking

All specimens were oil-quenched from 1800°F, tempered at indicated temperatures for 2 hours, stressed at 70,000 psi and tested in an atmosphere of 5% NaCl.

Tempering	Steel A1 0% Ferrite*			Steel A2 5% Ferrite			Steel A3 10% Ferrite		
		Time in Days			Time in Days			Time in Days	
Temperature	Rc	F*	NF**	Rc	F	NF	Rc	F	NF
700°F	40		75	38		75	39		75
			75			75			75
800°F	41	53		38		75	39		75
			75			75			75
900°F	42	6		40	50		39	30	
		9				75			75
950°F	41	11		39		75	38		75
		3				75			75
1000°F	34	11		34		75	34		75
		11				75			75
1050°F	28		75	27		75	27		75
			75			75			75

*This steel in the as-quenched condition and when tempered at 300; 400; 500 and 600°F did not fail in 75 days under the same testing conditions.
**F—Failure by cracking.
NF—No Failure; test discontinued.

Table III
Effect of Tempering on the Susceptibility of Type 420 to Stress Corrosion Cracking

All specimens were oil-quenched from 1850°F, tempered at indicated temperatures for 2 hours, stressed at 100,000 psi and tested in an atmosphere of 5% NaCl.

Tempering	Steel C1*			Steel C2*		
		Time in Days			Time in Days	
Temperature	Rc	F*	NF**	Rc	F	NF
700°F	50		75	45		75
800°F	50	4		46	13	
900°F	51	½		47	1	
1000°F	39	6		35	5	
1100°F	31		75	29		75

*These steels in the as-quenched condition and when tempered at 300; 400; 500 and 600°F did not fail in 75 days under the same testing conditions.
**F—Failure by cracking.
NF—No Failure; test discontinued.

Table IV
Effect of Tempering on the Susceptibility of Type 422 to Stress Corrosion Cracking

All specimens were oil-quenched from 1900°F, tempered at indicated temperatures for 2 hours, stressed at 100,000 psi and tested in an atmosphere of 5% NaCl.

Tempering	Steel B1 0% Ferrite			Steel B2 6% Ferrite			Steel B3 10% Ferrite		
		Time in Days			Time in Days			Time in Days	
Temperature	Rc	F*	NF*	Rc	F	NF	Rc	F	NF
700°F	47		75						
			75						
950°F	49	2		50	6		48	3	
		2			9			8	
1000°F	46	3		44	8		45	9	
		4			7			9	
1050°F	40	8		41		75	40		75
		9				75			75
1100°F	38	21		38		75	36		75
		32				75			75
1200°F	33		120						
			120						

*F—Failure.
NF—No Failure; test discontinued.

Table V
Effect of Tempering on the Susceptibility of Type 436 to Stress Corrosion Cracking

All specimens were oil-quenched from 1900°F, tempered at indicated temperatures for 2 hours, stressed at 100,000 psi and tested in an atmosphere of 5% NaCl.

Tempering Temperature	Steel D1 0% Ferrite Rc	Time in Days F*	NF*	Steel D2 5% Ferrite Rc	Time in Days F	NF
700°F	46		75	45		75
			75			75
900°F	47	5		47	11	
		3				75
1000°F	41	22		41		75
			75			75
1050°F	38		75	38		75
			75			75
1100°F	34		75	33		75
			75			75

*F—Failure.
NF—No Failure; test discontinued.

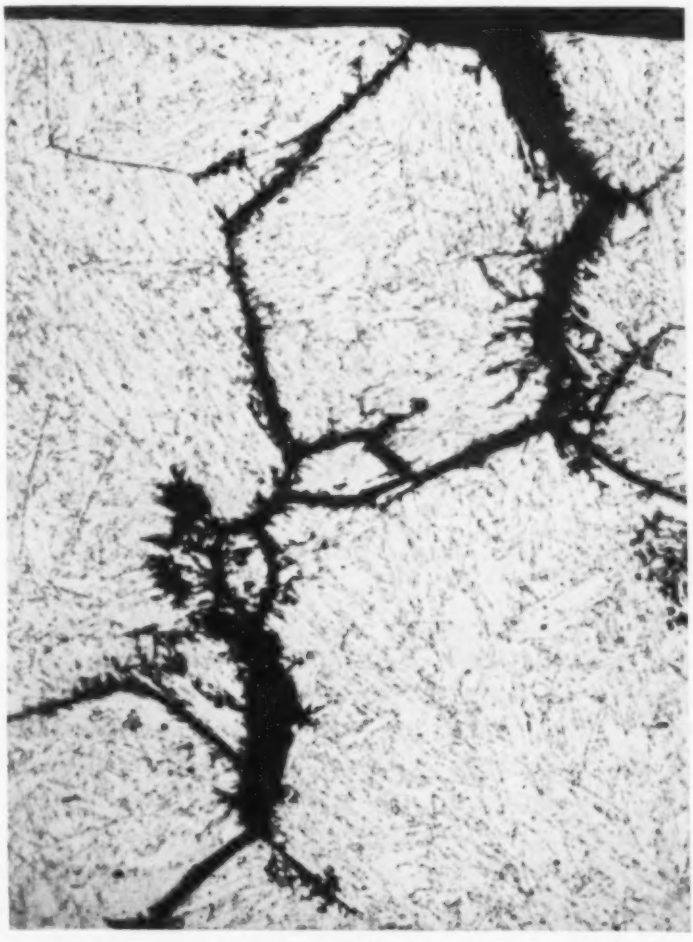


Fig. 2—Steel A1 (Type 410) Oil-Quenched from 1800°F and Tempered at 1000°F. Specimen stressed at 70,000 psi and tested in an atmosphere of 5% NaCl. Specimen failed in 11 days. Top of micrograph tension side. Etched in 5% picral + 0.5% HCl. ×500.

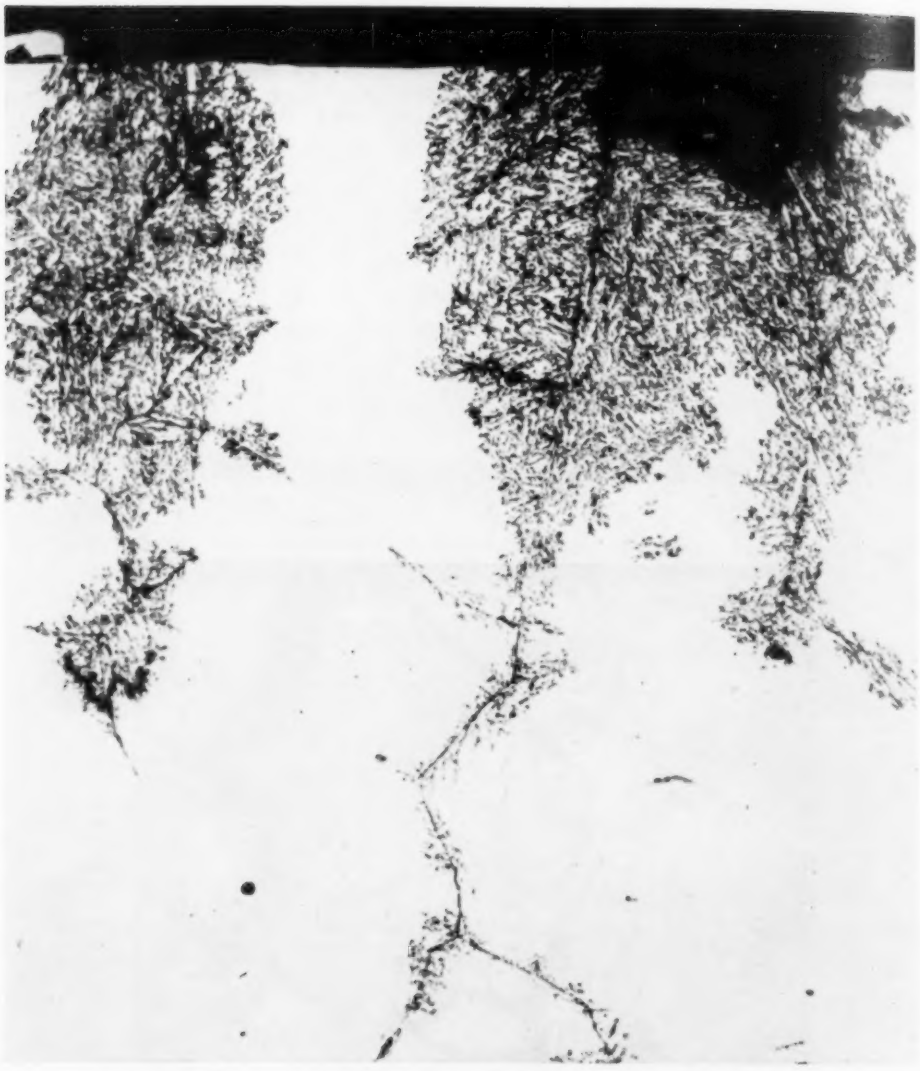


Fig. 3—Steel B1 (422 0% ferrite) Oil-Quenched from 2100°F to Produce Grain Coarsening. Tempered at 1100°F. Specimen stressed at 100,000 psi and tested in an atmosphere of 5% NaCl. Specimen failed in 15 days. Unetched. ×75.

corrosion cracking were found to exhibit general corrosion as well as intergranular cracking. This is illustrated by Fig. 3.

The cracking produced in the specimens tempered at 900°F was observed to be both intergranular and transgranular. The mode of cracking for the specimens tempered at 800°F could not readily be evaluated since the etchants employed did not adequately develop the grain boundaries and grain structure.

One effect of delta ferrite as mentioned previously is to restrict the range of tempering temperatures which promote stress corrosion cracking. Fig. 4 illustrates this effect. Type 422 containing no delta ferrite when tempered at 1050°F failed by intergranular cracking when stressed to the 100,000 psi level and exposed to the salt spray

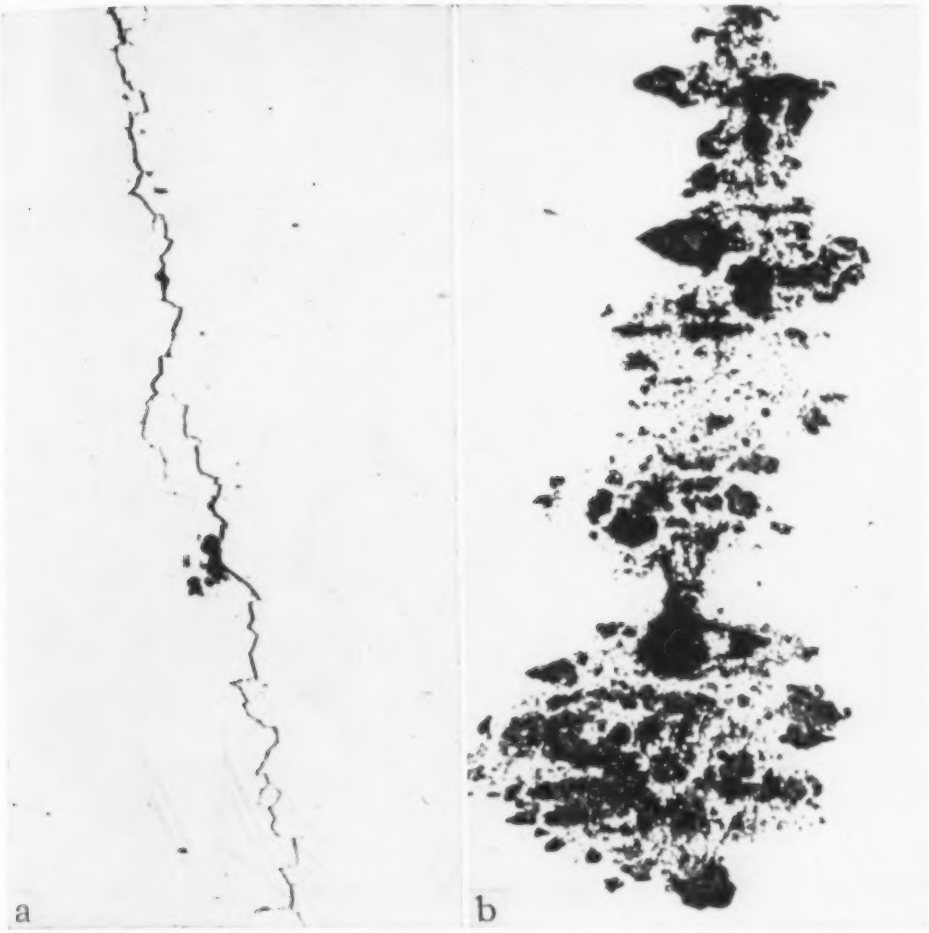


Fig. 4—Effect of Delta Ferrite on Stress Corrosion Cracking of Type 422. Specimens were austenitized at 1900°F, oil-quenched, tempered 2 hours at 1050°F, stressed to 100,000 psi and exposed to 5% NaCl spray. Top of photo micrograph is tension side. Unetched. ×75. (a) Steel B1 No Delta Ferrite Failed in 8 days; (b) Steel B3 10% Delta Ferrite No Failure after 75 days.

atmosphere. Type 422 stainless containing 10% delta ferrite did not fail when tempered at the same temperature and tested under the same conditions. Corrosion pits were observed, as Fig. 4b indicates, but there was no evidence of intergranular cracking.

It has also been mentioned that delta ferrite increases the time required for failure by stress corrosion cracking. Fig. 5 suggests an explanation for this observation. It appears that the ferrite interrupts crack propagation. Note that in several instances in this single micrograph cracking appears to have been stopped when a ferrite grain was encountered. Actually, the crack probably changes direction when it comes in contact with the delta ferrite. It would seem reasonable to expect that the rate of crack propagation would decrease when the crack deviates from the direction which is normal to the applied stress.

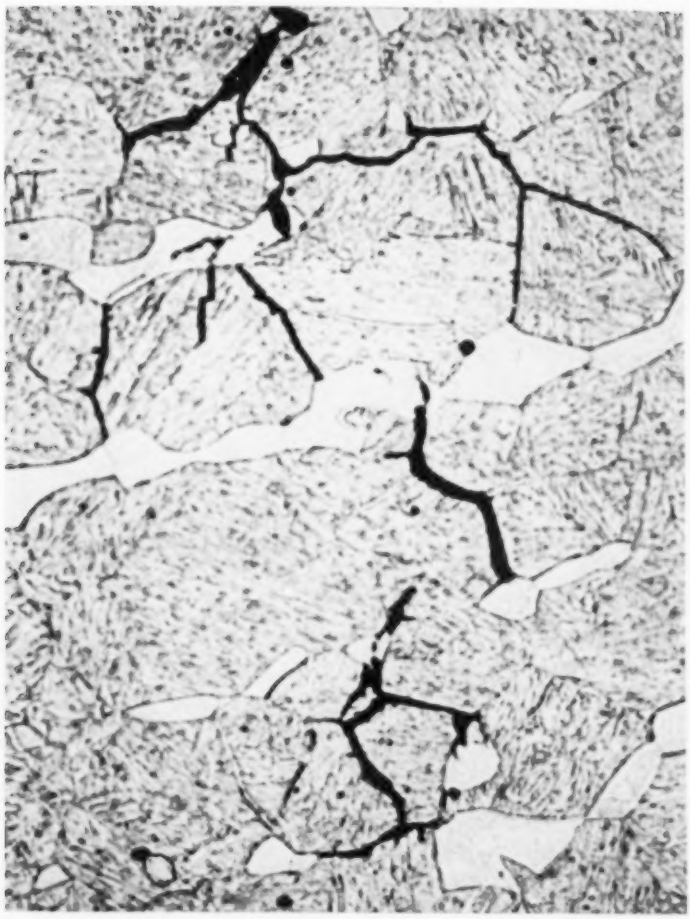


Fig. 5—Steel A3 (410, 10% ferrite) Oil-Quenched from 1800°F and Tempered at 900°F. Specimen stressed at 70,000 psi and tested in an atmosphere of 5% NaCl. Specimen failed in 30 days. Top of micrograph is tension side. Etched in 5% picral + 0.5% HCl. ×1000.

Fig. 6 indicates that delta ferrite minimizes the amount of precipitation in the former austenite grain boundaries. When there is no delta ferrite present the prior austenite grain boundaries are clearly outlined with a precipitate, presumably carbide, after a temper at 950°F as Fig. 6a indicates. When delta ferrite is present there is little precipitation in the former austenite grain boundaries. (Fig. 6b) There are two reasons for this observation. In the first place, when delta ferrite is present there is a tendency for the precipitation to occur preferentially at the ferrite former austenite grain boundaries. This was observed not only in the present investigation but in earlier investigations as well. Secondly, when delta ferrite is present the austenite grain size is smaller at a given austenitizing temperature so that a given amount of precipitate will be less concentrated when distributed over a greater grain boundary area. The grain size of the steel of Fig. 6a is about ASTM No. 5 compared with a grain size of

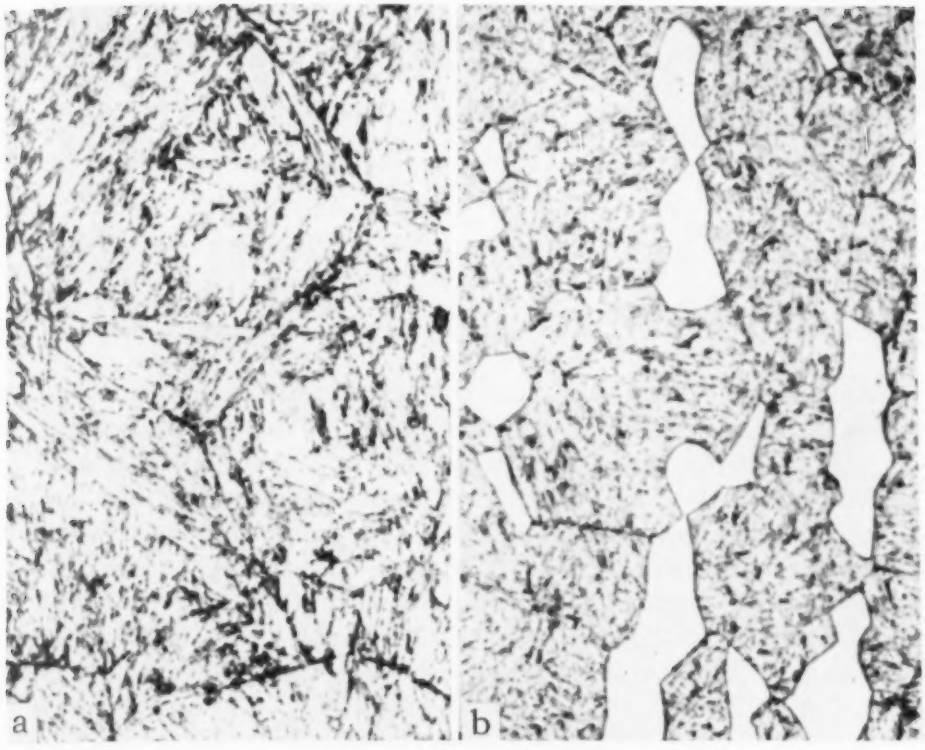


Fig. 6—Effect of Delta Ferrite on Precipitation at Parent Austenite Grain Boundaries. Specimens austenitized at 1800°F, oil-quenched and tempered at 950°F 2 hours. Etched in 5% picral + 0.1% HCl. ×1000. (a) Steel A1 (410) No Delta Ferrite; (b) Steel A3 (410) 10% Delta Ferrite.

about ASTM 7 or 8 for the steel containing delta ferrite illustrated by Fig. 6b. No effort was made during the course of this investigation to ascertain the effect of grain size on susceptibility to stress corrosion cracking. It is planned that the effect of grain size will be explored in the work on stress corrosion cracking which is to be continued.

Effect of Hydrogen Liberated During Corrosion

It might be argued that the failures which have been described are attributable to hydrogen embrittlement rather than to stress corrosion. In an attempt to resolve this issue the following experiment was carried out. Specimens of Steel Al (Type 410) which was known to fail by cracking in about 7 days when tempered at 900°F, stressed to the 70,000 psi level and exposed to the 5% salt spray atmosphere were used. Specimens of this steel were removed after exposures to salt spray of ½, 1½ and 3 days and were baked at 400°F for 2 hours to remove any hydrogen which may have been produced by the corrosion occurring during the initial exposure and absorbed by the specimen. The specimens were then returned to the salt spray cabinet for further exposure. If hydrogen embrittlement were in-

Table VI
Tests to Determine if Hydrogen Embrittlement is a Factor in Stress Corrosion Cracking of Type 410

Specimens of steel A1 were oil-quenched from 1800°F, tempered at 900°F for 2 hours, stressed at 70,000 psi and tested in an atmosphere of 5% NaCl. Control samples were exposed continuously until failure. Other specimens were removed after indicated times, baked at 400°F for 2 hours, restressed to 70,000 psi and returned for further exposure in salt atmosphere until failure.

Time in Test Before Removal for Baking, Days	Total Time for Failure in Days
Control	6, 8, 8
½	5, 5, 8
1½	5, 6, 6
3	6, 7, 8

volved it would be expected that the failures would all occur in about 7 days after the specimens were reexposed. It was found, however, as Table VI indicates that the specimens failed at various times with the result that the sum of the two exposure times equalled about 7 days, the time required for failure during continuous exposure. It seems reasonable to conclude, therefore, that hydrogen liberated by the corrosion process is not an important factor in the cracking failure of these steels. The failures which have been described so far are perhaps best designated as stress corrosion failures.

Hydrogen Embrittlement

There is evidence, however, that the 12% Cr martensitic stainless steels may, under some conditions of exposure, fail by hydrogen embrittlement (9,19). It seemed of interest, therefore, to ascertain if susceptibility to hydrogen embrittlement, like susceptibility to stress corrosion cracking is affected by variations in tempering temperature.

It was found that Type 410, 420 and 422 stainless all showed a similar relationship between tempering temperature and susceptibility to hydrogen embrittlement. Only the data obtained for Type 410 are presented and discussed in this paper.

Specimens of steel Al stressed to 100,000 psi were charged with hydrogen by arranging them as the cathode in a cell containing 0.1 normal sulphuric acid plus 3 mg per liter of arsenic as the electrolyte. The time for failure under these test conditions was noted.

The data obtained are summarized in Table VII. Failure was observed to occur in 1 hour or less when the specimens were in the quenched condition, or tempered at temperatures of 1000°F or less. With increasing tempering temperature up to 500°F the time for failure increased. With a further increase in tempering temperature from 500 to 850 or 900°F the time for failure decreased. Finally, as the tempering temperature was increased above 900°F the time for failure again increased. No failures were observed after 3 hours of exposure when a tempering temperature of 1050°F or higher was employed.

Table VII
Effect of Tempering Temperature on the Susceptibility of Type 410 to Hydrogen Embrittlement

Specimens of Steel A1 oil-quenched from 1800°F and tempered at indicated temperatures for 2 hours. Specimens stressed at 100,000 psi and tested in 0.1 N H_2SO_4 + 3 mg arsenic/liter of solution as cathodes of a cell.

Tempering Temperature	Hardness Rc	Time For Failure In Minutes	Type of Failure
None	43	16	Transgranular
300°F	42	28	Transgranular
400°F	41	40	Transgranular
500°F	40	60	Transgranular
600°F	39	40	Transgranular
700°F	40	30	Transgranular
800°F	41	15	Transgranular
850°F	42	5	Transgranular + Intergranular
900°F	42	5	Transgranular + Intergranular
950°F	41	20	Transgranular + Intergranular
1000°F	34	40	Intergranular
1050°F	28	No Failure	

Also, it is of interest that the mode of cracking varies with tempering temperature. The failures were entirely transgranular for tempering temperatures of 800°F or below. Cracking was partly transgranular and partly intergranular when an 850 to 950°F temper was used. The specimens tempered at 1000°F failed only by intergranular cracking. These three modes of cracking are illustrated by Figs. 7a,7b and 7c, respectively.

Discussion of Results

The data of Table VII are plotted as the upper curve of Fig. 8. The lower curve indicates the effect of tempering temperature on the room temperature Izod impact values for Type 410. The similarity in shape of the two curves is striking. It has been demonstrated by Klingler and his associates (20) that the shape of the impact versus tempering temperature curve for 4340 can be related to the changes which occur during tempering. Similarly, then, it should be possible to relate the shape of the impact and hydrogen embrittlement susceptibility curves to the various stages of tempering in the 12% Cr steels.

Klingler et al (20) found that the peak which occurs at about 400°F for 4340 when the tempering time is about 1 hour corresponds with the end of the first stage of tempering or the start of the third stage (cementite formation). As increasing amounts of cementite form during tempering of martensite at increasing temperatures above 400°F the impact values for 4340 and other low alloy steels decrease until minimum values are obtained after a temper in the range from about 500 to 700°F. There is an increase in impact values with increasing tempering temperature above about 700°F and this seems to be associated with the agglomeration of cementite.

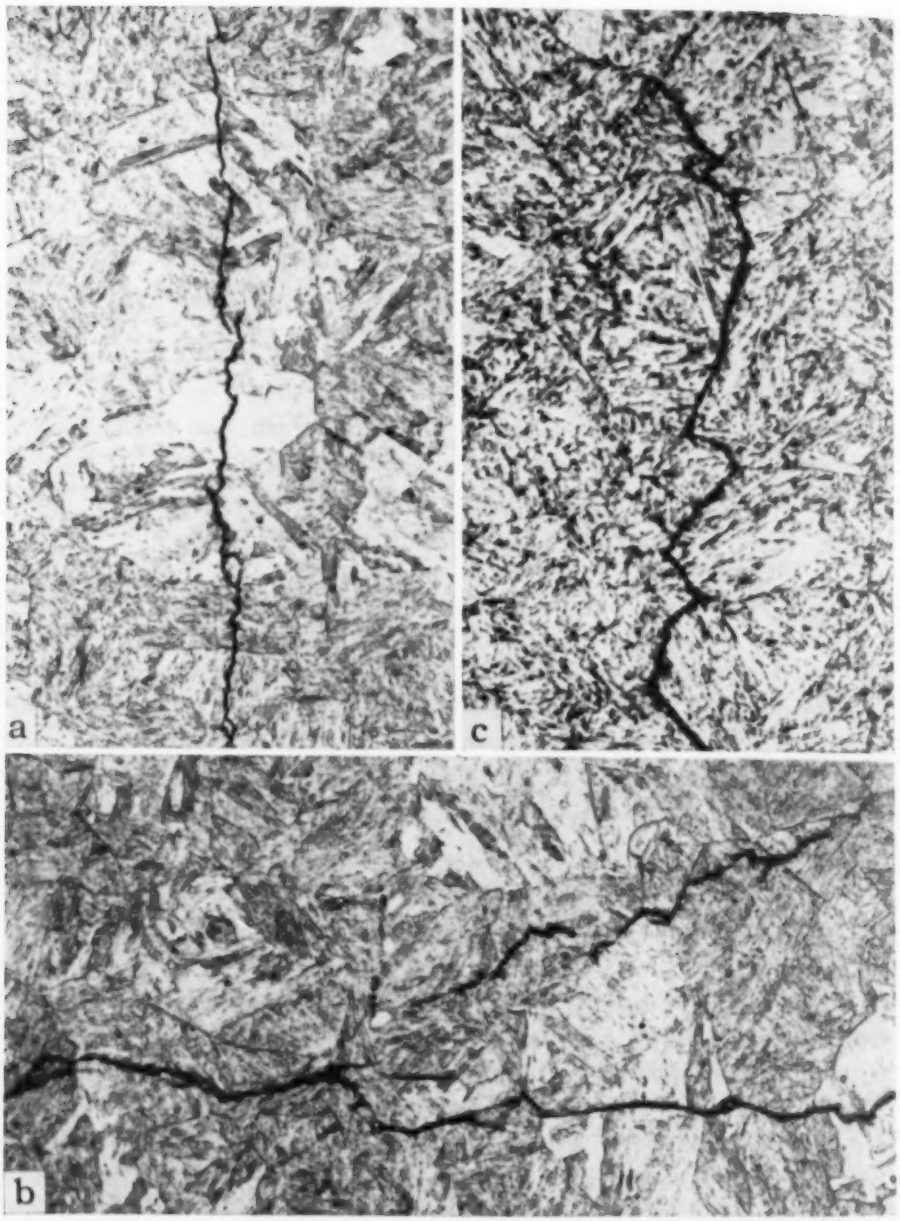


Fig. 7—Effect of Tempering Temperature on the Mode of Cracking of Type 410 Charged with Hydrogen. Specimens of steel A1 austenitized at 1800°F, oil-quenched and tempered at indicated temperatures for 2 hours. Specimens stressed at 100,000 psi and charged with hydrogen in a solution of 0.1 N sulphuric acid containing 3 mg of arsenic per liter of solution (a) failed in 30 minutes (b) failed in 5 minutes (c) failed in 40 minutes. Top of photo micrograph is tension side. Etched in 5% picral + 5% HCl. ×500. (a) 700°F; (b) 850°F; (c) 1000°F.

The shape of the impact versus tempering temperature curve for Type 410 stainless follows the same general pattern. The peak for Type 410 occurs after a 1 hour temper at 500°F instead of 400°F and the minimum value is obtained after a temper at 900°F, rather than at 500 to 700°F. Dilatometric work which need not be reported here

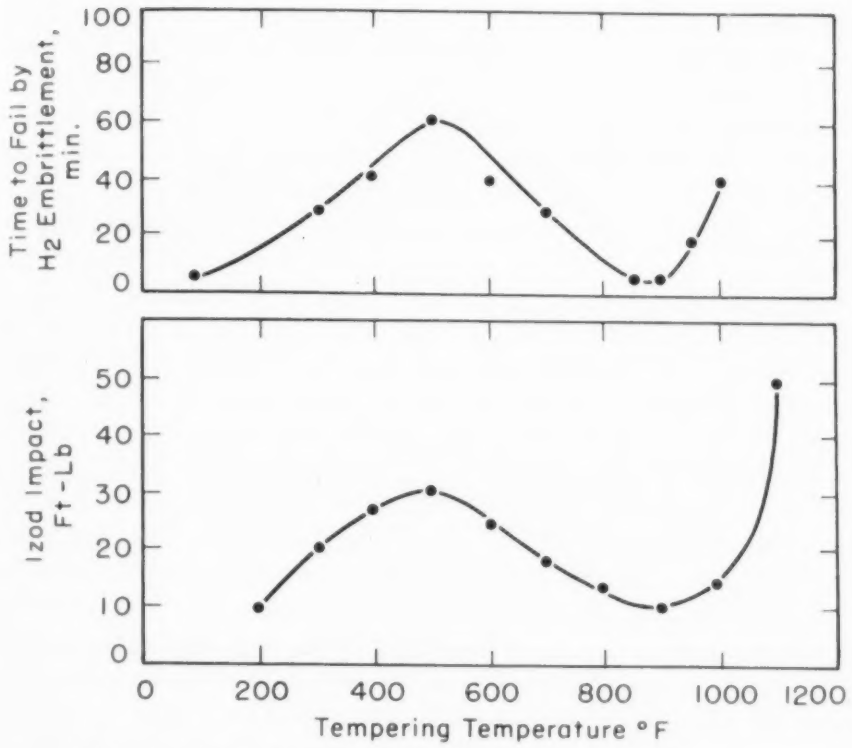


Fig. 8—Effect of Tempering Temperature on the Notch Impact Strength and Susceptibility of Type 410 to Hydrogen Embrittlement. Average of impact values for ten commercial heats of 410.

has indicated that the third stage of tempering starts at about 500°F for Type 410 stainless (21). Thus, in this steel also it appears that the initial decrease in impact value with increasing tempering temperature is associated with the early stages of cementite formation. The cementite reaction seems virtually complete, on the basis of dilatometric evidence, when a tempering temperature of about 600 to 650°F is reached, so the continued lowering of impact values with increasing tempering temperature above these temperatures cannot be attributed to continued cementite formation.

The hardness versus tempering temperature curves shown in Fig. 9 indicate that secondary hardening is observed when the martensitic stainless steels are tempered at temperatures above about 700°F. It seems reasonable to attribute this secondary hardening to the formation of a coherent chromium carbide. The maximum amount of secondary hardening occurs on tempering at 850 to 900°F. This treatment produces the minimum impact values. With increasing tempering temperature above 900°F the hardness drops off rapidly and the impact values increase abruptly. This softening is attributable to loss of coherency.

It has been observed that chromium retards the softening of steels during tempering in the third stage by retarding the coales-

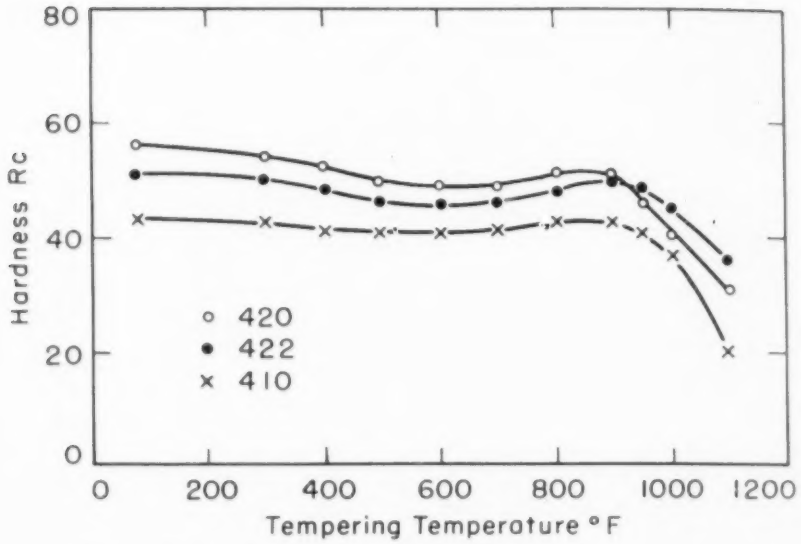


Fig. 9—Plot of Hardness Versus Tempering Temperature for Type 410, 420 and 422.

cence of the cementite particles (22). This may be a factor which contributes to part of the plateau at 500 to 700°F in the hardness versus tempering temperature curves.

In an earlier section of this paper it was mentioned during the discussion of microstructures that the lowest tempering temperature which produced grain boundary precipitation detectable by a light microscope is 850°F. This precipitate presumably is an incoherent chromium carbide. It appears that a somewhat higher tempering temperature is required to produce general precipitation of the chromium carbide throughout the matrix, and softening.

The association between microstructural changes on tempering and mode of cracking by stress corrosion and hydrogen embrittlement does not seem to be well defined. Evidence of precipitation in the parent austenite grain boundaries could be detected after a temper at 850°F. Cracking which was exclusively intergranular was not observed until after a 950°F temper in the case of the specimens exposed to the 5% NaCl atmosphere, and after a 1000°F temper for the specimens subjected to hydrogen embrittlement.

Summary and Conclusions

Specimens of hardened Types 410, 420, 422 and 436 stainless were tempered at various temperatures in the range 300 to 1200°F, stressed by bending to a stress level generally well below the elastic limit and were subjected to stress corrosion and hydrogen embrittlement.

For the stress corrosion studies an atmosphere of 5% NaCl was employed. It was found that these steels when free from delta ferrite

are susceptible to stress corrosion cracking when tempered in the range 800 to 1000°F. Delta ferrite minimizes the tendency for stress corrosion cracking in these steels by narrowing the range of tempering temperatures which produce susceptibility to stress corrosion cracking and by interfering with crack propagation. The tempering temperature which produces maximum susceptibility to stress corrosion cracking is 900°F.

It was also shown that the times for failure by hydrogen embrittlement vary with tempering temperature in the same manner as impact values vary with tempering temperature in these steels. For high levels of hardness, minimum susceptibility to failure by hydrogen embrittlement results from a temper at about 500°F. Maximum susceptibility was observed when 850 or 900°F is employed for the tempering. These variations in susceptibility seem to bear a definite relationship to the various stages in the tempering process. The tendency for hydrogen embrittlement in the steel heat treated to high strength levels is a minimum at the temperature at which cementite begins to form (500°F) and is a maximum at about the temperature at which an incoherent chromium carbide begins to form at the parent austenite grain boundaries.

This investigation has indicated that the 12% chromium stainless steels can be made to fail by hydrogen embrittlement, as other investigators have previously reported, when they are tempered at a temperature of 1000°F or lower. Failures were also obtained by exposing these steels to a 5% NaCl atmosphere. It does not necessarily follow, however, that these failures must also be the result of hydrogen embrittlement. The failures observed in salt spray are considered to be stress corrosion failures. During the tempering process chemical inhomogeneities are developed along crystallographic planes and at parent austenite grain boundaries so that localized corrosion by the electrochemical mechanism is possible.

Acknowledgment

The authors are grateful to the management of Crucible Steel Company of America for giving us permission to publish this work and appreciate the encouragement and advice given them by Mr. Peter Payson, Assistant Director of Research.

The authors are indebted to many of their colleagues including A. Simon, R. Frenkel, J. Stolte, F. Baureis, J. Stefanelli and H. Owsick who assisted us in various phases of the work.

References

1. Russell Franks, W. O. Binder, Charles M. Brown, "The Susceptibility of Austenitic Stainless Steels to Stress-Corrosion Cracking," American Society for Testing Materials-American Institute of Mining and Metallurgical Engineers, *Symposium on Stress Corrosion of Metals*, 1944, p. 411.

2. J. J. Heger, "Stress Corrosion of Stainless Steels," METAL PROGRESS, American Society for Metals, March 1955, p. 109.
3. R. B. Mears, R. H. Brown, E. H. Dix, Jr., "A Generalized Theory of Stress Corrosion of Alloys," American Society for Testing Materials-American Institute of Mining and Metallurgical Engineers, *Symposium on Stress Corrosion of Metals*, 1944, p. 323.
4. M. A. Scheil, "Some Observations of Stress-Corrosion Cracking in Austenitic Stainless Alloys," American Society for Testing Materials-American Institute of Mining and Metallurgical Engineers, *Symposium on Stress Corrosion of Metals*, 1944, p. 395.
5. M. A. Scheil, Authors' Closure, American Society for Testing Materials-American Institute of Mining and Metallurgical Engineers, *Symposium on Stress Corrosion of Metals*, 1944, p. 432.
6. F. W. Davis, "Stress Corrosion in a Stainless Steel Compressor," TRANSACTIONS, American Society for Metals, Vol. 42, 1950, p. 1233.
7. E. H. Dix, Jr., "Acceleration of the Rate of Corrosion by High Constant Stresses," *Transactions*, American Institute of Mining and Metallurgical Engineers, Institute of Metals Division, Vol. 137, 1940, p. 11.
8. D. K. Priest, F. H. Beck and M. G. Fontana, "Stress Corrosion Mechanism in a Magnesium-Base Alloy," TRANSACTIONS, American Society for Metals, Vol. 47, 1955.
9. H. H. Uhlig, "Action of Corrosion and Stress on 13% Chromium Stainless Steel," METAL PROGRESS, American Society for Metals, April, 1950, p. 486.
10. J. P. Fraser and R. S. Treseder, "Cracking of High Strength Steels in Hydrogen Sulfide Solutions," *Corrosion*, Oct. 1952, p. 342.
11. F. A. Prange, "Hydrogen Embrittlement Tests on Various Steels," *Corrosion*, Oct. 1952, p. 355.
12. John W. Juppenlatz, Discussion of Ref. 10, *Corrosion*, Oct. 1952, p. 357.
13. W. D. Robertson, Discussion of Ref. 10, *Corrosion*, Oct. 1952, p. 359.
14. W. L. Badger, "Stress Corrosion of 12% Cr Stainless Steel," Society of Automotive Engineers, Preprint No. 221, Jan. 1954, Annual Meeting.
15. R. H. Thielemann, J. C. Mertz and W. P. Eddy, Jr., "Trends in Gas Turbine Engine Materials," *Journal* Society of Automotive Engineers, April, 1952, p. 58.
16. Stuart and U. R. Evans, "The Effect of Zinc on the Corrosion Fatigue Life of Steel," *Journal*, Iron and Steel Institute, Vol. 147, 1943, p. 131.
17. R. T. Howard and M. Cohen, "Quantitative Metallography by Point Counting and Lineal Analysis," *Transactions*, American Institute of Mining and Metallurgical Engineers, Vol. 172, 1947, p. 413.
18. A. E. Nehrenberg, "Modified Picral for Higher Alloy Steels," METAL PROGRESS, American Society for Metals, Vol. 62, July 1952, p. 91.
19. A. E. Durkin, "Corrosion Cracking of Martensitic Stainless Steel," METAL PROGRESS, American Society for Metals, July, 1953, p. 72.
20. L. J. Klingler, W. J. Barnett, R. P. Frohmberg and A. R. Troiano, "The Embrittlement of Alloy Steel at High Strength Levels," TRANSACTIONS, American Society for Metals, Vol. 46, 1954, p. 1557.
21. Unpublished Crucible Steel Company of America Research Laboratory Report.
22. R. W. Balluffi, M. Cohen and B. L. Averbach, "The Tempering of Chromium Steels," TRANSACTIONS, American Society for Metals, Vol. 43, 1951, p. 497.

DISCUSSION

Written Discussion: By D. K. Hanink, chief metallurgist, Allison Division, General Motors Corp., Indianapolis, Indiana.

The clear and concise manner in which the authors have presented the results of their carefully conducted investigation increases the importance of their work as additional reference data in broadening our background on this subject. It

seems proper that this discussion should be limited to our experience with gas turbine engine compressor blading since the thermal treatments currently being used may seem to contradict conclusions reached by the authors.

It has been recognized for some time that the choice of thermal treatments on ferritic stainless steels is governed by many factors influenced occasionally by the required manufacturing procedures dictated by the particular part being made. More often however, processing procedures can be the result of determining required durability after making an accurate appraisal of the component under simulated operating environment. Then, recognizing these requirements, a suitable compromise may have to be determined which will produce an overall combination of acceptable properties.

Specifically, if we consider Type 410 steel one of the materials covered in this paper and which is currently a popular gas turbine compressor blade alloy, we wish to make the following comments based on extensive bench vibration fatigue tests in both air and corrosive sea water fog atmosphere:

1. Generally, regardless of thermal treatment, cracking can be produced through surface corrosion pits before the material exhibits an intergranular type of stress corrosion.

Air Atmosphere

2. In comparing new blades processed with 1100 to 1025°F tempering temperatures we find:
   (a) 1100°F tempered blades are 21% lower in endurance strength.
   (b) In comparing used blades the 1100°F tempered parts were 7% lower in endurance strength.

Corrosion Atmosphere

Per ASTM D1141-52 Temperature 92°F – 97°F.

(a) Comparing 1100°F tempered new blades, the endurance strength was 10% higher.
(b) Comparing 1100°F tempered used blades, the endurance strength was 16% lower.

3. The improvement of endurance limit in corrosive atmosphere representing the 1100°F tempered blades could not be attributed to the higher damping capacity since the actual engine running air damping minimizes influence of initial damping capacity of material.
4. After examining these test results it became obvious that to improve corrosion resistance of blading there might also be sacrifice in fatigue strength. Since it was also recognized that cracking was generally associated with the corrosion pits, it was decided that possibly superficial stresses imposed by finishing operations after thermal treatment were a major contributing factor. A stress relief of 950°F after finishing seems to have eliminated residual surface stresses which with superimposed dynamic stress during operation was accelerating corrosion susceptibility.

This experience suggests that a strict extrapolation of test results, such as covered in this paper, may not be justified. This is particularly true in consideration of the lower dynamic stresses experienced in actual blade application, and the higher static stress of 70,000 psi used on Type 410 steel in this investigation.

It has become apparent with development of this and other additional background data that further major improvement in blade durability requires serious consideration of higher chromium content and nickel bearing alloys of higher fatigue endurance limits without accompanying deterioration under corrosive environment.

Written Discussion: By V. W. Cooke, Materials Development Laboratory, Pratt & Whitney Aircraft, Division of United Aircraft Corp., East Hartford, Conn.

We wish to compliment the authors and their associates upon their excellent presentation of data regarding stress-corrosion and hydrogen embrittlement of the hardenable stainless steels. The fact that this class of very useful steels is subject to stress-corrosion type failure has been of quite some concern to the aircraft industry. We have conducted a parallel series of tests over a period of some years, although with slightly different techniques. PWA tests employed threaded tensile specimens loaded in cages and subjected to 20% salt spray at 95°F, so that the conditions were probably more severe than those of the Crucible strip tests. Our tests essentially confirm the results in this paper; namely, that maximum susceptibility to stress-corrosion cracking occurs when these steels have been tempered in the 800 to 1000°F range. This does not mean that they are free

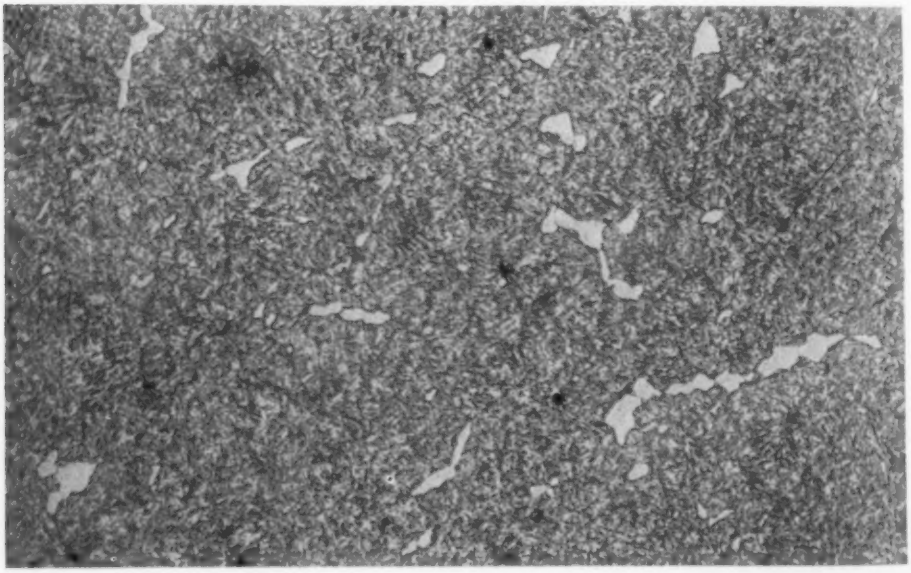


Fig. 10—Microstructure of Crucible 422 Stainless Steel Disk: Stress-Corrosion Specimen from This Heat Failed in Nine Days at 100,000 psi. ×100. Etchant: Vilella's Reagent.

from danger when tempered in most favorable ranges, however, since the time to failure merely takes longer. The limiting time of 75 to 120 days used for both investigations could mean little compared to actual service life of parts. Also, we feel that it is not fair to generalize that delta ferrite minimizes the tendency for stress-corrosion cracking. It is agreed that if the stress is applied in such a manner as to propagate cracks transverse to the grainflow, ferrite may have a beneficial effect. However, if crack propagation is parallel to the grainflow, delta ferrite appears to offer no benefit. An example of random ferrite orientation is shown in

Fig. 10a photomicrograph of a Crucible 422 disk section. This specimen has approximately 5% delta ferrite, and failed in salt spray tensile test in 9 days at 100,000 psi. This disk has been tempered at 1200°F to Rockwell C-32–34.

One further comment, in case anyone feels that salt spray tests are too severe, we also found that cracking could occur on tensile specimens subjected to a plain humidity environment, although times to failure were longer.

As indicated by the authors, some PWA data are reported by Thielemann et al in reference 15. A more recent presentation has been given by H. J. Noble and W. H. Sharp at the SAE meeting in Atlantic City in June 1955.

Despite the accumulation of test data I am left with the feeling that we still do not have a good answer to the problem. If some heats are more resistant to stress-corrosion than others, it should be possible to produce an overall improvement if we can obtain a better idea of the mechanism involved. If the difficulty is truly one of chromium carbide particle size and distribution, we might be able to improve this by columbium additions and perhaps heat treat variations. What few tests we do have on a columbium bearing steel do not indicate such a solution.

Written Discussion: By Julius J. Harwood, head, Metallurgy Branch, Office of Naval Research, Washington, D. C.

This paper by Messrs. Lillys and Nehrenberg is an excellent report of experimental data which is highly valuable for achieving a better understanding of cracking of the martensitic stainless steels in certain environments. Data concerning the correlation between metallurgical structure and cracking tendencies has been sorely needed and this paper is, therefore, a valuable contribution to this subject. The cracking of the 12% chromium and other martensitic stainless steels is becoming an important problem and the present expedient of tempering at high temperatures (~1100°F), while it apparently solves the cracking problem, does not permit taking advantage of the higher strength potentialities of these steels and often places them in an unfavorable competitive position with respect to other materials.

The question of whether the cracking of the martensitic stainless steels in chloride and other environments is due to hydrogen embrittlement or stress-corrosion cracking is a most intriguing one and the critical and definitive experiments are yet to be performed to resolve this issue. In this respect, the results of the baking experiments reported by the authors are not sufficient to draw the conclusion that hydrogen liberated by the corrosion process is not a contributing factor in the cracking failure of these steels. The fact that the same cracking times (about 7 days) in salt spray tests were found for specimens which were continuously exposed and for those which were given baking treatments at various time periods is no conclusive argument against the possibility of hydrogen playing a role in the cracking process. Indeed, the results which were obtained in this set of experiments are what might be expected.

There is increasing evidence that the causative agent in promoting brittle stress-corrosion cracking and related phenomena plays its greatest role shortly before final failure occurs.[2] This is particularly true of those alloys or of those experimental conditions in which once the crack is initiated, it is rapidly propagated through the specimen. For example, it has been shown, in some cases of stress-corrosion cracking, that the time to failure was the same for specimens which were

[2] J. J. Harwood, "The Phenomena and Mechanism of Stress-Corrosion Cracking," to be published in Symposium on Stress-Corrosion Cracking by Electrochemical Society.

stressed throughout the test as for those for which the stress was applied shortly before failure occurred.[3] These findings are of some significance to the observations of Messrs. Lillys and Nehrenberg. It appears that the major portion of the time required for the initiation of stress-corrosion cracking is associated with the time necessary to develop a corrosion fissure of critical length and radius required to establish the necessary stress field around the base of the corrosion fissure, which then triggers the stress-corrosion cracking process.

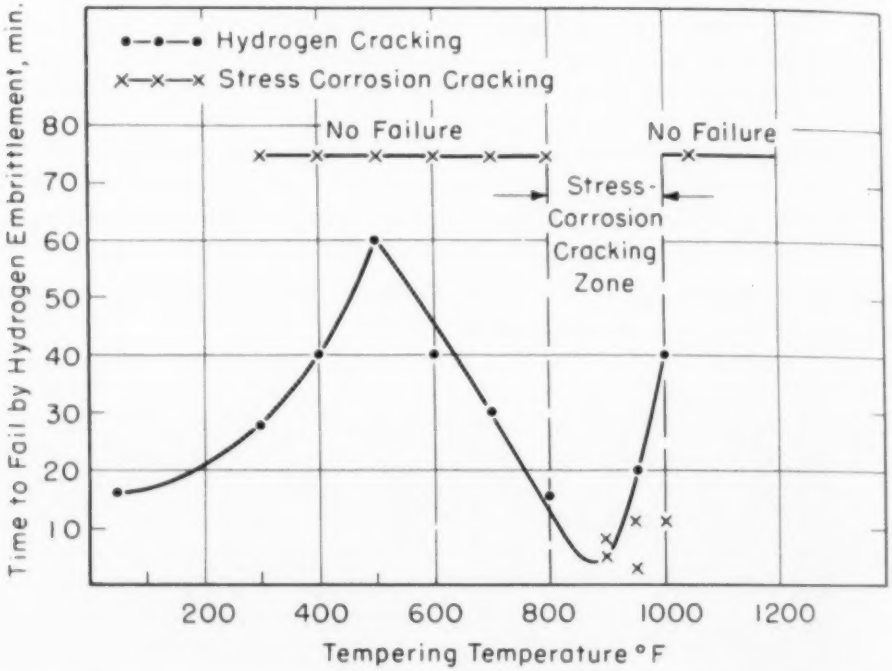


Fig. 11—Influence of Tempering Temperature on Hydrogen Cracking and Stress-Corrosion Cracking of Type 410.

In the authors' experiments a similar situation might well prevail. The time to failure may be, primarily, the time required to develop the necessary conditions for the growth of the corrosion fissure and the hydrogen produced by the corrosion reaction would become most effective when a corrosion crack of critical length and radius exists. Baking treatments at earlier intervals to remove any hydrogen which may have been produced would not negate the possibility of the action of hydrogen generated upon the crack surfaces at the critical time in promoting a brittle cracking process. Gas analyses to determine the hydrogen content of the specimens (in the vicinity of the crack, if possible) before and after exposure to salt spray tests may provide some meaningful data to help resolve this matter. It does not appear, from the data which is currently available, that we can differentiate between a hydrogen cracking mechanism or another type of stress-corrosion cracking mechanism.

The data reported by the authors contain a point of interest upon which they did not elaborate. They showed a striking correlation between impact properties and hydrogen embrittlement as a function of tempering temperature. From the

[3] C. Edeleanu, "A Mechanism of Stress-Corrosion in Aluminum-Magnesium Alloys," *Journal, Institute of Metals*, Vol. 80, 1952, p. 187.

authors' data another interesting correlation can be drawn between hydrogen cracking and stress-corrosion cracking. In Fig. 11, the data for time to failure of Type 410 in salt spray tests as a function of tempering temperature has been superimposed upon the authors' curve of susceptibility to hydrogen cracking. Note that sensitivity to cracking in salt spray environment is limited to specimens tempered within the temperature range of 800 to 1000°F which corresponds to same tempering range for maximum susceptibility to hydrogen embrittlement. It should be noted also that there is a close correspondence between the modes of cracking in the salt spray and hydrogen embrittlement tests, as a function of tempering temperature, as shown in Table VIII.

Table VIII
Influence of Tempering Temperature Upon Mode of Cracking

Tempering Temperature, °F	Mode of Cracking: Hydrogen Embrittlement Tests	Mode of Cracking: Salt Spray Tests
Up to 800	Transgranular	No Failure
850	Transgranular + Intergranular	—
900	Transgranular + Intergranular	Transgranular + Intergranular
950	Transgranular + Intergranular	Intergranular
1000	Intergranular	Intergranular
1050	No Failure	No Failure

These correlations strongly suggest that the structural factors responsible for the cracking of hydrogen charged specimens are also responsible for promoting stress-corrosion cracking in salt spray. Some evidence has been presented by the authors that cracking may be associated with a grain boundary precipitate, which they suggest is a chromium carbide. This is quite reasonable and it may be postulated, similar to the stress-corrosion cracking of steels in nitrate solutions,[4] that the strains at the grain boundary associated with the formation of a coherent chromium carbide may sensitize the grain boundary area (make it more anodic) and thus lead to a presusceptibility to intergranular corrosion. This could result in the development of corrosion fissures of the appropriate length and sharpness to trigger the stress-corrosion cracking process. The mixed cracking which was observed might be more closely associated with the propagation of the brittle cracks rather than with their initiation. Alternatively, the depletion of chromium from the solid solution adjacent to the grain boundaries, as a result of the precipitation of the chromium carbide, may also be a factor in making the grain boundaries anodic and susceptible to intergranular attack. The possibility of hydrogen, produced as a product of the corrosion reaction, contributing to the cracking process cannot be completely ignored.

The implication that the formation of chromium carbides is associated with the susceptibility to stress-corrosion cracking and hydrogen embrittlement leads to the interesting speculation of the possible advantageous effects of additions of columbium or titanium to the martensitic stainless steels. If columbium or titanium, as in the case of the stabilized austenitic stainless steels, can retard the precipitation of chromium carbide, susceptibility to stress-corrosion cracking

[4] R. N. Parkins, "The Stress-Corrosion Cracking of Mild Steels in Nitrate Solution," *Journal*, Iron and Steel Institute, Vol. 172, 1952, p. 149.

might be inhibited also. The decreased cracking susceptibility of martensitic stainless steels containing delta ferrite, as reported by the authors, provides some basis for this type of reasoning, since the delta ferrite not only acted as a barrier to the propagation of cracks but also acted to decrease the extent of grain boundary precipitation.

The results reported in the paper by Messrs. Lillys and Nehrenberg are quite consistent with recent advances in our understanding of the mechanism of stress-corrosion cracking,[2] and the authors are to be commended on their efforts to correlate structural changes with cracking tendencies. It is hoped that these efforts will be continued, since this type of research is essential for arriving at the mechanism of cracking in the 12% Cr and other types of martensitic stainless steels.

Written Discussion: By R. H. Gassner, chief metallurgist, and C. C. Angstadt, group leader-Metallurgy, Douglas Aircraft Company, Inc., El Segundo, California.

The authors are to be congratulated for their contribution to the understanding of stress-corrosion and hydrogen embrittlement phenomena in martensitic stainless steels. Some results of the writers' investigation involving low (2%) and high (10%) delta ferrite heats of Type 431 stainless steel (hardened by preheating at 1400°F for 1 hour, austenitizing at 1875°F for 30 minutes, quenching, and tempering at 550°F for three hours) corroborate the authors' views. However, the writers' data indicate that some of the authors' deductions require qualification.

The conclusion regarding interruption of crack propagation by delta ferrite is corroborated by the results of tests on specimens embrittled by hydrogen infusion from "protective" austenitizing atmospheres. Diffusion of hydrogen into the low ferrite heat caused lower ductility in direct proportion to both hydrogen and water vapor content of the austenitizing atmosphere. No ductility loss was evident in similarly treated specimens from the high ferrite heat. This was considered a manifestation of the crack deterrent characteristics of the ferrite, rather than indicative of absence of hydrogen.

Slow quenching caused selective grain boundary carbide precipitation similar to that observed by the authors on tempering. In specimens from the low ferrite heat, the precipitate was distributed throughout all grain boundaries while the precipitate in specimens from the high ferrite heat was concentrated at the bound-

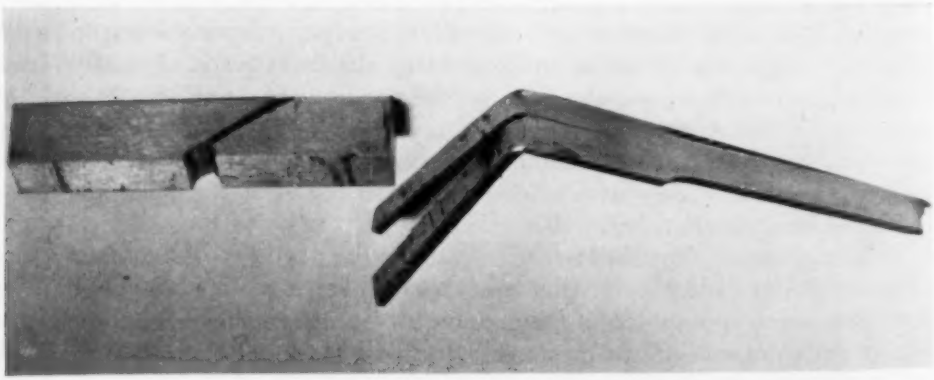


Fig. 12—Directional Embrittlement of Slow Quenched Type 431 Stainless Steel Containing 10% Delta Ferrite. The bend test specimen fractured after 90° deflection when bent across rolling direction and split after 5–10° deflection when bent parallel to the rolling direction. The longitudinal charpy V-notch specimen fractured diagonally at 41 ft-lbs. (A similarly treated short transverse specimen fractured at 1 ft-lb)

aries between the ferrite and tempered martensite grains. (The carbides were electrolytically extracted and identified by X-ray diffraction as the $M_{23}C_6$ type).

Evaluation of the ductility of slow quenched specimens indicated that the grain boundary precipitate severely lowered transverse ductility in the high ferrite heat with no detectable effect on longitudinal ductility. In the low ferrite heat, the embrittling effect of the precipitate was detectable in all directions. These effects are obvious when one considers that the delta ferrite is elongated by reduction of the ingot to the finished mill product. Fig. 12 dramatically illustrates



Fig. 13—Stress-Corrosion Test Specimen From Type 431 Stainless Steel Containing 10% Delta Ferrite. Failure occurred after 470 hours exposure to salt spray per QQ-M-151. Note fracture parallel to direction of applied stress.

how extreme transverse brittleness may be disguised by good longitudinal ductility.

It is considered that the effect of selective grain boundary precipitation on ductility should parallel its effect on stress-corrosion cracking. Therefore, the writers suggest that the authors' views regarding the beneficial effects of delta ferrite content are applicable to longitudinally stress specimens only. It seems likely that resistance to stress-corrosion cracking under transverse stress would be inversely proportional to the delta ferrite content. This hypothesis is supported by Fig. 13 which shows a stress corrosion test specimen from the high ferrite heat which cracked longitudinally, parallel to both the direction of rolling and the direction of maximum applied stress.

Authors' Reply

The authors wish to thank the discussers for their valuable contributions to this paper.

The authors were pleased that Mr. Cooke's results essentially confirm those reported in this paper.

We agree with Mr. Cooke that the hardenable stainless steels studied may not be free from danger when tempered at temperatures which were found to provide immunity to stress-corrosion cracking when a time limit of 75 days of ex-

posure to the salt atmosphere is imposed. Steels tempered somewhat above the susceptibility range of temperatures, although free from cracking after 75 days of exposure might be expected to fail after extremely long exposures to the salt atmosphere.

Both Mr. Cooke's and Mr. Gassner's observations that the presence of delta ferrite appears to offer little or no benefit to stress-corrosion cracking when the stress is applied normal to the grain flow, is quite interesting. In our studies of stress-corrosion cracking, the stress was applied in such a manner that the direction of crack propagation was normal to the ferrite stringers. Under these conditions, the observations of the authors and those of the discussers are in agreement as to the beneficial effects of delta ferrite in interrupting crack propagation. It is entirely possible as both Mr. Cooke and Mr. Gassner pointed out that ferrite may not have a beneficial effect, as one might expect on the basis of our studies, when the stress is applied such that a crack will propagate parallel to the grain flow.

We attempted during this investigation to obtain material containing varying amounts of delta ferrite of a size suitable for extracting specimens for testing in the transverse direction. However, in all cases the steels contained traces of no delta ferrite and were of little use in evaluating the effect of delta ferrite when stresses are applied in the transverse direction. Additional work is planned to study the effect of grain size and delta ferrite on stress-corrosion cracking in both directions.

In reply to Mr. Hanink, the data presented in our paper show the effect of tempering temperature on a single property of the hardenable stainless steels, that is, their susceptibility to stress-corrosion cracking or hydrogen embrittlement when subjected to a static stress. The performance of a component in service will generally depend upon a variety of properties not discussed in this paper. The endurance limit as affected by tempering temperature, notch sensitivity, surface condition, residual stress level, etc. are among the many factors other than susceptibility to stress-corrosion cracking which affect the performance of turbine blading. A combination of maximum endurance limit and at the same time, minimum susceptibility to stress-corrosion cracking in a corrosive atmosphere is not possible. In general, the endurance limit decreases with increase in tempering temperature above 1000°F whereas susceptibility to stress-corrosion cracking decreases. Thus, the optimum tempering temperature will be the tempering temperature which affords the best compromise. On the basis of considerations such as these, the results reported by Mr. Hanink can be rationalized and we do not see anything contradictory in his data.

In reply to Mr. Harwood, the authors visualize that hydrogen liberated by the corrosion process may play an important role in triggering the stress-corrosion process once the necessary stress field is established around the base of the corrosion fissure. However, this does not preclude the theory that hydrogen may not be a contributing factor and that external stresses present produce high stress concentrations at the base of the corrosion fissure which tend to tear the metal apart at that point and set off the stress-corrosion process. The authors agree, therefore, with Mr. Harwood that the baking experiments cannot be taken as conclusive evidence that hydrogen liberated by the corrosion process is not a contributing factor in the cracking of these steels. Certainly, more work is necessary to establish the role played by hydrogen in the failure of these steels as well as in other metals.

We are pleased that Mr. Harwood feels that there is an association between the structural changes which occur on tempering and susceptibility to failure by hydrogen embrittlement and stress-corrosion. Whether this susceptibility is the result of localized strains associated with the formation of a coherent chromium carbide or chromium impoverishment at the prior austenite grain boundaries remains an open question just as it does in the case of austenitic steels susceptible to intergranular corrosion.

Mr. Cooke and Mr. Harwood suggested that columbium or titanium additions to these steels might minimize susceptibility to stress-corrosion cracking and hydrogen embrittlement. Our feeling on this matter is that if enough of either of these strong carbide forming elements is added to prevent the precipitation of chromium carbide on tempering, little or no carbon would be available for hardening these steels. Possibly a somewhat smaller addition than that required for complete stabilization would result in a reasonable compromise between attainable hardness and susceptibility to stress-corrosion cracking and hydrogen embrittlement.

AUSTENITIC Fe-Cr-C-N STAINLESS STEELS

By G. F. Tisinai, J. K. Stanley and C. H. Samans

Abstract

Completely austenitic structures are formed at temperatures above about 2200° F in nickel-free steels containing 21 to 33% chromium provided proper additions of carbon and nitrogen are made. Rapid cooling retains the austenite but on slow cooling it decomposes to a mixture of ferrite, carbides and nitrides. Completely austenitic structures have been produced by casting, by nitrogenizing lower nitrogen alloys, and by powder metallurgy techniques. The austenitic structures are moderately strong and hard in the annealed state and work harden rapidly. Machining is not difficult in the ferritic state but is difficult in the austenitic state. (ASM-SLA Classification: N8, M27, Q general, SS)

Introduction

THE austenitic iron-chromium-nickel and iron-manganese-carbon alloys are well known and have useful, distinctive corrosion resisting, and/or mechanical properties. Another system of completely austenitic alloys, also with distinctive properties but based on the iron-chromium-carbon-nitrogen system, now has been developed.

Ordinarily the iron-chromium-carbon alloys are ferritic. However, it has been known for some time that, with the introduction of sizable amounts of nitrogen, the higher chromium (above about 22%) alloys could be made partially but not completely austenitic (1)[1]. It now has been found that if the higher chromium alloys contain up to 1% carbon, the amount of nitrogen which can be retained is increased tremendously. The high carbon and nitrogen appear to act synergistically, so that completely austenitic alloys result.

The iron-chromium-carbon system already has been studied extensively (2–7); an excellent summary was given by Kinzel and Crafts (8). Tofaute, Küttner and Büttinghaus (2) showed in detail the manner in which increased chromium restricted the austenite field, and how this is counteracted by increasing carbon. They showed also that the single phase austenitic field, i.e., in which neither ferrite nor carbide is present, cannot be extended beyond a maximum of about 20% chromium. Krivobok and Grossmann (6)

[1]The figures appearing in parentheses pertain to the references appended to this paper.

A paper presented before the Thirty-Seventh Annual Convention of the Society, held in Philadelphia, October 17–21, 1955. Of the authors, G. F. Tisinai is research engineer, and C. H. Samans is associate director, Materials Division, Engineering Research Department, Standard Oil Co., Whiting, Ind. J. K. Stanley, formerly with this department, now is associated with Crucible Steel Co. of America, Pittsburgh. Manuscript received April 8, 1955.

reported that they could produce a completely austenitic structure in a 21% chromium–0.62% carbon alloy, and that this could be retained completely by rapid cooling from elevated temperatures. On the other hand, a predominantly austenitic structure, but with some ferrite, was obtained with a 21% chromium–0.35% carbon composition. In an extension of their work to 28 and 33% chromium alloys of variable carbon content (up to 0.70%), they produced only minor amounts of austenite. On the basis of these results they postulated that in alloys containing as much as 33% chromium, a completely austenitic structure could be obtained with carbon contents in excess of 0.70% but subsequent studies have not supported these deductions.

In none of these early studies is there evidence that the effect of nitrogen was given any serious consideration. However, in 1926 Adcock (9) observed that iron-chromium alloys could dissolve more nitrogen than plain carbon steels. In 1935, both Krivobok (10) and Franks (11) reported that high chromium steels containing more than nominal amounts of nitrogen contained increased amounts of austenite after being quenched from above 2000°F, and they attributed this effect to the austenitizing power of nitrogen. Colbeck and Garner (12), in 1939, studied the austenite-forming tendencies of nitrogen in iron-chromium alloys in more detail, and found that they could produce 24% chromium alloys which were as much as 60% austenitic and 27% chromium alloys which were as much as 50% austenitic. About this time, it was realized that nitrogen could be substituted for nickel in the iron-chromium-nickel alloys and the emphasis in this field switched to the study of iron-chromium-nickel-nitrogen alloys.

The purpose of this paper is to show that completely austenitic structures, without ferrite, carbides and nitrides, can be obtained in 21 to 33% chromium alloys by a proper combination of carbon and nitrogen. The austenite is produced by heating above 2000°F and is retained by rapid cooling. This austenite decomposes to ferrite, carbides and nitrides, at temperatures somewhat below the stated austenitizing temperature, in accordance with a "C" type of reaction curve. The martensite transformation is suppressed although it can be obtained in alloys in certain ranges of composition.

Experimental Procedure and Results

Compositions for the study of the iron-chromium-carbon-nitrogen system were produced in several ways, the most useful of which were casting, powder metallurgy, and nitrogenization (solid-gas reaction). In casting, the addition to a low carbon (less than 0.1%) melt, of more nitrogen than 1/75 to 1/100 of the chromium content, results in considerable loss of nitrogen during solidification. How-

ever, if the carbon content of the melt is increased (say up to 1%), this loss of nitrogen is minimized or prevented so that high nitrogen alloys (containing up to 0.7% nitrogen) can be cast directly. The retention, in alloys containing less than 0.3% carbon, of the large percentages of nitrogen needed to produce completely austenitic structures is difficult to do by melting at atmospheric pressure, but may be simpler if nitrogen pressure casting is used. Some typical

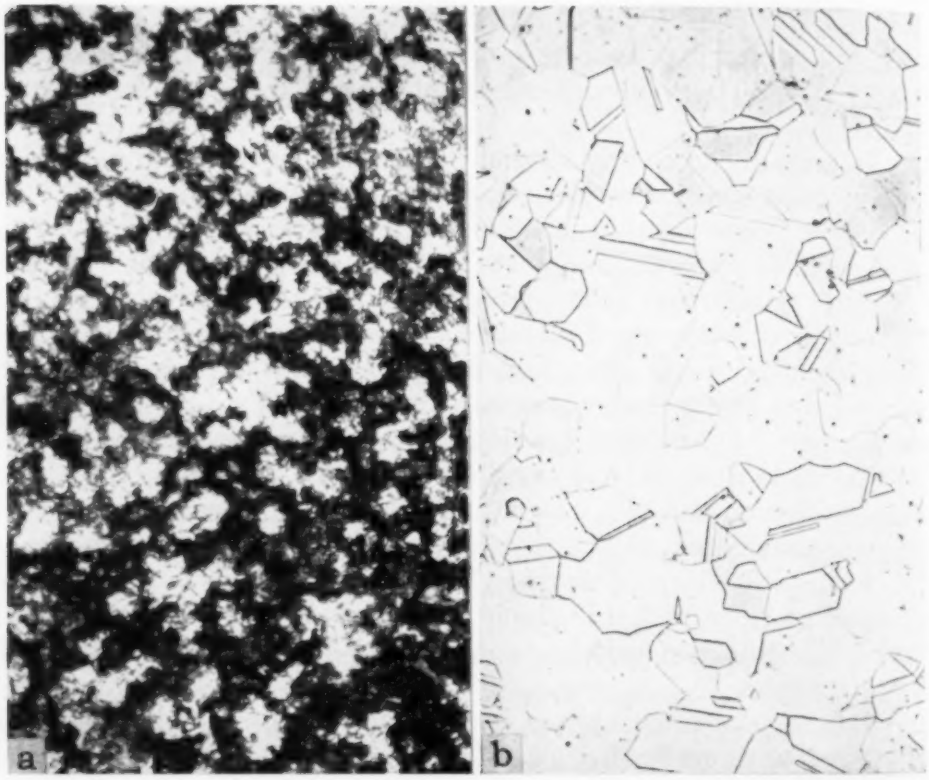


Fig. 1—Alloy 78. (a) Cast Alloy Showing a Considerable Degree of Decomposition; White is Austenite; Dark Areas are Mixtures of Ferrite, Carbides and Nitrides; (b) Wrought Alloy Held at 2200°F for 20 Hours and Water-Quenched; the Material is Entirely Austenitic. Aqua Regia etch. ×100.

austenitic compositions that have been made using ordinary casting techniques are 21% chromium–0.3% carbon–0.3% nitrogen, 24% chromium–0.4% carbon–0.4% nitrogen, and 27% chromium–0.5% carbon–0.5% nitrogen. Although the austenitic grain size is quite large in the cast alloys, it can be refined for control of mechanical properties by decomposing the alloys to ferrite, carbides and nitrides and then reaustenitizing for short periods of time at 2200–2300°F. Fig. 1 illustrates typical structures obtained in the decomposed cast, and reaustenitized states. Cast ingots of analyses which can be made completely austenitic have been satisfactorily reduced in size by forging.

Another method of producing the desired compositions is by nitrogenizing iron-chromium-carbon alloys in dry nitrogen at temperatures above 2000°F, preferably at 2200–2300°F. The nitrogen is absorbed by the alloy and produces a case of austenite. By nitrogenization, the completely austenitic structure can be obtained in the presence of much lower carbon contents than are required for the casting technique. For example, a ferritic 27% chromium steel containing 0.05% carbon can be nitrogenized to a completely austenitic structure. The rate of penetration of the nitrogen in amounts sufficient to form the austenitic case is a function of the carbon content and the nitrogen pressure. Fig. 2 illustrates typical structures obtained by nitrogenization. A technique similar to the above is to use conventional nitriding. The iron-chromium-carbon alloys can be nitrided at 1000–1200°F, and then homogenized, in either a vacuum (about a max. of 3 mm.) or a protective atmosphere, at 2200–2300°F.

A third method used to obtain these compositions was powder metallurgy. Proper proportions of iron carbide (Fe_3C), chromium nitride (Cr_2N), chromium and iron powders were mixed thoroughly, compacted into pellets, sealed in evacuated Vycor tubes, and sintered at 2200 to 2250°F. Graphite also has been used as a source of carbon, instead of the carbides. Compacting pressures above 80,000 psi were used. Sintering times of 16 hours proved satisfactory. Once the percentage recoveries of chromium, carbon and nitrogen were established, compositions could be compounded quite accurately. Fig. 3 illustrates typical structures obtained in such pellets. It was this technique, in particular, that permitted a rapid and accurate determination of the phase boundaries in the quaternary system.

The powders used to prepare these mixtures were relatively pure. Therefore, the percentages of other elements, ordinarily present as steelmaking impurities, were very low. This fact is reflected in the microstructure of some of the 21 and 24% chromium pellets which have relatively low carbon and nitrogen contents. These alloys become martensitic when quenched to room temperature. Since comparable compositions of the cast and forged material did not undergo the martensitic transformation, it appears reasonable that the steelmaking impurities suppressed the transformation. In fact, alloy 51 of Table II, which was prepared by melting, did not transform martensitically even when cooled to liquid nitrogen temperature.

The approximate limits of the austenite field in the iron-chromium-carbon-nitrogen system at 2200°F are given in Fig. 4 for five different chromium levels. These boundaries were determined from the data obtained from alloys produced by casting, by powder metallurgy and by nitrogenizing. The incidental variation in composition due to minor elements which results from the use of the three preparation techniques did not appear to affect the location of the phase

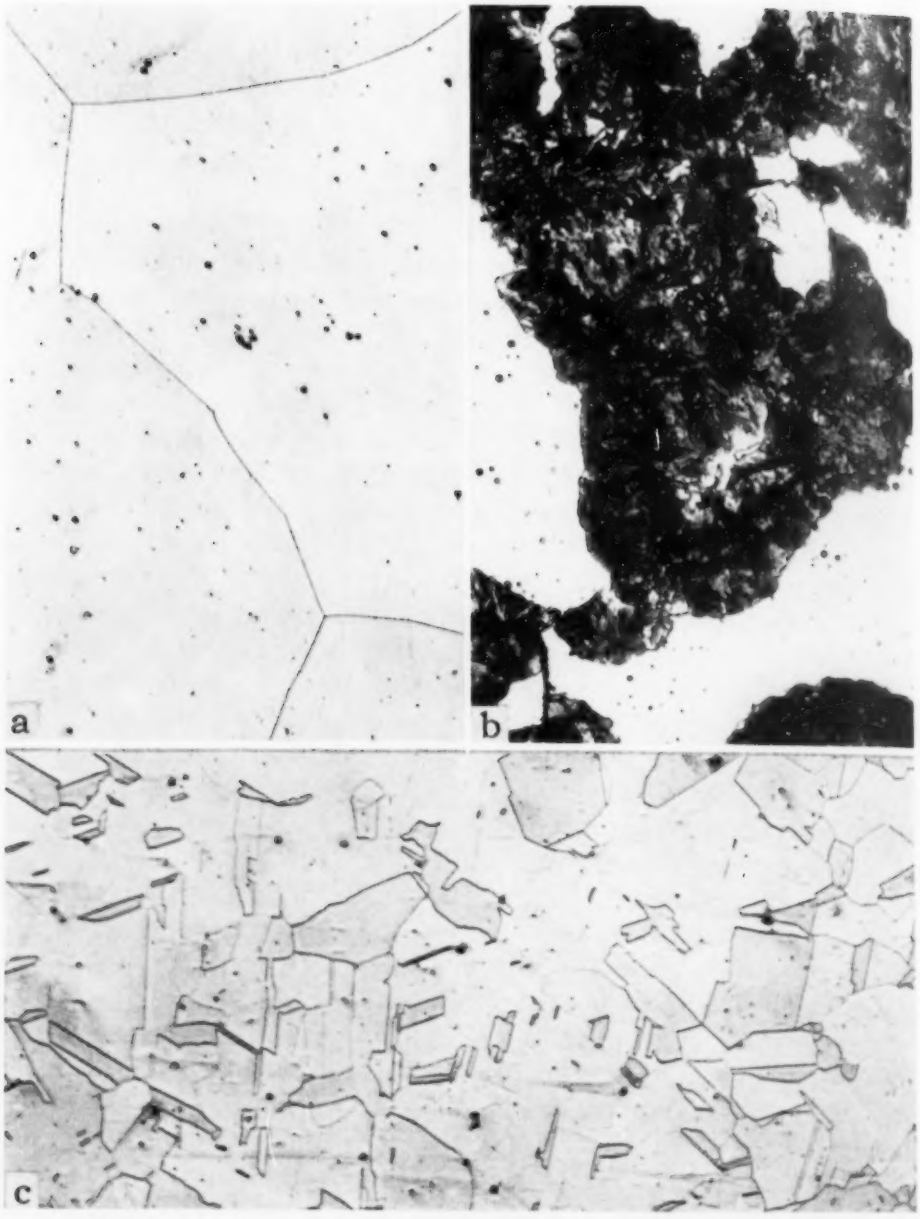


Fig. 2—Alloy 91. (a) As Nitrogenized, Showing Huge Austenite Grains, (b) Decomposed Partially into Ferrite, Carbide and Nitride (dark mixture) by Holding for 1 minute at 1600°F, (c) A Completely Decomposed Sample Reaustenitized at 2200°F (70 minutes) and Water-quenched. The grain structure is considerably refined. Aqua Regia etch. ×100.

boundaries. See Tables I, II and III. The austenite-austenite plus ferrite boundaries have been determined to rather close limits but the austenite-austenite plus carbide boundaries are known only approximately because less sampling was done on these alloys. All other boundaries are based on more limited information. The amounts of nitrogen and carbon required to produce the pure austenite field increase with increasing chromium content.

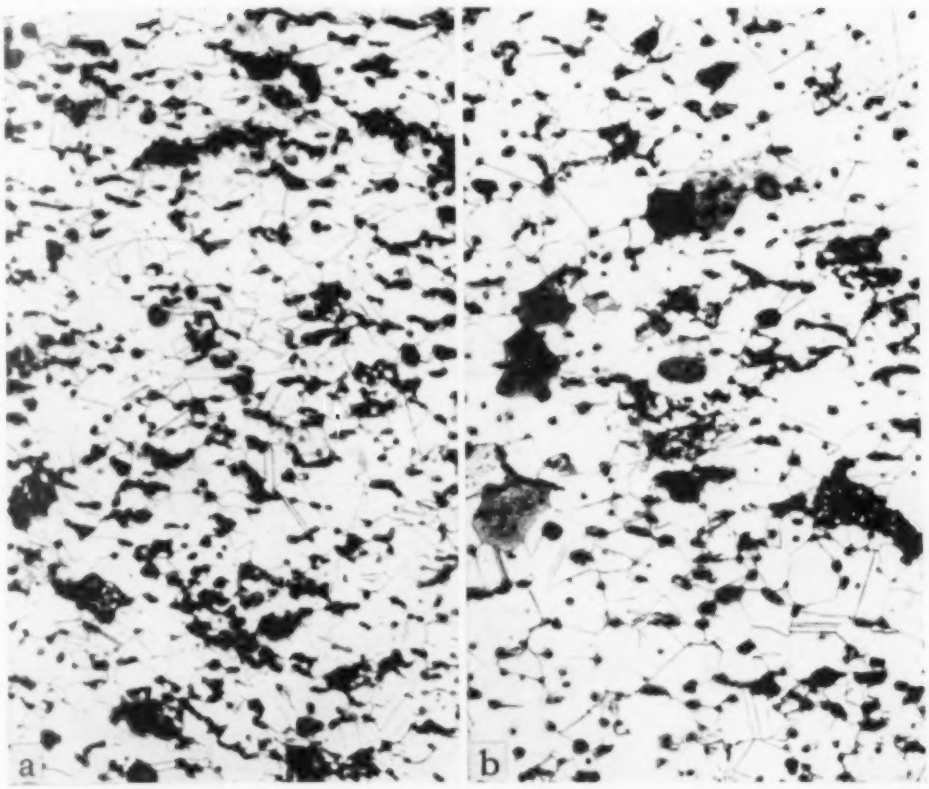


Fig. 3—(a) Alloy 18. A Sintered Compact Which is Predominantly Austenitic but Has Faint Traces of Martensite. Almost All of the Black Zones are Voids. (b) Alloy 37. A Sintered Compact Which is Predominantly Austenitic but Contains a Small Amount of Ferrite (dark mottled grains); the Black Zones are Voids; and the Dark Particle Almost in the Center of the Photograph is Oxide. Glycera Regia etch. ×100.

For the 21% chromium alloys containing 0.62 and 0.35% carbon, quoted by Krivobok and Grossmann (6), about 0.05 and 0.18% nitrogen, respectively, is required to obtain a completely austenitic structure at 2200°F. Thus, if such alloys picked up about 0.15% nitrogen from the atmosphere during melting, an amount which is conceivable, the results of Krivobok and Grossmann (6) as compared to those of Tofaute et al (2), could be explained. However, as the chromium content is increased beyond 21%, 0.15% nitrogen is too low a concentration to yield a completely austenitic structure. Also, it becomes clear why the alloys of Colbeck and Garner (12) fall into the two phase, ferrite plus austenite, field. The results of Tofaute et al (2) showing that large percentages of carbon act to precipitate carbides rather than to increase the limits of the pure austenite field also becomes clear. On the other hand, the present work shows clearly (Fig. 4) that nitrogen, if increased to more than about 1.0%, will cause alloys containing as much as 33% chromium to become completely austenitic even when the carbon contents are relatively low (0.20% carbon).

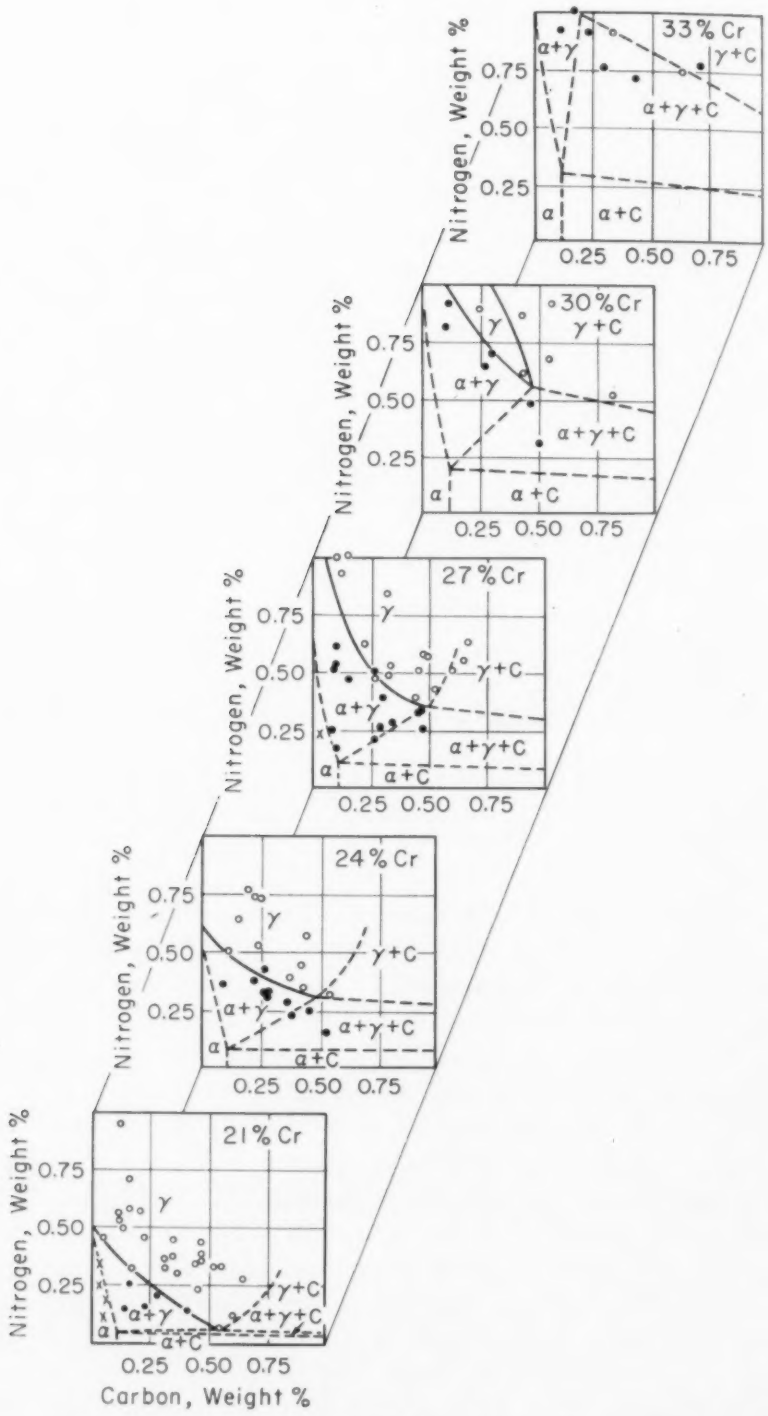


Fig. 4—Tentative Phase Relationships for the Quaternary System Iron-Chromium-Carbon-Nitrogen at 2200°F.

Table I
Compositions (%) of Sintered Compacts and Phases Present After Quenching From 2200F

Compact	Cr	C	N	Phases*	Compact	Cr	C	N	Phases
1	21.22	0.56	0.071	A-M-C	26	26.05	0.44	0.393	A
2	20.38	0.61	0.119	A	27	27.32	0.30	0.396	F-A
3	21.24	0.41	0.148	M-A-F	28	27.39	0.52	0.425	A
4	22.18	0.22	0.154	M-A-F	29	25.85	0.33	0.497	A
5	20.16	0.37	0.301	A-M	30	27.38	0.09	0.509	F-A
6	20.48	0.18	0.316	M	31	27.28	0.10	0.616	A-F
7	20.02	0.36	0.450	A	32	25.79	0.22	0.621	A
8	19.54	0.23	0.455	M-A	33	29.00	0.50	0.302	A-F-C
9	19.92	0.14	0.497	M-A	34	30.34	0.46	0.488	A-F-C
10	20.18	0.12	0.528	M-A	35	29.81	0.81	0.521	A-C
11	20.13	0.21	0.569	A-M	36	29.14	0.44	0.613	A
12	24.34	0.52	0.154	A-F-C	37	28.66	0.28	0.641	A-F
13	24.68	0.55	0.309	A-C	38	30.95	0.54	0.686	A-C
14	23.56	0.27	0.321	A-F	39	30.40	0.30	0.700	A-F-C
15	24.38	0.27	0.428	A-F	40	30.48	0.10	0.817	A-F
16	23.40	0.43	0.445	A	41	28.92	0.42	0.869	A-C
17	23.70	0.11	0.504	A-M	42	28.92	0.25	0.889	A
18	22.90	0.24	0.522	A-M	43	31.27	0.56	0.920	A-C
19	23.32	0.45	0.574	A	44	30.38	0.11	0.921	F-A
20	23.10	0.16	0.635	A-M	45	32.95	0.63	0.739	A-C
21	23.14	0.25	0.724	A	46	34.11	0.23	0.906	A-F-C
22	23.44	0.22	0.736	A	47	32.04	0.34	0.910	A-C
23	23.56	0.20	0.772	A	48	33.88	0.11	0.921	F-A
24	26.21	0.10	0.176	F-A	49	34.24	0.17	1.019	A-F
25	26.21	0.33	0.285	A-F					

*A—Austenite
F—Ferrite
C—Cubic Carbide
M—Martensite

Preliminary studies of the physical properties of the austenitic iron-chromium-carbon-nitrogen alloys reveal some distinctive characteristics. Similar to the iron-manganese-carbon Hadfield steels, the chromium alloys show extreme work hardening. This effect is reflected in their resistance both to cutting and to deformation in the tensile test. Even though this austenite shows a hardness value of only about Rockwell C-20, it is virtually impossible to cut it with ordinary tool steels although the materials can be cut readily with carbide tools. However, when the alloys are decomposed to ferrite, carbides and nitrides, they may be machined readily with ordinary cutting tools. In the tensile test, very little localized necking occurs even though reduction of area values of 50% are attained. The tensile strength of a 27% chromium-0.5% carbon-0.7% nitrogen alloy is 138,000 psi and the yield strength 90,000 psi. The alloys, of course, are nonmagnetic when in the completely austenitic state.

These alloys should have a potential usefulness in corrosive environment (because of their high chromium contents) where strength and abrasion resistance are required. The alloys may not be too suitable for elevated temperature application because they tend to decompose to ferrite, carbides and nitrides, above about 800°F.

Summary

Combined additions of carbon and nitrogen can convert steels containing between 21 to 33% chromium to a completely austenitic

Table II
Compositions (%) of Wrought Alloys and Phases Present After Quenching from 2200°F

Alloy	Si	Mn	S	P	C	Ni	Cr	N	Phases
50	0.96	0.80	0.017	0.008	0.28	0.64	20.12	0.204	A-F
51	0.75	0.83	0.010	0.014	0.46	0.72	20.81	0.230	A
52	0.87	0.86	0.013	0.024	0.65	0.64	21.05	0.289	A
53	0.80	0.97	0.023	0.014	0.31	0.66	21.27	0.320	A
54	0.82	1.02	0.011	0.023	0.52	0.59	20.60	0.325	A
55	0.94	0.95	0.024	0.012	0.56	0.64	20.88	0.330	A
56	0.80	0.81	0.016	0.012	0.45	0.71	22.20	0.350	A
57	1.29	0.98	0.010	0.010	0.32	0.63	21.11	0.359	A
58	0.72	0.84	0.024	0.020	0.48	0.68	22.24	0.362	A
59	1.17	0.86	0.018	0.017	0.35	0.02	21.15	0.380	A
60	1.24	0.75	0.013	0.012	0.47	0.75	21.93	0.385	A
61	0.84	0.79	0.010	0.020	0.48	0.64	22.30	0.440	A
62	0.93	0.80	0.010	0.008	0.39	0.64	24.14	0.220	A-F
63	0.96	0.83	0.023	0.010	0.46	0.71	25.34	0.240	A-F
64	0.61	0.77	0.014	0.026	0.36	0.13	23.98	0.290	A-F
65	0.65	0.99	0.012	0.008	0.28	0.18	25.46	0.310	F-A
66	0.61	1.05	0.020	0.012	0.29	0.71	22.60	0.328	F-A
67	0.68	0.95	0.013	0.012	0.43	0.63	24.14	0.344	A
68	0.63	0.75	0.014	0.012	0.09	0.63	22.53	0.361	F-A
69	0.63	1.01	0.008	0.014	0.22	0.63	22.77	0.382	F-A
70	0.68	0.82	0.013	0.010	0.38	0.55	24.58	0.392	A
71	0.59	0.64	0.023	0.018	0.26	0.02	27.03	0.206	F-A
72	1.01	0.98	0.010	0.012	0.47	0.25	26.55	0.260	F-A
73	0.72	0.85	0.007	0.020	0.29	0.40	27.18	0.263	F-A
74	0.82	0.86	0.010	0.010	0.45	0.20	27.00	0.325	F-A
75	0.68	0.71	0.019	0.014	0.46	0.40	26.28	0.330	A-F
76	0.70	1.04	0.012	0.012	0.15	0.63	26.99	0.476	F-A
77	0.84	0.86	0.016	0.014	0.60	0.71	26.96	0.501	A
78	0.68	0.96	0.012	0.012	0.45	0.71	25.57	0.505	A
79	0.87	0.80	0.014	0.012	0.28	0.63	26.38	0.507	A-F
80	0.82	0.86	0.017	0.014	0.33	0.71	27.57	0.538	A
81	0.77	0.90	0.034	0.014	0.65	0.67	26.79	0.550	A
82	0.80	0.84	0.020	0.020	0.49	0.67	26.62	0.580	A
83	1.15	0.98	0.010	0.008	0.47	0.25	26.89	0.587	A
84	0.77	0.90	0.020	0.022	0.68	0.67	25.74	0.638	A
85	0.91	0.81	0.017	0.016	0.30	0.71	33.73	0.768	F-A
86	0.91	0.95	0.019	0.016	0.44	0.71	33.59	0.710	F-A
87	0.72	0.87	0.020	0.018	0.71	0.63	33.46	0.781	A-F

Table III
Nitrogenization Data

COMPOSITIONS (%) OF STEELS BEFORE NITROGENIZATION								
		Si	Mn	S	P	C	Ni	Cr
	88	0.61	0.32	0.014	0.032	0.06	0.04	21.86
	89	0.63	0.77	0.017	0.026	0.32	0.08	21.21
	90	0.71	0.90	0.016	0.016	0.09	0.23	26.61
	91	0.61	0.51	0.017	0.024	0.28	0.18	27.50
CARBON AND NITROGEN CONTENTS AND PHASES AFTER NITROGENIZATION								
88	C	0.12	0.12	0.05	0.04	0.03	0.06	0.05
	N	0.946	0.568	0.462	0.350	0.262	0.193	0.112
	Phases	A	A	A	F	F	F	F
89	C	0.17	0.17	0.17	0.15			
	N	0.710	0.579	0.259	0.140			
	Phases	A	A	A+F	F+A			
90	C	0.15	0.10	0.12	0.10	0.08	0.04	
	N	1.055	1.039	0.932	0.535	0.266	0.224	
	Phases	A	A	A	A+F	F+A	F	
91	C	0.31	0.27					
	N	0.836	0.483					
	Phases	A	A					

structure at temperatures approximating 2200°F or higher. This austenite can be prevented from decomposing to ferrite, carbides and nitrides by rapid cooling to room temperature. The amounts of carbon and nitrogen required to produce a completely austenitic structure increase with increasing chromium content.

Alloys having the desired composition can be produced in several ways. The casting technique is feasible providing the carbon content is not too low. Nitrogenizing of iron-chromium-carbon alloys causes a case of austenite to form, the rate of penetration of the nitrogen which produces this case being proportional to the carbon content and the nitrogen pressure. The alloys also can be made by powder metallurgy techniques using carbides, nitrides, chromium and iron. Graphite has been used successfully, instead of carbides, as a source of carbon.

The austenite has some interesting properties in that it exhibits a high degree of work hardening as well as high tensile and yield strengths.

ACKNOWLEDGMENT

The authors are indebted to Messrs. L. Poremba and H. R. Seagren for assistance provided in this work. Many of the data were secured as parts of a cooperative program on stainless steels between Standard Oil Company (Indiana) and Crane Co. The permission of both companies to publish this work is gratefully acknowledged.

References

1. C. B. Post and W. S. Eberly, "Formation of Austenite in High-Chromium Stainless Steels," TRANSACTIONS, American Society for Metals, Vol. 43, 1951, p. 243.
2. W. Tofaute, C. Küttner and A. Büttinghaus, "Das System Eisen-Chrom-Chromkarbid Cr_7C_3-Zementit (The Iron-Chromium-Chromium Carbide Cr_7C_3-Cementite System)," *Archiv für das Eisenhüttenwesen*, Vol. 9, 1936, p. 606.
3. T. Murakami, K. Ora and S. Nishigori, "The Transformation and Constitution of High Chromium Steels," Technical Report Sendai, Vol. 9, 1929–1930, p. 405.
4. W. Tofaute, A. Sponheure and H. Bennek, "Umwandlungs, Härtungs-und Anlassvorgänge in Stählen mit Gehalten bis 1% C und bis 12% Cr, (Transformation, Hardening and Tempering Phenomena in Steels with up to 1% C and up to 12% Cr)" *Archiv für das Eisenhüttenwesen*, Vol. 8, 1934–1935, p. 499.
5. A. Westgren, G. Phragmen and T. Negresco, "On the Structure of the Iron-Chromium-Carbon System," *Journal*, Iron and Steel Institute, Vol. 117, 1928, p. 383.
6. V. N. Krivobok and M. A. Grossmann, "A Study of the Iron-Chromium-Carbon Constitutional Diagram," *Transactions*, American Society for Steel Treating, Vol. 18, 1930, p. 760.
7. M. Schmidt and O. Jungwirth, "Ein Beitrag Zur Kenntnis Hochhitzebeständiger Chromstähle (Highly Heat-Resistant Chromium Steels), *Archiv für das Eisenhüttenwesen*, Vol. 5, 1931–1932, p. 419.
8. A. B. Kinzel and W. Crafts, "Alloys of Iron and Chromium," Vol. 1, *Low-Chromium*, Engineering Foundation, published by McGraw-Hill Book Co., 1937, New York.

9. F. Adcock, "The Effect of Nitrogen on Chromium and Some Iron-Chromium Alloys," *Journal*, Iron and Steel Institute, 1926, p. 117.
10. V. N. Krivobok, "Alloys of Iron and Chromium," TRANSACTIONS, American Society for Metals, Vol. 23, 1935, p. 1.
11. R. Franks, "Chromium Steels of High Nitrogen Content," TRANSACTIONS, American Society for Metals, Vol. 23, 1935, p. 968.
12. E. W. Colbeck and R. P. Garner, "The Effect of Nitrogen Additions and Heat Treatment on the Properties of High Chromium Steels," *Journal*, Iron and Steel Institute, Vol. 193, p. 99.

DISCUSSION

Written Discussion: By Oscar E. Harder, consultant in Metallurgy, Battelle Memorial Institute, Columbus.

The authors have made a valuable contribution to our knowledge of this type of alloy by extending our knowledge of the relation of chromium to nitrogen and carbon to higher chromium contents in alloys which may be made wholly austenitic. They have plotted these relations for different chromium levels with ordinates of nitrogen and carbon in Fig. 4. James T. Gow and the writer[2] had studied the relation of carbon and nitrogen in cast 25% Cr-12% Ni type alloys.

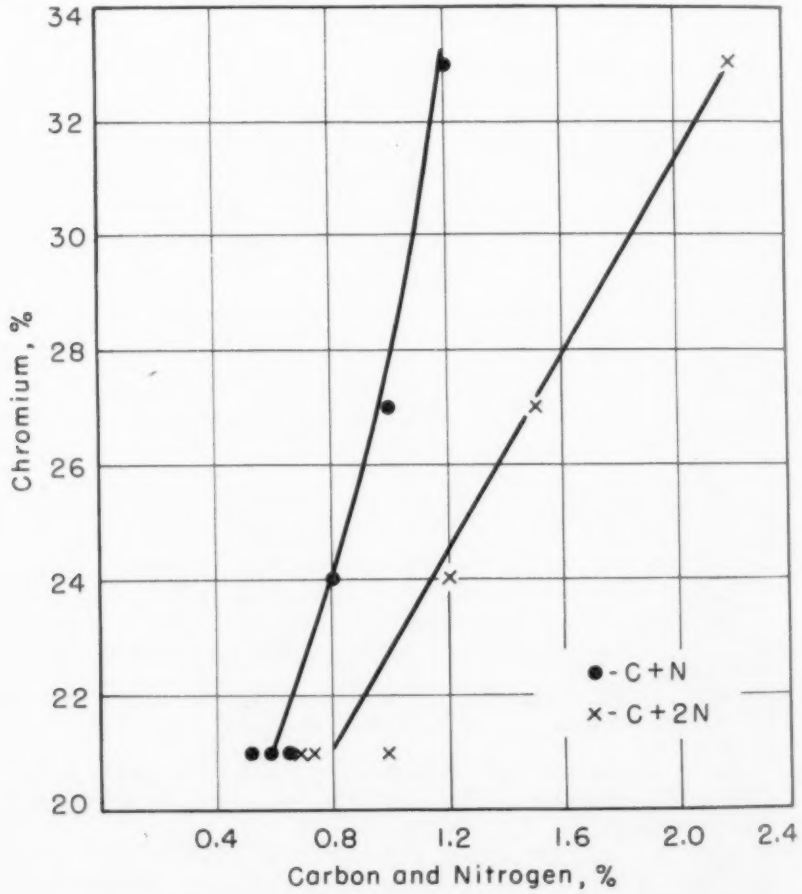


Fig. 5—Relation of Carbon and Nitrogen to Structures in Fe-Cr-C-N Stainless Steels.

[2]James T. Gow and Oscar E. Harder, "Balancing the Composition of Cast 25 Per Cent Chromium-12 Per Cent Nickel Type Alloys," TRANSACTIONS, American Society for Metals, Vol. 30, 1942, p. 855.

In that publication, Fig. 9 showed the relation of yield strength to carbon and nitrogen content when the abscissa was carbon plus two times nitrogen (C+2N) at 1600°F. Figs. 18 and 19 showed a similar relation for the tensile strength and yield strength at 1800°F. It was therefore of interest to see if a simple, but reasonable, correlation could be found between chromium and the nitrogen and carbon for alloys which could be made wholly austenitic by using the authors' data. In the accompanying figure (Fig. 5), the chromium content and the carbon plus nitrogen is plotted in one curve and the carbon plus two times the nitrogen in the second curve. Both of these curves suggest reasonable relations but the curve representing C+2N appears to be more nearly a straight line. While the authors have drawn diagram for these relations in Fig. 4, it would be of interest to see if these curves can be used to give a first approximation; and if further experience shows this to be the case, the work of selecting compositions would be greatly simplified. Further, if this relation is found to hold, it would seem possible to work out a nomographic chart such as Fig. 17 in the above reference for various combinations of carbon and nitrogen to produce alloys, which can be made austenitic by annealing, at various chromium levels. Possibly, within limits, combinations of carbon and nitrogen for the curve for C+2N (Fig. 5) can be used for rough approximations.

Authors' Reply

The authors wish to thank Dr. Harder for his discussion of this paper. We agree that the representation of compositions of fully austenitic alloys by a nomographic chart would be useful. The first approximations of either C plus N or C plus 2N, however, do not appear to yield the desired results. For example, Dr. Harder's plot shows a value of 1.5 at 27% chromium for the C+2N curve. Assuming a value of 0.1% carbon, this would result in an alloy with 0.7% nitrogen. Such an alloy would be almost 50% ferritic. However, if a more complex equation were developed to fit the austenite/austenite plus ferrite boundaries, it would be useful in simplifying the presentation of these data.

NOTCH DUCTILITY OF TYPE 410 (12% Cr) STAINLESS STEEL

By F. A. Brandt, H. F. Bishop and W. S. Pellini

Abstract

The influence of composition and heat treatment variables on the notch ductility of 12% Cr (Type 410) cast stainless steels were investigated. Sharp crack tests of large specimens were used to establish the temperature range of transition from notch-ductile to notch-brittle behavior and correlation was established with results of conventional Charpy V tests. It was demonstrated by the sharp crack tests that conventional Type 410 steels (normalized and tempered to 90,000 psi. T.S.) are susceptible to brittle fracture at "warm" service temperatures. The addition of approximately 0.70% molybdenum and nickel and the lowering of silicon from the normal 1.0/1.2% to approximately 0.50% results in material which is highly resistant to brittle fracture at low winter temperatures. It is concluded that the brittle failures of Type 410 castings experienced in various applications may be prevented by the use of the improved material. (ASM-SLA Classification: Q23, SS)

Introduction

THE ADDITION of 12% chromium to steels imparts sufficient resistance to corrosion to justify the term "stainless." Such steels are not stainless to the degree which is characteristic of 18% Cr grades; however, unlike the 18% Cr grades, it is possible to heat treat these steels to high hardness (martensitic grades) and to temper the hardened material to a wide range of strength and ductility. The straight 18% Cr grades are ferritic, and therefore nonhardenable, while the familiar 18% Cr-8% Ni grades are austenitic, i.e., the high temperature austenite phase is retained in metastable form by rapid cooling to ambient temperatures. Type 410 stainless represents a straight chromium steel of the martensitic class with the maximum (12–14%) chromium content which permits full response to heat treatment.

Because of its economy, high strength and good corrosion resistance Type 410 stainless has been used for ship propellers, water turbine wheels, oil well pressure valves and similar critical applications. Service experience involving the brittle fracture of Type 410 castings, particularly for the case of propellers, has indicated the

A paper presented before the Thirty-Seventh Annual Convention of the Society, held in Philadelphia, October 17–21, 1955. The authors, F. A. Brandt, H. F. Bishop and W. S. Pellini, are associated with the Metallurgy Division, Naval Research Laboratory, Washington, D. C. Manuscript received January 22, 1955.

need for improved notch ductility. This investigation is concerned with studies of the effects of alloy modifications and heat treatment procedures on the notch ductility of Type 410 stainless with the aim of developing material which would be expected to be resistant to brittle fracture at low service temperatures.

The general problem of the brittle behavior of steels of apparently high tensile ductility has been studied extensively for the case of structural mild steel and it has been established that such brittleness is a manifestation of inadequate notch ductility; i.e., a steel may show high ductility in the absence of notches, such as is the case of tensile tests, and no measurable ductility when notches are present. Such notches may be in the form of sharp fillets, threads and other design details or material defects in the form of nicks, casting imperfections, corrosion fatigue cracks, weld flaws, etc.

Testing Procedures

The general method of evaluating notch ductility involves the use of small notch-bend specimens such as the Charpy V or keyhole types. The specimens are broken at various temperatures and the temperature range of transition from high to low values of energy absorption serves to define the relative resistance of the steels to brittle fracture. Extensive correlation of service data with the results of these tests is necessary to determine values of energy absorption in the fracture of the small specimens which are required to provide resistance to brittle fracture in service.

As a more direct method of evaluating resistance to the initiation and propagation of brittle fracture, the Naval Research Laboratory has developed a procedure by which a sharp notch (considered equivalent to a crack-like defect in a service part) is introduced into a specimen of sufficient size to be representative of a section of the structural item. The crack defect is developed by means of a bead of brittle, hard surfacing weld metal. On loading, the bead cracks in a brittle manner thus injecting a sharp, crack-like notch into the test material. The method has been described previously (1,2,3)[1]; loading is by drop-weight or explosion depending on the severity desired. The drop-weight test, Fig. 1 (left), is aimed at determining if fracture is possible in the presence of a sharp notch when the conditions of loading are such as to develop only incipient yielding. For this test, a stop is used to limit the bend deformation of the test specimen to very low values. Fig. 2 illustrates a test series with the abrupt change from no fracture to fracture in a 10°F interval which is characteristic of the test. The highest temperature of fracture is defined as the D.W.T. (Drop-Weight Transition) which is a transition to nil ductility (%EL = nil value) in the pres-

[1] The figures appearing in parentheses pertain to the references appended to this paper.

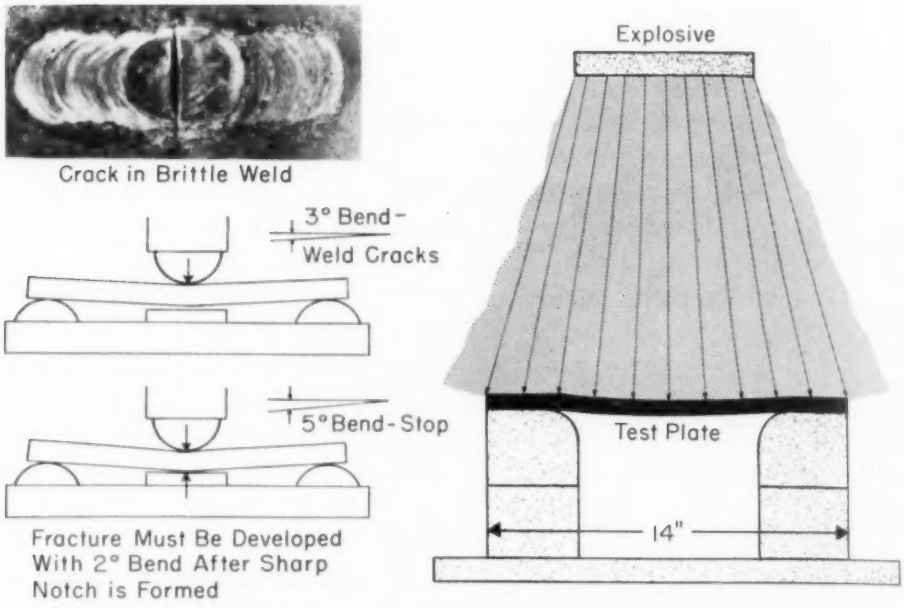


Fig. 1—(Left top) Crack Starter Weld. (Left bottom) Loading of $3\frac{1}{2} \times 14 \times 1$ inch specimen with crack starter weld by means of drop-weight; deformation limited to incipient yielding. (Right) Explosion loading of $14 \times 14 \times 1$ inch plate with crack starter weld; severe deformation developed to "force" initiation and propagation of brittle fractures.

ence of a crack-like defect. All steels develop such a sharp transition; however, the exact temperatures of the change vary widely depending on the specific notch ductilities of the materials.

The explosion test, Fig. 1 (right) uses the same crack starting weld bead as the drop-weight test, placed on the center of a $14'' \times 14'' \times 1''$ plate. Fig. 3 illustrates a test series for a 12% Cr steel having a D.W.T. of 0°F. It should be noted that 60°F above the highest fracture temperature in the drop-weight test (temperature of easy initiation of brittle fracture) the resistance to fracture is of high order. Despite the explosive loading, only short fractures in the central part of the bulge were developed at 60°F (fracture propagation was resisted). All of the wide variety of steels investigated to date have demonstrated such high resistance to fracture propagation in explosion tests at temperatures 40 to 60°F above the D.W.T.

It is apparent that the drop-weight test and the explosion test establish two broad limits of performance in relation to temperature. For example, the steel of Fig. 3 is denoted as highly susceptible to fracture initiation below 0°F (prefers to fracture rather than to deform) and is described as essentially immune to fracture propagation at temperatures in excess of 60°F. In the range of 0 to 60°F fracture may or may not occur depending on the severity of plastic overloading (forcing of fracture initiation) in the presence of a notch. Above 60°F brittle fracture cannot be "forced" to occur and

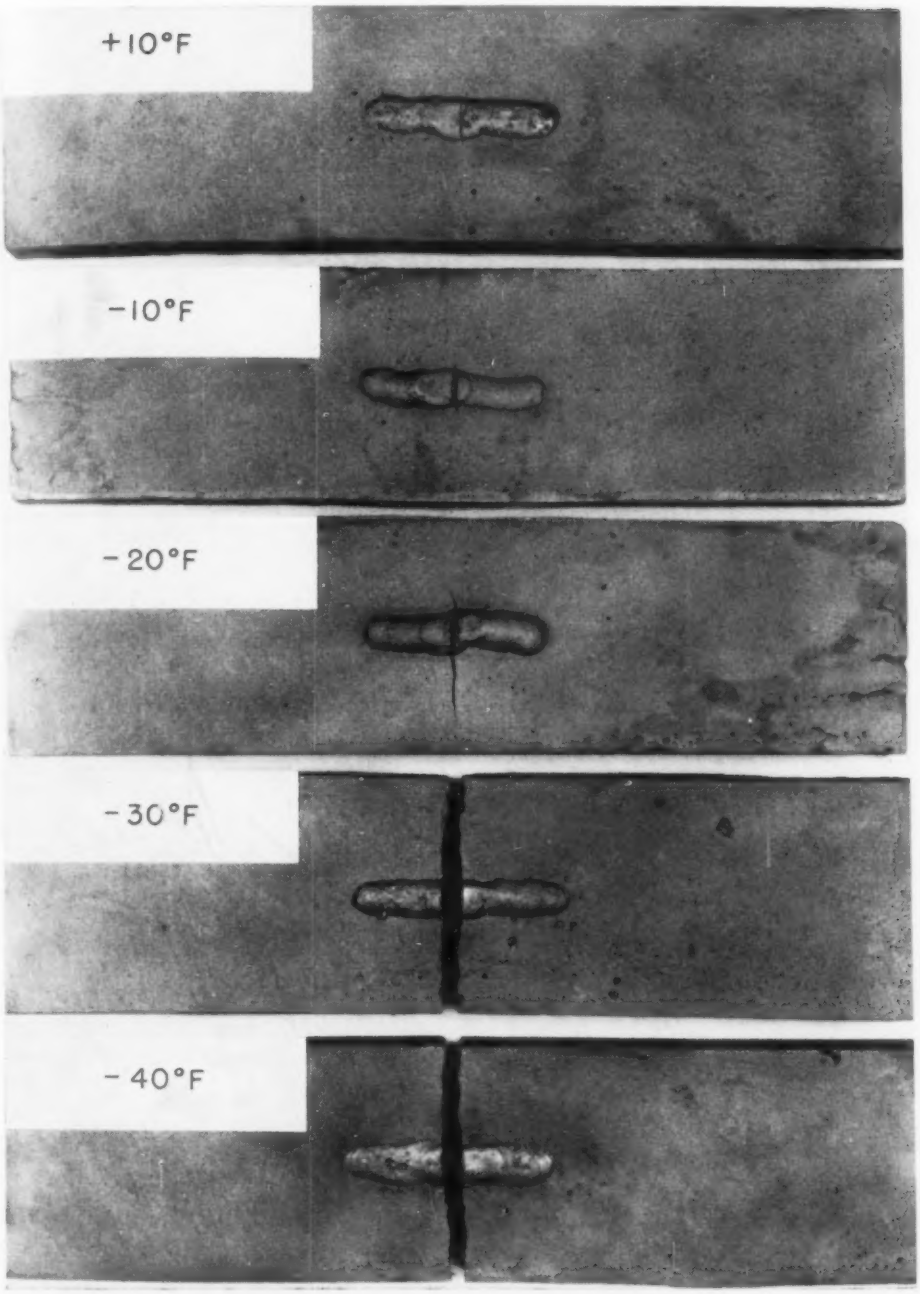


Fig. 2—Illustrating a Drop-Weight Test Series for a 12% Chromium Steel; D.W.T. is −30°F. Specimens are 14×3½×1 inches.

failure may be considered to be possible only by a mechanism of ductile tearing. The +60°F correlation, as will be demonstrated, permits full evaluation of the material on the basis of simple drop-weight tests.

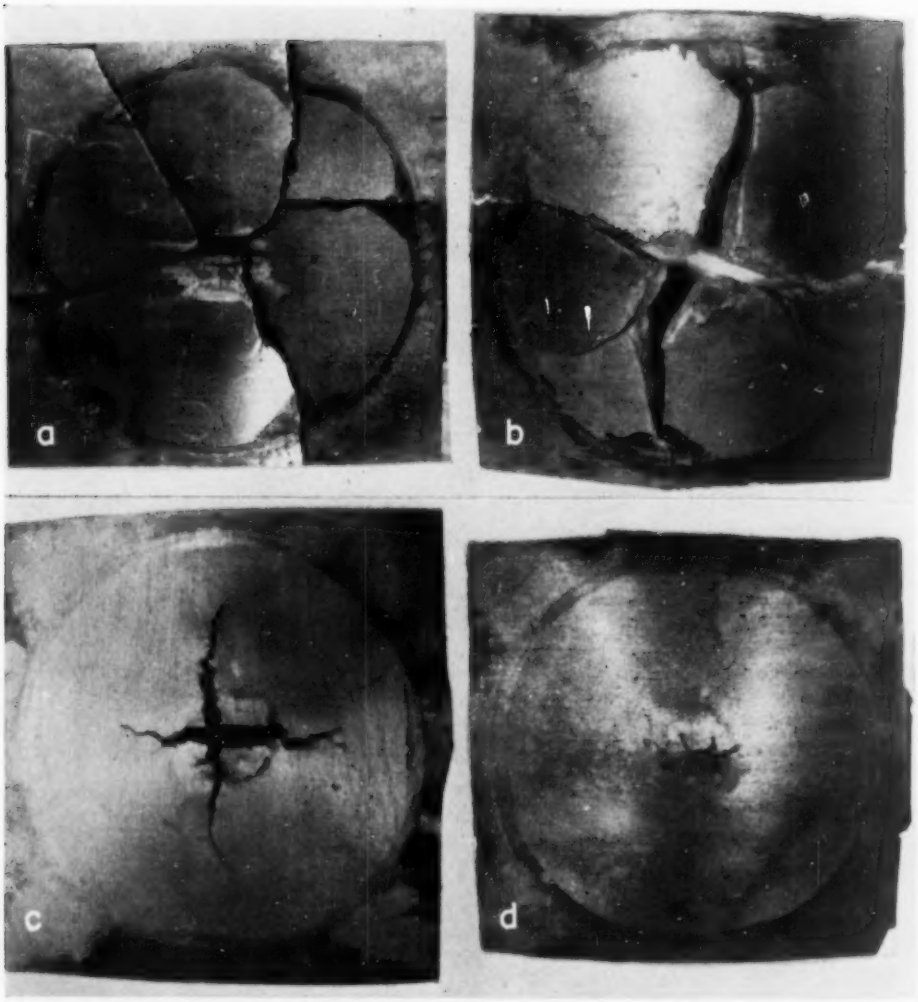


Fig. 3—Series of Explosion Loaded Test Plates (14×14×1 inch) with Crack Starter Welds to Provide a Sharp Notch Condition. (a) 0°F, (b) 20°F, (c) 60°F, (d) 100°F. Type 410 Steel with a D.W.T. of 0°F illustrating essentially complete resistance to brittle fracture 60°F above D.W.T. Temperature.

It is recognized that prototype tests such as the drop-weight and explosion crack starter tests require special equipment and that the usual procedure is to specify notch ductility as a minimum Charpy V energy value at a specific temperature. Extensive investigations of various steels have demonstrated that the drop-weight transition temperature corresponds to temperatures of the lower "tail" region of the Charpy V transition curve; i.e., low energy values in the range of 10 to 20 ft-lb, depending on the class of steel involved, (1,3,4). Accordingly, a correlation was developed between the D.W.T. temperatures and Charpy V energy values (at the D.W.T. temperatures) so that the Charpy test could be used to specify values which would preclude the development of brittle fracture at selected service temperatures.

Screening of Composition Effects

In order to evaluate the effects of variations in analysis on tensile properties and notch ductility, a series of keel blocks (1″×1″×12″ test sections projecting from a massive feeder block) were cast with systematic variations in composition. The heats were melted in an induction furnace from Armco iron stock to which ferro-alloy additions were made. The castings were poured at approximately 2900°F. In the screening heats 0.10% titanium was added to the

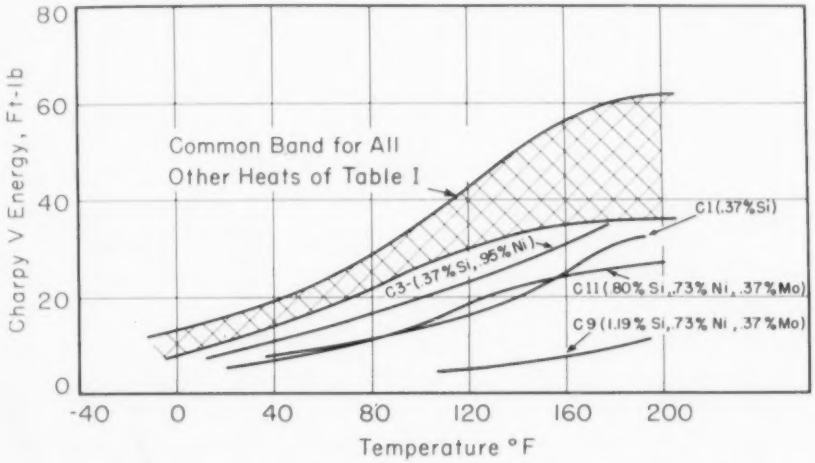


Fig. 4—Charpy V Transition Curves of Steels Listed in Table I (1850°F, 4 hours, A.C.—1200°F, 4 hours, A.C.).

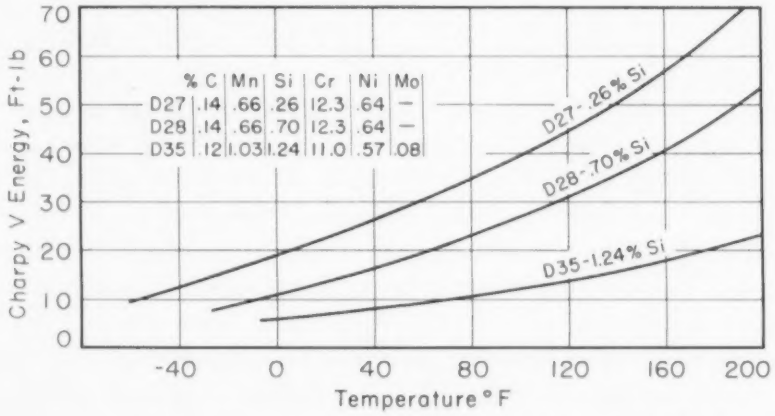


Fig. 5—Effect of Silicon on Charpy V Transition Curves (1850°F, 4 hours, A.C.—1300°F, 4 hours, A.C.).

ladle as a final deoxidizer but in subsequent heats no final addition was made. Charpy and tensile bars were machined from the 1″×1″×12″ bars following heat treatment. The elements which were indicated to be critical to the fracture problem were then to be explored further with drop-weight tests. The chemical analysis and tensile

Table I
Effect of Composition on Tensile Properties

Heat No.	C%	Mn%	Si%	Cr%	Ni%	Mo%	Temper* °F	YS (KIPS/in²)	TS (KIPS/in²)	RA%	EL%
C-4	0.10	0.80	0.52	12.0	0.66	0.43	1200	100	114	49	17
C-7	0.12	0.69	0.30	12.4	0.78	0.38	1200	101	116	43	15
C-15	0.13	0.75	0.24	12.1	0.73	0.37	1200	98	112	48	16
C-18	0.14	0.67	0.24	12.1	0.73	0.40	1200	103	117	22	11
C-16	0.11	0.54	0.24	12.1	0.73	0.37	1200	98	110	55	17
C-15	0.13	0.75	0.24	12.1	0.73	0.37	1200	98	112	48	16
C-14	0.13	0.88	0.24	12.1	0.73	0.37	1200	103	116	46	15
C-13	0.13	1.02	0.24	12.1	0.73	0.37	1200	99	114	44	15
C-15	0.13	0.75	0.24	12.1	0.73	0.37	1200	98	110	55	17
C-12	0.14	0.73	0.44	12.1	0.73	0.37	1200	102	115	47	15
C-11	0.14	0.72	0.80	12.1	0.73	0.37	1200	103	114	46	15
C-9	0.14	0.77	1.19	12.1	0.73	0.37	1200	96	117	41	16
C-5	0.15	0.69	0.34	11.2	0.73	0.40	1200	100	117	39	16
C-6	0.14	0.69	0.34	11.5	0.73	0.37	1200	100	115	46	15
C-15	0.13	0.75	0.24	12.1	0.73	0.37	1200	98	112	48	16
C-8	0.16	0.71	0.32	13.0	0.73	0.37	1200	102	118	40	15
D-30	0.12	0.55	0.50	11.0	0.74	—	1250	79	98	62	22
D-33	0.12	0.55	0.30	11.6	0.73	—	1250	76	95	66	23
D-17	0.12	0.70	0.37	13.4	0.54	0.18	1250	62	100	49	21
D-18	0.12	0.70	0.37	13.6	0.54	0.18	1250	60	99	48	21
D-19	0.12	0.65	0.35	14.4	0.54	0.18	1250	64	95	37	18
C-1	0.12	0.67	0.37	12.4	—	—	1200	86	102	50	17
C-3	0.13	0.70	0.37	12.3	0.95	—	1200	91	106	41	15
C-1	0.12	0.67	0.37	12.4	—	—	1200	86	102	50	17
C-4	0.12	0.70	0.34	12.3	—	0.53	1200	88	107	46	16
C-15	0.13	0.75	0.24	12.1	0.73	0.37	1200	98	112	48	16

*All heats austenitized 4 hours and air-cooled.

properties of the various groups are listed in Table I. The base composition which consisted of a nominal 0.12% carbon, 0.30% silicon, 12% chromium, 0.70% nickel, 0.35% molybdenum was modified by changes in the individual elements. Charpy data, presented in Fig. 4, indicated essentially common notch ductility for all heats (common band in Fig. 4) with the exception of the two high silicon heats and the two heats without molybdenum. It should be noted that the heat which contained molybdenum but no nickel fell into the common band. These data indicate that high silicon contents and the absence of molybdenum are detrimental to the notch ductility of these steels. The harmful effect of silicon on notch ductility was verified by the Charpy test data of a second silicon series which involved a 1300°F tempering treatment, Fig. 5.

Effects of Tempering Temperature

The preliminary screening tests indicated that tempering at 1200°F developed high strength properties at the expense of ductility, Table I. In order to establish the effects of tempering temperature on tensile properties, two keel block heats were normalized

Table II
Effect of Tempering Temperature on Tensile Properties

Heat No.	C%	Mn%	Si%	Cr%	Ni%	Temper °F	Y.S. (KIPS/in²)	T.S. (KIPS/in²)	RA%	EL%
D27	0.14	0.66	0.26	12.3	0.64	1100	144	193	11	5
						1200	90	109	56	20
						1300	79	100	58	22
						1400	69	99	60	23
D28	0.14	0.66	0.70	12.3	0.64	1200	94	114	50	19
						1300	84	106	57	21

(1850°F 4 hrs. A.C.) and tempered (4 hrs. A.C.) as indicated in Table II.

The effects of tempering temperature on notch ductility were investigated by the drop-weight test. For this purpose drop-weight specimens were cast in a cluster, as shown in Fig. 6, and heat treated by normalizing (1850°F, 4 hrs., A.C.) and tempering (4 hrs., A.C.) as indicated in Fig. 7 and Table III.

Fig. 7 and Table III indicate that tempering at 1300°F developed maximum notch ductility for the case of the low silicon material. The loss in notch ductility indicated by the 1400°F and particularly by the 1500°F tempering treatments is due to partial reaustenitization during tempering. A check of the critical temperature by dilatometer measurements indicated a range from 1380°F for low silicon material to 1480°F for high silicon material. This is in agreement with the D.W.T. data of the low silicon material which indicate damage from 1400°F tempering. The data presented in Table III show that high silicon material may be tempered at 1400°F without embrittlement as is predicted by the dilatometer data which indicate no austenitization at this temperature for high silicon material. It should be noted that increasing the silicon content has a detrimental effect on notch ductility as indicated by the increase in the D.W.T. from −30°F for the two low silicon heats to +70°F for the high silicon heat.

Table III
Comparison of the Effects of Tempering at 1300°F and 1400°F for Steels of Low and High Silicon Contents

Heat No.	C%	Mn%	Si%	Cr%	Ni%	Mo%	Temper °F	D.W.T. °F	Charpy V ft-lb at D.W.T.
D49	0.09	0.55	0.31	12.5	0.60	1.50	1300	−30	12
							1400	>0	—
D42	0.08	0.96	0.54	12.5	0.70	0.55	1300	−30	18
							1400	>0	—
D45	0.11	1.17	1.40	12.2	0.50	0.14	1300	70	15
							1400	60	—

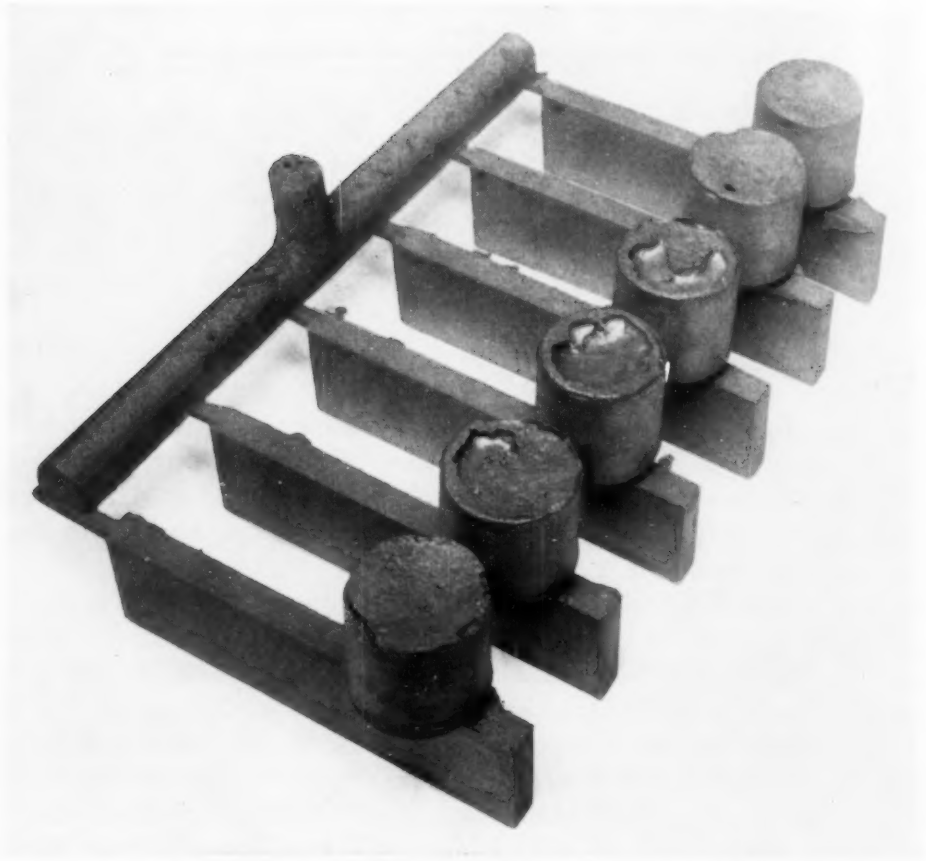


Fig. 6—Drop-Weight Test Specimens as Removed from Mold.

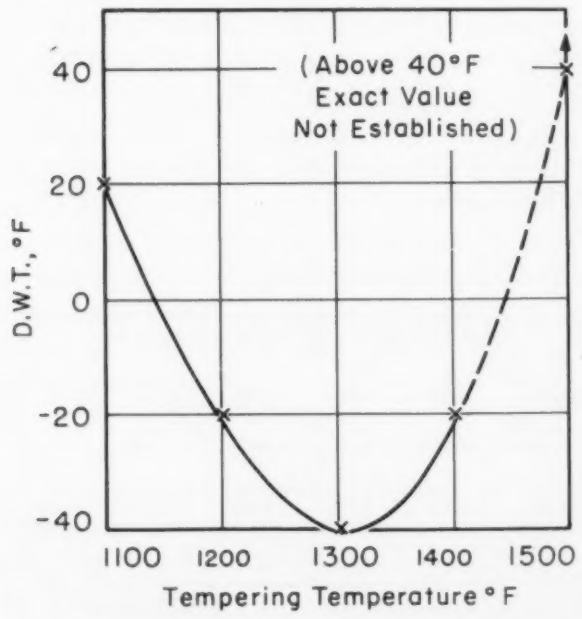


Fig. 7—Effect of Tempering Temperatures on D.W.T. (C 0.13%, Mn 0.67%, Si 0.26%, Cr 12.2%, Ni 0.64%, Mo 0.62%).

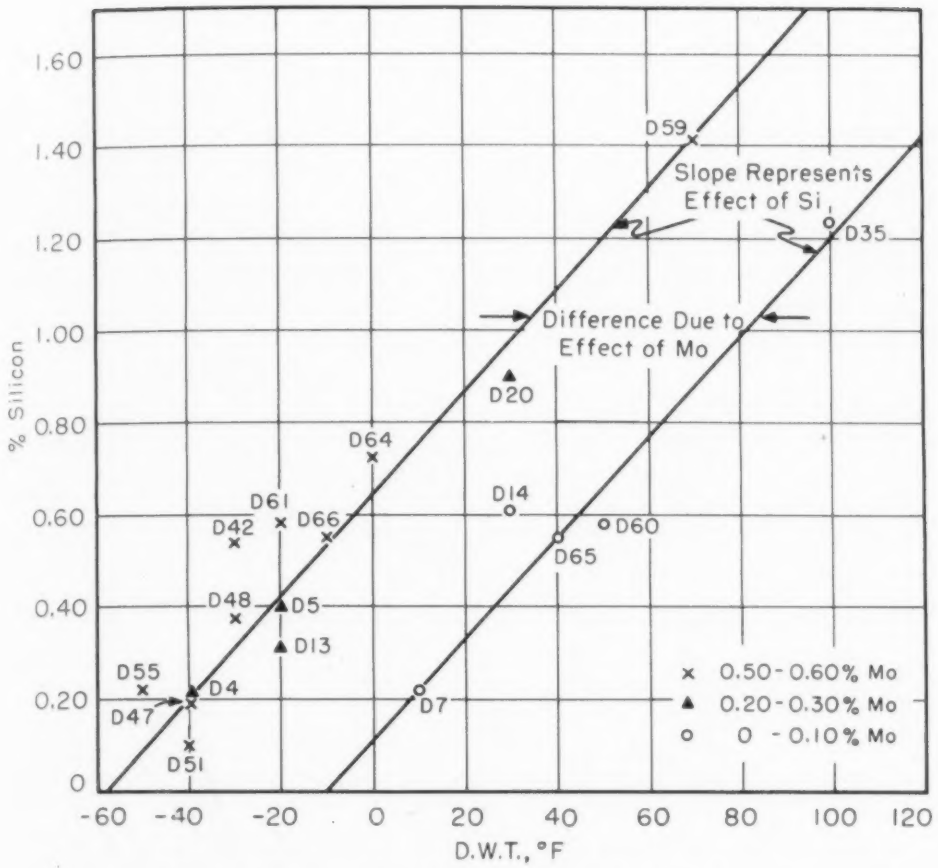


Fig. 8—Effect of Silicon and Molybdenum on D.W.T. of 1-inch Sections (1850°F, 4 hours, A.C.—1300°F, 4 hours, A.C.).

Effects of Si, Mo, Ni—1-inch Sections

The adverse effect of silicon and the beneficial effect of molybdenum indicated by the screening and tempering tests were further evaluated by additional heats of drop-weight test specimens. It was particularly desired to establish the inter-relationship of these two elements with respect to notch ductility. These additional heats were normalized (1850°F, 4 hrs., A.C.) and tempered (1300°F, 4 hrs., A.C.). The results of these tests are listed in Table IV and presented graphically in Fig. 8.

Fig. 8 illustrates that the effects of silicon and molybdenum on notch ductility are opposite and additive. For any level of molybdenum each 0.10% silicon increase has the effect of raising the D.W.T. by approximately 10°F. For any given level of silicon the addition of 0.20/0.30% molybdenum serves to lower the D.W.T. by approximately 50°F; the results of further increases of the molybdenum content to 0.50/0.60% are either very small or not significant for sections of 1-inch thickness.

Table V summarizes the results of various tests related to nickel effects.

Table IV
Effects of Si and Mo-1″ Sections

EFFECT OF Si (0.50–0.65% Mo)

Heat No.	C%	Mn%	Si%	Cr%	Ni%	Mo%	D.W.T. °F	Charpy V ft-lb at D.W.T
D51	0.08	0.34	0.10	12.5	0.50	0.64	−40	—
D47	0.10	0.41	0.19	12.3	0.73	0.60	−40	26
D55	0.13	0.37	0.22	12.0	0.75	0.65	−50	—
D48	0.12	0.75	0.37	12.3	0.73	0.52	−30	9
D42	0.08	0.96	0.54	12.5	0.70	0.55	−30	18
D66	0.12	0.75	0.55	12.5	—	0.55	−10	—
D61	0.13	0.80	0.58	12.6	0.67	0.54	−20	—
D64	0.11	0.58	0.72	11.8	0.82	0.66	0	—
D59	0.12	0.89	1.42	12.5	0.73	0.50	+70	—

EFFECT OF Si (0.20–0.30% Mo)

Heat No.	C%	Mn%	Si%	Cr%	Ni%	Mo%	D.W.T. °F	Charpy V ft-lb at D.W.T.
D4	0.12	0.54	0.21	12.5	0.65	0.25	−40	12
D13	0.12	0.50	0.31	12.5	0.50	0.30	−20	21
D5	0.12	0.55	0.40	12.5	0.68	0.28	−20	17
D20	0.10	1.05	0.90	12.0	0.40	0.20	+30	15

EFFECT OF Si (0–0.10% Mo)

Heat No.	C%	Mn%	Si%	Cr%	Ni%	Mo%	D.W.T. °F	Charpy V ft-lb at D.W.T.
D7	0.15	0.50	0.22	12.0	0.10	—	+10	—
D65	0.12	0.75	0.55	12.5	—	—	+40	—
D60	0.13	0.82	0.58	12.6	0.70	—	+50	—
D14	0.11	0.65	0.61	11.6	0.15	—	+30	—
D35	0.12	1.03	1.24	11.0	0.57	.08	+100	14

It is indicated that the addition of 0.70% nickel to a molybdenum free steel has no significant effect on notch ductility (D65, D14, D60), however, the improvement in notch ductility obtained by molybdenum is slightly enhanced by the addition of nickel.

It should be recognized that the effect of silicon is one of solid solution embrittlement and therefore is not a function of section size. In other respects these data indicate effects which are specific to the 1-inch section size of the test pieces. The possibility that increasing the molybdenum from the 0.20/0.30% range to 0.50/0.60% range may be beneficial for thicker sections and that the addition of nickel may provide for additional improvements will be discussed in the following sections.

Table V
Effect of Nickel—1-Inch Sections

Heat No.	C%	Mn%	Si%	Cr%	Ni%	Mo%	D.W.T. (°F)
D65	0.12	0.75	0.55	12.5	—	—	+40
D14	0.11	0.65	0.61	11.6	0.15	—	+30
D60	0.13	0.82	0.58	12.6	0.70	—	+50
D66	0.12	0.75	0.55	12.5	—	0.55	−10
D26	0.12	0.68	0.49	11.9	0.55	0.17	0
D61	0.13	0.80	0.58	12.6	0.67	0.54	−20
D42	0.08	0.96	0.54	12.5	0.70	0.55	−30

Effects of Section Size and Cooling Rate

Prior to evaluating the effects of slow cooling rates such as are obtained with massive sections it was necessary to establish if optimum notch ductility was obtained by air cooling 1-inch sections from the 1850°F austenitizing temperature. Accordingly, comparisons were made of the notch ductility of 1-inch sections (drop-weight specimens) resulting from the standard normalizing treatment with that obtained as the result of oil quenching from 1850°F; both types were tempered at 1300°F for 4 hours. The effects of double tempering treatments were also investigated to establish if any benefit resulted, Table VI.

Table VI
Effect of Quenching 1-Inch Sections

Heat No.	C%	Mn%	Si%	Cr%	Ni%	Mo%	Heat-Treat	D.W.T. °F	Charpy ft-lb at D.W.T.
D47	0.10	0.41	0.19	12.3	0.73	0.60	Standard	−40	26
							1850-OQ,Temp	−40	—
							1850-OQ,Dbl.Temp	−40	—
D38	0.12	0.49	0.25	10.8	1.21	0.43	Standard	−40	14
							1850 AC,Dbl.Temp	−40	—
							1850-OQ,Temp	−40	—
D48	0.12	0.75	0.37	12.3	0.73	0.52	Standard	−30	9
							1850-OQ,Temp	−30	—
							1850-OQ,Dbl.Temp	−40	—

The results of these tests show that the notch ductility of the 1-inch sections of steels containing molybdenum is not improved by quenching treatments. Similarly, there appears to be no benefit resulting from double tempering treatments.

To determine the notch ductility characteristics of more massive sections, plates having dimensions of 4×14×14 inches were cast and normalized as such (in two cases the 4-inch sections were oil-quenched). In all cases the treatments consisted of austenitization for 4 hours at 1850°F (A.C.) and tempering for 4 hours at 1300°F (A.C.). Standard, 1-inch thick specimens were also cast from the same heat for comparison purposes. The D.W.T. determined with the cast-to-size 1-inch specimens were also compared with those determined with 1-inch thick specimens removed from the 4-inch thick plate, Table VII.

These data indicate that the slower cooling rate obtained with the thick plates has no significant effect on notch ductility in the case of the high molybdenum steels; the D.W.T. is raised only 10°F. For the case of the low molybdenum (and nickel only) steels an increase in D.W.T. of 30 to 60°F is obtained. The notch ductility of 1-inch thick sections cut from the 4-inch plate prior to heat treatment (D39) shows no significant difference when compared to that

Table VII
Effect of Section Size

Heat No.	C%	Mn%	Si%	Cr%	Ni%	Mo%	Section Heat Cast	Section Heat Treat	Heat-Treat	Charpy D.W.T. °F	Charpy ft-lb at D.W.T.
D39	0.12	0.40	0.66	10.8	0.74	0.13	1″	1″	Standard	+20	10
							4″	4″	Standard	+80	20
							4″	1″	Standard	+10	—
D45	0.11	1.17	1.40	12.2	0.50	0.14	1″	1″	Standard	+60	15
							4″	4″	Standard	+100	16
D83	0.12	0.54	0.49	11.4	0.60	0.37	1″	1″	Standard	0	—
							4″	4″	Standard	+20	—
D48	0.12	0.75	0.37	12.3	0.73	0.52	1″	1″	Standard	−30	9
							4″	4″	Standard	−20	14
							4″	4″	1850-OQ-Temp	−30	—
D42	0.08	0.96	0.54	12.5	0.70	0.55	1″	1″	Standard	−30	18
							4″	4″	Standard	−20	13
D53	0.11	0.56	0.18	12.1	0.61	0.64	1″	1″	Standard	−40	30
							4″	4″	Standard	−30	12
D60	0.13	0.82	0.58	12.6	0.70	—	1″	1″	Standard	+50	—
							4″	4″	Standard	+80	—
							4″	4″	1850-OQ-Temp	+40	—

of the cast-to-size 1-inch sections. Quenching of the 4-inch sections develops properties equivalent to those of the 1-inch thick sections even for the case of the low molybdenum steels.

It may be concluded that a molybdenum content in the order of 0.20/0.30% is required to develop optimum properties for sections which cool in air at rates equivalent to 1-inch thick plates. At these cooling rates the difference between no molybdenum and 0.20/0.30% molybdenum involves a 50°F difference in D.W.T. but increasing the molybdenum content above 0.20/0.30% does not improve notch ductility. For cooling rates corresponding to 4-inch thick plates, 0.50/0.60% molybdenum appears to be sufficient to develop optimum notch ductility. Oil quenching of a 4-inch thick molybdenum-free plate lowered the D.W.T. from 80 to 40°F. Therefore, quenching treatments applied to molybdenum-free 12% chromium steels appear to be relatively ineffective compared to that which may be accomplished by the addition of molybdenum which results in a D.W.T. as low as −30°F for normalized 4-inch thick plates. The effect of silicon is essentially independent of section size or heat treatment as is expected of a solid solution embrittling element.

Additional tests were conducted to further evaluate the effects of nickel in combination with molybdenum. It should be noted that all the high molybdenum heats of Table VII also contained 0.60 to 0.70% nickel. In consideration of the strategic value of nickel it was considered important to determine with certainty if its addition is necessary for heavy sections.

Sections of 4″×14″×14″ size were cast of the compositions listed in Table VIII and heat treated 1850°F (4) A.C., 1300°F (4) A.C.

Table VIII
Effect of Nickel in Combination with Molybdenum

Heat	C%	Mn%	Si%	Cr%	Ni%	Mo%	D.W.T. (°F)
72A	0.11	0.64	0.41	12.0	0.10	0.05	+40
B	0.11	0.64	0.41	12.0	0.10	0.52	+10
C	0.11	0.64	0.41	12.0	0.77	0.52	−10
80A	0.11	0.66	0.56	12.2	0.09	0.05	+30
B	0.11	0.66	0.56	12.2	0.09	0.57	0
C	0.11	0.66	0.56	12.2	0.71	0.57	−20

It is evident from these data that nickel in combination with molybdenum is beneficial for the case of heavy sections. Values of D.W.T. below 0°F are developed only for the two heats which contained both nickel and molybdenum.

For sections somewhat in excess of 4-inch thickness a question arises as to the possible need of molybdenum contents higher than 0.50/0.60% for cooling rates slower than obtained with 4-inch thick sections. To establish this fact, furnace cooling treatments were applied to the standard 1-inch thick drop-weight specimens. Slow cooling rates of 20 to 30°F per hour through the critical transformation temperatures (750 to 500°F) were used. While the thickness of the section cooling in air, to which these cooling rates are comparable, is not known, it would necessarily be great when it is considered that 1-inch and 4-inch sections cooled in air have been found to cool through the transformation range at average rates of 2000°F per hour and 500°F per hour respectively. The results obtained from the furnace cooled specimens are presented in Table IX.

Table IX
Effect of Slow Cooling

Heat No.	C%	Mn%	Si%	Cr%	Ni%	Mo%	Heat-Treat °F	D.W.T. °F	Charpy Ft-lb at D.W.T.
D55	0.13	0.37	0.22	12.0	0.75	0.65	Standard	−50	—
							1850 FC-1300 AC	−30	—
D36	0.12	0.45	0.28	10.7	0.60	0.18	Standard	0	20
							1850 FC-1300 AC	50	14
D60	0.13	0.82	0.58	12.6	0.70	—	Standard	50	—
							1850 FC-1300 AC	100	—

These data demonstrate that in the presence of nickel, 0.65% molybdenum is sufficient to develop good notch ductility even for exceedingly slow cooling rates, i.e., corresponding to sections thicker than the 4-inch plate size used in this investigation. It is noted that when molybdenum is low or absent, the presence of 0.60/0.70%

nickel is not effective in developing optimum properties and the D.W.T. of the furnace-cooled material is raised 50°F. It may be concluded that nickel by itself is ineffective but added to 12% chromium steel containing molybdenum it is beneficial and should be used.

The effect of high molybdenum contents for material cooled at normal rates was further investigated by casting two heats of 1.50% molybdenum material for comparison with the 0.70% molybdenum grades. The heat treatment cycle 1850°F (4 hours) A.C., 1350°F (4 hours) A.C. was used for both the 1-inch and 4-inch sections which were investigated.

Table X
Effect of High Molybdenum Content

Heat	C%	Mn%	Si%	Cr%	Ni%	Mo%	Section	D.W.T. (°F)
D49	0.09	0.55	0.31	12.5	0.60	1.50	4″	0°
							1″	−30°
D52	0.13	0.59	0.37	12.1	0.67	1.42	4″	−10°
							1″	−30°
D48	0.12	0.75	0.37	12.3	0.73	0.52	4″	−20°
							1″	−30°
D61	0.13	0.80	0.58	12.6	0.67	0.54	4″	+10°
							1″	−10°
D42	0.08	0.96	0.54	12.5	0.70	0.55	4″	−20°
							1″	−30°

The comparisons Table X indicate that there is no advantage, insofar as notch ductility is concerned, resulting from higher molybdenum contents. As predicted by the furnace cooling experiments 0.60/0.70% molybdenum is sufficient to develop optimum notch ductility in heavy sections. The tensile and Charpy V properties of the two high molybdenum type heats were as follows:

	Y.S. (psi)	T.S. (psi)	%EL	%RA	Charpy V Ft-lb at D.W.T.
D49 4″ Section	73,000	98,000	21	55	15
D49 1″ Section	77,000	102,000	23	64	10
D52 4″ Section	—	—	—	—	17
D52 1″ Section	83,000	109,000	23	58	13

Relation of Notch Ductility to Microstructure

The 12% chromium steels border the gamma loop and therefore are sensitive to composition changes. Additions of ferrite forming elements such as silicon and molybdenum contract the gamma loop; conversely, austenite forming elements (Ni, C, N, Mn) act to expand the gamma loop. Whether a given composition will be entirely within the gamma loop or in a partially ferrite region at austenitizing temperatures may be established in terms of "chromium equiva-

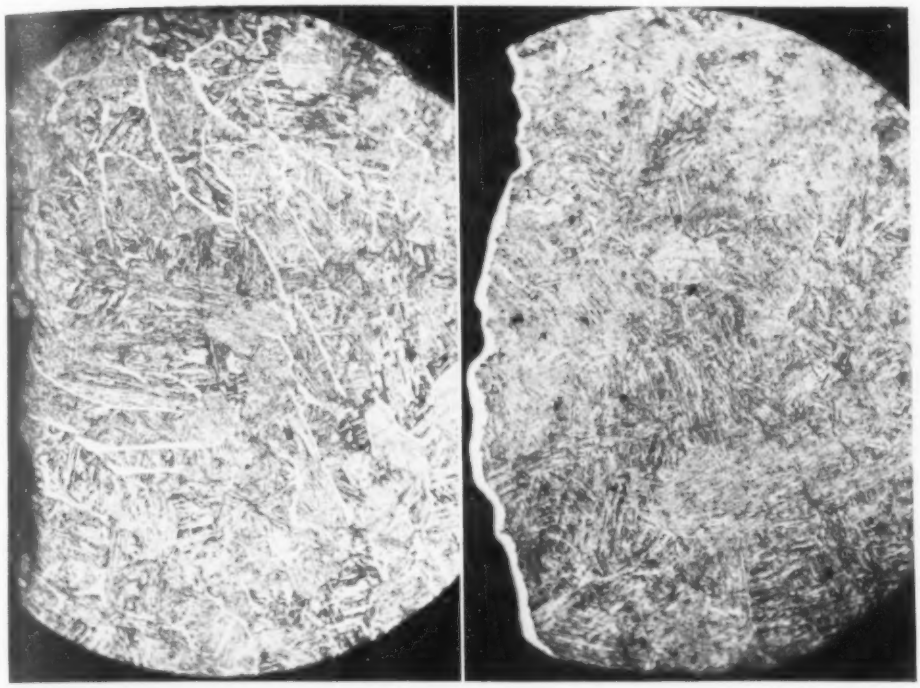


Fig. 9—Microstructures at Fracture Surfaces of D.W.T. Specimens (Right Nickel Plated) Left, Si 0.55% Cr Equivalent 10.0 D.W.T.—10°F; Right, Si 1.24% Cr equivalent 4.9 D.W.T. 100°F (×100).

lent" according to the following formula which is the authors' modification of Rickett's original formula (5).

Chromium Equivalent = 1Cr + 2Si + 1.5Mo − 2Ni − 1Mn − 15N − 27C. Values of C. E. above 7.3 indicate that ferrite will be present in the microstructure. The effects of such untransformed ferrite was of concern since it has been considered that brittle fractures of 12% chromium steels may have been related, in part, to the presence of ferrite networks. As the result of metallographic studies of the various heats of this investigation it appears that the presence of free ferrite is due to the high silicon contents and while it thus indicates a brittle material it is not per se the cause of brittleness. Fig. 9 presents representative microstructures in relation to notch ductility for a high silicon material with sufficient additions of austenite forming elements to result in a chromium equivalent of less than 7.3 (no ferrite present) as compared to a lower silicon material with a chromium equivalent of more than 7.3 (ferrite present). The conclusion that free ferrite is not deleterious to the notch ductility of 12% chromium steels is justified only for ferrite contents as high as 10%; no data are available for higher amounts.

The microstructures resulting from the various heat treatments and alloy variations consisted of acicular, low temperature products which are difficult to resolve and differentiate. It was found microstructural appearance could not be correlated with notch ductility.

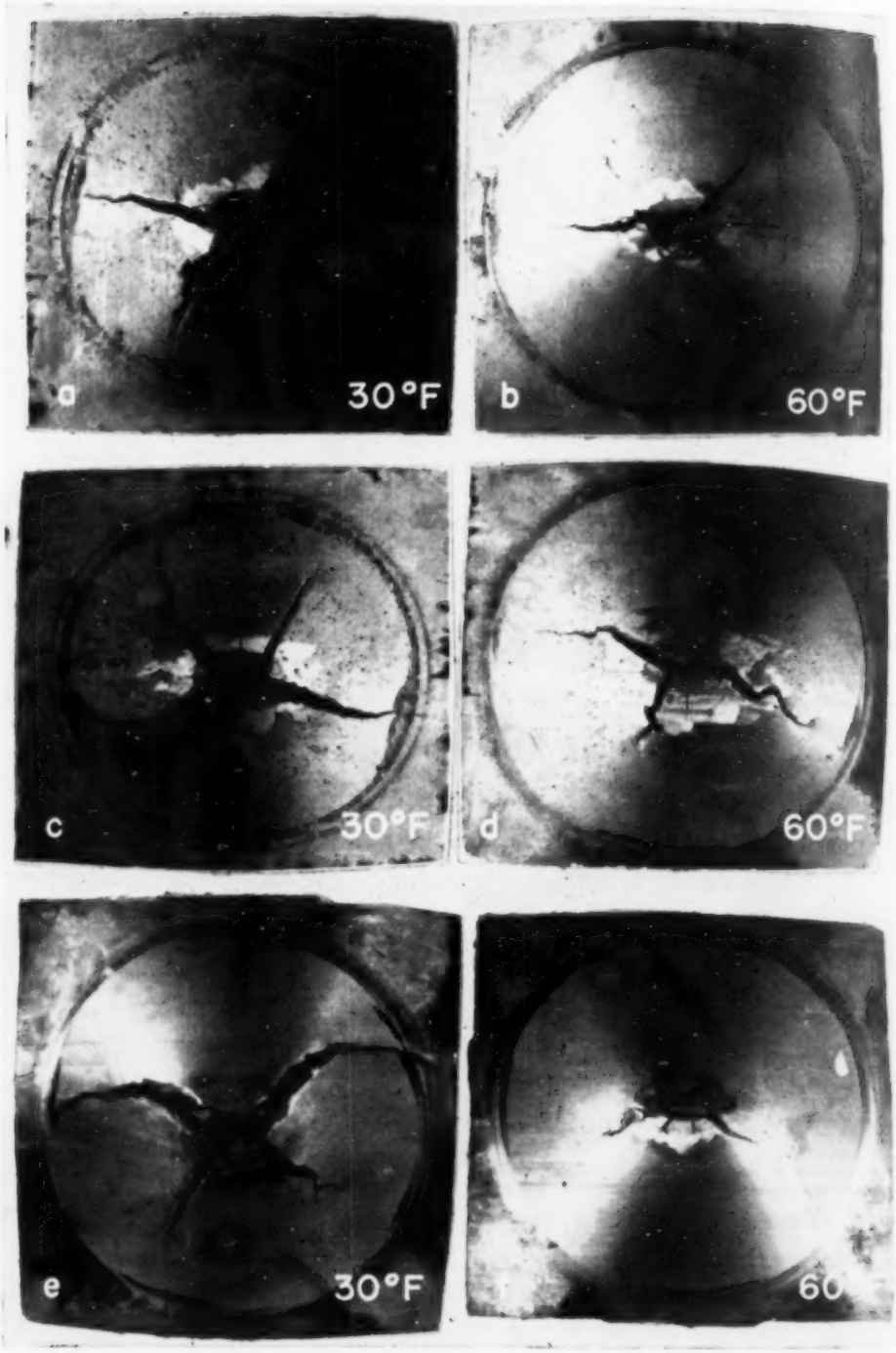


Fig. 10—Explosion Loaded 14×14×1 inch Plates with Crack Starter Welds, Illustrating High Resistance to Fracture at Freezing and Higher Temperatures Despite Drastic Loading. Materials have D.W.T. temperatures 50 to 70°F below freezing temperature. (a and b) Steel D5, D.W.T. −20°F; (c and d) Steel D13 D.W.T. −20°F; and (e and f) Steel D47 D.W.T. −40°F.

Explosion Tests

As described in the introductory section, the D.W.T. signifies the highest temperature at which the steel is unable to deform

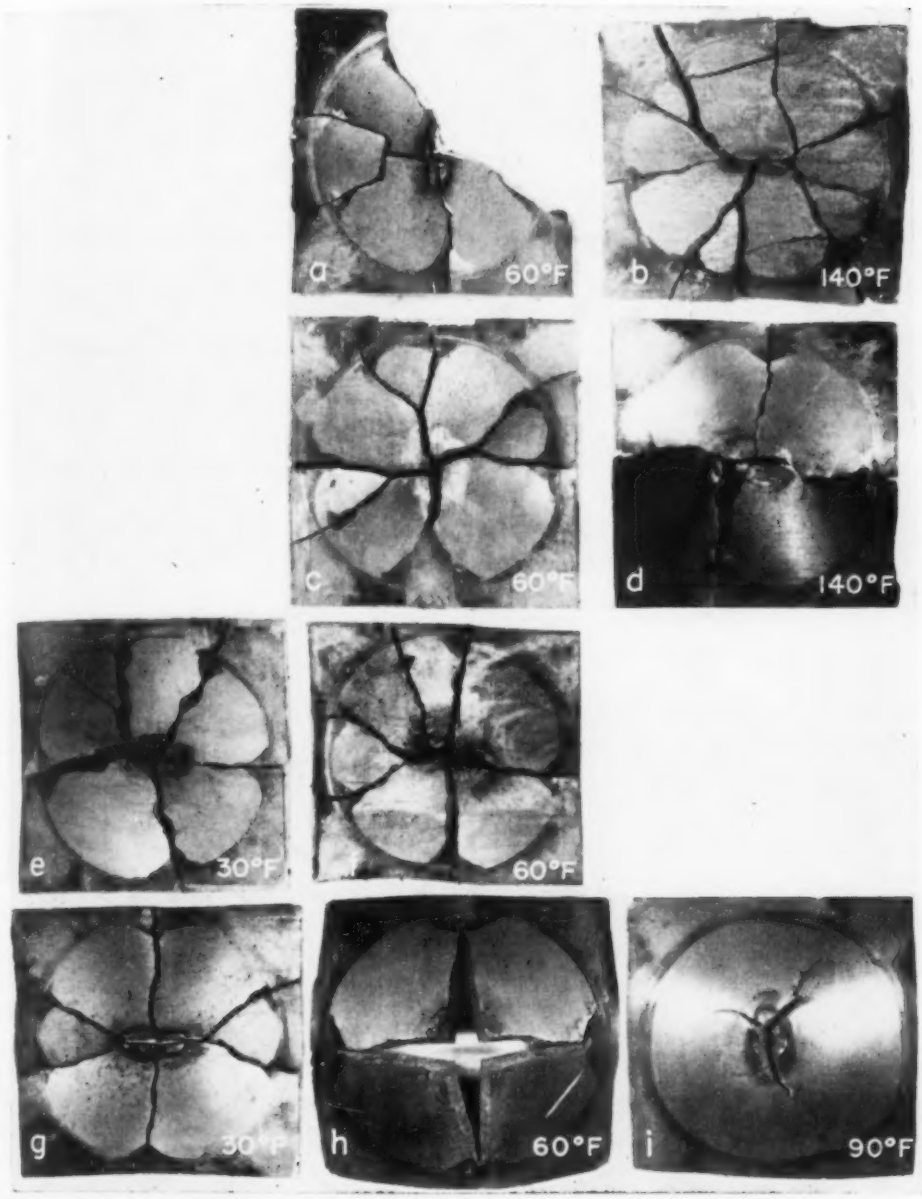


Fig. 11—Explosion Loaded Plates Tested Under Same Conditions as Plates of Fig. 10 Illustrating Brittleness at Warm Temperatures Developed by Drastic Loading for Materials with D.W.T. Temperatures Above 0°F. (a and b) Steel D35 D.W.T. 100°F; (c and d) Steel D45 D.W.T. 60°F; (e and f) Steel D14 D.W.T. 30°F; and Steel D36 D.W.T. 0°F.

even slightly in the presence of a crack or a notch-like flaw. If service conditions are considered to entail drastic deformation, safety from fracture will not be assured by steels having D.W.T. temperatures which are only slightly below the lowest temperature of service. For such loading conditions it is necessary to have steels with D.W.T.'s which fall approximately 60°F below the lowest temperature of service. This is established on the basis of explosion tests which demonstrate that temperatures 60°F above the D.W.T. are

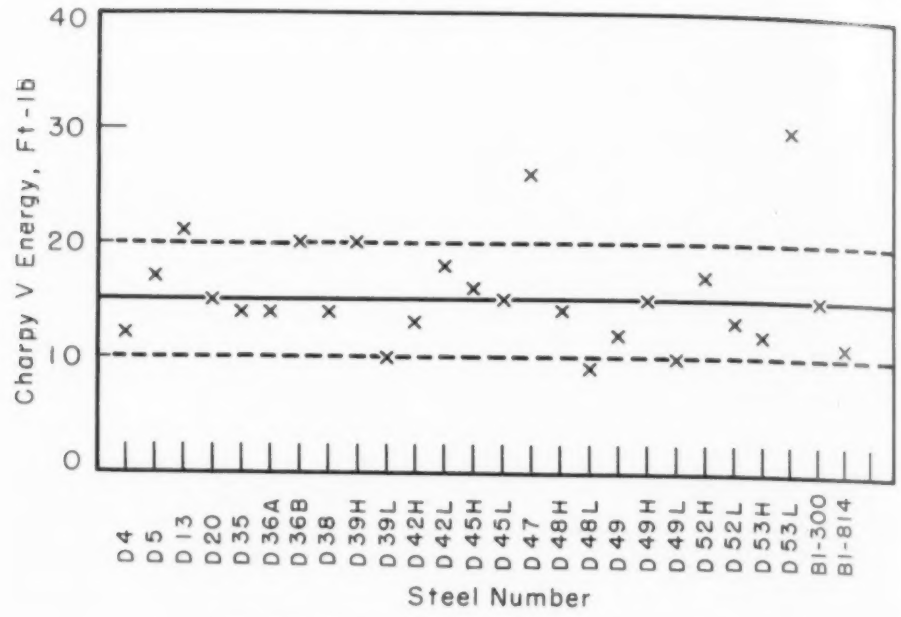


Fig. 12—Charpy V Energy Values at D.W.T. of 26 Heats of 12% Chromium Steels.

required to prevent the forced initiation and propagation of brittle fractures as the result of drastic loading. Figs. 10 and 11 present evidence of the behavior, at 30 to 90°F, of various 12% chromium steels of different D.W.T. characteristics. Note that steels with D.W.T. of −20°F, or lower, are highly resistant to fracture in explosion tests at 30 to 60°F; steels with 0°F D.W.T. fragment at 30°F and barely manage to hold together at 60°F; steels with D.W.T. of 60°F and higher fragment when tested at temperatures as high as 140°F.

It should be emphasized that whether a steel with a D.W.T. slightly below the lowest service temperature or one with D.W.T. 60°F below the lowest service temperature is desired, depends on the severity of service which is expected. If the loading conditions are assumed to be mild, i.e., entailing only yield point loading, the former material would be satisfactory; however, if severe loads resulting in large plastic deformations are expected, the latter material should be required. In all cases an assumption is made that notches will be present and that the problem is one of preventing the triggering of a brittle fracture from these notches.

Correlation with Charpy V Tests

In the various tables of this report the Charpy V ft-lb values developed at the drop-weight transition temperature (D.W.T.) were reported. Fig. 12 presents a summary of this correlation from which it is concluded that the D.W.T. temperatures occur at temperatures of Charpy V 10 to 20 ft-lb (most frequently 15 ft-lb). To insure that

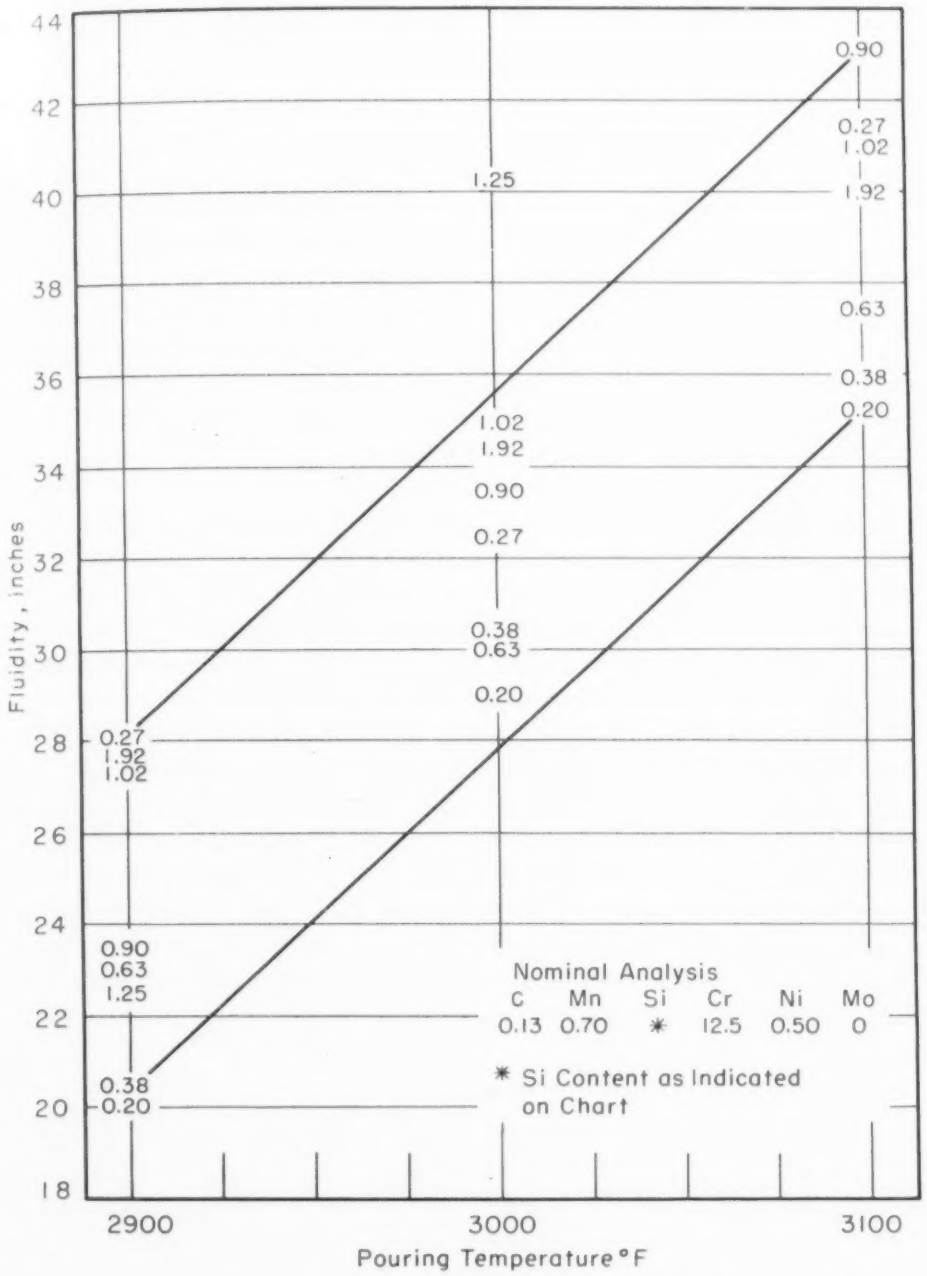


Fig. 13—Fluidity of 12% Chromium Steels of Various Silicon Contents.

the D.W.T. would be below any given temperature a minimum value of 20 ft-lb should be specified for the desired temperature. Depending upon the criteria of service severity described in the previous section this would mean that 20 ft-lb minimum should be set slightly below the lowest temperature of service or 60°F below this temperature. It is apparent from the results of various tests that low silicon, Mo-Ni, 12% chromium steels of 90,000 psi tensile strength are suitable for nondeformation type service to as low as

−40°F; for severe service entailing deformation the lowest suitable temperature is approximately +20°F.

Castability of 12% Chromium Steels

High chromium steels are not as easily cast as the lower alloy steels and have a tendency to exhibit wrinkles, laps, and incompletely filled corners on the cope surfaces of the castings. Such defects are commonly ascribed to inadequate fluidity and have lead to the prevalent belief that high silicon with its reported beneficial effect on fluidity is necessary to obtain good surfaces on 12% chromium steel castings. In this investigation these defects were noted on test castings made with either high or low silicon and are ascribed primarily to the tenacious chromium oxide surface film which is characteristic of these steels.

In order to quantitatively determine the fluidity of these steels, fluidity spirals were poured at temperatures varying between 2900 and 3100°F with 12% chromium steels in which silicon content varied from 0.20 to 1.9%. The interrelation between spiral length, silicon content and pouring temperature, Fig. 13, shows that at any given pouring temperature the maximum variation between the most fluid and the least fluid steel is 8 inches of spiral length, and that for each 100°F increment in pouring temperature the spiral length for any analysis is increased approximately 8 inches. A reproducibility of ±2 inches is usually the best which can be obtained in such tests. Inasmuch as silicon lowers the liquidus temperature, the moderate increase in fluidity obtained at a given pouring temperature with increasing silicon content may be ascribed to this effect. These data show that the small losses in fluidity resulting from lowering the silicon content can be regained with moderate increases in superheat.

Summary

The factors which influence the resistance to brittle fracture of 12% chromium steels were investigated by Charpy V tests and by sharp crack tests of large specimens involving drop-weight and explosion loading. The investigation was aimed at finding a solution to the problem of the brittle fractures of 12% chromium castings such as propellers and valve bodies. The following general conclusions were indicated:

1. As was firmly established for the case of structural mild steels, brittle fracture is possible for 12% chromium steels which show high tensile ductility (50–60% RA and 20–22% EL). Evaluation of the relative resistance to catastrophic, brittle failures requires the use of notch ductility tests.

2. Optimum notch ductility for any given composition is developed by tempering in the range of 1300 to 1400°F; high silicon

contents permit the use of the higher temperatures because of an increase in the critical temperature.

3. The addition of molybdenum and nickel is required to develop optimum notch ductility in heavy sections. Approximately 0.70% molybdenum and nickel permits full hardening on normalizing of sections equivalent at least, to 4-inch thick plates; approximately 0.25% molybdenum is required for a similar effect for sections equivalent to 1-inch thick plates.

4. Decreasing the silicon content from the normal 1.0/1.2% to 0.40/0.50% results in a marked improvement in notch ductility. The improvement is additive to that obtained by increased hardenability.

5. The following analyses and heat treatment are recommended for 12% chromium steels expected to resist brittle fracture to low temperatures.

(a) 1-inch section size: 0.50% silicon (max), 0.25% molybdenum (carbon, manganese, chromium, sulphur and phosphorus within existing specifications)

(b) 4-inch section size: 0.50% silicon (max), 0.50/0.60% molybdenum, 0.60/0.70% nickel, (carbon, manganese, chromium, sulphur and phosphorus within existing specifications). Normalize 1850°F (1 hr/in of section) A.C. temper 1300°F (4) A.C.

6. In the presence of sharp crack flaws (worst case) the above material resists the development of brittle fracture as follows:

(a) to as low as −40°F for conditions of loading involving only incipient yielding.

(b) to as low as +20°F for conditions of loading involving drastic deformations such as obtained by explosions.

In comparison, the conventional Mo and Ni free, type 410 material which has frequently failed in service has equivalent critical temperatures of approximately 80°F and 140°F. Increasing silicon above the 0.50% max specified increases the critical temperatures by 10°F for each 0.10% silicon.

7. Charpy V test correlation with the sharp crack tests indicates that a 20 ft-lb minimum value at the lowest expected service temperatures are required to preclude the development of brittle fractures under conditions of 6 (a) and 20 ft-lb minimum values 60°F below the lowest service temperature are required for conditions of 6 (b).

Acknowledgment

The support of this investigation by Code 582 USN Bureau of Ships, Mr. W. H. Baer and T. Griffin is acknowledged by the authors.

References

1. W. S. Pellini, "Significance of Charpy Tests to Service Performance," American Society for Testing Materials, 1953 Symposium on Metallic Materials at Low Temperatures.

2. W. S. Pellini, G. Sandoz and H. F. Bishop, "Notch Ductility of Nodular Iron," TRANSACTIONS, American Society for Metals, Vol. 46, 1954, p. 418.
3. P. P. Puzak, M. E. Schuster and W. S. Pellini, "Crack Starter Tests of Ship Fracture and Project Steels," *Welding Journal*, Vol. 33, October 1954, p. 481S.
4. P. P. Puzak, M. E. Schuster and W. S. Pellini, "Applicability of Charpy Test Data," *Welding Journal*, Vol. 33, September 1954, p. 433S.
5. R. L. Rickett, W. F. White, C. S. Walton and J. C. Butler, "Isothermal Transformation, Hardening and Tempering of 12% Chromium Steel," TRANSACTIONS, American Society for Metals, Vol. 44, 1952, p. 138.

DISCUSSION

Written Discussion: By J. J. Connelly, metallurgist American Brake Shoe Company, Mahwah, New Jersey.

The effect of silicon noted by the authors confirms the results of unpublished research conducted at Battelle Memorial Institute under the sponsorship of the Alloy Casting Institute. To have this effect further defined by the Drop-Weight Transition Test is a valuable addition to the literature on 12% chromium stainless steel castings.

Since the authors state that service experience involving brittle fractures of Type 410 propellers was one of the prime reasons for conducting this research, the question of why stainless is considered rather than a copper-base alloy for this application appears appropriate. The British[2] have recently made public a new copper-base alloy and claim that service results prove it to be ideal as a propeller material. Its chemistry (12–14% manganese, 7–8% aluminum with small amounts of iron and nickel, balance copper) is so adjusted to give a low melting point (about 1800°F). This, together with an aluminum content which is lower than the amounts normally contained in aluminum bronze of comparable strengths, makes this alloy an excellent foundry material with good fluidity at low pouring temperatures.

Work performed at our laboratories on this alloy has indicated that the following physical properties are obtainable in the as-cast condition:

Table XI

Tensile Properties:	
Yield strength (0.5% elongation)	40,000–46,000 psi.
Tensile Strength	85,000–100,000 psi.
Elongation	26–45%
Brinell hardness	145–190
Impact Properties—Charpy V Notch	
212°F.	36 ft. lbs.
75°F.	26 ft. lbs.
— 40°F.	22 ft. lbs.
— 80°F.	20 ft. lbs.

Fatigue test data developed in England[3] certify the alloy to be equivalent to high strength aluminum bronze and superior to manganese bronze under both air and salt spray test conditions.

In view of the above properties and also the fact that these properties are obtainable without heat treatment in an alloy which has far superior foundry characteristics to those of Type 410 stainless; the original question will be restated: ie., why not use a copper-base alloy of the type described as a propeller material instead of Type 410 stainless?

[2]Payne and Webb, U. S. Patent No. 297,976, April 1955.
[3]Private Correspondence, J. Stone and Company, Ltd., Charlton, London.

INFLUENCE OF ALLOYING ELEMENTS ON THE IMPACT TRANSITION BEHAVIOR OF 12% CHROMIUM STEELS AGED AT 900°F

By E. J. Whittenberger and E. R. Rosenow

Abstract

The effect of varying amounts of carbon, chromium, molybdenum, aluminum and titanium upon the V-notch Charpy transition temperature of 12% chromium steels aged for 10,000 hours at 900°F was determined. Higher (0.08%) carbon content favored slightly lower transition temperatures for AISI Type 410 steels in the annealed condition, however, an increase in transition temperature was observed for all combinations of carbon and chromium contents after aging for 10,000 hours at 900°F. Contrary to published information, 0.25% aluminum (AISI Type 405) appeared to have no influence on the transition temperature. While the addition of 0.50% molybdenum minimized the increase in transition temperature, the combined addition of molybdenum and aluminum appeared to eliminate it entirely. Evidence of a grain boundary network of a very fine lamellar precipitate which appeared to be carbides and/or nitrides appeared to correlate in every case with an increase in transition temperature. (ASM-SLA Classification: Q6, Q23, SS)

CONFLICTING data have been presented in the literature concerning the effect of composition upon the 885°F embrittlement of 12% chromium steels. Attention has been concentrated particularly on Type 405 steel which contains 0.10 to 0.30% aluminum. Newell(1)[1] reported embrittlement and failure of the lining of a hot oil separator after five years of service at elevated temperature of about 735°F. Since the Type 405 strip composing the lining had been welded to a regular Type 410 strip, the two grades were compared. He stated that Type 410 was still ductile, whereas Type 405 was badly embrittled.

In reply to Newell, Scheil (2) presented data which justified the application and the use of Type 405. His investigation showed that, of six reported instances of embrittlement upon prolonged service exposure at elevated temperatures, five cases were attributable to composition irregularities and one to stress corrosion. Scheil investi-

[1]The figures appearing in parentheses pertain to the references appended to this paper.

A paper presented before the Thirty-Seventh Annual Convention of the Society, held in Philadelphia, October 17–21, 1955. Of the authors, E. J. Whittenberger is chief development metallurgist and E. R. Rosenow is physicist, South Works, United States Steel Corp., Chicago. Manuscript received April 11, 1955.

gated the material, which was reported by Newell as embrittled, and concluded that both alloys had age hardened but exhibited no tendencies to embrittle at room temperature.

The commercial importance of 12% chromium steels is such that additional data are required on the effect of alloying elements on their embrittling behavior. This investigation was therefore undertaken to obtain these data on the basis of a study of impact properties. The change in impact transition temperature offers a convenient method for evaluating embrittlement since embrittlement generally causes a shift in impact transition temperature to higher temperatures. The Charpy "V" notch test shows a marked drop in impact values in the transition zone and permits a reasonably accurate evaluation of the effect of variations in chemical compositions on susceptibility to embrittlement.

Experimental Procedure

Steel from thirteen laboratory induction furnace heats and three commercial electric arc furnace heats was studied in this experimental program. In addition to the base 12 Cr composition (AISI Type 410), steels containing lower carbon contents (12 Cr-low C), molybdenum (12 Cr-Mo), aluminum (12 Cr-Al or AISI Type 405), aluminum plus molybdenum (12 Cr-Al-Mo) and aluminum plus titanium (12 Cr-Al-Ti) were investigated. Within each grade, heats containing low (12.0%) and high (13.5%) chromium contents were studied to determine whether chromium content alone affected transition behavior during aging and also whether an interaction existed between chromium and the other elements with regard to transition. Also included in the experimental program were single low carbon heats of 17% chromium (17 Cr-low C) and 27% chromium (27 Cr-low C) steel which have known embrittling tendencies and which were expected to contain sigma after extended

Table I
Chemical Composition of the 12 Per Cent Chromium Steels Investigated

Steel Code	Type	Special Characteristics	Composition—Per Cent C	Mn	Si	Ni	Cr	Mo	Al	Ti	N
1	12 Cr-Low C	0.03% max.C—Low Chromium	0.026	0.35	0.28	0.33	11.62	—	0.010	—	0.055
2	12 Cr-Low C	0.03% max.C—High Chromium	0.018	0.40	0.34	0.30	13.48	—	0.006	—	0.053
3	12 Cr	Low Carbon—Low Chromium	0.080	0.45	0.37	0.29	11.64	—	0.015	—	0.058
4	12 Cr	Low Carbon—High Chromium	0.060	0.41	0.38	0.32	13.73	—	0.009	—	0.062
5	12 Cr	High Carbon—High Chromium	0.100	0.50	0.21	0.18	13.35	0.02	0.008	—	0.029
6	12 Cr-Mo	Low Carbon—Low Chromium	0.080	0.27	0.36	0.30	11.96	0.43	0.030	—	0.056
7	12 Cr-Mo	Low Carbon—High Chromium	0.080	0.34	0.41	0.26	13.56	0.50	0.040	—	0.041
8	12 Cr-Mo	Low Carbon—Low Chromium	0.080	0.39	0.27	0.30	12.14	0.52	0.010	—	0.038
9	12 Cr-Al	Low Carbon—Low Chromium	0.080	0.32	0.22	0.10	12.06	—	0.250	—	0.032
10	12 Cr-Al	Low Carbon—High Chromium	0.070	0.38	0.45	0.30	13.61	—	0.250	—	0.055
11	12 Cr-Al-Mo	Low Carbon—Low Chromium	0.070	0.34	0.44	0.23	11.92	0.49	0.250	—	0.046
12	12 Cr-Al-Mo	Low Carbon—High Chromium	0.070	0.36	0.45	0.30	13.61	0.49	0.230	—	0.080
13	12 Cr-Al-Ti	Low Carbon—Low Chromium	0.070	0.34	0.48	0.24	12.04	—	0.210	0.11	0.049
14	12 Cr-Al-Ti	Low Carbon—High Chromium	0.080	0.37	0.46	0.38	13.67	—	0.230	0.10	0.073
15	17 Cr-Low C	0.03% max.C 17 Cr	0.030	0.44	0.38	0.22	16.28	—	0.040	—	0.064
16	27 Cr-Low C	0.03% max.C 27 Cr	0.020	0.30	0.42	0.31	25.04	—	0.005	—	0.081

elevated temperature aging. The chemical compositions of all steels are presented in Table I.

The twenty-six pound laboratory induction furnace ingots were forged directly to one-half inch square bars. Specimens representing commercial arc furnace heats were secured from rolled billet product varying in size from 3⅞ x 3⅞ inches to 6 x 5 inches and were forged to one-half inch square bars. Charpy impact coupons were annealed, machined and notched according to the standard "V" notch Charpy testing procedure.

All forged bars of the 12% chromium steel series were annealed at 1550°F for one-half hour and cooled at the rate of 50°F per hour to 1100°F, followed by air cooling. Forged bars of the 17% chromium steel were annealed at 1500°F for one-half hour and air-cooled. The annealing treatment for the 27% chromium steel consisted of heating at 1500°F for one-half hour and water quenching.

One-half inch square bars for impact testing were aged at 900°F for 10,000 hours. Duplicate metallographic specimens were cold reduced 75% prior to aging for 10,000 hours at 900 and 1050°F. Cold working was employed to accelerate phase changes during aging. The aging treatments were conducted at the Lorain Works of the National Tube Division. Rockwell hardness measurements for each heat were made on Charpy specimens representing both the annealed and the aged conditions.

"V" notch Charpy impact tests were conducted over a temperature range of −100 to +260°F. For testing temperatures of 50°F or lower, specimens were brought to thermal equilibrium in a mixture of alcohol and dry ice; tap water was used for temperatures of 50 to 212°F; above 212°F, clear quenching oil was used.

The average energy transition temperatures were selected at an average energy level which was the same for all heats within a particular grade, except for the 12 Cr-Al-Ti heats. In this grade, the average energy levels were not consistent for the two heats involved. No adequate explanation for this difference can be offered. The average energy level selected varied from grade to grade and some judgment was exercised in making the selections.

There are no standard procedures for selecting transition temperatures for "V" notch Charpy impact data for 12% chromium steels. The method used consisted of plotting the average of the impact values obtained at each testing temperature in the transition range. The intersection of the best straight line which could be drawn through these average values with a line representing the selected average energy level, Fig. 1, denoted the average energy transition temperature. Use of the average energy transition temperature permitted an evaluation of the increase in transition temperature associated with the aging treatment.

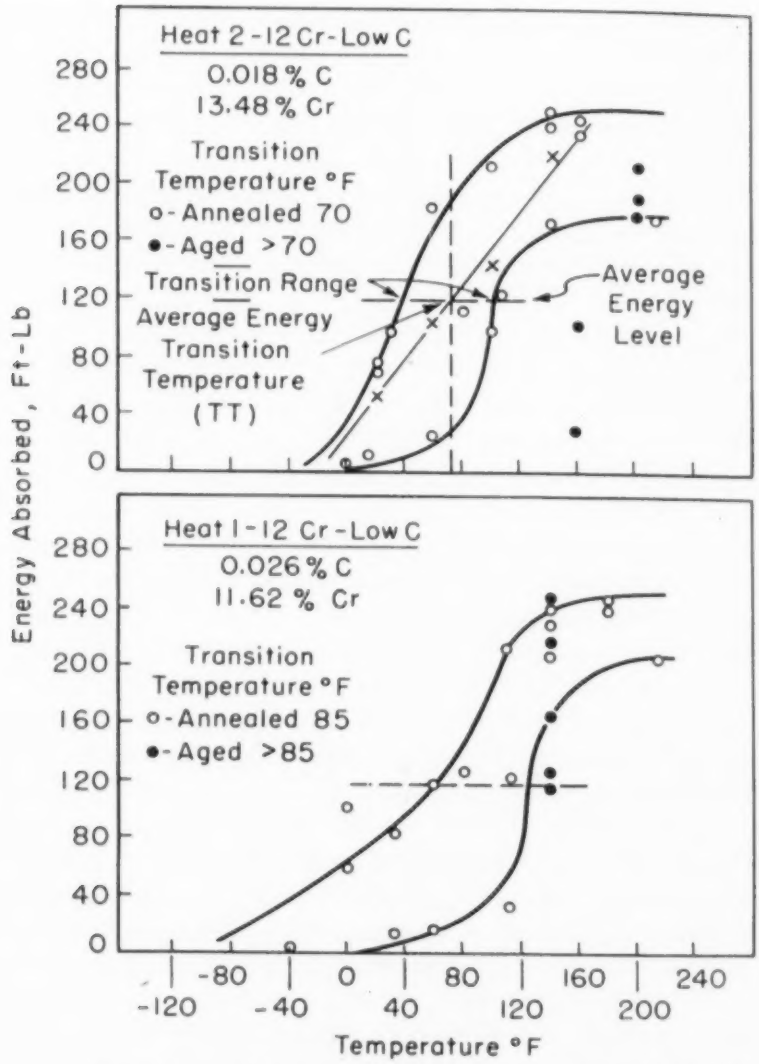


Fig. 1—V Notch Charpy Impact Results of 12 Cr-Low C Steels Used to Determine Average Energy Transition Temperatures in the Annealed and Aged Condition.

Average energy transition temperatures were determined for all modifications of Types 410 and 405 steels in the annealed condition. Average energy transition temperatures for the aged condition were determined for 12 Cr, 12 Cr-Mo, 12 Cr-Al and 12 Cr-Al-Ti for which ample material was available for Charpy impact specimens. For these heats for which only a limited number of specimens were available, it was only possible to determine qualitatively whether the transition temperature increased upon extended exposure of 10,000 hours at 900°F. For these heats, the temperatures selected for impact testing of the aged specimens were 20°F above the beginning of transition from high to low impact values (the "knee" of the transition curve). At the testing temperature selected, a minimum

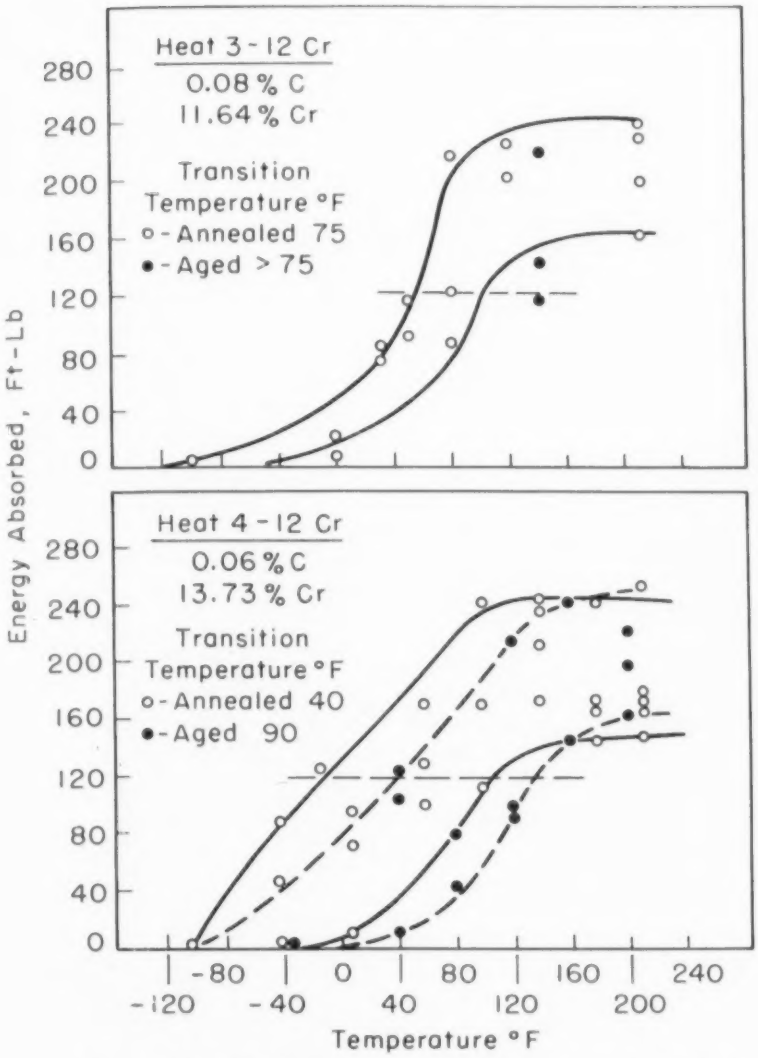


Fig. 2—V Notch Charpy Impact Results Used to Determine Average Energy Transition Temperatures of 12 Cr Steel in the Annealed and Aged Condition.

shift in transition temperature resulted in a maximum decrease in impact values. The steels with "V" notch Charpy impact values for the aged condition which were below the annealed transition curve were considered to have embrittlement tendencies, and conclusions were derived on this basis. Typical results of the "V" notch Charpy impact values at various testing temperatures for the modifications of Types 410 and 405 are presented in Figs. 1 through 5.

Metallographic studies were conducted on specimens in the annealed and aged conditions. Duplicate annealed specimens from each heat were cold reduced 75% prior to aging at 900 and 1050°F for 10,000 hours. Since cold work accelerates the formation of sigma, it was necessary to examine identical Charpy specimens which were

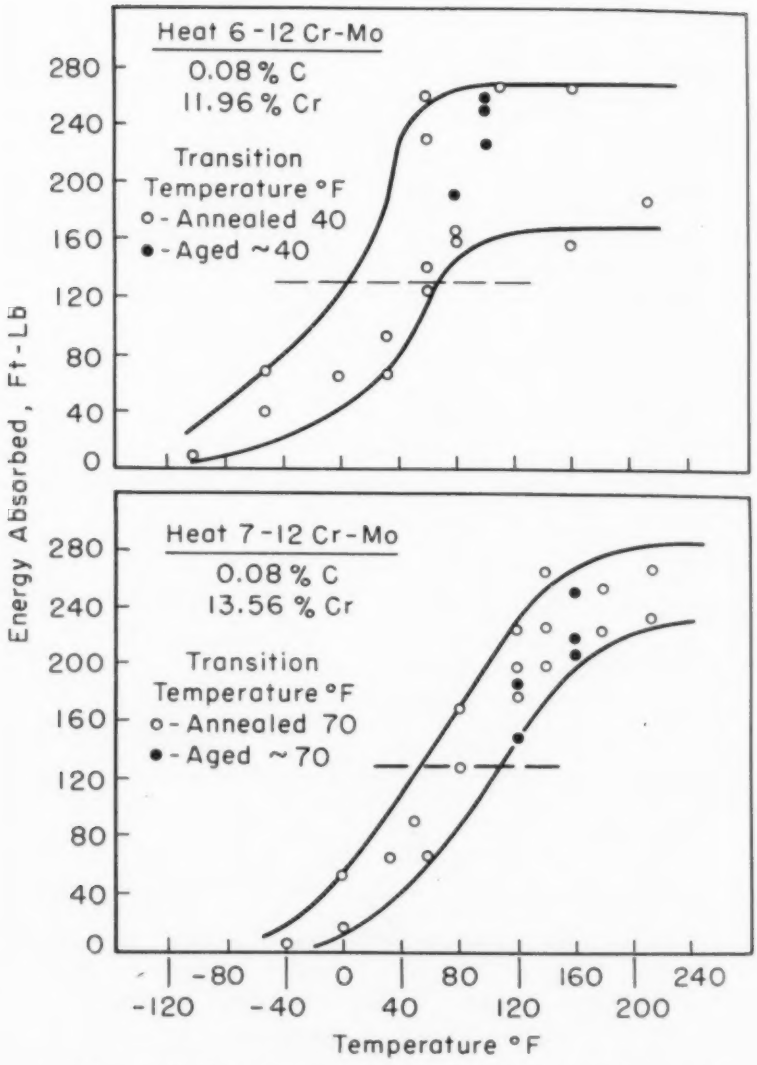


Fig. 3—V Notch Charpy Impact Results Used to Determine Average Energy Transition Temperatures of 12 Cr-Mo Steels in the Annealed and Aged Condition.

not cold-worked for a direct correlation between microstructure and embrittling behavior. X-ray and electron diffraction studies to identify dispersed phases were also conducted on selected samples.

Discussion

The impact testing program was arranged to provide information on the effect of the different alloying elements on (a) the average energy transition temperature for the annealed condition, and (b) the change in average energy transition temperature after aging for 10,000 hours at 900°F. The discussion of the data has therefore been subdivided into these two categories.

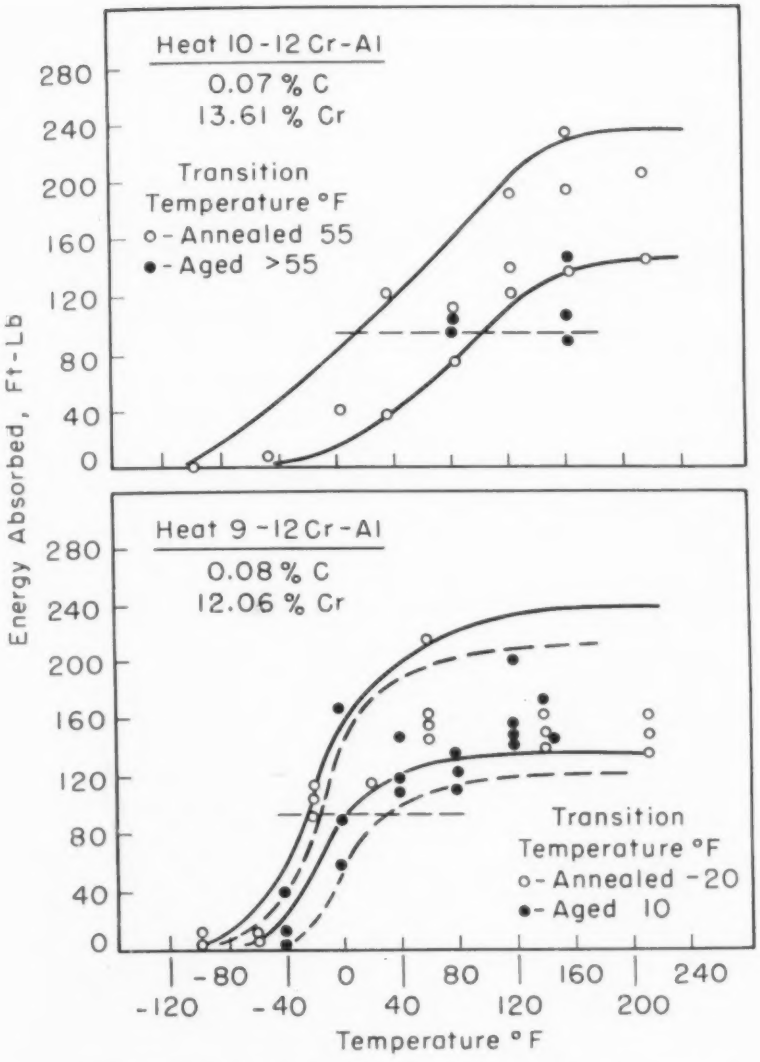


Fig. 4—V Notch Charpy Impact Results Used to Determine Average Energy Transition Temperatures of 12 Cr-Al Steels in the Annealed and Aged Condition.

The Effect of Alloying Elements on the Average Energy Transition Temperature for the Annealed Condition

The results of "V" notch Charpy impact testing of the various 12 Cr steels in the annealed condition indicated that the average energy transition temperature occurred over a temperature range of 110 to −30°F and, after aging for 10,000 hours at 900°F, the range was 125 to 10°F, see Table II.

Carbon—The results of testing 12 Cr steel indicated that increasing the carbon content from 0.018 to 0.10% decreased the average energy transition temperature 61.5 and 46.3°F for the high and low chromium 12 Cr steels, respectively, see Fig. 6. High

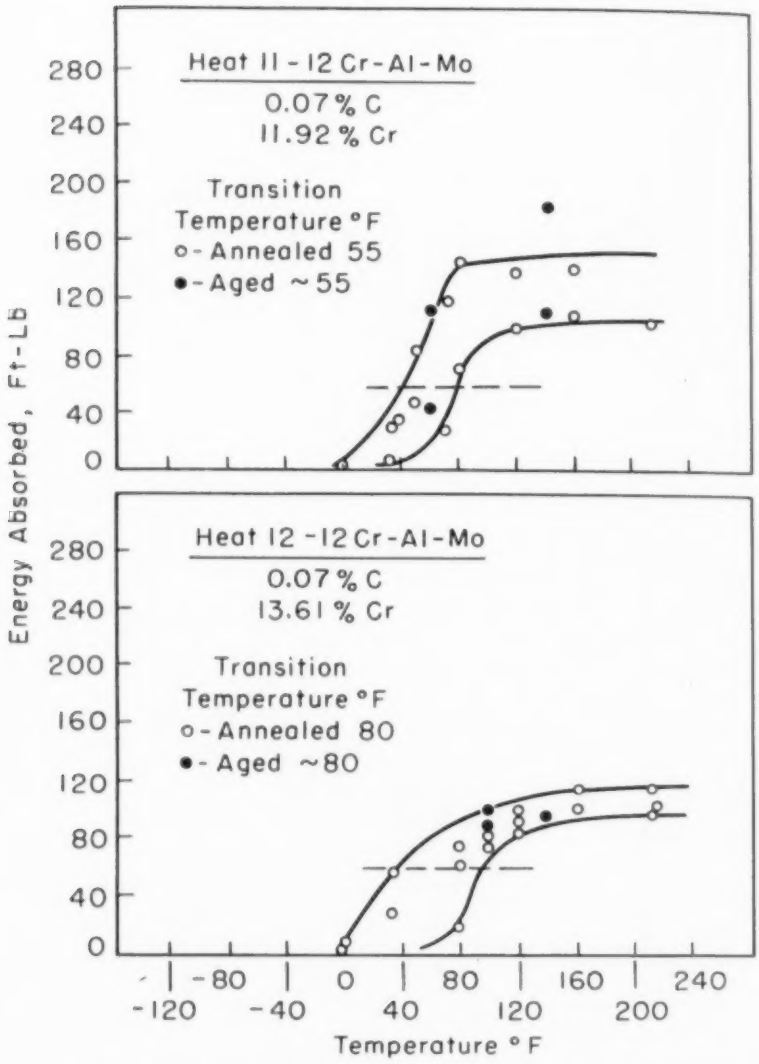


Fig. 5—V Notch Charpy Impact Results Used to Determine Average Energy Transition Temperatures of 12 Cr-Al-Mo Steels in the Annealed and Aged Condition.

chromium heats 2, 4 and 5, with respective carbon contents of 0.018, 0.06 and 0.10%, exhibited decreasing average energy transition temperatures (70, 40 and 20°F, respectively). Low chromium heats 1 and 3, with carbon contents of 0.026 and 0.08%, Fig. 6, indicate the effectiveness of carbon in lowering the transition temperature (from 85 to 60°F, respectively). The effect of variations in carbon content upon transition temperature was only evaluated for Type 410 stainless steels.

Chromium—The study of the effect of chromium on the average energy transition temperature, in the annealed condition for 12 Cr (Type 410), 12 Cr-low C and 12 Cr-Al-Ti, Fig. 7, shows a decrease of 23.5 (heats 3 and 5), 8.0 (heats 1 and 2), and 49.1 (heats 13 and

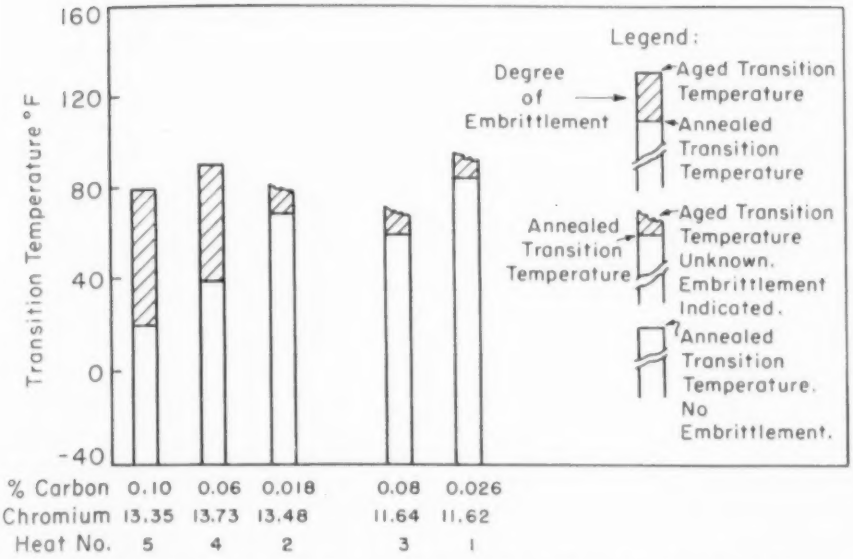


Fig. 6—The Effect of Carbon at High and Low Chromium Levels of 12 Cr Stainless Steels on the Average Transition Temperatures in the Annealed and Aged Conditions.[2]

Table II
Average Energy Transition Temperatures and Grain Size of the 12% Chromium Steels Investigated

Steel Code	Type	Average Energy Transition Temp.—°F Annealed*	Average Energy Transition Temp.—°F 10,000 hrs. @ 900°F[2]	Change in Transition Temperature	ASTM Grain Size Number
1	12 Cr-Low C	85	>85	Increase	6
2	12 Cr-Low C	70	>70	Increase	5
3	12 Cr	75	>75	Increase	7-8
4	12 Cr	40	90	50 degrees	7-8
5	12 Cr	20	80	60 degrees	8
6	12 Cr-Mo	40	~40	None	8-9
7	12 Cr-Mo	70	~70	None	7
8	12 Cr-Mo	40	125	90 degrees	6
9	12 Cr-Al	−20	10	30 degrees	8
10	12 Cr-Al	55	>55	Increase	1 & 4 (duplex)
11	12 Cr-Al-Mo	55	~55	None	1 & 8 (duplex)
12	12 Cr-Al-Mo	80	~80	None	1 & 5 (duplex)
13	12 Cr-Al-Ti	110	~110	None	2 & 8 (duplex)
14	12 Cr-Al-Ti	30	60	30 degrees	8
15	17 Cr-Low C	105	>105	Increase	4
16	27 Cr-Low C	55	>55	Increase	1 & 6 (duplex)

*See Table III.

14) Fahrenheit degrees in transition temperature, respectively, for 1% increases in chromium content. However, for 12 Cr-Mo, 12 Cr-Al (Type 405) and 12 Cr-Al-Mo, Fig. 2, the average annealed transition temperature increased 24.6, 45.0 and 14.8°F per 1% increase in chromium content for the respective grades. The reason for this inconsistent effect of chromium upon the transition temperature is not apparent from the available data.

Type 410 stainless steel heats 3 (11.64% chromium) and 5 (13.35% chromium) exhibited respective transition temperatures of

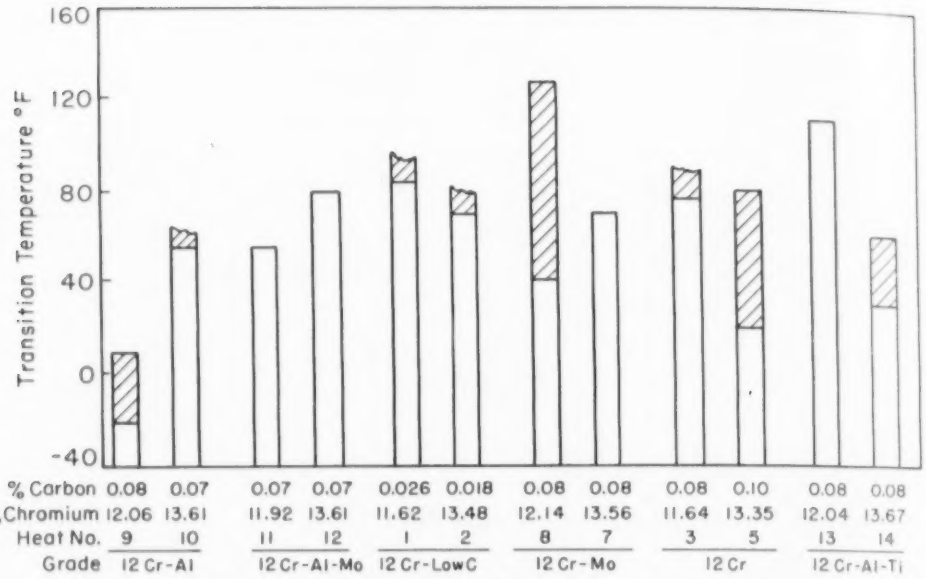


Fig. 7—The Effect of Chromium on the Average Transition Temperatures of 12 Cr and 12 Cr-Al Stainless Steels in the Annealed and Aged Conditions. See Legend—Fig. 6.

75 and 20°F. This large difference may be attributed in part to the lower nickel and silicon contents and the higher carbon content of the latter heat. Of the two 12 Cr-low C heats, the lower chromium heat 1 (11.62% chromium) had a transition temperature of 85°F which was 15°F higher than the transition temperature of the higher chromium heat 2 (13.48% chromium). The 12 Cr-Al-Ti heat 14 (13.67% chromium) had a transition temperature of 30°F, a substantial decrease in transition temperature as compared with heat 13 (12.04% chromium) which had a transition temperature of 110°F. Molybdenum, aluminum and molybdenum plus aluminum increased the transition temperature at the higher chromium contents. This may have resulted from an interaction effect of molybdenum and/or aluminum with chromium which produced an adverse effect upon the transition temperature for these steels.

Molybdenum—Contradictory influences of molybdenum upon the average energy transition temperature were obtained for 12 Cr heats in the annealed condition. At the lower chromium level, heats 3, 6 and 8 in Fig. 8, the addition of approximately 0.50% molybdenum resulted in a decrease (about 15°F) in transition temperature. However, at the higher chromium level, heats 4 and 7 in Fig. 3, a similar molybdenum addition raised the transition temperature approximately 30°F. This contradictory behavior may have resulted from an interaction between molybdenum and chromium as suggested in the previous section.

Aluminum—The addition of 0.25% aluminum to the 12 Cr steels (Type 405) resulted in average energy transition temperatures

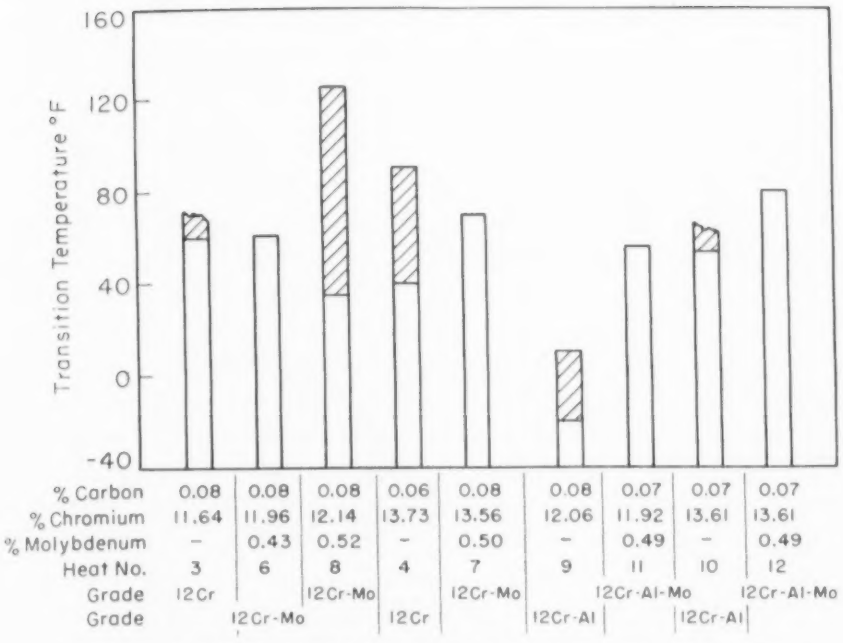


Fig. 8—The Effect of Molybdenum on Average Transition Temperatures of 12 Cr and 12 Cr-Al Stainless Steels in the Annealed and Aged Conditions.

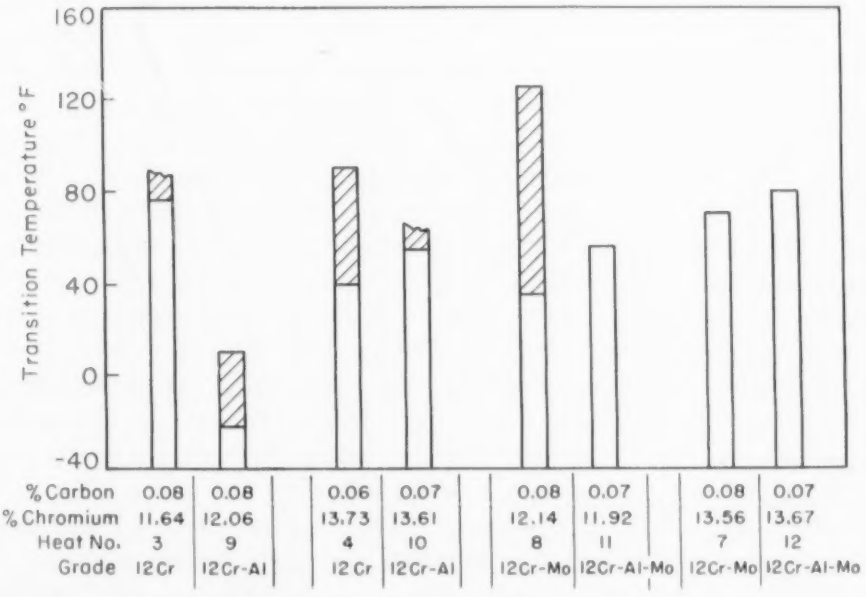


Fig. 9—The Effect of Aluminum on Average Transition Temperatures of 12 Cr and 12 Cr-Mo Steels in the Annealed and Aged Conditions.

for the annealed condition ranging from 55 to −20°F. Comparison of heats 3 and 9, 12 Cr (Type 410) and 12 Cr-Al (Type 405), respectively, in Fig. 9, at the same carbon and similar low chromium levels indicates that a decrease in transition temperature of 95°F accompanied the 0.25% aluminum addition. A possible explanation

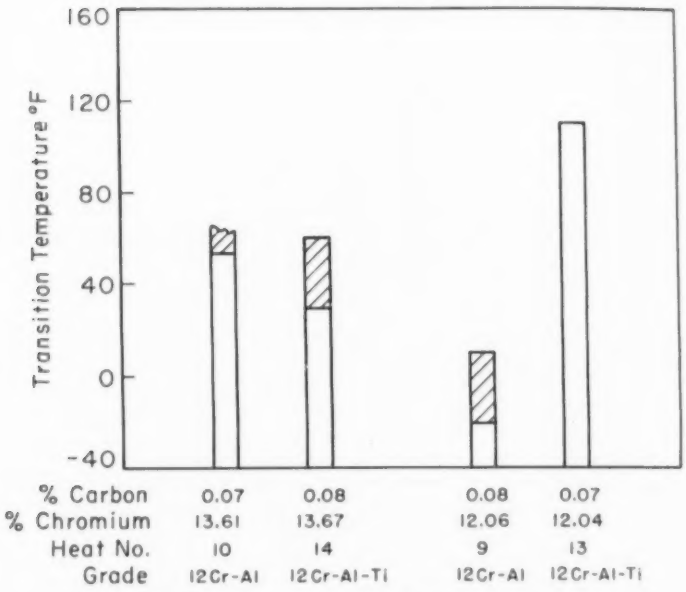


Fig. 10—The Effect of Titanium on Average Transition Temperatures of 12 Cr-Al Stainless Steels in the Annealed and Aged Conditions.

for the low transition temperature (−20°F) obtained for heat 9 is the lower manganese, nickel and silicon contents of this heat. A comparison of heats 4 and 10 containing similar high chromium contents and the same carbon contents indicates that an increase in the average transition temperature of 15.5°F accompanied the 0.25% aluminum addition. It was apparent from a comparison of heats 9 and 10, that in annealed 12 Cr-Al (Type 405) steels, lower chromium contents result in lower transition temperatures. For lower chromium steels containing molybdenum, the addition of 0.25% aluminum resulted in an increase in the average energy transition temperature of 21°F. At higher chromium levels, the presence of 0.25% aluminum increased the average transition temperature 13°F.

Except at the lower (12%) chromium level, aluminum when added to 12 Cr and 12 Cr-Mo steels, appeared to increase the transition temperature of the annealed product.

Titanium—The addition of 0.10% titanium to 12 Cr-Al high chromium steels decreased the average energy transition temperature 25°F while at lower chromium levels the opposite effect was obtained, Fig. 10. These results suggest a possible interaction between chromium and titanium but more data would be necessary to firmly establish this point.

Summary of Data for the Annealed Condition

Considering only the transition temperatures for the various compositions of 12% chromium steels in the annealed condition,

higher carbon contents generally lowered the transition temperature. Chromium, aluminum, molybdenum and titanium additions gave inconsistent results.

The Effect of Alloying Elements on the Change in Average Energy Transition Temperature During Aging

Sufficient impact specimens to establish the average energy transition temperatures for the aged condition were available for two 12 Cr (Type 410), one 12 Cr-Mo, one 12 Cr-Al (Type 405) and one 12 Cr-Al-Ti heats, Table II. For these steels, aged 10,000 hours at 900°F, the transition temperatures ranged from 125 to 10°F as compared to 40 to −30°F for the annealed condition. Because of a limited number of specimens on the balance of the steels, only partial transition curves were obtained, and only a qualitative evaluation of the effect of aging upon impact properties could be made.

Carbon—For all heats of 12 Cr chromium steels studied, an increase in transition temperature occurred over the full range of 0.018 to 0.10% carbon. The limited data do not permit a quantitative correlation of the degree of increase with carbon content, see Fig. 6. The carbon range was not varied for the balance of 12 Cr steels included in this study.

Chromium—Increases in transition temperature occurred in all of the straight chromium steels, 12 Cr (Type 410), 12 Cr-low C, 17 Cr-low C, 27 Cr-low C and also 12 Cr-Al (Type 405), Table II. In general, the higher chromium steels exhibited a greater increase than the lower chromium steels. However, in the case of 12 Cr-Al (Type 405) and 12 Cr-Mo steels, marked increases in transition temperature occurred at the lower chromium level, see Fig. 7.

Since sigma precipitation is favored by higher chromium contents, the failure to obtain a direct correlation between the increase in transition temperature and higher chromium contents provides indirect evidence that sigma precipitation may not be responsible for the embrittlement which reportedly occurs in some 12% chromium steels during elevated temperature service.

Molybdenum—Of the three 12 Cr-Mo and two 12 Cr-Al-Mo steels investigated, only the low chromium 12 Cr-Mo heat, 8 in Fig. 8, exhibited an increase in transition temperature after aging. It should be noted that no change was found for a similar heat, 6 in Fig. 8. This anomaly cannot be readily explained by differences in the base composition, see Table I. It should be acknowledged that heat 8 was the only heat for which sufficient aged impact specimens were available to establish a reasonably accurate transition temperature for the aged condition. That no increase in transition temperature was observed for four of the five heats which contained molybdenum suggests that molybdenum and molybdenum plus

aluminum may be effective in minimizing embrittlement during elevated temperature service. However, this advantage is accompanied by the disadvantage that the molybdenum bearing steels exhibited higher transition temperatures for the annealed condition than did the regular 12 Cr and 12 Cr-Al steels. This was particularly true when comparing higher chromium 12 Cr heats 4 and 7 and all of the 12 Cr-Al (Type 405) and 12 Cr-Al-Mo heats in Fig. 8.

Aluminum—Both of the 12 Cr-Al (Type 405) heats studied in this investigation exhibited increases in transition temperature after aging for 10,000 hours at 900°F, Fig. 9. This suggests that the addition of aluminum alone to 12% chromium steels will not eliminate the possibility of embrittlement during elevated temperature service. Contrary to previous evidence (1), these data do not indicate that aluminum increases the degree of embrittlement.

Titanium—Based on one impact result, the addition of approximately 0.10% titanium to 12 Cr-Al steel appeared to minimize embrittlement tendencies, while a companion heat with higher chromium content exhibited slight embrittlement, Fig. 10. It should be noted that, although the transition temperature of the low chromium 12 Cr-Al-Ti steel, heat 13, appeared to be unaffected by aging, the very high transition temperature for this steel in the annealed condition (110°F) suggests that it would be notch sensitive at room temperature.

Summary of Data for the Aged Condition

Summarizing the effect of all the alloying elements studied on the transition behavior of aged 12% chromium steels, the combined addition of aluminum and molybdenum (regardless of chromium content) and molybdenum alone at the higher chromium level, minimized tendencies toward increases in transition temperature, Table II. The qualitative nature of many of the results do not permit associating the actual increase in transition temperature during aging with several of the alloying elements investigated.

Metallographic and Hardness Studies

The annealed microstructures showed a random distribution of carbides in a ferrite matrix, with slight banding and duplexed coarse and fine grain structures evident in several laboratory heats containing 0.25% aluminum. A comparison of the grain sizes of the various steels with their transition behavior, Table II, does not reveal any relationship between the two. Heats 5, 10 and 14 all were fine-grained (ASTM grain sizes of No. 8 or finer) but yet exhibited an increase in transition temperature after aging. Laboratory induction furnace heats 10, 11, 12, 13 and 16 exhibited duplexed grain structures. Heats 10 and 16 increased in transition temperature

while the balance did not. As would be expected, no change in grain size occurred during the 10,000 hour aging treatment at 900°F.

The hardness change during aging did not appear to correlate with the changes in transition temperature, c.f. the hardness increases for heats 6, 7, 11, 12 and 13 which did not change in transition temperature with similar increases for heats 1, 2, 3, 9 and 14, hardness decreases for heats 4 and 10 and no change in hardness for heats 5 and 8, all of which exhibited an increase in transition temperature. These data suggest that hardness measurement cannot be used as an indication of "900°F embrittlement" in these 12% chromium steels and that some more sensitive indication, such as the impact transition temperature concept used in this investigation, should be employed as a criterion.

Since prior cold work has been found to enhance sigma precipitation during subsequent elevated temperature aging (3), samples of each heat in this program were cold-worked prior to aging. Metallographic specimens of the 12 Cr (Type 410) and 12 Cr-Al (Type 405) steels, cold reduced 75% and aged 10,000 hours at 900°F and at 1050°F, were examined for the presence of sigma. No sigma was observed in any of the steels with chromium contents less than 13%. In the 12 Cr (Type 410) steels, sigma precipitate was identified in heat 4 containing 13.73% chromium and 0.06% carbon after aging 10,000 hours at 900°F, Figs. 11a and 11b. Failure to identify sigma in a companion sample, also cold reduced 75% but aged 10,000 hours at 1050°F, Table III, confirms a similar observation

Table III
Metallographic Observations and Hardness Measurements for the Various Compositions and Conditions Investigated

Steel Code	Type	Annealed* Rb Hardness	Annealed* and Aged** Rb Hardness	% Sigma	Grain Boundary Precipitate?	Change in Transition Temperature	Cold Reduced 75% Aged 10,000 hrs. @ 900°F % Sigma	Cold Reduced 75% Aged 10,000 hrs. @ 1050°F % Sigma
1	12 Cr-Low C	68.2	72.0	None identified	Yes	Increase	0	0
2	12 Cr-Low C	70.7	78.5	None identified	Trace	Increase	0	0
3	12 Cr	76.2	79.0	None identified	Yes	Increase	0	0
4	12 Cr	82.0	80.0	None identified	Yes	Increase	3	0
5	12 Cr	81.0	81.0	None identified	Yes	Increase	0	0
6	12 Cr-Mo	78.1	81.5	None identified	None	None	0	0
7	12 Cr-Mo	79.4	80.0	None identified	None	None	0	0
8	12 Cr-Mo	83.0	83.0	None identified	Yes—semi-continuous	Increase	0	0
9	12 Cr-Al	82.5	81.0	None identified	Yes	Increase	0	0
10	12 Cr-Al	74.1	77.0	None identified	Yes	Increase	8	2
11	12 Cr-Al-Mo	81.8	83.5	None identified	None	None	0	0
12	12 Cr-Al-Mo	76.2	78.0	None identified	None	None	0	0
13	12 Cr-Al-Ti	73.4	75.5	None identified	None	None	0	0
14	12 Cr-Al-Ti	83.0	84.0	None identified	Yes	Increase	8	4
15	17 Cr-Low C	75.5	Rc 22.0	None identified	Yes—conuous	Increase	Trace	3
16	27 Cr-Low C	84.8	Rc 36.5	None identified	Yes—semi-continuous	Increase	15	20

*17 Cr-Low C annealed 30 minutes @ 1500°F and air-cooled. 27 Cr-Low C annealed 30 minutes @ 1500°F and water-quenched. All other steels annealed 30 minutes @ 1550°F, cooled 50°F per hour to 1100°F and air-cooled.

**Aged 10,000 hrs. @ 900°F and air-cooled.

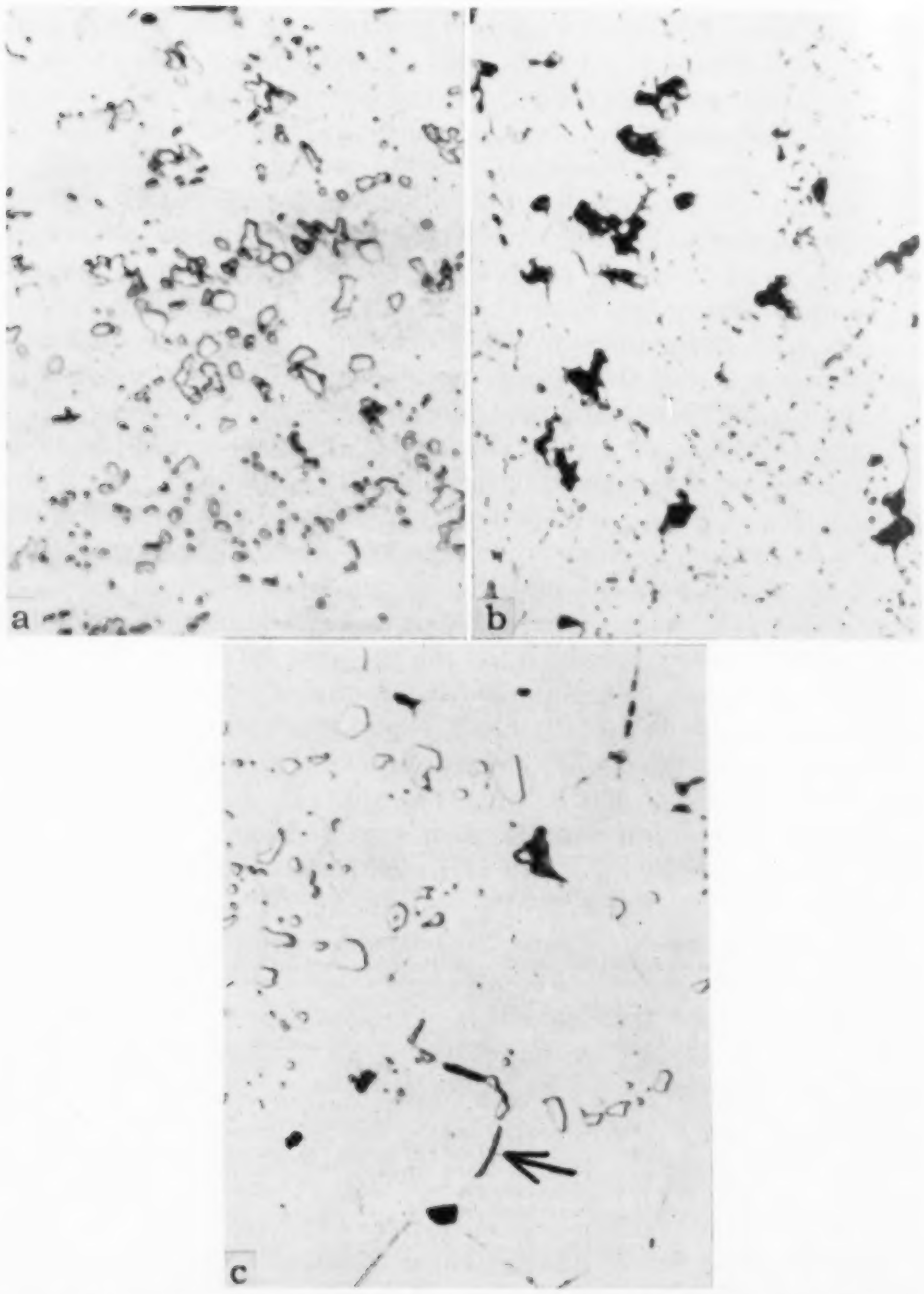


Fig. 11—Effect of Prior Treatment on the Microstructure of 12 Cr (13.73% Chromium) Heat 4, After Aging for 10,000 Hours at 900°F. ×2000. (a) Cold reduced 75% and aged. Etched in Vilella's reagent to outline carbides and sigma; (b) Cold reduced 75% and aged. Etched in glyceregia to attack sigma and outline carbides. The black constituent is sigma (about 3%); (c) Annealed (Table III) and aged. Etched in glyceregia showing the absence of identifiable sigma and the presence of discontinuous grain boundary precipitate responsible for embrittlement.

for a commercial purity 13% chromium steel by Link and Marshall (3). Examination of heat 2 containing 13.48% chromium and 0.018% carbon and heat 5 containing 13.35% chromium and 0.10% carbon

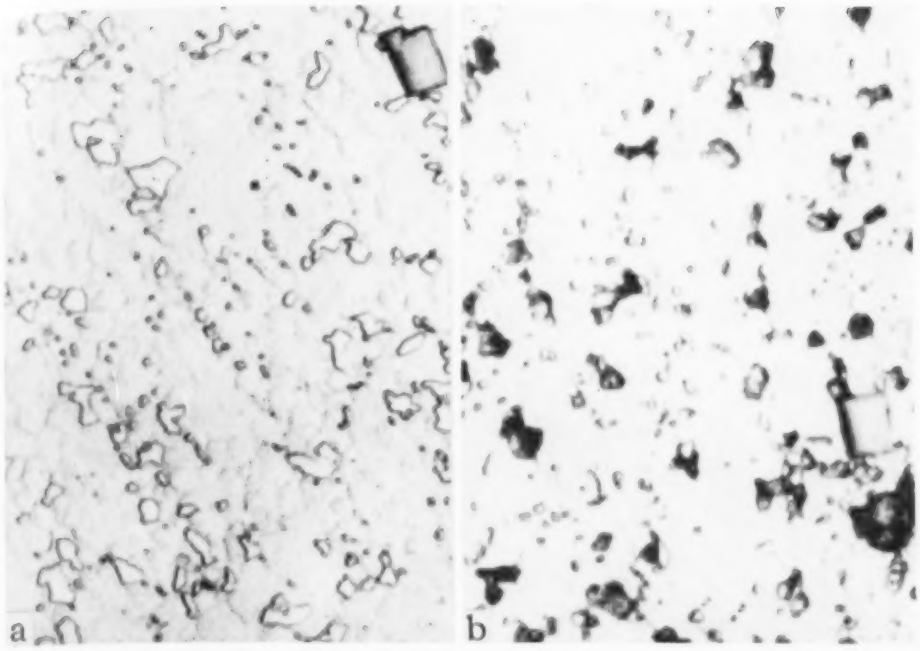


Fig. 12—Microstructures of 12 Cr-Al-Ti (13.6% Chromium) Heat 14, Cold Reduced 75% and then Aged for 10,000 Hours at 900°F. ×2000. (a) Etched in Vilella's reagent to outline carbides and sigma; (b) Etched in glyceregia to attack sigma and outline carbides. The black constituent is sigma (about 8%).

did not reveal the presence of sigma after aging cold-reduced samples at either 900 or 1050°F. These observations suggest that the ferrite (plus carbides)—ferrite plus sigma (plus carbides) phase boundary for these steels may be located at a slightly higher chromium content (about 13.60% chromium at 900°F) than that proposed by Link and Marshall.

The balance of 12 Cr (Type 410) steels with lower chromium contents (approximately 11.50%) did not contain sigma after being cold-reduced 75% and aged for 10,000 hours at either 900 or 1050°F, Table III. Neither was sigma detected in 12 Cr steels containing 0.50% molybdenum regardless of the chromium content (11.96 to 13.56%).

Sigma was identified in the high chromium 12 Cr-Al (Type 405) steel after cold working and elevated temperature aging. Heat 10 containing 13.61% chromium had approximately 8% sigma after aging at 900°F and approximately 2% sigma after aging at 1050°F. Heat 14, containing 0.10% titanium and 13.67% chromium, had 8% sigma after aging at 900°F, Fig. 12, and 4% at 1050°F, Table III. 12 Cr-Al with 0.50% molybdenum and 13.61% chromium did not contain sigma, Fig. 13, suggesting that molybdenum suppresses sigma formation even when the samples are cold-worked prior to elevated temperature aging. As in the case of the 12 Cr (Type 410)

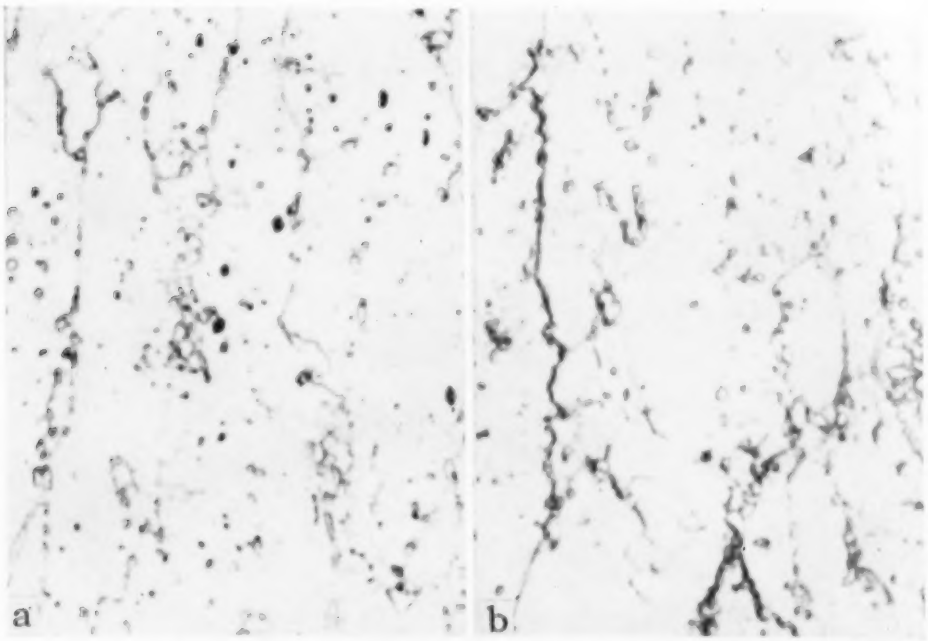


Fig. 13—Microstructure of 12 Cr-Al-Mo (13.61% Chromium) Heat 12, Cold Reduced 75% and Then Aged for 10,000 Hours at 900°F. ×2000. (a) Etched in Vilella's reagent to outline carbides and sigma; (b) Etched in glyceregia to attack sigma and outline carbides. The structure shows carbides at the grain boundaries and does not appear to contain sigma.

steels, the 12 Cr-Al (Type 405) steel with lower chromium contents (11.92 to 12.06%) did not show evidence of sigma.

Low carbon 17 Cr (heat 15) when cold-reduced 75% prior to aging, contained a trace of sigma after 10,000 hours at 900°F and 3% sigma after 10,000 hours at 1050°F, Table III. Although less sigma was observed than in the 16% chromium steel studied by Link and Marshall (3), the greater amount of cold reduction (95.4%) used by those investigators may account for the difference. The smaller amount of cold reduction (75%) used in the present research may also account for the failure to find more sigma after the 1050°F treatment than after the 900°F treatment. This discrepancy was not found for the low carbon 27 Cr (heat 16) where the cold-worked and aged samples contained approximately 15% sigma after heating 10,000 hours at 900°F and approximately 20% sigma after heating 10,000 hours at 1050°F, Fig. 14 and Table III.

To develop an explanation for the changes in transition temperature, a metallographic study was made on the annealed and aged impact specimens of all the compositions investigated. Sigma phase could not be identified in any of the 12% chromium steels in the annealed and aged condition. The absence of sigma after annealing and aging in steels which contained sigma after cold reducing and aging, Table III, constitutes another example of the effect of cold work in accelerating solid state reactions. That an increase in

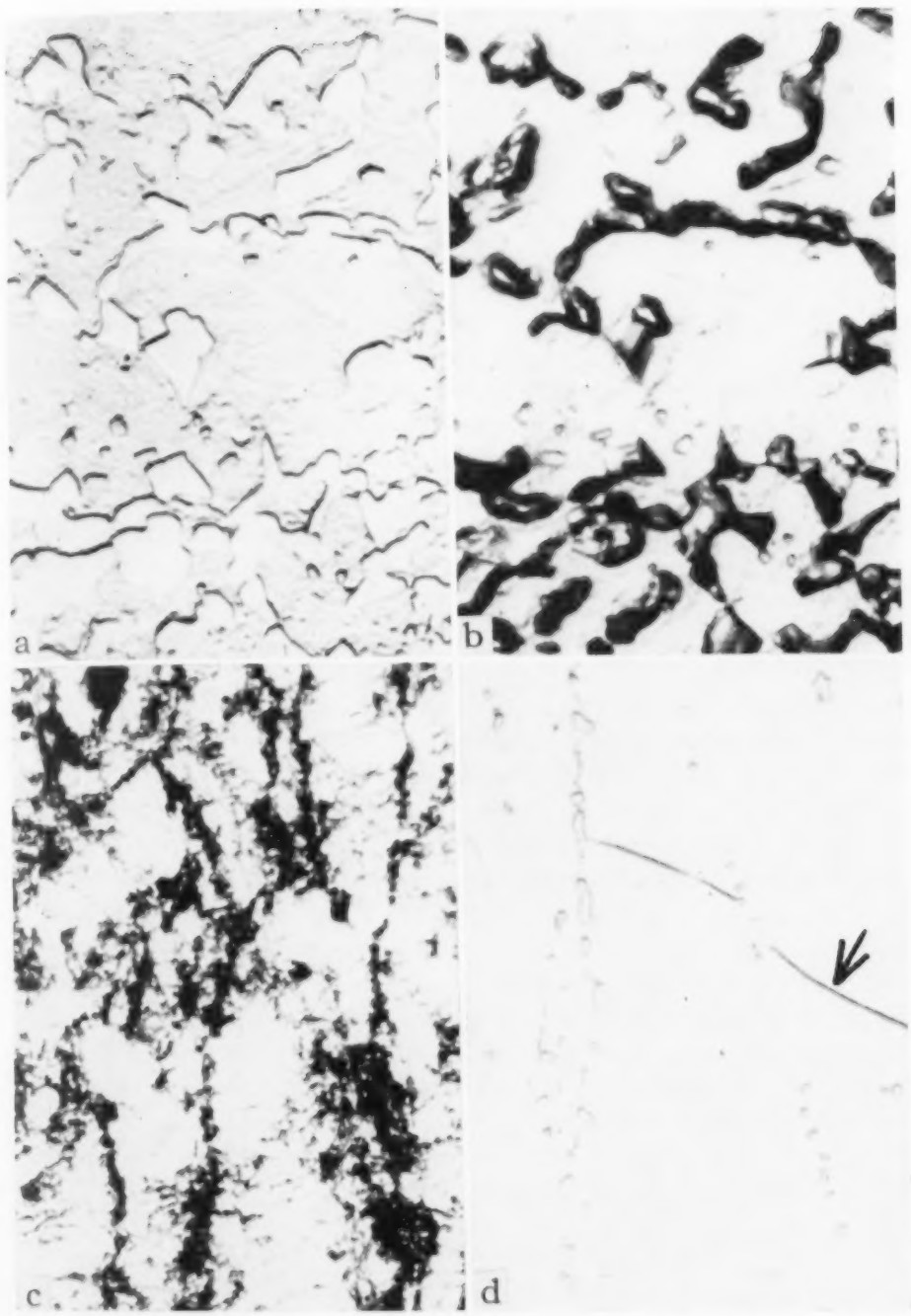


Fig. 14—Effect of Prior Treatment on the Microstructure of 27 Cr-Low C (25.04% Chromium) Heat 16 After Elevated Temperature Aging. (a) Cold-reduced 75% and aged 10,000 hours at 1050°F. Etched in Vilella's reagent to outline carbides and sigma. ×2000; (b) Same field as (a) but etched in glyceregia to darken sigma (about 20%). ×2000; (c) Cold-reduced 75% and aged 10,000 hours at 900°F. Etched lightly in glyceregia to attack sigma (about 15%). ×500; (d) Annealed (Table III) and aged 10,000 hours at 900°F. Etched in glyceregia and showing only carbides and fine semi-continuous grain boundary precipitate. ×2000.

transition temperature occurred in both the low and high chromium steels (11.62 to 13.73%) in the annealed and aged condition, and that sigma was identified only in the high chromium compositions (containing more than 13.60% chromium) after cold reducing and aging suggests that the so-called "885°F embrittlement" may not be a result of incipient sigma precipitation.

Further metallographic studies revealed that annealed and aged impact specimens from all of the heats investigated that exhibited an increase in transition temperature after aging contained a very fine precipitate at the ferrite grain boundaries. This grain boundary network is illustrated in Fig. 11c, a photomicrograph of a 12 Cr (Type 410) steel (heat 4) that embrittled,—i.e. the transition temperature after aging 10,000 hours at 900°F was 50°F higher than before aging. This photomicrograph and that of Fig. 14d are typical of all the heats tested that increased in transition temperature after aging 10,000 hours at 900°F. The balance of the heats of 12 Cr (Type 410) and 12 Cr-Al (Type 405) steel that did not increase in transition temperature did not contain this grain boundary precipitate. The microstructure of a representative heat of such a steel is shown in Fig. 15. Because of the extreme fineness of the grain boundary precipitate, positive metallographic identification of this material could not be made. Its etching behavior more closely paralleled that of carbides or carbo-nitrides rather than sigma. However, the fact that all of the heats which contained sigma after cold reducing and aging, heats 4, 9, 14, 15 and 16 in Table I, did not exhibit the fine grain boundary precipitate, Figs. 11b and 14b, while the annealed and aged impact specimens from these same heats did have the grain-boundary precipitate, Figs. 11c and 14d, suggests that this precipitate may be a transition phase which precedes the formation of readily identifiable sigma. This argument is refuted, in part, by the presence of the grain boundary precipitate in the annealed and aged specimens of low chromium heats 1, 3, 8 and 10, Table III, which did not form sigma after being cold-reduced 75% and aged 10,000 hours at either 900°F or 1050°F. The latter observation provides indirect evidence that grain boundary precipitate is not a preliminary step in sigma formation.

Electron Microscopic Examination

Electron microscopy did not confirm the presence of the fine intergranular precipitate previously observed with the light microscope. Examination of selected specimens in the electron microscope by means of uranium shadowed collodion replicas failed to reveal any significant differences between specimens considered to be embrittled and the others, Table IV. Extraction replicas of the specimens showed a small amount of a thin lamellar precipitate in brittle

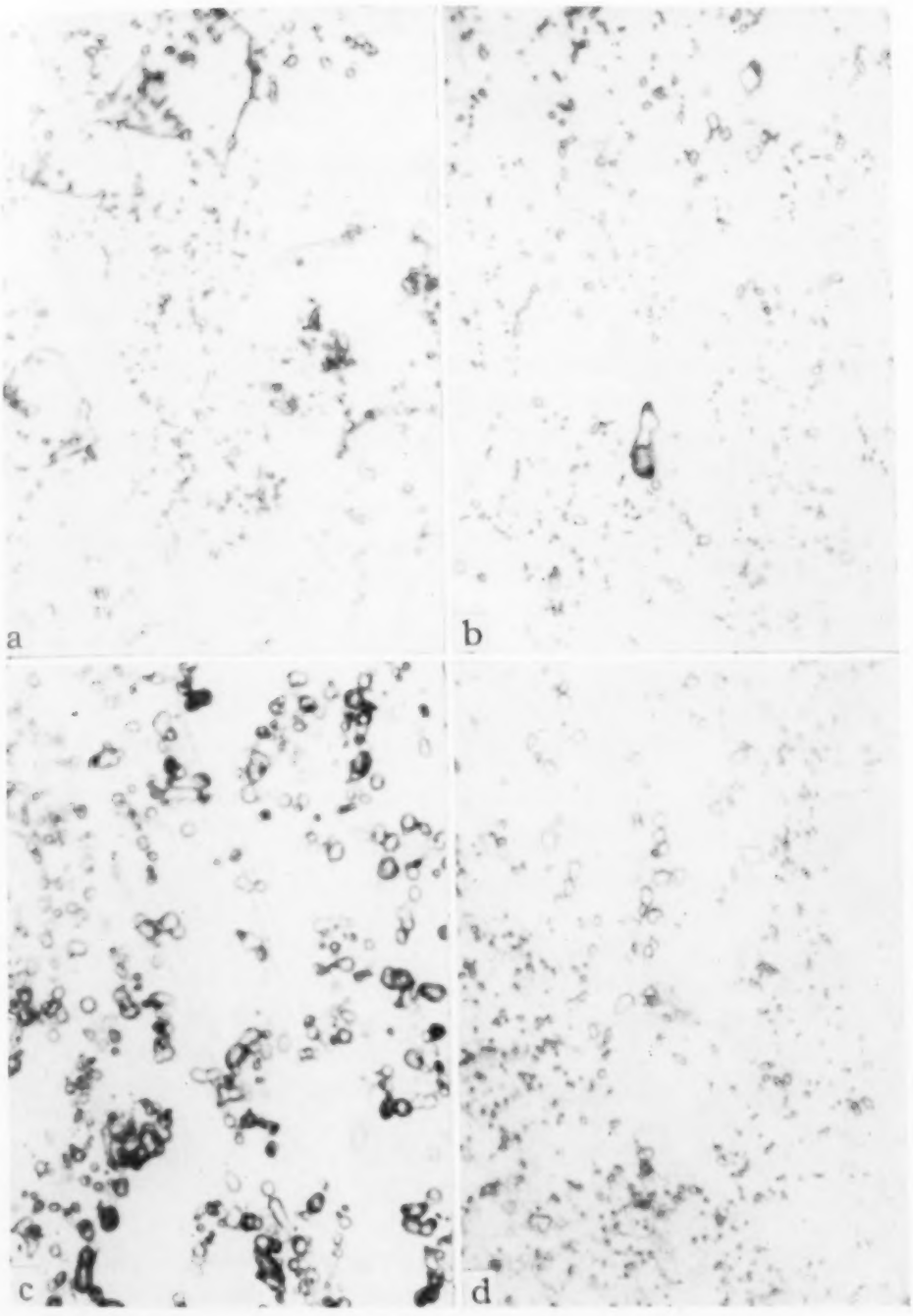


Fig. 15—Microstructure of 12 Cr-Mo Heat 6 Which Did Not Embrittle During Aging. 10,000 Hours at 900°F. ×2000. Annealed (Table III) Prior to Aging (a) Etched in Vilella's reagent showing fine carbides in a ferrite matrix and the absence of a grain boundary precipitate; (b) Etched in glyceregia which outlines carbides and attacks sigma. Neither sigma or a grain boundary precipitate are in evidence; (c) Light electrolytic chromic acid etch which attacks carbides but not ferrite grain boundaries. Note absence of grain boundary precipitate; cold-reduced 75% prior to aging. (d) Etched in glyceregia showing presence of carbides and absence of both sigma and grain boundary precipitate.

Table IV
Summary of X-Ray and Electron Diffraction Investigation of Samples Aged 10,000 Hours @ 900°F

Steel Code	Type	Change in Transition Temperature	Chemical Composition—% C	N	Cr	Mo	Al	X-ray Diffraction $Cr_{23}C_6$	Cr N	Electron Diffraction 885°F B.C.C.	Filmy Cr_2N
1	12 Cr-Low C	Increase	0.026	0.055	11.62	—	0.01	No	S	No	Yes
4	12 Cr	Increase	0.06	0.062	13.73	—	0.009	S	S	Yes	No
6	12 Cr-Mo	No	0.08	0.056	11.96	0.43	0.03	MS	S	No	No
8	12 Cr-Mo	Increase	0.08	0.038	12.14	0.52	0.01	S	MS	No	Yes
9	12 Cr-Al	Increase	0.08	0.032	12.06	—	0.25	S	No	No	Yes
12	12 Cr-Al-Mo	No	0.07	0.08	13.61	0.49	0.23	S	No	No	No

S—Strong
MS—Medium Strong

samples 1, 10 and 8. This material was identified by electron diffraction to be hexagonal chromium nitride Cr_2N. There was only a small amount of this lamellar precipitate present in these samples. This material did not appear to occur primarily at grain boundaries. An appreciable amount of the chromium rich body-centered cubic precipitate (chromium ferrite), found in higher chromium steels aged at 900°F (4), was present in sample 4 (high chromium, 12 Cr steel). Dark regions corresponding to areas of body-centered cubic precipitation could be seen at 1000X in the light microscope. None of this precipitate was found in any of the other samples examined by electron diffraction. Previous experience has shown that this precipitate cannot be detected in earliest stages of 885°F embrittlement.

X-ray Examination

A portion of each specimen listed in Table IV was dissolved in grain size reagent and the residue collected for X-ray diffraction examination. Carbide of the type $(Cr, Fe, W, Mo)_{23}C_6$ was found in all but specimen 1. This specimen contained only 0.026% carbon which is apparently below the solubility limit for chromium ferrite at 900°F. Chromium nitride (Cr_2N) was found in all specimens examined but numbers 10 and 12. Both of these samples had aluminum additions and apparently all nitrogen had combined as AlN which was soluble in the extracting solution.

Identification of the body-centered cubic precipitate in high (13.73%) chromium embrittled 12 Cr sample 4, and failure to identify it in high (13.61%) chromium unembrittled 12 Cr-Al-Mo sample 12, Table IV, suggests that, in these higher chromium steels, embrittlement may be associated with the presence of this new phase which is too fine to be resolved by the light microscope. However, reference to Table IV shows that this body-centered cubic phase could not be identified in the lower chromium steels which embrittled while a film-like Cr_2N precipitate was present in each. The latter evidence suggests that, in these steels, nitrides or carbonitrides participated in the embrittling process.

Summary

(a) A series of 12% chromium steels containing varying amounts of carbon, aluminum, molybdenum and titanium at two levels of chromium exhibited average energy transition temperatures ranging from −30 to 110°F for the annealed condition. After aging for 10,000 hours at 900°F, the same group of steels had transition temperatures in the range from 10 to 125°F or higher.

(b) While the higher (0.08%) carbon content favored slightly lower transition temperatures for the 12 Cr (Type 410) steels in the annealed condition, an increase in transition temperature was observed for all combinations of carbon and chromium contents in these steels after aging for 10,000 hours at 900°F. However, in no steel was this increase of a serious nature.

(c) Contrary to published information, 0.25% aluminum does not appear to favor an increase in transition temperature after aging. Low transition temperatures for both the annealed and aged conditions were obtained for a low (12%) chromium Type 405 steel.

(d) The addition of 0.50% molybdenum to high and low chromium 12 Cr (Type 410) and 12 Cr-Al (Type 405) steels resulted in intermediate transition temperatures for the annealed condition. After aging, the low chromium 12 Cr-Mo steel increased in transition temperature but the high chromium 12 Cr-Mo steel and both the high and low chromium 12 Cr-Al-Mo steels *did not*. The combined addition of molybdenum and aluminum appeared to effectively eliminate the so-called "885°F embrittlement" of the 12 Cr steels.

(e) The addition of 0.10% titanium to both high and low chromium 12 Cr-Al (Type 405) steels did not consistently lower the transition temperatures for both the annealed and the aged conditions.

(f) Sigma phase could not be identified in any of the steels in the annealed and aged condition. After cold reducing and aging, sigma was observed in a high chromium 12 Cr (Type 410) steel after heating at 900°F and in a high chromium 12 Cr-Al (Type 405) steel, the low carbon 17 Cr steel and the low carbon 27 Cr steel after heating at both 900 and 1050°F.

(g) Neither the grain size, the hardness change during aging nor the presence or absence of sigma in metallographic specimens, which had been cold-reduced prior to aging, could be correlated with the changes in transition temperature which occurred during aging.

(h) A fine intergranular precipitate which etched like carbides or nitrides was present in *every* impact specimen which showed an increase in transition temperature after aging. This finely dispersed phase was not found preferentially at the grain boundaries of steels

which did not show this increase nor was it observed in any of the steels after cold working and aging.

(i) The body-centered cubic precipitate previously associated with 885°F embrittlement in higher chromium steels (4), was identified by electron diffraction in an embrittled 13.73% chromium 12 Cr (Type 410) steel in the present work. In samples of lower chromium content, a lamellar Cr_2N precipitate appeared to correlate with impact transition behavior.

The impact data for the various compositions and conditions investigated suggest that for commercial applications comprising prolonged service at elevated temperatures where no increase in transition temperature can be tolerated, 12 Cr-Al-Mo steel should be used. It should be pointed out, however, that these steels exhibited average energy transition temperatures for both the annealed and the aged condition in the range from 55 to 80°F. For cold weather applications or service comprising only occasional brief intervals at elevated temperatures where low transition temperatures are of primary importance and minor elevated temperature embrittlement could be tolerated in the interest of achieving lower initial transition temperatures, the data suggest that low chromium (about 12.00%) 12 Cr-Al (Type 405) steel might be used to advantage.

ACKNOWLEDGMENT

The authors wish to express their appreciation to Mr. J. J. Heger for his constructive criticism and advice, to Mr. R. M. Fisher for the X-ray and electron diffraction analyses, to Mr. T. L. Batina who performed a portion of the testing and to Miss Mary E. Potter for much of the metallographic preparation and examination.

References

1. H. O. Newell, "High Chromium Irons," METAL PROGRESS, American Society for Metals, Vol. 51, April 1947, No. 4, p. 617.
2. M. A. Scheil, "Modified Type 405 Stainless Iron," METAL PROGRESS, American Society for Metals, Vol. 52, July 1947, No. 1, p. 91.
3. H. S. Link and P. W. Marshall, "The Formation of Sigma Phase in 13 to 16% Chromium Steels," TRANSACTIONS, American Society for Metals, Vol. 44, 1952, p. 549.
4. R. M. Fisher, E. J. Dulis and K. G. Carroll, "Identification of the Precipitate Accompanying 885°F Embrittlement in Chromium Steels," *Journal of Metals*, Transactions Supplement, Vol. 5, No. 5—Section 2, May 1953, p. 690.
5. A. J. Lena and M. F. Hawkes, "475°C (885°F) Embrittlement in Stainless Steels," *Journal of Metals*, Transactions Section, Vol. 6, No. 5—Section 2, May 1954, p. 607.

DISCUSSION

Written Discussion: By W. C. Hagel, applied-research metallurgist, Materials and Processes Laboratory, General Electric Company, Schenectady, New York.

In view of the complexity of embrittlement phenomena, the authors have presented additional information which is most welcome. The nature of precipitation reactions in certain modified 12-chromium alloys has been recently pursued in our laboratory, and it may be that our results will add to or clarify those of the authors.

Sigma was found, from X-ray diffraction patterns of electrolytically extracted residues, to form in stressed 12 Cr-Co-W-V specimens (containing 0.10 C, 12.5 Cr, 5.0 Co, 3.0 W and 0.25 V) after aging for only 1000 hours at 1050°F. This precipitation reaction causes little increase in hardness (although about 10 weight % sigma is present) and an extreme decrease in impact resistance to the extent that no impact transition temperature exists up to 1000°F. It would have been most interesting if the authors had further tested the impact properties of those specimens in which sigma appeared to form after cold reduction and aging. The use of glyceregia alone for sigma identification is liable to error, particularly if one reports a visual volume % of sigma as done in Table III. X-ray diffraction patterns are more reliable, and one can arrive at a satisfactory weight % of sigma in each specimen using quantitative electrolytic and chemical digestion techniques.

Chromium-rich ferrite (the cause of 885°F embrittlement) was found, from electron-diffraction patterns of extraction replicas, to precipitate in stressed and

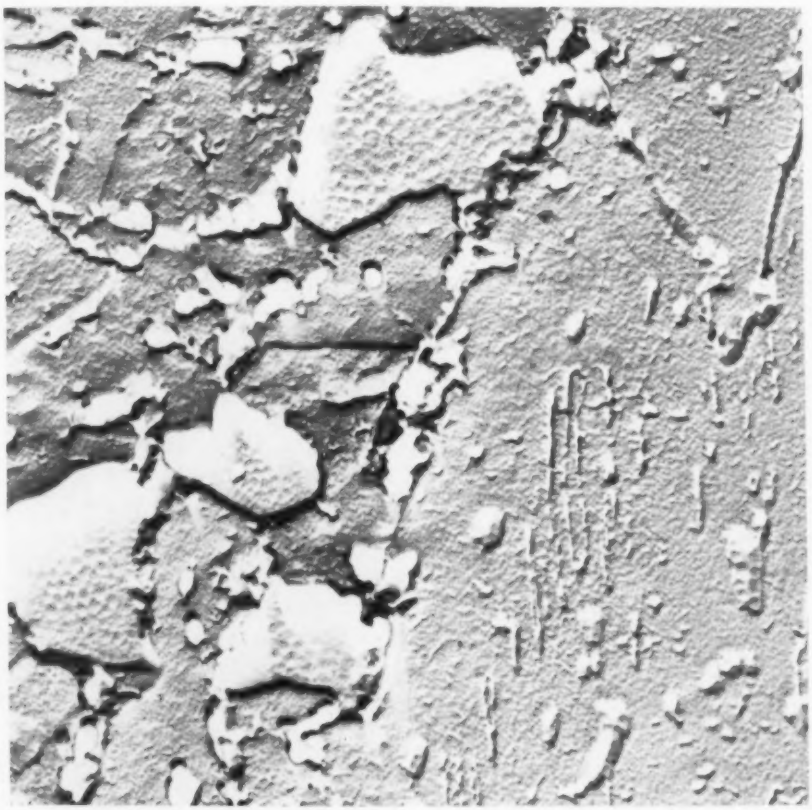


Fig. 16—Electron Micrograph at ×18,000 of 12 Cr-Co-W-V Alloy After Service Exposure for 22,000 Hours at 1000°F. Chromium-shadowed negative replica shows the presence of blocky sigma, globular $M_{23}C_6$ and lamellar precipitate.

unstressed 12 Cr-Co-W-V specimens after aging for 200 hours at 800 to 950°F. Specimen hardness increased from 340 to 360 BHN, and impact transition temperature increased from 200 to 900°F. The authors might find similar unaged transition temperatures if their specimens were austenitized, quenched and tempered at 1200°F rather than annealed at 1500 to 1550°F and air-cooled to a very ductile condition. Alone or jointly, sigma and chromium-rich ferrite account for the damaging embrittlement observed on long-time service exposure at 900 to 1050°F.

The small increases in transition temperature observed by the authors appear to result from the minor embrittlement caused by gas absorption during processing and aging. The enclosed electron micrograph shows the presence of a fine lamellar precipitate which is frequently observed in most 12-chromium alloys aged for long times in air. X-ray diffraction patterns of extracted residues were not found to give sufficient identification of this phase, although (using chromium Kα radiation) there are low intensity lines at 2θ positions of 62.0 and 66.0 which one can compare with patterns of pure Cr_2N or many other phases. The writer would appreciate seeing some of the original electron and X-ray diffraction patterns from which the authors made a positive identification of Cr_2N.

If the minor embrittling precipitate is Cr_2N, then many of the reported anomolous increases in impact transition temperature may be caused by processing rather than alloy compositional variables; the wide scatter in impact data does not allow one to attach great significance to transition-temperature increases of less than about 20°F. The detection of sigma in a high chromium 12 Cr-Al alloy appears to confirm, rather than refute, Newell's original observation that Type 405 can badly embrittle during long-time service exposure by sigma and/or chromium-rich ferrite precipitation. The authors may have studied only the minor and unpredictable effect of gas absorption.

Authors' Reply

The authors wish to thank Mr. Hagel for his interesting and informative discussion. Perhaps a brief definition of the objective of the investigation described in the paper would more clearly explain the testing conditions and techniques employed.

An important commercial application of 12 Cr steels comprises welded, corrosion-resistant linings in vessels used at elevated temperatures in oil refineries and other chemical industries. Here, the corrosion resistance of 12 Cr steel is adequate and these steels are not so susceptible to embrittlement by sigma precipitation at temperatures up to 900°F as were the 17 Cr steels formerly used. Because of the forming operations involved, these vessels are fabricated from annealed material—rarely is quenched and tempered material used. Therefore, this investigation was concerned with the embrittling behavior or shift in transition temperature of annealed specimens of various compositions which were heated for an extended period at 900°F.

A secondary objective was that of determining, if possible, what precipitate was responsible for any embrittlement observed, and the technique of metallographically evaluating the presence of sigma in the aged samples seemed adequate for this purpose. It should be pointed out, however, that in the 12 Cr-Al steels sigma was identified only in a cold reduced and aged sample of the high chromium

(13.61%) steel, Code 10 in Table III, and could not be discerned in annealed and aged samples of the same heat or in the low chromium (12.06%) steel, Code 9, whether the aging was carried out on annealed or cold-reduced specimens. The chromium content of this high chromium steel was above the commercial specification (11.50/13.50%) for AISI Type 405 while the steel which Newell reported as embrittled contained 13.18% Cr. Comparing the annealed and the aged transition temperatures of 12 Cr and 12 Cr-Al steels at similar carbon and chromium levels, c.f. heats 3 and 9, and 4 and 10 in Table II, does not suggest that the presence of 0.25% Al produced a larger increase in transition temperature during the 10,000 hour aging treatment at 900°F. As pointed out by Scheil (2) who quoted satisfactory service performance at 850 to 900°F of many modified Type 405 vessel linings, 12 Cr-Al (Type 405) steel containing not more than 13% chromium and approximately 0.08% carbon would not be expected to embrittle during prolonged heating at temperatures as high as 900°F.

No chemical analyses were made of the extraction residues upon which the X-ray diffraction analyses given in Table IV were made. The medium to high intensity lines of four of the diffraction patterns definitely showed that the material was isomorphous with pure Cr_2N. Certainly the presence of this phase would be expected in 12 Cr steels which did not contain significant amounts of elements with stronger nitride forming tendencies than chromium.

A comparison of total nitrogen contents of aged impact specimens with original nitrogen contents of drillings from the as-cast ingot, Table V, does not suggest that any significant absorption of nitrogen occurred during hot working, annealing, or the 10,000 hour aging treatment at 900°F. In fact, the data indicate only an average total nitrogen increase for the fourteen heats of 0.001%, a value less than the experimental error of the analytical technique.

Table V
Change in Total Nitrogen Content of the 12 Cr Steels During the Processing and Aging (10,000 Hrs. @ 900°F) Treatments

Steel Code	Type	% Nitrogen in Ingot	Change in Transition Temperature	% Nitrogen in Aged Impact Specimen
1	12 Cr-Low C	0.055	Increase	0.058
2	12 Cr-Low C	0.053	Increase	0.055
3	12 Cr	0.058	Increase	—
4	12 Cr	0.062	Increase	0.059
5	12 Cr	0.029	Increase	0.029
6	12 Cr-Mo	0.056	None	0.060
7	12 Cr-Mo	0.041	None	0.043
8	12 Cr-Mo	0.038	Increase	0.035
9	12 Cr-Al	0.032	Increase	0.024
10	12 Cr-Al	0.055	Increase	0.052
11	12 Cr-Al-Mo	0.046	None	—
12	12 Cr-Al-Mo	0.080	None	0.084
13	12 Cr-Al-Ti	0.049	None	0.048
14	12 Cr-Al-Ti	0.073	Increase	0.076
15	17 Cr-Low C	0.064	Increase	0.068
16	27 Cr-Low C	0.081	Increase	0.083

It would appear, therefore, that the data do not represent the minor effect of nitrogen absorption upon impact properties although nitride precipitation as the equilibrium structure at 900°F was approached, may have exerted some influence upon the transition temperature.

THE EFFECT OF COMPOSITION AND STRUCTURE ON THE CREEP-RUPTURE PROPERTIES OF 18-8 STAINLESS STEELS

By Forest C. Monkman, Peter E. Price and Nicholas J. Grant

Abstract

Twenty-seven simple unstabilized stainless steels of the 18 chromium-8 nickel variety were prepared in which amounts of chromium, nickel, and carbon plus nitrogen were varied. Stress-rupture tests were conducted on these alloys at temperatures of 1000, 1200, and 1300°F for rupture lives of about thirty seconds to five hundred hours. Variations in the chromium, nickel, or carbon plus nitrogen contents while holding the other two constant were studied to establish the effects of such composition changes on the strength and structure of the alloys at elevated temperatures. The effects of the formation and growth of carbides, ferrite, and sigma during testing were evaluated. (ASM-SLA Classification: Q3, Q4, SS)

THE relatively high cost and limited supply of many elements currently being used in high temperature alloys necessitate the development and better utilization of lower alloyed steels. This is, of course, especially important if there is to be a large scale expansion in the gas turbine and other high temperature fields. In this regard, a better understanding of the 18-8 type of stainless steel and the development of improved stainless steels as a substitute for some of the higher alloyed materials appears to be very promising.

To improve existing stainless steel alloys, it is first desirable to know exactly what are the effects of variations in chemical composition on alloy stability and on high temperature rupture strength and creep resistance. Thus it is desirable to understand the effects of phase changes on the strength properties, because relatively small changes in the chemical composition of the 18-8 type stainless steels result in structural changes, such as the formation of carbides, sigma or ferrite and their subsequent growth in the temperature range where stainless steels are normally used.

This paper is based on theses submitted for partial fulfillment of the requirements for the degree of Doctor of Science for Forest C. Monkman, and for the degree of Master of Science, for Peter E. Price.

A paper presented before the Thirty-Seventh Annual Convention of the Society, held in Philadelphia, October 17–21, 1955. Of the authors, Forest C. Monkman is DIC Staff member, Peter E. Price is research assistant, and Nicholas J. Grant is associate professor, Department of Metallurgy, Massachusetts Institute of Technology, Cambridge. Manuscript received April 1, 1955.

Experimental Procedure

A series of simple iron-chromium-nickel stainless steels containing carbon and nitrogen were investigated, omitting other alloying and stabilizing elements usually found in commercial stainless steels. While the general effects of alloying elements on the high temperature rupture strength and structure are known, their specific effects are still subject to considerable speculation. A previous investigation by Hum and Grant (1)[1] indicated a strong dependency of rupture strength on the carbon plus nitrogen content in a series of unstabilized 18-8 stainless steels. Therefore, in this study, which is an extension of the former work, the sum of the carbon and nitrogen contents was kept relatively constant when the nickel or chromium was varied. The chemical compositions of the alloys studied are listed in Table I.

Table I
Compositions and Initial Structures of the Alloys

Alloy No.	% Cr	% Ni	% C	% N	% Si	% Mn	% O	M_s°F	Structure*
1	18.50	6.15	0.032	0.033	0.39	0.10		+100	$\bar{\gamma}$, M, δ
2	15.7	8.7	0.030	0.030	—	—	—	+100	$\bar{\gamma}$, M
3	17.35	8.28	0.020	0.024	0.29	0.09	0.044	− 25	$\bar{\gamma}$, M, δ
4	19.61	8.46	0.029	0.027	0.26	—	0.054	−110	$\bar{\gamma}$, δ
5	16.01	11.08	0.025	0.025	0.25	—	—	< −320	$\bar{\gamma}$
6	16.16	9.38	0.037	0.031	—	—	—	−125	$\bar{\gamma}$
7	19.60	8.07	0.110	0.031	0.33	0.12	0.027	< −320	$\bar{\gamma}$
9	17.24	8.18	0.126	0.034	—	0.09	—	−250	$\bar{\gamma}$
10	18.49	6.09	0.116	0.035	—	0.09	—	−150	$\bar{\gamma}$, M
11	18.68	10.92	0.032	0.036	—	0.07	—	< −320	$\bar{\gamma}$
12	18.28	10.97	0.104	0.039	—	—	—	< −320	$\bar{\gamma}$
13	18.28	11.18	0.067	0.042	0.25	0.16	—	< −320	$\bar{\gamma}$
15	16.59	8.17	0.067	0.034	0.18	—	0.029	− 75	$\bar{\gamma}$, M
16	14.52	6.66	0.040	0.023	—	0.07	—	+150	$\bar{\gamma}$, M
19	19.78	8.17	0.061	0.038	—	0.06	0.035	< −320	$\bar{\gamma}$, δ
20	18.45	8.20	0.098	0.025	0.19	—	0.037	−200	$\bar{\gamma}$
21	18.52	8.10	0.081	0.030	—	0.03	0.041	−200	$\bar{\gamma}$
29	18.31	5.85	0.062	0.035	0.18	0.06	—	+ 75	$\bar{\gamma}$, M
35	18.26	8.17	0.027	0.038	0.21	—	—	−140	$\bar{\gamma}$, M
50	10.71	11.78	0.024	0.025	—	—	—	275	$\bar{\gamma}$, M
53	13.31	12.19	0.023	0.028	—	—	—	−150	$\bar{\gamma}$
55	15.37	11.98	0.032	0.038	—	—	—	−200	$\bar{\gamma}$
89	18.06	7.92	0.016	0.019	—	—	—	+ 50	$\bar{\gamma}$, M
103	19.28	15.03	0.020	0.028	—	—	—	< −320	$\bar{\gamma}$
104	14.10	18.38	0.030	0.036	—	—	—	< −320	$\bar{\gamma}$
105	16.28	14.78	0.028	0.028	—	—	—	< −320	$\bar{\gamma}$
106	13.06	15.31	0.026	0.016	—	—	—	< −320	$\bar{\gamma}$

*Structure after one-half hour solution treatment at 2000°F, followed by a water quench.

Heats 50, 53, and 55 were prepared in a six-pound indirect graphite arc furnace while the remaining heats were melted in a 25-pound induction furnace. The melts were deoxidized with a calcium-manganese-silicon alloy and cast at 1550°C (2820°F) into graphite molds. The ingots were forged to one half inch diameter rods at a maximum forging temperature of 2200°F. The rods were solution treated one half hour at 2000°F and water-quenched.

Stress-rupture test specimens were machined which had a test section of 0.250-inch diameter by 1.0-inch gage length. Stress-rupture

[1]The figures appearing in parentheses pertain to the references appended to this paper.

tests were run on equipment previously described (2). Tests were conducted at temperatures of 1000, 1200 and 1300°F and at stresses which resulted in rupture lives from about 30 seconds to 500 hours.

Metallographic samples were prepared from selected stress-rupture specimens in order to follow structural changes which occurred during testing. X-ray diffraction patterns were obtained on a Norelco X-ray spectrometer using chromium radiation. A high temperature X-ray camera was used for structure determination at the testing temperatures. It was found possible to determine accurately

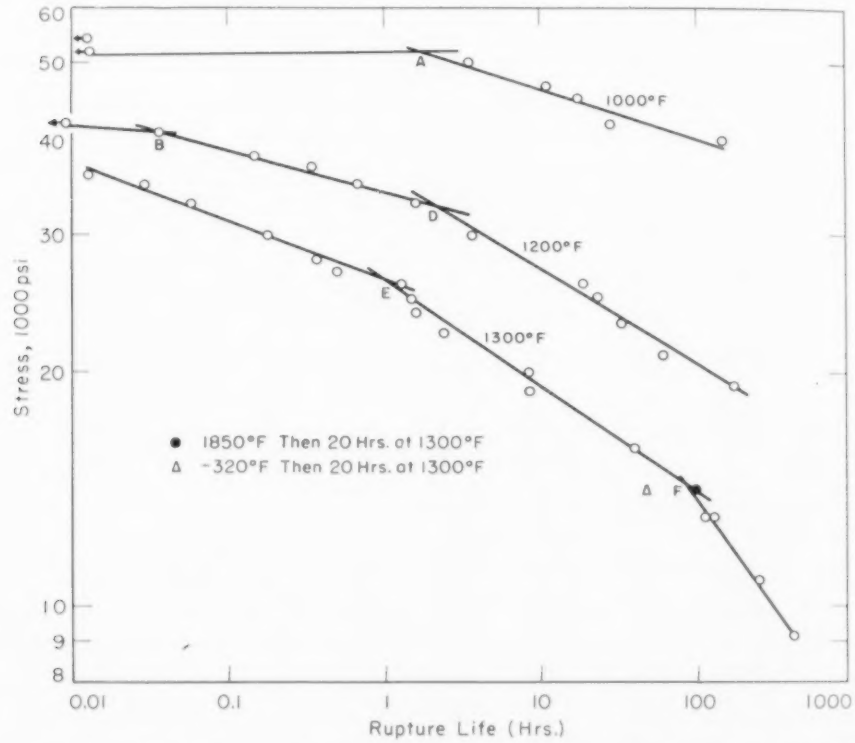


Fig. 1—Plot of Log Stress Versus Log Rupture Time at 1000, 1200, and 1300°F for Alloy 4 (19.6% Cr, 8.5% Ni, 0.056% C+N).

the formation and reversion temperatures of martensite by means of resistivity measurements with a Kelvin double bridge. In addition, a Magnegage, which measures the force necessary to pull a magnet off the surface of the specimen, was utilized to determine the amount of magnetic phase present in the alloys.

Experimental Results

Carbon and Nitrogen Series—Figs. 1 and 2 show typical log stress versus log rupture life and log stress versus log minimum creep rate plots for one of the alloys. In every case the best curves were drawn on the basis of the test values, supported by metallographic examina-

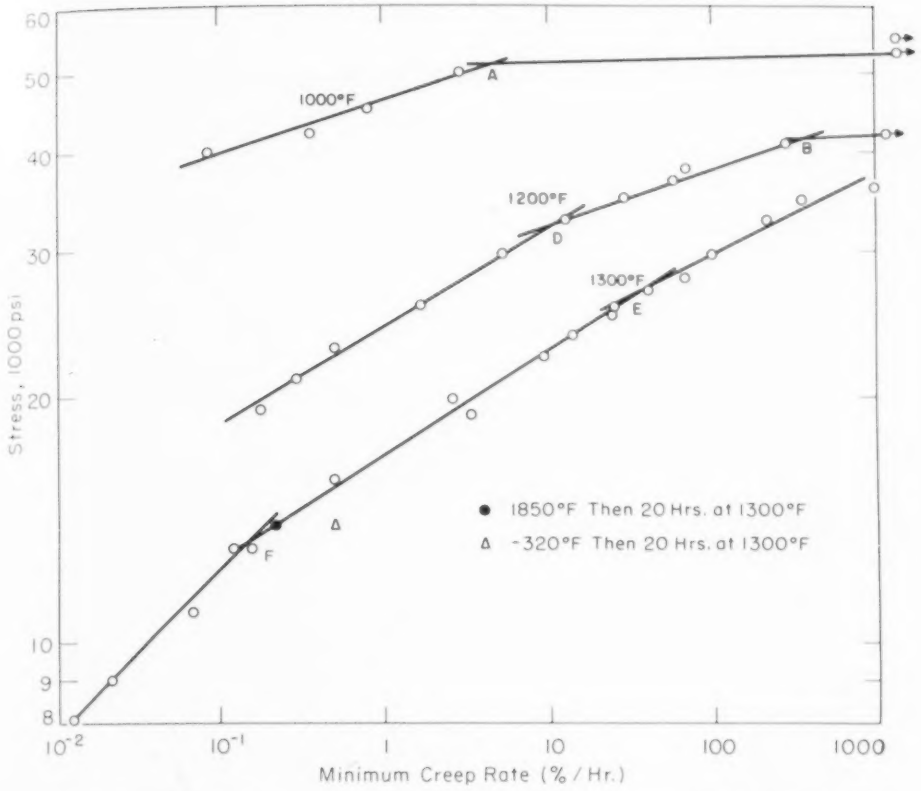


Fig. 2—Plot of Log Stress Versus Log Minimum Creep Rate at 1000, 1200, and 1300°F for Alloy 4 (19.6% Cr, 8.5% Ni, 0.056% C+N).

tion of the specimens. Such plots were obtained, using about the same number of tests, for each of the alloys, and the point scatter is representative of that of the other alloys; but because of the large number of individual plots, they have been omitted, and only the summary plots of log stress versus log rupture life are included and are shown in Figs. 3 to 7.

Metallographic examination of the stress-rupture specimens revealed that the breaks in the curves labeled A, B and C at 1000, 1200 and 1300°F, respectively, were due to a transition from a transcrystalline type of fracture to an intercrystalline one. The breaks in the curves labeled D and E at 1200 and 1300°F were associated with a grain boundary precipitate or precipitates as seen in Fig. 8.

Metallographic examination, magnetic tests, heat treatments, and X-ray diffraction were used in an attempt to identify the grain boundary precipitate or precipitates. The etching characteristics indicated that the precipitate was a combination of carbides, nitrides, and ferrite in each of the alloys of this series. Magnetic measurements showed that a magnetic phase was present in the stress-rupture specimens which broke beyond the breaks labeled D and E in the

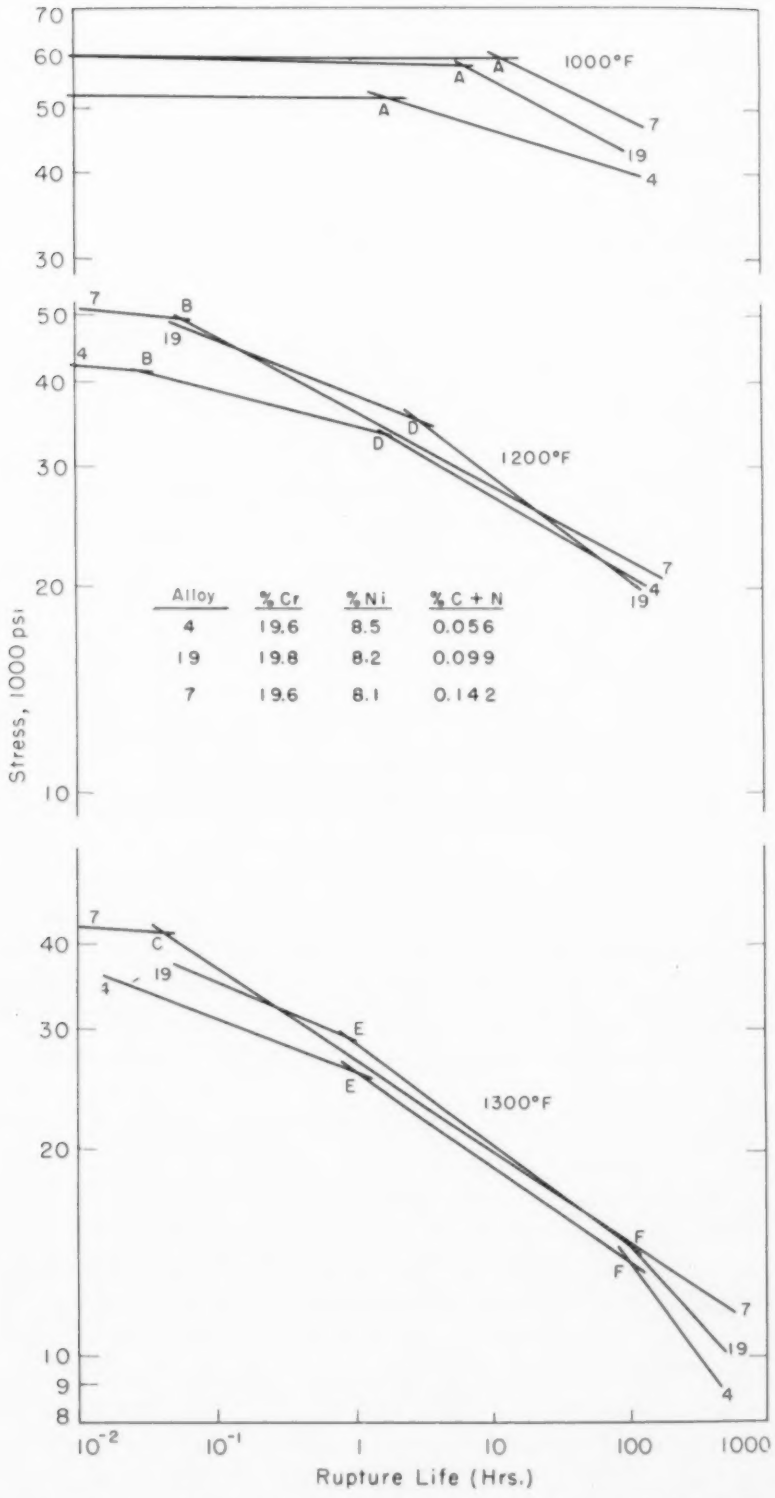


Fig. 3—Summary Plot of Log Stress Versus Log Rupture Life at 1000, 1200, and 1300°F for Alloys 4, 7, and 19.

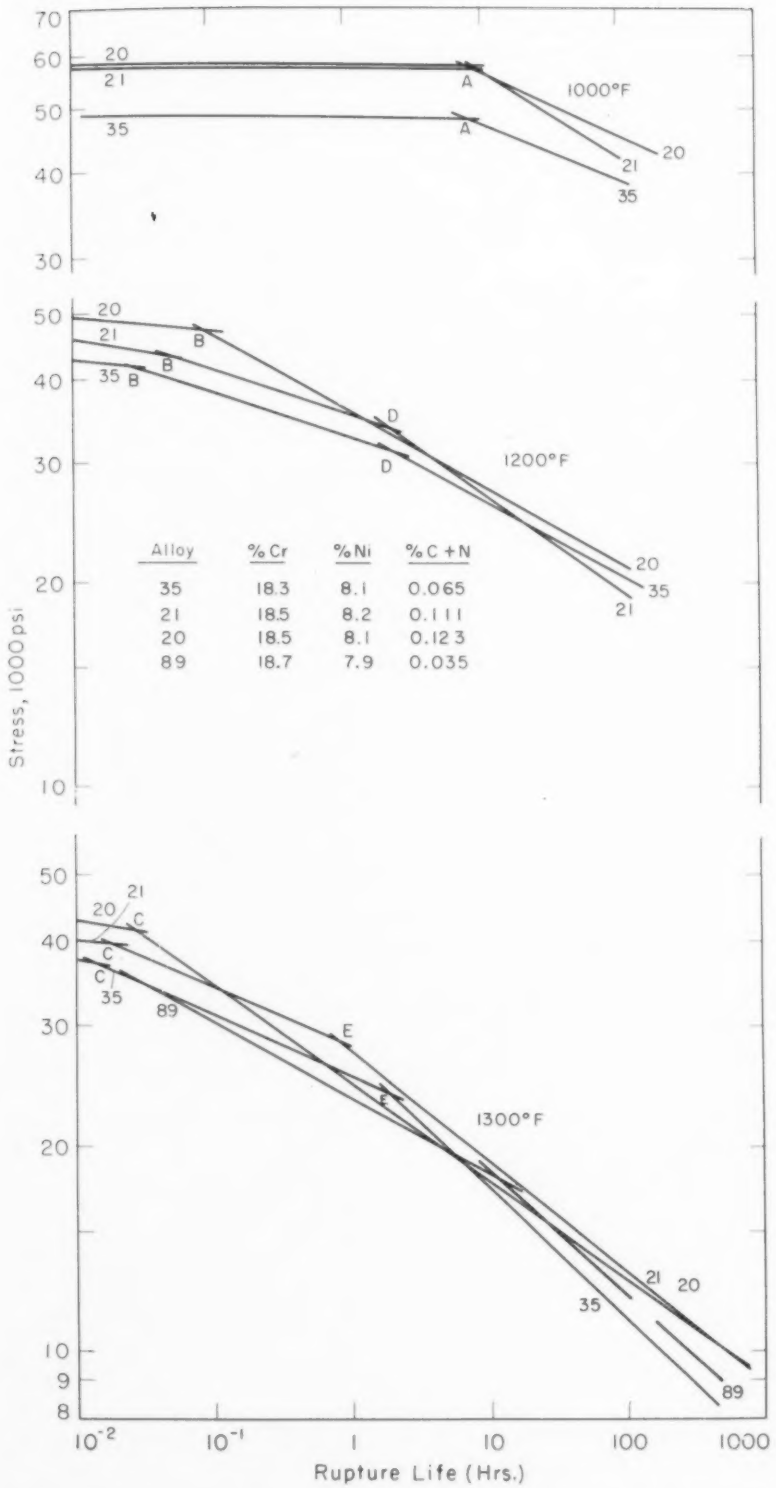


Fig. 4—Summary Plot of Log Stress Versus Log Rupture Life at 1000, 1200, and 1300°F for Alloys 35, 21, 20 and 89.

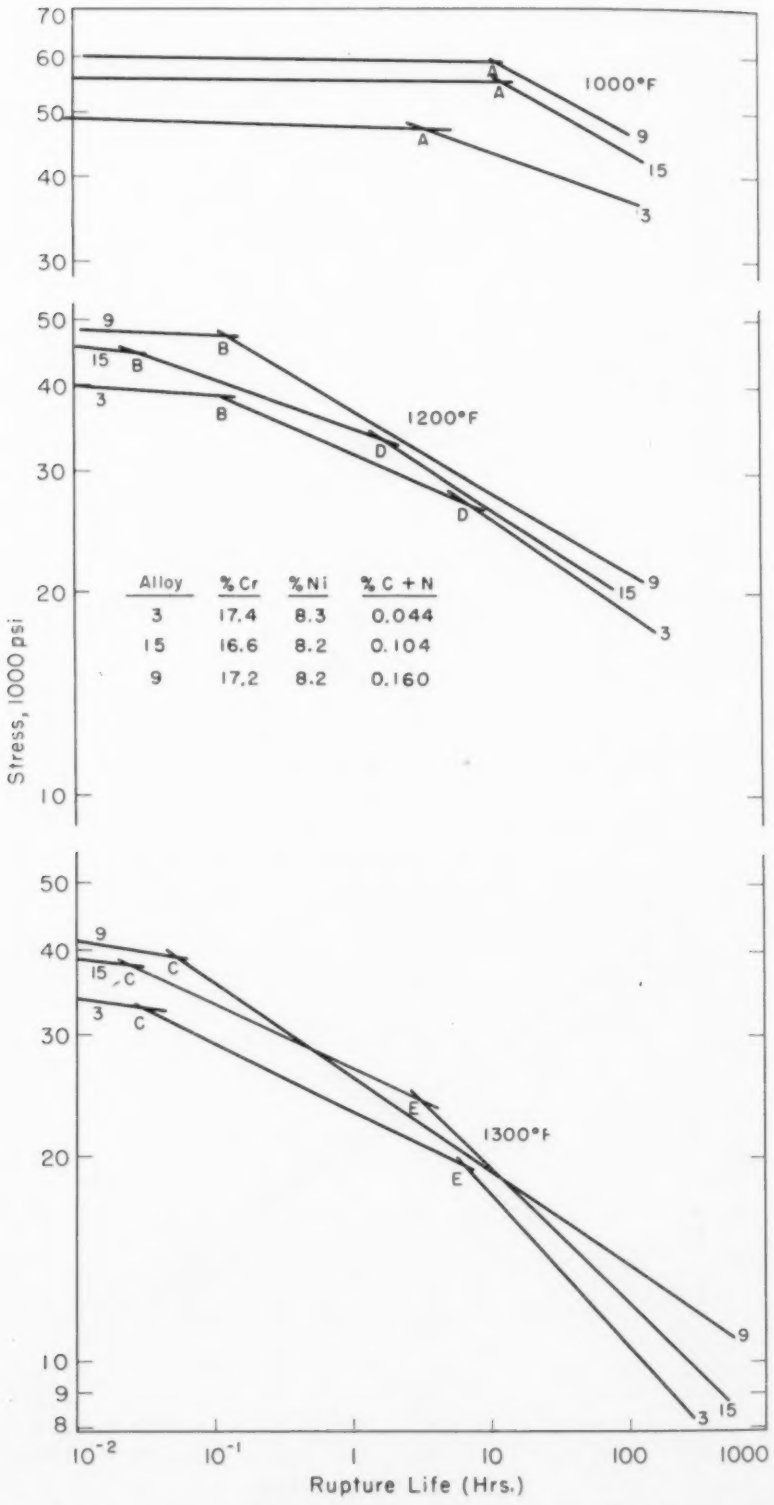


Fig. 5—Summary Plot of Log Stress Versus Log Rupture Life at 1000, 1200, and 1300°F for Alloys 3, 15, and 9.

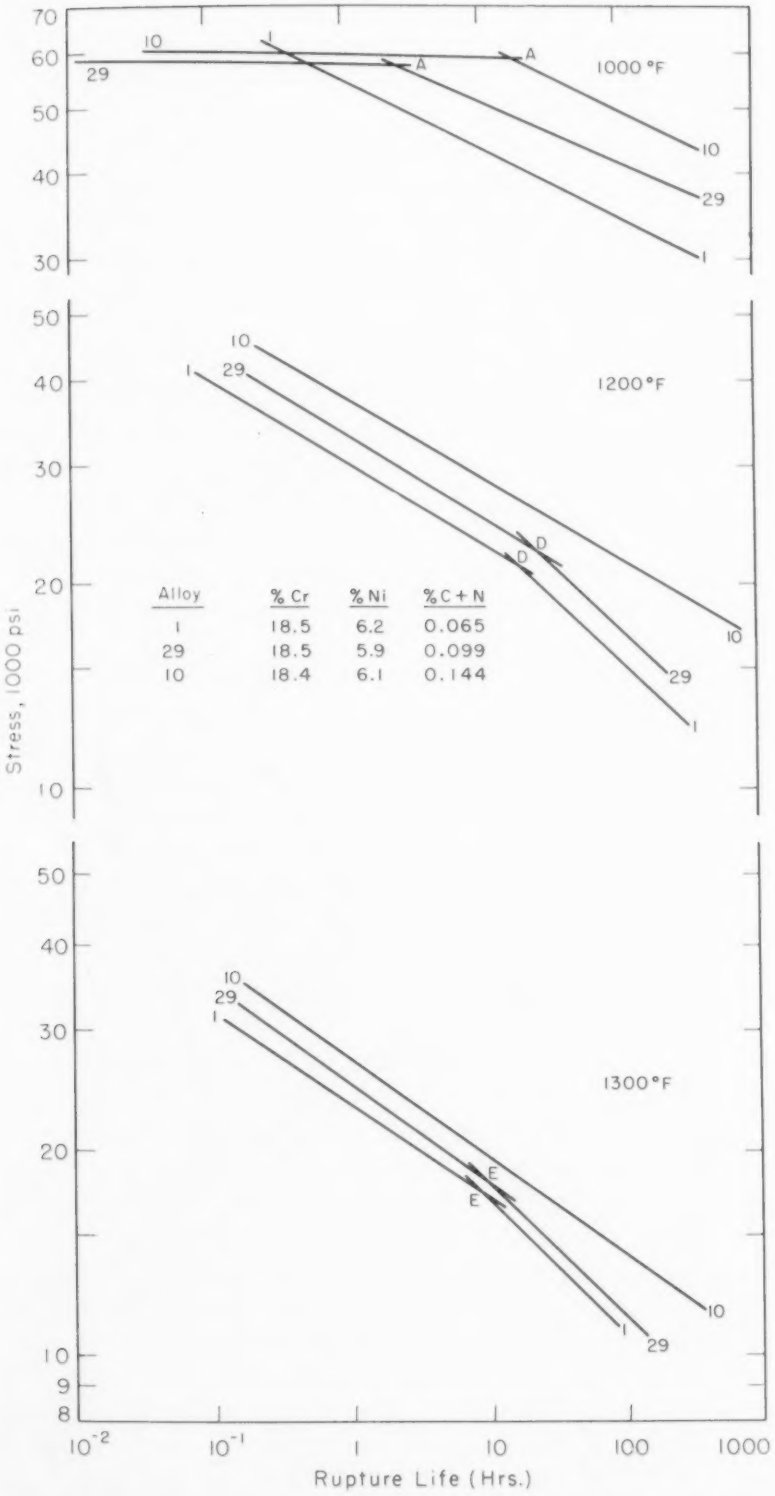


Fig. 6—Summary Plot of Log Stress Versus Log Rupture Life at 1000, 1200, and 1300°F for Alloys 1, 29, and 10.

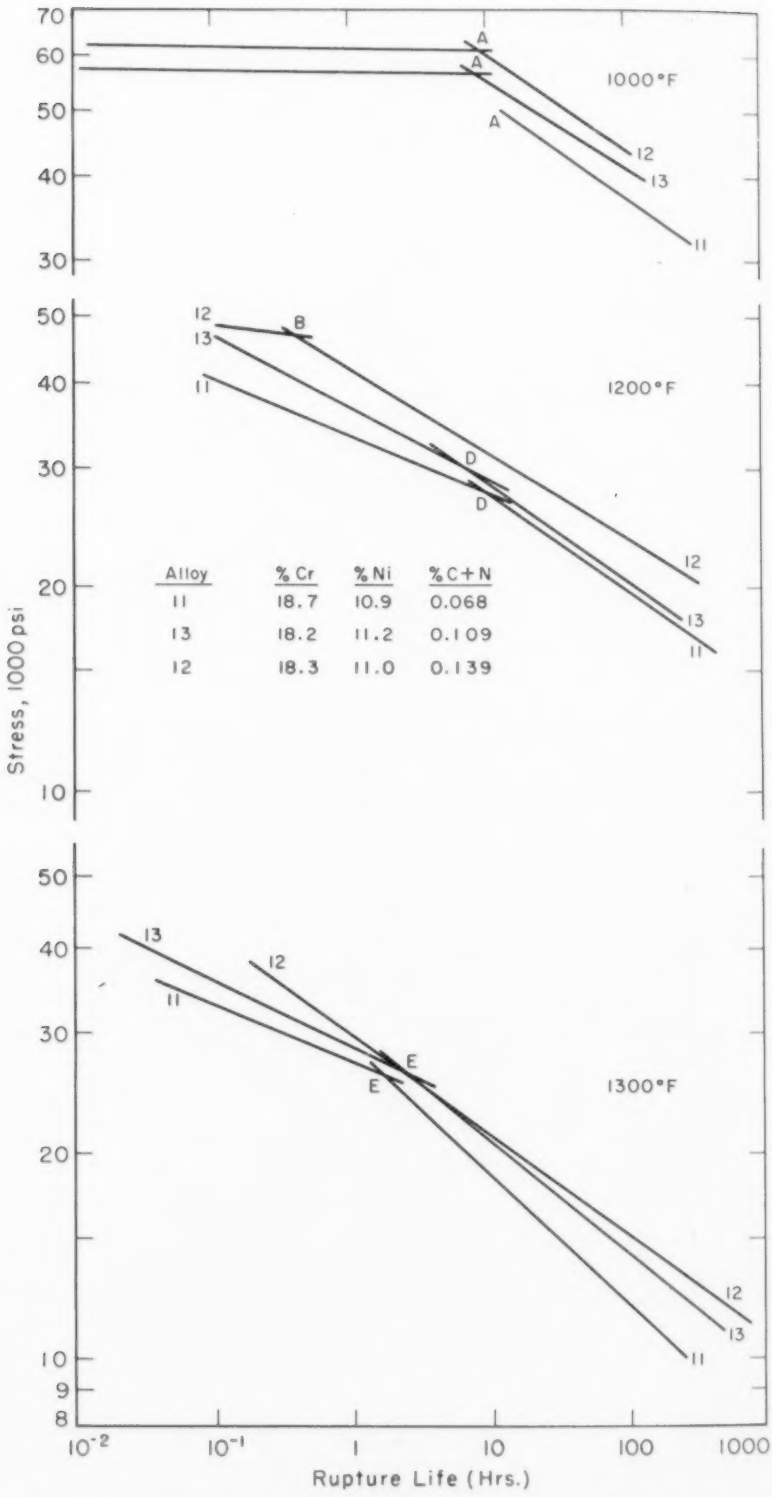


Fig. 7—Summary Plot of Log Stress Versus Log Rupture Life at 1000, 1200, and 1300°F for Alloys 11, 12, and 13.

curves. It is quite possible that the noted magnetism was due to martensite which formed in the long time rupture specimens of the alloys in this series due to the fact that the M_s temperatures of the alloys were raised above room temperature when carbon and nitrogen were precipitated out of solid solution during testing. To identify the magnetic phase, sections of the ruptured test specimens were heat treated for 100 hours at 1800°F which is above the solution temperature for sigma, carbides and nitrides, but not for ferrite. In every case a portion of the precipitate remained at the grain boundary, indicating that some of the precipitate was ferrite. In addition, an $M_{23}C_6$ carbide X-ray diffraction pattern was obtained from the residues electrolytically separated from the long time rupture specimens of the alloys in this series. On the basis of these tests, it was decided that the breaks in the stress-rupture curves (D and E) at 1200 and 1300°F were due to the growth of ferrite at the grain boundaries. This is supported by the observation that the instability breaks are suppressed by increasing carbon plus nitrogen content (they are strong austenite stabilizers) at constant chromium and nickel levels.

The third instability, denoted as "F" in the stress-rupture curves at 1300°F for alloys 4 and 19 (Fig. 3), is believed to be caused by the precipitation of sigma, even though the characteristic X-ray pattern of sigma was not found in the diffraction patterns of the electrolytically separated residue. Etching studies (3) did indicate that sigma was present; however, this is not positive proof since the etching characteristics of sigma are similar to those of the carbides and nitrides. The summary plots show that this instability "F" is enhanced by decreasing carbon and nitrogen content and with increasing chromium content, both changes promoting the formation of sigma (4,5,6).

It is evident from Figs. 3 to 7 that carbon and nitrogen increase the rupture strength of these alloys in the temperature range investigated; however, the magnitude of the strengthening effect is dependent upon both testing temperature and the time of the test (or stress). Table II summarizes the stress for rupture at specified times at 1000 to 1300°F. The range of stress values attainable through variation in the carbon plus nitrogen content can be seen to vary considerably at all temperatures. The precipitation of carbides and nitrides and the adjustment of the matrix to these changes takes place over a sufficiently long time to result in the observed variations of strength with time and temperature. In addition to the relatively large solid solution strengthening effect noted in the short time tests, carbon and nitrogen maintain the strength at long times by suppressing the formation of ferrite and sigma. This effect can be seen in Figs. 3 to 7 where instability breaks of the type D and E, due to

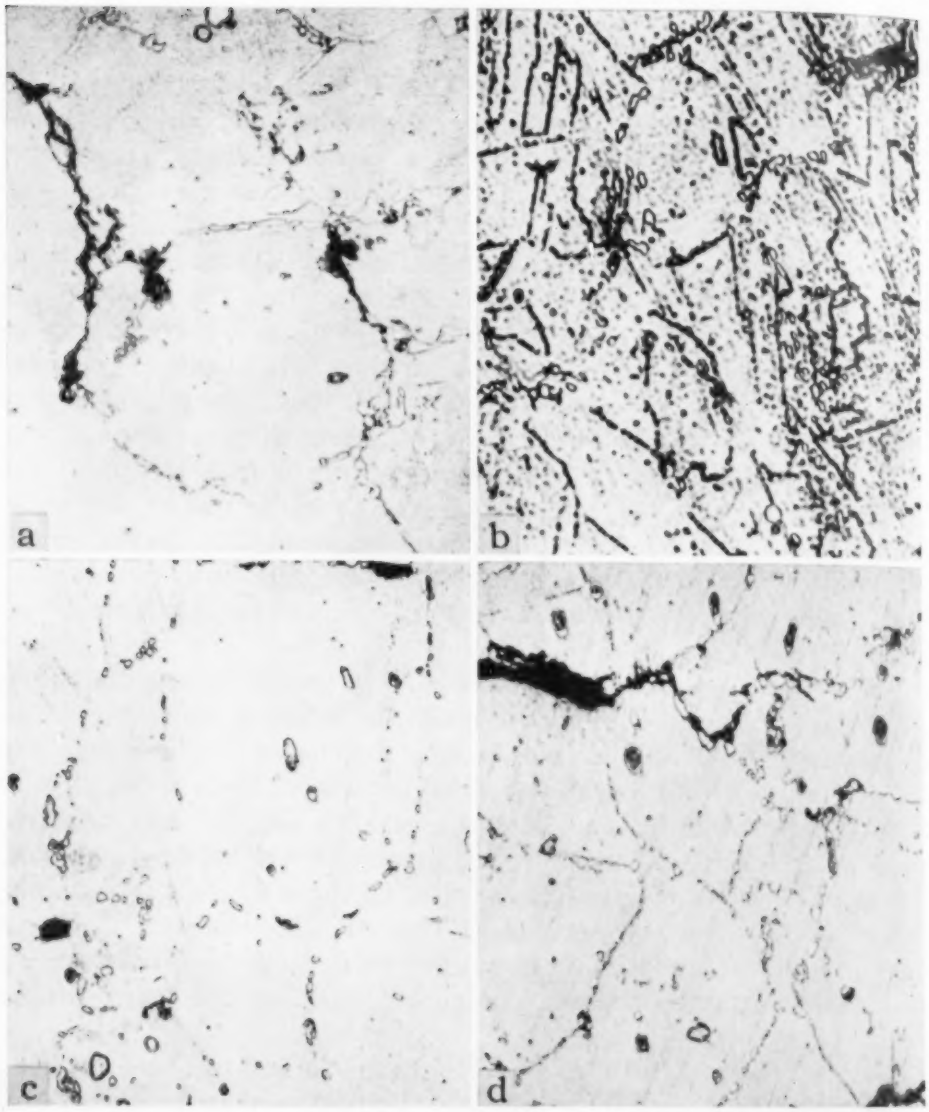


Fig. 8—Photomicrographs of Selected Stress-Rupture Specimens of Alloys 3, 4, 9, and 19, Showing Precipitates Formed During Testing. Ferritic Chloride Etch.
(a) Alloy 3. 1300°F 410 hours. X 500. (17.4 Cr, 8.3 Ni, 0.04 C+N); (b) Alloy 9. 1300°F 890 hours. X 750. (17.2 Cr, 8.2 Ni, 0.16 C+N); (c) Alloy 4. 1300°F 390 hours. X 750. (19.6 Cr, 8.5 Ni, 0.06 C+N); (d) Alloy 19. 1300°F 490 hours. X 500. (19.8 Cr, 8.2 Ni, .10 C+N).

the precipitation of ferrite, and F, due to the precipitation of sigma, were prevented by increasing carbon and nitrogen content.

It is important to note that the initial formation of ferrite and sigma is generally not detrimental to the high temperature strength. In fact, the summary plots show that the strength of the alloys which exhibit a ferrite instability break (D and E) is maintained at a higher level of stress (smaller slope) than the alloys without such an instability break up to a period of time just prior to the appearance of the instability break; compare alloys 4 and 19 to alloy 7 at 1200 and

Table II
Variations in Stress to Rupture for Specified Times at 1000, 1200, and 1300°F For the Alloys in the Carbon Plus Nitrogen Series

Alloy No.	% Cr	% Ni	% C+N	1000°F		1200°F		1300°F	
				10 hrs.	100 hrs.	10 hrs.	100 hrs.	10 hrs.	500 hrs.
				19½ Cr—8 Ni varying C plus N					
4	19.6	8.5	0.056	46,000	40,000	27,000	20,500	19,000	8,900
19	19.8	8.2	0.099	56,000	44,000	29,500	21,000	20,500	10,000
7	19.6	8.1	0.141	59,000	48,500	28,000	21,600	20,000	11,700
				17 Cr—8 Ni varying C plus N					
3	17.4	8.3	0.044	43,500	37,000	25,700	18,700	17,800	7,500
15	16.6	8.2	0.104	55,000	44,000	26,500	19,500	19,000	8,800
9	17.2	8.2	0.160	60,000	47,500	28,500	21,800	19,500	11,400
				18 Cr—8 Ni varying C plus N					
89	18.1	7.9	0.036	—	—	—	—	18,500	9,000
35	18.3	8.2	0.065	47,500	39,500	26,400	20,500	17,500	8,100
21	18.5	8.2	0.111	56,000	42,000	26,200	18,800	18,600	10,000
20	18.5	8.2	0.123	55,400	44,000	27,000	20,600	17,500	10,000
				18 Cr—6 Ni varying C plus N					
1	18.5	6.2	0.065	44,000	35,000	23,000	15,500	17,000	7,800
29	18.5	5.9	0.099	51,000	41,500	25,000	17,000	18,000	8,200
10	18.4	6.1	0.144	60,000	50,000	28,500	22,000	19,500	11,000
				18 Cr—11 Ni varying C plus N					
11	18.7	10.9	0.068	49,000	37,500	27,500	20,000	18,500	9,000
13	18.2	11.2	0.109	55,500	42,000	28,500	20,500	20,500	11,000
12	18.3	11.0	0.139	60,000	44,500	31,500	24,000	21,000	12,000

1300°F in Fig. 3. This indicates that the initial formation of ferrite (and sigma) actually strengthens the alloys; however, the subsequent growth and agglomeration of ferrite (and sigma) at the grain boundaries weaken the structure and result in the noted instability breaks D and E, after which there is a more rapid decrease in strength with increasing rupture life.

The Effect of Chromium Variations—The summary plots of log stress versus log rupture life for the chromium series are presented in Figs. 9 to 13. The instability breaks labeled A, B, and C at 1000, 1200, and 1300°F, respectively, were again determined to be due to the transition from a transcrystalline to an intercrystalline type failure. The instability breaks D and E were again found to be associated with the same type of grain boundary precipitation.

While the most recent iron-nickel-chromium phase diagram (4) at 1200°F indicates that it is impossible to form ferrite in stainless steels containing more than about 8 to 10% nickel, magnetic tests with a Magnegage showed small but discernible amounts of magnetic phase present in the chromium series of alloys containing as much as 12 and 15% nickel. A section from a stress-rupture specimen of alloy 103 (19 chromium-15 nickel) was tested in a search coil in a strong magnetic field. An amount of ferro-magnetic phase equivalent to 0.05% iron was measured, which corresponds approximately to the amount of grain boundary precipitate observed in this alloy (about equal to the amount of precipitate in alloy 53 in Fig. 20). Besides responding to etches for ferrite, this precipitate did not dissolve even after being held at 1800°F for 100 hours.

Table III
Variation in Stress to Rupture for Specified Times at 1000, 1200 and 1300°F For the Alloys in the Chromium Series

Alloy No.	% Cr	% Ni	% C+N	1000°F		1200°F		1300°F	
				10 hrs.	100 hrs.	10 hrs.	100 hrs.	10 hrs.	500 hrs.
				8 Ni—.14 C+N varying Cr					
9	17.2	8.2	0.160	60,000	47,500	28,500	21,800	19,500	11,400
20	18.5	8.2	0.123	55,400	44,600	27,000	20,600	17,500	10,000
7	19.6	8.1	0.141	59,000	48,500	28,000	21,600	20,000	11,700
				8 Ni—.10 C+N varying Cr					
15	16.6	8.2	0.104	55,000	44,000	26,500	19,500	19,000	8,800
21	18.5	8.1	0.111	56,000	42,000	26,200	18,800	18,600	10,000
19	19.8	8.2	0.099	56,000	44,000	29,500	21,000	20,500	10,000
				8 Ni—.06 C+N varying Cr					
2	15.7	8.7	0.056	—	—	26,000	19,000	—	—
3	17.4	8.3	0.044	43,500	37,000	25,700	18,700	17,800	7,500
35	18.3	8.2	0.064	47,500	39,500	26,400	20,400	17,500	8,100
4	19.6	8.5	0.056	46,000	40,000	27,000	20,500	19,000	8,900
				12 Ni—.06 C+N varying Cr					
50	10.7	11.8	0.049	—	—	—	—	21,000	7,200
53	13.3	12.2	0.051	—	—	—	—	18,000	7,800
55	15.4	12.0	0.070	—	—	—	—	17,600	8,500
11	18.7	10.9	0.068	49,000	37,500	27,500	20,000	18,500	9,000
				15 Ni—.06 C+N varying Cr					
106	13.1	15.3	0.042	—	—	—	—	14,100	7,900
105	16.3	14.8	0.056	—	—	26,000	17,500	18,000	8,300
103	19.3	15.0	0.048	—	—	—	—	18,200	7,700

On the basis of these summary plots, it is seen that chromium in solid solution increases the high temperature strength up to the point where sigma is formed as a relatively coarse product. The stress for rupture at specified times at 1000, 1200 and 1300°F is summarized in Table III. The strengthening effect at short times due to chromium is less than that of carbon and nitrogen as can be seen in comparing Figs. 5 and 12. In these figures, an increase in carbon plus nitrogen content from 0.04 to 0.16% increased the 36 second rupture life 6,000 psi, while an increase in chromium content from 10.7 to 18.7% only increased it 4000 psi. As in the case of the initial formation of carbides and ferrite, sigma formation strengthens the alloys at short test times, as evidenced by the flat slope of the curves in Figs. 9,10, and 13 (see for example alloy 4 at 1300°F, Fig. 9, and alloy 19 in Fig. 10, also at 1300°F). The subsequent growth of the sigma into a massive phase results in the "F" instability beyond which the slope of the strength curve becomes much steeper.

The Effect of Nickel Variations—The summary plots for the alloys in the nickel series are shown in Figs. 14 to 19. Again the transition from a transcrystalline to an intercrystalline type fracture results in an instability break labeled A, B, and C, whereas the other instability breaks labeled D and E and F were found to be associated with grain boundary precipitation, as explained above. The stress for rupture at specified times at 1000, 1200, and 1300°F is summarized in Table IV.

Table IV
Variation in Stress to Rupture for Specified Times at 1000, 1200, and 1300°F For the Alloys in the Nickel Series

Alloy No.	% Cr	% Ni	% C+N	1000°F		1200°F		1300°F	
				10 hrs.	100 hrs.	10 hrs.	100 hrs.	10 hrs.	500 hrs.
				18 Cr—.06 C+N varying Ni					
1	18.5	6.2	0.065	44,000	35,000	23,000	15,500	17,000	7,800
35	18.3	8.2	0.065	47,500	39,500	26,400	20,400	17,500	8,100
11	18.7	10.9	0.068	49,000	37,500	27,500	20,000	18,500	9,000
				18 Cr—.10 C+N varying Ni					
29	18.5	5.9	0.099	51,000	41,500	25,000	17,000	18,000	8,200
21	18.5	8.1	0.111	56,000	42,000	26,200	18,800	18,600	10,000
13	18.2	11.2	0.109	55,500	42,000	28,500	20,500	20,500	11,000
				18 Cr .14 C+N varying Ni					
10	18.4	6.1	0.144	60,000	50,000	28,500	22,000	19,500	11,000
20	18.5	8.2	0.123	55,400	44,000	27,000	20,600	17,500	10,000
12	18.3	11.0	0.139	60,000	44,500	31,500	24,000	21,000	12,000
				16 Cr—.06 C+N varying Ni					
2	15.7	8.7	0.058	—	—	26,000	19,000	—	—
6	16.2	9.4	0.068	—	—	26,000	20,500	—	—
5	16.0	11.1	0.050	—	—	26,000	17,000	—	—
105	16.3	14.8	0.056	—	—	26,000	17,500	18,000	8,300
				15 Cr—.06 C+N varying Ni					
16	14.5	6.7	0.063	55,000	49,800	31,700	20,500	19,000	7,400
55	15.4	12.0	0.070	—	—	—	—	17,600	8,500
105	16.3	14.8	0.056	—	—	26,000	17,500	18,000	8,300
104	14.1	18.4	0.066	—	—	—	—	17,100	7,700
				19 Cr—.05 C+N varying Ni					
4	19.6	8.5	0.056	46,000	40,000	27,000	20,500	19,000	8,900
103	19.3	15.0	0.048	—	—	—	—	18,200	7,700

Comparison of the summary plots indicates that nickel has a small direct effect on the stress-rupture properties. Small variations in the chromium or the carbon plus nitrogen content can be seen to have a greater effect than the relatively larger variations in nickel content in Figs. 14 to 19. However, since nickel has an important effect on the stability of austenite, nickel would be expected to suppress the formation of ferrite, and thereby to maintain the strength of the alloys through increased stability. Unfortunately, as can be seen in Fig. 20, an increase in nickel content from 12 percent to 18% (at about 13% chromium and 0.05% carbon plus nitrogen) was insufficient to suppress grain boundary precipitation. Both alloy 106 (13% chromium, 15% nickel, 0.04% carbon plus nitrogen) after 610 hours at 1300°F, and alloy 103 (19% chromium, 15% nickel, 0.05% carbon plus nitrogen) after 380 hours at 1300°F, had some magnetic phase after test. It is highly improbable that the ferrite formed under these conditions in these alloys is an equilibrium structure. In this regard, Rosenberg and Irish (7) found that a transition ferrite precipitate preceded the formation of equilibrium sigma in several 18 chromium-10 nickel high purity stainless steels.

Effect of Martensite—A martensitic transformation of austenite to ferrite takes place in stainless steel alloys which results in improved strength properties at room temperature. In addition, the

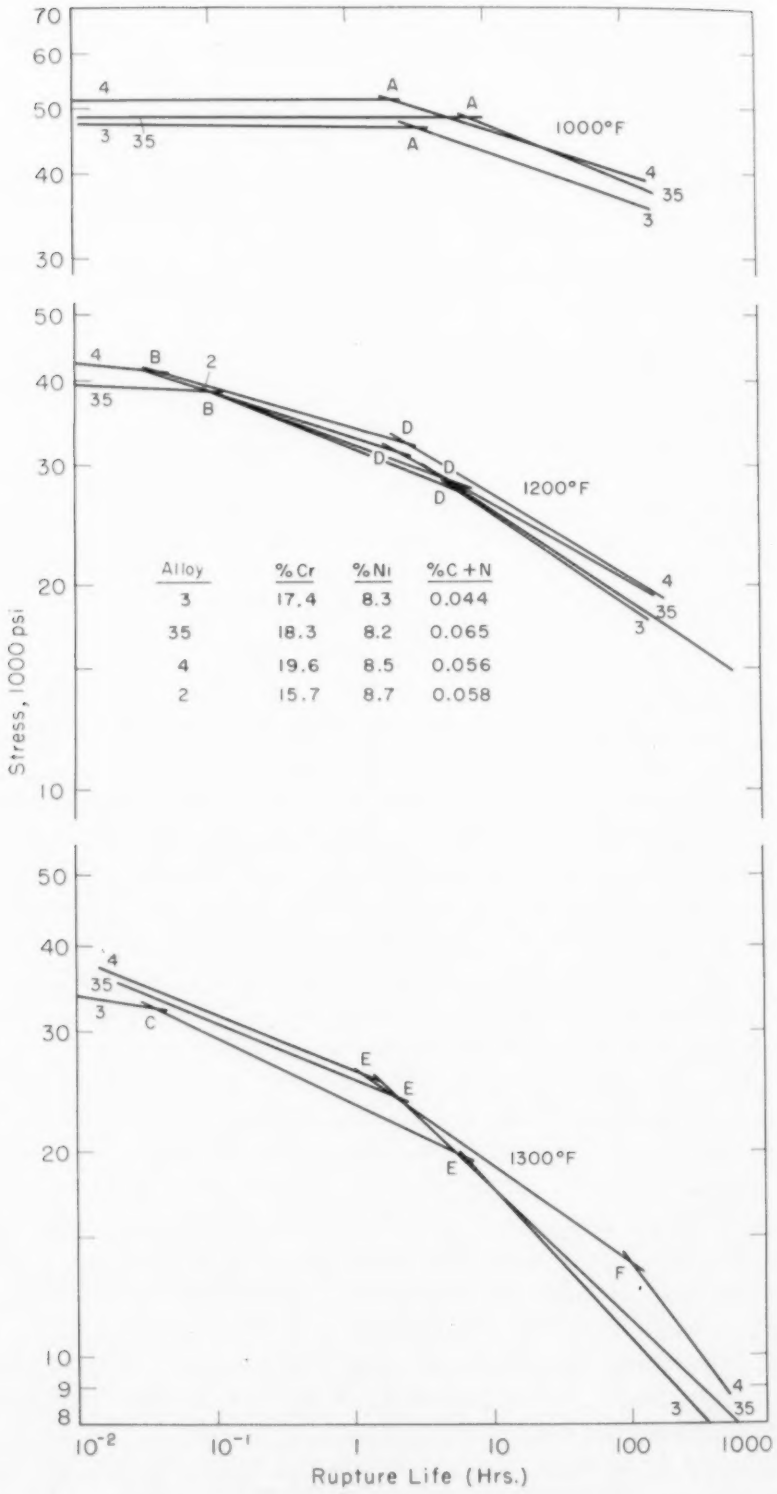


Fig. 9—Summary Plot of Log Stress Versus Log Rupture Life at 1000, 1200, and 1300°F for Alloys 3, 35, 4 and 2.

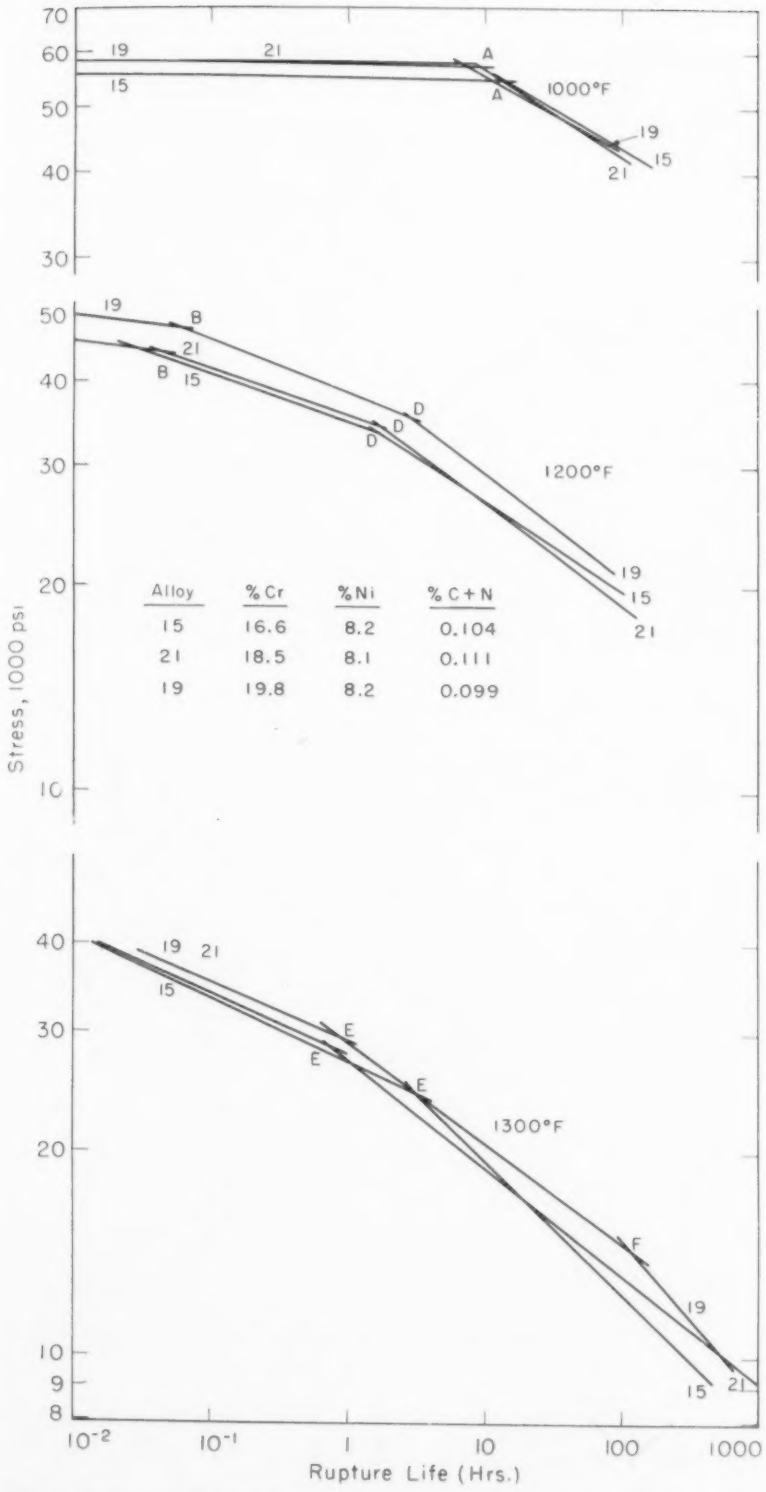


Fig. 10—Summary Plot of Log Stress Versus Log Rupture Life at 1000, 1200, and 1300°F for Alloys 15, 19, and 21.

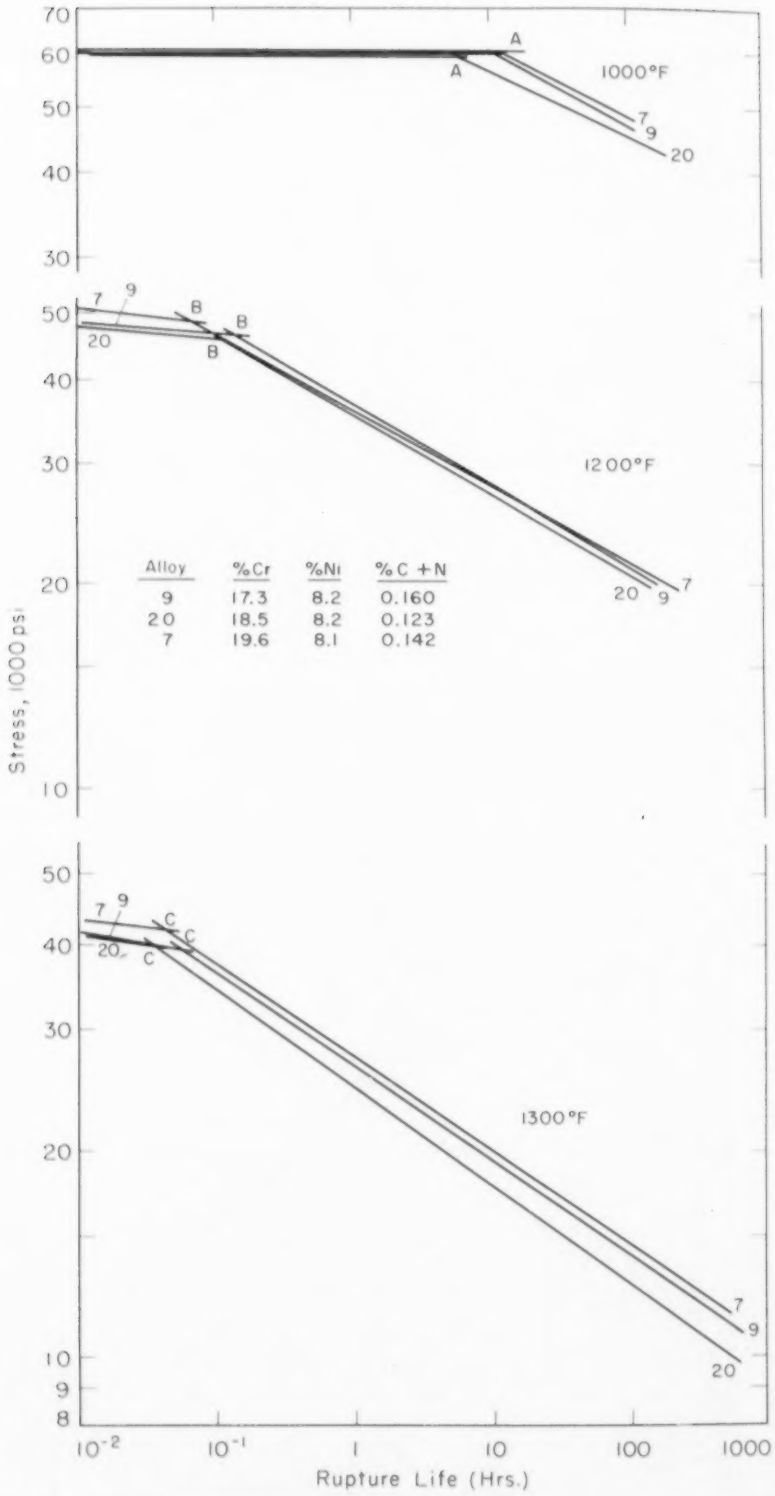


Fig. 11—Summary Plot of Log Stress Versus Log Rupture Life at 1000, 1200, and 1300°F for Alloys 7, 9, and 20.

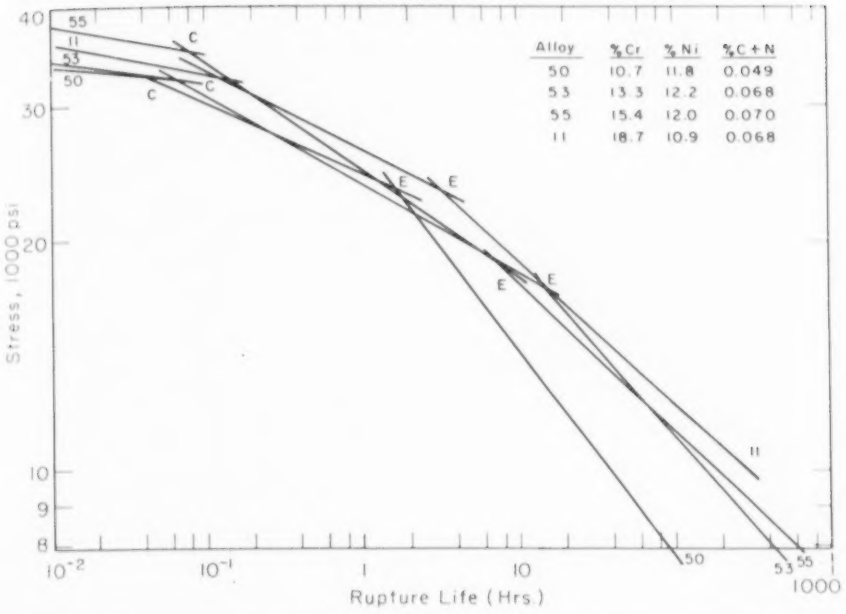


Fig. 12—Summary Plot of Log Stress Versus Log Rupture Life at 1300°F for Alloys 50, 53, 55, and 11.

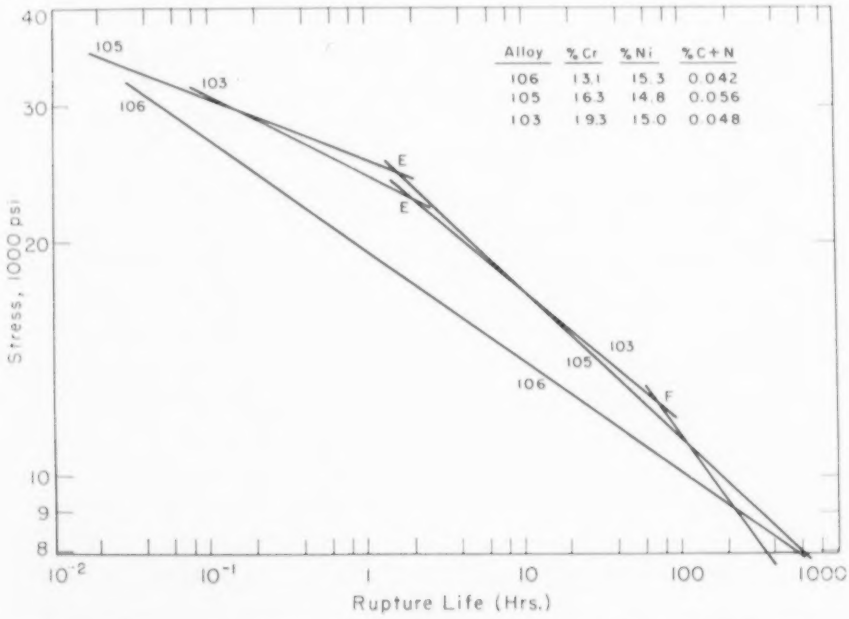


Fig. 13—Summary Plot of Log Stress Versus Log Rupture Life at 1300°F for Alloys 103, 105, and 106.

presence of an acicular ferritic phase was found in a stainless steel alloy which exhibited excellent stress-rupture properties at 1300°F (1). As listed in Table I, a number of the alloys in this investigation contained martensite at room temperature. Furthermore, martensite has been reported to exist up to temperatures approaching 1300°F (8).

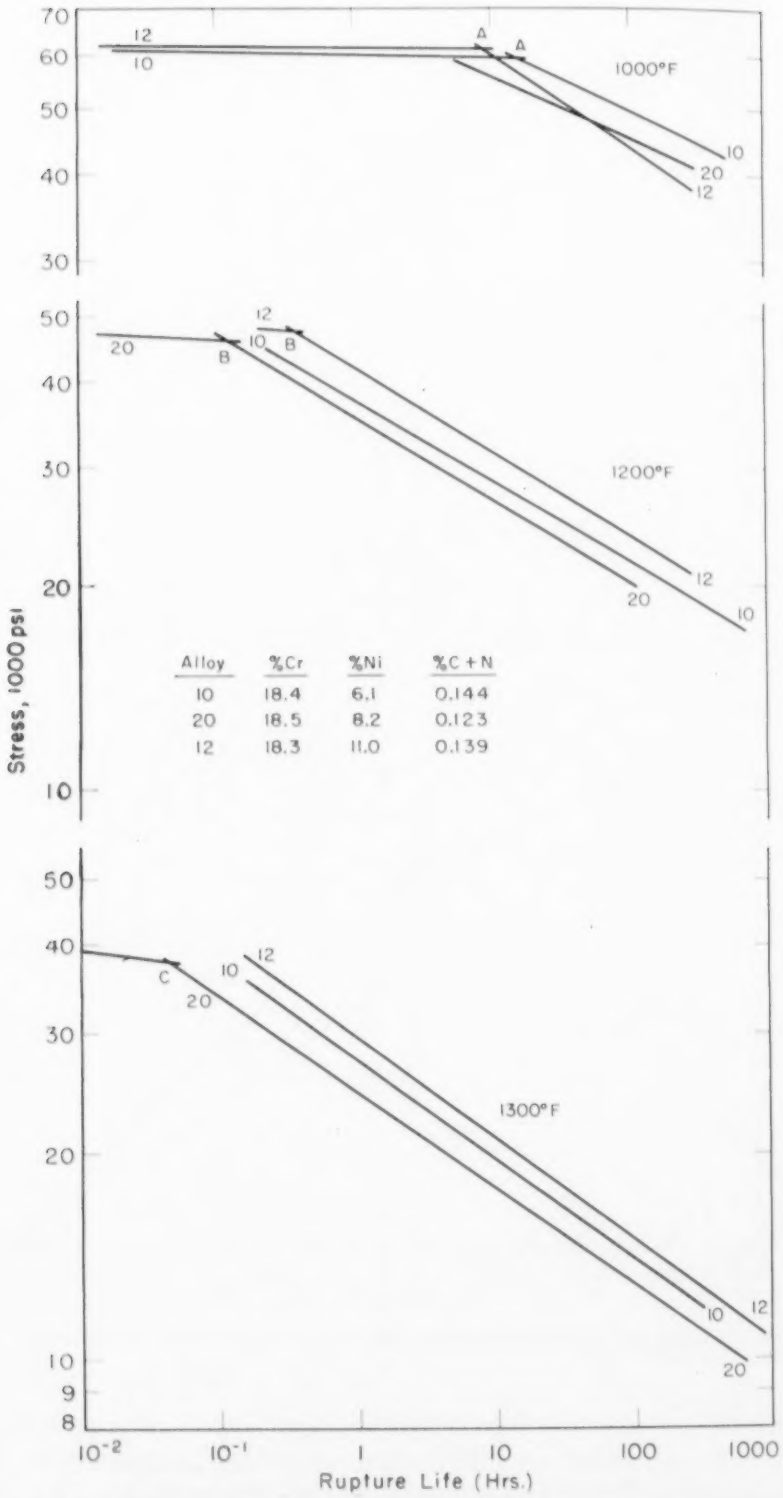


Fig. 14—Summary Plot of Log Stress Versus Log Rupture Life at 1000, 1200, and 1300°F for Alloys 10, 20, and 12.

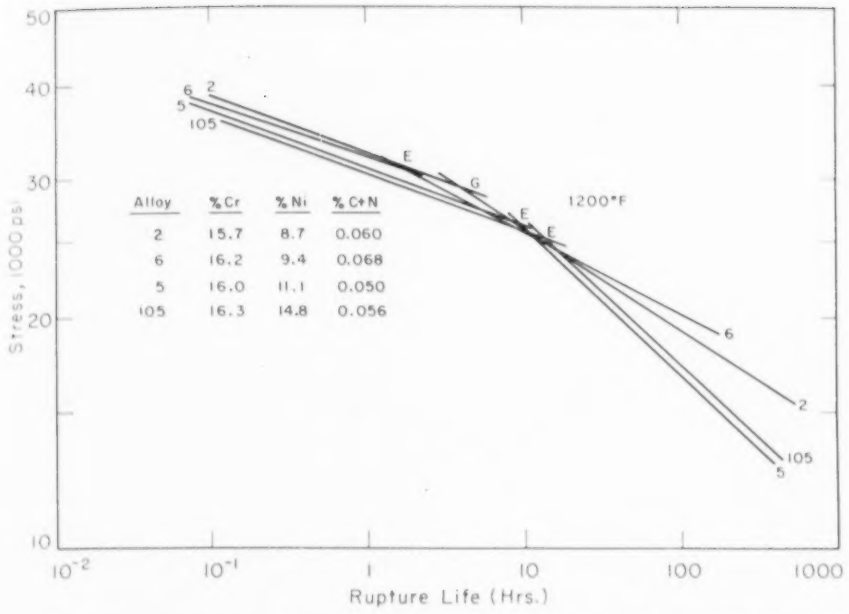


Fig. 15—Summary Plot of Log Stress Versus Log Rupture Life at 1200°F for Alloys 2, 5, 6 and 105.

For this reason, it was necessary to determine the effect of martensite and its decomposition products on the high temperature creep strength.

Inasmuch as the martensitic transformation of austenite to ferrite involves the change of a nonmagnetic phase to a magnetic one, electrical resistivity was found to be an excellent method of following this reaction. To verify the resistivity results, X-ray diffraction studies were made with a high temperature camera wherein the decomposition was followed by measuring the intensity of the lines of the martensite pattern.

Resistivity and X-ray experiments showed further that significant amounts of martensite could be formed in alloys 3, 4, 15, 35, and 53 by quenching in liquid nitrogen, and that most of this martensite was stable at 1000°F. Stress-rupture specimens of these alloys were prepared by quenching in liquid nitrogen followed by testing at 1000°F to determine the effect of martensite. Within experimental error, the rupture lives and the minimum creep rates of these specimens were equal to but not superior to those which contained no martensite.

To investigate the effect of the decomposition products of martensite, samples of alloys 3, 4, and 35 were quenched in liquid nitrogen to form martensite, and were then aged 20 hours at 1200 and 1300°F, which was found to be sufficient to decompose the martensite as evidenced by X-ray and resistivity experiments. These specimens were then tested and found to be weaker and to have lower

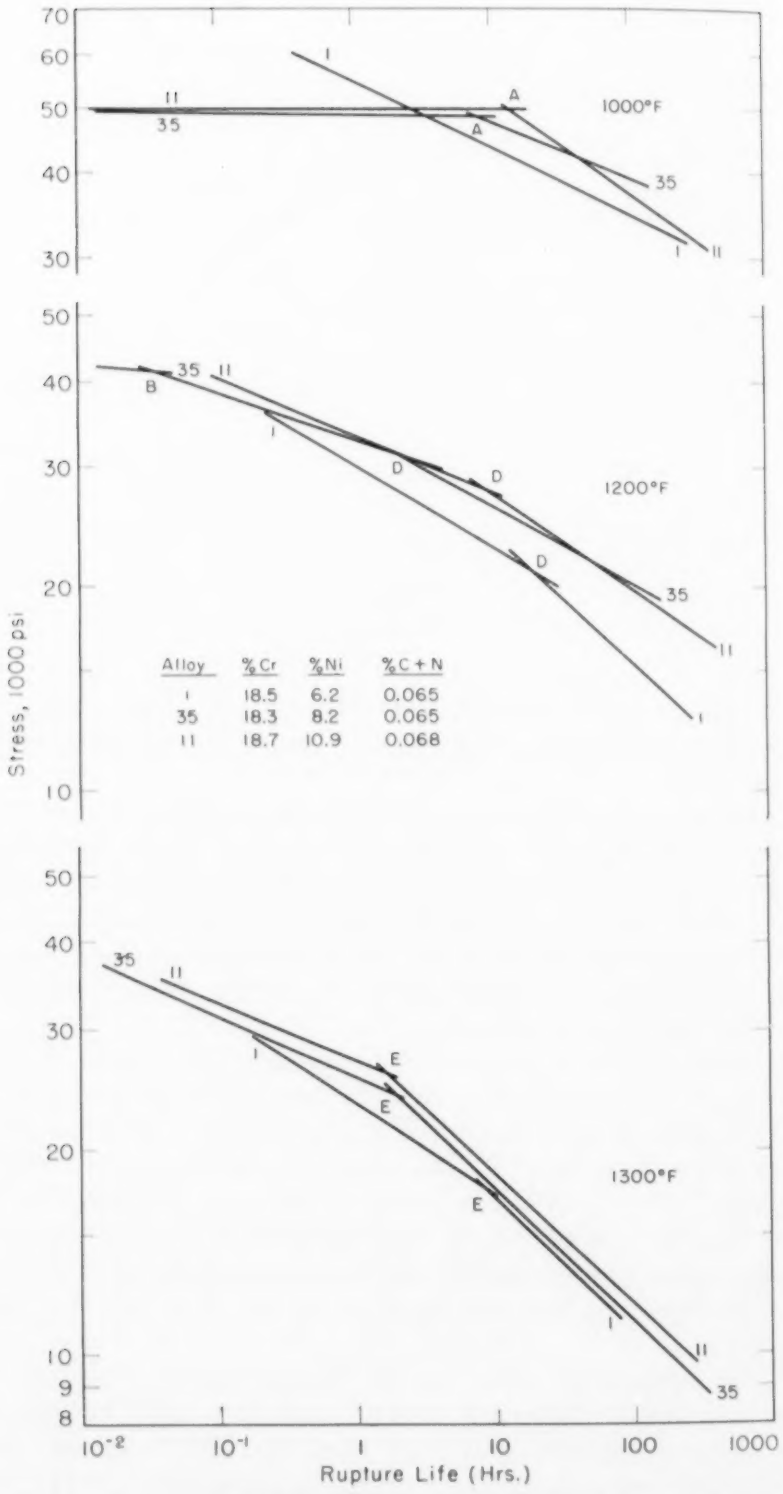


Fig. 16—Summary Plot of Log Stress Versus Log Rupture Life at 1000, 1200, and 1300°F for Alloys 1, 35, and 11.

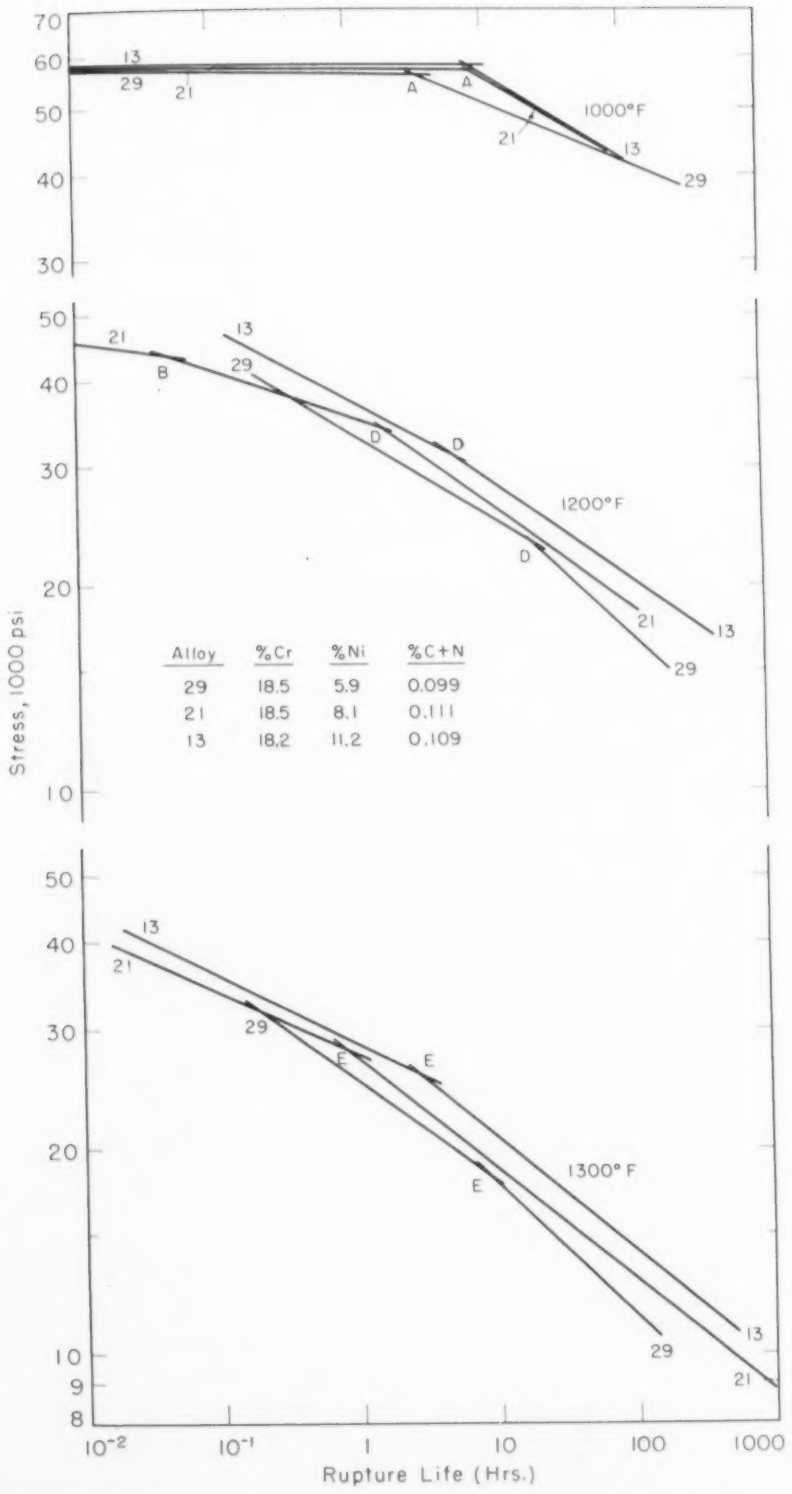


Fig. 17—Summary Plot of Log Stress Versus Log Rupture Life at 1000, 1200, and 1300°F of Alloys 13, 21, and 29.

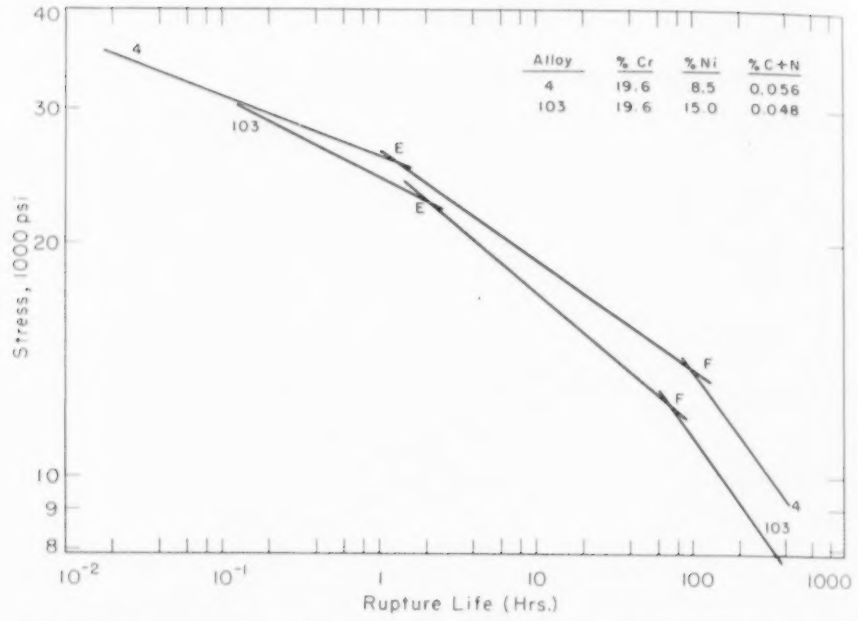


Fig. 18—Summary Plot of Log Stress Versus Log Rupture Life at 1300°F for Alloys 4 and 103.

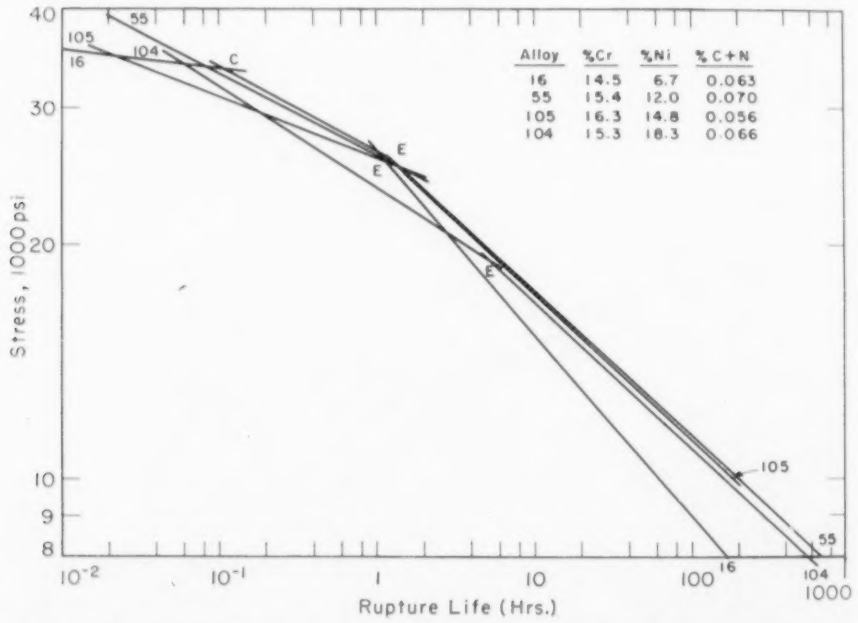


Fig. 19—Summary Plot of Log Stress Versus Log Rupture Life at 1300°F for Alloys 16, 55, 105, and 104.

ductility at these temperatures than specimens receiving only the 20 hour aging treatment. Metallographic examination of the specimens in which martensite was found and then decomposed showed that carbide and ferrite precipitation had taken place within the austenitic grains as well as at the grain boundaries. The martensite

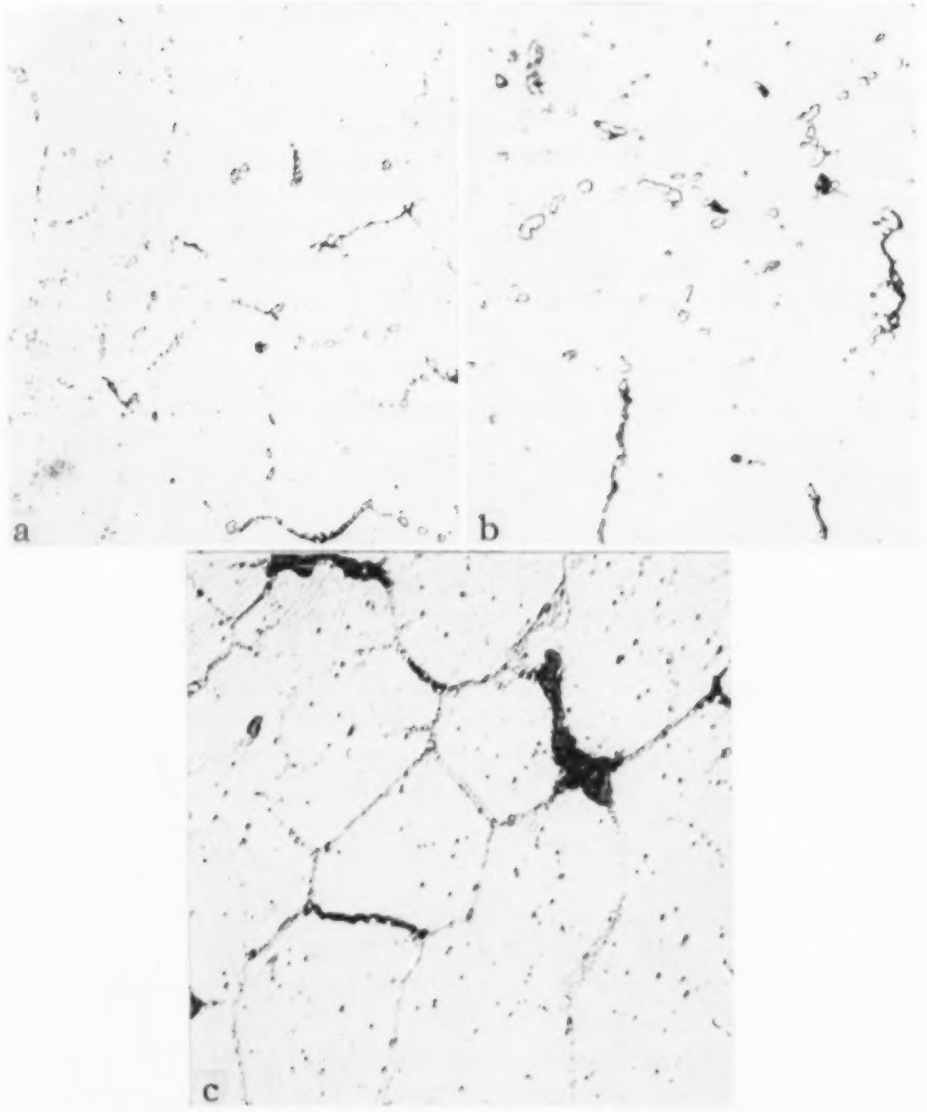


Fig. 20—Photomicrographs of Selected Stress-Rupture Specimens of Alloys 53, 106, and 104 Showing Precipitates Found During Testing. Ferric Chloride Etch.
(a) Alloy 53. 1300°F 380 hours. X 500. (13 Cr, 12 Ni, .05 C+N); (b) Alloy 106. 1300°F 610 hours. X 500. (13 Cr, 15 Ni, .04 C+N); (c) Alloy 104. 1300°F, 380 hours. X 500. (14 Cr, 18 Ni, .07 C+N).

probably transformed to carbides, nitrides, and austenite of low carbon and nitrogen content. With increasing time at temperature, the equilibrium ferrite precipitated out of the low carbon-nitrogen austenite, and thereby weakened the alloys.

Effect of Composition on Ductility—The elongation in a one inch long gage section, and the reduction in area at the fracture, were measured for each stress-rupture test. In every alloy a sharp decrease in ductility accompanied the transition from a transcrystalline to an intercrystalline type fracture. In addition, the ductility was found to

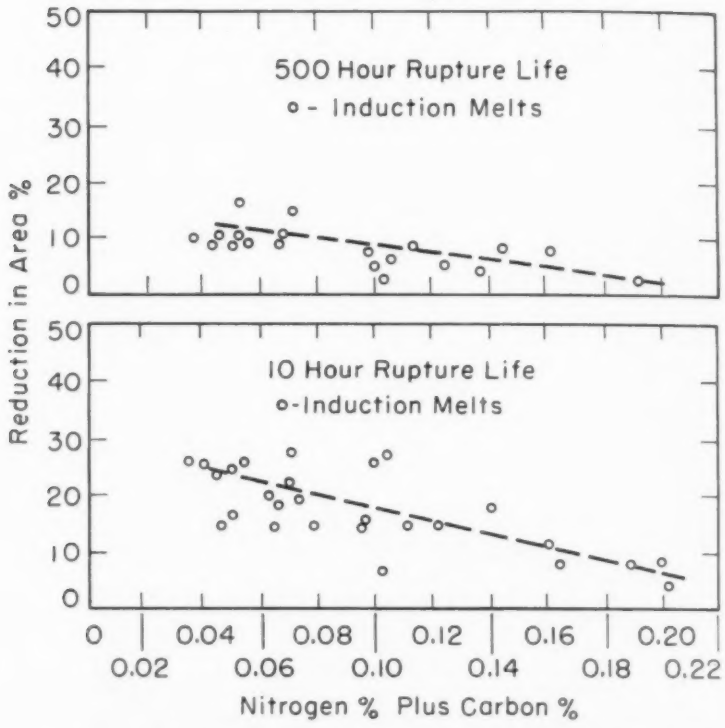


Fig. 21—Plot of Reduction in Area Versus Nitrogen Plus Carbon Content for 10 and 500 Hours Rupture Life at 1300°F.

decrease as the rupture life increased. The reduction in area values and the elongation values for specimens having a rupture life of 10, 100, and 500 hours were plotted against chromium content, nickel content, and carbon plus nitrogen content. Within experimental error, the ductility was independent of both chromium and nickel content but varied inversely with respect to the carbon plus nitrogen content; as can be seen in Fig. 21, the ductility was found to decrease linearly with carbon plus nitrogen content as a first approximation.

Discussion and Summary

It was found that increasing amounts of carbon and nitrogen in solid solution strengthen stainless steels at elevated temperatures both by alloying the austenitic matrix and by suppressing the formation of sigma and ferrite. However, carbon and nitrogen are precipitated out of solid solution as carbides and nitrides so that the strengthening effect is time and temperature dependent. This was especially evident at 1200 and 1300°F where the rate of carbide and nitride precipitation is relatively rapid. At 1000°F, on the other hand, the precipitation rate is much slower and the rupture life of the stainless steel alloys in this investigation exhibited a significant increase in strength out to 500 hours or more as a result of the increased carbon plus nitrogen content.

Carbon and nitrogen were found to be instrumental in maintaining the high temperature strength by suppressing other structural changes which occur at the testing temperatures. Because these elements stabilize the austenitic matrix, increasing the carbon and nitrogen content was found to eliminate the instability break in the stress versus rupture life curves which was caused by ferrite growth at the grain boundaries. The initial formation of ferrite, however, was seen to actually increase the high temperature strength as contrasted to the weakening effect due to subsequent growth and agglomeration of the ferrite.

The third instability break caused by the precipitation of sigma was also eliminated by increasing amounts of carbon and nitrogen. Presumably this was due to the precipitation of iron-chromium carbides which suppressed the formation of sigma by decreasing the chromium content of the matrix.

Chromium was also found to affect the high temperature strength of stainless steel alloys both as an alloying element in the austenitic matrix and by influencing the structural changes which can take place in these alloys. As an alloying element in the austenitic matrix, chromium was found to have an important strengthening effect at the testing temperatures. This strengthening effect was found to be considerably smaller than that of carbon and nitrogen; however, the benefit was not found to diminish with time at temperature to any great extent.

On the other hand, chromium was found to be detrimental to the high temperature strength when it promoted the formation of massive sigma. The initial precipitation, as with the ferrite, resulted in improved strength, but the subsequent growth of this phase at the grain boundaries was found to severely weaken the high temperature strength.

Nickel was not found to have an important strengthening effect on the high temperature rupture properties. The unavoidable small variations of chromium, nitrogen, and carbon contents in the alloys of the nickel series had as great an effect on the strength as the large variations in the nickel content. This is in agreement with the results of Borzdyka (9) who reported that nickel variations up to eighty percent in iron-chromium-nickel alloys had very little effect on their high temperature strength.

As determined experimentally, the martensitic ferrite which was formed in these alloys by cooling below the M_s temperature, was not found to have a significant effect on the rupture and creep properties of stainless steel at 1000°F. On the other hand, the decomposition of martensite which was found to occur above about 1100°F decreased the high temperature strength and ductility at 1200 and 1300°F. This is probably due to the fact that martensite decomposes to carbides, and austenite of low carbon and nitrogen content.

The formation of ferrite from this austenite as well as the decrease in the carbon and nitrogen content of the matrix, would account for the decrease in high temperature strength.

The ductility of these alloys were found to decrease with increasing rupture life. In addition, within the composition range of this investigation, the ductility was essentially independent of both chromium and nickel contents, but varied inversely to the carbon plus nitrogen content.

ACKNOWLEDGMENTS

The authors wish to express their appreciation to Mr. Alvin Boltax for his assistance with some of the magnetic tests, and to Mr. Frank Cuff for important assistance with the M_s measurements on these steels. We are especially grateful to the Bureau of Ships, under whose sponsorship this program was initiated, and to the Office of Naval Research for the current sponsorship.

References

1. J. Hum and N. J. Grant, "Austenite Stability and Creep-Rupture Properties of 18-8 Stainless Steels," TRANSACTIONS, American Society for Metals, Vol. 45, 1953, p. 105.
2. A. G. Bucklin and N. J. Grant, "On the Extrapolation of Short-Time Stress Rupture Data," TRANSACTIONS, American Society for Metals, Vol. 42, 1950, p. 720.
3. J. Gilman, "Etching Steels Which Contain the Sigma Phase," METAL PROGRESS, American Society for Metals, Vol. 59, 1951.
4. A. Cook and R. Brown, "Digest of the Constitution of the Iron-Nickel-Chromium Alloys 550 to 800°C," *Journal*, Iron and Steel Institute, Vol. 171, 1952, p. 345.
5. N. Lismer and K. Andrews, "Occurrence of Sigma Phase in a High Chromium-Nickel Steel and the Effect of Carbon Content," *Journal*, Iron and Steel Institute, Vol. 171, 1952, p. 49.
6. A. Bindari, P. Koh and O. Zmeskal, "Sigma Phase Formation in Wrought Heat Resistant Steels," TRANSACTIONS, American Society for Metals, Vol. 43, 1951, p. 226.
7. S. Rosenberg and C. Irish, "Sigma Phase in High Purity 18-10," METAL PROGRESS, American Society for Metals, Vol. 61, 1952, p. 92.
8. H. Fiedler, "The Martensite Transformation in Austenitic Stainless Steel," Sc. D. Thesis, Massachusetts Institute of Technology, 1953.
9. A. Borzdyka, "Relationship of Creep of Austenitic Alloys to Their Phase Diagram," Doklady Akademi Nauk USSR, Vol. 75, 1950, p. 37, Russian Brutcher Trans. 2597.

DISCUSSION

Written Discussion: By W. L. Badger, manager, Small Aircraft Engine Lab., General Electric Co., West Lynn, Mass.

This work, apparently part of an overall program on stainless steels, gives information which has not been available in such detail. With the earlier work of Hum and Grant, this paper covers very well the changes in the 18-8 steels which can be produced through alloying.

However, this work does not cover one area which would have seemed of most interest—that of composition variations in vacuum melted alloys. The

vacuum melted high strength heats reported by Hum and Grant should prove a better base for chromium and nickel variations than the 0.14% carbon and nitrogen series, which would be undesirable from a welding standpoint. In this connection, it would be interesting to also evaluate the effects of manganese and silicon on low carbon and nitrogen heats, both vacuum and air melts.

Authors' Reply

In reply to Mr. Badger's comments, we have in fact done some work with the vacuum melted stainless steels of ultra low carbon content. The variable which was studied was the carbon-plus-nitrogen content. The results substantiated the high strength and ductility values reported by Messrs. Hum and Grant and clearly show the importance of both vacuum melting and the low carbon-plus nitrogen content. Primarily it appears that the elimination of carbon and nitrogen produces an austenitic alloy which is very stable at high temperatures since it is not subject to carbide and nitride precipitation (overaging) or sigma formation (low chromium content). These interesting results have been submitted for publication. Further, we plan to study variations of vacuum melted composition reported by Messrs. Hum and Grant.

CREEP-RUPTURE PROPERTIES OF COLD-WORKED TYPE 347 STAINLESS STEEL

By N. J. Grant, Albert G. Bucklin, and Warren Rowland

Abstract

Type 347, columbium stabilized stainless steel, was cold-worked up to 60%. Recrystallization temperatures were determined for 0.5, 5, and 50-hour intervals. In addition to tensile testing at room temperature, creep rupture tests were performed at 1200, 1300, and 1500°F to study the effects of cold work on the high temperature properties; and to relate the time-temperature values for the incidence of intercrystalline fracture to the static recrystallization temperature. (ASM-SLA Classification: Q3, Q4, N5, SS)

BENEFITS due to cold working or warm working are a recognized method of improving both the low temperature and the high temperature properties of metals and alloys (1,2,3)[1]. In fact, the use of warm-worked 16-25-6 Timken alloy for jet engine disks is a standard operation (4). The use of 17 chromium—13 nickel—3 tungsten-titanium stabilized alloy in the warm-worked condition as an inexpensive rotor bucket in gas turbines for relatively long life at temperatures below 1200°F is a fine example of the profitable application of an alloy otherwise too weak for the application (3). The alternate choice of a substitute would require a higher alloyed product at considerably higher cost.

Unknown at the present are the relative advantages of various stainless compositions for cold or warm work strengthening. The recrystallation temperature is undoubtedly one of the best, if not the best, measures of useful work hardening for high temperature applications. This in turn suggests that the presence or appearance of ferrite in an otherwise austenitic structure may be undesirable.

The results presented below illustrate the benefits to be derived from cold-worked type 347 stainless steel for use in the relatively high temperature range 1200 to 1500°F, it being accepted that at lower temperatures the benefits for long time applications are quite safe for prior warm work up to 50% reduction of area.

[1]The figures appearing in parentheses pertain to the references appended to this paper.

A paper presented before the Thirty-Seventh Annual Convention of the Society, held in Philadelphia, October 17–21, 1955. Of the authors, N. J. Grant is associate professor, Albert G. Bucklin is DIC Staff member, and Warren Rowland was formerly research assistant, Department of Metallurgy, Massachusetts Institute of Technology, Cambridge, Mass. Manuscript received March 3, 1955.

Procedure

Type 347 stainless steel was obtained as ⅝ inch bar stock. Its composition was: 0.057 C; 0.040 N_2; 18.28 Cr; 9.42 Ni; 1.36 Mn; 0.65 Si; 0.58 Cb; balance Fe.

The bars were hot-forged to ½ inch round at a maximum of 2200°F and were then solution treated for 1 hour at 2000°F and water-quenched.

Sections were cold swaged to give reductions of area of 10.0, 20.8, 30.4, 37.6, 58.0, and 81.2% (they will be referred to as 10, 20, 30, 40, 60, and 80% in the text) for the purpose of determining the recrystallization parameters.

In addition room temperature tensile tests and creep-rupture tests at 1200, 1300, and 1500°F were performed on the solution treated, 10, 20, and 30% cold-worked grades. The specimens were of 0.250-inch diameter, 1-inch gage length size.

Results

Recrystallization Data—After cold work, specimens were held for periods of time from 0.5 to 50 hours (some for 500 hours) at temperatures from 1200 to 1700°F. Hardness values were taken and plotted as a function of temperature for various annealing times. The inflection of the curve was taken as an arbitrary measure of recrystallization for purposes of comparison.

Fig. 1 shows a summary plot of percent cold work versus temperature for three time periods of 0.5, 5, and 50 hours, giving the minimum recrystallization temperature as a function of cold work and annealing time. For a severely cold-worked condition, recrystallization in 50 hours will not occur below about 1325°F, in fact, even 500 hours should not produce recrystallization at 1300°F.

Room Temperature Mechanical Properties—Fig. 2 shows room temperature yield strength (0.2% offset), tensile strength, percent elongation in 2 inches, and reduction of area for various degrees of prior cold work up to 30%. Fig. 2 also shows the increase in hardness (Rockwell A) and ferrite content as a function of cold work up to 80% reduction of area. It is noted that both yield strength and tensile strength are still increasing rapidly after 30% cold work; but whereas the elongation has decreased as sharply as strength has increased, the reduction of area (in tensile tests) has changed remarkably little.

Beyond about 40% cold work, the hardness increases very little, reaching a maximum slightly above Rockwell A-65. Ferrite was not detected magnetically (by means of a Magnegage) until over 30% reduction of area by cold work was achieved. At 80% cold work the quantity of ferrite indicated is between 20 and 25%. The

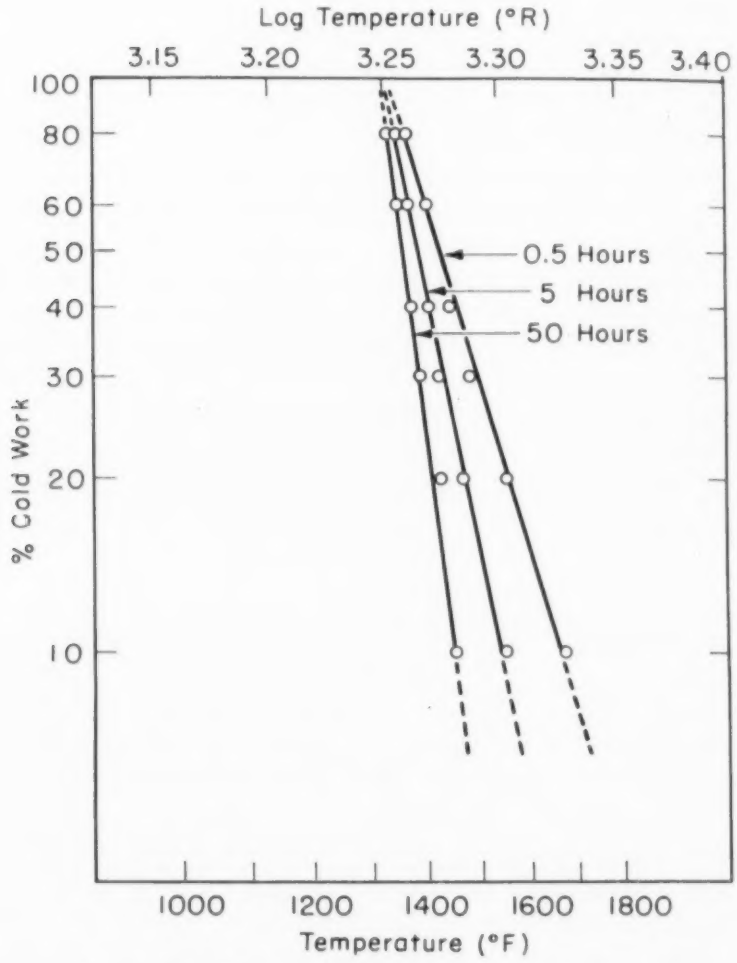


Fig. 1—Plot of Cold Work Versus Temperature for Recrystallization of Type 347 for Time Periods of 0.5, 5, and 50 Hours.

measurements indicate greater ferrite content in the center of the specimen than at the surface, by about 5%.

Creep-Rupture Data—Figs. 3,4, and 5 are log stress versus log rupture life plots at 1200, 1300 and 1500°F, respectively, in each instance for the annealed (solution treated) 10, 20, and 30% prior cold-worked conditions. Test times are from about 0.01 hour (about 36 seconds) to 500 hours. Fig. 3 shows that there is an increase in hot strength for all degrees of prior cold work up to 30% for rupture times up to at least 1000 hours. At 1300°F, however, (Fig. 4) after about 20 to 50 hours rupture life, the 20 and 30% cold-worked structures are weaker than the 10% cold-worked alloy, and are weaker than the solution treated condition for rupture times of about 200 hours. The 10% cold-worked alloy continues to show improved strength out beyond about 1000 hours. At 1500°F (Fig. 5) all benefits due to cold work are lost beyond a rupture life of about

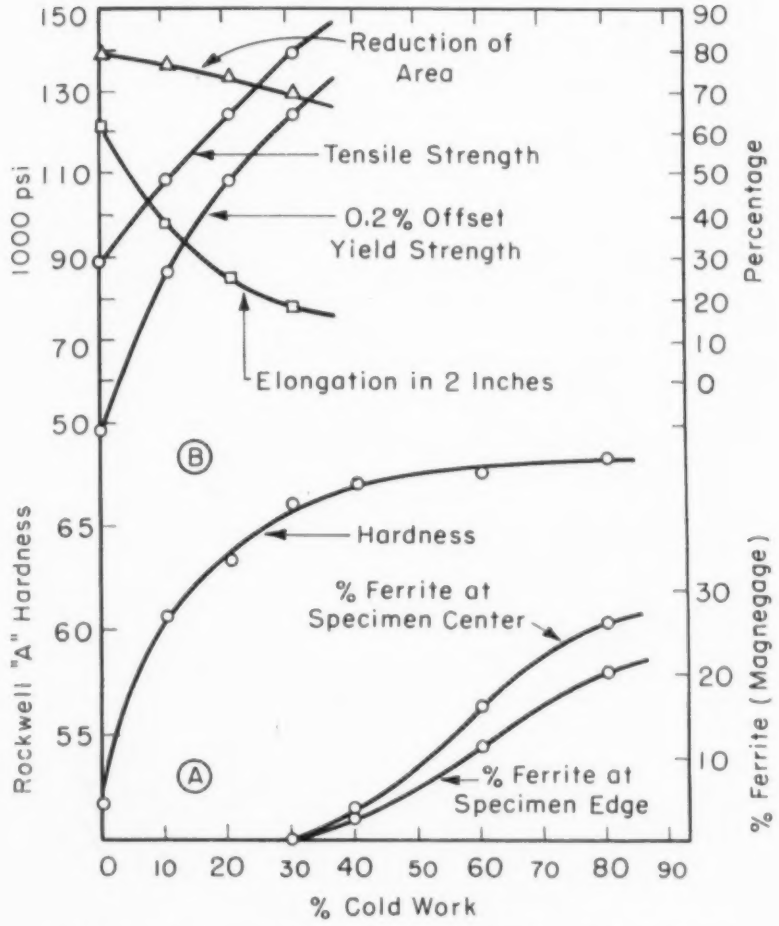


Fig. 2—Influence of Cold Work on the Room Temperature Properties and Ferrite Content of Type 347.

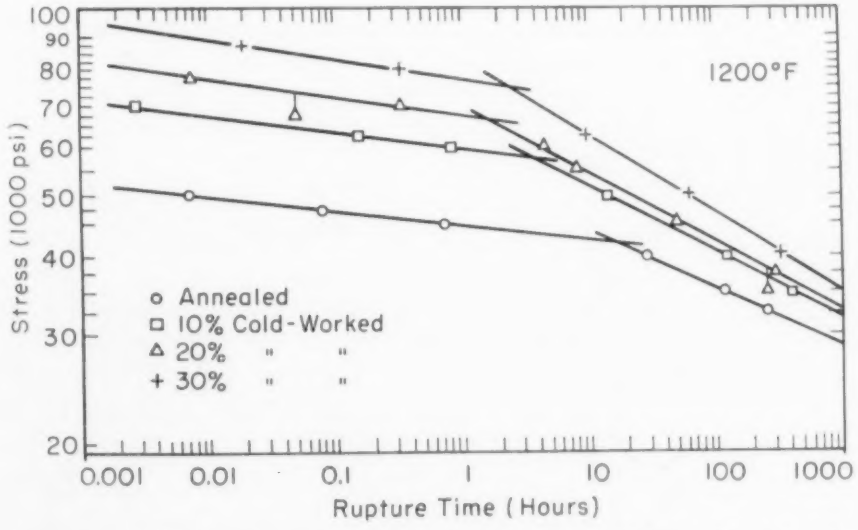


Fig. 3—Log Stress Versus Log Rupture Life Plot for Solution Treated and Cold-Worked Type 347 at 1200°F.

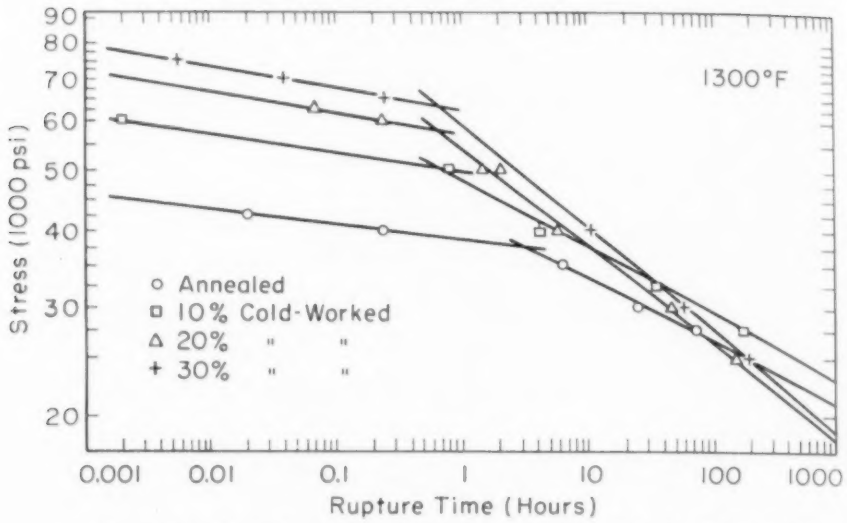


Fig. 4—Log Stress Versus Log Rupture Life Plot for Solution Treated and Cold-Worked Type 347 at 1300°F.

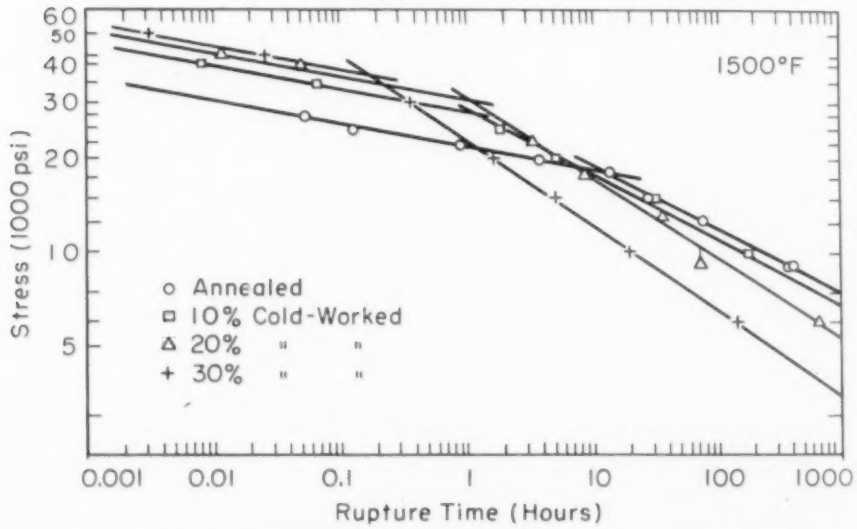


Fig. 5—Log Stress Versus Log Rupture Life Plot for Solution Treated and Cold-Worked Type 347 at 1500°F.

10 hours and the solution treated condition is appreciably stronger for a 1000-hour life. The 10, 20, and 30% cold-worked conditions are weaker in the order shown.

Table I summarizes the values of stress to rupture in 10, 100, and 1000 hours at 1200, 1300, and 1500°F for the four conditions.

Very similar trends were obtained for secondary creep rates as a function of cold work and temperature. Table II lists the stress for secondary creep rates of 1, 0.01, and 0.001% per hour.

Discussion

It was shown in studies of cold-worked Monel that evidence of

Table I
Effect of Cold Work on the Stress for Rupture (psi)

	10 Hours	100 Hours	1000 Hours
1200°F			
Annealed	42,200	35,500	28,700
10% cold-worked	52,000	40,700	32,000
20% cold-worked	54,300	42,000	32,500
30% cold-worked	62,700	46,700	34,900
1300°F			
Annealed	33,300	26,400	21,000
10% cold-worked	37,500	29,300	23,000
20% cold-worked	37,800	26,300	18,200
30% cold-worked	40,300	27,600	18,800
1500°F			
Annealed	18,300	11,800	7,500
10% cold-worked	17,800	11,000	6,800
20% cold-worked	17,200	9,600	5,300
30% cold-worked	12,200	6,500	3,500

Table II
Stress for Specified Secondary Creep Rates

	1% per Hour	0.01% per Hour	0.001% per Hour
1200°F			
Solution treated	42,000	35,500	31,500
10% cold-worked	58,000	41,000	33,000
20% cold-worked	67,000	42,500	33,000
30% cold-worked	72,000	47,000	36,000
1300°F			
Solution treated	35,000	28,000	25,000
10% cold-worked	41,000	29,000	25,500
20% cold-worked	50,000	28,500	22,000
30% cold-worked	52,000	30,000	22,500
1500°F			
Solution treated	20,000	8,500	6,000
10% cold-worked	22,000	8,000	5,200
20% cold-worked	25,000	6,500	3,000
30% cold-worked	16,000	3,500	900

Table III
Total Elongation for Specified Rupture Lives

	0.1 Hours	10 Hours	100 Hours	1000 Hours
1200°F				
Solution treated	45(T)*	25(T)	5.0	3.0
10% cold-worked	22(T)	3.0	2.5	1.5
20% cold-worked	6(T)	2.5	2.5	1.5
30% cold-worked	7(T)	1.8	2.5	1.5
1300°F				
Solution treated	40(T)	10	10	10
10% cold-worked	15(T)	2.5	2.3	2
20% cold-worked	7(T)	2.5	1.5	1.5
30% cold-worked	17(T)	16	1.8	1.5
1500°F				
Solution treated	30(T)	25	23	15
10% cold-worked	10(T)	10	12	12
20% cold-worked	10(T)	12	21	18
30% cold-worked	12(T)	35	40	40

*Designates transcrystalline fracture. Others are intercrystalline.

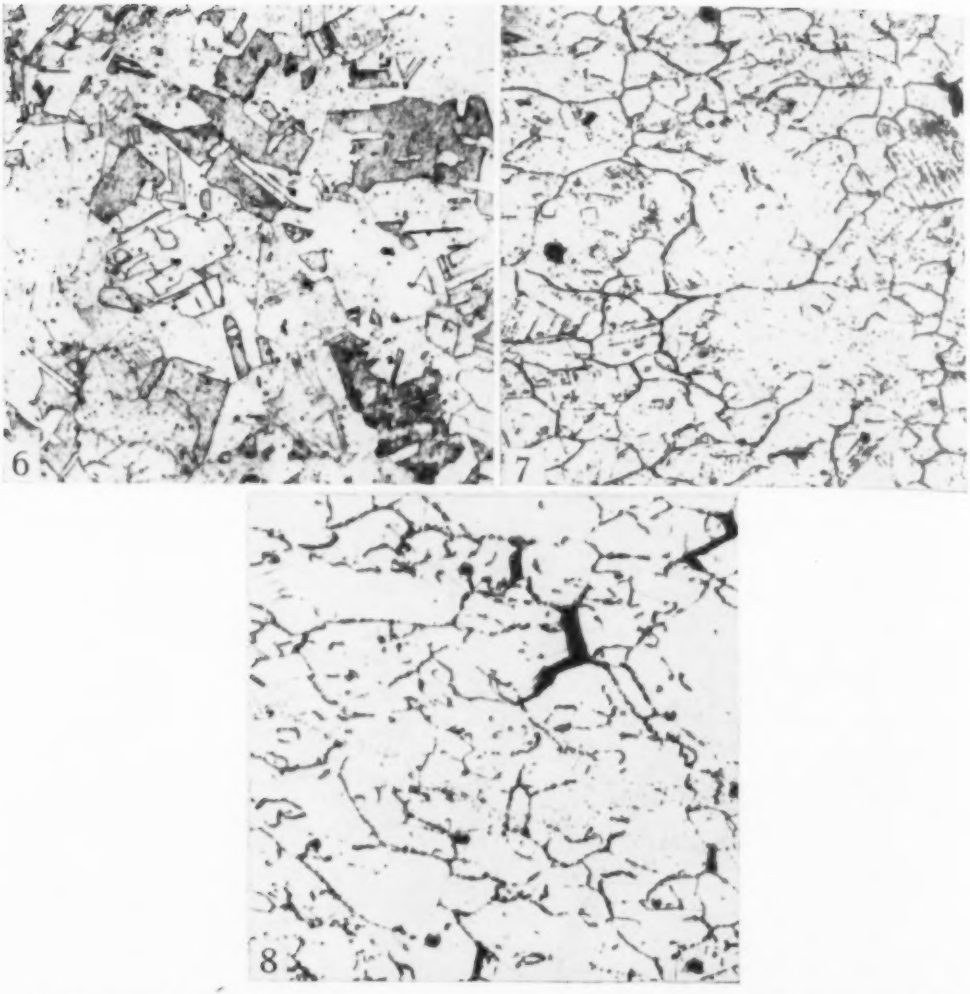


Fig. 6—Original Grain Structure of Annealed Type 347. 10% oxalic acid, electrolytic etch. ×100.

Fig. 7—Structure at Point Removed from Fracture in Test at 1200°F, 55,000 psi. Note considerable grain growth after only 8 hours. 10% oxalic acid, electrolytic etch. ×100.

Fig. 8—Point Removed from Fracture in Annealed Specimen Tested at 1300°F, 30,000 psi (to the right of equi-cohesion zone). Note intercrystalline cracking. Appreciable grain growth also apparent. 10% oxalic acid, electrolytic etch. ×100.

recrystallization is present in creep-rupture specimens at temperatures up to 200°F lower than the lowest recrystallization temperature based on static tests (2). The same behavior is evidenced in the present data. Fig. 6 shows the solution treated structure of the steel prior to cold work. Fig. 7 shows the structure of the 20% cold-worked alloy after being tested at 1200°F at a stress of 55,000 psi. Fracture occurred in about eight hours and the alloy underwent a total elongation of 2.5% and a reduction of area of 7.9%.

Fig. 8 shows that the solution treated alloy also recrystallized during the course of creep-rupture testing at 1300°F and at 30,000

psi. Rupture life was 24.6 hours, elongation about 15%. Note the intercrystalline cracks at a point away from the fracture.

Fig. 1 indicates a minimum recrystallization temperature of about 1400°F for an equivalent amount of cold deformation and an equivalent annealing time as the specimen in Fig. 8. These results confirm the observations made in studying Monel (2), namely, that

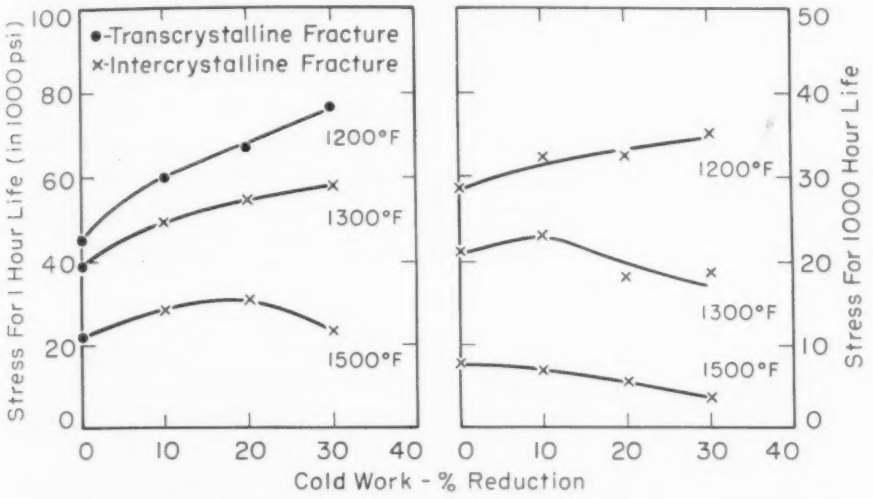


Fig. 9—Effect of Cold Work on the Stress for Rupture in 1 Hour and 1000 Hours at 1200, 1300, and 1500°F.

the first evidence of recrystallization in specimens tested in creep-rupture occurs at or beyond the equi-cohesive break in a log stress—log rupture life plot (see Fig. 3), and that this evidence of recrystallization occurs up to several hundred degrees lower than the lowest measured static recrystallization temperature.

These observations also indicate severe grain boundary deformation of an order of magnitude sufficient to promote recrystallization processes at temperatures much lower than would ordinarily be expected. It is important to emphasize that the mode of failure for stresses below the break (to the right of the break) shown in the curves of Figs. 3,4, and 5 was in all instances intercrystalline.

Unfortunately, whether there was a gain in rupture strength or not, cold work reduced the ductility (both elongation and reduction of area) at fracture at 1200 and 1300°F. The elongation values are tabulated in Table III for selected rupture life values of 0.1 to 1000 hours. As long as the fracture was of the transcrystalline variety, ductility remained usefully high as is shown by the 0.1-hour rupture life values. Where the fracture was intercrystalline, at 1200 and 1300°F, the elongation values were quite low for the cold-worked conditions. The solution treated condition was also embrittled at 1200°F, although not so rapidly, but at 1300°F showed a high level of ductility out to 1000 hours.

At 1500°F, where recrystallization occurred rapidly, frequently being well under way by the time loading was completed (average time to adjust temperature and load was about 20 to 25 minutes), the total ductility values were again high.

Fig. 9 shows that for short time use (under 1 hour) there is a steady increase in stress for rupture up to 30% cold reduction with no evidence of a maximum. This same trend continues at 1300°F but with a decreasing rate, suggesting a maximum soon after 30% cold work. At 1500°F all benefits are lost beyond about 20% cold reduction.

For a 1000-hour life, 30% cold work still shows an improvement at 1200°F. At 1300°F, only 10% reduction produces a small improvement, whereas at 1500°F the solution treated condition is significantly stronger than any of the cold-worked structures.

Conclusions

1. Static recrystallization studies as well as creep-rupture tests of solution treated and cold-worked type 347 stainless steel confirm that recrystallization occurs up to 200°F lower during creep-rupture than in static tests.

2. Useful high temperature strengthening in creep-rupture can be achieved through cold work (or warm work) as follows:

(a) At 1200°F, up to 30% cold reduction yields improvement up to at least 1000 hours.

(b) At 1300°F, up to 10% cold reduction for a 1000 hour life and over 30% for a one hour life or less.

(c) At 1500°F, up to 20% cold reduction for a one hour life but avoid cold work for rupture lives of greater than about one hour (the solution treated condition is best).

(d) At 1100°F and lower, it appears that very significant improvements can be achieved for long time use with cold work up to 30% or more.

Acknowledgments

The authors wish to thank the Bureau of Ships, Department of the Navy, for their sponsorship of this program.

References

1. D. N. Frey, J. W. Freeman and A. E. White, "Fundamental Effects of Cold Working on Creep Properties of Low-Carbon N-155 Alloy," NACA TN 2472, 1951.
2. N. J. Grant and A. G. Bucklin, "Creep-Rupture and Recrystallization of Monel from 700 to 1700°F", Transactions, American Society for Metals, Vol. 45, 1953, p. 151.
3. H. R. Zschokke, "Raising the Creep Limit by Cold Working," *Brown-Boveri Review*, Vol. 33, 1946, p. 227.
4. M. Fleischmann, "16-25-6 Alloy for Gas Turbines," *Iron Age*, Vol. 157, January 1946, p. 50.

DISCUSSION

Written Discussion: By W. L. Badger, manager, Small Aircraft Engine Lab., General Electric Co., West Lynn, Mass.

This paper, together with the other papers from the same group, adds to available information on use of stainless steels at elevated temperatures, information which should eventually promote economies of strategic materials through controlled working and alloy modification.

Can any of the observed results be ascribed to changes in orientation and grain shape during cold working? Admittedly, it would be difficult to hold the effective grain size constant during working, but could not X-ray measurements be used to determine strain levels in the cold-worked material?

Another point of interest is the effect of cold work and subsequent aging on room temperature properties, such as impact strength and corrosion resistance. This should be especially interesting in view of the very low ductility values recorded here at 1200°F.

Authors' Reply

It would not be expected that large changes in creep rupture properties would result from the small increases in preferred orientation of a face-centered cubic alloy associated with these amounts of cold work of the 347 stainless steel. On the other hand, the change in grain shape would probably have a larger effect, the magnitude of which is not known. Presumably one could stress relieve the cold-worked structure without recrystallizing to measure the effect of the change in grain shape, but the introduction of a sub-structure would introduce an unknown effect.

X-ray measurements certainly could be utilized to measure line broadening as a measure of cold work but would hardly be an accurate measure of the strain level. We wish that this were a practical tool. We are sorry that the program did not permit a study of the impact properties and corrosion resistance, or of the notch stress rupture properties too, in view of the drop in ductility.

EFFECTS OF CHEMICAL COMPOSITION AND HEAT TREATMENT UPON THE MICROSTRUCTURE AND CORROSION RESISTANCE OF AISI TYPES 309 AND 310

By D. J. Carney and E. R. Rosenow

Abstract

AISI Types 309 and 310 with varying carbon and nitrogen contents were subjected to different solution annealing treatments and cooling rates. Corrosion tests were conducted in boiling 65% nitric acid and copper sulphate-sulphuric acid. The effects of carbon and nitrogen on intergranular corrosion resistance were noted. Variations in the processing affected microstructures to such an extent that in some cases heats containing higher carbon contents yielded improved intergranular corrosion resistance. (ASM-SLA Classification: R2, M27, J general, SS)

THE American Iron and Steel Institute in its standard chemical compositions lists, at present, 0.20 and 0.25 maximum weight percent carbon for Types 309 (25% Cr-12% Ni) and 310 (25% Cr-20% Ni) respectively. For welded applications that involve corrosion service, 0.08% maximum carbon is generally recommended for the above grades (309S and 310S). This recommendation follows the reasoning applied to the use of lower carbon contents in the 18–8 compositions such as Type 304L. The desire for low carbon contents is associated with the need for the prevention of intergranular chromium carbide precipitation during air cooling following welding. The formation of a network of intergranular carbides in austenitic stainless steel results in reduced corrosion resistance in many types of industrial solutions and atmospheres.

While many investigations (1,2,3)[1] have been made concerning the effect of carbon content and heat treatment on the corrosion resistance of 18% Cr-8% Ni types of stainless steels, little data of this nature have been published for the stainless steels of high alloy content such as Types 309 and 310. Consequently, a laboratory investigation was initiated in which heats of Type 309 of different carbon and nitrogen contents and heats of Type 310 of different carbon

[1]The figures appearing in parentheses pertain to the references appended to this paper.

A paper presented before the Thirty-Seventh Annual Convention of the Society, held in Philadelphia, October 17–21, 1955. Of the authors, D. J. Carney is chief development metallurgist, and E. R. Rosenow is physical metallurgist, United States Steel Corp., South Works, Chicago. Manuscript received January 11, 1955.

contents were subjected to variations in solution annealing temperatures and cooling rates from the solution temperature. The effect of the variations in composition and heat treatment on microstructure and intergranular corrosion resistance were determined. Variations in the processing of these stainless steels affected microstructures to such an extent that in some cases heats containing higher carbon contents yielded improved intergranular corrosion resistance.

Experimental Procedure

Melting and Processing—Seven AISI Type 309 heats and two Type 310 heats were produced in a 26 lb. laboratory induction furnace for this investigation. Ingots, 3 inches in diameter and 16 inches long, were hammer forged to ½×1 inch flat bars. These bars were machined to remove surface defects and subsequently cold reduced 50% on a laboratory rolling mill before heat treatment.

Heat Treatment—For austenitic stainless steels, a common solution annealing treatment consists of holding at 1950°F for 0.5 hour followed by water quenching. For grades such as 309 and 310 depending upon the carbon content and other factors, some chromium carbides can remain undissolved following this solution treatment. It will be shown later that the degree of carbide solution following the annealing treatment has a marked influence upon carbide precipitation either during welding, cooling from annealing or during sensitization. To investigate this effect for both Types 309 and 310, two solution annealing temperatures were used—one, a higher temperature to insure complete solution of the carbides or carbonitrides and the other, a lower temperature to dissolve only approximately 50% of the carbides present in the as-forged or as-rolled structure. The two carbon levels used (0.06% and 0.16%) in this study required different solution temperatures to produce a comparable degree of carbide solution. Solution temperatures required to accomplish the above purpose were determined by heat treating pilot specimens. Specimens from each heat were given the two required solution treatments followed by, (a) water quenching, (b) cooling at 1300°F per hour and (c) cooling at 300°F per hour after being held 30 minutes at the solution temperature. The above cooling cycles were used to roughly approximate a range of cooling conditions which can exist in a welded structure. The specific heat treating cycle used for each heat is presented in Table I.

Corrosion Testing—Samples from each heat having each of the listed heat treating cycles were tested to determine their susceptibility to intergranular corrosion by means of the boiling 65% nitric acid test and the boiling copper sulphate-sulphuric acid test. The procedures used in conducting each of these tests is listed below:

Table I
Heat Treatment Conditions for AISI Type 310 and Type 309 Stainless Steels Investigated

Heat Number	Solution Treatment	Cooling Rates From Solution Temperatures No. 1	No. 2	No. 3
		TREATMENT I—All Carbides Dissolved		
A	30 min. @ 2025°F	Water-Quenched from Solution Temperature	Cooled 1300°F per Hour from Solution Temperature	Cooled 300°F per Hour from Solution Temperature
B	30 min. @ 2200°F	Water-Quenched from Solution Temperature	Cooled 1300°F per Hour from Solution Temperature	Cooled 300°F per Hour from Solution Temperature
C	30 min. @ 2025°F	Water-Quenched from Solution Temperature	Cooled 1300°F per Hour from Solution Temperature	Cooled 300°F per Hour from Solution Temperature
D	30 min. @ 2025°F	Water-Quenched from Solution Temperature	Cooled 1300°F per Hour from Solution Temperature	Cooled 300°F per Hour from Solution Temperature
E	30 min. @ 2025°F	Water-Quenched from Solution Temperature	Cooled 1300°F per Hour from Solution Temperature	Cooled 300°F per Hour from Solution Temperature
F	30 min. @ 2200°F	Water-Quenched from Solution Temperature	Cooled 1300°F per Hour from Solution Temperature	Cooled 300°F per Hour from Solution Temperature
G	30 min. @ 2200°F	Water-Quenched from Solution Temperature	Cooled 1300°F per Hour from Solution Temperature	Cooled 300°F per Hour from Solution Temperature
H	30 min. @ 2200°F	Water-Quenched from Solution Temperature	Cooled 1300°F per Hour from Solution Temperature	Cooled 300°F per Hour from Solution Temperature
I	30 min. @ 2025°F	Water-Quenched from Solution Temperature	Cooled 1300°F per Hour from Solution Temperature	Cooled 300°F per Hour from Solution Temperature
		TREATMENT II—Approximately 50% Carbides Dissolved		
A	30 min. @ 1800°F	Water-Quenched from Solution Temperature	Cooled 1300°F per Hour from Solution Temperature	Cooled 300°F per Hour from Solution Temperature
B	30 min. @ 2025°F	Water-Quenched from Solution Temperature	Cooled 1300°F per Hour from Solution Temperature	Cooled 300°F per Hour from Solution Temperature
C	30 min. @ 1800°F	Water-Quenched from Solution Temperature	Cooled 1300°F per Hour from Solution Temperature	Cooled 300°F per Hour from Solution Temperature
D	30 min. @ 1800°F	Water-Quenched from Solution Temperature	Cooled 1300°F per Hour from Solution Temperature	Cooled 300°F per Hour from Solution Temperature
E	30 min. @ 1800°F	Water-Quenched from Solution Temperature	Cooled 1300°F per Hour from Solution Temperature	Cooled 300°F per Hour from Solution Temperature
F	30 min. @ 2025°F	Water-Quenched from Solution Temperature	Cooled 1300°F per Hour from Solution Temperature	Cooled 300°F per Hour from Solution Temperature
G	30 min. @ 2025°F	Water-Quenched from Solution Temperature	Cooled 1300°F per Hour from Solution Temperature	Cooled 300°F per Hour from Solution Temperature
H	30 min. @ 2025°F	Water-Quenched from Solution Temperature	Cooled 1300°F per Hour from Solution Temperature	Cooled 300°F per Hour from Solution Temperature
I	30 min. @ 1800°F	Water-Quenched from Solution Temperature	Cooled 1300°F per Hour from Solution Temperature	Cooled 300°F per Hour from Solution Temperature

Boiling 65% Nitric Acid Test

For the boiling 65% nitric acid test, specimens ($\frac{1}{4} \times 1 \times 2$ inches) were machined from the heat treated strips, were surface ground and hand finished on 120 grit emery paper. The samples were cleaned in isopropyl alcohol and preboiled 30 minutes in a boiling 20% nitric acid solution. Each specimen was tested individually in a flask containing boiling 65% nitric acid in accordance with the test

Table II
Chemical Compositions of Laboratory Induction Furnace Heats of AISI Type 310 and Type 309 Stainless Steels Investigated

A.I.S.I. Type	Heat Number	Ladle Analysis C	Mn	P	S	Si	Cr	Ni	N
310	A	0.06	1.57	0.008	0.005	0.78	24.56	21.54	0.085
310	B	0.16	1.52	0.007	0.008	0.73	25.68	21.29	0.058
309	C	0.06	1.56	0.009	0.024	0.84	22.44	14.05	0.069
309	D	0.06	1.58	0.006	0.006	0.50	21.23	15.03	0.080
309	E	0.05	1.56	0.008	0.006	0.65	23.26	14.04	0.190
309	F	0.16	1.50	0.010	0.020	0.75	24.39	14.29	0.042
309	G	0.16	1.50	0.010	0.006	0.54	23.41	14.06	0.069
309	H	0.15	1.58	0.007	0.006	0.64	23.68	14.16	0.170
309	I	0.06	1.47	0.010	0.007	0.75	25.00	12.04	0.089

procedure as outlined in the ASTM Specifications (4). The weight losses occurring during each 48-hour exposure were determined and converted into corrosion rates measured as inches penetration per month. If the corrosion rate exceeded 0.005 inches penetration per month during any of the 48-hour boiling periods other than the first period the test was discontinued.

Boiling Copper Sulphate-Sulphuric Acid Test

For the boiling copper sulphate-sulphuric acid test, duplicate samples ($\frac{1}{8}\times\frac{3}{8}\times 3$ inches) were machined from each heat treated strip. The specimens were surface ground, hand finished on 120 grit emery paper and cleaned in isopropyl alcohol. They were immersed for 72 hours in a flask containing acidified copper sulphate (47 ml H_2SO_4—specific gravity 1.84, 13 grams $CuSO_4 \cdot 5H_2O$ and 950 ml distilled water). After removal from the solution each specimen was bent 180 degrees around a diameter equal to its thickness. If no surface cracking developed during bending, the specimen was considered to have exhibited a satisfactory resistance to intergranular corrosion by this test.

Microscopic Examination—Samples for microscopic examination were cut from the $\frac{1}{4}\times 1$ inch flat bars after each of the heat treating cycles. These samples were prepared for microscopic examination in accordance with standard metallurgical procedures so as to correlate the microstructure, particularly carbide distribution, with the results of the corrosion tests.

Results and Discussion

The chemical compositions of the two Type 310 heats and seven Type 309 heats are listed in Table II. For each grade, a low (0.06%) and a high (0.16%) carbon content was obtained and, for Type 309, the nitrogen content was varied from approximately 0.04 to 0.19%. In addition, to illustrate the effect of a chemical composition for Type 309 which results in the formation of considerable amounts of delta ferrite, a low carbon Type 309 heat with low nickel and high chromium content was included in this study.

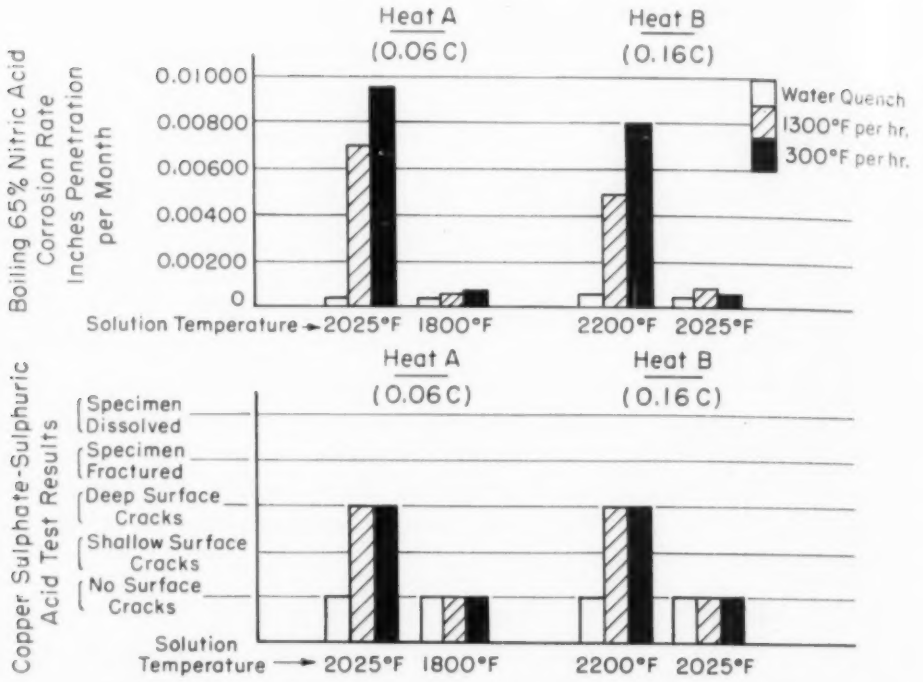


Fig. 1—Effect of Heat Treatment and Carbon Content Upon the Susceptibility of AISI Type 310 to Intergranular Attack in Boiling 65% Nitric Acid and Boiling Copper Suphate-Sulphuric Acid Tests.

AISI Type 310—Heats A and B, low and high carbon Type 310 were annealed at two different temperatures such that in one case undissolved carbides were present after annealing and in the other, all visible carbides were dissolved. Decreasing cooling velocities consisting of a water quench, 1300°F per hour and 300°F per hour cooling rates were used following each of the two annealing treatments. Fig. 1 illustrates the corrosion resistance of the two Type 310 heats given the above variations in heat treatment as measured by the boiling nitric acid test and the boiling copper sulphate-sulphuric acid test. These data showed that in the case of both high and low carbon Type 310 heats, excellent corrosion resistance was obtained when undissolved carbides were present at the annealing temperature. This was true for all three cooling rates which followed the annealing treatment. On the other hand, when the annealing treatment for both high and low carbon heats was such as to dissolve all visible carbides, a satisfactory corrosion resistance was obtained only in water-quenched specimens. Specimens cooled at either 1300 or 300°F following the high temperature annealing treatment failed in both types of acid solutions.

The examination of the microstructures of all specimens tested for corrosion revealed the following. All Type 310 specimens which failed in the boiling nitric acid and boiling copper sulphate-sulphuric

acid test had microstructures which consisted of complete encirclement of the austenite grains with carbides or carbo-nitrides. Conversely, all specimens which showed excellent corrosion resistance as determined by these two tests showed either very few or no visible carbides at the austenite grain boundary. However, many of these specimens had a large number of randomly distributed carbides. Specimens of intermediate corrosion resistance showed a partial or semi-continuous grain boundary network of carbides. These results illustrated a very close relationship between the distribution of carbides in Type 310 and the susceptibility to intergranular corrosion. This relationship, although not unexpected, was powerfully magnified in this study since large variations in carbon contents and cooling rates were used which resulted in large variations in carbide distribution. As illustrated in Fig. 1, the Type 310 heat with the highest carbon content had corrosion resistance equal to if not better than the low carbon Type 310, as long as the processing or heat treatment was such as to yield a microstructure relatively free of intergranular carbides even though there may have been many randomly distributed carbides. The corrosion data and microstructures showed that when undissolved carbides were present at the annealing temperature, good corrosion resistance was obtained and few intergranular carbides were observed even when the relatively slow cooling rate of 300°F per hour was used from the annealing temperature. If these same steels were heated high enough during annealing to dissolve all the visible carbides and cooled at the same rate, poor corrosion resistance was obtained and the majority of carbides observed at room temperature were at the grain boundary. This indicated that when all or most of the carbon is in solution at the annealing temperature, during cooling, the carbon precipitates as a carbide preferentially at the grain boundaries. However, when a portion of the carbon is present as an undissolved carbide at the solution temperature; during cooling, a large portion of the carbon apparently precipitates preferentially upon the existing carbides rather than at the grain boundaries. Both the corrosion resistance obtained, and most important, the microstructures observed supported the above hypothesis in the case of the two Type 310 heats studied in this report.

The variations in degree of carbon solution discussed above was accompanied by a large variation in grain size. The high solution temperatures which were required in both the low and the high carbon 310 heats to dissolve all the carbides resulted in a marked coarsening of the austenite grains. Specimens treated at the lower solution temperature which contained undissolved carbides were relatively fine-grained. It was not possible in this study to entirely isolate the effect of grain size, if any, upon corrosion resistance.

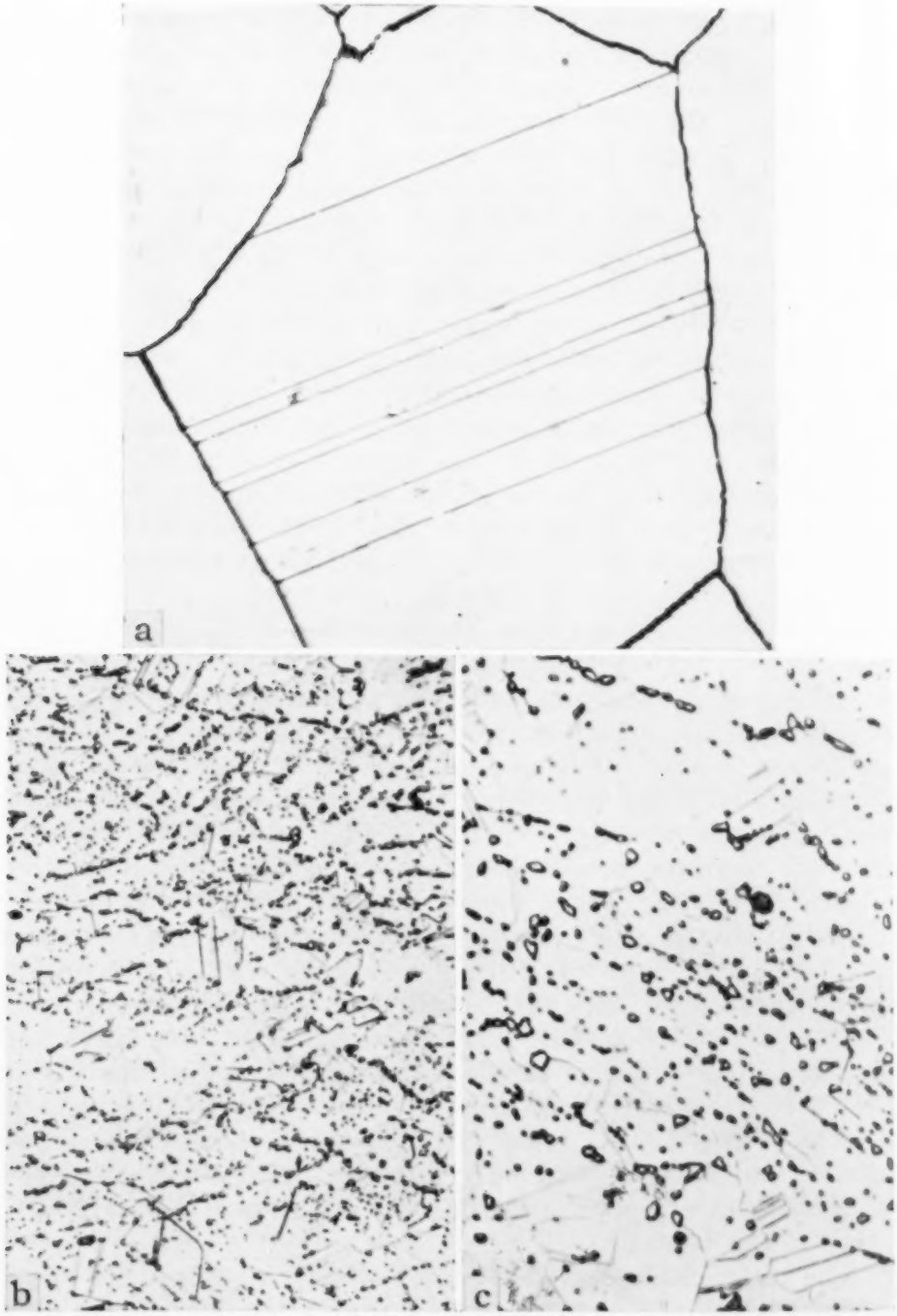


Fig. 2—Photomicrographs of AISI Type 310 Stainless Steel Heat B Showing Differences in Structure Resulting From the Use of Different Solution Temperatures Followed by Cooling at 1300°F per Hour. Etch: Hydrochloric and nitric acid in glycerine. (a) Dissolved carbides (2200°F solution temperature). ×500. (b) Undissolved carbides (2025°F solution temperature). ×500. (c) Undissolved carbides (2025°F solution temperature). ×1000.

To illustrate the variations in microstructures observed, a few typical specimens are shown in Fig. 2. In this figure the high carbon Type 310 heat, B, which had been heated to 2025 and 2200°F and

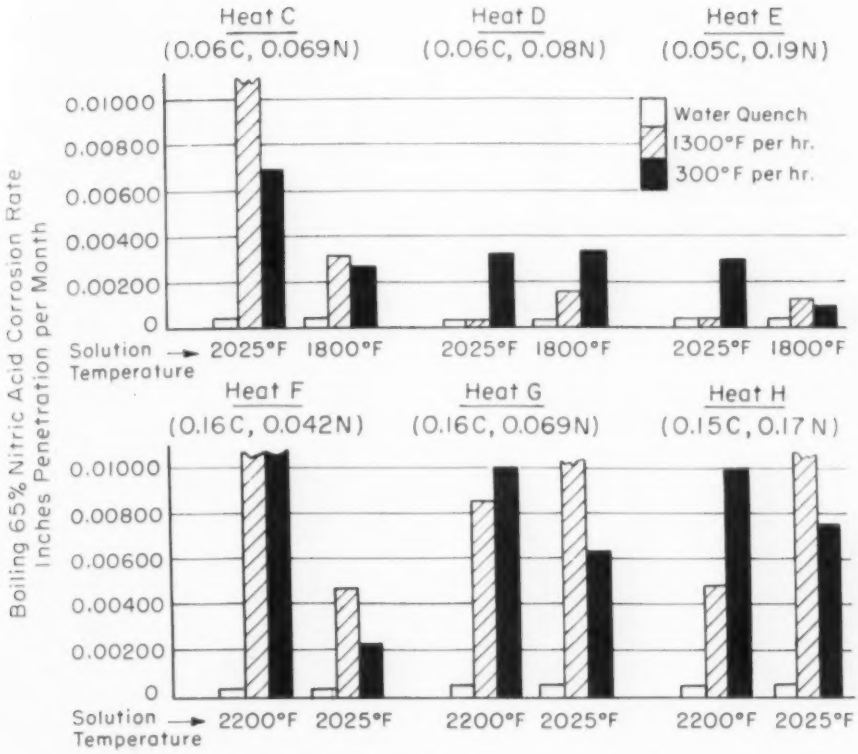


Fig. 3—Effect of Heat Treatment, Carbon and Nitrogen Content Upon the Susceptibility of AISI Type 309 Stainless Steel to Intergranular Attack in the Boiling 65% Nitric Acid Test.

cooled at the rate of 1300°F per hour is shown. These microstructures show that the use of the higher annealing temperature, where all or most of the carbon was in solution, resulted in a complete network of intergranular carbide following the above cooling treatment whereas the same steel heated to a lower solution temperature which left many randomly distributed undissolved carbides resulted in practically no intergranular carbides following the same cooling treatment. Instead, there was a random distribution of many chromium carbides. These data yield marked evidence for the above discussion of the effect of carbon distribution at the annealing temperature on the corrosion resistance of Type 310 steel.

AISI Type 309—The chemical compositions of the seven Type 309 steels studied in this investigation are listed in Table II. The composition of all these steels is within the present AISI chemical specification. Four of the steels were produced with a low carbon content (0.06%) and three were produced with a high carbon content (0.16%). The nitrogen content was varied at each carbon level over the range of approximately 0.04 to 0.19%. Heat I was purposely produced with a high chromium content and a low nickel content so as to investigate the effect of delta ferrite on corrosion resistance and microstructure.

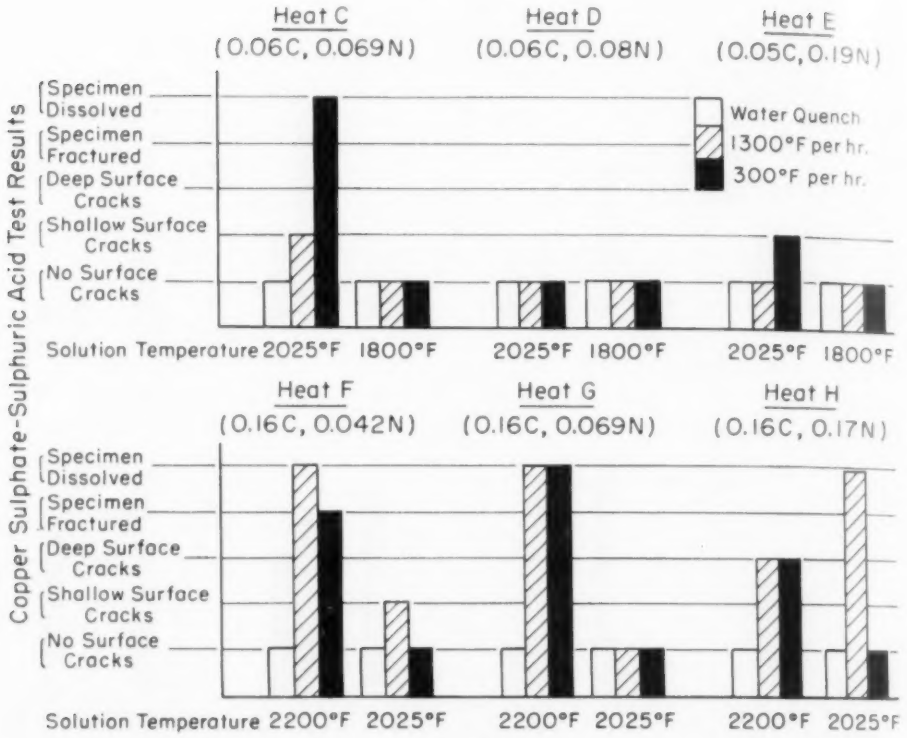


Fig. 4—Effect of Heat Treatment Carbon and Nitrogen Content Upon the Susceptibility of AISI Type 309 Stainless Steel to Intergranular Attack in the Boiling Copper Sulphate-Sulphuric Acid Test.

All of the above Type 309 steels were tested in boiling 65% nitric acid and boiling copper sulphate-sulphuric acid. Results of these corrosion tests are shown in Figs. 3 and 4 for all heats, except heat I which contained a high percentage of delta ferrite. For the heat treatments at the high and low solution temperature followed by water quenching, all steels investigated had satisfactory corrosion resistance in both types of acid solutions. For both the low and high carbon Type 309 heats at the lowest nitrogen levels, corrosion resistance of specimens which had the slower cooling rates from the solution temperature was improved when using the lower solution temperatures at which undissolved carbides were present as compared to the higher solution temperature which dissolved all carbides. In this respect these data are similar to those obtained for Type 310. However, the corrosion resistance obtained at the lower solution temperature and slow cooling rates was not sufficient to allow these Type 309 steels to meet the present acceptance limits in the boiling 65% nitric acid solution. This behavior differs from that of Type 310.

The data in Figs. 3 and 4 also showed that improved corrosion resistance was obtained with increasing nitrogen content at both low and high carbon levels, but with the most significant improvement

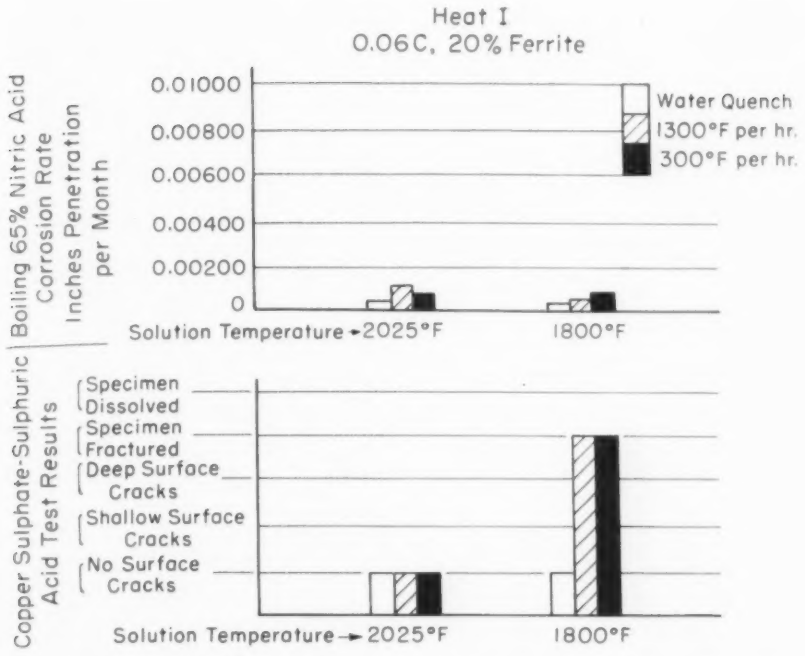


Fig. 5—Effect of Heat Treatment and Delta Ferrite Upon the Susceptibility of AISI Type 309 Stainless Steel to Intergranular Attack in the Boiling 65% Nitric Acid Test and the Boiling Copper Sulphate-Sulphuric Acid Test.

obtained at the lowest carbon level. Further, for the higher nitrogen content Type 309 heats there did not appear to be a marked improvement in corrosion resistance with the use of the lower solution temperatures as compared to the high solution temperatures as was the case for the low nitrogen steels studied and as was discovered for the Type 310 steels. The reason for this behavior is not known.

Results of corrosion testing of heat I, with the chemical composition which resulted in approximately 20% delta ferrite, are shown in Fig. 5. This steel exhibited satisfactory corrosion resistance in boiling 65% nitric acid at all solution temperatures and cooling rates investigated. However, there was severe embrittlement of the specimens containing undissolved carbides at the lower solution temperatures when cooled at 1300 and 300°F per hour. This embrittlement resulted in bend test failures even in the absence of exposure to the copper sulphate-sulphuric acid solution. This condition therefore does not indicate however, susceptibility to corrosion either of the general or intergranular type.

Examination of the microstructure of all Type 309 steels tested indicated, as with Type 310, a good correlation between distribution of carbides and intergranular corrosion resistance. When the austenite grains were completely surrounded by a precipitate, failure occurred in either of the two corrosive media studied. When a continuous plus a discontinuous or a discontinuous carbide network

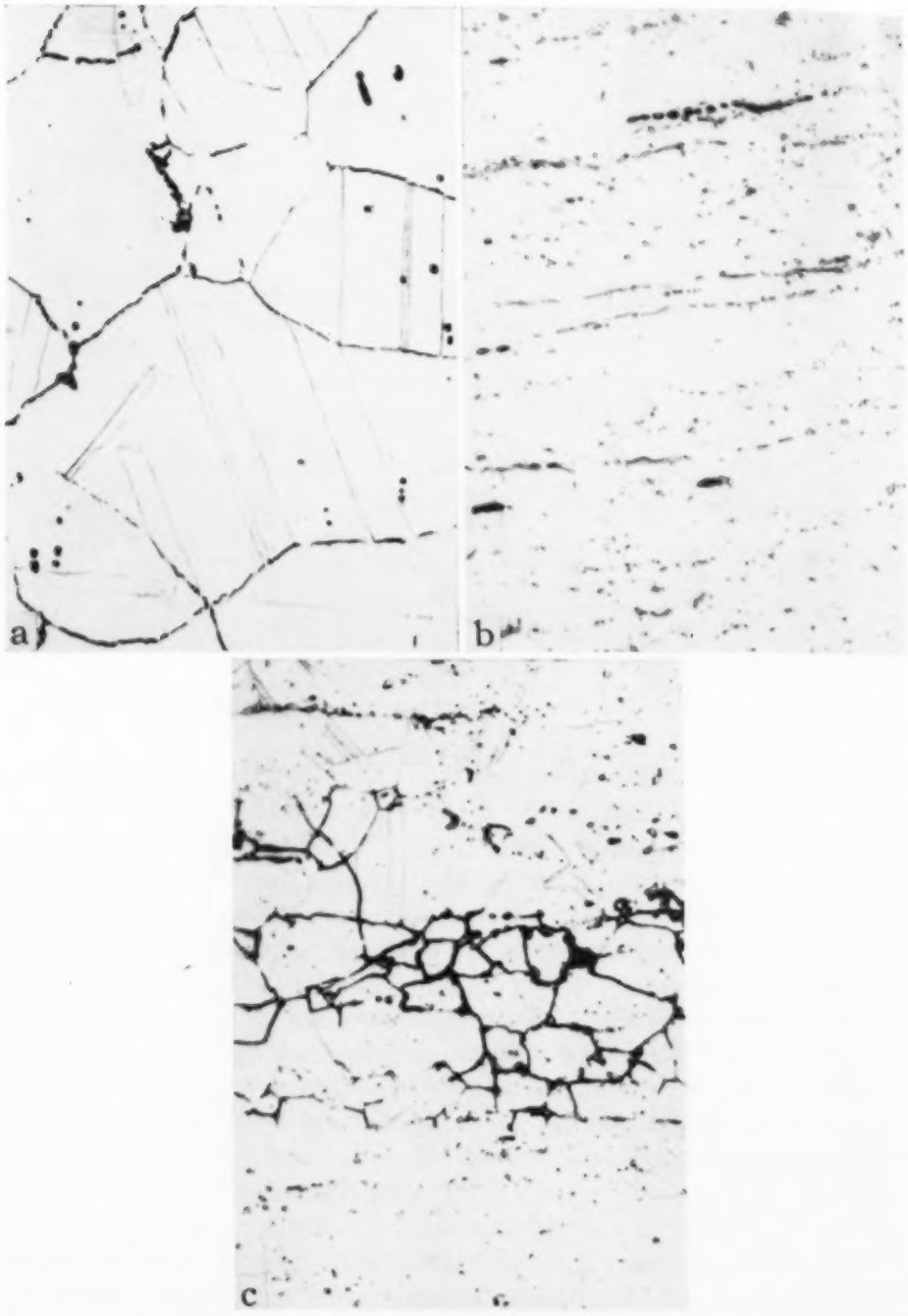


Fig. 6—Photomicrographs of AISI Type 309 Stainless Steel, Heat C Showing Differences in Structure Resulting from the Use of Different Solution Temperatures and the Mode of Corrosive Attack After Solution Treatment at the Lower Temperature. Etch: Hydrochloric and nitric acid in glycerine. (a) Solution treated 30 minutes at 2025°F and cooled 300°F/hour. ×500. (b) Solution treated 30 minutes at 1800°F and cooled 300°F/hour. ×500. (c) Nature of edge corrosion attack in boiling 65% nitric acid. ×500.

was observed, corrosion properties were poor to fair. When the grain boundaries were free of a precipitate, corrosion resistance was good. However, this relationship of microstructure to corrosion resistance

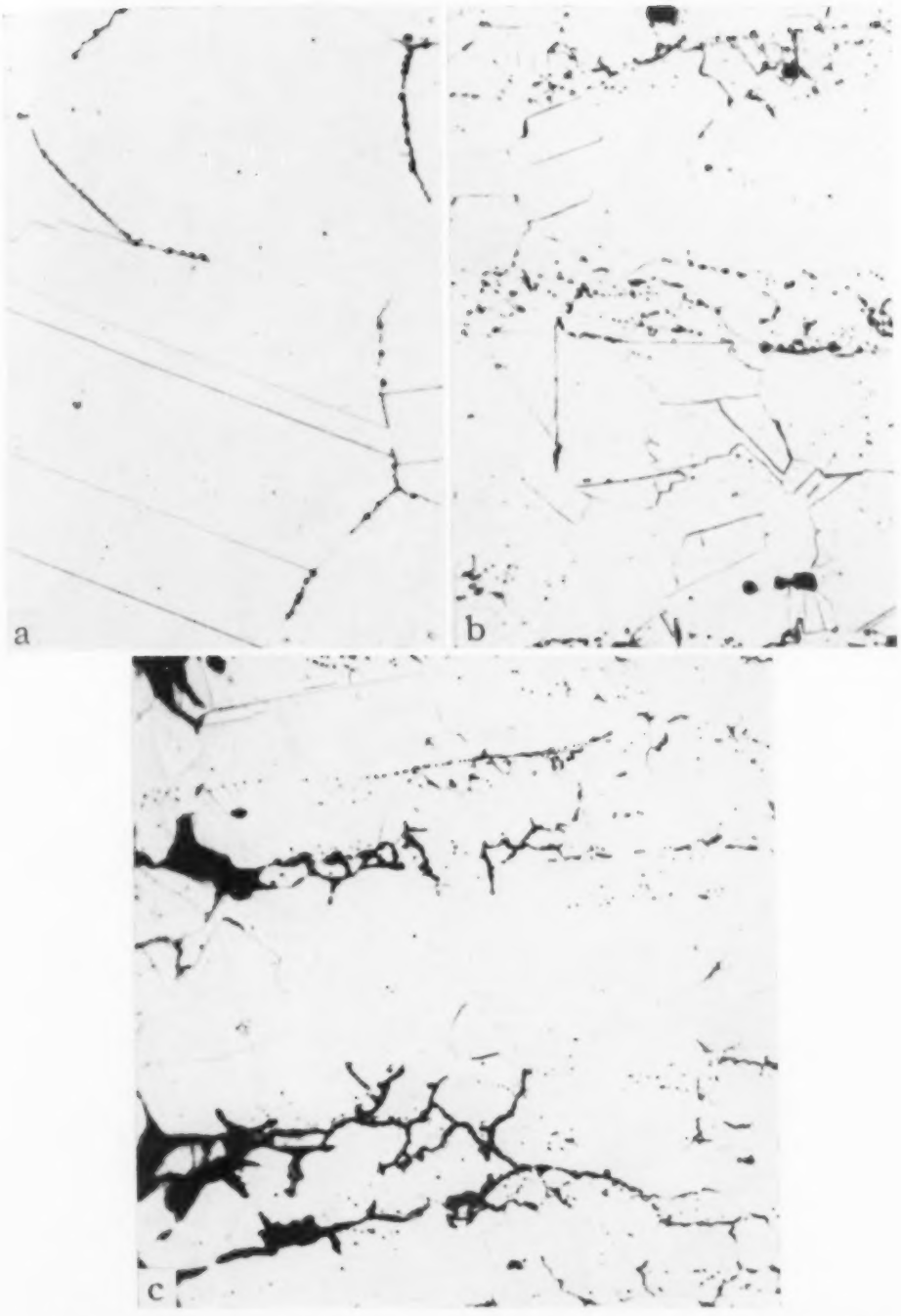


Fig. 7—Photomicrographs of AISI Type 309 Stainless Steel, Heat E Showing Differences in Structure Resulting from the Use of Different Solution Temperatures and the Mode of Corrosive Attack After Solution Treatment at the Lower Temperature. Etch: Hydrochloric and nitric acid in glycerine. (a) Solution treated 30 minutes at 2025°F and cooled 300°F/hour. ×500. (b) Solution treated 30 minutes at 1800°F and cooled 300°F/hour. ×500. (c) Nature of edge corrosion attack in boiling 65% nitric acid. ×500.

was not as clear-cut for Type 309 as it was for the Type 310 steels studied. In the case of Type 309 other factors affected corrosion resistance. For example, heats D, E, G and H exhibited carbide

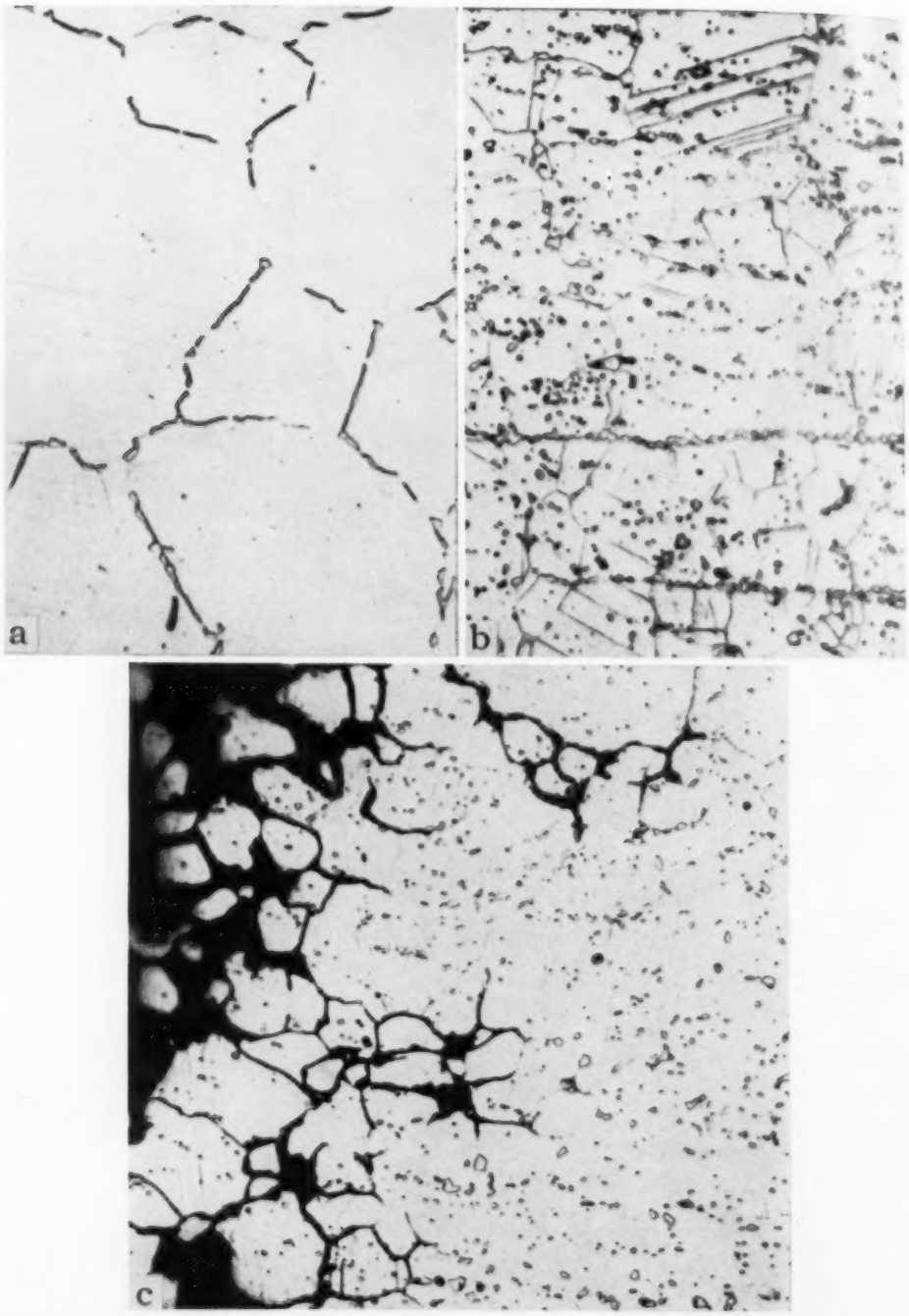


Fig. 8—Photomicrographs of AISI Type 309 Stainless Steel, Heat F Showing Differences in Structure Resulting From the Use of Different Solution Temperatures and the Mode of Corrosive Attack After Solution Treatment at the Lower Temperature. Etch: Hydrochloric and Nitric Acid in Glycerine. (a) Solution treated 30 minutes at 2200°F and cooled 300°F/hour. ×500. (b) Solution treated 30 minutes at 2025°F and cooled 300°F/hour. ×500. (c) Nature of edge corrosion attack in boiling 65% nitric acid. ×500.

segregation or banding which accelerated corrosion rates in boiling 65% nitric acid particularly after annealing at the lower temperatures. Further, heats C and F possessed carbide stringers which

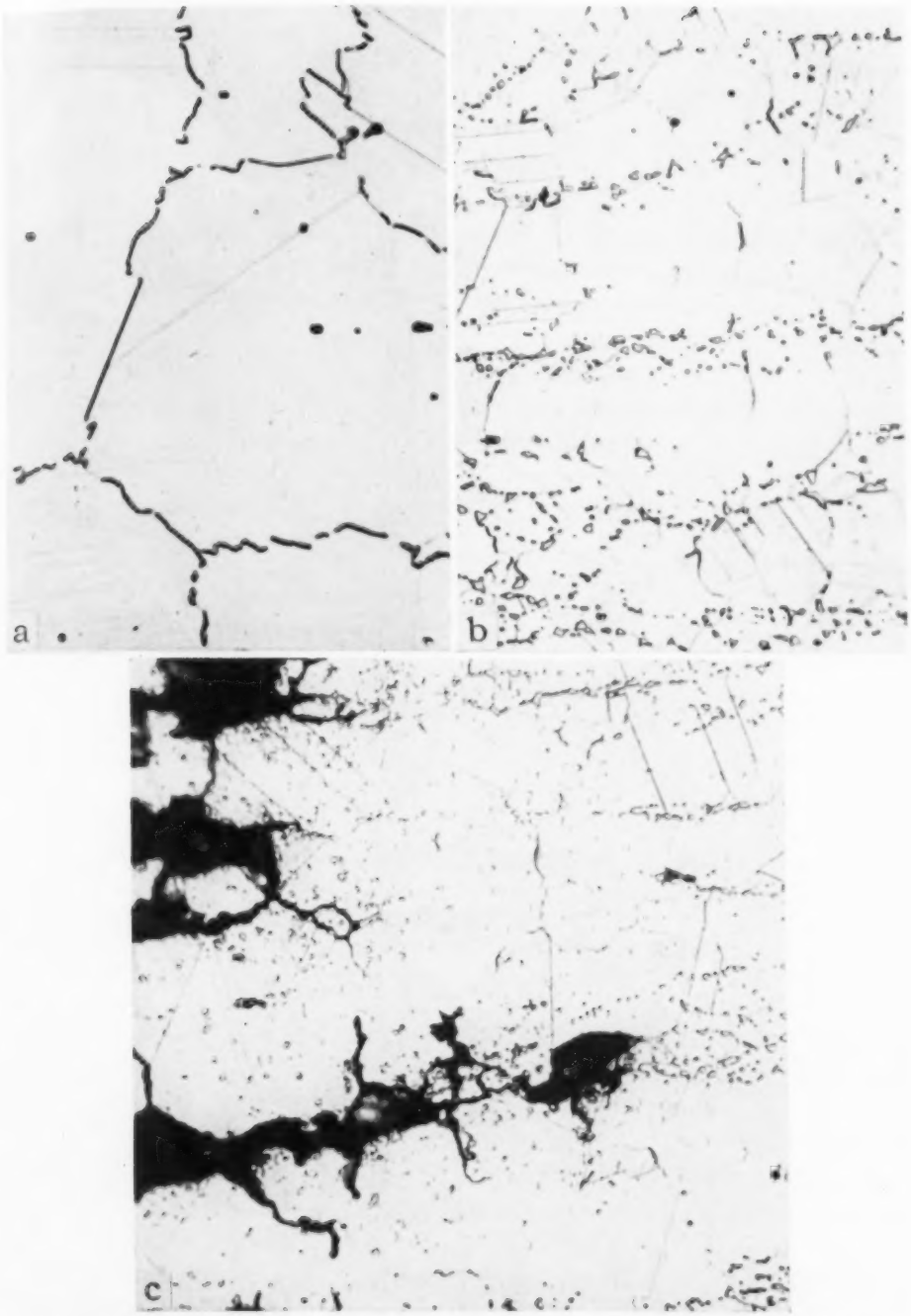


Fig. 9—Photomicrographs of AISI Type 309 Stainless Steel, Heat H Showing Differences in Structure Resulting from the Use of Different Solution Temperatures and the Mode of Corrosive Attack After Solution Treatment at the Lower Temperature. Etch: Hydrochloric and nitric acid in glycerine. (a) Solution treated 30 minutes at 2200°F and cooled 300°F/hour. ×500. (b) Solution treated 30 minutes at 2025°F and cooled 300°F/hour. ×500. (c) Nature of edge corrosion attack in boiling 65% nitric acid. ×500.

tended to increase the corrosion rate in boiling 65% nitric acid. As would be expected, this visible segregation of carbides was eliminated by the use of higher solution temperatures. The two solution

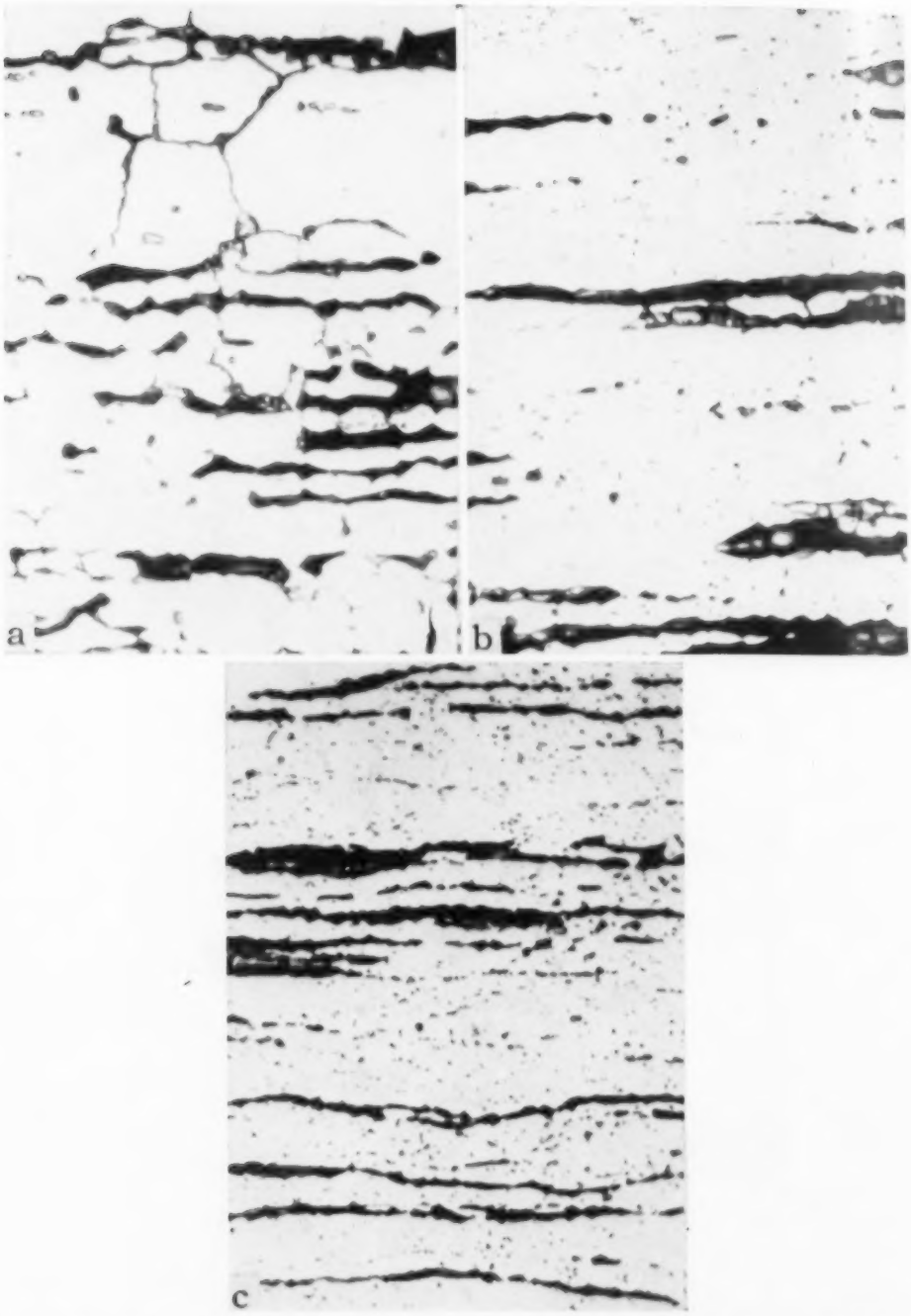


Fig. 10—Photomicrographs of AISI Type 309 Stainless Steel Heat I Showing the Effect of Delta Ferrite on the Distribution of Carbides. Etch: Electrolytic Chromic Acid. (a) Solution treated 30 minutes at 2025°F and cooled 1300°F per hour. ×500. (b) Solution treated 30 minutes at 1800°F and water-quenched. ×500. (c) Solution treated 30 minutes at 1800°F and cooled 1300°F per hour. ×500.

temperatures used for each heat resulted in a marked increase in grain size for the higher solution temperature. The difference in grain size and degree of carbide segregation produced by the two

solution treatments did not permit a clear differentiation of the individual effects, if any, of grain size and chemical homogeneity.

Typical microstructures of the Type 309 steels investigated showing the distribution of carbides and particularly the banding and carbide rich stringers and their effect on corrosion resistance are shown in Figs. 6,7,8 and 9.

Microstructures of heat I which contained an appreciable percentage of delta ferrite are shown in Fig. 10. This figure shows the occurrence of a fine precipitate of carbide within the delta ferrite. This precipitation occurred particularly following the slower cooling rates from the lower solution temperature. Precipitation of carbides within the ferrite is believed to be the cause of the severe embrittlement occurring in the specimens mentioned above. Less ferrite was present at the higher solution temperature.

Examination of heat I revealed that the presence of delta ferrite is very effective in improving intergranular corrosion resistance of Type 309 by affecting the distribution of the carbides formed during cooling in such a manner as to prevent their formation at the austenite grain boundaries. The majority of carbides precipitated during cooling in this latter steel were found at the ferrite grain boundaries and within the ferrite. This type of carbide precipitation did not result in corrosion failure in the two media used for testing.

Conclusions

The effects of chemical composition and heat treatment on the microstructure and the corrosion resistance of AISI Types 310 and 309 as determined in this study were as follows.

AISI Type 310

(a) Excellent correlation was observed between distribution of carbides and corrosion resistance in both boiling 65% nitric acid and copper sulphate-sulphuric acid tests.

(b) The best resistance to corrosion after slow cooling from the solution annealing temperature was obtained when the microstructure contained a random distribution of undissolved carbides which acted as nuclei for the carbon precipitation.

(c) When the microstructure prior to solution annealing contained intergranular carbides or when the carbides were completely dissolved during solution annealing, the steel became susceptible to intergranular corrosion after slow cooling from the solution annealing temperature.

(d) When the carbides were randomly dispersed and when the solution annealing temperature was such that only approximately 50% of the carbides were dissolved, corrosion resistance of the 0.16% carbon Type 310 steel was equal to that of the 0.06% carbon

Type 310 steel after slow cooling from the solution annealing temperature.

AISI Type 309

(a) A fair correlation was observed between the distribution of carbides and corrosion resistance in boiling 65% nitric acid and copper sulphate-sulphuric acid. Banding and segregation of carbides were more prevalent in the Type 309 steels than in Type 310 steels and this in turn affected somewhat the correlation between the grain boundary carbides and corrosion resistance.

(b) At the low or commercial nitrogen levels tested, improved corrosion resistance was obtained in Type 309 with the use of a low solution temperature which resulted in only partial solution of randomly distributed carbides. In this respect, the data were similar to those of Type 310. With the higher nitrogen levels the use of low solution temperatures did not greatly improve corrosion resistance when slow cooling rates were used from the solution temperature.

(c) Increasing the nitrogen content of the low (0.06%) carbon Type 309 heats appeared to be beneficial in increasing intergranular corrosion resistance. However, increasing the nitrogen content at the high (0.16%) carbon level had little affect on the intergranular corrosion resistance of the Type 309 steels investigated.

(d) In Type 309 steels if rate of cooling from the solution annealing temperatures is slow, adjustment of the composition to produce 20% delta ferrite will markedly improve intergranular corrosion resistance by minimizing intergranular carbide precipitation. However, in some cases severe embrittlement was observed in Type 309 containing a higher percentage of delta ferrite.

Acknowledgment

The authors would like to express their appreciation for the helpful assistance of Miss Mary Potter in conducting corrosion tests and the metallographic examinations.

References

1. E. C. Bain, R. H. Aborn and J. J. B. Rutherford, "The Nature and Prevention of Intergranular Corrosion in Austenitic Stainless Steels," *Transactions*, American Society for Steel Treating, Vol. 21, 1933, p. 481.
2. S. J. Rosenberg and J. H. Darr, "Stabilization of Austenitic Stainless Steel," TRANSACTIONS, American Society for Metals, Vol. 41, 1949, p. 1261.
3. D. C. Buck, J. J. Heger, F. J. Phillips and B. R. Queneau, "Corrosion Resistance and Mechanical Properties of Low Carbon Austenitic Stainless Steels," Special Publication No. 93, American Society for Testing Materials, 1949.
4. Book of ASTM Standards, 1952, Part I, p. 998.

DISCUSSION

Written Discussion: By D. E. Nulk, associate manager, Materials Laboratory, Jet Division, Thompson Products, Inc., Cleveland.

The authors are to be congratulated for their contribution to the metallurgy of these alloys. We have had these alloys so long yet little is known about them.

The writer has been one of those instrumental in convincing the steel mills to supply Type 310 free from a continuous network of carbides. One reason was this corrosion resistance problem which becomes important during pickling procedures in sheet metal fabrication.

This paper illustrates that corrosion resistance can be good if complete solution is realized or under certain conditions which are usually associated with dispersed carbide patterns. It is quite possible that the latter case is due to stabilization of the chromium deplete areas adjacent to the carbides formed during the primary working of the ingot. This stabilization could occur partially during the primary working and partially at the lower temperature anneal. Whether or not such a condition could be duplicated in mill practice is questionable.

Although the authors encountered severe attack of the corrosive solutions whenever complete carbide envelopment of the grains occurred, it will not always be so. If precipitation is induced in completely solution annealed material, it will occur at the grain boundaries. If the precipitation is at a temperature and time that will result in stabilization (or enrichment of the chromium deplete areas adjacent to the precipitate) the steel will resist corrosive attack.

It was noted by this writer that some of the physical properties of Type 310 were poor in some cases when the carbide networks completely surrounded grains of the steel. This along with the low corrosive resistance in some of these heats lead this writer to work toward the establishment of a solution anneal requirement on this steel. For example, a series of specimens of the same heat were furnace cooled from a 2050°F solution anneal. Specimens were water-quenched from a wide range of temperatures during the cooling cycle. All those quenched from 1300°F or above resisted acid attack. Those quenched from 1100 and 1200°F had low corrosion resistance.

On the basis of some work recently done there is good reason to believe that the low physical properties are associated with something other than carbides. Carbides formed at 1200°F seem to have less corrosion resistance than those formed at 1600°F.

There is a tendency for brittleness to occur in this lower temperature range. So far it has not been possible to induce brittleness by the 1100 to 1200°F heat treatment if the steel is first stabilized at 1650°F. It is possible that the low physical properties as well as the low corrosion resistance can be avoided by using a 1650°F stabilizing treatment for post welding or interstage annealing (drawing operations) during fabrication. If it is necessary to anneal at a higher temperature for interstage annealing it could be followed by a stabilization treatment.

It is possible that industry might best be served by: (a) the mills emphasizing the control of grain size and insuring a rapid quench from the annealing sequence rather than complete solution of the carbides; and (b) the fabricators using the 1650°F heat treatment for in-process heat treatments.

Authors' Reply

The authors appreciate the comments of Mr. Nulk. In our experience, we found no instance of good corrosion resistance when there was *complete* carbide envelopment of grain boundaries. We made no measurements of physical properties of the steels studied and thus cannot comment on Mr. Nulk's studies.

THE INFLUENCE OF STRAIN RATE AND TEMPERATURE ON THE DUCTILITY OF AUSTENITIC STAINLESS STEEL

By G. W. Form and W. M. Baldwin, Jr.

Abstract

The ductility of AISI 303 and 310 austenitic stainless steels was determined in tensile tests over a range of strain rates from 0.01 in./in./min. up to 19000 in./in./min., and over a range of temperatures from −321 up to +750°F. Ductility drops as strain rate is increased, the drop being greatest at room temperature. The ductility shows a maximum at room temperature at low strain rate, but at high strain rates it increases slowly and steadily with the test temperature. Magnetic measurements on broken specimens showed that the γ-α transformation can not account for all these behaviors. (ASM-SLA Classification: Q23, Q27, SS)

STAINLESS steels lose ductility at high strain rates at room temperature (1–4).[1] The factors which cause this strain rate sensitivity have not been satisfactorily rationalized yet. It has been inferred at times that the strain rate sensitivity is due to the γ-α transformation. The ASTM Subcommittee V on Mechanical Tests (5), for example, reports "Since austenitic stainless steels transform when cold-worked, the amount of transformation being dependent upon the amount of work and likely upon the rate of working, it is to be expected that rate of strain would affect the tensile properties." Yet an attempt to link the γ-α transformation with the ductility drop leads to a paradox. Binder (6) maintains the γ-α transformation lowers the ductility of 18-8 stainless steels. Cohen (7) states likewise, that if austenite could withstand decomposition it would display higher ductility. If the α-phase formed during a tensile test lowers the ductility of 18-8 stainless steel, it would then be natural to conclude that, at low strain rates, where ductility is high, less α-phase is present than at high strain rates, where ductility is low. This, however, contradicts Mathieu's results (8) which clearly show that the amount of α-phase drops markedly when the testing speed is increased. Confusing the issue even further is the fact that ductility drops at low temperatures where increased α-phase formation is known to exist (8).

[1]The figures appearing in parentheses pertain to the references appended to this paper.

This paper is based upon a portion of a research program conducted in the Metals Research Laboratory, Case Institute of Technology in cooperation with the Office of Naval Research.

A paper presented before the Thirty-Seventh Annual Convention of the Society, held in Philadelphia, October 17–21, 1955. Of the authors, G. W. Form is associated with Ecole Polytechnique, Montreal, Canada and was formerly associated with Case Institute of Technology. W. M. Baldwin, Jr. is research professor, Metals Research Laboratory, Case Institute of Technology, Cleveland. Manuscript received November 11, 1954.

In the present investigation—designed to shed light on this discrepancy—tensile tests were conducted over a wide range of temperatures and strain rates in order to evaluate the influence of these factors on the ductility behavior of austenitic stainless steels. In addition, magnetic measurements supplemented by microhardness tests were made on broken test specimens to determine to what extent, if any, the γ-α transformation is involved in the strain rate sensitivity of this material.

Material and Procedure

Material—The two steels selected for this investigation were AISI 303 (an 18% Cr, 8% Ni steel) and AISI 310 (a 25% Cr, 20% Ni steel).[2] The tensile specimens, 1½ inch long with a minimum diameter of 0.212 inch, were machined from fully annealed rod.

Tensile Test Procedure—Tensile tests were made at various temperatures and strain rates. The low strain rate tests (0.01 to 10 in./in./min.) were carried out on a Riehle and a Baldwin-Southwark tensile-testing machine, with the speed of the cross-head held constant. This, of course, yielded a variable strain rate as the specimen lengthened, but the true strain rate did not vary by more than a factor of 4 since the greatest reduction in area recorded was 75%. Since the strain rate was intentionally changed by a factor of almost two million in the various tests, the variability in strain rate during a given test can be reasonably overlooked. The strain rate of 100 in./in./min. was obtained on a hydraulic type draw bench, and the 8000 and 19000 in./in./min. on a drop-hammer. For the subzero temperature tests the specimens were immersed in a bath of liquid nitrogen (−321°F), a mixture of liquid nitrogen and isopentane (−200°F), or a mixture of isopentane and dry ice (−50°F). The room temperature tests (+70°F) were carried out in air, while all higher temperatures (+200, +300, +500 and +750°F) were obtained with an electrically heated furnace. In the tests carried out at low strain rates (0.01 to 10 in./in./min.) the specimens were held in a low temperature box containing the cooling liquid or in a furnace so that the test temperature could be kept constant during the test period. At high strain rates, however, the specimens were transferred from the cold liquid or from the furnace after having reached the desired temperature and tested while surrounded by air at room temperature. The elapsed transfer and testing time was about four seconds.

The ductility, $\epsilon = 2 \ln \frac{d_o}{d_f}$, was obtained as an average of six

[2]The analyses ran: 303—Si, 0.54%; S, 0.300%; P, 0.016%; Mn, 1.37%; C, 0.045%; Cr, 17.49%; Ni, 10.30%; 310—Si, 0.35%; S, 0.006%; P, 0.023%; Mn, 1.82%; C, 0.044%; Cr, 22.72%; Ni, 19.72%.

measurements of the initial and final diameter, d_o and d_f, respectively on an optical comparator.

Magnetic Measurements—Magnetic measurements were made on the broken tensile test specimens in order to detect how much α-phase (martensite) had been formed during the tensile test. A relatively simple setup based on the induction principle was used, Fig. 1. The energizing magnetic field was produced in a coil of about 2700 turns, which was connected to an AC-source.

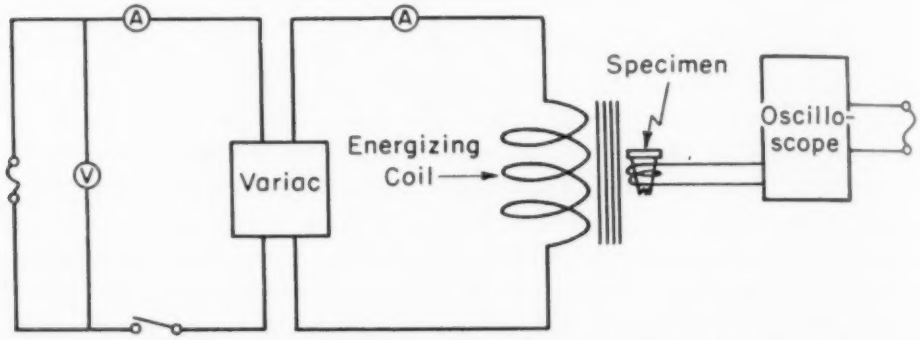


Fig. 1—Electric Circuit Used in the Magnetic Induction Method.

One half of a broken specimen was placed into a search-coil, whose shape was conical in order to minimize the air gap.[3] The specimen and search coil were inserted into the center of the energizing coil and connected to the grid of an oscilloscope. The amount of α-phase formed in a specimen determined the potential difference between grid and ground of the oscilloscope as indicated by the height of the sine wave amplitude on the screen. This amplitude was measured and expressed in terms of screen units (length of a square of the screen net). Both halves of a broken specimen were measured and the readings added. The amplitude produced by a nonmagnetic specimen was then subtracted and the difference taken as a qualitative measure of the α-phase formed.[4]

In order to reveal the distribution of martensite formed during the tensile test, a few broken specimens were inspected by a magnetic powder method. A colloidal magnetite was prepared according to Elmore (9) and the sol stabilized with soap. A broken specimen-half was sectioned lengthwise, one half mounted in lucite and polished. The mount was inserted into a core of Swedish iron, and the assembly placed into the same energizing coil as used previously.

[3]The air gap varied from specimen-to-specimen. However, the error thus involved was found to be negligibly small and therefore not taken into consideration when plotting the oscilloscope readings.

[4]This difference could be converted directly into the amount of α-phase formed, e.g. by a lineal analysis. Since the variation of α-phase under different test conditions is more important than absolute values for the present problems, it was not necessary to convert the oscilloscope readings into the equivalent of permeability or amount of martensite.

The magnetic sol was applied so that it covered the entire top surface of the mounting. The coil was connected to a DC source, thereby attracting the magnetic particles in the sol to those areas of the polished specimen surface which had undergone a γ-α transformation. The resulting patterns were photographed while the

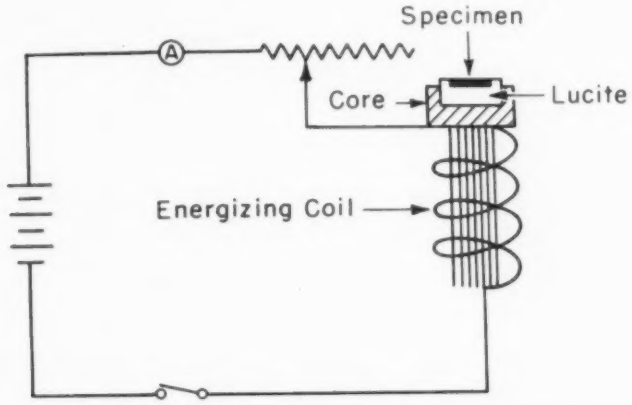


Fig. 2—Electric Circuit Used in the Magnetic Powder Method.

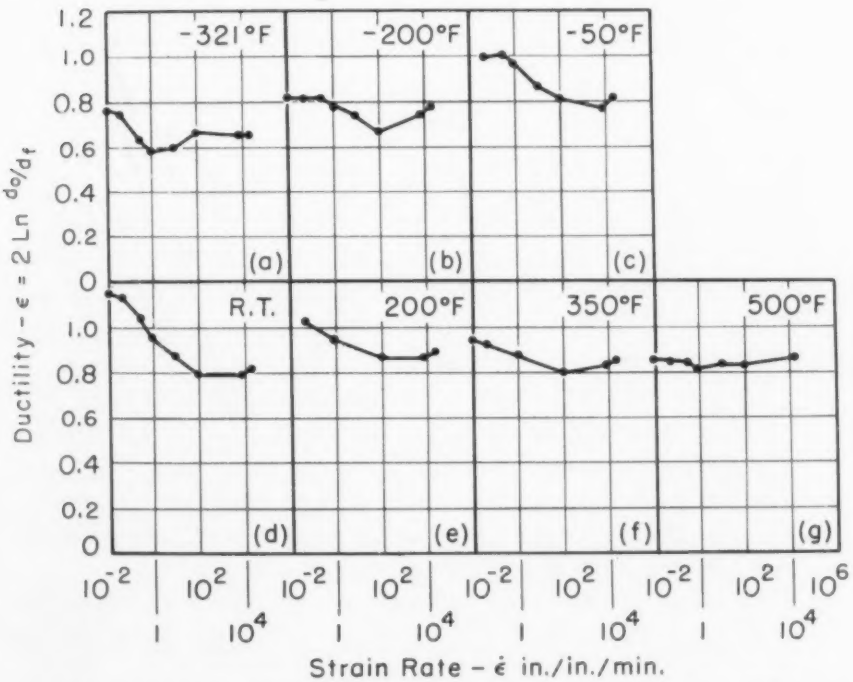


Fig. 3—(a-g): Ductility of AISI 303 Stainless Steel as a Function of Strain Rate at Various Test Temperatures.

magnetic field was still in effect. The electrical circuit used in the magnetic powder method is shown in Fig. 2.

Microhardness Tests—The samples that were inspected magnetically for martensite distribution were subjected to microhard-

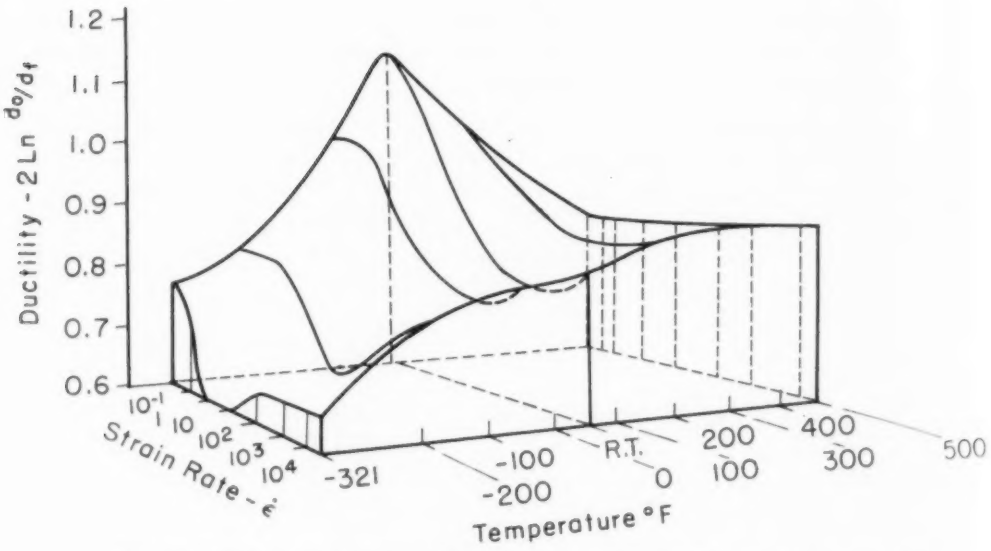


Fig. 4—Ductility of AISI 303 Stainless Steel as a Function of Strain Rate and Test Temperature.

ness tests. Readings were taken with a Knoop indenter and a load of 1000 grams on a Tukon tester and converted to Rockwell A Units.

Results

AISI 303 Stainless Steel

The ductility, ϵ, is plotted as a function of strain rate, $\dot{\epsilon}$, for various temperatures in Fig. 3. The three-dimensional graph of Fig. 4 represents the ductile behavior of AISI 303 steel over the entire range of temperatures and strain rates. These plots reveal three major characteristics of the ductility behavior:

(a) The strain rate sensitivity is most pronounced at room temperature, while it is relatively small at low temperatures and disappears at +500°F.

(b) At low strain rates the ductility increases sharply with temperature, reaches a maximum at room temperature and decreases at higher test temperatures.

(c) At high strain rates (19000 in./in./min.) the ductility increases slowly if irregularly as the test temperature increases.

In Figs. 5 and 6 the oscilloscope readings which were obtained as a measure of the martensite present are plotted as a function of strain rate for four different tensile test temperatures. All measurements on the test specimens were made at room temperature. It is seen that at a given temperature the amount of α-phase is less at high strain rates; also at a given strain rate the amount of α-phase is less

the higher the temperature.[5] No α-phase could be detected in the specimens pulled at +200°F or higher. The temperature above which no transformation can be induced by deformation before fracture (M_d temperature) must therefore lie between room temperature and +200°F. This agrees with results reported in the literature for stainless steels of similar analyses (8,10). In contrast with the

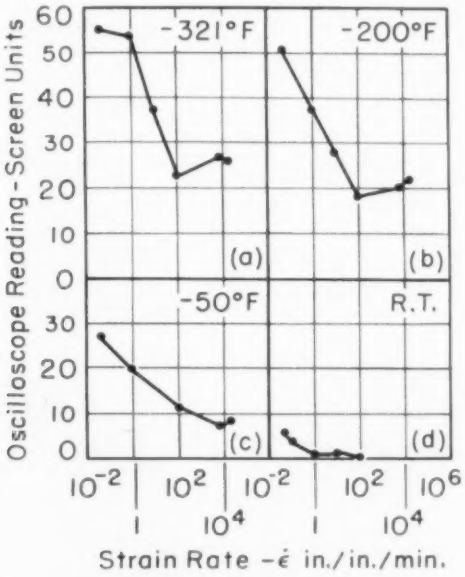


Fig. 5—(a-g): Effect of Strain Rate on the Magnetic Behavior of AISI 303 Stainless Steel at Various Tensile Test Temperatures.

ductility curves the strain rate sensitivity of the γ-α transformation is more pronounced at −321°F than at room temperature, i.e., the drop in oscilloscope reading over the total range of strain rates is larger at −321°F than at room temperature. The specimens broken at −321°F were magnetically tested at both −321°F and room temperature. The results indicated that no α-phase present at low temperature had reverted to austenite when brought up to room temperature.

The distribution of the α-phase in four fractured specimens—

[5]Scheil's theory of martensite formation (12) predicts the increase in martensite formed at low temperatures under constant strain rate found in Fig. 6. According to this theory a critical shear stress resolved in the slip plane has to be exceeded in order to overcome the resistance towards martensite formation. Once this critical value is surpassed, the amount of martensite formed increases with increasing plastic strain. It is further postulated that the shear resistance to martensite formation decreases with decreasing temperature, while the shear resistance towards slip ncreases with decreasing temperature.

The decrease in martensite with increasing strain rate at a given test temperature could be anticipated from either a) the increased heat retained in samples deformed at high speeds (which would by Scheil's theory give less martensite), or b) an increase in the stress required for martensite formation with increasing strain rate (which could be expected on dynamical grounds).

(If the stress reached during deformation drops with strain rate a decrease in martensite formation would also be expected, since this would mean that the resistance towards martensite formation might not be as readily overcome. At room temperature, for example, the fracture stress varied from 257,000 psi. at 0.05 in./in./min. to 237,000 psi at 10 in./in./min.)

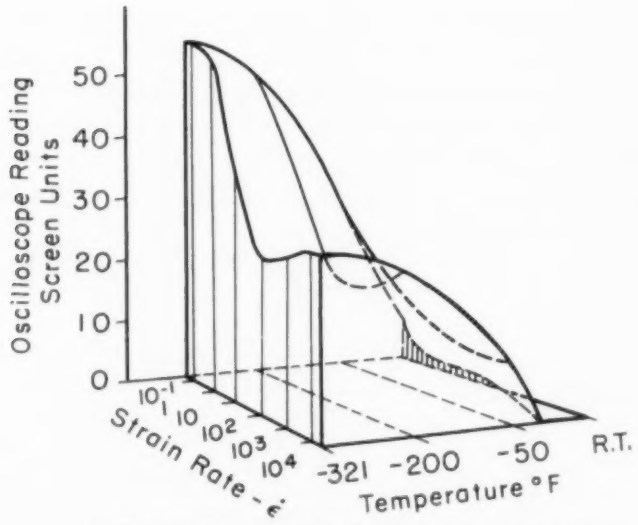


Fig. 6—Effect of Test Temperature and Strain Rate on the Magnetic Behavior of AISI 303 Stainless Steel.

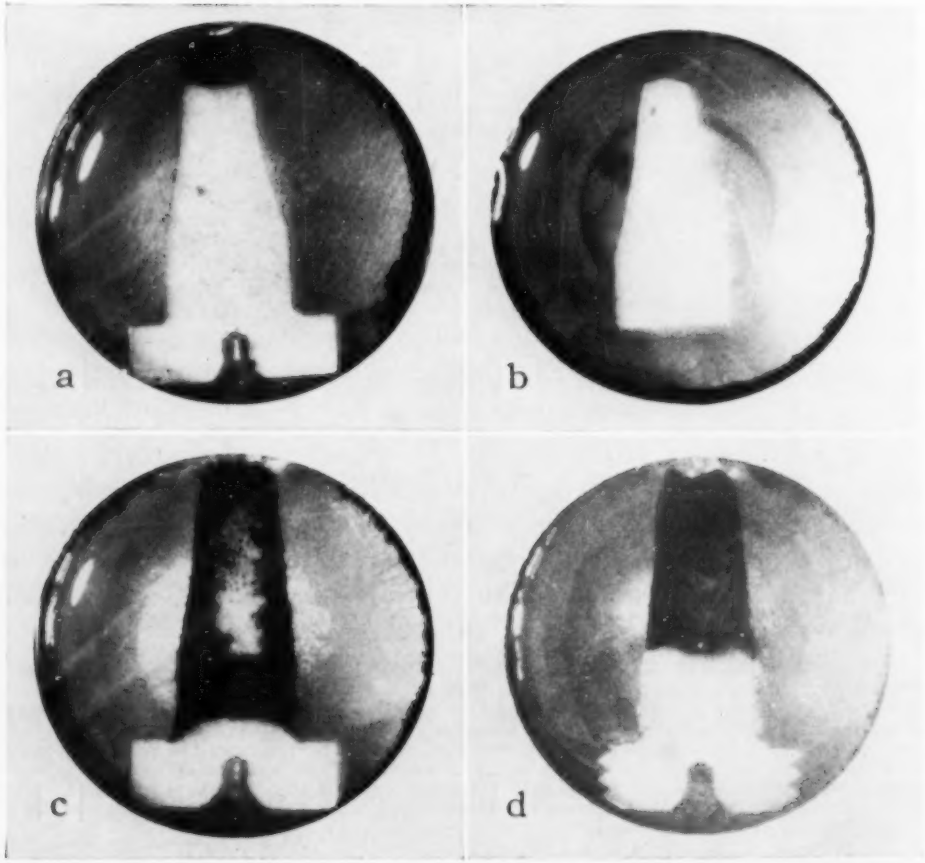


Fig. 7—(a-d): Magnetic Powder Patterns on Broken AISI 303 Stainless Steel Specimens. ×15.
(a) Specimen Pulled At: R.T.; 0.05 in./in./min.
(b) Specimen Pulled At: R. T.19,000 in./in./min.
(c) Specimen Pulled At: −321°; 0.05 in./in./min.
(d) Specimen Pulled At: −321°; 19,000 in./in./min

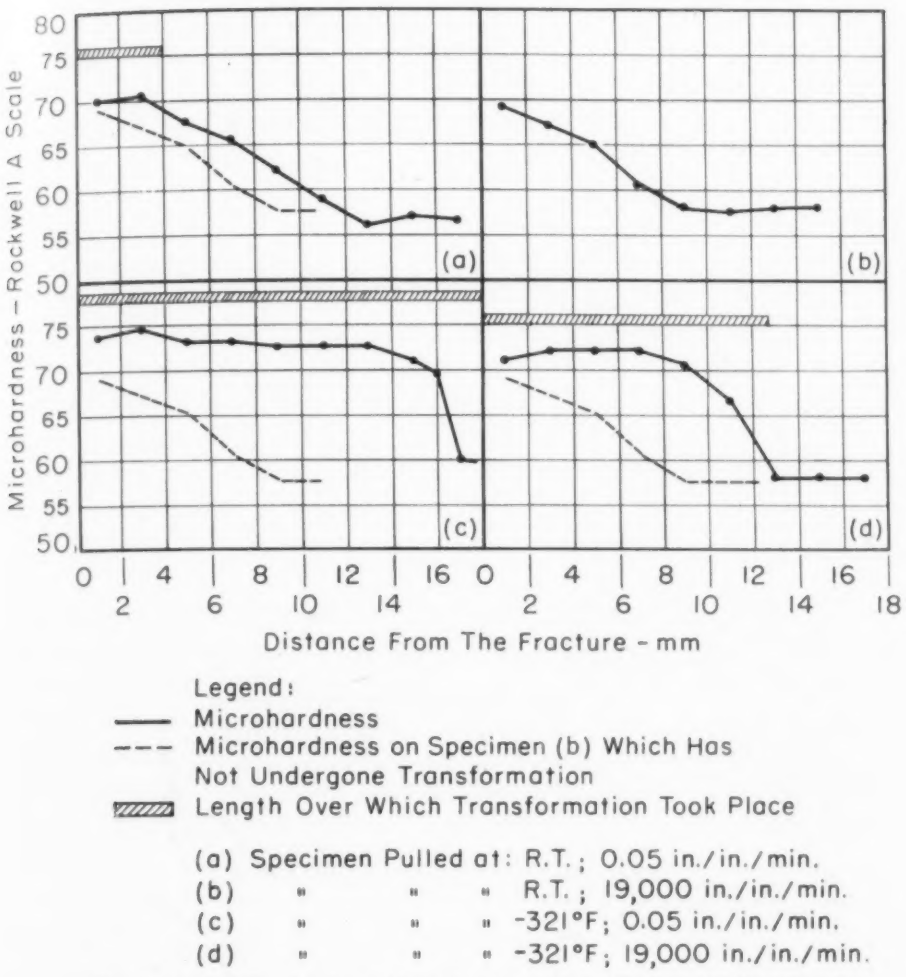


Fig. 8—(a-d): Microhardness Along the Centerline of Broken AISI 303 Tensile Specimens.

two specimens pulled at room temperature (0.05 and 19000 in./in./min., respectively), and two at −321°F (0.05 and 19000 in./in./min., respectively)—is shown by the magnetic powder patterns in Fig. 7. The amount of magnetic particles attached to the samples agrees qualitatively with the result obtained by the induction method in that they indicate that the amount of α-phase decreases with both increasing strain rate and temperature. The specimen tested at room temperature at a strain rate of 19000 in./in./min. did not undergo any detectable transformation, which is in agreement with results given by Krivobok and Talbot (11).

The microhardness tests made along the longitudinal centerline of the above four specimens are given in Fig. 8. The three samples which had undergone transformation show an excess in hardness over that of the sample pulled at 19000 in./in./min. at room tem-

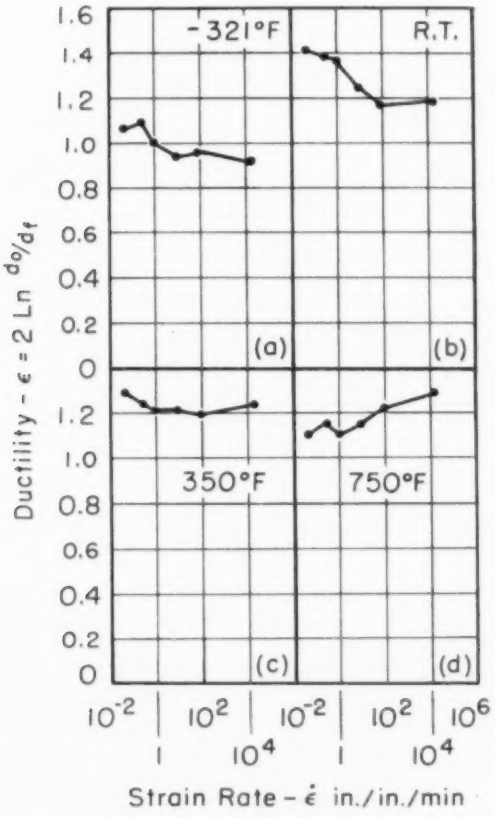


Fig. 9—(a-d): Ductility of AISI 310 Stainless Steel as a Function of Strain Rate at Various Test Temperatures.

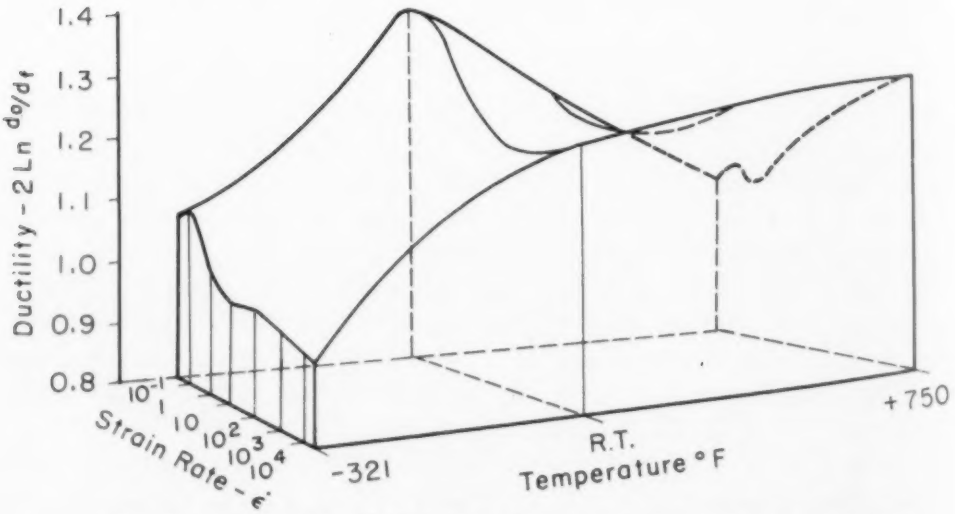


Fig. 10—Ductility of AISI 310 Stainless Steel as a Function of Strain Rate and Test Temperature.

perature which had undergone no transformation. At the same time the length of that portion of the specimen that evidences transformation in the magnetic sol test is greater than that over which the hardness shows a constant high value.

AISI 310 Stainless Steel

The ductility of the 310 stainless steel as a function of strain rate at various temperatures is given in Figs. 9 and 10. The temperature effect on the ductility of the AISI 310 steel is similar to that of the AISI 303 steel. At low strain rates the ductility first rises with temperature, reaches a maximum at room temperature, and then decreases at higher test temperatures. At high strain rates the ductility increases slowly with increasing test temperature.

Magnetic measurements did not reveal any α-phase in any of the 310 specimens, even those deformed at $-321°F$.[5a]

Discussion

It appears that most if not all of the peculiarities in the ductility behavior of austenitic steels must be explained on some other basis than the γ-α transformation. The principal evidence for this conclusion is:

i) Both the 303 (18-8) and 310 (25-20) stainless steel possess similarly shaped ductility *vs.* temperature and strain rate surfaces, yet the 310 steel shows no γ-α transformation at any temperature or strain rate.

ii) Even in the 303 (18-8) steel no γ-α transformation is found above room temperature where ductility drops with increasing strain rate.

iii) Where the γ-α transformation is found in 303 (18-8) steel (room temperature and below) it is found in amounts that bear no direct relationship with ductility behavior; at constant strain rates a drop in temperature increases the amount of α-phase formed but decreases ductility; at constant test temperature an increase in strain rate drops *both* ductility and the amount of α-phase formed.

iv) Sundry experiments appear to show that the amount of α-phase can be without influence on ductility; A 303 stainless steel test specimen, for example, was prestrained at $-321°F$ and 0.05 in./in./min. to the "upper yield point," which becomes very pronounced at this low temperature. The purpose of this operation was to render the specimen magnetic at the smallest prestrain possible. (The diameter after prestraining was 0.002 inch smaller than before.) The specimen was easily attracted by a hand magnet, indicating that transformation had taken place during prestraining at $-321°F$. The

[5a] X-ray diffraction patterns of 310 steel deformed at $-321°F$ showed no α-phase lines although patterns from the 303 steel deformed at $-321°F$ did.

specimen was then pulled at room temperature and a strain rate of 0.05 in./in./min. The total ductility thus obtained equaled the one of the specimen which was tested at room temperature and 0.05 in./in./min. without prestraining. The broken halves of the prestrained specimen were magnetically inspected by means of the induction method and revealed an oscilloscope reading of 18 screen units. Although the amount of α-phase formed was more than 3 times as high as in the nonprestrained specimen (which Fig. 5a shows ran about 5.5 units), the ductility in the two specimens was the same.[6]

To complete the record, it should be mentioned that the gradual drop in ductility with increasing strain rate observed here in austenitic stainless steels is not to be confused with the sudden drop in ductility with strain rate that von Kármán predicts for all metals because of the finite speed of propagation of plastic deformation (13). The velocity at which this sudden drop in ductility should occur has been variously calculated and determined experimentally to be between 3600 inches per minute and 144000 inches per minute (1,4,14), whereas the gradual drop in ductility described here occurs at strain rates as low as 0.01 in./in./min.

Conclusions

1. At low strain rates 303 and 310 austenitic stainless steels have a maximum ductility at room temperature as test temperature is varied.
2. At high strain rates ductility increases steadily as the test temperature is increased.
3. The loss in ductility at high strain rates is greatest at room temperature.
4. The γ-α transformation can not account for these unusual features in ductility.

References

1. D. S. Clark and G. Dätwyler, "Stress-Strain Relation Under Tension Impact Loading," *Proceedings*, American Society for Testing Materials, Vol. 38, 1938, p. 98.

[6]The microhardness results of the low carbon AISI 303 steel (C = 0.045%) seem to indicate that the α-formation is of little, if any, influence on the hardness. By comparing the data of the two specimens pulled at room temperature at strain rates of 0.05 and 19000 in./in./min., Fig. 7a and b, it can be seen that the hardness near the fracture is practically the same for both specimens, although only the one pulled at 0.05 in./in./min. has undergone transformation. Furthermore the true stress—true strain curve of the AISI 303 steel obtained at room temperature is similar to that of the AISI 310 steel, and the increase in fracture stress is about 65% for both the stable and the metastable steel, if the test temperature is lowered from room temperature to −321°F. One could conclude from these results that the high work hardening in stainless steel is rather a property of the austenitic phase and not due to the γ-α transformation. On this basis it can also be understood why the hardness in Fig. 8 does not show a discontinuity at that point of the centerline where the transformation ceases to take place. The fact that the distance from the cross-section over which α-phase was formed exceeds the length over which the hardness is constant, indicates that the maximum resolved shear stress built up in the specimen is higher than the stress necessary to initiate the γ-α transformation. The above discussion, however, does not exclude the possibility that the influence of the α-phase on the work hardening becomes more pronounced, if the carbon content is considerably higher than in the AISI 303 stainless steel.

2. G. Jones and H. F. Moore, "An Investigation of the Effect of Rate of Strain on the Results of Tension Tests of Metals," *Proceedings*, American Society for Testing Materials, Vol. 40, 1940, p. 610.
3. E. R. Parker and C. Ferguson, "The Effect of Strain Rate on the Tensile Impact Strength of Some Metals," TRANSACTIONS, American Society for Metals, Vol. 30, 1942, p. 68.
4. D. S. Clark and D. S. Wood, "The Tensile Impact Properties of Some Metals and Alloys," TRANSACTIONS, American Society for Metals, Vol. 42, 1950, p. 45.
5. "Cooperative Study of the Effect of Rate of Strain on the Tensile Properties of Stainless Steel," Report of Subcommittee V on Mechanical Tests, *Proceedings*, American Society for Testing Materials, Vol. 44, 1944, p. 133.
6. W. O. Binder, "Effect of Cold Work at Low Temperature on Austenitic 18-8 Stainless Steel," METAL PROGRESS, American Society for Metals, Vol. 58, August 1950, p. 201.
7. M. Cohen, "Principles of the Austenite-Martensite Reaction," TRANSACTIONS, American Society for Metals, Vol. 41, 1949, p. 35.
8. K. Mathieu, "Einfluss von Legierungsgehalt und Versuchsbedingungen auf die γ-α Umwandlung bei der Kaltverformung austenitischer Stahle," Mitteilungen aus dem Kaiser Wilhelm Institut fur Eisenforschung, Vol. 24, 1942, p. 243.
9. W. C. Elmore, "Ferromagnetic Colloid for Studying Magnetic Structures," *Physical Review*, Vol. 54, 1938, p. 309.
10. B. L. Averbach, S. A. Kulin, M. Cohen, "The Effect of Plastic Deformation on Solid Reactions," COLD WORKING OF METALS, American Society for Metals, 1949, p. 309.
11. V. N. Krivobok and A. M. Talbot, "Effect of Temperature on the Mechanical Properties, Characteristics and Processing of Austenitic Stainless Steel," *Proceedings*, American Society for Testing Materials, Vol. 50, 1950, p. 895.
12. E. Scheil, "Uber die Umwandlung des Austenits in Martensit in Eisen-Nickel-Legierungen unter Belastung," *Zeitschrift fur anogranische und allegmeine Chemie*, Vol. 207, 1932, p. 21.
13. Th. von Kármán, "On the Propagation of Plastic Deformation in Solids," National Defence Research Committee Report No. A-29 OSRD, No. 365, February 2, 1942.
14. H. C. Mann, "The Relation Between the Tension Static and Dynamic Test," *Proceedings*, American Society for Testing Materials, Vol. 35, 1935, p. 323.

ROOM AND ELEVATED TEMPERATURE MECHANICAL PROPERTIES OF AISI TYPE 414 AND TYPE 431 STAINLESS STEELS

By E. J. Dulis, S. J. Parker, and P. W. Marshall

Abstract

Room temperature tensile properties, elevated temperature tensile properties in the range 700 to 1100°F, and creep and creep-rupture properties in the range 900 to 1200°F were determined for normal nitrogen (0.015%) AISI Type 414, for high-nitrogen (0.124%) AISI Type 414, for normal nitrogen (0.010%) Type 431, and for high nitrogen (0.063%) Type 431 steels. Also, keyhole-notch transition temperatures were determined for the normal nitrogen steels. (ASM-SLA Classification: Q27, Q3, Q4, Q6, SS)

ALTHOUGH AISI Type 414 (12% Cr, 2% Ni) and Type 431 (16% Cr, 2% Ni) stainless steels have been used for many years, little information is available on the mechanical properties of these steels at elevated temperatures. To evaluate the applicability of these steels as materials for the construction of equipment that is used under stress at elevated temperatures, the Applied Research Laboratory of the United States Steel Corporation determined the room temperature tensile properties, the elevated temperature tensile properties in the range 700 to 1100°F, the creep and creep-rupture properties in the range 900 to 1200°F, and the keyhole-notch Charpy transition temperatures of the steels.

In addition, the room temperature and elevated temperature tensile properties and the creep and creep-rupture properties of Type 414 and Type 431 steels with high nitrogen contents (0.124 and 0.063%, respectively) were determined to evaluate the effect of nitrogen on the properties of these steels.

Materials and Experimental Work

Materials

Two of the four steels for the present investigation, a high-nitrogen Type 414 and a high-nitrogen Type 431 steel, were cast as 30-pound induction furnace ingots. The third, a normal nitrogen Type 414 steel, was cast as a 100-pound induction furnace ingot. These three ingots were forged to ⅝ and 1½-inch square bars. The

Of the authors, S. J. Parker and P. W. Marshall are associated with the United States Steel Corp., Applied Research Laboratory, Monroeville, Pa. E. J. Dulis was formerly associated with this department and is now supervisor, Research Laboratory, Crucible Steel Co. of America, Pittsburgh. Manuscript received May 2, 1955.

fourth steel, a normal nitrogen Type 431 steel, was obtained from a commercial electric furnace heat as ¾-inch diameter forged bars. Table IA shows the chemical composition of the steels.

That the compositions of the steels meet the requirements of AISI specifications (1)[1] is evident from the information given in Tables IA and IB. Although no limits are set by the AISI on nitrogen content, the nitrogen contents of Steel B (0.124%) and Steel D (0.063%) are very high in comparison with the nitrogen content of Steel C (0.010%), a commercial steel with a normal nitrogen content.

Table IA
Compositions of Steels Investigated—Per Cent Ladle Analyses

Steel	AISI Type	C	Mn	P	S	Si	Ni	Cr	N
A	414 (Normal N)	0.13	0.78	0.008	0.017	0.71	1.88	12.31	0.015
B	414 (High N)	0.13	0.58	0.022	0.017	0.52	1.82	12.37	0.124
C	431 (Normal N)	0.11	0.37	0.007	0.018	0.17	1.87	15.60	0.010
D	431 (High N)	0.16	0.58	0.021	0.022	0.53	1.82	16.13	0.063

Inasmuch as the mechanical properties of the present steels are subsequently compared with those of 12 and 17% chromium, nickel-free stainless steels, the AISI chemical composition limits for the nickel-free steels, Types 410 and 430, are also shown in Table IB.

Table IB
AISI Composition Limits for Types 414, 431, 410, and 430 Stainless Steel—Per Cent

AISI Type	C	Mn	P	S	Si	Ni	Cr
414	0.15	1.00	0.04	0.03	1.00	1.25	11.5
	max	max	max	max	max	2.50	13.5
431	0.20	1.00	0.04	0.03	1.00	1.25	15.0
	max	max	max	max	max	2.50	17.0
410	0.15	1.00	0.04	0.03	1.00	—	11.5
	max	max	max	max	max		13.0
430	0.12	1.00	0.04	0.03	1.00	—	14.0
	max	max	max	max	max		18.0

Heat Treatments and Hardnesses

Prior to being tested, bars of each of the four steels were austenitized at 1800°F for ½ hour, oil-quenched, tempered at 1225°F for 4 hours, and oil-quenched. (Hereafter, reference to a steel in the quenched condition means a steel oil-quenched from 1800°F.) The Rockwell hardness of the steels in the quenched condition and the Brinell hardness of the steels in the quenched and tempered condition were determined. The Brinell hardness values were subsequently converted to Rockwell C hardness values.

[1]The figures appearing in parentheses pertain to the references appended to this paper.

Tension Tests

Room temperature tension tests were made on each of the four steels in the quenched and tempered condition. Subsize (0.252-inch diameter) specimens were tested in duplicate.

Elevated temperature tension tests at 700, 900, and 1100°F were made on each of the four steels in the quenched and tempered condition. In these tests, special 0.254-inch diameter tensile specimens were used.

Creep-Rupture Tests

Creep-rupture tests were conducted at 900, 1100, and 1200°F on each of the four quenched and tempered steels, 0.252-inch diameter specimens being used. Creep data for the steels were obtained from the autographic time-elongation curves recorded during the creep-rupture tests. In addition, the Rockwell B hardness of each steel was determined on the specimens that ruptured after the longest time at each test temperature.

Impact Tests

Keyhole-notch Charpy impact tests were made on the normal nitrogen steels of each type (Steels A and C, Table IA) in the quenched and tempered condition. The specimens were broken at temperatures in the range room temperature to —320°F so that ductility-transition temperatures might be determined.

Because all the material from the two high nitrogen steels (Steels B and D, Table I) was used in making specimens for the aforementioned tension and creep-rupture tests and because the main interest in impact strength was in the normal-nitrogen steels, we did not believe that the making of additional high nitrogen steels for impact test studies was warranted. Therefore, impact tests were not made on the high nitrogen steels.

Metallographic and X-ray Studies

Metallographic examinations were made on specimens of each of the four steels in the quenched and tempered condition prior to testing and after the longest exposure time at each creep-rupture test temperature. The austenite grain size of each steel was estimated by a comparison of the microstructure of quenched and tempered specimens with ASTM standard grain size charts.

Furthermore, microhardness measurements were made on the regions of untempered martensite observed in the matrix of quenched and tempered specimens of the high nitrogen Type 431 steel (Steel D).

X-ray diffraction patterns were obtained for each of the four steels in the quenched and in the quenched and tempered condition.

From these diffraction patterns, the amount of retained austenite in the steels in each condition was determined.

Results and Discussion

Heat Treatments and Hardnesses

The hardness of each of the steels in the quenched and in the quenched and tempered condition is shown in Table II. The hardness of the oil-quenched normal nitrogen Type 414 steel, Rockwell C-47.2, is about the same as that reported (2) for 0.13% carbon, 12% chromium steels, Rockwell C-48, but the hardness of the high nitrogen Type 414 steel is slightly higher, Rockwell C-50.8. For the

Table II
Hardness and Grain Size of the Steels

Steel	AISI Type	Hardness, Rockwell C: Quenched Condition*	Hardness, Rockwell C: Quenched and Tempered Condition**	Austenite Grain Size, ASTM No.
A	414 (Normal N)	47.2	22.2	6 to 7
B	414 (High N)	50.8	20.9	6 to 7
C	431 (Normal N)	45.5	22.0	6
D	431 (High N)	49.7	36.7	8

*Oil-quenched from 1800°F.
**Oil-quenched from 1800°F and tempered at 1225°F. For the quenched and tempered steels, Brinell hardness measurements were made and were converted to Rockwell C hardnesses.

oil-quenched Type 431 steels, the hardness of the normal nitrogen steel is about the same as that reported (2) for 0.11% carbon, 12% chromium steels, Rockwell C-45.5; the hardness of the high nitrogen steel is lower than expected in view of the carbon and nitrogen contents of the steel. However, as will be discussed in a subsequent section of this report, the retained austenite in the high nitrogen Type 431 steel in the quenched condition probably accounts for the low hardness of the steel.

After being tempered for 4 hours at 1225°F, the two Type 414 steels and the low nitrogen Type 431 steel exhibit about the same hardness, Table II. The hardness of the high nitrogen Type 431 steel after an identical tempering treatment, however, is markedly higher than that of the other three steels. The high hardness is probably a consequence of the transformation of the aforementioned austenite to martensite during cooling from the tempering temperature.

The austenite grain size of the four steels is also shown in Table II. It is evident that except for the high nitrogen Type 431 steel, the steels have about the same austenite grain size, ASTM No. 6 to 7. The austenite grain size of the high nitrogen Type 431 steel is finer than those of the other steels by about 1½ to 2 ASTM numbers.

Tension Tests

Room Temperature Tensile Properties. The room temperature tensile data in Table III indicate that the tensile properties of the normal nitrogen steels of both types, Steels A and C, do not differ markedly. Each of the high nitrogen steels (Steels B and D) has a higher tensile strength and a lower tensile ductility than its normal nitrogen counterpart. Inasmuch as it has been shown previously (3) that the transformations in iron-nitrogen alloys are similar to those in iron-carbon alloys, one might expect the strength and ductility of the high nitrogen steels to be similar to those of steels with higher carbon contents than those of the present steels. The tensile strength of Steel B (with the highest nitrogen content) is only about 10,000 psi higher than that of Steel A, whereas the tensile strength of Steel D (with about half the nitrogen of Steel B but with the highest carbon content) is about 50,000 psi higher than that of Steel C. The very high tensile strength, the low yield-tensile ratio, and the low ductility of Steel D are probably associated with the untempered martensite that apparently formed in this steel during cooling from the tempering temperature. Although Steel D exhibits a low yield-tensile ratio, the yield strength of this steel is the highest of the steels investigated. Because of the previously mentioned simi-

Table III
Room Temperature Tensile Properties of AISI Types 414, 431, 410, and 430 Stainless Steel

A. Data Obtained in the Present Investigation

Steel	AISI Type	Yield Strength (0.2% Offset), psi	Tensile Strength, psi	Elongation in 1 Inch, %	Reduction of Area, %
A	414 (Normal N)	94,000	116,400	21.5	64.6
B	414 (High N)	90,400	126,800	14.0	34.7
C	431 (Normal N)	83,200	112,500	21.5	60.4
D	431 (High N)	107,800	163,100	8.0	12.7

B. Data Reported in the Literature*

AISI Type	Heat Treatment	Yield Strength (0.2% Offset), psi	Tensile Strength, psi	Elongation in 2 Inches, %	Reduction of Area, %
414	Oil-quenched from 1800°F and tempered at 1200°F	105,000	120,000	20.0	65.0
431	Oil-quenched from 1900°F and tempered at 1200°F.	95,000	125,000	20.0	60.0
410	Oil-quenched from 1800°F and tempered at 1200°F.	85,000	110,000	23.0	65.0
430	Annealed	45,000	75,000	30.0	65.0

*Data from Reference 1.
Note: In the present investigation, ⅝-inch-square bars of Steels A, B and D and ¾-inch-diameter bars of Steel C were austenitized for ½ hour at 1800°F, oil-quenched, tempered for 4 hours at 1225°F, and oil-quenched. Subsize (0.252-inch-diameter) specimens were tested in duplicate.

larity in the effect of carbon and nitrogen on the transformations in iron, the high nitrogen content of Steel D probably contributed to the retention of austenite on quenching and to the subsequent formation of martensite during cooling from the tempering temperature. Further discussion of the effect of the martensite formed during cooling from the tempering temperature is presented later.

Shown in Table III are tensile properties reported to be representative of commercial Type 414 and Type 431 steels (1). It will be noted that the yield and the tensile strengths of the present normal nitrogen steels (Steels A and C) are somewhat lower than the nominal yield and tensile strengths reported (1) for these grades. That the present steels were tempered at a higher temperature than were the steels for which the nominal properties are reported, probably accounts for the differences in strength. The tensile ductility of each of the present steels is similar to the tensile ductility reported for the commercial steels.

The nominal tensile properties reported (1) for Type 410 and Type 430 steel—the nickel-free counterparts of Type 414 and Type 431 steels, respectively—are also listed in Table III. Although the yield and tensile strengths of the present Type 414 steel (Steel A) are only slightly higher than those of the Type 410 steel, the yield and tensile strengths of the present Type 431 steel (Steel C) are considerably higher than those of the Type 430 steel. The latter circumstance is to be expected because Type 430 steel is a nonhardenable steel, and the properties reported are for an annealed steel. The tensile ductility of the present Type 414 steel is similar to that of the Type 410 steel, but as might be expected, the tensile ductility of the Type 431 steel is lower than that of the Type 430 steel.

Elevated Temperature Tensile Properties. The results of the elevated temperature tension tests at 700, 900, and 1100°F are given in Table IV. At 700°F, the normal nitrogen Type 414 steel (Steel A) has a higher yield and a higher tensile strength than the normal nitrogen Type 431 steel (Steel C); at 900°F, the Type 414 steel has only slightly higher strength; and at 1100°F, the Type 431 steel has slightly higher strength. Both the elongation and the reduction of area of the Type 414 steel are higher than those of the Type 431 steel.

A comparison of the properties of Steels A and B and of Steels C and D, Table IV, indicates that in general, the effect of nitrogen is to raise the yield and the tensile strengths and to lower the ductility of the two grades of steel at elevated temperatures. It is evident, however, that as the test temperature increases, the effect of nitrogen becomes less pronounced. That the strength of the high nitrogen Type 431 steel (Steel D) decreases greatly and that the

Table IV
Elevated Temperature Tensile Properties of AISI Types 414, 431, 410, and 430 Stainless Steel

Steel	AISI Type	Test Temp, °F	Yield Strength (0.2% Offset), psi	Tensile Strength, psi	Elongation in 1 Inch, %	Reduction of Area, %
		A. Data Obtained in the Present Investigation				
A	414 (Normal N)	700	78,400	101,300	18.0	59.0
		900	*	77,200	26.3	73.0
		1100	29,600	45,700	42.3	87.0
B	414 (High N)	700	86,500	122,500	11.0	15.0
		900	67,000	87,000	22.5	53.0
		1100	35,400	49,700	**	89.0
C	431 (Normal N)	700	71,500	89,800	15.0	43.0
		900	61,800	75,200	16.0	46.0
		1100	33,200	49,100	27.0	77.0
D	431 (High N)	700	112,200	156,400	6.0	10.0
		900	92,200	135,000	11.0	62.0
		1100	31,000	51,400	52.5	86.0
		B. Data Reported in the Literature+				
	410	700	—	71,000	21	70
		900	—	58,000	23	73
		1100	—	34,000	41	87
	430	700	33,000	58,000	28	70
		900	28,500	48,500	34	74
		1100	18,000	30,500	47	87

*The autographic stress-strain curve obtained was unsatisfactory for the determination of the yield strength.
**Fracture of test specimen occurred outside of the gage marks.
+Data from Reference 4.
Notes: In the present investigation, ⅝-inch square bars of Steels A, B, and D were austenitized for ½ hour at 1800°F, oil-quenched, tempered for 4 hours at 1225°F, and oil-quenched. Special 0.254-inch diameter specimens were tested in duplicate. Also, ¾-inch diameter bars of Steel C were heat treated by the aforementioned practice, and then standard 0.505-inch diameter specimens were tested in duplicate. Therefore, the elongation in 2 inches is reported for Steel C.
For the data from the literature, the elongation is in 2 inches.

ductility increases greatly as the test temperature is increased from 900 to 1100°F, can be attributed, at least in part, to the softening of the untempered martensite that was formed during cooling from the tempering temperature.

Table IV also shows that in the range 700 to 1100°F, the normal nitrogen Types 414 and 431 steels have higher strength and lower ductility than their nickel-free counterparts, Types 410 and 430 steels, respectively. Furthermore, the difference between the elevated temperature tensile strengths of the nickel and the nickel-free steels decreases as the test temperature increases. However, it is important to note that the data given in Table IV for Type 410 and Type 430 steels (4) represent conservative averages of data from many sources and for the steels in different heat treated conditions.

Creep-Rupture Tests

The results of the creep-rupture tests are summarized in Table V and are plotted in Figs. 1 to 8. At 900°F, the 1000-hour creep-

Table V
Creep-Rupture Properties of AISI Types 414, 431, 410, and 430 Stainless Steel

Steel	AISI Type	Test Temperature, °F	Stress, 1000 psi, for Rupture in 1000 hr	Stress, 1000 psi, for Rupture in 10,000 hr*	Stress*, 1000 psi, for a Creep Rate of 0.001 Per Cent Per Hour (1% in 1000 hr)
		A. Data Obtained in the Present Investigation			
A	414 (Normal N)	900	26.0	19.2	15.8
		1100	8.7	5.6	5.2
		1200	6.3	4.0	4.0
B	414 (High N)	900	28.0	20.0	19.0
		1100	8.8	5.1	4.6
		1200	5.6	3.2	2.7
C	431 (Normal N)	900	34.0	23.0	20.0
		1100	10.5	6.8	5.3
		1200	5.7	3.5	3.3
D	431 (High N)	900	34.5	24.0	21.0
		1100	10.8	7.1	5.9
		1200	6.0	3.7	3.4
		B. Data Reported in the Literature			
	410	900	34.0[1]	26.0[1]	**
		1100	10.0[1]	6.9[1]	**
		1200	4.9[2]	3.0[2]	**
	430	900	30.0[1]	24.0[1]	**
		1100	9.1[1]	6.5[1]	**
		1200	5.0[1]	3.4[1]	**

*Extrapolated values.
**No data available.
[1] Data from Reference 4.
[2] Data from Reference 5.

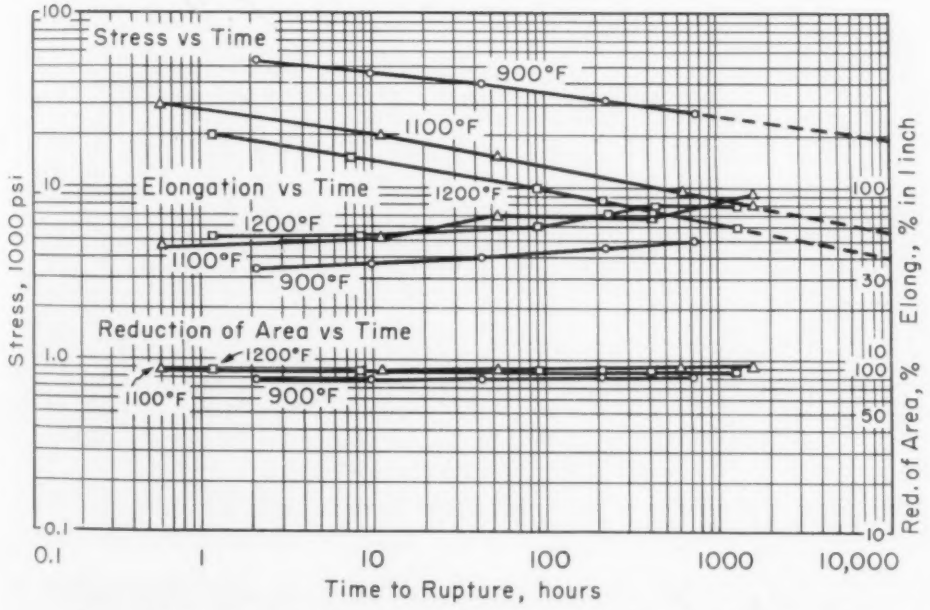


Fig. 1—Creep-Rupture Properties of Normal Nitrogen Type 414 Stainless Steel (Steel A) at 900, 1100, and 1200°F.

rupture strength of the normal nitrogen Type 431 steel (Steel C) is 8000 psi higher than that of the normal nitrogen Type 414 steel

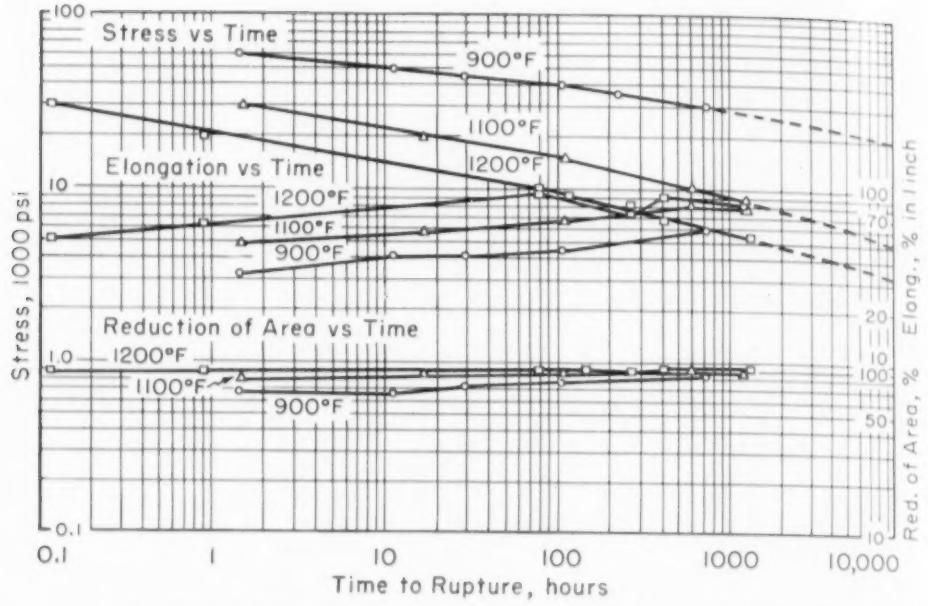


Fig. 2—Creep-Rupture Properties of High Nitrogen Type 414 Stainless Steel (Steel B) at 900, 1100, and 1200°F.

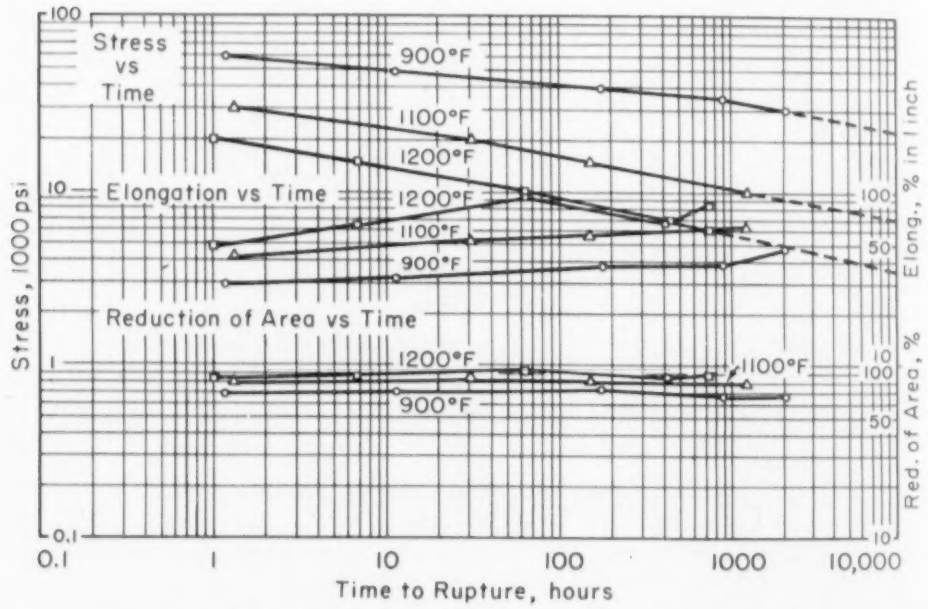


Fig. 3—Creep-Rupture Properties of Normal Nitrogen Type 431 Stainless Steel (Steel C) at 900, 1100, and 1200°F.

(Steel A); at 1100°F, the strength of Steel C is only about 2000 psi higher than that of Steel A; and at 1200°F, the strength of Steel A is slightly higher than that of Steel C. A similar trend with increasing temperature may be observed for the 10,000-hour creep-rupture strengths of the two steels.

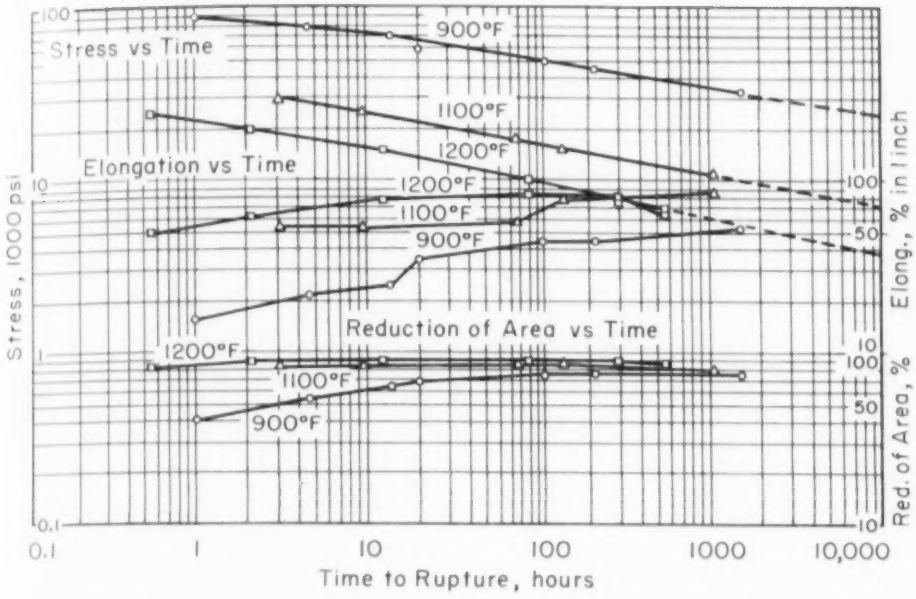


Fig. 4—Creep-Rupture Properties of High Nitrogen Type 431 Stainless Steel (Steel D) at 900, 1100, and 1200°F.

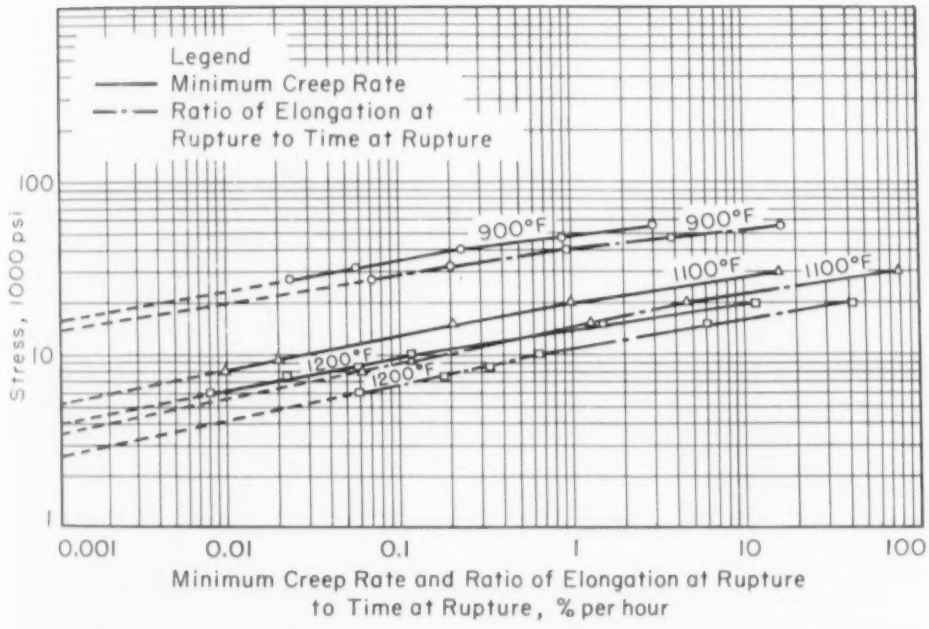


Fig. 5—Creep-Rupture Properties of Normal Nitrogen Type 414 Stainless Steel (Steel A) at 900, 1100, and 1200°F.

That high nitrogen contents contribute little to long time creep-rupture strength is evident from the similarity in the strengths of Steel A and Steel B and in those of Steel C and Steel D. Indeed, except for the differences at 900°F, the creep-rupture strengths of the four steels are very nearly the same. This may also be seen

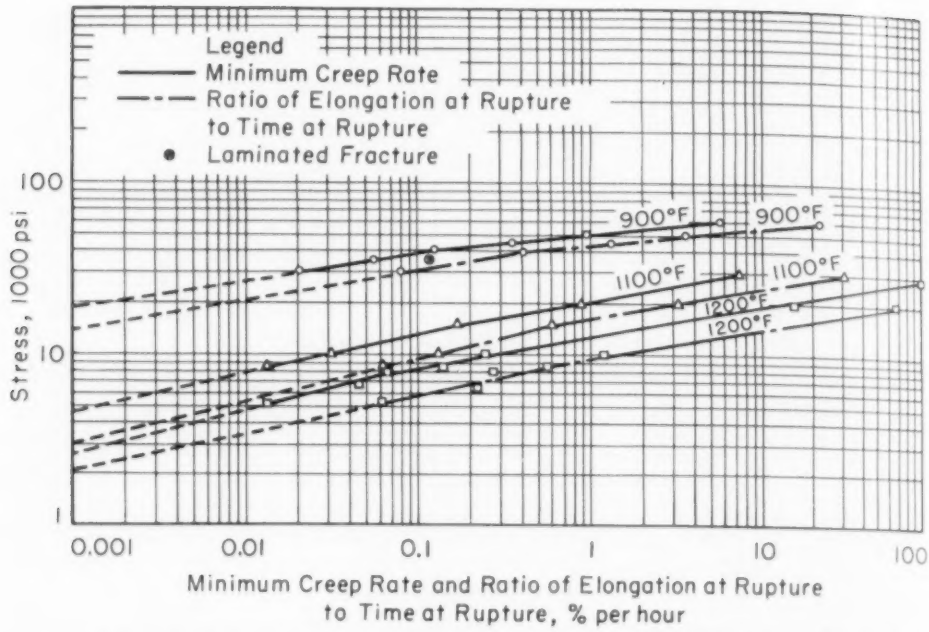


Fig. 6—Creep-Rupture Properties of High Nitrogen Type 414 Stainless Steel (Steel B) at 900, 1100, and 1200°F.

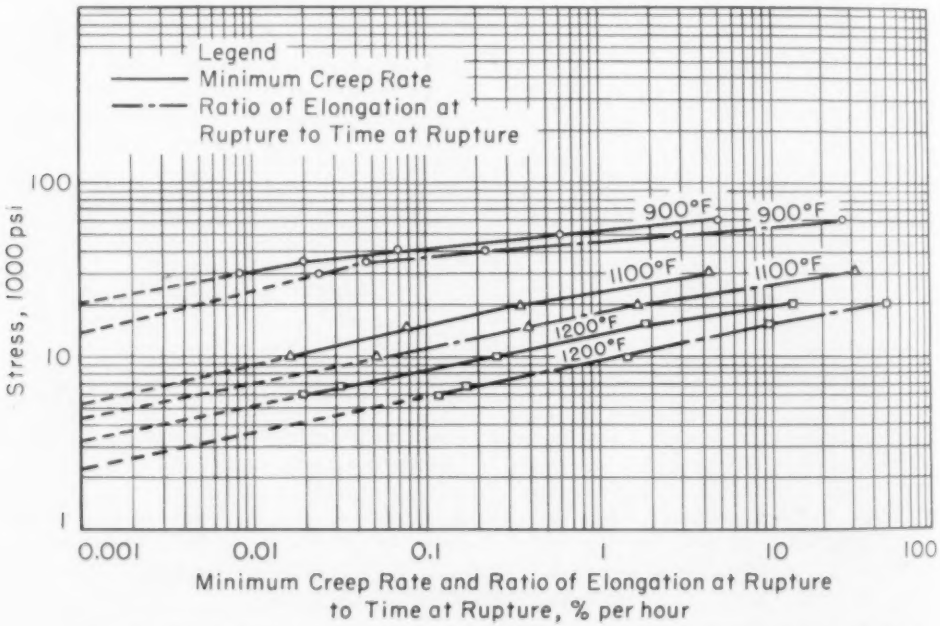


Fig. 7—Creep-Rupture Properties of Normal Nitrogen Type 431 Stainless Steel (Steel C) at 900, 1100, and 1200°F.

from the curves of Fig. 9, which were plotted from the creep-rupture data in Table V. The creep-data listed in Table V are also plotted in Fig. 9, and it appears that except for the differences between Steels A and B at 900 and 1200°F, the high nitrogen contents do not have a significant effect on the stress for a minimum creep rate of 0.001%

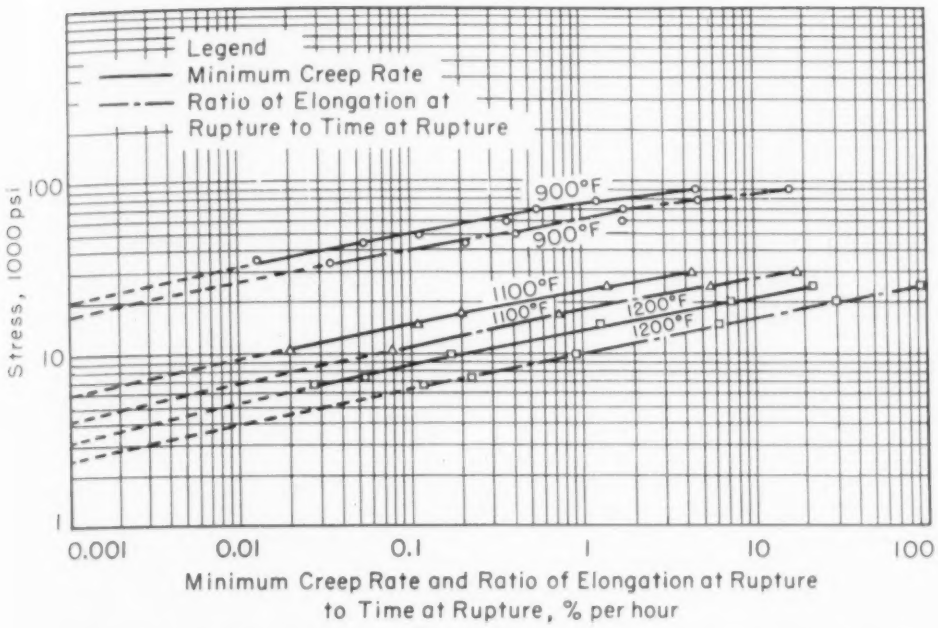


Fig. 8—Creep-Rupture Properties of High Nitrogen Type 431 Stainless Steel (Steel D) at 900, 1100, and 1200°F.

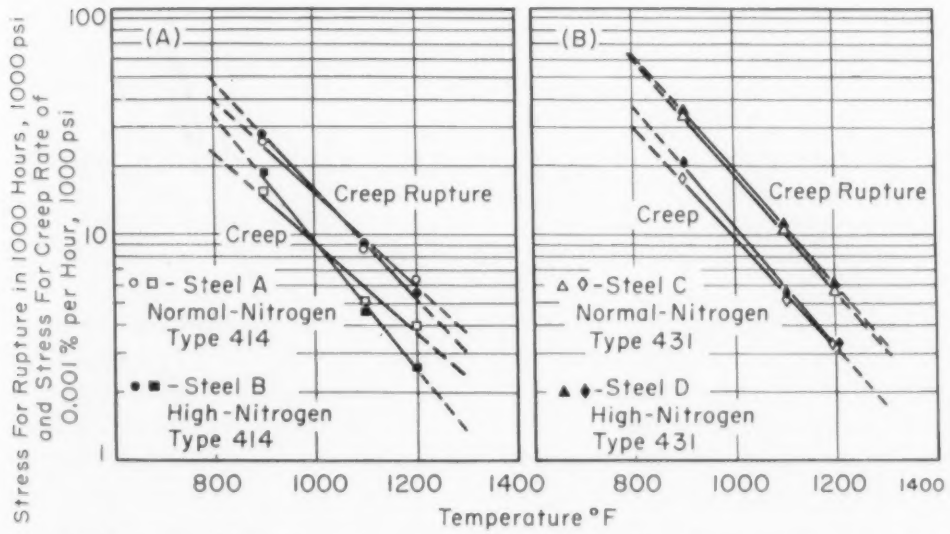


Fig. 9—Creep-Rupture and Creep Strength as a Function of Temperature for Type 414 and Type 431 Stainless Steel.

per hour. At 900°F the high nitrogen Type 414 steel has a creep strength about 3000 psi higher than that of the normal nitrogen Type 414 steel, but at 1200°F the high nitrogen steel has a creep strength about 1300 psi lower than that of the normal nitrogen steel, Table V. The creep strength of the high nitrogen Type 431 steel at 900°F is higher than that of the normal nitrogen Type 431 steel, but both steels have about the same creep strength at 1200°F.

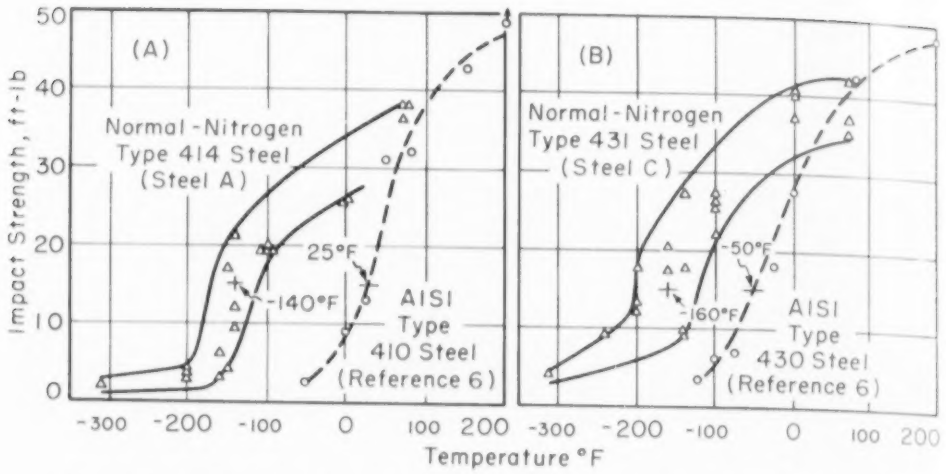


Fig. 10—Keyhole-Notch Charpy Impact Curves for Normal Nitrogen Type 414 and 431 Steels and for Type 410 and 430 Steels.

Some creep-rupture data reported in the literature (4,5) for 12% chromium steel (Type 410) and for 17% chromium steel (Type 430) are included in Table V. It is apparent from these data that the 1000 and 10,000-hour strengths of the 12% chromium steel at 900 and 1100°F are greater than those of the 12% chromium, 2% nickel steel (Type 414), but that these creep-rupture strengths of the straight chromium steels at 1200°F are slightly lower than those of the chromium-nickel steels at 1200°F. In the range 900 to 1200°F, the 1000-hour creep-rupture strengths of the 16% chromium, 2% nickel steel (Type 431) are slightly higher than those of the 17% chromium steel, but the 10,000-hour strengths of the two steels are about the same.

Impact Tests

The results of keyhole-notch Charpy impact tests on quenched and tempered specimens of the normal nitrogen Type 414 and Type 431 steels (Steels A and C) are plotted as a function of test temperature in Fig. 10. The ductility-transition temperatures at the 15 foot-pound energy level are shown in the figure; the Type 414 steel has a transition temperature of about −140°F, and the Type 431 steel has a transition temperature of about −160°F. That the steels have similar transition temperatures might be expected inasmuch as the steels were quenched and tempered to about the same hardness, Rockwell C-22.

Keyhole-notch impact data (6) for the nickel-free counterparts of the present steels (Type 410 and Type 430 steels) are also shown in Fig. 10. Inasmuch as only average curves were reported for the Type 410 and Type 430 steels, the ductility-transition temperatures were selected at the same energy level as were those for the Type 414 and Type 431 steels. The transition temperature of the Type

410 steel, +25°F, is about 165°F higher than that of the Type 414 steel, and the transition temperature of the Type 430 steel, −50°F, is about 110°F higher than that of the Type 431 steel.

The impact data reported for the Type 410 steel are for the annealed condition, and one might expect the steel to exhibit a somewhat higher transition temperature in this condition than if the steel had been quenched and tempered. The Type 430 steel, on the other hand, is nonhardenable and the reported impact data are presumably for the optimum heat treatment. Thus the low temperature impact properties of the nickel steels appear to be better than those of similar steels without nickel.

Metallographic and X-Ray Studies

The microstructures of the steels before testing and after long time creep-rupture tests at 900, 1100, and 1200°F are shown in Figs. 11 to 14. In each figure, the photomicrographs marked A show the microstructure of the steel prior to testing, that is, after being oil-quenched from 1800°F and tempered for 4 hours at 1225°F. These photomicrographs show that the microstructure of the normal nitrogen Type 414 and Type 431 steels (Steels A and C) consist chiefly of tempered martensite, Figs. 11A and 13A. On the other hand, Figs. 12A and 14A show that the microstructures of the high nitrogen steels (Steels B and D) consist of both tempered and untempered martensite. As was mentioned earlier in this report, the martensite is believed to have formed from austenite that was retained on oil quenching the steels from 1800°F and that transformed when the steel was quenched from the tempering temperatures.

Microhardness measurements showed that the hardness of the light etching areas in the microstructure of Steel D was about 515 KHN (Knoop hardness number), or Rockwell C-48, a hardness nearly the same as that of the steel in the oil-quenched condition, Rockwell C-49.7. That this steel in the oil-quenched condition contained austenite was confirmed by X-ray determinations, which indicate 11.6% austenite. As is indicated in Fig. 14a, the martensite in this steel is present in bands.

No austenite was detected by the X-ray studies of the oil-quenched and tempered specimens of Steel D or of the oil-quenched and tempered specimens of the other steels. However, the lower limit of precision of the X-ray method used is 2% austenite.

The results of metallographic examination showed no untempered martensite (resulting from the transformation of retained austenite) in the microstructures of oil-quenched and tempered specimens of Steels A and C, Figs. 11a and 13a, but did show a

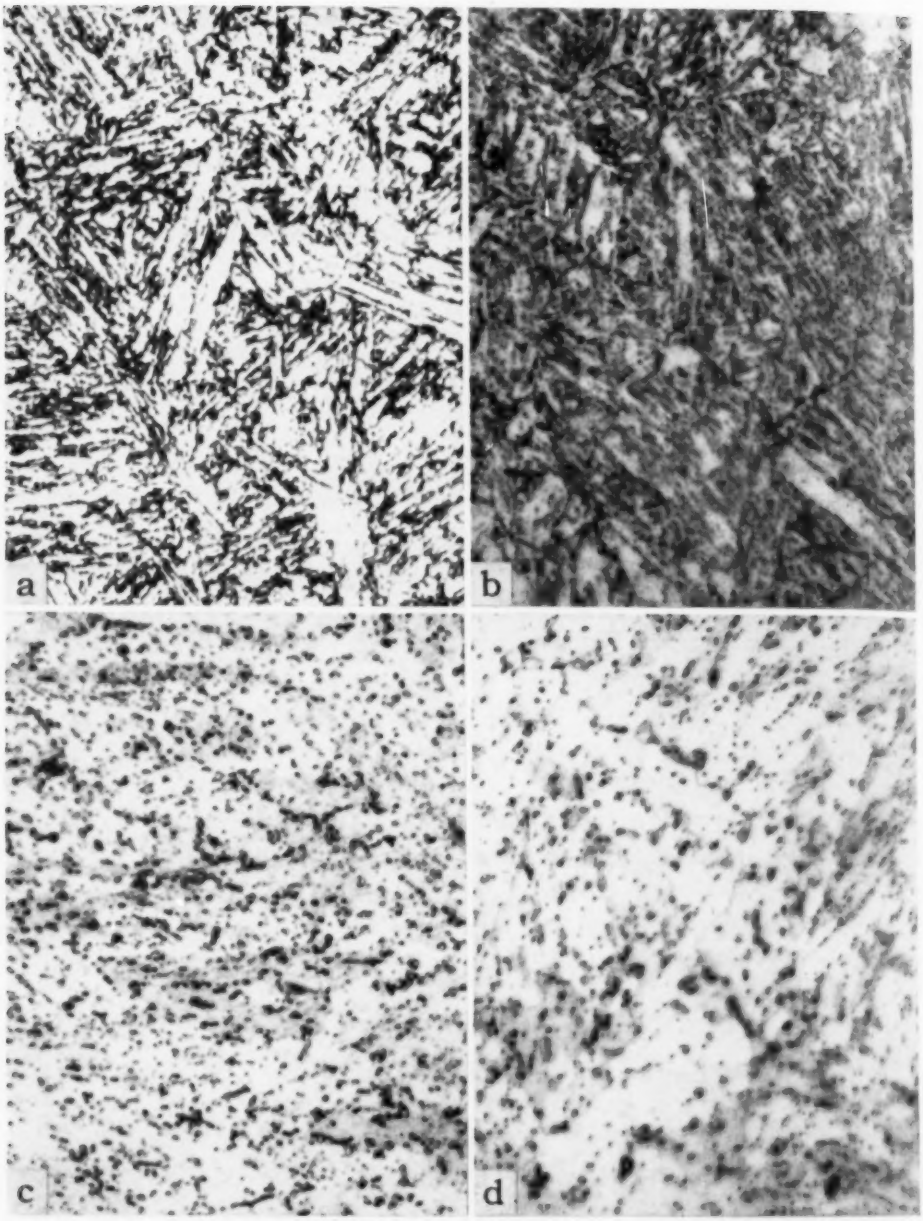


Fig. 11—Microstructures of the Normal Nitrogen Type 414 Stainless Steel (Steel A) in the Quenched and Tempered Condition, and After Long-time Creep-Rupture Tests at 900, 1100, and 1200°F. Photomicrographs taken near the fracture of the ruptured specimens. Etched in Vilella's reagent. X 750.

(a) Prior to test. Heat treatment: ½ hr. at 1800°F, oil-quenched; 4 hr. at 1225°F, oil-quenched. Rockwell C-22.2; (b) After rupturing in 730.5 hr. at 900°F. Stress 27,500 psi. Rockwell B-93.5; (c) After rupturing in 1520 hr. at 1100°F. Stress 8,000 psi. Rockwell B-85.4; (d) After rupturing in 1298 hr at 1200°F. Stress 6,000 psi. Rockwell B-85.3.

significant amount, approaching the 2% limit of the X-ray method for austenite, in the microstructure of the oil-quenched and tempered specimen of Steel B, Fig. 12a. As was observed for Steel D, the martensite in Steel B is present in bands, indicative of areas with a composition higher in carbon and alloys than the nominal

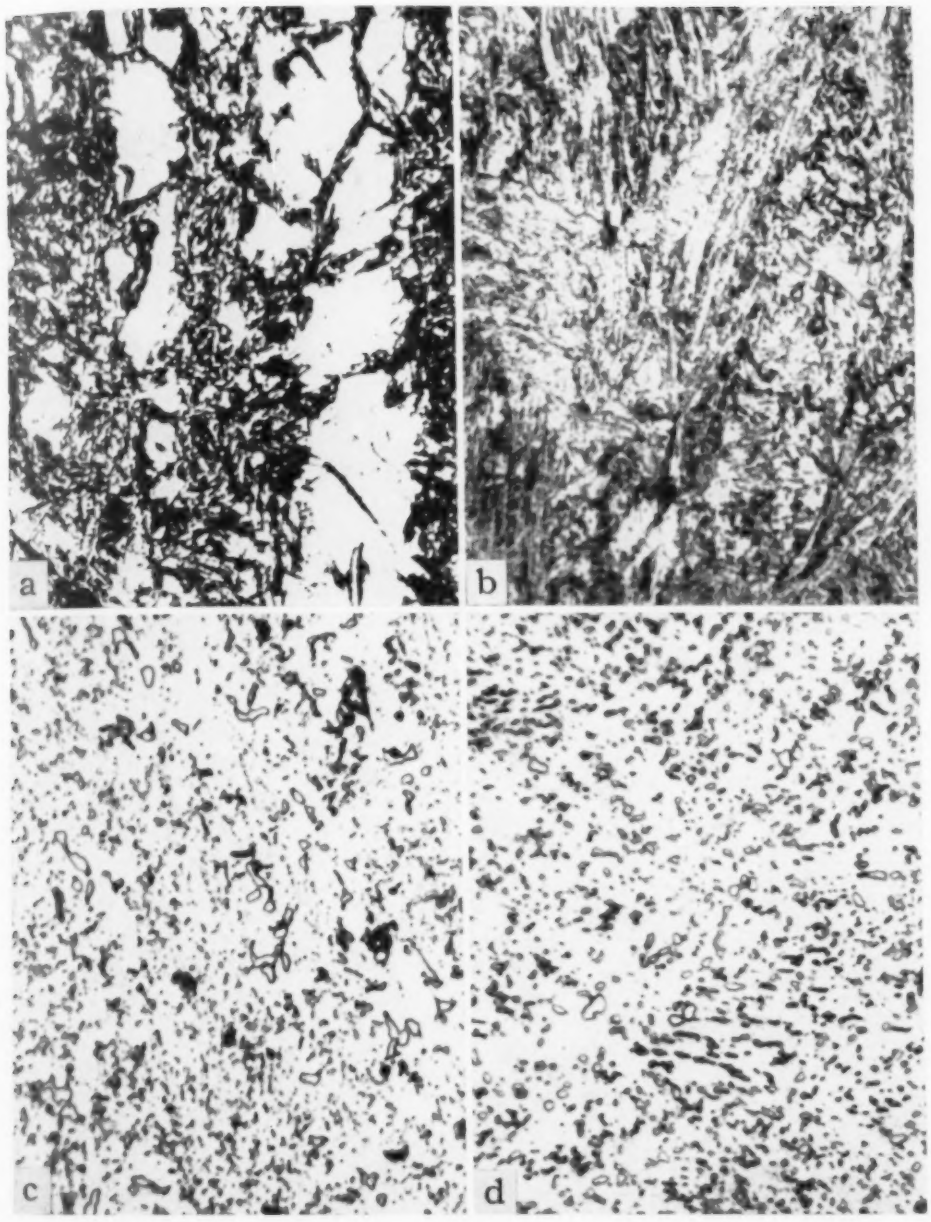


Fig. 12—Microstructures of the High Nitrogen Type 414 Stainless Steel (Steel B) in the Quenched and Tempered Condition, and After Long time Creep-rupture Tests at 900, 1100, and 1200°F. Photomicrographs taken near the fracture of the ruptured specimens. Etched in Vilella's reagent. X 750.

(a) Prior to test. Heat treatment: ½ hr. at 1800°F, oil-quenched; 4 hours at 1225°F, oil-quenched. Rockwell C-20.9; (b) After rupturing in 712 hours at 900°F. Stress 30,000 psi. Rockwell B-95.1; (c) After rupturing in 1213 hours at 1100°F. Stress 8,500 psi. Rockwell B-83.8; (d) After rupturing in 1295 hours at 1200°F. Stress 5,200 psi. Rockwell B-86.3.

composition. Apparently, the high nitrogen content of Steels B and D augments the effect of carbon and the alloying elements in stabilizing the austenite.

In all the steels, the acicular appearance of the original micro-

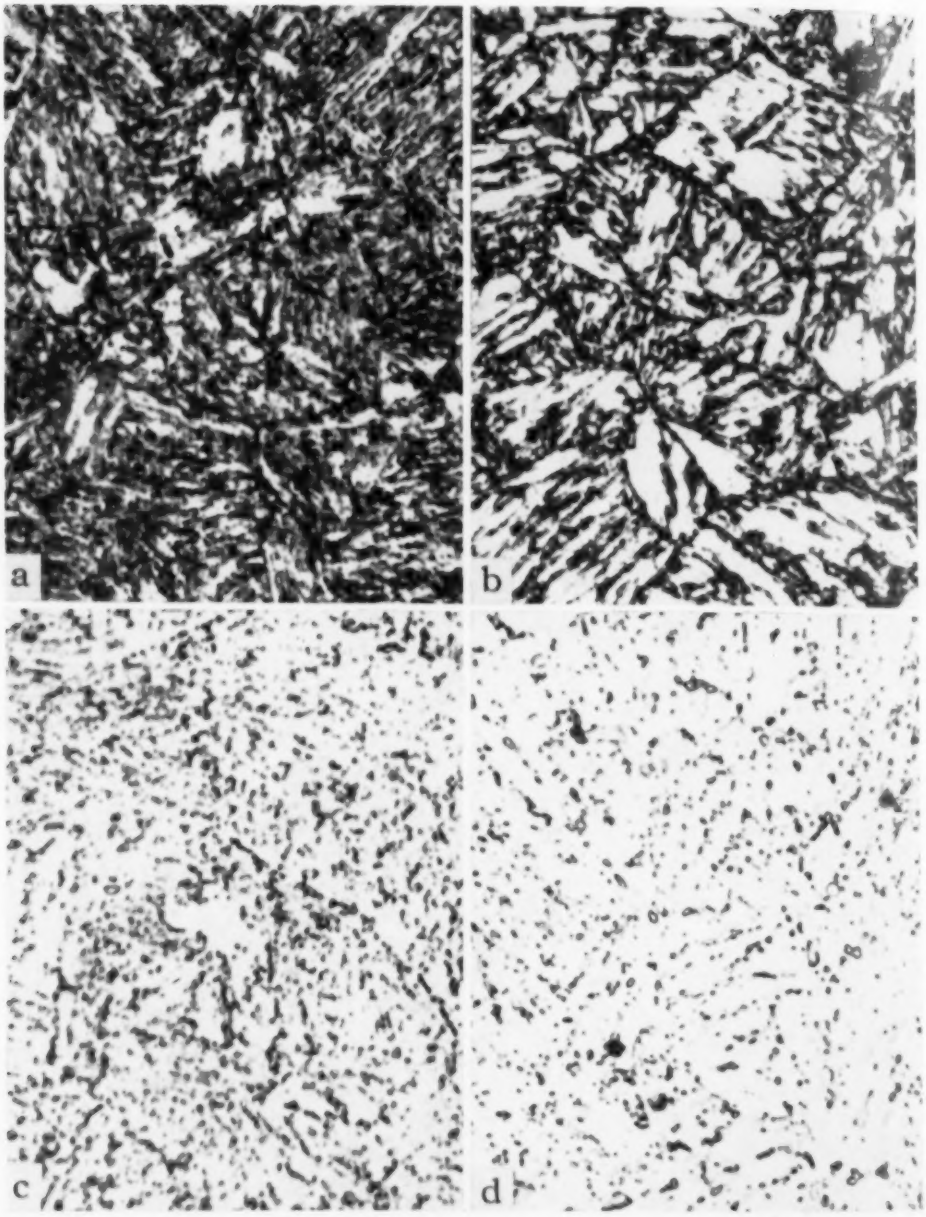


Fig. 13—Microstructures of the Normal Nitrogen Type 431 Stainless Steel (Steel C) in the Quenched and Tempered Condition, and After Long Time Creep-Rupture Tests at 900, 1100, and 1200°F. Photomicrographs taken near the fracture of the ruptured specimens. Etched in Vilella's reagent. X 750. (a) Prior to test. Heat treatment: ½ hour at 1800°F, oil-quenched; 4 hours at 1225°F, oil-quenched. Rockwell C-22; (b) After rupturing in 2042 hours at 900°F. Stress 30,000 psi. Rockwell B-94.9; (c) After rupturing in 1223 hours at 1100°F. Stress 10,000 psi. Rockwell B-84.1; (d) After rupturing in 735.5 hours at 1200°F. Stress 6,000 psi. Rockwell B-82.8.

structure remains after the longest times at 900°F. Steel A exhibits a general precipitation of fine carbides (Fig. 11b); Steel B exhibits a fine grain boundary carbide precipitation (Fig. 12b); Steel C exhibits a fine grain boundary carbide precipitation (Fig. 13b); and Steel D exhibits a general precipitation of fine carbides (Fig. 14b).

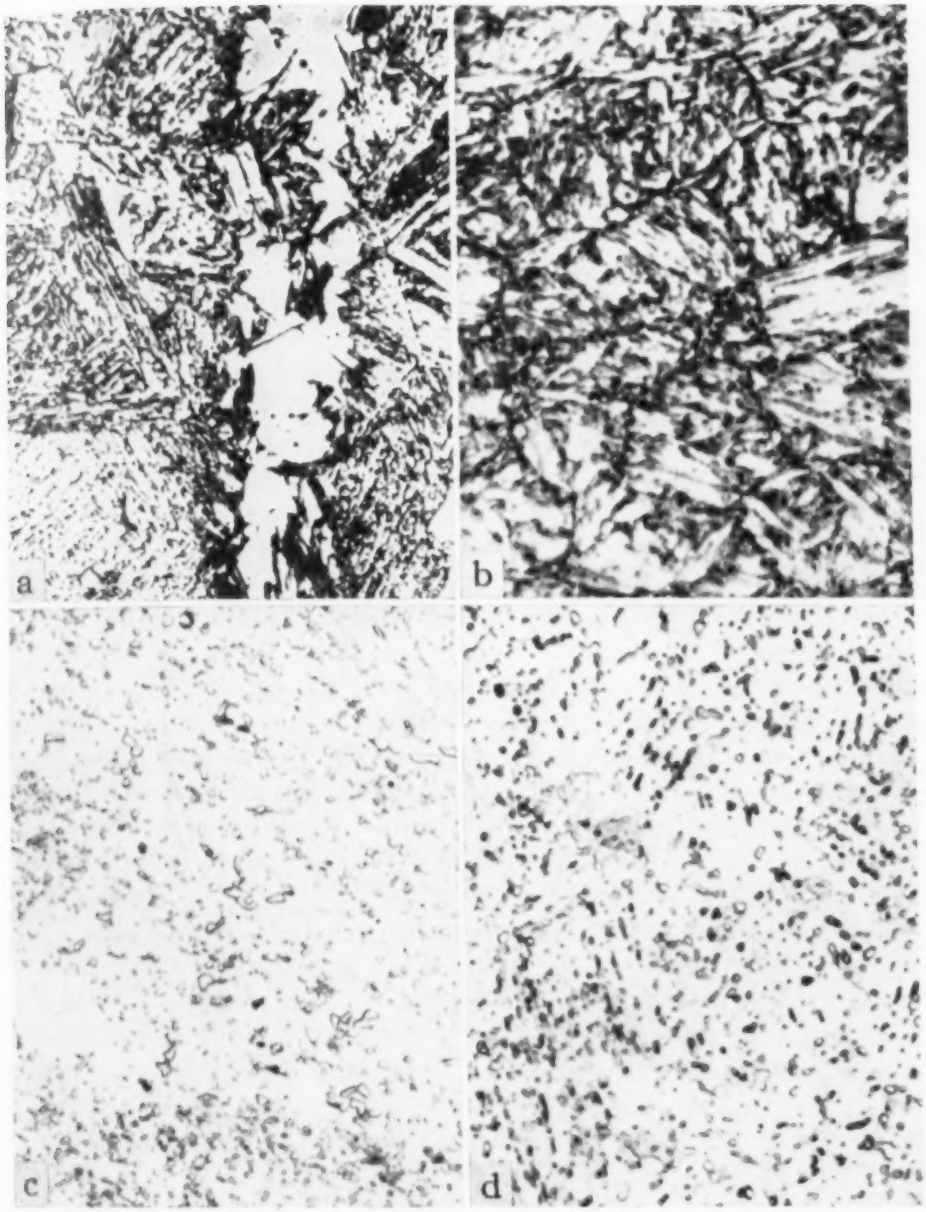


Fig. 14—Microstructures of the High Nitrogen Type 431 Stainless Steel (Steel D) in the Quenched and Tempered Condition, and After Long Time Creep-Rupture Tests at 900, 1100, and 1200°F. Photomicrographs taken near the fracture of the ruptured specimens. Etched in Vilella's reagent. X 750. (a) Prior to test. Heat treatment: ½ hour at 1800°F, oil-quenched; 4 hours at 1225°F, oil-quenched. Rockwell C-36.7; (b) After rupturing in 1559 hours at 900°F. Stress 34,400 psi. Rockwell B-98.7; (c) After rupturing in 1087 hours at 1100°F. Stress 10,700 psi. Rockwell B-90.6; (d) After rupturing in 550 hours at 1200°F. Stress 6,800 psi. Rockwell B-90.8.

The microstructures of all the steels after the longest times at 1100°F consist of spheroidized carbides (and possibly nitrides) in a ferrite matrix, Figs. 11c,12c,13c, and 14c. The photomicrographs in Figs. 11d,12d,13d, and 14d indicate that as the test temperature is increased to 1200°F, the carbides (and possibly nitrides) coalesce

more than at 1100°F. In general, this microstructural trend might be expected and is confirmed by the lower strengths obtained at 1200 than at 1100°F.

Summary

The results of the present investigation of mechanical properties of Type 414 and Type 431 stainless steels can be summarized as follows:

1. The room temperature tensile properties of the normal nitrogen steels (0.010 to 0.015% N) do not differ greatly from those reported in the literature for the two grades of steel. High nitrogen contents (0.063 to 0.124%) raise the tensile strength and lower the yield-tensile ratio and the ductility of each grade. The tendency for austenite to be retained in Type 414 and Type 431 steels during the quench from the austenitizing temperature is apparently increased by high nitrogen contents.

2. At 700 and 900°F, the yield and tensile strengths of the normal nitrogen Type 414 steel are higher than those of the normal nitrogen Type 431 steel; however, at 1100°F the Type 431 steel is stronger. The strength of each steel at each temperature is higher than the reported strength of its nickel-free counterpart (that is, Type 410 and 430, respectively), although the difference between the strengths decreases as the test temperature increases. However, the reported strengths of the nickel-free steels are based on a conservative average of data from many sources and for steels in various heat treated conditions. In the range 700 to 1100°F, the elevated temperature yield and tensile strengths of the high nitrogen steels are higher than those of the normal nitrogen steels, the difference between the strengths at 1100°F being relatively small.

3. In the range 900 to 1200°F, the 1000-hour creep-rupture strengths of the normal nitrogen Type 431 steel are higher than those of the nickel-free, 17% chromium Type 430 steel; the 10,000-hour strengths of the two steels are about the same. At 900 and 1100°F, the normal nitrogen Type 414 steel is not so strong as the nickel-free, 12% chromium steel, Type 410, but at 1200°F the Type 414 steel is stronger than the nickel-free steel.

4. Although the 0.001% per hour creep strength and the 1000- and 10,000-hour creep-rupture strengths of the normal nitrogen Type 431 steel are somewhat higher than those of the normal nitrogen Type 414 steel at 900 and 1100°F, the strengths of Type 414 are slightly higher at 1200°F. In general, a high nitrogen content appears to have an almost negligible effect on the creep and creep-rupture strengths of these steels. An exception to this effect is that the creep strength of high nitrogen Type 414 steel at 1200°F is somewhat lower than that of normal nitrogen Type 414 steel.

5. The ductility transition temperatures of the normal nitrogen Type 414 and Type 431 steels are about 110 to 165°F lower than those of the nickel-free, 12 and 17% chromium steels, Type 410 and Type 430, respectively.

We conclude that so far as mechanical properties are concerned, for applications in which high room temperature and elevated temperature tensile strength and/or good low temperature notch toughness are necessary, Type 414 and Type 431 steels seem to be preferable to Type 410 and Type 430 steels, respectively. However, for applications in which creep and creep-rupture strengths are the prime requisites there is no advantage to be gained by using Type 414 steel instead of Type 410 steel or by using Type 431 steel instead of Type 430 steel.

ACKNOWLEDGMENTS

The authors are pleased to acknowledge the assistance of D. C. Buck and J. J. Heger, U. S. Steel Corporation, for their part in planning this investigation; of R. D. Manning, Applied Research Laboratory, U. S. Steel Corporation, for his part in planning and reviewing this work; of Wood Works, U. S. Steel Corporation for making the elevated temperature tension tests; and of members of the Applied Research Laboratory staff for assistance in various phases of this investigation.

References

1. "Stainless and Heat Resisting Steels," *Steel Products Manual*, American Iron and Steel Institute, Section 24, April 1950, pp. 27, 39 and 83.
2. R. L. Rickett, W. F. White, C. S. Walton and J. C. Butler, "Isothermal Transformation, Hardening and Tempering of 12% Chromium Steel," TRANSACTIONS, American Society for Metals, Vol. 44, 1952, p. 138.
3. B. N. Bose and M. F. Hawkes, "Kinetics of the Eutectoid Transformation in Alloys of Iron and Nitrogen," *Transactions*, American Institute of Mining and Metallurgical Engineers, Vol. 188, 1950, p. 307; also *Journal of Metals*, February, 1950.
4. "Steels for Elevated Temperature Service," U. S. Steel Corporation, 1949.
5. E. J. Dulis and G. V. Smith, "Creep and Creep-Rupture Properties of Some Ferritic Steels Containing 5 to 17% Chromium," American Society for Testing Materials, Preprint No. 66, 1953.
6. G. V. Smith, W. B. Seens, H. S. Link and P. R. Malenock, "Microstructural Instability of Steels for Elevated Temperature Service," *Proceedings*, American Society for Testing Materials, Vol. 51, 1951, p. 895.

DISCUSSION

Written Discussion: By Edward A. Loria, staff metallurgist, Crucible Steel Company of America, Pittsburgh.

This paper introducing the effect of nitrogen in Types 414 and 431 stainless is very interesting. The aircraft industry wishes to eliminate ferrite in Type 431 bars which are fabricated into a variety of pressure vessels and fittings. The presence of ferrite weakens the matrix structure and is particularly damaging to transverse impact and fatigue. The addition of nitrogen to Type 431 may be the answer

to this major problem if it eliminates ferrite. It is realized that the authors show in their photomicrographs that no free ferrite existed in the small sections that they studied but, nevertheless, this subject is the most important one to the consumer who has to utilize heavier sections.

Do the authors have data on the effect of tempering temperature on the mechanical properties of Types 414 and 431, with and without nitrogen? Are the tensile strength and hardness less subject to scatter in the high nitrogen steels? This may be possible if the presence of nitrogen reduces the amount of ferrite as the presence of nickel in Type 436 does in comparison with Type 410. Are data available for tempering temperatures in the 600 to 800°F range? Also, would the authors comment on the results of single or double tempering treatments for their high nitrogen Type 431 with respect to raising yield strength and impact values? Any data which show the importance of varying the austenitizing temperature in achieving maximum properties on tempering at 600 to 800°F would be worthwhile.

It is well known that high chromium and low carbon in martensitic chromium steels favors formation of ferrite which may not be removed by ordinary heat treatment. The presence of ferrite can reduce the fatigue strength of engine parts. Free ferrite can confer serious directional effects for properties other than fatigue. Parts will be more prone to fracture under static or impact loading. Do the authors have any data on transverse tensile and impact properties for the four steels studied? What are the impact transition curves for the high nitrogen steels B and D? Data on transverse tests where the grain flow was split would be of considerable value. Indeed, the beneficial effect of nitrogen in bar sections susceptible to ferrite formation would be evaluated by such studies.

Would the authors comment on the relative amounts of free ferrite in their steels in the as-received condition? Material free from ferrite usually has a coarser grain size than ferrite containing steel. A comment on the effect of nitrogen on grain coarsening would be appreciated. Would the authors discuss the notch sensitivity in fatigue and rupture of their normal versus high nitrogen steels? It is hoped that they will continue their study of the effect of nitrogen on ferrite formation along the lines of this discussion.

Written Discussion: By Chi-Mei Hsiao, research metallurgist, Research and Development Laboratory, Crucible Steel Co. of America, Pittsburgh.

The authors are to be congratulated for their noteworthy and timely additions to the knowledge of mechanical properties of stainless steels at room and elevated temperatures.

The authors' finding of the existence of 11.6% retained austenite in steel D in the oil-quenched condition is very interesting. According to recent published work[2] the Ms temperature of the stainless steel can be calculated from its chemical composition. In addition, the percentage of martensite formed at various temperatures below the Ms was found to be dependent upon the Ms itself[3] or the temperature interval below Ms.[4]

The Ms temperatures and the temperatures at which 80, 90 and 99% of the austenite of the four steels investigated by the authors will transform to martensite

---

[2]G. H. Eichelham and F. C. Hull, "The Effect of Composition on the Temperature of Spontaneous Transformation of Austenite to Martensite in 18-8 Type Stainless Steel," TRANSACTIONS, American Society for Metals, Vol. 45, 1953, p. 77.

[3]Discussion by L. D. Jaffe of paper by R. A. Grange and H. M. Stewart, "The Temperature Range of Martensite Formation," *Transactions*, American Institute of Mining and Metallurgical Engineers, Vol. 167, 1946, p. 493.

[4]W. J. Harris and M. Cohen, "Stabilization of the Austenite-Martensite Transformation," *Transactions*, American Institute of Mining and Metallurgical Engineers, Vol. 180, 1949, p. 447.

Table VI

Steel	Ms (°F)	Temperature at Which Various Quantities of Martensite Form		
		80%	90%	99%
A	734	—	649°F	599°F
B	431	—	246°F	171°F
C	607	—	482°F	417°F
D	242	64°F	17°F	—

have been calculated from the aforementioned relationships, and the results are listed in the following table.

The calculations are in general agreement, at least semiquantitatively, with the authors' findings that in the oil-quenched condition, there is 11.6% austenite in steel D, 2% in steel B, and no austenite in steels A and C.

The transformation of the retained austenite in steels B and D after tempering at 1225°F for 4 hours is most probably due to the fact that the precipitation of carbide (and nitride) during tempering raise the Ms temperatures above room temperature.

It appears to the writer, at least academically, that it is not proper to compare steel D in a duplex structure (tempered and untempered martensite) with other steels. It would be interesting to transform steel D in a wholly tempered martensite structure either by double aging or by refrigeration and then compare its properties with other steels.

On the same line of thinking, it will be worthwhile to consider the Ms temperature in designing the chemical composition of stainless steel so as to prevent the necessity to use more complicated heat treatment (double aging or refrigeration) for improving its ductility.

Authors' Reply

We wish to thank Mr. Loria for his comments on our paper. Free ferrite formation in Type 431 steel is a function of austenitizing temperature and of the composition balance between (a) the ferrite forming elements chromium, silicon, etc., and (b) the austenite forming elements nickel, carbon, and nitrogen. Increasing the amounts of the latter elements decreases the tendency for free ferrite formation; however, as has been shown in the paper, increasing the nitrogen content over that normally found in Type 431 steel also increases the tendency for retained austenite to exist in this steel after austenitizing and quenching to room temperature. Indeed, after austenitizing at 1800°F and oil quenching to room temperature, the high-nitrogen (0.063%) Type 431 stainless steel (⅝-inch square bars) contained about 11% retained austenite.

If a steel that has retained austenite (a) is subsequently double tempered at sufficiently high temperatures, for example, about 1200°F or (b) is refrigerated to a temperature below M_f prior to a single tempering treatment, the resultant structure is essentially all tempered martensite. However, if high strength requirements limit the tempering temperatures to about 600 to 800°F, which reportedly is the case in the aircraft industry, the retained austenite probably cannot be transformed by a double tempering heat treatment. In this case, the temperature of the first tempering heat treatment may be too low to "condition" the retained austenite so that a martensitic transformation will not occur during cooling to room temperature. To transform the retained austenite in this case, a refrigeration treatment below M_f is needed. Thus, although the formation of free ferrite is minimized or eliminated by increasing the nitrogen content in Type 431 steel, our

studies show that retained austenite and its associated problems can result from increasing the nitrogen content. However, by properly balancing the amount of ferrite and austenite formers within the AISI specification limits, the elimination of both free ferrite and retained austenite may be possible.

Inasmuch as the main objective of the present study was to determine the tensile and creep-rupture properties of Types 414 and 431 stainless steels in the temperature range 900 to 1200°F, studying the effects of tempering in the range 600 and 800°F prior to testing at the elevated temperature was not attempted. Nor did we conduct the extensive study that would have been required to answer Mr. Loria's numerous questions about the effects of various heat treatments, particularly of tempering in the range 600 to 800°F, on room-temperature mechanical properties.

In reference to the impact tests on the high nitrogen Steels B and D over a temperature range that would enable the ductlity transition temperature to be determined, we explained on page 487 of the paper that this had not been done and our reasons for not doing this work.

The amount of ferrite in the as-received condition was not determined. However, because the size of heats varied from the experimental 30-lb. heats to a commercial heat, the processing of the steels was different and, therefore, we doubt that the determination of free ferrite in these steels would be meaningful.

The grain sizes of the steels investigated are given in Table II. As explained in the paper, the austenite grain size of the high-nitrogen Type 431 steel is finer than that of the normal-nitrogen Type 431 steel by about 2 ASTM numbers. However, the austenite grain size of the high-nitrogen and the normal-nitrogen Type 414 steels is the same.

We believe that considerable research work remains to be done on these steels, particularly the Type 431 steel, to establish such factors as the chemical composition balances to minimize or eliminate free ferrite and/or retained austenite, the effects of various heat treatments on microstructure and mechanical properties, and the susceptibility to corrosion and stress corrosion in various environments.

We are pleased to have Dr. Hsiao's comments and very interesting observation on the agreement between calculated and experimentally determined quantities of retained austenite. The relationship between the Ms temperature and the extent of transformation of austenite to martensite during cooling to room temperature (see table VI in Dr. Hsiao's discussion) explains the reason for the greater amount of retained austenite in Steel D (16.1% Cr and 0.223% C plus N) as compared to that in Steel B (12.4% Cr and 0.254% C plus N). Also, we agree that by balancing the chemical composition of these steels according to the known relationships between composition and Ms temperature, a good first approximation can be made of the maximum carbon plus nitrogen addition that could be made and still avoid retained austenite. This maximum carbon plus nitrogen level would in turn minimize or eliminate the formation of delta ferrite during the austenitizing heat treatment.

Dr. Hsiao's observation concerning the comparison of the properties of Steel D with those of the other steels is certainly worthwhile. If one wished to determine the effect of nitrogen per se on the properties of Type 431 stainless steel, it would be necessary to determine the properties of the steels after they were heat treated to the same microstructure.

HIGH NITROGEN AUSTENITIC CR-MN STEELS

By V. F. Zackay, J. F. Carlson and P. L. Jackson

Abstract

High nitrogen Cr-Mn austenitic steels were prepared by a pressure-melting and -casting technique. Nitrogen levels of one-half weight percent and higher were achieved. The creep-rupture properties of the base composition, 16 Cr-14 Mn-2 Mo-½ N, were approximately equivalent to those of 16-25-6, a commercial heat resistant alloy. The unusually high interstitial nitrogen content resulted in excellent combinations of strength and ductility in both the annealed and cold-worked state. (ASM-SLA Classification: Q3, Q4, Q23, SS)

THE advent of World War II ushered in a period of intense research activity in the field of elevated temperature materials. Early metallurgical efforts were concentrated on iron-base chromium-nickel alloys for supercharger applications. This was followed by the development of nickel and cobalt base alloys of the precipitation hardening type for jet engine components. Although continued progress is being made in pushing the strength and temperature limits of these alloys to still higher levels, a new area of research has received considerable attention in recent years. Briefly, this may be described as an effort to produce economically, materials capable of sustaining high loads at elevated temperatures which have a minimum of strategic, scarce, or critical elements. The growing possibility of application of these steels to mass-produced automobile gas-turbine engines greatly accelerates this phase of research.

The investigation described herein is aimed at the development of iron-base austenitic alloys capable of service in the temperature range of 1200–1400°F.

Selection of Base Material

Generically speaking, alloys designed for service in this temperature range may be considered related to the base composition of the commercial 18 Cr-8 Ni type stainless steels. The addition of 2 to 3% of the ferrite-forming and hot-strengthening element molybdenum to this base requires about 4% more of austenite

A paper presented before the Thirty-Seventh Annual Convention of the Society, held in Philadelphia, October 17–21, 1955. Of the authors, V. F. Zackay is supervisor, Scientific Laboratory, Ford Motor Co., Dearborn, Mich., J. L. Carlson is metallurgical engineer, Hoskins Manufacturing Co., Detroit, and P. L. Jackson is research metallurgist, Misco Precision Casting Co., Whitehall, Mich. Manuscript received April 19, 1955.

stabilizing nickel to form the best of the commercial elevated temperature stainless steels, namely, AISI 316, type 18-8 M. A further advance came with the design of a balanced composition of 16% chromium, 25% nickel, and 6% molybdenum known commercially as Timken 16-25-6. This iron-base alloy is superior in the annealed condition to AISI 316 and has the further advantage that it responds to hot-cold working. The latter term denotes the process of working the steel in the 1200–1400°F range so as to leave residual stresses in the material which in turn strengthen it up to 1350°F. These two alloys, AISI 316 and Timken 16-25-6, are used as a basis of comparison for the alloys described in this report.

The search for a substitute for nickel in alloys of the type referred to above has occupied the attention of numerous investigators, particularly in Germany and Russia, where nickel was in short supply in the late thirties and early forties. An obvious substitute, manganese, immediately suggests itself, although it is common knowledge that the austenite forming capacity of manganese is weak compared to nickel. The structural constitution of chromium-manganese steels has been recently reviewed in considerable detail by Franks et al (1)[1]. Critical reviews (2) of the considerable literature on the subject give confirmation that it is virtually impossible to build sufficient hot strength into the iron-base chromium-manganese steels without the resultant breakdown of the metastable austenite at relatively low temperatures. This hot strength is achieved almost always by the use of ferrite-forming molybdenum or wolfram.

The addition of the element nitrogen, with its intense austenite forming capacity has been recommended to supplement the manganese (3) in chromium-manganese steels. This element was found to confer significant hot strength, toughness, and ductility as well as to retain the austenitic structure under the combined action of thermal and mechanical forces. Also, the chromium level necessary for the formation of sigma phase is raised by nitrogen (4). Although chromium, manganese, and molybdenum lower the activity of nitrogen and therefore aid in increasing the solid solubility of nitrogen, present practice is to hold the nitrogen level to about 1/75th of the chromium content. Above this ratio ingot gas porosity may be encountered.

If chromium-manganese austenitic steels are to be developed, comparable to those containing nickel, it seems imperative that a technique be developed wherein lower chromium-nitrogen ratios are obtained. Brick and Creevy (5) have shown that nitrogen solubility in liquid iron-chromium alloys is proportional to the square root of the pressure. A concept of pressure-melting was developed

[1]The figures appearing in parentheses pertain to the references appended to this paper.

by the authors of this paper wherein alloys are melted and cast under superatmospheric nitrogen pressures. By this procedure and with the added use of nitrogen-bearing ferro-alloys, sound ingots of chromium-manganese nitrogen alloys for elevated temperature service have been made having about ½% nitrogen in interstitial solid solution.

A study of both the influence of nitrogen on the Fe-Cr-Mn ternary phase diagram (4) and the results of elevated temperature studies conducted by German workers (6) led to the exploration of the properties of a base composition of 16% chromium, 14% manganese, 2% molybdenum, and ½% nitrogen. In this alloy, chromium performs the dual function of imparting oxidation resistance and increasing the nitrogen solubility (as does the manganese); manganese and nitrogen stabilize the austenitic structure; while molybdenum and, again nitrogen, act as hot strengtheners.

Preparation of Alloys

The raw materials consisted of electrolytic iron, nickel, silicon, and molybdenum metal, hydrogen deoxidized electrolytic manganese (1850°F for 6 hours) and chromium in the form of 2½ inch cubes of AISI 430 or 446 stainless steel. The stainless steel, electrolytic iron (if needed) and molybdenum were melted in vacuo (1 micron Hg). Prepurified nitrogen was then introduced until a pressure of two atmospheres absolute was attained. The manganese was then added to the crucible by means of charging buckets and the melt cast under the nitrogen atmosphere. The temperature of the melt was kept as close to the liquidus as possible as the nitrogen solubility in the liquid showed an apparent decrease with increasing temperature. A further refinement, later added, was to raise the nitrogen content by the addition of hydrogen deoxidized nitrided manganese (Mn_4N). Approximately one-half of the manganese added was in this form.

The tendency of the ingot to gas upon solidification is a function of alloy composition, the amount of nitrogen-bearing alloy additions, nitrogen pressure, melt temperature, and the ingot solidification rate. A fundamental investigation of several of the important variables influencing nitrogen solubility is currently in progress. In cooperation with the Armour Research Foundation, equipment has been built to permit the melting and casting of Cr-Mn-N steels at pressures of up to ten atmospheres of nitrogen.

The composition of the alloys discussed in this paper are shown in Table I.

Processing of Ingots

The as-cast 2½ inch diameter ingots (12 to 20 pounds) were

THE UNIVERSITY OF MICHIGAN LIBRARIES

Table I
Alloy Composition

Alloy	Cr	Mn	Mo	C	Si	N	Ni	Others
47	15.9	13.3	2.02	0.03	0.25	0.46	—	—
49	15.9	13.7	1.79	0.03	0.27	0.44	—	—
69	14.6	16.0	4.39	0.06	0.28	0.49	—	—
73	15.6	15.0	2.88	0.07	1.32	0.46	1.15	—
75	15.7	15.4	1.94	0.08	1.42	0.40	1.45	—
76	15.6	15.2	1.94	0.07	1.08	0.39	2.44	—
91	15.1	13.0	2.80	0.10	0.18	0.44	—	0.01B
153	15.9	12.6	1.75	0.08	—	0.57	—	—
155	16.5	11.6	2.08	0.18	—	0.77	—	—

hot-rolled at initial temperatures of 2250 to 2350°F into 5/8 inch rounds. The temperature at which these steels were worked was determined not only by the composition balance but also by the nature of the available processing equipment. The hot strength of these alloys necessitates very high forging temperatures particularly in view of the power limitations of laboratory-type mills. On the other hand, temperatures in excess of 2200°F invite the formation of delta ferrite with resultant tearing in the initial stages of hot working (1).

The 5/8 inch hot-worked rod or the machined 1/4 inch round creep-rupture specimens were solution heat treated at 2012°F and water-quenched.

Elevated Temperature Properties

The austenitic structure in iron-base Cr-Mn-N alloys is metastably retained by rapid cooling from elevated temperatures. This nonequilibrium phase tends to decompose when subjected to the combined action of thermal and mechanical forces. The degree of austenitic stability in any given environment is closely dependent upon the relative proportion of the alpha- or gamma-forming elements in the alloy. Thus the guiding principle in the alloy chemistry of these steels is to achieve the greatest austenitic stability over the desired temperature range consistent with the hot strength requirements of the particular service application.

The creep-rupture characteristics of the base composition, represented by alloy 47 and 49, are shown in Fig. 1, on a Larson-Miller plot (7). For convenience, dotted vertical lines defining the 100-hour rupture life at the indicated temperatures are shown. Values for the normal scatter of creep-rupture properties of commercial alloys 316 and 16-25-6 taken from several sources in the published literature are shown as bands superimposed on the Larson-Miller plots.

The creep-rupture parameters for alloys 47 and 49 are seen to lie within the lower half of the 16-25-6 band falling off somewhat at values corresponding to short-time rupture tests at 1500°F. The excellent ductility to fracture for several typical rupture tests is shown in Table II.

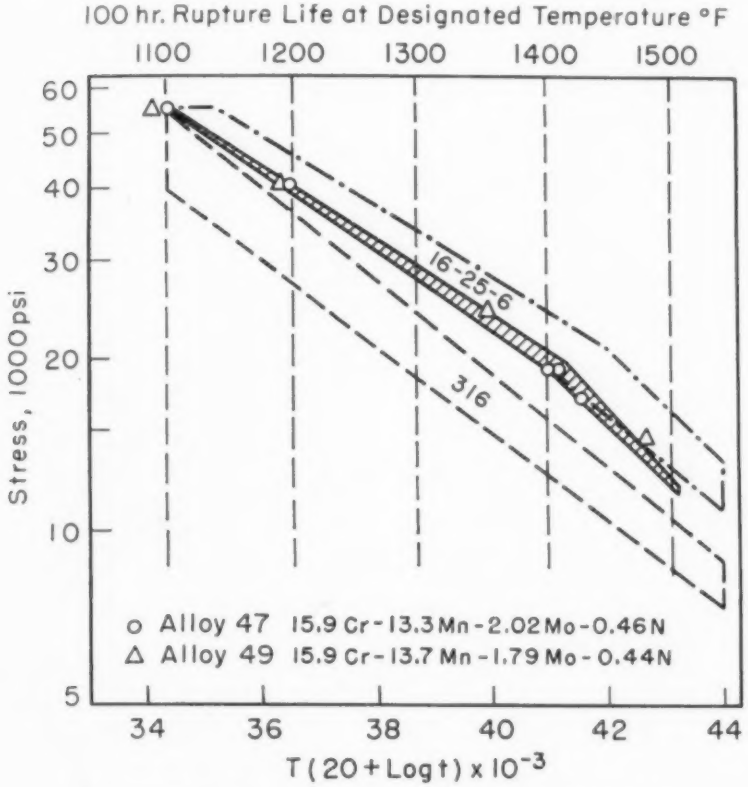


Fig. 1—Creep-Rupture Properties of the Base Composition 16 Cr-14 Mn-2 Mo-½ N.

Precipitation of nitrides during creep is probably a factor in the plastic behavior of these alloys although no evidence for this could be established metallographically. However, the fall in ductility after several hundred hours of testing, as shown in Table III, probably attests to some precipitation taking place.

The effect of increased molybdenum on the elevated temperature properties of the base composition, alloy 47 (or 49) is shown in Fig. 2. At relatively low temperatures the creep-rupture lives of

Table II
Typical Ductility Values from Stress-Rupture Tests of Cr-Mn-Mo-N Steels

Alloy	Nominal Composition	Temp. °F	Stress Psi	Rupture Time (Hours)	Elong. %	R.A.%
47	16 Cr-14 Mn-2 Mo-0.5 N	1200	40,000	86.6	14	28
		1350	20,000	400.9	13	18
		1500	10,000	246.6	47	36.5
76	16 Cr-15 Mn-2 Mo-2½ Ni-0.5 N-1 Si	1200	40,000	189.8	13	15
		1350	20,000	273.5	35	28
		1500	10,000	126.3	41	30
91	15 Cr-13 Mn-3 Mo-0.5 N-0.01 B	1200	40,000	310.9	11	17
		1350	20,000	668.9	31	30
		1500	10,000	157.0	19	21

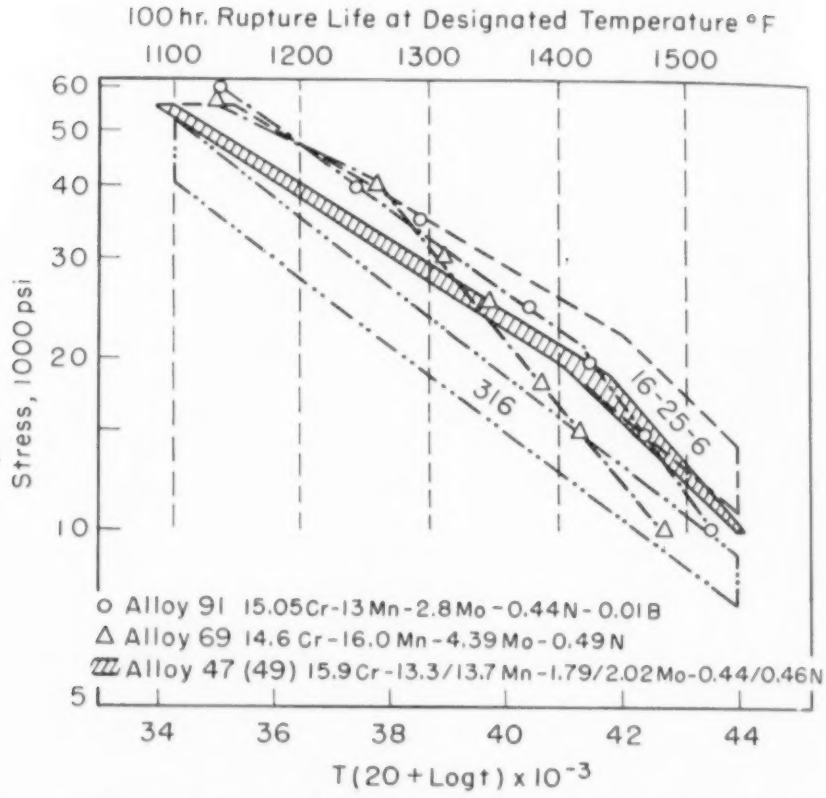


Fig. 2—Effect of Molybdenum Additions on Creep-Rupture Life of Cr-Mn-Mo-N alloys.

these steels are considerably improved by molybdenum additions. At higher temperatures, however, the rupture values are observed to fall off with increasing molybdenum content. Alloy 91 with approximately 3 percent molybdenum and 0.01 percent boron, although somewhat weaker than the base composition at quite elevated temperatures, shows excellent short time rupture strength up to 1500°F.

A similar dependence upon composition can be shown by changes in the proportion of austenite forming constituents such as nickel. To improve the oxidation resistance of alloy 91 about 1% silicon was added. It was intended to off-set the ferrite forming tendency of the silicon by the addition of small amounts of nickel. The properties of this alloy, number 73, are shown in Fig. 3. The very low nickel in alloy 73, is apparently insufficient in the presence of the high silicon to retain the creep-rupture properties of alloy 91. Further lowering of the molybdenum content results in the loss of strength at lower temperatures without real improvement at higher temperatures. A compromise is reached by increasing the nickel and slightly decreasing the silicon levels as shown by alloy 76. The effect of nickel at the 2 to 3% level is to raise the creep parameter curve for

Table III
Residual Ductility of Creep-Rupture Specimens

Alloy & Heat Treatment***	Creep Data: Temp. °F	Creep Data: Stress Psi	Creep Data: Time at Temp. (Hrs.)	Tensile Test Data: As Quenched Y.S.*	As Quenched T.S.	As Quenched R.A.	As Quenched E.**	After Creep Testing Y.S.*	After Creep Testing T.S.	After Creep Testing R.A.	After Creep Testing E.**
49 W.Q.	1200	35,000	355.4	59,100	121,250	69	68	68,200	111,200	12	17
49 W.Q.	1350	15,000	235.9	59,100	121,250	69	68	75,000	113,000	13	17
	1350	20,000	119.0								
47 W.Q.	1200	35,000	212.7	61,400	119,000	71	65	79,800	107,500	8	14
49 A.C.	1200	30,000	240.9	71,500	118,750	77	68	80,000	115,200	30	30
47 A.C.	1200	30,000	168.8	67,900	118,200	74	72	76,800	117,500	37	40

***Quenched from 2012°F
**In 1-inch, percent
*0.2 Off-set, percent

UNIVERSITY OF MICHIGAN LIBRARIES

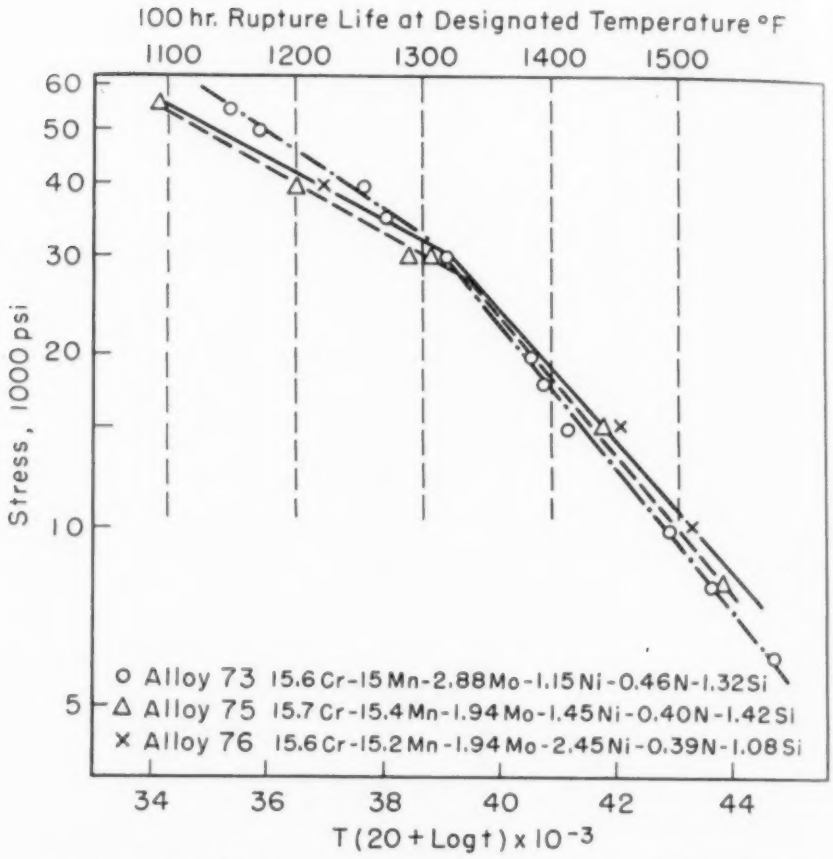


Fig. 3—Effect of Austenite Forming Elements on the Creep-Rupture Properties of Cr-Mn-N Steels.

alloy 76 over the complete temperature range. Unfortunately, nickel even at these concentrations has an adverse effect on nitrogen solubility and therefore must be used with caution.

Alloys 76, 91 and the base compositions are representative of those alloys having the best creep rupture properties of nickel-free and very low nickel Cr-Mn-Mo-N steels.

Other alloying elements were qualitatively appraised for their effect on the properties of Cr-Mn-N steels. The behavior of wolfram, as would be expected, was similar to the less costly element molybdenum. Silicon, although a poor hot strengthener, confers added oxidation resistance on the nickel-free austenitics. Niobium alloys exhibited poor creep rupture strength while vanadium, even at very low levels, caused embrittlement and rendered the nitrogen ineffective by nitride precipitation.

Attempts to devise mechanical-thermal treatments to improve the creep rupture life of the Cr-Mn-N alloys, generally proved unsuccessful. Hot-cold working (1400–1600°F) of the ingots during

the rolling operation either proved ineffective or actually decreased the rupture life.

Similar negative results were found with various combinations of aging times and temperatures. Failure to improve elevated temperature properties by aging and by hot-cold working is undoubtedly related to the metastable nature of these steels. Water quenching from 2000°F was considered to be the optimum heat treatment.

Room Temperature Properties

The Cr-Mn steels have been suggested as high strength aircraft construction materials when used in the cold-worked state (8). Tensile tests of the high nitrogen Cr-Mn steels as shown in Table IV gave sufficient promise to warrant further testing of the room temperature mechanical properties. Two typical Cr-Mn-Mo-N alloys, one single phase (153) and the other duplex (155) were alternately cold-rolled and annealed to 0.090 inch strip and subsequently cold-rolled as far as the roll pressures of the laboratory-type mill permitted.

Table IV
Room Temperature Tensile Tests of Cr-Mn-Mo-N Steels

Alloy	Nominal Composition	Tensile Test Data Y.P. Psi	T.S. Psi	Elong. %
47	16 Cr-14 Mn-2 Mo-0.5 N	61,400	119,000	70
49	16 Cr-14 Mn-2 Mo-0.5 N	59,100	121,250	68
153	16 Cr-13 Mn-2 Mo-0.6 N	61,500	120,000	65
155	17 Cr-12 Mn-2 Mo-0.75 N	75,000	140,000	50

Table V
Tensile Properties of Cold-Worked Austenitic Steels

Nominal Composition	A.I.S.I. 301	A.I.S.I. 302	Type CM*	Ford 153	Ford 155
Cr	17	18	16	16	17
Ni	7	9	1	—	—
Mn	—	—	15	14	13
Mo	—	—	—	2	2.5
N	—	—	—	0.6	0.75
Cold-Work, %	40	60	40	33	25
Y.S. Psi	150,000	180,000	145,000	183,000	176,000
T.S. Psi	200,000	195,000	185,000	207,000	205,000
Elong. %	10	3	5	13	11.5

*A commercial Cr-Mn stainless steel produced during World War II.

Table VI
Tensile Properties of a Hot-Cold Worked Cr-Mn-Si-N Steel

Alloy	Nominal Composition	Condition	Y.S. Psi	T.S. Psi	Elong. %
158	14 Cr-14 Mn-2 Si-.½ N	Solution Quenched	70,700	134,000	62
		Hot-Cold Worked 15%	145,500	174,250	29
		Hot-Cold Worked 25%	161,500	184,000	28

As shown in Table V, combinations of high tensile strengths and good residual ductility were obtained at relatively low amounts of cold reduction. Representative values of commercial stainless steels, including a Cr-Mn steel (CM) produced during World War II, are shown for comparison. Increased yield and tensile strength of these steels also results when they are hot-cold worked as shown in Table VI for a 14 Cr-14 Mn-2 Si-½ N alloy.

Welding Characteristics

A detailed study of the welding characteristics of high nitrogen Cr-Mn steels is currently being undertaken. Preliminary results indicate that sound fusion welds can be produced provided certain precautions are taken. Welds made by the metallic arc with coated electrode process exhibited good fusion, nonporosity, and adequate mechanical properties. The short time at temperature and rapid freezing associated with this process probably aids in preventing nitrogen evolution by the solidifying metal.

Welds fabricated by the inert gas, shielded arc process with argon as the shield gas were highly porous. However, the employment of nitrogen or mixtures of nitrogen and argon as a protective atmosphere allowed consistent production of sound nonporous welded joints.

Oxidation Resistance

Oxidation tests of Cr-Mn-N steels, including several commercial stainless steels for comparative purposes were conducted in still air on carefully prepared strip material measuring approximately 0.060 inch × 1 inch × 2 inch. After exposure for 100 hours at a given temperature the strips were wire brushed, cathodically descaled, and weighed, according to the method of Brasunas et al (9).

Although the test results must be regarded as qualitative in nature since the humidity was not precisely controlled, certain conclusions may be drawn. The chromium level, as in commercial stainless steels, is of paramount importance in establishing the overall level of oxidation resistance. Those Cr-Mn-N steels having 16% or more chromium were roughly equivalent in scaling resistance to AISI 18-8 or AISI 430 type stainless up to 1700°F. For intermittent service, i.e., cyclic heating and cooling, an upper limit of 1600°F would seem to be the maximum operating service temperature.

Summary

Very high nitrogen Cr-Mn austenitic steels have been prepared using special pressure-melting and -casting techniques. With

the aid of nitrogen-bearing ferroalloys as charging materials and an external pressure of several atmospheres nitrogen gas, sound ingots were cast containing about one-half weight percent nitrogen in solid solution.

The elevated temperature properties of the base composition, 16 Cr-14 Mn-2 Mo-½ N, and several of its modifications, were found to be equivalent to those of the commercial alloy 16-25-6, in the temperature range of 1200–1400°F. The hot strength and satisfactory ductility of these alloys plus the retention of an austenitic matrix at elevated temperatures can be attributed, in large measure, to the unusually high nitrogen content.

The alloying elements wolfram, silicon, niobium, vanadium, and nickel, were qualitatively appraised for their effect on the creep-rupture strength of Cr-Mn-N steels. None of these elements was found to be superior to molybdenum. While several percent nickel appears to be beneficial in stabilizing the austenitic matrix at higher temperatures, its presence severely decreases the nitrogen solid solubility.

The room temperature tensile properties of nickel-free high nitrogen austenitic steels are characterized by yield, tensile, and ductility values generally superior to those of commercial austenitic stainless steels. In the cold-worked state, these alloys possess both high tensile strength and good residual ductility.

The oxidation resistance of Cr-Mn-N steels appears to be comparable to those of commercial stainless steels of the same chromium content.

Exploratory studies indicate that conventional welding techniques are applicable. A possible exception is the inert gas, shielded arc process wherein nitrogen or mixtures of nitrogen and argon must be substituted for the usual inert gas.

References

1. R. Franks, W. O. Binder and K. Thompson, "Austenitic Chromium-Manganese-Nickel Steels Containing Nitrogen," TRANSACTIONS, American Society for Metals, Vol. 47, 1955, p. 231.
2. D. J. Mack, "High Manganese Stainless Steels," *Metals and Alloys*, Vol. 18, 1943, p. 507.
3. H. K. Legat, "Austenitic Cr-Mn Steels are Unusually Creep Resistant," METAL PROGRESS, American Society for Metals, Vol. 33, 1938, p. 284.
4. H. Krainer and O. Mirt, "Constitution Diagram of Nitrogen-Containing Chromium and Chrome-Manganese Steels," *Archiv Eisenhuttenwesen*, Vol. 15, 1942, p. 467.
5. R. M. Brick and J. A. Creevy, "Solubility of Nitrogen in Liquid Fe-Cr and Fe-V Alloys," American Institute of Mining and Metallurgical Engineers, Technical Publication No. 1165, 1940, p. 10.
6. F. Rapat, "Applications of Stainless and Heat Resisting Steels Alloyed with Nitrogen," *Stahl und Eisen*, Vol. 61, 1941, p. 1073.
7. F. R. Larson and James Miller, "A Time-Temperature Relationship for Rupture and Creep Stresses," *Transactions*, American Society of Mechanical Engineers, Vol. 74, 1952, p. 765.

UNIVERSITY OF MICHIGAN LIBRARIES

8. R. Franks, W. O. Binder and C. M. Brown, "High Manganese Austenitic Steels," *Iron Age*, Vol. 150, October 1942, p. 51.
9. Anton DeS. Brasunas, James T. Gow and Oscar E. Harder, "Resistance of Iron-Nickel-Chromium Alloys to Corrosion in Air at 1600 to 2200°F," Symposium on Materials for Gas Turbines, 49th Annual Meeting, American Society for Testing Materials, July 24-28, 1946.

DISCUSSION

Written Discussion: By Martin Fleischmann, Metallurgical Engineer, The Timken Roller Bearing Company, Canton.

The authors deserve our thanks for this thought provoking paper. Everybody who is concerned with austenitic steels for high temperature service knows the importance of developing economic materials of low strategic alloy content, capable of high load carrying characteristics.

The pressure melting and casting technique described in the paper deserves our attention. It indicates a new approach to a problem. An approach from the opposite direction compared to vacuum melting and casting of high temperature alloys which, in recent years, created considerable interest.

In laboratory furnaces the authors were successful to produce a base composition of 16Cr-14Mn-2Mo-½N which exhibited high temperature properties approximately equivalent to the commercial 16-25-6 alloy. The elimination of all nickel as an alloying element, replacing it with manganese and increased nitrogen content, was accomplished, employing a pressure melting and casting technique.

We, at Timken, have worked on the problem of lowering the strategic alloy content of the 16-25-6 composition for a number of years. A paper presented before the midwinter meeting of the Society in 1954 dealt with the substitution of manganese for nickel in the 16-25-6 alloy. By replacing 10% of the nickel with 6% of manganese a new modification of this alloy was produced which exhibited essentially the same high temperature properties as the original 16-25-6 material with improved ductility. By lowering the nickel content, the nitrogen could be increased to 0.20% from a 0.15% average composition specified for the standard 16-25-6 alloy.

In the meantime, we have learned to further increase the nitrogen content in the modified 16-15-6 alloy to about 0.30/0.40% without resorting to pressure casting resulting in a material which does not require cold working to obtain hardness levels of 250 to 300 Brinell in the as-rolled or forged condition, an alloy which may be precipitation hardened to a marked degree.

Written Discussion: By H. E. McCune and R. A. Lula, Research Laboratory, Allegheny Ludlum Steel Corporation, Brackenridge, Pa.

The authors have brought a valuable contribution to the knowledge of the high temperature properties of austenitic chromium-manganese steels with high nitrogen which might open the possibilities for the development of new economical high temperature alloys. The strengthening effect of nitrogen extends also to room temperature tensile properties. We have studied this effect in the laboratory using 3 to 60-pound induction and arc furnace heats of straight chromium-manganese steels with up to 0.70% nitrogen. The nitrogen was added as high nitrogen ferrochrome, and no special atmosphere was used.

The plot in Fig. 4 illustrates the influence of nitrogen on the strength and the elongation of the material annealed at 1900 to 2000°F. The maximum strength is

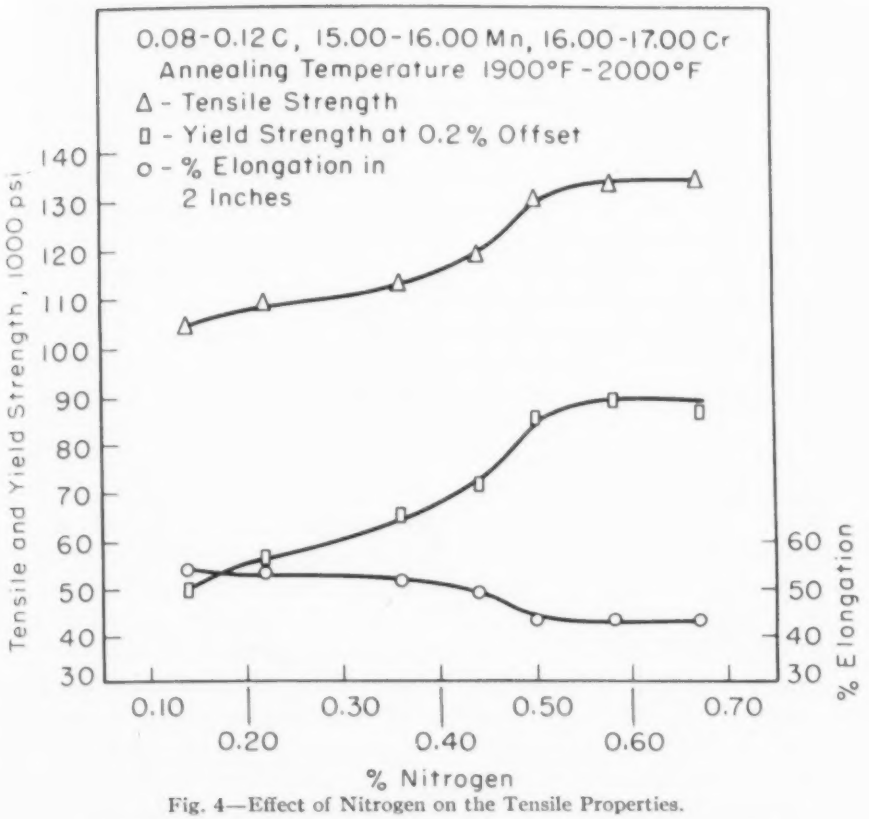


Fig. 4—Effect of Nitrogen on the Tensile Properties.

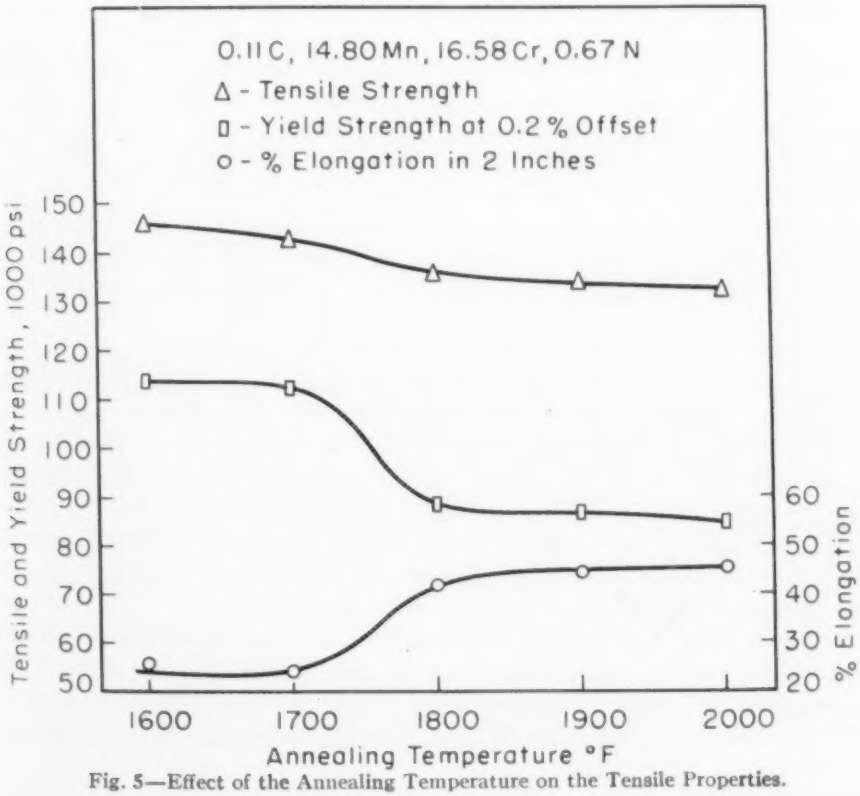


Fig. 5—Effect of the Annealing Temperature on the Tensile Properties.

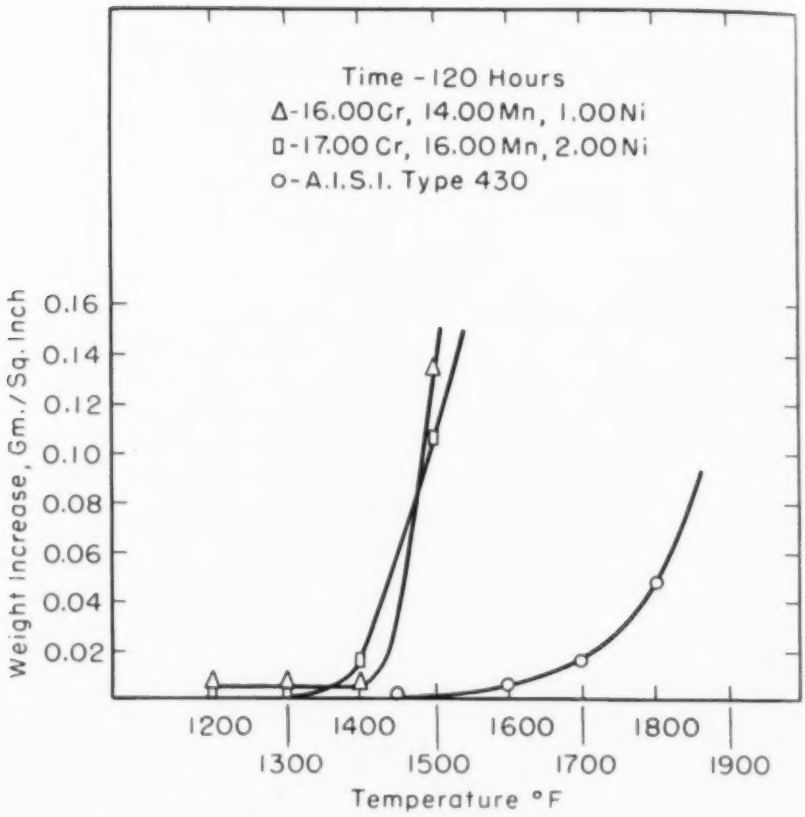


Fig. 6—Oxidation Rates of Types 16-14-1, 17-16-2, and 430.

attained at about 0.50% nitrogen. The elongation decreases continuously up to 0.50% nitrogen, and then it remains more or less constant. The tensile properties are seriously affected by the annealing temperature as shown in Fig. 5. With a 1600 to 1700°F anneal the tensile strength and especially the yield strength are considerably higher than with the 1800 to 2000°F anneal. A lower elongation corresponds to the higher strengths. The compressive 0.2% offset yield strength in the longitudinal direction of a high nitrogen austenitic chromium-manganese steel with a 0.67% nitrogen is 116,000 psi after a 1700°F anneal and 91,000 psi after a 1900°F anneal.

A comparison of the properties of annealed chromium-manganese steel with the properties of cold-rolled AISI Type 301 shows that the longitudinal tensiles of the chromium-manganese steel with a high temperature anneal are equivalent to quarter hard Type 301, and with a low temperature anneal the tensiles are equivalent to half hard Type 301. Based on compressive strength, the chromium-manganese high nitrogen steel is equivalent to full hard Type 301 since the longitudinal compressive yield strength of full hard Type 301 is 90,000 psi. These results point out some very interesting mechanical properties of the chromium-manganese high nitrogen steel for structural applications.

Oxidation tests using the weight gained method carried out in our laboratory show a lower resistance to oxidation than the data obtained by the authors. Fig. 6 shows the weight gain versus temperature of two chromium-manganese steels as compared with a straight chromium steel with approximately the same chromium

content. Above 1400°F the resistance to oxidation of the chromium-manganese steels is lower than the chromium steel indicating that high manganese impairs the oxidation properties of these steels.

Written Discussion: By Edward A. Loria, staff metallurgist, Crucible Steel Company of America, Pittsburgh.

The development of high nitrogen austenitic steels is an important one. This paper ties in directly with the technical note on cast steels[2] which the authors have recently presented, and the writer will direct some questions pertaining to both. First, have the authors extended their work beyond the 12 to 20-pound ingot stage? What final sheet gage was achieved in the cold rolling of alloys 153 and 155? Also, comments on the rate of work hardening on rolling any of the steels would be worthwhile. What stress rupture properties were obtained on welded sheet and how do these values compare with those obtained on the unwelded steels? Was it possible to weld the phosphorus bearing steels?

The writer has been associated with the development of Crucible CMN which is a high C-Cr-Mn-N austenitic steel that has good elevated temperature properties.[3] Its nominal chemical composition is 0.65 C, 12.0 Mn, 25.0 Cr, 0.40 N. The carbon and chromium contents are higher than the subject alloys but, nevertheless, this steel has been utilized principally in sheet form. Furnace rider sheet, 36 x 96 x 0.037 inches thick with an annealed hardness of Rockwell C-25 to 30 (2000°F for 4 minutes) is being produced commercially. CMN has a high hardness in the as-cast or hot-rolled condition which may possibly be explained by a rapid aging reaction that cannot be suppressed. What were the hardness values for the author's steels at different stages of processing? Their comment that improved elevated temperature properties could not be realized with aging treatments or by hot-cold working is noteworthy. Despite its high initial hardness, stress rupture results showed that the strength of CMN increased with increasing stabilization temperature and decreased with longer time at the solution temperature.

Authors' Reply

The authors of this paper are deeply indebted to those who have made both written and oral contributions. We are especially grateful for the high caliber and instructive nature of the comments made.

The beneficial properties which nitrogen confers on elevated temperature alloys has been quickly recognized by the metallurgists of the Timken Roller Bearing Company and put to good use in their high nitrogen modified 16-15-6 alloy. All of us look forward to hearing more about this new precipitation hardening, low strategic index alloy.

The data presented by Messrs. McCune and Lula are most welcome to the growing knowledge of nitrogen as a major alloying element in austenitic steels. It is certainly agreed that the room temperature properties of high nitrogen steels are equally as interesting as those at elevated temperatures.

The relatively low ductility values of the steels reported by McCune and Lula is apparently due to the fact that they used sheet specimens while we employed ¼-inch diameter round tensile bars. The lowest ductility obtained in any solution quenched Cr-Mn-N steel was about 50% elongation. The decreased

[2] J. F. Carlson and V. F. Zackay, "High Nitrogen Cast Austenitic Steels," *Journal of Metals* Vol. 7, October 1955, p. 1112.

[3] E. A. Loria, "New Stainless Steels Qualify for High-Temperature Service: Part 2—Nickel-Free Grade," *Iron Age*, Vol. 176, October 1955, p. 65.

ductility of this steel is probably due to the rather high carbon content, viz., eighteen points. All other steels tested possessed more than 60% elongation. We regard this retention of excellent ductility with increased tensile and yield strength as one of the outstanding characteristics of high nitrogen steels, viz., those containing 40 to 80 points of nitrogen.

The interesting comments made by Messrs. McCune and Lula with reference to the potential use of high nitrogen Cr-Mn alloys for structural applications deserves much attention. In this regard, the atmospheric corrosion and elevated temperature oxidation resistance are of importance. A re-examination of the data gathered by the authors reveals, as McCune and Lula rightly point out; that the oxidation resistance of Cr-Mn-Mo-N steels is definitely inferior to either straight chromium or to the nickel-containing austenitic steels of the same chromium content. A considerable improvement in oxidation resistance of Cr-Mn-N steels was noted in high silicon alloys.

A few comments regarding pressure melting and casting are in order. Since the submission of this paper considerable effort has been devoted to development of techniques designed to add nitrogen at high levels without the use of super-atmospheric pressure. Several methods can now be recommended.

Centrifugal casting was successfully used by the present authors in production of Cr-Mn-Mo-N castings containing more than 70 points of nitrogen.

A process applicable to the production of large ingots of high nitrogen steels is suggested by low carbon rimming steel practice. Gas holes formed during ingot solidification are not detrimental if they weld shut during hot rolling. An economic advantage of gassing ingots is the increased ingot-to-slab yield. This process is especially suited to those steels containing elements which increase the activity, hence the vapor pressure of nitrogen in liquid steel. Molybdenum above 3%, nickel above 2%, and silicon at any level, are a few of the elements acting in this manner. Pressure melting and casting was used in this investigation primarily for alloys containing these elements. Most of the alloys made did not require pressure melting and casting to produce sound ingots.

Lastly, the excellent high temperature strength of the boron-containing chromium-manganese steels shown by Mr. Dyrkacz of Allegheny-Ludlum is most encouraging. Apparently iron-base "superalloys" have finally arrived. It is our humble opinion that further work of this caliber promises to significantly alter the economics of refractory metals and of course to ensure their more widespread utilization.

Dr. Loria's interesting comments on the properties of Crucible CMN, a nickel-free austenitic, and the subject high nitrogen alloys are very much appreciated. The authors, in cooperation with the Allegheny-Ludlum Steel Corp., have made heats of 1000 lbs. of the Cr-Mn-Mo-N alloys. The U. S. Steel Co. has made ingots of the Cr-Mn-N type as large as 30 tons. The final sheet thickness of alloys 153 and 155 was about 0.050 inches. These alloys were cold-rolled to the final thickness from 0.100 inches. The last reductions were of the order of 5%. As other investigators have observed, alloys of this type work-harden at a rate intermediate between that of austenitic stainless steels AISI Types 301 and 302. No elevated temperature stress-rupture properties were obtained on welded sheet.

The element phosphorus functions as a precipitation-hardening agent only in the presence of high carbon.[4] Since all the subject alloys were low carbon, little

[4] J. K. Y. Hum and N. J. Grant, "Austenite Stability and Creep-Rupture Properties of 18-8 Stainless Steels," TRANSACTIONS, American Society for Metals, Vol. 45, 1953, p. 105.

benefit was derived from the addition of phosphorus as an alloying element. By the same token, no increase in hardness or stress-rupture life was observed with various heat treatments since the relatively low carbon content does not allow for extensive chromium carbide precipitation. Chromium nitrides are not effective precipitation-hardening compounds. The addition of vanadium does initiate precipitation of vanadium nitrides, thereby making the high nitrogen alloys amenable to heat treatment.

HARVARD UNIV. OF BUILDING LIBRARIES

ROLLING TEXTURES IN TANTALUM

By J. W. Pugh and W. R. Hibbard, Jr.

Abstract

Cold-rolled and recrystallized textures of tantalum are presented as pole figures. Pole figures for cold-rolled metal were interpreted in terms of the "ideal" orientations {112} <011>, {100} <011>, and {111} <112>. Similarity with other body-centered cubic textures was observed, but the existence of discrete orientations near the {112} <011> is unusual. Analysis by means of the Pickus-Mathewson criterion indicates that slip takes place on the {110} plane. Interpretation of the recrystallized texture has been made in terms of a single orientation, {111} <112>. The usual split {100} <011> ±15° orientation was not observed. It is suggested that the dominant recrystallization mechanism for tantalum is that of growth selectivity. (ASM-SLA Classification: Q24, Ta)

Introduction

THE earliest work on the sheet textures of body-centered cubic metals was concerned with iron and steel. The cold-rolled texture was found to be primarily {100} <011> with a deviation from this position chiefly about the rolling direction as an axis (1)[1]. Textures in mild steel have been shown to have orientations which are rotated up to about 55 degrees about the rolling direction from the ideal {100} <011> orientation (2). There is evidence that this range of deviation decreases with increasing amounts of cold rolling (3). Kurdjumow and Sachs have published pole figures of cold-rolled iron which are described in terms of ideal orientations {112} <011> and {111} <112>, as well as {100} <011> (4). Pole figures for iron containing 4.6% silicon have been published which are almost identical to those of Kurdjumow and Sachs (5). However, increasing carbon content has been shown to cause an increasing randomness of the texture (6).

Kurdjumow and Sachs have also analyzed the recrystallized texture of iron and steel (4). In this case, the texture can be described in terms of two orientations. These are {111} <112> and {100} <011> ±15 degrees of rotation about the normal to the roll-

[1]The figures appearing in parentheses pertain to the references appended to this paper.

A paper presented before the Thirty-Seventh Annual Convention of the Society, held in Philadelphia, October 17–21, 1955. The authors, J. W. Pugh and W. R. Hibbard, Jr., are associated with the Metallurgy and Ceramics Research Department, General Electric Co., Schenectady. Manuscript received June 9, 1955.

ing plane. Recrystallized textures reported for iron-silicon alloys are not consistent. They have been found to be similar to those for iron (5) and, in another case, to be describable in terms of the {110} <001> orientation (7).[2]

The cold-rolled texture for molybdenum is very similar to that of iron. The principal orientation is again the {100} <011> with a similar spread about the rolling direction (8). The recrystallized texture is reported to be identical to the cold-rolled texture, except that less spread about the {100} <011> orientation is observed.

Vanadium appears to have a cold-rolled texture like iron also, and has been described in terms of the orientations {100} <011>, {112} <011>, and {111} <112> or by a ±55-degree spread about the {100} <011> (9). Pole figures made for recrystallized vanadium are also very similar to the recrystallized pole figures of iron. They represent a texture which is described as centered about the orientation {111} <112> and the orientation {100} <011> rotated ±15 degrees about the normal to the rolling plane.

The texture of another body-centered cubic metal, chromium, has been investigated recently (10). The cold-rolled texture is reported to be mainly {100} <011> with some evidence of the {111} <112> orientation. A determination for recrystallized chromium sheet indicated no preferred orientation.

Zirconium-niobium alloys containing 18% niobium are body-centered cubic. A recent analysis of the rolling textures of such an alloy indicates that both the cold-rolled and recrystallized textures are comparable to those of iron (11). In this case, the cold-rolled texture was described as the {100} <011> orientation with ±47-degree spread about the rolling direction. Recrystallized textures were said to consist of two {100} <011> orientations displaced ±23 to 26 degrees from the rolling direction about a normal to the rolling plane as an axis of rotation.

It is apparent that the textures of body-centered cubic metals are strikingly similar. Cold-rolled textures are consistent and can usually be described by the {100} <011> orientation with a large spread (40 to 60 degrees) about the rolling direction in the plane of the sheet. Much smaller spreads are observed around the cross direction as an axis. Alternate descriptions of this texture can be made based on the three "ideal" orientations {100} <011>, {112} <011>, and {111} <112>. For recrystallized body-centered cubic metals the most frequent components reported are the {111} <112> orientation and a split {100} <011>, each component of which is rotated (15 to 25 degrees) from the rolling direction about the pole of the rolling plane.

[2]It is likely that the difference is due to obtaining primary recrystallization in the first case and secondary recrystallization in the latter.

Experimental Procedure

Tantalum was received as 95% reduced cold-rolled strip from the Fansteel Metallurgical Corporation. Fig. 1 is a photomicrograph of the as-received metal. A series of annealing treatments which subjected the tantalum to various temperatures for ½-hour periods were applied. The hardness measurements and the metallographic examination of these samples indicated that recrystallization could



Fig. 1—Tantalum Cold-Rolled 95%. ×250.

be expected to take place between 1830 and 2550°F. Fig. 2 shows hardness plotted as a function of annealing temperature. Strip which had been recrystallized at 0.010-inch thick was further cold-rolled 95% to 0.0005-inch thick in a Sendzimir rolling mill. X-ray diffraction samples were cut from this strip and annealed at 2010, 2190, 2370, 2550, and 4530°F. Attempts to polish and etch this very thin strip for metallographic comparison with the thicker strip were unsuccessful. Figs. 3 to 7 are photomicrographs of the thicker strip which had the same annealing treatments as were used for the X-ray diffraction specimens.

Chemical analysis for this material is as follows:

Element	Weight Per Cent Present
oxygen	0.0056
nitrogen	0.013
niobium	0.10
tungsten	0.01
iron	0.015
carbon	0.02

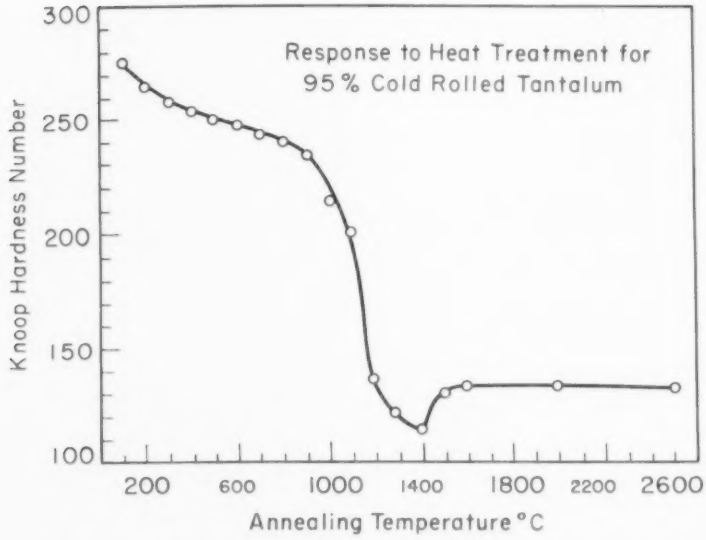


Fig. 2—Effect of Annealing Temperature On The Hardness of Cold-Rolled Tantalum.

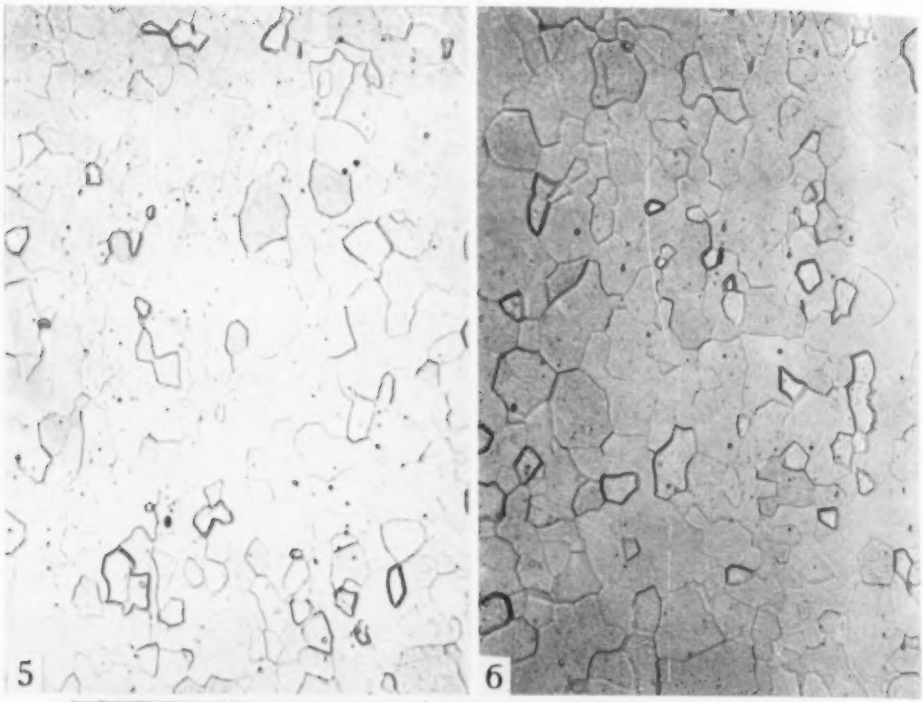




Fig. 3—Tantalum Cold-Rolled 95%—Annealed at 1100°C (2010°F) For 30 Minutes, ×250.

Fig. 4—Tantalum Cold-Rolled 95%—Annealed at 1200°C (2190°F) For 30 Minutes, ×250.

Pole figures were made by a technique devised by Geisler (12). It involved the use of an integrating pole figure goniometer which permits the continuous rotation about a perpendicular to the sheet



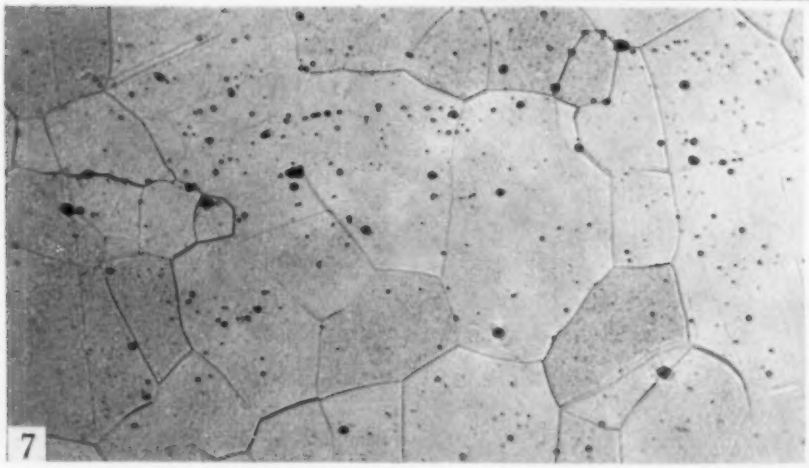


Fig. 5—Tantalum Cold-Rolled 95%—Annealed at 1300°C (2370°F) For 30 Minutes. ×250.

Fig. 6—Tantalum Cold-Rolled 95%—Annealed at 1400°C (2550°F) For 30 Minutes. ×250.

Fig. 7—Tantalum Cold-Rolled 95%—Annealed at 2500°C (4530°F) For 30 Minutes. ×250.

as an axis (β angles) and a 5-degree incremental rotation about a direction parallel to the plane of the sheet (α angles). The specimen was raised and lowered a distance of one inch at a rate of one cycle per second so that a large area could be covered by the incident X-rays. Diffracted X-rays were detected by a stationary Geiger-counter detector mounted at the appropriate 2Θ angle. Intensities were calibrated by comparison with diffraction from a random sample. The effect of a changing α angle on the absorption factor (μt)

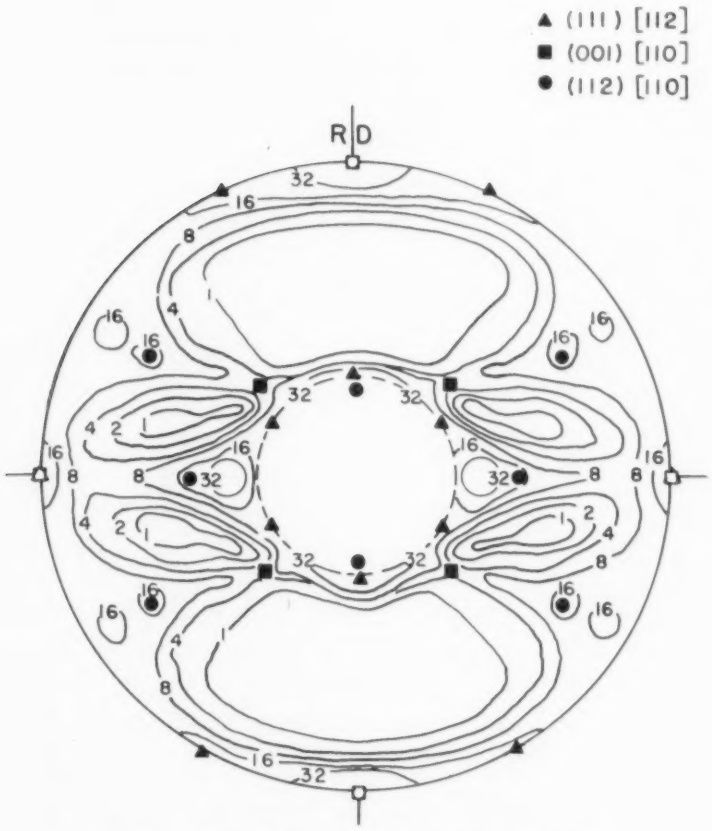


Fig. 8—110 Pole Figure For Cold-Rolled Tantalum.

was compensated for by calibrated resistances in the pick-up circuit. Intensity data were recorded autographically on a chart recorder and on an automatic pole figure recorder (12).

Molybdenum Kα radiation was used with a zirconium filter. A 3-degree slit in the XRD-3 spectrogoniometer was used so that the total exposed area on the specimen was 0.3 square inches. Rotation of the specimen beyond an α angle of 55 degrees was not possible because of the interference of the specimen holder. This limitation is indicated in the pole figures published here by a dotted circle.

Spurious intensities which resulted from white radiation were identified in two ways. The first was to take new data in questionable areas using an auxiliary strontium filter to remove Kα and making a comparison with the original data. The second technique was to compare the results obtained by diminishing the spectrogoniometer slit to 1 degree.

Results

The cold-rolled texture of tantalum is revealed in the 110 pole figure of Fig. 8 and the 200 pole figure of Fig. 9. These pole figures

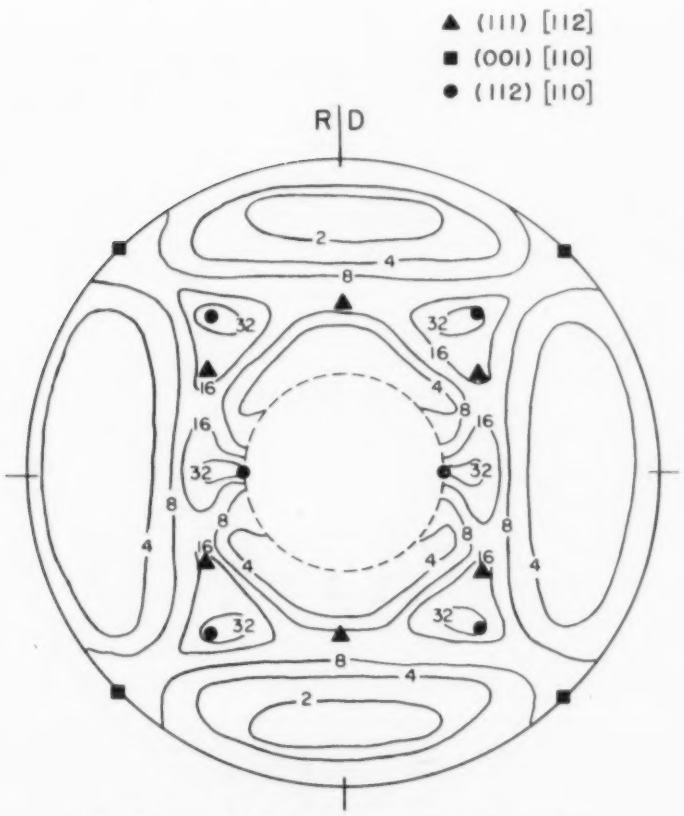


Fig. 9—200 Pole Figure For Cold-Rolled Tantalum.

may be observed to be similar to those already published for other body-centered cubic metals. This texture can be interpreted in terms of the orientations {100} <011>, {112} <011>, and {111} <112>. The last two are double textures which are disposed to cause symmetry in the cross direction and the rolling direction respectively. The intensity peaks associated with {112} <011> are not all centered precisely on this orientation. The component having the highest intensity in the contour plot of Fig. 8 is displaced about 12 degrees from {112} and it corresponds approximately to the orientation {223} <011>. Description of the cold-rolled texture in terms of a single spread about the rolling direction as an axis is not satisfactory in this case in view of the discrete intensity peaks associated with these other orientations.

Fig. 10 is the 110 pole figure of the sheet annealed at 2010°F. The intensity spread is somewhat diminished and the primary texture is now definitely near the {223} <011> orientation. Fig. 11, the pole figure of the 2190°F annealed sheet, shows what may be described as the effect of recrystallization on the texture. The intensity peak at {223} <011> has disappeared and a new one appears at approximately the orientation {115} <011>. In the sam-

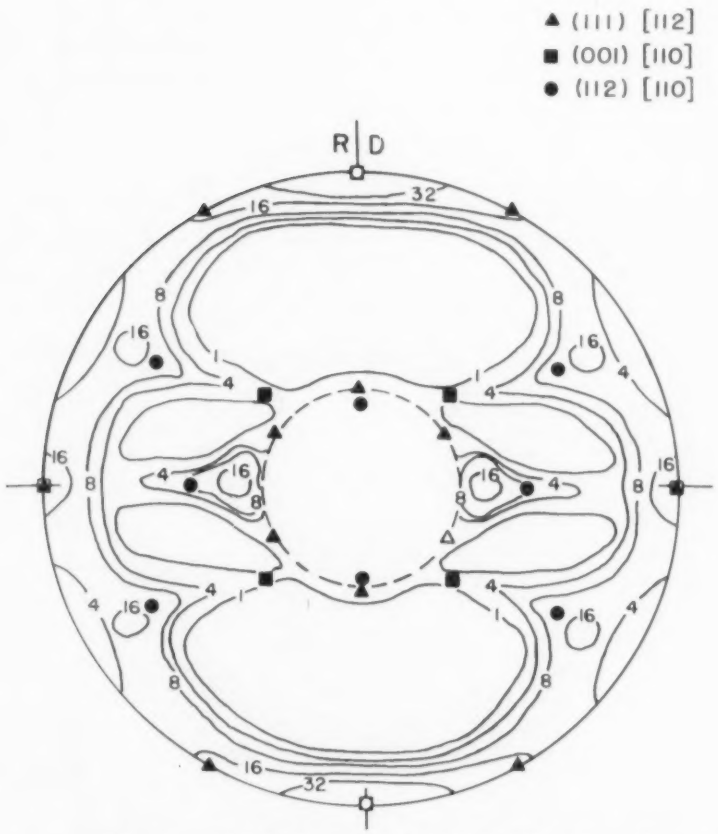


Fig. 10—110 Pole Figure For Cold-Rolled Tantalum After Annealing at 1100°C (2010°F).

ple annealed at 2370°F, Fig. 12, the component near {115} <011> in Fig. 11 is less in evidence, otherwise there is little difference between the two pole figures.

Figs. 2 and 6 both indicate that full recrystallization has been reached at 2550°F. Fig. 13 is the 110 pole figure and Fig. 14 is the 200 pole figure for sheet specimens having this treatment. They are in good agreement and show the existence of a texture attributable only to the {111} <112> orientation. Fig. 15 is the 110 pole figure of the 4530°F treated sheet. This texture is like that of Figs. 13 and 14 except that it is considerably sharper.

Discussion

The cold-rolled texture of tantalum is similar to those published for other body-centered cubic metals. It is not, however, satisfactory to describe this texture entirely as a spread of the {100} <011> orientation, because there are evidences of other discrete orientations.

Two sets of "ideal" orientations have been proposed for body-centered cubic metals. The first are the {100} <011>, {112}

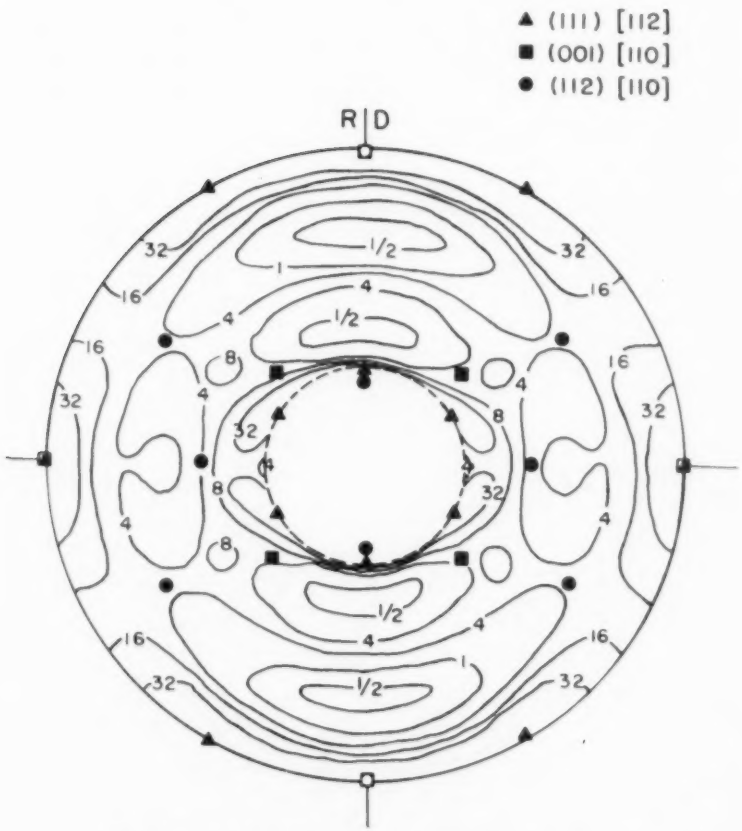


Fig. 11—110 Pole Figure For Cold-Rolled Tantalum After Annealing at 1200°C (2190°F).

<011>, and {111} <112>. These have frequently been used to describe various body-centered cubic metal textures and have been reported as the stable end orientations of rolled single crystals (13). The other set which consists of {100} <011>, {111} <112>, and {111} <011> were proposed as stable orientations by Hibbard and Yen (14). They are based on calculations which assume that the body-centered cubic slip system is {110} <111>. They considered the {100} <011> orientation the most favorable because the <111> active slip directions lie in the plane containing the rolling direction and perpendicular to the rolling plane. Such an orientation would preclude transverse spread. It is less important that this plane be perpendicular to the rolling plane when the active <111> slip directions are symmetrically disposed, as they are for the pole figures of this investigation.

New calculations were made using the Pickus and Mathewson (15) criterion that the product $\cos \chi \cos \lambda \cos \phi$ is a maximum for the most stable end orientations. The angles are defined as follows: χ is the angle between the stress axis and the pole of the operating slip plane, λ is the angle between the stress axis and the slip direc-

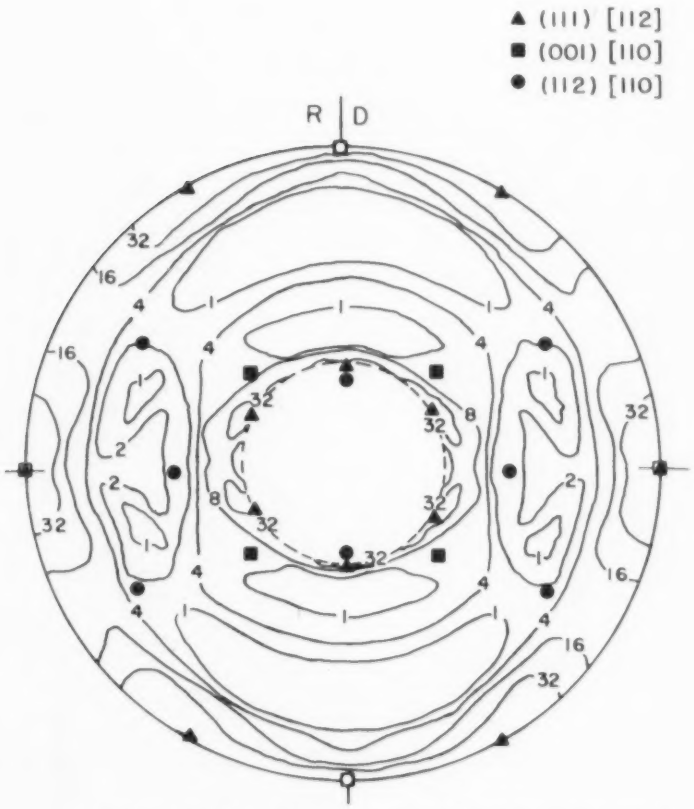


Fig. 12—110 Pole Figure For Cold-Rolled Tantalum After Annealing at 1300°C (2370°F).

tion, and ϕ is the angle between the operating slip direction and the flow direction. The normal to the rolling plane is considered the stress axis and the rolling direction is the flow direction. Table I

Table I

Orientation		110 Slip Plane				112 Slip Plane				123 Slip Plane			
		χ	λ	ϕ	Cos Prod.	χ	λ	ϕ	Cos Prod.	χ	λ	ϕ	Cos Prod.
112	011	30	60	35	0.36	33	60	35	0.34	29	60	35	0.36
100	011	45	54	35	0.34	35	54	35	0.40	37	54	35	0.39
111	112	35	70	19	0.25	19	70	19	0.29	22	70	19	0.30
111	011	35	70	35	0.23	19	70	35	0.26	22	70	35	0.26

contains the results of these calculations. For {110}-type slip, the stable end orientations are in order of stability {112} <011>, {100} <011>, {111} <112>, and {111} <011>. If {112}-type slip is postulated, the order is {100} <011>, {112} <011>, {111} <112>, and {111} <011>. For {123}-type slip, the order is the same as for {112}. These results indicate the importance of the choice of slip plane and suggest a method for selecting a slip system

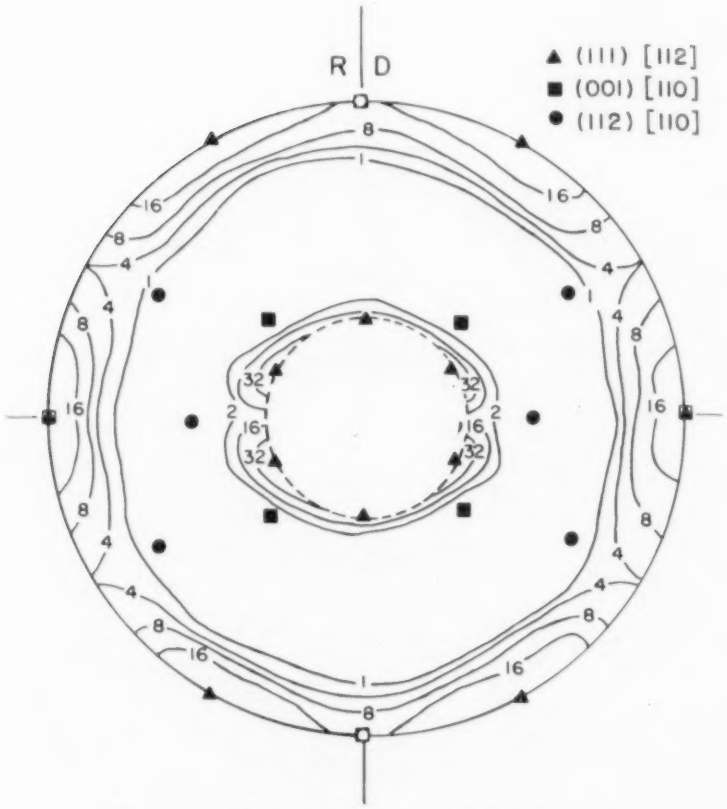


Fig. 13—110 Pole Figure For Cold-Rolled Tantalum After Annealing at 1400°C (2550°F).

for body-centered cubic metals consistent with the Pickus-Mathewson criterion. The application of this suggestion to the tantalum data of this investigation implies that the {110}-type slip plane is operative. Furthermore, such metals as iron (1), molybdenum (8), vanadium (9), and chromium (10), which have a predominant {100} <011> rolling texture, ought to have {112}-type slip.

Annealing appears to have caused (a) a sharpening of the texture near {112} <011> during recovery, (b) a strengthening of the {111} <112> texture during recrystallization, (c) a monopoly of the texture by the single orientation {111} <112> after recrystallization, and finally (d) a sharpening of the {111} <112> texture after grain growth. This sequence suggests that recrystallization takes place in tantalum by a growth selectivity mechanism. The {111} <112> orientation which was present in the cold-rolled metal appears to have grown at the expense of other orientations.

The crystallographic relationship between deformation orientation and recrystallized orientations for certain face-centered cubic metals has been shown to involve a rotation about a pole of the active slip plane as an axis (17,18). In addition, it has been re-

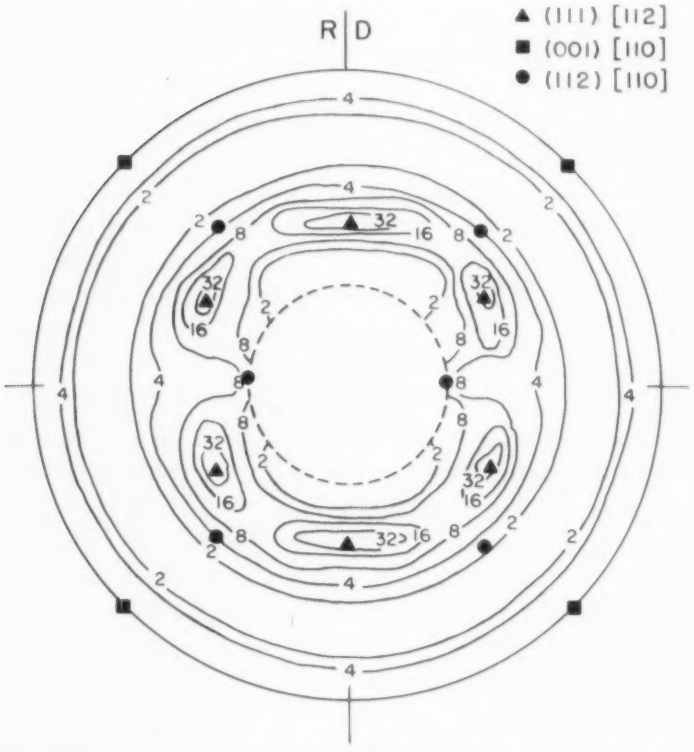


Fig. 14—200 Pole Figure For Cold-Rolled Tantalum After Annealing at 1400°C.

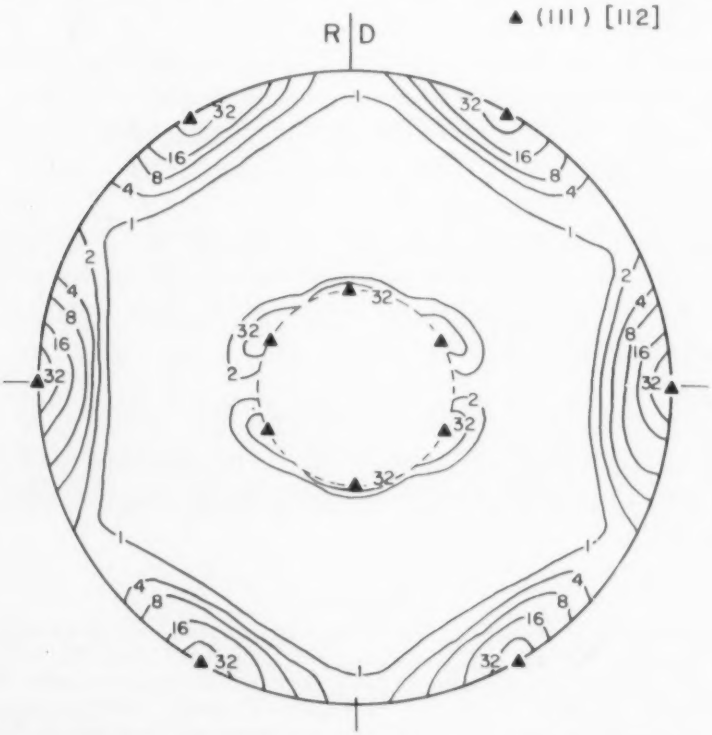


Fig. 15—110 Pole Figure For Cold-Rolled Tantalum After Annealing at 2500°C.

ported that the deformation itself seems to produce rotation about the active slip plane normal (19). This suggests that in these cases, the deformation process itself may control the orientation and that the recrystallization mechanism is one of oriented nucleation.

For the orientation changes which appear to take place for tantalum, that is, {112} <011> to {111} <112> and {001} <011> to {111} <112>, simple rotation about a pole of an active slip plane has not occurred. It must be concluded, therefore, that the conception of oriented nucleation which depends on a rotational deviation about the pole of an active slip plane does not apply for the recrystallization of tantalum.

It is interesting to observe that there is apparently a fundamental difference between the recrystallization of tantalum, as described here, and that of silicon-iron. In tantalum the {111} <112> component does not recrystallize to {110} <001>, as in silicon-iron, but remains "in situ." This suggests that the predominate mechanism in the two cases is different. It may be, for example, that the recrystallization of tantalum is a matter of growth selectivity, while the recrystallization of silicon-iron may, on the other hand, involve oriented nucleation.

Summary

Tantalum has been shown to develop a rolling texture which is predominately {112} <011> and contains the components {100} <011> and {111} <112>. On annealing, the {112} <011> and {100} <011> orientations disappear and after recrystallization the {111} <112> remains as the single orientation in the texture. Annealing at very high temperatures produces a very sharp {111} <112> texture.

These results, when analyzed on the basis of existing theories, indicate that slip and flow take place on 110 planes in the 111 direction in tantalum and that growth selectivity is the preponderant factor during recrystallization.

Acknowledgment

The authors wish to acknowledge the assistance of Mrs. Ann Cooper, who operated the X-ray equipment and prepared the pole figure data.

References

1. Zay Jeffries, "The Trend in the Science of Metals," *Transactions*, American Institute of Mining and Metallurgical Engineers, Vol. 70, 1924, p. 303.
2. Franz Wever, "Uber die Walzstruktur kubisch kristallisierender Metalle (On the Cold Worked Structure of Cubic Metals)," Mitteilungen aus dem Kaiser-Wilhelm-Institut für Eisenforschung zu Dusseldorf, Vol. 5, 1924, p. 69.

3. Carl B. Post, "Preferred Orientation and Rolling Characteristics of Low Carbon Strip Steels," TRANSACTIONS, American Society for Metals, Vol. 24, 1936, p. 679. D. McLachlan, Jr. and Wheeler P. Davey, "An X-Ray Study of Preferred Orientations in Pure Cold Rolled Iron-Nickel Alloys," TRANSACTIONS, American Society for Metals, Vol. 25, 1937, p. 1084.
4. G. Kurdjumow and G. Sachs, "Walz-und Rekristallisationstextur von Eisenblech (Cold Worked and Recrystallized Textures of Iron Sheet)," *Zeitschrift für Physik*, Vol. 62, 1930, p. 592.
5. C. S. Barrett, G. Ansel, and R. F. Mehl, "Preferred Orientations in Iron-Silicon Alloys," *Transactions*, American Institute of Mining and Metallurgical Engineers, Vol. 125, 1937, p. 516.
6. George Lindenberg Clark, *Applied X-Rays*, Third Edition, 1940, p. 532, 577, McGraw Hill Book Company, Inc.
7. Richard M. Bozorth, "The Orientation of Crystals in Silicon Iron," TRANSACTIONS, American Society for Metals, Vol. 23, 1935, p. 1107. J. T. Burwell, "Crystal Orientations in Silicon-Iron Sheet," *Transactions*, American Institute of Mining and Metallurgical Engineers, Vol. 140, 1940, p. 353.
8. M. Semchyshen and G. A. Timmons, "Preferred Orientation of Arc-Cast Molybdenum Sheet," *Transactions*, American Institute of Mining and Metallurgical Engineers, Vol. 194, 1952, p. 279.
9. Carl J. McHargue and Joseph P. Hammond, "Preferred Orientation in Vanadium," *Transactions*, American Institute of Mining and Metallurgical Engineers, Vol. 194, 1952, p. 745.
10. W. H. Smith, "On the Casting, Rolling, and Annealing Textures of Chromium," *Journal of Metals*, Vol. 7, No. 9, Section 2, September 1955, p. 1064.
11. J. H. Keeler and A. H. Geisler, "Preferred Orientations in Beta-Annealed Zirconium," General Electric Research Laboratory Report No. RL 1148, August 1954.
12. A. H. Geisler, "Crystal Orientation and Pole Figure Determination," MODERN RESEARCH TECHNIQUES IN PHYSICAL METALLURGY, 1953, p. 131, American Society for Metals.
13. C. S. Barrett and L. H. Levenson, "Analysis of the Cold Rolling Texture of Iron," *Transactions*, American Institute for Mining and Metallurgical Engineers, Vol. 145, 1941, p. 281.
14. Walter R. Hibbard, Jr. and Ming-Kao Yen, "Wire Textures of Copper and Its Binary Alpha Solid Solution Alloys with Aluminum, Nickel, and Zinc," *Transactions*, American Institute of Mining and Metallurgical Engineers, Vol. 175, 1948, p. 126.
15. M. R. Pickus and C. H. Mathewson, "On the Theory of the Origin of Rolling Textures in Face Centered Cubic Metals," *Journal*, Institute of Metals, Vol. 64, 1939, p. 237.
16. C. G. Dunn, "Cold Rolled and Primary Recrystallization Textures in Cold Rolled Single Crystals of Silicon Iron," ACTA METALLURGICA, Vol. 2, 1954, p. 173.
17. Robert Maddin, C. H. Mathewson, and Walter R. Hibbard, Jr., "The Origin of Annealing Twins in Brass," *Transactions*, American Institute of Mining and Metallurgical Engineers, Vol. 185, 1949, p. 655.
18. J. E. Burke and D. Turnbull, "Recrystallization and Grain Growth," *Progress in Metal Physics*, Vol. 3, 1952, p. 220, Pergamon Press Ltd.
19. R. D. Heidenreich and W. Shockley, "Study of Slip in Aluminum Crystals by Electron Microscope and Electron Diffraction Methods," Report of a Conference on Strength of Solids, The Physical Society, 1948, p. 57.

THE INITIATION OF DISCONTINUOUS YIELDING IN DUCTILE MOLYBDENUM

By J. A. Hendrickson, D. S. Wood, and D. S. Clark

Abstract

This paper presents the results of an experimental investigation of the initiation of yielding in fine-grained ductile molybdenum under rapidly applied constant stress. Two lots of material, one produced by arc-casting and the other by powder metallurgy methods were investigated. The experiments were conducted at temperatures of −74°F (−59°C), +76°F (24°C), and +200°F (93°C).

The results show that fine-grained ductile molybdenum exhibits the phenomenon of delayed yielding as well as a distinct yield point in the static stress-strain relation. The dependence of the delay time for yielding upon stress and temperature is found to be similar to that exhibited in low carbon steel. These results, together with others obtained in this investigation, indicate that the mechanism of the initiation of yielding in ductile molybdenum is substantially the same as for annealed low carbon steel. This lends further support to the dislocation theory of yield point phenomena based upon the concept of the anchoring of dislocations in body-centered cubic metals by interstitial solute atoms. (ASM-SLA Classification: Q23, Mo)

THE investigation of delayed yielding has been in progress for several years at California Institute of Technology. The technique involves the application of a constant tensile stress to a specimen while deformation is measured as a function of time. The stress is increased from zero to its final value in a continuous manner within a total time of from 5 to 10 millisec. The stress is then held constant for the remainder of the test.

Rapid loading tests of this type have been made previously on annealed low carbon steel (1,2,3).[1] The results showed that a well defined period of time was required for the initiation of plastic deformation at stresses exceeding the static upper yield stress. This observed period of time has been defined as the "delay time for yielding."

The delay time for a given material depends upon the tem-

[1]The figures appearing in parentheses pertain to the references appended to this paper.

A paper presented before the Thirty-Seventh Annual Convention of the Society, held in Philadelphia, October 17–21, 1955. Of the authors, J. A. Hendrickson is research assistant, D. S. Wood is assistant professor of mechanical engineering, and D. S. Clark is professor of mechanical engineering, California Institute of Technology, Pasadena, Calif. Manuscript received April 8, 1955.

perature of the material and the applied stress. For mild steel it is found that at any given temperature, the relation between the logarithm of the delay time and the applied stress may be represented by a straight line along which the logarithm of the delay time decreases as the stress is increased to values above the static upper yield stress. The logarithm of the delay time at a constant stress level is found to vary approximately as the inverse of the absolute temperature.

Delayed yielding has been shown previously to exist in single crystals of the body-centered cubic metal, beta brass, as well as in mild steel (4). There has not been any evidence of delayed yielding in single crystals of the face-centered cubic metals, alpha brass and aluminum (4).

A very small amount of inelastic strain has been found to occur in rapid load tests on annealed mild steel during the period of delay before yielding (5, 6). The rate at which this inelastic microstrain develops is greatest at the beginning of constant load and decreases until a microstrain of about 30×10^{-6} in./in. is present. After the strain has reached a value of this order of magnitude, yielding occurs. Such microstrains also occur when the test stress is less than the static upper yield stress but greater than about one-half that value. When stresses in this range are applied the microstrain increases with time and asymptotically approaches an equilibrium value which is a function of the applied stress and test temperature.

A theoretical model of a yield nucleus has been proposed (6,7), which is capable of quantitatively describing the experimental observations of delayed yielding and pre-yield inelastic microstrain in terms of the generation and motion of dislocations. This model is based upon the concept of the thermally activated release of dislocations from carbon and nitrogen "atmospheres" as proposed by Cottrell and Bilby, (8), the Frank-Read dislocation source (9), and the obstruction of dislocation motion by grain boundaries proposed by Cottrell (10).

Carbon and nitrogen atoms in interstitial solid solution are believed to produce a shear distortion as well as a simple volume expansion of the body-centered cubic iron lattice. For this reason these atoms are capable of forming relatively tightly bound "atmospheres" around screw dislocations (11,12), as well as edge dislocations in iron and steel, and thus give rise to the yield point phenomena. On the other hand solute atoms are not expected to produce appreciable shear distortions in face-centered cubic lattices, and hence will not form tightly bound "atmospheres" around screw dislocations. This then explains the fact that marked yield point phenomena are not observed in the face-centered cubic metals.

These theoretical considerations thus indicate that the phenomenon of delayed yielding should always be found for materials that have the body-centered cubic crystal structure and that exhibit distinct upper and lower yield points in their static stress-strain relations. Therefore, it is of some interest to determine whether materials of the body-centered cubic type, other than iron and beta brass, exhibit delayed yielding and the associated pre-yield inelastic microstrain effects. One such material is molybdenum. Bechtold and Scott (13) have shown that fine grained ductile molybdenum exhibits distinct upper and lower yield points in its static stress-strain relation. The purpose of this paper is to present the results of an investigation to determine if molybdenum exhibits delayed yielding under rapidly applied loads, and to compare its behavior with that of low carbon steel over suitable ranges of applied stress and temperature.

Material, Test Specimens and Treatment

The material used in this investigation is high purity molybdenum, cold-worked and completely recrystallized to obtain a uniform, fine grain structure. The investigations were made on molybdenum produced by two different processes. One type of molybdenum was produced by arc-casting and the other was produced by powder metallurgy methods, hereafter referred to as sintered molybdenum.

The arc-cast molybdenum was supplied by the Climax Molybdenum Company and the sintered molybdenum was obtained from the Westinghouse Electric Corporation. The analyses of these materials as provided by the suppliers are as follows:

Climax (Arc-Cast) Heat No. 4-1050		Westinghouse (Sintered) Lot No. WNS-8000S	
Carbon	0.033%	Carbon	0.006–0.007%
Oxygen	0.003% (max.)*	Oxygen	0.0019–0.0023%
Nitrogen	0.0002% (max.)*	Nitrogen	0.011–0.013%

*Based on actual analysis of other similar heats.

The molybdenum was received in the form of 5/8 inch diameter bar rolled at a temperature below the recrystallization temperature. Specimen lengths were cut from the bar stock, machined to approximate dimensions, and finish ground.

The specimens were recrystallized in a purified dry hydrogen atmosphere after finish grinding. The furnace schedule for the arc-cast molybdenum specimens was as follows:

1) heat to 2350°F at normal furnace rate under full power,
2) hold at 2350°F for 1 hour,
3) cool from 2350°F to room temperature at normal furnace rate with power off.

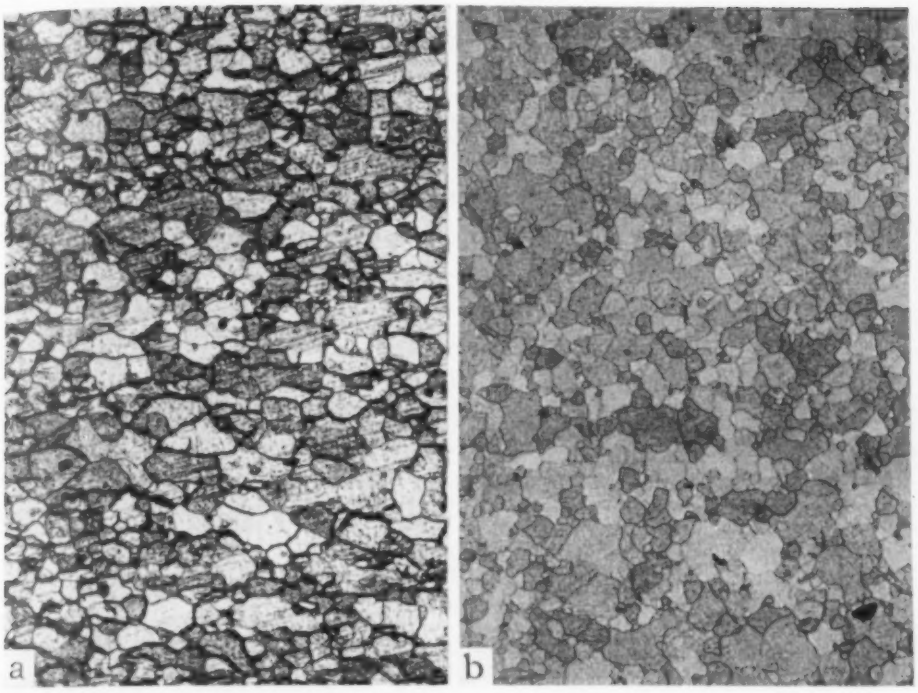


Fig. 1—Structure of Arc-Cast and Sintered Molybdenum. (a) Arc-cast molybdenum; (b) Sintered molybdenum. ×100.

The furnace schedule for the sintered molybdenum specimens was as follows:

1) heat to 2100°F at normal furnace rate under full power,
2) hold at 2100°F for 1 hour,
3) cool from 2100°F to room temperature at normal furnace rate with power off.

These recrystallization treatments are essentially the same as those which were found by Bechtold and Scott (13) to give completely recrystallized uniform fine grain structures. The photomicrographs presented in Fig. 1 show that such structures are present in the specimens employed in the present investigation.

Two types of specimens were used in this investigation. The design of the first type of specimen in which threads were used to transmit the applied force to the specimen is shown in Fig. 2. Specimens of this type are the same as those used in previous investigations (1). The stress concentration caused by the threads in rapid-load tests on arc-cast molybdenum at stresses above 95,000 psi produced fracture in the thread reliefs of the specimens. The specimen design designated as type 2 and shown in Fig. 2, which eliminates the need for threads on the specimen, was used for rapid-load tests at stresses above 95,000 psi on arc-cast molybdenum and for all the tests on sintered molybdenum. Both types of specimens have a round gage section 0.300 inch in diameter and 1 inch in length.

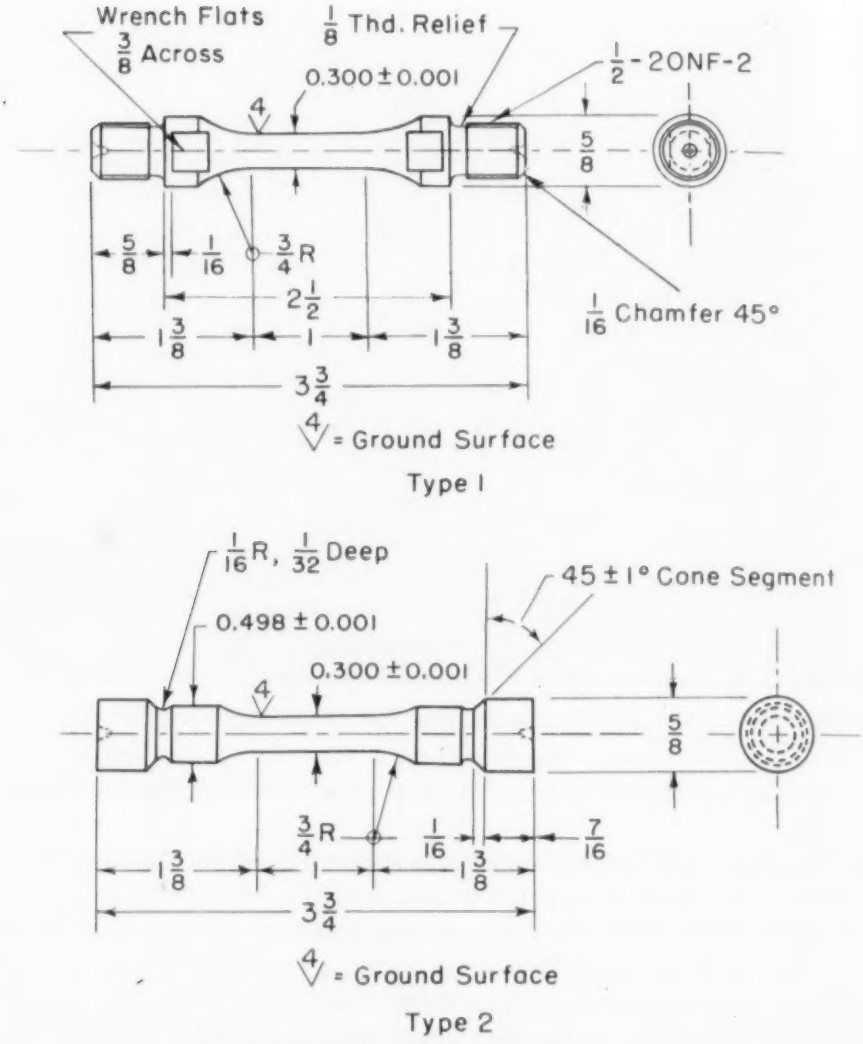


Fig. 2—Dimensions and Shape of Test Specimens.

Test Procedure

The rapid load tests in this investigation were made by rapidly but smoothly applying the load to the specimen within a period of about 10 millisec, and maintaining the load constant thereafter until the test was terminated by yielding and/or fracture. This was accomplished by use of a rapid-load tensile testing machine of special design, hydro-pneumatically operated, which has been described previously (1).

The applied load and the extension of the specimen were determined as functions of time during the tests. Two means of detecting the extension of the specimen during a test were used simultaneously. Tensile strains were measured by means of two type A-5, SR-4 resistance sensitive wire strain gages bonded diametrically

opposite to one another on the gage section of the specimens. Suitable electrical connections between the specimen gages and temperature compensating dummy specimen gages completed the strain gage bridge circuits. A less sensitive measurement of strain, giving an over-all indication of the specimen deformation during a test was obtained by means of two extensometers, diametrically opposite to one another and attached to the specimen grips. The extensometers are the same ones previously used in work of this type (1). The load acting on the specimen was measured by means of a dynamometer, described previously (1), employing type AB-14, SR-4 strain gages.

The signals from the extensometers, strain gages, and dynamometer were recorded on photographic paper by a recording oscillograph manufactured by the Consolidated Engineering Corporation, Pasadena, California. This recording system provides a minimum resolving time of 0.001 second.

The load acting on the specimen was determined within an estimated over-all accuracy of 4%. The output of the extensometer and strain gages was determined within an accuracy of about 5%.

The tests were conducted at temperatures of −74°F (−59°C), +76°F (24°C), and +200°F (93°C). The temperature of −74°F was attained by bubbling liquid nitrogen at a controlled rate through a kerosene bath surrounding the specimen. The tests at +76°F were made without a thermostatic bath. The temperature of +200°F was attained by a bath of SAE 10 lubricating oil and a controlled electric immersion heater. The specimen temperatures were determined by means of copper-constantan thermocouples secured to the specimen gage section with electrician's rubber tape, together with a Leeds and Northrup portable precision potentiometer. At −74°F (−59°C) the temperature variations along the gage length and from test to test were within ±10°F. At the temperatures of 76 and 200°F (24 and 93°C) these variations were within ±1°F.

The assembly of a specimen of type 2 with grips and hard rubber cup for the thermostatic baths is shown in Fig. 3. These grips employ toroidal seats which transmit the applied force to conical sections of the specimen. With this arrangement all fractures occurred within the gage section of the specimens, whereas specimens of type 1 fractured in the threads. These grips also incorporate hard rubber thermal insulation to reduce the heat flux between the specimen and the testing machine to a reasonable value.

The stresses at which the tests were made were chosen to obtain a reasonably uniform distribution of test points in the plots of delay-time versus stress within the time range from 10 millisec to 1 hour. The lower time limit was dictated by the stress rise time characteristic of the rapid-load testing machine. The long time limit was governed by patience and the ability to maintain a constant specimen temperature.

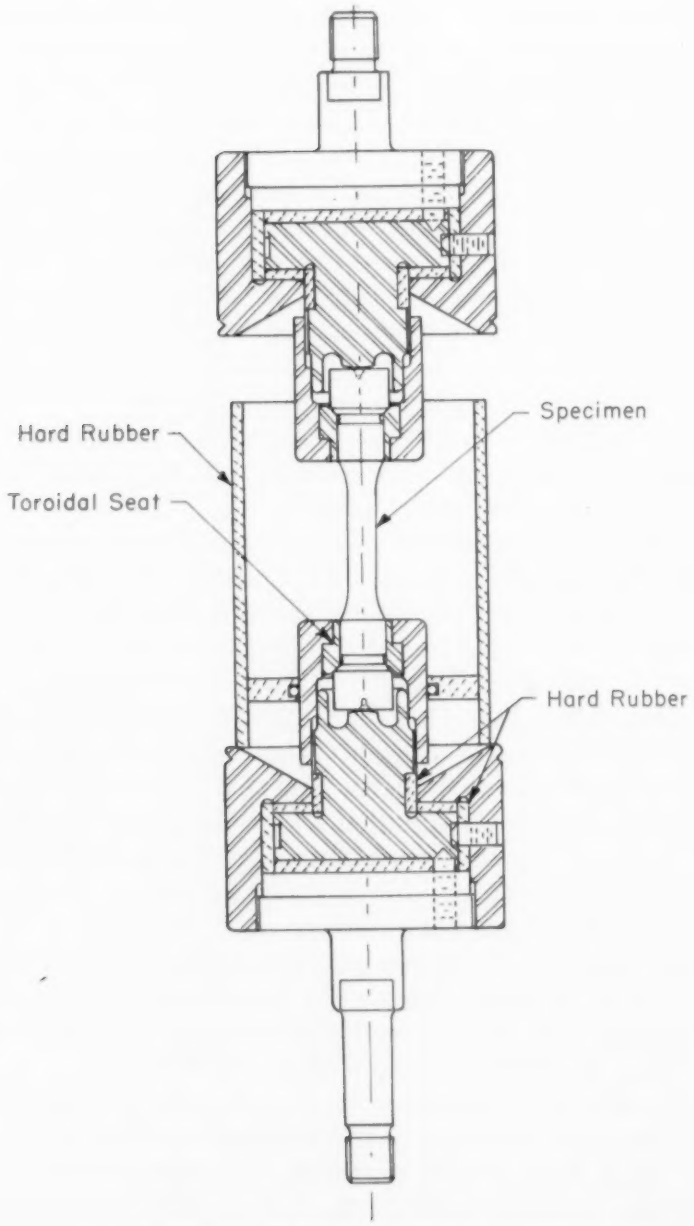


Fig. 3—Test Specimen and Grip Assembly.

Static tension tests were performed for both arc-cast and sintered molybdenum at temperatures of −74°F (−59°C), +76°F (24°C), and +200°F (93°C). The static tension tests were made in the rapid-load machine, using the same grips and temperature control arrangements as for rapid-load tests. The static tests were performed by controlling the applied load with the various manually operated valves associated with the machine in such a manner that the load was applied in steps. A short length of record was taken

Table I
Results of Static Tests
Arc-Cast Molybdenum

Temperature	Upper Yield Stress 10^3lb/in.^{2}	Lower Yield Stress 10^3lb/in.^{2}	Yield Elongation %	Specimen Number
−74°F (−59°C)	87.5	77	2.0	47
	89.0	77	1.8	46
+76°F (24°C)	40.4	38.5	0.30	1
	40.2	33	2.05	44
+200°F (93°C)	20.0	20.0	0.40	23
	16.5	16.5	0.30	24

on the oscillograph after the stress and the strain attained equilibrium values. This operation was performed after each load increment was applied. The maximum strain to which the specimens could be subjected was 5% since this was the maximum range of the extensometer. The total time for such a static test was approximately 1 hour. Two static tests were made for each temperature investigated for both sintered and arc-cast molybdenum.

Experimental Results

The values of upper yield stress, lower yield stress, and yield elongation obtained in the static tests at temperatures of −74°F (−59°C), +76°F (24°C), and +200°F (93°C) are given in Tables I and II for arc-cast and sintered molybdenum respectively. Fracture within the specimen gage length occurred in two of the four static tests performed at −74°F (−59°C), one in an arc-cast and the other in a sintered molybdenum specimen. These fractures took place at strains of 2.7 and 4.5% respectively, and appeared to be of the cleavage type. No other static test specimens fractured within the 5% strain limit of the tests.

Two typical oscillograph records of stress, strain in gage section, and over-all specimen extension as functions of time during rapid-load tests are shown in Figs. 4 and 5. The manner in which the delay time for yielding is obtained from the extensometer trace

Table II
Results of Static Tests
Sintered Molybdenum

Temperature	Upper Yield Stress 10^3lb/in.^{2}	Lower Yield Stress 10^3lb/in.^{2}	Yield Elongation %	Specimen Number
−74°F (−59°C)	84.8	74	1.10	026
	84.9	71.5	1.50	030
+76°F (24°C)	48.5	35	1.90	01
	46.2	40	1.90	028
+200°F (93°C)	34.8	30	0.90	029
	34.0	27.5	0.90	031

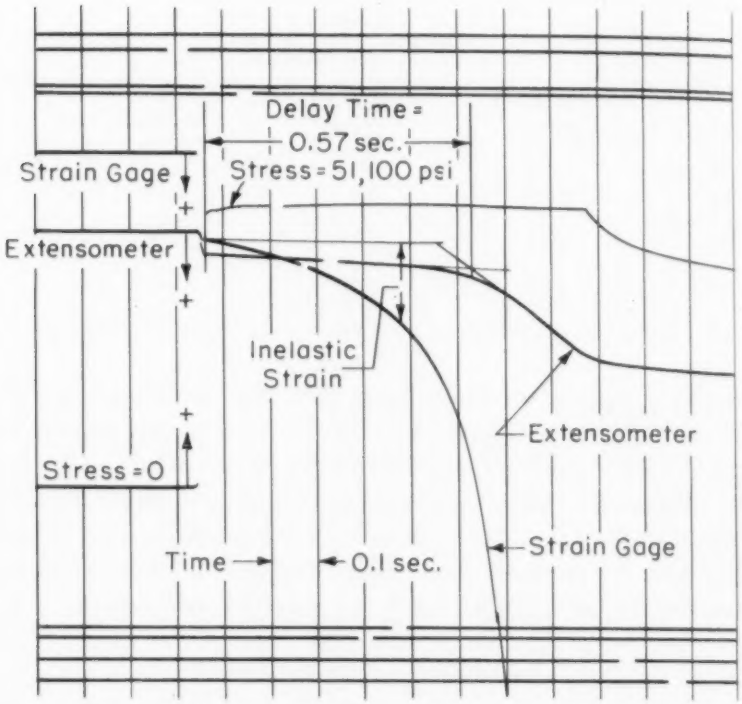


Fig. 4—Rapid Load Test Record for Arc-Cast Molybdenum at 200°F., Specimen 15.

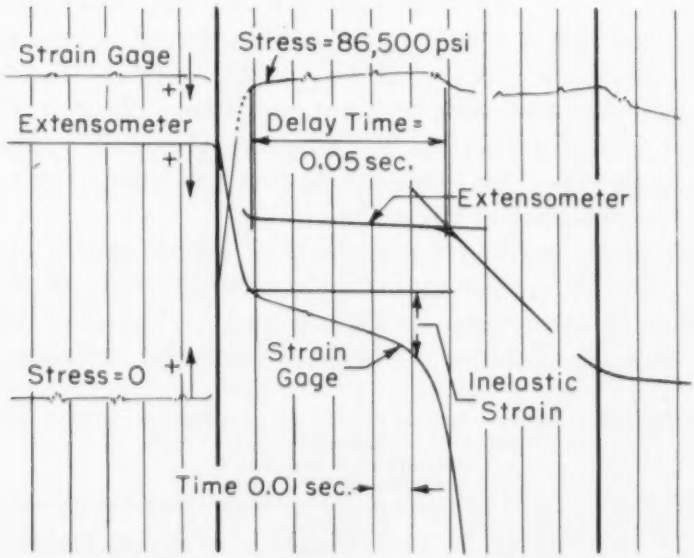


Fig. 5—Rapid Load Test Record for Sintered Molybdenum at 76°F., Specimen 013.

is indicated on these records. The traces obtained from the SR-4 strain gages show the pre-yield plastic strains which occur in the two types of molybdenum tested.

Table III
Results of Rapid-Load Tests
Arc-Cast Molybdenum

Temperature	Stress 10^3 lb/in.^{2}	Delay Time Sec	Specimen Number
−74°F (−59°C)	79.5	3000 + 1000	38
	84.8	590	41
	88.7	150	42
	95.1	79	34
	98.6	7.8	37
	102.0	3.9	35
	107.0	1.3	30
	117.5	0.87	40
	120.0	0.06	39
76°F (24°C)	48.0	3600	5
	51.3	48	10
	58.0	18	12
	63.3	9.2	16
	68.0	3.8	4
	76.8	1.2	26
	87.0	0.15	2
	95.2	0.09	3
	102.0	0.011	27
200°F (93°C)	20.8	280	22
	26.2	39	20
	33.7	12	19
	36.2	9.0	18
	45.7	1.4	17
	51.1	0.57	15
	64.5	0.12	13
	66.5	0.043	21
	75.6	0.016	11

Table IV
Results of Rapid-Load Tests
Sintered Molybdenum

Temperature	Stress 10^3 lb/in.^{2}	Delay Time Sec	Specimen Number
−74°F (−59°C)	72.3	3600	018
	76.5	800	014
	83.6	200	019
	87.1	120	016
	92.5	66	09
	96.0	30	017
	102.0	0.20	011
	104.0	<0.01	05
76°F (24°C)	47.5	160	010
	50.2	85	07
	52.7	330	04
	58.6	30	03
	62.2	16	012
	69.0	0.86	02
	77.1	0.20	06
	86.5	0.050	013
	99.5	0.020	08
200°F (93°C)	34.9	1100	020
	40.8	140	023
	44.5	18	025
	47.5	0.40	027
	51.2	1.3	024
	59.1	0.22	021
	62.5	0.067	015

The corresponding values of stress and delay time for yielding obtained in the rapid-load tests are given in Tables III and IV, and in Figs. 6 and 7, in which the experimental points of stress vs.

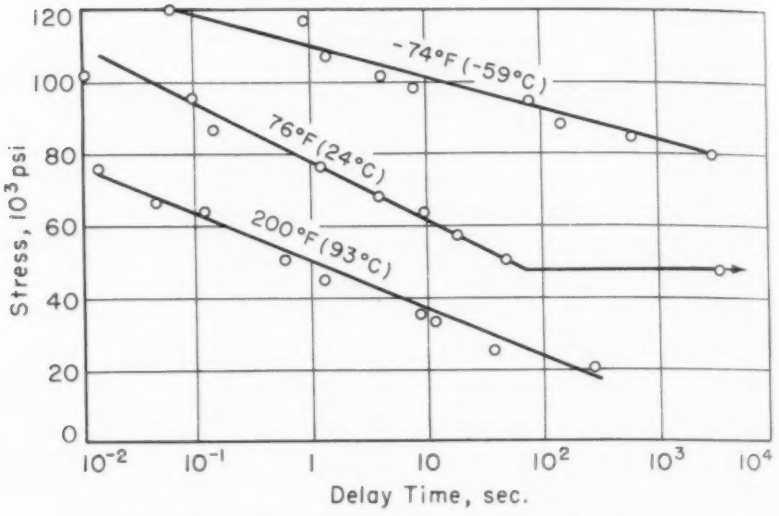


Fig. 6—Stress Versus Delay Time for Arc-Cast Molybdenum.

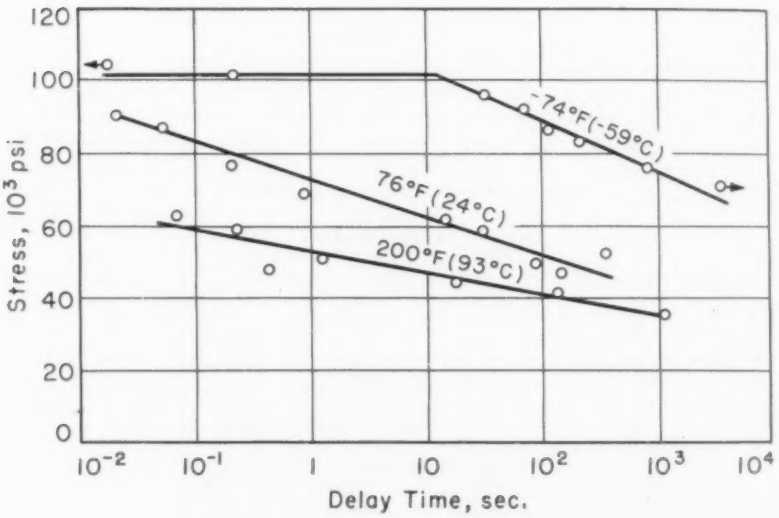


Fig. 7—Stress Versus Delay Time for Sintered Molybdenum.

logarithm of the delay time for yielding are plotted. The average trends of the experimental points of Figs. 6 and 7 are represented by straight lines.

The type of fracture observed in the static tests at a temperature of −74°F (−59°C) occurred in four of the eight rapid-load tests performed on sintered molybdenum and in seven of the nine tests on arc-cast molybdenum at that temperature. Such fractures also occurred in one of the nine rapid-load tests on sintered molybdenum and in two of the nine tests on arc-cast molybdenum at a temperature of +76°F (24°C). Undoubtedly, more such fractures would have been observed if the maximum specimen extension had not been limited to 5%. There were no fractures in any of the rapid-

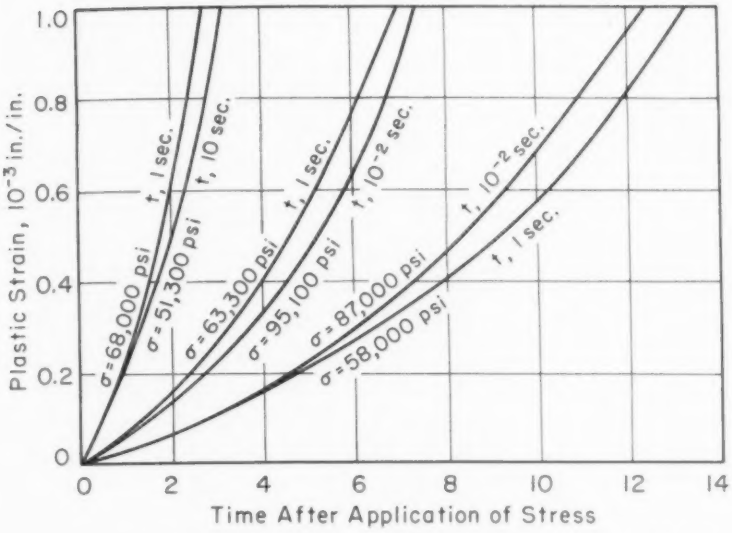


Fig. 8—Preyield Plastic Strain Versus Time for Arc-Cast Molybdenum at 76°F, σ and τ Values Give the Constant Test Stress and Time Scale Multiplying Factor Respectively for Each Curve.

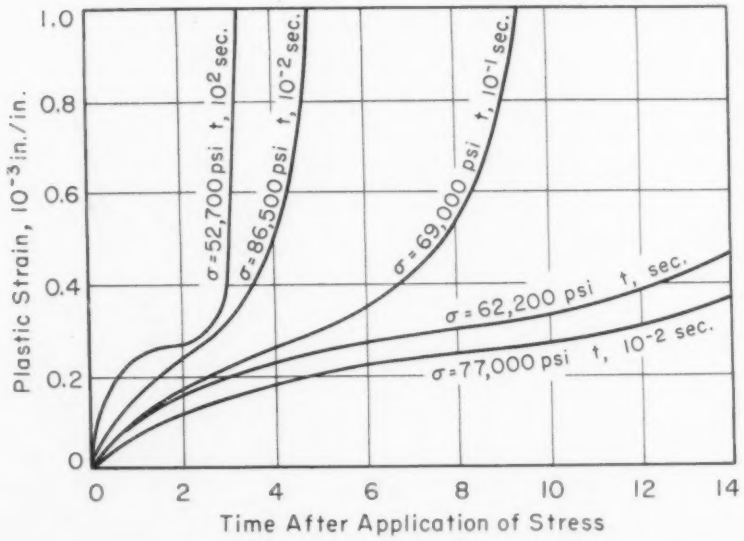


Fig. 9—Preyield Plastic Strain Versus Time for Sintered Molybdenum at 76°F., σ and τ Values Give the Constant Test Stress and Time Scale Multiplying Factor Respectively for Each Curve.

load tests at a temperature of +200°F (93°C). Pre-yield plastic strain vs. time for a series of constant stresses applied to specimens of arc-cast and sintered molybdenum at a temperature of +76°F (24°C), are shown in Figs. 8 and 9. Similar results were obtained at the other two test temperatures. The applied stresses in each case were above the static upper yield stress. These values of pre-yield plastic strains are the differences between the total strain indicated by the SR-4 strain gages at any instant and the elastic strain. The

elastic strain is substantially constant during any given test and is taken to be the total strain at the instant the stress attains the constant test value.

Discussion of Results

The results of the static tension tests are substantially in agreement with those obtained by Bechtold and Scott (13) on similar materials. These show clearly that fine-grained ductile molybdenum, produced by either the arc-casting or powder metallurgy processes, exhibits the phenomenon of a distinct yield point and that the yield point is quite temperature sensitive. Thus these materials exhibit a yielding behavior which is quite similar to that commonly observed in iron and low carbon steels. However, some quantitative differences between the molybdenum employed in this investigation and annealed low carbon steels previously investigated are indicated by the static tests. First, the upper yield stress of the molybdenum continuously decreases as the temperature is increased in the range from −74°F (−59°C) and +200°F (93°C) and no multiple yield points are observed in molybdenum during static tests at +200°F (93°C). Annealed low carbon steel on the other hand exhibits a decrease in upper yield stress with increasing temperature up to about room temperature after which the upper yield stress remains about constant up to at least +250°F (121°C), (1). Also, at +150°F (66°C) and +250°F (121°C) annealed low carbon steels exhibit multiple yield points (1). These features of the behavior of low carbon steel may be attributed to the thermal diffusion of carbon and/or nitrogen to dislocations during testing and may be considered as strain aging effects. The absence of such behavior in molybdenum in the same temperature range may be due to lower diffusion coefficients of the interstitial atoms, or the lower concentrations of these atoms in the molybdenum tested, or both.

Second, the molybdenum exhibits larger deviations from linear elasticity just prior to yielding than does low carbon steel. Also, the arc-cast molybdenum tested at +200°F (93°C) actually does not exhibit a drop in load at the yield point, although it shows a yield point elongation at constant stress. This is also probably due to the rather low concentration of carbon and/or nitrogen in the molybdenum. Similar behavior has been observed in steel in which the carbon and nitrogen concentrations have been reduced to values comparable with those in the molybdenum (2).

The results of the rapid-load tests show clearly that ductile molybdenum exhibits the phenomenon of delayed yielding under rapidly applied constant stress. The dependence of the delay time for yielding upon stress and temperature as shown in Fig. 6 and 7

is, on the whole, similar in form to that found for annealed low carbon steel (1).

The stress versus delay time curves for the molybdenum tested, with the possible exception of the curve for the arc-cast material tested at 76°F (24°C), do not appear to show a lower limiting stress (horizontal portion at a low stress and long delay times), such as that found in normal low carbon steel. However, a similar behavior has been observed in steel in which the carbon and nitrogen concentrations were exceptionally low (2). Thus the observed behavior of molybdenum in this respect is consistent with the relatively low concentrations of carbon and nitrogen in the material tested. The single case in which such a lower limiting stress is indicated for molybdenum is based upon only one experimental point and is, therefore, somewhat doubtful.

The stress versus delay time curve for sintered molybdenum tested at −74°F (−59°C) exhibits an upper limiting stress (horizontal portion at high stress and short delay times). Similar behavior is exhibited by low-carbon steel at −320°F (−196°C), (3). The fact that such an upper limiting stress may be observed in molybdenum at a higher temperature than in low carbon steel may be related to its higher melting point and is consistent with Bechtold and Scott's observation (13) that the transition temperature in unnotched tensile specimens is considerably higher for molybdenum than for Armco iron.

The absence of an upper limiting stress in the stress vs. delay time relation for arc-cast molybdenum tested at −74°F (−59°C) does not indicate that a fundamental difference exists between the two types of molybdenum. Rather, it indicates a quantitative difference in their behavior in which the upper limiting stress for arc-cast molybdenum at a temperature of −74°F (−59°C) occurs in a range of delay times which are shorter than those which can be investigated with the testing technique employed in the present investigation. This quantitative difference between the delayed yielding behavior of the two types of molybdenum tested is probably associated with the differences in carbon, nitrogen, or oxygen contents in these materials.

The measurements of pre-yield plastic strain in molybdenum given in Figs. 8 and 9 show that this material exhibits considerably larger pre-yield plastic strains than those which have been previously observed in low carbon steel (6). The latter material exhibits pre-yield plastic strains of about 30 x 10^{-6} in/in. whereas the molybdenum exhibits pre-yield plastic strains ranging from about 100 x 10^{-6} in/in. to about 1000 x 10^{-6} in/in. The arc-cast material exhibits particularly large strains of this type. Furthermore, in the arc-cast material the pre-yield plastic strain rate increases continu-

ously with time during any particular test at constant stress. Conversely, in the sintered molybdenum, as in low carbon steel, the pre-yield plastic strain rate decreases with time at constant stress up until the time when macroscopic yielding begins. The latter behavior is consistent with the dislocation model of a yield nucleus which has been developed previously (6,7), while the behavior of the arc-cast molybdenum is not consistent with this model.

This difference between the behavior of arc-cast molybdenum on the one hand and sintered molybdenum and low carbon steel on the other, may be associated with the relative differences in the carbon and nitrogen contents of the materials. The arc-cast material contains considerably more carbon and less nitrogen than the sintered material. If the assumption is made that dislocations in molybdenum interact strongly with nitrogen atoms, but only relatively weakly with carbon atoms, then the arc-cast material might be expected to contain many more dislocations which are unanchored by Cottrell "atmospheres" than the sintered material. Hence the behavior of the yield nuclei would be different in the arc-cast material than is predicted by the theoretical dislocation model. However, this point of view may be subject to criticism in that even the very small concentration of nitrogen present in the arc-cast material should be sufficient to provide complete "atmospheres" for all the dislocations which are expected to be present initially in the material. Thus if the initial density of dislocations is $10^8/cm^2$ the concentration of nitrogen required to provide one nitrogen atom per atomic length along each dislocation is only about 10^{-6} weight %.

An alternative hypothesis for the effect of different carbon and nitrogen contents upon the pre-yield plastic strains in molybdenum is that the grain boundaries in molybdenum are markedly strengthened by nitrogen but not by carbon. According to the theory, the ability of grain boundaries to impede the motion of dislocations plays an important part in the development of pre-yield plastic strain. Thus weaker grain boundaries in the arc-cast molybdenum, due to low nitrogen content, could explain the observed behavior. Since the saturation of all the grain boundaries would require larger amounts of nitrogen than the saturation of all the dislocations, this second explanation may be preferable to the first.

Since the pre-yield plastic strain in the sintered molybdenum occurs in a manner which is qualitatively in accord with the dislocation theory (7) of a yield nucleus, it may be compared with that theory quantitatively. Specifically, experimental values of the initial rate of the pre-yield plastic strain as a function of applied stress, may be compared with the theoretical relationship between these

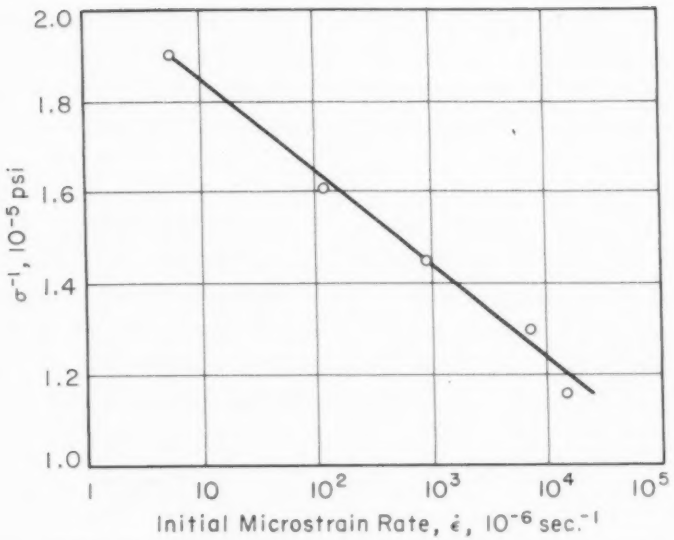


Fig. 10—Reciprocal of the Tensile Stress Versus the Initial Preyield Plastic Strain Rate for Sintered Molybdenum at 76°F.

two quantities. Sufficient reliable data for this comparison were only obtained in the case of the sintered molybdenum tested at +76°F (24°C). These initial pre-yield plastic strain rates are found by determining the initial slopes of the experimental curves given in Fig. 9, and the values are plotted in Fig. 10 to a logarithmic abscissa scale versus the reciprocals of the corresponding values of the applied stress on the ordinate scale. The experimental points are seen to correspond to a straight line in this plot.

The theoretical relationship between the initial pre-yield plastic strain rate and the applied stress is (7)

$$\ln\dot{\epsilon}_0 = -\frac{2\gamma_0^2 f(\gamma/\gamma_0)}{\sigma bKT} + C \qquad \text{Equation 1}$$

where $\dot{\epsilon}_0$ = initial pre-yield plastic strain rate,
γ_0 = energy per unit length of a dislocation not bound by a Cottrell "atmosphere,"
γ = energy per unit length of a dislocation bound by a Cottrell "atmosphere,"
σ = applied tensile stress,
b = The Burger's vector of a slip dislocation in molybdenum,
K = Boltzmann's constant,
T = absolute temperature,
C = an undetermined constant.

and $f(\gamma/\gamma_0) = \cos^{-1}(\gamma/\gamma_0) - \gamma/\gamma_0(1-\gamma^2/\gamma_0^2)^{\frac{1}{2}}$.

Thus the theory predicts a linear relationship between the logarithm of the initial strain rate and the reciprocal of the applied stress in agreement with experiment as shown in Fig. 10. The theoretical value of the slope of this relationship is

$$\frac{\partial(\ln\dot{\epsilon}_0)}{\partial(1/\sigma)} = -\frac{2\gamma_0^2 f(\gamma/\gamma_0)}{bKT} \qquad \text{Equation 2}$$

and this may be compared quantitatively with the experimental value determined from the slope of the line in Fig. 10. The quantities in Equation 2 are all accurately known except γ_0 and γ. The energy per unit length of a free dislocation, γ_0, may reasonably be taken as

$$\gamma_0 = \tfrac{1}{2}Gb^2 \qquad \text{Equation 3}$$

where G is the shear modulus of molybdenum ($G = 6.6 \times 10^{11}$ dynes/cm^2 according to ASM Metals Handbook, 1948). This corresponds to 4.2 electron volts per atomic distance along the dislocation. Using this value of γ_0 and the known values of b, K and T in Equation 2, a value for the binding energy $(\gamma_0 - \gamma)$ of a dislocation in molybdenum with an "atmosphere" of interstitial solute atoms may be obtained by substituting the experimental value of the slope, $\partial(\ln\dot{\epsilon}_0)/\partial\left(\frac{1}{\sigma}\right)$ in the equation. This leads to a value of the binding energy of $(\gamma_0 - \gamma) = 0.022$ electron volt per atomic distance along the dislocation line. This value is about three and one-half times as large as the value for dislocations in iron determined in the same manner. However, it is only about one-twentieth of the value estimated by Cottrell and Bilby (8). Thus the values of the binding energy determined in the above manner for dislocations in both iron and molybdenum deviate from the theoretical values by the same order of magnitude. A satisfactory resolution of this discrepancy has not yet been found.

Summary and Conclusions

The initiation of yielding under rapidly applied constant stress has been investigated in two lots of fine-grained ductile molybdenum. One lot was produced by the arc-casting method and the other by the powder metallurgy method. Both lots were worked at temperatures below the recrystallization temperature, followed by a recrystallization treatment which produced a rather uniform fine-grained structure. These materials were found to exhibit distinct yield points in their static stress-strain relations, in agreement with the work of Bechtold and Scott (13).

The results of this investigation show that fine-grained ductile molybdenum exhibits the phenomenon of delayed yielding in a form very similar to that observed in annealed low carbon steels. This result lends further support to the view proposed by Cottrell (10) on theoretical grounds that yield point and delayed yield phenomena are a consequence of the anchoring of dislocations in body-centered cubic metals by interstitial solutes such as carbon and nitrogen. The present work gives a tentative indication that nitrogen may be more effective than carbon in anchoring dislocations or in strengthening grain boundaries in molybdenum.

A quantitative difference between the delayed yielding behavior of molybdenum and low carbon steel which is shown by the present work is that the upper limiting stress in the stress versus delay time relations may be observed at higher temperatures in molybdenum than in steel. Thus experimental studies of this upper limiting stress phenomenon with a view toward its possible relationship to conventional transition temperatures might be more conveniently carried out with molybdenum than with iron or steel.

The initial rate of pre-yield plastic strain in the sintered molybdenum tested at room temperature is found to depend upon the applied stress in a manner which is in agreement with a dislocation theory of delayed yielding. Quantitative comparison of theory and experiment in this respect yields a value for the binding energy of a dislocation in molybdenum with an "atmosphere" of interstitial solute atoms, which is of the same order of magnitude as that found for iron.

Acknowledgments

This research was conducted under the sponsorship of the Office of Naval Research and the authors express their thanks for support of this work. The arc-cast molybdenum employed in this investigation was supplied by the Climax Molybdenum Company, and the molybdenum produced by powder metallurgy was prepared by the Research Laboratories of the Westinghouse Electric Corporation. Appreciation is expressed to these companies for their cooperation in providing these materials.

References

1. D. S. Wood and D. S. Clark, "The Influence of Temperature Upon the Time Delay for Yielding in Annealed Mild Steel," TRANSACTIONS, American Society for Metals, Vol. 43, 1951, p. 571.
2. D. S. Wood and D. S. Clark, "Delayed Yield in Annealed Steels of Very Low Carbon and Nitrogen Content," TRANSACTIONS, American Society for Metals, Vol. 44, 1952, p. 726.
3. D. S. Wood and D. S. Clark, "Delayed Yielding in Annealed Mild Steel with Special Reference to Yielding at Low Temperature," Fourth Technical Report submitted to Office of Naval Research, Contract N6onr-24418, December 1951.
4. I. R. Kramer and R. Maddin, "Delay Time for the Initiation of Slip in Metal Single Crystals," *Journal of Metals*, Vol. 4, 1952, p. 197.
5. T. Vreeland, Jr., D. S. Wood, and D. S. Clark, "A Study of the Mechanism of the Delayed Yield Phenomenon," TRANSACTIONS, American Society for Metals, Vol. 45, 1953, p. 620.
6. T. Vreeland, Jr., D. S. Wood, and D. S. Clark, "Preyield Plastic and Anelastic Microstrain in Low-Carbon Steel," *Acta Metallurgica*, Vol. 1, July 1953, p. 414.
7. T. Vreeland, Jr., and D. S. Wood, "A Comparison Between Dislocation Theory and Experimental Measurements of Delayed Yield in Steel," Eighth Technical Report under Office of Naval Research, Contract N6onr-24418, April 1954.

8. A. H. Cottrell, and B. A. Bilby, "Dislocation Theory of Yielding and Strain Aging of Iron," *Proceedings*, Physical Society of London, Sec. A, Vol. 62, Part 1, 1949, p. 49.
9. F. C. Frank, and W. T. Read, "Multiplication Processes for Slow Moving Dislocations," *Physical Review*, Vol. 79, 1950, p. 722.
10. A. H. Cottrell, "The Yield Point in Single Crystal and Polycrystalline Metals," *Symposium on the Plastic Deformation of Crystalline Solids*, Mellon Institute, 1950.
11. F. R. N. Nabarro, "Mechanical Effects of Carbon and Iron," Report on Strength of Solids, Physical Society of London, 1948, p. 38.
12. C. Crussard, "The Physics of Metals—Diffusion and Interaction of Impurities and Defects of Structure in Metals," *Metaux et Corrosion*, Vol. 25, 1950, p. 203.
13. J. H. Bechtold, and H. Scott, "Mechanical Properties of Arc-Cast and Powder Metallurgy Molybdenum," *Journal*, Electrochemical Society, Vol. 98, 1951, p. 495.

Also "Properties of Molybdenum Made by Arc Casting and Powder Metallurgy," Metal Progress, American Society for Metals, Vol. 61, (4), 1952, p. 82.

DISCUSSION

Written Discussion: By Irvin R. Kramer, Mercast Corp., New York, New York.

This paper on the discontinuous yielding in molybdenum makes an excellent contribution to the understanding of this little understood phenomenon, and the authors are to be congratulated for this and other fine contributions they have made to this subject. The authors show that a delay time for the initiation of plastic flow is associated with the existence of a yield point. While I am inclined to agree with the authors, I also feel that a certain amount of caution should also be exercised. While it is true that, of the metals tested to date, only those which exhibited a yield point had a delay time, it should be noted that these metals all had a body-centered cubic structure. In a recent work[2] single crystals of zinc were studied and found to exhibit a pronounced delay time. The zinc used was 99.99% and the crystals were prepared in vacuum. Unfortunately stress-strain curves were not obtained so that it cannot be stated definitely whether a yield point existed. However, judging from the work of Wain and Cottrell[3] a yield point should not have existed. These authors found that a yield point was not present in pure zinc but did exist when nitrogen was held in solid solution. Ardley and Cottrell[4] were able to find a yield point in alpha brass containing nitrogen.

I would like to suggest that a series of delay time experiments be run with alpha brass and zinc containing enough nitrogen to develop a yield point. The stress-strain curves and the delay time measurements should be obtained at various temperatures to determine whether the delay time and yield point exist together.

The authors' observations on the type of fracture of the molybdenum specimens are interesting. They state that at −74°F brittle type fracture occurred in four of the eight rapidly loaded specimens of the sintered molybdenum while seven of the nine arc-melted molybdenum specimens failed in a brittle manner. This indicated that the arc-melted molybdenum is more brittle than the sintered molyb-

[2]T. S. Liu, I. R. Kramer and M. A. Steinberg, to be published.
[3]H. L. Wain and A. H. Cottrell, "Yield Points in Zinc Crystals," *Proceedings*, Physical Society, Vol. 63, Sec. B, May 1950, p. 339.
[4]G. W. Ardley and A. H. Cottrell, "Yield Points in Brass Crystals," *Proceedings*, Royal Society, Vol. 219, Ser. A, September 1953, p. 328.

denum. In general the delay times for the arc-melted specimens are larger than those of the sintered molybdenum specimens and is in accord with the theory for brittle fracture postulated by this author.[5]

Authors' Reply

The authors appreciate Dr. Kramer's comments on this paper and agree with him that a generalization should not be made at this time on the relationship between yield point, crystal structure, and delay phenomenon. However, the information available so far points to the existence of delayed yielding in materials that exhibit the yield phenomenon. The authors have shown that while the distinct yield point may be eliminated by removal of nitrogen, there still remains a definite delay. This situation may also be observed in such a material as zinc.

Investigations are now in progress on zinc single crystals to determine the presence or absence of a yield point and to obtain information on delay phenomenon in this material. Furthermore the influence of nitrogen on these characteristics will be studied.

[5] I. R. Kramer and R. Maddin, "Delay Time for the Initiation of Slip in Metal Single Crystals," *Transactions*, American Institute of Mining and Metallurgical Engineers, Vol. 194, 1952, p. 197

THE MECHANICAL PROPERTIES OF VANADIUM-BASE ALLOYS

By W. Rostoker, A. S. Yamamoto and R. E. Riley

Abstract

The tensile properties of unalloyed vanadium, its binary and ternary alloys have been surveyed extensively. It has been shown that small additions of titanium and zirconium have a markedly beneficial effect on the ductility of vanadium. Binary alloys containing other than titanium or zirconium show little promise. High strengths have been developed on ternary alloys containing 20–50% Ti and third element additions of chromium, aluminum and silicon. An extensive study of hot tensile properties revealed interesting possibilities of high strength at elevated temperatures. Selected alloys have been tested for stress-rupture behavior. Aluminum has been shown superior to chromium as a third metal addition. At least one alloy has stress-rupture properties equal to the best currently available from titanium alloys. Alumino-thermic vanadium is compared with calcium-reduced vanadium as an alloy base for selected alloys. Carbon additions of 0.5% have been shown to improve forgeability but to have little influence on mechanical properties. (ASM-SLA Classification: Q general, V)

THIS PAPER summarizes the results of a portion of a research program sponsored by the Materials Laboratory of the Wright Air Development Center, Ohio, which sought to explore the potential usefulness of vanadium-base alloys. Research of this nature became possible only within the last few years with the development of the calcium reduction process for vanadium pentoxide. The vanadium metal which is produced by this process is low enough in interstitials and metallic impurities to permit severe mechanical deformation both hot and cold. The term "ductile" has therefore been applied to this metal. A typical chemical analysis of the ductile vanadium as supplied by the Electro Metallurgical Corporation of Niagara Falls, New York is as follows:

Carbon 0.077%; Oxygen 0.056%; Nitrogen 0.086%; Hydrogen 0.002%

Based on work on Contract No. AF 33(038)-8517 for Materials Laboratory, Wright Air Development Center, Ohio.

A paper presented before the Thirty-Seventh Annual Convention of the Society, held in Philadelphia, October 17–21, 1955. Of the authors, W. Rostoker is supervisor, Physical Metallurgy Research and A. S. Yamamoto is associate metallurgist, Armour Research Foundation of Illinois Institute of Technology, Chicago, and R. E. Riley is research metallurgist, Rem-Cru Titanium Corp., Midland, Pa.

A study of the alloying behavior of vanadium was summarized in an earlier paper (1).[1] It was demonstrated that at least 13 elements had solid solubility limits in vanadium of 5% or more. In spite of reported allotropy (2), there was no evidence of transformation type structures in any of the alloys examined. Accordingly, the improvement of mechanical properties must be expected through solid solution hardening, through cold working, and through age hardening, in the instances where forging proved feasible in the region of the solid solubility limit. It cannot be said that the potentialities of each of these mechanisms have been exhaustively evaluated. The intention of this work was to concentrate on trends of behavior rather than the optimum properties of singular alloy compositions. The pattern of evaluation of mechanical properties has included in succession: room temperature tensile behavior, elevated temperature tensile behavior, and stress-rupture behavior. The results of each stage were used to restrict effort in the next stage to alloy compositions of likeliest interest.

Melting and Forging Methods

All alloys were produced by melting of the elemental components in the proper proportions in a nonconsumable electrode, water-cooled copper crucible, arc melting furnace. Pancake shaped ingots of 125–200 gram weight were generally made. A few 450 gram ingots were produced. Compositions referred to in the text of this paper are nominal unless otherwise specified. The vanadium metal was supplied by the producer in the form of selectively sized lumps. The metal was melted in the as-received form.

Cast ingots were forged to ½ inch diameter rods for machining directly to tensile test pieces or to blocks for subsequent cold rolling. Forging was performed by drop hammers using open dies or swaging dies as needed. Forging temperatures varied from 1150 to 1450°C (2100 to 2640°F), depending on the stiffness of the alloy. It was found generally unfeasible to forge below 1150°C (2100°F), the risk of cracking being too great. Heating was conducted in gas-fired muffle furnaces with no protective atmosphere. Vanadium and its alloys oxidize very rapidly above about 675°C (1240°F). Above this temperature, V_2O_5 is molten and the alloy ingot is covered with a fluid, slag-like film during the forging operation. Experience demonstrated that, provided the total furnace time was less than 15 minutes, surface contamination was not severe.

Infusion of oxygen and nitrogen does have a profound surface hardening effect. A typical microhardness traverse through a forged block of unalloyed vanadium is shown in Fig. 1. It is seen that an extremely hard case exists in the first millimeter. Machining is quite

[1]The figures appearing in parentheses pertain to the references appended to this paper.

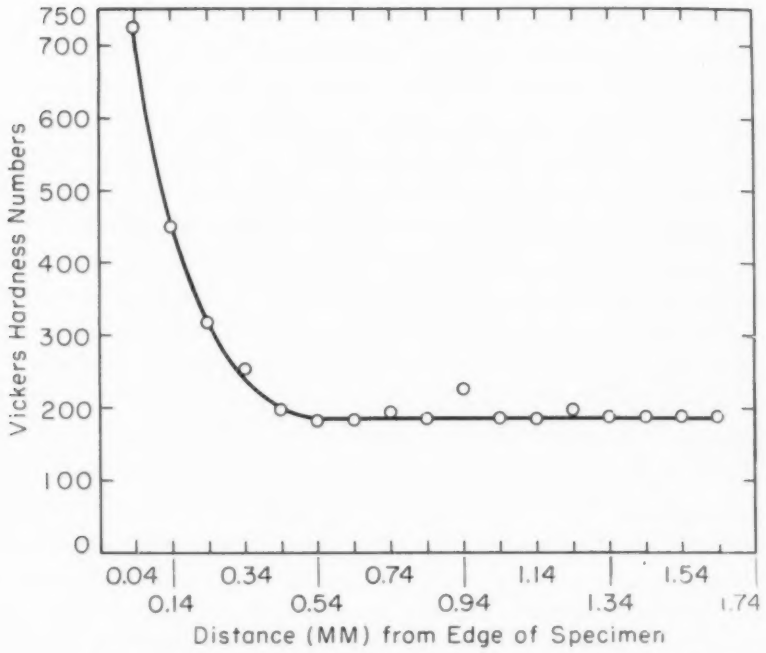


Fig. 1—Micro-hardness Traverse at Surface of Forged Block of Unalloyed Vanadium.

difficult if the first cut is not deep enough to undercut the whole hardened case. Provided that the first roughing cut was deep enough, all of the alloys studied proved machinable.

Forging failures occurred almost invariably after the first few blows of the hammer. Generally, after the cast structure was broken up, the alloys were more easily forgeable. The poor forgeability of the as-cast structure was related to the pronounced columnar-type grain structure in the ingots. It is unfortunate that the cold mold, arc melting method accentuates tendencies toward columnar type grain configurations. Casting of larger size ingots did not alleviate the problem. The rather high cost of vanadium metal made it advisable, therefore, to work almost exclusively with the small ingots.

Later in the program, in an attempt to improve stress-rupture properties of certain alloys by the addition of a dispersed phase, carbon was added to the melts. The carbon appears largely as carbides (V_2C or VC), the solid solubility being very small (1). It was immediately noted that the melts deliberately inoculated with carbon had superior forgeability. Additions of carbon to a number of alloys of marginal forgeability showed improvement in forging characteristics in every instance.

The influence of carbon can be appreciated from Fig. 2, which shows the macrostructures of four ingots of the same basic metallic content but with successively larger carbon contents. The progressive suppression of the columnar grains in the cast structures is ob-

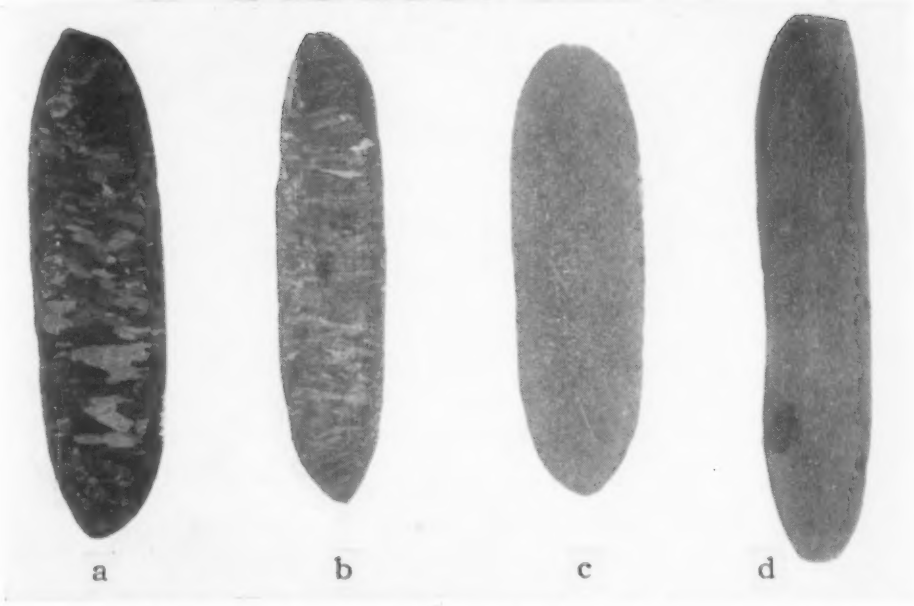


Fig. 2—Influence of Carbon Additions on the Suppression of Columnar As-Cast Structure in an Alloy V-50% Ti-7% Al. Etched with 60 glycerine —20 HNO_3—20 HF. X 1. (a)—0% C; (b)—0.47% C; (c)—0.96% C; (d)—1.40% C.

vious. It was a conclusion from this phase of the work that the general addition of 0.5% C to vanadium alloys had definite advantages in improving forgeability without, as will be seen, any disadvantageous influence on tensile properties. Carbon can be added either in the elemental or master alloy form. Analyzed contents agreed more closely with nominal when carbon master alloy additions were used.

Mechanical Testing

Shoulder type tensile test pieces were machined from ½ inch diameter forged rods to the following specifications: test diameter = 0.252 inch; gage length = 1 inch; overall length = 3 inches. Testing was performed in a conventional Baldwin-Southwark, hydraulically operated, universal testing machine.

For tensile testing at elevated temperatures between 100 and 900°C (210 and 1650°F), controlled heating and an adequate uniform temperature zone were provided by a vertical tube furnace surrounding the sample during the test. A uniform temperature zone of about 2 inches was maintained. Actual testing temperatures were measured by two thermocouples bound to the test length of the specimen. Test pieces were machined to the same test length and diameter as the room temperature specimens, but the shoulders were threaded for insertion into long Inconel connecting shackles which transmitted the load from the machines to the test piece. Above 500°C (930°F), a measure of protection against oxidation was provided by an upward current of argon in the tube furnace.

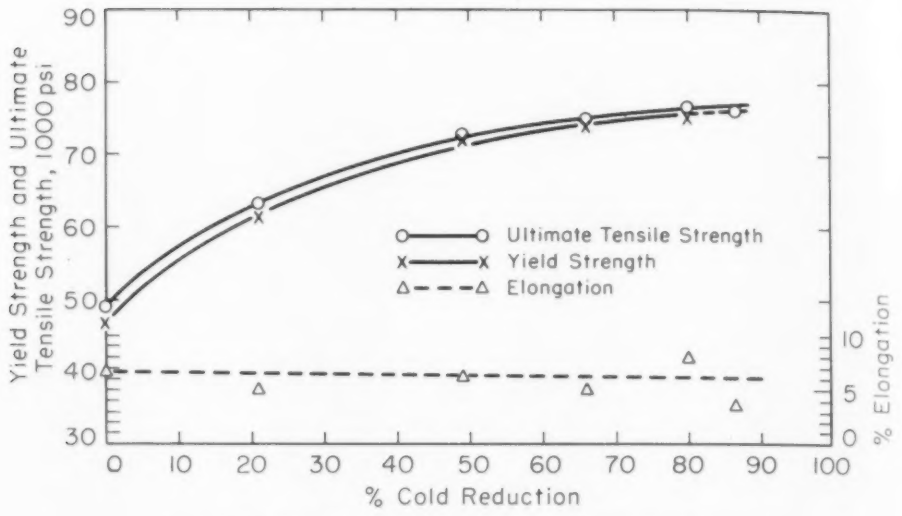


Fig. 3—Tensile Properties of Cold-Rolled Vanadium Sheet.

Stress-rupture measurements were conducted on lever-arm type stress-rupture test machines. Test pieces employed were of the standard 0.252 inch diameter tensile test type specimens. Extensometers were attached to the shoulders of the test specimens to obtain stress-rupture data. The selected testing temperatures were 500, 600 and 700°C (930, 1110 and 1290°F); these were measured by three recording thermocouples attached to the test section of each specimen.

The Room Temperature Tensile Properties of Vanadium and Its Alloys

The unalloyed vanadium used in this investigation in the as-forged state had the following mechanical properties:

Yield Strength (0.2% offset)	46,600 psi
Ultimate Tensile Strength	49,100 psi
Reduction in Area	2.4%
Elongation	6.0%
Modulus of Elasticity	19.7×10^{-6} psi
Hardness	182 VHN

In spite of the apparently poor ductility, the annealed metal can be cold-rolled to at least 90% reduction in area without intervening anneal. The tensile properties of strip test pieces, all of the same gage (0.056 inch), with various stages of cold work are summarized in Fig. 3. A high ratio of yield to ultimate strength is seen to obtain throughout the history of deformation. This is also reflected in the consistently low percentage elongation values.

A preliminary survey of hardnesses showed that most binary alloy additions hardened vanadium very rapidly to levels greater than 300 VHN. The elements Al, Si, Ti, Cr, Ta, Ni, Zr and Mo were

Table I
Mechanical Properties of Binary Vanadium Alloys

Composition	Ultimate Tensile Strength psi	Elongation %	Reduction in Area %	Hardness (VHN)
1% Al	74,330	0	0	198
2.5% Al	93,430	0	0	175
5% Al	80,120	0	0	242
7.5% Al	81,330	0	0	271
1% Cr	65,530	0	0	184
2.5% Cr	60,350	0	0	193
5% Cr	79,320	0	0	218
1% Fe	66,460	0	0	204
2.5% Fe	74,900	0	0	246
5% Fe	91,970	0	0	260
7.5% Fe	75,910	0	0	267
10% Fe	74,200	0	0	307
1% Mo	81,250	0	0	228
2.5% Mo	68,270	0	0	193
5% Mo	62,350	0	0	170
7.5% Mo	63,650	0	0	194
10% Mo	70,880	0	0	194
1% Ni	65,580	0	0	221
2.5% Ni	70,320	0	0	227
5% Ni	74,300	0	0	247
7.5% Ni	83,300	0	0	256
10% Ni	101,830	0	0	269
0.25% Si	56,200	0	0	—
0.50%	64,200	0	0	—
1% Si	84,000	32.8	35.0	—
2% Si	84,400	0	0	—
3% Si	58,000	0	0	—
4% Si	41,000	0	0	—
1% Ti	99,200	0	0	292
2.5% Ti	90,160	12.5	23.7	191
5% Ti	78,540	26.5	77.9	172
7.5% Ti	80,520	25.0	70.5	190
10% Ti	91,570	27.4	66.5	194
1% Zr	49,600	34.1	51.5	118
2.5% Zr	53,800	23.1	74.4	109

most moderate in their alloy hardening behavior. The results of tensile testing of forged binary alloys containing these elements at various alloy content levels is summarized in Table I. The highest alloy contents in the case of Al, Si, Cr, Fe, Mo and Ni represent approximate forgeability limits. Excepting Ti and Zr, all binary additions to vanadium developed extremely brittle alloys (the 1% Si alloy is a singular exception). The V-Ti and V-Zr alloys by contrast were extremely ductile. In fact, the 1% Zr alloy has a lower yield strength and much more ductility than unalloyed vanadium itself. Unfortunately, beyond 3% Zr, alloys become hot short.

The vanadium-titanium series was extended to 50% Ti additions. The trend of tensile behavior is graphically summarized in Fig. 4. It was obvious from these results that potential high strength vanadium alloys would have to be based on the V-Ti binary compositions with third and fourth element additions.

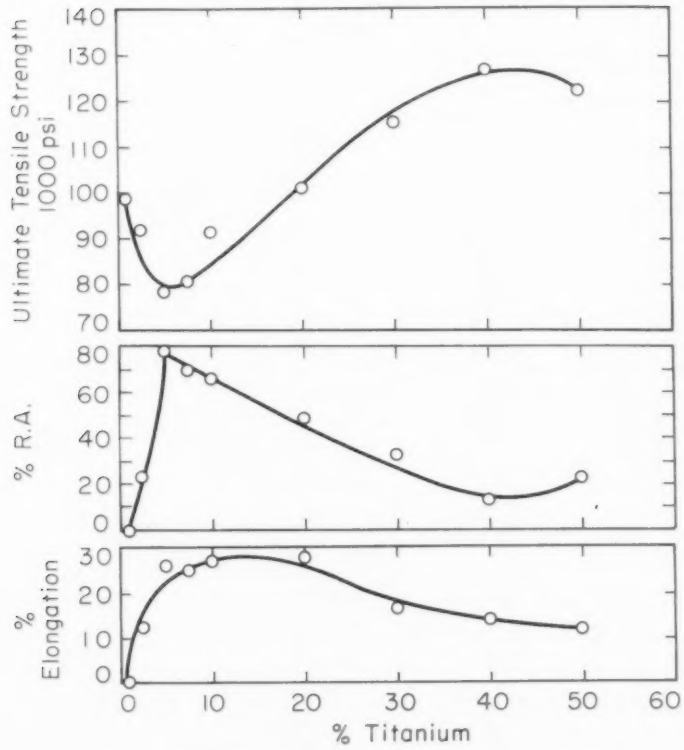


Fig. 4—Tensile Properties of Vanadium-Titanium Alloys.

The curves of tensile strength and ductility in Fig. 4 have one unusual feature. Very small additions of titanium embrittle vanadium almost completely. By 5% Ti additions the trend has been so radically reversed that this alloy is more ductile than unalloyed vanadium. Coincident with the low alloy addition embrittlement, the microstructures show the presence of a very finely dispersed second phase. This was illustrated and remarked upon in a previous paper (1). With larger titanium additions, the dispersed phase gradually disappears and the 10% Ti alloy is single phase. It does not appear that these effects are characteristic of pure binary alloys. The interpretation is advanced that the effects are related to the oxygen and nitrogen contents intrinsic in the unalloyed vanadium. It is suggested that the terminal solid solubility surface in the system V-Ti-O is more sharply re-entrant in the range O-10% Ti than in the binary vanadium-oxygen system. If the estimate of Allen et al (3) is correct, that the solubility limit of oxygen in vanadium is of the order of 0.25%, then a portion of the oxygen (and presumably nitrogen) could be bound up as an interstitial-rich second phase and the matrix solid solution depleted with titanium additions. This is a sort of deoxidation mechanism. The result should be to improve the ductility of the alloy, provided the second phase causes no secondary

Table II
Mechanical Properties of Vanadium Alloys
With Small Additions of Titanium and Zirconium

Composition	Ultimate Tensile Strength psi	Elongation %	Reduction in Area %
5% Fe-5% Ti	76,800	0	0
10% Fe-5% Ti	84,000	20.0	10.0
0.25% Si-5% Ti	71,500	15.6	37.0
0.5% Si-5% Ti	68,100	18.8	33.0
0.75% Si-5% Ti	79,200	21.9	34.0
1% Si-5% Ti	82,000	24.0	48.0
2% Si-5% Ti	93,000	3.1	10.0
3% Si-5% Ti	90,200	3.1	3.0
5% Cr-2.5% Zr	42,700	9.4	19.0
10% Cr-2.5% Zr	63,100	7.0	10.0
0.25% Si-2.5% Zr	58,100	21.9	66.0
0.5% Si-2.5% Zr	53,200	25.0	58.0
1% Si-2.5% Zr	71,900	18.8	48.0
3% Si-2.5% Zr	106,000	9.4	6.0

effects. The embrittlement at 1% Ti and enhancement of ductility at 5% Ti are rationalized in terms of possible age hardening or dispersion hardening effects which under appropriate phase equilibrium conditions can be more serious at certain alloy concentrations than at others. The same explanation might reasonably be used to account for the behavior of zirconium.

Small additions of both titanium and zirconium act to improve ductility in otherwise brittle alloys. Selected instances of this are collected in Table II.

The next logical step in the pursuit of high strength vanadium alloys was the addition of third elements. Chromium, aluminum and silicon were added to alloys containing 5-50% Ti in amounts up to 10%. In only one instance, V-50% Ti-15% Cr, was an alloy forgeable with more than 10% of a third element. Silicon appears to exert a stronger solid solution hardening influence than either aluminum or chromium. A direct comparison might be made between the tensile strengths of vanadium alloys containing 50% Ti and 5% Al, Cr, and Si, respectively.

Aluminum.....126,000 psi
Chromium.....133,400 psi
Silicon.....160,200 psi

The strongest alloy encountered contained 50% Ti and 7% Si. Its tensile properties included 173,200 psi ultimate strength, 1.6% reduction in area and zero elongation. Another alloy containing 50% Ti and 2% Si delivered 150,000 psi tensile strength with much better ductility, 17.5% reduction in area and 12.5% elongation. The possibilities of developing better high strength alloys are by no means exhausted, but it seems clear that the optimum alloys will be based on the 20-50% Ti with third and fourth element additions.

Table III
Mechanical Properties of Some Vanadium Alloys With Carbon Additions

Composition	Ultimate Tensile Strength psi	Elongation %	R.A. %
50% Ti- 5% Cr	130,000	9.4	9.6
50% Ti- 5% Cr-0.5% C	121,200	15.6	28.7
50% Ti- 5% Cr-1% C	124,000	16.5	33.7
50% Ti- 5% Cr-1.5% C	125,000	4.0	7.6
50% Ti-15% Cr	145,800	1.5	0
50% Ti-15% Cr-0.5% C	151,200*	>9.0	21.7
40% Ti- 5% Al	134,600	23.4	25.8
40% Ti- 5% Al-0.5% C	138,400	13.0	33.7
50% Ti-10% Al	84,000	0	0
50% Ti-10% Al-0.5% C	123,200*	—	—

*Fractured at a shoulder.

Tensile Properties of Vanadium Alloys with Carbon Additions

It has already been remarked that carbon additions proved very beneficial to forgeability. A limited study was also made of the effect of carbon (largely as carbides) on the room temperature tensile properties of forged alloys. Various carbon additions were added to four (4) alloys. The results of the four alloys are summarized in Table III. Wherever possible, comparable data on alloys without carbon additions have been included.

It appears that there is no consistent indication that the presence of free carbides influences the tensile strength of any of the alloys. Tensile ductilities of alloys containing carbon additions are generally better than for the same alloys without carbon. There are some singular instances of remarkable superiority. The nature of the improvement in ductility is something of a puzzle. The effect on the as-cast structure can be readily rationalized, but the tensile test work was done on alloys which had been hot-worked beyond any residual cast structure. One is forced to believe that the presence of carbon acts in some constitutional fashion to reduce the content of the other interstitial elements (oxygen and nitrogen) in solid solution.

Elevated Temperature Tensile Properties of Vanadium Alloys

Hot tensile testing was conducted on a wide variety of alloys at temperatures ranging up to 900°C (1650°F). Unalloyed vanadium, although initially low in strength at room temperature, retains considerable strength even at 900°C (1650°F). The trend of behavior is shown in Fig. 5. The rise in strength from room temperature to 300°C (570°F) is indicative of an aging effect and one more instance

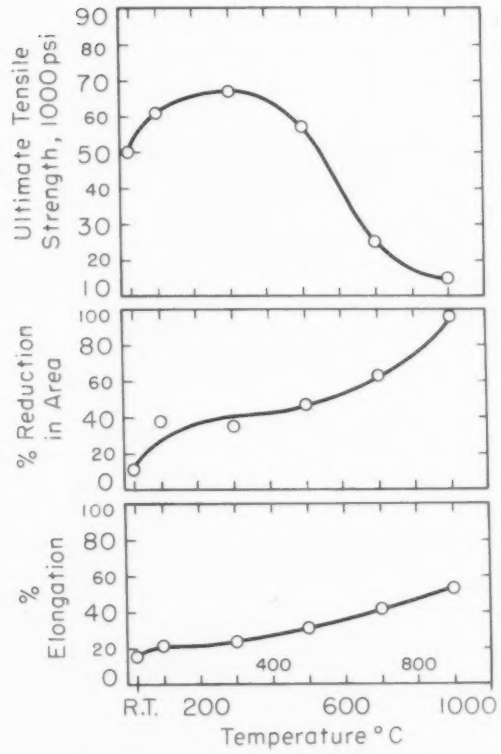


Fig. 5—Elevated Temperature Tensile Properties of Unalloyed Vanadium.

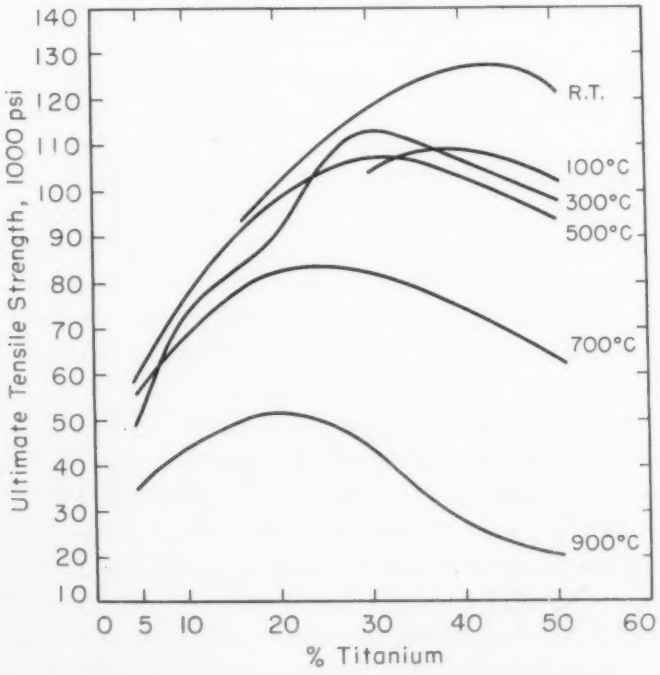


Fig. 6—Comparison of Hot Tensile Strengths of Vanadium-Titanium Alloys.

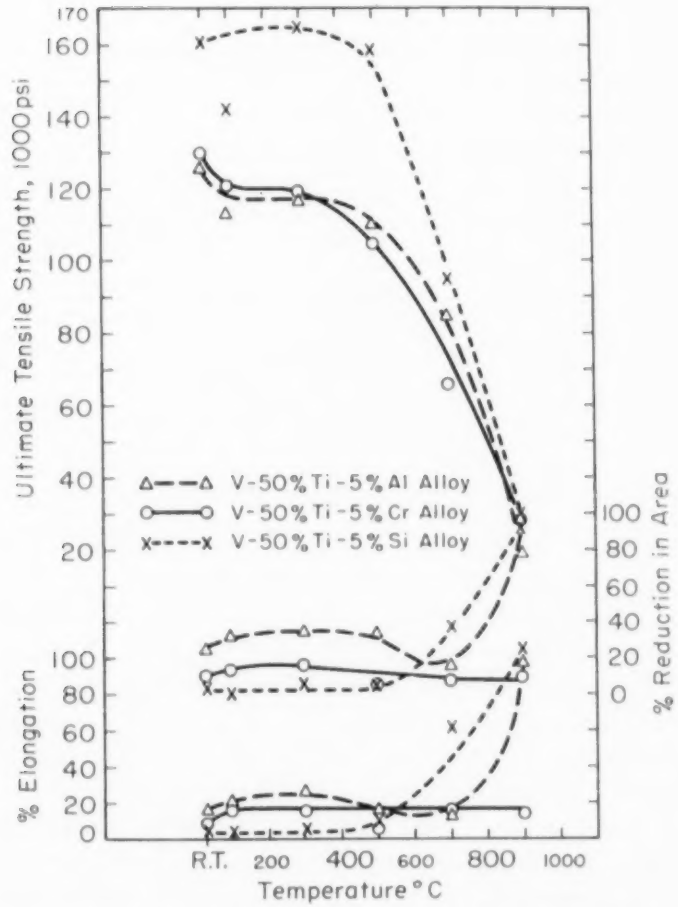


Fig. 7—Comparison of Strengthening Effects of Aluminum, Chromium and Silicon on Hot Tensile Properties of 50% Titanium Alloy.

where the intrinsic interstitial content is probably exercising an influence. A comprehensive picture of the performance of V-Ti alloys is shown in Fig. 6. It is seen that the peak strength occurs at room temperature near 40% Ti, but with increasing temperatures the peak moves toward 20% Ti. The 20% Ti has a strength of over 50,000 psi at 900°C (1650°F) with associated ductility values of 43% elongation and 20% reduction in area.

A 5% Cr addition increases the tensile strength of V-Ti alloys over the whole range of alloys tested. Aluminum additions were confined to the 40% and 50% Ti alloys and silicon additions to the 50% Ti alloy. A comparison of the strengthening behavior of 5% additions of these elements on a 50% Ti alloy is shown in Fig. 7. Clearly, none of these elements changes the fundamental trend in the binary alloy of steeply falling strength with increasing temperature above 400–500°C (750–930°F). It might be noted that 10% Cr and 10% Al additions, while rendering forgeability poorer, appeared to offer no

advantage in strength over the 5% additions of these elements. The same can be said of silicon additions of over 5% to the V-50% Ti alloy, although the forgeability limit in this instance is only 7 %.

Tensile Properties of V-Ti-Al Alloys made from Alumino-Thermic Vanadium

Recently the Electro Metallurgical Company of Niagara Falls, New York made available a new vanadium-rich material which is the product of an alumino-thermic reduction of V_2O_5. Its very significantly cheaper cost makes the material of considerable interest. The metal has the following representative composition:

V	84.17%	O	0.26%
Al	13.99%	N	0.03%
Fe	0.50%	C	0.03%
Si	<0.40%	H	0.005%

The high aluminum content renders the metal brittle, but since V-Ti-Al alloys in the range 40-50% Ti and 0-10% Al proved to have interesting mechanical properties it is a point of some interest to determine whether such alloys made from alumino-thermic vanadium by alloying directly with titanium would have comparable properties. It should be noted at this point that the total interstitial content in this metal is considerably higher than in calcium-reduced vanadium and this might be expected to inhibit ductility.

Ternary alloys were prepared by melting alumino-thermic vanadium with sponge titanium (120 BHN). The ratio of vanadium to aluminum was therefore fixed. A number of these alloys proved unforgeable without the benefit of carbon additions. Accordingly, the influence of carbon content on each of the basic ternary compositions was investigated. The following alloys were included in this program:

V+45% Ti+7.5% Al+0-1.5% C
V+50% Ti+6.9% Al+0-1.5% C
V+55% Ti+6.2% Al+0-1.5% C
V+60% Ti+5.5% Al+0-1.5% C

Tensile properties at room temperature, 500°C (930°F), and 700°C (1290°F), respectively, are summarized in Table IV. A number of observations can be made from the results. There is a continuous decrease in tensile strength at all temperatures with increasing titanium content. The same trend obtains in binary V-Ti alloys.

By interpolation of results with ternary V-Ti-Al alloys produced from calcium-reduced vanadium, it appears that alloys based on alumino-thermic vanadium offer higher tensile strengths at room temperature and 500°C (930°F), but not at 700°C (1290°F). The lower temperature strength superiority is probably due to the higher content of interstitial elements—0.32% (O+N+C) as compared with 0.17% for calcium-reduced vanadium.

Table IV
Tensile Properties of Alumino-Thermic Vanadium Alloys With Various Titanium, Aluminum and Carbon Contents

Composition	Ultimate Tensile Strength psi	Elongation %	Reduction in Area %	Analyzed Carbon Content %
Room Temperature				
V-60% Ti-5.6% Al	131,400	9.9	26.5	—
V-60% Ti-5.5% Al-0.5% C	129,800	12.1	27.7	0.15
V-60% Ti-5.5% Al-1% C	132,000	11.0	24.3	0.21
V-60% Ti-5.4% Al-1.5% C	131,000	9.6	17.3	0.40
V-55% Ti-6.3% Al	137,600	11.2	32.3	—
V-55% Ti-6.2% Al-0.5% C	139,200	9.8	13.7	0.25
V-55% Ti-6.2% Al-1% C	143,200	11.1	29.1	0.80
V-55% Ti-6.1% Al-1.5% C	143,200	5.0	7.6	1.14 (M)
V-50% Ti-6.9% Al-0.5% C	142,600	13.4	31.1	0.41
V-50% Ti-6.9% Al-1% C	144,600	9.0	6.8	1.17 (M)
V-50% Ti-6.8% Al-1.5% C	142,400	2.0	6.2	0.33
	132,800	2.0	1.4	1.13 (M)
V-45% Ti-7.6% Al-0.5% C	154,400	8.0	9.2	0.17
V-45% Ti-7.6% Al-1% C	162,800	11.0	20.1	0.34
V-45% Ti-7.5% Al-1.5% C	133,200	0	0	0.32
500 °C				
V-60% Ti-5.5% Al-0.5% C	116,000	19.0	34.9	—
V-60% Ti-5.5% Al-1% C	118,600	17.5	30.5	—
V-60% Ti-5.4% Al-1.5% C	115,600	8.0	14.5	—
V-55% Ti-6.2% Al-0.5% C	116,800	18.5	28.5	—
V-55% Ti-6.2% Al-0.5% C	128,600	18.0	30.4 (M)	—
V-55% Ti-6.2% Al-1% C	124,200	18.5	31.9	—
V-55% Ti-6.2% Al-1% C	125,800	7.5	11.3 (M)	—
V-55% Ti-6.1% Al-1.5% C	131,800	15.0	22.5	—
V-50% Ti-6.9% Al-0.5% C	128,800	31.0	24.3	—
V-50% Ti-6.9% Al-1% C	136,200	11.0	15.3 (M)	—
V-50% Ti-6.8% Al-1.5% C	131,800	16.0	21.7	—
V-50% Ti-6.8% Al-1.5% C	131,400	3.5	7.8 (M)	—
700 °C				
V-60% Ti-5.6% Al	44,400	48.3	93.6	—
V-60% Ti-5.5% Al-0.5% C	37,600	49.2	84.5	0.15
V-60% Ti-5.5% Al-1% C	40,600	43.3	84.5	0.52
V-60% Ti-5.4% Al-1.5% C	59,000	20.7	41.4	0.40
V-55% Ti-6.3% Al	55,600	42.5	89.2	—
V-55% Ti-6.2% Al-0.5% C	48,100	56.8	86.1	0.25
V-55% Ti-6.2% Al-0.5% C	58,800	66.5	74.9	0.44 (M)
V-55% Ti-6.2% Al-1% C	55,800	40.9	79.1	0.80
V-55% Ti-6.2% Al-1% C	63,000	43.5	73.8	0.95 (M)
V-55% Ti-6.1% Al-1.5% C	69,400	39.0	55.4	1.14 (M)
V-50% Ti-6.9% Al-0.5% C	50,200	26.6	71.7	0.41
V-50% Ti-6.9% Al-1% C	53,600	38.0	77.3	—
V-50% Ti-6.9% Al-1% C	72,000	32.0	52.0	0.63 (M)
V-50% Ti-6.8% Al-1.5% C	76,600	23.7	61.6	0.93

(M) Vanadium-carbon master alloy (20% carbon) used.

The V+50% Ti+6.9% Al and V+45% Ti+7.5% Al alloys made from alumino-thermic vanadium were unforgeable. Carbon additions were necessary to permit forgeability. The analogous ternary alloys based on calcium-reduced vanadium permitted forgeability with aluminum contents as high as 10%.

Additions of up to 1.17% C (analyzed) were made on certain alloys, but only at 700°C (1290°F) is there any obvious effect of in-

crease in strength with carbon content. At room temperature and at 500°C (930°F), tensile strengths are substantially independent of carbon content. Ductilities, however, appear to be reduced at higher carbon levels. It appears, therefore, that carbon is a desirable addition as a general safeguard of forgeability, but that it confers little advantage in tensile properties.

The tensile behavior of alloys based on alumino-thermic vanadium, when rendered satisfactorily forgeable by carbon additions, is as good as or superior to that of the same alloys produced from the purer and considerably more expensive calcium-reduced vanadium.

Stress-Rupture Behavior of Vanadium Alloys

From the elevated temperature tensile results, the most obvious potential usefulness of vanadium alloys seemed to be in applications where high creep strength to density is a governing design parameter. The fundamentally lower densities of V-Ti alloys place these in the forefront of the new alloy development picture.

A program of stress-rupture testing is considerably more involved than hot tensile testing and accordingly the range of alloys had to be considerably more restricted. It is planned to publish another paper describing the oxidation behavior of vanadium alloys which was studied concurrently. The alloys selected for stress-rupture testing were those which, at the time, seemed most likely to provide superior oxidation resistance. In all, 14 alloys were studied in the temperature range 500–700°C (930–1290°F). The selection provided an insight into the relative influence of aluminum and chromium, the contribution of free carbides, and the comparative behavior of calcium and aluminum-reduced vanadium.

In all but a few instances, the time-stress dependency of rupture at any given temperature could be represented by a straight line. Table V summarizes the hot tensile strengths and the interpolated 100 hour stress-to-rupture values. A review of these test results indicates the following trends:

(a) The stress-rupture limits are sharply dependent on temperature. This can be more easily appreciated from Fig. 8, which illustrates for a characteristic selection of alloys the temperature dependence of the stress for 100 hour rupture. It will be noted that there is a general tendency for curves of all the alloys to converge at about 700°C. Above that temperature level, it would appear that creep rupture behavior is not strongly composition dependent. There are major differences in 100 hour strength at 500°C (930°F) between the alloys. The general indications are that the stress for rupture approaches an independency from time at or below 500°C (930°F), i.e., rupture stresses approach the hot tensile strengths.

(b) Aluminum confers more creep rupture strength on a 50%

Table V
Hot Tensile Strengths and Stress-Rupture Strengths of Some Vanadium Alloys

Composition	Testing Temperature °C	Hot Tensile Strength psi	Interpolated 100 Hour Stress-Rupture Value psi
50%Ti-5% Cr	500	105,200	60,000
	700	66,200	9,500
50% Ti-10% Cr	500	110,000	63,000
	700	82,900	9,500
50% Ti-15% Cr	500	137,300	95,000
	700	80,200	11,500
50% Ti-5% Al	500	110,400	95,000
	600	—	37,000
	700	84,600	—
50% Ti-10% Al	500	107,400	83,000
	600	—	47,000
	700	104,000	—
40% Ti-5% Al	500	109,600	100,000
	600	—	45,000
	700	96,600	8,000
50% Ti-5% Cr-0.5% C	500	119,200	76,000
	600	—	26,000
50% Ti-5% Al-0.5% C	500	—	94,000
	600	109,000	36,000
40% Ti-5% Al-0.5% C	500	132,800	112,000
	600	118,800	41,500
50% Ti-6.9% Al-0.5% C	600	—	40,000
50% Ti-6.8% Al-1.5% C	600	—	46,000
50% Ti-6.9% Al-0.5% C	500	128,800	104,000
	600	—	29,500
55% Ti-6.2% Al-1% C	600	107,800	29,000
60% Ti-5.5% Al-0.5% C	600	89,600	18,000

Table VI
Stress-Rupture Properties of Some Alloys

Temperature °C	Stress psi	Rupture Time, Hrs.,—(brackets indicate % elongation) V-40% Ti-5% Al	V-50% Ti-10% Cr	V-50% Ti-15% Cr
700	65,000		0.2 (17.2%)	0.1 (4.7%)
	50,000	0.58 (48.4%)		
	40,000			0.8 (14.1%)
	20,000	21.0 (84.4%)		
	15,000		28.9 (106%)	
	10,000	49.7 (–)	60.6+(145.3%)	120.3+(130%)
600	85,000	7.2 (17.2%)		
	70,000	18.1 (23.4%)		
	55,000			5.0 (7.8%)
	46,000	43.2 (25.0%)	16.6 (29.7%)	
	35,000			30.5 (9.4%)
	29,500		75.6 (34.4%)	
	25,000			250.8 (43.8%)
	22,500		193.1 (137.5%)	
500	107,500	56.8 (3.1%)		
	98,000	109.0 (3.1%)		
	65,000		43.6 (7.8%)	
	59,000		259.2 (9.4%)	

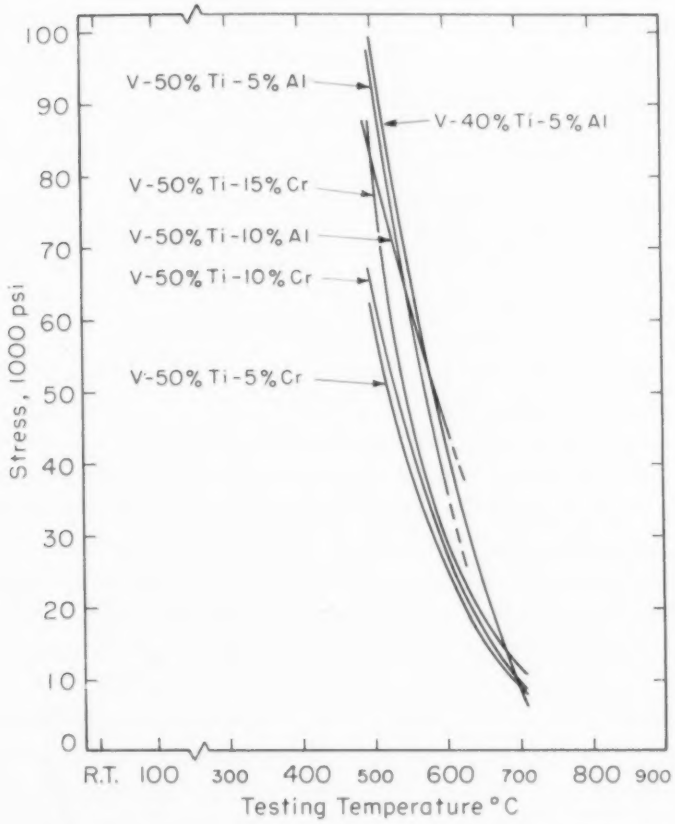


Fig. 8—100 Hour Rupture Life of Selected Vanadium Alloys as a Function of Temperature.

V-50% Ti alloy than does chromium. The differences in behavior are more apparent at 500 and 600°C (930 and 1110°F). A 10% Al level offers no more 100 hour strength than a 5% Al level.

(c) The presence of carbon as free carbides adds little or nothing to the stress-rupture strength. Although the 40% Ti-5% Al-0.5% C alloy showed the highest 100 hour strength at 500°C (930°F), its superiority over the equivalent alloy with no intentional carbon addition is only about 10,000 psi. The alloy containing 50% Ti-6.9% Al-0.5% C has a stress-rupture curve at 600°C (1110°F) almost identical to that of the same alloy with 1.5% C added.

(d) The 600°C (1110°F) stress-rupture behavior of a 50% Ti-6.9% Al-0.5% C alloy based on alumino-thermic vanadium is identical, within the limits of experimental error, to that of the 50% Ti-5% Al-0.5% C alloy based on calcium-reduced vanadium. It appears, therefore, that the initial purity of the vanadium is not a crucial point at these temperature levels of testing.

(e) At 500°C (930°F), the highest stress for a 100 hour rupture condition is delivered by a vanadium alloy containing 40% Ti,

5% Al, and 0.5% C. At 600°C (1110°F), three alloys are tied for first place:

40% Ti+5% Al+0.5% C
50% Ti+10% Al
50% Ti+6.8% Al+1.5% C (alumino-thermic vanadium)

All of the alloys exhibited ductile behavior at the testing temperature. Table VI summarizes ductility values at fracture for several alloys.

Summary

In its unalloyed form, vanadium may be regarded as a low strength, very ductile metal. Its ductility, as in titanium, zirconium, and other high melting point transition elements, is most severely limited by the content of interstitial elements—oxygen and nitrogen—held in solid solution. Accordingly, melting and heat treatments must be designed to prevent any increase in the existent level of interstitials. Because of this and because of its very high melting point (~1900°C), it would seem that vanadium and its alloys will have to be melted in the cold mold, arc melting furnaces currently in use for titanium and zirconium alloys.

Although a large number of elements have appreciable solid solubilities in vanadium, only one of the binary systems, vanadium-titanium, permitted forgeability beyond 10% alloy addition. The V-Ti alloys proved forgeable over the whole range of compositions.

Certain elements in small additions developed anomalous minima in hardness and tensile strengths which in some instances were significantly lower than even for unalloyed vanadium itself. Titanium and zirconium were particularly remarkable in this respect. An alloy containing 2.5% Zr has considerably more tensile ductility than unalloyed vanadium and the sheet specimens cold-rolled to more than 90% reduction in area can still be bent over a sharp mandrel to nearly 180 degrees.

Nearly all of the forgeable binary alloys proved to have low tensile strengths and negligible tensile ductilities. Outstanding exceptions were binary alloys containing up to 50% Ti and up to 3% Zr. These results showed that the goal of high strength-high ductility could be achieved only in polycomponent alloys based on vanadium-titanium and vanadium-zirconium. On the basis of considerable testing, it was shown that only the V-Ti-X alloys, where X is a third addition or more, could develop very high strength levels. Single phase solid solution alloys based on V+40-50% Ti can develop room temperature strengths up to 170,000 psi.

While the overall strength of unalloyed vanadium is relatively low, the rate of decrease with temperature is also low, with the result that even at 900°C (1650°F), vanadium retains strengths of the

order of 15,000 psi. Judged on a strength to density basis (density of vanadium = 6.0 gms/cc), this is nearly equal to molybdenum. A systematic program of hot tensile testing of vanadium alloys showed that the elevated temperature strengths in the range room temperature to 500°C (930°F) could be raised to substantially higher levels than those shown by unalloyed vanadium. For instance, unalloyed vanadium at 500°C (930°F) has a tensile strength of 57,000 psi, whereas an alloy containing 50% Ti and 5% Si had a strength of 158,000 psi. Above 500°C (930°F), all alloys showed sharp progressive drops in strength converging near 900°C (1650°F). At this temperature strengths vary between 15,000 and 50,000 psi. It would appear that at about 1100°C (2010°F), all alloys would have about the same strength, irrespective of composition.

The excellent high temperature tensile strengths were taken as a preliminary indication of useful creep strengths, especially when judged on a strength to density basis. The stress-rupture behavior of a number of alloys was studied in the temperature range 500–700°C (930-1290°F). Alloy groups included V-Ti-Cr, V-Ti-Al, and V-Ti-Al-C, as well as alloys of V-Ti-Al using alumino-thermic vanadium as an alloy base. The scope of work was necessarily limited by time and funds. A considerable area of promising alloy compositions remains to be studied. Nevertheless, with this limited survey, certain vanadium alloys were developed which were at least equal, and probably marginally superior, to the best so far developed, at the time of writing, in titanium-base alloys. In the temperature range 400–500°C (750-930°F), there is an unquestioned superiority of the vanadium and titanium alloys over the nickel-base, cobalt-base and iron-base alloys when judged on a stress-to-rupture by density parameter.

Carbon additions have been shown to improve the forging characteristics of vanadium alloys without impairing mechanical properties. In fact, in certain instances, carbon additions developed superior ductilities. The presence of free carbides does not seem to affect the stress-rupture behavior.

The majority of this work made use of vanadium metal produced by a calcium reduction process. This metal is of comparatively high purity and is ductile in the unalloyed state. A new vanadium metal is currently available, which is produced by an alumino-thermic reduction process. This metal contains appreciable amounts of aluminum in solid solution as well as a higher level of interstitials. Accordingly, it is not ductile in its "unalloyed" state. It was, however, shown that when the alumino-thermic metal was used as base material to prepare the V+40-50% Ti+5-10% Al alloys, the alloys were similar in mechanical behavior to the same compositions produced with calcium-reduced vanadium.

Vanadium alloys have potential application as high strength

materials at elevated temperatures up to 675°C (1240°F), at which temperature V_2O_5 melts and catastrophic oxidation occurs. Above that temperature suitable oxidation preventive measures are necessary. The work presently reported is of a preliminary nature, but it serves to define areas of interest for further investigation.

Acknowledgments

This work was performed under the sponsorship of the Materials Laboratory of the Wright Air Development Center, Wright-Patterson Air Force Base, Ohio. The authors wish to express their gratitude for this support and for permission to publish this paper. Acknowledgment is due also to Mr. W. Carew of the Foundation for his supervision of the stress-rupture testing.

References

1. W. Rostoker and A. S. Yamamoto, "A Survey of Vanadium Binary Systems," Transactions, American Society for Metals, Vol. 46, 1954, p. 1136.
2. A. U. Seybolt and H. T. Sumsion, "Vanadium-Oxygen Solid Solutions," *Transactions*, American Institute of Mining and Metallurgical Engineers, Vol. 5, 1953, p. 292.
3. N. P. Allen, O. Kubaschewski and O. von Goldbek, "The Free Energy Diagram of the Vanadium-Oxygen System," *Journal*, Electrochemical Society, Vol. 98, November 1951, p. 417.

PROPERTIES OF VANADIUM CONSOLIDATED BY EXTRUSION

By C. E. Lacy and C. J. Beck

Abstract

Ductile vanadium, produced by the bomb reduction of V_2O_5 with calcium, was simultaneously consolidated and reduced to shape by hot extrusion. Chemical analyses, mechanical properties, recrystallization behavior, metallographic structure, and cold fabrication behavior were used to evaluate the extruded products.

Consolidation by extrusion produced a dense, sound product with satisfactory tensile properties and excellent cold fabrication characteristics. Contamination of the reactive vanadium with oxygen and nitrogen during processing was minimized. A ¾ inch O.D. by ⅛ inch wall extruded tube was readily cold drawn to 0.080 inch O.D. by 0.010 inch wall capillary tubing.

Properties reported include standard tensile data, true stress—true strain tensile data, hardness, moduli, and density.

Hardness versus annealing temperature data are presented for extruded vanadium which had been given a 60% cold reduction. An anomaly attributed to age hardening was observed in these data. (ASM-SLA Classification: F24, Q general, V)

Properties of Vanadium Consolidated by Extrusion

MASSIVE ductile vanadium can be prepared by the bomb reduction of V_2O_5 with calcium (1,2,3).[1] The product of this reduction is a button or regulus which is not particularly suitable for processing directly into usable forms because it has an irregular shape and generally contains entrapped slag. Since vanadium is a reactive metal similar to titanium and zirconium, the reguli cannot be melted into ingots by normal melting techniques without producing serious embrittlement. As little as 0.05% oxygen causes a serious loss in the cold ductility.

The vanadium reguli have been converted into usable forms by arc melting and fabrication of the ingots using a metal sheath or salt as protective coating. However, care must be exercised in

[1]The figures appearing in parentheses pertain to the references appended to this paper.

A paper presented before the Thirty-Seventh Annual Convention of the Society, held in Philadelphia, October 17–21, 1955. Of the authors, C. E. Lacy is research associate and C. J. Beck is metallurgist at the Knolls Atomic Power Laboratory, General Electric Company, Schenectady. Manuscript received March 10, 1955.

both the melting and fabrication operations to prevent oxygen contamination. Another possible method of consolidating the reguli is by hot extrusion. This technique has the advantages of eliminating the arc melting step and providing a short work cycle, which minimize chances for contamination. The present paper gives data on the properties of ductile, bomb-reduced vanadium which has been consolidated by hot extrusion.

Experimental Procedure

General—In the consolidation of a metal by extrusion, small particles are pressure welded into a solid mass by hot working. Consolidation and reduction to shape are accomplished in a single operation. The general technique of pressure welding is not new, but there is increasing interest in extrusion for this purpose because of its speed and versatility in regard to starting materials and shape of product. Extrusion is particularly suitable for a reactive material like vanadium because the metal can be confined readily in a protective jacket and the short work cycle minimizes possible contamination during fabrication.

Extrusion Procedure—Ductile vanadium buttons or reguli (Fig. 1) were cold-rolled to 0.030 inch sheet which was in turn sheared into ¼ inch squares. The total cold reduction was in excess of 90%. This amount of reduction caused some splitting and edge cracking, but this condition was unimportant since the purpose was to make small pieces which could be packed uniformly for extrusion. Rolling to sheet also served to permit the elimination of any slag entrapped in the buttons. Since slag-bearing areas produced defects in the sheet, the slag could be removed by discarding these defective areas in the shearing operation or by leaching in subsequent acid pickling.

To prepare an extrusion billet, approximately 850 grams of these vanadium squares were degreased, pickled in dilute nitric acid, and vibration packed to 50% of theorical density in a 2⅜ inch O.D. by 0.060 inch wall steel can (see Fig. 2). A steel plug was welded in the top of the can, and the can was evacuated through a steel tube in the plug. A seal was made while the can was under vacuum by cold pinching the steel tube.

Extrusion of the billet assemblies was done on a 500-ton press with a 2.48 inch diameter container. The billets were heated for one hour at 1100 to 1150°C (2010 to 2100°F) in an argon atmosphere prior to extrusion. Lubricants were the conventional graphite-oil and mica-asphalt type. Delivery speed of the extruded product was approximately 60 feet per minute.

A list of the five extrusions made in this study and the pertinent extrusion data are given in Table I. Vanadium squares for Extrusions 1 through 3 were obtained from 125 to 1000 gram buttons prepared by the calcium reduction of V_2O_5 as described in References 1



Fig. 1—Vanadium Button or Regulus Produced by Bomb Reduction of V_2O_5 with Calcium.

and 2; those for Extrusions 82 and 94 were obtained from larger reductions made by a commercial supplier of vanadium. Material for Extrusion 82 was prepared by hydriding, crushing, and dehydriding regulus vanadium rather than by cold rolling and shearing. This vanadium was supposedly typical of regulus metal which had borderline cold fabricability after being processed to rod by com-

Table I
Extrusion Conditions for Vanadium Consolidated by Extrusion

Extrusion Number	Extruded Form	Billet Temp. —°C	Extrusion Ratio	Extrusion Constant-PSI*
KAPL-1	¾ inch Rod	1150	10.9 to 1	50,000
KAPL-2	¾ inch x ½ inch Tube	1150	18.9 to 1	52,000
KAPL-3	¾ inch Rod	1100	10.9 to 1	50,000
UC-82	¾ inch Rod	1100	10.9 to 1	—
UC-94	¾ inch Rod	1100	10.9 to 1	—

*Extrusion Constant $= \dfrac{\text{Ram Pressure (Psi)}}{\log_e \dfrac{\text{Original Area}}{\text{Final Area}}}$



Fig. 2—Vanadium Squares and Steel Can Used in the Preparation of Extrusion Billet Assemblies.

mercial techniques. The billet assembly for the tubing extrusion was similar to those used for rod extrusions except that a 0.550 inch I.D. by 0.060 inch wall mild steel tube was inserted through the axis of the assembly and welded to the steel jacket at each end. The vanadium chips were packed between the inner and outer jacketing tubes. Extrusion of this assembly into tubing was made using a floating mandrel.

Methods of Evaluation—To evaluate the extruded product, the following data were obtained: (a) chemical analyses, (b) mechanical properties, (c) recrystallization behavior, (d) metallographic structure, and (e) cold fabrication behavior. Further information on methods of obtaining these data is given in the following sections on experimental results.

Experimental Results

Chemical Analyses—Analytical data were obtained on samples from the extruded product in either the "as extruded" or extruded and cold worked condition. Values determined on Extrusions 1, 2, 82, and 94 are given in Table II. A typical composition of a 1000 gram vanadium button of the type used for Extrusions 1 through 3 is included for comparison.

Table II
Chemical Analyses of Extruded Vanadium

Element	Typical 1000 Gram Button	Weight Per Cent of Element KAPL-1	KAPL-2	UC-82	UC-94
O_2	0.03	0.045	0.034	0.031	0.0324
N_2	0.009	0.0072	0.0052	0.026	0.0009
H_2	0.002	0.0043	0.0028	0.0021	0.0025
C	0.13	0.130	0.119	0.146	0.075
Fe	0.2*	0.22	0.025	0.17	0.33
Si	0.05	0.054	0.51	0.069	0.040
Al	0.1*	0.051	0.25	0.056	0.025
Ca	0.1*	0.048	0.096	0.079	0.101

*Spectrographic values

Tensile Properties—Tensile tests were run on Rod Extrusions 1, 82, and 94 in three different conditions: (a) as-extruded and cold straightened, (b) cold-reduced 50 to 60% by swaging or rolling, and (c) annealed after cold working. To obtain material for the tensile specimens the extruded rods were cold-straightened by swaging and the steel jackets were removed by machining. The as-extruded specimens were machined from lengths of the dejacketed rod. Portions of the dejacketed rod from each of the three extrusions were cold-swaged a total of 50 to 60% reduction in area using 15% reductions per swaging pass. A portion of Extrusion 1 was also reduced 60% by cold rolling in hand round grooves using 10 to 15% reduction per pass. Part of each of the cold-worked rods was an-

nealed 1 hour at 900 to 950°C (1650 to 1740°F) in vacuum to provide material for the annealed specimens.

Tensile data were obtained on standard ¼ inch diameter, 1 inch gage length specimens. Duplicate tests were made on the as-extruded and the annealed specimens; single tests were run on the cold-worked specimens. A microformer averaging extensometer was used to obtain yield and rough modulus data. Simultaneous load-diameter measurements were made on the annealed specimens to permit computation of true stress-true strain curves. The specimens were strained at a rate of 0.005 to 0.01 in./in./minute.

Properties determined in the tensile tests are presented in Table III. All except the cold-worked specimens exhibited a yield point; for these the upper and lower yield point values are reported.

Table III
Tensile Properties of Vanadium Consolidated by Extrusion

Specimen Identity and Condition	Upper Yld. Point Psi	Lower Yld. Point Psi	Tensile Strength Psi	Young's Modulus Psi $\times 10^{-6}$	Elong. in 1 in. %	Red Area %
As-Extruded						
KAPL-1 (5)	57,800[c]		61,500	19.4	35	64
UC-82	51,700	48,900	63,600	19.8	31	56
UC-94	47,200	44,300	60,800	19.6	31.5	70.5
Cold-Worked						
KAPL-1[a] (63)	71,600[c]		75,800	19.3	18	64
KAPL-1[b] (62)	78,500[c]		85,100		17	58
UC-82[a] (50)	73,500[c]		77,700	18.1	18	53
UC-94[a] (47)	71,400[c]		75,100	18.1	19	66
C. W. + Anneal						
KAPL-1[a] (63)	47,800	41,900	56,000	19.1	44.5	78.5
KAPL-1[b] (62)	51,700	46,200	56,400	17	35	79
UC-82[a] (50)	55,100	49,800	61,700	19.2	37	64
UC-94[a] (47)	48,600	45,800	58,400	19.2	33	80.5

[a] = Cold-Swaged
[b] = Cold-Rolled
[c] = 0.2% Yield Strength
( ) = Per cent Cold Work
Anneal = 1 hour at 900–950°C (1650–1740°F)

Yield strengths for the cold-worked specimens are the stresses required to give 0.2% permanent deformation. Table IV lists the strain hardening exponent and strength coefficients for the annealed specimens. These are the n and A constants in the true stress-true strain equation $\sigma = A\epsilon^n$ where $\epsilon = \int_{l_o}^{l_1} \frac{dl}{l} = \log_e \frac{l_1}{l_o}$ or $\log_e \frac{A_o}{A_1}$. Values for n and A were determined from log-log plots of the true stress-true strain data; averages of two determinations made from the duplicate tensile tests are reported in the Table.

Values for Young's modulus and the shear modulus of Extrusion 1 in the as-extruded condition were determined dynamically. These were calculated from the longitudinal and shear wave veloci-

Table IV
Strain Hardening Exponents and Strength Coefficients for Annealed Vanadium

Extrusion Number	Type of Cold Work Prior to Anneal*	Strain Hardening Coefficient	Strength Coefficient, Psi
KAPL-1	Swaged 63%	0.16	87,500
KAPL-1	Rolled 62%	0.21	96,000
UC-82	Swaged 50%	0.17	98,000
UC-94	Swaged 47%	0.20	98,000

*Annealed 1 hour at 900–950°C in vacuum

ties obtained by the ultrasonic pulse technique (4). Following are these values:

Young's Modulus	18,400,000 psi
Shear Modulus	6,730,000 psi
Poisson Ratio	0.36

The density of the machined cylinder used for these measurements, as determined from its size and weight, was 6.10 grams/^{cm3}.

Hardness—Diamond pyramid hardness data for the five extrusions are presented in Table V; hardness was determined on metallographically polished specimens using a 10 kilogram load. In most cases data were obtained on samples cut both parallel and perpendicular to the working direction. The data for the two types of samples are reported separately in the table. Each value listed is the average determined from three to five hardness impressions.

Recrystallization Data—In order to determine the proper temperature for heat treating the annealed specimens, hardness versus annealing temperature data were determined on cold-swaged and

Table V
Hardness of Extruded Vanadium

Extrusion Number	Condition	Longitudinal DPH-10 Kg. Load	Transverse DPH-10 Kg. Load
KAPL-1	As-Extruded	134	—
	Cold-Swaged 62%	179	—
	Cold-Rolled 63%	196	190
	Cold-Swaged—Annealed	125	—
	Cold-Rolled—Annealed	130	148
KAPL-2	As-Extruded Tubing	109	129
	Drawn to 0.30 in. x 0.25 in.		
	¼ Hard	123	140
	Annealed	105	107
	Drawn to 0.080 in. x 0.060 in.		
	¼ Hard	162*	181*
	Annealed	135*	151*
KAPL-3	As-Extruded	137	139
UC-82	As-Extruded	148	146
	Cold-Swaged 50%	180	184
	Cold-Swaged—Annealed	144	140
UC-94	As-Extruded	136	134
	Cold-Swaged 47%	178	170
	Cold-Swaged—Annealed	144	124

*Converted from Knoop Readings

cold-rolled samples from KAPL-1 rod. These data are plotted in Fig. 3. All samples were annealed in vacuum using a constant annealing time of 1 hour.

The irregularity in the hardness-temperature curve between 600 and 800°C (1110 and 1470°F) is real since it was duplicated on three sets of samples, each of which was processed separately. The anomaly was first observed in data from a set of cold-swaged

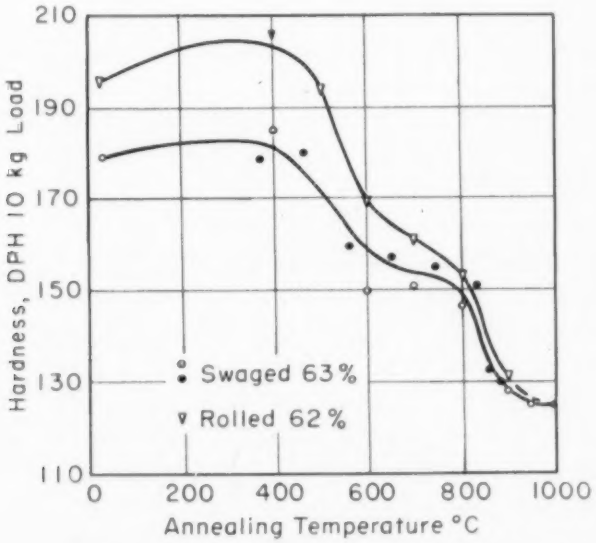


Fig. 3—Effect of Annealing Temperature on the Hardness of Cold-Worked Vanadium.

samples represented by the open circles in Fig. 3. A second set of cold-swaged samples and a set of cold-rolled samples were processed with similar results.

In the metallographic examination of the samples, no observable recrystallization was noted until a temperature in excess of 750°C (1380°F) was reached. Microscopic recrystallization was complete after a 1 hour anneal at 850 to 900°C (1560 to 1650°F).

Metallography—Photomicrographs of longitudinal sections of the five extrusions are shown in Figs. 4a, 4b, 4c, 4e, and 4f. For comparison a photomicrograph (Fig. 4d) of a transverse section has been included; this transverse section is typical of those for all extrusions. The as-extruded material has an annealed grain structure. Further, the pieces of vanadium used in the extrusion have welded together leaving no trace of the original particle surfaces.

Longitudinal sections of Extrusion 1 at high magnification are shown in Figs. 5a and 5b in the as-extruded condition and the cold-worked and annealed condition, respectively. There is a small amount of a second phase at the grain boundaries of the as-extruded

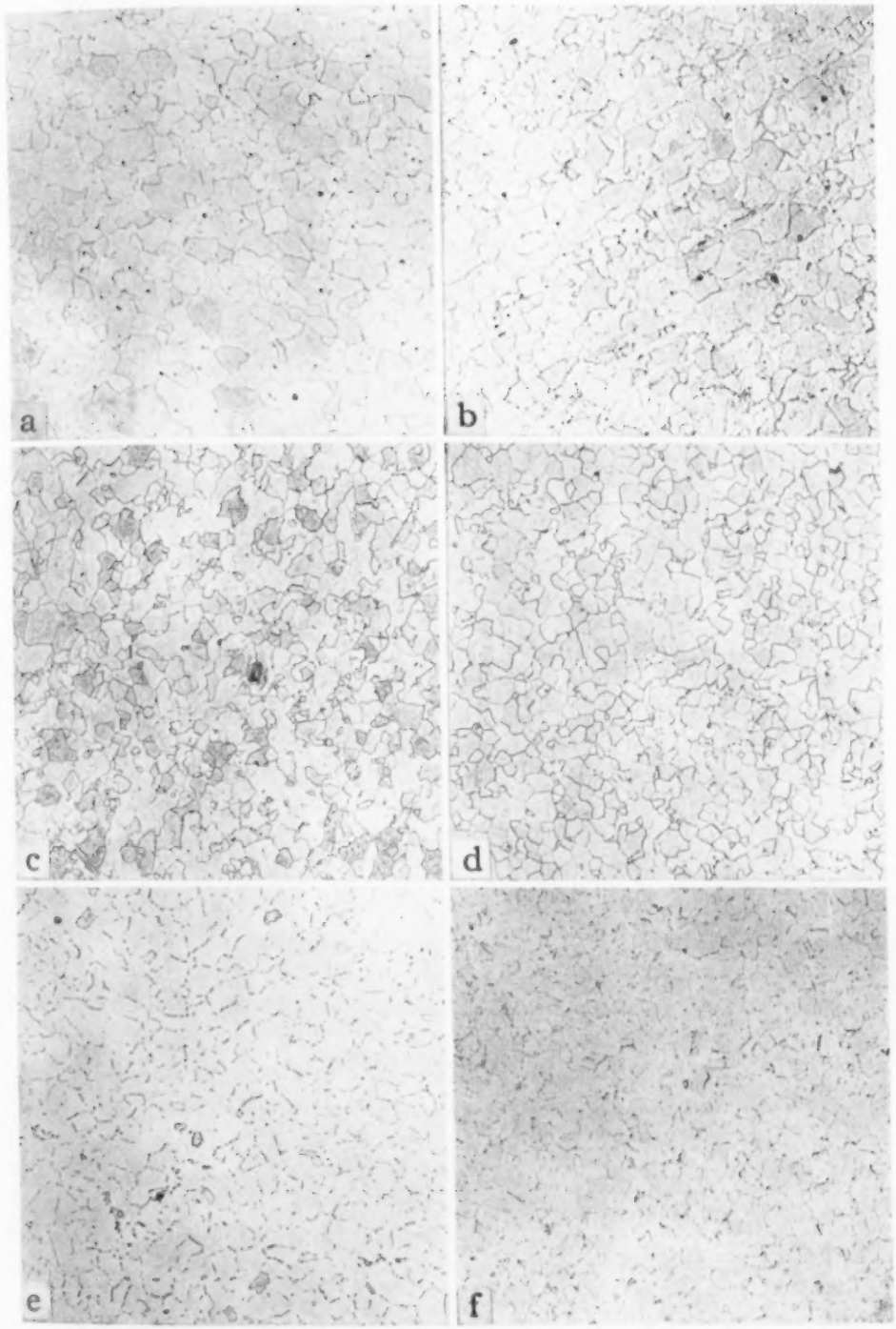


Fig. 4—Structure of Bomb-Reduced Vanadium as Consolidated by Extrusion. Etchant-Aqua regia and Glycerine. × 100. (a) Longitudinal Section of KAPL-1, (b) Longitudinal Section of KAPL-2, (c) Longitudinal Section of KAPL-3, (d) Transverse Section of KAPL-3, (e) Longitudinal Section of UC-84, (f) Longitudinal Section of UC-94.

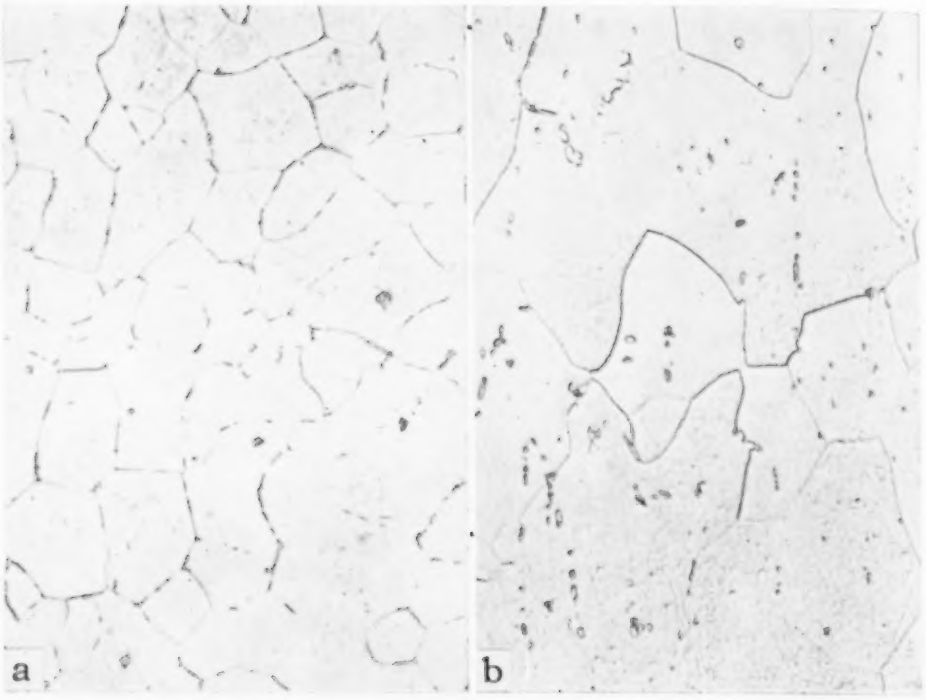


Fig. 5—Longitudinal Sections of Vanadium Extrusion KAPL-1. Etchant-Aqua regia and Glycerine. × 500. (a) As-Extruded (b) Cold-Swaged 62% and Annealed One Hour at 950°C (1740°F).

rod. As is evident in Fig. 5b, this phase remained in situ during cold working and annealing of the extruded rod; thus it did not go into solution during annealing at 950°C (1740°F). Based on known solubilities of impurities present in the vanadium, it is believed the second phase is a carbide, VC.

Cold Fabrication Characteristics—Since contamination of vanadium with oxygen causes embrittlement at room temperature, the cold fabrication behavior is a good measure of vanadium quality. Swaging, rolling, and drawing were used to check the cold fabrication characteristics of the vanadium extrusions.

Rod Extrusions 1, 82, and 94 were cold-swaged to 63, 50, and 47% reductions in area, respectively, without annealing as described in the section on tensile properties. The material swaged easily and could have been reduced further. Extrusion 1 was also readily cold-rolled to a total reduction in area of 62%.

Extrusion 2, a ¾ inch O.D. by ½ inch I.D. tube, was used solely for checking the cold working qualities of extrusion consolidated vanadium. The inner and outer steel jackets on the extruded tube were removed by pickling in dilute HCl. This pickling treatment produced hydrogen embrittlement of the tube, but vacuum annealing 6 hours at 1000°C (1830°F) removed the hydrogen and restored the original hardness. The surface of the vanadium was rough after removal of the steel jacket, and machining was

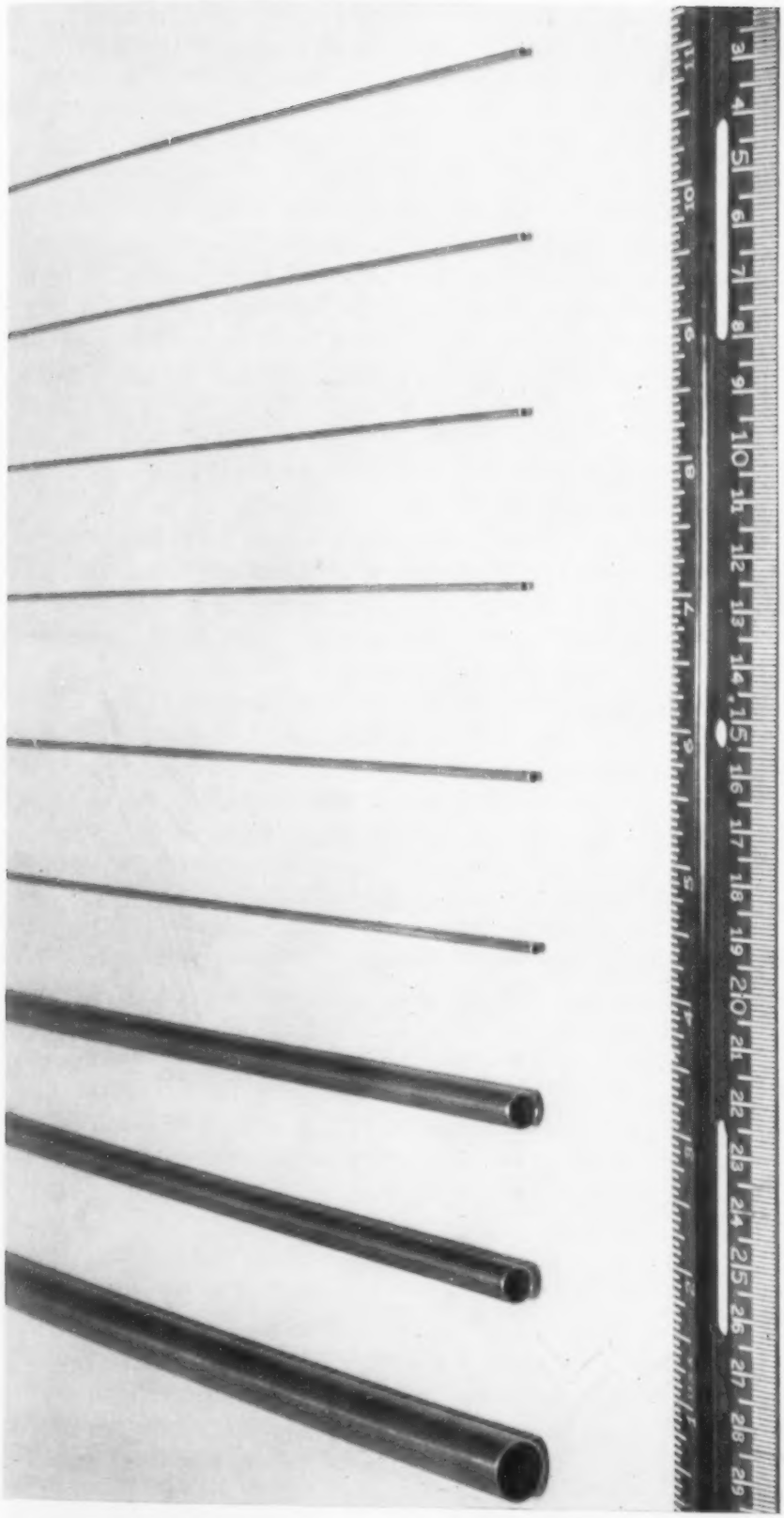


Fig. 6—Vanadium Tubing Drawn from Extrusion KAPL-2. Sizes Left to Right: One Length 0.500 inch O.D. by 0.025 inch Wall, Two Lengths 0.310 inch O.D. by 0.025 inch Wall, Two Lengths 0.100 inch O.D. by 0.010 inch Wall, and Four Lengths 0.082 inch O.D. by 0.010 inch Wall.

required to produce a tube suitable for drawing. After surface conditioning the tubing was successfully drawn into the four sizes of tubing shown in Fig. 6. Annealing in the drawing operation was done in vacuum. The total reduction in area of the starting tube in drawing to the smallest size, 0.062 inch I.D. by 0.010 inch wall, was in excess of 98%.

In an inspection of the six small tubes, they were found to be leak tight by mass spectrometer leak testing. The six small diameter tubes were pressure tested at a maximum hoop stress of 8000 psi without observable permanent change in dimensions. One of the tubes, pressure tested to rupture, failed at a hoop stress of 34,500 psi; this is approximately the proportional limit for the vanadium.

Discussion of Results

The data obtained in this work show that extrusion is a feasible technique for consolidating ductile vanadium reguli produced by bomb reduction. Extrusion produces a dense sound product with satisfactory mechanical properties and excellent cold fabrication characteristics. Hardness and analytical data indicate that the quality of the extruded vanadium is practically equivalent to that of the as-reduced regulus or buttons.

The tensile properties of the extruded vanadium are similar to those of ingot iron; they are characterized by moderate strength and excellent ductility. A comparison of the properties of the extruded vanadium with those reported by Kinzel (3), Nash et al (5), and Brown (6) for commercial, iodide, and "high purity" vanadium, respectively, is given in Table VI. The properties in general are intermediate to those of commercial and iodide vanadium and are

Table VI
Comparison of Properties of Extrusion Consolidated Vanadium with Data Reported in the Literature

Property*	Extruded Vanadium	Commercial Vanadium (3)	High Purity Vanadium (6)	Iodide Vanadium (5)
Upper Yield Point, Psi	48 to 55,000			
Lower Yield Point, Psi	42 to 50,000			
0.2% Yield Strength, Psi		76,000		16,700
Tensile Strength, Psi	56 to 62,000	81,000	60 to 70,000	31,600
Elongation %	33 to 44 (1 in.)	7 (2 in.)	≤25	17 (1 in.)**
Reduction in Area %	64 to 80		≤65	75
Strain Hardening Coefficient	0.16 to 0.21			0.20
Strength Coefficient, Psi	87 to 98,000			53,200

*Properties in all cases are for annealed specimens.
**Sheet specimen—broke outside of gage mark.

nearly equivalent to those of the "high purity" vanadium. Since an increase in the impurity content increases the strength and lowers the ductility, the data indicate that the purity of the extruded vanadium is intermediate to that of the crystal bar and "high

purity" metal. Thus the data confirm that consolidation of vanadium by extrusion minimizes contamination. The use of cold working operations and vacuum annealing during subsequent fabrication serves to maintain the impurity content at a low level.

The yield point phenomenon exhibited by the extruded vanadium is similar to the yield point in low carbon iron. Both have body-centered cubic crystal structures; hence yielding in vanadium is probably associated with carbon and nitrogen impurities, as it is in iron. Elimination of the impurities, as is the case for crystal bar vanadium, or cold working eliminates the yield point.

In Tables III and IV, small differences may be noted in the properties of the three extrusions, but there is no direct correlation of these variations with analytical data. Extrusion 82 in the annealed condition has a slightly higher tensile strength and significantly lower reduction in area than the other two extrusions; this might be expected since this extrusion has the largest total gas and carbon impurities. However, on this impurity basis, Extrusion 1 should be somewhat stronger and less ductile than Extrusion UC-94, but the reverse is true. There is an appreciable difference between the cold-swaged and cold-rolled properties of Extrusion 1 even though reductions in cross sectional area were approximately the same. The cold-rolled rod obviously was subjected to a considerable amount of transverse deformation which was not taken into account in determining the amount of deformation from the original and final dimensions of the rod.

With reference to the hardness versus annealing temperature data on the cold-worked vanadium, rapid softening began at 500 to 600°C (930 to 1110°F) and ceased at 850 to 900°C (1560 to 1650°F). Metallographic recrystallization occurred between 750 and 900°C (1380 and 1650°F); thus it did not start until softening was well under way. The temperature range of softening agrees with those reported by Nash et al (5) for crystal bar vanadium and Rostoker and Yamamoto (7) for a "pure" vanadium; however, their data indicate that metallographic recrystallization occurred between 650 and 800°C (1200 and 1470°F). It would be expected that the higher purity iodide metal would recrystallize at a lower temperature, but the reason for the lack of agreement with Rostoker's data is not apparent.

No irregularity in the hardness versus annealing temperature curve for cold-worked vanadium is indicated in the data of Nash or Rostoker. However, since the irregularity observed on extruded vanadium from Extrusion 1 was duplicated on three sets of samples, the effect is real. This behavior very likely is an aging phenomenon, similar to strain aging in steel and titanium (8), although the temperature range in which it occurs, 650 to 800°C (1200 to 1470°F),

is much higher than the low ductility temperature range for iron and titanium.

The technique of loosely packing the small vanadium squares in a steel can for extrusion worked satisfactorily. However, the extruded pieces did have a rough surface after the steel was removed by pickling. The surface of the extruded vanadium could be improved by increasing the density of packing of the vanadium in the cans. A simple cold compacting operation could be used to increase the density from the 50% of theoretical value achieved by tamp packing to approximately 75% of theoretical density.

Summary

Extrusion was demonstrated to be a feasible technique for consolidating ductile vanadium reguli produced by the bomb reduction of V_2O_5 with calcium. Simultaneous consolidation and shaping of vanadium by extrusion resulted in a dense, sound product with satisfactory mechanical properties and excellent cold fabrication characteristics. Contamination of the reactive vanadium with oxygen and nitrogen during processing was minimized.

The tensile properties of the extruded vanadium were similar to those of ingot iron; they are characterized by moderate strength and high ductility. The ductility of the extruded product was further demonstrated by the excellent cold fabrication characteristics in tube drawing.

The temperature range of softening for extruded vanadium, which was cold-reduced 60% in area and annealed 1 hour at temperature, was 500 to 900°C (930 to 1650°F). Metallographically, recrystallization occurred between 750 and 900°C (1380 and 1650°F). An anomaly, attributed to age hardening, was observed in the softening curve between 600 and 800°C (1110 and 1470°F).

Acknowledgments

Vanadium for Extrusions 1 through 3 was prepared at the Knolls Atomic Power Laboratory by A. P. Beard and D. D. Crooks. Vanadium for Extrusions 82 and 94 was supplied through the courtesy of C. M. Brown of the Electro Metallurgical Company, a commercial source of vanadium. The tubing shown in Fig. 6 was drawn from the extruded tube by the Superior Tube Co. Dynamic modulus and density data were determined by M. B. Reynolds, analytical data were obtained by L. P. Pepkowitz and W. S. Horton, and metallographic work was done by J. W. Czarkowski and his staff, all of the Knolls Atomic Power Laboratory. A. J. Palmer assisted in the experimental portion of the work. The help of these and other Laboratory personnel who made contributions to the work is gratefully acknowledged.

References

1. R. K. McKechnie and A. U. Seybolt, "Preparation of Ductile Vanadium by Calcium Reduction," *Journal*, Electrochemical Society, Vol. 97, 1950, p. 311.
2. A. P. Beard and D. D. Crooks, "Kilogram Scale Reductions of Vanadium Pentoxide to Vanadium Metal," *Journal*, Electrochemical Society, Vol. 101, December 1954, p. 597.
3. A. B. Kinzel, "Vanadium Metal—A New Article of Commerce," METAL PROGRESS, American Society for Metals, Vol. 58, 1950, p. 315.
4. M. B. Reynolds, "The Determination of the Elastic Constants of Metals by the Ultrasonic Pulse Technique," TRANSACTIONS, American Society for Metals, Vol. 45, 1953, p. 839.
5. J. W. Nash, H. R. Ogden, R. E. Durtschi, and I. E. Campbell, "Preparation and Properties of Iodide Vanadium," *Transactions*, Electrochemical Society, Vol. 100, 1953, p. 272.
6. C. M. Brown, "Mechanical Properties of High Purity Vanadium," Spring Meeting, Electrochemical Society, April 1953.
7. W. Rostoker and A. Yamamoto, "Vanadium Binary Systems," TRANSACTIONS, American Society for Metals, Vol. 46, 1954, p. 1136.
8. F. D. Rosi and F. C. Perkins, "Mechanical Properties and Strain Aging Effects in Titanium," TRANSACTIONS, American Society for Metals, Vol. 45, 1953, p. 972.

DISCUSSION

Written Discussion: By J. W. Pugh; General Electric Research Laboratory, Schenectady, New York.

It is interesting to compare the results described in this paper with some obtained recently on aro-melted vanadium. This metal was arc-melted under argon from powder pellets, rolled to 0.100-inch thick sheet at 850°C (1560°F), finished to 0.020 inch thick cold, and annealed for an hour at 1000°C (1830°F). A chemical analysis of this material indicated the following.

Element	Weight % Present
O	0.057
N	0.071
H	0.0063
W	<0.02
Fe	<0.005
Si	<0.005
C	0.09

Hardness as a function of annealing temperature for this material is shown in Fig. 7. Note that there is an anomaly in this relationship similar to that of Messrs. Lacy and Beck and that recrystallization has taken place in the same temperature range. The irregularity in the temperature dependence of hardness prior to recrystallization is, as the authors have suggested, undoubtedly due to strain aging. Additional observation on the arc-melted material which confirm this are inverse temperature dependences for the strain-hardening coefficient, strain-rate sensitivity, elongation, and strength in the same temperature range as the anomaly noted for hardness. Yield points and serrated stress-strain curves at the appropriate temperatures provide additional confirmation.

The tensile properties of the arc-melted vanadium at room temperature were as follows.

Property	Value
Yield Strength	53,700 psi
Ultimate Tensile Strength	60,600 psi
Per Cent Elongation	18.9
Strain Hardening Coefficient	0.116

It appears that this material has slightly higher strength, but lower ductility than that of Messrs. Lacy and Beck.

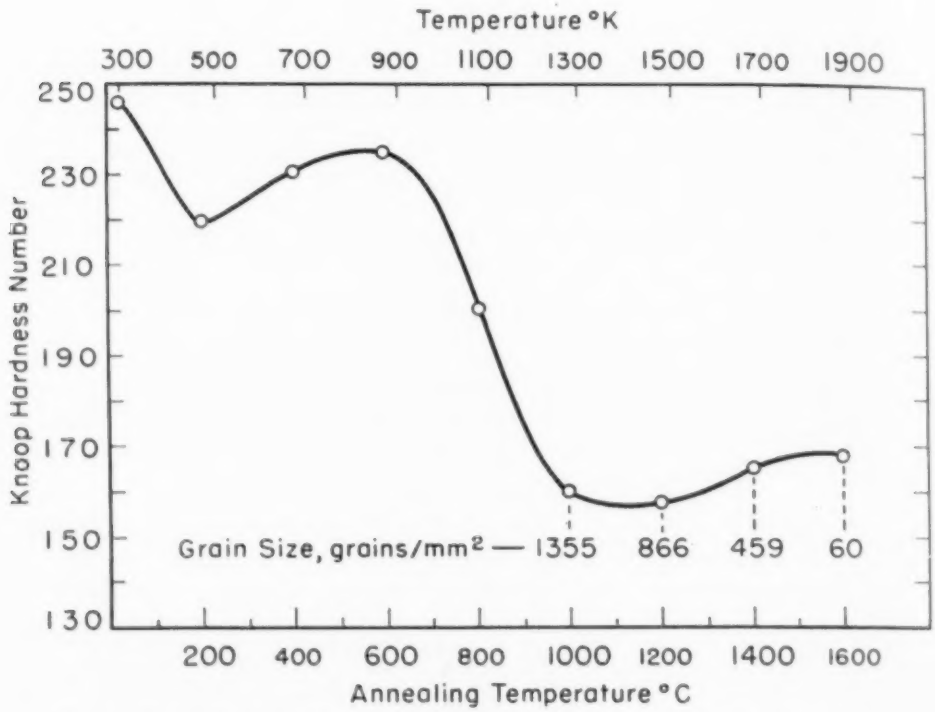


Fig. 7—Knoop Hardness Versus Annealing Temperature on Cold-Rolled Vanadium.

Authors' Reply

The authors appreciate having Dr. Pugh's data on arc-melted vanadium powder. As Dr. Pugh mentions, his data are in general agreement with the data on the extrusion-consolidated bomb-reduced vanadium, except for ductility.

A point of interest is the degree of contamination which occurs in arc-melting. However, since Dr. Pugh's starting material was powder pellets, a comparison of the two sets of data cannot be used to check this point.

FABRICATION AND EVALUATION OF THIN CLAD SHEETS OF MOLYBDENUM

By M. H. LaChance and R. I. Jaffee

Abstract

Techniques for producing thin sections of clad molybdenum and for edge protecting the sheared edges of the composite sheet are described. A method for selecting cladding materials was developed. This method consisted of simulating the conditions existing when clad molybdenum is exposed at elevated air temperatures. The high temperature air oxidation of iron, cobalt, and alloys containing significant quantities of iron or cobalt was drastically accelerated by contact with molybdenum and its oxidation products. Oxidation of chromium, nickel, and high nickel alloys was relatively mild in the presence of molybdenum and MoO_3. Iron-base alloy claddings proved to be markedly inferior to high nickel claddings for service at elevated air temperatures. Of the cladding materials tested, molybdenum was best protected by the 80 w/o nickel-20 w/o chromium alloy. (ASM-SLA Classification: L22, Mo)

FOR structural applications at 1800°F or above, it is now rather generally conceded that of all the possible high melting metals molybdenum has the most promise. The very low resistance of molybdenum to oxidation, beginning about 900°F, requires that a protective coating be used. The present work is concerned with metallic coatings and continues the work described earlier for thick clads by Bruckart and Jaffee (1)[1]. There are several obvious advantages to protective metallic coatings, the most important being their ductility. As the work described will show, thin metallic coatings can provide adequate oxidation protection for molybdenum at 1800°F for long times, even during thermal cycling.

Objective and Scope

The purpose of this work was to produce thin clad composite sheet for limited service life in air at elevated temperatures. A cladding material was rated as satisfactory for service at 1800, 2000, or 2200°F if 3 mils provided protection for: (a) 100 hr. at constant temperature, and (b) 40 1-hour cycles from testing temperature.

[1]The figures appearing in parentheses pertain to the references appended to this paper.

Work performed under AEC Contract No. W-7405-eng-92.

Of the authors, M. H. LaChance is principal metallurgist and R. I. Jaffee is division chief, Nonferrous Physical Metallurgy, Battelle Memorial Institute, Columbus, Ohio. Manuscript received September 20, 1954.

Initial efforts were concentrated on (a) the development of a cladding technique which would yield good metallurgical bonding, and (b) perfecting a method of edge sealing the sheared composite sheet. A total of some 30 alloys were block tested[2] for possible use in cladding molybdenum. Molybdenum was clad with 12 different alloys and air-oxidation tested to determine which material provided satisfactory protection. Throughout the work, an effort was made to classify commercial and experimental heat resistant alloys according to their oxidation resistance, both in air and in air plus MoO_3. It is believed that the findings of this work will augment existing data and lead to a better understanding of surface phenomena for the eventual protection of molybdenum on a commercial scale.

Background Research

It was noted in the initial research work (1) that claddings of "A" nickel, Inconel, and Types 302 and 446 stainless steels (nickel contents decreasing in the order listed) yielded progressively weaker metallurgical bonds, demonstrating that nickel is a desirable alloying element in cladding materials. Utilizing this property, 1 mil of nickel was plated on the contact surfaces of a Type 446 stainless cladding prior to assembly and rolling. No improvement in bond strength was noted with the 1-mil thick interlayer of nickel. The sheared edges of the plus 40-mil thick composite sheets were sealed with nickel, applied with an oxyacetylene torch. It was demonstrated that, at 1800°F under stress, 15 mils of nickel protected the molybdenum base metal from oxidation for approximately 1800 hour.

Materials and Preparation of Clad Sheet

Cladding Components

Westinghouse hydrogen-sintered molybdenum in the wrought condition was used for the core sections. This was machined to the size shown in Fig. 1.

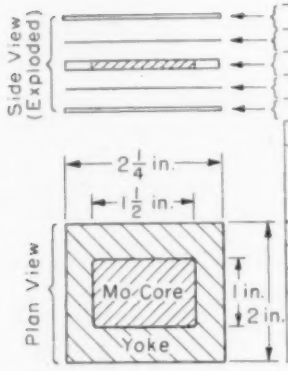
The frame sections, or yokes, were machined from commercial "A" nickel, Inconel, or 80 w/o nickel-20 w/o chromium. Since the edges of the cladding assemblies were sealed by welding, the choice of alloy for the frame depended on its compatibility with the cladding material. Frame sections were shaped to size and milled to accommodate the cores (see Fig. 1).

Commercially available materials which were satisfactorily bonded to molybdenum were "A" nickel, "Z" nickel, 80 w/o nickel-20 w/o chromium, Inconel, Inconel X, and Types 310 and

[2]Accelerated oxidation tests developed for screening intended cladding materials. Detailed description is given later under Oxidation Resistance.

Table I
Experimental Cladding Alloys

Nominal Alloy Composition, w/o	Melting Technique	Forgeability
		From 2200°F
Ni-5.2Ta	Induction melted in air under slag cover	Good
Ni-2.3Ti-2.7Si	Slag composition, w/o: $50Al_2O_3$-42CaO-8MgO	Good
Ni-1.9Ti-2.1Si-1.9Al		Good
Fe-15Cr-5Al		Good
		From 2050°F
Ni-5.1Zr	Arc-cast in argon	Good
Ni-5.2Zr	Induction melted in vacuum	Good
Ni-5.0Zr-2.5Al	Induction melted in vacuum	Good



	Thickness Prior to Roll Cladding, in.		
Cladding Plate	0.0235	0.0205	0.016
"A" Nickel Bonding Layer	None	0.003	0.007
Molybdenum Core	0.110	0.110	0.110
"A" Nickel Bonding Layer	None	0.003	0.007
Cladding Plate	0.0235	0.0205	0.016
Total Thickness	0.157	0.157	0.156

	Thickness After Roll Cladding, in.		
Cladding	0.003	0.0026	0.002
"A" Nickel	None	0.0004	0.001
Molybdenum Core	0.014	0.014	0.014
"A" Nickel	None	0.0004	0.001
Cladding	0.003	0.0026	0.002
Total Thickness	0.020	0.020	0.020

Fig. 1—Cladding Assembly and Thicknesses Used.

446 stainless steel. Some experimental cladding alloys (Table I) were also evaluated as bonded to molybdenum.

Seven additional experimental alloys containing more than 90 w/o nickel were made. These alloys, described subsequently, were tested for resistance to attack in air and in air plus MoO_3 atmospheres but were not evaluated as cladding materials.

Cladding Assembly

A cladding assembly of the conventional picture-frame type was used. As shown in Fig. 1, claddings were made without bonding layers and also with 3- and 7-mil thick bonding layers of "A" nickel. All contact surfaces of the assembly were sanded and degreased in ethylene trichloride vapor before edge welding.

The tendency of oxidation-resistant alloys to form stable surface oxides when heated in air was found to be very detrimental to bond adherence. It was found that, even in an edge-welded assembly, sufficient air was occluded to allow such films to form. Two methods were employed to prevent this.

One method consisted of electroplating 3 mils of nickel on the contact surface of the heat resistant cover plates. As illustrated in

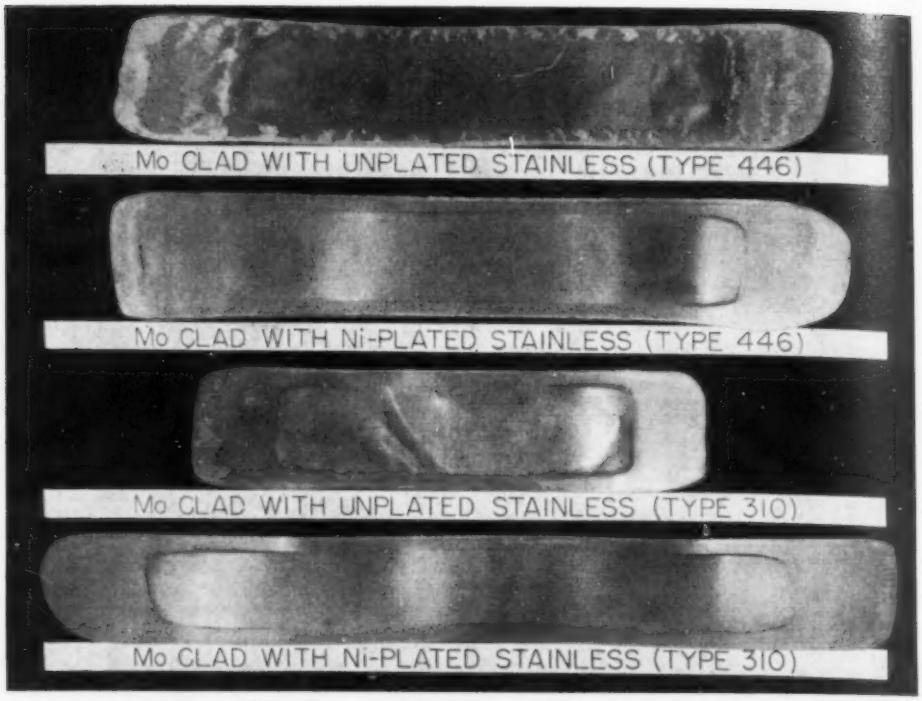


Fig. 2—Effect of a 3-Mil Thick Interlayer of Nickel Plate on the Bonding of Molybdenum to Types 446 and 310 Stainless Claddings. Assemblies not scaled under vacuum; reheat temperature, 2280°F; nominal reductions, 20% per pass ×⅜.

Fig. 2, the nickel plating resulted in successful cladding with Types 446 and 310 stainless steel.

Frequently, internal air pressure, created by heating an assembly prior to rolling, would either prevent bonding or would rupture the bond after the first rolling pass. When this occurred, the probability of bonding on subsequent passes was greatly reduced. To eliminate difficulties stemming from the presence of air in a cladding assembly, evacuation of the pack was found to be necessary. This alternate method consisted of welding a nickel tube into the edge of an assembly, pressure testing under water for defects, evacuating the air, and sealing the tube by hot forging while the assembly was still under vacuum.

Bonding by Roll Cladding

Initially, the assemblies were heated to 2280°F in hydrogen for rolling. After considerable reduction in thickness, rupture of the cladding layers at the core-frame junction was frequently observed (see Fig. 2). This difficulty was minimized by lowering the heating temperature to 2190°F.

All composites were rolled to a thickness of 20 mils without intermediate annealing. Normally, reductions of 20% per pass were used. To increase the probability of bonding on the crucial first pass

Table II
Undercutting Conditions for 20-mil Clad Sheet[a]

(Optimum conditions are underlined)

Bath composition, per cent NaOH	10, **25**, 50
Bath temperature, °F	**77**, 140
Electrolytic current, ma[b]	**150**, 300
Current density, amp/sq in.[c]	**0.1**, 0.2

[a] 14 mils of molybdenum; 3 mils of nickel per side.
[b] Specimen anodic.
[c] Based on total specimen area where total area = 32 × area of exposed molybdenum.

through the rolls, reductions of 40 per cent were very effective. The finish-rolled composite sheet was annealed for 30 min. in hydrogen. Heating for rolling and annealing in a hydrogen-atmosphere furnace produced a smooth adherent oxide coating on the sheet. The underlying metal surface was also smooth and free of defects.

Edge Protection

In the production of clad sheets it is customary to finish roll to the desired thickness and shear to size. For clad molybdenum, protection of sheared edges from high temperature oxidation then becomes mandatory.

Direct application of a nickel edge bead with an oxyacetylene torch was satisfactory for sheets of greater than 40-mil thickness, but this method yielded uneven and discontinuous beads on 20-mil material. Efforts were therefore concentrated on finding a method of undercutting the molybdenum at a sheared edge to permit insertion and fusion of a filler wire. Successful undercutting was achieved by electrolytically dissolving the exposed molybdenum in a sodium hydroxide solution. Table II gives data on undercutting conditions.

A comparison was made of the relative merits of NaOH and KOH solutions as undercutting media. Fig. 3 shows that the rate of attack with KOH is double that obtained with NaOH. The concave bottom of the KOH undercut permits closer contact between the core and filler wire during fusion. Fig. 4 shows a filler wire in position with the claddings lapped to hold it in place and a sealed edge after fusion with an oxyacetylene torch.

Formability of Clad Molybdenum

Test Method

A special bend test was used to evaluate the bend ductility of clad molybdenum and the bond. Bend specimens $\frac{3}{4} \times \frac{3}{8} \times 0.020$ inch were placed horizontally across a 75-deg. V-notch die block. Bending was at 90 degrees to the rolling direction and was done at a rate of 0.5 in./min. by a 75-degree male wedge block, the acute edge

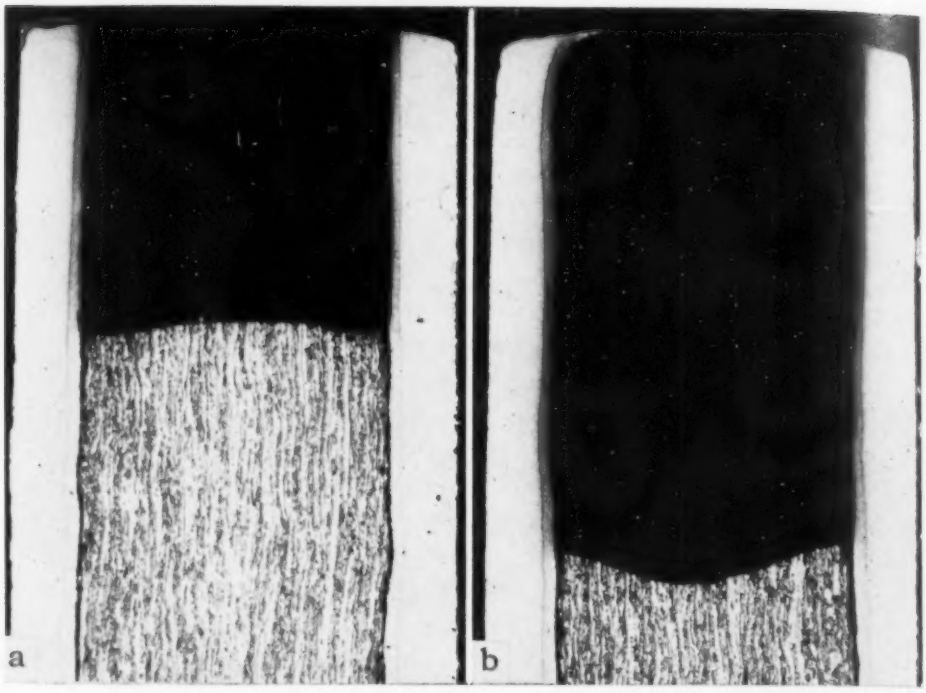


Fig. 3—Comparison of the Rates of Undercutting Obtained in 25% Solutions of Sodium and Potassium Hydroxides. (a) Undercutting rate: 0.00024 inch per minute; (b) undercutting rate 0.00046 inch per minute ×100.
Current density: 0.125 amp/sq in. of total area
Immersion time: 60 min
Bath temperature: 77°F
Core material: Hydrogen-sintered molybdenum (0.014 in. thick)
Cladding material: 80 w/o iron-15 w/o chromium-5 w/o aluminum (0.003 in. thick per side)

of which had a radius of 1/64 inch. Evaluation of bend ductility was made by sectioning and macroscopic examination.

Test Results

Fig. 5 shows excellent bend ductility for 20-mil clad molybdenum sheet. Macroscopic examination revealed no bending failures. The reduction in thickness of the claddings on the tension side of the bends indicates that cladding integrity and bonding is retained beyond the elastic limit.

Oxidation Resistance

Screening of Cladding Materials

In the early stages of this investigation, it was noted that claddings high in iron, such as Types 446 and 310 stainless steel, failed sooner than would be expected from their normal excellent air-oxidation resistance. This led to the development of a test for determining the corrosive effect of molybdenum oxide vapor on intended cladding materials. This test will be referred to subsequently as the "block test."

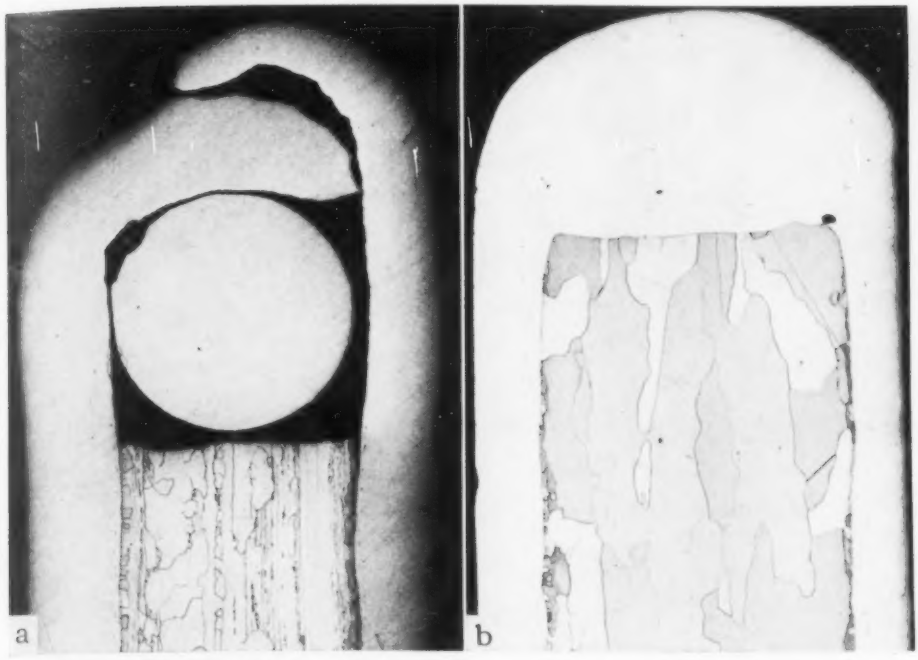


Fig. 4—Edge Sections of Clad Molybdenum Showing a Positioned Filler Wire and a Fused Edge. (a) Before fusion; (b) after fusion ×100.
Core material: Hydrogen-sintered molybdenum (0.014 in. thick)
Cladding material: "A" nickel (0.003 in. thick per side)
Fusion method: Oxyacetylene

A preliminary series of nickel-chromium-iron specimens with decreasing nickel (and increasing iron) contents were placed on small molybdenum blocks in an air atmosphere and heated at 1800°F for 14.5 hours. Results are shown in Fig. 6. The detrimental effect of iron as an alloy constituent is apparent.

Screening-Test Method

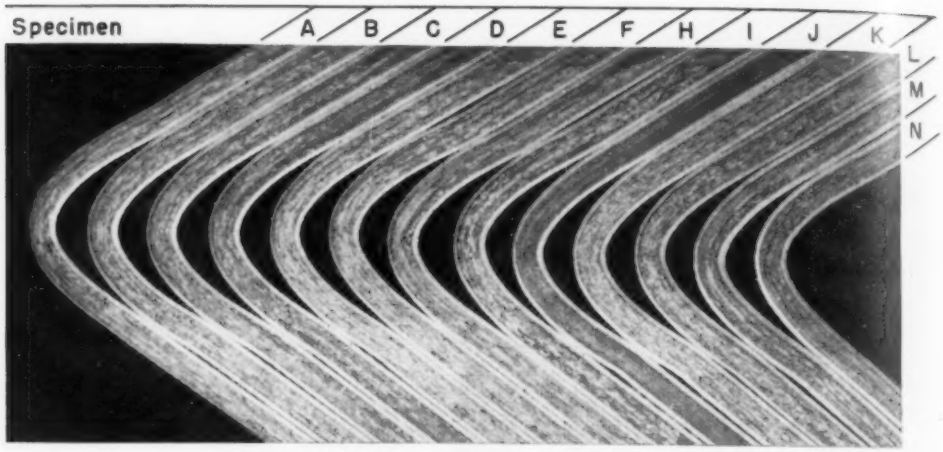
Failure of a cladding layer at elevated air temperatures results in the formation of volatile MoO_3, which in turn accelerates the oxidation of many cladding materials. Therefore, screening tests were

Table III
Exposure Conditions for Block Tests

(10-hr exposures at 1800°F)

Test Designation	Exposure Conditions	
	0.75 ×0.75 ×0.1-In. Specimens Mounted	Atmosphere
A—Contact Test	Horizontally in contact with molybdenum block[a]	Air plus MoO_3[b]
B—Base-Line Test	Horizontally in contact with Alundum slab	Uncontaminated air
C—Suspended Test	Vertically on Alundum cylinder over molybdenum block	Air plus MoO_3

[a] Molybdenum mounting block was approximately the same size as the specimens.
[b] MoO_3 generated by oxidation of molybdenum mounting block.



105-deg bends over 1/64-in. radius; bending rate = ½ in. per min

Specimen	Surface-Cladding Material	Thickness, mils: Cladding, per side	"A" Nickel Interlayers, per side	Molybdenum Core	Total Composite
A	Inconel	3	0	14	20
B	Inconel	2.6	0.4	14	20
C	Inconel	2	1	14	20
D	Inconel X	3	0	14	20
E	Inconel X	2.6	0.4	14	20
F	Inconel X	2	1	14	20
H	"A" nickel	3	—	14	20
I	80Ni-20Cr	3	0	14	20
J	80Ni-20Cr	2.6	0.4	14	20
K	80Ni-20Cr	2	1	14	20
L	"Z" nickel	3	0	14	20
M	"Z" nickel	2.6	0.4	14	20
N	"Z" nickel	2	1	14	20

Fig. 5—Cross Section of Clad Molybdenum Specimens after Room Temperature Bend Testing Demonstrating Satisfactory Bend Ductility and Bond Strength. ×12.

conducted to evaluate the resistance to MoO_3 attack of some 35 intended cladding materials. Specimens were exposed to the test conditions given in Table III. After exposure, the specimens were cathodically descaled in a molten caustic bath (60 w/o NaOH–40 w/o Na_2CO_3) and weighed. Corrosion rates were calculated as grams lost per square inch of initial specimen area per hour.

Screening-Test Results

Block-test results for 18 wrought alloys are listed in Table IV and for 18 cast alloys in Table V. The metals and alloys tested are listed in order of increasing attack in the contact block test.

Fig. 7 shows the effect of block testing on unalloyed materials. High purity chromium was the most resistant material in the contact test, followed by "A" nickel, high purity cobalt, and Armco iron. Of the four metals, nickel appears to be the most promising for use as an alloy base. Fig. 7 also shows the "worm track" corrosion on one cobalt specimen where it was in contact with the molybdenum block. This erosive effect is referred to later under Discussion.

Table IV
Corrosion Rates of Various Wrought Alloys When Exposed for 10 Hours at 1800°F in Still Air and in Still Air-MoO_3 Mixtures

(Specimen Size—¾ ×¾ ×0.1 in.)

Alloy	Nominal Composition, w/o	Weight Loss, g/(sq.in.)(hr) Specimen Mounted on Mo Block[a]	Specimen Mounted on Al_2O_3 Block[b]	Specimen Suspended Over Mo Block[c]
1	"D" Nickel (Ni-4.5 Mn)	0.0037	0.0186	0.0047
2	Chromium (High Purity)	0.0049	0.0189	0.0072
3	Ni-0.25Zr	0.0059	0.0125	—
4	"A" Nickel (Commercial Purity)	0.0069	0.0093	0.0029
5	"Z" Nickel (Ni-4.5Al-1Ti)	0.0073	0.0084	0.0031
6	Ni-5.1Zr (Melted in Argon)	0.0090	0.0117	0.0022
7	Ni-5.0Zr-2.5Al (Melted Under Vacuum)	0.0100	0.0098	0.0024
8	Ni-20Cr (Melted at BMI)	0.0277[e]	—	0.0017
9	Monel (Ni-30Cu)	0.0359	0.1948	—
10	Hastelloy B (Ni-30Mo-6Fe)	0.0405	0.0506	—
11	Ni-20Cr (Commercial Grade)	0.1905	0.0004	0.0048
12	Inconel X (Ni-5Cr-7Fe-2.5Ti-1Al-1Cb)	0.2358	0.0020	0.0355
13	Inconel (Ni-15Cr-5Fe)	0.2643	0.0018	0.0136
14	Type 302 (Fe-18Cr-9Ni)	0.3600	0.0034	C.O.[d]
15	Type 446 (Fe-25Cr)	0.3759	0.0035	C.O.[d]
16	Type 430 (Fe-15Cr)	0.4307	0.0025	0.4181
17	Armco Iron	0.4676	0.1622	0.3159
18	Type 310 (Fe-25Cr-20Ni)	C.O.[d]	0.0010	0.3789

[a]Atmosphere: air plus molybdenum trioxide. Specimen in direct contact with molybdenum.
[b]Atmosphere: uncontaminated air.
[c]Atmosphere: air plus molybdenum trioxide. Specimen in proximity, but not in contact, with molybdenum.
[d]C.O.: completely oxidized.
[e]Corrosion loss of 0.0277 g/(sq in.)(hr) is lower than obtained with Alloy 11 because of lower concentration of MoO_3.

Table V
Corrosion Rates of Various Cast Alloys when Exposed for 10 Hours at 1800°F in Still Air and in Still Air-MoO_3 Mixtures

(Specimen Size—¾ ×¾ ×0.1 in.)

Alloy	Actual Composition, w/o	Weight Loss, g/(sq in.)(hr) Specimen Mounted on Mo Block[a]	Specimen Mounted on Al_2O_3 Block[b]	Specimen Suspended Over Mo Block[c]
19	Ni-6.1Al	0.0050	0.0046	0.0034
20	Ni-5.5Zr	0.0053	0.0009	0.0000
21	Nickel (+99% Purity)	0.0054	0.0126	0.0041
22	Ni-5.2Ta	0.0054	0.0068	0.0035
23	Ni-2.3Ti-2.7Si	0.0054	0.0069	0.0034
24	Ni-1.9Ti-2.1Si-1.9Al	0.0058	0.0070	0.0034
25	Ni-5.0Cb	0.0066	0.0069	0.0028
26	Ni-2.8Al-4.3Ti	0.0069	0.0074	0.0037
27	Ni-5.0Ti	0.0070	0.0074	0.0034
28	Ni-5.2Si	0.0089	0.0024	0.0140
29	Ni-5.0Mn	0.0099	0.0137	0.0021
30	Ni-2.8Al-4.1Si	0.0270	0.0004	0.0032
31	Ni-31Al(NiAl)	0.0577	0.0064	—
32	Cobalt (High Purity)	0.0988	0.0466	0.0107
33	Co-26.4Cr-14.4Ni	0.1892	0.0004	—
34	Co-20.3Cr	0.2061	0.0012	—
35	Fe-15Cr-5Al	0.3966	0.0013	C.O.[d]
36	Co-27.8Cr-5.4Mo(Stellite No. 21)	0.4582	0.0013	0.1005

[a]Atmosphere: air plus molybdenum Trioxide. Specimen in direct contact with molybdenum.
[b]Atmosphere: uncontaminated air.
[c]Atmosphere: air plus molybdenum Trioxide. Specimen in proximity, but not in contact, with molybdenum.
[d]C.O.: completely oxidized.

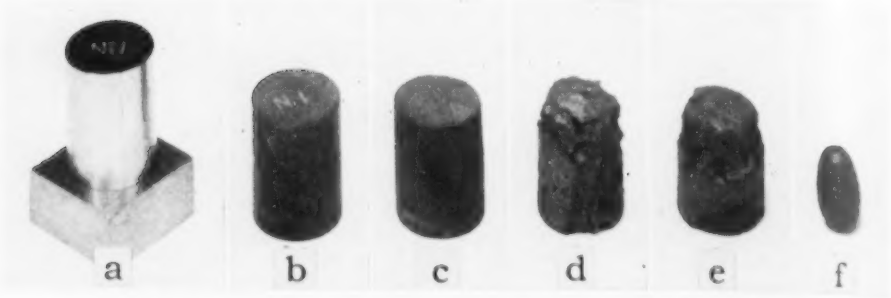


Fig. 6—Effect of Decreasing Nickel Content on the Corrosion of Cast Nickel-Chromium-Iron Alloys when Exposed in Direct Contact with Molybdenum in Static Air at 1800°F. Specimen (a) initial appearance of specimen on molybdenum block; remaining five appearance after 14.5-hour exposure at 1800°F in static air and molybdenum trioxide. ×1.

	Initial appearance (Specimen on molybdenum block)				
Nickel, w/o	99.9	65.0	38.5	34.4	3.1
Chromium, w/o	0.0	17.7	19.8	16.5	27.6
Iron, w/o	0.0	14.9	39.4	46.7	67.1
Weight Loss, per cent	0.57	3.8	25.8	21.1	87.8
Weight Loss, g/(sq in.)(hr)	0.004	0.024	0.159	0.128	0.511

Note: The ferritic stainless alloy at the upper right had an oxidation rate of 0.0007 g/(sq in.)(hr) in uncontaminated air, based on 100 hr at 1800°F.

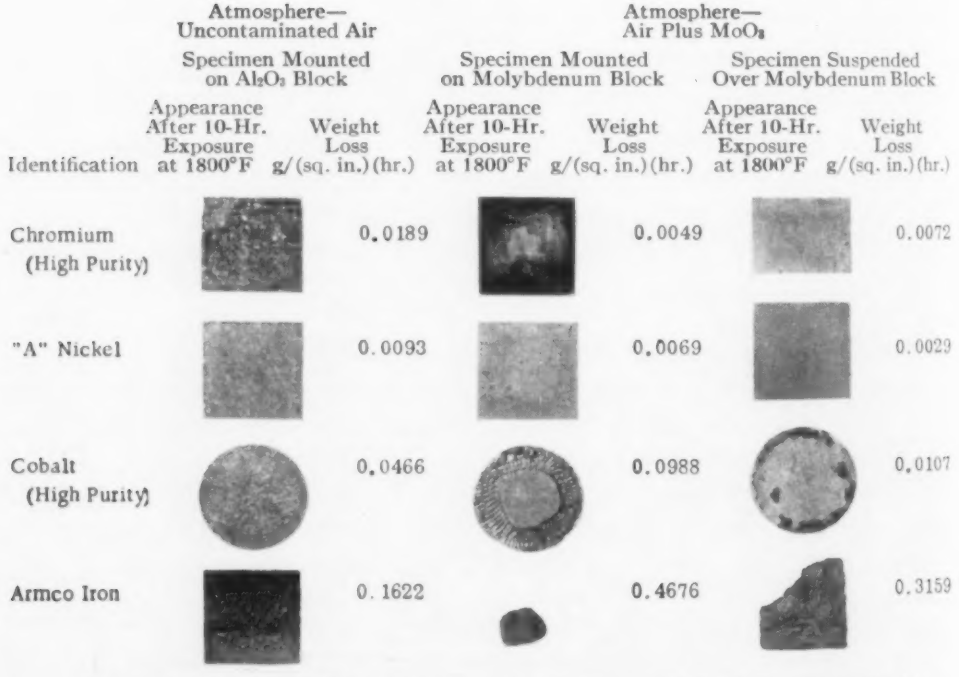
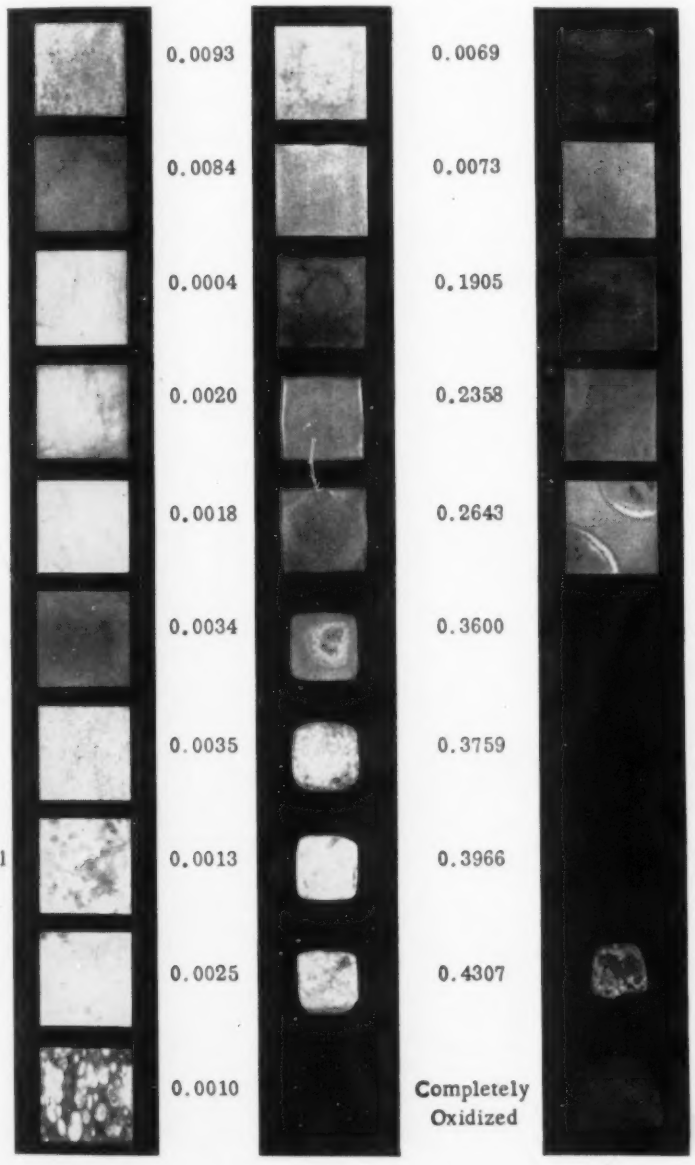


Fig. 7—Effect of Molybdenum Trioxide on the Oxidation of Metals Commonly Used in Oxidation Resistant Alloys. ×¾.



Identification	Atmosphere—Uncontaminated Air: Specimen Mounted on Al_2O_3 Block — Appearance After 10-Hr. Exposure at 1800°F	Atmosphere—Uncontaminated Air: Specimen Mounted on Al_2O_3 Block — Weight Loss g/(sq. in.)(hr.)	Atmosphere—Air Plus MoO_3: Specimen Mounted on Molybdenum Block — Appearance After 10-Hr. Exposure at 1800°F	Atmosphere—Air Plus MoO_3: Specimen Mounted on Molybdenum Block — Weight Loss g/(sq. in.)(hr.)	Atmosphere—Air Plus MoO_3: Specimen Suspended Over Molybdenum Block — Appearance After 10-Hr. Exposure at 1800°F	Atmosphere—Air Plus MoO_3: Specimen Suspended Over Molybdenum Block — Weight Loss g/(sq. in.)(hr.)
"A" Nickel		0.0093		0.0069		0.0029
"Z" Nickel		0.0084		0.0073		0.0031
80Ni-20Cr		0.0004		0.1905		0.0048
Inconel X		0.0020		0.2358		0.0355
Inconel		0.0018		0.2643		0.0136
302 Stainless Steel		0.0034		0.3600		Completely Oxidized
446 Stainless Steel		0.0035		0.3759		Completely Oxidized
80Fe-15Cr-5Al (As Cast)		0.0013		0.3966		Completely Oxidized
430 Stainless Steel		0.0025		0.4307		0.4181
310 Stainless Steel		0.0010		Completely Oxidized		0.3789

Fig. 8—Effect of Molybdenum Trioxide on the Oxidation of Wrought Heat Resistant Alloys. ×¾

Table VI
Constant-Temperature Oxidation Data for Clad Molybdenum Exposed for 100 Hours in Still Air

[Initial Specimen Size—1 ×0.75 ×0.02 in.
Initial Specimen Weight—approx. 2 g]

Cladding Material (Alloy Compositions are in w/o)	Thickness[a]	Edge Wire Used	Exposed at 1800°F Weight Change %	Exposed at 1800°F Mode of Oxidation	Exposed at 2000°F Weight Change %	Exposed at 2000°F Mode of Oxidation	Exposed at 2200°F Weight Change %	Exposed at 2200°F Mode of Oxidation
"A" Nickel (99.5 Ni)	A	"A" Nickel	−17.7	Uniform	−32.8	Uniform	−45.2	Uniform
"A" Nickel (99.5 Ni)	A	"A" Nickel	−16.6	Uniform	−33.8	Uniform	−46.7	Uniform
"Z" Nickel (Ni-4.5Al-1Ti)	A	80Ni-20Cr	+2.8	Uniform	−28.8	Localized	−100	Total
"Z" Nickel (Ni-4.5Al-1Ti)	C	80Ni-20Cr	+3.2	Uniform	−32.6	Uniform	−100	Total
Inconel (Ni-15Cr-5Fe)	A	80Ni-20Cr	+0.2	Uniform	−0.04	Uniform	−100	Total
Inconel (Ni-15Cr-5Fe)	A	80Ni-20Cr	+0.3	Uniform	+1.5	Uniform	−100	Total
Inconel (Same as above)	B	80Ni-20Cr	+0.6	Uniform	+1.4	Uniform	−100	Total
Inconel (Same as above)	B	80Ni-20Cr	+0.4	Uniform	+1.2	Uniform	−100	Total
Inconel (Same as above)	C	80Ni-20Cr	0.0	Uniform	+0.2	Uniform	−100	Total
Inconel X (Ni-15Cr-7Fe-2.5Ti-1Al-1Cb)	A	80Ni-20Cr	+1.0	Uniform	+2.2	Uniform	−100	Total
Inconel X (Same as above)	C	80Ni-20Cr	+1.0	Uniform	+1.2	Uniform	−100	Total
80Ni-20Cr	A	80Ni-20Cr	−0.2	Uniform	−13.1	Localized	−100	Total
80Ni-20Cr	C	80Ni-20Cr	+0.1	Uniform	+0.3	Uniform	−100	Total
Type 310 Stainless Steel (Fe-15Cr-20Ni)	B	310 Stainless Steel	−100	Total				
Type 310 Stainless Steel (Same as above)	B	310 Stainless Steel	−100	Total				

Table VI—Con't

Cladding Material (Alloy Compositions are in w/o)	Thickness(a)	Edge Wire Used	Exposed at 1800°F Weight Change %	Exposed at 1800°F Mode of Oxidation	Exposed at 2000°F Weight Change %	Exposed at 2000°F Mode of Oxidation	Exposed at 2200°F Weight Change %	Exposed at 2200°F Mode of Oxidation
Type 310 Stainless Steel (Same as above)	B	310 Stainless Steel	−100	Total	Test data not obtained at 2000° and 2200°F			
Type 446 Stainless Steel (Fe-25Cr)	B	430 Stainless Steel	−100	Total				
Type 446 Stainless Steel (Same as above)	B	430 Stainless Steel	−100	Total				
Type 446 Stainless Steel (Same as above)	B	430 Stainless Steel	−100	Total				
Ni-5.2Ta	C	Ni-1.9Ti-2.1Si-1.9Al	−17.0	Uniform(b)	−33.9	Uniform(b)	−100	Total
Ni-5.2Ta	C		−17.7	Uniform	−29.1	Uniform	−100	Total
Ni-5.0Zr-2.5Al	C	"A" Nickel	−21.7	Uniform	−37.6	Uniform	−100	Total
Ni-5.0Zr-2.5Al	C	"A" Nickel	−21.1	Uniform	−86.6	Localized(c)	−100	Total
Ni-2.3Ti-2.7Si	C	Ni-1.9Ti-2.1Si-1.9Al	+3.3	Uniform	−27.1	Uniform	−100	Total
Ni-2.3Ti-2.7Si	C		+2.8	Uniform	−27.3	Uniform	−100	Total
Ni-1.9Ti-2.1Si-1.9Al	C	Ni-1.9Ti-2.1Si-1.9Al	+4.8	Uniform	−28.6	Uniform	−100	Total
Ni-1.9Ti-2.1Si-1.9Al	C		+5.3	Uniform	−29.7	Uniform	−100	Total

(a) Thickness Code

	A	B	C
Thickness of outer (alloy) cladding per side	3 mils	2.6 mils	2 mils
Thickness of inner (nickel) cladding per side	None	0.4 mil	1 mil
Thickness of molybdenum core	14 mils	14 mils	14 mils
Thickness of total composite	20 mils	20 mils	20 mils

(b) Some localized attack at edges.

(c) Advanced state of oxidation precludes evaluation of mode of oxidation. Rapid oxidation probably started at edge, otherwise the rate of attack would have approximated that of duplicate specimen.

Fig. 8 shows the effect of the presence of molybdenum on the oxidation of selected alloys. Here again, the superior resistance of nickel and high nickel alloys to attack by MoO_3 is apparent. Conversely, the iron-base alloys (Types 302, 446, 430, and 310 stainless steel, and 80 w/o iron—15 w/o chromium—5 w/o aluminum) were catastrophically attacked in the presence of MoO_3.

Air-Oxidation Resistance of Clad Sheet

100-Hour Constant-Temperature Tests—Tests of 100-hour duration were conducted at 1800, 2000, and 2200°F on specimens $1 \times 0.75 \times 0.02$ inch with 3 mils of cladding per side. The specimens were edge sealed according to the procedure previously described. The furnace atmosphere was still air, and the specimens were placed in individual Alundum crucibles permitting the access of air to both faces.

Table VI gives elevated temperature oxidation data for the composite sheet tested. With thin cladding materials other than nickel, the change in specimen weight is generally either very small or, when the cladding is disrupted, appreciable.

As shown in Table VI nickel cladding exhibited unique behavior in the 100-hour constant temperature tests. At 1800°F, the nickel-coated specimens showed no significant loss in thickness but had a 17% weight loss. At 2000°F, the weight loss from scaling was greater, but 1.5 mils of the original 3 mils of nickel remained after 100 hours. At 2200°F, all of the nickel was oxidized, leaving only the oxidation products. These still afforded some protection, evidenced by the fact that more than half of the initial specimen thickness remained after 100 hours. This is discussed further under Intentional-Defect Test. Despite the protection afforded molybdenum by nickel, it cannot be considered satisfactory for service even at 1800°F, because of the rapid scaling rate of nickel itself and the tendency of the oxidation products to spall during cooling. Types 446 and 310 stainless steel claddings were completely oxidized in less than 100 hours at 1800°F. "Z" nickel, Inconel, Inconel X, 80Ni-20Cr, Ni-2.3Ti-2.7Si, and Ni-1.9Ti-2.1Si-1.9Al provided good protection for 100 hours at 1800°F.

At 2000°F, Inconel, Inconel X, and 80 w/o nickel-20 w/o chromium provided the best protection to the underlying molybdenum.

At 2200°F, only the "A" nickel cladding provided a degree of protection; all others permitted total oxidation of the molybdenum in less than 100 hours.

It was anticipated that intermediate layers of nickel would retard oxidation of thin composite sheet; however, the data of Table VI do not verify this. Superior bond strength is apparently the principal advantage of nickel-bonded claddings.

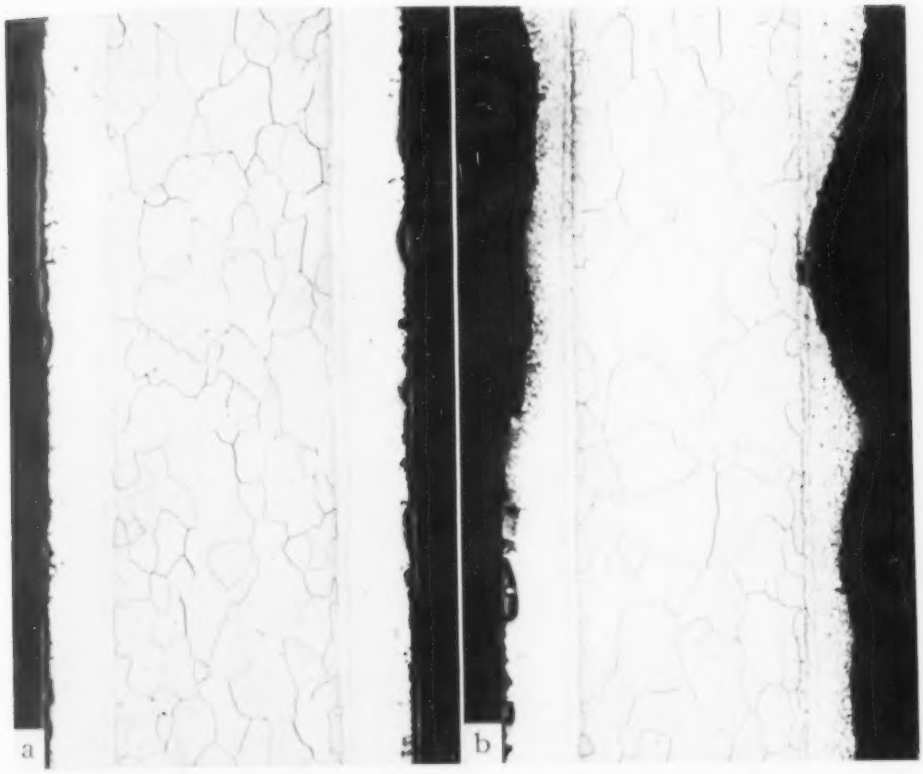


Fig. 9—Molybdenum Clad with Inconel (Specimen CR-15% Cladding Per Side) after 50-Hour Exposure at 2200°F in Still Air. (a) Uniform oxidation; (b) localized oxidation. ×100

Fig. 9 illustrates uniform and localized oxidation of an Inconel cladding. The example of localized oxidation in Fig. 9 illustrates imminent cladding failure.

Intentional Defect Tests. An intentional defect test was utilized to evaluate the effect of cladding integrity on oxidation rate. These tests were conducted at constant temperatures. Standard oxidation specimens 1×0.75×0.02 inch with 3 mils of cladding per side were used. Three types of specimens were used: (a) completely edge sealed, (b) edge sealed but with a 47-mil-diameter hole drilled through the specimen center, and (c) in the as-sheared condition. These specimens were exposed for 100 hours in still air. Defect testing was carried out at 1800, 2000, and 2200°F with the test specimens contained in high purity Alundum crucibles.

"A" nickel and high-nickel claddings (>92% nickel) provided the best protection when exposed in a defective condition. The data of Table VII demonstrate the defect sensitivity of molybdenum clad with various materials. Fig. 10 illustrates the relatively slow rate at which nickel-clad molybdenum oxidizes at a defect location. The decreasing thickness of nickel remaining on the surface of the molybdenum at the successively higher temperatures is also illustrated in Fig. 10. Despite the fact that little or no nickel remains on

Table VII
Constant-Temperature Air-Oxidation Data for Clad Molybdenum Fully Edge Protected, With Intentional Defects, and in the As-Sheared Conditions

[Initial Specimen Size—¾ ×1 ×0.020 in.
Initial Specimen Weight—Approx. 2 g]

Specimen Description	Exposed 100 Hr at 1800°F Weight Change %	Exposed 100 Hr at 2000°F Weight Change %	Exposed 100 Hr at 2200°F Weight Change %
		3-Mil "A" Nickel Cladding	
Standard Edge Seal [a]	+2.0	−33.3	−50.4
Edge Sealed, With Defect [b]	−4.7	−43.2	−52.4
As-Sheared Edge [c]	−36.1	−100	−63.1
		3-Mil Inconel Cladding (With No Nickel Underlayer)	
Standard Edge Seal [a]	−0.1	+1.1	−100
Edge Sealed, With Defect [b]	−28.5	−45.2	—
As-Sheared Edge [c]	−100	−100	—
		2-Mil Inconel Cladding (With 1-Mil Nickel Underlayer)	
Standard Edge Seal [a]	0.0	+0.2	−100
Edge Sealed, With Defect [b]	−100	−48.5	—
As-Sheared Edge [c]	−100	−100	—
		2-Mil "Z" Nickel Cladding (With 1-Mil Nickel Underlayer)	
Standard Edge Seal [a]	+3.2	−32.6	−100
Edge Sealed, With Defect [b]	−8.1	−60.2	−100
As-Sheared Edge [c]	−52.5	−100	−100

Table VII—Con't

Specimen Description	Exposed 100 Hr at 1800°F Weight Change %	Exposed 100 Hr at 2000°F Weight Change %	Exposed 100 Hr at 2200°F Weight Change %
		2-Mil Inconel-X Cladding (With 1-Mil Nickel Underlayer)	
Standard Edge Seal[a]	+1.0	+1.2	−100
Edge Sealed, With Defect[b]	−100	−100	"
As-Sheared Edge[c]	−100	−100	"
		2-Mil 80 Ni-20Cr Cladding (With 1-Mil Nickel Underlayer)	
Standard Edge Seal[a]	+0.1	+0.3	−100
Edge Sealed, With Defect[b]	−100	−100	"
As-Sheared Edge[c]	−100	−100	"
		2-Mil Ni-5.2Ta Cladding (With 1-Mil Nickel Underlayer)	
Standard edge seal[a]	−14.0	−30.2	
Edge sealed, with defect[b]	−6.2	−44.2	
As-sheared edge[c]	−53.9	−100	
		2-Mil Ni-5.OZr-2.5 Al Cladding (With 1-Mil Nickel Underlayer)	
Standard edge seal[a]	−23.4	−37.9	
Edge sealed, with defect[b]	−9.1	−50.8	
As-sheared edge[c]	−100	−100	
		2-Mil Ni-2.3Ti-2.7Si Cladding (With 1-Mil Nickel Underlayer)	
Standard edge seal[a]	+2.0	−27.9	
Edge sealed, with defect[b]	−6.0	−27.9	
As-sheared edge[c]	−62.3	−100	
		2-Mil Ni-1.9Ti-2.1Si-1.9Al Cladding (With 1-Mil Nickel Underlayer)	
Standard edge seal[a]	+5.6	−35.5	
Edge sealed, with defect[b]	−6.4	−41.5	
As-sheared edge[c]	−58.2	−100	

[a]Standard Edge—Edge initially undercut by anodic immersion in 25 per cent KOH, filler wire positioned in groove so formed and oxyacetylene welded.
[b]Edge Sealed, With Defect—Edge sealed as in Footnote (a). In addition, a 0.047-in.-diameter hole drilled through center of specimen.
[c]As-Sheared Edge—No attempt made to protect edge.



Fig. 10—Effects of Complete and Incomplete Sealing on the Air-Oxidation of Nickel-Clad Molybdenum. Initial specimen thickness was 14 mils, with 3 mils of cladding per side. (a) Standard edge—Edge initially undercut by anodic immersion in 25% KOH solution, nickel wire placed in groove so formed, and acetylene welded (b) Intentional defect—This consisted of a 0.047-in.-diameter hole drilled through the center of the specimen (c) Sheared edge—No attempt made to protect edge. ×8.

the surface of the specimens exposed at 2200°F, complete oxidation of the core material did not occur. The higher sensitivity of Inconel-clad molybdenum to defects is clearly illustrated in Fig. 11. Fig. 11 also shows that even a perfectly sealed specimen of Inconel-clad molybdenum was completely oxidized in 100 hours at 2200°F. The data of Table VII do not indicate any protective advantage in the presence of defects for the Inconel-nickel duplex cladding.

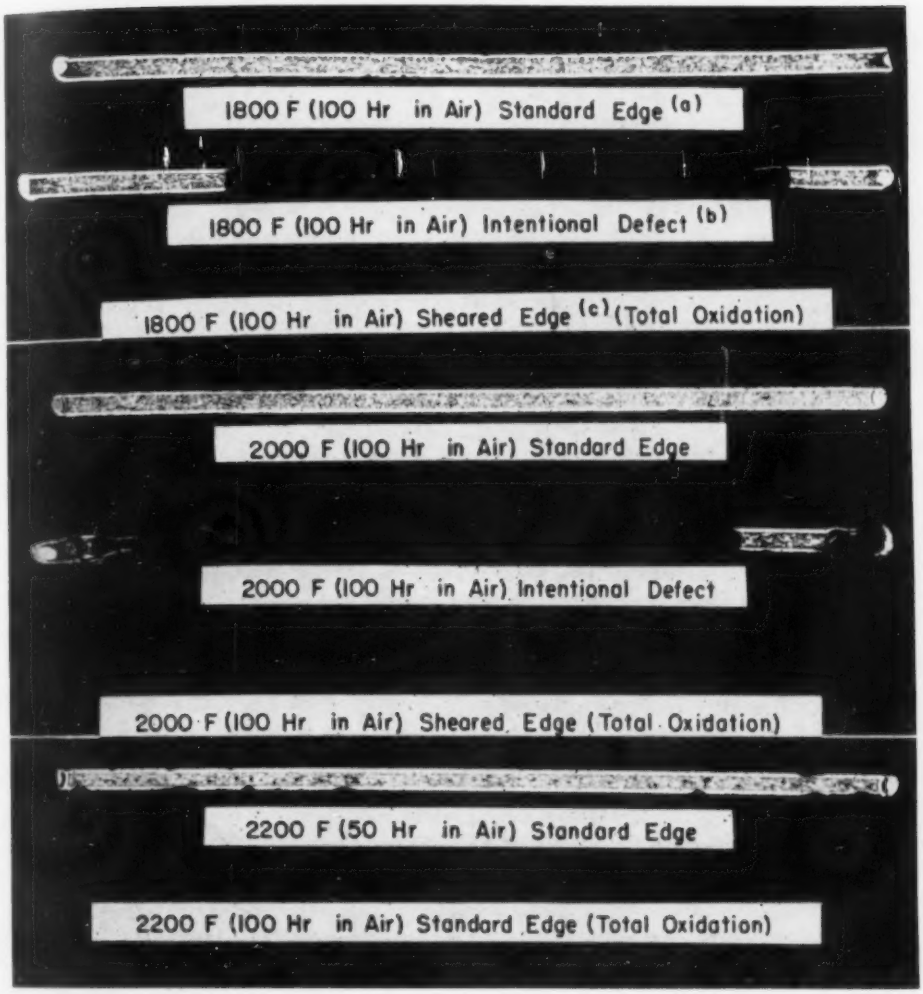


Fig. 11—Effects of Complete and Incomplete Scaling on the Air-Oxidation of Inconel-Clad Molybdenum. Initial specimen thickness was 14 mils, with 3 mils of cladding per side. (a) Standard edge—Edge initially undercut by anodic immersion in 25% KOH solution, nickel wire placed in groove so formed, and acetylene welded (b) Intentional defect—This consisted of a 0.047-in.-diameter hole drilled through the center of the specimen (c) Sheared edge—No attempt made to protect edge. ×8.

40-Hour Cyclic Temperature Tests. Forty-hour cyclic temperature tests were conducted according to the following schedule:

Time at temperature per cycle	1 hour
Number of cycles per test	40
Total time at temperature	40 hours
Average heating and cooling rate	275°F/min.

Specimen size was $1 \times \frac{3}{4} \times 0.020$ in., with 3 mils of cladding per side (the same as for the constant-temperature oxidation tests), and the specimens were placed in individual Alundum crucibles as previously discussed.

Listed in Table VIII are cyclic-temperature oxidation data for

Table VIII
Air Oxidation of Clad Molybdenum Based on 40 Hr. of Cycling from 1800, 2000, and 2200°F[a]

Cladding Alloy	Chemical Composition, w/o	Thickness[b]	Specimens Cycled From 1800°F: Weight Change After 40 Cycles, %	First Signs of Failure After, cycles	Completely Oxidized After, cycles	Specimens Cycled From 2000°F: Weight Change After 40 Cycles, %	First Signs of Failure After, cycles	Completely Oxidized After, cycles	Specimens Cycled From 2200°F: Weight Change After 40 Cycles, %	First Signs of Failure After, cycles	Completely Oxidized After, cycles
"A" Nickel	Commercial purity (99.5 Ni)	A	−100[d]	22	34	−100[d]	4	18	−100[d]	9	14
"Z" Nickel	Ni-4.5Al-1.0Ti	A	−100[d]	1[c]	19	−100[d]	10	18	−100[d]	9	25
"Z" Nickel	Ni-4.5Al-1.0Ti	C	+0.9	—	—[e]	−100[d]	24	38	−100[d]	9	16
Inconel	Ni-15Cr-5Fe	A	+0.4	—	—[e]	−34.0	26	—	−100[d]	15	32
Inconel	Ni-15Cr-5Fe	C	+0.6	—	—[e]	+1.0	—	—[e]	−100[d]	8	23
Inconel X	Ni-15Cr-7Fe-2.5Ti-1Al-1Cb	A	+0.5	—	—[e]	−100[d]	10	31	−100[d]	13	23
Inconel X		C	−29.5	1[c]	—	−100[d]	26	39	−100[d]	13	25
80Ni-20Cr	Ni-20Cr	A	+0.1	—	—[e]	+0.3	—	—[e]	−69.7	15	—
80Ni-20Cr	Ni-20Cr	C	+0.1	—	—[e]	+0.1	—	—[e]	+0.2	—	—[e]
Ni-Ta	Ni-5.2Ta	C	−14.4	24[f]	—	−100[d]	1[f]	26	−100[d]	9	13
Ni-Ta	Ni-5.2Ta	C	−15.2	6[f]	—	−100[d]	10[f]	27	−100[d]	10	13
Ni-Zr-Al	Ni-5.0Zr-2.5Al	C	+0.4	32[c]	—	−100[d]	10[f]	23	−100[d]	2	5
Ni-Zr-Al	Ni-5.0Zr-2.5Al	C	−24.0	34[c]	—	−100[d]	8[f]	17	−100[d]	3	5
Ni-Ti-Si	Ni-2.3Ti-2.7Si	C	+1.9	6[c]	—	−100[d]	17[f]	29	−100[d]	7	11
Ni-Ti-Si	Ni-2.3Ti-2.7Si	C	+2.3	33[c]	—	−100[d]	10[f]	28	−100[d]	10	13
Ni-Ti-Si-Al	Ni-1.9Ti-2.1Si-1.9Al	C	+3.8	32[c]	—	−100[d]	9[f]	18	−100[d]	3	5
Ni-Ti-Si-Al	Ni-1.9Ti-2.1Si-1.9Al	C	+3.1	33[c]	—	−100[d]	10[f]	23	−100[d]	3	5

[a] Cycling temperatures: 1800↔400F; 2000↔400F; 2200↔400F
Time at temperature per cycle: 1 hr
Number of cycles per test: 40
Total time at temperature: 40 hr
Average heating and cooling rate: 275 F/min

[b] Thickness Code

	A	C
Thickness of outer (alloy) cladding per side	3 mils	2 mils
Thickness of inner (nickel) cladding per side	None	1 mil
Thickness of molybdenum core	14 mils	14 mils
Thickness of total composite	20 mils	20 mils

[c] Initial failure at specimen edge.
[d] Completely oxidized.
[e] Specimen intact after 40 cycles.
[f] First sign of failure was spalling of surface coating.

clad molybdenum. As shown in Table VIII, "A" nickel, which provided some protection for molybdenum at constant temperatures, up to 2200°F, was ineffective when thermally cycled. At 1800°F, however, good protection was obtained with "Z" nickel, Inconel, Inconel X, 80Ni-20Cr, Ni-2.3Ti-2.7Si, and Ni-1.9Ti-2.1Si-1.9Al. At 2000°F, only Inconel and 80 nickel—20 chromium withstood 40 cycles, while at 2200°F, only 80 nickel—20 chromium afforded protection throughout the exposure. Oxidation failure during cycling generally initiated at a welded edge, either (a) because of a defective edge seal and the thinner metal coverage encountered here or (b) because of the concentration of thermal stresses. It is believed that, with improved edge-sealing techniques, the life of the claddings could be prolonged.

Discussion

If a defect-free cladding were applied to molybdenum and the resulting composite exposed in air at elevated temperatures, its life would depend primarily on the oxidation resistance of the cladding. However, if a cladding is initially defective or if it is penetrated by local oxidation, molybdenum trioxide begins to form. This oxide is highly volatile and potentially corrosive to the cladding itself. It is therefore essential, particularly where specifications require very thin cladding layers, to select cladding materials having good resistance to both air and molybdenum trioxide attack.

Data presented in this report show that the high temperature air oxidation of iron and cobalt, as well as that of alloys containing significant quantities of these two elements, is drastically accelerated by contact with molybdenum and molybdenum trioxide. On the other hand, the corrosion of chromium, nickel, and high nickel alloys is relatively unaffected by molybdenum or its volatile oxide.

The corrosive effect of molybdenum trioxide has been noted by other investigators (3,4) whose studies have been concerned primarily with the corrosion at elevated temperature of alloys containing molybdenum, rather than with the corrosion of pure metals and molybdenum-free alloys in close proximity to molybdenum. Leslie and Fontana (3) offered evidence that above 1500°F appreciable dissociation of MoO_3 occurs, accompanied by the liberation of nascent oxygen, which in turn results in the markedly accelerated oxidation of 16 w/o chromium—25 w/o nickel—6 w/o molybdenum and similar iron-base alloys containing substantial amounts of molybdenum. Service conditions conducive to such attack were reported to be: (a) insufficient circulation of the furnace atmosphere to remove the MoO_3 vapors as they form on a metal surface, and (b) porous scale or oxide layers which render the base metal accessible to the nascent oxygen of dissociation. A corrosive com-

bination of MoO_3 and limited circulation prevails at the bimetal interface between a block-test specimen and its molybdenum mount. Radial grooves are visible on one of the cobalt samples shown in Fig. 7. These grooves clearly define the corrosion advance at an interface. Such a pattern of attack, frequently referred to as "worm tracking," would be expected if corrosion were accelerated by localized concentrations of nascent oxygen.

Molybdenum trioxide is similar to vanadium pentoxide in that, when combined in complex form with oxides such as Cr_2O_3, Fe_2O_3, and NiO, an appreciable decrease in melting point results. The "fluxing" tendency of such low-melting complexes, when in a liquid or semi-liquid state, is another probable factor which accelerates corrosion. Brasunas and Grant (4) have determined the melting temperatures tabulated below for molybdic oxide complexes.

Oxide Complex	Melting Point or Decomposition Temperature, °F
$MoO_3 \cdot Fe_2O_3$	1650
$MoO_3 \cdot Cr_2O_3$	1830
$MoO_3 \cdot NiO$	2425

The 67 w/o iron specimen shown in Fig. 6 indicates that, when exposed in air—MoO_3 atmosphere, the surface corrosion product which formed was liquid or partially so at 1800°F, resulting in an evenly rounded surface. A similar result would be expected if the specimen had been immersed in a liquid corrodent. The physical evidence suggests that a liquefied scale may act as a vehicle in conveying oxygen to the unprotected base metal, resulting in extremely rapid attack.

Of considerable interest was the scale which formed on nickel-clad molybdenum when exposed in air at 2200°F. Such scale was observed to provide a remarkable degree of protection, even after the nickel cladding had been completely converted to scale (see Fig. 10). Upon cooling, however, this scale was observed to spall in a series of minute bursts to a fine green residue. By X-ray diffraction at room temperature, only the suboxides Mo_2O_3 and MoO_2 could be positively identified as remaining on the surface of the molybdenum base metal. Fig. 12 shows this surface at high magnification. Subsequent exposure of the specimen in air at 1800°F resulted in unretarded oxidation of the base metal, as is normal for molybdenum.

An attempt was made to identify (by X-ray diffraction) the green residue resulting from spalling. The resulting line pattern (Fig. 13) shows that the strongest lines match the face-centered cubic structure of NiO with a lattice constant of 4. 18A (NiO is given as slightly over 4. 17A). Additional fainter lines match very well the diffraction data for a green oxide formed on a molybdenum—15 w/o nickel alloy and also synthesized from mixed oxides of nickel and molybdenum (5). The X-ray data strongly suggest that an im-

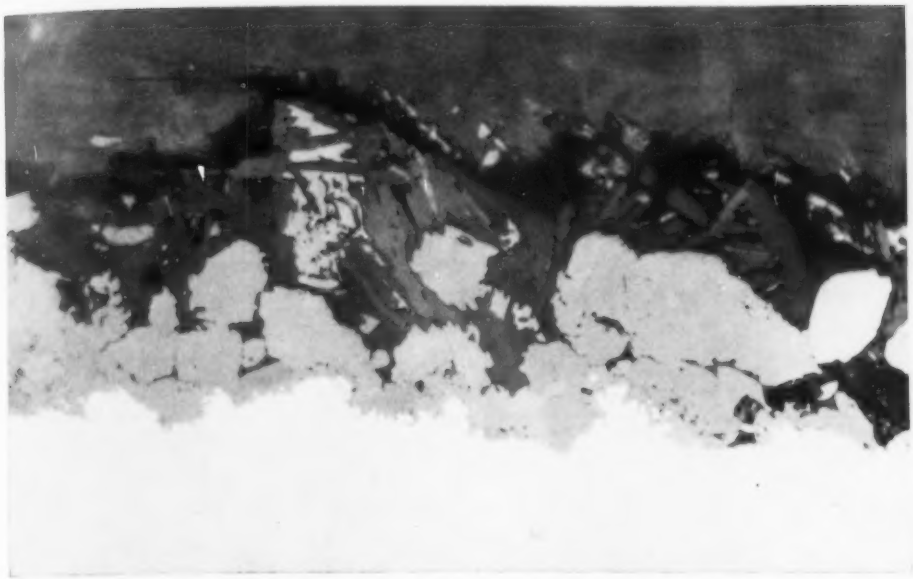
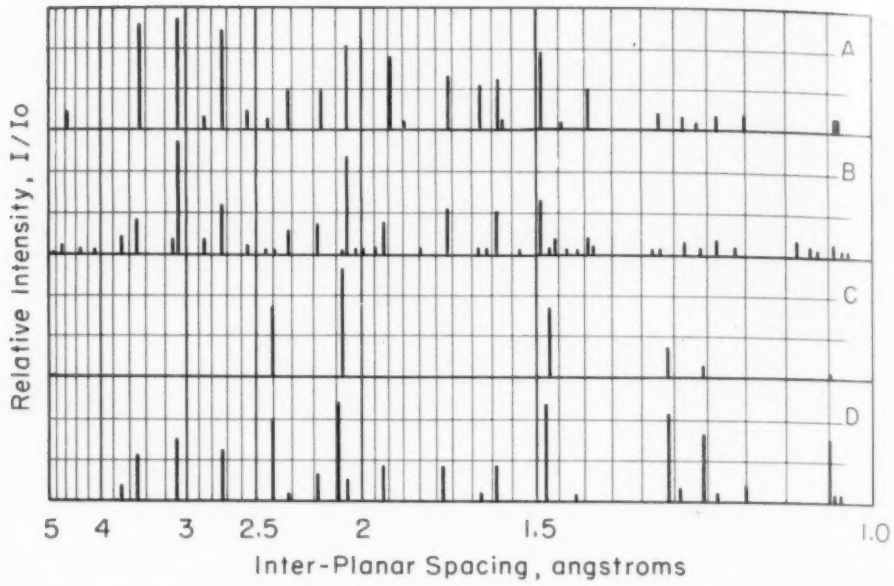


Fig. 12—Oxides, Identified by X-ray Diffraction as Mo_2O_3 and MoO_2, on the Surface of Molybdenum Initially Clad with Nickel and Exposed for 100 Hr at 2200°F in Still Air. ×250

pervious oxide complex of nickel and molybdenum is formed at elevated temperatures. This complex has been identified by Ohio State University (6) using an X-ray spectrometer, as being the high temperature form of nickel molybdate. Recent data (6) indicate that spalling occurs only under certain conditions of cooling, although there appears to be some doubt as to whether such spalling is the result of a phase change or strain.

Only nickel and high nickel alloys (plus 75 w/o nickel) provided satisfactory protection against air oxidation at elevated temperatures (see Tables VI and VIII). As shown in Fig. 10, even in the event of defective claddings or edge seals, nickel claddings provide molybdenum with a remarkable degree of protection. In Table VI, several specimens clad with nickel-base alloys are shown to have been only partially oxidized in 100 hours at test temperature (i.e., they lost less than 100% of their initial weight). Of the cladding alloys tested, 80 w/o nickel—20 w/o chromium was the most protective. Table VIII shows that one of the specimens clad with 80Ni-20Cr was completely intact after 40 1-hour cycles from 2200°F, while the other specimen lost 70% of its initial weight as a result of cycling. That the one specimen was not completely oxidized attests to the retarding of oxidation by the 80 w/o nickel—20 w/o chromium alloy, even after the cladding had lost its integrity.

Considerable effort was devoted to the development of nickel-base cladding alloys having superior resistance to air and MoO_3 attack. These alloys (see Alloys 19 to 30 in Table V) had a maximum of 7.5 w/o of alloy addition and contained no chromium. The data.



A Data for Oxidation Product Appearing on Surface of a Molybdenum-15 w/o Nickel Alloy Heated in Air at 1600 and 1800°F for 5 hr [Ohio State University (5)]

C Standard Line Data for NiO

B Data for Synthesized Nickel Molybdate (Prolonged Heating of $NiCO_3$ and MoO_3 Suspended in H_2O) Heated in Air at 1875°F [Ohio State University (5)]

D Data for Fine Green Powder Which Spalled Off the Surface of Molybdenum Sample Initially Clad with 3 mils of Nickel and Heated in Air at 2200°F for 100 hr

Fig. 13—Comparison of X-ray Diffraction Data for (a) Naturally Formed Oxidation Product from Molybdenum-15 w/o Nickel Alloy, (b) Synthesized Nickel Molybdate, (c) NiO, and (d) Spalled Product from Surface of Molybdenum Sample Initially Clad with 3 Mils of Nickel. Height of plotted peaks are relative to estimated intensities on the individual films.

of Table V) show that they were generally more oxidation resistant at 1800°F than was nickel, with no marked decrease in resistance to MoO_3. Clad composites were made from Alloys 7, 22, 23, and 24 (Tables IV and V) and subsequently tested in air at 1800, 2000, and 2200°F. The data of Table VI show that at 2000°F (constant temperature), these chromium-free claddings were no more protective than was unalloyed nickel. In contrast, nickel-base claddings containing 15 to 20% chromium were very protective when similarly exposed. Likewise (Table VII), when thermally cycled from 2000°F, the chromium-free claddings were generally only slightly more protective than unalloyed nickel. In contrast, claddings containing 15 to 20% chromium more than doubled the number of cycles required for complete oxidation.

The present data indicate that a nickel-chromium base, rather than a nickel-base, would be the most promising starting point for further alloy development work. However, the inherent ability of the higher nickel claddings to retard the oxidation of molybdenum in the presence of small cladding defects is certainly a unique property and of potential value to the molybdenum industry.

Conclusions

A reliable way to insure metallurgical bonding of molybdenum with its cladding is to seal the cladding assembly under vacuum prior to rolling. An alternate, but slightly less reliable, method of bonding claddings which form stable oxide films (when heated) is to nickel plate their contact faces. Thin sheets of nickel may be substituted for the electrodeposited nickel if the air occluded in the assembly is evacuated. This combination technique resulted in the most consistent bonding.

A satisfactory method of sealing the sheared edges of double-clad molybdenum sheet consists of undercutting the molybdenum core section by anodic immersion in caustic solution, inserting filler wire in the groove so formed, and fusing the edges with an oxy-acetylene torch.

The bend ductility of composite sheet (14 mils of molybdenum with 3 mils of nickel-alloy cladding per side) was adequate to permit bending through a 105 deg. arc over a 1/64-inch radius without failure of the composite or of its bond.

Test samples of iron, iron-base alloys, cobalt, and cobalt-base alloys were catastrophically oxidized when heated to 1800°F in an atmosphere of air plus molybdenum trioxide. In some instances, oxidation was still more rapid when the samples were heated in physical contact with molybdenum.

Test samples of chromium, nickel, and nickel-base alloys had relatively high resistance to attack by air-molybdenum trioxide mixtures at 1800°F.

Three-mil-thick claddings of Inconel, Inconel X, and 80 w/o nickel-20 w/o chromium on molybdenum provided good protection when test samples were heated for 100 hr. at a constant temperature of 2000°F in air. Three-mil claddings of Inconel and 80 nickel-20 chromium on molybdenum were also protective when test samples were thermally cycled from 2000°F.

For still-air conditions at constant temperature, where the cladding had been penetrated (intentionally or by localized oxidation) leaving the molybdenum partially unprotected, unalloyed nickel and high-nickel alloys (>92% nickel) gave superior protection. The ability of nickel-rich claddings to protect under such conditions is attributed to the formation of a surface compound which closely resembles the high-temperature form of nickel molybdate (6).

For thermal-cycling conditions, where there were no defects in the cladding, excellent protection was provided by 80Ni-20Cr, Inconel, and Inconel X. Nickel-base claddings containing substantial amounts of chromium form thermally stable oxide films which make them relatively impervious to rapid oxidation under conditions of rapid temperature change.

ACKNOWLEDGMENTS

The authors express their appreciation to the following Battelle personnel for their assistance in this research: C. M. Craighead and W. L. Bruckart, for consultation; J. T. Sunderlin and R. D. Mico, fabrication and testing; C. B. Disbennett, welding; R. D. Buchheit and G. A. Wheeler, metallography; and O. E. Huber, X-ray diffraction. The permission to publish this work, performed under AEC Contract No. W7405-eng-92, is acknowledged.

References

1. W. L. Bruckart and R. I. Jaffee, "Cladding of Molybdenum for Service in Air at Elevated Temperature," TRANSACTIONS, American Society for Metals, Vol. 44, 1951, p. 176.
2. W. L. Bruckart, M. H. LaChance, C. M. Craighead, and R. I. Jaffee, "Investigation of Molybdenum and Molybdenum-Base Alloys by Powder-Metallurgy Techniques," Progress Report No. 9 under Contract No. AF 33(038)-12641, Battelle Memorial Institute, September 1, 1952.
3. W. D. Leslie and M. G. Fontana, "Mechanism of the Rapid Oxidation of High-Temperature, High-Strength Alloys Containing Molybdenum," TRANSACTIONS, American Society for Metals, Vol. 41, 1949, p. 1213.
4. A. de S. Brasunas and N. J. Grant, "Accelerated Oxidation of Metals at High Temperatures," TRANSACTIONS, American Society for Metals, Vol. 44, 1952, p. 1117.
5. "Protection of Molybdenum Against Corrosion at High Temperature," Ohio State University Research Foundation Report No. 6 under ONR Contract N6 onr-22528 (NR 039-005).
6. "Protection of Molybdenum Against Corrosion at High Temperature" Ohio State Research Foundation Report No. 7 under ONR Contract N6 onr-22528 (NR 039-005).

DISCUSSION

Written Discussion: By William L. Larsen, research associate, The Ohio State University, Columbus, Ohio.

The authors are to be commended for their attempts to identify the oxidation products observed in their work. However, the compound Mo_2O_3, reported to occur on the surface of a molybdenum sample, probably does not exist. The ASTM X-ray Diffraction Data Cards list on Card #1-0615 the X-ray diffraction data for a material which is supposedly Mo_2O_3. It may easily be shown by reference to Card #2-0422 or to Card #5-0452 that all the lines of Mo_2O_3 can be accounted for by assuming the sample is a mixture of MoO_2 and Mo. This fact has been noted by Hickman and Gulbransen[3] and confirmed in a private communication to them by H. W. Rinn.

[3] J. W. Hickman and E. A. Gulbransen, Discussion, Institute of Metals Division, Metals Technology, Vol. 47, #3, 1947.

The oxidation product nickel molybdate ($NiMoO_4$) has been observed by the writer to form on the surface of molybdenum-base molybdenum-nickel alloys of widely varying composition. Since the time of writing of references (5) and (6), additional work has confirmed the existence of nickel molybdate in two crystal structures, one existing at the usual oxidizing temperatures and the other resulting from the crystalline transformation to the form usually existing at room temperature. The spalling of the green scale ($NiMoO_4$) noted by the authors is undoubtedly associated with this phase transformation. The X-ray diffraction patterns reported by the authors are those of the phase apparently stable at room temperature. A complete discussion of the spalling and stabilization of nickel molybdate is being published.[4] This reference also lists X-ray data for both the protective form existing at high temperature and the spalled form. The term "high temperature form" used in references (5) and (6) for the spalled product is a misnomer.

The existence of a liquid phase in oxide mixtures containing MoO_3 or MoO_2 has been reported and discussed in detail by Rathenau and Meijering.[5] They propose that the effect of molybdenum upon the oxidation of other metals is not only a result of the release of nascent oxygen but also results from the formation of liquid oxides. Their experimental work shows liquid phases to exist at the following temperatures:

System	Eutectic Temperature
MoO_3+MoO_2	778°C
$MoO_3+MoO_2+Cr_2O_3$	772°C
MoO_3+MoO_2+NiO	764°C
$MoO_3+MoO_2+(Fe_2O_3+Fe)$*	705°C
$MoO_3+(Fe_2O_3+Fe)$*	715°C

*In proportions equivalent to FeO.

In alloys containing both iron and chromium with molybdenum, it is noted that attack of the alloy does not begin at the temperature of the oxide eutectic, but at the higher temperature where the otherwise protective Cr_2O_3 is attacked by the molybdenum.

Apparently a liquid does not exist in the system MoO_3-MoO_2-NiO at 764°C (1400°F) for all compositions, as is evidenced by the stability of $NiMoO_4$ at temperatures above 764°C (1400°F). However, the temperatures cited by Rathenau and Meijering indicate at least the approximate temperatures at which liquids can exist in systems containing molybdenum of oxides.

Written Discussion: By E. D. Sayre, metallurgical engineer, Materials Laboratory, AGT Development Department, General Electric Co., Cincinnati, Ohio.

This paper is quite a contribution to the problem of oxidation protection of molybdenum sheet at elevated temperatures. The fabrication process consisting of hot rolling evacuated packs apparently is quite successful, and the systematic survey of cladding materials adequately demonstrated the superior protection of high nickel chromium alloys.

Certain interesting deductions may be made from this work, and other work in this field, which indicate problems requiring further exploration.

[4]M. Gleiser, W. L. Larsen, R. Speiser and J. W. Spretnak, Symposium on Basic Effects of Environment on the Strength, Scaling and Embrittlement of Metals at High Temperatures, American Society for Testing Materials Special Technical Publication, No. 171, September 1955.

[5]G. W. Rathenau and J. L. Meijering, "Rapid Oxidation of Metals and Alloys in the Presence of MoO_3," *Metallurgia*, Vol. 42, September 1950, p. 167.

As is indicated in Figs. 9,10, and 11, the molybdenum cores are completely recrystallized after a short time at temperatures over 1800°F. This recrystallization, which is a result of the great amount of cold work involved in producing the clad sheet by rolling the thick starting material, will drastically reduce the high temperature properties of the material. This problem could be mitigated by starting with thinner material, but this would undoubtedly be less practical and uneconomical. Recrystallization of the molybdenum part way through the rolling operation is a complex problem, because of the effects on the cladding. This problem is certainly worthy of further study.

The edge protecting method is quite satisfactory when applied to the small test samples, but may prove to be very costly and difficult to apply to large fabricated parts. Other approaches to the edge protection problem, such as undercutting and brazing are worthy of consideration.

The use of nickel as a bonding agent is quite successful, but effects of diffusion into the base molybdenum and the brittle intermetallics formed, may be harmful to structural use of the material.

As evidenced by the authors' survey of the clad materials, nickel-chromium alloys are the superior cladding for molybdenum sheet, however, the alloy has not yet been optimized. Continued search for improved cladding materials is certainly in order.

This work certainly indicates that clad molybdenum sheet has a considerable potential for high temperature structural members and warrants further development.

Written Discussion: By D. C. Goldberg, division manager, Metallurgical Division, Westinghouse Electric Corp., East Pittsburgh, Pa.

The approach of the authors, Messrs. LaChance and Jaffee, is to be congratulated. The data obtained by their "block" test technique indicates by a new quantitative tool what has been known for several years by move qualitative measurements, that is, nickel clad molybdenum has high oxidation resistance as compared iron and cobalt base clad molybdenum.

The roll bond cladding technique has been under investigation in various organizations of the Westinghouse Electric Corporation—Research Laboratories, Materials Engineering, Bloomfield, and the Aviation Gas Turbine Division. Several jet engine components have been fabricated from clad molybdenum and tested. As a result of our experience in this field, the following comments are offered.

The authors point out in their discussion that the life of clad molybdenum is primarily dependent upon the oxidation resistance of the cladding. This is true when the specimen is under no load. However, this is not the case under conditions of steady or vibratory stress. It is felt that the prime limiting factor becomes the molybdenum cladding interface. This brittle layer, caused by a diffusion mechanism as discussed below, is highly sensitive to prior forming history, thermal impact, fatigue, and creep. It is wondered if the authors have any data on this subject.

In fact, thermal impact and forming have been found to be move definitive in establishing the adequacy of cladding in producing oxidation resistant coatings for molybdenum by Westinghouse. For example, a study of the Mo-Ni phase diagram in the range of 1600 to 2200°F reveals that molybdenum is soluble in nickel forming a brittle intermetallic compound "δ" at 50-50 atomic % Ni-Mo. At

1630°F a compound γ forms a peritectoid reaction of α Ni-Mo solid solution with δ, at 1540°F, a third compound β forms by a peritectoid reaction of Mo-Ni and γ.

When a nickel or nickel-base alloy clad sample is heated in this critical temperature range, nickel will diffuse into the molybdenum and molybdenum into the nickle or nickel alloy clad forming α Ni-Mo and ϵ Mo-Ni solid solutions and a film of the hard brittle "δ" compound at the interface. The extent of diffusion and the thickness of the "δ" film is dependent on time and temperature.

It is seen from the above that the apparent adequacy of nickel-base alloy cladding is not a true one as the brittle interface developed between the nickel and molybdenum could not be tolerated in actual service conditions. In order to overcome this problem, Westinghouse has employed most successfully the technique of employing a barrier layer between the Mo and Ni. Improvements in bond strength in the order of 3 to 400% have been obtained.

Complete data are not available at this time, but it is intended that this work will be published when completed.

Written Discussion: By W. L. Bruckart, development engineer, Universal-Cyclops Steel Corporation, Bridgeville, Pa.

This paper represents a very extensive piece of research work which is well reported, and for which the authors should be congratulated. Much of the information presented here verifies earlier work reported by Dr. Jaffee and myself (1), as well as work on the corrosive attack of iron base materials by molybdenum oxide.

I should like to offer a few points of value in connection with this general subject, particularly with respect to the preparation and rolling operations. It was noted that the description under the heading "Cladding Assembly" is of a picture frame type yoke. Recent experience in developing a scaled-up cladding operation has indicated that a differently designed yoke would be superior to the picture frame type cut from a single plate of nickel or nickel-base alloy. The design of the new type yoke calls for construction of a picture frame surrounding a molybdenum or molybdenum alloy core, as is illustrated in Fig. 14. The main difference in the new design is that the picture frame is constructed from bar stock and is welded at the four corners. The advantage of such construction is many fold. First, the size of cladding which can be constructed by this technique is not limited to the size of flat nickel plate which is available in a single piece, from which a frame may be cut. Secondly, the expense of removing the center section to an exact set of dimensions is eliminated by use of the new design. Third, the core section does not necessarily have to be edge ground to precisely the dimensions of the cladding yoke. Fourth, the welded joints not only provide great strength, but serve to shrink the yoke very tightly around the core section as the joints freeze. Fifth, the versatility of this type of yoke design shows itself greatest when in a series of cores, one or two develop edgecracks which need to be ground off, thus yielding material of slightly different dimensions than those of the balance of the lot. Any last minute shift in dimensions in the core is automatically compensated for in this design.

Under the heading of "Bonding by Roll Cladding," commercial experience has been had with molybdenum alloy claddings covered with nickel-base alloys which were rolled in air after heating them in a gas fired furnace. Normally, molybdenum and its alloys can be rolled to 2300°F very satisfactorily. For the claddings, 2150 to 2200°F is very satisfactory in commercial practice. There is another ad-

vantage to the use of a temperature not in excess of 2200°F commercially: that is the avoiding of liquation at the clad-to-core interface. While the use of 2300°F is preferable, it is too close to the liquation temperature for practical application in commercial practice because of the greater variation in furnace temperature and lack of close control which would be normally associated with a laboratory operation.

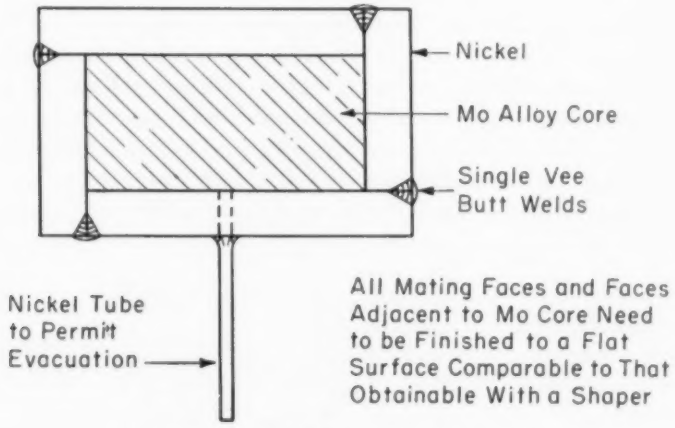


Fig. 14—Details of Cladding Yoke Design.

One of the foremost conclusions which I believe should be drawn from the data presented here is that nickel-base alloys do provide a reliable protection for molybdenum and its alloys at extremely high temperatures in air. The weak-link in the whole process of protection, namely edge protection, apparently has been taken care of. I believe now that we are far enough along in the development of protective coatings for molybdenum that industry may make use of them. The above statement is made with the understanding that one must think in terms of limited parameters when considering behavior of any materials at elevated temperatures. In other words, the limits of time, temperature, environment, and stress are now generous enough to permit economic application of nickel-base-alloy clad molybdenum. As more development work is done we shall undoubtedly see these limits extended so that we may operate in a still more generous area.

We all know that cladding is only one of the satisfactory means to protect molybdenum at elevated temperature. Among other means are: siliconizing, electro-plating, metal spray coatings, ceramic coatings, inert atmospheres and vacuum. Each of these methods enjoys advantages and disadvantages. Some of the disadvantages and advantages are common among several of the protective means. Some are unique. On this basis of thinking, then, each of the protective means is justified for certain applications. It is therefore, reasonable to assume that combinations of all of the protective methods will be employed where ever molybdenum is used, and that the protective methods employed will be those which are most suitable to the application.

The very fact that there is a need for pushing back the limitations on temperature, time, stress and environment points obviously to the need for further research on protection of molybdenum. At present the protective means under conditions of severe stress, deformation, and abrasion are not adequate to fully utilize the stress-bearing characteristics and the recrystallization temperature of

the better molybdenum-base alloys. It is hoped that there will be a continuation of research work toward the improvement of ductile metallic claddings and that this information will be dissemenated among producers and potential users. The advantages to be enjoyed by the use of ductile metallic coatings on molybdenum, in the majority of cases, far outweigh the advantages of any other type of protective means.

Authors' Reply

The authors wish to thank Messrs. Sayre, Larsen, Bruckart, and Goldberg for their interesting and valuable discussions of this paper.

Mr. Sayre cites, as problems to be answered by future research, 1). the accelerating effect of large amounts of cold work on subsequent recrystallization, 2). the high cost of edge protecting clad sheet by welding, and 3). the formation of brittle intermetallics when nickel is used as a bonding agent. These points are very well taken. The amount of recrystallization in service can be decreased by limiting the amount of reduction after recrystallization and by using molybdenum alloys that are more resistant to recrystallization than molybdenum, such as Mo-0.5Ti. We consider the latter expedient the preferable one. Also, we agree that an improved method suitable for production for protecting the edges of clad sheet and development of superior cladding alloys would be most desirable.

In response to Dr. Larsen's discussion, the X-ray diffraction data used for identification of the oxide layers were the ASTM data issued in 1950, the only information available at the time the work was done. We are very glad to have Dr. Larsen's comment that the pattern for Mo_2O_3 was a composite of the molybdenum and MoO_2 structures. The Mo_2O_3 data were deleted in the 1953 revision of the ASTM data files (published in mid-1954).

The correlation made between the basic research at The Ohio State University and our work is most valuable, particularly with regard to the crystal structures and phase transformations of $NiMoO_4$.

Mr. Bruckart's description of a more economical cladding assembly has considerable industrial merit. With regard to the temperatures to which assemblies may be preheated for roll cladding, 2200°F would appear to be a practical maximum for nickel-base alloys. There is no apparent advantage in exceeding this temperature, but there may be certain disadvantages, one of which is pointed out in the first sentence of the section entitled "Bonding by Roll Cladding."

A completely satisfactory method of edge protecting clad molybdenum sheet has not yet been developed. The method of undercutting the edges of clad sheet by anodic solution, disclosed here, constitutes what is believed to be a start in the right direction. However, as Mr. Sayre has pointed out, undercutting followed by a brazing operation would be worthy of consideration. Aside from the cost saving involved, certain brazes might be applied below the recrystallization temperature of the load-bearing component, whereas welding causes overheating and edge recrystallization.

The various methods of protecting molybdenum, their peculiar advantages, disadvantages, and limitations certainly must all be considered. When the individual methods of coating have been evaluated, multiple coatings offer a still broader field for exploration. The achievement of self-regenerating and self-healing coatings for molybdenum is the ultimate, though possibly remote, objective being sought.

Evaluation of the relative merits of iron-, cobalt-, and nickel-base alloys, as cladding materials for molybdenum, is perhaps the most important of the findings reported. In lieu of specific references, it is assumed that Mr. Goldberg's statement to the effect that such information "has been known for several years" refers to unpublished results obtained by his organization. He discussed quite thoroughly the detrimental effect of the brittle intermetallic layer which forms at the interface in nickel-clad molybdenum. This is an important consideration which becomes increasingly serious with decreasing thickness of the core section. The deleterious effect of interdiffusion was not fully recognized in November of 1953, when this research was completed. However, at least two distinct intermetallic phases, and possibly a third, have since been observed in nickel-clad samples after diffusion treatments. In addition, terminal solid solutions of Ni-Mo and Mo-Ni have been observed, corroborating Mr. Goldberg's observations. When released for publication, the data on barrier coatings used by Westinghouse to combat the problem of interdiffusion will constitute an important contribution to further application of clad molybdenum.

MECHANICAL PROPERTIES OF TI-CR-MO ALLOYS AS AFFECTED BY GRAIN SIZE AND GRAIN SHAPE

By H. R. Ogden, F. C. Holden and R. I. Jaffee

Abstract

The mechanical properties of an alpha, a metastable-beta, and an alpha-beta alloy are not altered significantly by changes in grain size or grain shape. Acicular types of structures obtained by heating into the beta field prior to annealing in the alpha or alpha-beta field cause a lowering of unnotched tensile ductilities to about the same values as notched tensile ductilities. Fatigue endurance limit is unaffected by grain size or shape and appears to be relatively unaffected by alloy content. (ASM-SLA Classification: Q general, M27, N3, Ti)

DURING the past six years, much effort has been devoted to studying the effects of heat treatment and composition on the mechanical properties of titanium alloys. In many instances, large grain size and acicular structures have been blamed when poor properties are obtained. As will be shown, large grain size or acicular structures are not necessarily detrimental to mechanical properties.

The purpose of this research was to determine how variations of grain size and shape would affect the mechanical properties of titanium and of representative titanium-base alloys. The mechanical properties of interest were those that describe fabrication and performance capabilities and that also may be affected by grain size. These include tensile properties, hardness, bend properties, impact properties, and fatigue endurance limits.

The three alloys that were chosen for this study included commercial titanium as representative of an alpha-type alloy, Ti-7.5Cr-7.5Mo as representative of a metastable-beta alloy, and Ti-2.5Cr-2.5Mo as representative of an alpha-beta alloy.

Experimental Procedures

Preparation of Alloys

The alloys for this study were prepared as 30-pound ingots, using commercial purity titanium and high purity additions of

A paper presented before the Thirty-Seventh Annual Convention of the Society, held in Philadelphia, October 17–21, 1955. Of the authors, H. R. Ogden is assistant chief, F. C. Holden is principal metallurgist and R. I. Jaffee is chief, Nonferrous Physical Metallurgy Division, Battelle Memorial Institute, Columbus. Manuscript received April 11, 1955.

chromium and molybdenum. The ingots were arc melted in cold wall copper crucibles with an inert tungsten electrode. To reduce segregation, the alloys containing chromium and molybdenum additions were melted three times. Despite the triple melting procedure, microstructures of the Ti-7.5Cr-7.5Mo alloy showed some particles of unmelted molybdenum. These were uniformly distributed and probably do not affect the properties of the alloy significantly. Analyzed compositions are shown below.

Nominal Composition	Analyzed Composition, per cent						
	Cr	Mo	N	C	Fe	O	H, ppm
Commercial Ti	—	—	0.014	0.03	0.29	0.10	31
Ti-7.5Cr-7.5Mo	7.60	6.66	0.026	0.03	0.32	0.13	44
Ti-2.5Cr-2.5Mo	2.32	2.58	0.015	0.04	0.27	0.13	60

Fabrication

Material for test specimens was prepared from the ingots by forging, rolling, and swaging operations. All fabrication and heating was done in air. The temperatures are given below.

Alloy Composition	Forging Temperature, °F	Rolling Temperature, °F	Swaging Temperature, °F
Commercial Ti	1600	1400	1300
Ti-7.5Cr-7.5Mo	1800 to 1600[a]	1400	1500 to 1550
Ti-2.5Cr-2.5Mo	1600	1400	1400

(a) Forging finished at 1600°F

Heat Treatments

Heat treatments were done in potentiometer-controlled electric furnaces. Specimens annealed at temperatures above 1380°F were encapsulated in Vycor under a partial pressure of argon; specimens annealed at the lower temperature were done in air.

Mechanical Testing

The testing program was designed to provide as much information as could reasonably be obtained from the available material. Tensile and bend-test specimens were cut from 1/16-inch sheet. Tensile, notched-tensile, micro impact, and fatigue specimens were cut from 0.302-inch diameter rod, and V-notch Charpy impact test specimens were made from 0.625-inch rod. Specifications for the test specimens are shown in Figs. 1 and 2.

Tensile Testing—Tensile properties were determined for each test condition, using duplicate sheet and round unnotched specimens, and round notched specimens. Details of the testing procedures have been presented previously (1).[1]

Impact Testing—The effects of grain size and other structural

[1]The figures appearing in parentheses pertain to the references appended to this paper.

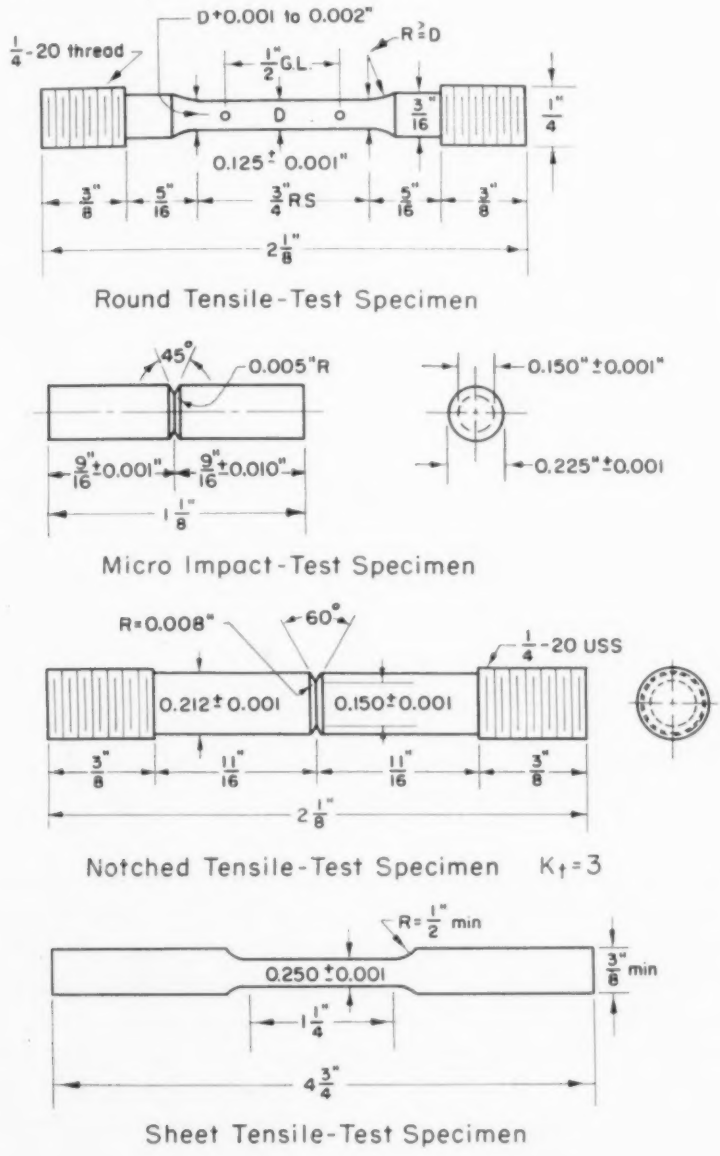
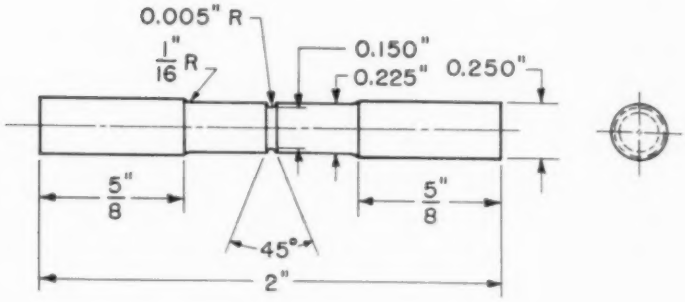


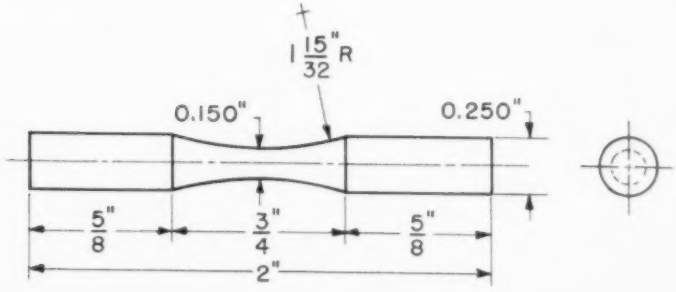
Fig. 1—Specifications for Test Specimens.

variables on notched-bar impact resistance were studied, using the micro impact test. Duplicate specimens were used for each testing temperature over a temperature range of −320 to 750°F. In addition, standard V-notch Charpy test specimens were used for a single testing condition for each alloy. Testing procedures and correlations have been discussed previously (1).

Bend Testing—The bend ductility of titanium sheet was measured by use of a progressive-bend test. Tests were conducted in quadruplicate on specimens cut transverse and longitudinal with respect to the rolling direction. The test specimens used were



a. Rotating-Beam Notched Fatigue Specimen, $K_t = 3$



b. Rotating-Beam Unnotched Fatigue Specimen

Fig. 2—Specifications for Rotating Beam Fatigue Specimens.

approximately $\frac{1}{16} \times 1 \times 3$ inches. Bend tests were conducted on a laboratory press with 75-degree bend dies. Specimens were bent progressively over decreasing radii until a visible crack appeared. The results are presented as the ratio of the radius of the last good die to the specimen thickness.

Fatigue Testing—The effects of grain size and other structural variables on resistance to alternating stresses were studied by means of rotating-beam fatigue specimens. Tests were conducted under a limited number of conditions with notched and unnotched test specimens. The tests were made on Krouse cantilever-type rotating beam machines, at a rotational speed of 8000 to 10,000 rpm. Approximately 20 specimens were used in the determination of the endurance limit. Specimens were machined and hand polished before testing. Contrary to the results of other investigators (2), no heating of the specimens was apparent during the tests.

Grain Size Determinations

Because grain size effects were of primary interest in this study, the effects of annealing time and temperature on grain size

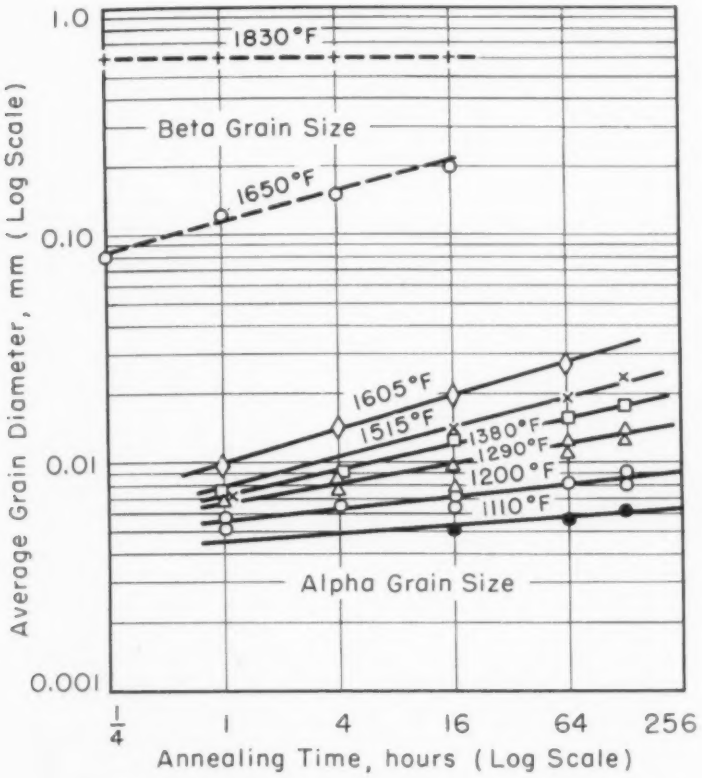


Fig. 3—Effect of Heat Treating Temperature and Time on the Grain Size of Commercial Titanium.

were investigated. Microstructure specimens were annealed at temperatures in the range of interest and water-quenched after various times. Grain size measurements were made by counting the grains contained in a specified area (Jeffries' Method). At least two fields were measured on each specimen. The heat treatments used in the alloy testing program were selected on the basis of these grain size determinations.

Commercial Titanium

Unalloyed high purity titanium exists in two allotropic forms, of which the hexagonal alpha phase is stable at room temperature. The body-centered cubic beta phase is stable at temperatures above about 1625°F. The beta structure cannot be retained at lower temperatures, but transforms on cooling to plates of alpha phase, which tend to form serrated colonies of alpha. The presence of impurities in commercial titanium, however, introduces a two-phase transformation region in place of a single transformation temperature. The retention of small quantities of beta phase is made possible by the presence of beta-stabilizing impurities.

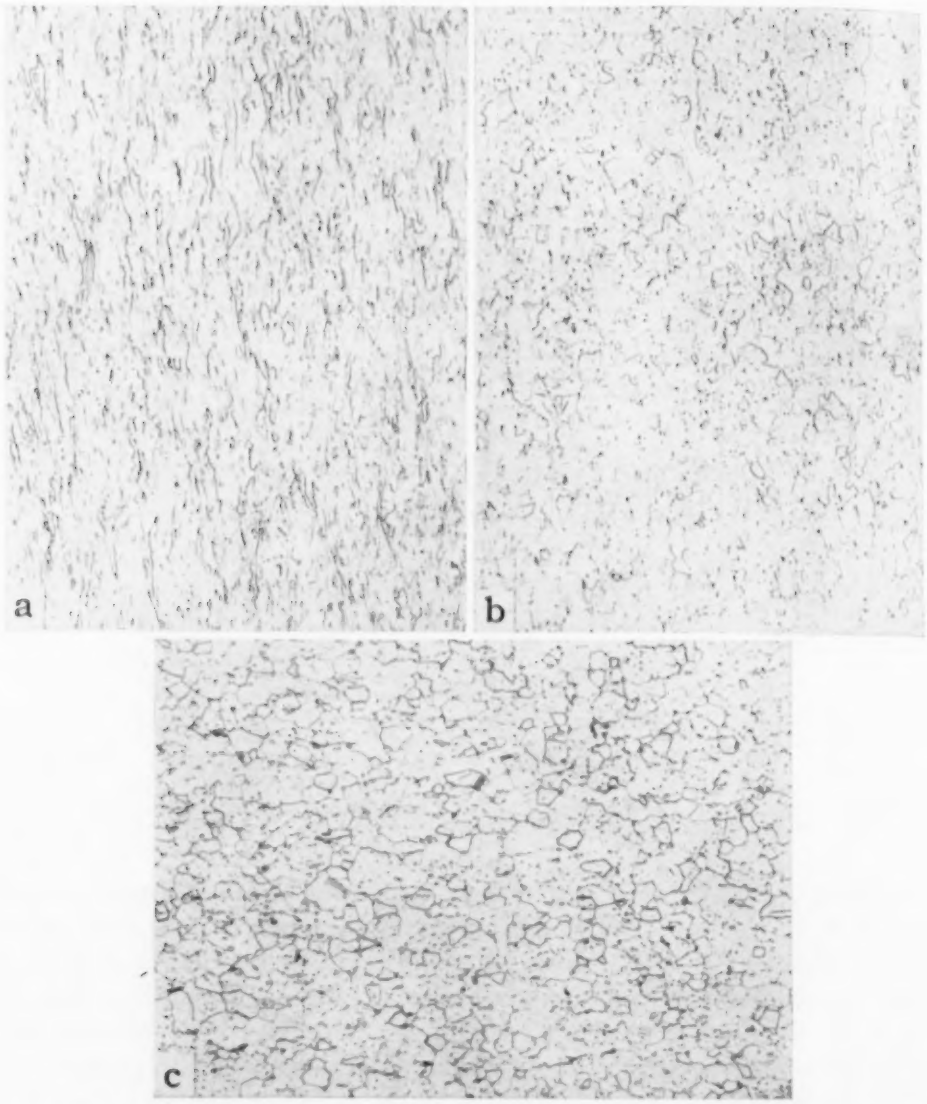


Fig. 4—Photomicrographs of Commercial Titanium Annealed at 1110 and 1290°F (a)—As Fabricated at 1400°F; (b)—Annealed 1 Hour at 1110°F and Air-Cooled; (c)—Annealed 2 Hours at 1290°F and Air-Cooled. ×250.

Grain Size and Microstructure

The effects of annealing time and temperature on the grain size of commercial titanium as hot-rolled at 1400°F are shown in Fig. 3. It may be noted that the two upper curves, which represent beta-grain size, are considerably above the curves representing alpha-grain size. Also, the annealing temperature, rather than annealing time, is the dominant factor in determining the final grain size. Photomicrographs of samples of unalloyed titanium in the conditions of testing are given in Figs. 4,5, and 6.

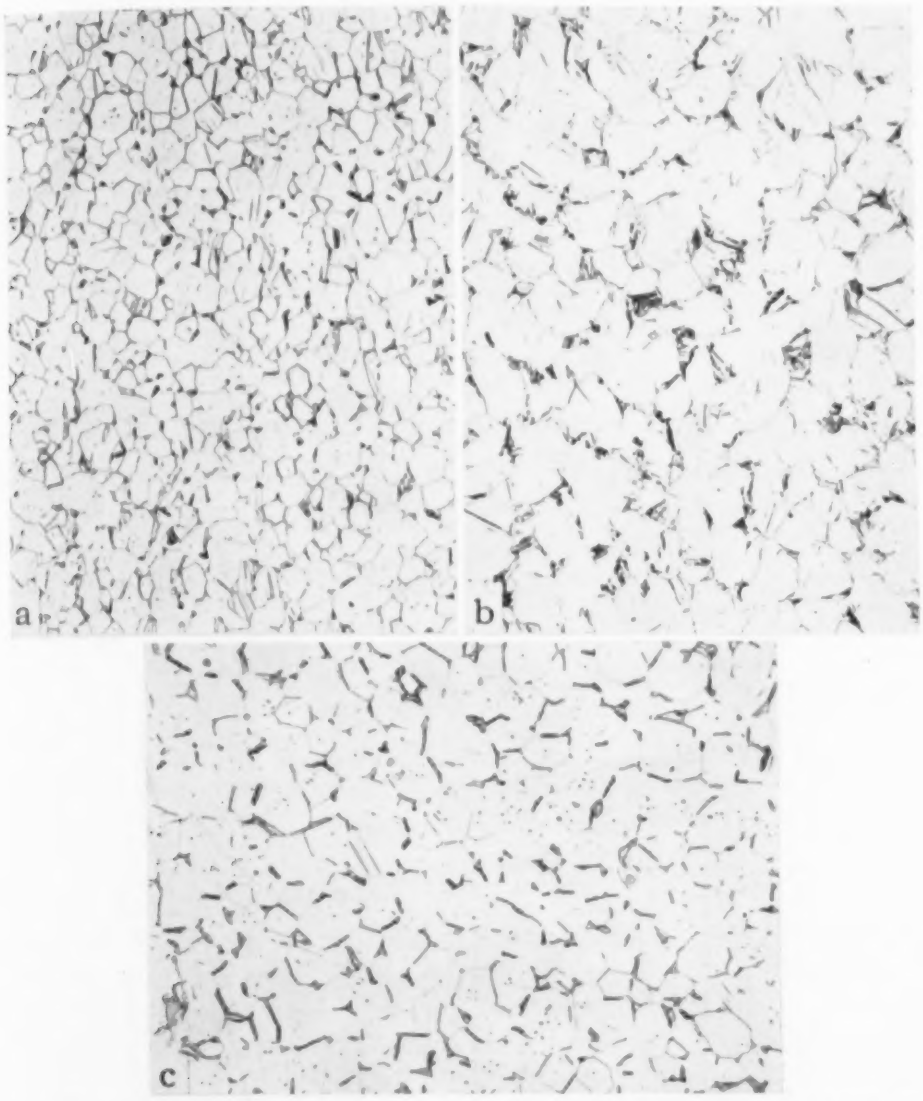


Fig. 5—Photomicrographs of Commercial Titanium Annealed at 1515 and 1605°F. (a)—Annealed 4 Hours at 1515°F and Air-Cooled; (b)—Annealed 16 Hours at 1605°F and Air-Cooled; (c)—Vacuum Annealed 18 Hours at 1605°F and Furnace-Cooled. ×250.

Mechanical Properties

With the exception of the partially recrystallized specimen (1110°F—annealed condition), tensile strengths as shown in Fig. 7 are insensitive to microstructure. A slight decrease in yield strength occurs for specimens annealed in the range at which alpha and beta phases coexist (1605 to 1650°F). This is associated with the disappearance of the yield point, which occurs in the equiaxed-alpha specimens. The yield-point behavior occurs in specimens annealed at 1110 or 1290°F. Similar yield points have been observed previ-

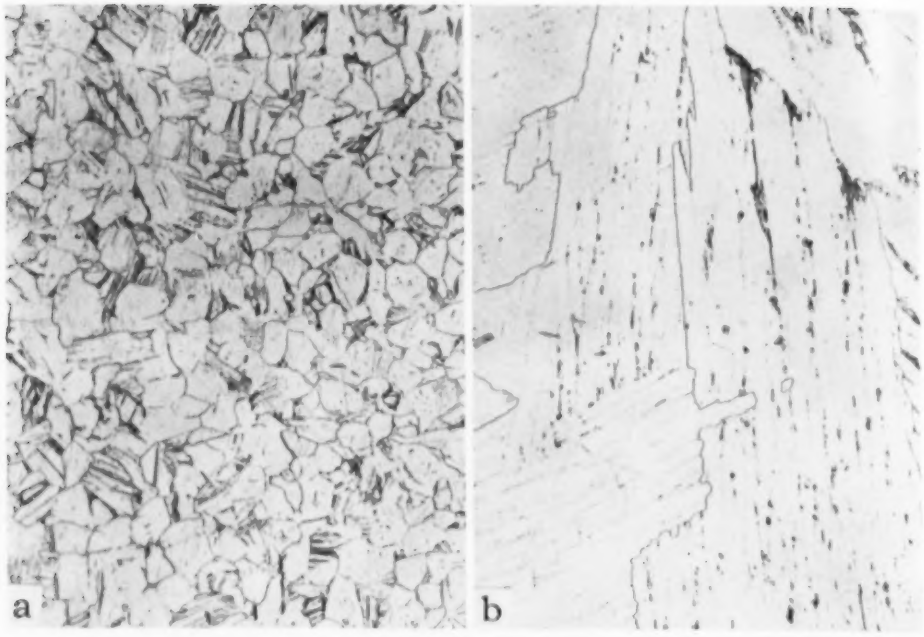


Fig. 6—Photomicrographs of Commercial Titanium Annealed at 1650 and 1830°F. (a)—Annealed 1 Hour at 1650°F and Air-Cooled; (b)—Annealed 2 Hours at 1830°F and Air-Cooled. ×250.

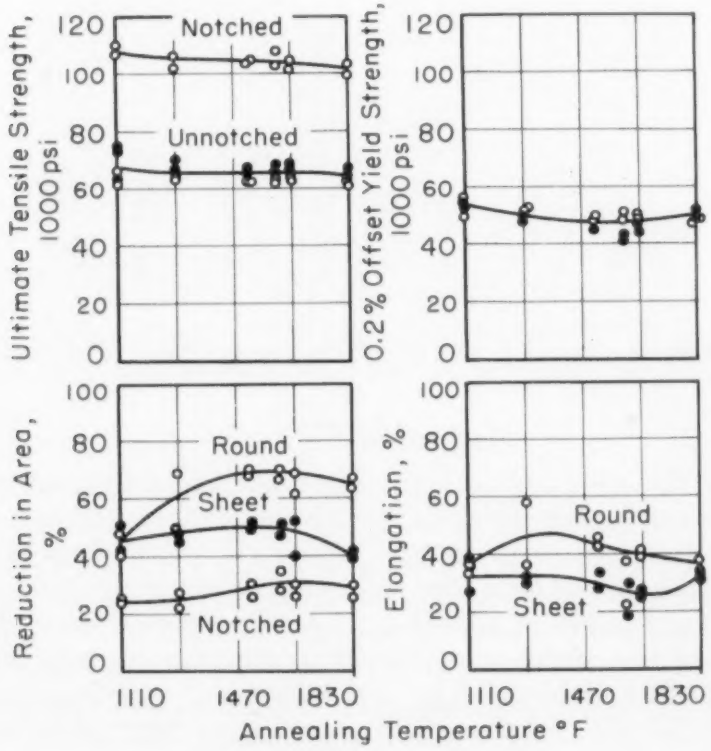


Fig. 7—Tensile Properties of Commercial Titanium.

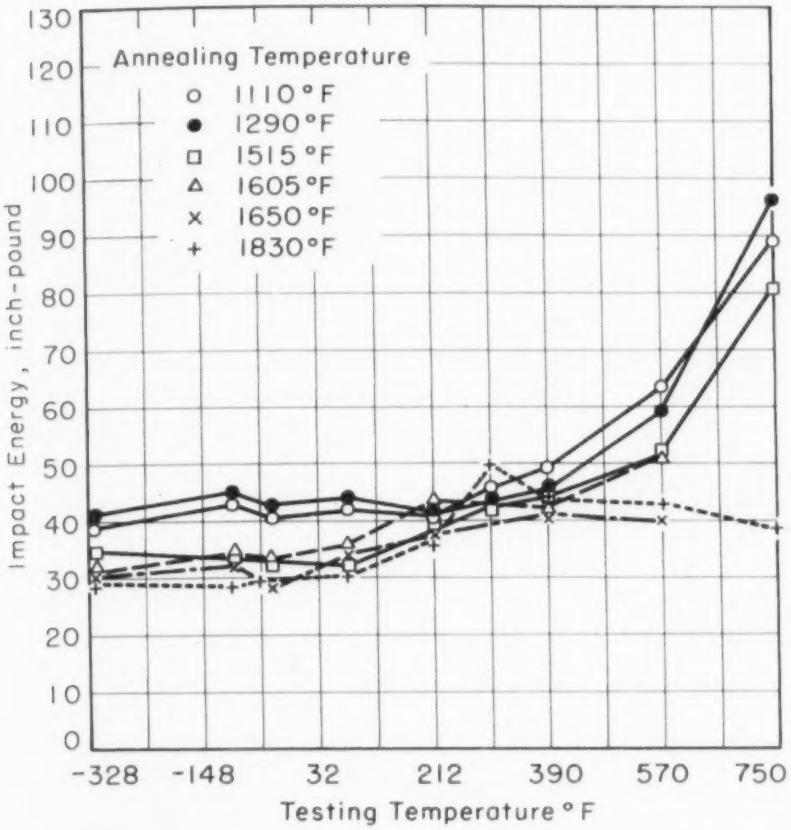


Fig. 8—Effect of Testing Temperature on the Impact-Energy Values of Commercial Titanium.

ously in high-purity alloys containing interstitial alpha-stabilizing additions (carbon and nitrogen) (3,4), but do not appear in unalloyed high purity titanium (1). The presence of the interstitial impurities in commercial titanium undoubtedly accounts for the appearance of the yield point phenomenon in the equiaxed-alpha condition.

Tensile ductilities, as measured by reduction in area and elongation, show more dependency on grain size and shape than do the strength properties. The partially recrystallized specimens have lower ductilities than do the specimens with fully recrystallized structures. The ductilities of the specimens annealed at 1830°F are slightly lower than those for specimens annealed at lower temperatures. In general, the dependence of ductility on microstructure is slight, with highest values obtained for the specimens annealed at 1515 to 1650°F.

The same strength values were obtained from both the sheet and the round unnotched specimens. The effect of geometry is reflected in the ductility, however, since both reductions in area and elongations are higher for the round specimens. Per cent

Table I
Fatigue Strengths of Commercial Titanium

Annealing Treatment		Mean Stress at 10^7 Cycles, psi		Tensile Strength, psi	Endurance-Limit Tensile-Strength Ratio	
Time, hr	Temp., °F	Unnotched	Notched		Unnotched	Notched
2	1290	52,700 ± 1300	27,700 ± 2500	64,000	0.82	0.43
16	1605	51,200 ± 1300	27,700 ± 1100	64,000	0.80	0.43
1	1650	53,400 ± 2500	28,000 ± 800	64,000	0.83	0.44

elongation was measured over a 1-inch gage length for the flat specimens, and a ½-inch gage length for the rounds. The ultimate tensile strengths of the notched specimens are increased over those of the unnotched specimens by 56 to 70%. Ductility, as measured by reduction in area, is reduced to 41 to 55% of the unnotched condition. The notched-tensile-test values obtained show that this material is notch insensitive in all conditions according to the usual standards.

The fatigue endurance limit of commercial titanium was determined for a limited number of microstructural conditions. The values obtained for both notched and unnotched specimens are given in Table I. As for most of the other mechanical properties, no effect of grain size or shape on the endurance limit was observed. The unnotched endurance limit at 10^7 cycles is about 80%, and that of the notched specimens about 43%, of the ultimate tensile strength.

The bend ductilities of commercial titanium are excellent. Minimum bend radii in the range of zero to 1 T were obtained for all conditions of testing. No dependence of bend ductility on grain size or shape was found.

The specimens with partially recrystallized and small alpha-grain sizes have the highest resistance to impact. Impact-energy values obtained for specimens with large alpha-grain sizes and with transformed-beta structures are about 25% lower than those for the fine-grained alpha specimens. As shown in Fig. 8, no effect of testing temperature is observed from −320°F to room temperature. From room temperature up to 750°F, the specimens with equiaxed-alpha structures show a considerable increase in impact resistance, whereas those with transformed-beta structures show only a slight increase.

Metastable-Beta Alloy (Ti-7.5Cr-7.5Mo)

A titanium alloy containing additions of 7.5% chromium and 7.5% molybdenum was studied as an example of a metastable-beta alloy. Specimens quenched from the beta field have a retained-beta structure that is unstable when reheated to temperatures below the beta transus. The precipitation of alpha under such conditions

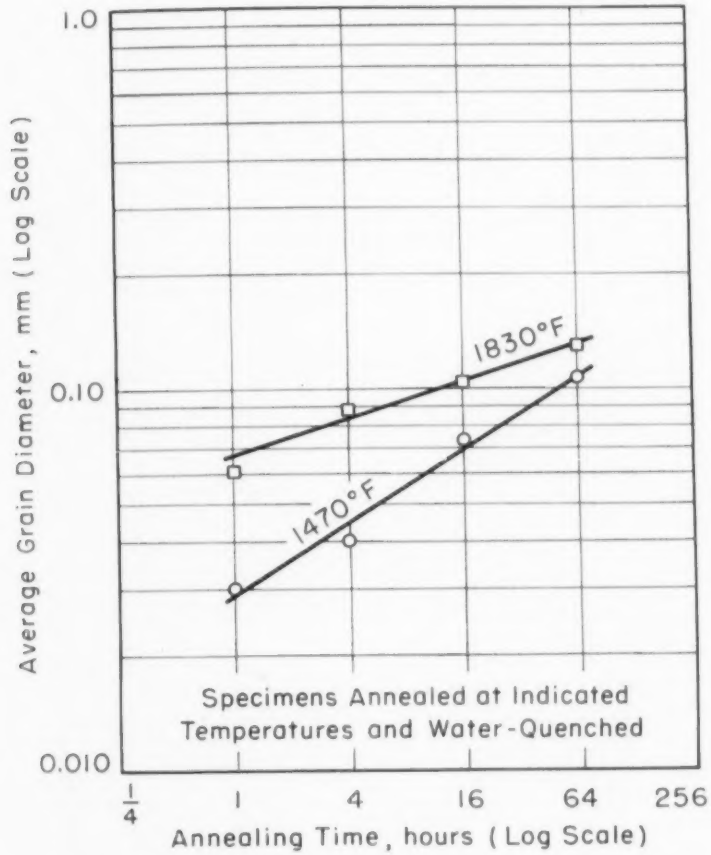


Fig. 9—Effect of Annealing Temperature and Time on the Grain Size of a Ti-7.5Cr-7.5Mo Alloy.

may have considerable effect on the microstructure and mechanical properties.

The basic heat treatments for this alloy were designed to determine the effects of beta-grain size on the mechanical properties. These studies also included the effects of prior beta anneals on specimens slow cooled to 1290°F. These treatments were intended to separate the effects of beta-grain size from those of quenching temperature. The 1290°F anneal, however, was slightly below the beta transus, so that approximately 5% of equilibrium alpha was formed.

Grain Size and Microstructure

The effects of annealing time and temperature on beta-grain size of specimens hot-rolled at 1400°F are illustrated in the curves of Fig. 9. It is seen that both time and temperature are significant factors in the control of grain size, but that the rate of grain growth decreases with increasing annealing temperature. Photomicrographs of typical microstructures are presented in Fig. 10. The particles

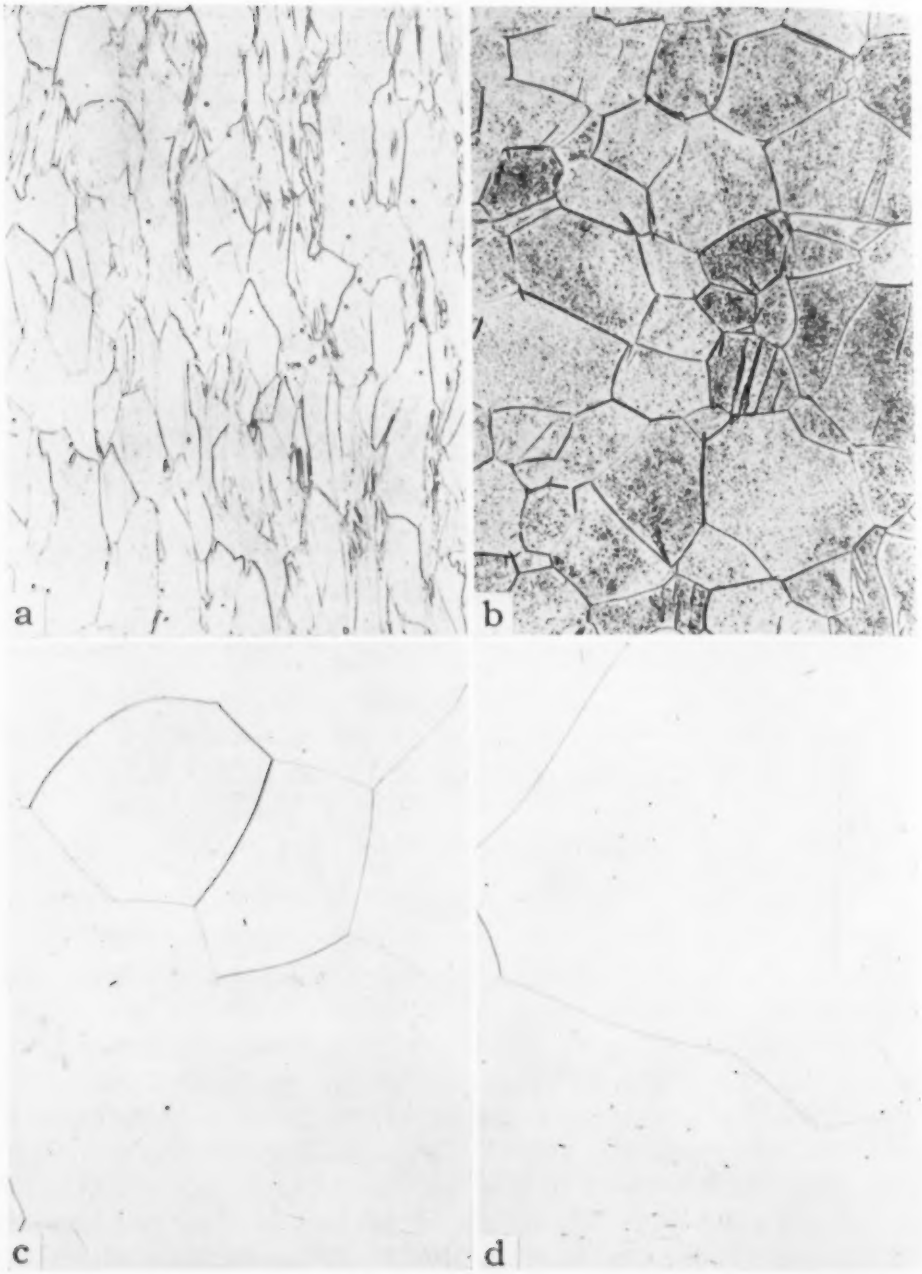


Fig. 10—Photomicrographs of a Ti-7.5Cr-7.5Mo Alloy in Various Microstructural Conditions. (a)—As Fabricated at 1400°F (760°C); (b)—Annealed 1 Hour at 700°C (1290°F) and Quenched; (c)—Annealed 2 Hours at 850°C (1560°F) and Quenched; (d)—Annealed 4 Hours at 1000°C (1830°F) and Quenched. ×250.

in the microstructure of the specimen quenched from 1830°F have not been identified, but probably are associated with the interstitial content of the alloy. Similar structures have been observed in high purity beta-stabilized alloys to which intentional nitrogen additions have been made (5).

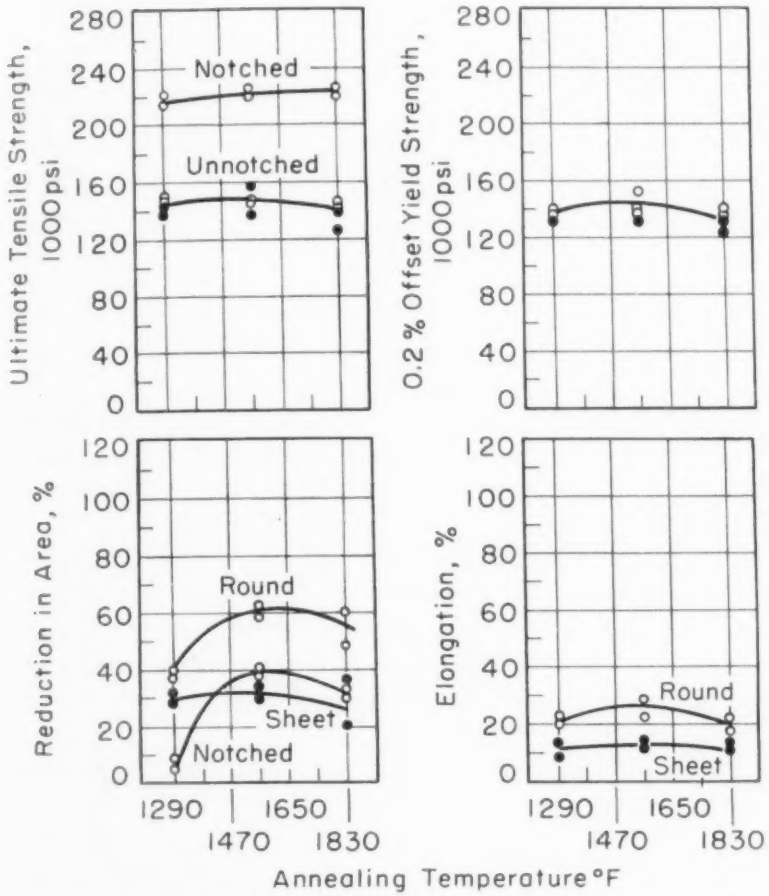


Fig. 11—Tensile Properties of a Ti-7.5Cr-7.5Mo Alloy Quenched From Various Temperatures.

Mechanical Properties

Unnotched tensile strengths of the metastable-beta alloy show no significant variation with beta annealing temperature, as shown in Fig. 11. This is also the case for tensile ductility, except for the reduction-in-area values for the 1290°F anneal which, because of the presence of alpha phase, showed some loss of ductility. Elongations are not affected appreciably by annealing temperature. The unidentified precipitate in the microstructure of the 1830°F quenched specimens does not appear to affect the tensile properties.

The notched strength is unaffected by annealing temperature. Reductions in area, however, are lowered considerably by the presence of alpha phase in the specimens annealed at 1290°F. Using the ratio of notched to unnotched reduction in areas as a measure of notch sensitivity, the alloy is more sensitive to notches when alpha is present in the microstructure. The ratio of notched-to-unnotched tensile strengths is unaffected by annealing temperature.

Table II
Fatigue Strengths of a Ti-7.5Cr-7.5Mo Alloy

Annealing Treatment[a] Time Hr.	Temp. °F	Mean Stress at 10^7 Cycles, psi Unnotched	Notched	Tensile Strength, psi	Endurance-Limit Tensile-Strength Ratio Unnotched	Notched
1	1290	66,500 ± 5700	33,000 ± 4200	144,000	0.46	0.23
4	1830	57,200 ± 4100	32,600 ± 3700	141,000	0.41	0.23

[a]Quenched from the annealing treatment.

The fatigue endurance limits were obtained for specimens annealed at 1290 and 1830°F. The endurance limit in the unnotched condition was higher for the specimens annealed at 1290°F, as shown by the data in Table II. On the basis of ultimate tensile strength, the endurance limit of the 1290°F annealed condition is 46% of 144,000 psi, and that of the 1830°F annealed condition is 41% of 141,000 psi.

In the notched condition, the endurance limit was found to be the same for both the 1290°F and 1830°F annealed conditions. Ratios of endurance limit to ultimate tensile strength were 0.23 for both conditions. Both notched and unnotched endurance-limit ratios (to ultimate tensile strength) are considerably lower than those for the unalloyed titanium.

Bend ductility is improved as the quenching temperature is increased, as shown below.

Quenching Temp. °F	Average Bend Radius, T
1290	3.2
1560	0.8
1830	0.2

This probably is caused both by the elimination of the alpha phase and the increase in beta-grain size as the temperature is increased. From these results, it may be concluded that specimens having retained-beta structures have good bend ductility. Ductility is increased slightly as the beta-grain size is increased. The presence of alpha phase in the microstructure, however, decreases bend ductility. No effect of rolling direction on bend ductility was observed.

The effects of beta-grain size on impact behavior, as determined by comparison of specimens annealed at 1560 and at 1830°F, are minor. The level of room temperature impact energy values for the specimens containing all retained beta is high (36 to 39 inch-pounds), and compares favorably with that for unalloyed titanium. The presence of alpha in the 1290°F quenched specimens, however, lowers the impact resistance considerably (9 inch-pounds).

The effects of testing temperature on impact properties are shown in Fig. 12. A definite transition behavior is apparent for this

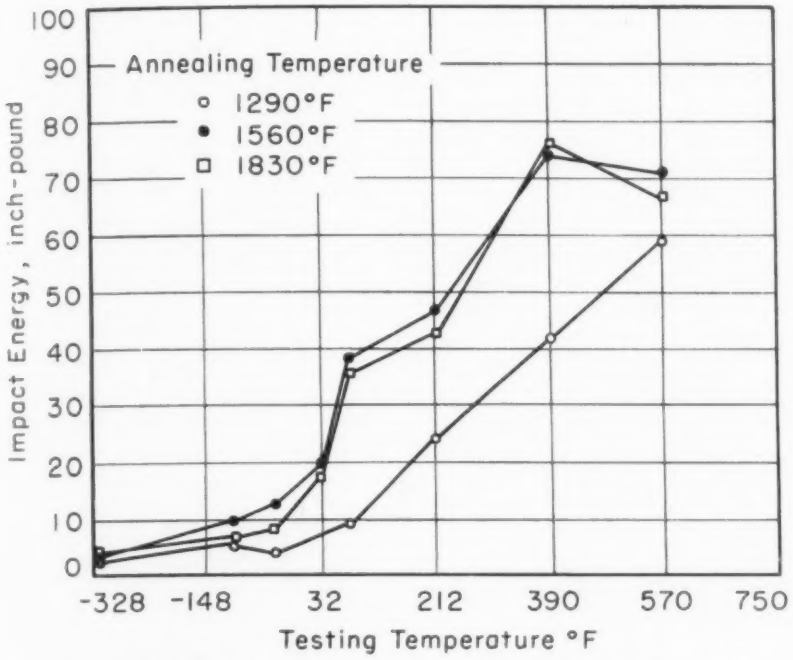


Fig. 12—Effect of Testing Temperature on the Impact Behavior of a Ti-7.5Cr-7.5Mo Alloy Quenched From Various Temperatures.

alloy. This is typical of retained-beta alloys. The transition occurs between —58 and 390°F for the specimens annealed at 1560 and 1830°F. The transition behavior of the 1290°F annealed specimens is less apparent because of the presence of the alpha phase. The impact-energy values for this condition are lower for a given temperature, and the transition temperature is increased. There is no distinct difference between the curves for the 1560°F and 1830°F annealed material.

Effect of Prior Treatment on Properties of the Metastable-Beta Alloy Quenched from 1290°F

Because beta-grain size is largely controlled by annealing temperature, specimens were annealed at 1560 and 1830°F to develop large beta-grain structures. These specimens were then slow cooled to 1290°F and quenched. This provided material of three beta-grain sizes quenched from the same temperature, so that quenching temperature could be eliminated as a variable. The structure of samples annealed at 1290°F after fabrication in the beta field is composed of equiaxed beta with an intragranular coarse alpha precipitate. However, when samples are furnace-cooled from the beta, the structure is composed of equiaxed beta with intragranular alpha plates. Microstructures of these conditions are presented in Fig. 13.

The ultimate tensile strengths of these alloys are affected only

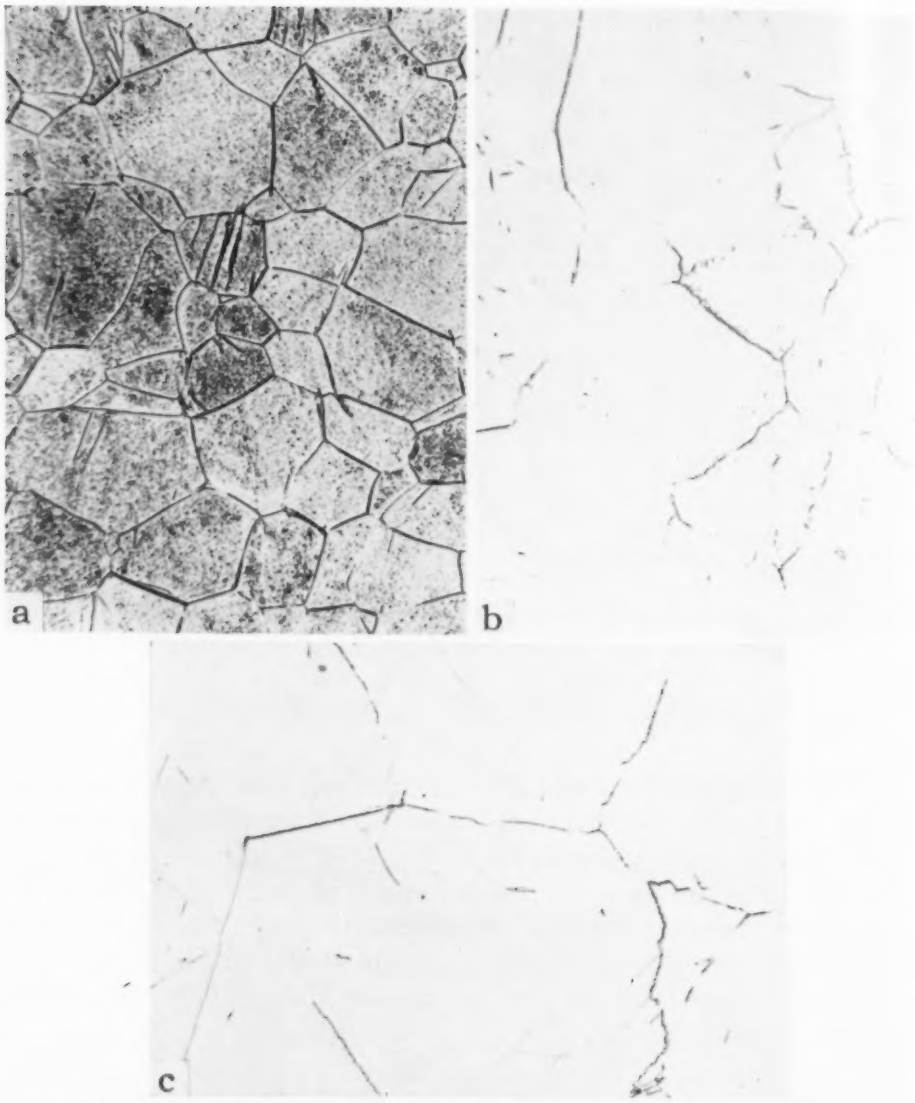


Fig. 13—Photomicrographs of a Ti-7.5Cr7.5-Mo Alloy Quenched From 700°C (1290°F). (a)—Annealed 1 Hour at 700°C (1290°F) and Quenched; (b)—Annealed 2 Hours at 850°C (1560°F); Furnace-Cooled to 700°C (1290°F), Held 1 Hour, and Quenched; (c)—Annealed 4 Hours at 1000°C (1830°F); Furnace-Cooled to 700°C (1290°F), Held 1 Hour, and Quenched. ×250.

slightly by beta-grain size, as shown in Fig. 14. Both notched and unnotched specimens, however, show a slight decrease in tensile strength with an increase in beta-grain size. Yield strengths remain constant with increasing annealing temperature, and are very close to the ultimate tensile strengths. Neither the reduction-in-area nor elongation values appear to be affected by annealing temperature.

The ratio of notched to unnotched tensile strength is nearly constant, ranging from 1.5 to 1.45. Reductions in area of the notched specimens are reduced to 16 to 24% of the unnotched values. This indicates a more notch-sensitive condition than for the same

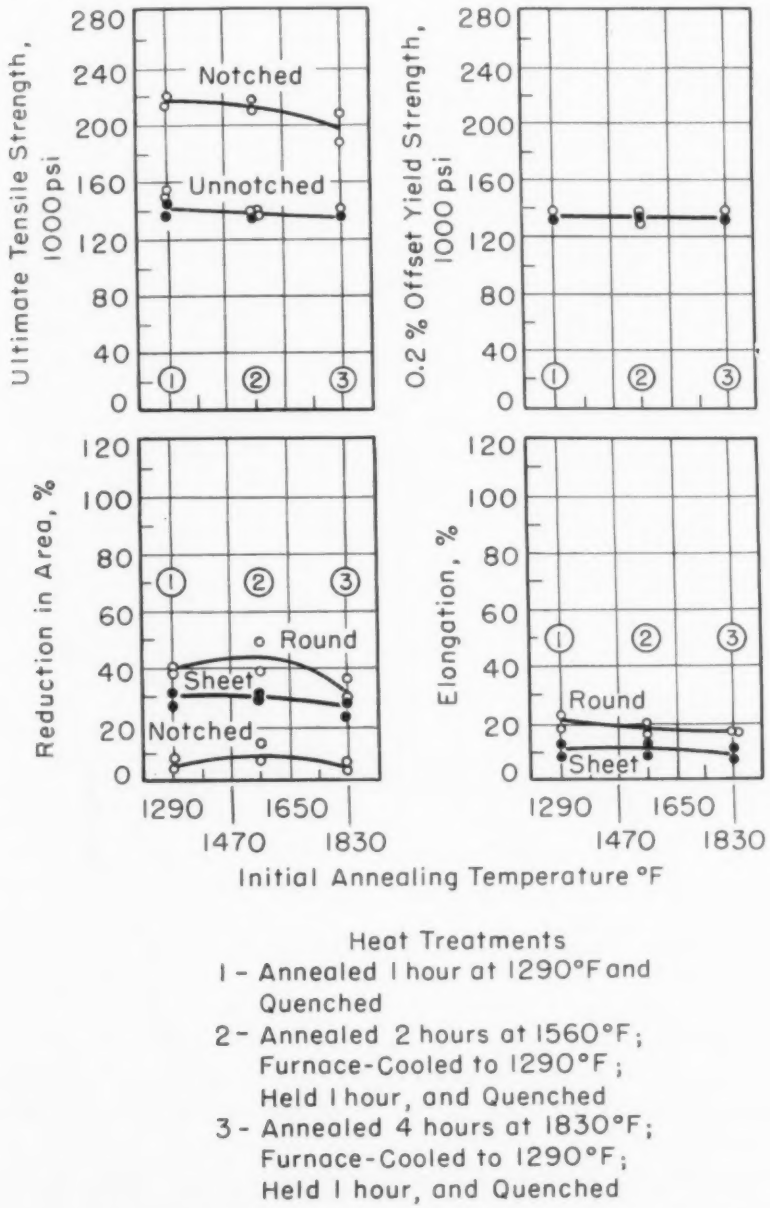


Fig. 14—Effect of Previous Beta Annealing Treatment on Tensile Properties of a Ti-7.5Cr-7.5Mo Alloy. All specimens quenched from 700°C (1290°F).

alloy in the all-beta condition. The notch sensitivity of the 1290°F quenched specimens was not affected by beta-grain size.

The fatigue-endurance limit of 10^7 cycles for the 1290°F quenched condition and for the 1830°F furnace-cooled to 1290°F and quenched condition are given in Table III. There is no significant difference between the notched endurance limits for these two conditions. However, the unnotched endurance limit for the fur-

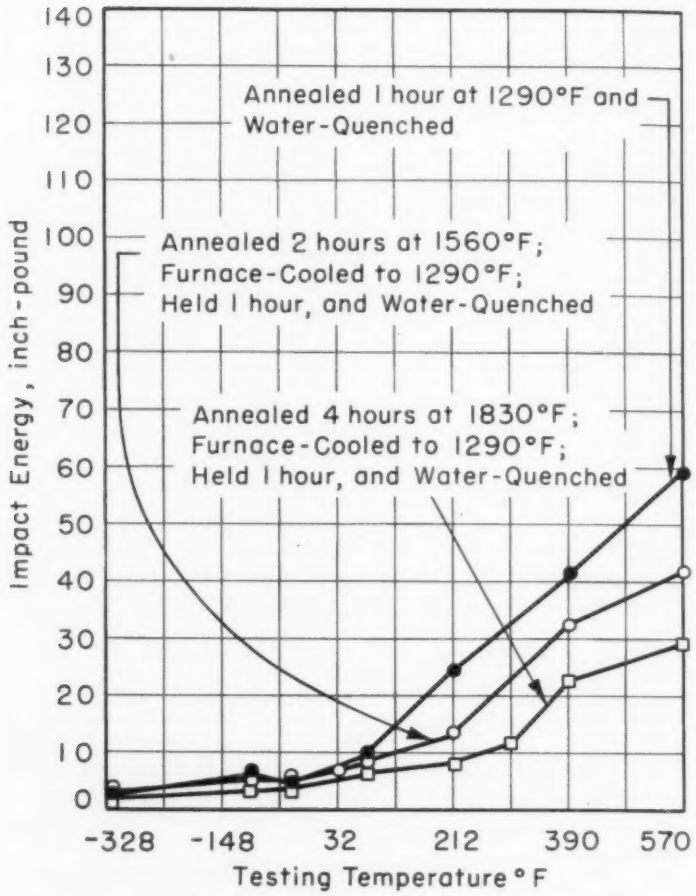


Fig. 15—Effect of Previous Beta Annealing Treatment on Impact Behavior of a Ti-7.5Cr-7.5Mo Alloy. All specimens quenched from 1290°F.

nace cooled to 1290°F sample is much lower than that for the 1290°F quenched sample. This indicates that the alpha plates present probably act as stress raisers, similar to notches, and decrease the fatigue resistance.

Bend ductilities, both longitudinal and transverse, were determined for these conditions. Four specimens were used for each test. Although the scatter of the data points was large, at least one specimen in the 1560°F and 1830°F annealed conditions failed in a brittle manner. Average values are shown below.

Initial Annealing Temp. °F (Quenched From 1290)	Average Bend Radius, T
—	3.2
1560	8.5
1830	19.0

This indicates that the specimens slow-cooled to 1290°F and quenched are more susceptible to embrittlement than the speci-

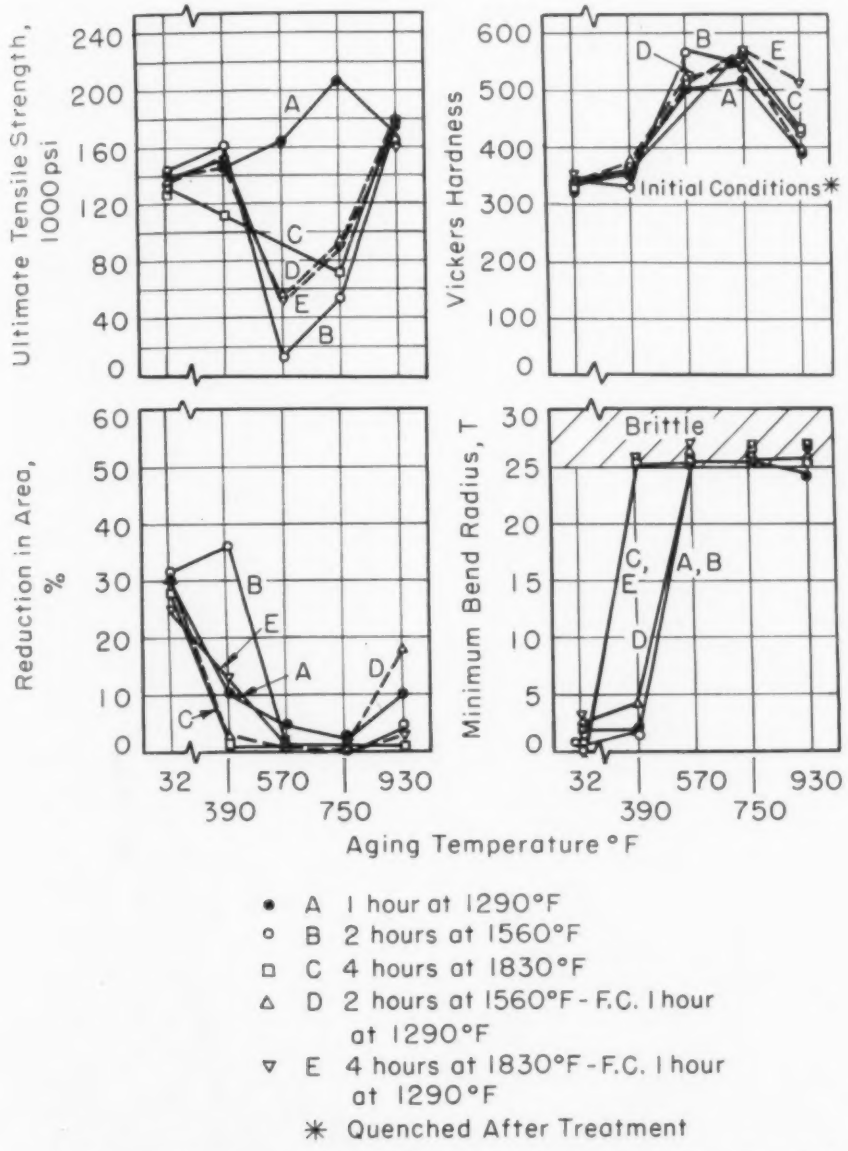


Fig. 16—Effect of Aging Temperature on the Properties of a Beta-Quenched Ti-7.5Cr-7.5Mo Alloy Aged for 200 Hours.

Table III
Fatigue Properties of a Ti-7.5Cr-7.5Mo Alloy Quenched from 1290°F

Heat Treatment	Mean Stress at 10^7 Cycles, psi		Tensile Strength, psi	Endurance-Limit Tensile-Strength Ratio	
	Unnotched	Notched		Unnotched	Notched
1 hr. at 1290°F and quenched	66,500 ± 5700	33,000 ± 4200	144,000	0.46	0.23
4 hr. at 1830°F, furnace-cooled to 1290°F, held 1 hr. at 1290°F, and quenched	48,000 ± 1400	32,900 ± 1400	138,000	0.35	0.24

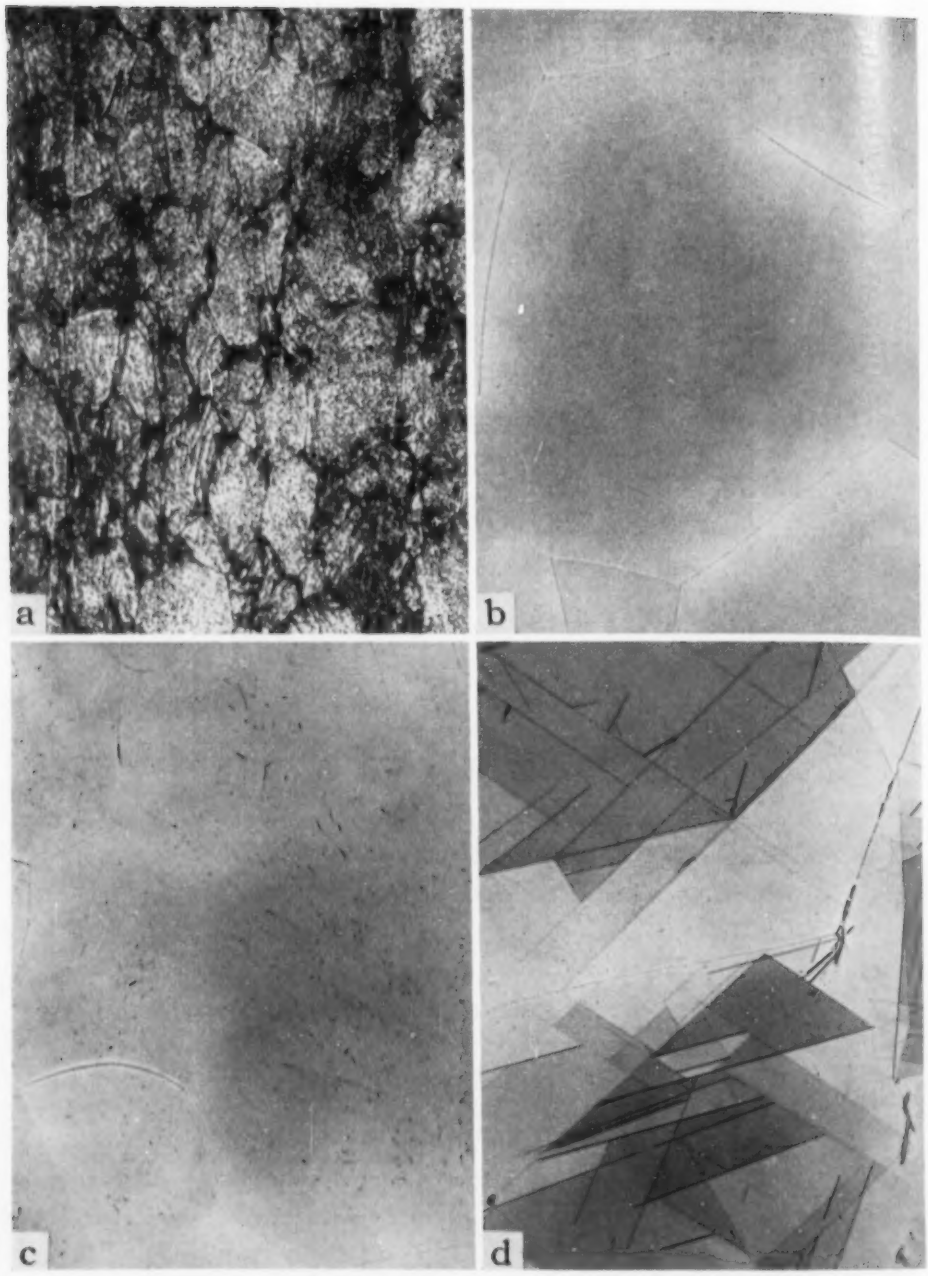


Fig. 17—Microstructures of a Ti-7.5Cr-7.5Mo Alloy in Aged Conditions. (a)—1 Hour at 1290°F and Quenched Plus 200 Hours at 750°F; (b)—2 Hours at 1560°F and Quenched Plus 200 Hours at 750°F; (c)—4 Hours at 1830°F and Quenched Plus 200 Hours at 750°F; (d)—4 Hours at 1830°F, Furnace-Cooled to 700°C (1290°F), Held 1 Hour and Quenched, Plus 400 Hours at 750°F. ×250.

mens annealed at 1290°F and quenched. This, again, points out the detrimental effect on properties of the alpha plates in the microstructure.

Impact-energy values at room temperature decrease with an increase in beta-grain size. This is pointed out further by the transi-

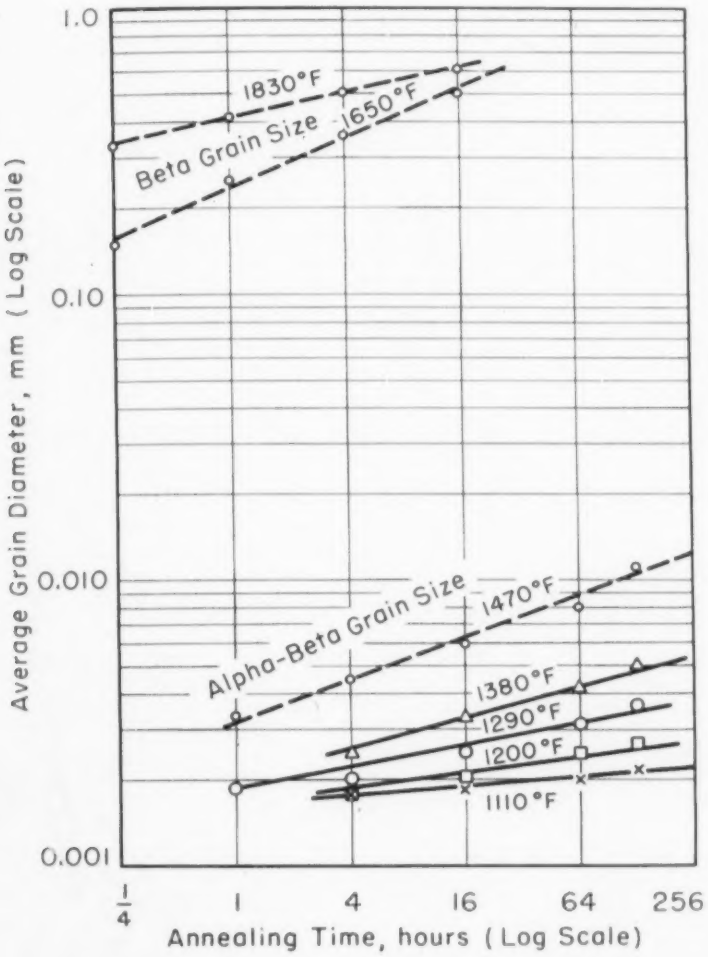


Fig. 18—Effect of Annealing Temperature and Time on the Grain Size of a Ti-2.5Cr-2.5Mo Alloy.

tion behavior, shown in Fig. 15. The energy level is lower and the transition temperature is higher for the specimens with the larger beta-grain sizes. This behavior is opposite to that observed for the same alloys when the alpha phase is not present, again illustrating the detrimental effect of the alpha plates in the structure.

Stability of the Metastable-Beta Alloy

To evaluate the stability of this alloy, a series of stability checks was made on the five conditions previously described. The stability checks were made, using 100-hour treatments at 390, 570, 750, and 930°F. The evaluation was made on a single sheet tensile specimen and a longitudinal bend test specimen. The results of these tests are presented in Fig. 16.

In almost every case, ductility is markedly decreased by the 100-hour treatment. Some ductility remains after the 390°F treat-

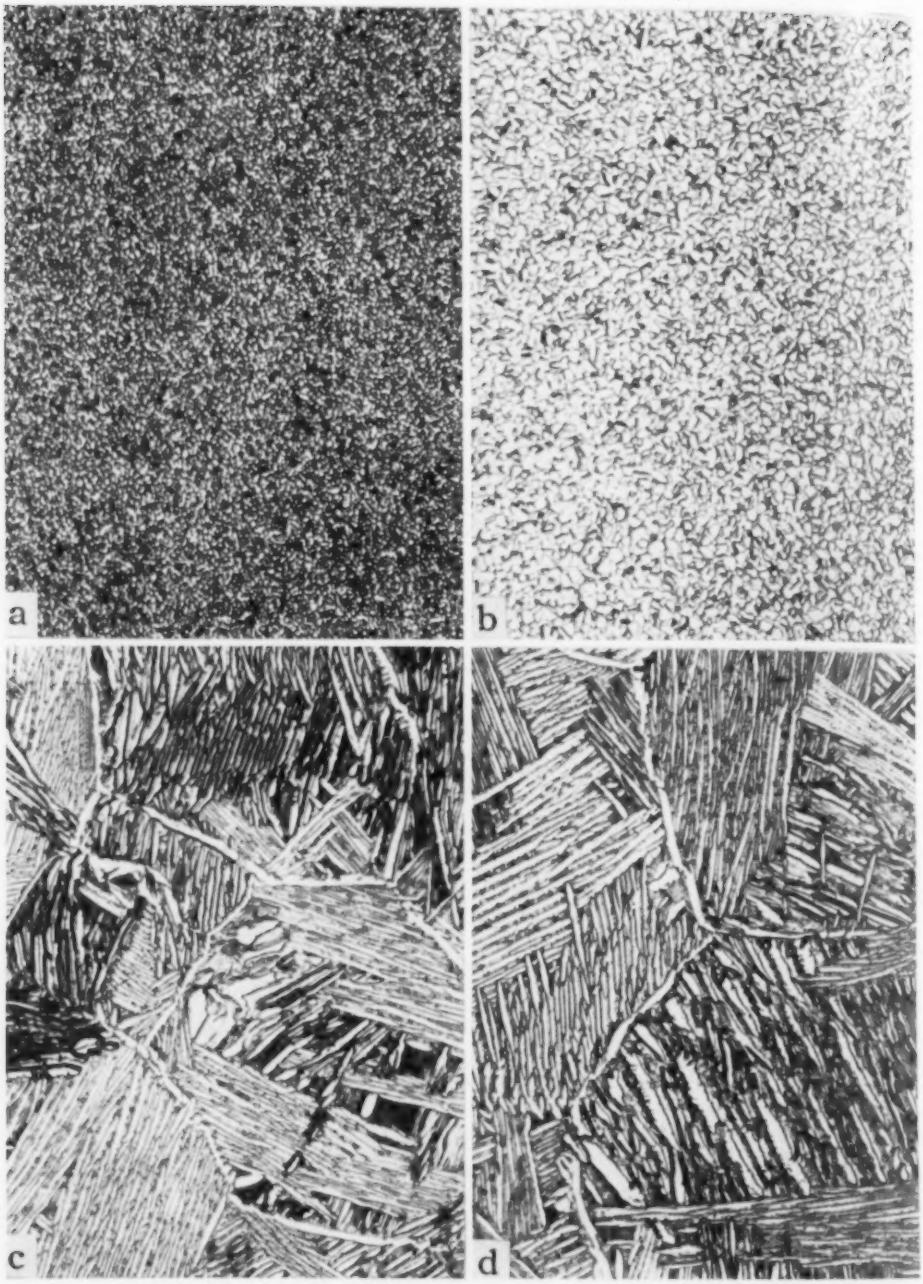


Fig. 19—Microstructures of a Ti2.5Cr-2.5Mo Alloy. (a)—Annealed 1 Hour at 1380°F, Furnace-Cooled to 1200°F, and Air-Cooled; (b)—Annealed 64 Hours at 1380°F, Furnace-Cooled to 1200°F, and Air-Cooled; (c)—Annealed ½ Hour at 1650°F, Furnace-Cooled to 1380°F, Held 1 Hour, Furnace Cooled to 650°C (1200°F), and Air-Cooled; (d)—Annealed 1 Hour at 1830°F, Furnace-Cooled to 1380°F, Held 1 Hour, Furnace-Cooled to 1200°F, and Air-Cooled. ×250.

ment. Embrittlement is very severe at 570 and 750°F, and overaging is apparent after the 930°F treatments. Hardness values increase to a maximum at 570 to 750°F, and decrease as the temperature is increased to 930°F. Tensile strengths do not follow the same

pattern because of the excessive embrittlement. Bend ductilities are lowered to a minimum at 570 to 750°F, and some ductility is recovered by overaging at 930°F.

The effects of prior condition on stability are not entirely clear from these data. In general, the stability of specimens with large beta-grain sizes appears to be less than that for the smaller beta-grain size. This is also observed in the microstructures, in which the alpha precipitation appears to be more extensive for the larger beta-grain sizes for any one stability check. This is shown in Fig. 17. The unusual microstructure of Fig. 17d is composed of alpha plates formed during the 1290°F anneal. The dark-etching alpha precipitate formed during the subsequent exposure at 750°F.

A more complete evaluation of stability was made on samples annealed for 100 hours at 570°F after initially quenching from 1290°F. The results, as compared with the as-quenched condition, are given in Table IV.

Table IV
Mechanical Properties of a Ti-7.5Cr-7.5Mo Alloy Before and After Aging at 570°F

Property	Annealed 1 Hour at 1290°F and Water-Quenched	Annealed 1 Hour at 1290°F and Water-Quenched; Annealed 100 Hours at 570°F and Water-Quenched
Vickers Hardness	334	484
Ultimate Tensile Strength, psi	143,000	111,000–163,000
0.2% Offset Yield Strength, psi	135,000	—
Reduction in Area, %	34	0
Elongation, %	16	0
Notched Tensile Strength, psi	217,000	101,000
Notched Reduction in Area, %	7	5
Minimum Bend Radius, T	3	>24 (Brittle)
Room-Temperature Impact Energy, inch-pounds	10	2
Endurance Limit (10^7 Cycles), psi		
Unnotched Specimen	66,500 (±5800)	68,100 (±26,200)
Notched Specimen	33,000 (±4200)	39,500 (±3400)

The lack of tensile ductility accounts for the erratic tensile strength observed for the 570°F treated specimens. Vickers hardness values are increased from an average of 334 to 484, indicating that considerable aging is taking place as a result of beta instability. Tensile and bend ductilities are reduced, as is the room temperature impact resistance. The ratio of notched to unnotched tensile strength is difficult to evaluate because of erratic behavior. However, it is definitely reduced from about 1.5 to less than 1.0, indicating a change to a notch-sensitive condition. Unlike the tensile and bend properties, the fatigue endurance limit is not changed significantly by the aging treatment. Thus, it appears that the embrittlement caused by the low temperature precipitation of alpha is not shown up by fatigue tests. However, appreciable scatter was obtained in the endurance limits of these samples, with the greatest deviations occurring for the unnotched specimens in the aged condition.

Alpha-Beta Alloy (Ti-2.5Cr-2.5Mo)

This alloy was selected as an example of an alpha-beta-type alloy. The beta transus is at about 1515°F, and beta of this composition transforms to martensite on quenching. The fabrication of this alloy was completed in the alpha-beta field, so that an equiaxed-alpha-beta structure could be produced by subsequent anneals. An acicular type of structure may be produced by first annealing in the beta field and then equilibrating in the alpha-beta field. Microstructural variables include the grain size and shape of the equilibrated alpha-beta structures, and the prior beta-grain size of the transformed structures.

The heat treatments in the alpha-beta field may be designated as equilibrating or as stabilizing treatments. An equilibrating treatment is usually done at a relatively high temperature and has the effect of decreasing the alpha-to-beta ratio as the equilibrating temperature increases. A stabilizing treatment may consist of either an isothermal anneal or a slow cooling or step-cooling process, finishing at a relatively low temperature in the alpha-beta field. Its primary objective is to reject sufficient alpha so that subsequent heating in the service-temperature range of 570 to 930°F will not cause precipitation of fine alpha, with a resultant loss in ductility.

Grain Size and Microstructure

The testing program for the Ti-2.5Cr-2.5Mo alloy was carried out, using two equiaxed-alpha-beta-grain sizes and equilibrated acicular-alpha-beta structures of two prior beta-grain sizes. The effects of annealing time and temperature on grain size were studied, and the results are shown graphically in Fig. 18. The equiaxed-alpha-beta-grain sizes are small, and the rate of grain growth increases with increasing annealing temperature. Beta-grain sizes are much larger, and the rate of growth decreases as the annealing temperature is increased. Typical microstructures are presented in Fig. 19.

Mechanical Properties

The unnotched tensile strength of the alpha-beta alloy, as shown in Fig. 20, is not affected appreciably by either the shape or the size of the alpha-beta structure. Yield strengths, except for the small equiaxed alpha-beta structure, also are relatively unaffected by microstructure. The increased yield strength observed for the small equiaxed alpha-beta structure may be the result of yield-point behavior observed in this condition. The yield point was observed in this alloy only for the shortest annealing time at lowest annealing temperature, 1 hour at 1380°F. The factors governing its appearance are not known. Such behavior usually is associated with interstitial additions, but is not uncommon in alpha-beta alloys.

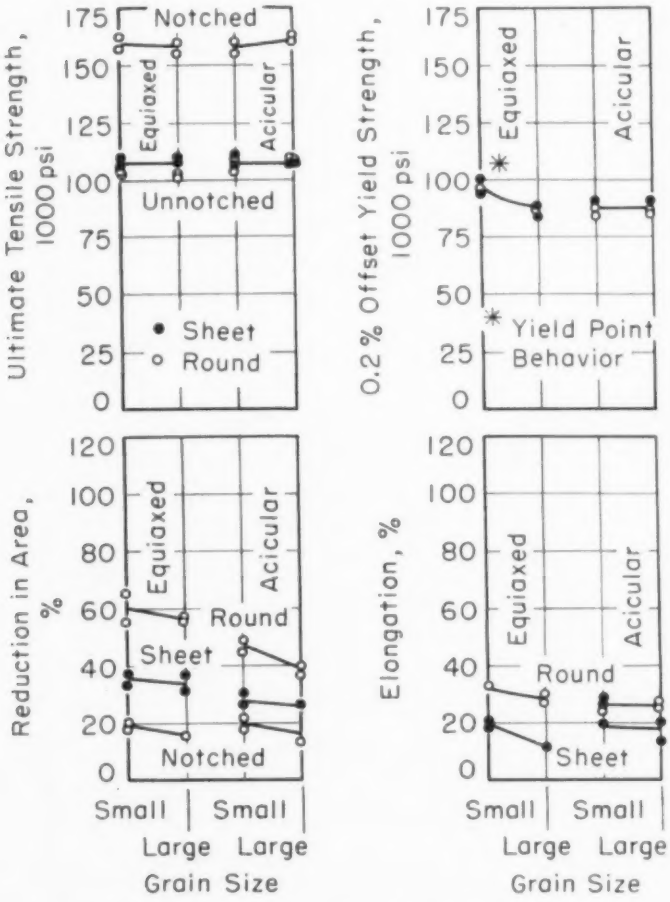


Fig. 20—Effect of Alpha-Beta Grain Size and Shape on Tensile Properties of a Ti-2.5Cr-2.5Mo Alloy.

Ductilities, particularly reductions in area, are higher for the equiaxed than for the acicular-type structures. Ductilities also are better for the finer grained equiaxed alpha-beta specimens than for the coarse-grained specimens.

The ratio of notched to unnotched tensile strength varies from 1.50 to 1.55, indicating no structural effect and a generally notch-insensitive condition. Although the reduction-in-area values of unnotched equiaxed specimens are greater than those of the unnotched acicular specimens (about 60% as compared with 45%), the reduction in area of notched specimens is about the same in both conditions, about 20%. These high reduction-in-area values for notched tensile specimens also indicate lack of notch sensitivity at room temperature.

The results of the fatigue tests are given in Table V. Except for the small-acicular-grain-size condition (½ hour at 1650°F), there is no significant change in endurance limit of both the notched and

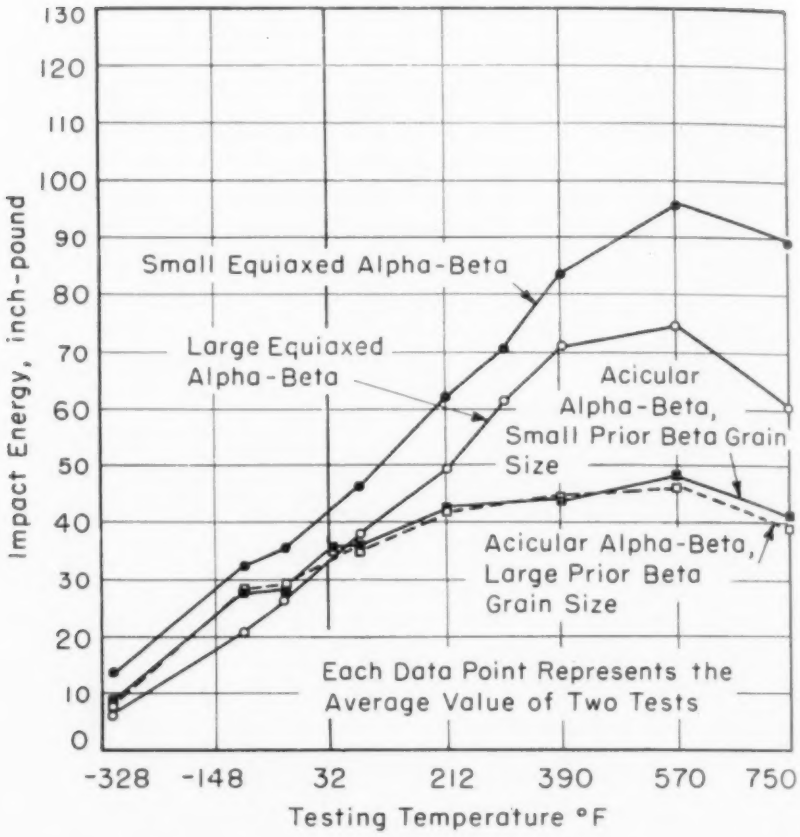


Fig. 21—Effect of Testing Temperature on Impact Behavior of a Ti-2.5Cr-2.5Mo Alloy in the Equiaxed and Acicular Alpha-Beta Conditions.

unnotched specimens with change in microstructure. The unnotched endurance limit for the small-acicular-grain-size condition is the highest obtained for this alloy. The ratio of endurance limit to tensile strength is excellent for all conditions, ranging from 0.44 to 0.55 for the unnotched condition and from 0.26 to 0.29 for the notched condition. These data show that alpha-beta alloys can be produced that have high endurance-limit ratios.

Bend ductility, both longitudinal and transverse, was found to be high for both equiaxed and acicular conditions, as shown below:

Microstructural Condition	Average Bend Radius, T
Fine equiaxed alpha-beta	0.7
Coarse equiaxed alpha-beta	1.0
Acicular alpha-beta, small prior beta-grain size	0.9
Acicular alpha-beta, large prior beta-grain size	1.1

No dependence of bend ductility on microstructure or rolling direction was observed.

The room temperature impact resistance was found to be greater for small than for large equiaxed-grain sizes. Also, the specimens

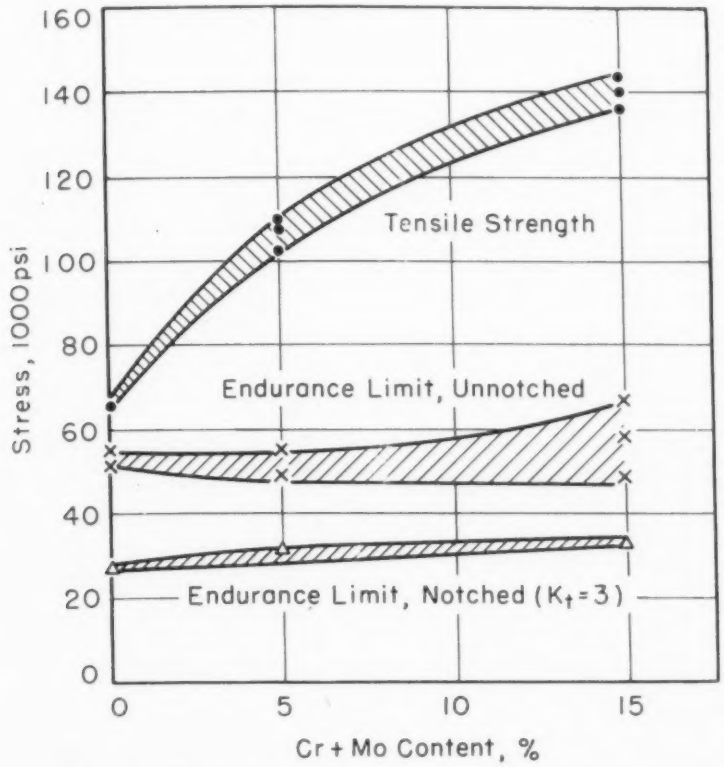


Fig. 22—Effect of Alloy Content on the Fatigue Properties of Ti-Cr-Mo Alloys.

with equiaxed structures are more resistant to impact than those with acicular structures. The effects of grain size and shape on impact-energy values are more pronounced at higher temperatures. This is illustrated by the curves of Fig. 21.

Table V
Fatigue Properties of a Ti-2.5Cr-2.5Mo Alloy

Heat Treatment	Mean Stress at 10^7 Cycles, psi		Tensile Strength, psi	Endurance-Limit Tensile-Strength Ratio	
	Unnotched	Notched		Unnotched	Notched
1 hr. at 1380°F, furnace-cooled to 1200°F, air-cooled	48,200 ± 1300	31,500 ± 2600	109,000	0.44	0.29
64 hr. at 1380°F, furnace-cooled to 1200°F, air-cooled	49,100 ± 2900	27,800 ± 2100	102,000	0.48	0.27
½ hr. at 1650°F, furnace-cooled to 1380°F, held 1 hr., furnace-cooled to 1200°F, air-cooled	55,000 ± 4000	27,200 ± 1300	106,000	0.52	0.26
1 hr. at 1830°F, furnace-cooled to 1380°F, held 1 hr., furnace-cooled to 1200°F, air-cooled	48,000 ± 3800	28,200 ± 1700	108,000	0.45	0.26

The impact resistance of equiaxed alpha-beta specimens increases almost linearly with testing temperature up to about 570°F, with higher values apparent for the smaller grain size. Impact-energy values for the specimens with acicular structures also increase with testing temperature, but much less rapidly. In the acicular structures, no effect of prior beta-grain size is apparent.

The impact-energy-temperature curves of this type are typical of alpha-beta alloys, and illustrate a condition between transition (beta) and nontransition (alpha) behavior. The advantage of the fine-grained equiaxed alpha-beta structure is apparent from these data.

Summary

For unalloyed titanium, grain size or shape has only a minor effect on the mechanical properties. Yield strengths are decreased slightly for specimens annealed in the alpha-beta range because of the partition of impurities to the nonmatrix alpha. Impact resistance is highest for the smallest alpha-grain sizes. Bend ductility and tensile ductility are excellent for all grain sizes. The fatigue endurance limit at 10^7 cycles is 79% of ultimate strength for unnotched and 42% for notched specimens.

The grain size of the metastable-beta alloy (Ti-7.5Cr-7.5Mo) also has only a minor effect on the mechanical properties so long as the alloy is single phase. The presence of alpha in the structure lowered the bend ductility, tensile ductility, and impact resistance. Notched fatigue properties appear to be relatively unaffected by changes in grain size or microstructural condition. The plates of alpha phase in the beta matrix act as stress raisers similar to notches and lower the unnotched endurance limit.

The alpha-beta alloy (Ti-2.5Cr-2.5Mo) was tested in the stabilized condition so that the only variables would be grain size and grain shape. Only minor changes in properties occurred as a result of changing the alpha-beta grain size. Strengths were unaffected by changing grain shape, although the equiaxed alpha-beta specimens had higher tensile ductilities and impact resistance than the acicular alpha-beta specimens. The fatigue endurance limits generally were unaffected by grain size or shape. The unnotched fatigue strength was 34% of the ultimate tensile strength, and the notched fatigue strength was 20% of the ultimate tensile strength.

One interesting observation on the fatigue properties of the alloys studied is shown in Fig. 22. The fatigue endurance limit of the alloys appears to be unchanged, regardless of alloy content, although the tensile strength is greatly increased as a result of alloy content. Thus, these data indicate that the fatigue endurance limit of titanium, at least for rotating-beam tests, probably will not be increased greatly by alloying.

ACKNOWLEDGMENTS

The authors wish to thank W. S. Hyler and R. R. Spencer of Battelle's Applied Mechanics Division for conducting the fatigue tests. The work described in this paper is based on research done at Battelle Memorial Institute under Air Force Contract No. AF 33(616)-412. The authors are grateful to the Materials Laboratory, Wright Air Development Center, for permission to publish this information.

References

1. F. C. Holden, H. R. Ogden, and R. I. Jaffee, "Microstructure and Mechanical Properties of Iodide Titanium," *Transactions*, American Institute of Mining and Metallurgical Engineers, Vol. 197, 1953, p. 238.
2. J. P. Romualdi and E. D'Appolonia, "Research and Development of Effect of Range of Stress and Prestrain on the Fatigue Properties of Titanium and Its Alloys," Final Report for Office of Chief of Ordnance, Research and Development Branch, October 1952, Contract No. DA-36-061-ORD-68.
3. H. R. Ogden, R. I. Jaffee and F. C. Holden, "Structure and Properties of Ti-C Alloys," *Transactions*, American Institute of Mining and Metallurgical Engineers, Vol. 203, 1955, p. 73.
4. R. I. Jaffee, F. C. Holden and H. R. Ogden, "Mechanical Properties of Alpha Titanium as Affected by Structure and Composition," *Transactions*, American Institute of Mining and Metallurgical Engineers, Vol. 200, 1954, p. 1282.
5. H. R. Ogden, F. C. Holden and R. I. Jaffee, "Effect of Alpha Solutes on the Heat-Treatment Response of Ti-Mn Alloys," *Transactions*, American Institute of Mining and Metallurgical Engineers, Vol. 203, 1955, p. 105.

DISCUSSION

Written Discussion: By Donald C. Buffum, Watertown Arsenal, Watertown, Mass.

In the presentation of data you stated that the presence of alpha caused decreases in the mechanical properties. Since alpha is present in the microstructure, it would indicate that the beta has decomposed and that it would be possible for omega to be present. Could the presence of omega cause the decreases which were obtained? Did you check for the presence of omega?

Authors' Reply

In the tests that were conducted on the metastable-beta alloy, it was noted that the presence of small amounts of alpha phase obtained by annealing just below the beta transus had a deleterious effect on ductility and toughness. In addition, it was noted that the shape and distribution of this alpha phase affected toughness particularly. We believe these effects to be directly attributable to the presence of a small amount of acicular alpha phase in the grains and grain boundary areas, and not to the presence of omega. The interstitials would tend to concentrate in the alpha and make it less ductile. Thus, the alpha platelets would act as though they were internal stress concentrators.

The alpha phase that can be seen in the microstructures of Fig. 13 is formed at the annealing temperature, which was 700°C (1290°F). This temperature is much higher than the temperature range of 200 to 500°C (390 to 930°F), where omega formation generally occurs. Thus, it would not be expected that annealing

this alloy at 700°C (1290°F) would involve the beta-to-omega reaction. It is possible that omega formation could occur during the subsequent quench to room temperature. Two factors would suggest that this is not the case. First, the beta alloy content of this alloy (Ti-7.5Cr-7.5Mo) is much higher than that where omega formation occurs on quenching from the beta field, and, second, the formation of omega is invariably accompanied by marked hardening. No such hardening occurred in these samples. More typical of the effects of omega formation are the properties shown in Fig. 16, where extreme hardening is found when the metastable-beta alloy is reheated at temperatures of 200 to 500°C (390 to 930°F).

We did not check for the presence of omega in these alloys for the reasons set forth above. We do not believe that the loss in ductility and toughness of the Ti-7.5Cr-7.5Mo alloy annealed at 700°C (1290°F) is caused by omega, but believe it is directly associated with the presence of small amounts of acicular alpha phase, in which the interstitial concentration was concentrated by alpha-beta partition.

INVESTIGATION OF THE HEAT TREATABILITY OF THE 6% ALUMINUM-4% VANADIUM TITANIUM-BASE ALLOY

By R. G. Sherman and H. D. Kessler

Abstract

Heat treatment, stress-stability, section size, elevated temperature tensile and fatigue studies were carried out on material from production ingots of the Ti-6Al-4V alloy. The results show that the alloy is moderately heat treatable; in ½-inch sections, tensile strengths from 130,000 to 175,000 psi and yield strengths from 100,000 to 165,000 psi combined with high ductilities may be obtained. The alloy is stable under stress to 800° F and has excellent tensile properties at this temperature; its fatigue endurance ratio is greater than 0.55 for the heat treatments evaluated. (ASM-SLA Classification: J general, Q general, Ti)

THE Ti-6Al-4V alloy was developed by the Armour Research Foundation under government sponsorship. Early studies showed it to have an excellent combination of tensile strength and ductility with good resistance to impact, and high strength at elevated temperatures. Production of the alloy was initiated early in 1954; and at the present time, the alloy is one of the most popular of the commercial compositions. It is being used in large quantities in ordnance, airframe and aircraft engine applications; and is currently available as wire, sheet, bar and forging billet mill products.

This paper presents the results of an extensive study by the Titanium Metals Corporation of America of the heat treating characteristics of the alloy, with special emphasis on solid solution plus aging heat treatments. Effect of section size on the tensile properties obtained by these duplex heat treatments, stability under stress at elevated temperatures, short-time elevated temperature properties, and some fatigue data are presented. All results were obtained on material from production ingots of the Ti-6Al-4V alloy.

Experimental Procedure

Rolling Practice and Forging Practice

All the data in this paper other than the work on effect of section size were obtained on material rolled to 0.550-inch round, using

A paper presented before the Thirty-Seventh Annual Convention of the Society, held in Philadelphia, October 17–21, 1955. Of the authors, R. G. Sherman is research metallurgist, and H. D. Kessler is supervisor, Metallurgical Division, Technical Department, Titanium Metals Corporation of America, Henderson, Nevada. Manuscript received April 25, 1955.

a 30% reduction in area following the final reheat. A pre-heating temperature of 1700°F was used, except for the work on the effect of rolling temperature.

The section size data was obtained on material forged from a 3¾-inch diameter section. One forging schedule, from 1850°F, resulted in a 35% reduction in area to each size following the final reheat. Six-inch lengths of these sections were heat treated at 1750°F (1 hr.) WQ, cut in half, and 3-inch lengths aged at 1100°F (24 hrs.). The second forging schedule, from 1750°F, resulted in a 60% reduction in area after the last reheating operation. These sections were heat treated at 1550°F (1 hr.) WQ, cut in two, and one-half aged at 1000°F (24 hrs.). Tensile specimens were machined from the centers of all sections and from the edges of the larger sizes.

Delayed Water and Jominy End Quench

To study the effect of a delayed water quench from the solution temperatures, specimens removed from the furnace were air-cooled 3, 6, 10, 15, 25, 40, 60 and 100 seconds, and then water-quenched.

A ½-inch diameter by 4-inch long sample was used in conjunction with a 7/32-inch water jet for the end-quench hardenability test from 1550°F. Vickers hardness tests were made with a diamond penetrator and a 10-kilogram load. The end quenched bar was then aged at 900°F (24 hrs.) and hardness measurements made again.

Stress-Stability and Fatigue

Test bars were stressed at 50,000 psi in stress-rupture units at temperatures of 600 and 800°F. The specimens were measured for length before and after the stability tests to obtain total deformation measurements; after 200 hours, the bars were removed and tensile tested at room temperature.

The fatigue testing was carried out on hand polished specimens run at 10,000 RPM on Moore rotating beam machines.

Tensile Specimens

All tensile testing was done on 0.250-inch diameter, 1-inch gage length specimens tested at a head speed of 0.05-in/minute. The 0.2% yield strengths were obtained using a Peters microformer extensometer.

Material

The table below lists the chemical analyses of the two ingots used for this study. Both ingots were made with TMCA 140 BHN sponge.

	Al,%	V,%	Fe,%	N_2,%	C,%	H_2,%
1.	6.26	4.13	0.102	0.013	0.021	0.006
2.*	6.09	4.06	0.147	0.013	0.015	0.004

*(Fatigue tests only)

Discussion

Rolling Temperature—The as-rolled tensile strength varied inversely and the ductility varied directly with rolling temperature. However, there was little difference in the strength levels of the heat treated conditions (See Fig. 1). Because of somewhat lower ductilities of specimens rolled at 1800°F, 1700°F was selected as the best

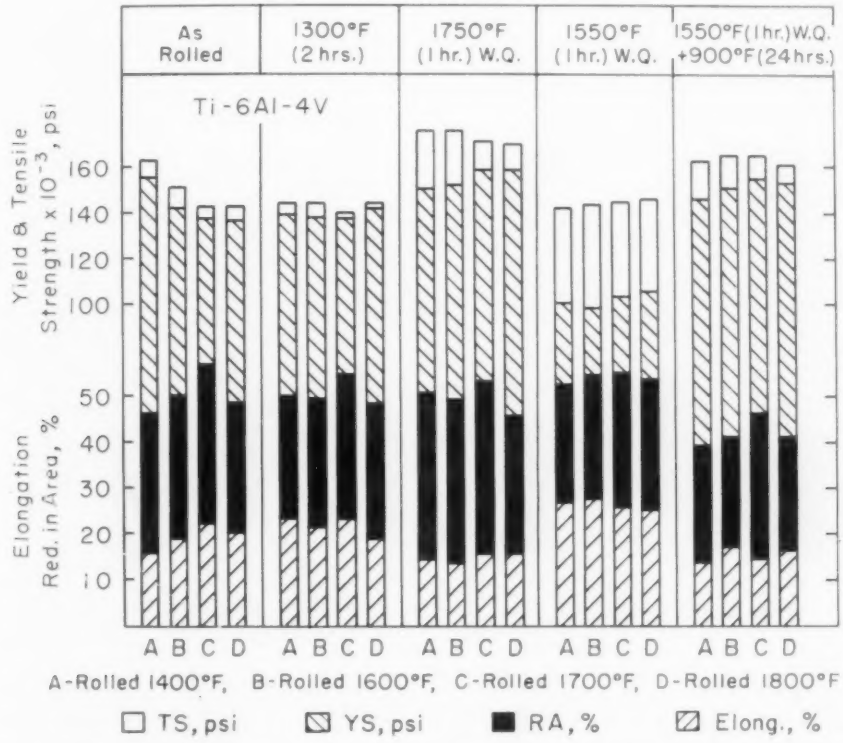


Fig. 1—The Effect of Rolling Temperature on Variously Heat-Treated Specimens.

temperature for ease of rolling compatible with good mechanical properties.

Solution Treatment—The beta transus temperature, established by metallographic examination, was 1825°F ± 15°F for the two heats studied. To determine the effect of various solution temperatures, a series of specimens were heated for 1 hour at temperatures between 1300 and 1850°F, and water-quenched (See Table I and Fig. 2). The 1550°F temperature was selected for further investigation of duplex heat treatments, because the minimum yield-tensile strength ratio of about 0.7 was obtained. In this low yield strength, soft condition, the material offers the advantages of good machinability and excellent low temperature formability, and can be subsequently aged to maximum strength levels. The other solution temperature selected was 1750°F because this treatment gave an excellent combination

Table I
Effect of Solution Temperature on Tensile Properties of Ti-6Al-4V

Heat Treatment	U.T.S., psi	Y.S.(0.2%) psi	Elong., %	R.A., %	Hardness R_a	YS/TS
1300°F(1 hr.)WQ	139,000	137,500	21	53	33	0.99
1400°F(1 hr.)WQ	135,000	124,000	20	56	33	0.92
1450°F(1 hr.)WQ	144,000	114,500	22	47	30	0.80
1500°F(1 hr.)WQ	141,000	101,000	22	53	33	0.72
1550°F(1 hr.)WQ	145,000	103,000	26	55	34	0.71
1600°F(1 hr.)WQ	148,000	119,000	23	55	34	0.81
1650°F(1 hr.)WQ	160,000	141,000	21	55	41	0.88
1750°F(1 hr.)WQ	172,000	148,500	15	53	43	0.86
1850°F(1 hr.)WQ	167,500	145,500	5	10	43	0.87

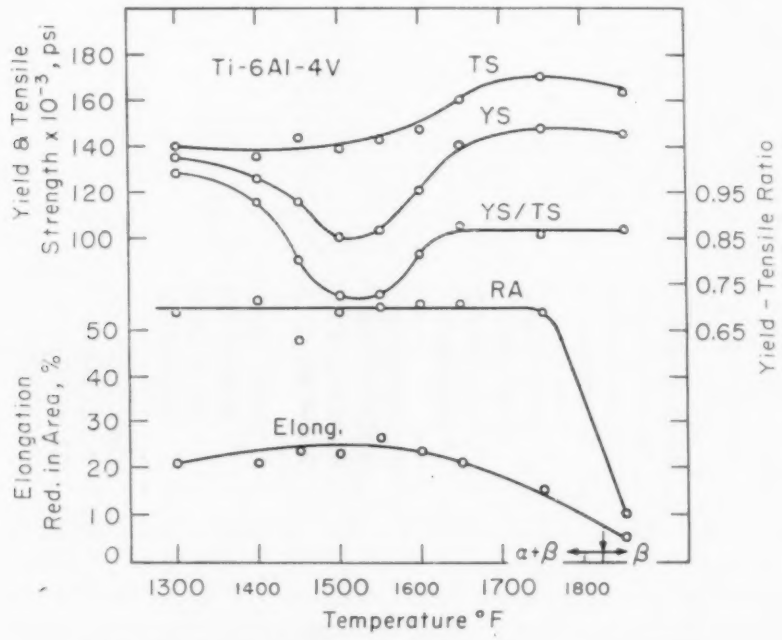


Fig. 2—The Effect of Solution Temperature on Tensile Properties.

of quenched properties and amenability to aging. Figs. 3 and 4 show the microstructures of the two solution-treated conditions.

Figs. 5 and 6 show the effect of a delayed water quench on the mechanical properties of specimens quenched from the two solution temperatures. There was no microstructural difference between any of the specimens given a delayed quench from 1550°F. The only effect of the delayed quench from this temperature is the loss of the low yield strength. Delaying the quench from 1750°F results in widely different properties, depending on the length of delay. The microstructures of the specimens delayed for longer times indicate that they had cooled below the Ms before quenching; and as a result, instead of an alpha prime background there was a coarse basket-weave alpha-beta structure. This structure became coarser for the longer time delays (Figs. 7,8,9). Although the mechanical proper-

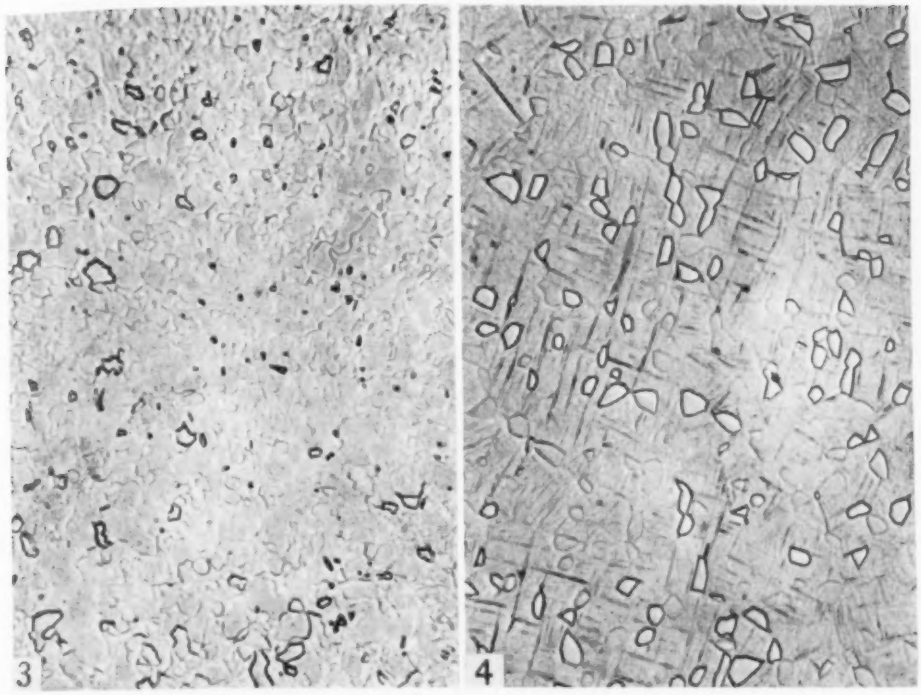


Fig. 3—Fine-grained Alpha Plus Retained Beta Structure. 1550°F (1 hr.) WQ ×500

TS psi	145,000
YS(0.2%) psi	103,000
Elong. %	26
R.A. %	55

Fig. 4—Small Amount of Primary Alpha in Transformed Beta Matrix. 1750°F (1 hr.) WQ ×500

TS psi	172,000
YS(0.2%) psi	148,500
Elong. %	16
R.A. %	53

ties of the specimen delayed 25 seconds before quenching were similar to those resulting from the 1550°F (1 hr.) WQ, the microstructures were quite different. (Compare Fig. 3 with Fig. 8). The results indicate that the composition of the beta prior to quenching is the governing factor in controlling the yield-tensile ratio.

The effect of time at solution temperature and cooling rates from these temperatures on tensile properties are shown in Table II. Times at the 1550°F solution temperature as short as 15 minutes

Table II
Effect of Total Time and Cooling Rate from Solution Temperature on the Tensile Properties of Ti-6A1-4V

Heat Treatment	U.T.S., psi	Y.S.(0.2%) psi	Elong., %	R.A., %	Hardness R_c
1550°F(¼ hr.)WQ	147,000	100,000	21	56	33
1550°F(½ hr.)WQ	146,000	97,000	21	55	32
1550°F(¾ hr.)WQ	147,000	97,500	22	55	31
1550°F(1 hr.)WQ	145,000	103,000	26	55	34
1550°F(24 hr.)WQ	136,000	112,000	25	55	32
1550°F(1 hr.)AC	144,000	123,500	21	50	35
1550°F(1 hr.)FC 50°/hr.	139,000	130,000	20	49	33
1750°F(1 hr.)FC 50°/hr.	134,500	124,000	20	44	33

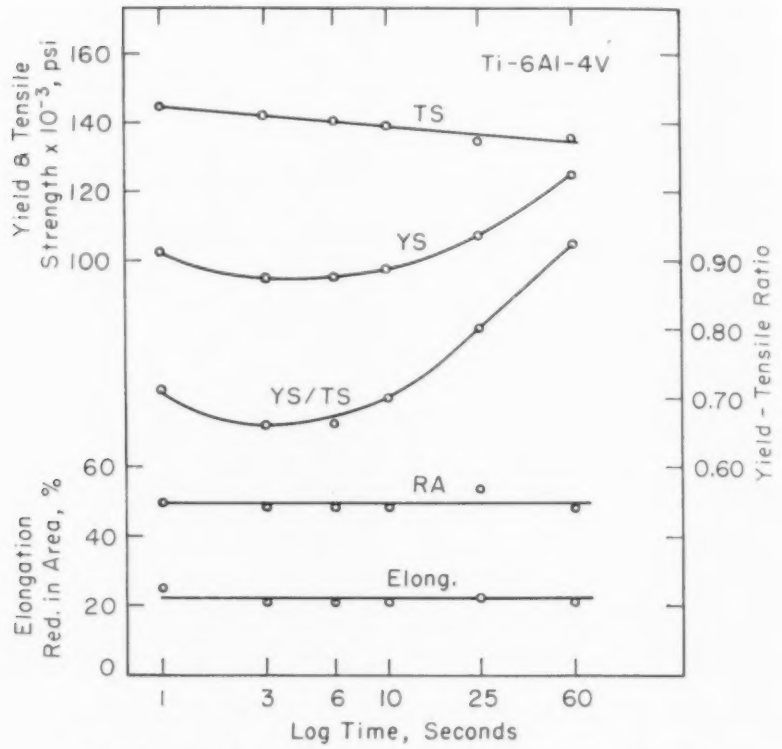


Fig. 5—The Effect of Delayed Water Quenching from 1550°F on the Tensile Properties.

produce properties similar to those obtained from 1 hour at temperature. However, the properties after 24 hours at the solution temperature were quite different. Fig. 10 shows the coarse-grained structure resulting from the longer solution treatment. As might be expected from viewing the delayed quench data, an air cool from 1550°F had no effect on the ductility and tensile strength, but raised the yield strength; indicating some aging had occurred. The very slow cooling rate (50°F/hr.) of the furnace cool from both 1550 and 1750°F produced very low strengths; the higher temperature treatment resulted in one of the lowest strength conditions obtained in the study.

Solution-Plus Aging Treatment—A low temperature aging treatment was investigated to simulate pickling conditions. The treatment of 400°F (½ hr.) slightly increased the yield strength of both solution treated conditions without effecting the tensile strength or the ductilities (See Fig. 11). Therefore, it is evident that solution-treated material can be descaled or pickled at temperatures to 400°F without significant aging occurring. The effect on the mechanical properties of 24-hour aging treatments at 900, 950, and 1000°F is presented in Fig. 11. It is interesting to note the differences in properties resulting from these small variations in aging temperatures. Figs. 12 and 13 show the typical aged structures following the two solution treatments.

Table III
Effect of Aging Treatments Following Various 1550 and 1750°F Treatments on the Tensile Properties of Ti-6Al-4V

Heat Treatment	U.T.S., psi	Y.S.(0.2%) psi	Elong., %	R.A., %	Hardness R_c
1550°F(1 hr.)WQ	145,000	103,000	26	55	34
1550°F(1 hr.)WQ + 900°F(24 hr.)	165,000	155,000	14	47	40
1550°F(1 hr.)WQ + 1000°F(24 hr.)	149,000	147,000	20	52	33
1550°F(1 hr.)AC	144,000	123,500	21	50	35
1550°F(1 hr.)AC + 900°F(24 hr.)	151,000	139,000	20	50	35
1550°F(1 hr.)AC + 1000°F(24 hr.)	143,000	140,500	23	54	34
1550°F(1 hr.)FC 50°F/hr.	139,000	130,000	20	49	33
1550°F(1 hr.)FC + 900°F(24 hr.)	137,000	137,000	19	51	33
1550°F(1 hr.)FC + 1000°F(24 hr.)	136,000	136,000	20	53	34
1750°F(1 hr.)FC 50°F/hr.	134,500	124,000	20	44	33
1750°F(1 hr.)FC + 900°F(24 hr.)	132,000	123,000	21	46	32
1750°F(1 hr.)FC + 1000°F(24 hr.)	133,000	124,000	23	44	32
1550°F(24 hr.)WQ	136,000	112,000	25	55	32
1550°F(24 hr.)WQ + 900°F(24 hr.)	154,000	140,000	18	44	38
1550°F(24 hr.)WQ + 1000°F(24 hr.)	153,000	144,000	19	43	36

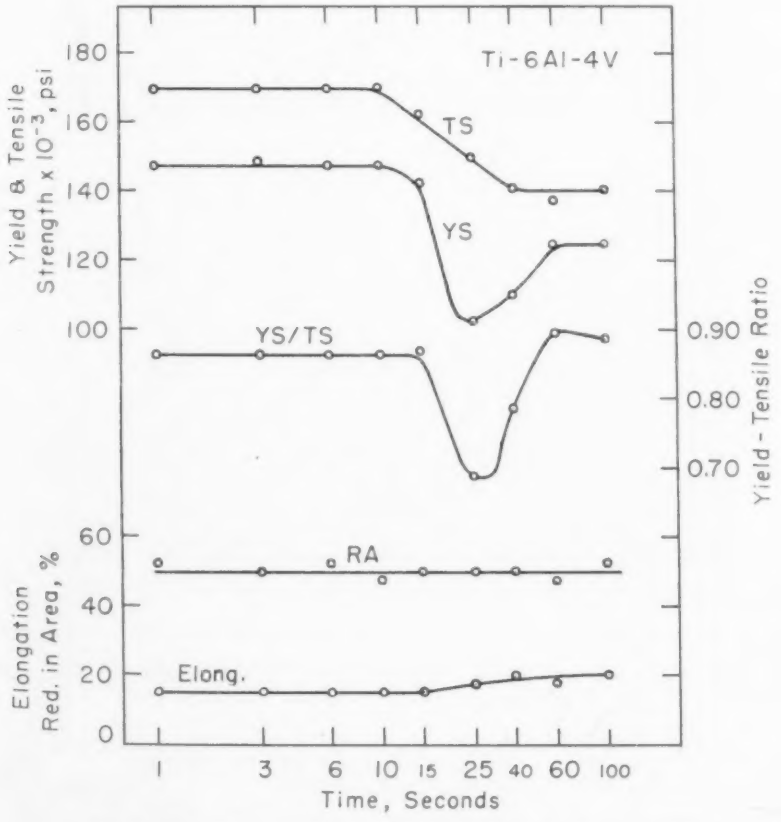


Fig. 6—The Effect of Delayed Water Quenching from 1750°F on the Tensile Properties.

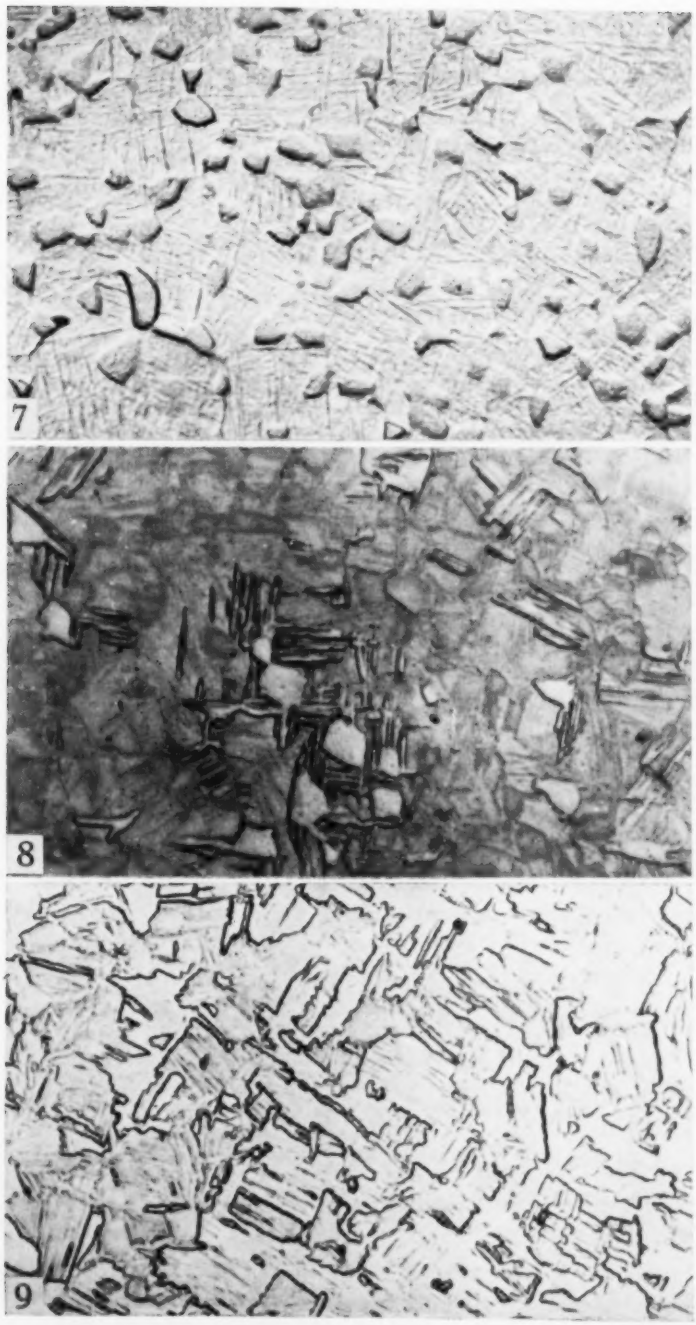


Fig. 7—Primary Alpha in Transformed Beta Matrix. 1750°F (1 hr.) Delay 6 Sec. WQ. ×750

Fig. 8—Primary Alpha in Basket-Weave Alpha-Beta Matrix. 1750°F (1 hr.) Delay 25 Sec. WQ. ×750

Fig. 9—Primary Alpha in Coarse Basket-Weave Alpha-Beta Matrix. 1750°F (1 hr.) Delay 60 Sec. WQ. ×750

Fig. 7		Fig. 8		Fig. 9	
TS psi	172,000	TS psi	149,000	TS psi	138,000
YS(0.2%) psi	148,000	YS(0.2%) psi	102,000	YS(0.2%) psi	124,000
Elong. %	15	Elong. %	18	Elong. %	17
RA %	54	RA %	49	RA %	46

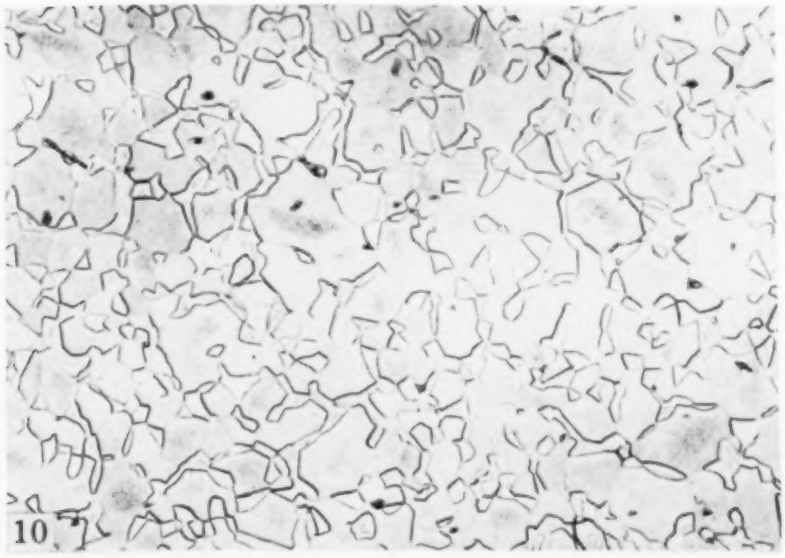


Fig. 10—Coarse Alpha Plus Beta Structure Resulting from Long Solution Treatment. Pattern in beta would indicate that some transformation has occurred. ×500. Heat treatment—1550°F (24 hrs.) WQ. Properties:—TS psi 139,000; YS(0.2%) psi 111,000; Elong. % 25; R A % 55.

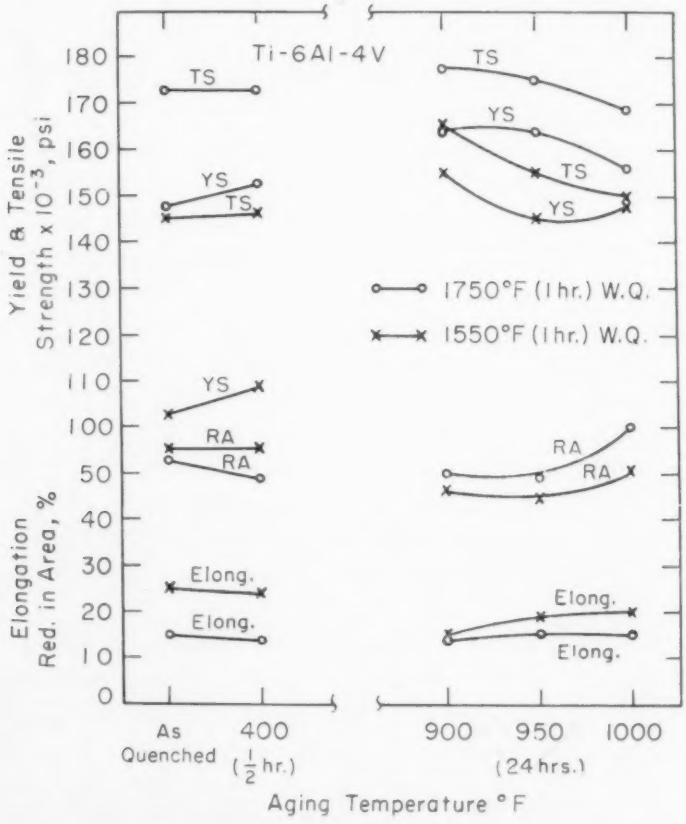


Fig. 11—The Effect of Various Aging Treatments on the Tensile Properties of Solution-Treated Specimens.

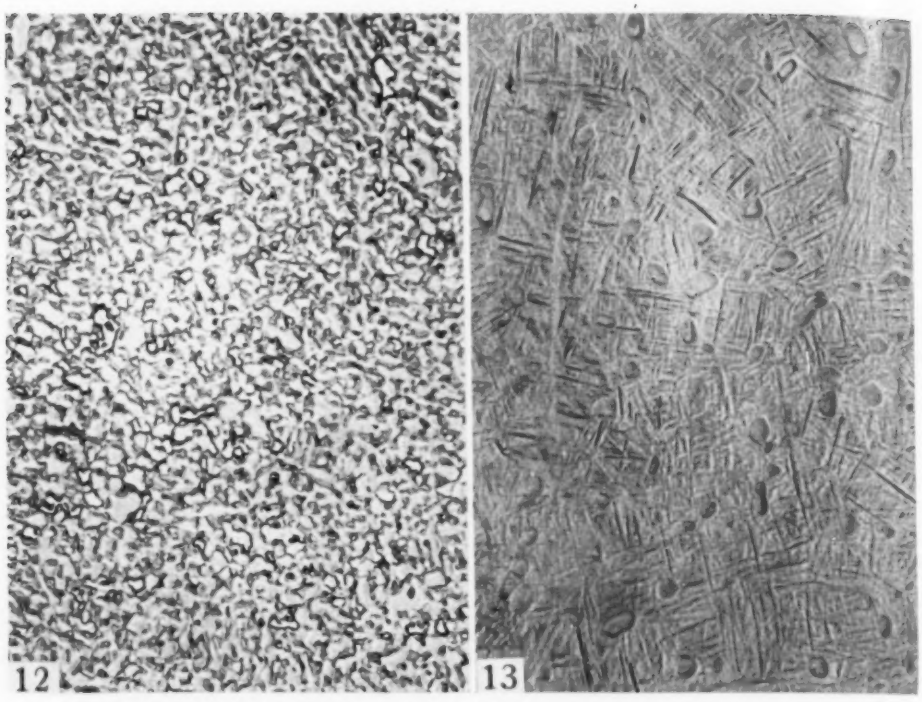


Fig. 12—Alpha and Age-Hardened Beta. (Compare with Fig. 3) ×500. Heat treatment —1550°F (1 hr.) WQ+1000°F (24 hrs.). Properties: TS psi 149,000; YS(0.2%) psi 147,000; Elong. % 20; R A % 52.

Fig. 13—Primary Alpha in an Aged, Formerly Alpha Prime-Beta Matrix. (Compare with Fig. 4) ×500. Heat Treatment-1750°F (1 hr.) WQ+1000°F (24 hrs.).

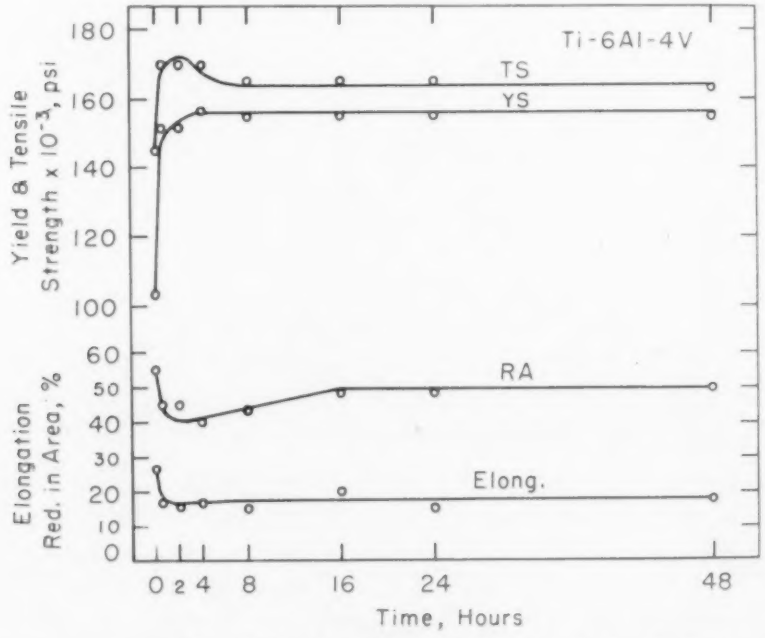


Fig. 14—The Effect of Aging Time at 900°F on the Tensile Properties of Specimens Solution-Treated at 1550°F.

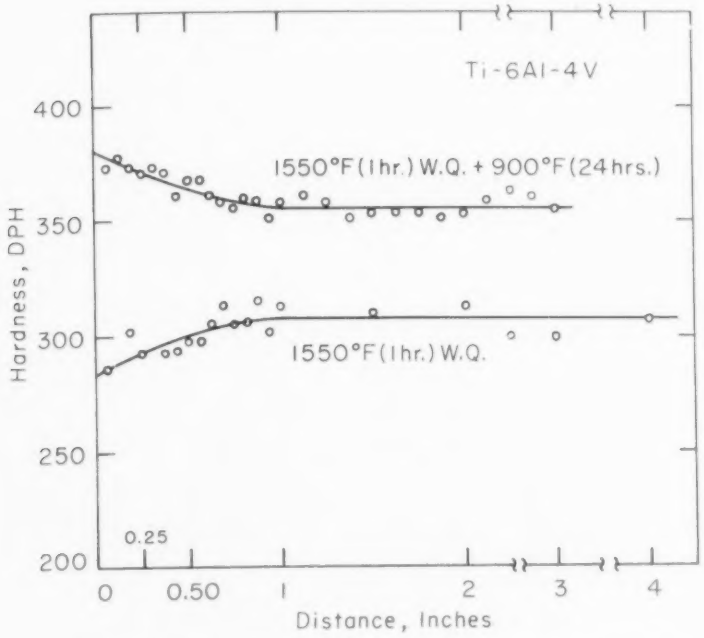


Fig. 15—The Effect of Aging on the Hardness of a Specimen End Quenched from 1550°F.

Age hardening relationships resulting from treatments of ½ hour to 48 hours duration at 900°F following the 1550°F solution treatment are shown in Fig. 14. The aging response at 900°F is quite rapid, inasmuch as the highest tensile and yield strengths were obtained at ½ hour. Thereafter, the tensile strength decreased while the yield strength remained constant.

Table III shows the effect of two 24-hour aging cycles following various 1550 and 1750°F treatments. It is evident from the lower strengths resulting from these two aging treatments after an air cool that water quenching is necessary for maximum retention of beta for subsequent aging. As might be expected, there was no aging response following a 1750°F (1 hr.) F.C.; however, some aging occurred following the 1550°F (1 hr.) F.C. as indicated by a slight decrease in tensile strength and an increase in yield strength. It is interesting to note that the aging response following a 24-hour solution treatment at 1550°F is not the same as that following a 1-hour solution treatment.

Effect of Section Size—From the limited hardenability investigation made, it is apparent that there is some strength advantage to be gained from aging solution-treated sections as large as 3¾-inch diameter. These results are also supported by the Jominy end quench data, which show that the sample increased in hardness after aging as far as 3½-inch from the quenched end (Fig. 15). The core

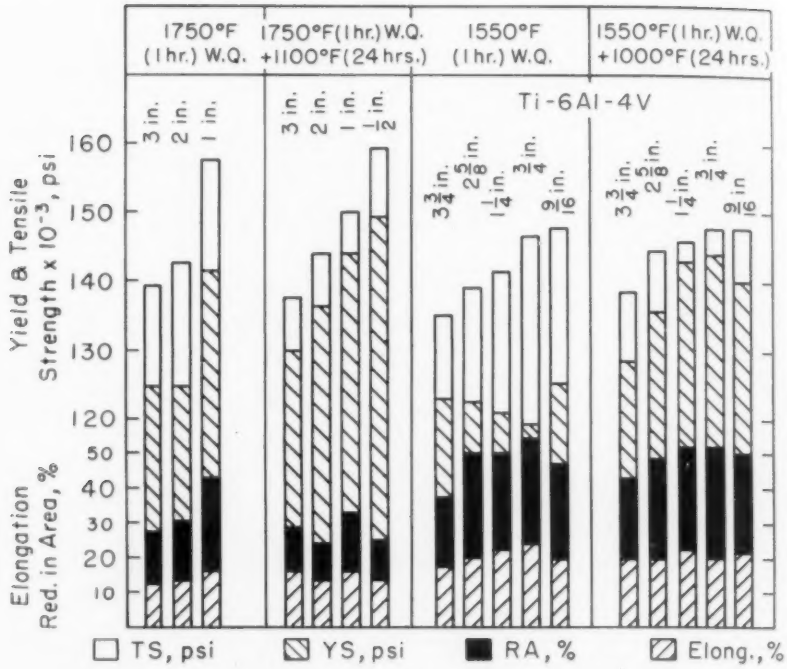


Fig. 16—The Effect of Section Size on the Tensile Properties.

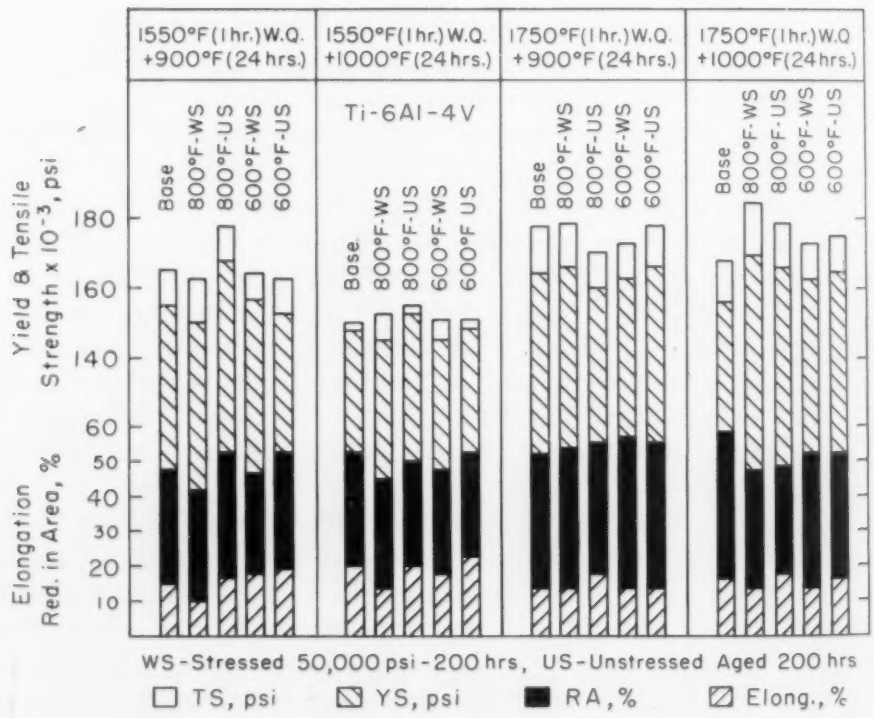


Fig. 17—Tensile Properties Before and After Stability Testing.

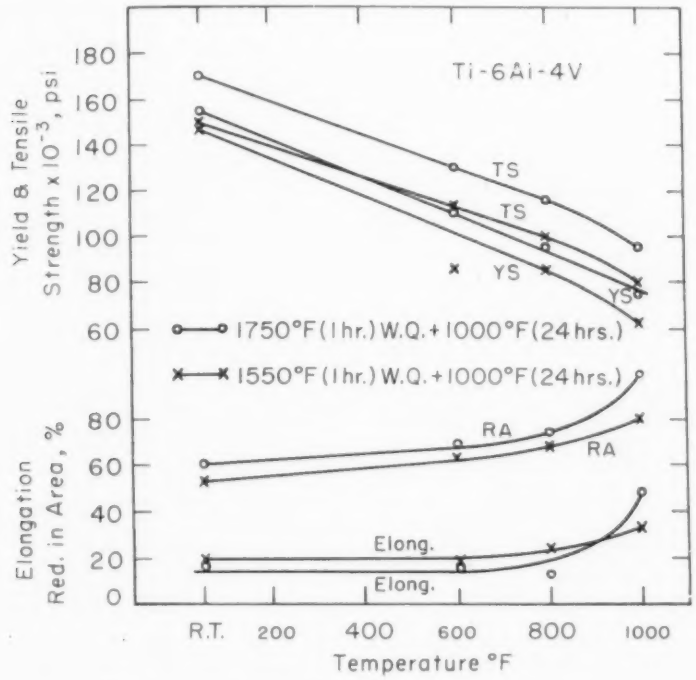


Fig. 18—Elevated Temperature Tensile Properties.

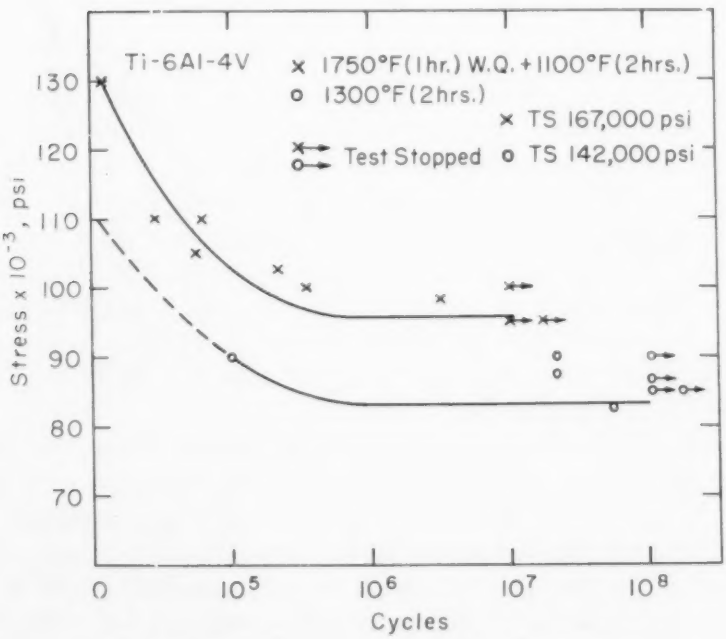


Fig. 19—Fatigue Strength for Two Heat Treatments.

strength varied inversely with section; and for the heat treatments used, it would appear to be very difficult to obtain yield strengths over 140,000 psi in sections larger than 1½-inches or 130,000 psi in sections larger than 3 inches (See Fig. 16). The results of aging

Table IV
Tensile Properties of Ti-6Al-4V Before and After Stability Tests

Heat Treatment	Stress psi	Temp. °F	Time (hrs.)	Total Def. %	U.T.S., psi	Y.S. (.2%) psi	Elong. %	R.A. %	Hardness R_c
1550°F(1 hr.)WQ + 900°F(24 hr.)					165,000	155,000	14	46	39
1550°F(1 hr.)WQ + 900°F(24 hr.)	50,000	800	200	2.0	163,000	151,000	11	41	40
1550°F(1 hr.)WQ + 900°F(24 hr.)	50,000	600	200	0.25	164,000	157,000	17	46	38
1550°F(1 hr.)WQ + 900°F(24 hr.)	—	800	200	—	177,000	166,000	16	51	41
1550°F(1 hr.)WQ + 900°F(24 hr.)	—	600	200	—	163,000	152,000	19	52	40
1550°F(1 hr.)WQ + 1000°F(24 hr.)					149,000	147,000	20	52	33
1550°F(1 hr.)WQ + 1000°F(24 hr.)	50,000	800	200	1.5	152,500	145,000	14	45	36
1550°F(1 hr.)WQ + 1000°F(24 hr.)	50,000	600	200	0.25	151,000	144,500	19	48	37
1550°F(1 hr.)WQ + 1000°F(24 hr.)	—	800	200	—	154,000	154,000	20	50	38
1550°F(1 hr.)WQ + 1000°F(24 hr.)	—	600	200	—	151,000	149,000	22	52	36
1750°F(1 hr.)WQ + 900°F(24 hr.)					177,000	163,500	14	51	41
1750°F(1 hr.)WQ + 900°F(24 hr.)	50,000	800	200	0.8	179,000	166,000	14	53	40
1750°F(1 hr.)WQ + 900°F(24 hr.)	50,000	600	200	0.1	173,000	162,000	15	55	39
1750°F(1 hr.)WQ + 900°F(24 hr.)	—	800	200	—	169,000	160,000	17	54	41
1750°F(1 hr.)WQ + 900°F(24 hr.)	—	600	200	—	177,000	165,500	15	54	39
1750°F(1 hr.)WQ + 1000°F(24 hr.)					168,000	156,500	16	59	40
1750°F(1 hr.)WQ + 1000°F(24 hr.)	50,000	800	200	0.4	184,000	169,000	13	48	44
1750°F(1 hr.)WQ + 1000°F(24 hr.)	50,000	600	200	0.2	172,000	163,000	14	52	40
1750°F(1 hr.)WQ + 1000°F(24 hr.)	—	800	200	—	179,000	167,000	16	49	42
1750°F(1 hr.)WQ + 1000°F(24 hr.)	—	600	200	—	175,000	164,500	16	52	41

studies indicate that at some sacrifice in ductility, higher strengths could have been obtained in even the larger sections using lower temperature aging treatments.

Stress-Stability and Elevated Temperature Tensile Tests

To separate the effect of aging with and without stress, duplicate bars were aged in both conditions for 200 hours at 600 and 800°F. The results indicate the alloy is quite stable under a stress of 50,000 psi for 200 hours at temperatures to 800°F (Fig. 17). It is interesting to note that in several instances, increased strength resulting from the test conditions was not accompanied by a decrease in ductility. It is evident from the deformation measurements that prior heat treatment has an effect on the short-time creep properties. The smallest deformations were obtained on bars heat treated to the highest strengths (See Table IV).

The results of elevated temperature tensile tests indicate that prior heat treatment affects the short time elevated temperature properties (Fig. 18). The better high temperature properties were obtained using the higher strength heat treatment.

Fatigue—The results of fatigue tests shown in Fig. 19 illustrate the improvement in endurance strength which can be realized using duplex heat treatments. Endurance ratios greater than 0.55 were obtained in both cases.

Summary of Results

The Ti-6Al-4V alloy has a wide range of hot working temperatures. Varying the working temperature between 1400 and 1750°F

has little effect on the mechanical properties resulting from any particular heat treatment.

Duplex heat treatments can be used to advantage to obtain moderately high strength levels accompanied by good ductilities. A wide range of mechanical properties, 140,000 to 175,000 psi tensile strength and 100,000 to 165,000 psi yield strength, may be achieved using solution treatments from 1550 to 1750°F and aging at temperatures from 900 to 1000°F. Strengths as low as 130,000 psi may be obtained by very slow cooling from the solution temperatures.

The 1550°F solution treatment results in the lowest yield-tensile ratio and offers the possible advantages of good machinability and excellent low temperature formability. Subsequent aging can then be used to increase the strength to maximum levels.

With good forging practice, yield strengths of 130,000 psi can be obtained in sections to three inches; and 140,000 psi in sections to one and one-half inches, with ductility values of 20% elongation and 50% reduction in area.

The alloy is stable under conditions of 50,000 psi for 200 hours at temperatures to 800°F. Total deformations of less than 1% under these conditions may be achieved by the use of a 1750°F (1 hr.) WQ +1000°F (24 hrs.) heat treatment. With this heat treatment, the alloy has an 800°F tensile strength of 115,000 psi and yield strength of 97,000 psi.

The results of two heat treated conditions indicate the alloy has 10^7 cycle endurance ratio greater than 0.55.

Acknowledgments

The authors wish to thank their associates at the Titanium Metals Corporation of America for the help they received during the investigation. Particular thanks are due to D. L. Day for the Jominy data, to R. S. Richards for the fatigue data and to L. Dudas for the metallographic work.

DISCUSSION

Written Discussion: By Frank A. Crossley, research metallurgist, Armour Research Foundation, Chicago.

The authors are to be commended for this excellent addition to the literature on commercial titanium alloys. It is most welcome.

Considering the statement, "The microstructure of the specimens delayed for longer times indicate that they had cooled below the M_s before quenching; and as a result, instead of an alpha-prime background there was a coarse basket weave alpha-beta structure." The second part of this statement contradicts the first part. Furthermore, the first part is inconsistent with the microstructures shown in Figs. 7 to 9. The alpha-prime structure results from cooling the beta phase below its M_s temperature, whether this cooling be in air or in water. It

should be understood that a specific M_s temperature for an alloy is defined only with respect to quenching from the high temperature single phase field. The alloy quenched from the two-phase field has a lower M_s temperature depending upon the degree of enrichment of the remaining beta. The change in structures of which the authors speak, depicted by Figs. 7 to 9, is the result of rapid growth of the alpha grains (existant at 1750°F) at the expense of the beta during the cooling in air prior to the water quench. The basket-weave structure shown in Fig. 9 is characteristic of alpha titanium alloys air-cooled from the beta field and is formed by nucleation and growth.

Written Discussion: By S. R. Carpenter, supervisor of producibility, Convair, Division of General Dynamics Corp., San Diego, California.

Requirements for increased titanium usage are appearing in sharper focus. Within its scope of operational limits, titanium is an efficient material when considered from a strength-weight standpoint. It is now fulfilling this purpose with current production alloys in the annealed condition. Titanium alloys in the heat treated condition are elevated to a high position of prominence as a material of construction.

The work of Messrs. Sherman and Kessler, with heat treatment of Ti-6Al-4V alloy is an important contribution leading to its production use. One of the highlights of their research are the conditions for best formability and subsequent heat treatments for maximum strength. The many other facets of the work opens the door of confidence to higher strength levels through the medium of heat treatment.

It is the purpose of this discussion to review the authors' work in terms of its meaning to engineering design and production use.

One of the problems in contour stretch formed sheet metal titanium angles, zees and channels stems from the high ratio of yield/ultimate. Yield strength of commercial titanium alloy sheets ranges up to 95% of the ultimate tensile strength. This high ratio is a source of trouble in stretching operations. The stretch machine operator has very little margin between yield strength and the material breaking point.

Successful extruding of Ti-6Al-4V alloy, to replace sheet metal shapes, and duplex heat treatment opens the way for ease of forming with the end product at a strength level far in excess of current sheet alloys. Direction of this route is found in Fig. 2. It will be noted Ti-6Al-4V has a yield/ultimate ratio of 0.71 in the 1550°F solution-treated condition. Elongation is at a maximum. It was increased from 23% in the annealed condition to 26%. The stage is now set to make everyone happy. The shop has a large margin between yield and ultimate with a consequent reduction in scrap loss. The designer benefits because he can engineer for more severe curvature due to increased elongation in the solution treated condition. Finally, his part can be aged after forming to a high strength level for structural efficiency.

Application of Ti-6Al-4V alloy in extruded shapes has been mentioned. This alloy and versions thereof are now being produced in sheet form under pilot production conditions. Confirming data showing the behavior of sheet material similar to that of Fig. 2 for bar stock will be a major factor in accelerating large usage of titanium alloy sheet. Benefits to be derived from the solution treated condition have been reviewed. Intensive effort is required on the part of the material suppliers to produce and to deliver a sheet material in the solution treated condition. It is necessary in the overall cost picture. Fabricators of titanium alloy

sheet generally are not equipped to cope with warpage problems after solution treatment. The mills are the logical place to handle the problem.

It is desired to re-emphasize the implications of Fig. 2. Potential is attractive for ease of production of high strength structural members. The pattern of Fig. 2 is a characteristic desired in future alloys having forming properties.

The aging time of a heat treat cycle is an important consideration from a shop standpoint and facilities requirements. Long aging times tie up expensive furnace equipment. In large scale production, valuable floor space is needed for additional furnaces when the aging time is extended. Shift changes of operating personnel must also be considered, in order to avoid the need for overlapping coordination when the aging cycle extends beyond one shift.

Wherever possible we like to establish an aging time of 6 hours. It is a workable time span in which to complete an aging cycle within an 8 hour shift. Convair's major effort in the heat treatment of titanium is directed to this end. It is suggested research institutions working with heat treatment of titanium alloys, include shorter aging times in their programs. This may seem insignificant, but in actual practice the long aging cycles can be a substantial cost item. We must yield, of course, on this point when longer aging times have been definitely established as necessary.

Fortunately, Ti-6Al-4V alloy seems amenable to a 6-hour aging cycle for the 1550°F solution treatment. Fig. 14 shows maximum strength and elongation can be attained with the 6-hour cycle. Reduction in area is lowered from 55 to 43%. This loss can be accepted for the gains derived from shorter aging times.

Mechanical properties look very promising from the data of Table IV. Unfortunately, they must be revised downward for design purposes. The condition is brought about by minimum guarantees for Ti-6Al-4V. They have been quoted in the annealed condition as:

Ultimate Tensile Strength	130,000 psi
Yield Tensile Strength (0.2%)	120,000 psi
Elongation (1")	10%
Reduction of Area	30%

Experience has shown that the majority of titanium alloys exceed minimum guarantees by a considerable amount. A small percentage, however, is received with minimum guarantees. It must be taken into account for design purposes.

In the absence of additional test data, Convair is pegging design values for heat treated titanium by adding minimum guarantees to the change due to heat treatment. This assumes the change from heat treatment is constant for all strength levels in the annealed condition. On this premise, tentative minimum values are established as follows:

Annealed Properties of Test Material	
Ultimate Tensile Strength	140,000 psi
Yield Tensile Strength (0.2%)	139,000 psi
Elongation (1")	23%

From Table IV and the annealed properties of test material, changes due to heat treating are:

For a Heat Treatment of 1550°F (1 Hr.) WQ+900°F (24 Hr.)	
Ultimate Tensile Strength	Increased 25,000 psi
Yield Tensile Strength (0.2%)	Increased 16,000 psi
Elongation (1")	Changed from 23% to 14% or a reduction of 39%

For a Heat Treatment of 1750°F (1 Hr.) WQ+900°F (24 Hr.)	
Ultimate Tensile Strength	Increased 37,000 psi
Yield Tensile Strength (0.2%)	Increased 24,500 psi
Elongation (1")	Changed from 23% to 14% or a reduction of 39%

The changes in properties, as a result of heat treatment, when applied to minimum guarantees in ½-inch section tentatively become:

For a Heat Treatment of 1550°F (1 Hr.) WQ +900°F (24 Hr.)	
Ultimate Tensile Strength	155,000 psi
Yield Tensile Strength (0.2%)	136,000 psi
Elongation (1")	6%
For a Heat Treatment of 1750°F (1 Hr.) WQ +900°F (24 Hr.)	
Ultimate Tensile Strength	167,000 psi
Yield Tensile Strength (0.2%)	144,500 psi
Elongation (1")	6%

The tentative minimums may be subjected to a slight revision downward after heat treat response is checked from other heats. Transverse properties must be determined. The values given are for longitudinal direction only. It is necessary to determine effect of furnace temperature tolerances during the heat treat cycle. At Convair the tolerances have been established at ±25°F for solution treatment and ±10°F for aging. These tolerances were chosen in order to use existing heat treat equipment for steel and aluminum alloys.

Foregoing properties of heat treated material are for ½-inch section size. Fig. 16 shows these strength values may be expected to prevail up to 1-inch section for the 1550°F solution treatment and age. A noticeable drop in strength can be expected in 1-inch sections for the 1750°F solution treatment and age. However, the latter treatment shows some strength advantage in 1-inch sections over the 1550°F solution treatment and age. Although Ti-6Al-4V does not have deep hardening properties, the material can be used to good advantage. A fairly large percentage of aircraft structural sections are 1-inch or less after completion of manufacture. There is an advantage strength-wise over current production alloy bars and forgings in the annealed condition. Much greater advantage will be realized in sheet and extruded forms to replace parts now fabricated from commercial alloy sheet.

In conclusion the following points are emphasized:

1. Excellent formability is anticipated in the solution treated condition.
2. An aging cycle of 6 hours is desired to reduce cost of heat treatment. Ti-6Al-4V meets this requirement for the 1550°F solution treatment.
3. Bar and forgings in the heat treated condition can be used with a weight advantage in many aircraft parts. There will be superior weight advantage in the form of sheet and extrusions.
4. Change in mechanical properties from heat treatment should be added to minimum guarantees in order to establish design allowables.
5. Transverse properties must be determined for the heat treated condition.
6. There is a need for development of an alloy sheet to be supplied by the mills in the solution treated condition.

Written Discussion: By R. H. Gassner, chief metallurgist, Douglas Aircraft Company, Inc., El Segundo, California.

This extensive study is a welcome addition to titanium alloy metallurgy. Many of the properties ascribed to this alloy appear particularly attractive to the aircraft industry, but it is not considered that the data presented fully justify all of the conclusions.

We have recently hot-formed some S-shaped slat tracks from another titanium alloy utilizing resistance heating. Because of the low thermal conductivity of titanium, controlled cycling of the current was necessary to allow the heat to diffuse uniformly through the part and avoid localized overheating. The "excellent

low temperature formability" ascribed to the 6% aluminum, 4% vanadium alloy after the 1550°F solution heat treatment should permit room temperature forming of such complex shapes. However, the low yield-tensile strength ratio, high elongation and high reduction of area do not necessarily connote excellent formability. The values cited could indicate that the elongation occurred primarily in the "necked down" region of the specimen. This type of ductility may be valuable from a toughness standpoint, but hardly from a formability standpoint, because most of the elongation is concentrated near the fracture. The uniform elongation, elongation at ultimate stress prior to necking, or complete stress-strain curves are much better criteria for evaluating stretch-formability. Such evaluation does not necessarily correlate with bending or deep drawing formability; evaluation of these properties should be based upon bend test and cup test results.

The fatigue curves of Fig. 19 show the advantage of a duplex heat treatment 1750°F (1 hour) WQ+1100°F (2 hours) over the single heat treatment 1300°F (2 hours). The data indicate that other duplex heat treatments 1750°F (1 hour) WQ+900°F (24 hours) and 1550°F (1 hour) WQ+900°F (24 hours) offer more attractive combinations of tensile properties. Can similar fatigue properties be expected from these other treatments?

Authors' Reply

The authors wish to express their thanks to Messrs. Crossley, Carpenter, and Gassner for their interest as shown by the written discussions of this paper.

We are grateful to Dr. Crossley for pointing out the sentence referred to as contradictory, and in its place we submit the following: "The specimens quenched after a delay of less than 25 seconds had an alpha prime background (Fig. 7). The microstructures of specimens delayed for longer times indicate that the majority of the beta had transformed to a basket-weave alpha-beta structure prior to quenching (Figs. 8 and 9). This structure became coarser with increasing time of delay. The formation of the coarse alpha plates and the subsequent enrichment of the remaining beta during the initial slow cooling resulted in a beta phase sufficiently rich to be retained upon quenching, and no alpha prime was formed."

The authors agree with Mr. Gassner that the low yield/tensile ratio obtained for this alloy in the 1550°F solution treated condition does not necessarily connote excellent formability. Considerable additional work will have to be done along the line of testing long gage length sheet specimens and the forming of actual parts before conclusions can be reached with regard to the forming advantages offered by the solution treatment giving the low yield/tensile ratio. There seems to be little question but that other duplex treatments beside the 1750°F (1 hour) WQ+1100°F (2 hours) treatment which gives high strength values will result in better fatigue properties than those obtained in the mill annealed condition.

The authors appreciate Mr. Carpenter's remarks and the fact that he recognizes the valuable benefits which can be derived by heat treating titanium alloys. Providing that the solution treated condition giving a low yield/tensile ratio proves to have a definite advantage, Mr. Carpenter can be sure that the producers of titanium mill products will give careful consideration to the possibility of making available a solution treated product. It must be recognized, however, that many problems will have to be solved by the producers before a satisfactory flat, properly descaled, and uniformly quenched sheet product can be marketed.

There is little question but that 6 hours aging at temperatures in the range

of 900°F will produce excellent strength levels, however the authors caution prospective users of such treatments to thoroughly investigate the notch sensitivity and thermal stress-stability of the alloy prior to application. The Titanium Metals Corporation is currently studying the notched properties and stress stability characteristics of short time heat treated Ti-6Al-4V, and hopes that some of this data will be available in the near future.

With regard to the inclusion in specifications of mechanical properties resulting from heat treatment, considerable production statistical data will be required before this type of specification can be considered. Whenever heat treatment is involved, product form and section size must be taken into account.

TEMPERATURE DEPENDENCE OF THE TENSILE PROPERTIES OF TANTALUM

By J. W. Pugh

Abstract

The tensile properties of tantalum sheet have been measured in vacuum for the temperature range 78 to 1500°K. The temperature dependences of strength, ductility, strain hardening and strain-rate sensitivity were evaluated. Discontinuous yielding was observed as yield points and as serrated load-elongation curves. Susceptibility to strain aging was demonstrated, and the anomalies in mechanical parameters and the discontinuous yielding was attributed to this phenomenon. An explanation of this behavior was made in terms of dislocation theory.

Introduction

TANTALUM is a refractory metal which has a very high melting point (3270°K). Its use has been chiefly limited to applications based on its corrosion resistance, but its melting point suggests good load carrying capacity at very high temperatures. At moderate temperatures the mechanical properties of tantalum are comparable to those of mild steel. In this report an analysis is made of the tensile properties of sheet metal for constant strain rate and at temperatures between 78 and 1500°K.

Fabrication and Testing Procedure

Production and fabrication of the metal used was accomplished at the Fansteel Metallurgical Corporation. A powder metallurgy ingot was made and rolled to 0.010-inch thick. This sheet material was vacuum-annealed to produce the structure shown in Fig. 1. The recrystallized grain size here is ASTM 6–7. Chemical analysis revealed that the important impurities are as follows:

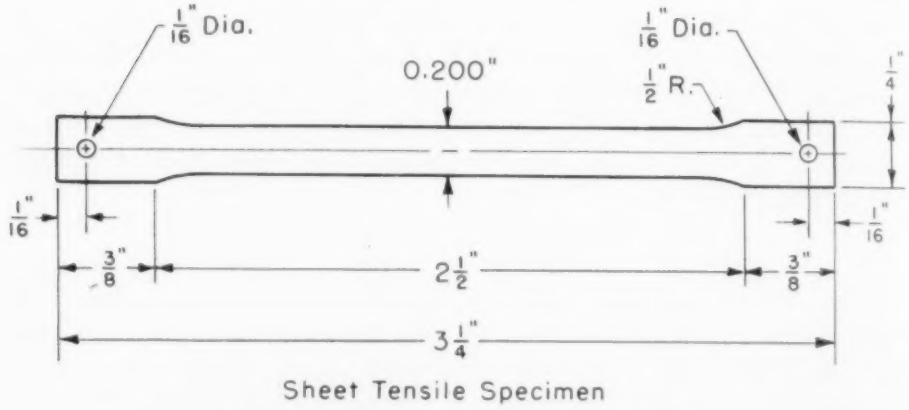
Element	Weight % Present
Oxygen	0.0056
Nitrogen	0.013
Carbon	0.02
Niobium	0.10
Tungsten	0.01
Iron	0.015

Test specimens were cut from the sheet parallel to the rolling direction. The texture of recrystallized tantalum sheet metal has

The author, J. W. Pugh is associated with the General Electric Co., Metallurgy and Ceramics Research Department, Schenectady. Manuscript received August 8, 1955



Fig. 1—Longitudinal Section of Tantalum Sheet, Cold-Rolled and Recrystallized. ×250



Sheet Tensile Specimen

Fig. 2—Sheet Tensile Specimen, 0.010-inch thick.

been shown to be {111} <112> (1).[1] Fig. 2 is a drawing of the specimen used. Tests were made on an Instron testing machine at 0.09 inches per inch per minute and at temperatures from 78 to 1500°K. In order to determine the effect of strain rate on flow stress, the rate was changed momentarily to 0.009 during each test. These changes were made at 0.05 strain, except at 78°K, where they had to be made at 0.015. Data were plotted autographically. Elevated-temperature tests were made in vacuum, and temperatures were recorded by means of a platinum-platinum rhodium thermocouple embedded in the test fixture.

[1]The figures appearing in parentheses pertain to the references appended to this paper.

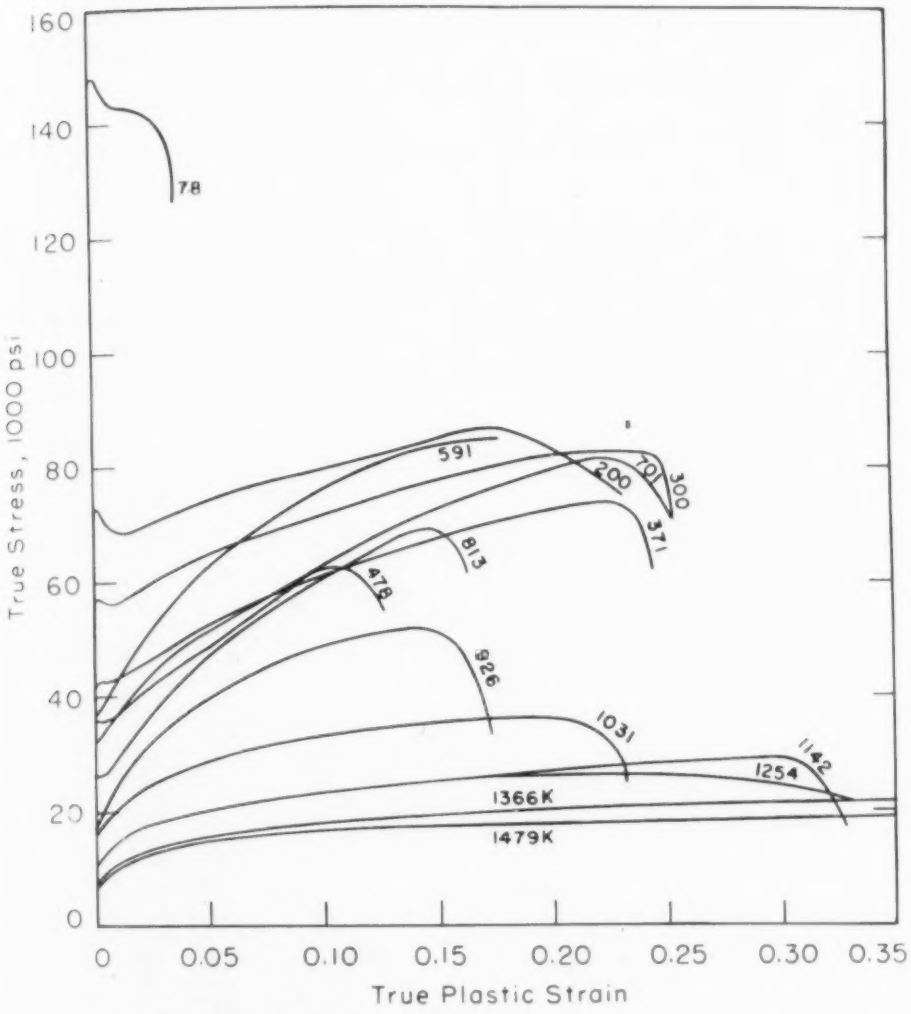


Fig. 3—True Stress-Strain Curves. Temperature in degrees Kelvin is printed adjacent to each curve.

Results

Tensile flow curves are presented in Fig. 3. Some kind of yield point is observed for these tests as high as 813°K, and the original autographic curves made between 371 and 926°K were jagged, indicating some degree of discontinuous yielding. However, the serrated curve made at 591°K exceeded all the others by at least a factor of three with respect to the frequency and load deviation involved in the discontinuities.

Logarithmic plots of true stress-strain are shown in Fig. 4. Many of these curves show rather drastic deviation from linearity. Most are, however, fairly straight at the strain associated with maximum load. Strain hardening was evaluated in terms of the slope (m) of these logarithmic curves at this point.

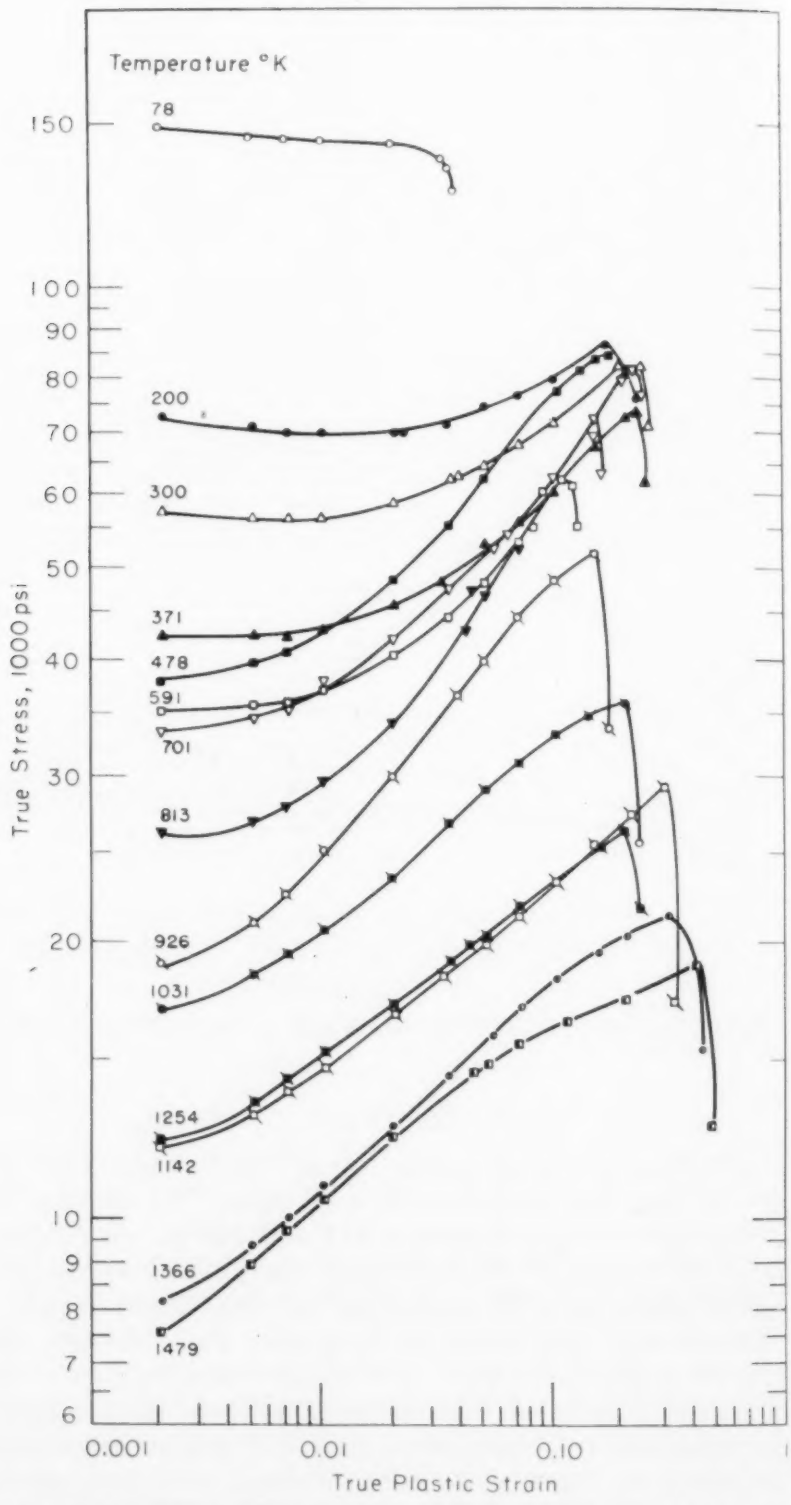


Fig. 4—Logarithmic True Stress-Strain Curves. Temperature in degrees Kelvin is printed adjacent to each curve.

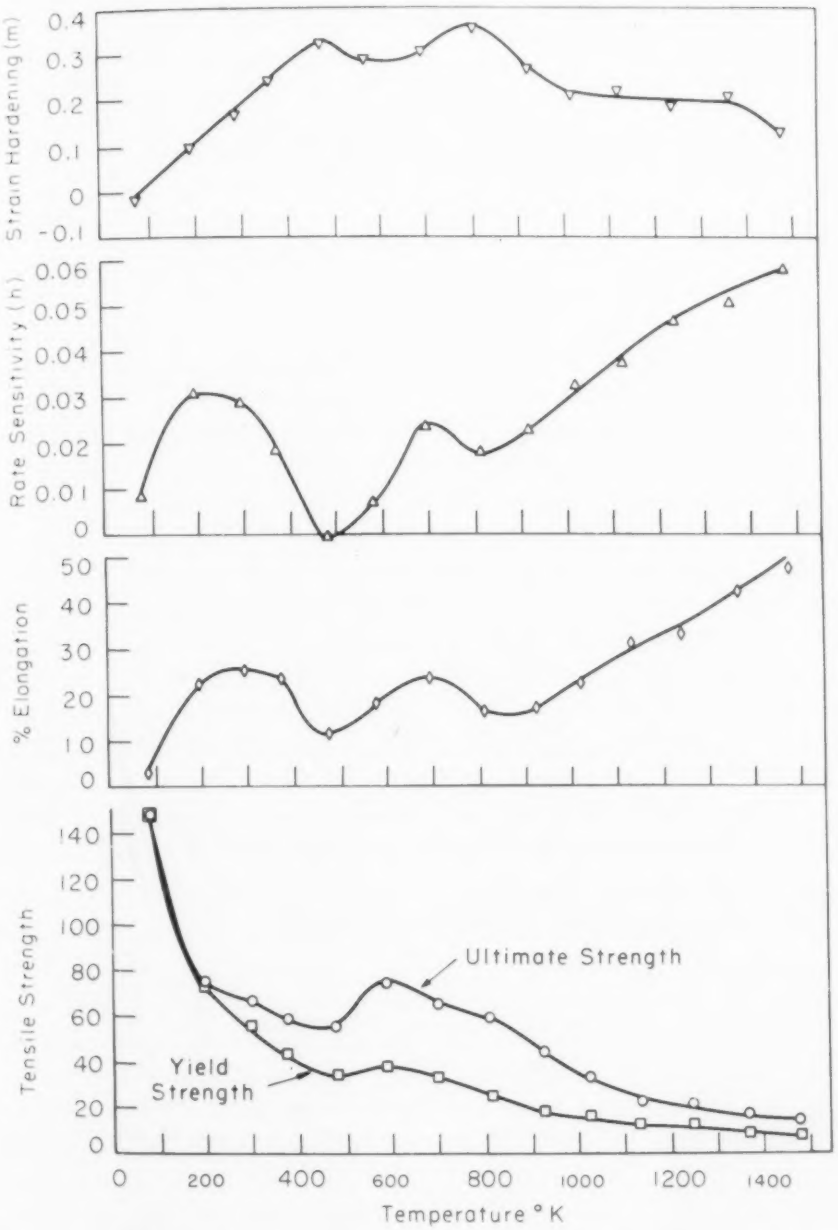


Fig. 5—Temperature Dependence of the Tensile Parameters.

$$m = \frac{\partial \log \sigma}{\partial \log \epsilon}\Big|_{\dot{\epsilon},\, T} \qquad \text{Equation 1}$$

where m is called the strain-hardening coefficient, σ is the flow stress and ϵ is the true strain. The temperature dependence of these slopes is presented in Fig. 5. Strain hardening is observed to rise rapidly with temperature at first, to reach maxima at 508 and 800°K, and to diminish at higher temperatures.

Strain rate sensitivity is defined as

$$n = \frac{\partial \log \sigma}{\partial \log \dot{\epsilon}}\Bigg|_{\epsilon,\ T} \qquad \text{Equation 2}$$

It was evaluated by comparing the flow stress at two different strain rates.

$$n = \frac{\log \frac{\sigma 1}{\sigma 2}}{\log \frac{\dot{\epsilon} 1}{\dot{\epsilon} 2}}\Bigg|_{\epsilon,\ T}$$

where n = strain rate sensitivity, σ_1 = flow stress at the faster rate, σ_2 = flow stress at the slower rate, $\dot{\epsilon}_1$ = the faster rate = 0.09 inch per inch per minute, and $\dot{\epsilon}_2$ = the slower rate = 0.009 inch per inch per minute. The temperature dependence of n is shown in Fig. 5. These data indicate a maximum at 200 to 300°K and a minimum at about 500°K, and possibly a second minimum at 800°K.

Elongation and strength parameters as a function of temperature are also presented in Fig. 5. The elongation maxima and minima compare very well with the irregularities observed in the temperature dependence of strain rate sensitivity and strain hardening. Yield strength (0.2% offset) and ultimate tensile strength show inverse temperature dependence in the range 500 to 600°K. This has the effect of causing the strength to be higher than an extrapolation of low temperature data in the temperature range 500 to 1000°K. This anomaly corresponds with those observed for the other tensile parameters plotted in Fig. 5.

Table I summarizes the data obtained.

Table I
Tensile Properties of Tantalum

Temp., °K	Yield Strength 0.2%	Ultimate Tensile Strength	% Elongation	m	n
78	148,000	148,000	3.7	—0.018	0.0075
200	72,450	73,190	23.1	0.099	0.0307
300	57,350	67,140	25.3	0.164	0.0285
371	42,520	59,280	24.6	0.243	0.0175
478	35,430	56,073	12.7	0.326	—0.0012
591	37,930	73,990	18.0	0.298	0.006
701	33,380	65,260	24.3	0.316	0.0240
813	26,120	59,940	16.2	0.356	0.0176
926	18,890	44,730	17.3	0.266	0.0220
1031	16,940	30,320	23.1	0.205	0.0321
1142	12,110	22,230	32.8	0.212	0.0374
1254	12,350	21,620	33.1	0.181	0.0461
1366	8,130	16,804	43.2	0.217	0.0506
1479	7,520	14,719	47.5	0.130	0.0581

Discussion

The temperature dependences of the mechanical parameters evaluated in this report are similar in character to those for many

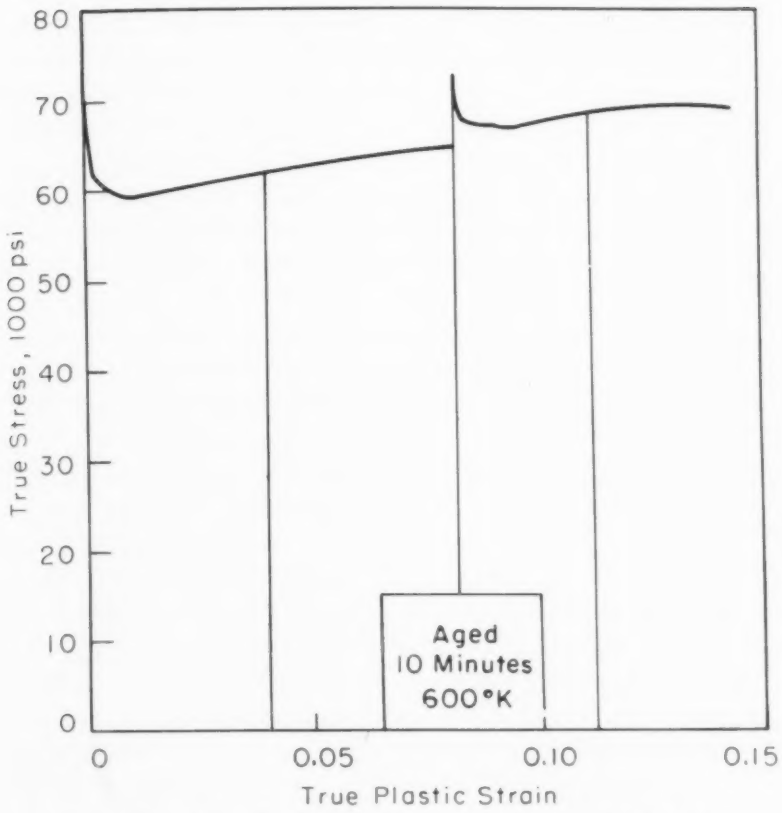


Fig. 6—True Stress-Strain Curve Illustrating Strain Aging Behavior.

other metals. The strength maxima and elongation minima in the 400 to 1000°K range is strikingly like those for iron and steel in the so-called "blue brittleness range" (2,3). The strain hardening maxima and the minima in rate sensitivity appear in this same temperature range. These observations, together with the discontinuous yielding demonstrated by the yield points and serrated load-elongation curves indicate that tantalum is subject to strain aging. Similar effects have frequently been observed for other strain aging metals (4,5,6).

Yield points due to a strain aging mechanism can be reproduced in a given specimen if it is tested and annealed at an appropriate temperature prior to retesting. Fig. 6 illustrates this sequence for tantalum. The test represented here was started at 200°K, strained through the yield point to about 0.04 strain and unloaded. When the specimen was reloaded immediately, a smooth continuation of the flow curve was produced as indicated. The specimen was then unloaded, aged ten minutes at 600°K, and the test was repeated. A new yield point and a slightly higher flow curve were the result.

This behavior has been explained in terms of the dislocation model (7). It is expected to result from the presence of interstitial

elements in solution. Such interstitial elements (usually carbon, nitrogen or oxygen) can cause the relief of stresses around a dislocation by migrating to the dilatation side of the dislocation field. The "atmosphere" of solute atoms which migrate to dislocation sites exerts an anchoring effect which inhibits the motion of the dislocation and strengthens the metal. When sufficient stress is applied, however, dislocations do break away from the solute atmospheres, and subsequent plastic flow takes place suddenly and at lower stress than that required to initiate flow. A yield point such as the one in Fig. 6 is the result. In order to re-establish the yield point, the interstitials must diffuse to dislocations and "recondense" on them. The annealing treatment at 600°K is sufficient to permit this diffusion in tantalum.

The inverse effects of temperature on strength and ductility in the range 300 to 600°K can also be explained. It has been proposed that when the temperature is sufficiently high that a solute atom can change its site while interacting with a dislocation, the new site is not random but has a lower interaction energy (8). As the interstitial atoms become reoriented preferentially on lower energy sites, the result is an increase in flow stress. The magnitude of this effect ought to increase with strain since the number of new interaction sites increases with strain. This appears to be the case for tantalum and explains the increase in strain hardening with increase in temperature in the lower temperature range. Another indication is the large maximum in temperature dependence for ultimate tensile strength compared to the considerably smaller one for yield strength (Fig. 5).

Strain aging behavior was expected for tantalum, although it had not been previously demonstrated. This prediction was based on some internal friction measurements which were published recently (9,10). Acoustic absorption peaks were observed for tantalum at 425, 445 and 625°K for a frequency of one cycle per second. These were attributed to the interstitial solute elements, carbon, oxygen and nitrogen, respectively. This phenomenon is related to strain aging insofar as it is attributed to the stress-induced interstitial diffusion of solute atoms. The temperatures at which the peaks occur depend upon the mobility of the interstitials in the tantalum lattice.

It is possible that the double maxima and minima associated with strain hardening, rate sensitivity and elongation in Fig. 5 result from the interaction of dislocations with different interstitials. For example, carbon and/or oxygen may account for the anomalies at 500°K, while nitrogen may be responsible for those at 800°K.

Mott has explained strain hardening in terms of back stress on dislocation mills caused by piling up dislocations on obstacles such as sessile dislocations (11). This back stress causes the generation of dislocation loops at each source to stop until more stress is applied.

The net effect of this phenomenon is to increase the resistance to deformation as a function of the number of dislocation loops generated, or, in other words, as a function of strain. The theory also accounts for a diminuation of the strain hardening effect with increasing temperature. Above a certain temperature level, deformation-created lattice vacancies become sufficiently mobile to permit them to diffuse and relieve piled-up dislocations. At still higher temperatures, these anchored dislocation arrays can be dispersed more effectively by the process of "climb."

These statements with respect to the theoretical mechanism imply that for very low temperatures, strain hardening ought to be relatively high. When the temperature is sufficiently high to permit vacancies to move, it ought to diminish slightly with temperature, and in the range where self-diffusion is practical it ought to descend more rapidly with temperature.

Fig. 5 indicates how the temperature dependence of strain-hardening for tantalum deviates from that just described. The low values of strain hardening-coefficient in the temperature range 200 to 370°K can to some extent be attributed to the fact that the exponent m is inversely dependent on flow stress. The significant deviation in this range is, however, very likely due to the strain-aging phenomena. The negative value for 78°K is not readily explainable. It may result, of course, from crack propagation or from early necking.

The characteristic temperature dependence, whether it be most affected by strain aging or by lattice vacancy migration, is related to diffusion processes. It will be different for different relationships between these diffusion processes and the strain rate used. It is likely that the characteristic maxima and minima in Fig. 5 would be shifted upward for faster strain rates and downward for slower rates.

The temperature dependence of the strain rate sensitivity (Fig. 5) is thought also to be determined by the characteristic diffusion mechanisms. Vacancy migration and self-diffusion diminish the effective flow stress. Faster rates reduce this effect by giving these processes less time to operate and produce higher flow stresses than the slower rates. At lower temperatures, where the diffusion rates are slower, equivalent changes in deformation rate have less effect on flow stress. A continuous increase in strain rate sensitivity is predicted from these considerations. However, the diffusion and condensation of interstitials on dislocations (strain aging) have an opposite effect, just as they did for strain hardening. In the temperature range where strain aging can take place, flow stress depends less upon strain rate because now the impediment to dislocation movement is primarily the condensed interstitial cloud. Rate

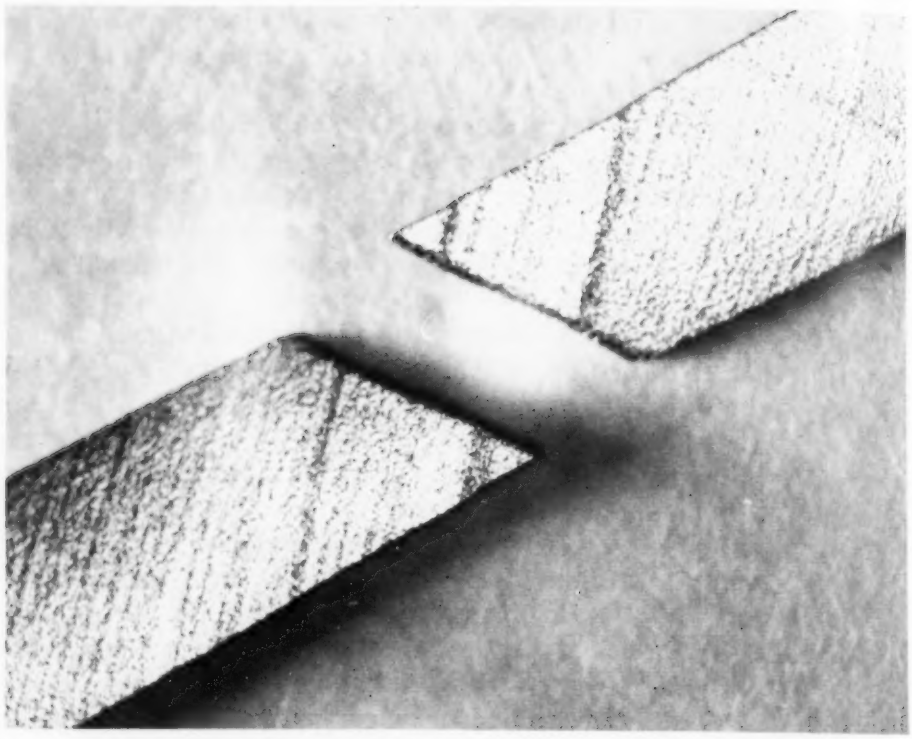


Fig. 7—Strain Markings on a Polished Tensile Specimen Tested at 600°K. ×5

sensitivity for tantalum is relatively high at 200 to 300°K, but diminishes at about 400°K because the interstitial solute atoms are mobile enough to interact with moving dislocations. It is likely that as the temperature is raised, strain aging becomes less effective, because the interstitial solute atoms offer less resistance to dislocation movement when they are more mobile. At some critical temperature it is probable that they are completely "uncondensed" and ineffective (12). Thus, at temperatures higher than 800°K, the rate sensitivity for tantalum rises very steeply.

The minimum in the rate sensitivity caused by strain aging should be displaced to lower temperatures if relatively lower rates are compared, and to higher temperatures if higher rates are compared. This results again from the fact that the characteristic temperature dependence is determined by the relationship between strain rate and atomic mobility.

Strain markings were produced on test specimens at all temperatures up to 1140°K. It is thought that they result from discontinuous yielding and may be expected to accompany yield points and serrated load-elongation curves. The strain marking evidence was most pronounced at 600°K where the serrated deviations were greatest. Fig. 7 is a picture of a polished specimen which was pulled to fracture at 600°K. The crossed markings on the surface of the

specimen are typical of those tested in the temperature range where strain aging was most effective.

Fig. 8 indicates how the strength of tantalum compares to other body-centered cubic metals as a function of homologous temperature. Homologous temperature is defined for this comparison as

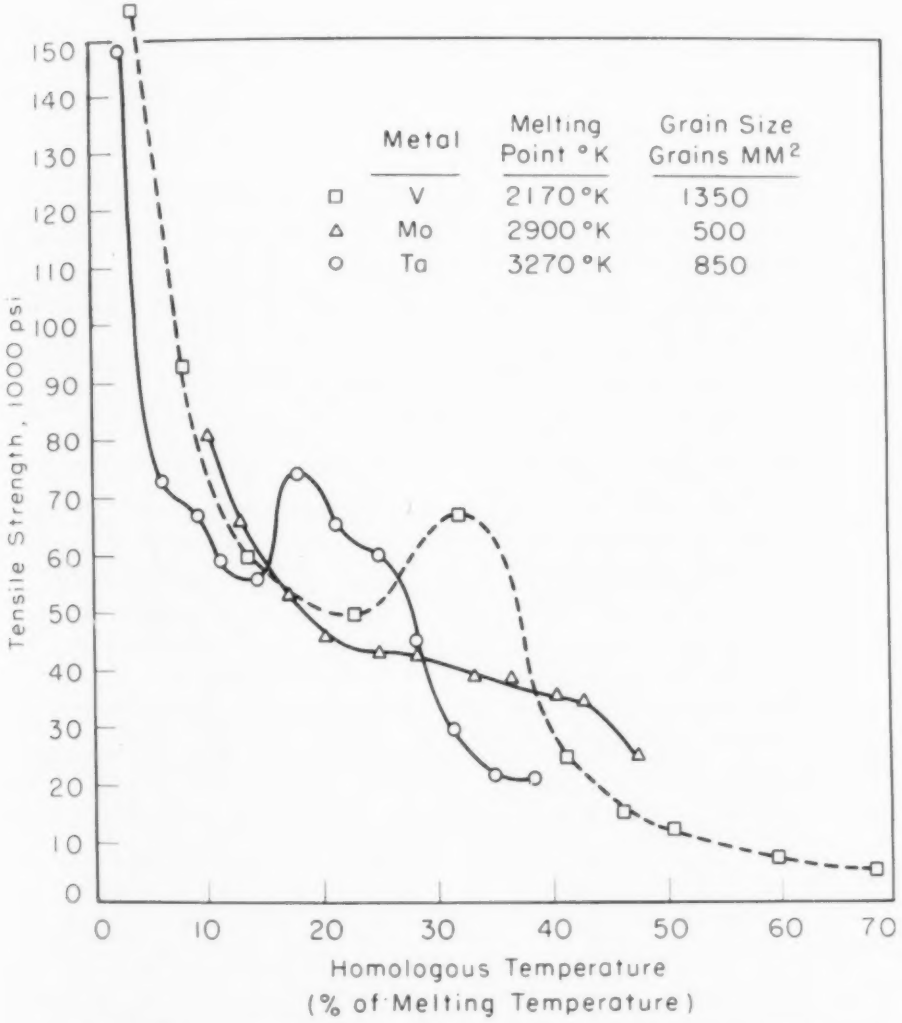


Fig. 8—Comparison of the Relative Strengths of Tantalum, Molybdenum and Vanadium. Homologous temperature is defined as the ratio of the test temperature and the melting point of the metal. It is plotted here as a percentage.

the ratio of the absolute test temperature and the absolute melting point of the metal involved. Vanadium (13) and molybdenum (4) data were obtained under conditions similar to those for tantalum. The inverse temperature effects which result from strain aging somewhat obscure the results at higher temperatures, but tantalum appears to be somewhat weaker than its high melting point suggests.

Conclusion

Tantalum has been shown to have a temperature dependence of tensile properties similar to those for iron and steel. Yield points, serrated stress-strain curves and anomalies in the temperature dependence of strength, ductility, strain hardening, and rate-sensitivity indicate strain aging. Moreover, a specific demonstration of strain aging was made by reproducing a yield point at 200°K after aging at 600°K. The characteristic temperature dependence of the tensile parameters can be explained in terms of current dislocation theory.

References

1. J. W. Pugh and W. R. Hibbard, Jr., "Rolling Textures in Tantalum," Transactions, American Society for Metals, Vol. 48, 1956.
2. J. L. Everhard, et al, "Mechanical Properties of Metals and Alloys," National Bureau of Standards, Cir. C447,265, 1943.
3. G. W. Geil and N. L. Carwide, "Tensile Properties of Ingot Iron at Low Temperatures," National Bureau of Standards, *Journal of Research*, Vol. 45, 1950, p. 129.
4. J. W. Pugh, "The Tensile Properties of Molybdenum at Elevated Temperatures," Transactions, American Society for Metals, Vol. 47, 1955, p. 984.
5. J. H. Hollomon and L. D. Jaffe, *Ferrous Metallurgical Design*, 1947, p. 76, published by John Wiley and Sons, New York.
6. J. D. Lubahn, "Strain Aging Effects," Transactions, American Society for Metals, Vol. 44, 1952, p. 643.
7. A. H. Cottrell, *Dislocations and Plastic Flow in Crystals*, 1953, published by Oxford University Press, Oxford.
8. A. H. Cottrell, "Interaction of Dislocations and Solute Atoms," Relation of Properties to Microstructure, 1954, p. 131, published by American Society for Metals.
9. T. S. Ke, "Internal Friction in the Interstitial Solid Solutions of C and O in Tantalum," *Physical Research*, Vol. 74, July 1, 1948, p. 9.
10. T. S. Ke, "Internal Friction and Precipitation from the Solid Solution of N in Tantalum," *Physical Research*, Vol. 74, Oct. 15, 1948, p. 914.
11. N. F. Mott, "Theory of Work-hardening of Metal Crystals," *Philosophical Magazine*, Vol. 43, 1952, p. 912.
12. A. H. Cottrell, "Theory of Dislocations," *Progress in Metal Physics*, Interscience Publishers, Inc., Vol. 4, 1953, p. 204.
13. J. W. Pugh, "Tensile Properties of Vanadium," to be published.

PHASE RELATIONS IN MAGNESIUM-LITHIUM-ALUMINUM ALLOYS

By D. W. Levinson and D. J. McPherson

Abstract

A study was made of equilibrium phase relations in the system Mg-Li-Al by the methods of metallographic and X-ray diffraction analysis. Isothermal sections are presented for the temperatures of 400, 300, 200 and 100°C and a vertical section, derived from the isotherms, is presented also.

The existence of the ternary phase at approximately the stoichiometry Mg Li Al_2 was verified. The ternary phase Mg Li_2 Al was not found to be an equilibrium phase at any of the temperatures studied. (ASM-SLA Classification: M24, Mg, Li, Al)

Introduction

A STUDY of phase relations in the system magnesium-lithium-aluminum was made by Shamrai (1)[1] largely by the methods of thermal analysis. The essential features of the 400°C (750°F) isotherm derived from this study are reproduced in Fig. 1. A ternary phase forming peritectically and having very nearly the stoichiometry of $MgLiAl_2$ is reported.

Studies of mechanical properties of magnesium lithium-base alloys (2,3,4,5) have resulted in the concept that the rejection of a different ternary intermediate phase, $MgLi_2Al$, from the β solid solution is responsible for age hardening and embrittlement of the β solid solution. $MgLi_2Al$ is reported to be cubic with $a_o = 6.7$ Å. This phase was not observed by Shamrai.

A study of phase relations in the vicinity of the magnesium corner by Jones et al (6,7), including some alloys in the range of the previously mentioned mechanical property studies, failed to confirm the existence of either ternary intermediate phase. The isotherm given for 372°C (700°F) (Fig. 8) by Jones et al shows the presence of a 2 phase (Mg)+AlLi field which is incompatible with the 2 phase β+$MgLiAl_2$ field of Shamrai (see Fig. 1).

In order to shed light on the source of mechanical property difficulties in the Mg-Li base alloys and to resolve the inconsistencies in the available knowledge of phase relationships in this system, a

[1]The figures appearing in parentheses pertain to the references appended to this paper.

Of the authors, D. W. Levinson is supervisor, Nonferrous Metallurgy Research, and D. J. McPherson is assistant manager, Metals Research, Armour Research Foundation, Chicago. Manuscript received December 30, 1954.

study of phase relations in the vicinity of the alloy Mg-33Li-7.5Al (Mg-12.5Li-10Al by weight) was undertaken.

Experimental Method

Alloys for this study were prepared from the high purity materials listed in Table I.

The lithium was received in the form of massive blocks which were scraped clean of surface scale and forged to ½ inch round rod.

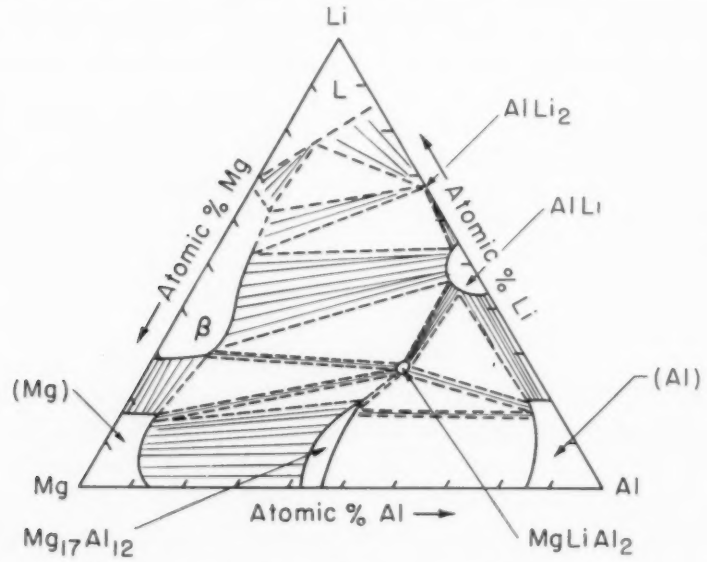


Fig. 1—400°C (750°F) Isotherm of Shamrai.

The lithium remained bright as long as it was kept under kerosene and could readily be cut into pieces suitable for weighing and charging. The lithium was carefully dried prior to weighing. The charging materials were weighed to the nearest 0.01 gram and heats were calculated to have a total weight of 10 grams. During weighing the lithium was observed to develop a brown, almost transparent tarnish, but no weight gain was evident. The tarnish, which is known to be lithium nitride, was not removed prior to charging and further tarnishing was prevented by restoring the weighed lithium in kerosene until melting.

Melting was carried out in molybdenum crucibles fabricated

Table I
Material Used

Material	Source	Purity
Lithium	Maywood Chemical Co. Maywood, N. J.	"Special grade Low Na, low Cl lithium." Na guaranteed <0.02.%
Magnesium	Dow Chemical Co.	Redistilled high purity magnesium. Total impurity content <0.05%.*
Aluminum	Aluminum Co. of America	High purity Al Sheet. 99.994% Al.*

*Analysis furnished with material.

Table II
Chemical Analyses of Selected Mg-Li-Al Alloys

Nominal Composition (Wt. %)			Analyzed Composition (Wt. %)		
Mg	Li	Al	Mg	Li	Al
89.1	10.9	—	89.2	10.8	—
—	20.5	79.5	—	20.5	79.5
73.1	18.8	8.1	Bal	19.5	7.7
69.4	22.0	8.6	Bal	20.6	8.7
65.3	25.6	9.1	Bal	22.9	9.2
72.3	13.1	14.6	Bal	16.0	14.1
61.2	21.8	17.0	Bal	20.9	17.2
56.6	25.4	18.0	Bal	22.8	16.9
65.2	13.1	21.7	Bal	14.5	20.4
57.6	18.5	23.9	Bal	18.7	23.5
53.1	21.6	25.3	Bal	18.6	25.5
48.1	25.2	26.7	Bal	25.0	26.6
37.3	21.3	41.4	37.9	21.2	Bal
31.5	24.8	43.7	38.6	24.0	Bal
44.7	12.8	42.5	44.8	11.8	Bal
40.2	15.3	44.5	Bal	13.8	44.0
35.2	18.0	46.8	35.3	17.8	Bal
23.5	24.5	52.0	23.4	23.5	Bal
46.6	8.3	45.1	Bal	9.0	45.0
22.0	21.0	57.0	23.3	19.6	Bal
23.8	10.2	66.0	23.5	11.5	Bal
6.8	17.5	75.7	5.7	16.9	Bal

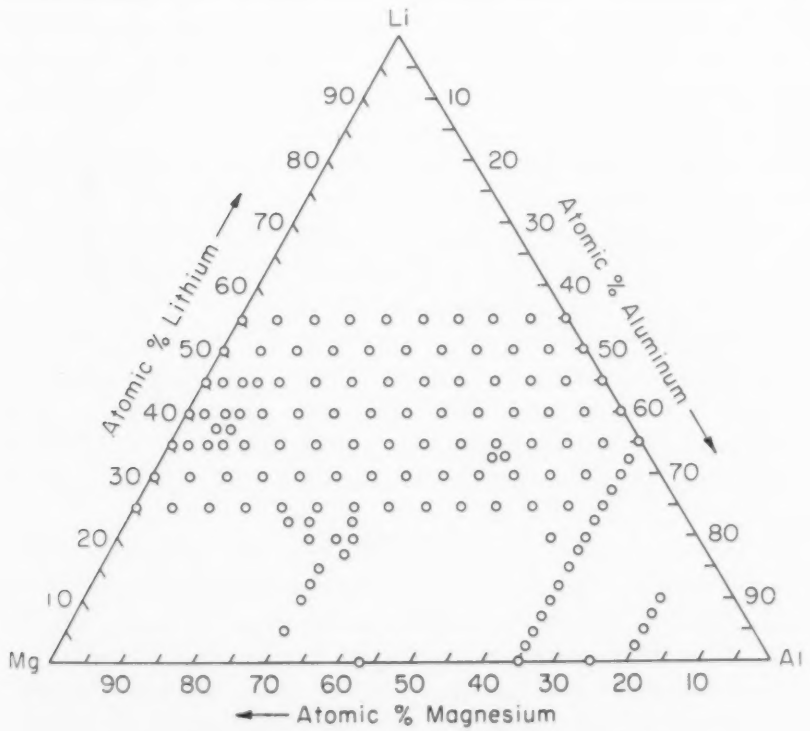


Fig. 2—Nominal Composition of Alloys Studied.

from sheet and rod stock to form a thin walled (0.003 inch) cylinder with a removable solid bottom. The sleeves were discarded after each melt while the bottoms were cleaned and re-used. An interlocking crimp seam rendered the sleeve liquid-tight, while the bottom was secured in place with iron wire wrapped about the outside of the assembly. This type of crucible was found necessary since

preliminary tests in iron and stainless steel crucibles showed appreciable iron contamination. Because of the reactivity of the alloys, no suitable refractory crucibles could be found. The crucible measured approximately 5/8 inch I.D. ×3 inch long.

Spectographic analysis of several trial melts of widely varying composition over the range investigated showed no significant contamination by crucible materials. These heats were held liquid in the crucibles for 15 minutes and allowed to freeze in place, a condition far more likely to give contamination by the crucible than the melting schedule for the experimental alloys.

Melting was carried out with the crucible placed in an argon filled stainless steel chamber inserted in a small resistance furnace. The melt was covered at all times with a flux consisting of 3 parts LiCl and 1 part LiF by weight. The flux, which normally amounted to about 25% of the charge weight, was charged with the aluminum and magnesium. In this way the flux, which was rather deliquescent, was dehydrated before the metals became molten. The lithium portion of the charge was then dried of kerosene and pushed under the flux cover with a molybdenum stirring rod. The melting and mixing operation was carried out between 700 and 750°C (1290 and 1380°F) and normally required about 5 minutes total time.

The alloys were then poured into a cold iron mold of square cross section resulting in a 1 cm ×1 cm ×2 to 4 inch long chill cast ingot. Ingots showing any obvious evidence of segregation were discarded, as were any heats for which the weight loss exceeded 0.2 gram.

General control of chemical composition was excellent as may be appreciated from Table II. Because of the generally good control of composition afforded by the melting technique employed, only those alloys were analyzed which appeared to delineate phase boundaries, or those for which analyzed compositions were, for other reasons, desired. The nominal compositions of alloys prepared for study are shown in Fig. 2.

With the exception of alloys lying in the vicinity of the magnesium-lithium axis, the alloys were generally far too brittle to permit any working operation prior to the equilibration anneals. Because of this the ingots were simply broken or cut into samples approximately one-quarter inch on a side. These samples were wrapped in aluminum foil with a stamped identification tag and were sealed under a partial pressure of argon in pyrex bulbs.

All bulbs were given an initial homogenization anneal of 2 hours at 400°C (750°F) whereupon the bulbs were either broken in chilled kerosene or furnace-cooled to 300, 200 or 100°C (570, 390, 210°F) and held for approximately 40, 100, and 300 hours respectively. These were quenched, as in the case of the 400°C (750°F) bulbs, by breaking the bulb under chilled kerosene.

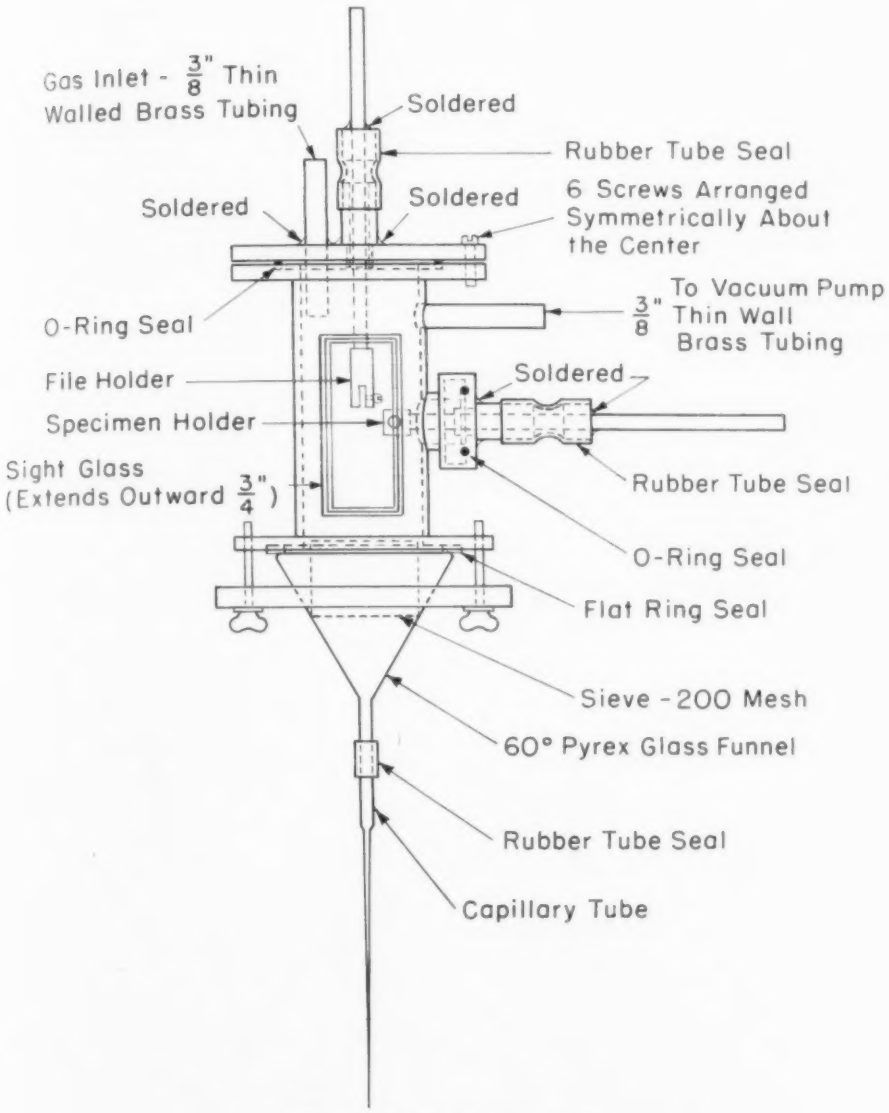


Fig. 3—Powdering Apparatus.

Heat treated samples were mounted in a room temperature setting resin which remained below 50°C during curing. Samples were polished by conventional techniques except in the case of the more reactive alloys which were ground and polished under mineral oil. Samples were etched with suitable reagents which are listed in Table III. Phases could generally be identified from the microstructures once positively identified by X-ray diffraction.

Specimens were prepared for X-ray diffraction by powdering heat treated samples in the apparatus pictured in Fig. 3. The illustration is largely self-explanatory and permits the preparation of a sealed off capillary filled with —200 mesh powder. The entire operation is carried out under either high vacuum or a partial pressure of

Table III
Etchants Employed for This Study

Reagent	Action
1. 10 Gr. Citric Acid 90 ml. Ethanol (95%) "Citral" (C)	Mild etch for outlining AlLi. Darkens β, slightly darkens $MgLiAl_2$ and (Mg)
2. 4 gr. Picric Acid 100 ml Ethanol (95%) 10 ml H_2O 5 ml Glacial Acetic Acid "Acetic-Picral" (AP)	Stains β, attacks AlLi, severely if β is not present. Outlines (Mg) in the presence of β
3. 10 ml Acetic Picral 90 ml Ethanol (95%) "Modified Acetic-Picral" (MAP)	Slower acting version of (AP)
4. 20 ml conc. HF 20 ml conc. HNO_3 60 ml glycerol "Mixed acids in glycerol" (MAG)	Stains $MgLiAl_2$ tan to brown, $Mg_{17}Al_{12}$ gray; (Mg) white and severely attacks AlLi
5. 60 ml ethylene glycol 19 ml H_2O 20 ml glacial acetic acid 1 ml conc. HNO_3 "Glycol-Acetic-Nitric" (GAN)	Stains (Mg) blue to brown, $Mg_{17}Al_{12}$ tan to brown; $MgLiAl_2$ remains white

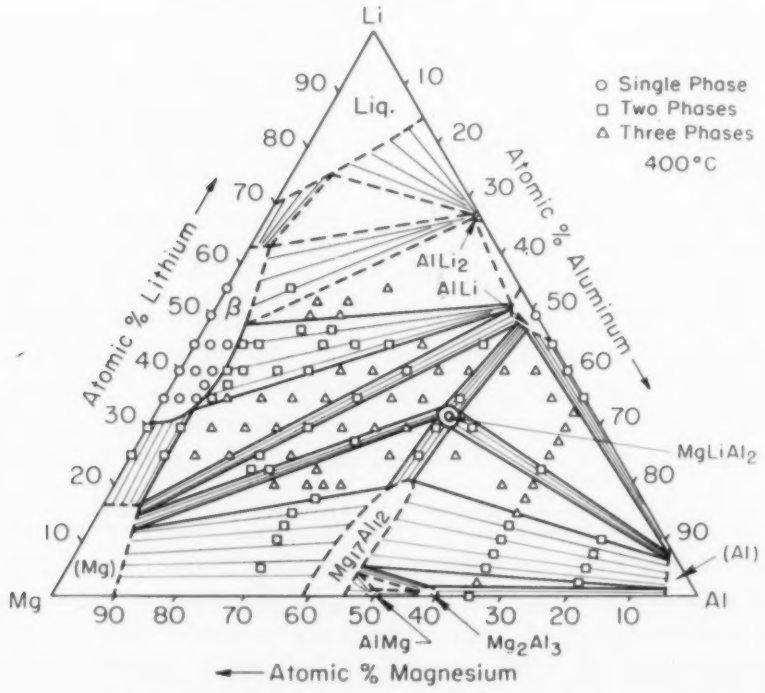


Fig. 4—400°C (750°F) Isothermal Section.

inert gas. Samples were not annealed after filing except for one series of binary Mg-Li β alloys used for a parametric study described later.

X-ray patterns were obtained in 14.4 cm DeBye cameras using nickel filtered copper radiation. Some additional data were obtained from mounted metallographic samples in a Norelco Geiger-counter spectrometer unit.

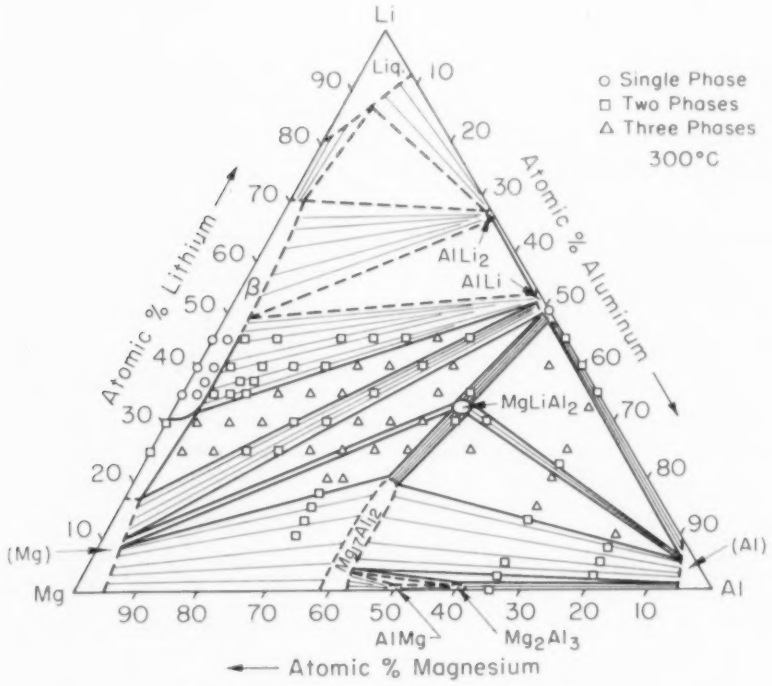


Fig. 5—300°C (570°F) Isothermal Section.

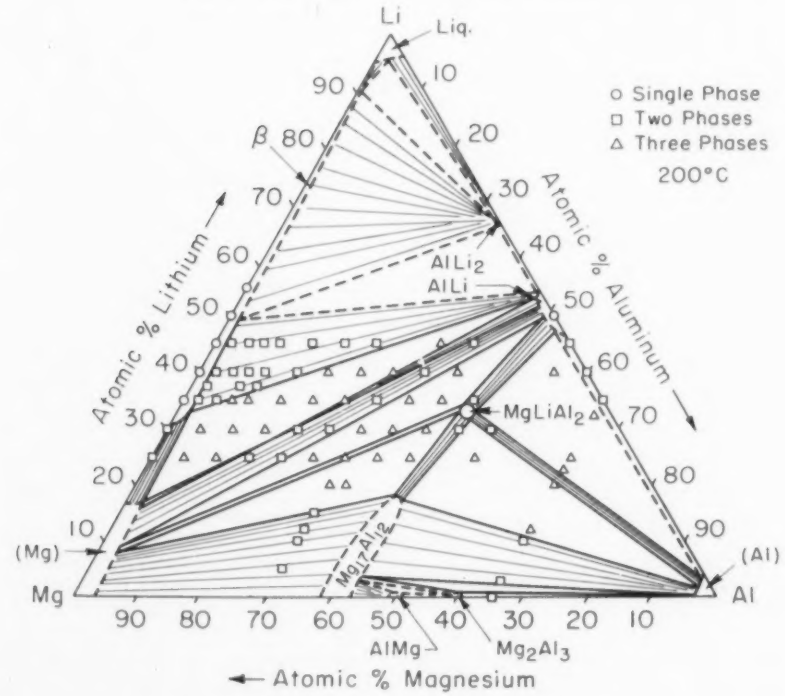


Fig. 6—200°C (390°F) Isothermal Section.

In order to be certain that the reflections observed were produced by the alloys themselves and not by any oxidation product which formed during specimen preparation in spite of all precautions,

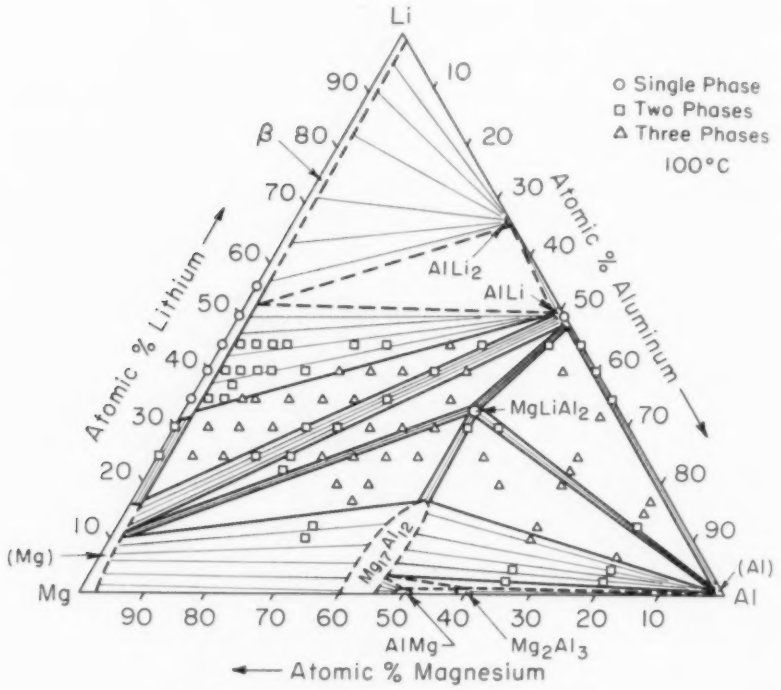


Fig. 7—100°C (210°F) Isothermal Section.

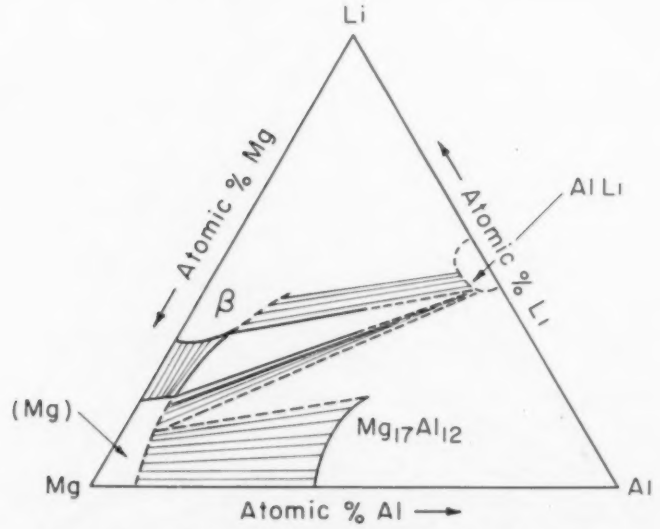


Fig. 8—372°C (700°F) Isothermal Section of Jones.

solid pieces of reactive alloys from representative regions of the ternary diagram were allowed to scale in air for several days. Samples of the scale were taken and powder patterns were made of these surface scales. Six such "oxide" patterns were made and the d values were recorded. In this way all patterns made could be readily checked for the presence of these atmospheric reaction products.

Results and Discussion

The data are summarized in the isotherms of Figs. 4,5,6 and 7. Note that the tie lines shown are hypothetical and serve only to delineate the two-phase fields. For comparative purposes, isothermal sections for the highest temperature of study of Shamrai (1) and of Jones (6) are shown in Figs. 1 and 8.

The solid lines shown on the isotherms summarizing the results of the present study are believed to be accurate since they are, in all cases, delineated by at least several alloys in which a phase appears or disappears, or both. Dashed lines are used to outline probable phase relationships in areas for which there were an insufficient number of experimental alloys for positive location of the boundaries.

A number of aspects of this ternary system are of particular interest. A ternary intermediate phase was identified having nearly the stoichiometry of $MgLiAl_2$. This is precisely the phase first claimed by Shamrai (1). The intersection of four two-phase fields places the composition at 46 at. % Al, 31 at. % Li and 23 at. % Mg. Fig. 9 shows the single phase microstructure of an alloy prepared to have this composition and equilibrated at 400°C (750°F).

The ternary intermediate phase $MgLiAl_2$ was found to co-exist with the (Mg), AlLi, (Al) and $Mg_{17}Al_{12}$ phases[2] at all temperatures investigated, and these two-phase structures are shown for 400°C (750°F) in Figs. 10–13. No evidence of the $[\beta+MgLiAl_2]$ phase field reported by Shamrai (see Fig. 1) was found, and the presence of the [(Mg)+AlLi] field reported by Jones and corroborated by this study renders a $[\beta+MgLiAl_2]$ field impossible at the temperatures investigated.

Alloys from the surrounding three-phase fields are shown in Figs. 14–17. Representative microstructures from the other phase fields investigated are shown in Figs. 18–27.

An attempt was made to determine the structure and compositional variation of lattice constants of all equilibrium phases for this system. This attempt was singularly unsuccessful only in the instance of the $AlLi_2$ phase which proved to be so chemically active as to defy all attempts to produce a satisfactory powder or solid spectrometer sample. It is significant that the structure of this phase has never been reported.

The binary (AlMg) phase, which occurs at 50 at. % Al has been reported to have low symmetry (8) and was not encountered in any of the experimental alloys. The structure and gross compositional parametric variations for phases whose structures are well known are given in Table IV. The indexed reflections found for the ternary ($MgLiAl_2$) phase are given in Table V.

[2]The terminology used to describe the various phases is that in common use. (Mg) and (Al) refer respectively to the primary magnesium and aluminum solid solutions.

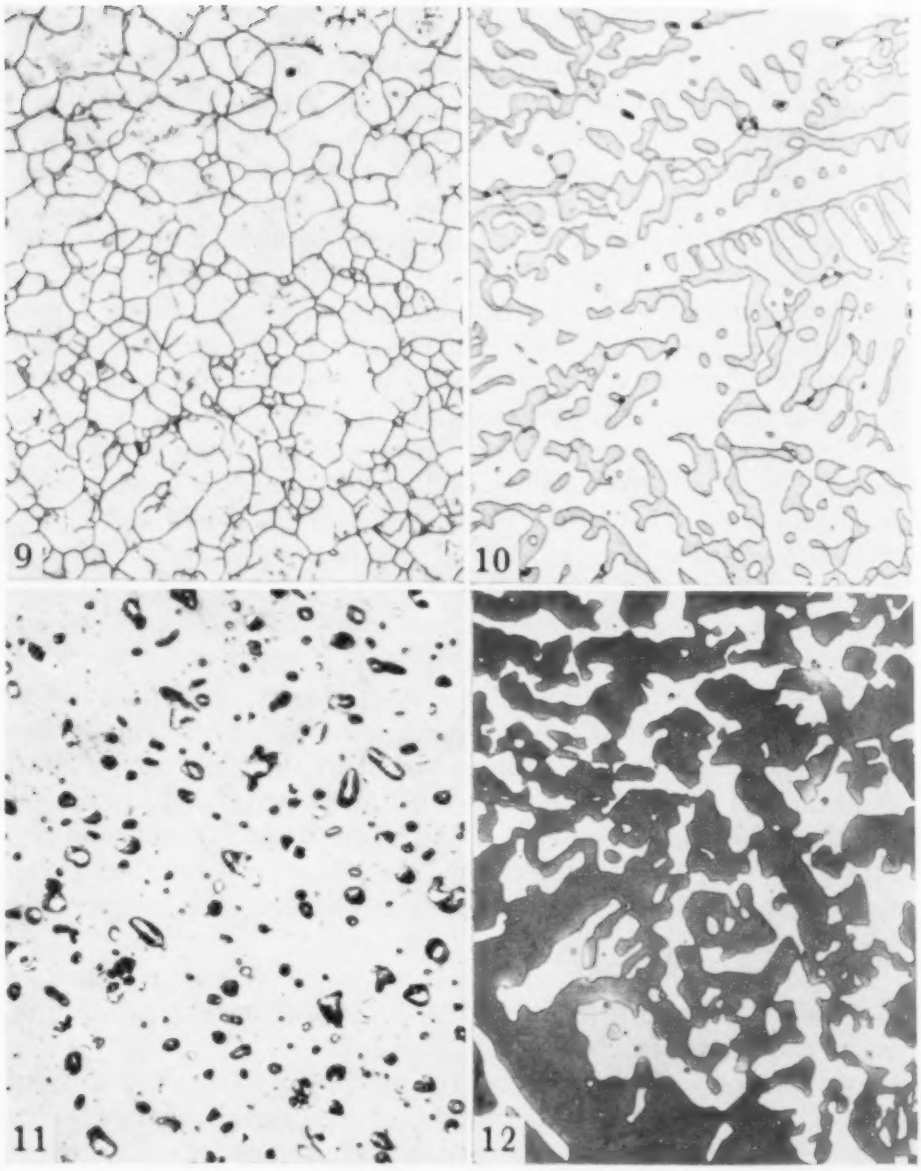


Fig. 9—Ternary Intermediate Phase $MgLiAl_2$ — ×250 Aqueous HF-HNO_3 Etch.
Fig. 10—(Mg) + $MgLiAl_2$ Phases. Matrix is (Mg) — ×250 MAG Etch.
Fig. 11—AlLi + $MgLiAl_2$ Phases. AlLi partly dissolved out— ×250 AP Etch.
Fig. 12—(Al) + $MgLiAl_2$ (matrix) Phases— ×250 MAG Etch.

Two features of these data are unusual. Firstly, the lattice constant of the β phase shows approximately linear variation to a pronounced minimum at 50 at. % Li for Mg-Li binary alloys (see Table IV). This variation is most probably due to a Brillouin zone overlap and is discussed more fully elsewhere (9). If this is the case, the effect of addition of trivalent Al to the solid solution would be to shift the minimum toward the lithium-rich side so that the β parametric surface would be cusped, with the cusp following the Mg-Al ratio

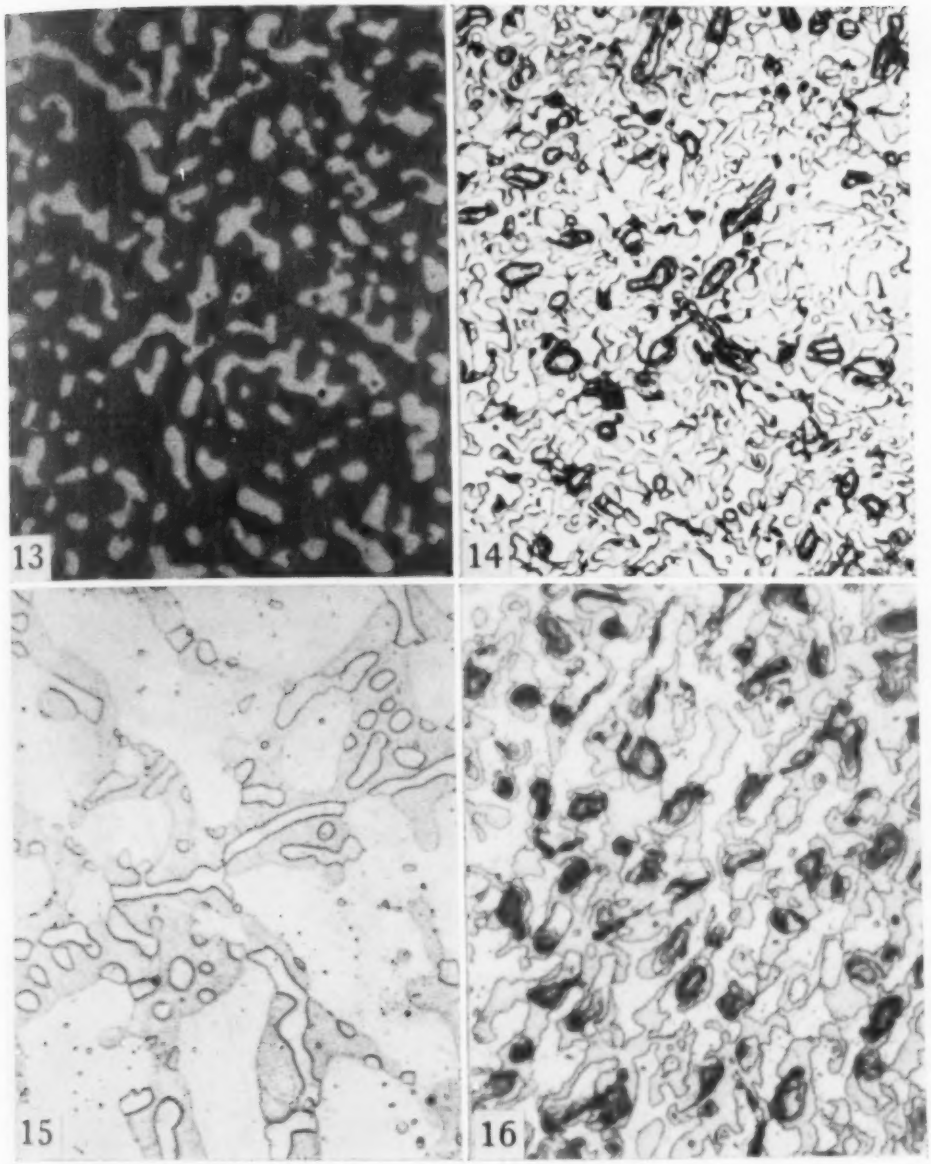


Fig. 13—$Mg_{17}Al_{12}+MgLiAl_2$ (gray matrix)—×250 MAG Etch.
Fig. 14—(Mg)+AlLi+$MgLiAl_2$.—×250 AP Etch.
Fig. 15—(Mg)+$MgLiAl_2$+$Mg_{17}Al_{12}$. Matrix is (Mg)—×500 MAG Etch.
Fig. 16—(Al)+$MgLiAl_2$+AlLi—×500 MAG Etch.

which maintains an electron concentration of 1.5 per atom. Because these alloys were somewhat richer in lithium than most of those studied, this could be only superficially verified.

Secondly, examination of the data in Table V for the ternary phase, which was found to be most satisfactory indexed as cubic with $a_o \cong 20.2$ Å, indicates that there exists an overlap with the reflections previously assigned to what has been called the $MgLi_2Al$

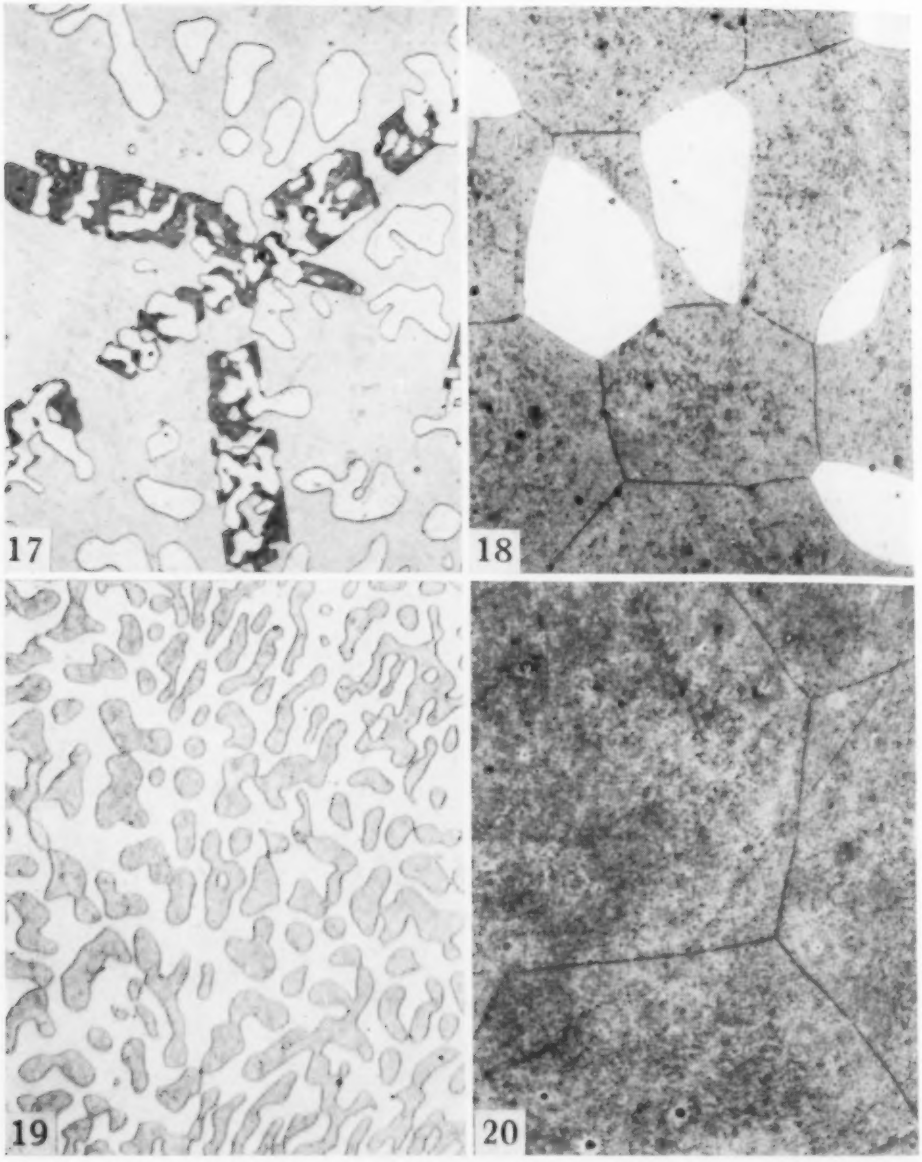


Fig. 17—(Al) + $MgLiAl_2$ (dark) + $Mg_{17}Al_{12}$. Matrix is $Mg_{17}Al_{12}$ — ×250 MAG Etch.
Fig. 18—(Mg) + β (dark)— ×250 Citral Etch.
Fig. 19—(Mg) + $Mg_{17}Al_{12}$ (gray)— ×500 Citral Etch.
Fig. 20—β— ×250 Citral Etch.

phase (cubic, NaTl type, $a_o \cong 6.7$ Å). Note that this value is almost exactly ⅓ the parameter of the $MgLiAl_2$ phase. The assignment of these reflections and, consequently, this cubic structure to the $MgLiAl_2$ phase is based on approximately 20 experimental alloys rich in this phase. The alloy which was single phase metallographically showed a small quantity of the ternary solution based on $Mg_{17}Al_{12}$ after filing. The $MgLi_2Al$ cannot, based on the general data of this

Table IV
Structure and Parameters of Phases Studied

Phase	Structure	Parameters	
(Mg)	HCP	a = 3.16A c/a = 1.63	—Li rich Mg-Li binary—Practically no change for compositions in equilibrium with different phases
(Al)	FCC	a = 4.04Å	—Pure Al. ½% increase if in equilibrium with $Mg_{17}Al_{12}$ or $MgLiAl_2$. Slightly greater increase when saturated with Li
β	BCC	a = 3.51Å	—Pure Li. Addition of Mg linearly decreases parameter to a minimum of 3.485Å at 50 at. % Mg. Parameter increases upon further addition of Mg to a = 3.516Å at β/β+(Mg) phase boundary
AlLi	Cubic (NaTl)	a = 6.36Å	(binary) Max. increase of 1% in equilibrium with the β phase. Somewhat smaller increases for equilibrium with phases less rich in lithium
$Mg_{17}Al_{12}$	Cubic (αMn)	a = 10.52Å	(binary) Parameter decreases with addition of either Al or Li. Max. decrease of 1.5% in equilibrium with $MgLiAl_2$
Mg_2Al_3	Cubic	a = 28.2Å	Value in equilibrium with (Al)
$MgLiAl_2$	Cubic	a = 20.2Å (See Table V)	[equilibrium with (Al)] increase in parameter up to 1.5% when in equilibrium with (Mg) or AlLi
Transition ($MgLi_2Al$) Phase	Cubic (NaTl)	a = 6.7 Å	Found only in several delayed-quenched beta alloys

Table V
X-Ray Identification of the $MgLiAl_2$ Phase

I	d_{obs}**	d_{calc}*	Indices
vw	7.129	7.12	220
w	6.071	6.07	311
w	4.652	4.62	331
vw	4.500	4.50	420
s	4.109	4.11	422
s	3.870	3.87	511
w	3.556	3.56	440
vw	3.398	3.41	531
w	2.831	2.83	711
ft	2.702	2.70	642
w	2.623	2.62	731
vw	2.519	2.52	800
ms	2.454	2.46	733
vs	2.371	2.37	822
w	2.327	2.32	751
ms	2.204	2.20	842
mw	2.146	2.15	664
w	2.112	2.12	931
ms	2.024	2.03	933
m	1.976	1.98	1020

*Based on a cubic structure cell with $a_o = 20.2$ Å
**Only the first 20 lines observed are recorded. An additional 63 lines were indexed. The indices obey the systematic selecting rule h k l ie., the sum of any 2 indices is always even.

Table VI
Summary of Results for Transition Phase Study on Extruded Wire
Sample Alloy is
Dow No. 76066
(Mg, 40Li,4.8Al)(at. %)

Heat Treatment	Phases Present*
400°C→WQ(1)	β+"$MgLi_2Al$"+trace (Mg)
400°C→WQ(1)+150°C (2 hrs)	β+"$MgLi_2Al$"+trace AlLi+trace (Mg)
400°C→WQ(1)+150°C (16 hrs)	β+trace "$MgLi_2Al$"+AlLi+trace (Mg)
400°C→WQ(1)+150°C (30 hrs)	β+AlLi+trace (Mg)
400°C→WQ(1)+150°C (2 hrs)+177°C (2 hrs)	β+AlLi+trace (Mg)
400°C→WQ(2)	β+trace "$MgLi_2Al$"
400°C→WQ(2)+100°C (½ hr)	β+"$MgLi_2Al$" (more than above)
400°C→WQ(2)+100°C (1 hr)	β+"$MgLi_2Al$" (still more)
400°C→WQ(2)+100°C (2 hrs)	β+"$MgLi_2Al$" (still more)
400°C→WQ(2)+100°C (25 hrs)	β+ AlLi+trace (Mg)+trace "$MgLi_2Al$"

*X-ray study of the extruded wire sample.
(1)Delayed 5 sec. in air before quenching.
(2)Rapid quench.

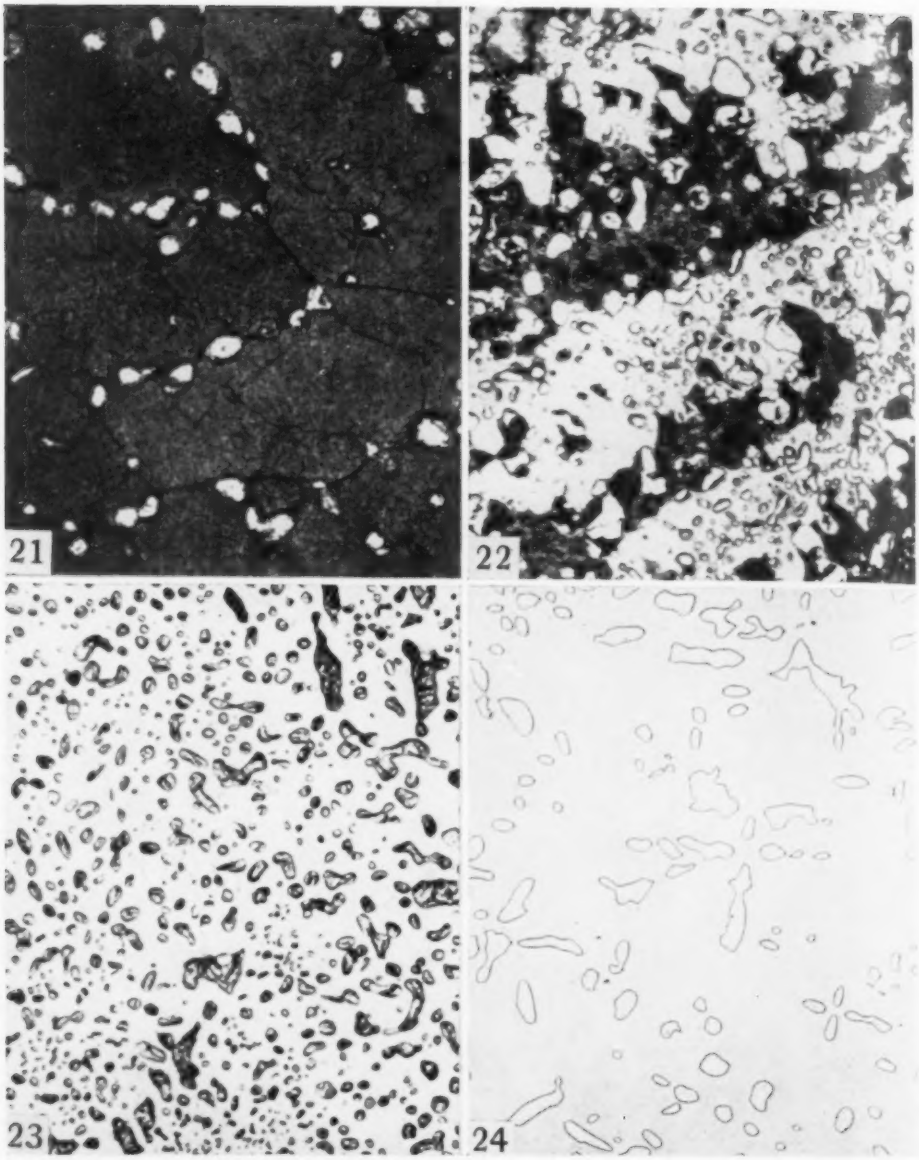


Fig. 21—β+AlLi—×250 Citral Etch.
Fig. 22—(Mg)+β+AlLi. AlLi is Outlined and Partly Dissolved—×250 AP Etch.
Fig. 23—(Mg)+AlLi—×250 Citral Etch.
Fig. 24—(Al)+Mg_2Al_3 (matrix)—×100 MAG Etch.

study, exist as an equilibrium phase in this system. This phase ($MgLi_2Al$) was encountered in several samples of β alloys near the β/β+AlLi boundary quenched from 400°C (750°F). Metallographic examination of these alloys showed only the β phase. These X-ray observations were made on alloys powdered after quenching and also on extruded wire samples of alloys of similar composition kindly furnished by J. B. Clark of the Dow Chemical Company. Subse-

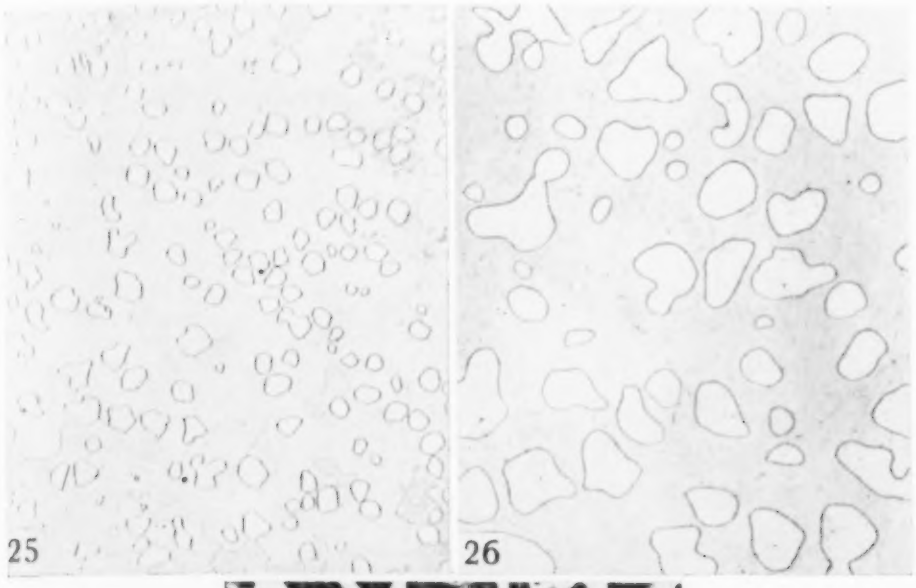




Fig. 25—$Mg_2Al_3+Mg_{17}Al_{12}+(Al)$. (Al) is white and outlined—×100 MAG Etch.
Fig. 26—$(Al)+Mg_{17}Al_{12}$ (matrix)—×250 MAG Etch.
Fig. 27—(Al)+AlLi (dark)—×250 Citral Etch.

quent annealing of these samples at several temperatures in the β+AlLi field indicated that the X-ray pattern corresponding to $MgLi_2Al$ at first increased in intensity and then disappeared at the expense of AlLi reflections. These data are summarized in Table VI. The transformation appeared to be of the discontinuous type, that is, AlLi lines co-existed with lines of the $MgLi_2Al$ phase and became more intense with time as the latter lines diminished to zero in intensity. It would thus appear that the $MgLi_2Al$ phase is a

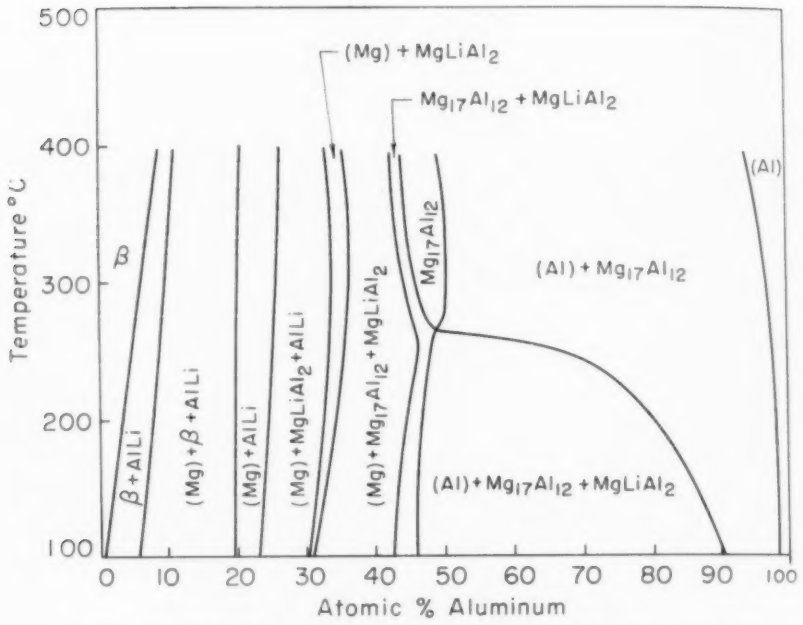


Fig. 28—Vertical Section through the Al Corner and the β Phase Field.

transition phase preceding the rejection of AlLi from the β phase. It remains to be convincingly shown that the composition of this phase actually corresponds to the stoichiometry $MgLi_2Al$.

The surprisingly large ternary solubility of the binary $Mg_{17}Al_{12}$ phase reported by Shamrai was confirmed in the present study.

The general effect of temperature on the phase space surfaces can be appreciated from the vertical section of Fig. 28. This vertical section, which was constructed from the isothermal data, is drawn from the aluminum corner to the Mg-Li axis intersecting the axis at approximately 36.5 at. % Li.

Summary

The study by metallographic and X-ray diffraction methods of approximately 150 alloys has permitted the construction of partial isothermal sections for the temperatures of 400, 300, 200 and 100°C (750, 570, 390, 210°F) for this system.

A ternary intermediate phase first reported by Shamrai was found at the composition 46 at. % Al, 31 at. % Li and 23 at. % Mg. The miscibility field of this phase was found to be small and the structure of the phase was found to be cubic with $a_o = 20.2$ Å.

It was found that the "$MgLi_2Al$" phase is not an equilibrium phase in this system at any temperature investigated. An experiment demonstrating the transitional nature of this phase is reported.

ACKNOWLEDGMENT

The authors wish to express their appreciation of the sponsorship of this research by the Metallurgy Research Laboratory, Frankford Arsenal, Philadelphia, Pennsylvania, and for permission to publish this paper.

The work was supported on Contract No. DA-11-022-ORD-906.

References

1. F. I. Shamrai, "The Ternary System; Aluminum-Magnesium-Lithium. Part I. Method of Working with Lithium. Binary Systems. Part II. Phase Diagrams for Additional Cross Sections. Part III. Projection of the Surface of the Liquidus; Isotherms at 400 and 20°C and Process of Crystallization," Bulletin of the Academy of Sciences of the U.S.S.R., Section of Chemical Science, 1947, Part I, p. 605, 1948, Part II, p. 83 and Part III, p. 290.
2. J. H. Jackson, P. D. Frost, A. Loonam, L. Eastwood and C. Lorig, "Magnesium Lithium Base Alloys, Preparation, Fabrication and General Characteristics," *Transactions*, American Institute of Mining and Metallurgical Engineers, Vol. 185, 1949, p. 149.
3. R. S. Busk, D. L. Leman and J. J. Casey, "The Properties of Some Magnesium-Lithium Alloys Containing Aluminum and Zinc," *Transactions*, American Institute of Mining and Metallurgical Engineers, Vol. 188, 1950, p. 945.
4. P. D. Frost, J. G. Kura and L. W. Eastwood, "Aging Characteristics of Magnesium-Lithium Base Alloys," *Transactions*, American Institute of Mining and Metallurgical Engineers, Vol. 188, 1950, p. 1277.
5. P. D. Frost, J. H. Jackson, A. C. Loonam and C. H. Lorig, "The Effect of Sodium Contamination on Magnesium-Lithium Base Alloys," *Transactions*, American Institute of Mining and Metallurgical Engineers, Vol. 188, 1950, p. 1171.
6. A. Jones, WADCTR, 1951, p. 52.
7. A. Jones, J. Lennon, R. Nash, W. Chang and E. MacPeek, WADCTR, 1952, p. 52.
8. K. Eickhoff and H. Vosskuhler, "Phase Diagram of Aluminum-Magnesium System," Zeitschrift fur Metallkunde, 1953, 44:223 ff.
9. D. W. Levinson, "On the Lattice Parameter of Mg-Li β Alloys," *Acta Metallurgica*, Vol. 3, 1955, p 294.

THE CONSTITUTION OF INDIUM-ARSENIC-ANTIMONY ALLOYS

By C. H. Shih and E. A. Peretti

Abstract

The alloys have been investigated over the entire compositional range by thermal analysis, microscopic and X-ray methods.

The valid tie lines connecting the compound InAs with the binary compound InSb and Sb divide the diagram into three subternary areas. No ternary compounds were found to exist.

In the system InAs-InSb-In an InAs-rich solid solution is the primary phase upon cooling of the liquid, regardless of composition. The secondary precipitation consists of almost pure InSb, and all alloys complete their freezing at 154.5°C (310°F).

The InAs-InSb-Sb region of the diagram has a eutectic valley whose maximum point lies on the InAs-Sb tie line at 82.5% Sb and 17.5% InAs and with a melting point of 582°C (1080°F). The minimum point is on the terminal InSb-Sb binary at 494°C and 69.5% antimony. The primary phase for all compositions lying on the InAs side of the eutectic trough is an InAs-rich solid solution, and antimony is the first phase to precipitate on the other side of the eutectic line. The temperature of the ternary eutectic plane is identical with that of the binary InSb-Sb eutectic, 494°C.

The third sub-ternary area, involving InAs, antimony and arsenic contains a eutectic trough running from the InAs-As binary eutectic, 731°C, 82% arsenic, to the InAs-Sb binary eutectic at 582°C and 82.5% antimony. Depending upon which side of the eutectic valley an alloy lies, it may have as a primary phase either an As-Sb-rich or an InAs-rich solid solution. The temperature of final solidification in this region depends upon composition and may vary from 731 to 582°C. (ASM-SLA Classification: M24, In, As, Sb)

AS PART of a research program on indium alloys, begun in the Metallurgy Laboratories of the University of Notre Dame several years ago, there have been determined and published the phase relationships in the systems In-Bi (1),[1] In-Cd-Zn (2), In-As

Abstracted from a dissertation submitted by C. H. Shih to the Graduate School, University of Notre Dame, in partial fulfillment of the requirements for the degree of Doctor of Philosophy.

Of the authors, C. H. Shih is research associate Massachusetts Institute of Technology, Cambridge, Mass. and E. A. Peretti is professor of metallurgy, University of Notre Dame, Notre Dame, Ind. Manuscript received April 13, 1955.

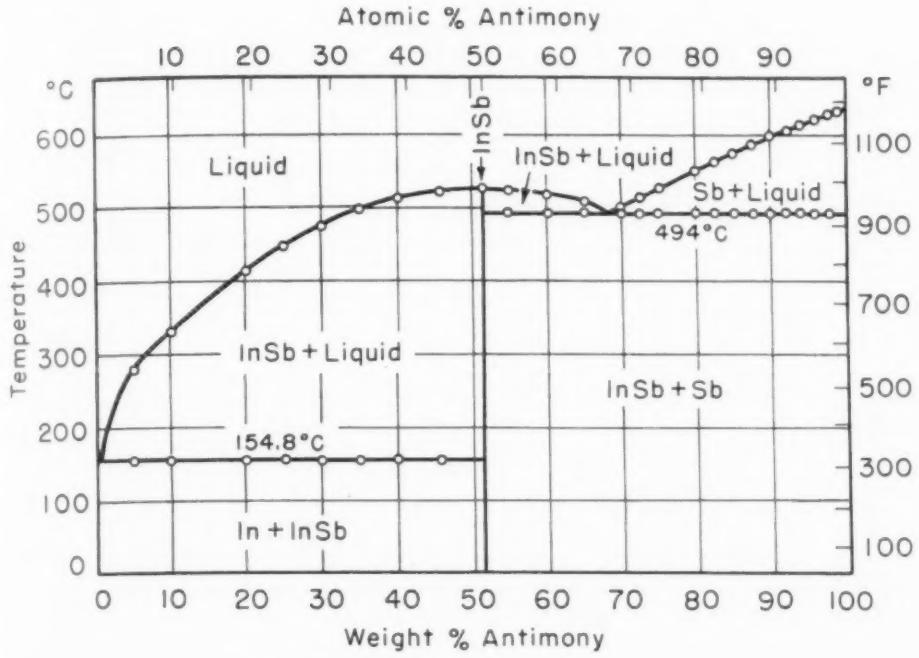


Fig. 1—The Indium-Antimony Phase Diagram.

(3), In-Sb (4), InAs-InSb (5) and InAs-Sb (6). Preliminary X-ray studies showed that the valid tie lines in the In-As-Sb ternary system were those connecting InAs with Sb and InSb. These tie lines divide the ternary into three sub-ternaries: namely, InAs-InSb-Sb, InAs-Sb-As and In-InAs-InSb. It was the object of this work to determine the liquidus and solidus of the complete ternary system. As far as is known, other than our own work cited above, no description of the ternary indium-arsenic-antimony system has appeared in the literature.

Previous Work

The Binary Indium-Antimony System—The phase diagram of the indium-antimony alloys is shown in Fig. 1. This is based on the work of Liu and Peretti (4). An intermediate phase exists whose composition corresponds closely to InSb. It melts congruently at 525°C (970°F) and has a face centered cubic, zinc blende-type structure, with a lattice parameter of 6.4760Å. It forms eutectics with both antimony and indium. The antimony-rich eutectic contains 69.5% antimony and melts at 494°C (920°F), and the indium-rich contains 0.7% antimony and melts at 154.8°C (310°F). The solid solubility of each element in the other is very small.

The Binary Indium-Arsenic System—Fig. 2 shows the indium-arsenic diagram according to Liu and Peretti (3). As in the indium-

[1]The figures appearing in parentheses pertain to the references appended to this paper.

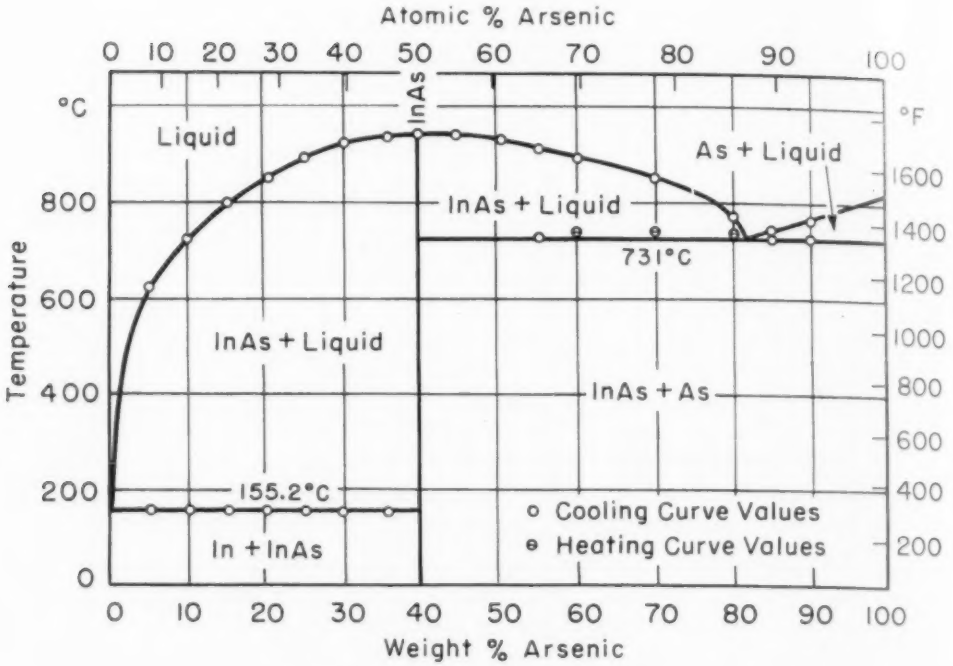


Fig. 2—The Indium-Arsenic Phase Diagram.

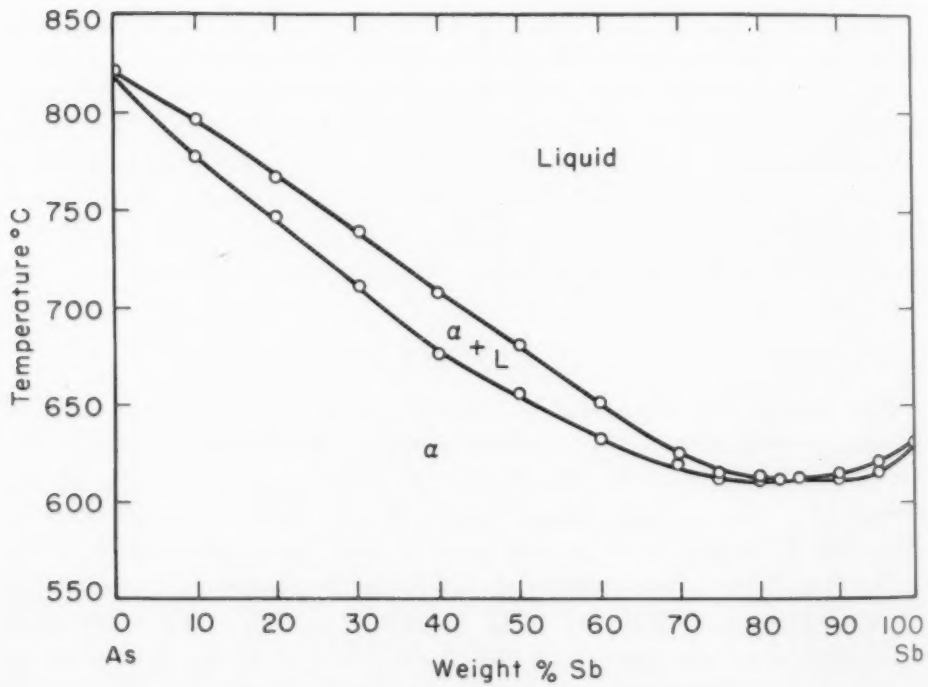


Fig. 3—The Arsenic-Antimony Phase Diagram.

antimony system an intermediate phase is formed of very narrow compositional limits. InAs melts at 942°C (1725°F), and like the InSb it has a face-centered cubic, zinc blende-type structure with a

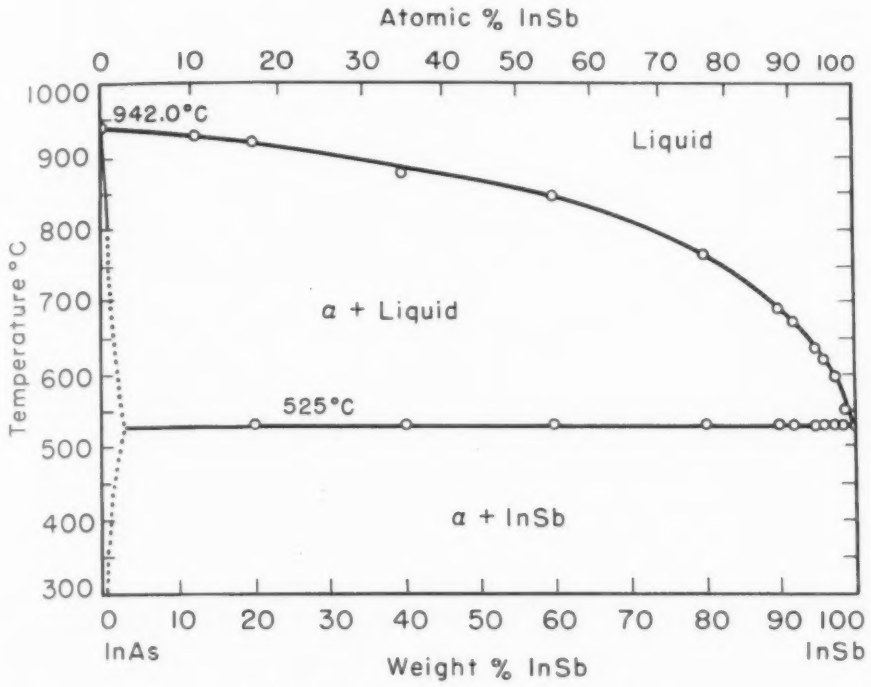


Fig. 4—The InAs-InSb Phase Diagram.

lattice parameter of 6.0584Å. The two eutectics melt at 731°C and 155.2°C (1350 and 310°F) and contain 82% and 0.02% arsenic, respectively.

The Binary Arsenic-Antimony System—Two investigations on this system are reported. Parravano and deCesaris (7) conducted thermal analyses in open clay crucibles under a hydrogen atmosphere on alloys containing up to 35% arsenic. Mansuri (8) made his studies with the alloys in evacuated glass tubes and was able to analyze alloys with up to 80% arsenic. As these investigators agree as to the broad outlines of the diagram, but differ on details, we thought it advisable to remeasure some of the liquidus and solidus points. The results of our experiments are shown in Fig. 3. These agree fairly well with Parravano and Mansuri for the high antimony compositions but, in general, the solidus and liquidus are lower for the higher arsenic alloys. Our experiments were carried out in open crucibles for alloys containing more than 75% antimony and in sealed evacuated containers for those with less than 75% antimony. As Mansuri had a residual pressure of 15 mm. of mercury in his capsules his final total pressure would be higher, and this might account for the differences. In any event the pressure is not constant over the whole compositional range, so Fig. 3 does not represent a true equilibrium diagram. X-ray patterns confirmed the existence of a continuous, single solid solution across the diagram. We found the

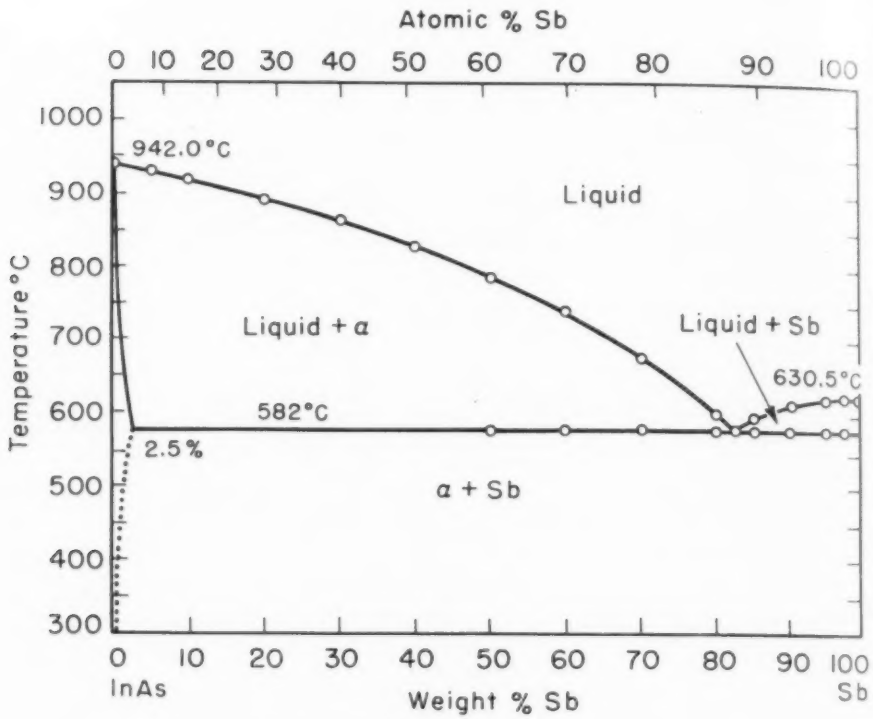


Fig. 5—The InAs-Sb Phase Diagram.

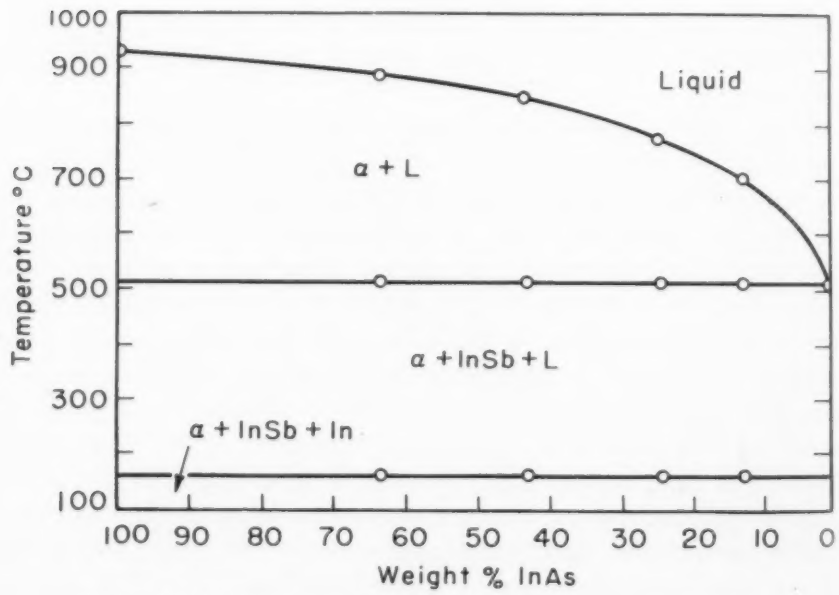


Fig. 6—Vertical Section in the In-InAs-InSb System, InSb: In = 3:7.

temperature of the minimum to agree exactly with the value given by Parravano and deCesaris, i.e. 612°C, and it lies between 80 and 85% Sb.

The System InAs-InSb—The results of Shih and Peretti (5) on

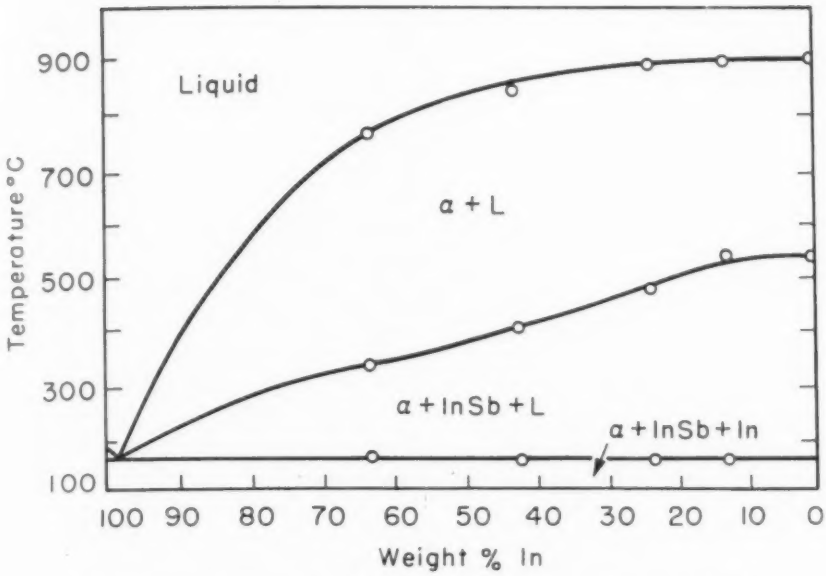


Fig. 7—Vertical Section in the In-InAs-InSb System, InSb:InAs = 3:7.

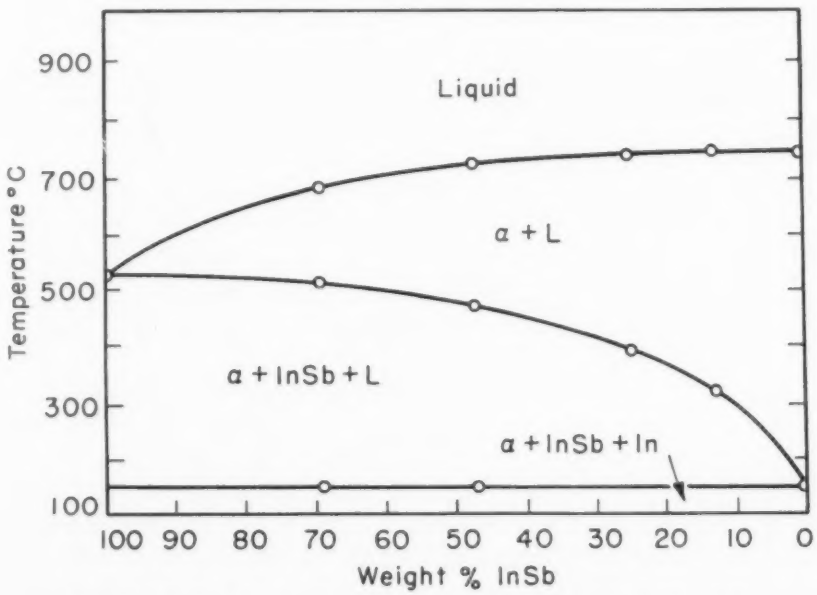


Fig. 8—Vertical Section in the In-InAs-InSb System, InAs:In = 3:7.

this pair are shown in Fig. 4. The liquidus is a continuous line running from the freezing point of InAs (942°C) to a eutectic point experimentally indistinguishable from the freezing point of InSb (525°C). A one-phase region in the InAs end of the diagram extends out to about 2% InSb at the eutectic temperature.

The System InAs-Sb—Fig. 5 shows the relationships in this system as reported by Shih and Peretti (6). A eutectic occurs at 582°C (1080°F), containing 82.5% antimony and 17.5% InAs by

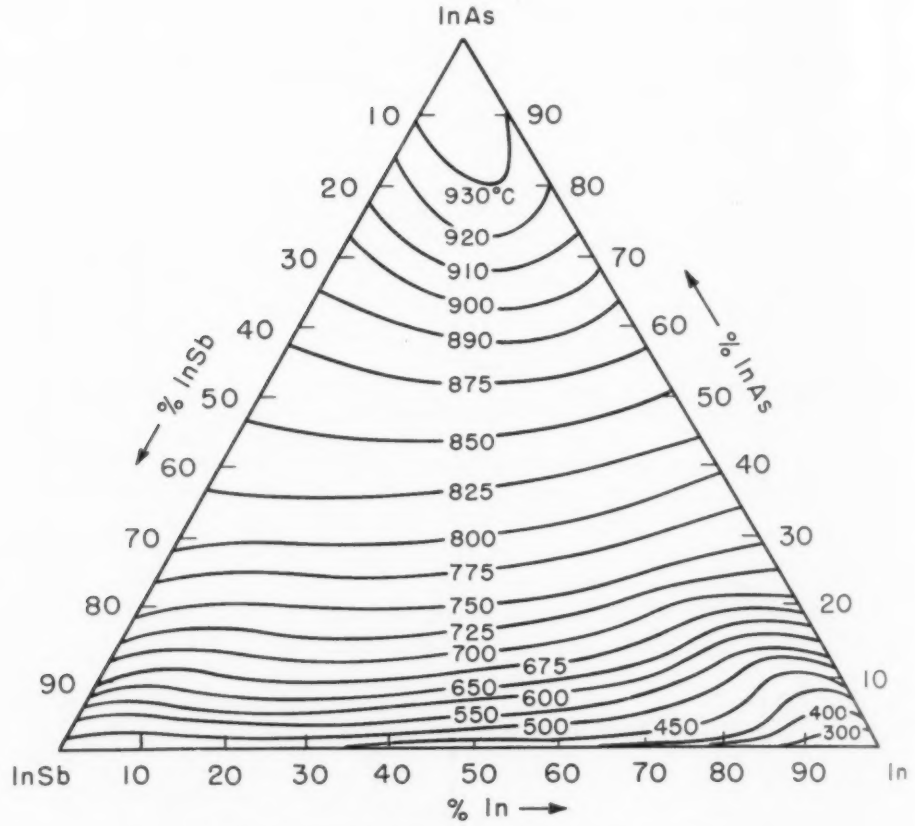


Fig. 9—The Liquidus Isotherms in the System In-InAs-InSb.

weight. The InAs-rich solid solution contains a maximum of 2.5% antimony at the eutectic temperature.

Experimental Methods

Materials

All alloys were prepared from materials of the highest purity available. The indium was loaned to us by the Indium Corporation of America. It had a guaranteed purity of 99.97% with the following chemical analysis: 0.002 wt.—% copper, 0.006% lead, 0.01% tin and 0.01% zinc.

The antimony came from two sources, Johnson, Mathey and Company, London and J. T. Baker Chemical Company, Phillipsburg, New Jersey. That from the first source contained 0.031 wt.—% arsenic, 0.001% copper, 0.015% iron, 0.001% nickel, 0.012% sulphur, 0.017% lead, 0.00005% bismuth, 0.005% aluminum and 0.006% silicon. The Baker antimony analyzed 0.007 wt.—% iron, 0.03% sulphur, 0.005% arsenic, 0.02% lead and 0.002% copper.

J. T. Baker's purified lump arsenic crystals were employed. A spectrographic analysis of this material is as follows: 0.00X% cop-

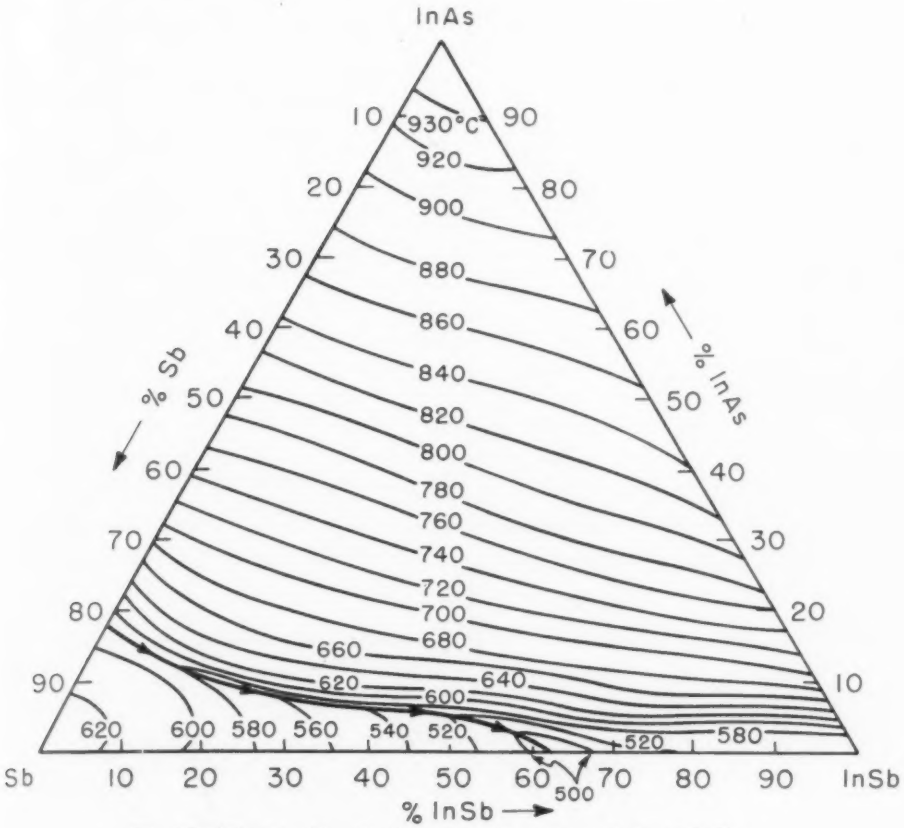


Fig. 10—The Liquidus Isotherms in the System Sb-InAs-InSb.

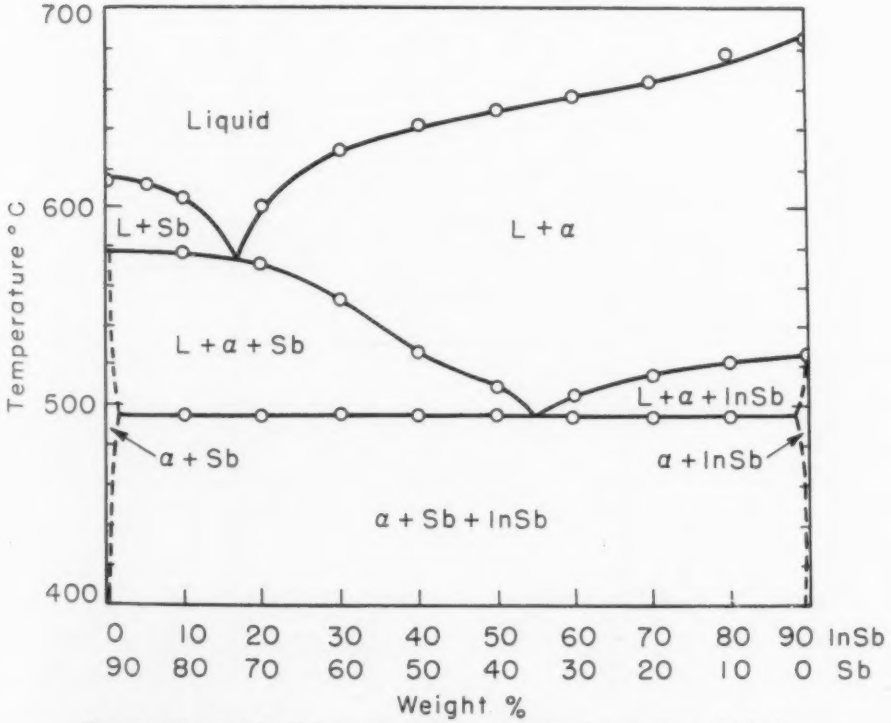


Fig. 11—Vertical Section in the Sb-InAs-InSb System at 10 wt. % InAs.

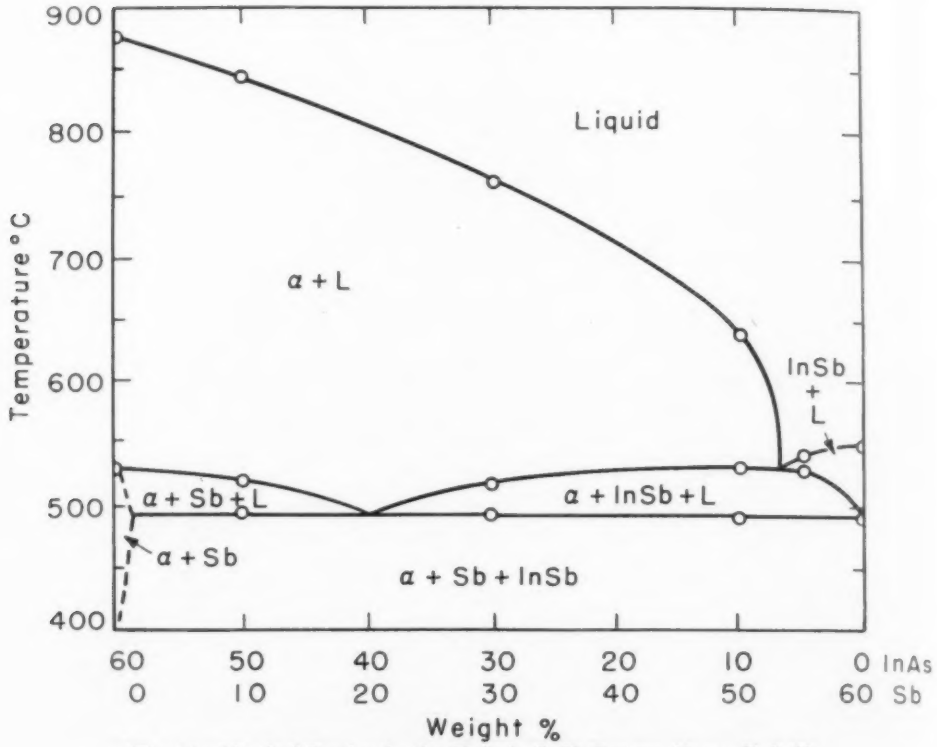


Fig. 12—Vertical Section in the Sb-InAs-InSb System 40 wt. % InSb.

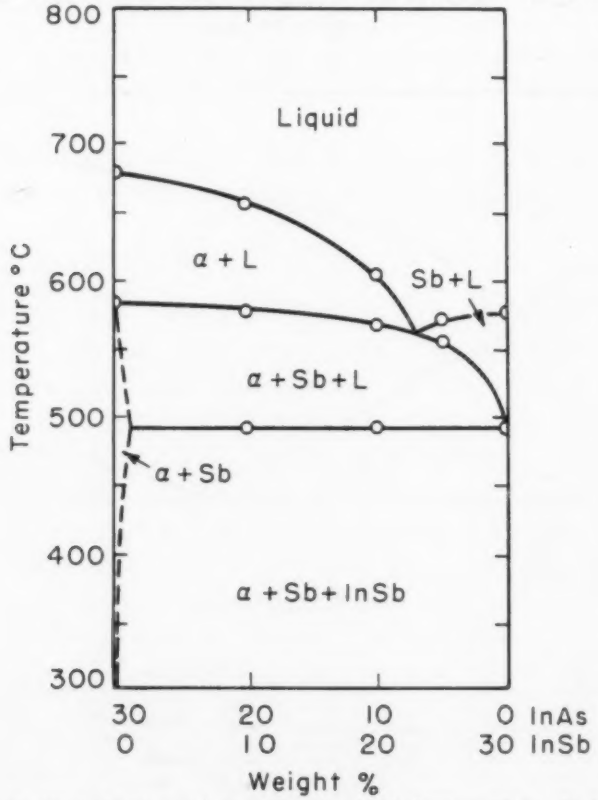


Fig. 13—Vertical Section in the Sb-InAs-InSb System 70 wt. % Antimony.

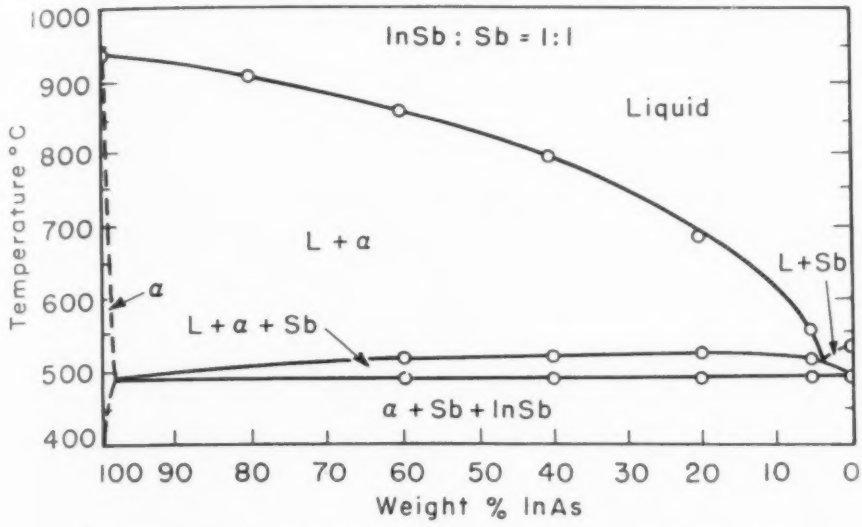


Fig. 14—Vertical Section in the Sb-InAs-InSb System with InSb:Sb 1:1.

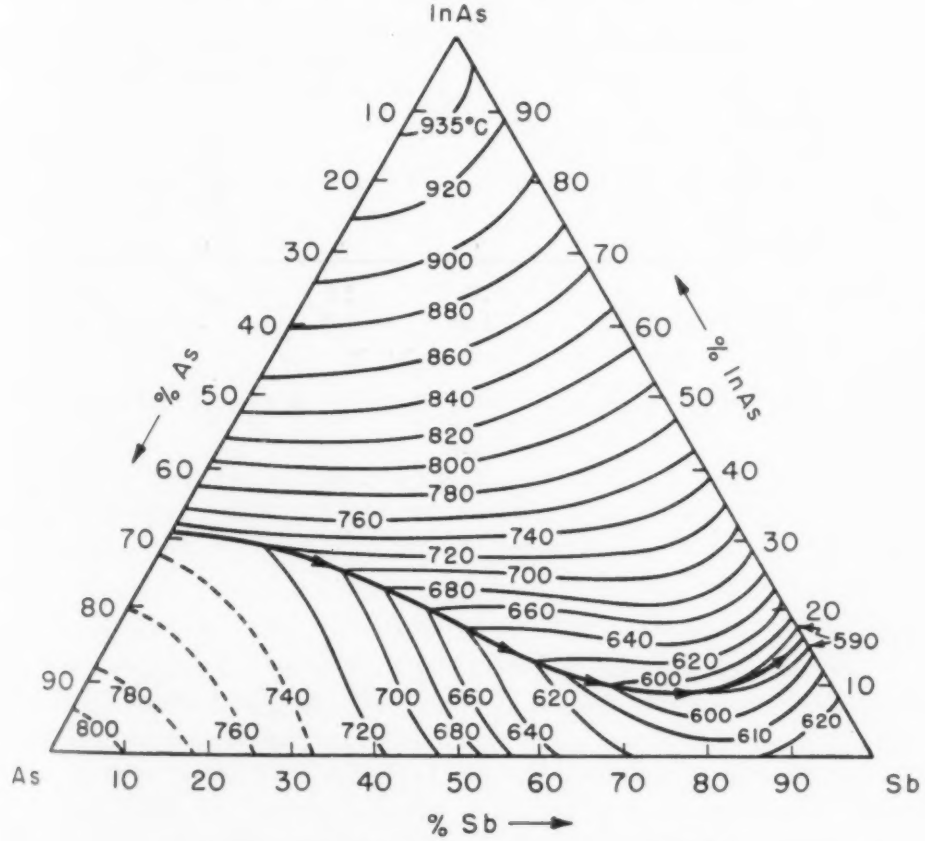


Fig. 15—Liquidus Isotherms in the System Sb-As-InAs.

per, 0.00X% lead, 0.0X% antimony, 0.0X% bismuth and 0.000X% iron. This arsenic was further purified before use by heating in vacuo at 350°C (660°F) to sublime oxides. The element was then

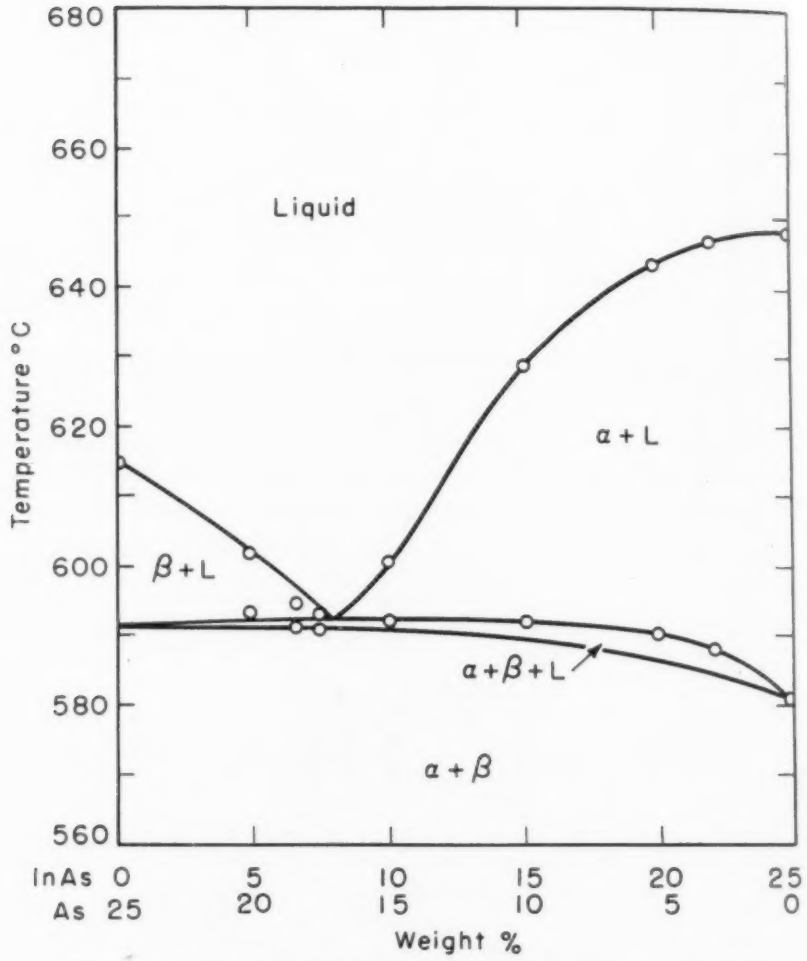


Fig. 16—Vertical Section in the InAs-Sb-As System, 75 wt.% Antimony.

sealed in evacuated Pyrex tubes, and the arsenic sublimed at 600°C (1110°F). The sublimate was condensed in the cooler portions of the tube, where it was stored, free from contact with air, until ready for alloying.

Alloy Preparation

Every alloy used in this investigation was made in evacuated, sealed Vycor or quartz tubes. The carefully weighed elements (to an accuracy of 0.0001 grams) were sealed in the closed capsules under a pressure of less than five microns. In order to minimize the quantity of arsenic vapor, the capsules were filled and sealed off with as little excess volume as possible. Melting was carried out in a muffle furnace at a temperature of 20 to 50° higher than the melting point of the alloy to be made. To insure complete dissolution the alloys were vigorously shaken while molten and held liquid for at least one half hour.

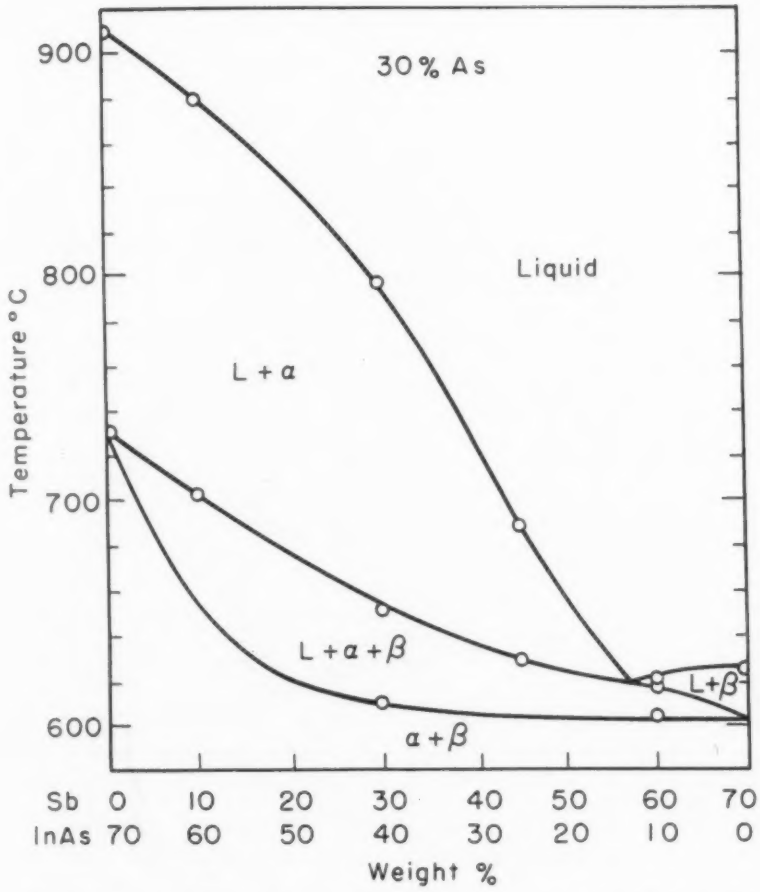


Fig. 17—Vertical Section in the InAs-Sb-As System, 30 wt. % Arsenic.

The three elements alloyed quite readily and little difficulty was encountered except with high arsenic compositions. These had a great tendency to explode, if overheated, due to the high arsenic pressure generated.

The weight of alloy made for thermal analysis was dependent upon whether open or closed tubes could be employed, i.e. it was largely determined by the arsenic content. For analyses in sealed tubes 10 to 15 grams of metal were used, while 30 to 70 grams could be conveniently worked with in open tubes under an inert atmosphere.

Thermal Analysis

Cooling curves were taken of the alloys at cooling rates of 0.5 to 5°C per minute by means of calibrated platinum versus platinum-rhodium or chromel-alumel thermocouples and a White single potentiometer with a high-sensitivity galvanometer. A thin-walled quartz tube protected the thermocouple from the molten metal. An

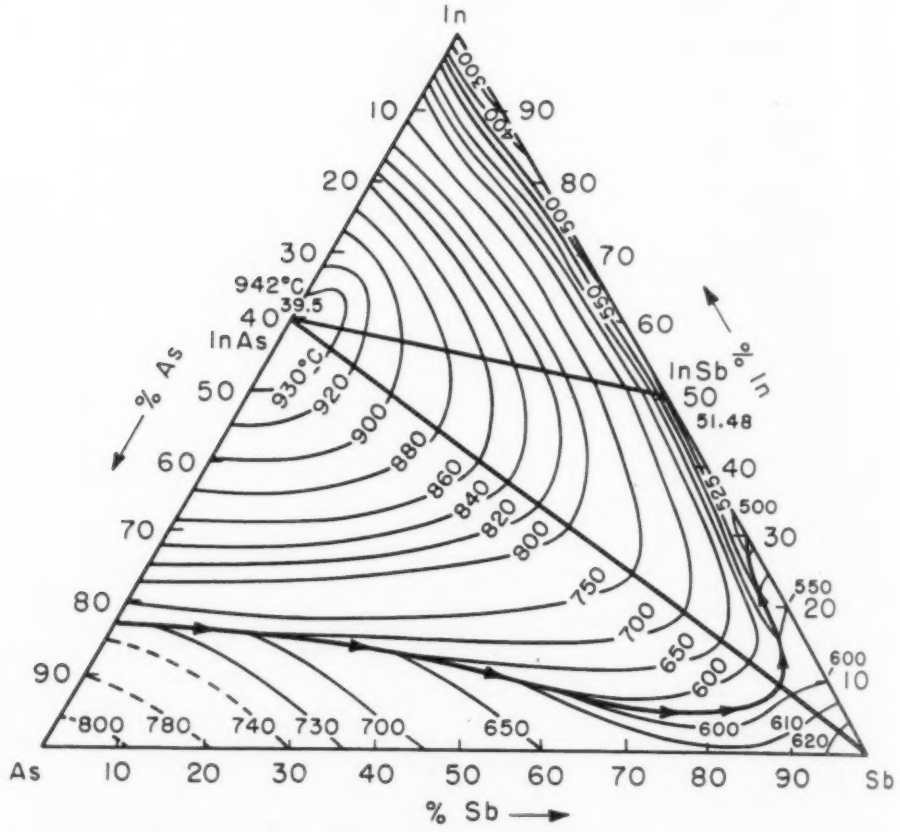


Fig. 18—The Liquidus Surface of the System In-As-Sb.

Table I
Thermal Arrests in the System In-InAs-InSb

InSb	InAs	In	Liquidus °C	Secondary °C	Solidus °C
0.0	100.0	0.0	942.0	—	942.0
11.5	62.0	26.5	897.8	396.4	154.6
11.5	26.5	62.5	755.0	324.5	155.7
12.5	87.5	0.0	926.3	—	—
17.5	41.0	41.5	836.7	394.3	155.7
20.0	80.0	0.0	917.5	—	524.8
23.0	23.0	54.0	747.9	—	154.6
23.0	54.0	23.0	880.9	474.4	155.5
26.5	62.0	11.5	893.3	530.3	154.4
26.5	11.5	62.0	658.4	401.6	155.5
33.3	33.3	33.3	814.6	473.3	155.5
40.0	60.0	0.0	875.1	—	525.3
41.0	17.5	41.5	730.5	473.3	155.1
41.1	41.1	17.8	845.3	528.8	154.6
54.0	23.0	23.0	777.3	527.3	155.4
60.0	40.0	0.0	844.6	—	526.2
62.0	26.5	11.5	788.2	523.3	154.2
62.0	11.5	26.5	702.6	530.3	154.5
80.0	20.0	0.0	760.6	—	524.8
90.0	10.0	0.0	684.7	—	527.3
92.0	8.0	0.0	670.5	—	524.9
95.0	5.0	0.0	632.0	—	525.8
96.0	4.0	0.0	618.3	—	526.3
97.0	2.5	0.0	595.2	—	524.2
100.0	0.0	0.0	525.0	—	525.0

Table II
Thermal Arrests in the Sb-InAs-InSb System

Weight % InAs	Sb	InSb	Liquidus, °C	Secondary, °C	Solidus, °C
0.0	100.0	0.0	630.5	—	630.5
2.5	97.5	0.0	629.3	—	580.0
5.0	95.0	0.0	624.0	—	580.0
5.0	10.0	85.0	620.5	524.8	492.3
5.0	40.0	55.0	580.6	504.0	495.0
5.0	50.0	45.0	528.8	525.8	495.5
5.0	55.0	40.0	539.4	526.2	496.3
5.0	60.0	35.0	550.6	535.8	495.8
5.0	85.0	10.0	616.7	564.3	496.3
10.0	10.0	80.0	677.9	521.7	492.3
10.0	20.0	70.0	663.5	515.7	493.5
10.0	30.0	60.0	656.5	504.5	495.5
10.0	40.0	50.0	648.5	508.5	495.3
10.0	50.0	40.0	639.2	526.2	494.0
10.0	60.0	30.0	629.8	552.6	496.3
10.0	70.0	20.0	600.6	571.7	494.3
10.0	80.0	10.0	605.0	575.7	496.5
10.0	90.0	0.0	613.0	—	580.0
15.0	85.0	0.0	598.9	—	582.9
17.5	82.5	0.0	582.6	—	—
20.0	40.0	40.0	686.2	520.9	495.2
20.0	50.0	30.0	679.0	550.9	496.3
20.0	70.0	10.0	653.0	576.9	497.3
20.0	80.0	0.0	600.1	—	582.1
30.0	10.0	60.0	789.0	508.2	495.0
30.0	30.0	40.0	759.4	509.2	494.5
30.0	70.0	0.0	677.8	—	582.1
40.0	30.0	30.0	798.3	517.8	493.5
40.0	50.0	10.0	760.4	559.1	492.4
40.0	60.0	0.0	743.5	—	575.0
50.0	10.0	40.0	843.0	515.3	494.0
50.0	30.0	20.0	820.5	526.9	492.5
60.0	20.0	20.0	855.2	515.0	—
60.0	40.0	0.0	827.2	—	572.0
70.0	20.0	10.0	858.3	—	—
70.0	30.0	0.0	864.2	—	—
80.0	10.0	10.0	904.9	—	—
80.0	20.0	0.0	892.7	—	—
90.0	10.0	0.0	919.8	—	—
95.0	5.0	0.0	931.7	—	—
100.0	0.0	0.0	942.0	—	—

almost constant cooling rate was achieved by the use of devices described previously (2).

Most of the runs could be made in crucibles made of either Vycor, quartz or graphite with a protective atmosphere of purified argon. The melts were stirred vigorously by a motor stirrer as the cooling proceeded. As the arsenic content was increased volatilization losses increased unduly, and hence the thermal analysis had to be carried out in evacuated, sealed Vycor tubes. In these cases the total pressure was unknown, and stirring was not possible; therefore, the high arsenic portion of the system is not considered to be very accurate.

All alloys used for thermal analysis were made from the elements as described in the previous section. These were then placed in appropriate crucibles and remelted prior to taking the cooling curves.

Metallographic and X-Ray Examinations

Conventional polishing techniques could be used for the greater

Table III
Thermal Arrests in the System InAs-As-Sb

Weight % InAs	As	Sb	Primary Arrest, °C	Secondary Arrest, °C
3.0	5.0	92.0	613.6	584.1
3.0	10.0	87.0	606.2	590.0
3.0	15.0	82.0	604.2	591.0
3.0	17.0	80.0	603.2	590.5
3.0	20.0	77.0	605.2	593.5
3.0	25.0	72.0	610.1	596.3
5.0	10.0	85.0	603.7	589.0
5.0	15.0	80.0	601.7	591.0
5.0	17.0	78.0	600.2	592.0
5.0	20.0	75.0	602.7	594.4
5.0	25.0	70.0	607.8	597.8
7.0	10.0	83.0	598.1	589.8
7.0	13.0	80.0	594.5	589.3
7.0	15.0	78.0	593.1	588.7
7.0	18.0	75.0	594.4	590.8
7.0	30.0	63.0	609.8	603.2
8.0	17.0	75.0	590.5	588.8
9.0	10.0	81.0	590.2	589.9
9.0	6.0	85.0	596.4	588.2
10.0	10.0	80.0	591.0	590.0
10.0	15.0	75.0	601.7	592.4
10.0	20.0	70.0	609.5	597.4
10.0	30.0	60.0	618.4	615.8
10.0	45.0	45.0	663.0	646.0
10.0	60.0	30.0	686.0	648.0
11.0	10.0	79.0	590.3	589.8
12.0	2.0	86.0	593.9	588.2
13.0	10.0	77.0	613.8	590.1
13.0	5.0	82.0	588.5	588.0
15.0	0.5	84.5	586.5	584.1
15.0	5.0	80.0	592.0	589.6
15.0	10.0	75.0	632.2	592.0
17.0	3.0	80.0	598.3	587.1
20.0	5.0	75.0	647.8	590.0
20.0	10.0	70.0	668.5	592.9
20.0	40.0	40.0	657.8	—
22.0	3.0	75.0	651.2	588.0
25.0	15.0	60.0	711.0	595.5
25.0	30.0	45.0	688.0	627.8
25.0	45.0	30.0	694.2	679.5
25.0	60.0	15.0	725.0	717.5
40.0	30.0	30.0	798.2	650.2
40.0	45.0	15.0	801.8	709.3
45.0	10.0	45.0	794.7	600.0
60.0	10.0	30.0	851.0	608.5
60.0	20.0	20.0	870.5	652.7
60.0	30.0	10.0	878.7	703.0
80.0	10.0	10.0	919.0	—
90.0	5.0	5.0	936.5	—

part of the alloy system. Those specimens with a high indium content were polished according to the procedure described by Carapella and Peretti (9). Satisfactory etching was attained by the use of Vilella's reagent (400 ml ethyl alcohol, 20 ml HCl and 40 grams of picric acid) for high indium and high antimony alloys. For high arsenic compositions the standard dichromate etchant for zinc and a solution containing one part H_2O_2, 5 parts H_2O and 10 parts NH_4OH were used. Eden's etchant (20 grams $Fe(NO_3)_3$, 20 grams NH_4NO_3, 2 ml. HNO_3 and 500 ml water) was also used, alone and with equal parts of Vilella's reagent.

In the arsenic-antimony alloys containing from 75 to 100 wt. % antimony the solidus was determined by homogenizing these alloys at 450°C (840°F) for prolonged periods of time, followed by

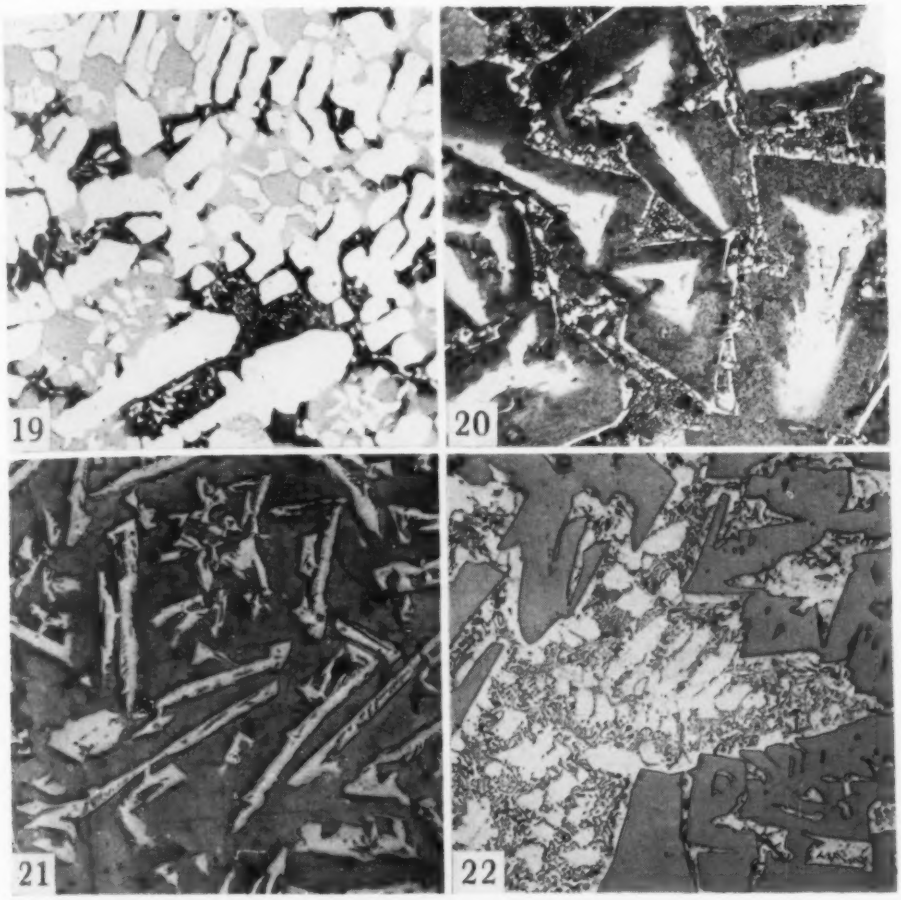


Fig. 19—5% InAs, 60% Sb, 35% InSb, As-cast. Primary Sb, secondary alpha, and eutectic of Sb and InSb. Etchant: Vilella's reagent. ×150

Fig. 20—10% InAs, 10% Sb, 80% InSb. Primary alpha, secondary InSb and eutectic of Sb and InSb. Etchant: Vilella's reagent. ×150

Fig. 21—70% InSb, 30% InAs. Primary alpha and secondary InSb. Etchant: Equal volumes of Vilella and Eden's reagents. ×150

Fig. 22—46% InAs, 10.8% As, 43.2% Sb. Primary alpha plus eutectic of alpha and beta. Etchant: Dichromate. ×250

heat treatments at 2°C intervals and metallographic examination to detect incipient fusion.

In order to confirm the conclusions arrived at by thermal analysis and the microscopic examinations, each alloy was X-rayed with Cr-K alpha radiation.

Experimental Results

The System In-InAs-InSb—Because of the nature of the border binary systems and the lack of ternary compound formation within this region it was possible to determine the relatively simple phase relationships with about 25 alloys. The results of the thermal analyses are given in Table I. Figs. 6, 7 and 8 show typical vertical sections with a 3 to 7 ratio of InSb to In, InSb to InAs and InAs to In, re-

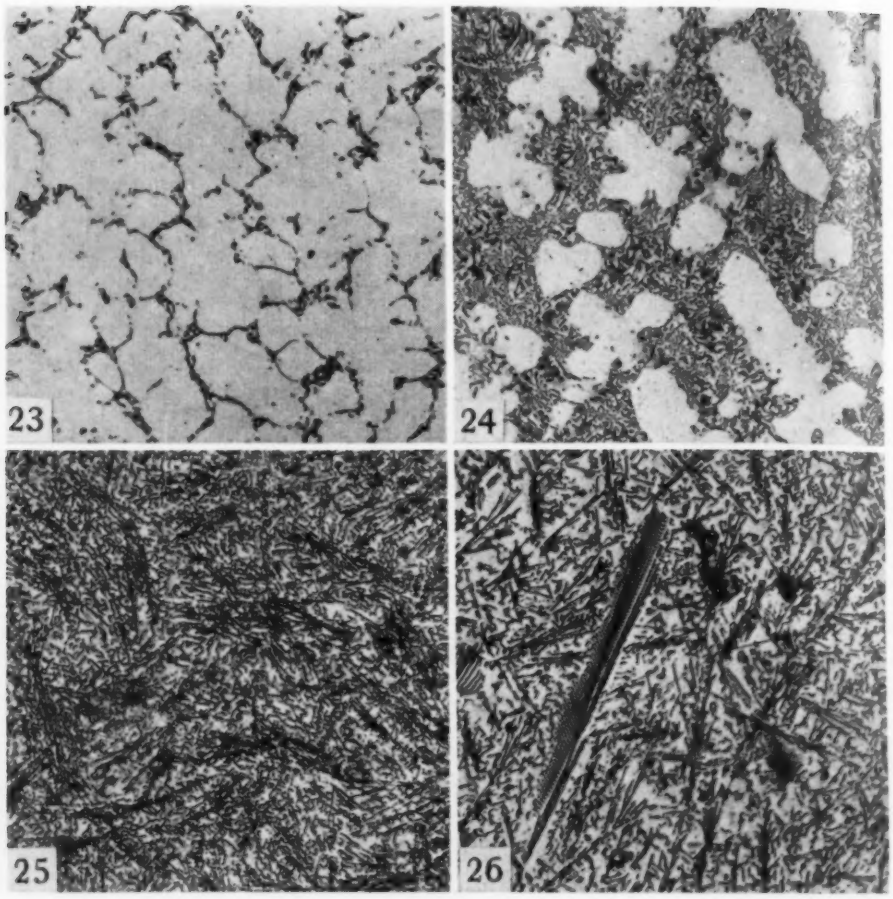


Fig. 23—3% InAs, 17% As, 80% Sb. Primary beta plus eutectic of alpha and beta. Etchant: Dichromate. ×250

Fig. 24—5% InAs, 17% As, 78% Sb. Primary beta plus eutectic of alpha and beta. Etchant: Dichromate. ×250

Fig. 25—8% As, 12% InAs, 80% Sb. Eutectic of alpha and beta. Etchant: Dichromate. ×250

Fig. 26—25% As, 10% InAs, 65% Sb. Eutectic of alpha and beta. Etchant: Dichromate. ×250

spectively. The liquidus isotherms for this region are portrayed in Fig. 9. Over practically the entire compositional range, the primary phase to precipitate upon cooling from above the liquidus is the InAs-rich solid solution. The secondary precipitation consists of almost pure InSb, and freezing is complete at a temperature of 154.5°C. The exact composition of the eutectic was not determined, but it must be quite close to the 100% indium point on the diagram.

The System InAs-InSb-Sb—No ternary compounds were encountered in this area, and the phase diagram is relatively simple (Fig. 10). The InAs-rich solid solution is the primary phase for all compositions lying in the InAs side of the eutectic valley. On the other side of this line, antimony is the first phase to precipitate

upon cooling the liquid. All alloys in this region complete their solidification at the temperature of the InSb-Sb eutectic, 494°C. Table II gives the thermal data for this system. Figs. 11, 12, 13 and 14 show some typical vertical sections.

The System As-Sb-InAs—This portion of the In-As-Sb system proved to be the most difficult to work with. For a large number of the alloys the cooling curves had to be made in sealed evacuated quartz tubes to prevent loss of arsenic. Stirring of the melts could

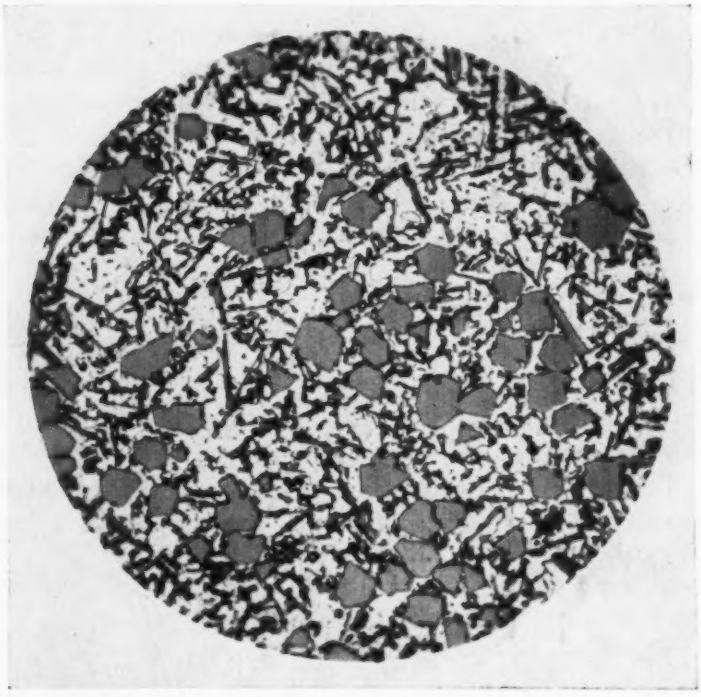


Fig. 27—70% Sb, 30% InAs. Primary alpha plus eutectic of alpha and Sb. Etchant: Vilella's reagent. ×75

not be carried out, and results obtained were often questionable. Explosions occurred rather frequently with the high arsenic compositions. The liquidus isotherms are shown in Fig. 15. The binary eutectic valley runs from one side of the diagram (the InAs-Sb eutectic) without going through a minimum. Two vertical sections are given by Figs. 16 and 17.

The X-ray patterns in this area showed all alloys to be made up of the InAs-rich solid solution and the Sb-As solid solution. Most compositions gave two well defined arrest points; these are given in Table III.

Fig. 18 portrays the liquidus surface for the entire In-As-Sb system. Typical structures obtained are shown in Figs. 19–27.

Summary

The liquidus and solidus for the In-As-Sb system have been determined. The valid tie lines, connecting InAs with InSb and Sb divide the diagram into three sub-ternaries. No ternary compounds were encountered.

1. In the In-InAs-InSb region the primary phase to solidify upon cooling is an InAs-rich solid solution. The secondary precipitation consists of almost pure InSb. The ternary eutectic plane lies at 154.5°C.

2. The InAs-InSb-Sb area has a eutectic valley whose maximum point lies on the InAs-Sb tie line, (82.5% Sb and 17.5% InAs) and has a melting temperature of 582°C. The minimum point is the InSb-Sb binary eutectic at 494°C, containing 69.5% antimony. The primary phase for all compositions lying on the InAs side of the eutectic trough is an InAs-rich solid solution. On the other side of the eutectic line antimony is the first phase to precipitate upon cooling. The temperature of the ternary eutectic plane is identical with that of the binary InSb-Sb eutectic—namely, 494°C.

3. The InAs-Sb-As area contains a eutectic trough running from the InAs-As binary eutectic (731°C, 82% arsenic) to the InAs-Sb binary eutectic at 582°C and 82.5% antimony. The primary phase of solidification may be either an As-Sb-rich or an InAs-rich solid solution depending upon which side of the eutectic valley the alloy lies. The temperature of final solidification varies from 731 to 582°C, depending upon composition, and the solid alloys consist of two solid solutions.

Acknowledgments

The authors wish to thank the Studebaker Corporation for financial assistance and the Indium Corporation of America for the loan of the indium used in this investigation.

References

1. E. A. Peretti and S. C. Carapella, Jr., "The Indium-Bismuth Phase Diagrams," TRANSACTIONS, American Society for Metals, Vol. 41, 1949, p. 947.
2. S. C. Carapella, Jr. and E. A. Peretti, "The Ternary System Indium-Cadmium-Zinc," TRANSACTIONS, American Society for Metals, Vol. 43, 1951, p. 853.
3. T. S. Liu and E. A. Peretti, "The Indium-Arsenic System," TRANSACTIONS, American Society for Metals, Vol. 45, 1953, p. 677.
4. T. S. Liu and E. A. Peretti, "The Indium-Antimony System," TRANSACTIONS, American Society for Metals, Vol. 44, 1952, p. 539.
5. C. Shih and E. A. Peretti, "The System InAs-InSb," *Journal*, American Chemical Society, Vol. 75, 1953, p. 608.
6. C. Shih and E. A. Peretti, "The Phase Diagram of the System InAs-Sb," TRANSACTIONS, American Society for Metals, Vol. 46, 1954, p. 389.
7. N. Parravano and P. de Cesaris, *International Zeitschrift fur Metallographie*, Vol. 2, 1912, p. 70.
8. Q. A. Mansuri, "Equilibrium Diagram of the System Indium-Arsenic," *Journal*, Chemical Society, London, Vol. 131, Part II, p. 2107.

9. S. C. Carapella and E. A. Peretti, "Metallography of Indium and Indium-Rich Alloys," METAL PROGRESS, American Society for Metals, Vol. 56, November 1949, p. 666.

DISCUSSION

Written Discussion: By Earl C. Roberts, associate professor, Metallurgical Engineering, University of Washington, Seattle, Washington.

The authors have carried out what appears to be a careful investigation of the In-As-Sb ternary system. In this day of highly complex research facilities, it is a pleasure to find that the relatively simple techniques of thermal analysis and metallographic examination can still be used to determine the major portion of a complete ternary system.

The major indefinite feature of this work seems to be the unknown influence of pressure on the positions of the lines, particularly in the high arsenic portion of the diagram. Since the experimental points established in both the open crucibles and the sealed containers can be connected by continuous lines, it might well be concluded that the effect of pressure is rather small.

It seems quite possible that the experimental data of Figs. 3 and 7 have been interpreted just a little more closely than is justifiable. In Fig. 3 both the liquidus and solidus lines are probably continuous smooth curves, and in Fig. 7 the line between the α+L and α+InSb+L fields might well be drawn without the minor inflection points.

There also is a slight inconsistency between Figs. 9 and 10 in the temperatures of the liquidus isotherms which intersect the InAs-InSb lines between 95 and 100% InSb.

Authors' Reply

The authors wish to thank Dr. Roberts for his very careful examination of the drawings and his kind comments. It was not intended to indicate an inflection point in Fig. 3, but a rather flat portion in the liquidus and solidus curves. We can agree with the criticism of how the line was drawn in Fig. 7; and as Dr. Roberts correctly points out, the 500 degrees isotherm in Fig. 9 should terminate on the InSb-In binary line.

HYDROGEN CONTAMINATION IN DESCALING AND ACID PICKLING OF TITANIUM

By G. A. Lenning, C. M. Craighead, and R. I. Jaffee

Abstract

Significant hydrogen absorption in titanium can occur in a sodium hydride descaling bath and in a 10% nitric—2% hydrofluoric acid pickle. The amount of hydrogen absorbed increased with increasing ratio of surface area to mass and also with time in the baths. There was a minimum at about 800°F in the hydrogen pickup from the sodium hydride descaling bath. No hydrogen pickup occurred with the Virgo bath, but this treatment resulted in surface pitting. The 8% manganese alpha-beta alloy (C-110M) absorbed more hydrogen than did the alpha commercially pure (A55) titanium. (ASM-SLA Classification: L12, Ti)

Introduction

As part of a general investigation of the effects of hydrogen on titanium, descaling and pickling operations were investigated as probable sources of hydrogen contamination. Preliminary tests were made in a commercial sodium hydride descaling bath. Subsequently, the study was extended on a laboratory scale to cover the effects of time and temperature on hydrogen absorption in sodium hydride, Virgo, and acid pickling baths.

At the time this investigation was started, the deleterious effects of hydrogen in alpha titanium and alpha-beta titanium alloys had been established. Hydrogen in alpha titanium and alpha alloys had been shown to lower the notch-bend impact strength (1)[1]. In the alpha-beta-type alloys, like the 8% manganese alloy, however, the notch-bend impact strength was relatively unaffected by hydrogen, but low-speed tensile ductility was markedly decreased at approximately 200 ppm hydrogen (2).

Subsequent to the initiation of this work, the jet-engine and airframe industries encountered problems that were traceable to hydrogen contamination in titanium alloys. Thus, it became of increased importance to keep hydrogen out of the material.

The object of the present work was to demonstrate the magnitude of hydrogen contamination in titanium under various conditions. The sodium hydride bath is a 1.5 to 2% solution of sodium

[1]The figures appearing in parentheses pertain to the references appended to this paper.

Of the authors, G. A. Lenning is principal metallurgist, C. M. Craighead is consultant, and R. I. Jaffee is chief. Nonferrous Physical Metallurgy Division, Battelle Memorial Institute, Columbus. Manuscript received April 11, 1955.

hydride in molten sodium hydroxide. The Virgo bath has a sodium hydroxide base with some additives. The acid pickle investigated was a 10% nitric—2% hydrofluoric acid bath.

Materials and Fabrication

The commercial-purity titanium (A-55) and Ti-8Mn (C-110M) materials used in this investigation were received in the form of ⅝-inch bar stock. This stock was hot swaged or rolled at 1300°F to prepare the ¼-inch rod and 0.040-inch sheet needed for this work. Next, the A-55 material was air annealed for 1 hour at 1470°F. The C-110M alloy was stabilized by annealing in air for 1 hour at 1300°F, furnace cooling to 1100°F, and subsequent cooling in air to room temperature.

Hydrogen analyses for the various lots of ¼-inch-diameter rod are shown in Table I.

Table I
Hydrogen Analyses of A-55 and C-110M Titanium Alloys

Alloy	Lot Number	Hydrogen Content(a), ppm
A-55	C-9	59
A-55	C-11	38
C-110M	C-10	57
C-110M	C-12	55
C-110M	C-14	49

(a) Vacuum-fusion analyses by the low-pressure fractional-freezing method(3). Tolerance ±10 relative per cent of value reported.

The values reported are within the expected hydrogen range for these alloys in the form of bar stock.

Procedures for Laboratory Descaling and Pickling

The descaling salts were heated in mild-steel containers in an electric resistance furnace. Virgo descaling was done according to directions in Hooker Electrochemical Company's Bulletin No. 25. The sodium hydride descaling practice used was that outlined in Du Pont Bulletin No. SP-28-351. The dimensions of the caustic container and sodium hydride generator were modified from those given for Du Pont's laboratory model to fit an existing electric resistance furnace. This type of heating permitted temperature control within ±5°F of the desired temperature. All material descaled in either the Virgo or sodium hydride bath was subsequently dipped briefly in a 10% nitric-2% hydrofluoric acid bath at room temperature to assure removal of surface films.

The same nitric-hydrofluoric acid bath was also used in the pickling investigation. The bath was contained in a hard-rubber battery case immersed in a hot-water bath for temperature control.

Table II
Hydrogen Absorption For Rod and Sheet Titanium in Sodium Hydride Descaling

Descaling Treatment(a)	Original Hydrogen(b), ppm	Final Hydrogen(b), ppm	Hydrogen Absorption, ppm
	A-55 Titanium (¼-In.-Diameter Rod)		
15 min at 720°F	59	79	20
20 min at 720°F	59	80	21
	(0.040-In. Sheet)		
15 min at 720°F	64	110	46
30 min at 720°F	64	110	46
	C-110M Ti-8Mn Alloy (¼-In.-Diameter Rod)		
15 min at 720°F	57	110	53
30 min at 720°F	57	120	63
	(0.040-In. Sheet)		
15 min at 720°F	64	200	136
30 min at 720°F	64	230	166

(a) Descaling bath contained 1.7% sodium hydride. The descaling treatment was followed by a brief dip in a nitric-hydrofluoric acid bath for brightening.
(b) Hydrogen determined by vacuum-fusion analyses. Tolerance is ±10 relative per cent of the value reported.

Trials with water in place of the acid indicated that the liquid in the battery case could be held within ±5°F of the desired temperature. At the 160°F pickling temperature, however, the acid bath overheated due to rapid solution of the metal, and the maximum immersion time was limited to 10 minutes.

Sodium Hydride Descaling

Effect of Ratio of Surface Area to Mass

Before the laboratory descaling bath was set up at Battelle, tests were made in the sodium hydride descaling bath at Rem-Cru Titanium, Incorporated. The purpose of these tests was to determine the effect of the ratio of surface area to mass on hydrogen absorption in titanium. Descaling times of 15 and 30 minutes were used with the bath temperature at 720°F. The sodium hydride content of the bath analyzed 1.7%.

The results of these tests are given in Table II, and show the effect of the ratio of surface area to mass on hydrogen pickup.

The ¼-inch diameter rod had approximately 1.4 cm^2 of surface area per gram of metal, while the 0.040-inch sheet had 4.6 cm^2. The greater surface-area-to-mass ratio for the sheet (approximately 3 times) resulted in higher absorption with sheet specimens of both alloys. The data in Table II also permitted further observations. First, they indicated that the rate of hydrogen absorption decreased with time in the bath, since the amount of hydrogen absorbed after 30 minutes was not appreciably greater than for 15 minutes. Second, the alpha-beta alloy (C-110M) absorbed considerably more hydrogen than did the alpha material (A-55), as might be expected from the higher diffusion rate of hydrogen in beta than in alpha titanium.

Effect of Time and Temperature

The effects of increasing the sodium hydride bath temperature and extending the descaling time were studied in the small laboratory bath. The ¼-inch rods were tested both with and without the scale produced by the fabrication and annealing or stabilizing treatments. To determine whether the scale acted as a barrier to hydrogen absorption in the baths, a portion of the rods was shot blasted to remove the scale, while the scale on the remaining rods was left on.

Metal-loss and hydrogen-absorption data are given for the unalloyed titanium in Table III, and similar results are given for the Ti-8Mn alloy in Table IV. The sodium hydride content of the bath was maintained at 1.9% at all temperatures except at 900°F, at which temperature the reaction rate was sufficiently rapid to reduce the concentration to 1.7%. For both alloys, the longest descal-

Table III
Hydrogen Analyses and Metal Loss for Sodium Hydride Descaling of A-55 Titanium Alloy in the Form of ¼-Inch Rod

Descaling Treatment Time, min	Temperature, °F	Weight Loss, mg/cm²	Original Hydrogen, ppm	Final Hydrogen, ppm	Hydrogen Absorption, ppm
Scale free					
15	700	0.7	38	87	49
60	700	5.4	38	150	112
15	800	3.0	38	75	37
60	800	8.2	38	160	122
15	900	8.2	38	110	72
60	900	68	38	200	162
Scaled					
15	700	1.2	38	85	47
60	700	8.0	38	150	112
15	800	4.6	38	70	32
60	800	11.3	38	85	47
15	900	9.0	38	110	72
60	900	94.5	38	240	202

Table IV
Hydrogen Analyses and Metal Loss for Sodium Hydride Descaling of Ti-8Mn Alloy in the Form of ¼-inch Rod

Descaling Treatment Time, min	Temperature, °F	Weight Loss, mg/cm²	Original Hydrogen, ppm	Final Hydrogen ppm	Hydrogen Absorption, ppm
Scale free					
15	700	0.8	49	140	91
60	700	8.3	49	250	201
15	800	5.3	49	95	46
60	800	12.9	49	180	131
15	900	10	49	130	81
60	900	38	49	300	251
Scaled					
15	700	0.8	49	130	81
60	700	8.3	49	270	221
15	800	5.3	49	98	49
60	800	12.9	49	190	141
15	900	9.7	49	160	111
60	900	37.9	49	310	261

ing times gave the greatest hydrogen absorption, although the rate of absorption of hydrogen decreased with time. The variation of hydrogen absorption with temperature, which is also shown in Tables III and IV, was rather surprising in that the lowest hydrogen pickup generally occurred at 800°F, rather than at 700°F. Because the tendency of titanium to absorb hydrogen normally increases with temperature, one would have expected just the opposite behavior. Moreover, the weight-loss data show that the rate of reac-

Table V
Hydrogen Analyses and Metal Loss for Virgo Descaling of A-55 Titanium Alloy in the Form of ¼-inch Rod

Descaling Treatment		Weight Loss, mg/cm²	Original Hydrogen, ppm	Final Hydrogen, ppm	Hydrogen Absorption, ppm
Time, min	Temperature, °F				
Scale free					
30	850	3.1	38	43	5
60	850	5.4	38	43	5
5	930	2.3	38	47	9
15	930	6.1	38	42	4
30	930	7.5	38	45	7
60	930	11.2	38	44	6
1	1000	1.3	38	47	9
5	1000	4.1	38	42	4
15	1000	8.6	38	43	5
Scaled					
15	850	4.4	38	48	10
15	930	11.4	38	46	8
15	1000	27.3	38	50	12

tion responsible for metal loss increased progressively with temperature. Thus, it appears that the reaction responsible for hydrogen pickup is not directly associated with the descaling reaction, which generally is considered to be the metal-loss reaction.

The condition of the metal surface before descaling, i.e., whether it was scaled or shot blasted, did not appear to affect hydrogen absorption appreciably for the times and temperatures investigated. After the sodium hydride treatments at 700 and 800°F, the surfaces of the rods were bright and lustrous. However, after the 900°F treatment, the rod surfaces showed slight localized pitting.

Examination of the microstructure of transverse sections of the A-55 alloy before and after descaling did not reveal a detectable increase in the amount of hydride phase after any of the treatments. No hydride-rich surface layer was detected at the edges of mounted specimens when special caution was taken to avoid rounding off of the corners.

Virgo Descaling

Descaling in the Virgo bath was done at 850, 930, and 1000°F. The 930°F temperature is recommended by the vendor. The data for hydrogen absorption and metal loss are shown in Table V for the

unalloyed A-55 material and in Table VI for the Ti-8Mn alloy (C-110M). Since the small hydrogen pickup in these tests was within the limit of error inherent in the vacuum-fusion technique applied to single samples (±10 relative per cent), it appears that there is virtually no hydrogen pickup in the Virgo bath.

Acid Pickling

A 10% nitric-2% hydrofluoric acid bath was used to pickle alpha and alpha-beta titanium alloys. The results for A-55 titanium are given in Table VII, and those for Ti-8Mn (C-110M) alloy are given in Table VIII. Hydrogen pickup for the A-55 titanium was not appreciable. Hydrogen pickup for the scale-free Ti-8Mn alloy became appreciable after 15 minutes at 120°F, and after 10 minutes at 160°F. Considerably less absorption of hydrogen occurred when the scale was left on the Ti-8Mn alloy before pickling. Apparently scale acts as a barrier to hydrogen absorption in acid pickling, just as it acts in decreasing the rate of hydrogen absorption from hydrogen-containing atmospheres.

After this work was completed, the effect of nitric acid concentration on hydrogen pickup was reported by Rem-Cru (4). The Rem-Cru work indicated that a 20 to 30% nitric acid solution gives much lower hydrogen absorption for an equivalent amount of metal removed than the 10% solution.

Summary and Conclusions

No significant hydrogen absorption was encountered in this investigation with the Virgo bath. The surface of the Virgo-descaled material was covered with shallow pits, and it lacked a bright finish. The sodium hydride-descaled material, on the other hand, was generally lustrous at 700 and 800°F, but at 900°F, shallow pitting caused a loss of luster.

Hydrogen absorption in the sodium hydride bath was appreciable for the conditions investigated. The amount of hydrogen absorbed appears to be primarily a function of alloy type, ratio of surface area to mass in the piece to be descaled, and the time and temperature of descaling. The alpha-beta-type C-110M alloy picked up more hydrogen than did the alpha A-55 alloy. Hydrogen absorption in sheet material was shown to be greater than in rod. Increasing the descaling time increased the amount of hydrogen absorbed at all temperatures, as would be expected. The effect of increasing the temperature from 800 to 900°F was to increase hydrogen absorption; however, increasing the temperature from 700 to 800°F decreased the amount of hydrogen absorbed. This decrease in the amount of hydrogen absorbed with increasing temperature is not consistent with the picture of a simple diffusion-controlled reaction.

Table VI
Hydrogen Analyses and Metal Loss for Virgo Descaling of Ti-8Mn Alloy in the Form of ¼-inch Rod

Descaling Treatment Time, min	Temperature, °F	Weight Loss, mg/cm²	Original Hydrogen, ppm	Final Hydrogen, ppm	Hydrogen Absorption, ppm
Scale free					
30	850	5.1	55	50	−5
60	850	8.3	55	48	−7
5	930	4.2	55	47	−8
15	930	7.2	55	50	−5
30	930	12	55	49	−6
60	930	15.5	55	58	+3
1	1000	1.7	55	55	0
5	1000	5.5	55	55	0
15	1000	13.5	55	57	+2
Scaled					
15	850	6.4	49	53	4
15	930	16.6	49	54	5
15	1000	27.7	49	55	6

Table VII
Hydrogen Analyses and Metal Loss for Acid Pickling of A-55 Titanium Alloy in the Form of ¼-inch Rod

Pickling Treatment Time, min	Temperature, °F	Weight Loss, mg/cm²	Original Hydrogen, ppm	Final Hydrogen, ppm	Hydrogen Absorption, ppm
Scale free					
30	72	1.4	38	48	10
60	72	2.6	38	48	10
15	120	42.6	38	42	4
30	120	304	38	42	4
10	160	583	38	43	5
Scaled					
30	72	0.1	38	41	3
60	72	0.3	38	41	3
15	120	0.7	38	41	3
30	120	4.8	38	46	8
10	160	10.6	38	42	4

Table VIII
Hydrogen Analyses and Metal Loss for Acid Pickling of Ti-8Mn Alloy in the Form of ¼-inch Rod

Pickling Treatment Time, min	Temperature, °F	Weight Loss, mg/cm²	Original Hydrogen, ppm	Final Hydrogen, ppm	Hydrogen Absorption, ppm
Scale free					
30	72	1.8	49	50	1
60	72	2.4	49	50	1
15	120	136	49	60	11
30	120	358	49	110	61
10	160	786	49	100	51
Scaled					
30	72	0.3	49	52	3
60	72	0.2	49	50	1
15	120	0.5	49	55	6
30	120	4.9	49	51	2
10	160	5.2	49	52	3

Acknowledgment

The authors wish to express their appreciation to Watertown Arsenal, under whose sponsorship on Contract DA1-33-019-505-

ORD-(P)-1 this work was done, for permission to publish this information. The assistance of Dr. W. L. Finlay and his associates at Rem-Cru Titanium, Inc., in connection with preliminary studies of sodium hydride descaling, was most helpful in this work. The vacuum-fusion analyses were made by C. B. Griffith and W. M. Hansen.

References

1. G. A. Lenning, C. M. Craighead, and R. I. Jaffee, "Constitution and Mechanical Properties of Titanium-Hydrogen Alloys," *Transactions*, American Institute of Mining and Metallurgical Engineers, Vol. 200, 1954, p. 367.
2. C. M. Craighead, G. A. Lenning, and R. I. Jaffee, "Hydrogen Embrittlement of Beta-Stabilized Titanium Alloys," submitted to American Institute of Mining and Metallurgical Engineers, for publication.
3. M. W. Mallett, "A Versatile Vacuum-Fusion Apparatus," TRANSACTIONS, American Society for Metals, Vol. 41, 1949, p. 870.
4. Rem-Cru Titanium Review, October, 1954, p. 7.

DISCUSSION

Written Discussion: By S. Mitsui, chief engineer, Osaka Titanium Co., Ltd., Amagaski Hyogo-Ken, Japan.

It gives me a great pleasure to be given this opportunity of participating in the discussion of this paper.

I have had the experience of making researches in the past on the subject of descaling, acid pickling and hydrogen brittleness of various metals. However, for some time my study has been concentrated on the production of titanium sponge, for this reason, I should like to comment on the given subject of descaling and acid-pickling of titanium based chiefly on the results of experiments made by Mr. K. Kawamura of Sumitomo Metal Industries, Ltd., who assisted my researches in my Sumitomo Metal days. Details of Mr. K. Kawamura's experiments are given in "The Sumitomo Metal," house organ of the same company.

Mr. Kawamura's researches have made the following facts clear.

1. Almost all metals and intermetallic compounds, with the exception of Cr-carbides, can be dissolved by H_2O_2 solutions of suitable composition (H_2O_2 plus addition of HCl, H_2SO_4, HNO_3HF, or other organic acids).

2. Several inorganic compounds can likewise be dissolved by the same solutions.

3. For dissolving a certain specific substance a certain specific composition of H_2O_2 solution is required.

4. Scales hitherto considered difficult to remove by usual methods of pickling can mostly be descaled with ease by the above-mentioned solution. As an added advantage, the descaling can be made without loss of metal by choosing a solution of proper composition and proper temperature. In this case, the scales are disintegrated and come off the metal surface in a colloidal state.

5. Almost all kinds of metals can be thus chemically polished by finding a matching solution and temperature.

6. The descaling and the chemical polish are conducted in two different stages of treatment, using different compositions of solution and temperatures.

7. Gas producing in the processes of these treatments is mostly of O_2.

Mr. Kawamura is also doing research on titanium metal, and has had success in the descaling and chemical polishing of that metal. The process is easier and quicker than Na-hydride process. On top of it, there is naturally no absorption of hydrogen. (Results of several quantitative analyses give the hydrogen value well within the tolerance.)

In making use of titanium scrap returns, it is necessary that such scrap be carefully descaled and chemically polished, otherwise the scrap will bring a large amount of oxygen into the melting pot, resulting in the lowering of purity of the titanium melt. In this sense, I think the achievement of Mr. Kawamura's research offers food for much consideration by titanium producers.

The dissolving loss of metal, the volume of hydrogen generation, and the volume of hydrogen absorption by the metal, have no interrelations. In the processing of steel, acid brittleness is avoided by eliminating "S" as CuS by adding Cu ion in the bath or by oxidizing "S" with oxidizing agents such as $KMnO_4$. I should be grateful to you if you would enlighten me on the kinds of ions that are harmful to titanium.

When steel is heat treated to ultimate strength above certain limits, the hydrogen it absorbs in acid pickling will lower its tensile strength and will result in the appearance of many small flakes on the ruptured surface. In such a case it was my observation that the mechanical properties of the material could not be completely restored even if the hydrogen were dispelled out of the material. Is this also the case with titanium?

The speed of the hydrogen penetration through steel during acid pickling was about 5 mm/16 hour. The measurement was made by using a tube of 5 mm wall thickness, with the outer face acid pickled and the inside hollow containing mercury. We also measured the volume of hydrogen bubbles in the mercury at room temperature. Will you advise me of the hydrogen penetration speed through titanium?

Written Discussion: By W. J. Barth, Pigments Department, Research Division, E. I. duPont deNemours & Co., Wilmington, Delaware.

The authors are to be commended for their contribution to this critical phase of titanium processing. Their results are in close agreement with those obtained in our laboratory.

They clearly show the effect of ratio of surface area to mass on hydrogen absorption from the sodium hydride bath. The difference of behavior of C.P. and an alloy grade such as 8% manganese is conclusively demonstrated.

In the work at our laboratory for hydride descaling studies, the procedure employed was designed to divide titanium descaling into two stages: I—Descaling; II—Metal Attack. It was demonstrated hydrogen absorption does not occur until stage II is initiated. Hence, by very close control of bath immersion time hydrogen absorption can be minimized. This time can vary widely depending upon the type and thickness of scale. For instance, at 715°F, 1.3% NaH concentration for a mill-scale weighing 0.0040 gm/cm² about 10 minutes were required for scale removal. Under the same conditions a mill-scale of <0.0005 gm/cm² was removed in less than ½ minute.

With regard to the effect of temperature on hydrogen absorption from the hydride bath, we have observed the same tendency. If one considers the ratio of hydrogen absorbed per unit weight loss it is seen the ratio decreases with increasing temperature. This is true of Battelle's and our data as illustrated in Table IX.

Table IX

Battelle Data ¼″ A55 Rod*			Du Pont Data 0.060″ C.P. Sheet		
Temp. °F	Time Minutes	Ratio**	Temp. °F	Time Minutes	Ratio**
700	60	22	715	30	30
800	60	15	800	30	12
900	60	2.4			

*Reference Battelle Data, Table III.
**Ratio of hydrogen absorption (ppm) per unit weight loss (mg/cm²).

While the numerical values are not equal, the same tendency is observed.

To quote the authors, "this decrease in the amount of hydrogen absorbed with increasing temperature is not consistent with the picture of a simple diffusion-controlled reaction."

It may be associated with a change in NaH and TiH equilibria. The theory is of academic rather than practical interest. Although a study of the theory may aid in developing means of inhibiting hydrogen pick-up.

With regard to minimizing hydrogen pick-up, it was reported[2] that the hydride bath can be modified with titanium dioxide addition to reduce hydrogen absorption.

We essentially agree with the authors' conclusions concerning descaling with oxidizing caustic baths such as Virgo. In all of our work we have attempted to use sheet material of 0.020 to 0.030-inch gage to promote detection of hydrogen absorption by keeping a high ratio of surface to mass. Under these conditions we have detected hydrogen absorption when temperatures exceed 900°F for a 30-minute period. At 800°F hydrogen absorption is difficult to detect during 30 minutes of metal attack.

In addition, with oxidizing caustic baths we have observed the formation of acid insoluble nodules on sample surfaces above 900°F. These appear to be TiO_2. They do contribute to poor surface finish. At 800°F, we obtained good finishes and no nodules. Do the authors wish to comment on this point?

Based upon our experience we sincerely believe a new and better bath is needed. The hydride bath is most satisfactory from the standpoint of operability, product finish and safety; it has the disadvantage of promoting hydrogen absorption with exposure beyond that required for scale removal. The oxidizing caustic baths provide better control of hydrogen, however, surface finish is not as good, firing of sheet materials may occur and secondary effects such as nodule formation are observed.

Written Discussion: By J. N. Moore, Virgo sales supervisor, Hooker Electrochemical Company, Niagara Falls, New York.

The authors have pointed out that descaling of titanium and titanium alloys in Virgo descaling salt resulted in no hydrogen pick-up. This is in accordance with our experience and is inherent in the nature of the bath since it is a strongly oxidizing composition.

It is our feeling, however, that the indications that corrosion and pitting occurred when the descaling was done according to the manufacturers directions[3] may lead the reader to erroneous conclusions.

Generally, the application of Virgo to descaling titanium requires working

[2]Q. de L. Wheatley, "Hydride Modified to Reduce Hydrogen Absorption," METAL PROGRESS, American Society for Metals, Vol. 68, No. 2, August 1955, p. 119.
[3]Hooker Electrochemical Company Bulletin No. 25.

out a specific cycle for each specific application. Temperature of bath and time of immersion are very critical in titanium descaling.

Time cycles in the order of 1–2 minutes and temperatures in the range of 800–825°F are typical for light gage titanium sheet. The authors reported on immersion times up to 60 minutes and on temperatures up to 1000°F. Severe corrosion is to be expected under such drastic conditions.

We should like to emphasize that the descaling of titanium and titanium alloys in Virgo require careful handling and descaling according to cycles which must be worked out experimentally for each application. This has proven to be the case in instances where Virgo is currently being used successfully by several major titanium producers and fabricators to produce metal of low hydrogen content and satisfactory finish.

Written Discussion: By G. J. Adams and D. E. Yeomans, technical officers, Imperial Chemical Industries Ltd., Metals Division, Birmingham, England.

Research on descaling titanium and its alloys has been carried on in this laboratory over the past 2 years and it is planned to publish results of these investigations as soon as possible. Comparing the sodium hydride and Virgo processes, as Messrs. Lenning, Craighead and Jaffee have done, we also consider the hydride process superior to the Virgo process with regard to surface quality of the descaled product, and also because descaling times are much shorter for all types of scale. During our investigation, however, it became clear that if the processes were to be considered as methods of descaling a complete range of fabricated titanium products, then hydrogen contamination would be an important criterion of suitability. The hydride process was suspected of causing appreciable contamination by hydrogen.

To assess quantitatively hydrogen contamination in hydride and Virgo descaling, thin sheet was used to obtain high sensitivity to hydrogen pick-up. The material was 0.018 inch thick with an oxide film produced by annealing for 30 minutes at 650°C (1200°F), this being the customary annealing procedure. Using various bath conditions, specimens were immersed, water-quenched, washed in hot water and acid pickled. For accuracy, adjacent samples for hydrogen analysis were taken from every test piece before and after immersion in the caustic bath and further samples were taken after pickling. To establish the extent of the decrease in contamination by pickling, some specimens were given the customary 3 minutes brightening pickle, while others were pickled for 30 minutes to remove approximately 0.001 inch of metal. Pickle composition was 1% hydrofluoric acid and 4% nitric acid and it was used at room temperature. Hydrogen estimations were carried out by a vacuum extraction technique. Results are plotted in Figs. 1, 2 and 3 against immersion time in the descaling bath. Only immersion times up to 60 minutes are recorded, higher regions of the curves being linear. Fig. 1 records weight loss during immersion alone, while Fig. 2 indicates hydrogen contamination resulting from this treatment, and Fig. 3 that remaining after pickling.

Virgo Process—Results do not differ significantly from those reported by Messrs. Lenning, Craighead and Jaffee although in our experience considerable variations in rate of metal loss occur. Two other interesting points may be mentioned:—(a) Rates of weight loss corresponding to removal of scale and to subsequent dissolution of metal are similar; (b) Bright pickling decreases hydrogen content sharply but prolonged pickling has no useful effect.

As an example of hydrogen contamination that may be expected during

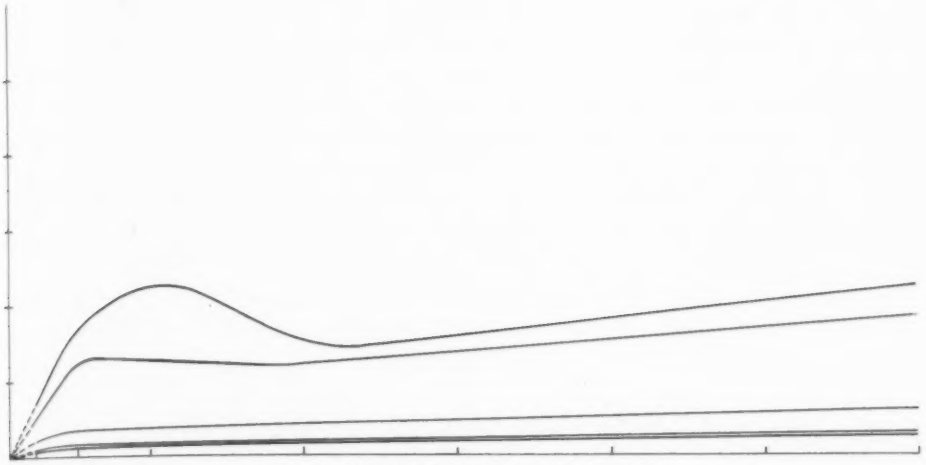


Fig. 1—Weight Loss During Immersion.

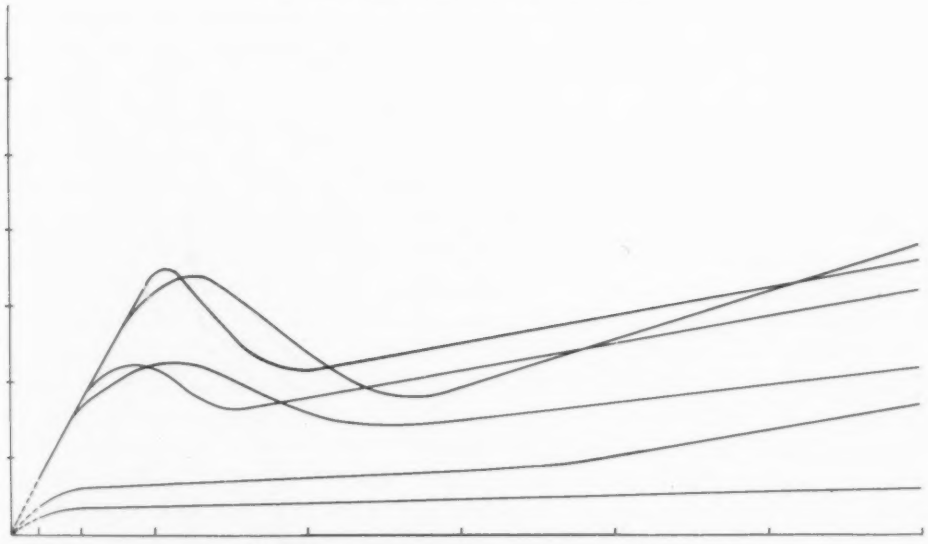


Fig. 2—Hydrogen Contamination Resulting from Immersion.

descaling by this process the following figures may be quoted.

Bath temperature 425°C (800°F).

0.018 inch thick annealed sheet.

Immersion time 30 minutes.

Hydrogen contamination after immersion in descaling bath 0.004 wt. % (40 ppm.).

Hydrogen contamination after immersion in descaling bath and subsequent bright pickling 0.002 wt. % (20 ppm.).

In view of increased contamination at higher operating temperatures, 425°C (800°F) would seem to be the optimum for Virgo descaling of thin sheet, but higher temperatures might be used for thick sections in which the greater contamination would be less serious.

Sodium Hydride Process—Results indicate a rapid weight loss during the descaling period, suggesting marked preferential attack on the scale. Hydrogen pick-up is also rapid during this period, but is followed by a temporary decrease.

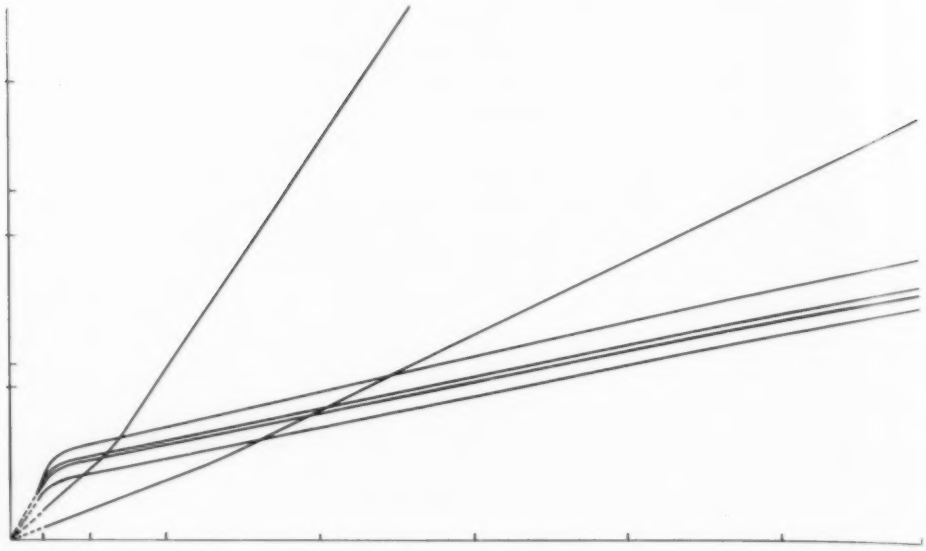


Fig. 3—Hydrgoen Contamination Remaining After Pickling.

In the final stages, metal loss and hydrogen pick-up are substantially linear with time. The occurrence and explanation of the initial rapid rise in hydrogen content are of the utmost importance to titanium descaling. Thus, it is considered that, at this stage, hydrogen is derived from the reaction of titanium dioxide with sodium hydride, and easily diffuses into the metal through the thin oxide layer. If this interpretation is correct, it is doubtful if control of descaling conditions or inhibition of the rate of the metal/bath reaction can prevent contamination.

The effect on hydrogen content of subsequent acid pickling suggests that appreciable hydrogen gradients are present in the metal after immersion in the descaling bath, but it is clear that the metal removal necessary to reduce hydrogen content to base value would be impracticable.

To minimize hydrogen contamination, hydride content and temperature should be kept to a minimum. We recommend 350°C (660°F) and not greater than 1% hydride, but even under these conditions serious contamination of thin material occurs.

As an example of the extent of hydrogen contamination that may be expected during hydride descaling the following figures may be quoted.

Bath temperature 350°C (660°F).

1% sodium hydride.

0.018 inch thick annealed sheet.

Immersion time 5 minutes.

Hydrogen contamination after immersion in the descaling bath 0.020 wt. % (200 ppm.).

Hydrogen contamination after immersion in descaling bath and subsequent bright pickling 0.018 wt. % (180 ppm.).

Operating Hazard in Caustic Soda Descaling—Discussion of molten caustic soda descaling of titanium is incomplete without mention of operating risks, in which hydrogen plays a major role. A number of cases are on record in which the reaction between titanium and caustic soda became violent. The reasons are not fully understood, but the effect is evolution of large quantities of hydrogen which

usually ignites spontaneously. As expected, the danger is greatest with thin material and at high bath temperatures, but the risk cannot be ignored even under normal operating conditions.

Descaling by Acid Pickling—It is our experience that commercially pure titanium and alpha-alloys are not susceptible to significant hydrogen pick-up in acid media. On the other hand alloys containing beta phase are susceptible, and the extent of contamination obviously depends on the proportion and distribution of this phase. We agree that with a high proportion of nitric acid present, contamination can be effectively eliminated.

The conclusion by Messrs Lenning, Craighead and Jaffee that scale acts as a barrier to hydrogen absorption may be true, but we feel that it is not necessarily a proper conclusion from their experimental results with titanium—8% manganese alloy. For evolution of hydrogen to occur from acid media, metal attack is surely necessary, but the recorded weight losses are in fact very small.

Written Discussion: By J. H. Shoemaker, president, Kolene Corporation, Detroit.

We note you have mentioned the proprietary product, Virgo, which causes us to call attention to other proprietary baths, Kolene.

The Virgo bath, as you know, is an oxidizing type of bath. We, too, have an oxidizing bath in use in several steel mills for the scale or oxide removal from stainless alloys.

Several of the manufacturers of titanium and its alloys also manufacture the stainless alloys and it is desirable, wherever possible, to use the same equipment and process for both materials—stainless steels and titanium.

We have done considerable experimental work with various manufacturers of titanium, some of this with laboratory size samples, other with 30″ x 30″ sheets and, again, with continuous strip up to more than 3′ in width. We have also used molten salt baths with various percentages of sodium hydroxide and oxidizing members.

We agree with your findings "it appears that the reaction responsible for hydrogen pickup is not directly associated with the descaling reaction" and we have also found "there is virtually no hydrogen pickup" in the Kolene oxidizing bath, just as you found the case with the Virgo bath. Our findings seem to indicate that the sodium hydroxide base baths show lesser hydrogen pickup as the sodium hydroxide percentages are decreased and the oxidizing members increased.

Authors' Reply

The authors are grateful for the many detailed discussions contributed. The large amount of additional information presented has added considerably to the value of this paper.

Mr. Mitsui asks about permanent damage effects due to hydrogen charging and degassing in titanium. Although specific investigations on this subject for titanium alloys have not been reported, it is well known that titanium and titanium alloys containing up to 400 ppm hydrogen can have their mechanical properties restored by degassing. We are not aware of any data on hydrogen penetration of titanium at room temperature, about which Mr. Mitsui asked.

The data of Messrs. Adams and Yeomans are very interesting and bring up a point not covered in investigations to date. Hydrogen distribution in a descaled sample is a very important consideration with respect to the mechanical

properties of descaled titanium. Hydrogen pickup, as indicated by analysis of the total section, may be small. However, when all this hydrogen is concentrated in a thin surface layer, surface cracking may result, which could decrease strength and/or ductility. The existence of a hydrogen-rich surface layer was established in the excellent work of Barth and Fields ("Sodium Hydride Descaling of Titanium," Metal Progress, page 114, August, 1955). The point regarding the possibility of a twofold barrier effect of the scale is well taken.

With regard to the comments of Messrs. Barth and Moore, we did not operate the Virgo bath below the 850°F temperature. However, we did note an improvement in surface condition of the descaled metal at 850°F compared with higher bath temperatures even for the relatively long times used in our work.

In view of the importance of hydrogen contamination in descaling to the technology of titanium, the results and comments of Dr. Wheatley and Mr. Shoemaker are very gratifying and should prove to be of considerable help to persons concerned with the operation of commercial descaling baths.

Written Discussion: By Q. D. Wheatley, E. I. du Pont de Nemours & Co., Buffalo, N. Y.

Dr. Wheatley asked the speaker what method of hydrogen analysis had been used, and whether he would comment on the reliability of available analytical techniques. Mr. Lenning replied that the vacuum fusion technique of hydrogen analysis had been used, but it was his impression that the equilibrium-pressure method was equally reliable.

Dr. Wheatley noted that the data presented by Mr. Lenning in general confirmed work on hydride descaling of titanium done at the Niagara Falls Laboratory of the Electrochemicals Department of the du Pont Company. In particular it was noted that treatment time, temperature, hydride concentration and sample geometry are all important factors in determining hydrogen pickup by titanium descaled in the conventional hydride bath.

Dr. Wheatley then commented as follows on the modified hydride bath developed by the Electrochemicals Department:

Research has disclosed that addition of titanium dioxide to the conventional hydride bath causes a marked decrease in hydrogen pickup by commercial purity titanium. Titanium dioxide reacts with the bath to give alkali titanates. When the bath is saturated with the reaction products, it contains the equivalent of about 0.35% dissolved titanium dioxide. While 0.030-inch pure titanium sheet treated in the conventional hydride bath may pick up several hundred ppm hydrogen, similar material treated under the same conditions in the titania-modified hydride bath absorbs only 8–25 ppm hydrogen in 5–40 minutes. The descaling rate is not affected by the addition of titanium dioxide, and a smooth, bright surface finish is obtained. The titania-modified bath performs just as well as the conventional hydride bath in descaling stainless and alloy steels. It has also been found that treatment time and sample geometry are the important factors governing hydrogen pickup in the titania-modified bath.

The titania-modified hydride bath is now in commercial use. Early reports of evaluations of the new bath have been received. One user reports that with the titania-modified bath he experiences only one-tenth the hydrogen pickup formerly found with the conventional hydride bath. These data were obtained by analyses of pure titanium and various titanium alloy rods. When ¼ inch diameter rods were treated for 1 hour at 700°F in the titania-modified bath containing 1.0%

NaH, hydrogen pickup was only 10–20 ppm. Maximum depth of hydrogen penetration was reported to be $\frac{1}{64}$ inch.

W. L. Finlay (co-chairman) asked for comments on the method of installing and controlling the titania-modified bath. Dr. Wheatley pointed out the possible hazards of evolved hydrogen when titanium dioxide is added to a hydride bath, and stressed that:

1. Pilot lights must always be lit and placed near the bath surface to ignite hydrogen if it is evolved too rapidly when titanium dioxide is added to the bath.

2. Pigment grades of titanium dioxide must not be used, for the fine size causes extremely rapid reaction; the bath might boil over. Du Pont's "Ti-Pure" VG grade of titanium dioxide is satisfactory.

3. The bath can be controlled simply by adding sufficient titanium dioxide on a regular schedule to maintain saturation of the bath with the reaction products, as calculated from the quantities of sodium and caustic added to the bath.

To Dr. R. I. Jaffee's query as to why a bath used to descale titanium does not automatically become a titania-modified bath by solution of scale and metal, Dr. Wheatley replied that in the case of baths used exclusively for titanium descaling this may be almost the case. It was pointed out, however, that most titanium processing is done by producers of stainless steel. The volume of steel normally put through the bath drags out dissolved titanates faster than the relatively small throughput of titanium replenishes them. Further, the titanates present even in relatively low concentrations markedly reduce the extent to which the bath attacks titanium metal. As a result, even baths used exclusively for titanium descaling seldom remove enough titanium to build up the optimum concentration desired.

THE RATE OF DIFFUSION OF CARBON IN ALPHA AND BETA TITANIUM

By F. C. Wagner, E. J. Bucur and M. A. Steinberg

Abstract

The diffusion rates of carbon in titanium were determined over a range of temperature from 736 to 1150°C, excluding the two phase region occurring between 882 to 920°C. The activation energies were obtained by application of the Arrhenius type equation, $D = D_0 e^{\frac{-Q}{RT}}$ *From a logarithmic plot of the diffusion coefficients versus the reciprocal of the absolute temperature, the values obtained for the alpha and beta temperature range are 43,500 cal/mol and 48,400 cal/mol respectively. The frequency factors obtained are 5.06 in the alpha range and 108 in the beta range.*

By substituting the respective D_0 *value and Q value for the alpha or beta temperature range in the Arrhenius type equation the diffusion coefficient for a specific temperature can be calculated directly. For example:*

$$D\alpha = 5.06\, e^{\frac{-43{,}500}{RT}} \quad (700 \text{ to } 880°C)$$

$$D\beta = 108\, e^{\frac{-48{,}400}{RT}} \quad (920 \text{ to } 1200°C)$$

It was also shown, within the limits of experimental error, that the rate of diffusion of carbon in titanium is independent of concentration. From the experimental work the limits of solid solubility of carbon in both alpha and beta titanium over the temperature range studied were determined. (ASM-SLA Classification: Nl, Ti)

THE effect of interstitial elements, such as carbon, oxygen, nitrogen, and hydrogen, on the physicial properties of titanium makes the study of these alloys important in view of the commercial significance of titanium-base alloys as structural components in the field of aircraft and ordnance production.

Studies on the rate of diffusion of oxygen, hydrogen, and nitrogen in titanium have just been completed (1).[1] However, no data are

[1]The figures appearing in parentheses pertain to the references appended to this paper.

This paper is based in part on work carried out by Horizons Incorporated for the Watertown Arsenal, Watertown, Massachusetts, under contract DA-36-034-ORD-1157-RD.

A paper presented before the Thirty-Seventh Annual Convention of the Society, held in Philadelphia, October 17–21, 1955. Of the authors, F. C. Wagner is section head, Physical Metallury, E. J. Bucur, project supervisor, and M. A. Steinberg is head, Metallurgy Department, Horizons Incorporated, Cleveland. Manuscript received March 20, 1955.

available on carbon diffusion in titanium. Since the diffusion of carbon in both alpha and beta titanium plays an important role in the metallurgical processes of heat-treatment, homogenization, and aging, a knowledge of the rate at which these processes occur requires data on the rate of carbon diffusion for a quantitative description of these processes.

Accordingly, an investigation was planned: (a) to determine the diffusion coefficients of carbon in high purity alpha and beta titanium, (b) to determine if the diffusivity is concentration dependent, (c) to determine the temperature variation of the diffusion coefficients over an extensive range of temperatures, and the activation energy for diffusion, and (d) to determine from the measured data, the limits of solid solubility of carbon in alpha and beta titanium over the temperature ranges studied.

Review of the Literature

There is little information on the diffusion of interstitial or substitutional elements in titanium. However, some data does exist on gas-metal reactions from which diffusivity data have been obtained.

One of the established relationships in diffusion is that the diffusivity depends inversely upon the solid solubility, usually being greatest for elements which are only slightly soluble, and least for elements with a wide solubility range (2). Self-diffusion is normally the slowest process. On this basis, one would expect a considerably greater diffusivity for carbon in titanium than either oxygen or nitrogen in the alpha range, and perhaps in the beta range. Such a relationship has been shown for carbon in iron, the diffusion coefficient of carbon in ferrite being greater than that in austenite at a given temperature (3,4).

While no precise trend of diffusion coefficients with atomic radius of solute has been found, it is apparent that other factors being equal, the smaller the atomic radius of an interstitial element, the lower the activation energy required for diffusion through a given solvent. This would indicate that nitrogen should have a lower Q value for diffusion than carbon, as the atomic radius is somewhat less.

In the study of the carbon diffusivity in alpha and beta titanium, the experimental work and results accomplished on carbon diffusion in gamma iron afford an excellent background for choice of experimental procedures to obtain reliable data for the value of the diffusion coefficients in titanium. An experimental method has been used by Paschke and Hauttmann (5) and others (6) which consists of (a) carefully resistance-butt-welding steels of different carbon contents, (b) the annealing of these in order to diffuse carbon along the specimens across the welded "interface," (c) the determination

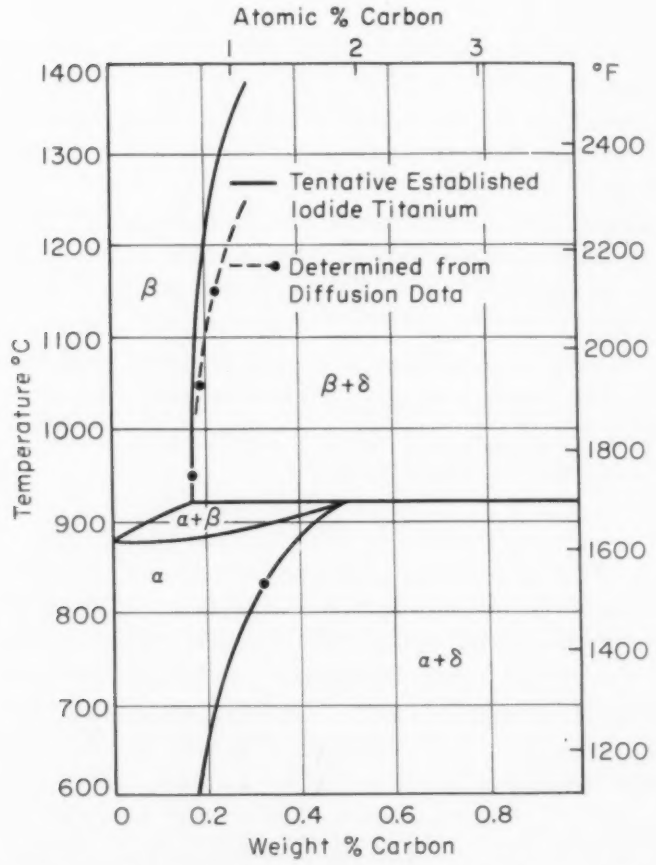


Fig. 1—Phase Diagram of Titanium-Carbon System (8,9).

of the carbon distribution across the diffusion zone, and (d) the plotting of concentration-penetration curves.

This procedure was adapted to the study of carbon diffusion in titanium. Here, however, the limited solubility of carbon in titanium requires a different method of calculation to obtain the diffusion constant, D. The working equations were determined from the following line of reasoning.

The diffusion studies were made with diffusion couples consisting of (a) high purity titanium containing 0.038% carbon, and (b) 0.4% carbon or higher carbon-titanium alloys. Thus, at most temperatures, excluding those between the allotropic transformation temperature (882°C) and the peritectoid temperature (920°C), the diffusion will occur from a conglomerate of $\alpha+\delta$ into α, or from a conglomerate of $\beta+\delta$ into β as shown in Fig. 1. The mechanism of diffusion in both of these cases is the same and can be treated in a similar manner. This method consists of allowing carbon to diffuse from an inexhaustible supply into an essentially carbon-free specimen. Jost and Wagner (7) treat this method in a manner which is

practicable. If a diffusion couple composed of pure titanium, with a 0.038% carbon content, and a titanium alloy, with a 1.30% carbon content, is vacuum annealed at 800°C (1470°F), carbon will diffuse out of the $\alpha+\delta$ into the α region. This depletes the δ region of carbon and results in a shift of the plane of discontinuity as shown in Fig. 2.

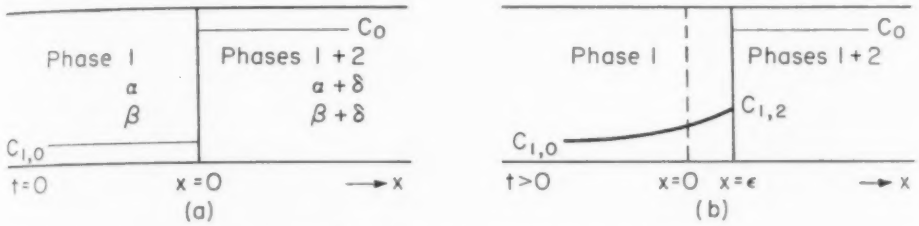


Fig. 2—Diffusion in a Titanium-Titanium Carbon Couple.

The diffusion will proceed in the α phase only, and obey Fick's second law:

$$\frac{\delta c}{\delta t} = D\alpha \frac{\delta^2 c}{\delta x^2} x < \epsilon \qquad \text{Equation 1}$$

provided that D is independent of concentration. A particular integral of this equation is,

$$C = C_{1,\,o} - B\left(1 + \text{erf}\frac{x}{2\sqrt{Dt}}\right) \qquad \text{Equation 2}$$

the initial conditions being,

$$C = C_{1,o} \text{ at } x<0 \text{ and } t=0$$
$$C = C_o \text{ at } x>0 \text{ and } t=0$$

the mass flow equation for this case is,

$$(C_o - C_{1,2})d\epsilon = -D\alpha\, dt \left(\frac{\delta c}{\delta x}\right) \qquad \text{Equation 3}$$

the remaining boundary conditions are,

$$C = C_{1,2} \text{ at } x = \epsilon_{-o} \text{ and } t>0$$
$$C = C_o \text{ at } x = \epsilon_{+o} \text{ and } t>0$$

assuming the relationship,

$$\epsilon = 2\gamma\sqrt{Dt} \qquad \text{Equation 4}$$

and combining equations 2 with 3 and 4 along with the boundary conditions, the resulting equation becomes,

$$\frac{C_{1,o} - C_{1,2}}{C_{1,2} - C_o} = \sqrt{\pi}\gamma e^{\gamma^2}(1 + \text{erf}\ \gamma) \qquad \text{Equation 5}$$

This solution was used for the diffusion studies in both the α and β temperature ranges. The entire derivation assumes D to be independent of concentration; however, the maximum solubility of

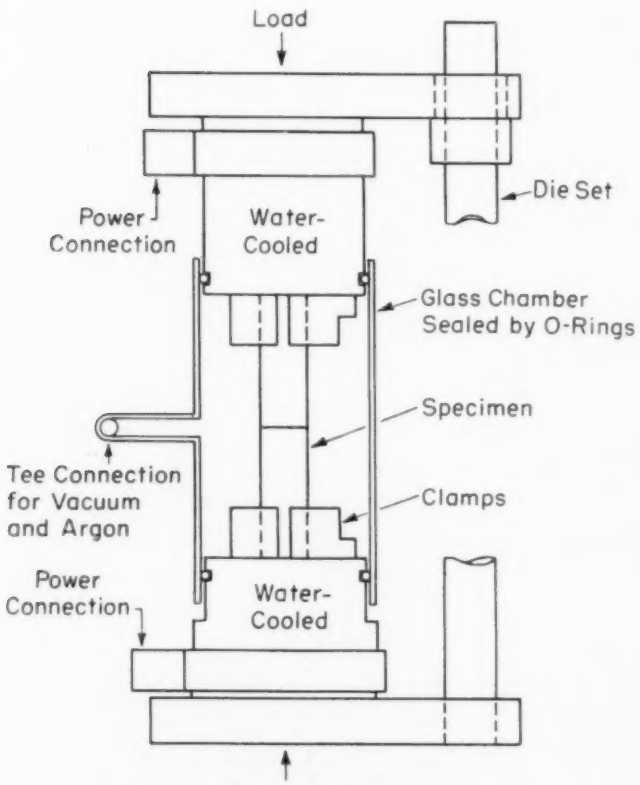


Fig. 3—Schematic of Butt-Welding Jig.

carbon in titanium is only about 0.38% and, therefore, the dependence of the diffusion coefficient on concentration should be very small and thus justify this assumption.

Determination of the activation energy was accomplished by assuming that D varies with temperature in accordance with the Arrhenius type equation,

$$D = D_o e^{\frac{-Q}{RT}} \qquad \text{Equation 6}$$

where D_o is the frequency factor and varies very little with temperature, and,

Q is the experimental activation energy,

R is the gas constant, and

T is the absolute temperature.

By taking the slope of a logarithmic plot of D versus 1/T and equating this to Q/R and knowing D and Q, D_o was calculated from this equation.

Experimental Procedure

The diffusion couples consist of two ¾-inch diameter by 2-inch long bars, butt-welded together; one bar being iodide titanium, and the other a high carbon-titanium alloy.

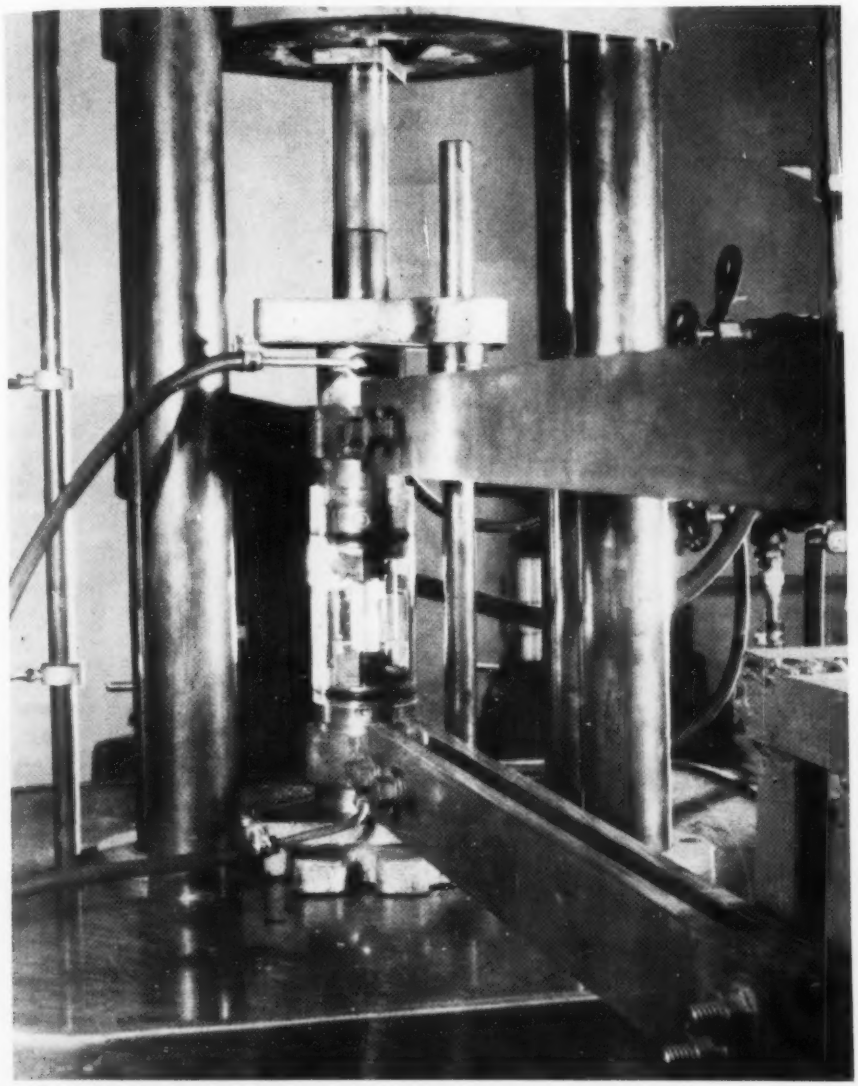


Fig. 4—Photograph Showing Butt Welding Apparatus as Used in Conjunction with Tensile Machine.

Specimen Preparation—The butt welder was made up of a movable and a stationary jaw into which the ends of the diffusion couple components were clamped for welding. These jaws were mounted in a die-set which provided alignment of the ends to be welded (see Fig. 3). A glass chamber, sealed by O-rings, surrounded the specimen and permitted welding in a purified argon atmosphere. The entire fixture was placed in a universal testing machine during the welding operation; thereby, permitting the pressure applied to the specimen during welding to be accurately controlled (see Fig. 4). A butt welder was used with a maximum capacity of 17,000 amps and 7.85 volts off the secondary.

The contact surfaces of the specimens to be welded were first

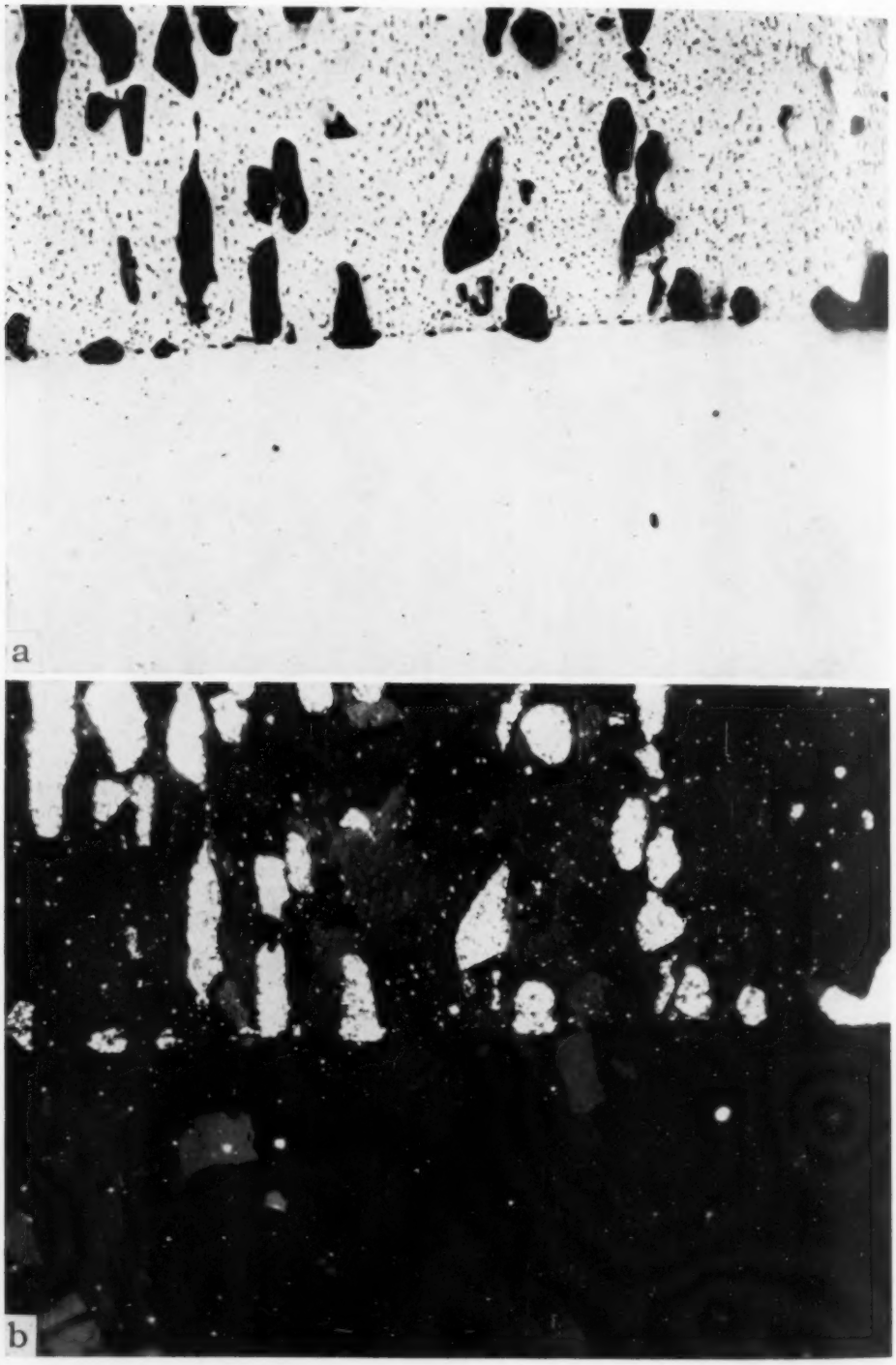


Fig. 5—Butt Weld of 0.038% C Iodide Titanium to 1.300% C Iodide Titanium. ¾-inch diameter bar. (a) Bright light; (b) Polarized light. ×250.

polished through 3/0 metallographic paper and then lightly etched with a 2% hydrofluoric-10% nitric acid solution. The welding cham-

ber was thoroughly evacuated and flushed with argon several times before butt-welding the specimen under a positive pressure of argon. An initial load was applied to insure good contact between the two surfaces, and yet provide a load high enough to have accurate control of the plastic flow at the interface during the welding. Initially during welding, the specimens expanded thermally with a resulting increase in load until the interface was hot enough to flow. By turn-

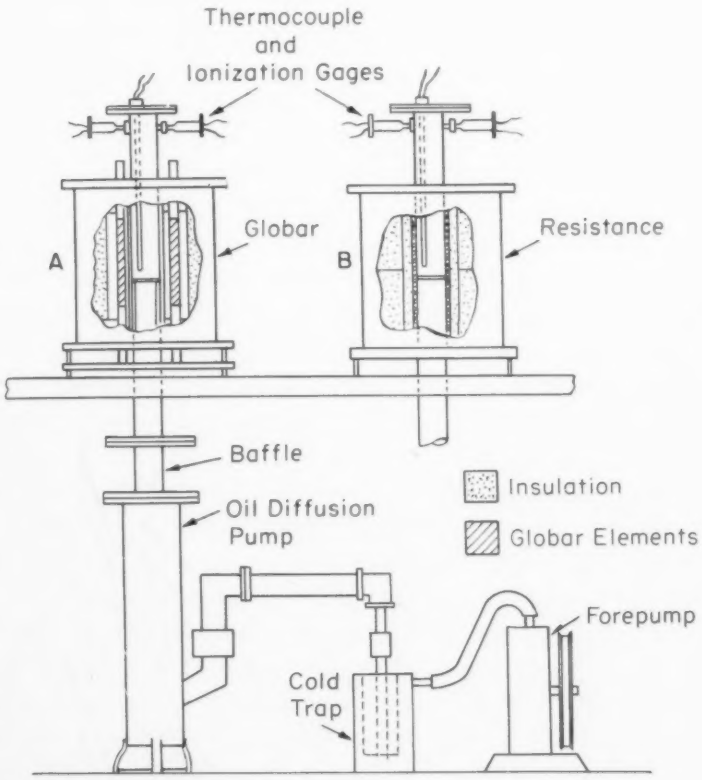


Fig. 6—Diagrammatic view of furnaces.

ing the power off at a definite load after the plastic flow began at the interface it was possible to obtain consistent welds. The welding time was 6–8 seconds. The diffusion which occurred during welding was considered negligible. Fig. 5 is a photomicrograph of a typical weld interface.

A tensile specimen with a 2-inch gage length was carefully machined from a welded couple. The tensile data obtained showed that the bond was as strong as the parent material.

Vacuum Annealing—The vacuum diffusion furnaces were of the vertical tube type as shown in Fig. 6. Globar resistance heating elements were used for temperatures above 950°C (1740°F), while nichrome windings were used in the lower temperature furnaces.

The controlling thermocouples were placed near the heat source and permitted temperatures within the heating chambers to be held to $\pm 2\frac{1}{2}$°F of the desired temperature. To supplement this control, a resistance was connected in parallel with the on-off power solenoid to permit continuous heating in the furnace tube. Full power to three-fourths power on the on-off controller cycle eliminated the rather extensive temperature lag characteristic of on-off type controllers. The thermocouples within the evacuated tube chambers were attached to an automatic Brown 12 point recorder for calibrating and maintaining a permanent record of each annealing run.

The vacuums obtained and maintained at room temperature were between 2 and 10^{-5} and 9×10^{-6} mm of Hg and between 1×10^{-4} and 1×10^{-5} mm of Hg at the annealing temperatures.

Determination of Interface Movement—After the couples were annealed, they were polished metallographically along the length and across the interface and examined for interface shift. The carbide particles very clearly denoted the new interface, and an accurate measurement of this movement was possible by overetching the specimen until the original interface, or weld, was clearly seen as shown in Figs. 7 and 8. A minimum of ten measurements were taken with the use of a filar eyepiece and averaged for each tabulated ϵ or interface shift value.

Whenever small interface movements (under 0.016 cm) were observed, the specimens were sectioned across the interface for measurements at different depths to determine if there was any change in ϵ with respect to distance from surface.

Analysis of Specimens—After determination of the interface movement the specimens were sectioned and machined in slices of 0.078 inch. After each slice was machined, visual inspection on a comparator determined the slice thickness and the accumulative thickness of the slice to an accuracy of ± 0.0002 inch. The chips from each layer were collected on aluminum foil to prevent any contamination. Specimens with very small interface shifts were not sectioned for carbon analyses since the carbon concentration gradient was too steep to obtain reliable data.

The material used for the couples was iodide titanium and iodide titanium alloyed with carbon. The material was supplied by Watertown Arsenal and the complete chemical analysis, as received, is shown in Table I. The 1.300% carbon alloy was prepared by adding carbon to iodide titanium and then casting the alloy into ingots which were then hot forged and rolled at 750°C (1380°F) into machinable bar stock. The oxygen content is somewhat higher than would be considered for an ideal material; this was probably the result of the alloying and melting procedure.

All carbon determinations were accomplished using a Leco semi-

Table I
Chemical Analysis of Iodide Titanium Used

	Iodide Titanium	1.3% C-Iodide Titanium Alloy	0.413% C-Iodide Titanium Alloy
Ti	Major	Major	Major
Al	.003	.003	.003
Fe	.001	.007	.002
Si	.002	.005	.002
Mg	.001	[1].001	[1].001
Mn	.001	.002	.003
Pb	[1].001	[1].001	[1].001
B	[1].001	[1].001	[1].001
Cd	[1].001	[1].001	[1].001
Mo	[1].001	[1].001	[1].001
Cu	[1].0005	[1].0005	[1].0005
Ni	[1].001	[1].001	[1].001
Co	[1].0005	[1].0005	[1].0005
Cr	[1].001	[1].001	[1].001
Ca	.10	.005	.005
Sn	[1].001	[1].001	[1].001
C	.038	1.300	.413
O	.018	.236	.076
H	.011	.020	.009
N	.011	.034	.017

Not Detected: Sb, As, V, Zn, W, Zr, Hf

[1]Less than.

automatic carbon determinator manufactured by the Laboratory Equipment Corporation. The principle of the apparatus is, namely, the combustion of a given sample followed by the collection of the evolved gases, adsorption of the CO_2, and measurement of this quantity as a loss in volume. The obtainable accuracy is $\pm 0.005\%$ carbon.

Errors—In general, the major sources of experimental error in determining diffusion constants in metals are (a) lack of precise control and measurement of temperature, (b) inaccurate determination of concentrations of the diffusing element, and (c) improper preparation of diffusion couples or use of impure materials in the couples.

In this work, precautions were taken to insure maximum control of all known factors. However, some scatter of results was obtained, particularly in the β range. The possible reasons for this are discussed below.

By estimating the welding temperature at the interface to be approximately 900°C (1650°F) and the time at temperature to be two seconds, it can be seen that the diffusion occurring during welding is negligible since the order of the diffusion rate is 1×10^{-7} cm^2 sec^{-1} at this temperature. Some diffusion was also caused by the heating and cooling cycle for each diffusion anneal. However, since the diffusion rate is more than ten times greater for each 100°C increase in temperature in the annealing range, and since the time for heating and cooling of the specimen is very small (about two hours) as compared to the actual time at temperature, this is not serious.

Measurement of the interface movement was done by metallographic examination with an accuracy of ± 0.002 mm. The tem-

Table II
Diffusion Coefficients Obtained with Respective Interface Movements

Spec. No.	Temp. °C	Time hrs.	mm	D values $cm^2/sec.$	Av. D Values for each temp. range
7	736	200	.0745	2.09×10^{-9}	
3	736	595	.1250	1.98×10^{-9}	2.02×10^{-9}
6	736	1006	.1636	2.00×10^{-9}	
2	782	400	.188	5.53×10^{-9}	
16	782	817	.228	4.05×10^{-9}	5.27×10^{-9}
15	782	1440	.3781	6.22×10^{-9}	
1	835	100	.182	1.22×10^{-8}	
12	835	500	.3075	1.06×10^{-8}	1.28×10^{-8}
13	835	904	.5031	1.57×10^{-8}	
21	950	72	1.300	3.66×10^{-7}	
10	950	92	.132	1.84×10^{-7}	
5	950	140	.4464	3.08×10^{-7}	
9	950	280	.2610	3.72×10^{-7}	$2.49 \times 10^{-}$
20	950	620	.4030	1.23×10^{-7}	
19	950	620	.4290	1.39×10^{-7}	
11	1050	93	.219	3.55×10^{-7}	
18	1050	116	.499	3.02×10^{-7}	
4	1050	140	.899	3.53×10^{-7}	1.02×10^{-6}
22	1057	68	4.78	3.10×10^{-6}	
23	1150	19	6.28	1.145×10^{-5}	
14	1150	30	.605	3.29×10^{-6}	4.34×10^{-6}
8	1150	99	.664	1.2×10^{-6}	
17	1150	125	.811	1.415×10^{-6}	

perature control was $\pm 2\frac{1}{2}$°F, which averaged out fairly well since the zero controlling point was set on temperature. Measurement and successive machining of layers also introduces an error of ± 0.0002 inch. Carbon analysis errors are approximately $\pm 0.005\%$ carbon. This again is fairly well averaged out when the curve is drawn through the experimental points. This source of error does not influence the diffusion coefficient determination if the solubility limit is known for the annealing temperature.

The accumulation of all these errors, although significant, is not too serious. Any attempt to apply a correction factor was therefore deemed impracticable in the presented program.

The oxygen content was found to be fairly high in the alloyed material, and may have contributed to scatter of results. Only a few of the specimens revealed the basket-weave structure characteristic of the presence of oxygen in titanium. Carbon content varied as much as 12% in the high carbon forgings. However, cylinders to be machined for the high carbon ends for the diffusion couples were homogeneous in carbon distribution within each couple.

Discussion of Results

The diffusion anneals for the specimens in the alpha temperature range were conducted at 736, 782, and 835°C; for the specimens in the beta temperature regions at 950, 1050, 1057, and 1150°C. Twenty-three couples were annealed at the temperature

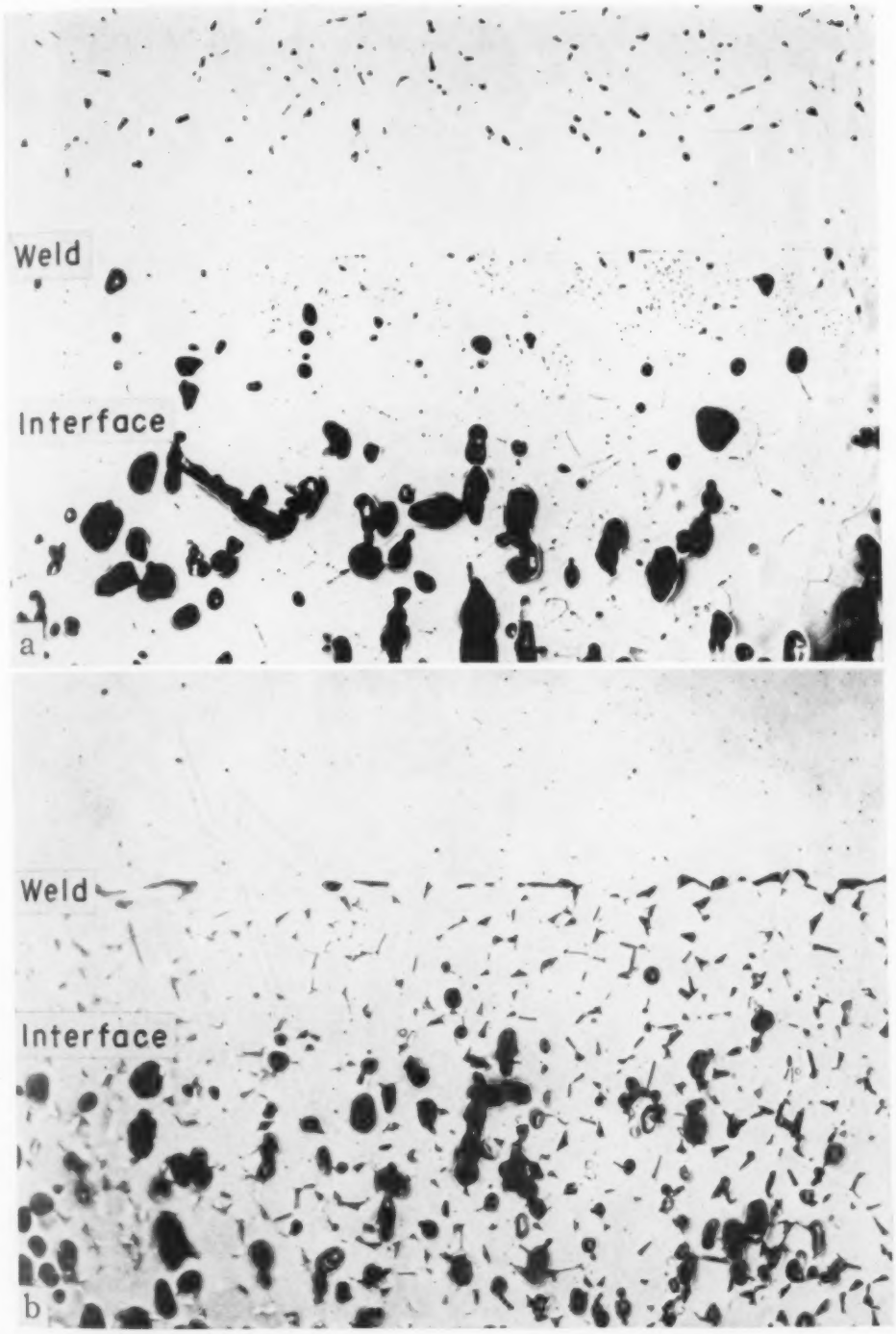


Fig. 7—Photomicrographs Showing Interface Shifts. (a)—Diffusion Couple No. 6—736°C for 1006 hours; (b)—Diffusion Couple No. 2—782°C for 400 hours. ×150.

and times shown in Table II. Figs. 7 and 8 show typical observed interface shifts. The weld is shown at the top of the photomicrographs with the α and β regions clearly bound by the γ phase. After

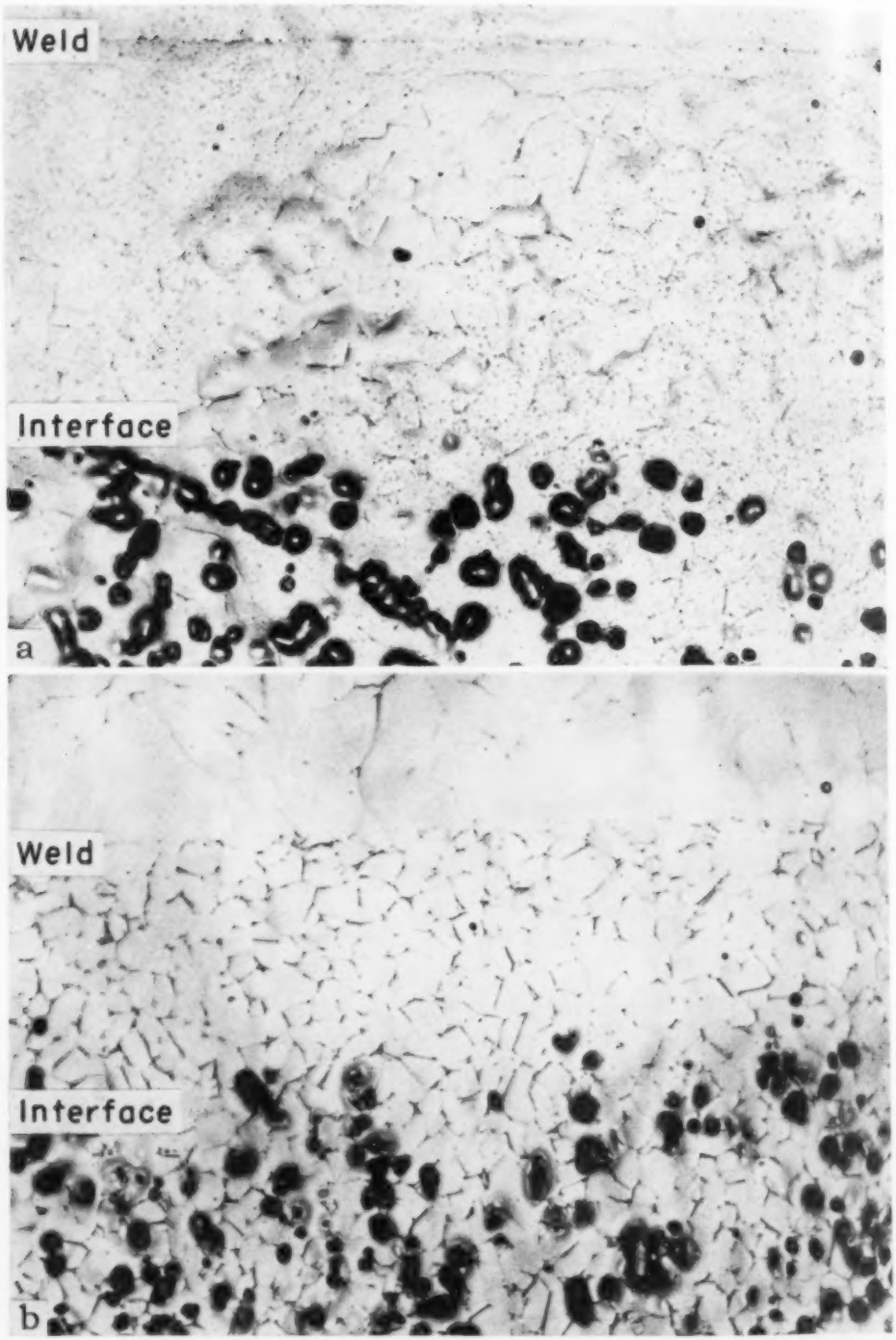


Fig. 8—Photomicrographs Showing Interface Shifts. (a)—Diffusion Couple No. 12—835°C for 500 hours; (b)—Diffusion Couple No. 1—835°C for 100 hours. ×150.

determining this interface movement by metallographic measurements, the specimen was machined in sections for carbon analysis.

The following procedure was used for plotting the carbon con-

Table III
γ Values Obtained with Corresponding Carbon Contents and Solubility Limits

Spec. No.	C_o	$C_{1,o}$	$C_{1,2}$	γ
7	1.300	.038	.240	.096
3	1.300	.038	.240	.096
6	1.300	.038	.240	.096
2	1.296	.037	.258	.105
16	1.296	.037	.258	.105
15	1.297	.037	.258	.105
1	1.296	.038	.316	.137
12	1.496	.050	.316	.111
13	1.496	.050	.316	.111
21	.413	.038	.160	.211
10	1.431	.098	.160	.027
5	1.300	.038	.160	.057
9	1.455	.110	.160	.021
20	1.455	.110	.160	.021
19	1.455	.110	.160	.021
11	1.367	.115	.188	.034
18	1.300	.038	.188	.070
4	1.367	.117	.188	.034
22	.413	.038	.190	.275
23	.413	.038	.224	.355
14	1.367	.115	.224	.051
8	1.367	.115	.224	.051
17	1.367	.115	.224	.051

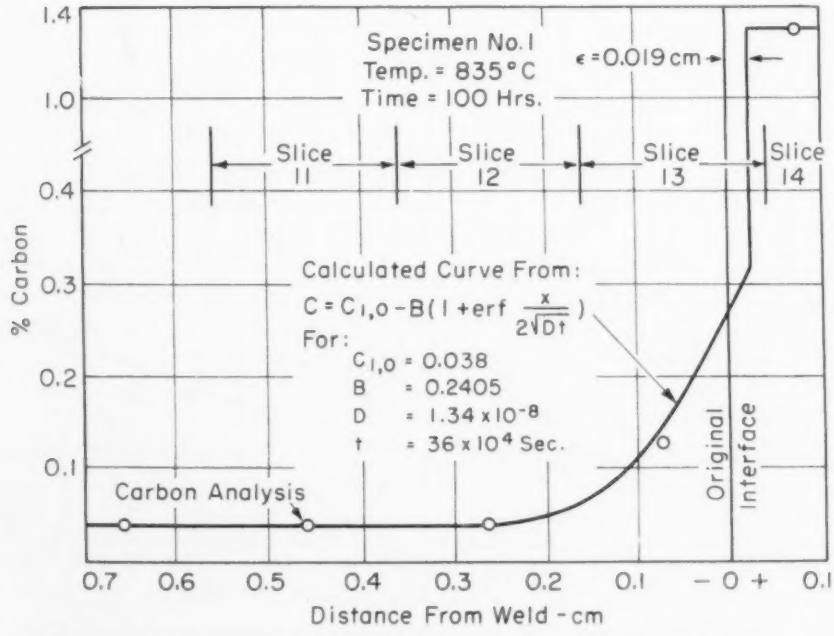


Fig. 9—Experimental Points Plotted for Comparison with Theoretical curve.

centration curve (Figs. 9 through 12). It can be seen by the small interface movements obtained with the high carbon content specimens (1.3% C) that accurate determinations of the α and β solubility limits would require extremely long annealing procedures. For

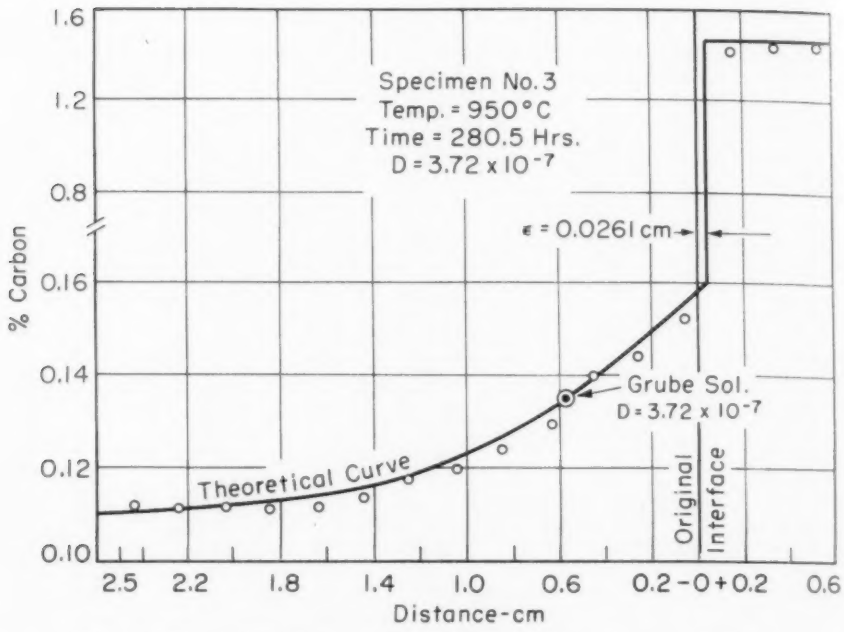


Fig. 10—Theoretical Concentration Curve with Experimental Points Superimposed.

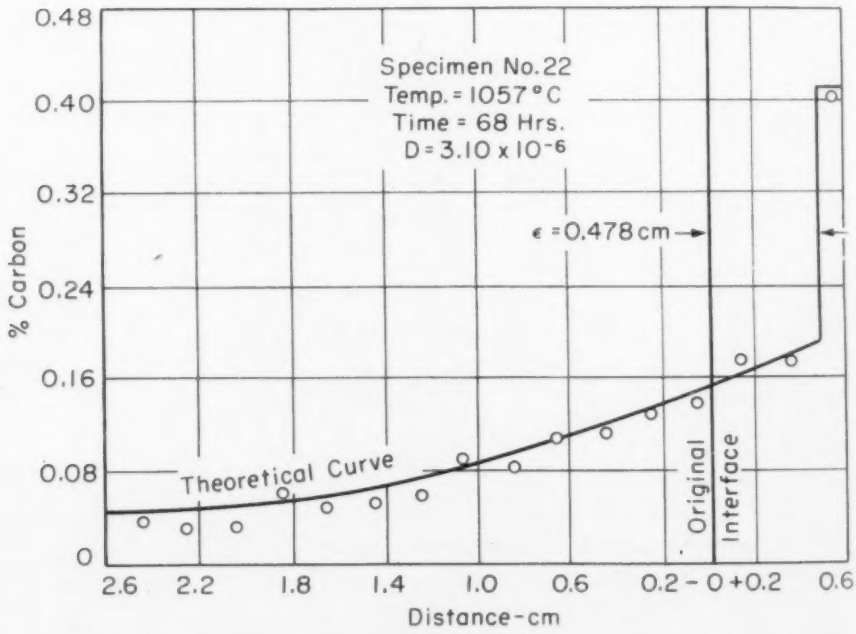


Fig. 11—Theoretical Concentration Curve with Experimental Points Superimposed.

this reason values for the α and β solubility limits ($C_{1,2}$) at the respective temperatures were taken from WADC Technical Report 53–41 (8) (see Fig. 1). The lower carbon content couples (0.413% carbon) gave slightly higher solubility limits for 1057 and 1150°C.

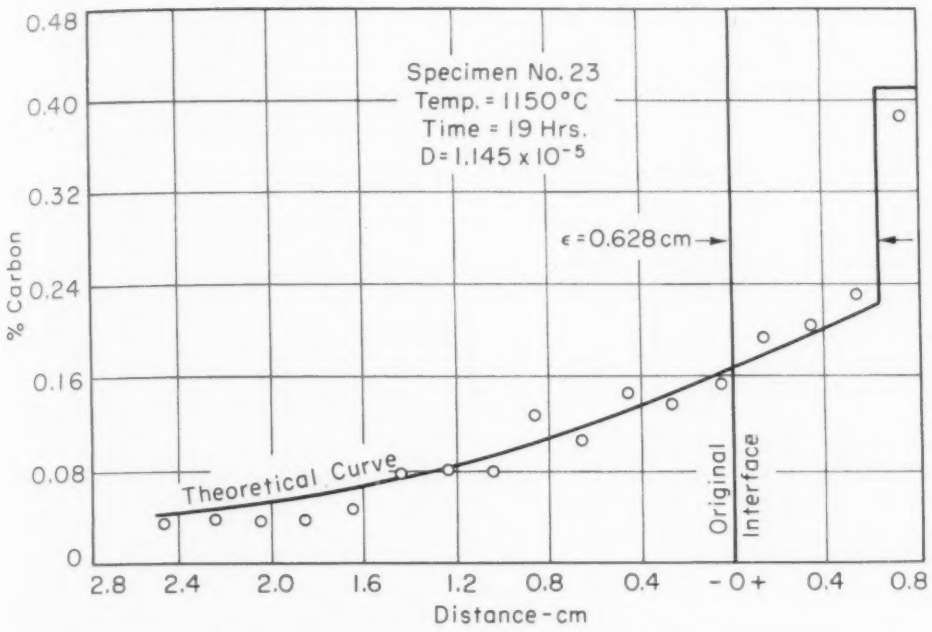


Fig. 12—Theoretical Concentration Curve with Experimental Points Superimposed.

For the purpose of calculating the diffusion coefficients (D), these solubility limits were approximated from the above mentioned report and the carbon concentration curves obtained from the lower carbon content couples.

The values of the parameter γ were determined by substituting the values given in Table III in Equation 5 below:

$$\frac{C_{1,2}-C_{1,2}}{C_{1,2}-C_o}=\sqrt{\pi}\gamma e\gamma^2(1+\text{erf}\gamma)$$

and then by substituting the calculated γ and measured ϵ into Equation 4:

$$\epsilon=2\gamma\sqrt{Dt},$$

the diffusion coefficients were determined for the α and β temperature range. By knowing D, the carbon contents, and the solubility limits at the respective temperatures, the theoretical concentration curves for the specimens were drawn according to Equation 2:

$$C=C_{1,o}-B\left(1+\text{erf}\frac{x}{2\sqrt{Dt}}\right)$$

The experimental points were, in turn, superimposed on the theoretical curve according to their relative positions to check the validity of the theory. It can be seen from Figs. 9 through 12 that the experimental points fall well within allowable experimental accuracy. It can be noted that the approximated solubility limits were justifiable in this temperature range. The location of the ex-

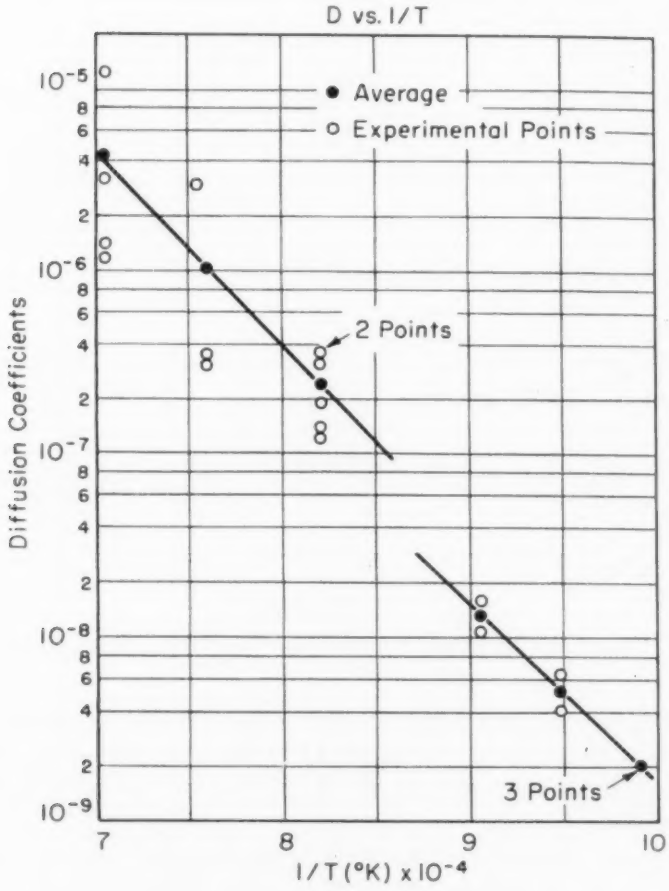


Fig. 13—Logarithmic Plot of D vs. $\frac{1}{T\ (°K)} \times 10^{-4}$ For the Diffusion of Carbon in Alpha and Beta Titanium.

perimental point in each case, within the volume where discontinuity occurred in the specimen, was determined by adjusting the carbon content for the respective volumes.

A plot of the square root of time versus interface movement also verified the assumption that:

$$\epsilon = 2\gamma\sqrt{Dt}$$

for a constant temperature. Where the γ was different, plots were substituted of $\frac{\epsilon}{\gamma}$ versus $\sqrt{\text{time.}}$

The activation energies for the alpha and beta regions were calculated from the slope of the logarithmic plots of D versus 1/T as shown in Fig. 13.

The activation energy for the alpha temperature range was slightly less than that obtained for the beta temperature range being 43,500 cal/mole and 48,400 cal/mole, respectively.

The diffusion rate of carbon in titanium was found to be independent of concentration within the limits of experimental error. This was confirmed by plotting the experimental data for carbon concentration along the curve calculated from:

$$C = C_{1,o} - B\left(1 + \text{erf}\frac{x}{2\sqrt{Dt}}\right)$$

Since the calculated and experimental curves superimposed very well, it was concluded that D was independent of concentration. With D independent of concentration, it was also possible to use the Grube solution of Fick's second law to check the values of diffusion coefficients obtained by the above method.

Thus from Fig. 10, one may consider the range $C_{1,2} - C_{1o}$, as equal to Co/2 and C at any value of x as equal to C-x-$C_{1,o}$. In this case, $C_{1,2} - C_{1,o} = 0.160 - 0.111 = 0.049$, and at 0.60 centimeters from the interface value of C-x-$C_{1,o} = 0.135 - 0.111 = 0.024$. The Grube expression is $\left(\frac{2C}{C_o} - 1\right) = \text{erf}\left(\frac{x}{2\sqrt{Dt}}\right)$, so that:

$$\left(\frac{0.024}{0.049}\right) - 1 = \text{erf}\left(\frac{0.600}{2\sqrt{Dt}}\right)$$

$$-0.510 = -\text{erf}\left(\frac{0.600}{2\sqrt{Dt}}\right)$$

$$0.489 = \frac{0.300}{\sqrt{Dt}}$$

$$Dt = \left(\frac{0.300}{0.489}\right)^2$$

$$D = \frac{0.376 \times 10^{-3} \times 10^{-4}}{0.280\ 5 \times 0.36} = 3.72 \times 10^{-7}\ \text{cm}^2\ \text{sec}^{-1}$$

This is the same value as obtained with the Wagner solution, using the expressions:

$$\frac{C_{1,\,o} - C_{1,\,2}}{C_{1,\,2} = C_o} = \sqrt{\pi}\ \gamma e\gamma^2(1 + \text{erf}\ \gamma)$$

and $\epsilon = 2\gamma\sqrt{Dt}$

Solubility of Carbon in Alpha and Beta Titanium—In theory, diffusion studies of systems such as the one in the present investigation offer a sensitive means of determining solubility limits of the diffusing element. Thus, in the titanium-carbon system, when diffusion occurs from the two phase regions of $\alpha+\beta$ into pure titanium, there occurs a discontinuous carbon concentration at the solubility limit. Since this concentration can be determined accurately by chemical analysis, the maximum solubility at the temperature of diffusion is pinpointed within the limits of accuracy of the carbon analyses.

By utilizing the data from these experiments, solubility limits were determined and, as indicated in Fig. 1, were slightly different

at high temperatures from those reported in the literature (8,9). The differences were slight, and probably insignificant for practical purposes. Thus at 1050°C, a C_s value of 0.19 wt. % was obtained in the diffusion studies, while the literature data indicated a carbon solubility of 0.16 wt. %. At 1150°C, the position of the β solvus was indicated to be 0.22 wt. % from diffusion analyses, and 0.17 wt. % from metallographic studies. At temperatures below 1050°C, the solubility limits obtained by both methods were in agreement.

The reasons for these differences are not obvious. It has been suggested, however, that oxygen content of the specimens may have been a factor (10). This may be the answer since the oxygen contents of the titanium-carbon alloys used in the diffusion experiments were higher than the iodide grade titanium (see Table I).

Conclusions

The diffusion rates of carbon in titanium were determined over a range of temperature from 736 to 1150°C (1355 to 2100°F). The D values obtained at the various diffusion temperatures were as follows:

Ti Modification	Temp °C	$D_{cm^2/sec}$
α	736	2.0×10^{-9}
α	782	5.0×10^{-9}
α	835	1.3×10^{-8}
β	950	2.5×10^{-7}
β	1050	1.0×10^{-6}
β	1150	4.0×10^{-6}

Activation energies were obtained from the D values in the α and β ranges, and were 43,500 cal/mol and 48,400 cal/mol respectively.

The scatter of results was somewhat greater in the β range than in the α range. However, a sufficient number of specimens were tested to obtain reliable average values of D at each temperature.

It was also shown, within the limits of experimental error, that the rate of diffusion of carbon in titanium is independent of concentration.

The solubility limits obtained for the alpha and beta temperature range were the following:

Ti Modification	Temp °C	Solubility Limit %C
α	736	0.240
α	782	0.258
α	835	0.316
β	960	0.160
β	1050	0.188
β	1057	0.190
β	1150	0.224

ACKNOWLEDGMENT

The authors are grateful to the Watertown Arsenal for their support of this work and permission to publish the results at this time.

The authors also acknowledge the work of the following in carrying out this research effort: R. H. Baskey, R. Kosar, G. Day, and P. M. Reif, all of Horizons Incorporated.

References

1. R. J. Wasilewaki and G. L. Kehl, Summary Report on Diffusion of Hydrogen, Nitrogen, and Oxygen in Titanium, Watertown Arsenal Report No. WAL 401/149-11A.
2. C. Smithells, Metals Reference Book, Butterworth 1949, p. 390.
3. D. Polder, "Theory of the Elastic After Effect and the Diffusion of Carbon in Alpha Iron," Phillips Research Reports, Vol. 1, No. 5, 1945, p. 1045.
4. J. K. Stanley, "The Diffusion and Solubility of Carbon in Alpha Iron," *Transactions*, American Institute of Mining and Metallurgical Engineers, Vol. 185, 1949, p. 752.
5. M. Paschke and Hauttmann, "Versuche uber die Diffusion von Kohlenstoff, Silizium, and Mangan in Testem und Flussigem Eisen," *Archiv fur das Eisenhuttenwessen*, Vol. 9, 1935–36, p. 305.
6. C. Wells and R. F. Mehl, "Rate of Diffusion of Carbon in Austenite in Plain Carbon in Nickel, and in Manganese Steels," *Metals Technology*, August 1940, TP 1180.
7. W. Jost, "Diffusion in Solids, Liquids, and Gases," Academic Press Inc. 1952, New York, p. 68.
8. WADC Technical Report 53–41, p. 26.
9. I. Cadoff and J. P. Nielson, "Titanium-Carbon Phase Diagram," *Transactions*, American Institute of Mining and Metallurgical Engineering, Vol. 197, 1953, pp. 248.
10. L. Stone and H. Margolin, "The Titanium Rich Regions of the Ti-C-N, Ti-C-O, and Ti-N-O Phase Diagrams," *Transactions*, American Institute of Mining and Metallurgical Engineers, Vol. 197, 1953, p. 1498.

DISCUSSION

Written Discussion: By J. E. Reynolds, Battelle Memorial Institute, Columbus, Ohio.

The authors are to be congratulated on this work. The comment that I would like to make is a minor one, and in no way is intended to detract from their excellent paper. With regard to the specimen preparation prior to butt welding the diffusion couples, the authors have indicated that the contact surfaces were first polished through 3/0 metallographic paper, etc. It has been my experience and the experience of others that one cannot retain flat surfaces in the usual manual polishing operation, and, in addition, parallelism of opposite end faces is lost. In the butt welding process, this would seemingly result in greater tendency toward undulation and uneven welding pressure across the interface. In the present work, these effects may not have introduced an appreciable error, but, in general, specimen faces surface ground to ± 0.0001 inch are to be desired over metallographically polished faces.

Authors' Reply

Because of the appreciable amounts of plastic flow occurring at the weld interface during the resistance butt welding operation, uniform contact of the ends of the prepared specimens was assured. If this plastic flow had not been obtained, the flatness and parallelism of the abutting specimens would have been more critical.

METALLOGRAPHY OF TEMPERING OF ALPHA-PRIME IN TITANIUM ALLOYS

By R. F. Domagala and W. Rostoker

Abstract

This paper describes a program which was designed to discover microscopically how the α' phase, a metastable supersaturated isomorph of the α phase changes on reheating to that of equilibrium α as dictated by the phase diagram. Specimens containing 13% Mo or 6% Cr were prepared, solution treated at 1000°C, and water quenched. By metallographically following changes in α' needles on tempering below the β transus, it was discovered that in the Mo alloy the α' needles generally temper by precipitating small particles of α while in the Cr alloy tempering occurred by diffusion across the α'/β interface. (ASM-SLA Classification: N6, Ti)

DURING quenching of alloyed titanium from the beta field, a martensitic transformation may occur. The product of this transformation is isomorphous with the alpha modification of titanium, but presumably has the composition of the original beta. As such, the martensitic phase is generally a supersaturated alpha, and the term alpha prime (α') is used to designate it. It should be remarked, however, that the supersaturated condition is not mandatory, since some quench products which metallographically appear to be α' occur in systems which have a single phase alpha field at low temperatures. This paper describes the changes in metallographic experience of α' in two beta-stabilized alloys during the process of tempering at various elevated temperatures.

The two binary alloys selected as representative of different types of beta-stabilized systems contained 13% Mo and 6% Cr, respectively. The quenched (from 1000°C) structures of these specific compositions contained relatively few alpha prime needles or platelets clearly resolved against a background of retained beta. Actually, the 13% Mo alloy developed α' in the quenched structure only after etching in a strong HF-HNO_3 acid bath.

Since α' in the 13% Mo alloy is metastable with respect to a phase mixture of $(\alpha+\beta)$, one might anticipate several possible configurations resulting from tempering:

(a) Rejection of a dispersion of alloy-rich β of the composition

---

A paper presented before the Thirty-Seventh Annual Convention of the Society, held in Philadelphia, October 17–21, 1955. Of the authors, R. F. Domagala is associate metallurgist, and W. Rostoker is supervisor, Physical Metallurgy Section, Metals Research Department, Armour Research Foundation of Illinois Institute of Technology, Chicago. Manuscript received March 31, 1955.

characteristic of the tempering temperature, causing depletion of the solute content of α'.

(b) Rejection of alloy-poor α, enriching the remaining α' until it reverts to an enriched beta.

(c) Mass transfer of solute and solvent atoms across the α'/β interface, causing no essential change in the configuration.

Above the eutectoid temperature, the 6% Cr alloy should behave in the same way as the 13% Mo alloy; but below, the added possibility exists that α' can deplete its solute content by rejection of $TiCr_2$.

The alloys were prepared from 120 BHN titanium sponge by arc melting in a nonconsumable electrode arc furnace. The pancake ingots were sliced to provide coarse grained specimens for subsequent heat treatment. They were homogenized by a prolonged anneal at 1000°C (1830°F). During all heat treatments, specimens were sealed in evacuated Vycor bulbs. The bulbs were broken under water at the instant of quenching. Early attempts were made to reexamine the same area in each sample after progressive tempering. Regardless of the care taken, however, no more than four successive anneals could be completed before the specimen required new metallographic preparation, which invariably cut through the original α' needles. For this reason, most of the observations recorded refer to average conditions throughout a specimen after a particular prior history.

Observations on the 13% Mo Alloy

The α' needles observed in this alloy were generally very simple in structure and configuration. Each needle appears to be a homogeneous orientation. Intersection of needles is common. A typical field is illustrated in Fig. 1.

A tempering temperature of 700°C (1290°F) was chosen for the first series of experiments. Cumulative times at temperature ranged from 0.5 to 31 hours. Only after 3 hours could even a slight precipitate be detected in the α' needles. After 6 hours, the dispersed precipitate etched more darkly (Fig. 2). After somewhat less than 31 hours, the original α' needles had blended indistinguishably into the fine $(\alpha+\beta)$ structure, which developed by concurrent isothermal transformation of the surrounding β matrix. The major point in question is whether the fine precipitate in the α' needles is alpha or beta. If the precipitate were β, then a β dispersion in an α matrix could not reasonably blend into an α dispersion in a β matrix, and the trace of the original needles should persist. Since the needles do disappear, they must ultimately form an α dispersion in a β matrix; this could only happen if the original precipitate were α.

In some of the specimens examined, a few tempered α' needles took on a duplex or banded configuration. Fig. 3 shows needles com-

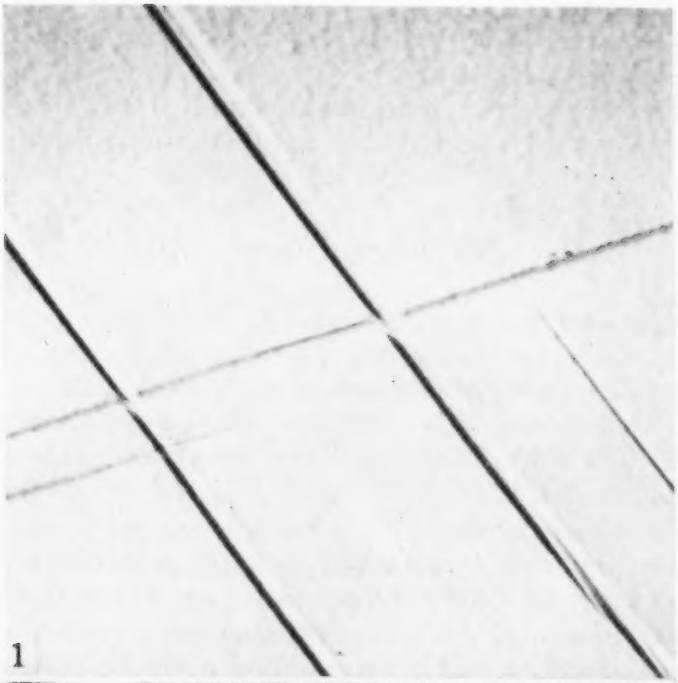




Fig. 1—α' Needles in a 13% Mo Alloy As-quenched from 1000°C (1830°F) (oblique illumination). ×750.

Fig. 2—α' Needles in a 13% Mo Alloy After Tempering at 700°C (1290°F) for 6 hours. (No additional metallographic treatment beyond that performed on the original specimen of Fig. 1). ×750.



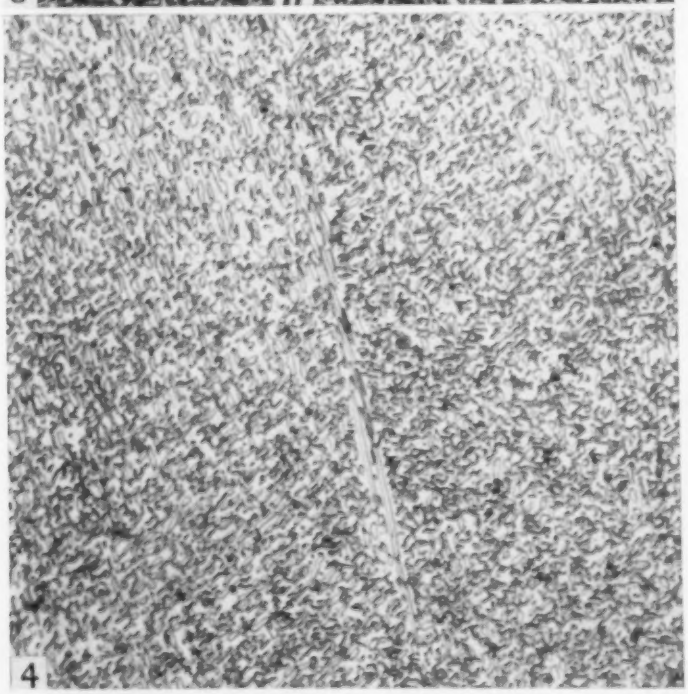
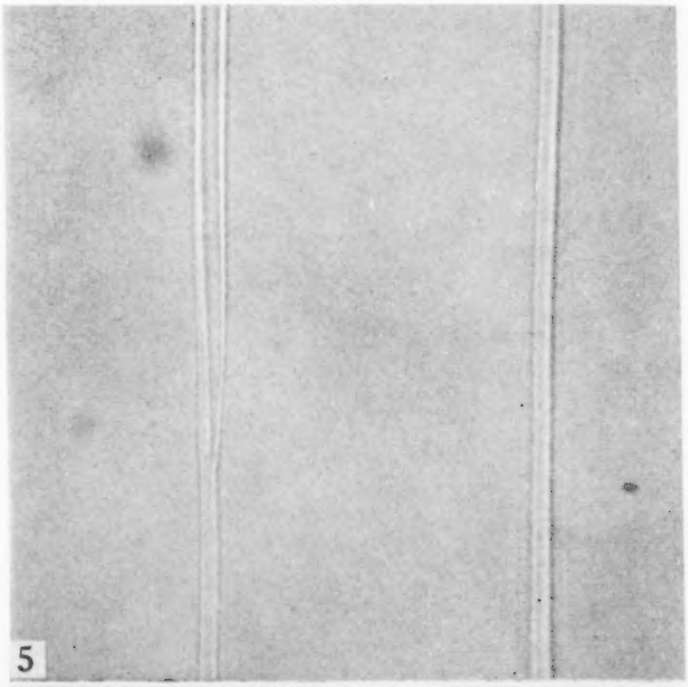


Fig. 3—α' Needles After Tempering at 750°C (1380°F) for 1 hour, Showing a Configuration of two side bands of α and a midrib of β. ×750.

Fig. 4—α' Needles After Tempering at 700°C (1290°F) for 31 Hours, Showing the Breakup of the Side Bands of α. ×750.



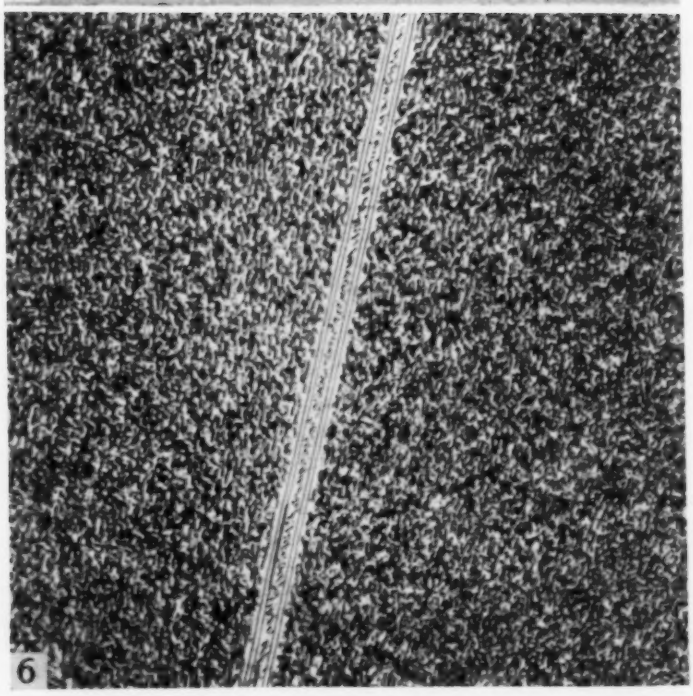


Fig. 5—Banded α' Needles in As-quenched 13% Mo Alloy. ×750.

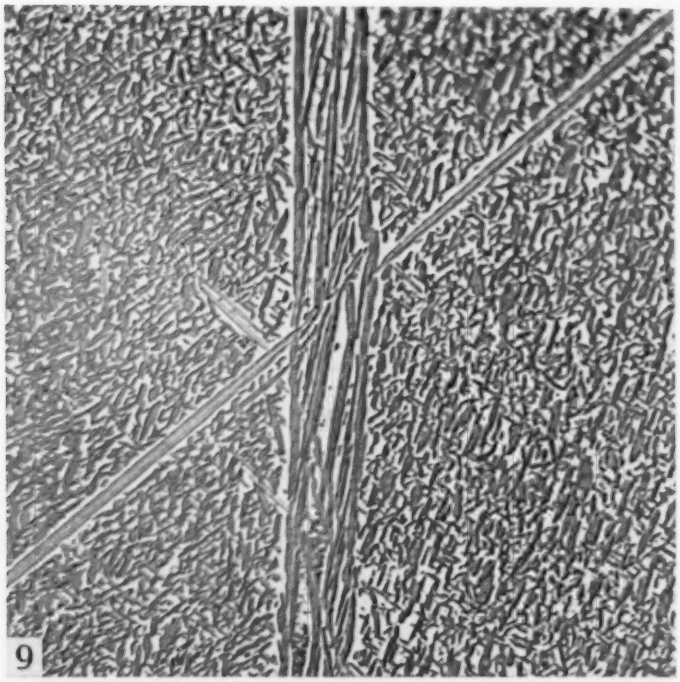
Fig. 6—α' Needle Tempered at 700°C (1290°F) for 10 Hours, Showing a Precipitate in the β Midrib. ×750.





Fig. 7—α' Needles in an As-quenched 6% Cr Alloy, Showing Simple and Complex Configurations. ×750.

Fig. 8—An α' Needle in As-quenched 6% Cr Alloy, Showing Fine Structure of a Complex Needle. ×750.



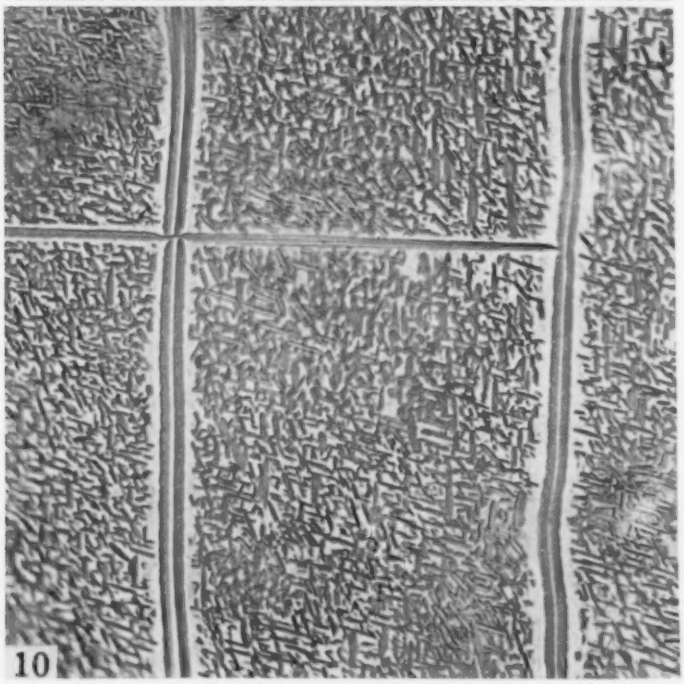
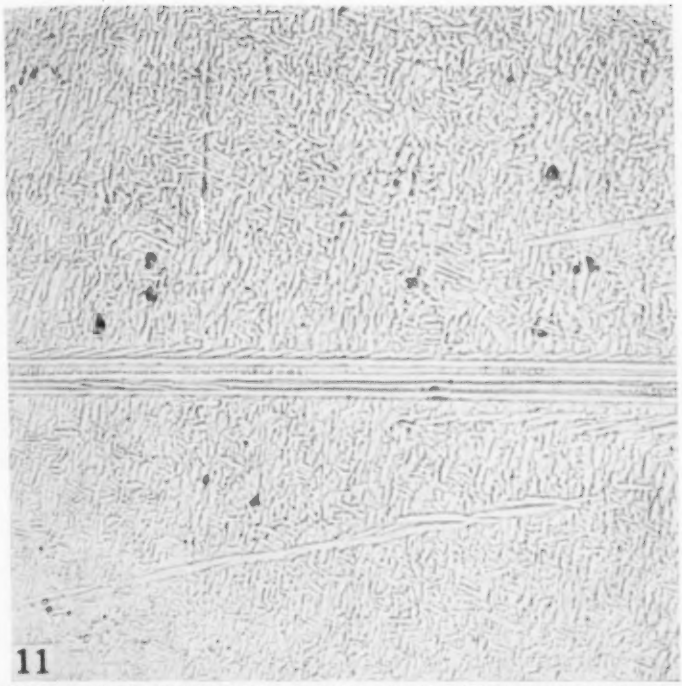


Fig. 9—α' Needle in a 6% Cr Alloy After Tempering at 700°C (1290°F) for 2 Hours, Showing Structure of Complex Needle. ×750.

Fig. 10—α' Needle in 6% Cr Alloy After Tempering at 750°C (1380°F) for 0.5 Hours, Showing Banded Configuration of α With a Midrib of β. ×750.



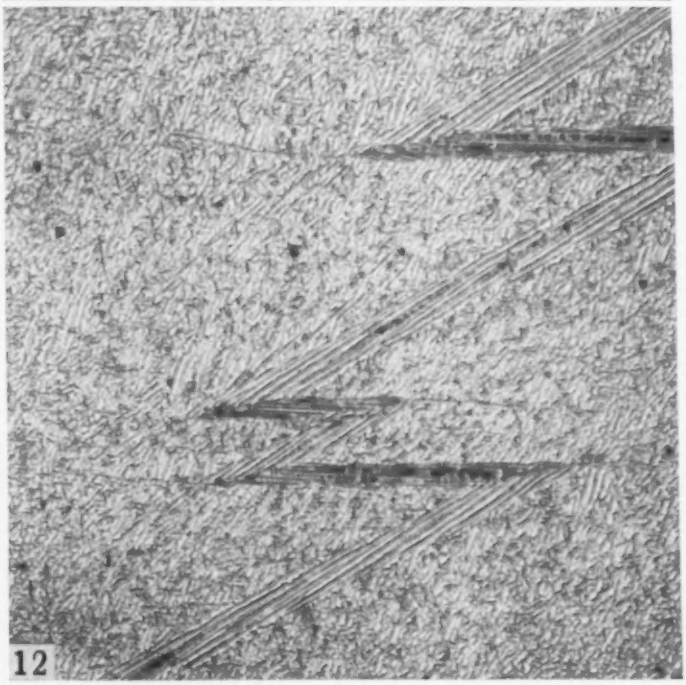


Fig. 11—α' Needle in 6% Cr Alloy Tempered at 700°C (1290°F) for 1 Hour, Showing Multiple Bands of α.

Fig. 12—Series of α' Needles in a 6% Cr Alloy After Tempering at 600°C (1110°F) for 5 Hours, Showing Unidentified Dark Etching Characteristic. ×750.

posed of two side bands of α and a center midrib of β. The midrib was identified as β for two reasons: (a) There is no optical reaction to rotation in polarized light. This is characteristic of β, while α and α' react by sharp changes in reflectivity. The side bands do react in this fashion. (b) On prolonged tempering the side bands break up (Fig. 4), and the midrib becomes continuous with the β matrix. The occurrence of these structures prompted a careful re-examination of as-quenched specimens. It was observed that on rare occasions α' needles originally form as a banded configuration (Fig. 5).

Additional proof that the banded needles are present initially in the specimens is presented in Fig. 6. This structure represents the state after tempering at 700°C (1290°F) for 10 hours. The midrib is peppered with a fine precipitate just as the surrounding beta matrix. This means that the center rib was nonequilibrium beta at the tempering temperature, i.e., it formed on quenching. If the rib had formed during tempering, it should be of the composition dictated by the equilibrium diagram for that temperature and should not show a precipitate.

The α' needles or bands on either side of the beta midrib do not show precipitate at any stage of tempering. Tempering must, therefore, occur by a diffusion process across the α'/β interface. Equilibrium is thus obtained without the nucleation of new orientations of either phase. The breakup of the alpha bands after prolonged annealing is probably a surface tension effect. At 700°C (1290°F), therefore, there appear to be two mechanisms of tempering.

At 750°C (1380°F), tempering is much accelerated. The α' needles developing a dispersed phase disappear in less than an hour. The banded needles persist for somewhat longer.

Tempering at 500°C (930°F) was extremely sluggish and the dispersed phase structures were too fine to resolve.

Observations on the 6% Cr Alloy

Two types of α' needles are observed in this alloy. One is a simple, narrow band of apparently single homogeneous orientation. The other is much broader and has a substructure of short fragments of α' interleaving the beta matrix. Typical examples of these are shown in Figs. 7 and 8.

On tempering at 700°C (1290°F), the configurations are essentially unchanged in form. The etching characteristics of the tempered α' approach those of alpha. With time the structure coarsens, breaks up, and blends into the $(\alpha+\beta)$ background of the matrix. No precipitates were observed in the α' plates. Tempering, therefore, must proceed by mass transfer across the α'/β interface until equilibrium concentration of α is achieved. The original fine structures of the complex α' shapes are more easily resolved after tempering (Fig. 9).

The banded configuration of tempered α' needles was also noted in this alloy (Fig. 10). In some instances, multiple banded structures were observed (Fig. 11). The significant remark at this point is that despite exhaustive study of as-quenched structures, no examples were discovered of banded configurations in the original α' needles. One is forced to the conclusion that these formed during tempering by oriented growth of the beta midrib or midribs within the α' needle. Furthermore, there were no precipitates observed in these beta midribs, indicating that they were of the composition characteristic of the tempering temperature.

On tempering at 600°C (1110°F), below the eutectoid temperature, irresolvable dark etching effects appear in some of the needles as shown in Figure 12. These might be fine particles of $TiCr_2$ but no positive identification could be made.

Summary

Alpha prime needles in a 13% Mo alloy are of simple construction. On rare occasions two needles form parallel to each other, entrapping a thin layer of retained beta. Tempering occurs slowly at 700°C (1290°F) by one of two processes. In one, a fine precipitate develops throughout the α' needle which, from the fact that the needle ultimately blended into the matrix, was inferred to be alpha. In the other process, which only occurred with symmetrically banded α' needles, there was a simple mass transfer across the α'/β interface until the α' was diluted to equilibrium alpha. With prolonged annealing times, surface tension effects broke up the long bands of alpha into small fragments.

Alpha prime needles in the 6% Cr alloy were either of the simple type found in the 13% Mo alloy; or were complex, made up of short, almost randomly oriented platelets of α' interleaving the beta matrix in a broad band. No instances of symmetrically banded needles were found in the as-quenched state.

Tempering occurred most frequently by mass transfer across the α'/β interfaces, yielding final structures which were essentially the same as the original but more clearly resolved. In a number of instances, tempered structures composed of two parallel bands of alpha bracketing a midrib of beta were noted. Since such structures were not observed in the as-quenched state, it is inferred that they formed by oriented growth of beta within the α' needle. At 600°C (1110°F) an irresolved dark etching effect was observed in some needles, but its nature could not be determined. It was not possible to identify the occurrence of $TiCr_2$ as a temper product.

Raising or lowering the tempering temperature appeared to influence only the kinetics of the processes, but not their nature.

ACKNOWLEDGMENT

The work herein reported was conducted under Contract No. AF 33(038)-8708 for the Materials Laboratory, and under Contract No. AF 33(616)-2559 for the Aeronautical Research Laboratory, both of the Wright Air Development Center, Ohio. This sponsorship and permission to publish are gratefully acknowledged.

Special thanks are due to the metallographic section of the Metals Department of Armour Research Foundation for the photomicroscopy.

DISCUSSION

Written Discussion: By D. N. Williams, Battelle Memorial Institute, Columbus, Ohio.

The authors, Messrs. Domagala and Rostoker have pointed out that there are only three possible mechanisms which might describe the decomposition of alpha prime (martensite) during tempering:

1. Precipitation of beta (or compound) with a gradual approach of the alpha prime matrix to an equilibrium alpha composition.
2. Precipitation of equilibrium alpha, followed by transformation (by a shear process?) of the increasingly alloy rich alpha prime to beta.
3. Mass transfer of atoms across the beta-alpha prime interface.

In their paper, and in a contemporary paper by Brotzen, et al.,[2] the results of tempering studies of three alloys are reported in which examples of each of these mechanisms are reported.

Messrs. Domagala and Rostoker found that a Ti-6Cr alloy showed Type 3 tempering at 1290°F, with some evidence that Type 1 tempering occurred below 1110°F. In a Ti-13Mo alloy, these authors reported that tempering occurred chiefly by a Type 2 process, but occasional Type 3 tempering was also observed. Brotzen, et al., reported that a Ti-7.5V alloy exhibited Type 1 tempering between 660 and 1020°F. On first examination, these two papers would indicate that tempering of alpha prime is exceedingly complex and varies considerably from alloy to alloy.

Such complexity is unexpected, particularly in the case of Ti-V and Ti-Mo alloys which have been found to behave quite similarly in most other respects. This leads one to question either the Ti-V or the Ti-Mo data, even though the tempering temperatures investigated for the Ti-Mo alloy, 930 to 1380°F, were somewhat higher than those investigated for the Ti-V alloy. Since a Ti-13Mo alloy is usually assumed to be 100% beta on quenching (the Ms has been reported to be at room temperature at about 11.5% Mo,[3] the possibility exists that the alpha prime needles observed in this alloy were strain-induced during sample preparation. The tempering process observed in strain-induced needles might not bear any relationship to that normally occurring in alpha prime formed during a quench.

If the observation of Type 2 tempering in the Ti-Mo alloy is disregarded on

[2]F. R. Brotzen, E. L. Harmon, and A. R. Troiano, "Nature and Decomposition Kinetics of Alpha Prime in Titanium-Vanadium Alloys," TRANSACTIONS, American Society for Metals, Vol. 48, 1956, (Preprint No. 24).

[3]D. J. DeLazaro, M. Hansen, R. E. Riley, and W. Rostoker, "Time-Temperature Transformation Characteristics of Titanium-Molybdenum Alloys," *Transactions*, American Institute of Mining and Metallurgical Engineers, Vol. 194, 1952, p. 265.

the assumption that these needles were probably strain-induced, the tempering reactions follow a consistent pattern for all three alloys; tempering by mass transfer across the beta-alpha prime interface at high temperatures where the diffusion rates are high, and precipitation of beta (or compound) at low temperatures where nucleation is rapid. Such a mechanistic picture of the tempering reaction would appear quite reasonable.

Authors' Reply

The major contention raised by Dr. Williams seems to be the differences in tempering mechanisms reported for Ti-Mo alloys in this paper and for Ti-V alloys suggested in the paper by Brotzen, et al. It should be noted that Brotzen's paper dealt only with kinetics of tempering rather than mechanism. Their mention of beta precipitation on tempering alpha prime is surmise not based on any experimental evidence.

Alpha prime needles in the 13% Mo alloy occurred during the cleaning of the specimens. There is probably some sort of "release of surface stress" origin to their formation. Since they are probably compositionally identical with the quench martensite and they are certainly structurally the same, there is little reason to expect that the etch-induced α' should temper by a different mechanism.

The best evidence supporting the precipitation of alpha particles in needles (Ti-13% Mo) during tempering is that ultimately there is a blending of the alpha prime needle sites into the matrix of alpha-in-beta formed during tempering of the beta. Restating from the text of the paper, precipitation of beta in an alpha matrix would not blend with the background of alpha in a beta matrix.

NATURE AND DECOMPOSITION KINETICS OF ALPHA PRIME IN TITANIUM-VANADIUM ALLOYS

By F. R. Brotzen, E. L. Harmon and A. R. Troiano

Abstract

The nature and the decomposition kinetics of martensitically transformed alpha titanium (α') were studied, utilizing X-ray diffraction techniques and electrical resistance and hardness measurements.

X-ray diffraction disclosed that the c parameter of the α' phase followed Vegard's Law for compositions up to about 10% vanadium. The α' parameter varied linearly with composition up to about 7.5% vanadium but deviated noticeably for a 10% vanadium alloy.

Supersaturation was found to increase the hardness of α' only slightly.

By correlating electrical resistance changes with the amount of α' transformed, it was established that the tempering of α' in a 7.5% vanadium-titanium alloy followed the same rate law as the first stage of martensite tempering in steel.

The results further indicated that the precipitation of equilibrium beta from supersaturated alpha titanium is a diffusion controlled process with an activation energy for the tempering reaction of about 15,000 cal/mole. (ASM-SLA Classification: N9, Ti)

TITANIUM-RICH alloys may undergo shear-type allotropic transformations similar to the formation of martensite in steel (1)[1]. The diffusionless nature of the transformation from the high temperature beta to the low temperature alpha phase precludes compositional changes, so that the alloy contents of matrix and precipitate are identical. This condition leads to supersaturated transformation products, which are thermodynamically unstable. When these products are tempered at slightly elevated temperatures, increased diffusion makes possible an approach to equilibrium conditions. At present, little information is available on the effect of supersaturation upon the structure of the alpha prime phase.[2] More-

[1]The figures appearing in parentheses pertain to the references appended to this paper.
[2]The martensitically formed phase will be referred to as alpha prime.

A paper presented before the Thirty-Seventh Annual Convention of the Society, held in Philadelphia, October 17–21, 1955. Of the authors, F. R. Brotzen is assistant professor, Department of Mechanical Engineering, Rice Institute, Houston, Texas; E. L. Harmon is research assistant and A. R. Troiano is professor, Department of Metallurgical Engineering, Case Institute of Technology, Cleveland. Manuscript received May 20, 1955.

over, there is only meager data on the decomposition of supersaturated alpha prime during tempering.

The present investigation of the formation and decomposition of alpha prime was conducted for titanium-vanadium alloys, in which transformations can be followed quite readily. Because of the mild stabilizing effect of vanadium on the high temperature beta phase, temperature changes correspond to easily detectable, large changes in the equilibrium composition of beta, Fig. 1 (2,3). Furthermore, in the titanium-vanadium system there are no intermetallic compounds which would unnecessarily complicate the transformation picture.

Material

The alloys used for X-ray diffraction and hardness studies were prepared by the Research Division, New York University from iodide titanium and electrolytic vanadium. These alloys, containing from 0 to 20% vanadium, were arc-melted in an inert atmosphere, in lots of 20 grams each.

The 7.5% vanadium-titanium alloy which was used for resistivity experiments was prepared by Battelle Memorial Institute from iodide titanium furnished by Watertown Arsenal, and vanadium of 99.8% purity. An 8 lb. ingot was prepared by arc-melting in an inert atmosphere with a tungsten electrode and water-cooled copper crucible. Following this, the ingots were remelted, forged and then rolled to half-inch square bars, which were subsequently grit blasted, pickled, and wire brushed.

Procedure

Heat Treating Procedure—Solution treatments were conducted in high vacuum, resistance furnaces at pressures below 5×10^{-5}mm of mercury. Tempering treatments were carried out in a salt bath. The specimens were not attacked by the salt in the temperature range studied (350–550°C) (660 to 1020°F). The quenching medium used in all cases was iced brine.

X-ray Diffraction and Hardness Measurements—Specimens used for hardness measurements and X-ray diffraction studies were $\frac{1}{4}'' \times \frac{1}{4}'' \times \frac{1}{32}''$ in size. The thin section facilitated rapid cooling.

A Geiger-counter spectrogoniometer was utilized for lattice parameter determinations. Because of the excessive broadness of the diffraction lines, intensities were scaled at regular angular intervals. The scaling results were evaluated by a modification of a method proposed by Finch (4).

Electrical Resistance Measurements—Specimens used for electrical resistance determinations measured $1\frac{1}{2}'' \times \frac{1}{32}'' \times \frac{1}{32}''$. The quenched specimens were suspended in a manner that allowed aging

in a salt bath and cooling to testing temperature without disconnecting the leads. The voltage drop across a constantan standard resistance, which corresponded to the current through the specimen, and the voltage drop across the specimen were measured with the same potentiometer. The temperature was determined with copper-constantan thermocouples at each end of the specimen. The thermocouple wires served also as potential leads in the measuring circuit.

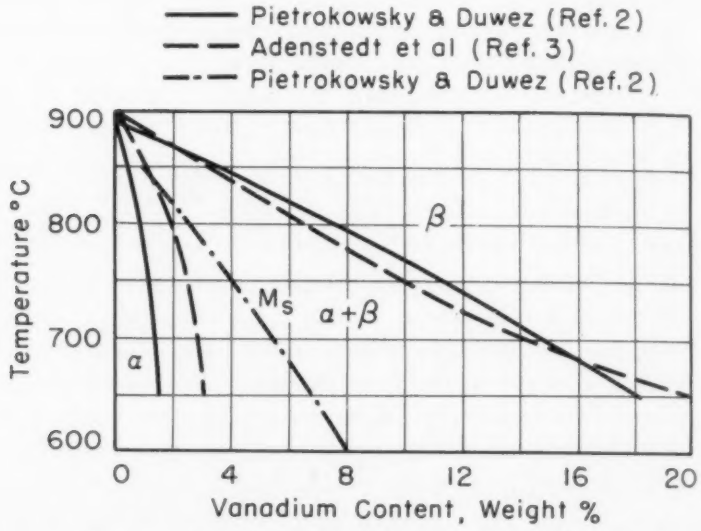


Fig. 1—Partial Titanium-Vanadium Diagram, Showing also M_s as a Function of Vanadium Content.

This method yielded reproducible results of relative resistance within about 0.05%, but did not lend itself to absolute resistivity measurements.

Results and Discussion

The Nature of Alpha Prime—In titanium-vanadium alloys the high temperature, body-centered cubic beta phase, when rapidly quenched, transforms martensitically into the close-packed hexagonal alpha phase. The temperature at which this transformation begins, Ms, becomes lower with increasing vanadium content, Fig. 1 (1,2). Since no diffusion takes place during the martensitic process, the transformation product retains the original composition of the alloy. As illustrated by the equilibrium diagram in Fig. 1, this would lead to alpha solutions supersaturated in vanadium.

The vanadium atom has a smaller volume than the titanium atom, so that the parameters of the alpha solution would be expected to decrease with higher vanadium content. X-ray diffraction results plotted in Fig. 2 illustrate that this is the case for equilibrium (0% V, 1% V, and 2.5% V) and supersaturated alpha solutions. The "most

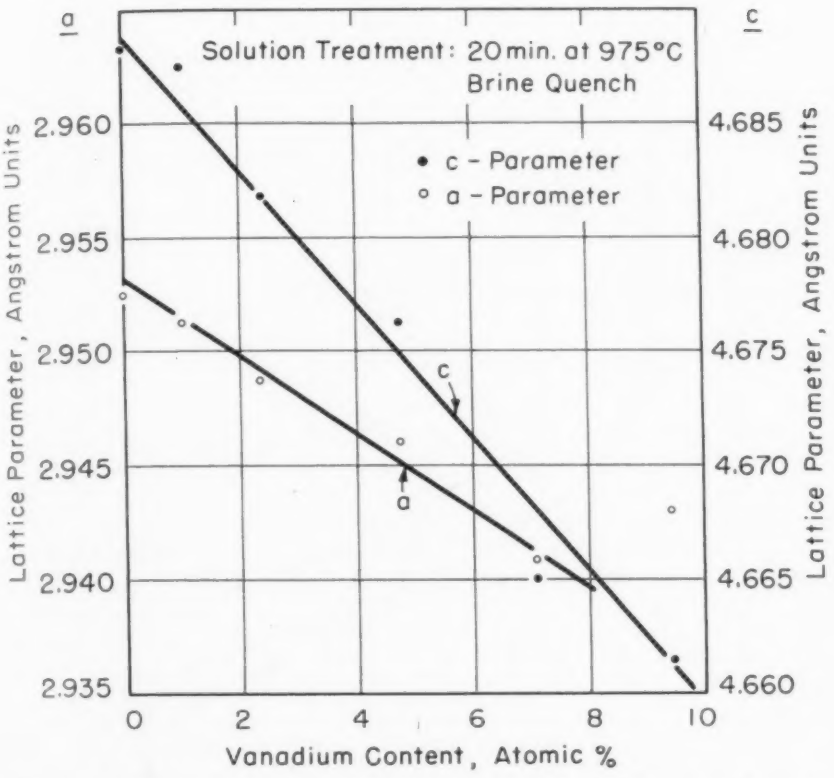


Fig. 2—Lattice Parameters of α' Titanium as a Function of Vanadium Content.

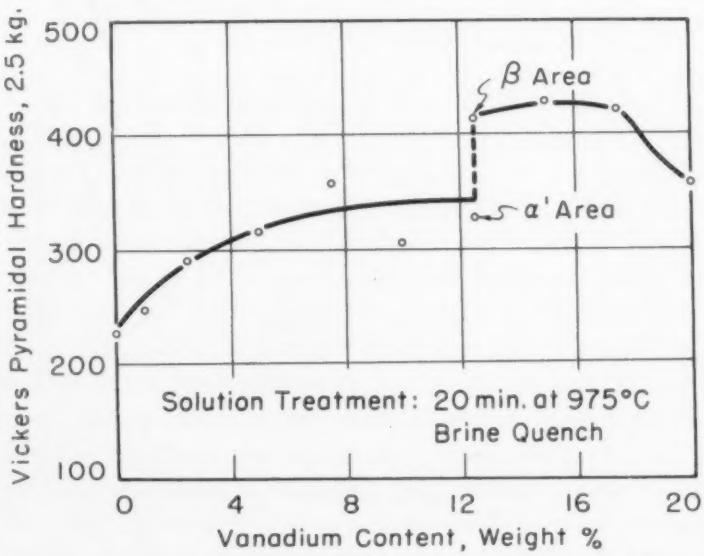


Fig. 3—Hardness of Quenched Titanium Alloys as a Function of Vanadium Content.

probable" lattice parameters given in Fig. 2 were determined by evaluation of broad diffraction lines, assuming a normal distribution of intensities. The results summarized in Fig. 2 reveal that Vegard's

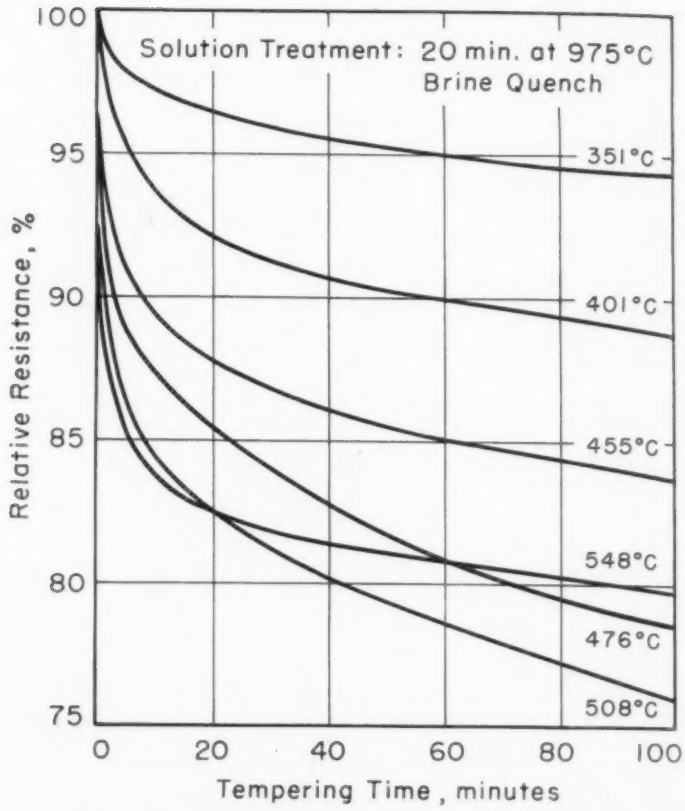


Fig. 4—Relative Electrical Resistance as a Function of Time at Various Tempering Temperatures for a Quenched 7.5% Vanadium-Titanium Alloy.

Law was followed quite closely by both the *c* and the *a* parameters of the close-packed hexagonal lattice. In the highest alloy tested, i.e., 10% vanadium by weight, the *a* parameter was larger than expected while the *c* parameter reached the value anticipated from Vegard's Law. Except for the 10% vanadium alloy, the c/a ratio was not affected by the alloy content.

The effect of composition on the hardness of rapidly quenched titanium-vanadium alloys is demonstrated in Fig. 3. The martensitically formed alpha prime is not associated with a particularly high hardness level, as is the case in iron-carbon alloys. A sudden increase in hardness was noticeable when large amounts of metastable beta were retained during quenching. The beta area referred to in Fig. 3 appeared to be untransformed beta, but X-ray diffraction revealed the presence of small amounts of the transition phase, omega, in the 12.5%, 15% and 17.5% vanadium alloys.

Kinetics of Alpha Prime Decomposition

The kinetics of the decomposition of alpha prime were investigated for a 7.5% vanadium-titanium alloy. This alloy when brine-

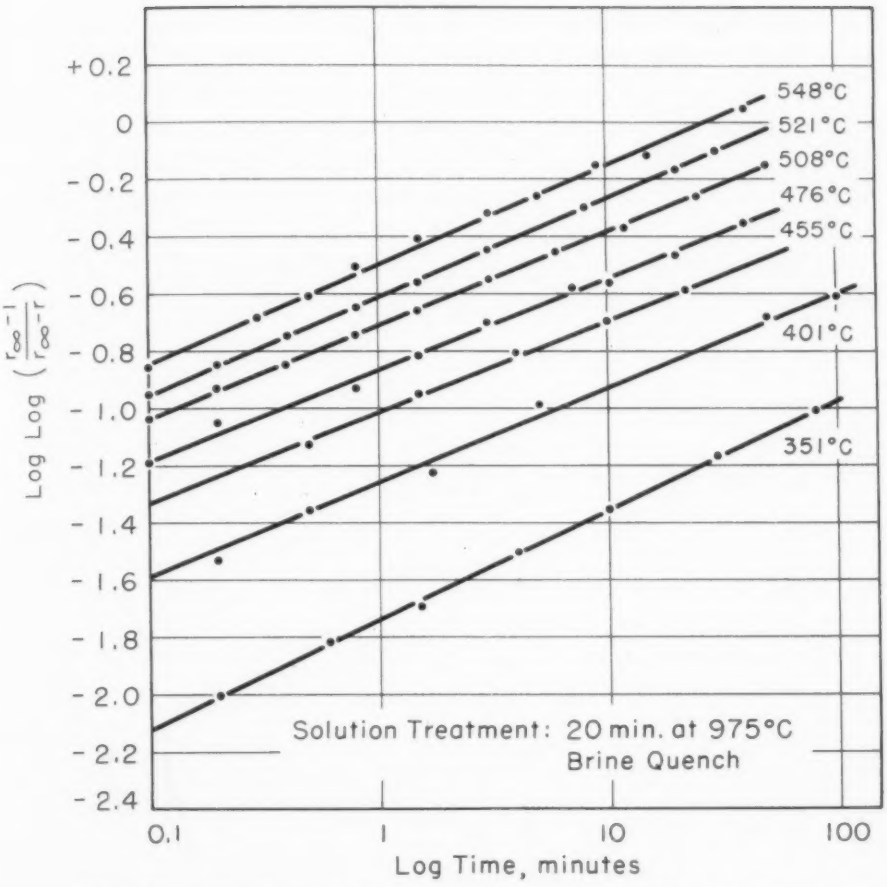


Fig. 5—Rate Equation at Various Tempering Temperatures for a Quenched 7.5% Vanadium-Titanium Alloy.

quenched from the beta phase region appeared to consist entirely of alpha prime. X-ray diffraction revealed no beta titanium lines.

Tempering of the 7.5% vanadium alloy in the temperature range from 660 to 1020°F produced a drop in electrical resistivity, Fig. 4. After sufficiently long holding times the resistivity curves leveled off, indicating that the tempering reaction had virtually come to an end. The resistivity at completion of the reaction decreased with lower tempering temperatures. Thus, longer tempering times than indicated in Fig. 4 eventually showed that at lower tempering temperatures the curves leveled off more slowly but reached a lower final value of resistivity. Because of the difficulty in evaluating final resistivity at lower temperatures, (660°F) was the minimum temperature investigated. X-ray parameter measurements disclosed that when the tempering reaction was completed the specimen consisted of high vanadium beta and alpha of composition lower than that of the original, untempered alpha prime phase. The compositions of the alpha and beta phases were in agreement with the

titanium-vanadium equilibrium diagram, Fig. 1, extrapolated to the tempering temperatures.

In order to follow the tempering reaction quantitatively, it was necessary to correlate resistance changes with the amounts of the phases present. For this purpose, it was assumed that the fraction of alpha prime transformed was proportional to the fractional change in resistivity.

Employing this assumption, the rate equation

$$\frac{df}{dt} = K(1-f)t^m, \qquad \text{Equation 1}$$

where f = fraction transformed
t = time
K = rate constant (temperature dependent)
m = constant

can be written in the form

$$\frac{dr}{dt} = K(r_\infty - r)t^m, \qquad \text{Equation 2}$$

where $r = \frac{\rho}{\rho_{\alpha'}}$ = relative resistivity
ρ = measured resistivity
$\rho_{\alpha'}$ = initial resistivity
r_∞ = relative resistivity after the tempering reaction was completed.

Integration of Equation 2 between the boundary values of

$r = 1$ at $t = 0$
$r = r$ at $t = t$

yields

$$\log \log \frac{(r_\infty - 1)}{(r_\infty - r)} = (m+1) \log t + \log \frac{K}{(m+1)2.3} \cdot \qquad \text{Equation 3}$$

A plot of $\log \log \left(\frac{r^\infty - 1}{r^\infty - r}\right)$ vs. $\log t$ at a given temperature then should yield a straight line with slope $m+1$. That this is the case at all temperatures studied is illustrated in Fig. 5.

The values of m and K for the various tempering temperatures are listed in Table I. The parameter m was independent of temperature while K, the rate constant, increased with temperature in the manner depicted in Fig. 6.

Table I
Values of m and K for Various Tempering Temperatures

t (°C)	m	K
351	−0.62	0.0159
401	−0.67	0.0417
455	−0.68	0.0720
476	−0.68	0.0995
508	−0.67	0.1445
521	−0.65	0.1980
548	−0.65	0.2545

Average m = −.66

The average value of m (−0.66), Table I, was close to that obtained by Roberts et al (−0.70) for the first stage of tempering of martensite in steel (5).

These authors interpret the constant *m* as being dependent only upon the geometry of the martensitic precipitate. This point of view is corroborated by the close-agreement of values of *m* in steel and titanium alloys, both of which possess acicular structures.

The variation of the rate constant, K, with temperature can be described by an Arrhenius-type plot, assuming that the activation

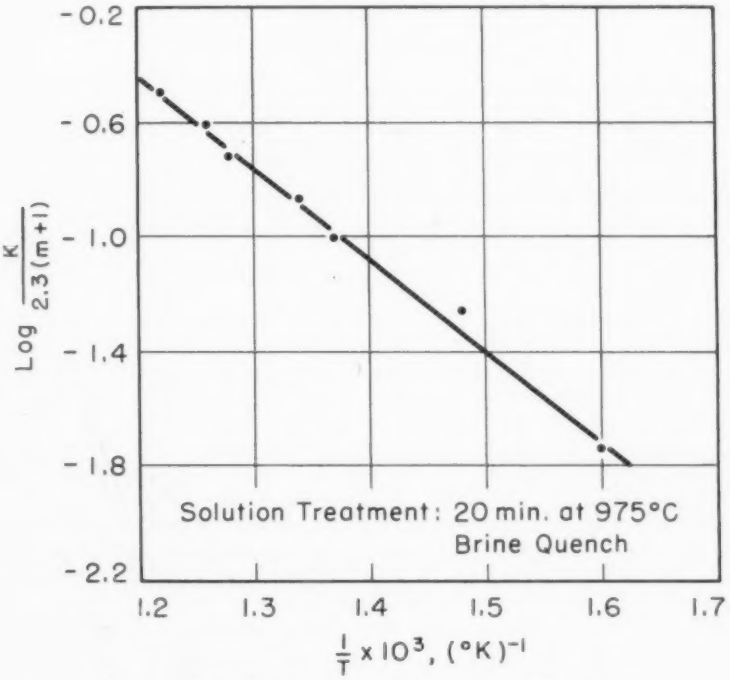


Fig. 6—Rate Constant, K, as a Function of Temperature for a Quenched 7.5% Vanadium-Titanium Alloy.

energy for the tempering reaction is independent of temperature. Thus, log K plotted against T^{-1} yields a linear relationship, Fig. 6. The activation energy obtained from the slope of this curve is approximately 15,000 cal/mol. for the tempering of alpha prime titanium.

Summary and Conclusions

Lattice parameter determinations disclosed that the *c* parameter of the hexagonal, supersaturated alpha lattice followed Vegard's Law for compositions up to 10% vanadium. The *a* parameter varied linearly with composition up to about 7.5% vanadium, but deviated noticeably for the 10% vanadium alloy.

The hardness was mildly increased by supersaturation.

The kinetics of α' decomposition were investigated for a 7.5% vanadium alloy by observing electrical resistance changes. By correlating the change in resistance with the amount of material transformed, it was established that the kinetics of α' decomposition in titanium were similar to those of the first stage of martensite tempering in steel.

The results further indicated that the precipitation of equilibrium beta from supersaturated alpha titanium is a diffusion controlled process with an activation energy for the tempering reaction of about 15,000 cal/mol.

Acknowledgments

This investigation was carried out under contract No. DA 33-019-ORD-941 with Army Ordnance Corps, Watertown Arsenal. The authors express their appreciation to the Ordnance Corps of the Army for permission to publish this research. The authors are also grateful for the cooperation of Watertown Arsenal Laboratory.

References

1. P. Duwez, "The Martensite Transformation Temperature in Titanium Binary Alloys," TRANSACTIONS, American Society for Metals, Vol. 45, 1953, p 934.
2. P. Pietrokowsky and P. Duwez, "Partial Titanium-Vanadium Phase Diagram," *Transactions*, American Institute of Mining and Metallurgical Engineers, Vol. 194, 1952, p. 627.
3. H. K. Adenstedt, J. R. Pequignot and J. M. Raymer, "The Titanium-Vanadium System," TRANSACTIONS, American Society for Metals, Vol. 44, 1952, p. 990.
4. L. G. Finch, "Correction to the Diameter Measurement of Diffuse X-Ray Diffraction Rings," *Nature*, Vol. 163, March 12, 1949, p. 402.
5. C. S. Roberts, B. L. Averbach and Morris Cohen, "The Mechanism and Kinetics of the First Stage of Tempering," TRANSACTIONS, American Society for Metals, Vol. 45, 1953, p. 576.

APPROXIMATE PHASE RELATIONSHIPS IN THE TITANIUM-VANADIUM-ALUMINUM SYSTEM AT 1800 AND AT 1400°F

By Charles B. Jordan and Pol Duwez

Abstract

Isothermal sections of the phase equilibrium diagram of the titanium-vanadium-aluminum system have been approximately determined at 1800 and at 1400°F, which temperatures lie respectively above and below the allotropic transformation point of titanium at 1620°F. No phases have been found other than those already encountered in the three binary systems, and no features of unusual interest have appeared among the phase relationships. Aluminum has been found to enter into solid solution in vanadium with an atomic size notably smaller than that to be expected on the basis of Goldschmidt's rules. (ASM-SLA Classification: M24, Ti, V, Al)

Introduction

THE recent active interest in the development of titanium has resulted in investigations of varying degrees of thoroughness, of a large number of binary titanium alloy systems, and of a somewhat smaller number of ternary titanium alloy systems (1).[1] Among the binary systems which have been worked out, that of titanium and aluminum is unique in that aluminum is the only metallic element which has been found to stabilize the alpha phase of titanium, that is, to raise the temperature of the alpha-beta transformation. The investigation of a ternary system composed of titanium, aluminum, and a third metal which is known to stabilize the beta phase of titanium therefore naturally suggests itself as a subject of research. Moreover, the titanium-aluminum system is one for which detailed results have been established by several groups of investigators (2,3,4). Accordingly, the titanium-vanadium-aluminum system was chosen for the present investigation, vanadium being selected as the third constituent since it is known to act as a beta-stabilizer for titanium (5), and because the complete titanium-vanadium system has been well established as being of a simple type (6,7). Isothermal sections at 1800 and at 1400°F were chosen because these temperatures lie about equally above and below the alpha-beta transformation temperature of pure titanium (1620°F).

[1]The figures appearing in parentheses pertain to the references appended to this paper.

Of the authors, Charles B. Jordan is research engineer and Pol Duwez is professor of Mechanical Engineering, California Institute of Technology, Pasadena, California. Manuscript received April 7, 1955.

Binary Systems

The titanium-aluminum system has been most completely determined by the work of Ogden, Maykuth, Finlay, and Jaffee (4) and by Bumps, Kessler, and Hansen (2). Although the phase diagrams proposed by these two groups are not in complete agreement, the phase boundaries at 1800 and at 1400°F, which are the only features relevant to the present investigation, are not greatly different. The locations of these phase boundaries are given in Table I. Since the differences reported are within the degree of accuracy

Table I
Location of Phase Boundaries in the Titanium-Aluminum System

Boundary	Location (wt % Al) Ref. 2	Ref. 4
At 1800°F:		
Beta/alpha-plus-beta	4.9	4.3
Alpha-plus-beta/alpha	6.2	5.6
Alpha/alpha-plus-gamma	25	26
Alpha-plus-gamma/gamma	35	33
Gamma/gamma-plus-delta	45	46
Delta	63	63
Liquid-plus-delta/liquid	*	90
At 1400°F:		
Alpha/alpha-plus-gamma	24	26
Alpha-plus-gamma/gamma	35	33
Gamma/gamma-plus-delta	44	46
Delta	63	63
Liquid-plus-delta/liquid	*	98

*The investigation of Ref. 2 did not extend beyond 70 wt % aluminum.

Table II
Location of Phase Boundaries in the Titanium-Vanadium System at 1400°F

Boundary	Location (wt % V) Ref. 6	Ref. 7	Ref. 8
Alpha/alpha-plus-beta	2.5	1.2	0.5
Alpha-plus-beta/beta	8.2	10.2	13

sought in the ternary investigation, the points used on the ternary diagram are a compromise between the reported points.

For the titanium-vanadium system, there are available the results of three groups of investigators (6,7,8). At 1800°F, the three results agree that titanium (beta phase) and vanadium form a continuous series of solid solutions. At 1400°F, the differences between the positions reported in Refs. 6 and 7 for the phase boundaries, as shown in Table II, are again not significant with respect to the degree of accuracy aimed at in the determination of the ternary system. The results of Powers and Wilhelm (8) diverge from those of Refs. 6 and 7, but since Powers and Wilhelm, unlike the other investigators cited, did not use iodide titanium in the preparation of their specimens, their results have not been taken into account.

The points used on the ternary are a compromise between those reported in Refs. 6 and 7.

No earlier investigation of the vanadium-aluminum binary was available. The existence and structure of the phase VAl_3 had, however, been reported (9), as had a determination of the solubility of vanadium in aluminum (10).

In the titanium-aluminum system, the phases found at 1800°F are (in the order in which they are encountered in going across the diagram from pure titanium to pure aluminum) beta, alpha, gamma, delta, and liquid. At 1400°F, the same system exists in the alpha, gamma, delta, and liquid phases. The titanium-vanadium system consists entirely of beta phase at 1800°F, and of alpha and beta phases at 1400°F. A description of these phases is given in the appendix of this report.

Experimental Procedure

The metals used throughout this investigation were iodide titanium from the New Jersey Zinc Company, 99.99% pure aluminum kindly furnished by the Aluminum Company of America, and vanadium bar from the Westinghouse Electric Corporation. The high purity of the vanadium is attested by the fact that bars initially about ¼ inch thick were consistently reduced to a thickness of about 0.010 inch by cold rolling, without any annealing.

Ternary alloys of about 100 different compositions were prepared by weighing out suitable amounts of the constituent metals on an analytical balance so as to make the total weight of each specimen 3 grams. Each alloy was first arc melted by the technique of Schramm, Gordon, and Kaufmann (11), then sectioned, rough polished, and inspected for homogeneity. If no macroscopic inhomogeneity could be observed, the specimen was accepted as satisfactory; otherwise it was remelted until satisfactory. Under the latter circumstances it was occasionally felt necessary to make up a new specimen, because of the possibility that the composition might have altered significantly as a result of the losses caused by sectioning and repeated melting.

When a sectioned as-melted specimen was accepted as having satisfactory homogeneity, both pieces were sealed in a silica tube which had been evacuated to a pressure not greater than 10^{-4} mm Hg, and heated at 1800°F for 1 week. Quenching from this heat treatment was then accomplished by dropping the sealed capsule into water and crushing it at once; the entire quenching operation required about 1 second. After removing any surface layer of oxide produced by quenching, one piece of the specimen was again sealed in an evacuated silica tube, heated for 2 weeks at 1400°F, and quenched as before. Powder for an X-ray diffraction pattern was

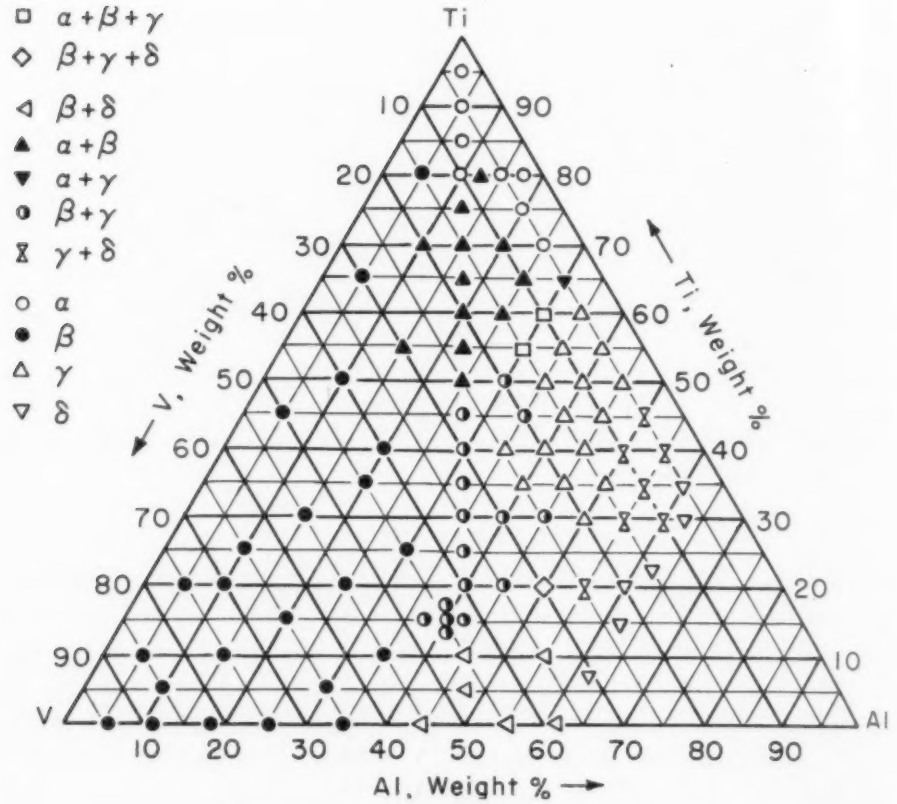


Fig. 1—Phases Found in Ti-V-Al System at 1800°F

obtained from each portion of each specimen by filing or crushing, according to the ductility, and passing through a 200-mesh screen. The screened powders were then sealed in thin-walled evacuated silica envelopes. The powder from that portion of the specimen which had been heated only 1 week at 1800°F was quenched after annealing for 1 minute at 1800°F, and the powder from the portion which had in addition been heated for 2 weeks at 1400°F was quenched after annealing 3 minutes at 1400°F. Annealing of the powders was carried out by suspending the sealed sample in a vertical furnace from which quenching was accomplished by dropping the sample beneath a simultaneously released brass weight, the weight serving to crush the silica tube on impact with a steel block in a vessel containing liquid argon. The powder enclosed in the silica tube was thus quenched very rapidly on contact with the liquid argon. Argon was used as the quenching medium because of its inertness; other possible media (such as water or liquid air) would have reacted with the hot titanium-alloy powder and caused serious contamination. The short annealing times were necessary because it was found that more prolonged heating caused serious evaporation from the powdered alloy.

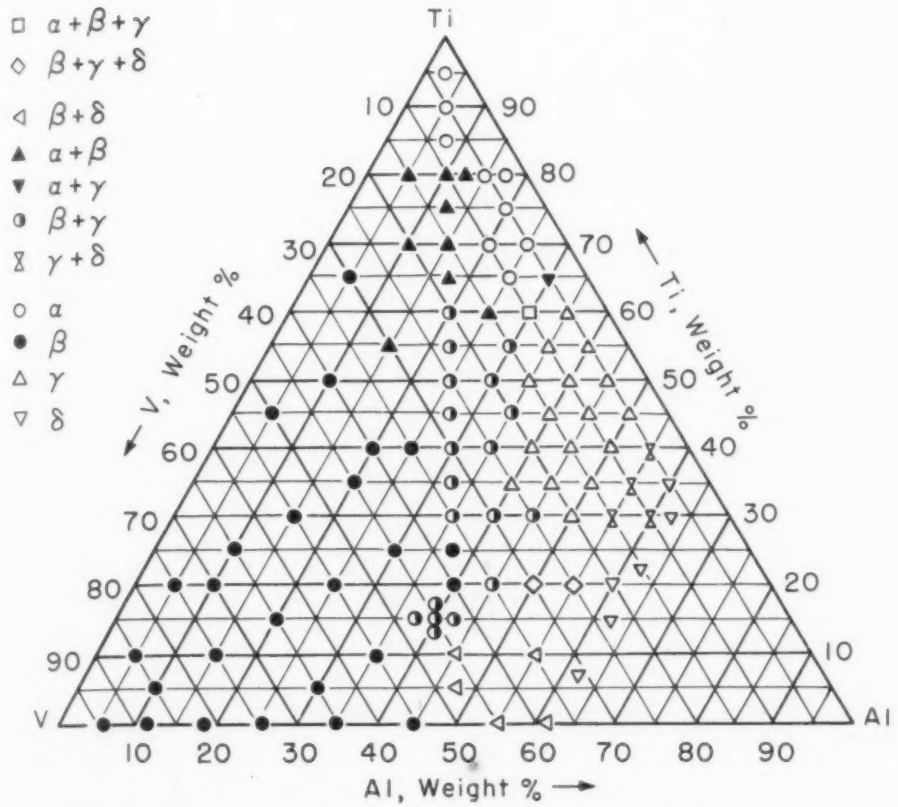


Fig. 2—Phases Found in Ti-V-Al System at 1400°F

X-ray diffraction patterns were made of all the powders thus prepared, using a powder camera of 14.32 cm diameter, copper radiation filtered through nickel foil, and a film arrangement of the Straumanis type. In addition, metallographic examinations of about 60 of the alloys were made after both the 1800 and the 1400°F heat treatment.

The nominal compositions of the alloys prepared are shown in Figs. 1 and 2. No further analysis of the specimens was made, either after arc melting or after powdering. Checks on a few samples indicated that the relative weight loss on melting was less than 1%.

Since both of the temperatures at which this investigation was carried out lie above the melting point of aluminum (1220°F), a liquid phase is encountered near the aluminum corner of the diagram. In order to avoid the presence of such a molten phase, the aluminum-rich portion of the diagram was omitted, the straight line from VAl_3 to $TiAl_3$ being taken as a convenient boundary.

Results

The phases found in the various alloys are shown in Figs. 1 and 2, and phase boundaries based on these results, the previously estab-

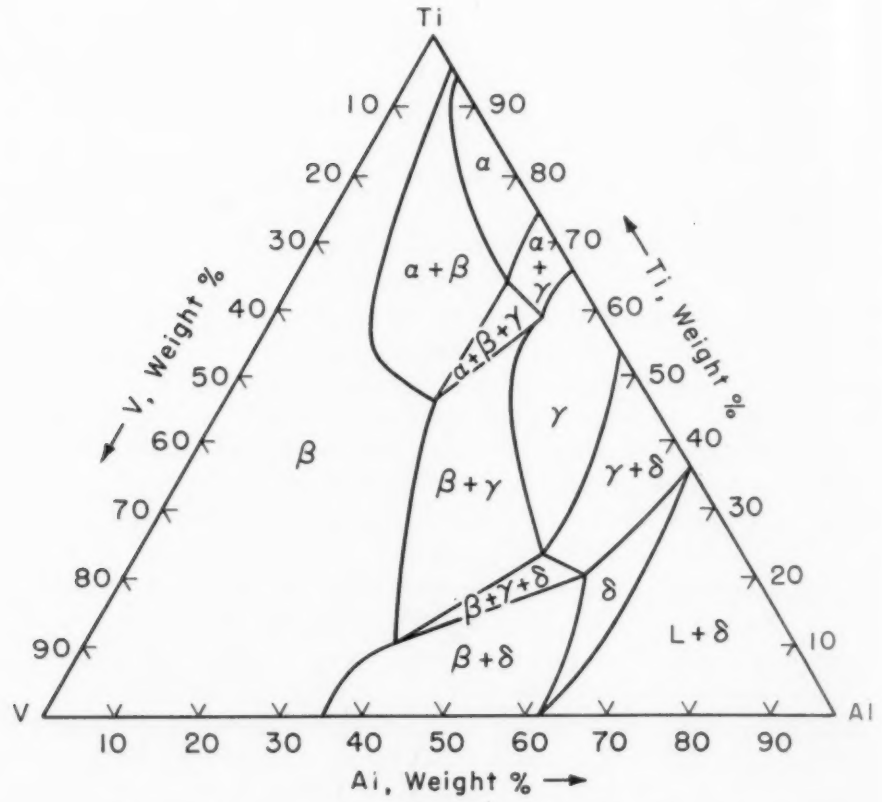


Fig. 3—Approximate Phase Boundaries in Ti-V-Al System at 1800°F

lished binary diagrams, and the requirements of thermodynamics (12) are shown in Figs. 3 and 4. Since a precise location of the various features of the phase equilibria was not the aim of this investigation, the resulting diagrams should not be considered as more than tentative in detail.

The general nature of the diagrams is found to be quite similar at 1800 and at 1400°F. In fact, the only difference, except for a shift in position of the phase boundaries, is that caused by the allotropic transformation of titanium: at 1800°F, the beta phase is contiguous to the entire titanium-vanadium boundary, whereas at 1400°F the titanium vertex must of course be contiguous to the alpha-phase region. Correspondingly, the alpha-plus-beta region is adjacent to the outside boundary of the diagram on the titanium-aluminum edge at 1800°F, and on the titanium-vanadium edge at 1400°F. Aside from this difference, the same one-phase, two-phase, and three-phase fields are found at both temperatures.

No intermediate phases are encountered in the ternary system other than those already known from the component binary systems. The compound $TiAl_3$ forms a continuous series of solid solutions with the compound VAl_3, and the phase thus formed is that desig-

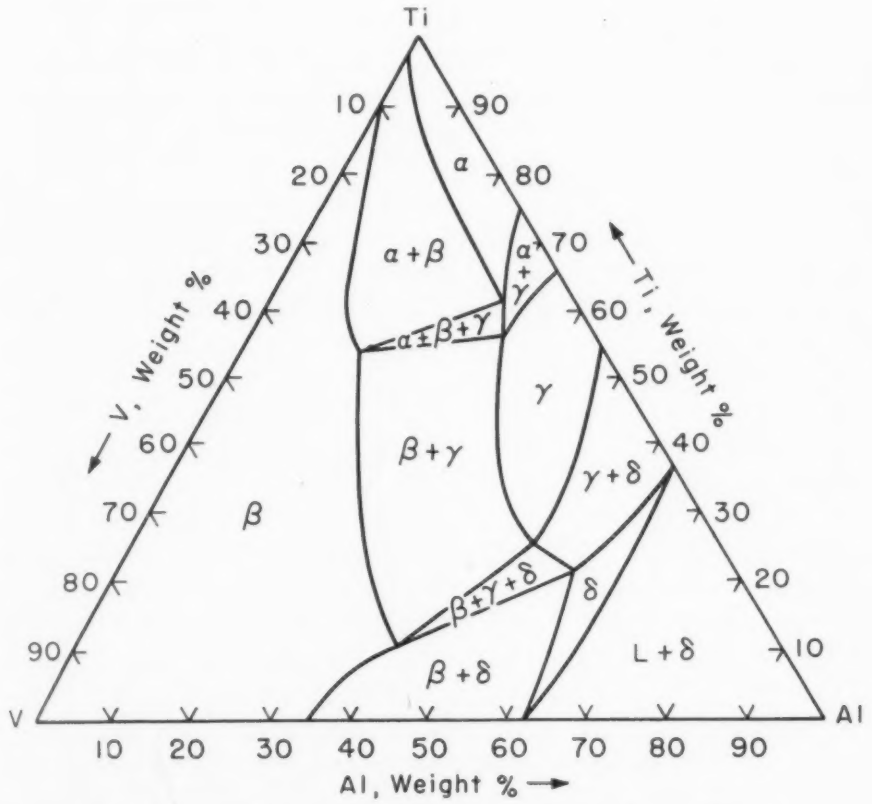


Fig. 4—Approximate Phase Boundaries in Ti-V-Al System at 1400°F

nated as the delta phase in the ternary system. (This series of solid solutions was the closest approach made to the aluminum corner of the diagram, as mentioned in the preceding section of this report.) The other single-phase regions of the ternary are simply extensions of the solid solutions found in the binary systems.

A feature of some interest is encountered in the vanadium-aluminum binary: aluminum enters into solid solution in vanadium with an atomic diameter much smaller than that with which it crystallizes as pure aluminum. According to Vegard's Law (13), it would be expected that the lattice parameters of solid solutions of aluminum in vanadium should, when plotted against atomic percentage of aluminum, lie on a straight line from the parameter of pure vanadium to the parameter which pure aluminum would have if crystallized in a body-centered cubic structure isomorphous with vanadium. In this investigation, however, it was found that although the lattice parameters of solutions of aluminum in vanadium lie on a straight line, this line does not extrapolate to the expected value at 100% aluminum, but rather to a markedly smaller value. The numerical results are given in Table III, together with similar results which have been reported by other investigators on the size of the

Table III
Size of the Aluminum Atom in Various Solid Solutions

Solute metal	Reference	Lattice parameter (Å) In A1 structure	Lattice parameter (Å) In A2 structure	Atomic Diameter (Å) In CN 12	Atomic Diameter (Å) In CN 8
Pure aluminum	18	4.049	3.207	2.863	2.777
Vanadium	this report	3.927	3.113	2.777	2.696
Iron	19	3.806	3.019	2.692	2.614
Chromium	20	3.915	3.104	2.769	2.688
Gold	21	3.938	3.119	2.784	2.700

Underlined values of parameters have been taken directly from experimental data; diameters in related CN were then calculated from these. Diameters in other CN were calculated by applying Goldschmidt 3% correction, and parameter in other structure type was calculated from latter diameter.

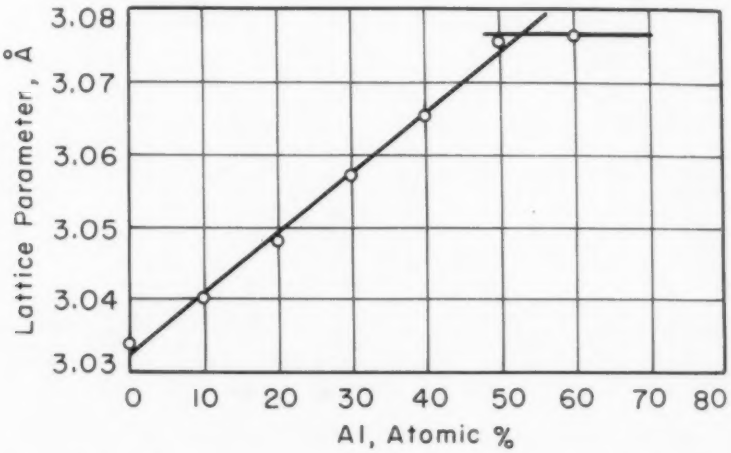


Fig. 5—Lattice Parameters of Solid Solutions of Aluminum in Vanadium

aluminum atom in solid solution with elements other than vanadium. Parameters taken from the reports of other workers have been extrapolated to 100% aluminum and converted from kx to Å units. For convenient comparison, diameters are tabulated both for CN (coordination number) 12 and for CN 8, one value having been computed from the extrapolated parameter, and the other value by applying the Goldschmidt (14) 3% contraction in going from CN 12 to CN 8. All reported values have been rounded to four significant figures. The parameters of the solutions of aluminum in vanadium were obtained by the extrapolation method of Nelson and Riley (15) applied to the X-ray patterns of the specimens which had been heat treated for 1 week at 1800°F subsequent to arc melting. A plot of these parameters vs. composition is shown in Fig. 5. (The 1800°F results were chosen because they exhibited better quantitative consistency than those measured directly after arc melting or after 2 weeks heat treatment at 1400°F; the qualitative results are, however, clearly similar in all three cases.) A discussion of the question of atomic diameters in crystals, with particular reference to aluminum, is given in Ref. 16.

Sources of Error

The approximate nature of the proposed phase diagrams is brought out by consideration of the possible errors introduced by the experimental procedure followed.

First, there is the error introduced by basing the results on nominal compositions, which amounts to assuming that composition changes caused by weight losses in arc melting are negligible, and that the compositions of the powders used for X-ray diffraction are essentially the same as those of the original specimens. Since the total weight loss on arc melting was found to be under 1% (as mentioned under "Experimental Procedure"), any change in composition due to this cause is probably negligible compared to the other sources of error. There are, however, several ways (which are in practise very difficult or impossible to control) in which significant variations of composition may be introduced in the preparation of the powder sample finally used for X-ray diffraction (17). Unfortunately, the only method of avoiding such errors is to make a precise chemical analysis of every powder sample. Such a procedure clearly involves a heavy expenditure of effort which was not felt to be justified for the type of exploratory investigation carried out in the present work.

Second, there is the possibility of quenching error; that is, that the quenching either was not sufficiently rapid to retain the high temperature state of the alloy, or that the quenched alloy underwent a change of structure at room temperature. Aside from the well-known transformation of beta phase to alpha phase in titanium-rich alloys, however, no evidence was found that such phase transitions had occurred in the present work. (The beta-to-alpha transformation is readily detected by metallographic examination.) Again, the only way of strictly eliminating such a possible error is one which involves considerable experimental difficulty, namely by taking the X-ray patterns in a high temperature camera.

Third, there are the inaccuracies arising from the fact that the X-ray patterns were often blurred to such an extent as to make their interpretation difficult. Thus, a phase actually present in an X-rayed sample may have escaped detection. In this connection, it must also be remembered that X-ray diffraction is inherently insensitive, and even in favorable circumstances (i.e. when sharp clear patterns are obtained) may fail to reveal minor constituents. Because of these possibilities, it is quite justifiable to include a few points on the ternary diagram in a two-phase field when only one phase was detected, or in a three-phase field when only two phases were detected, if such an inclusion is indicated in order to obtain consistency with the large majority of the data. It will be noted from a comparison of Figs. 1 and 2 with Figs. 3 and 4 that the phase boundaries have been drawn so as to attribute to several specimens a greater number of

phases than were actually detected, in accordance with the foregoing reasoning.

Finally, it can be seen from Figs. 1 and 2 that the distribution of the compositions investigated is such as to limit the accuracy with which the boundaries of the various regions of the diagram can be drawn. This spacing of the alloy compositions is of course again a reflection of the limitations set upon the degree of accuracy with which it was desired to carry out this investigation.

Appendix

Description of Phases Found in the Titanium-Vanadium-Aluminum System

1. The Alpha Phase

This phase is isomorphous with the low-temperature (below 1620°F) phase of titanium. It has the A3 or close-packed hexagonal structure with 2 atoms per unit cell, one at 000; the other at ⅔, ⅓, ½. For pure titanium, the lattice constants are a = 2.953 kx, c = 4.729 kx.

2. The Beta Phase

This phase is isomorphous with pure vanadium and with the high temperature (above 1620°F) form of titanium. It has the A2 or body-centered cubic structure with 2 atoms per unit cell, one at 000; the other at ½½½. For pure vanadium, the lattice constant is a = 3.034 kx; for pure beta-titanium, a = 3.32 kx at 1652°F.

3. The Gamma Phase

This phase exists over an extended range of composition in the titanium-aluminum system; in the titanium-vanadium-aluminum ternary, the binary gamma phase is able to dissolve a certain amount of vanadium, and thus to exist over an extended area of the ternary diagram. In the titanium-aluminum binary, the ideal composition of the gamma phase is TiAl, which has the tetragonal structure of ordered AuCu, with titanium atoms at 000 and ½½0, and aluminum atoms at 0½½ and ½0½ (3). At the ideal TiAl composition, the unit cell dimensions are a = 3.997 kx, c = 4.063 kx.

4. The Delta Phase

This phase is found in the vanadium-aluminum system at the composition VAl_3, and in the titanium-aluminum system at the composition $TiAl_3$. In both of these binary systems, the delta phase appears to have a sharply defined composition, in contrast with the variable composition found in the gamma phase. In the ternary investigation, VAl_3 and $TiAl_3$ were found, as expected, to form a continuous series of solid solutions.

The delta phase may be described (Ref. 9) on the basis of a body-centered tetragonal lattice with unit cell dimensions for $TiAl_3$ of a = 3.84 kx, c = 8.58 kx, and for VAl_3 of a = 3.77 kx, c = 8.31 kx. The titanium (or vanadium) atoms are at 000 and ½½½; the aluminum atoms are at 00½; ½½0; 0½¼; ½½, 0, ¾; ½0¼; and 0, ½, ¾.

ACKNOWLEDGMENT

This work was done at the Jet Propulsion Laboratory, California Institute of Technology, under contract number DA-04-495-ORD-18 with the Army Ordnance Corps, Washington, D. C. The authors wish to thank this agency for permission to publish the results of this investigation.

References

1. M. Hansen, D. J. McPherson and W. Rostoker, "Constitution of Titanium Alloy Systems," WADC Technical Report 53–41, Wright-Patterson Air Force Base, Ohio, February 1953.
2. E. S. Bumps, H. D. Kessler and M. Hansen, "Titanium-Aluminum System," *Transactions*, American Institute of Mining and Metallurgical Engineers, Vol. 194, 1952, p. 609.
3. P. Duwez and J. L. Taylor, "Crystal Structure of TiAl," *Transactions*, American Institute of Mining and Metallurgical Engineers, Vol. 194, 1952, p. 70.
4. H. R. Ogden, D. J. Maykuth, W. L. Finlay and R. I. Jaffee, "Constitution of Titanium-Aluminum Alloys," *Transactions*, American Institute of Mining and Metallurgical Engineers, Vol. 191, 1951, p. 1150.
5. C. M. Craighead, O. W. Simmons and L. W. Eastwood, "Titanium Binary Alloys," *Transactions*, American Institute of Mining and Metallurgical Engineers, Vol. 188, 1950, p. 485.
6. H. K. Adenstedt, J. R. Pequignot and J. M. Rayner, "The Titanium-Vanadium System," TRANSACTIONS, American Society for Metals, Vol. 44, 1952, p. 990.
7. P. Pietrokowsky and P. Duwez, "Partial Titanium-Vanadium Phase Diagram," *Transactions*, American Institute of Mining and Metallurgical Engineers, Vol. 194, 1952, p. 627.
8. R. M. Powers and H. A. Wilhelm, "The Titanium-Vanadium System," United States Atomic Energy Commission, ISC-228, Technical Information Service, Oak Ridge, Tennessee, September 1952.
9. G. Brauer, "Konstitution der Aluminum-Vanadin-Verbindung VAl_3," *Zeitschrift fur Elektrochemie*, Vol. 49, 1943, p. 208.
10. A. Roth, "Ein Beitrag zur Kenntnis des Systems Aluminum-Vanadium," *Zeitschrift fur Metallkunde*, Vol. 32, 1940, p. 356.
11. C. H. Schramm, P. Gordon and A. R. Kaufmann, "The Alloys Systems Uranium-Tungsten, Uranium-Tantalum and Tungsten-Tantalum," *Transactions*, American Institute of Mining and Metallurgical Engineers, Vol. 188, 1950, p. 195.
12. H. Lipson and A. J. C. Wilson, "Some Properties of Alloy Equilibrium Diagrams Derived from the Principle of Lowest Free Energy," *Journal*, Iron and Steel Institute, Vol. 142, 1940, p. 107P.
13. L. Vegard, "Die Konstitution der Mischkristalle und die Raumfullung der Atome," *Zeitschrift fur Physik*, Vol. 5, 1921, p. 17.
14. V. M. Goldschmidt, "Über Atomabstande in Metallen," *Zeitschrift fur Physikalische Chemie*, Vol. 133, 1928, p. 397.
15. J. B. Nelson and D. P. Riley, "An Experimental Investigation of Extrapolation Methods in the Derivation of Accurate Unit-Cell Dimensions of Crystals," *Proceedings*, Physical Society, Vol. 57, 1945, p. 160.

16. W. Hume-Rothery and G. V. Raynor, "The Apparent Sizes of Atoms in Metallic Crystals with Special Reference to Aluminum and Indium and the Electronic State of Magnesium," *Proceedings*, The Royal Society, Vol. A177, 1940, p. 27.
17. W. Hume-Rothery and G. V. Raynor, "The Application of X-Ray Methods to the Determination of Phase-Boundaries in Metallurgical Equilibrium Diagrams," *Journal*, Scientific Instruments, Vol. 18, 1941, p. 74.
18. A. J. C. Wilson (general editor), Structure Reports for 1947–1948, Vol. 11, p. 3; N. V. A. Oosthoek's Uitgevers Mij, Utrecht, 1951.
19. A. J. Bradley and A. H. Jay, "The Lattice Spacings of Iron-Aluminum Alloys," *Journal*, Iron and Steel Institute, Vol. 145, 1932, p. 339.
20. A. J. Bradley and S. S. Lu, "An X-Ray Study of the Chromium-Aluminum Equilibrium Diagram," *Journal*, Institute of Metals, Vol. 60, 1937, p. 319.
21. A. S. Coffinberry and R. Hultgren, "The Gold-Aluminum System," American Institute of Mining and Metallurgical Engineers, Technical Publication No. 885, 1938.

DISCUSSION

Written Discussion: By W. Rostoker, Armour Research Foundation of Illinois Institute of Technology, Chicago.

A paper appeared last year on the binary vanadium-aluminum system[2] in which it is stated that an intermediate phase occurs at 56% V having the structure of gamma brass. Since the present authors do not indicate such a phase field in Figs. 3 and 4, may we assume that they found no evidence for its existence?

Would the authors have sufficient lattice parameter data to indicate the directions of the tie-lines in the $(\alpha+\beta)$ phase fields at the two temperatures? This information would be of considerable value in interpreting heat treatment response of some of the newer titanium alloys.

Authors' Reply

The paper by O. N. Carlson, D. J. Kenney and H. A. Wilhelm mentioned by Dr. Rostoker appeared after our study of the ternary Ti-V-Al system was completed. Although we did not find a phase around 56% V in the Al-V system, we cannot claim that this phase does not exist, and additional work seems to be necessary to settle the question.

Concerning the question of the tie-lines in the alpha+beta field, we feel that the number of alloys prepared for this preliminary investigation was not large enough to obtain lattice parameter tie-lines with a sufficient degree of accuracy.

[2]O. N. Carlson, D. J. Kenney, and H. A. Wilhelm, "The Aluminum-Vanadium System," TRANSACTIONS, American Society for Metals, Vol. 47, 1955, p. 520.

ELEVATED TEMPERATURE STRENGTH OF SELECTED ZIRCONIUM-BASE ALLOYS

By R. J. Van Thyne and D. J. McPherson

Abstract

Zirconium-base alloys with high strength properties at 650 and 800°C (1200 and 1470°F) were investigated. Tensile data for the wrought, arc-melted alloys were obtained at room temperature, 650 and 800°C (1200 and 1470°F). At the elevated temperatures the test specimens were protected from air contamination by a helium atmosphere. Alloys containing aluminum and/or tin appeared superior. Preliminary Zr-Ta phase relationships, unknown at the initiation of this program, were investigated. Apparently the system is of the eutectoid type. (ASM-SLA Classification: Q23, Zr)

UNALLOYED zirconium is known to possess poor strength at elevated temperatures. An investigation was initiated[1] to develop zirconium-base alloys with improved strength properties at 650 and 800°C (1200 and 1470°F) and reasonable ductility at room temperature. Tensile testing was the only criterion employed for this initial survey.

A limited amount of work has been expended on the development of zirconium-base alloys for elevated temperature use. In the present investigation the alloy additions were generally the metallic elements which stabilize alpha-zirconium. Alloys of this type may be expected to possess optimum high temperature properties similar to titanium-base alloys. The compositions reported in this paper are in weight percent.

Experimental Procedure

Preparation of Alloys

High purity zirconium crystal bar (Grade I) was used in preparing the alloys. Commercial grade alloy additions were employed; nominal purity of the metals is shown in Table I. Zirconium-base "pancake" ingots weighing 250 grams were melted in a nonconsumable tungsten electrode arc furnace. The techniques were similar to those reported previously(1,2).[2] Melting conditions were non-con-

[1]This work was performed under the auspices of the Argonne National Laboratory and the Atomic Energy Commission.

[2]The figures appearing in parentheses pertain to the references appended to this paper.

Of the authors, R. J. Van Thyne is associate metallurgist and D. J. McPherson is supervisor of Nonferrous Metals Research, Armour Research Foundation of Illinois Institute of Technology, Chicago. Manuscript received April 13, 1955.

Table I
Alloying Additions

Metal	Form	Supplier	Nominal Purity (wt. %)
Zirconium	Crystal Bar	(Obtained from Argonne National Laboratory)	99.8 (Grade I)
Titanium	Sponge	E. I. DuPont de Nemours & Co.	99.7+ (124 BHN)
Aluminum	Sheet	Aluminum Co. of America	99+
Tin	Hemispherical Ingots	Vulcan Detinning Co.	99.99
Tantalum	Sheet	Fansteel Metallurgical Corp.	99.9
Chromium	Electrolytic Plate	Bureau of Mines	99.3

taminating as proved by the fact that no measurable hardness increase was obtained upon remelting control buttons of unalloyed metal. Each ingot was inverted without opening the furnace and remelted a number of times to insure homogeneity. The alloy charges and resultant ingots were weighed. Only small losses were observed, indicating that the actual compositions must follow the nominal compositions very closely. Chemical analyses were obtained for a few alloys containing aluminum and tin, since these appear to offer promise, and are presented in Table II. The analyses compare well with the nominal compositions.

Table II
Analysis of Selected Zirconium-Base Alloys

Nominal Composition		Chemical Analysis	
wt. % Al	wt. % Sn	wt. % Al	wt. % Sn
1.5	7	1.32	6.79
2	7	2.18	6.82, 6.75
1.5	10	1.39	—
2	10	2.25	9.79
0	10	—	9.81
3	0	2.96	—

Forging Practice

A drop forge was used for fabrication and the ingots were heated in a gas fired furnace; heating time was always held to a minimum. The zirconium-base "pancake" ingots were approximately $\frac{3}{8}$ inch thick by $2\frac{1}{2}$ inch in diameter. In forging, these ingots were extended in a direction parallel with the flat surfaces. Because of the poor geometry, the forging temperatures reported in Table III are probably higher than those which would be required to forge larger ingots of favorable geometry. The preheat temperatures varied from 1040 to 1400°C (1900 to 2550°F) which, for many alloys, represent temperatures appreciably above the $\beta/\alpha + \beta$ transus.

With the exception of Zr-Sn alloys, heavy scaling was encountered for the zirconium-base compositions. Early in the program it was found that finish forging in swaging dies formed deep seams in

Table III
Forging Conditions for Zirconium-Base Alloys

Alloy (wt. %)	Approximate Forging Temperatures (°F)	(°C)	Comparative Forging Scale
Zr	1950	1065	medium
Zr-2 Al	2100	1150	heavy
Zr-3 Al	2150	1175	very heavy
Zr-4 Al	2200	1205	very heavy
Zr-5 Al	2250	1230	very heavy
Zr-5 Ti	2100	1150	medium
Zr-10 Ti	2300	1260	medium
Zr-15 Ti	2300	1260	medium
Zr-25 Ti	2300	1260	heavy
Zr-45 Ti	2300	1260	heavy
Zr-5 Ta	2100	1150	medium
Zr-10 Ta	2250	1230	medium
Zr-15 Ta	2250	1230	heavy
Zr-20 Ta	2350	1290	heavy
Zr-3 Sn	1900	1040	light
Zr-7 Sn	2150	1175	light
Zr-10 Sn	2150	1175	light
Zr-1.5 Al-3 Sn	2150	1175	heavy
Zr-1.5 Al-7 Sn	2350	1260	heavy
Zr-1.5 Al-10 Sn	2300	1260	heavy
Zr-2 Al-3 Sn	2200	1205	heavy
Zr-2 Al-7 Sn	2300	1260	heavy
Zr-2 Al-10 Sn	2300	1260	heavy
Zr-2.5 Al-3 Sn	2250	1230	heavy
Zr-3 Al-3 Sn	2350	1290	heavy
Zr-5 Ti-3 Sn	2400	1315	very heavy
Zr-5 Ti-7 Sn	2350	1290	heavy
Zr-5 Ti-10 Sn	2400	1315	medium
Zr-5 Ti-15 Sn	2550	1400	medium
Zr-5 Ti-2 Al	2500	1370	very heavy
Zr-5 Ti-3 Al	2500	1370	very heavy
Zr-5 Ti-3 Sn-1 Al	2400	1315	very heavy
Zr-5 Ti-3 Cr	2400	1315	heavy
Zr-5 Ti-5 Ta	2400	1315	heavy
Zr-3 Sn-2 Mo	2250	1230	light
Zr-3 Sn-3 Cr	2300	1260	light
Zr-3 Sn-3 Ta	2200	1205	heavy

the surface. Therefore, the remainder of the alloys were forged only in open dies and better surface finish resulted. Finished rod size was ½ or 9/16 inch diameter. The forging characteristics of the ternary alloys could generally be anticipated from the binary data.

Testing Procedures

Standard tensile specimens with a gage section of 0.252 inch diameter and 1 inch length were machined from the forged rods. The only machining difficulties were encountered with the Zr-20% Ta alloy. Annealing treatments were performed in precision-controlled furnaces with the samples sealed in Vycor bulbs.

A Baldwin-Southwark tensile machine of 60,000-pound capacity was used. For both room and elevated temperature testing, a Baldwin-Lima-Hamilton elevated temperature, separable microformer extensometer was employed. A temperature-controlled Nichrome-wound furnace was used for the elevated temperature tests. Temperature measurements were made by means of thermocouples attached to the shoulders of the specimens. Testing was initiated when a constant temperature had been achieved. Test specimens

were protected from contamination by sealing the furnace surrounding the test bar and maintaining a positive pressure of helium. A limited amount of contamination occurred; however, microhardness data obtained on the cross section of a few tensile bars after testing indicated that contamination was slight and should not affect the results.

With the testing conditions employed, a strain rate of approximately 0.0035 in/in/min. through the elastic portion of the stress-strain curve resulted. Single samples were generally used so that the greatest number of compositions might be tested. However, the single test results appear to be reasonably accurate since consistent trends may be noted in the alloy systems.

Discussion of Results

Annealing Treatments

The zirconium-base alloys were tested after a simple heat treatment consisting of an anneal at the test temperature. Previous experience with titanium-base alloys has shown that, with a duplex annealing treatment, appreciable room temperature ductility may be obtained for certain alloys that are brittle with a simple anneal. Thus, in the present work an alloy that may at first be discarded because of poor room temperature ductility may actually be acceptable with a complex heat treatment. This project did not involve a study of the effects of heat treatment on the properties of zirconium-base alloys.

Tensile Data

Little information is available in the unclassified literature on the development of zirconium-base alloys for use at 650 to 800°C (1200 to 1470°F). Strength properties have been investigated at temperatures up to 500°C (930°F) in unpublished work (3). Data obtained at 980 to 1205°C (1800 to 2200°F) were presented in a recent contribution in which the alloy additions were beta-stabilizing (4). It is the premise of the present work that alpha alloys will possess the best high temperature properties for the same reasons that this is true with titanium-base alloys. Previous work with carbon-bearing zirconium-base alloys showed this to be true (5,6).

The first alloys studied were binary compositions chosen on the basis of phase relationships and previous work. The alloy systems selected were those with large solubility of the solute element in alpha zirconium. Although the phase relationships of the Zr-Ta system were not known, the alloys were investigated because of previous data and the possibility of extensive solubility in the alpha phase. Alloys were produced containing up to 5% aluminum, 45% titanium, 20% tantalum, and 10% tin. The phase diagrams for the

Table IV
Tensile Data at Room Temperature for Zirconium-Base Alloys
(Annealed at 650°C (1200°F) for 2 days and water quenched unless otherwise designated)

Alloy (wt. %)	Tensile Strength (psi)	Yield Strength (psi)	Modulus of Elasticity (psi x 10^{-6})	Elongation (%)	R.A. (%)
Zr	38,400	22,000	12*	42	58
Zr-2 Al	92,600	82,000	13	16	22
Zr-3 Al	112,000	99,000	14	10	26
Zr-4 Al	124,600	107,000	13	6	13
Zr-5 Al	128,800	114,000	16	2*	5*
Zr-5 Ti	52,200	33,000	9.5	42	
Zr-10 Ti	62,800	44,000	10.5	18	37
Zr-15 Ti	89,200	60,000	10.5	12	26
Zr-25 Ti+	122,400	104,000	12	6	10
Zr-45 Ti+	143,600	122,000	11	6	3
Zr-5 Ta	87,000	67,000	13	12	37
Zr-10 Ta	128,600	106,000	13.5	2	8
Zr-15 Ta	118,200	92,000*	13	2	4
Zr-3 Sn	55,400	40,000	11.5	32	53
Zr-7 Sn	76,000	65,000	13.5	24	12
Zr-10 Sn	95,000	75,000*	12	19	25
Zr-1.5 Al-3 Sn	91,000	72,000	11	20	31
Zr-1.5 Al-7 Sn		96,000			
Zr-2 Al-3 Sn	103,000	88,000	15	16	31
Zr-2 Al-7 Sn		>100,000			
Zr-2 Al-10 Sn	105,800	86,000	15	3	7
Zr-2.5 Al-3 Sn	110,400	92,000	13	14	30
Zr-3 Al-3 Sn	127,200	106,000	15	10	26
Zr-5 Ti-3 Sn	64,000	47,000	12	18	34
Zr-5 Ti-7 Sn	92,000	77,000	12	12	27
Zr-5 Ti-10 Sn	117,200	103,000	12	4	9
Zr-5 Ti-2 Al	100,400	81,000	9*	19	29
Zr-5 Ti-3 Al	123,000	108,000	13	4	9
Zr-5 Ti-3 Sn-1 Al	112,000	97,000	13	10	35
Zr-5 Ti-3 Cr	>93,000	84,000	14		
Zr-5 Ti-5 Ta	77,000	64,000	12	8	17
Zr-3 Sn-2 Mo	81,200	60,000	13	14	24
Zr-3 Sn-3 Cr	90,800	62,000	15	4	7
Zr-3 Sn-3 Ta	69,200			26	38

*Difficulties with the test but data considered valid.
+Annealed 500°C (930°F) for 3 days and water-quenched.

Zr-Al, Zr-Ti and Zr-Sn systems have been published (7,8,9). In the choice of alloys, an attempt was made to preserve about 10% room temperature tensile elongation. No emphasis was placed on oxidation resistance.

Upon completion of tensile testing of the binary alloys at room temperature, 650 and 800°C (1200 and 1470°F), the data were evaluated and promising ternary and quaternary alloys were prepared and tested. The alloys may not necessarily represent the optima but were "educated" selections made within the time limit of the research project. The tensile data are presented in Tables IV to VI. All alloys were given a simple annealing treatment. Although the properties are generally lower than for titanium-base alloys, the tensile results of the zirconium-base alloys are surprisingly good for such high temperatures.

It is evident from Table IV that to retain 10% tensile elongation at room temperature with the indicated annealing treatment, the maximum binary alloy addition is about 3% aluminum, 15% titanium, 5% tantalum, or an amount somewhat greater than 10%

Table V
Tensile Data at 650°C (1200°F) for Zirconium-Base Alloys
(Annealed at 650°C (1200°F) for 2 days and water-quenched)

Alloy (wt. %)	Tensile Strength (psi)	Yield Strength (psi)	Modulus of Elasticity (psi x 10^{-6})	Elongation (%)	R.A. (%)
Zr	5,800	4,700	4	60	98
Stainless Steel (Type 347)	51,200	41,000	22	46	71
Zr-2 Al	36,800	28,400	7	57	94
	35,800	30,000	7	58	93
Zr-3 Al	52,000	34,000	7	32	71
	51,600	34,000	8	49	79
Zr-4 Al	56,000	36,000	6.5	58	98
Zr-5 Al	52,400	31,000	6.5	72	99
Zr-5 Ti	24,200			60	96
Zr-5 Ti	19,700	17,400	4.5	90	95
Zr-10 Ti	26,800	16,600	5.5	44	97
Zr-15 Ti	18,400	16,000	3	78	99
Zr-15 Ti	17,100	13,600	2	170	99
Zr-25 Ti	4,400	4,000	4	>300	79
Zr-45 Ti	4,200	3,200	2.5	>300	92
Zr-5 Ta	24,800	22,400	6.5	34	99
Zr-10 Ta	30,600	27,200*		33	98
Zr-15 Ta	39,000	36,000	8	17	50
Zr-20 Ta	36,400	25,000	5.5	34	90
Zr-3 Sn	19,600	17,800	7.5	46	86
Zr-7 Sn	34,200	29,600	9.5	44	86
Zr-10 Sn	47,800	36,000	9.5	33	60
Zr-1.5 Al-3 Sn	50,000	39,000	9	58	99
Zr-1.5 Al-7 Sn	62,600	48,000	7	44	60
Zr-1.5 Al-10 Sn	48,000	36,000		35	61
Zr-2 Al-3 Sn	50,000	36,000		35	82
Zr-2 Al-7 Sn	68,000	50,000	8	19	10
Zr-2 Al-10 Sn	48,000	38,000	7	14	13
Zr-2.5 Al-3 Sn	59,200	38,000	8	28	65
Zr-3 Al-3 Sn	61,400	42,000	7	17	36
Zr-5 Ti-3 Sn	22,500	20,400	6	52	91
Zr-5 Ti-7 Sn	37,900	34,000	4.5	50	88
Zr-5 Ti-10 Sn	47,400	34,800	5	82	93
Zr-5 Ti-15 Sn	38,200	30,000	5	96	99
Zr-5 Ti-2 Al	40,000	38,000	6	65	90
Zr-5 Ti-3 Al	30,400	24,000	3.5	102	99
Zr-5 Ti-3 Sn-1 Al	37,700	36,400	6		99
Zr-5 Ti-3 Cr	30,800	20,000	1.5	46	97
Zr-5 Ti-5 Ta	23,600	20,000		64	99
Zr-3 Sn-2 Mo	27,600	22,000	7	30	99
Zr-3 Sn-3 Cr	32,000	24,000*	5		93
Zr-3 Sn-3 Ta	32,000	26,000	6.5	18	98

*Difficulties with the test but data considered valid.

tin. The tensile elongation values for the ternary alloys are essentially as anticipated from the binary information.

The properties at 650°C (1200°F), illustrated in Table V, may be compared to those for unalloyed zirconium and type 347 stainless steel, which are included in the table. For example, the Zr-3% Al-3% Sn alloy possesses tensile properties similar to type 347 stainless steel and is better than unalloyed zirconium by a factor of approximately ten. Because of the promising properties, duplicate tests were run on the binary 2 and 3% aluminum compositions and these check quite well.

At 650°C (1200°F) the alloys containing 25 and 45% titanium are weak because the structure is all beta at this temperature. However, at temperatures up to 500°C (930°F), the alloys would have an alpha structure and be appreciably stronger. For example, a tensile strength of 64,600 psi and a yield strength of 54,000 psi were

Table VI
Tensile Data at 800°C (1470°F) for Zirconium-Base Alloys
(Annealed at 800°C (1470°F) for 1 day and water-quenched)

Alloy (wt. %)	Tensile Strength (psi)	Yield Strength (psi)	Modulus of Elasticity (psi × 10^{-6})	Elongation (%)	R.A. (%)
Zr-2 Al	18,000			62	99
	15,800	13,200	5		99
Zr-3 Al	25,100	19,600	3	55*	91
Zr-5 Ti	3,900	2,800	3		98
Zr-10 Ti	3,400			>250	99
Zr-5 Ta	7,700	4,800	3.5	48	95
Zr-10 Ta	3,500	2,600	4*	>50	93
Zr-15 Ta	4,800	3,200	3.5*	77	99
Zr-3 Sn	7,600	6,400	4		97
Zr-7 Sn	18,000	15,800	4	70	83
Zr-10 Sn	27,700	24,000	4.5	74	94
Zr-1.5 Al-3 Sn	23,500	21,600	6	188	84
Zr-1.5 Al-7 Sn	24,200	19,200*	5.5	77	99
Zr-1.5 Al-10 Sn	24,400	20,600	5	>200	98
Zr-2 Al-3 Sn	19,500	16,400	5	108	99
Zr-2 Al-7 Sn	21,200	16,400	3.5	54	99
Zr-2 Al-10 Sn	17,100	16,400	3	92	99
Zr-5 Ti-3 Sn-1 Al	12,200	9,200	3.5		

*Difficulties with the test but data considered valid.

obtained at 500°C (930°F) for the Zr-25% Ti composition. Tensile elongations of 6% were obtained for the two Zr-Ti alloys at room temperature.

Additions of 5% titanium or 3% tin increased strength properties without greatly decreasing room temperature ductility values. For this reason these binary alloys were taken as a base for the preparation of ternary alloys containing molybdenum, chromium and tantalum. The quaternary, Zr-5% Ti-3% Sn-1% Al, alloy was also made. However, it can be seen from the tables that these compositions do not offer special promise. In general, zirconium-base alloys containing aluminum and/or tin appear to have maximum strength properties.

Data obtained at 800°C (1470°F) are presented in Table VI. The binary alloys containing titanium and tantalum are weak. At this temperature, the 5% titanium composition is apparently located in the beta field. Similar to the results at 650°C (1200°F), the zirconium-base alloys containing aluminum and/or tin appear best.

Zr-Ta Phase Relationships

Tantalum was chosen as one of the original binary additions to zirconium because the possibility of extensive solubility in the alpha phase existed. However, no phase diagram had been determined. Therefore, samples of forged bars (5,10,15,20% tantalum) were annealed at 600, 800 and 1000°C (1110, 1470, 1830°F) for 3, 2 and 1 days, respectively. The resulting metallographic data eliminate the possibility of extensive solubility of tantalum in alpha zirconium.

The tentative phase relationships obtained are as follows: the beta phase decomposes eutectoidally and the eutectoid point is

located between 800 and 865°C (1470 and 1590°F) and between 5 and 10% tantalum. Eutectoid decomposition was observed in samples annealed at 800°C (1470°F) for 2 days. The maximum solubility in the alpha phase is less than 5% tantalum. These phase relationships account for the low ductility values obtained for alloys containing more than 5% tantalum.

Summary

The tensile properties of zirconium-base alloys were investigated at room temperature, 650 and 800°C (1200 and 1470°F). Tensile testing was carried out under a helium atmosphere at the elevated temperatures. The first phase was the preparation and testing of binary alloys containing up to 5% aluminum, 45% titanium, 20% tantalum and 10% tin. The alloy additions were confined to those believed to be alpha stabilizers. All alloys were successfully forged, although rather heavy scaling was observed for all compositions except those containing tin. After results on the above alloys were obtained, ternary and quaternary compositions were designed. An attempt was made to retain approximately 10% room temperature tensile elongation.

The tensile data obtained are promising in that the strength of zirconium at 650°C (1200°F) was increased tenfold by alloying to a strength level similar to Type 347 stainless steel. Information is presented for a number of alloys. The optimum additions to zirconium for elevated temperature strength appear to be aluminum and/or tin. The data presented are based on a simple annealing treatment.

The phase diagram of the Zr-Ta system was unknown. As tantalum was one of the original binary additions, the phase relationships were surveyed. From the limited findings, the following tentative phase relationships were determined: the transformation temperature of zirconium is lowered by tantalum additions resulting in a eutectoid between 865 and 800°C (1590 and 1470°F) and between 5 and 10% tantalum. The poor ductility values observed for the Zr-Ta alloys may be explained by the above findings.

Acknowledgments

The authors are grateful to the Argonne National Laboratory, who sponsored this work under Subcontract 31-109-38-493, for permission to publish this paper. Mr. K. Smith of Argonne National Laboratory was contact engineer for this project. Special thanks are due to H. D. Kessler who contributed to the earlier part of the program.

References

1. M. Hansen, H. D. Kessler and D. J. McPherson, "The System Titanium-Silicon," Transactions, American Society for Metals, Vol. 44, 1952, p. 518.

2. M. Hansen, E. L. Kamen, H. D. Kessler and D. J. McPherson, "The Systems Titanium-Molybdenum and Titanium-Columbium," *Transactions*, American Institute of Mining and Metallurgical Engineers, Vol. 191, 1951, p. 881.
3. J. H. Keeler, "Development of Zirconium-Base Alloys," General Electric Research Laboratory Reports on Contract No. W-31-109-Eng-52 for the U.S. Atomic Energy Commission, 1952–1955.
4. H. A. Saller, J. T. Stacy and S. W. Porembka, "The Strength of Wrought Zirconium-Base Binary Alloys at 1800 to 2200°F," Preprint No. 37, TRANSACTIONS, American Society for Metals, Vol. 47, 1955.
5. S. M. Shelton, "Zirconium Alloys for High Temperature Service," AF-TR-5932, June, 1949.
6. C. T. Anderson, E. T. Hayes, A. H. Roberson and W. J. Kroll, "A Preliminary Survey of Zirconium Alloys," Bureau of Mines Report of Investigations No. 4658, March, 1950.
7. D. J. McPherson and M. Hansen, "The System Zirconium-Aluminum," TRANSACTIONS, American Society for Metals, Vol. 46, 1954, p. 354.
8. M. Hansen, D. J. McPherson and W. Rostoker, "Constitution of Titanium Alloy Systems," WADC-TR-53-41, February, 1953.
9. D. J. McPherson and M. Hansen, "The System Zirconium-Tin," TRANSACTIONS, American Society for Metals, Vol. 45, 1953, p. 915.

DISCUSSION

Written Discussion: By A. H. Roberson, chief, Branch of Process Metallurgy, United States Department of the Interior, Bureau of Mines, Albany, Oregon.

The authors are to be commended for an interesting and informative paper.

A question is raised regarding the advisability of heating the alloys in a gas fired furnace, apparently without protection, prior to forging.

The writer and his co-workers have shown[2,3] that when zirconium is heated above the $B/\alpha+B$ transus in air or several gases the surface attack becomes serious. This is especially true in the case of Zr+50 (atomic) or 35 (weight) Ti alloys. This alloy has been used as an efficient getter for oxygen, nitrogen, and water vapor at the Bureau of Mines laboratory in Albany, Oregon.

In contrast to air heating prior to forging, the authors were careful to minimize the exposure to air during tensile testing at lower temperatures, which seems rather inconsistent.

Tensile properties for Zr-Ti alloys annealed at 650°C (1200°F) and water-quenched[4] agree closely with those obtained by Bureau of Mines investigations when similar compositions were annealed at 950°C (1740°F) water-quenched and tested at room temperature.

Authors' Reply

As described in the discussion by A. H. Roberson, surface attack certainly does occur during forging in air. However, this contaminated surface was completely removed by machining, since the forged rod diameter was ½ or 9/16 inch and the tensile gage section was 0.252 inches in diameter. It would not seem inconsistent to protect the finished test specimen during testing since contamination would adversely affect the results.

[2] E. T. Hayes, and A. H. Roberson, "Some Effects of Heating Zirconium in Air, Oxygen and Nitrogen," *Journal*, Electrochemical Society, Vol. 96, September 1949, p. 142.
[3] E. T. Hayes, A. H. Roberson and R. H. Robertson, "Heat Resistance of Zirconium in Several Media," *Journal*, Electrochemical Society, Vol. 97, October 1950, p. 316.
[4] "Zirconium-Titanium System," *Constitution Diagram and Properties*, USBM Report of Investigations, 4826, November 1951.

PROGRESS IN THE DEVELOPMENT OF CREEP-RESISTANT ZIRCONIUM ALLOYS

By W. Chubb

Abstract

The development of creep-resistant zirconium alloys is described. The mechanical properties of binary alloys in selected alloy systems have been measured at room temperature, 260°C (500°F), and 500°C (930°F). On the basis of these results, ternary alloys in the zirconium-tin-aluminum, zirconium-tin-molybdenum, zirconium-tin-niobium, zirconium-aluminum-molybdenum, and zirconium-aluminum-niobium systems were prepared and tested. Alloys of the type zirconium-tin-molybdenum and zirconium-aluminum-niobium have been called "peritectoid-eutectoid hybrids." Alloys of this type are relatively easy to fabricate, exhibit good strength and ductility at room temperature, and show promise for the development of creep-resistant alloys at 500°C (930°F). (ASM-SLA Classification: Q3, Q general, Zr)

THE HISTORY of zirconium alloys dates from 1949 when the U. S. Bureau of Mines published the results of a survey of zirconium alloys (1).[1] Since that time, detailed information with respect to more than 25 zirconium binary constitutional diagrams has been published. The most important of these are the zirconium-aluminum (2), zirconium-chromium (3,4), zirconium-molybdenum (5), zirconium-niobium (6), zirconium-tin (7), zirconium-titanium (8), and zirconium-vanadium (9) systems. These constitutional diagrams are important in the sense that the higher strength alloys of zirconium are to be found in these systems, and that the useful, high-strength alloys of zirconium probably will contain one or more of these elements as alloying additions.

Since 1949, intensive efforts have been made to develop high-strength alloys of zirconium. Representative portions of the results have appeared in the literature (10,11,12,13). In general, the development of zirconium alloys has paralleled the development of titanium alloys; the similarities between titanium and zirconium-base alloys are more striking than the differences.

[1]The figures appearing in parentheses pertain to the references appended to this paper.

Work performed under AEC Contract W-7405-eng-92.

A paper presented before the Thirty-Seventh Annual Convention of the Society, held in Philadelphia, October 17–21, 1955. The author, W. Chubb, is associated with Battelle Memorial Institute, Columbus, Ohio. Manuscript received October 27, 1954.

Metallurgy of Zirconium Alloys

From room temperature to 865°C (1225°F), zirconium possesses a hexagonal close-packed crystal structure; from 865°C (1225°F) to the melting point, zirconium is body-centered cubic. Solid solutions based on the hexagonal structure are called "alpha zirconium"; solid solution based on the cubic structure are called "beta zirconium." Alloying elements which tend to raise the transformation temperature of zirconium are called "peritectoid-type" alloying elements. Aluminum and tin are representatives of this group. Alloying elements which tend to lower the transformation temperature of zirconium are called "eutectoid-type" alloying elements. Chromium, molybdenum, niobium, tantalum, titanium, and vanadium are representatives of this group. Titanium is completely soluble in both alpha and beta zirconium, and, hence, does not exhibit a eutectoid reaction. Titanium can be classed with the "eutectoid" group only because of its effect on the transformation temperature.

The transformation temperature of zirconium is to the mechanical properties of zirconium and its alloys much the same as the melting point of most metals is to their mechanical properties. For this reason, it is very important to distinguish between alloying elements which raise this temperature and those that lower it. The reason for this behavior may be found in the mechanical-property changes that occur at the transformation temperature. Fig. 1 shows a hot-hardness curve for pure zirconium. The loss in hardness at the transformation temperature is similar to the loss of hardness occurring in melting, even though the product in this case is a solid with a measurable hardness. It is possible to eliminate this drop in hardness at the transformation temperature by alloying to strengthen the beta phase, but this fact is of little practical use because no beta zirconium alloys are stable at room temperature, and the alloying elements that preferentially strengthen the beta phase precipitate from the alpha phase and tend to cause extreme brittleness at room temperature.

In designing alloys for creep resistance, it is generally observed that the metals with the higher melting points have the best creep strength. In zirconium, we have a case where the apparent melting point, the transformation temperature, can be controlled by alloying. On this basis, it might be expected that the "peritectoid-type" alloying elements are more effective than "eutectoid-type" alloying elements in improving the creep resistance of zirconium. Among binary alloys of zirconium, this is indeed found to be true.

A second general observation is that highly complex alloys tend to have better creep resistance than simple alloys. Unfortunately, the combination of aluminum and tin in a zirconium alloy results in such high hardness at elevated temperatures that alloys of this type

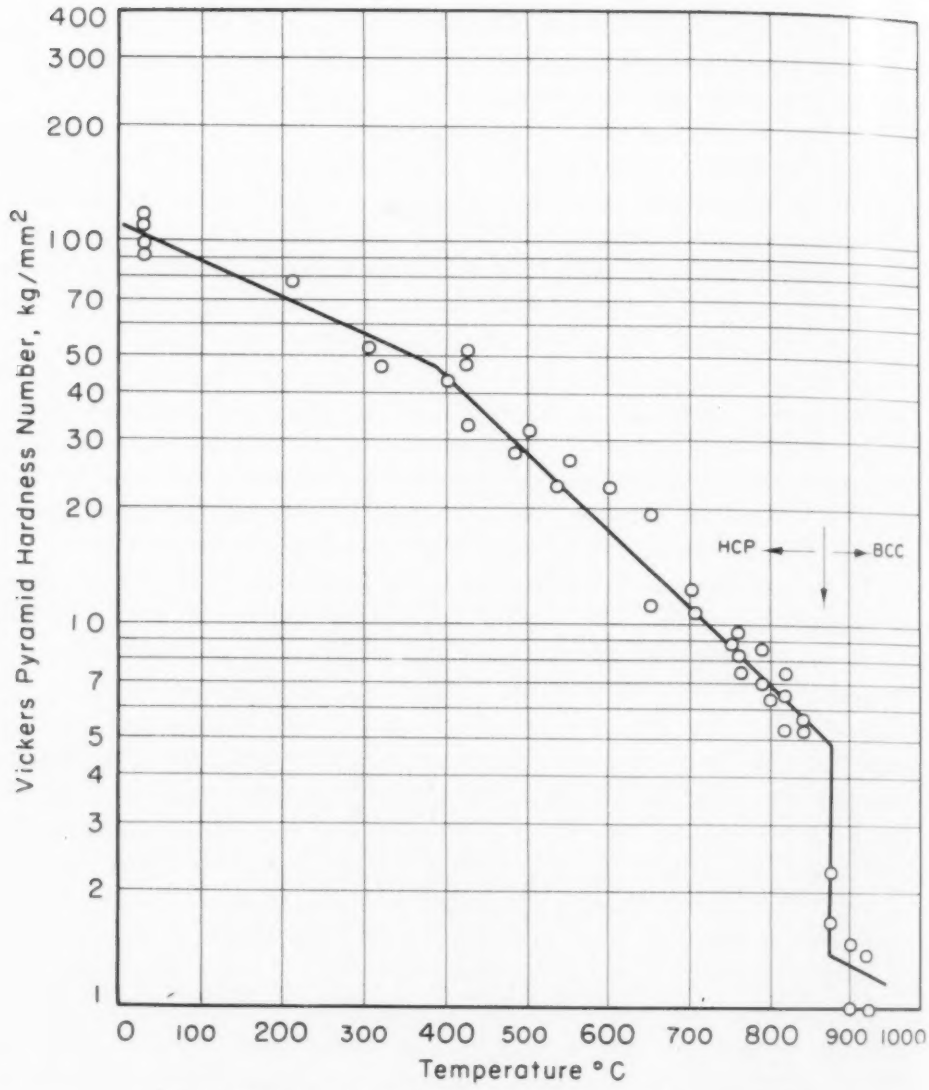


Fig. 1—Hardness of Iodide Zirconium at Elevated Temperatures.

developed up to the present time are quite unworkable at reasonable hot working temperatures. This circumstance has led to the development of the "peritectoid-eutectoid hybrid" zirconium alloys. In these alloys, the peritectoid-type alloying element is present to stabilize and strengthen the alpha-zirconium solid solution; the eutectoid-type alloying element is present primarily to lower the lower limit of the alpha-plus-beta phase region and hence reduce hardness at the hot rolling temperature. Secondarily, the eutectoid-type alloying element strengthens the alpha-zirconium solid solution, produces a precipitate in the microstructure, and makes the alloy heat treatable. The extremely wide range of properties to be found among the "peritectoid-eutectoid hybrid" alloys makes them the

most promising zirconium alloy family developed up to the present time.

Fabrication and Test Methods

Fabrication—The alloys described in this paper were prepared from Foote Mineral Company, Grade I, low hafnium iodide zirconium. Some of the alloys were compounded by induction melting in graphite; others were prepared by double arc melting in a water-cooled copper crucible using a tungsten electrode. The alloying elements used were commercial, high purity materials. In general, the induction-melted products were less ductile at room temperature than the arc-melted products.

The ingots weighing 200 to 2000 grams were hot-forged and rolled at temperatures between 800 and 1000°C (1470 and 1830°F). The hot-rolled sheet was cleaned by sandblasting and pickling. The pickle solution was 50% HNO_3 plus 2% NaF. The bright pickled sheet was cold-rolled as much as possible without cracking, or up to a limit of approximately 30%. The alloys were annealed for 3 hours at 730°C (1345°F) to reduce all alloys to the alpha-annealed condition. The annealed sheet was cut into tensile specimens with a reduced section approximately 2 ×0.5 ×0.06 inch.

Hot Hardness—Hardness data at elevated temperatures were obtained by means of hardness testing devices operating inside vacuum chambers. These machines are heated by commercial, resistance-type furnaces. Indentations are made by applying a dead-weight load of 500 to 1000 grams to a 136-degree pyramid indenter. By moving the specimen after each indentation, a large number of indentations can be made at any temperature or series of temperatures from room temperature to 1000°C (1830°F). This equipment has been described in greater detail elsewhere (14,15).

Tensile Tests—Duplicate tensile tests were made at 500°C (930°F) in argon or helium. Tests at room temperature and 260°C (500°F) were made in air. A clip-on extensometer with a 1-inch gage length was used to measure strain. This extensometer utilizes SR-4 gages on compression loops and is accurate to plus or minus 0.0001 in./in. Tests were run using a 20,000-pound Baldwin-Southwark universal testing machine. The speed of travel of the head of the testing machine was 0.02 in./min.

Creep Tests—Creep testing at 500°C (930°F) was performed in vacuum creep units. In a unit of this type, a constant load is applied to the specimen through a system of lever arms and a vacuum-tight bellows. Extensions are measured by means of platinum strips fastened to the specimen. The relative movement of these strips is measured with an optical comparator having a sensitivity of 50 microinches. Tests were designed to find the stress necessary to give

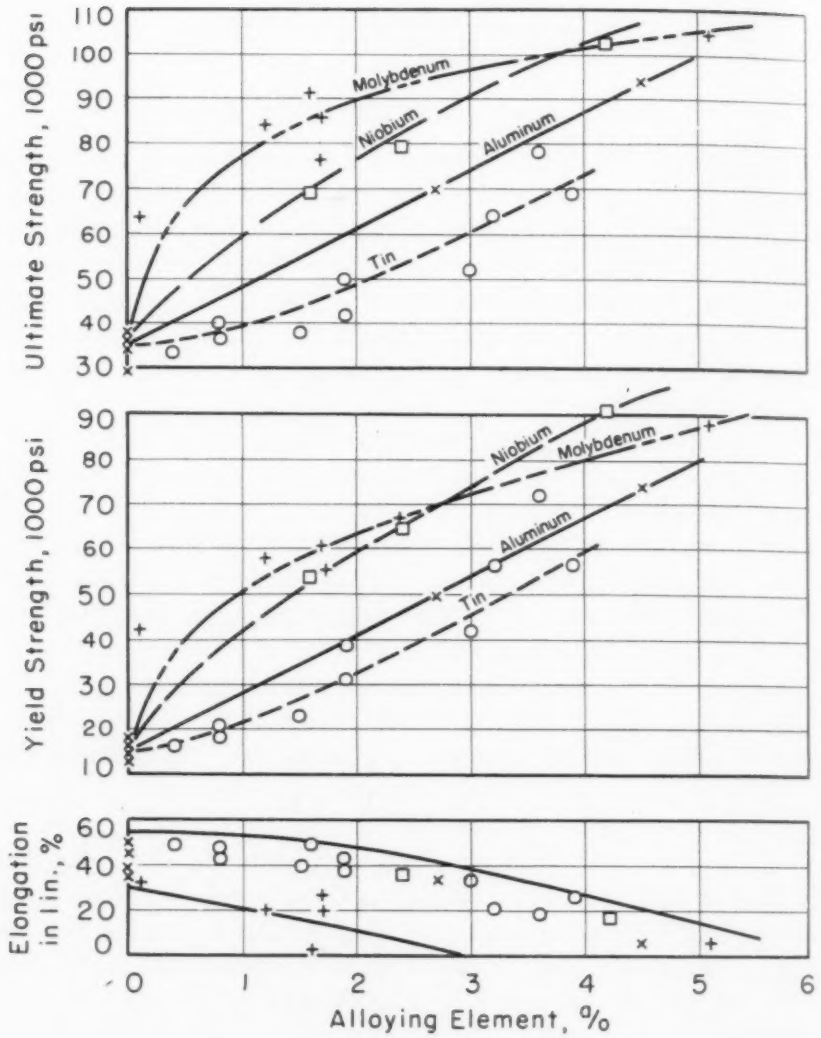


Fig. 2—Tensile Properties of Zirconium Alloys at Room Temperature.

a creep rate of 0.0001% per hour. Tests showing creep rates of this order of magnitude were continued for 1000 hours.

Tensile and Hardness Properties of Binary Alloys

To establish a sound basis for the development of creep-resistant zirconium alloys, it was first necessary to investigate a large number of binary alloys. As mentioned earlier, it was soon found that the alloying elements which produced the greatest strengthening effect in zirconium were aluminum, chromium, molybdenum, niobium, tin, titanium, and vanadium. The results of tests on binary zirconium alloys containing these elements are shown in Figs. 2,3,4,5, and 6. All compositions are given in atomic per cent.

These results show that at low temperatures molybdenum and niobium strengthen zirconium more rapidly than any of the other

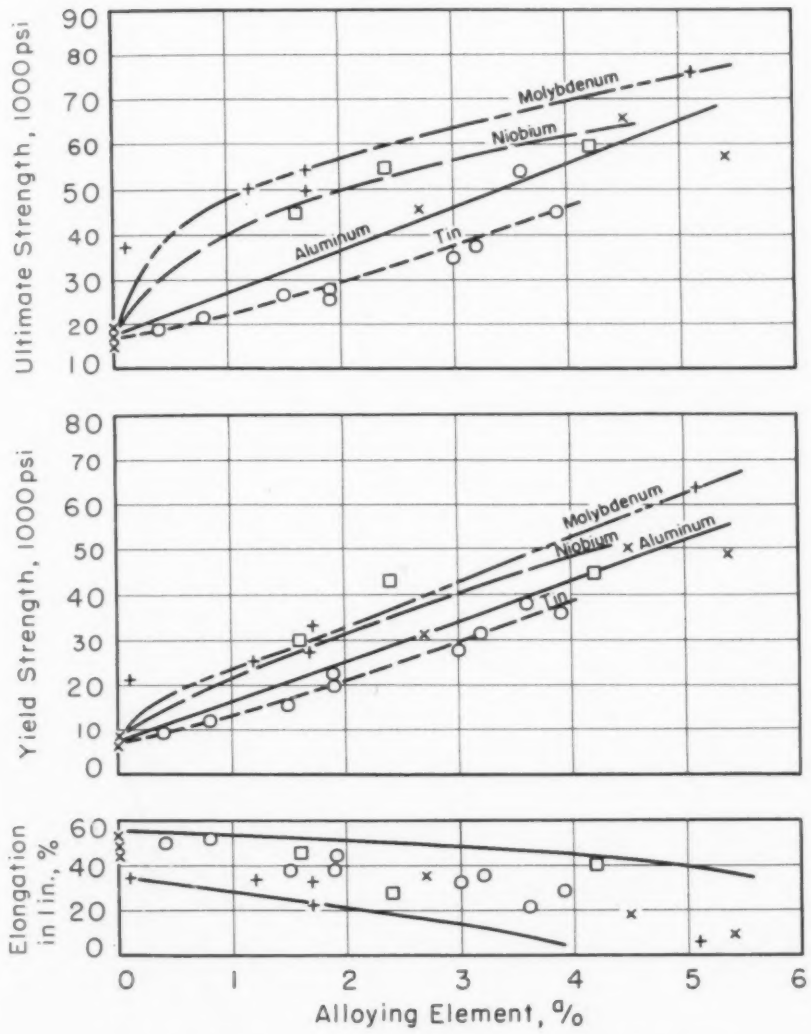


Fig. 3—Tensile Properties of Zirconium Alloys at 260°C (500°F).

elements examined. However, at 500°C (930°F) the strengthening effect of molybdenum and niobium is nearly the same as that of aluminum and tin. These data show that the rate of decrease of strength with increasing temperature is greater for zirconium-molybdenum and zirconium-niobium alloys than for zirconium-aluminum and zirconium-tin alloys. Carrying this relation a step further, it is possible to predict that at temperatures above 500°C (930°F), the strengthening effect of aluminum and tin is greater than the strengthening effect of molybdenum and niobium. That this is true is shown by hot-hardness data, Fig. 7.

These results confirm the concept that the transformation temperature of zirconium acts toward the tensile and hardness properties of zirconium as if it were the melting point. The eutectoid-type alloying elements lower the transformation temperature and

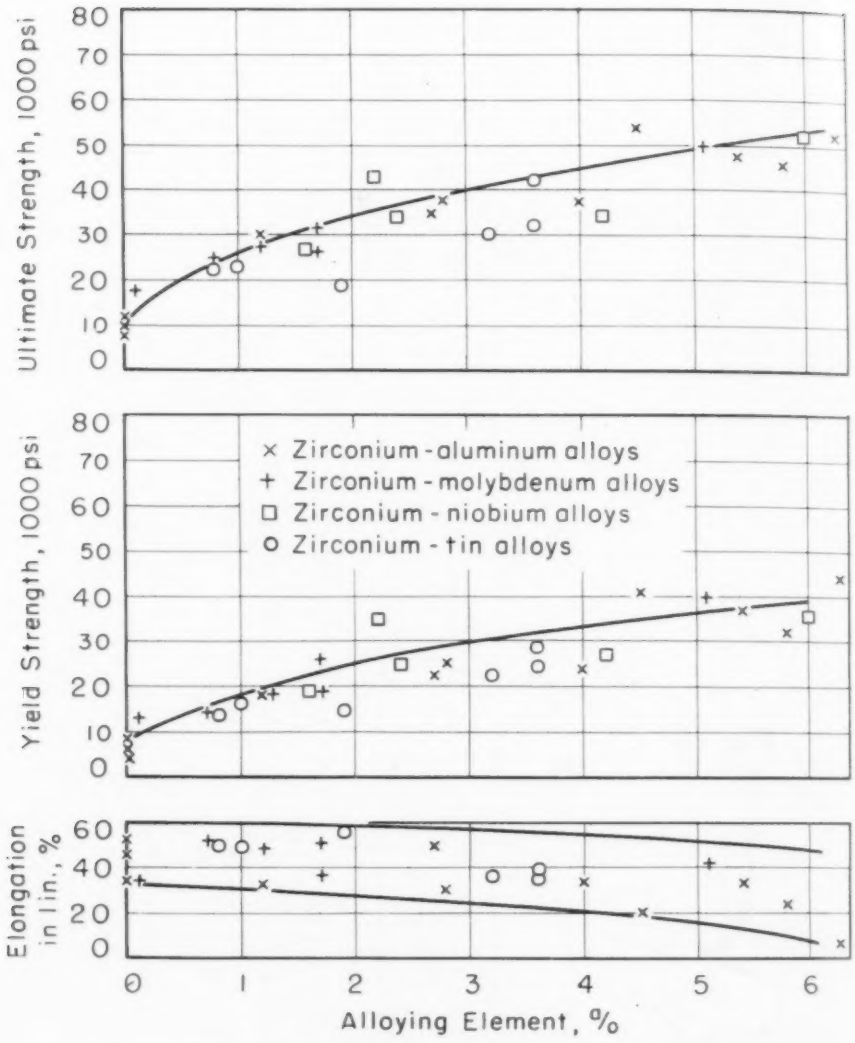


Fig. 4—Tensile Properties of Zirconium Alloys at 500°C (930°F).

result in alloys that tend to soften more rapidly with increasing temperature than alloys formed from peritectoid-type alloying elements.

Figs. 1 and 7 illustrate a related concept of importance to the development of creep-resistant zirconium alloys. In these plots, it will be noted that the portions of each curve between 25 and 400°C (77 and 750°F) and between 600 and 800°C (1110 and 1470°F) conform closely to a straight line. A short transition zone connects these two straight-line portions. The point of intersection of the two straight lines will be known as the "softening temperature" and will be understood to refer to the entire transition zone. A similar transition zone is found in semilogarithmic plots of tensile data versus temperature. This transition zone is variously known as the "equi-

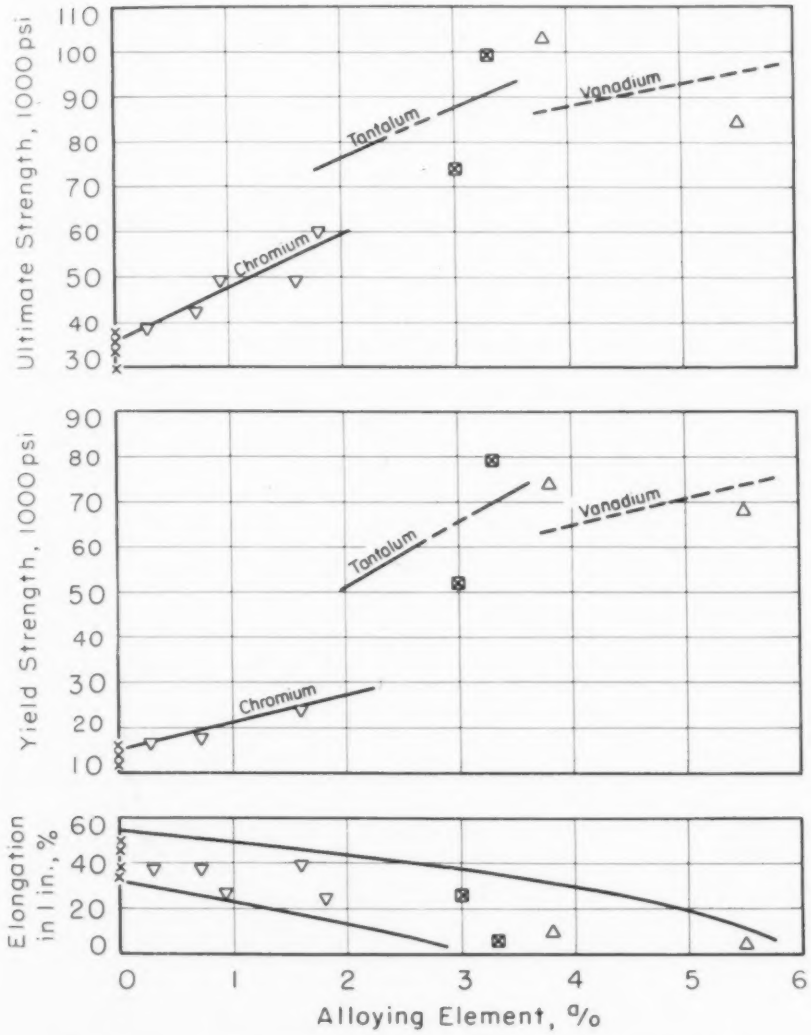


Fig. 5—Tensile Properties of Zirconium Alloys at Room Temperature.

cohesive temperature," the "grain-boundary relaxation temperature," the "lowest recrystallization temperature," and the "upper temperature limit for strain hardening in creep." However, these temperatures are definitely not the same, since they depend upon the condition of strain and the strain rate involved in the determination of each. However, these temperatures are related to one another in that they are manifestations of the same phenomenon, namely the onset of increased atomic mobility such that dislocations and dislocation atmospheres may diffuse to new sites within the time allowed by the particular test (16). Thus, the "softening temperature" is the temperature below which cold working takes place and above which hot working occurs. Since secondary creep rates are believed to represent a balance between cold working and

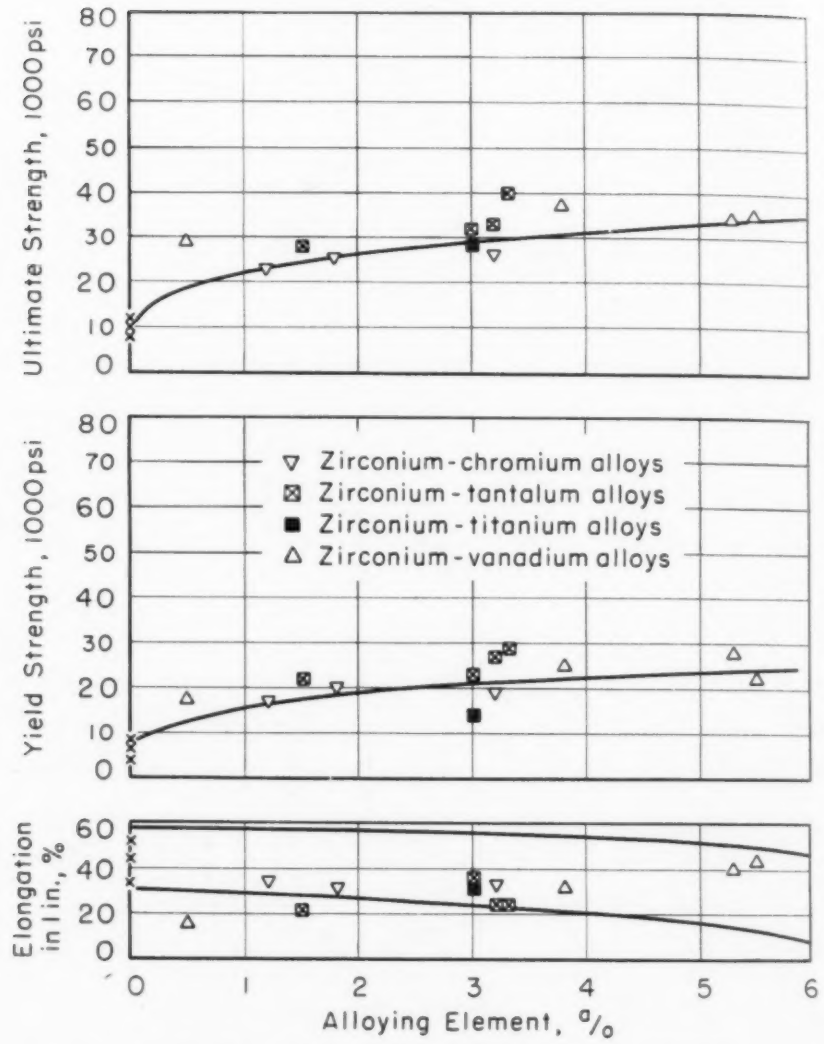


Fig. 6—Tensile Properties of Zirconium Alloys at 500°C (930°F).

stress relief by diffusion, it follows that for temperatures within the transition zone, those elements that raise the "softening temperature" most will reduce secondary creep rates most. As might be expected, all elements raise the softening temperature of zirconium, but Fig. 7 shows that the peritectoid-type alloying elements, aluminum and tin, raise it most. These data are the basis for postulating that the best creep-resistant alloys of zirconium for use in the temperature range 400 to 700°C (750 to 1290°F) will be based on the zirconium-aluminum and zirconium-tin systems.

Creep Properties of Binary Alloys

A standard for comparison purposes was established by running creep tests on arc-melted iodide zirconium and on arc-melted sponge

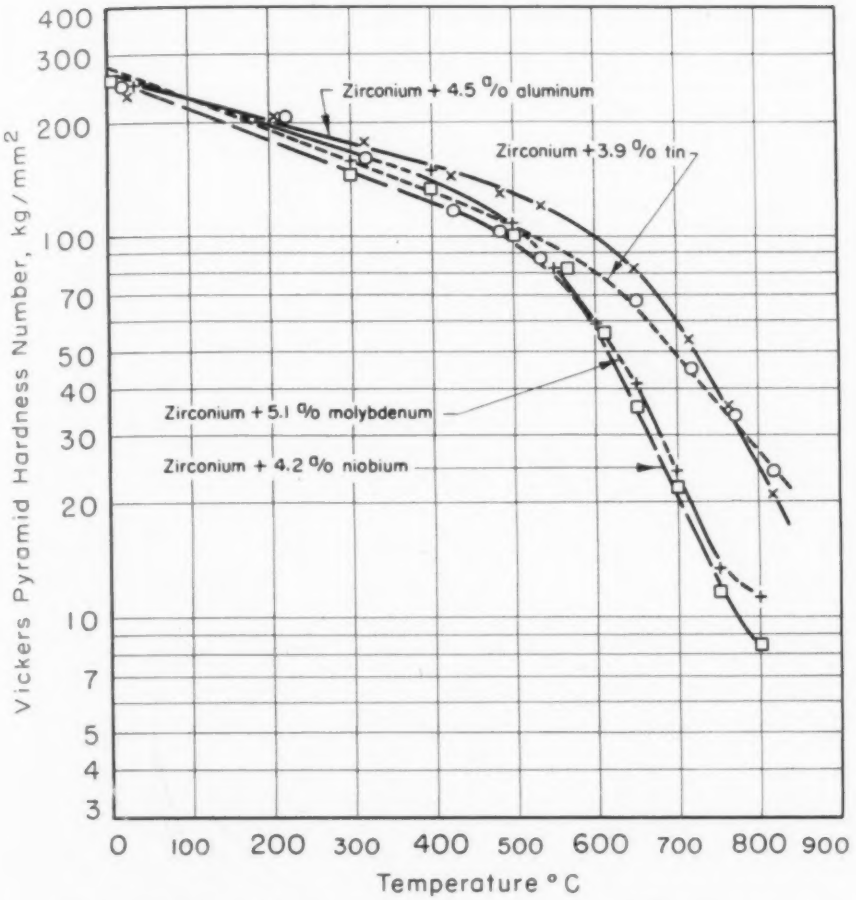


Fig. 7—Hardness of Binary Zirconium Alloys at Elevated Temperatures.

zirconium. Sponge zirconium is the product of the magnesium reduction process of the U. S. Bureau of Mines, and is essentially a zirconium-oxygen alloy. This standard was the only alloy prepared from sponge zirconium. The results of creep tests at 500°C (930°F) on binary zirconium alloys are shown in Figs. 8 and 9. The data points for 10,000 hours are based on creep-rate data for tests of only 1000-hour duration; and, hence, are not as reliable as the data for 100 and 1000 hours. The alloys are compared on the basis of the stress and time necessary to cause 1% total deformation.

Fig. 8 shows that increasing amounts of aluminum are beneficial to the creep resistance of zirconium, and that while small amounts of molybdenum have a beneficial effect on the creep resistance of zirconium at 500°C (930°F), further additions of molybdenum may actually decrease this benefit. Fig. 9 shows that the peritectoid-type alloying element, tin, is more beneficial to the creep resistance of zirconium than the eutectoid-type alloying elements, niobium, tantalum, titanium, and vanadium.

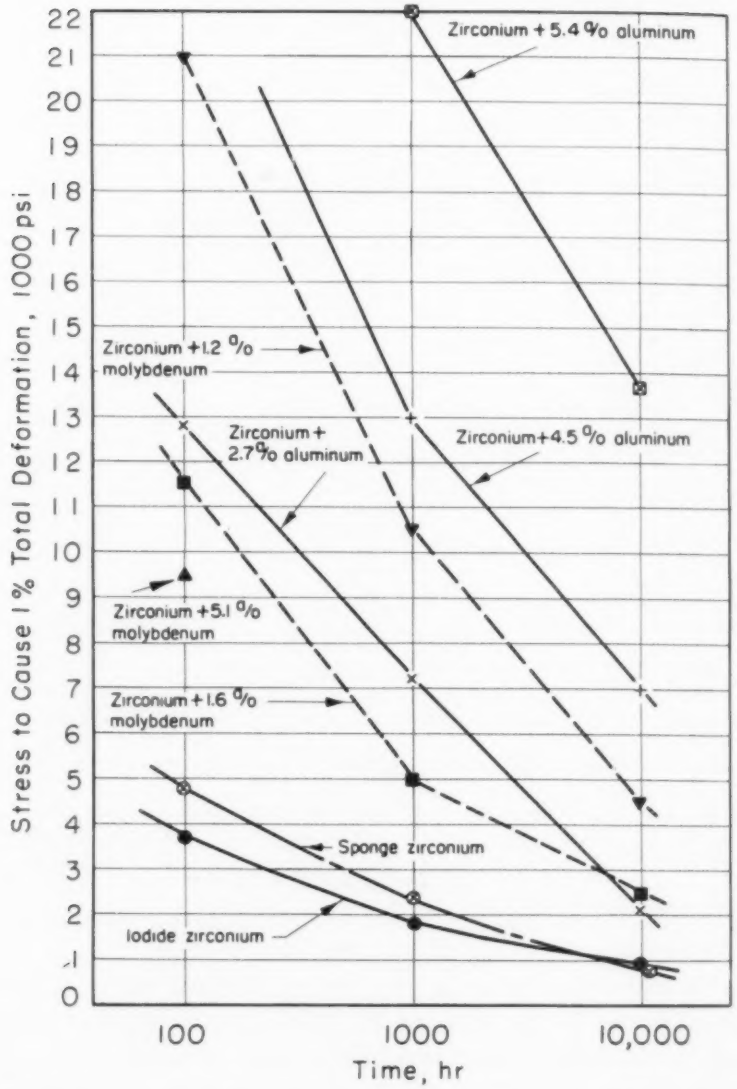


Fig. 8—Stress Versus Time for 1% Total Deformation at 500°C (930°F).

Tensile and Hardness Properties of Ternary Alloys

Long before the metallurgy of binary zirconium alloys was clearly understood, ternary alloys of zirconium were being prepared. These alloys were prepared on the theory that complex alloys tend to have better creep resistance than simple alloys. Of the first eleven ternary alloys prepared, only four were successfully fabricated to sheet tensile specimens. One of these four was an alloy containing 2.1 atomic % tin plus 1.7 atomic % aluminum, and it has since been determined that this composition is near the limit of fabricability of this system. As a rule of thumb, it has been found that alloys with a hardness in excess of 30 DPH at the hot-rolling temperature are difficult to roll without cracking; alloys with lower hardness may

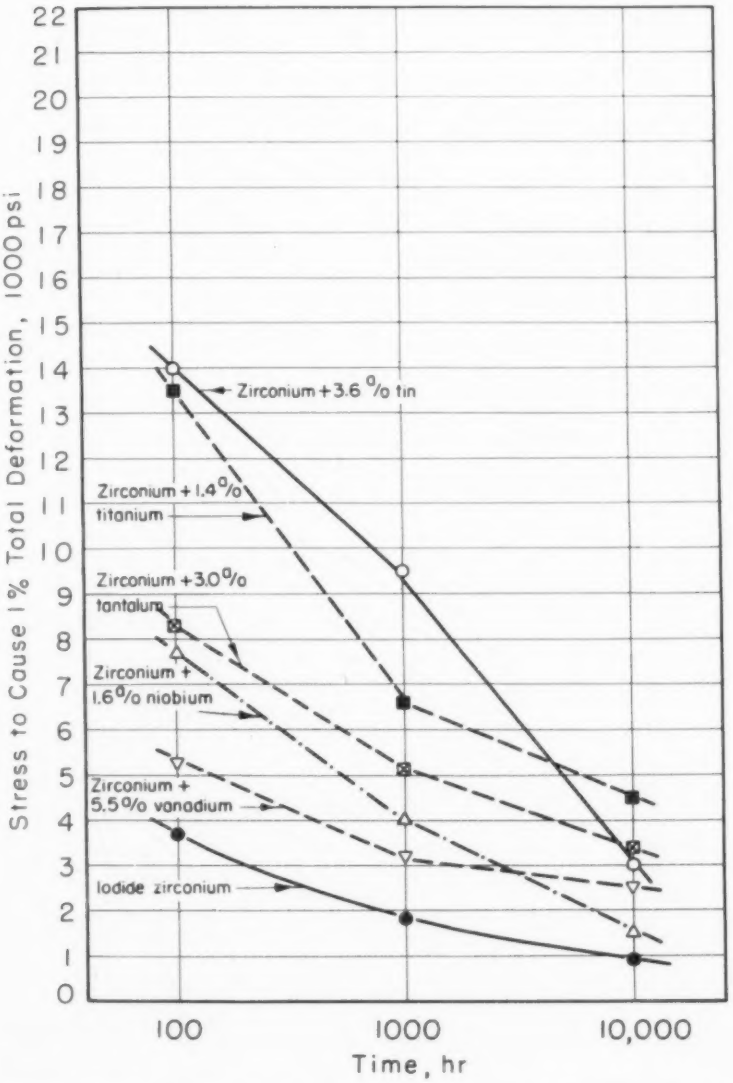


Fig. 9—Stress Versus Time for 1% Total Deformation at 500°C (930°F).

crack for other reasons such as casting defects or the presence of a weak second phase.

Since one of the possible applications of zirconium alloys is in nuclear devices where they compete with the stainless steels as structural materials, it is important that the thermal-neutron absorption cross section of zirconium alloys be kept as low as possible. Since chromium, tantalum, titanium, and vanadium have relatively high absorption cross sections as compared to aluminum, molybdenum, niobium, and tin, major emphasis in the development of ternary zirconium alloys has been upon alloys containing the latter elements.

As mentioned earlier, it soon became apparent that fabricability would be the limiting factor in the development of creep-resistant

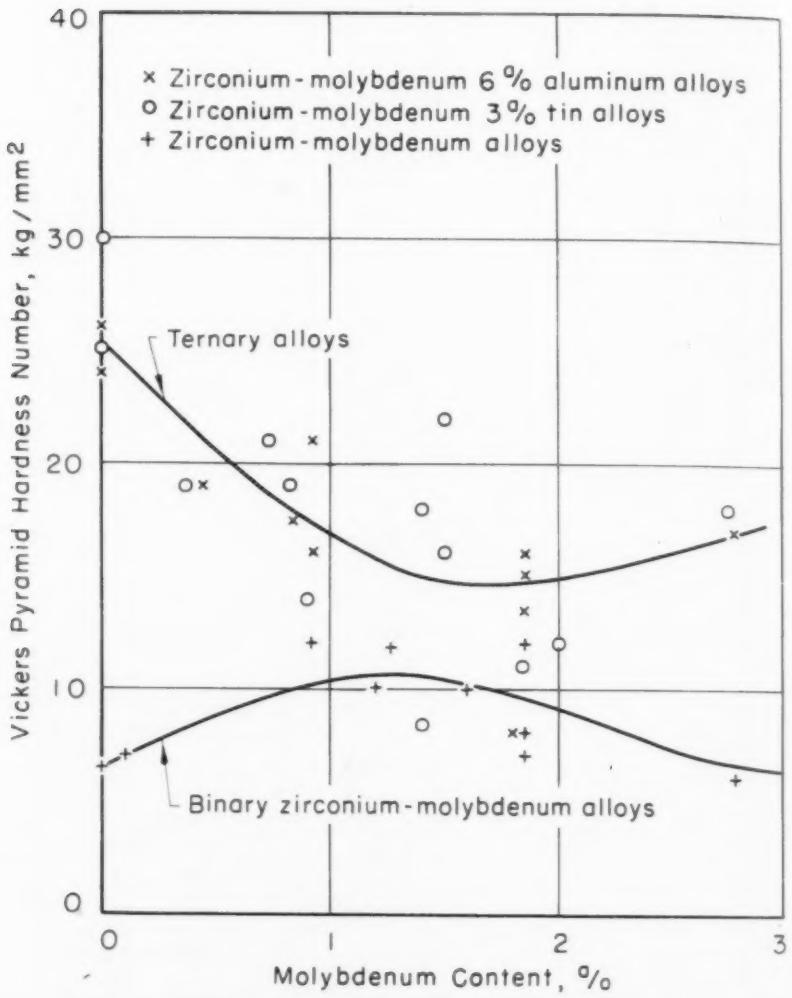


Fig. 10—Hardness of Zirconium-Aluminum-Molybdenum and Zirconium-Tin-Molybdenum Alloys at 800°C (1470°F).

zirconium alloys. For binary and ternary alloys containing only aluminum and tin, the limit of fabricability at a rolling temperature of 800°C (1470°F) occurs at a total alloy content of about 4 atomic %. This difficulty was partially overcome by the discovery that the addition of molybdenum or niobium to a zirconium-aluminum or a zirconium-tin alloy actually results in a ternary alloy with lower hardness at 800°C (1470°F). This lower hardness at 800°C (1470°F) is caused by the appearance of beta zirconium in the structure at this temperature. The effect of molybdenum additions upon the hardness of zirconium-aluminum and zirconium-tin alloys at 800°C (1470°F) is shown in Fig. 10. Zirconium alloys that utilize this principle are properly called "peritectoid-eutectoid hybrids." These hybrid alloys possess a feature in common with most other zirconium alloys, namely that rapidly cooled beta zirconium becomes hard and brittle. It follows that for maximum ductility they should be hot

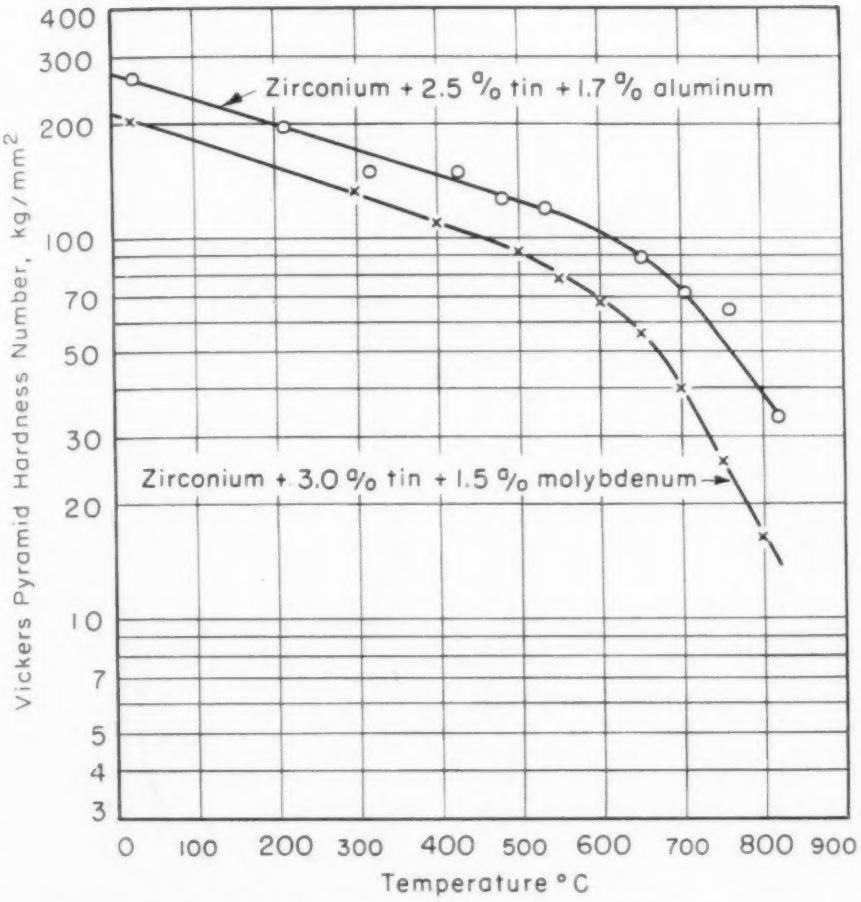


Fig. 11—Hardness of Ternary Zirconium Alloys at Elevated Temperatures.

rolled at as low a temperature as possible; and that higher strengths may be achieved by rolling or heat treating at temperatures above the minimum.

Table I shows the tensile properties of typical zirconium-tin-aluminum, zirconium-tin-molybdenum, zirconium-tin-niobium, zirconium-aluminum-molybdenum, and zirconium-aluminum-niobium alloys. In every case, the alloys were treated in an attempt to produce the state of maximum ductility. These data illustrate the low ductility of the zirconium-tin-aluminum alloys and the comparatively high ductility of the "peritectoid-eutectoid hybrids." For the same alloy content, the strength of the two types of alloys is quite similar.

Fig. 11 shows how the hot hardness of a "peritectoid-eutectoid hybrid" differs from the hot hardness of a straight peritectoid, zirconium-tin-aluminum alloy. At 800°C (1470°F) the zirconium-tin-aluminum alloy is more than twice as hard as the zirconium-tin-molybdenum alloy. The zirconium-tin-aluminum alloy was hot-rolled at 1000°C (1830°F); the zirconium-tin-molybdenum alloy was hot rolled at 760°C (1400°F).

Table I
Tensile Properties of Zirconium Alloys

Alloy Analysis (Balance Zirconium), Atomic Per Cent	Test Temperature, C	0.2 Per Cent Offset Yield, Strength, psi	Ultimate Strength, psi	Elongation to Maximum Load, %	Total Elongation in 1 Inch, %	Reduction of Area, %
3.3 Al+3.0 Sn[1]	25	78,900	84,300	3	3	—
3.3 Al+3.0 Sn[1]	260	54,200	68,000	9	25	35
3.3 Al+3.0 Sn[1]	500	39,400	44,700	2	6	9
2.5 Sn+2.0 Al[2]	25	72,100	72,600	1	3	10
2.5 Sn+2.0 Al[2]	260	—	38,300	0.3	—	—
2.5 Sn+2.0 Al[2]	500	32,300	34,400	4	4	6
2.5 Sn+1.9 Al[1]	260	45,500	52,100	9	19	24
2.5 Sn+1.9 Al[1]	500	31,400	37,700	6	13	12
2.5 Sn+1.7 Al[1]	25	79,400	98,100	7	14	19
2.5 Sn+1.7 Al[1]	260	54,300	68,400	5	11	18
2.5 Sn+1.7 Al[1]	500	44,200	55,100	6	8	11
3.8 Sn+1.3 Mo[1]	25	65,800	77,600	9	25	24
3.8 Sn+1.3 Mo[1]	500	32,700	42,100	7	29	35
3.4 Sn+2.0 Mo[2]	25	70,800	96,000	10	18	21
3.4 Sn+2.0 Mo[2]	260	50,700	71,800	8	16	34
3.4 Sn+2.0 Mo[2]	500	39,200	54,400	11	28	41
3.0 Sn+1.5 Mo[1]	25	59,000	86,700	13	25	43
3.0 Sn+1.5 Mo[1]	260	38,700	60,900	11	26	42
3.0 Sn+1.5 Mo[1]	500	30,400	45,900	11	42	65
3.0 Sn+1.5 Mo[2]	25	91,400	106,000	9	13	26
3.0 Sn+1.5 Mo[2]	260	53,600	71,600	5	16	35
3.0 Sn+1.5 Mo[2]	500	38,800	53,000	6	30	44
2.9 Sn+1.5 Mo[1]	25	71,200	90,600	10	20	24
2.9 Sn+1.5 Mo[1]	500	33,600	44,400	12	44	62
3.5 Sn+0.6 Nb[2]	25	89,000	103,800	9	18	26
3.5 Sn+0.6 Nb[2]	260	61,500	77,200	5	13	23
3.5 Sn+0.6 Nb[2]	500	40,000	55,200	12	24	30
2.3 Sn+1.7 Nb[2]	500	33,900	45,400	6	30	40
6.0 Al+1.8 Mo[1]	25	111,200	125,800	5	6	6
6.0 Al+1.8 Mo[1]	500	59,200	69,100	3	30	38
6.0 Al+0.8 Mo[1]	25	92,000	105,000	4	5	16
6.0 Al+0.8 Mo[1]	500	47,000	61,800	7	30	35
1.7 Al+1.0 Mo[2]	500	30,400	38,800	9	32	48
2.3 Al+1.5 Nb[2]	500	34,300	44,700	6	27	31

[1] Arc-melted alloy
[2] Induction-melted alloy

Table II shows how simple heat treatments affect the room-temperature tensile properties of a "peritectoid-eutectoid hybrid." These data show that the alloy is most ductile when its structure approximates an alpha-annealed, equilibrium structure. The highest strength and lowest ductility is found in the alloy when it is air-cooled from 900°C (1650°F). Lower strength is obtained in the alloy as water-quenched and as furnace-cooled. These data suggest that some relatively weak, beta zirconium is retained in the water-quenched alloy and that a precipitation hardening reaction proceeds in the material at slower cooling rates. It is obvious that transformed beta structures are not desirable for ductility.

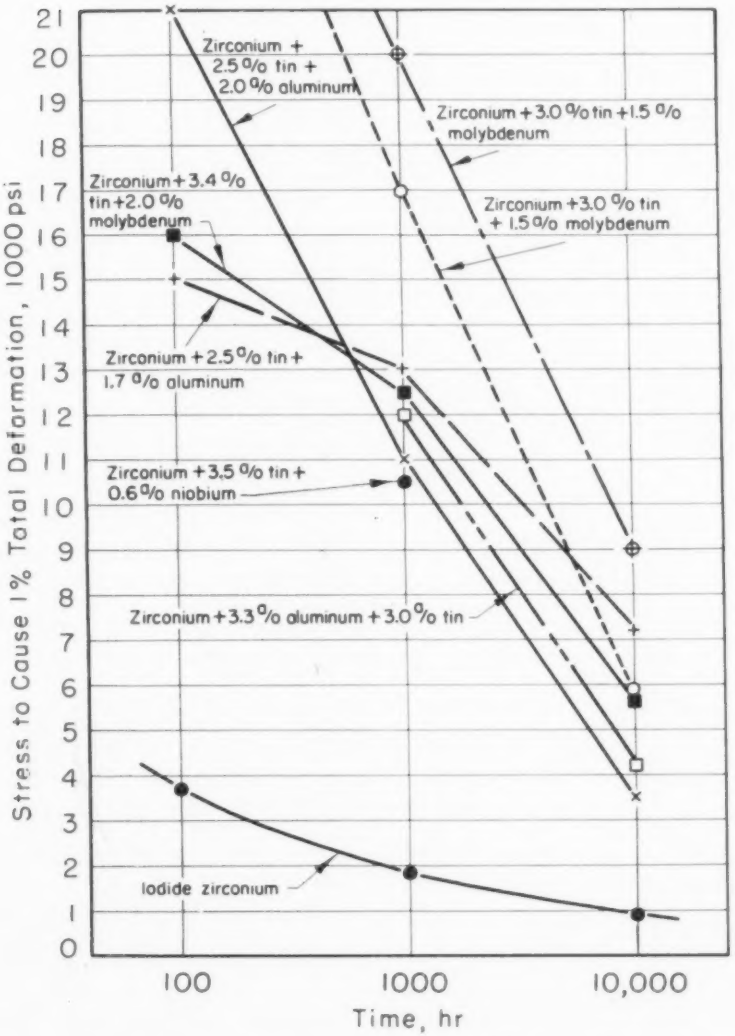


Fig. 12—Stress Versus Time for 1% Total Deformation at 500° (930°F).

Table II
Effect of Heat Treatment on the Tensile Properties of Zirconium+2.9 Atomic Per Cent Tin+1.5 Atomic Per Cent Molybdenum

Heat Treatment (a)	0.2% Offset Yield Strength, psi	Ultimate Strength, psi	Elongation to Maximum Load, %	Total Elongation in 1 Inch, %	Reduction of Area, %
1	71,200	90,600	10	20	24
2	89,000	103,300	3	3	2
3	123,800	143,300	2	2	1
4	74,900	97,600	10	12	3

(a) Treatment 1: Standard fabrication procedure consisting of hot roiling at 800°C (1470°F), cold rolling 30%, and annealing for 3 hours at 730°C.
Treatment 2: Material heated for 1 hour at 900°C (1650°F) and water-quenched.
Treatment 3: Material heated for 1 hour at 900°C (1650°F) and air-cooled in a Vycor capsule.
Treatment 4: Material heated for 1 hour at 900°C (1650°F) and furnace-cooled at a rate of 50°C per hour.

Creep Properties of Ternary Alloys

The development of creep-resistant zirconium alloys has just begun. However, zirconium alloys that will sustain a load of 10,000 psi at 500°C (930°F) with less than 1% total deformation in 1000 hours are no longer rare. The binary zirconium-aluminum alloys, the zirconium-tin-aluminum alloys, and the "peritectoid-eutectoid hybrid" family are prominent among the alloys that meet this specification. The available data for the creep resistance at 500°C (930°F) of alloys in the systems zirconium-tin-aluminum, zirconium-tin-molybdenum, and zirconium-tin-niobium are shown in Fig. 12. A comparison of Fig. 12 with Figs. 8 and 9 discloses that, except for two binary aluminum alloys, the creep resistance of the ternary alloys is generally superior to that of the binary alloys. These data suggest that alloys in the zirconium-aluminum-molybdenum and zirconium-aluminum-niobium systems will have even better creep properties than the alloys shown here. These ternary alloys will probably be the base for more complex alloys with still greater creep resistance.

Summary of Results

The metallurgy of zirconium has been developed on the basis of the effect of alloying elements on the transformation temperature. "Peritectoid-type" alloying elements tend to raise the transformation temperature; "eutectoid-type" alloying elements tend to lower the transformation temperature. These effects have been used to explain in part the mechanical behavior of zirconium alloys.

The various zirconium alloys systems have been investigated with respect to the effect of alloying elements upon tensile properties, creep properties, and hardness. The alloy systems have been screened, and those systems that produce the greatest increase in strength in the dilute range have been selected. The mechanical properties of binary alloys in these systems have been measured at room temperature, 260 and 500°C (500 and 930°F).

The "eutectoid-type" alloying elements, molybdenum, niobium, tantalum, and vanadium, are most effective in strengthening zirconium at temperatures below 500°C (930°F). The peritectoid-type alloying elements, aluminum and tin, are most effective in strengthening zirconium at temperatures above 500°C (930°F). The "peritectoid-type" alloying elements are also most effective in improving the creep strength of zirconium at 500°C (930°F).

Those ternary zirconium alloys that contain both "peritectoid" and "eutectoid-type" alloying elements have been called "peritectoid-eutectoid hybrids." These alloys show an extremely wide range of mechanical properties and are noted for the ease with which they can be hot fabricated. Alloys of this type exhibit good strength and

ductility at room temperature, and show promise for the development of creep-resistant alloys at 500°C (930°F).

The "peritectoid-eutectoid hybrids" are heat treatable, and can be strengthened by heating into and quenching from an alpha-plus-beta or beta-phase field. This strengthening effect is usually associated with a severe loss in ductility.

References

1. C. T. Anderson, E. T. Hayes, A. H. Roberson and W. J. Kroll, "A Preliminary Survey of Zirconium Alloys," U. S. Bureau of Mines Report of Investigation No. 4658, March 1950.
2. D. J. McPherson and M. Hansen, "The System Zirconium-Aluminum," TRANSACTIONS, American Society for Metals, Vol. 46, 1954, p. 354.
3. E. T. Hayes, A. H. Roberson and M. H. Davies, "Zirconium-Chromium Phase Diagram," *Transactions*, American Institute of Mining and Metallurgical Engineers, Vol. 194, 1952, p. 304.
4. R. F. Domagala, D. J. McPherson and M. Hansen, "System Zirconium-Chromium," *Transactions*, American Institute of Mining and Metallurgical Engineers, Vol. 197, 1953, p. 279.
5. R. F. Domagala, D. J. McPherson and M. Hansen, "Systems Zirconium-Molybdenum and Zirconium-Wolfram," *Transactions*, American Institute of Mining and Metallurgical Engineers, Vol. 197, 1953, p. 73.
6. B. A. Rogers and D. F. Atkins, "The Zirconium-Columbium Diagram," Iowa State College, Ames, Iowa, Ames Laboratory Report ISC-500, June 29, 1954.
7. D. J. McPherson and M. Hansen, "The System Zirconium-Tin," TRANSACTIONS, American Society for Metals, Vol. 45, 1953, p. 915.
8. E. T. Hayes, A. H. Roberson and O. G. Passche, "The Zirconium-Titanium System—Constitution Diagram and Properties," U. S. Bureau of Mines, Report of Investigation No. 4826, November 1951.
9. J. T. Williams, "The Vanadium-Zirconium Alloy System," Iowa State College Report No. ISC-491, June 15, 1954.
10. ZIRCONIUM AND ZIRCONIUM ALLOYS, 1953, published by the American Society for Metals, Cleveland, Ohio.
11. A. D. Schwope and W. Chubb, "Small Additions Raise Strength of Zirconium at Elevated Temperatures," *Journal of Metals*, Vol. 4, November 1952, p. 1138.
12. F. B. Litton, "Ten Zirconium Alloys Evaluated," *Iron Age*, Vol. 167, April 5 and 12, 1951, p. 95 and 112.
13. J. H. Keeler, "Development of Zirconium Base Alloys," General Electric Quarterly Technical Progress Reports, SO-2505 to SO-2515, May 1952 to July 1954.
14. W. Chubb and G. T. Muehlenkamp, "The Effects of Chromium, Iron, and Nickel on the Mechanical Properties of Zirconium," USAEC Document No. BMI-938, August 11, 1954.
15. W. Chubb, "The Contribution of Crystal Structure to the Hardness of Metals," *Transactions*, American Institute of Mining and Metallurgical Engineers, Vol. 203, Jan. 1955, p. 189.
16. A. D. Schwope, "Structure and Alloy Design," ASM TRANSACTIONS SUPPLEMENT, Vol. 46A, "Relation of Properties to Microstructure," 1954, p. 108.

DISCUSSION

Written Discussion: By G. L. Miller, research manager, Murex Ltd., Rainham, Essex, England.

The only point that I have to make is to complain that Dr. Chubb has done what so many other investigators have done in the case of metallurgical research

and that is not to give full details of the materials they employed in their investigations.

A short time ago when I was studying the work on zirconium in preparation for my book on this subject, I was appalled at the manner in which investigators proceeded to carry out research on the various aspects of zirconium, without even bothering to determine the purity of their basic materials. Dr. Chubb does at least state that the zirconium employed was of the low hafnium iodide type and that it was the Grade I quality supplied by the Foote Mineral Company, but surely it would not have taken up a great deal of space to have shown the actual content of impurities. Again, he states that some of these alloys were prepared by melting in a graphite crucible and others by using the double arc melting technique with a tungsten electrode, but he does not give the carbon content of the alloy after melting in graphite or indicate whether there was any tungsten contamination from the arc melting procedure. As far as the alloying elements are concerned, we are told that the elements used were commercial high purity materials. In the case of aluminum, copper, etc. this is probably sufficient but for niobium it would have been interesting to know what the oxygen content was and also the tantalum and titanium contents.

It seems to me that in an age when we know that small amounts of impurities can influence the properties of alloys, it is quite wrong not to give full details of the materials employed in the investigations.

Written Discussion: By F. A. Crossley and R. J. Van Thyne, Armour Research Foundation, Metals Research, Chicago, Ill.

The author has made a significant contribution to zirconium alloy metallurgy. At Armour Research Foundation zirconium-base alloys have also been investigated. Similar to results presented here, it was found that alloys containing aluminum and/or tin require working at high temperatures, but it would seem that this is generally what we want—strength at elevated temperatures. Compositions containing up to 5 wt % aluminum or 10 wt % tin were studied. The forging temperatures of binary and ternary alloys were from 1900 to 2200°F.

The prediction by the author that above 500°C (930°F) the strengthening effects of aluminum and tin are greater than those of the beta-stabilizers is certainly true. Our tensile data at 650 and 800°C (1470°F) demonstrate that a large difference exists between the two types at the elevated temperatures. Titanium is also an effective addition for elevated temperature strength. At temperatures up to 500°C (930°F) zirconium and titanium form a continuous series of alpha solid solutions. However, at higher temperatures titanium is less soluble in alpha zirconium because a minimum exists for the beta phase.

Heat treatment, microstructure, creep resistance, and stability are all interrelated. The author gives little attention to this interrelationship. This paper suffers from the fact that heat treatments used for evaluating the alloys are not given. Microstructures produced by these heat treatments are likewise omitted. A ternary, so-called "peritectoid-eutectoid hybrid," alloy may be single phase alpha, alpha-beta, alpha plus compound or even more complex, depending upon the specific additions, the amount of each addition, and the heat treatment applied. Designating alloys by their structural characteristics in the temperature range of usefulness would be of greater significance than the peritectoid-eutectoid nomenclature employed.

The statement, ". . . . alloying elements that preferentially strengthen the beta phase precipitate from the alpha phase. . . .," is perhaps in need of clarifica-

tion, considering the context in which it appears. Eutectoid-type additions have decreasing solubility in alpha below the eutectoid temperature, and consequently, compound may precipitate from the alpha phase. However, in beta alloys the beta phase may transform by several mechanisms, depending upon thermal history and the kinetics of the competing reactions. These reactions are: (a) diffusionless formation of alpha prime, (b) alpha rejection by nucleation and growth, and (c) eutectoidal decomposition.

Written Discussion: By J. H. Keeler, Metallurgy and Ceramics Research Department, General Electric Company, Schenectady, N. Y.

Dr. Chubb has presented a large amount of information that the zirconium-metallurgist should examine in detail. As a supplement to Dr. Chubb's data I would like to add some yield strength versus composition data for zirconium alloys containing only small amounts of niobium or tantalum.

Figs. 13 and 14 show that alloys containing up to about 3 atomic % niobium or tantalum showed less strengthening with a higher oxygen-nitrogen impurity

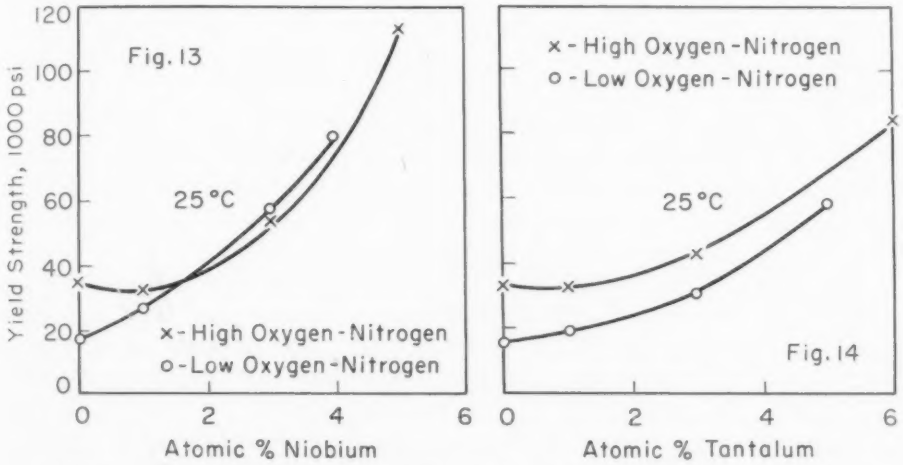


Fig. 13—Alloys Containing Up to 3 Atomic % Niobium Showed Less Strengthening With a Higher Oxygen-Nitrogen Impurity Content Than With a Lower Impurity Content.

Fig. 14—Alloys Containing Up to 3 Atomic % Tantalum Showed Less Strengthening With a Higher Oxygen-Nitrogen Impurity Content Than With a Lower Impurity Content.

content than with a lower impurity content. However, the higher oxygen-nitrogen alloys showed about the same compositional rate of strengthening when the niobium or tantalum content was greater than 3 atomic %. It is thought that an explanation of this behavior may be that the tantalum and niobium act as deoxidizers in the alloys with higher oxygen and nitrogen and thus do not contribute their full strengthening effect until higher compositional levels are reached.

Author's Reply

The discussion evoked by this paper is indicative of the widespread interest in zirconium and zirconium alloys at the present time. This interest is stimulated to a great extent by the growing need for neutron efficiency in thermal power reactors. Zirconium shows considerable promise of answering this need.

Dr. Miller is quite correct in stating that small amounts of impurities do affect the properties of metals, particularly zirconium, and it is quite imperative that we know the contaminants present. However, it seemed that to list the

impurities in Foote, Grade 1, low hafnium iodide zirconium was somewhat analogous to listing the impurities in electrolytic copper. For the benefit of those unfamiliar with iodide zirconium, the following figures are presented as typical of the zirconium used in these studies:

Carbon	300 ppm
Oxygen	200 ppm
Nitrogen	20 ppm
Hydrogen	40 ppm
Iron	300 ppm
Hafnium	200 ppm
All Other Impurities	400 ppm
Zirconium	more than 99.8%

The alloys used in these studies which were prepared by induction melting contained about 0.3 w/o carbon. This carbon was present as zirconium carbide in rather large particles. These particles affected ductility adversely, but showed only a minor strengthening effect and did not obscure the effects of alloying with other elements.

Contamination by tungsten in the arc melting of zirconium occurs by an intermittent process, so that the tungsten occurs in the zirconium as discrete droplets of pure tungsten or tungsten-rich alloy. The effect of these droplets on mechanical properties is insignificant, and an analytical figure could have little meaning.

The alloying elements, including niobium, were all purer than 99%. Since only about 6% alloy was used in these studies, a calculation will show that the alloying materials could, under the worst possible circumstances, introduce no more than 600 ppm of a single impurity. We were optimistic and felt that it was unnecessary to analyze for this amount of impurity.

The author is pleased to note that the results of Crossley and Van Thyne agree with his own. It was reported in 1952 that titanium effectively strengthened zirconium at temperatures up to 700°C (1292°F). Unfortunately, titanium greatly reduces the oxidation resistance of zirconium; it is difficult to hot roll such alloys without prohibitive losses due to oxidation. Furthermore, the thermal neutron efficiency of titanium is poor, so that eventually titanium was abandoned in favor of molybdenum and niobium as alloying elements.

Messrs. Crossley and Van Thyne are quite correct in stating that heat treatment, microstructure, creep resistance, and stability are all inter-related. They have evidently failed to notice that all alloys except that listed in Table 2 were prepared by cold rolling, and were annealed for 3 hours at 730°C (1345°F), fully 230°C (445°F) above the highest tensile or creep-test temperature. This annealing temperature was selected as a compromise between the lowest eutectoid temperature of the alloying elements and the temperature necessary to achieve recrystallization in a reasonable time. Only the temperature of the zirconium-niobium eutectoid is lower than 730°C (1345°F).

Only a few of the alloys were single phase at room temperature, most contained a very fine dispersion of second phase. This latter structure was considered to be eminently satisfactory for maximum creep resistance.

As Messrs. Crossley and Van Thyne indicate, the transformation of beta zirconium may occur in one or more of several different ways. These modes of transformation are very interesting to the physical metallurgist, and they undoubtedly will be described in great detail at some future date. This writer expects the transformation of beta zirconium to resemble in most respects the transformation of beta titanium.

TENSILE PROPERTIES OF ZR-CR ALLOYS—PARTICLE-STRENGTHENING EFFECTS

By J. H. Keeler

Abstract

The tensile properties of zirconium-chromium binary alloys containing up to 18 atomic % chromium are reported for the temperature range −195 to 500°C (−319 to 930°F). The highest yield strength obtained at 500°C (930°F) was about 26,000 psi (for the 18% chromium alloy). No significant solid-solution hardening in alpha zirconium was observed. A linear relation between the flow stress and volume fraction of the compound was observed. The particle-hardening effect increased with strain in the range of true strain 0.002 to 0.05, and made a greater total strengthening contribution at lower temperatures. The normalized (per cent) increase in strength was essentially independent of testing temperature except at the highest temperature where the alloys showed signs of instability. (ASM-SLA Classification: Q27, Zr)

Introduction

ZIRCONIUM, with its low neutron absorption, high temperature of melting, and good corrosion resistance, is of interest to the Atomic Energy Commission for use in reactors. It is desirable to raise its strength at elevated temperatures and at the same time maintain its low neutron absorption and good corrosion resistance as much as possible. Chromium is one of the alloying elements that might be used with zirconium because of its relatively moderate neutron absorption (2.9 barns) and known ability to impart elevated-temperature strength and oxidation resistance to other metals.

In addition, the zirconium-chromium system is interesting metallurgically since it is a eutectoid system with essentially no solid solubility in the low temperature alpha phase. The constitution diagram for the system as determined by Domagala, McPherson, and Hansen (1)[1] is shown in Fig. 1. With no solid solubility in the hexagonal close-packed alpha phase, strengthening is obtained only by particle hardening in alpha-annealed materials (annealed below 835°C (1535°F) in the temperature range wherein the alpha phase of

[1]The figures appearing in parentheses pertain to the references appended to this paper.

A paper presented before the Thirty-Seventh Annual Convention of the Society, held in Philadelphia, October 17–21, 1955. The author, J. H. Keeler, is associated with the Metallurgy and Ceramics Research Department, General Electric Co., Research Laboratory, Schenectady. Manuscript received April 8, 1955.

zirconium is stable). The effect of compound particles on strength can thus be studied without complications by solution hardening.

An earlier survey of zirconium alloys was conducted by the Bureau of Mines using chloride-process zirconium; and the tensile properties for zirconium-chromium alloys induction-melted in a graphite crucible, swaged at 850°C (1560°F) in iron sheaths, and annealed were among those reported (2). Recently, zirconium alloys

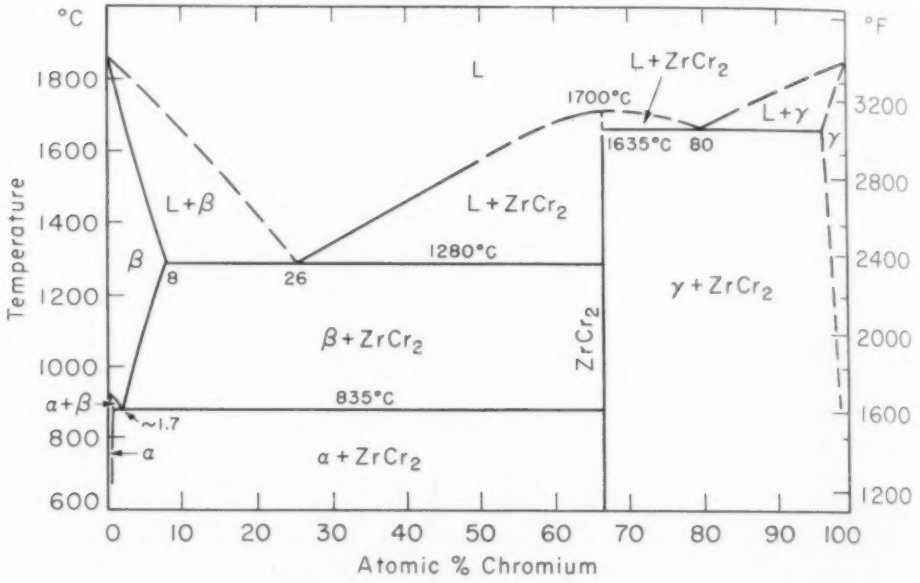


Fig. 1—Zirconium-Chromium Constitution Diagram After Domagala, McPherson and Hansen (1).

containing up to about 1.5 atomic % chromium were studied by Chubb and Muehlenkamp (3). These alloys were made using crystal-bar zirconium, and yield strength and ultimate tensile strength were determined at room temperature and at 316°C (600°F).

Experimental Procedure

The materials in this investigation were crystal-bar zirconium prepared by the iodide process and electrolytic chromium. The largest impurity in the zirconium was hafnium, which was less than 0.3%. The composition of the crystal-bar zirconium obtained by spectrographic analysis is given in Table I, as is the nominal analysis of the chromium.

Alloy ingots weighing 100 grams were melted in a single-crucible arc-melting furnace. This furnace was a conventional one using a water-cooled copper crucible, a tungsten-tipped electrode, and an atmosphere of purified argon. Although the furnace was evacuated to a pressure of about one micron before the argon was introduced, the oxygen and nitrogen remaining in the chamber as well as that

Table I
Composition of Melting Stock

Crystal-bar Zirconium		Electrolytic Chromium	
Element	Weight Per Cent	Element	Weight Per Cent
Hf	0.3 maximum	C	0.01
Fe	0.02–0.1	O	0.2
Al	0.005–0.02	N	0.009
Cr	0.02–0.1	H	0.02
Cu	0.001–0.005	Fe	0.080
Ni	0.005–0.02	Cu	0.01
Mg	0.001–0.005	Pb	0.001
Mo	0.01	S	0.15
N	0.007[x]		

[x]Chemical analysis

NOTE: Oxygen and carbon are estimated at 0.02% for the zirconium.

adsorbed on the charge and crucible were sufficient to contribute to the strengthening of the alloy.

The oxygen content was determined by vacuum-fusion methods for the 3 atomic % chromium alloy. The analytical result, 0.0531 ±0.0009 weight % oxygen for the product of this furnace, gives an idea of the relative amount of interstitial impurity.

Unalloyed zirconium ingots were made to be used as zero chromium compositions in data analysis.

The early alloy ingots, containing up to 3 atomic % chromium, were alternately cold-rolled and then annealed in order to produce alloy sheet approximately 0.020-inch in thickness. The annealing was carried out in evacuated tubes of Vycor or quartz containing zirconium foil to take up any remaining oxygen or nitrogen. The high chromium alloy ingots containing 10 and 18 atomic % chromium were hot rolled at 800 to 950°C (1470 to 1740°F) in welded iron or stainless steel sheathes. The fabrication history of the various alloys is given in Table II.

Table II
Fabrication History of Zirconium-Chromium Alloys

Melt No.	Nom. A/o Cr	Melting Furnace	Rolling Temp., °C	Final Reduction, %	Annealed[xx] Hardness VHN	Intermediate Annealing Temp., °C
556	1	S[x]	25	70	164	800
578	3	S	25	60	175	800
5029	10	S	925	90	218	
5028	18	S	925	90	231	

[x]Single hearth.
[xx]Hardness measurements were obtained on the sheet surface with a 5-kg load.

Tensile specimens of the dimensions reported previously(4) were machined from the sheets prior to final annealing treatments. Unless otherwise stated, the specimens were annealed 1 hour at 800°C (1470°F) (in the alpha region) prior to tensile testing.

Tensile tests were conducted with Instron Tensile Testing

machines, described earlier (4). Load-time curves were recorded automatically on a synchronously-driven chart. The relation of recorder chart speed to jaw speed is known, and therefore the time axis of the chart can be converted to strain.

Tensile tests were conducted in liquid nitrogen at −195°C (−319°F), in air in the temperature range from 25 to 370°C (77 to 700°F), and *in vacuo* at 500°C (930°F). True stress versus true strain and logarithm true stress versus logarithm true plastic strain were plotted for these tests. True stress at a true plastic strain of 0.002 (0.2% offset yield strength), true stress at true plastic strains of 0.02 and 0.05, tensile strength, reduction in area, and elongation are tabulated. The strain-hardening exponent, "m," from the stress-strain relationship, $\sigma = K\epsilon^m$, and obtained from the slope of the log true stress versus log true plastic strain plot, is also listed. In those instances where the log-log plot was not a straight line, the slope was taken from that portion of the curve in the vicinity of the strain at maximum load. When the log-log plot was not a straight line, the significance of m is uncertain and so the slope $d\sigma/d\epsilon$ of the linear true stress-true strain curve at $\epsilon\rho = 0.02$ was determined to provide a measure of the strain hardening. At least two tests were made for each alloy at each test condition.

The zirconium-rich end of the zirconium-chromium system is eutectoid in nature, and so heat treatments patterned after those used in the iron-carbon system might be considered. However, if the zirconium-chromium alloys are to be used at elevated temperatures, perhaps in the neighborhood of 300 to 500°C (570 to 930°F) or even higher, they would have to be stable at these temperatures. For this reason this investigation, with its goal a survey of the system, concerned primarily alpha-annealed alloys.

Results and Discussion

True stress-true plastic strain curves were derived from tensile tests of unalloyed zirconium and 1, 3, 10 and 18 atomic % chromium alloys at the several test temperatures. In most instances a single strain rate was used. However, in certain tests there was an instantaneous positive displacement of the flow curve in the stress direction resulting from an instantaneous ten-fold increase in the strain rate. This change in strain rate was used to determine the strain-rate sensitivity of the alloy under conditions which avoid specimen-to-specimen variation. In these instances the first part of the test, up to a true plastic strain of about 0.03 was carried out at a strain rate of 0.009 min^{-1}. The change in stress was obtained in psi and a measure of the "rate sensitivity" was calculated. The stress-strain rate relation has been expressed[5] as

$$\sigma = K\dot{\epsilon}^n \Big|_{\epsilon, T}$$

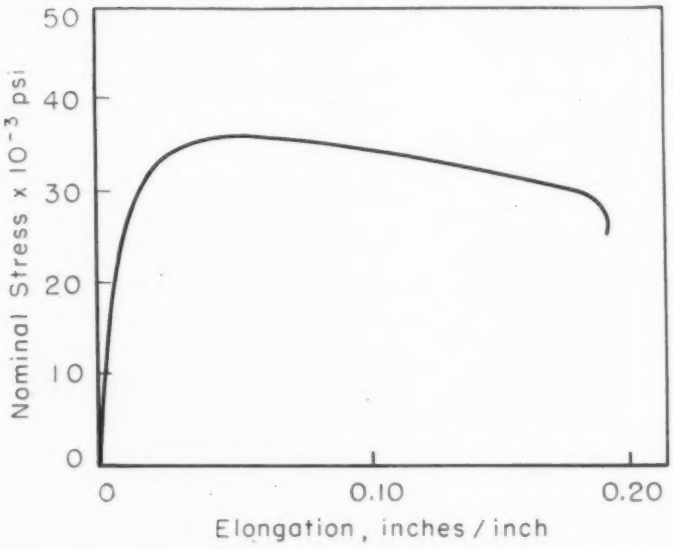


Fig. 2—Early Maximum-Load Type of Load-Elongation Curve Found for the Zirconium-10 chromium alloy at 500°C (930°F).

where K is a material constant, strain and temperature are held constant, and n is a constant called the strain-rate exponent. The term "rate sensitivity" has thus been defined (5–7) as the ratio of a small change in log stress to the resultant change in log rate for a given strain and temperature:

$$n = \left.\frac{\Delta \log \sigma}{\Delta \log \dot{\epsilon}}\right|_{\epsilon, T}$$

This rate sensitivity, n, can be obtained from a test wherein strain rate is changed quickly from one value to another (8) by the relation

$$n = \frac{\log S_2/S_1}{\log \dot{\epsilon}_2/\dot{\epsilon}_1}$$

in which S_2 is the stress obtained with strain rate $\dot{\epsilon}_2$, and S_1 the stress obtained with strain rate $\dot{\epsilon}_1$.

Greater tendency to deviate from a straight-line relation in log stress-log strain plots was observed with increasing test temperature, resulting from increasing participation of secondary reactions such as recovery.

Additional evidence of instabilities in these alloys was the observation of the early-maximum-load type of tensile curve (9) shown in Fig. 2, reported earlier for unalloyed zirconium (4). The early-maximum type of flow curve was observed for all of the alloys at 500°C (930°F), but not at 300°C (570°F). This observation was also true of unalloyed annealed zirconium.

It is characteristic of this type of load-extension curve to reach an early maximum load at a true plastic strain of about 0.04 to 0.09

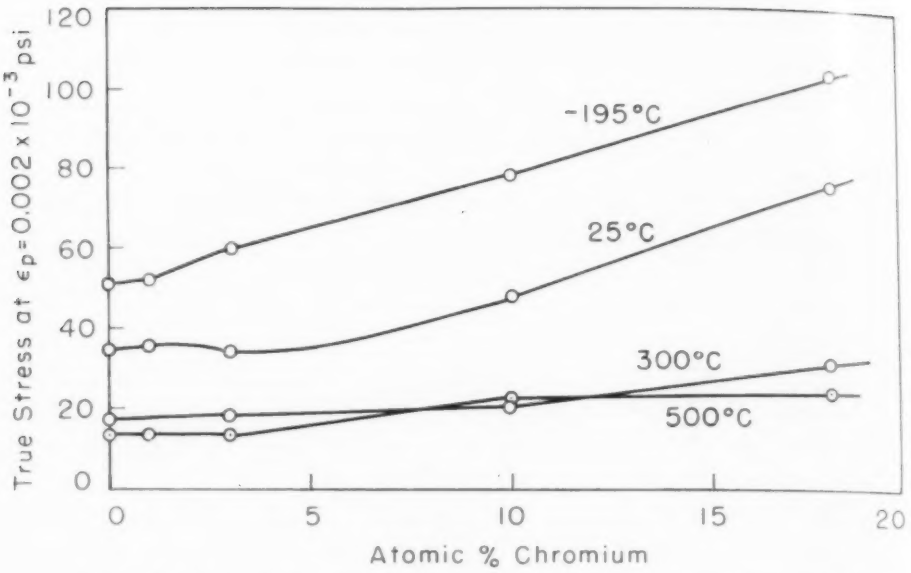


Fig. 3—True Stress at $\epsilon_p = 0.002$ (or 0.2% offset yield stress) Versus Chromium Content at Various Test Temperatures.

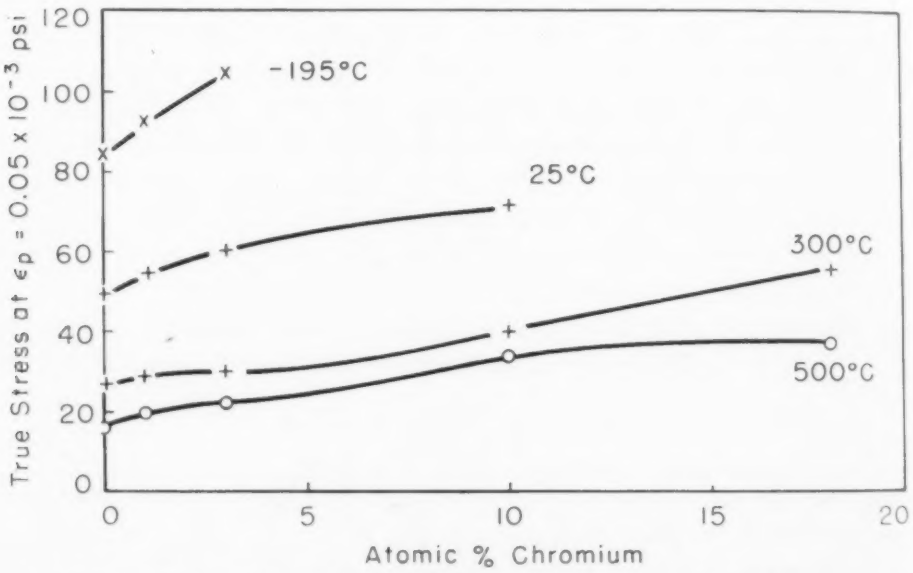


Fig. 4—True Stress at $\epsilon_p = 0.05$ Versus Chromium Content at Various Test Temperatures.

(or an elongation of approximately 4 to 9%) after which a long gradual falling-off of the load occurs. This latter portion of the curve is almost a straight line. Finally, true localized necking occurred at a strain 2 to 5 times that of maximum load and fracture occurred. Several of the tests on the zirconium-chromium alloys were stopped in the straight-line portion of the curve following the point of maximum load to see if localized necking was apparent. As was observed earlier for severely cold-worked zirconium, the specimen was smooth and

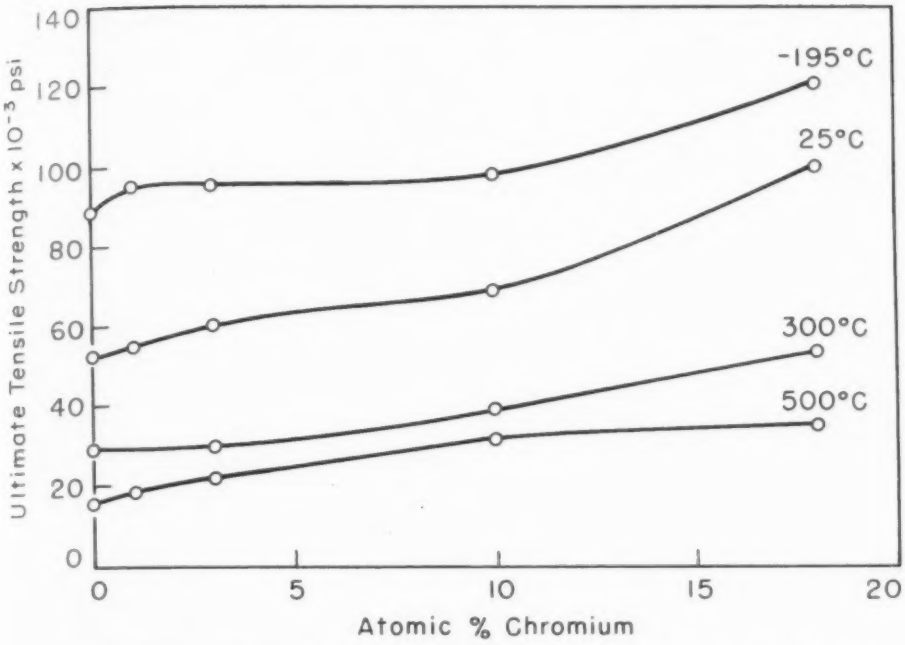


Fig. 5—Ultimate Tensile Strength Versus Chromium Content at Various Test Temperatures.

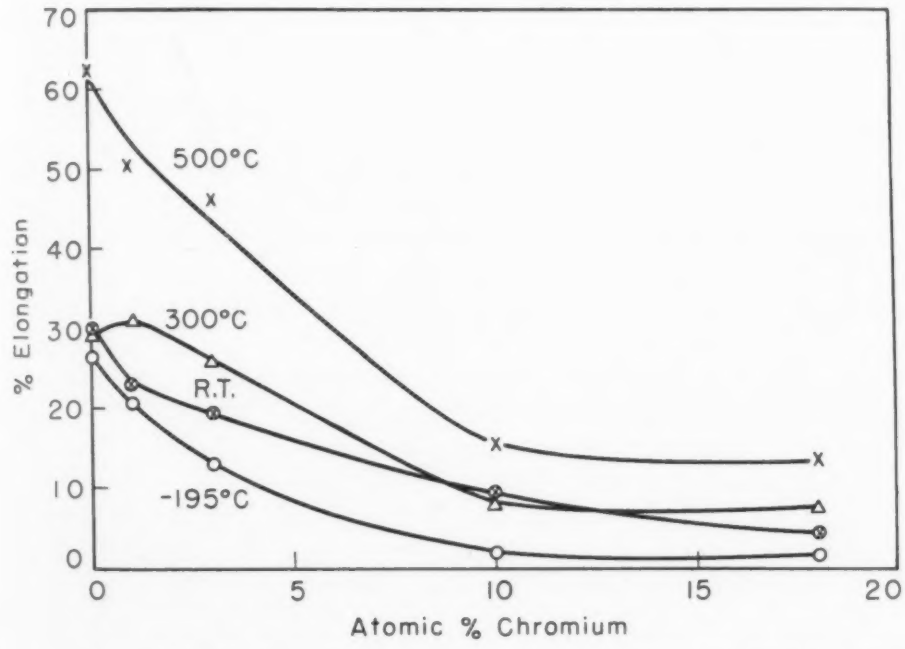


Fig. 6—Per Cent Elongation (in 2.25 inches) Versus Chromium Content at Various Test Temperatures.

did not exhibit localized necking. Also, the amount of localized strain near the fracture area in broken specimens was too small to account for the large amount of strain that followed the strain at maximum load. True stress versus true strain calculations for curves of this

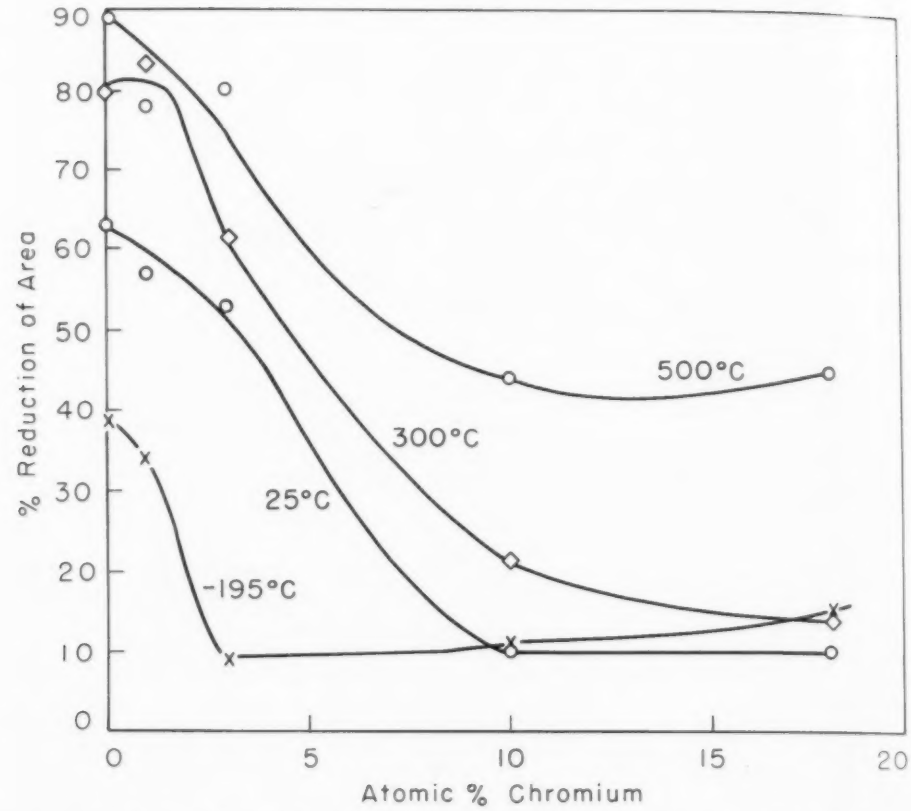


Fig. 7—Per Cent Reduction of Area Versus Chromium Content at Various Test Temperatures.

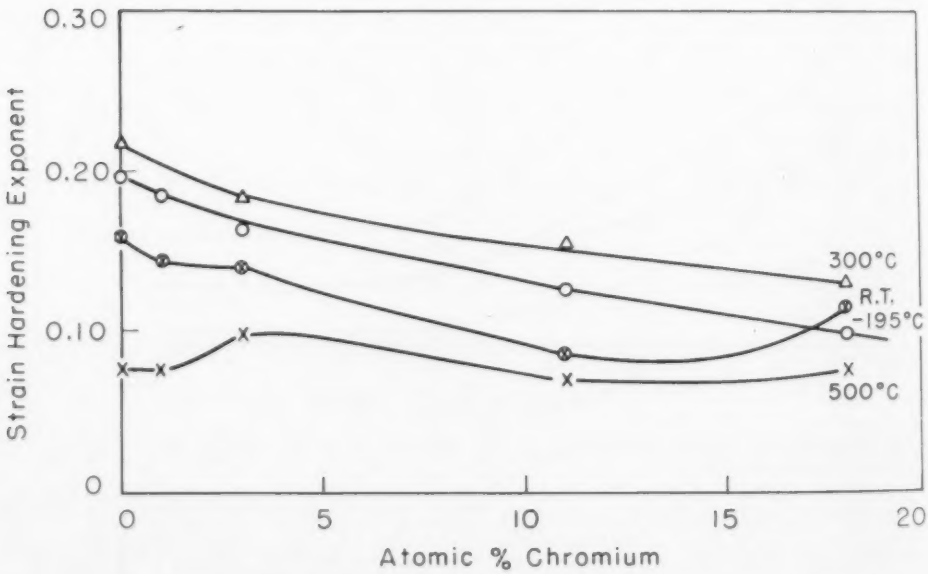


Fig. 8—Strain-Hardening Exponent Versus Chromium Content at Various Test Temperatures.

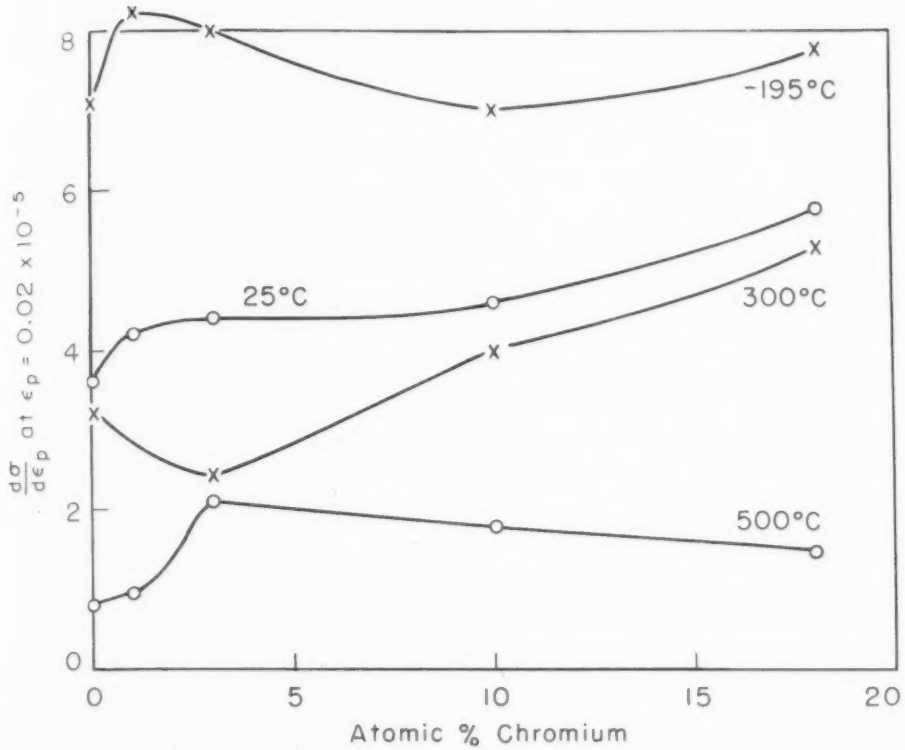


Fig. 9—Rate of Strain Hardening (slope of the true stress-true strain curve) at a Plastic Strain of 0.02 Versus Chromium Content at Various Test Temperatures.

type were plotted for points beyond the maximum load since uniform strain was apparently still taking place. As was true of unalloyed zirconium, these curves exhibited a flattening beyond the maximum load, with the slope of the curve approaching zero and even becoming slightly negative in the case of the 10 chromium alloy.

Recrystallization treatments for these alloys had been carried out at 800°C (1470°F) for one hour in order to obtain a fine grain size of about 0.005 to 0.007 mm average diameter essentially independent of composition. Annealing treatments at lower temperatures had not produced recrystallized grains in one hour.

Summarizing the data are plots of various tensile characteristics versus atomic per cent chromium at various temperatures (Figs. 3 to 9). See Table III.

Since the zirconium-chromium system is one in which there is little or no solid solubility in the alpha phase of hexagonal-close-packed zirconium, the strengthening effect of second-phase particles can be studied without the complications of accompanying solid solution. The crystal structure of the second phase $ZrCr_2$, is known (1,10,11,12) so the density of the compound and the volume frac-

Table III
Tensile Properties of Zirconium-Chromium Alloys

Property	Test Temp, °C	Atomic Per Cent Chromium 0	1	3	10	18
σ at 0.002 ϵ_p (psi)	—195	51,000	52,000	60,500	78,100	103,200
	25	35,000	36,000	34,300	47,600	75,500
	300	17,500	—	19,700	20,100	31,000
	500	13,750	13,700	14,000	22,700	25,900
σ at 0.02 ϵ_p (psi)	—195	71,700	76,900	88,500	104,000	—
	25	42,400	45,700	52,000	63,500	97,300
	300	21,500	23,800	25,900	33,600	47,300
	500	15,700	17,900	19,800	31,900	35,500
σ at 0.05 ϵ_p (psi)	—195	84,000	92,100	104,200	—	—
	25	49,500	54,400	60,100	71,200	—
	300	26,500	28,500	29,400	39,900	55,400
	500	16,700	19,400	22,100	34,000	37,000
Ultimate tensile strength, (psi)	—195	88,500	96,600	106,300	98,100	120,900
	25	52,000	55,300	60,100	68,500	99,900
	300	29,000	—	30,100	38,800	53,400
	500	16,000	18,600	21,800	32,300	35,300
Elongation in 2.25 inch, %	—195	26.5	21	8	2	1.5
	25	29.5	23	19.5	9	4
	300	29	32	27.5	8	7
	500	63.6	51	46	15	13
Reduction in area, %	—195	39	34	9	10.5	15
	25	63	57	53	10	10
	300	80	84	62	21	14
	500	87.5	78	80	44	46
Strain-hardening exponent, "m"	—195	0.196	0.184	0.164	0.127	0.098
	25	0.159	0.140	0.14	0.10	0.110
	300	0.215	0.20	0.18	0.151	0.130
	500	0.076	0.074	0.10	0.067	0.078
Rate sensitivity, "n"	—195	0.007	0.008	0.008	—	—
	25	0.021	—	—	—	—
	300	0.011	—	—	—	—
	500	0.048	—	—	0.10	0.07
$d\sigma/d\epsilon$ at $\epsilon_p=0.02$ ($\times 10^{-5}$)	—195	7.1	8.2	8.0	7.0	7.8
	25	3.6	4.2	4.4	4.6	5.8
	300	3.2	—	2.4	4.0	5.3
	500	0.8	0.95	2.1	1.8	1.5

tion of compound present can be calculated as follows. The density of the compound, 7.031 grams per cubic centimeter, is calculated from the relation

$$\rho = \frac{N \cdot M}{V \cdot A}$$

where N is the number of molecules in a unit cell, M is the gram molecular weight of the compound, V is the volume of the unit cell, and A is Avogadro's number. The volume fraction, f_1, of compound present in an alloy is calculated from the relation

$$f_1 = \frac{g_c}{\beta(g_a + g_c)}$$

where g_c is the amount by weight of compound present, g_a is the amount by weight of alpha-phase present, and β is the ratio of the density of the compound to the density of the alpha phase. The values for g_c and g_a were obtained from the constitution diagram.

Relations between true stress and volume fraction $ZrCr_2$ for true plastic strains of 0.002 and 0.05 are shown in Figs. 10 and 11. The true stress at a true strain of 0.002 can also be considered the 0.2% offset yield strength (Fig. 10). The straight lines through the data points of the alloys intersect zero volume fraction at the same stress values as those obtained from tests of the unalloyed zirconium. This fact strongly supports the assumption in this work, based upon the findings of Domagala and co-workers (1) and Hayes et al (11) that there is very little or no solid solution of $ZrCr_2$ in alpha zirconium.

Little attention was paid to controlling the size, shape, and distribution of the compound particles. Attempts were made to calculate mean particle radii, interparticle distances, and other relations after Fullman (13), but results indicated that the tiny particles of compound were not sufficiently resolved to allow accurate calculations to be made. Photomicrographs of the alloys are shown in Fig. 12. However, it was expected on the basis of earlier experimental work in the titanium-silicon system (14) that within a wide scatter band the data might be represented by a straight-line relation between true stress and volume fraction compound.

The true stress at $\epsilon_p = 0.002$ was plotted versus $\sqrt{f}$ as suggested by the modified Orowan relation (discussed later in this report) and true stress at $\epsilon_p = 0.05$ was plotted against $f^{3/2}$ as suggested by Fisher, Hart and Pry (15). Although the data did not clearly distinguish between the various ways of representing the volume fraction relation, nevertheless a better straight-line correspondence was obtained with f than with $\sqrt{f}$ or $f^{3/2}$.

The result that the flow stress is a nearly linear function of the volume fraction of $ZrCr_2$ for the range of particle sizes and numbers of particles shown in Fig. 12 suggests that the strengthening effect in this system is independent of the particular sizes, shapes, and number of particles and simply approaches the law of mixtures. This independence is not quite true since there are small positive deviations from linearity as seen in Fig. 11 for the 1 and 3% alloys with a larger number of smaller particles. However, large particles are essentially as effective in blocking dislocation motion as small particles and it is simply a matter of a larger volume of particles being able to hinder a larger number of dislocations.

In Figs. 13 and 14, the increase in strength at various temperatures is plotted against volume fraction $ZrCr_2$ for true stress at strains of 0.002 and 0.05. It is apparent that the numerical increase in strength due to the second phase is greater at lower temperatures. Part of these data are replotted in Fig. 15, where it can be seen that the effectiveness of the compound particles in raising the stress level

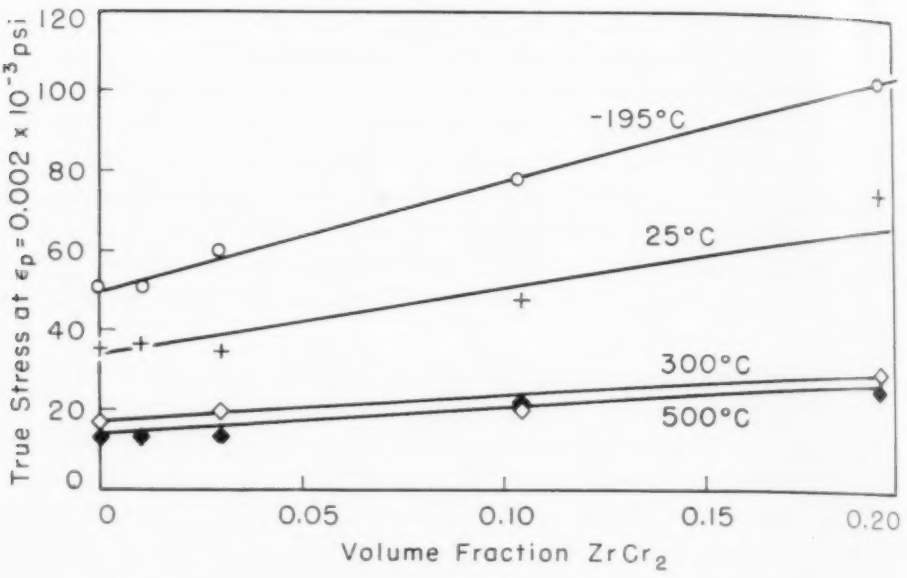


Fig. 10—True Stress at $\epsilon_p = 0.002$ (0.2% offset yield strength) Versus Volume Fraction $ZrCr_2$ at Various Test Temperatures.

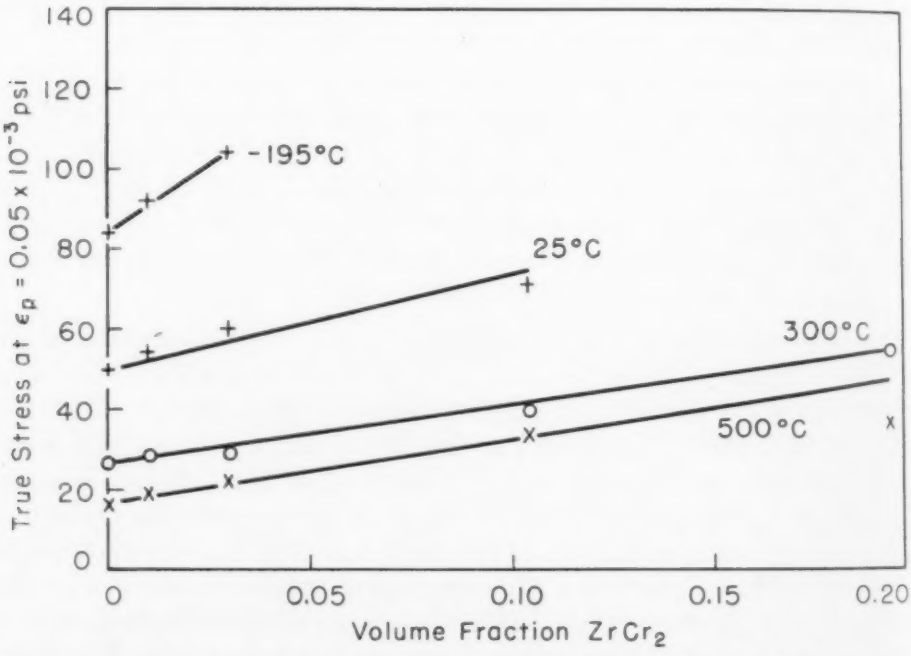


Fig. 11—True Stress at $\epsilon_p = 0.05$ Versus Volume Fraction $ZrCr_2$ at Various Test Temperatures.

of the flow curve is greater at larger strains. This would be anticipated from theory, since the function of particles would primarily be associated with strain hardening by piling up dislocation loops.

In contrast to the absolute increase in strength, the normalized or per cent increase in true stress at a given strain due to the presence of the second phase (calculated for a 0.1 volume fraction

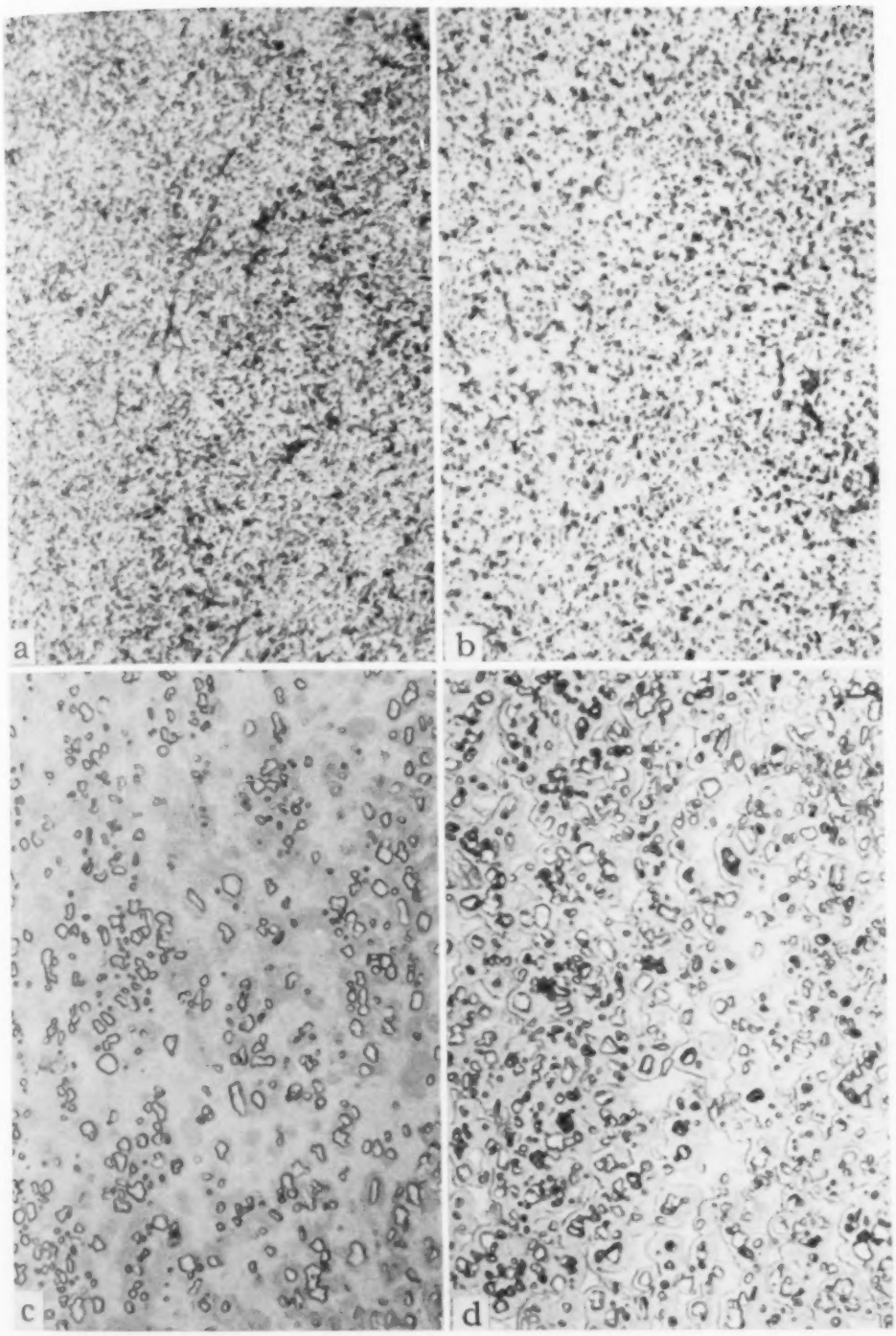


Fig. 12—Photomicrographs of Zirconium-Chromium Binary Alloys Showing Particles of $ZrCr_2$. Bright field, etchant: $HF+HNO_3$ and H_2O. (a)—1 Atomic % Chromium; (b)—3 atomic % chromium; (c)—10 atomic % chromium; (d)—18 atomic % chromium. ×1000.

$ZrCr_2$ alloy) is largest at 500°C (930°F), where the matrix unstrengthened by solution hardening is behaving as unalloyed zirconium and the particles may be acting to inhibit recovery or recrystallization.

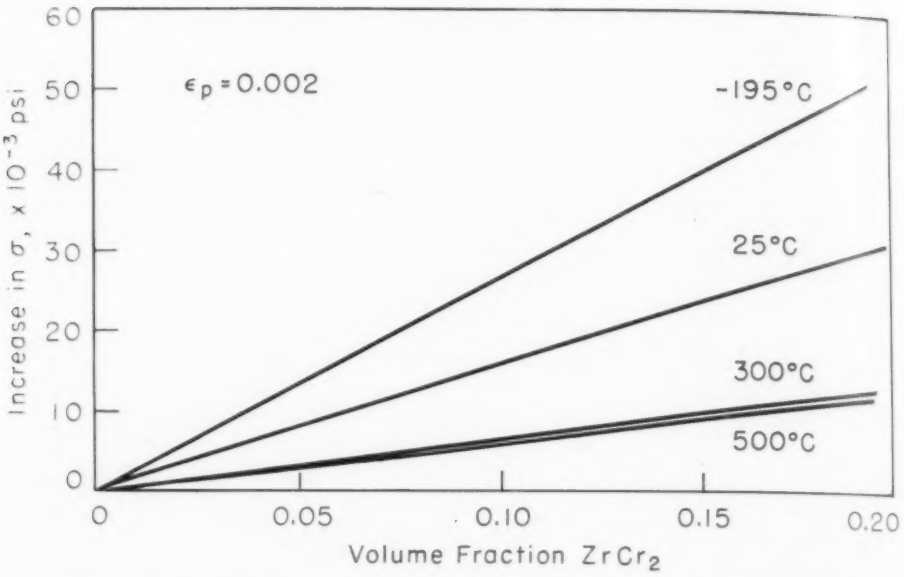


Fig. 13—Increase in True Stress at $\epsilon_p = 0.002$ (approximately the 0.2% offset yield stress) Versus Volume Fraction $ZrCr_2$ at Various Test Temperatures.

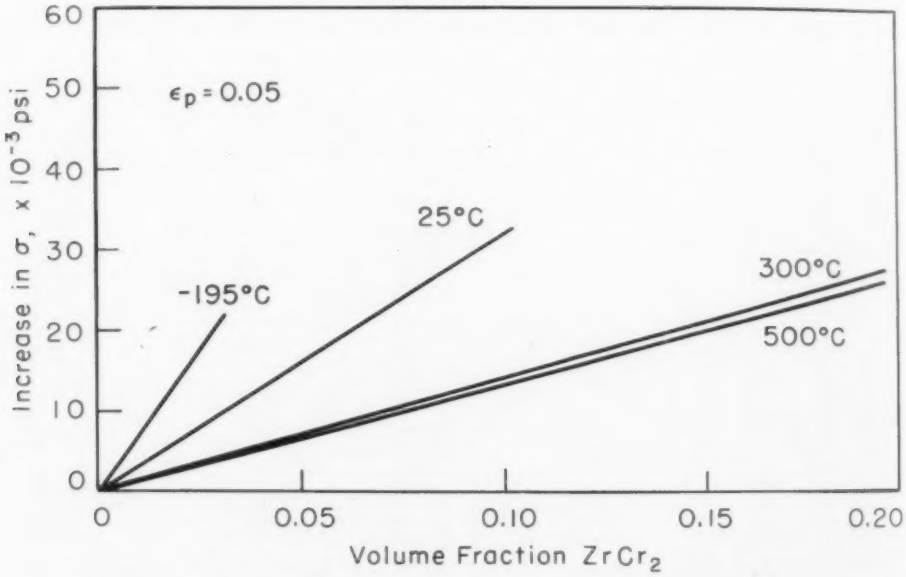


Fig. 14—Increase in True Stress at $\epsilon_p = 0.05$ Versus Volume Fraction $ZrCr_2$ at Various Test Temperatures.

The increases at —195, 25 and 300°C (—319, 77 and 570°F) were about the same (see Table IV). Similar to the absolute increase in strength, the normalized increase was greater at larger strains.

The theory of Fisher, Hart and Pry (15), an extension of Orowan's concept (16) of dislocation loops left encircling precipitate particles, suggests an appreciable hardening increment resulting from strain due to back stresses from the trapped loops. The maximum value of the stress increment, discussed further by Hart (17), is ob-

Table IV
Normalized Increase in Strength of a 0.1 Volume Fraction $ZrCr_2$ Alloy Due to Second-phase Particles

Test Temperature °C	Test Temperature °F	Per Cent Increase in True Stress at $\epsilon_p = 0.002$	$\epsilon_p = 0.02$	$\epsilon_p = 0.05$
−195	−319	52	65	67
25	77	58	57	75
300	570	40	61	60
500	930	45	80	88

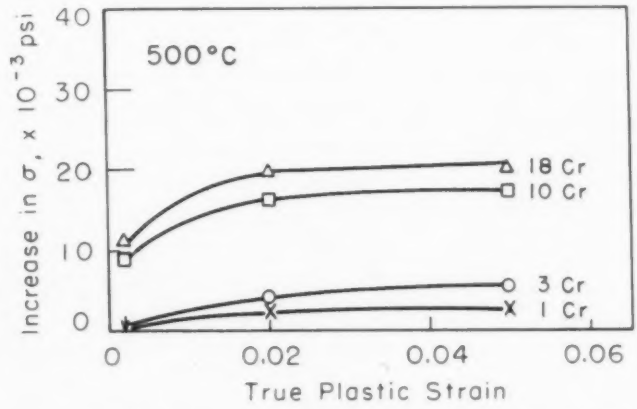


Fig. 15—Increase in True Stress Versus True Strain at 500°C (930°F) for the Several Zirconium-Chromium Alloys.

tained only after a finite amount of strain. Where there is no effect on yield strength and where there are spherical particles of uniform size, this maximum value is the steady-state value of the stress increment necessary to continue plastic deformation once shearing of the particles or surrounding matrix is sufficient to balance the resistance of newly-forming loops. Hart suggests a strain of about 10% to be necessary to achieve this steady-state maximum. In the case of copper-chromium alloys the maximum increment was reached after about 15% (18). The strains considered in the zirconium-chromium alloys are only as high as 5% because of the limited ductility of alloys rich in chromium, and so the increment of hardening due to $ZrCr_2$ should not be expected to be independent of strain. A marked effect of alloy additions on yield strength was found, as was a tendency toward a maximum strengthening increment in those alloys reaching larger strains. It seems apparent from these results, however, that alloys containing large amounts of second-phase particles are going to show a dependence of strengthening increment upon strain since the ductility is limited to strains less than 10%.

The modified[2] Orowan relation, $\sigma^* = Gb/r\sqrt{3f/2}$, was used to calculate the room-temperature yield stress due to particle harden-

[2]Using the relation from Fullman (13) for uniform spherical particles, $N_a = 3f/2\pi r^2$, where N_a is the number of particles per unit area, f is the volume fraction, and r is the radius of the particles; and the relation for the average distance of a particle from nearest neighbors in a plane, $D \cong 2/\sqrt{\pi N_a}$.

ing in a 10% chromium-zirconium alloy. The shear modulus value (19) was taken as 2540 kg/mm², b is the Burgers vector, r the average radius of the particles, and f the volume fraction. The calculation was made for the 0.104 volume fraction alloy (10 atomic % chromium) since the particles were large enough for an estimation of the particle radius (about 5×10^{-5} cm). The calculated value for σ^* was 900 psi, which is to be compared with the increment of increased stress due to particle hardening of about 13,000 and a yield strength of the particle hardened alloy, experimentally determined as 47,600 psi. (Since σ^* has been considered as an increment of strengthening due to particles as well as the actual yield strength which includes the strengthening due to particles, both values are compared here with the calculated σ^*.)

However, the calculated value of σ^* was considerably less than the yield stress of the unalloyed zirconium containing no $ZrCr_2$ particles and was also much less than the increment of strengthening due to the $ZrCr_2$ particles. Thus, the calculations from the Orowan relation are not consistent with these data. The limitations of the method of the Orowan Theory have been discussed by Hart (17).

Summary and Conclusions

1. The tensile properties of zirconium-chromium binary alloys containing up to 18 atomic % chromium are given for the temperature range −195 to 500°C (−319 to 930°F). The highest yield strength obtained at 500°C (930°F) was about 26,000 psi (for the 18% chromium alloy).

2. Stress-strain data indicate no significant solution hardening and thus no significant solid solubility of the compound in alpha zirconium in agreement with Domagala *et al*, (1), and Hayes and co-workers, (11).

3. A linear relation between flow stress and volume fraction of compound was observed, suggesting that the strengthening effect in this system follows the law of mixtures.

4. An increasing strengthening contribution by the particles of the compound was found at decreasing temperature, whereas the contribution in a normalized sense (per cent increase in strength compared to the matrix without $ZrCr_2$ compound particles) was essentially constant in the temperature range where the alloys were stable. At the highest temperature, a greater normalized contribution was made.

5. The particle-hardening effect was found to increase with increasing strain in the range 0.002 to 0.05 true strain.

Acknowledgments

The author wishes to acknowledge the many helpful comments

and criticisms of W. R. Hibbard, Jr., R. W. Guard, R. L. Fullman, and E. W. Hart. He is also indebted to L. J. Hartford and other members of the Metallurgy and Ceramics Research Department for the experimental portion of the work, and to Mrs. M. V. Doyle, Miss R. M. Kimura, and Miss B. J. Drummond for the calculations in reducing the experimental data. This work was supported by the United States Atomic Energy Commission under Contract No. W-31-109-Eng-52.

References

1. R. F. Domagala, D. J. McPherson and M. Hansen, "System Zirconium-Chromium," *Transactions*, American Institute of Mining and Metallurgical Engineers, Vol. 197, 1953, p. 279.
2. C. T. Anderson, E. T. Hayes, A. H. Roberson and W. J. Kroll, "A Preliminary Survey of Zirconium Alloys," Bureau of Mines, Report of Investigations, 4658, U. S. Department of Interior, March 1950.
3. W. Chubb and G. T. Muehlenkamp, Battelle Memorial Institute Report U. S. AEC BMI-938, August 11, 1954.
4. J. H. Keeler, "The Tensile Characteristics of Unalloyed Zirconium at Low and Moderate Temperatures," TRANSACTIONS, American Society for Metals, Vol. 47, 1955, p. 157.
5. J. H. Hollomon and J. D. Lubahn, "The Flow of Metals at Elevated Temperatures," General Electric Review, Part I, Vol. 50, February 1947, p. 28; Part II, Vol. 50, April 1947, p. 44.
6. J. D. Lubahn, "Simultaneous Aging and Deformation in Metals," TRANSACTIONS, American Institute of Mining and Metallurgical Engineers, Vol. 105, 1949, p. 702.
7. J. D. Lubahn, "Strain Aging Effects," TRANSACTIONS, American Society for Metals, Vol. 44, 1952, p. 643.
8. J. D. Lubahn, "Creep-Tension Relations at Low Temperatures," *Proceedings*, American Society for Testing Materials, Vol. 52, 1952, p. 905.
9. R. W. Guard, J. H. Keeler and S. F. Reiter, "Observations on Elevated Temperature Tensile Deformation," *Journal of Metals*, Vol. 6, February 1954, p. 266; *Transactions*, American Institute of Mining and Metallurgical Engineers, Vol. 200, 1954, p. 226.
10. H. Wallbaum, Naturwiss, Vol. 30, 1942, p. 149.
11. E. T. Hayes, A. H. Roberson and M. H. Davies, "Zirconium-Chromium Phase Diagram," *Journal of Metals*, March 1952; *Transactions*, American Institute of Mining and Metallurgical Engineers, Vol. 194, 1952, p. 304.
12. W. Rostoker, "Allotropy in the Phase $ZrCr_2$," *Journal of Metals*, Vol. 5, February 1953, p. 304; *Transactions*, American Institute of Mining and Metallurgical Engineers, Vol. 197, 1953, p. 304.
13. R. L. Fullman, "Measurement of Particle Sizes in Opaque Bodies," *Journal of Metals*, Vol. 5, March 1953; *Transactions*, American Institute of Mining and Metallurgical Engineers, Vol. 197, 1953, p. 447.
14. J. H. Keeler, to be published.
15. J. C. Fisher, E. W. Hart and R. H. Pry, "The Hardening of Metal Crystals by Precipitate Particles," ACTA METALLURIGICA, Vol. 1, 1953, p. 336.
16. E. Orowan, *Symposium on Internal Stress in Metals and Alloys*, Institute of Metals, London 1948, p. 451.
17. E. W. Hart, RELATION OF PROPERTIES TO MICROSTRUCTURE, 1954, p. 95, published by American Society for Metals, Cleveland.
18. W. R. Hibbard, Jr., and E. W. Hart, "Dispersion Hardening of Copper-Chromium Alloys," *Journal of Metals*, Vol. 7, January 1955, p. 200; *Transactions*, American Institute of Mining and Metallurgical Engineers, Vol. 203, 1955, p. 200.
19. W. Koster, American FIAT Review, Vol. 31, 1950, p. 55.

DISCUSSION

Written Discussion: By W. Chubb, metallurgical engineer, Battelle Memorial Institute, Columbus, Ohio.

Dr. Keeler's results on zirconium-chromium alloys show considerable variance from those obtained by Muehlenkamp and myself (3). In particular, I notice that Dr. Keeler gives a value of 35,000 psi for the 0.2% offset yield strength of arc-melted iodide zirconium annealed at 800°C (1470°F). Our value for arc-melted, iodide zirconium annealed at 700°C (1290°F) was 15,000 psi. Values of the yield strength of extremely pure zirconium range from 7000 to 10,000 psi.[3] R. M. Treco[4] gives 18,700 psi as the 0.2% offset yield strength of zirconium containing 0.055 weight % oxygen. I wonder if Dr. Keeler can offer an explanation for the unusually high value obtained.

As a word of caution to anyone else desiring to roll zirconium alloys in steel cans, there is a eutectic in the zirconium-iron system at 934°C (1705°F). Rolling of zirconium in contact with steel near, or above 934°C (1705°F), can easily result in catastrophe from rapid reaction of iron and zirconium to form liquid.

Author's Reply

The high value for the yield strength of unalloyed zirconium used in this investigation resulted from the presence of oxygen and nitrogen impurity. The unalloyed zirconium was prepared by arc-melting in a conventional single hearth furnace in the same manner that the zirconium-chromium binary alloys were prepared. In the early part of this investigation when the high chromium compositions were melted, only this one furnace was available for melting small ingots. Later a multihearth furnace was constructed and then ingots having the benefit of a prior "getter" melt and having a fine grain size exhibited a yield strength of 17,000 psi at room temperature. However, for proper interpretation and handling of results, the zero chromium composition (or unalloyed zirconium) must be prepared in a manner similar to that of the alloys containing chromium.

Later test data using zirconium and zirconium-chromium alloys with lower impurity content confirmed the relatively minor strengthening effect of chromium. In these data, however, the general stress level was lower as a result of the lower impurity level. Since only the low chromium levels were re-examined and the narrow composition range does not so clearly illustrate the effect of volume fraction second phase, the data was omitted for sake of briefness. (A report concerning lower impurity level material and volume fraction second phase effects is now being prepared for publication.)

If only the added strength due to chromium content is considered by subtracting the strength of unalloyed zirconium from that of the alloy, the results of Chubb and Muehlenkamp (3), Anderson, Hayes, Roberson, and Kroll (2), and this investigation do not differ widely.

In regard to sheath rolling, fortunately the oxide coating on the inner surfaces of the sheathes minimizes the metal to metal contact and bonding of the iron and zirconium is inhibited.

---

[3] B. Lustman and F. Kerze, "The Metallurgy of Zirconium," published by McGraw-Hill, 1955.
[4] "ZIRCONIUM AND ZIRCONIUM ALLOYS," 1953, published by the American Society for Metals, Cleveland.

ZIRCONIUM-GERMANIUM ALLOY SYSTEM

By O. N. Carlson, P. E. Armstrong and H. A. Wilhelm

Abstract

The zirconium-germanium system has been investigated by microscopic, thermal and X-ray methods. Four intermediate phases, Zr_3Ge, Zr_5Ge_3, ZrGe and $ZrGe_2$ have been proposed on the basis of microstructures and X-ray data. Zr_3Ge undergoes a peritectic transformation at 1585°C (2885°F), ZrGe at 2240°C (4065°F) and $ZrGe_2$ at 1520°C (2770°F). Zr_5Ge_3 melts congruently at approximately 2300°C (4170°F). There is a eutectic at 1535°C (2795°F) at the composition 7.7 weight per cent germanium. There is limited solid solubility of germanium in zirconium and negligible solid solubility of zirconium in germanium. (ASM-SLA Classification: M24, Zr, Ge)

Introduction

IN RECENT years zirconium metal, because of its favorable nuclear, mechanical and chemical properties, has assumed major importance as a structural material in nuclear reactors. The effect of alloying additions upon the mechanical properties and corrosion resistance of zirconium has therefore been of considerable interest.

Since data regarding the fundamental properties and phase relationships with other elements are important in considering applications of a metal, the investigation of the zirconium-germanium system has been undertaken. This work is a part of a research program on the physical metallurgy of zirconium and its alloys. Although one compound, $ZrGe_2$, has been reported by Smithells (1),[1] no reference to any work on the phase diagram of this system has been found in the literature.

Experimental Procedures

Materials. At the outset of this investigation the only zirconium readily obtainable was grade 3 crystal bar from Westinghouse Atomic Power Division at Pittsburgh, Pennsylvania. The surface film of corrosion product resulting from grade designation tests was removed by wire brushing. Later grade 1 crystal bar zirconium became available from the same source and this was used in most of the alloys investigated.

[1]The figures appearing in parentheses pertain to the references appended to this paper.

The authors, O. N. Carlson, P. E. Armstrong and H. A. Wilhelm are associated with Institute for Atomic Research and Department of Chemistry, Iowa State College, Ames, Iowa. Manuscript received April 18, 1955.

Germanium metal in the form of irregular lumps and in powder form was obtained from the Belmont Smelting and Refining Company. According to the suppliers' specifications the lump metal was of a 99.9% purity whereas the powder was spectrographically pure. The powder was converted to massive form by first heating to 650°C (1200°F) in a hydrogen atmosphere to reduce any residual oxide, then melting under a vacuum of less than 10^{-4} mm of mercury in a graphite container. This material was easily fractured into smaller pieces for use in sample preparation.

Preparation of Alloys

Alloys weighing 20 to 80 grams were prepared by arc melting the massive metals together under a helium atmosphere, using a water-cooled copper crucible and a tungsten electrode. Alloys containing greater than 80% germanium were prepared by co-melting in graphite in vacuo.

Samples were carefully weighed before and after arc melting, the loss in weight being ascribed to volatilization of germanium. Chemical analyses were obtained on several of the alloys and the results were found to agree quite well with the compositions calculated from weight losses.

In the preparation of alloys containing very low percentages of germanium, portions of a chemically analyzed 7.7% germanium alloy were added to zirconium. Weight losses on alloys thus prepared were extremely small, indicating reasonable accuracy in the estimated compositions. Table I lists the alloys employed in this investigation and the composition of each.

The analyst felt that the germanium analyses tended to be low while the zirconium values were considered to be more accurate. For

Table I
Zr-Ge Alloys Used in Investigation

Intended Composition wt. % Ge	Chemical Analysis wt. % Ge	Chemical Analysis wt. %Zr	Estimated from Weight Loss wt. % Ge	Intended Composition wt. % Ge	Chemical Analysis wt. % Ge	Chemical Analysis wt. % Zr	Estimated from Weight Loss wt. % Ge
0.17			0.17	25.0			24.0
0.50			0.47	30.0		70.82	27.4
0.60			0.50	32.0			30.7
1.00			0.95	35.0	30.60	68.75	31.2
3.0			—	37.5			35.3
7.0	5.96	93.8	6.1	40.0			34.7
8.0	6.0	92.3	7.7	41.0			38.5
10.0			10.0	44.0			43.0
12.0			12.0	46.0			45.1
14.0	13.0	87.2	13.8	54.3			51.0
16.0	12.5	85.0	15.0	56.0			53.3
18.0		82.1	18.0	61.4	56.6	39.0	61.0
18.5			15.8	70			68.1
19.5			17.6	80			78
20.0			17.8	83			83
20.0			19.5	96			96
22.0	20.4	80.5	20.2	98			98

this reason the compositions of most of the alloys will be referred to on the basis of the zirconium analysis or calculated from the weight loss.

Examination of Alloys

The presence of peritectic reactions in the system resulted in nonequilibrium structures in many of the alloys as-arc-melted. Homogenization treatments were conducted on most of the alloys in this investigation, the heating being carried out either in induction or graphite resistor furnaces in vacuo. The specimens were contained in a graphite crucible during this treatment. High temperature quenches were done by suspending the samples in the furnace with a fine tungsten wire. At the desired time, the tungsten wire was fused by a high electric current, dropping the sample into a reservoir of molten Wood's metal while still under vacuum.

The melting temperatures of most of the alloys in this system are above the range of commonly used thermocouples. Thus two other techniques have been employed in locating the eutectic and peritectic horizontals. In one method a small hole was drilled in the sample and the melting temperature was observed by sighting on the hole with an optical pyrometer during heating. The first appearance of liquid in the hole was readily detected and has been called the solidus temperature. The incipient melting method was used for temperatures around 2000°C (3630°F). This consists of heating small samples to various temperatures, quenching or rapidly cooling, and then examining the microstructures for evidence of partial melting.

For measuring transitions occurring in the lower temperature range, cooling curves were run using a differential thermocouple circuit. This circuit consisted of a chromel-alumel thermocouple placed in the alloy specimen and another in a reference specimen, usually of pure nickel. Both the sample and the neutral body were heated in a resistance furnace in vacuo. A Leeds and Northrup Speedomax x-y recorder measured simultaneously the specimen temperature and the temperature difference between the two bodies.

Experimental Results

On the basis of microscopic evidence, X-ray diffraction data, thermal analyses and melting observations, a phase diagram has been proposed. The proposed diagram together with a plot of the thermal data are shown in Fig. 1.

Four intermediate phases have been detected in the system and have been assigned formulae based upon microscopic and X-ray data. These phases are a stable high melting compound, Zr_5Ge_3, and peritectic compounds corresponding to Zr_3Ge, ZrGe and $ZrGe_2$.

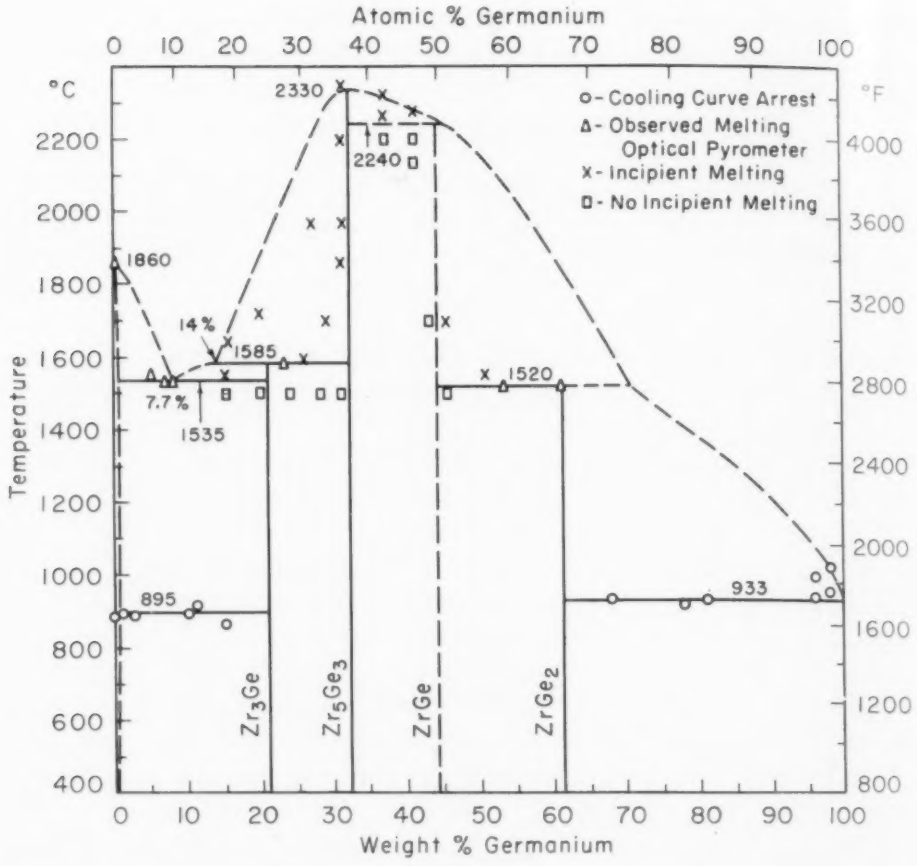


Fig. 1—Zirconium-Germanium Phase Diagram.

The melting point of zirconium is lowered by the addition of germanium forming a eutectic at 1535°C (2795°F). A 1.0 wt. % germanium alloy contains a small but detectable amount of the eutectic as can be seen in Fig. 2, and a 7.7% alloy (Fig. 3) is interpreted as lying very close to the eutectic composition. The peritectic compound, Zr_3Ge, can be seen in a 13% alloy (Fig. 4) as the primary phase in a eutectic matrix. The peritectic nature of this phase is evident in an as-arc-melted 15% alloy (Fig. 5) in which Zr_3Ge surrounds the initially precipitated crystals of Zr_5Ge_3. The reaction is Zr_5Ge_3+melt (14% Ge)$\rightleftharpoons Zr_3Ge$ at 1585°C (2885°F). This reaction causes considerable difficulty in attaining complete equilibrium in alloys close to the theoretical composition of Zr_3Ge. Fig. 6 is a micrograph of a 20.4% Ge alloy which has been annealed for 20 hours at 1500°C (2730°F). This alloy consists principally of Zr_3Ge but contains small areas of unreacted zirconium and Zr_5Ge_3. The peritectic horizontal has been located at 1585°C (2885°F) by observed partial melting and by quenching experiments as plotted in Fig. 1.

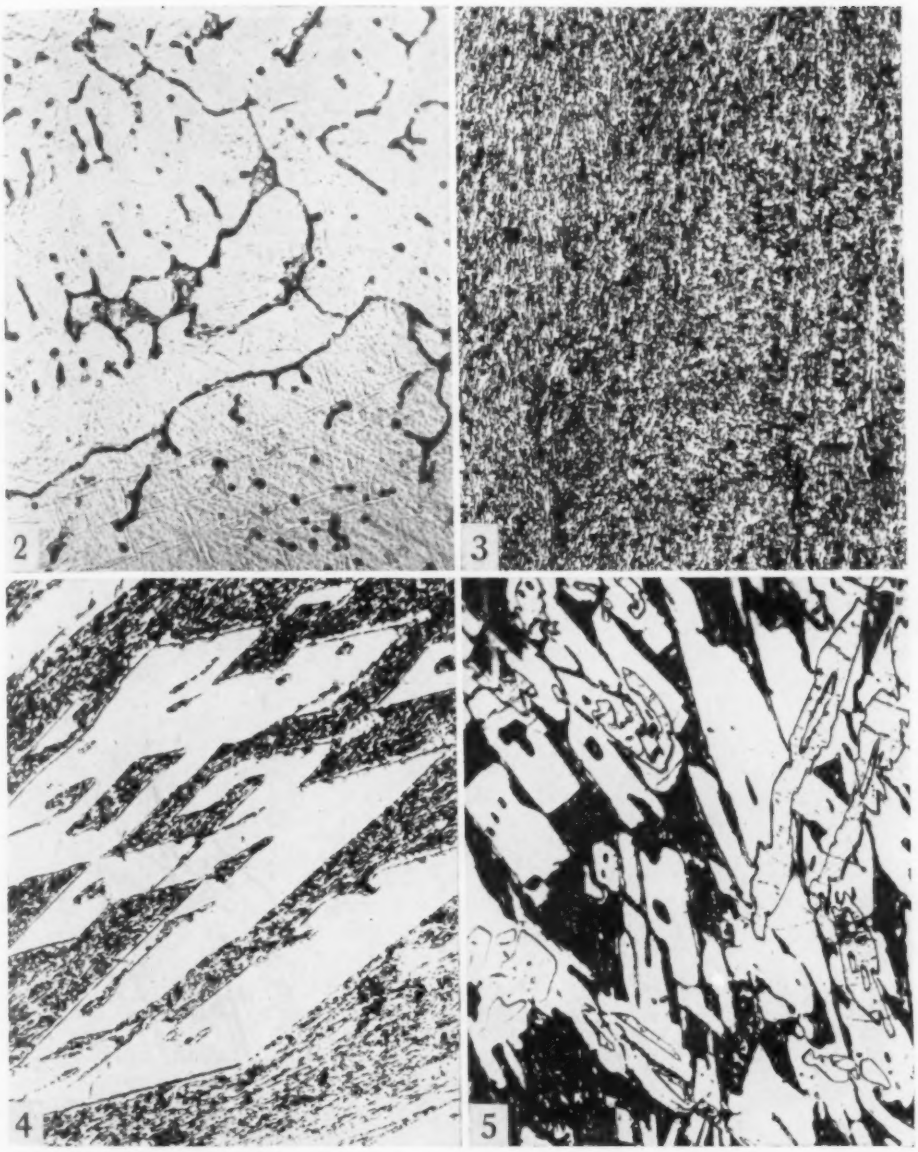


Fig. 2—1% Ge Alloy As-Arc-Melted. Primary zirconium with eutectic along grain boundaries. Etchant: 2 parts HNO_3, 1 part H_2SO_4, 1 part HF, 1 part H_2O. ×250.

Fig. 3—7.7% Germanium Alloy As-Arc-Melted. Eutectic structure. Etchant: 1% HF in conc. HNO_3. ×250.

Fig. 4—13% Germanium Alloy As-Arc-Melted. Primary Zr_3Ge in eutectic matrix. Etchant: 1% HF in conc. HNO_3. ×250.

Fig. 5—15% Germanium Alloy As-Arc-Melted. Primary Zr_5Ge_3 surrounded by peritectically formed Zr_3Ge, in eutectic matrix. Etchant: 1% HF in conc. HNO_3. ×250.

X-ray powder patterns of an 18% alloy have been indexed on the basis of a hexagonal lattice with a = 8.14 Å and c = 7.17 Å. From atomic volume and density considerations the phase corresponds most simply to the formula Zr_3Ge with 5 molecules/unit cell.

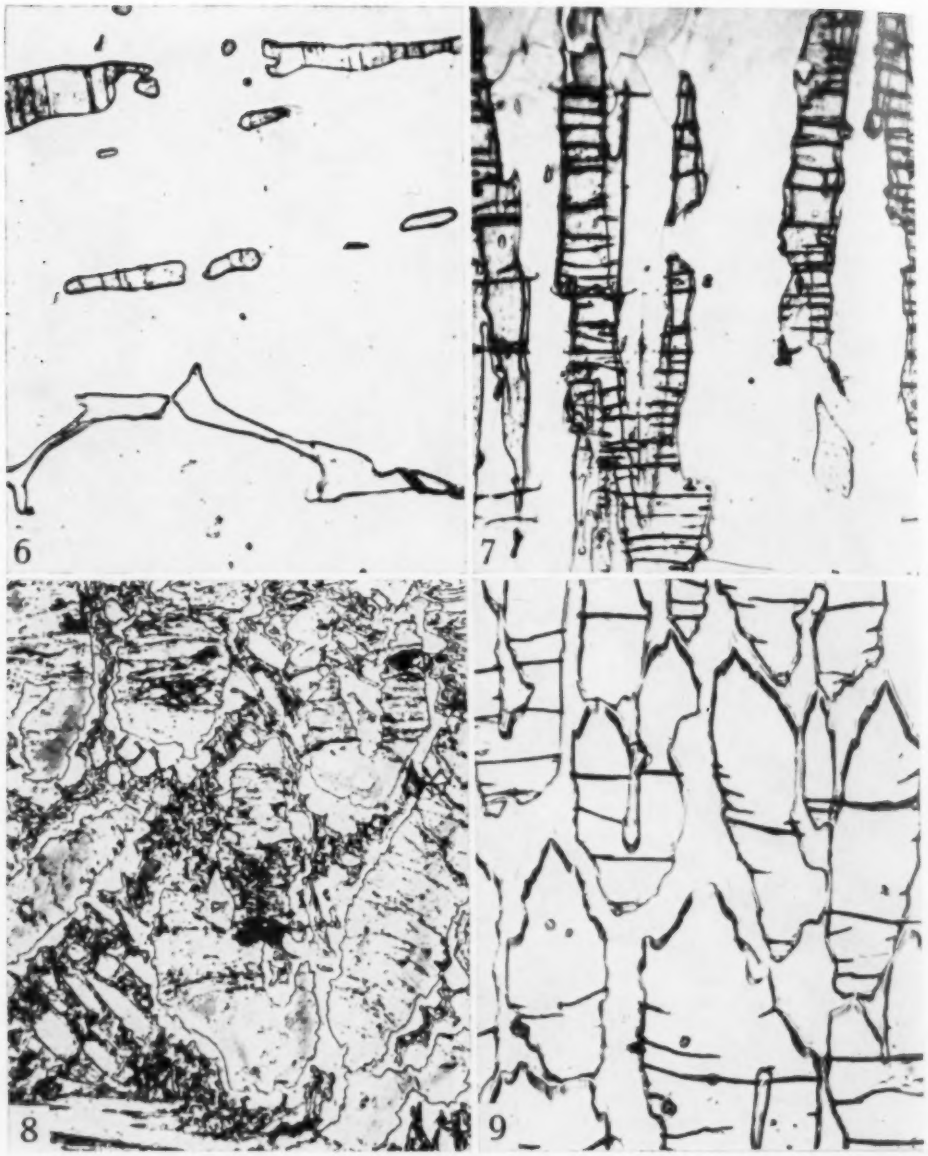


Fig. 6—20.4% Germanium Alloy Annealed at 1500°C (2732°F) for 20 Hours. Unreacted Zr (light phase) and Zr_5Ge_3 (cracked phase) in matrix of Zr_3Ge. Etchant: 2 parts HNO_3, 1 part H_2SO_4, 1 part HF, 1 part H_2O. ×250.

Fig. 7—24% Germanium Alloy Annealed at 1500°C (2732°F) for 5 Hours. Primary Zr_5Ge_3 in clear matrix of Zr_3Ge. Etchant: 2 parts HNO_3, 1 part H_2SO_4, 1 part HF, 1 part H_2O. ×250.

Fig. 8—24% Germanium Alloy Annealed at 1700°C (3092°F) for 10 Minutes and Quenched. Primary Zr_5Ge in coarsened eutectic matrix. Etchant: 1% HF in conc. HNO_3. ×250.

Fig. 9—27.5% Germanium Alloy Annealed at 1500°C (2732°F) for 20 Hours. Primary Zr_5Ge_3 in Zr_3Ge (clear phase) matrix. Etchant: 2 parts HNO_3, 1 part H_2SO_4, 1 part HF, 1 part H_2O. ×250.

A 24% alloy which has been annealed at 1500°C (2730°F) contains mixed crystals of Zr_3Ge and Zr_5Ge_3 as is evident from Fig. 7. That the Zr_3Ge phase of this alloy undergoes incongruent melting

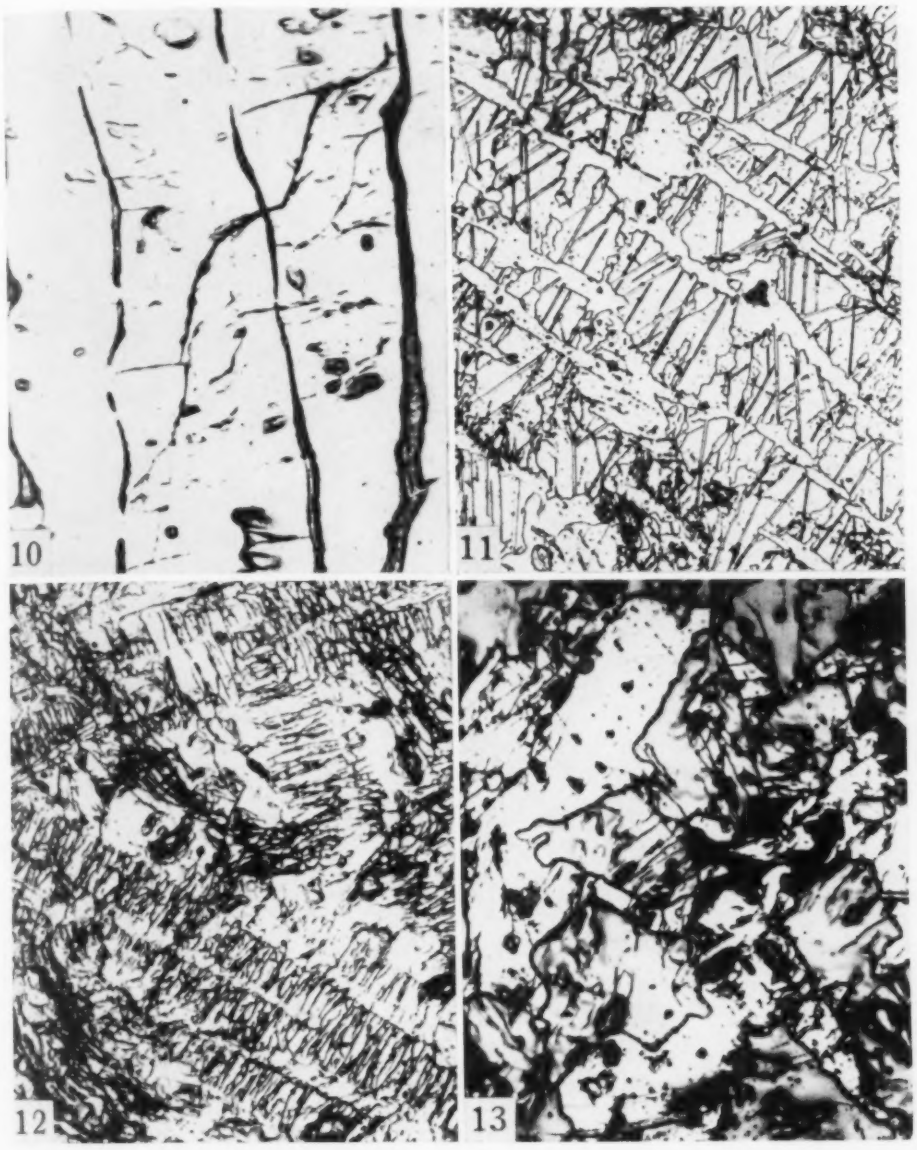


Fig. 10—31.2% Germanium Alloy Annealed at 1350°C (2462°F) for 20 Hours. Primary Zr_5Ge_3 with Zr_3Ge (dark areas) along crystal boundaries. Etchant: 2 parts HNO_3, 1 part H_2SO_4, 1 part HF, 1 part H_2O. ×250.

Fig. 11—35.3% Germanium Alloy Annealed at 1650°C (3002°F) for 20 Hours. Mixed crystals of Zr_5Ge_3 (with cracks) in ZrGe matrix. Etchant: 2 parts HNO_3, 1 part H_2SO_4, 1 part HF, 1 part H_2O. ×250.

Fig. 12—43% Germanium Alloy Annealed at 1700°C (3092°F) for 1½ Hours. Badly cracked one-phase alloy of ZrGe. Etchant: 2 parts HNO_3, 1 part H_2SO_4, 1 part HF, 1 part H_2O. ×250.

Fig. 13—53.3% Germanium Alloy Annealed at 1500°C (2732°F) for 4 Hours. Darker primary crystals of ZrGe in matrix of $ZrGe_2$. Etchant: 2 parts HNO_3, 1 part H_2SO_4, 1 part HF, 1 part H_2O. ×250.

above 1585°C (2885°F) is shown by quenching the alloy from 1700°C (3090°F) (see Fig. 8).

Microscopic investigation has provided evidence for another

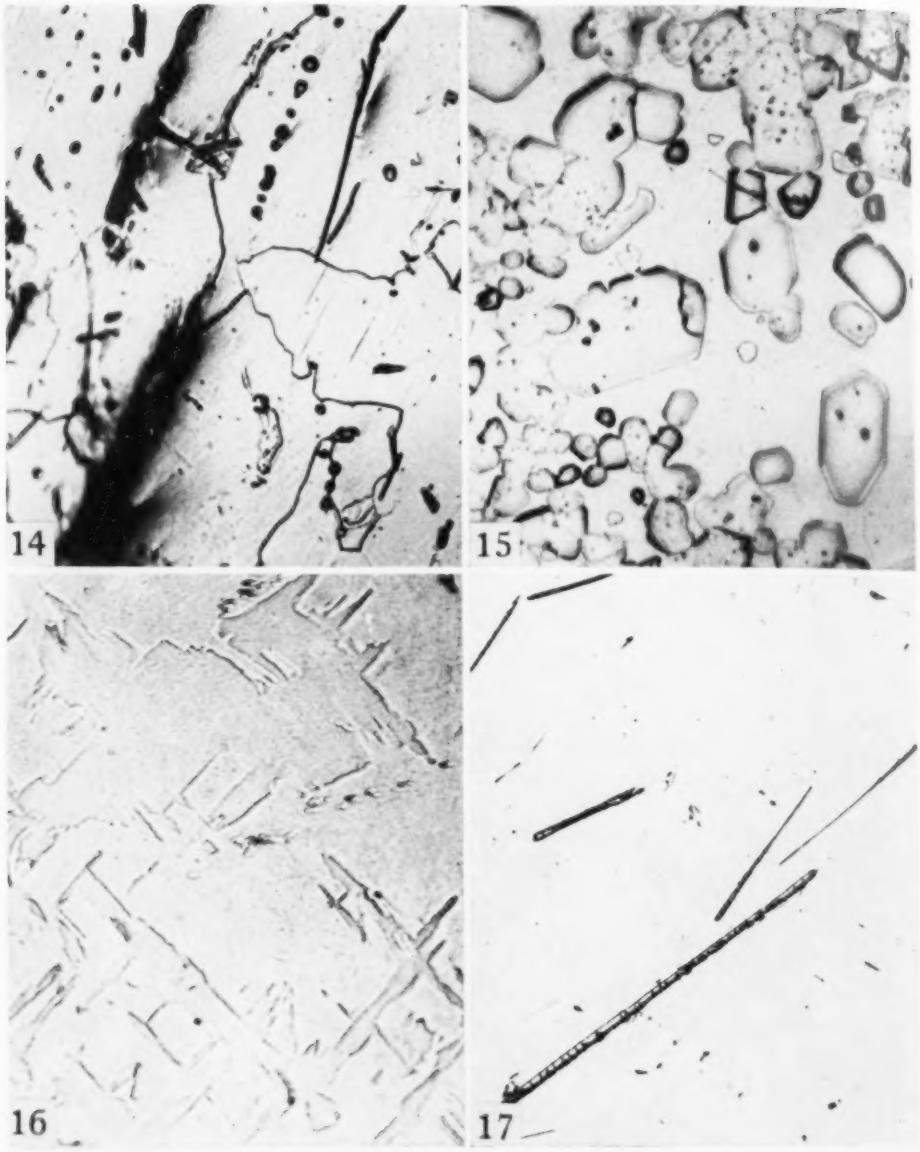


Fig. 14—61% Germanium Alloy Annealed at 1350°C (2462°F) for 20 Hours. Nearly single-phase $ZrGe_2$. Etchant: 2 parts HNO_3, 1 part H_2SO_4, 1 part HF, 1 part H_2O. ×250.

Fig. 15—81% Germanium Alloy As-Cast. $ZrGe_2$ crystals in a matrix of germanium. ×250.

Fig. 16—0.5% Germanium As-Arc-Melted. Decomposed beta zirconium with no evidence of a second phase. Etchant: 2 parts HNO_3, 1 part H_2SO_4, 1 part HF, 1 part H_2O. ×250.

Fig. 17—98% Germanium Alloy As-Cast. Needle-like crystals of $ZrGe_2$ in a germanium matrix. Etchant: 1% HF in conc. HNO_3. ×75.

one-phase region occurring around 32% germanium. Figs. 9 and 10 are micrographs of a 27.5% and a 31.2% germanium alloy respectively. From this and other similar evidence the formula Zr_5Ge_3 (theoretical composition 32.2% Ge) has been assigned to this phase.

The compound is quite brittle and cracks upon solidification, resulting in alloys which require very careful metallographic preparation in order to reveal their actual microstructures. Zr_5Ge_3 melts congruently at $2300 \pm 50°C$ ($4170 \pm 90°F$).

The 31.2% alloy was annealed at 1960°C (3550°F) and an X-ray powder pattern taken. This diffraction pattern has been indexed as hexagonal with $a = 7.99$ Å and $c = 5.54$ Å. The formula Zr_5Ge_3 with 2 molecules/unit cell is in agreement with atomic volume and density considerations. The X-ray density of 7.29 g./cc. calculated from atom weights and cell dimensions compares favorably with the measured density of 7.12 g./cc. of the 31.2% alloy. The volume of the unit cell, 306 Å^3, is only slightly smaller than the calculated cell volume of 326 Å^3 based on atom volumes in the respective metal lattices. This structure appears to be isomorphic to that of Zr_5Sn_3 as found by H. Smith (2), and to Ti_5Sn_3, Ti_5Ge_3, and Ti_5Si_3 reported by Pietrokowsky and Duwez (3).

At higher germanium compositions evidence for a third intermediate phase appears. A 35.3% Ge alloy (Fig. 11) is observed to contain mixed crystals of Zr_5Ge_3 and another equally brittle phase. As can be seen from Fig. 12 the 43% Ge alloy lies close to a one phase region. This phase has been tentatively assigned the formula ZrGe corresponding to 44.2% germanium. Based on incipient melting experiments ZrGe undergoes peritectic decomposition at about 2240°C (4065°F). These data have been plotted in Fig. 1. Efforts to index the complex powder pattern of this phase have been unsuccessful although the presence of such a phase has been confirmed by powder data.

At higher concentrations of germanium a fourth intermetallic phase, $ZrGe_2$, appears. A 53.3% germanium alloy contains about equal quantities of the phases ZrGe and $ZrGe_2$ (see Fig. 13), whereas a 61% alloy consists almost entirely of $ZrGe_2$ (Fig. 14). A single crystal of this phase was isolated and from precession data it was shown to belong to the orthorhombic space group D^{17}_{2h}-Cmcm with $a = 3.76$ Å, $b = 14.97$ Å and $c = 3.79$ Å. This was in agreement with values reported for $ZrGe_2$ by Smithells (1). J. F. Smith (4) has determined the structure for the compound from intensity data. There are 4 molecules/unit cell with atoms located at three four-fold positions:

$$0\ y\ \tfrac{1}{4};\ 0\ \bar{y}\ \tfrac{3}{4};\ \tfrac{1}{2},\ \tfrac{1}{2}+y,\ \tfrac{1}{4};\ \tfrac{1}{2},\ \tfrac{1}{2}-y,\ \tfrac{3}{4}$$

The parameters have been evaluated as follows:

$$y_{Zr} = 0.106,$$
$$y_{Ge_I} = 0.750,$$
$$y_{Ge_{II}} = 0.445.$$

Alloys in the composition region around $ZrGe_2$ undergo partial melting at 1520°C (2770°F) as can be seen from the data plot of Fig. 1. This is interpreted as a peritectic horizontal.

An alloy containing 81% germanium contains two distinct phases as shown by Fig. 15. X-ray powder patterns taken of this alloy identify the phases present as $ZrGe_2$ and germanium. The solidus in this region has been determined from cooling curves as a temperature horizontal at 933°C (1710°F), near the melting point of germanium.

There appears to be some solid solubility of germanium in zirconium. A 0.5% Ge alloy contains one phase as-arc-melted (see Fig. 16). This would indicate a maximum solid solubility at the 1535°C (2795°F) eutectic temperature of slightly more than 0.5% germanium since, as was shown in Fig. 2, a 1.0% germanium alloy contains areas of eutectic. The 0.5% alloy after annealing at 850°C (1560°F) for 72 hours contained only a single phase while the eutectic structure remained in the 1% alloy after the same treatment. This indicates an alpha solid solubility of at least 0.5% but less than 1% germanium at the transformation temperature.

There appears to be no solid solubility of zirconium in germanium. A 98% germanium alloy contains primary crystals of $ZrGe_2$ in a germanium matrix (see Fig. 17). The lattice constant was determined for the germanium phase in a 78% germanium alloy and found to be 5.655 ± 0.002 Å. This when compared with the measured value of 5.657 ± 0.002 Å for the germanium used in this work, indicates that there is little if any solid solubility of zirconium in germanium.

Discussion of Results

Although empirical formulae have been assigned to all four intermediate phases, only $ZrGe_2$ has been definitely identified. Although it has been established in this investigation that a one phase region occurs very close to the theoretical composition of Zr_3Ge, the structure and exact composition of this phase have not been fully determined. A powder pattern of the phase contains over 70 lines of which all but 6 or 8 can be adequately accounted for by the proposed hexagonal lattice. No intensity calculations have been made, however, and there is rather poor agreement between the X-ray density of 6.48 g./cc. and the measured density, 6.84 g./cc.

The compound, Zr_5Ge_3, seems to be adequately verified by the X-ray and metallographic evidence presented above and by its apparent isomorphism to identified compounds in similar systems.

The formula ZrGe has been tentatively assigned from microscopic evidence and also on the basis of analogous compounds ZrSi and ZrSn reported by Schachner (5) and by Lundin (6) respec-

tively. Several attempts have been made to isolate a single crystal of this phase. In all cases what appeared to be single crystals later were shown by rotation patterns to be oriented polycrystalline bundles.

The melting point of germanium was found to be quite sensitive to impurities and to vary from 933 to 948°C (1711 to 1740°F) for the germanium used in this study. In an effort to obtain a purer form of the metal for melting point studies C.P. GeO_2 was obtained from Fairmount Chemical Company. This was reduced with purified hydrogen at 650°C (1200°F) and melted in a graphite crucible under a high vacuum. The melting point was determined on several samples of this material as 925 ± 2°C (1697°F). This value is about 10 degrees lower than the value of 936°C (1717°F) reported by Greiner (7) for very pure germanium and far below the older literature value of 958°C (1756°F) (8). The electrical resistivity of the purest germanium used by the authors was 3.2 ohm-centimeters compared to 20 ohm-centimeters for the metal used by Greiner. A melting point of 936°C (1717°F) has been used in the construction of the phase diagram.

Data on the zirconium transformation horizontal at 895°C (1643°F) have been obtained from alloys prepared from grade 3 crystal bar. This material transforms over a range of temperatures from 860 to 880°C (1580 to 1615°F) probably due to oxygen contamination. The authors feel that the temperature of the 895°C horizontal would be somewhat lower if the alloys were prepared from grade 1 zirconium, but would still be peritectic in nature. Because of this degree of uncertainty in these data the phase relationships near the transformation temperature of pure zirconium have not been fully represented in the diagram.

Summary

An investigation of the zirconium-germanium system covering the complete composition range was conducted and the following salient features were established:

(a) The maximum solid solubility of germanium in zirconium is between 0.5 and 1.0% germanium.

(b) A eutectic forms between zirconium and the zirconium-rich compound, Zr_3Ge, at 7.7% germanium. The eutectic temperature is 1535°C (2795°F).

(c) The proposed compound, Zr_3Ge at 20.9% Ge decomposes peritectically at 1585°C (2885°F) according to the reaction $Zr_3Ge \rightleftharpoons Zr_5Ge_3$ + melt (14% Ge).

(d) Zr_5Ge_3 at 32.2% Ge melts congruently at 2300 ± 50°C (1470 ± 90°F).

(e) Another peritectic compound, ZrGe, has the proposed formula ZrGe at 44.2% Ge. It decomposes at 2240°C (4075°F) according to the reaction $ZrGe \rightleftharpoons Zr_5Ge_3 + \text{melt}$.

(f) The fourth compound of the system, $ZrGe_2$, exists at 61.4% Ge, and decomposes at 1520°C (2770°F) according to the reaction $ZrGe_2 \rightleftharpoons ZrGe + \text{melt}$.

(g) The solidus in the germanium-rich region occurs as a temperature horizontal at 933°C (1711°F).

Acknowledgments

The authors would like to express their thanks to Dr. C. V. Banks and Mr. Robert Bachman for the chemical analyses and to Dr. J. F. Smith and Mr. Harold Smith for their assistance and advice in the X-ray investigations.

References

1. C. J. Smithells, *Metals Reference Book*, 1949, p. 187, 214. Butterworths Scientific Publications, London.
2. H. Smith, Private Communication, Ames Laboratory, April 1955.
3. P. Pietrokowsky and P. Duwez, "Crystal Structure of Ti_5Si_3, Ti_5Ge_3, and Ti_5Sn_3," *Transactions*, American Institute of Mining and Metallurgical Engineers, Vol. 3, 1951; *Journal of Metals*, September 1951, p. 772.
4. J. F. Smith, Private Communication, Ames Laboratory, April 1955.
5. H. Schachner, H. Nowotny, and H. Kudielka, "Die Kristallstrukturen von ZrSi and $ZrSi_2$," *Monatschefte für Chemie*, Vol. 85, 1954, p. 1140.
6. C. E. Lundin, D. J. McPherson, and M. Hansen, "The System Zirconium-Silicon," TRANSACTIONS, American Society for Metals, Vol. 45, 1953, p. 901.
7. E. S. Greiner, "Specific Heat, Latent Heat of Fusion, and Melting Point of Germanium," *Transactions*, American Institute of Mining and Metallurgical Engineers, Vol. 4, 1952; *Journal of Metals*, October 1952, p. 1044.
8. METALS HANDBOOK, American Society for Metals, Cleveland, 1948.

PHASE RELATIONS IN MG-LI-ZN ALLOYS

By A. F. Weinberg, D. W. Levinson and W. Rostoker

Abstract

A study was made of equilibrium phase relations in the system Mg-Li-Zn by the methods of metallographic thermal and X-ray diffraction analysis. Isothermal sections are presented for the temperatures of 400, 300, 200 and 100°C (750, 570, 390 and 210°F). A vertical section, derived from the isotherms is also presented.

A ternary phase of wide miscibility was identified. The ternary phase Mg-Li_2-Zn was not found to be an equilibrium phase at any of the temperatures studied. (ASM-SLA Classification: M24, Mg, Li, Zn)

Introduction

THE results of an alloy development study on Mg-Li-Zn alloys were reported by Dow Chemical Company in 1951 (1).[1] In general, the alloys studied were characterized by very high compressive yield strength, but poor ductility. The high strength properties available in this system were not stable at room temperature or slightly elevated temperatures. It was found that the best combination of properties at a high strength level was obtained in the alloy Mg-7Li-16 to 20Zn (weight %).

Alloys of this system are age hardening. Precipitation occurs very rapidly upon quenching, though maximum properties are apparently not reached until several days of aging at room temperature. It was postulated (2) that the aging mechanism is due to the precipitation of the ternary compound, $MgLi_2Zn$. The only unambiguous evidence of this phase has been the observation of X-ray diffraction patterns whose lines can be indexed as a cubic lattice with a cell parameter of 6.70Å (see Table IX). It has never been positively established that the X-ray pattern corresponding to what is called $MgLi_2Zn$ actually corresponds to a phase with this stoichiometry. The phase-temperature relationships for the alloy Mg-7Li-16Zn were reported as follows:

Above 750°F (399°C)—two phase—cubic and hexagonal solid solutions.

Between 750°F (399°C) and 300°F (149°C)—three phase—cubic and hexagonal solid solutions plus MgLiZn.

[1]The figures appearing in parentheses pertain to the references appended to this paper.

Of the authors, A. F. Weinberg is with the U.S. Navy; D. W. Levinson is supervisor, Nonferrous Metallurgy Research, and W. Rostoker is supervisor, Physical Metallurgy Research, Armour Research Foundation, Chicago. Manuscript received February 10, 1955.

Below 300°F (149°C)—three phase—cubic and hexagonal solid solution plus $MgLi_2Zn$ with MgLiZn often present though not under equilibrium conditions.

A four phase reaction was postulated at about 300°F (149°C).

Further study on phase-temperature relationships was conducted by Jones, et al. (3). Isothermal diagrams at 700°F (371°C) and 500°F (260°C) were presented showing the extent of the β, (Mg+β) and (Mg) phase fields together with the identification of the fields bounding the above phase fields. A feathery precipitate appearing along the boundaries of large grains of beta solid solution was found in some alloys. This was identified as $MgLi_2Zn$ by X-ray diffraction. However, on the basis of the isotherms presented, these investigators concluded that $MgLi_2Zn$ was a nonequilibrium structure which formed from the beta during quenching.

The aim of the present investigation was to establish the equilibrium phase relationships more definitely by using a wider composition range than was formerly studied. This was done at several temperatures, and special interest was shown in the attempt to find whether $MgLi_2Zn$ exists as an equilibrium structure.

Experimental Procedure

Alloys for this study were prepared from high purity materials described in Table I. Because of the known influence of sodium on the mechanical properties of these alloys (4), metals and fluxes of the lowest possible sodium content were employed.

The charges were melted in molybdenum crucibles. The melting was done under both a LiCl-LiF flux and an argon blanket in a vertical tube furnace. The flux composition was 3 parts LiCl, 1 part LiF by weight and normally amounted to about 25% of the charge weight. All melts were chill cast in a cast iron mold. Spectrographic analysis was used on several samples to determine the molybdenum pick-up. In all cases the tests showed no contamination.

The nominal compositions studied are shown in graphical form in Fig. 1. Chemical analyses have been carried out on alloys which

Table I
Materials Used

Materials	Source	Purity
Lithium	Maywood Chemical Co. Maywood, New Jersey	"Special grade low Na, low Cl lithium." Na guaranteed <0.02% and should be <0.001%.
Magnesium	Dow Chemical Co.	Re-distilled high purity magnesium. Total impurity content <0.05%.
Zinc	Merck and Co. Rahway, New Jersey	High purity. Low As, Fe, Pb. Total impurity content <0.03%.

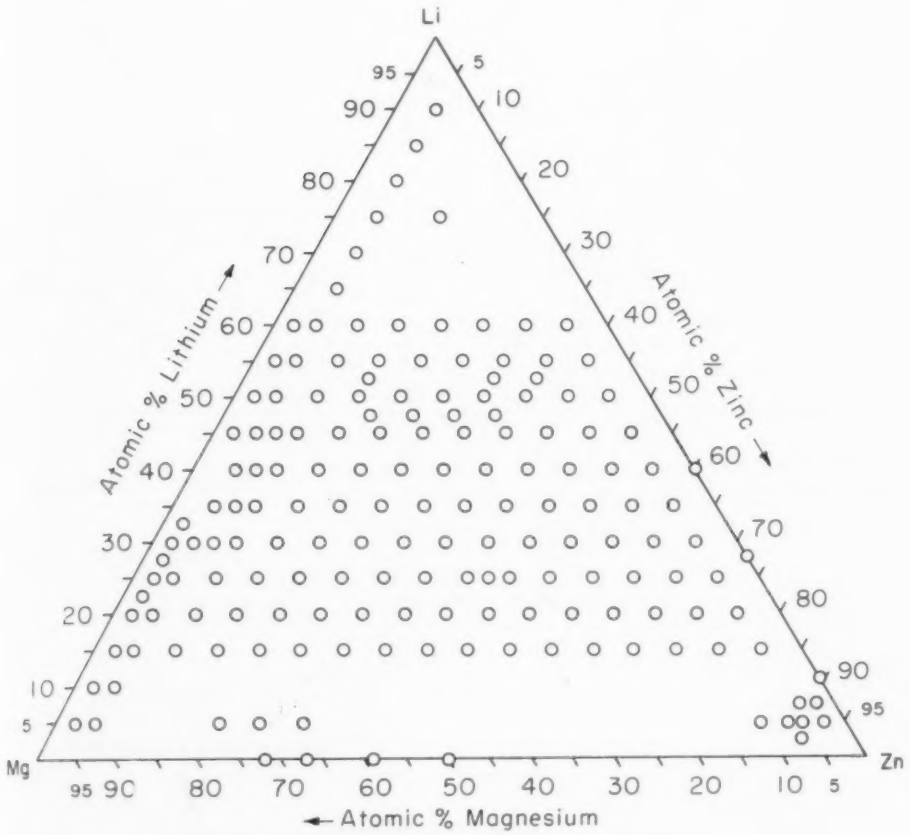


Fig. 1—Nominal Compositions of Mg-Li-Zn Alloys.

appear to delineate phase boundaries and on other alloys for which the analyzed composition was, for one reason or another, desired. Generally good control of alloy composition was indicated.

The ingots were broken or sawed into pieces suitable for heat treatment. The specimens were wrapped in aluminum foil, provided

Table II
Etchants Employed for This Study

Reagent	Composition	Action
Citral	10 gm citric acid 90 ml ethanol (95%)	β tan to black, θ light cream, (Mg gray, LiZn very light gray
Acetic Picral (AP)	4 gm picric acid 100 ml ethanol (95%) 10 ml H_2O 5 ml glacial acetic acid	β light brown to black, (Mg) tan, stains θ and LiZn
Modified acetic picral (MAP)	10 ml AP 90 ml ethanol (95%)	Slower acting version of AP
Glycol-acetic-nitric (GAN)	60 ml ethylene glycol 19 ml H_2O 20 ml glacial acetic acid 1 ml con. HNO_3	β light gray to black, θ very light cream, (Mg) light tan, LiZn gray

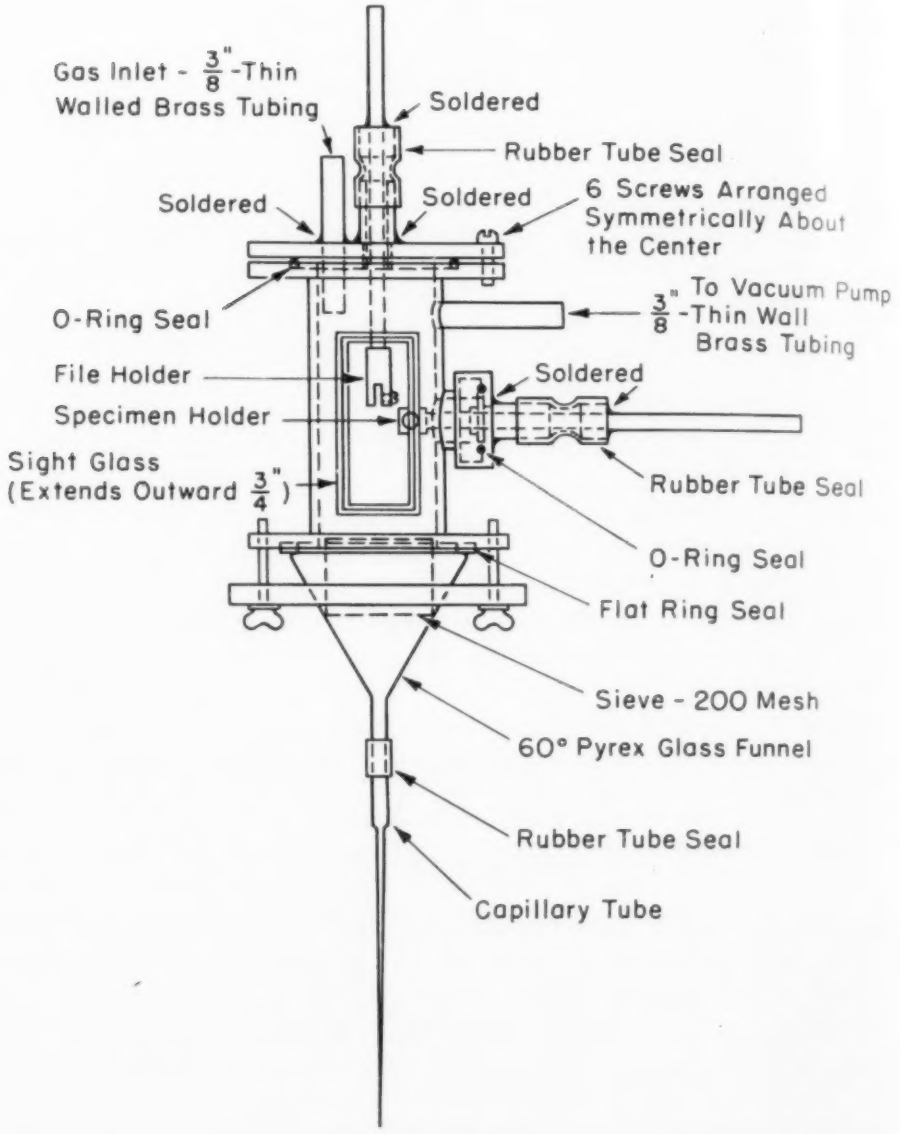


Fig. 2—Powdering Apparatus.

with a stamped tag for identification, and were sealed in pyrex bulbs under a partial pressure of argon. Heat treatments were conducted at temperatures of 400, 300, 200, and 100°C. Preliminary experiments indicated the following annealing times were sufficient for equilibration:

400°C (750°F)	24 hours
300°C (570°F)	42 hours
200°C (390°F)	100 hours
100°C (210°F)	310 hours

The heat treatment schedule was:

1. Homogenize 24 hours at 400°C (750°F).

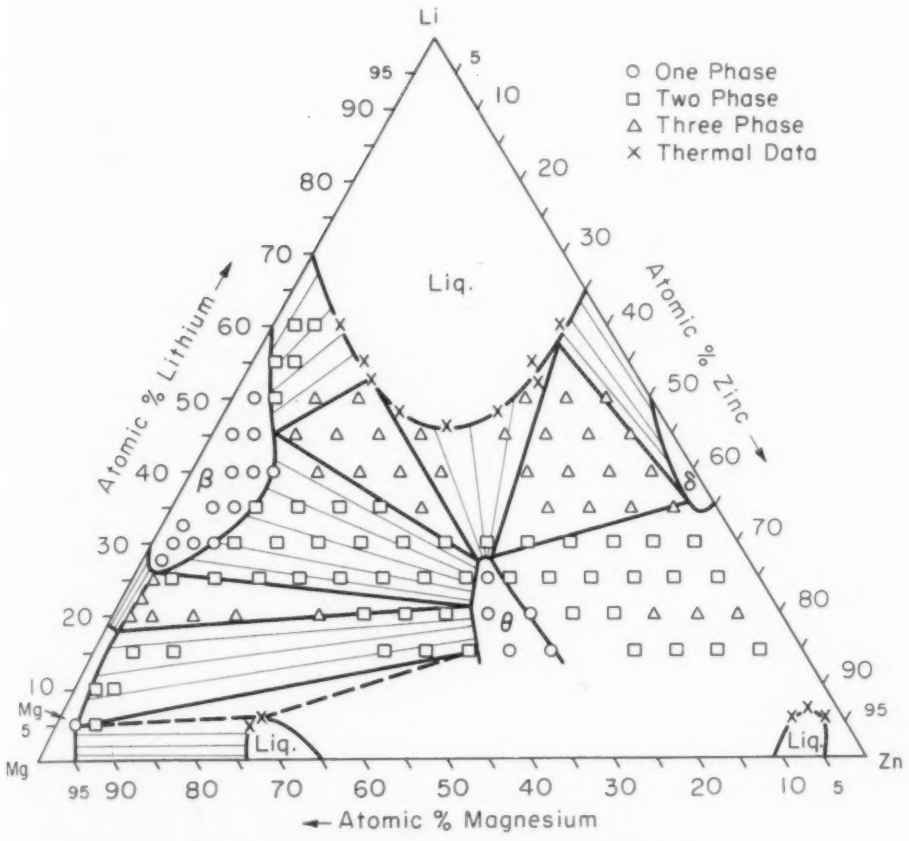


Fig. 3—400°C (750°F) Isotherm for System Mg-Li-Zn.

2. Furnace cool to annealing temperature and hold for times listed above.

3. Quench to room temperature.

Because of the possibility of destroying the desired isothermal equilibrium by low temperature aging, the specimens were mounted in a room temperature setting medium known as "Epon" manufactured by Shell Oil Company. The normal polishing procedure was followed except that some specimens which were very reactive received their final polishing on a wheel on which the carrier was mineral oil rather than water. Etching reagents employed in this study are listed in Table II.

Table III
Reported Structures of Phases Occurring in the Alloys Studied

Phase*	Structure	Parameter	Source
θ (MgLiZn)	cubic	7.45 Å	(5)
$MgZn_2$	hexagonal	a = 5.15 Å c/a = 1.65	
δ (LiZn)	NaTl (cubic)	6.20 Å	(5)
$MgLi_2Zn$	cubic	6.7 Å	(5)

*This terminology corresponds to that used in the isotherms presented.

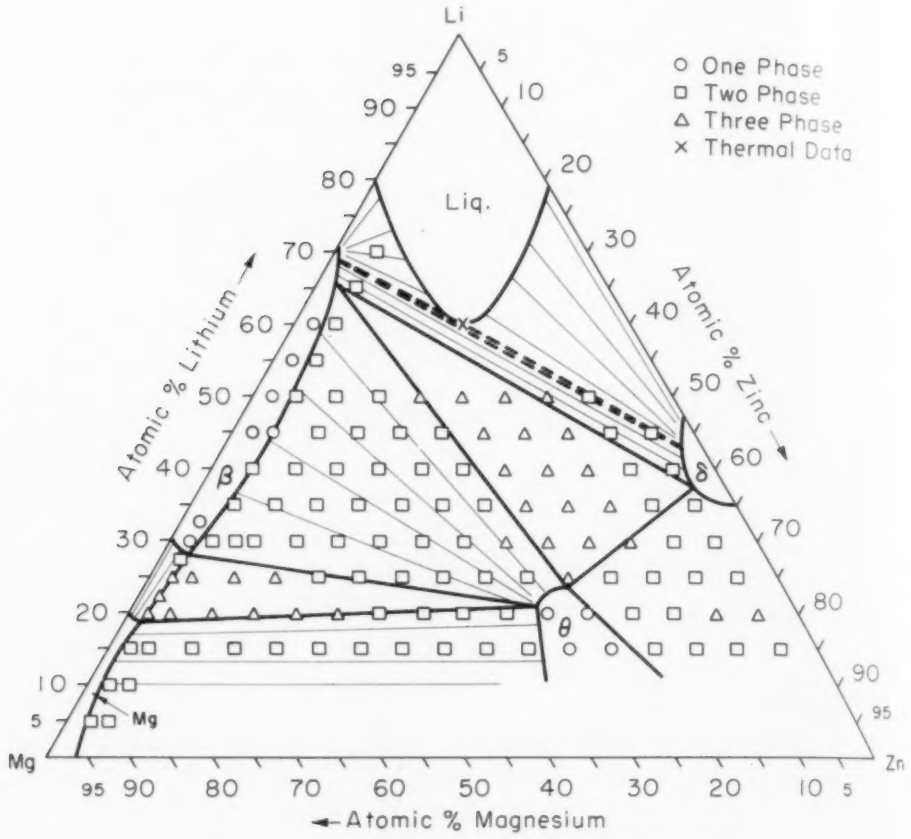


Fig. 4—300°C (570°F) Isotherm for System Mg-Li-Zn.

An X-ray diffraction program was conducted to supplement the metallographic study in order that the identification of phases in the system would be most positive. Specimens were prepared from the heat treated samples.

Due to the extreme reactivity of the alloys, the powdering was done under vacuum in the device pictured in Fig. 2. In no case was a stress relief annealing treatment used on these powders since it was found that during any such anneal there was appreciable reaction of the specimen with the glass capillary and distinct evidence of volatilization of magnesium and lithium. Patterns were obtained in 14.4 cm diameter Debye-Sherrer cameras with nickel-filtered copper radiation. The reflections were indexed by comparison with calculated d values from the reported structures of the phases. The structures and parameters of the phases previously reported are given in Table III.

To find the boundaries of the liquid fields which were present at some of the temperatures studied thermal analysis was used. A calibrated iron-constantan thermocouple, placed inside a protective molybdenum sheath, was inserted in 10 gm melts. The data were

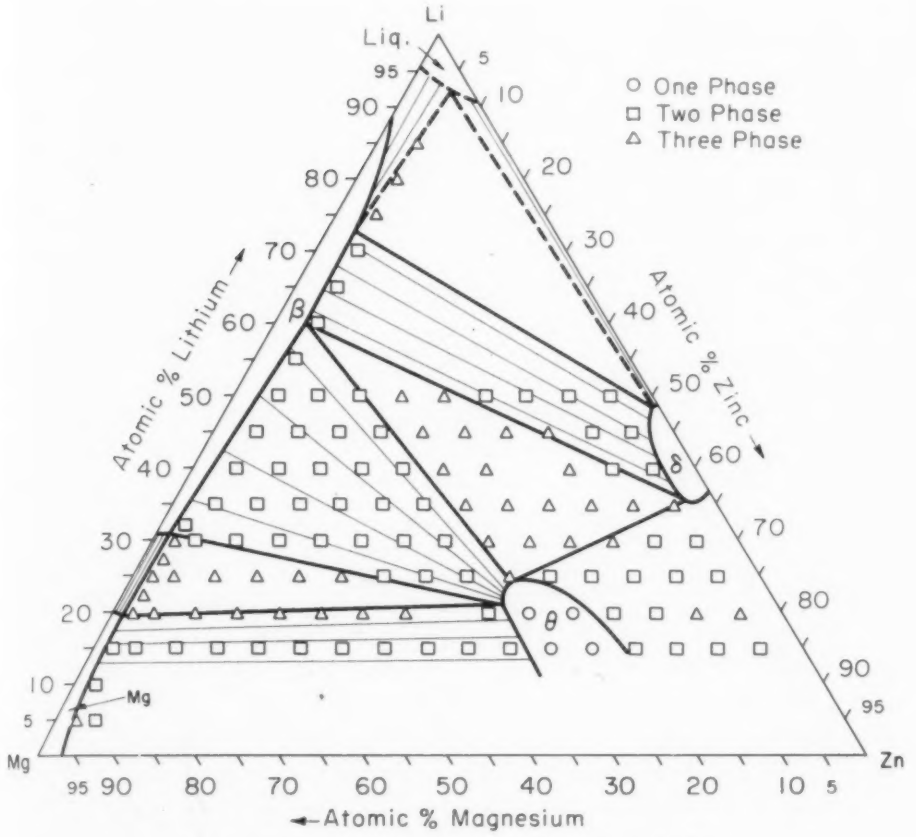


Fig. 5—200°C (390°F) Isotherm for System Mg-Li-Zn

recorded on a Leeds and Northrup "Azar Speedomax" with a chart speed of 2 inches per minute.

Results

Data obtained from the alloys studied are summarized in the isothermal diagrams, Figs. 3,4,5, and 6. These isotherms are presented on an atomic % scale due to the great disparity in density of one of the components. The tie lines shown are hypothetical and serve only to designate two-phase fields. The solid lines drawn on the isotherms are believed to be accurate since they are delineated in most cases by special study of several critical alloys. The one exception is the delta field, whose miscibility was fixed by the intersection of the sides of the three phase triangle terminating at this phase. The dashed lines represent a best guess at the location of boundaries in instances in which no actual experimental alloys, or prior knowledge, permitted a precise location. The liquid fields shown in the 400°C (750°F) and the 300°C (570°F) diagrams are based upon cooling data.

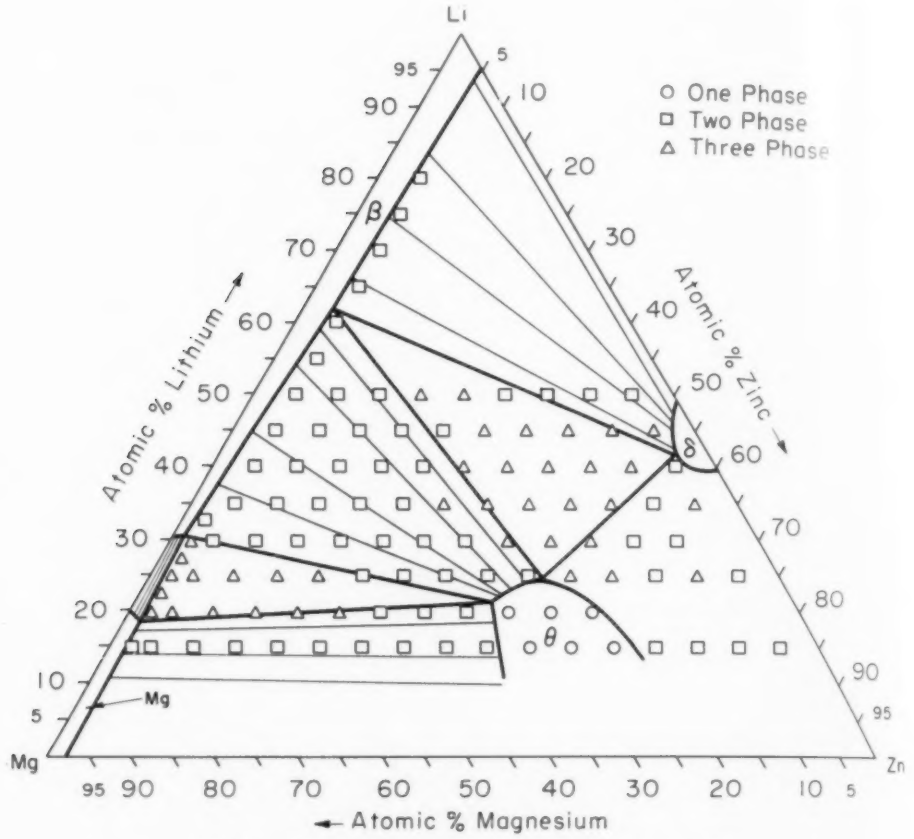


Fig. 6—100°C (210°F) Isotherm for System Mg-Li-Zn.

The phase field designations are based upon identification of the phases by the metallographic techniques described in a previous section. Corroboration of the metallographic interpretations was obtained by analysis of X-ray diffraction powder patterns. A summary of the phase verification program is given in Table IV.

Table IV
Summary of Phase Verification Program for the Mg-Li-Zn System

Alloy Composition At. %			Equilibration	Metal-	
Mg	Li	Zn	Temperature °C	lography	X-Ray
75	20	5	400	$Mg+\beta+\theta$	$Mg+\beta+\theta+MgLi_2Zn$
30	25	45	400	$\theta+?$	θ
35	30	35	400	$\beta+\theta$	$\beta+\theta$
25	30	45	400	$\theta+\delta$	$\theta+\delta$
50	35	15	400	$\beta+\theta$	$\beta+\theta+MgLi_2Zn$
15	40	45	400	$\theta+\delta+L$	$\theta+\delta+\beta+MgLi_2Zn$
40	45	15	400	$\beta+\theta+L$	$\theta+\delta+\beta+MgLi_2Zn$
30	65	5	300	$\beta+\delta$	$\beta+\delta$
25	25	50	300	$\theta+\delta+\beta$	$\theta+\delta+\beta$
25	40	35	300	$\theta+\delta+\beta$	$\theta+\delta+\beta+MgLi_2Zn$
25	45	30	300	$\theta+\delta+\beta$	$\theta+\delta+\beta+MgLi_2Zn$
30	50	20	300	$\theta+\delta+\beta$	$\theta+\delta+\beta+MgLi_2Zn$
75	20	5	200	$Mg+\beta+\theta$	$Mg+\beta+\theta+MgLi_2Zn$
70	25	5	200	$Mg+\beta+\theta$	$Mg+\beta+\theta+MgLi_2Zn$
82.5	15	2.5	200	$Mg+\theta$	$Mg+\theta$
75	22.5	2.5	200	$Mg+\beta+\theta$	$Mg+\beta+\theta+MgLi_2Zn$
15	50	35	200	$\beta+\delta$	$\beta+\delta+MgLi_2Zn$

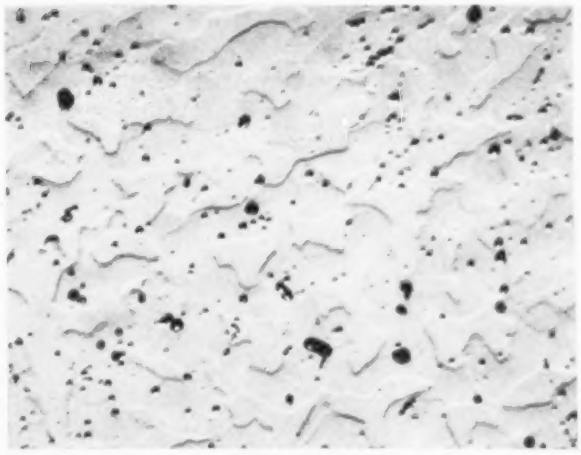


Fig. 7—Photomicrograph Showing the θ Phase.

The X-ray diffraction line sequences used for identification of β, (Mg), the ternary intermediate phase, θ (see discussion in a later section of this paper), $MgLi_2Zn$ (Dow designation), and LiZn (8) are given in Tables V, VI, VII, VIII, and IX. There was no indication of large parameter changes in θ and $MgLi_2Zn$ due to composition variation. LiZn (8) exhibited a large parameter change between the single phase specimen examined and specimens where delta coexisted with one or more other phases (see Table VIII).

The present investigation agrees with the results of Jones, et al as to the identification of the phase fields presented. Slight differences are noted in the extent of the miscibility of the beta field, and marked differences are seen in the directions of the phase field boundaries.

A phase was found to exist in many specimens whose etching characteristics, X-ray diffraction line sequence, and lattice parameter were the same as the phase called MgLiZn. Although this phase exhibits a wide range of miscibility, at none of the temperatures examined did the field include the stoichiometric composition MgLiZn. For this reason the symbolism θ has been used to designate

Table V
X-Ray Identification of β Phase

Heat No. BB 1 I	d_{obs}	d^*_{calc}	Identification
s	2.485	2.50	(110)
w	1.758	1.75	(200)
s	1.436	1.43	(211)
w	1.243	1.24	(220)
w	1.112	1.11	(310)
f	1.015	1.01	(222)
w	0.940	0.940	(321)
w	0.892	0.880	(400)
w	0.829	0.830	(411/330)
vw	0.787	0.784	(420)

*Based on BBC structure a_o=3.50 Å.

Table VI
X-Ray Identification of (Mg) Phase

Heat No. BB 1 I	d_{obs}	d^*_{calc}	Identification
s	2.769	2.75	(10.0)
s	2.567	2.57	(00.2)
vvs	2.435	2.42	(10.1)
m	1.881	1.87	(10.2)
s	1.597	1.58	(11.0)
vw	1.382	1.37	(20.0)
s	1.355	1.35	(11.2)
s	1.334	1.32	(20.1)
vw	1.282	1.28	(00.4)
vw	1.216	1.21	(20.2)
vw	1.161	1.16	(11.3)
w	1.075	1.07	(20.3)
vw	1.045	1.03	(00.5)
m	1.024	1.01	(12.1)
vw	1.000	0.998	(11.4)
vw	0.962	0.963	(10.5)
vw	0.824	0.821	(20.5)

*Based on hexagonal structure, a = 3.16 Å, c/a = 1.63.

Table VII
X-Ray Identification of θ Phase

Heat No. C-26 I	d_{obs}	d^*_{calc}	Identification
s	4.279	4.30	(111)
w	2.619	2.63	(220)
vs	2.234	2.25	(311)
s	2.141	2.15	(222)
wm	1.874	1.86	(400)
w	1.699	1.71	(331)
ft	1.513	1.52	(422)
m	1.426	1.43	(511/333)
m	1.309	1.32	(440)
vw	1.252	1.26	(531)
ft	1.170	1.18	(620)
vw	1.131	1.14	(533)
w	1.118	1.12	(622)
ft	1.071	1.08	(444)
ft	1.039	1.04	(711/551)

*Based on cubic structure, a = 7.45 Å. Density measurements on heat D-8 (heat treated at 400°C) indicate that the unit cell contains 24 atoms.

Table VIII
X-Ray Identification of LiZn (δ) Phase

Heat No. J-1 I	d_{obs}	d^*_{calc}	Identification
ft	3.541	3.55	(111)
vs	2.177	2.17	(220)
ft	1.855	1.85	(311)
wm	1.538	1.54	(400)
ft	1.426	1.41	(331)
m	1.257	1.26	(422)
ft	1.198	1.18	(333)
vw	1.088	1.09	(440)

*Based on cubic structure, a = 6.15 Å.

NOTE: This lattice parameter is based upon a binary alloy specimen. This phase in coexistence with other phases exhibits a larger parameter. For example, specimen C-28 (heat treated at 400°C) has a lattice parameter ~6.21.

this phase. Fig. 7 shows a microstructure of this single phase. The photograph was taken under oblique lighting conditions to show the

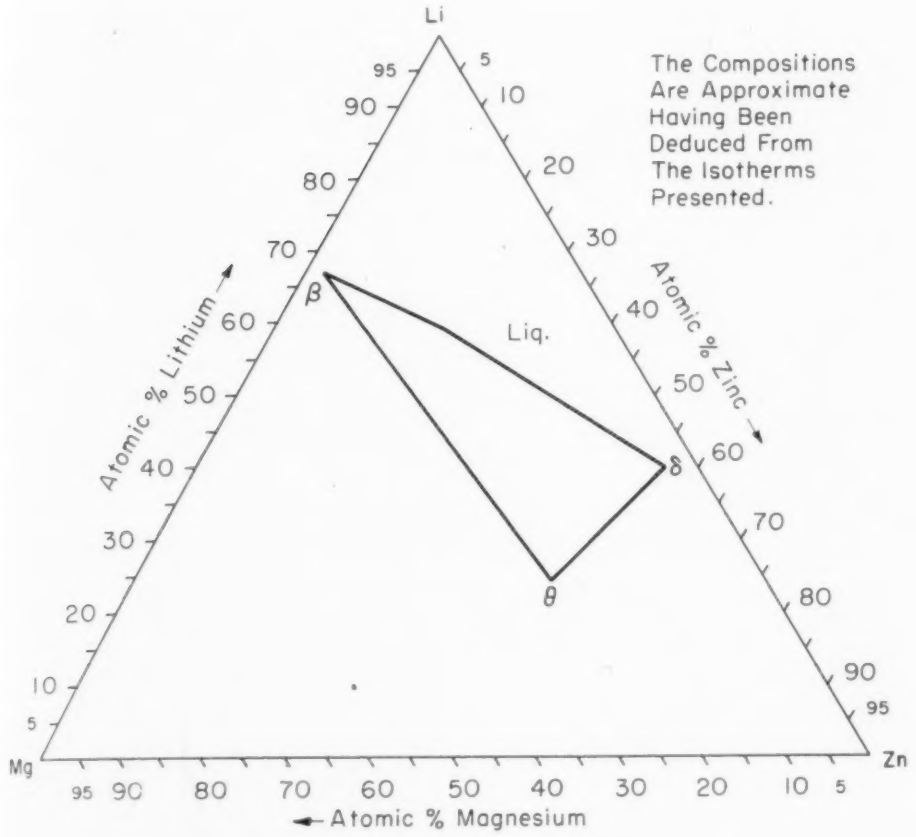


Fig. 8—Ternary Peritectic Quadrangle.

grain boundaries. The small spheres scattered throughout are etching effects, since the specimen had to be severely etched to bring out the low contrast between grains. This low contrast, even after heavy etching, is indicative that the specimen is single phase since a two phase specimen would have developed contrast between the grains much sooner.

Table IX
X-Ray Identification of $MgLi_2Zn$ Phase

Heat No. C-60 I	d_{obs}	d^*_{calc}	Identification
vw	3.844	3.87	(111)
vft	3.304	3.35	(200)
w	2.350	2.37	(220)
ft	1.998	2.02	(311)
vft	1.659	1.68	(400)
—	—	1.54	(331)
vw	1.354	1.37	(422)
ft	1.307	1.29	(333/511)
vft	1.175	1.18	(440)

*Based on cubic structure, a = 6.70 Å.

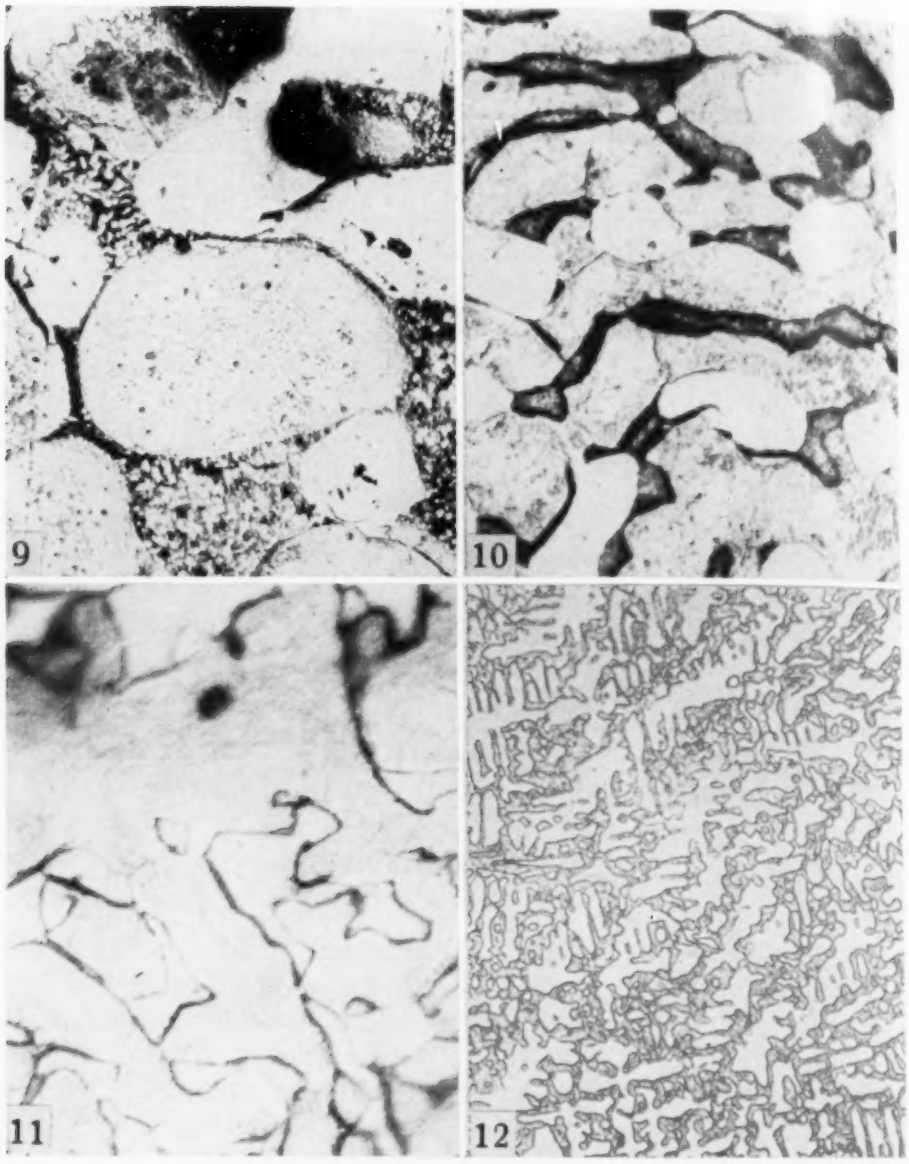


Fig. 9—Photomicrograph Showing $\delta+\theta+L$.
Fig. 10—Photomicrograph Showing $\delta+\theta+\beta$.
Fig. 11—Photomicrograph Showing $\delta+\beta$.
Fig. 12—Photomicrograph Showing $\theta+$(Mg).

In the temperature range 300 to 400°C (570 to 750°F) a ternary peritectic reaction, $L+\theta \rightleftarrows \beta+\delta$, occurs. The temperature of this reaction has been set at 317 ± 2°C by thermal analysis. The compositions of the participating phases have been estimated from the 300°C (570°F) isotherm. Fig. 8 shows the quadrangle corresponding to this invariant reaction. Fig. 9 illustrates the microstructure of a Mg-45Li-40Zn (at. %) alloy heat treated at 400°C (750°F) so that it occurs in the three-phase field ($\delta+\theta+L$). The three-phase struc-

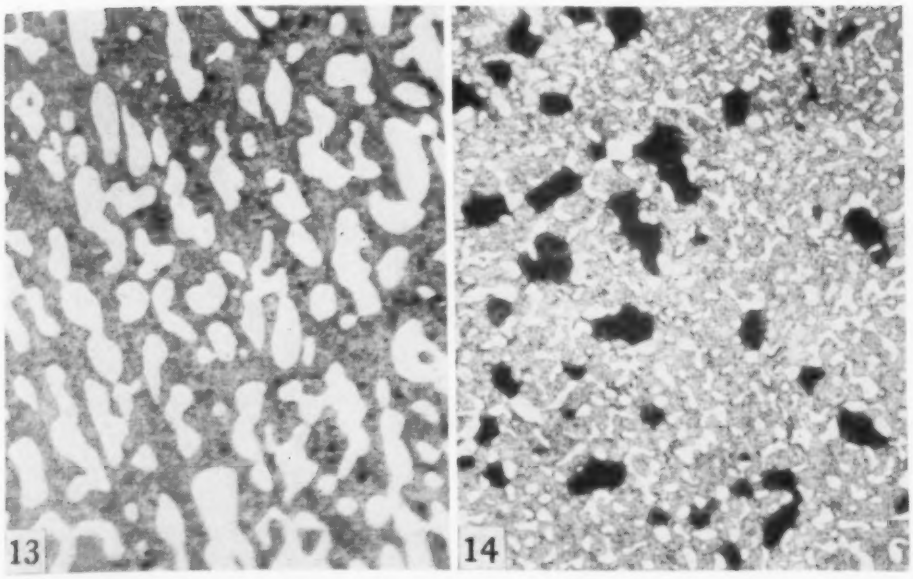


Fig. 13—Photomicrograph Showing $\theta+\beta$.
Fig. 14—Photomicrograph Showing (Mg) $+\beta+\theta$.

ture, $(\delta+\theta+\beta)$, in which this alloy exists below the ternary peritectic temperature was developed by annealing at 300°C (570°F) and is shown in Fig. 10. A specimen falling in the $(\delta+\beta)$ field formed by the reaction is shown in Fig. 11.

Other important characteristics of the system can be summarized as follows:

1. The coexistence of the θ phase with (Mg) and β has been established at all temperatures investigated. Figs. 12 and 13 show these two phase structures.

2. Other phase fields established at 400°C (750°F) are $(\theta+L)$ and the three phase fields $(\beta+L+\theta)$ and $(\delta+L+\theta)$.

3. The solid solution range of θ increases as the temperature is decreased.

4. All fields present in the 300°C (570°F) isotherm remain at the lower temperatures with the exception of the $(L+\delta)$, $(\beta+\delta+L)$ and liquid fields, which disappear at 186°C (360°F), the melting point of lithium. Fig. 14 shows the existence of the three phases $[(Mg)+\beta+\theta]$ at 300°C (570°F).

5. The $(\beta+\theta)$ and $(\beta+\delta)$ fields broaden as the temperature is decreased, but the other fields remain essentially the same.

6. As the temperature decreases the point of maximum zinc content on the trace of the surface separating the β and $(\beta+\theta)$ fields move toward a smaller percentage of zinc. The maximum solubility decreases from 10 atomic % zinc at 400°C (750°F) to 5 atomic % zinc at 300°C (570°F). This trend continues as the temperature is decreased to less than 5 atomic % at 200 and 100°C

(390 and 210°F). The exact value of the maximum solubility at these temperatures has not been determined.

It should be noted that difficulty was encountered in the interpretation of the specimens which were heat treated at 100°C due to the fineness of the structures, which is, of course, characteristic of the low annealing temperature. For this reason the 100°C isotherm is more uncertain than the other isotherms.

It can be seen from the isotherms presented that at no temperature was the hypothetical compound $MgLi_2Zn$ observed metallographically, and it would be expected that if it did occur as an

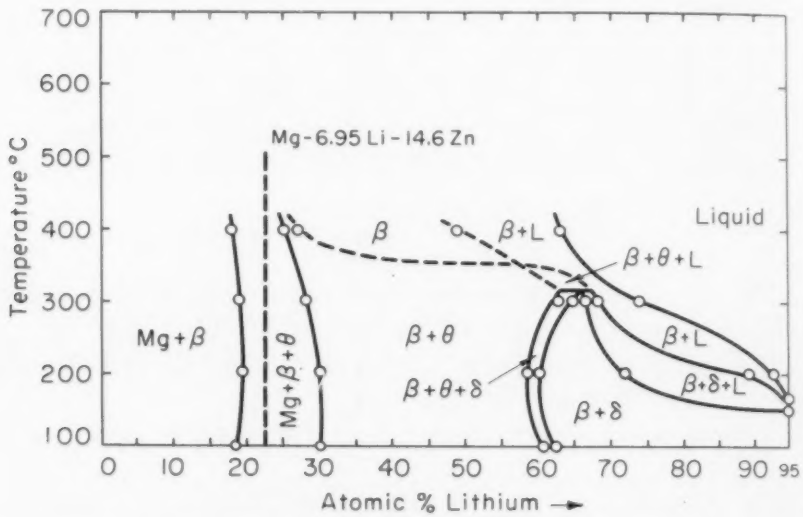


Fig. 15—Vertical Section Through Mg-Li-Zn System.

equilibrium phase, large amounts of it would have been found in some of the specimens examined. Further, the metallographic data are self consistent without the postulate of an additional ternary phase. Evidence of its presence was found in many specimens by X-ray diffraction methods. However, in all cases where $MgLi_2Zn$ was found, it occurred in addition to the phases which were found metallographically. This seems to contradict the evidence of many investigators that metallographic examination is invariably a much more sensitive means of detecting small amounts of precipitate than is X-ray diffraction using powder methods, but is consistent with the general inability of metallographic methods to detect transition phases.

On the basis of the isotherms presented, if $MgLi_2Zn$ were to form at a low temperature it would have to do so by a four-phase reaction. This is in agreement with the conclusions of Dow Chemical Company cited earlier. Since one of the phases participating in the invariant reaction would have to be liquid, according to the

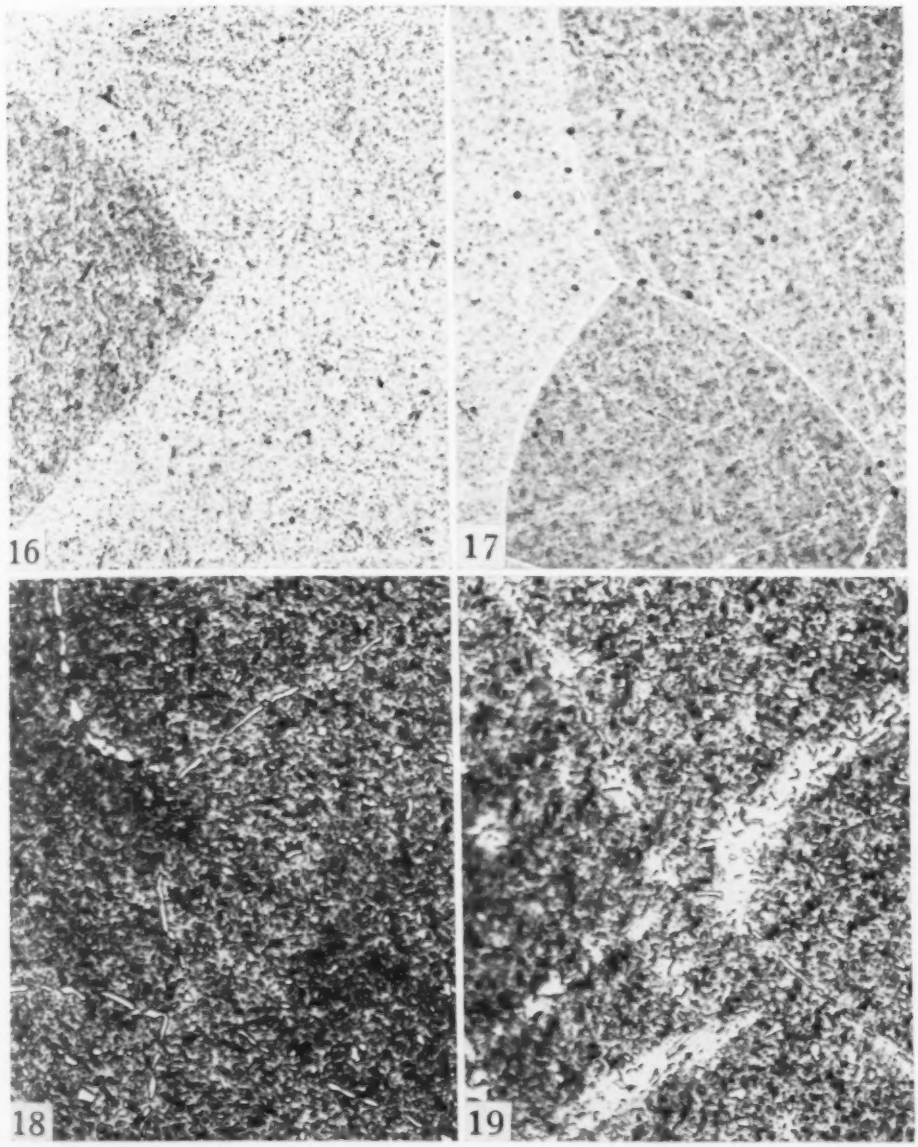


Fig. 16—Photomicrograph of a β Alloy at 400°C (750°F).
Fig. 17—Photomicrograph of a β Alloy at 300°C (570°F).
Fig. 18—Photomicrograph of a β Alloy at 200°C (390°F).
Fig. 19—Photomicrograph of a β Alloy at 100°C (210°F).

isotherms presented, it was thought that this reaction should show as a "hold" on cooling curves. Cooling curves were therefore run on alloys of composition Mg-85Li-5Zn and Mg-75Li-12.5Zn (at. %). No "holds" were observed for either alloy. Two "breaks" were observed in each curve with the final "break" being such that the final slope was steeper than the previous slope. This indicates the completion of solidification in the alloys and eliminates the possibility of the reaction occurring at a lower temperature.

The evidence all points, therefore, to an agreement with Jones (6) that the hypothetical $MgLi_2Zn$ is a nonequilibrium structure. However, in disagreement with previous work, configurations similar to the feathery precipitates reported were found in some lithium-rich specimens which were all beta at high temperatures, but fell into the $(\beta+\theta)$ field upon cooling, and these were identified metallographically as being due to the form of the theta precipitation rather than to precipitation of $MgLi_2Zn$. In the previous work the identification had been done by X-ray diffraction using powder methods. In the present investigation all X-ray diffraction work was also done by powder methods. It is also a possibility that the hypothetical $MgLi_2Zn$ is a metastable strain-induced phase developed by the powdering operation.

Fig. 15 shows a vertical section derived from the isotherms. It is seen that specimens quenched from beta can exist in either of two-phase fields, $(\beta+\theta)$ or $[(Mg)+\beta+\theta]$. This seems to indicate that two modes of aging are possible depending upon the alloy composition.

Figs. 16,17,18, and 19 show an alloy of composition Mg-32.5Li-2.5Zn (at. %) heat treated at 400, 300, 200, and 100°C (750, 570, 390 and 210°F). At 400°C (750°F) the specimen is all beta (the mottled surface of the specimen, as observed in the photograph, is due to the extreme severity of the reaction between beta and the etchant); at 300°C (570°F) there is some theta at the boundaries, but its distribution indicates that it developed during quenching, signifying that the specimen was all beta at the heat treatment temperature. A precipitate, identified as theta, begins to show in the specimen heat treated at 200°C (390°F), and the amount of precipitate is increased in the 100°C specimen.

Summary

Isothermal sections of the magnesium-lithium-zinc system at 400, 300, 200, and 100°C (750, 570, 390 and 210°F) have been established by metallographic, thermal and X-ray diffraction analysis.

A ternary intermediate phase has been identified and designated as θ. It has been shown that the phase $MgLi_2Zn$ could exist only as a nonequilibrium structure. The presence of a ternary peritectic reaction was established at 317 ± 2°C.

A study of the isotherms shows a decrease in the solubility of zinc in the beta field with a decrease in temperature, indicating an amenability to age hardening. It is shown that two different aging mechanisms may exist as alloys, depending upon composition, and can go from the beta field to either the $(\beta+\theta)$ field or the $[(Mg)+\beta+\theta]$ field upon quenching.

Acknowledgment

The authors wish to express their appreciation of the sponsorship of this research by the Metallurgy Research Laboratory, Frankford Arsenal, Philadelphia, Pennsylvania, and for permission to publish this paper.

The work was supported on Contract No. DA-11-022-ORD-906.

References

1. Dow Chemical Company Report No. 14468, 1951.
2. Dow Chemical Company Report No. 14468, 1951.
3. A. Jones, L. Lennon, R. Nash, W. H. Chang and E. G. MacPeek, "Magnesium Alloy Research Studies," WADC TR 52-169, September 1952.
4. P. D. Frost, J. H. Jackson, A. C. Loonam and C. H. Lorig, "The Effect of Sodium Contamination on Magnesium-Lithium Base Alloys," *Transactions*, American Institute of Mining and Metallurgical Engineers, Vol. 188, p. 1171.
5. Personal Communication, Dow Chemical Company.
6. Op. Cit., WADC TR 52-169, 1952.

FATIGUE AND ANISOTROPY IN COPPER

By M. L. Ebner and W. A. Backofen

Abstract

Copper of commercial purity has been found to exhibit a mechanical anisotropy under fatigue loading which is explained by postulating the presence of a fibrous structure of crack-like flaws aligned parallel to the axis of the wrought bar of test material. The presence of such a structure accounts for marked differences in the fatigue behavior of specimens prestrained by severe unidirectional twisting and also by equal amounts of twisting and untwisting. The orientation of the crack structure in the latter specimens was unchanged, while in the former it was reoriented in a helical pattern at the surface of each specimen nearly perpendicular to the axis of the specimen. Upon testing to failure it was found that specimens prestrained by twisting in only one direction (a) failed after fewer stress cycles at any stress level, (b) developed a helical, fibrous-appearing fracture rather than a fracture normal to the specimen axis, and (c) exhibited more rapid crack propagation than specimens that were twisted and then untwisted. These differences are attributed to the crack structure, nearly perpendicular to the direction of the maximum tensile stress, facilitating the development of fatigue cracks and their rapid growth.

From established curves relating stress and cycles to failure, it is suggested that permanent damage from the generation of cracks comparable to the postulated microcracks may have occurred after no more than the first thirty per cent of the expected life of twisted and untwisted specimens. (ASM-SLA Classification: Q7, Cu)

Introduction

RECENT work (1,2)[1] has provided evidence that wrought single-phase alloys and metals of moderately high purity may exhibit a pronounced anisotropy in tensile fracturing characteristics because of an oriented and extremely fine-scale crack structure, the elements of which have been termed microcracks. Experiments were carried out with materials processed by swaging, drawing, extrusion, and rolling. Many of the tests involved fracturing in tension after torsional prestraining. It was found that, after an amount of twisting

[1]The figures appearing in parentheses pertain to the references appended to this paper.

A paper presented before the Thirty-Seventh Annual Convention of the Society, held in Philadelphia, October 17–21, 1955. Of the authors, M. L. Ebner is a graduate student, and W. A. Backofen is assistant professor of metallurgy, Department of Metallurgy, Metals Processing Laboratory, Massachusetts Institute of Technology, Cambridge, Mass. Manuscript received April 13, 1955.

which introduced a shear strain of approximately 2 or more at the surface of the tension specimen, tensile fracture occurred by abrupt separation across a helical surface after little reduction in cross-sectional area and at a low value of average true fracture stress. However, tensile fracture following prestraining by equal amounts of forward and reverse torsion was of the commonly observed ductile type.

The peculiar effect of torsional prestrain upon fracturing in tension has been explained in terms of the reorientation of microcracks. In a heavily reduced rod, microcracks present initially or generated by the processing will be strongly aligned parallel to the rod axis, or direction of elongation. After prestraining a specimen from the rod by equal amounts of forward and reverse torsion, the cracks are still aligned parallel to the specimen axis so that a tensile load, before necking occurs, imposes no stress normal to the cracks, and flow and eventual fracture proceed in the usual way. After a critical amount of unidirectional twisting, however, the angle between the reoriented crack structure and the specimen axis along which load is applied has become appreciable. Then normal stresses can bring about the abrupt helical separation, accompanied by the drop in fracture stress and ductility, through growth and union of the microcracks. Such an explanation is further supported by a consistently accurate prediction of the angle between the axis of the specimen and the trace of the helical fracture in the specimen surface. This prediction is based on the shear strain and the assumption that the crack structure orientation in the twisted specimens follows the helical path described by a line initially parallel to the specimen axis.

Inclusions are invariably held at least partly responsible for the directionality in properties relating to fracture that is commonly encountered in wrought metal. Very striking evidence that inclusions do contribute to mechanical anisotropy of the kind studied in the present work is provided by Ransom (3) who found that the transverse fatigue strength of vacuum-melted, essentially inclusion-free, SAE 4340 steel averaged 50% higher than the same property of commercial quality SAE 4340. However, in the vacuum-melted steel the ratio of transverse to longitudinal fatigue strength was only 0.86. Thus even when inclusion content is practically nil, some fibrous structure might still be regarded as contributing to an anisotropy in properties. Aluminum of commercial purity has also been examined in this respect, and Jacquesson and Laurent (4) working with rolled sheet found a dependence of fatigue strength on direction in the plane of the sheet consistent with the presence of a fibrous structure. Therefore the evidence could reasonably be interpreted to imply that wrought metals of considerable purity and cleanliness are anisotropic with respect to fracture in fatigue as well as in tension, and

that a highly oriented, fibrous and crack-like, but as yet invisible, structure also contributes to this anisotropy. An interest in more detailed information about fatigue and anisotropy in pure metal prompted the work presented here.

In studying the contribution of a crack structure to anisotropy in fatigue, torsional prestraining again is a convenient way of producing different orientations relative to the stress axis. One set of specimens may be prestrained by severely twisting in only one direction; then the cracks will approach an alignment at right angles to the specimen axis. A second set may be prestrained by equal amounts of twisting and untwisting so that the total shear strain (forward plus reverse) will be the same as in the first set. Now both sets will be approximately the same with respect to hardness, yield strength, and tensile strength. Yet in the second set the crack structure will still be aligned parallel to the specimen axis. Therefore it might be expected that under fatigue loading the first set will: (a) fail at any stress level after fewer stress cycles, (b) develop a helical fibrous-appearing fracture rather than the more common fracture normal to the specimen axis, and (c) exhibit more rapid crack propagation. Such were the predictions to be investigated in the present work.

Experimental Procedures

Specimen Preparation—All specimens were taken from the same length of cold drawn, electrolytic tough-pitch copper. The torsion specimens illustrated in Fig. 1 were machined from the as-received stock and then annealed at 800°F (425°C) for one-half hour. Twenty specimens were twisted so that a shear strain of 5 was introduced at the surface of the minimum section in the fatigue specimens; another twenty were twisted to produce a strain of 2.5 at the same location and then completely untwisted so that the specimens of each set underwent approximately the same amount of cold working.

After twisting, the fatigue specimens shown in Fig. 1 were machined from the torsion bars, then polished with No. 1 emery paper until no machining marks were visible, next polished successively with 0, 2/0, 3/0, 4/0 emery papers, and finally polished with a No. 3 alumina suspension and broad cloth. The polishing technique, carried out as reproducibly as possible from specimen to specimen, resulted in a bright, nearly metallographic surface showing a uniform density of light scratch marks left by the No. 1 emery and of a depth about equal to that produced by prolonged polishing with 3/0 paper. Fatigue tests were conducted with such a finish to insure a uniform surface that could be described and reproduced with moderate accuracy, rather than a surface resulting from longer polishing that contained only a few scratches of widely varying size. It seemed reasonable to expect that a surface containing uniform irregularities could lead to more nearly reproducible results.

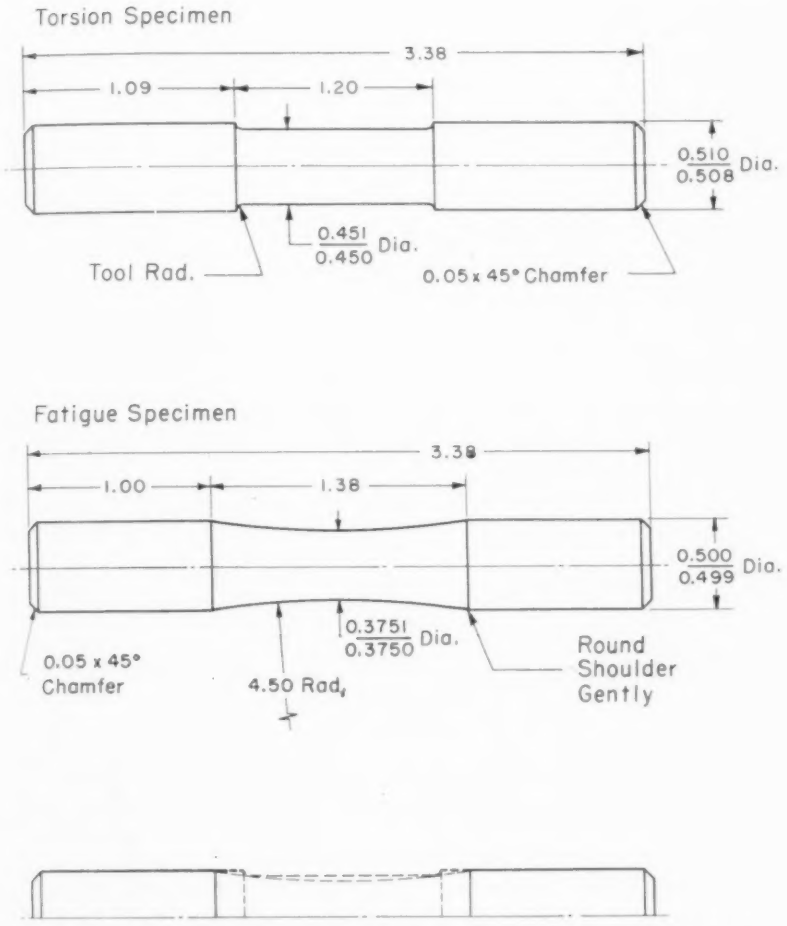


Fig. 1—Test Specimens. Method of taking fatigue specimens from torsion specimens is shown at bottom. All dimensions inches.

Fatigue Testing—Specimens were tested in alternating bending at maximum stresses of 20,000, 25,000, 30,000, and 35,000 psi at the top (and bottom) fiber of the minimum section. Five specimens from each of the two differently prestrained sets were tested at each of the different stress levels. Specimens were tested in groups of five in order that the confidence limits[2] for the mean of the population of cycles to failure from which the sample was taken be as tight as practical for a given confidence estimate. As the number of specimens tested at a given stress is increased from 1 to 5 or 6, the confidence limits for the mean of a normal population of cycles to failure, for perhaps 90% confidence, draw together very rapidly; further change proceeds much more gradually as the number of test specimens increases (5). Consequently, 5 specimens were chosen as representing a practical number for estimating the mean of the population of cycles to failure from which the sample was taken.

[2]The confidence limits define the band or range of cycles to failure at a given stress which would include the average of an infinite sample with a given probability (the confidence estimate).

A Rayflex bending beam, resonance-type fatigue testing apparatus[3] was used in the work. Because the Rayflex machine incorporates a magnetic driving unit, it was necessary to provide mild-steel chucks for holding the nonmagnetic copper specimens. A cathotometer consisting of a telescope with cross-hair reticule and vernier scale was used for measuring the deflection at the minimum section and was mounted between the driving magnets, as was a constant vibration amplitude servocontrol.

Calibration—By calibration, the stress corresponding to a given deflection at the minimum section was established. Part of the calibration was accomplished statically; the deflections at the minimum section caused by different moments applied to the chuck-specimen assembly were measured with the cathotometer. From the slope of the moment-deflection curve obtained,

$$\Delta = 2.90 \times 10^{-4} M \qquad \text{Equation 1}$$

where Δ = half deflection, centimeters
M = applied bending moment, inch-pounds

From beam theory,

$$\sigma_{max} = \frac{Mr_o}{I_m} = \frac{4M}{\pi r_o^3} = 1.94 \times 10^2 M \qquad \text{Equation 2}$$

where M = the applied bending moment, inch-pounds
σ_{max} = the normal stress at the top fiber of the minimum section, psi
r_o = the radius of the minimum section, inches
I_m = the minimum section area moment of inertia about the neutral axis, (inches)^4

Eliminating M between Equation 1 and Equation 2,

$$\sigma_{max} = 6.67 \times 10^5 \Delta \qquad \text{Equation 3}$$

Fig. 2 is a plot of Equation 3 with the deflections indicated that correspond to the chosen stress levels.

Definition of Failure—Failure was considered to have occurred the second time the specimen-chuck assembly fell out of resonance after cracks became visible. Since resonance was in the audible range, the fall-out produced a readily detected change in pitch. Requiring that cracks be visible eliminated the possibility of mistaking an occasional resonance fall-out, caused by drift in the electronic unit, for failure. Using the second fall-out allowed the first fall-out to serve as a warning to be ready for failure and permitted the cracks in the specimens to grow from about 2 to 5 mm in length when measured with the cathotometer as a projection at right angles to the plane of bending. All crack-length measurements were made in this way,

[3]Product of Raytheon Mfg. Co.

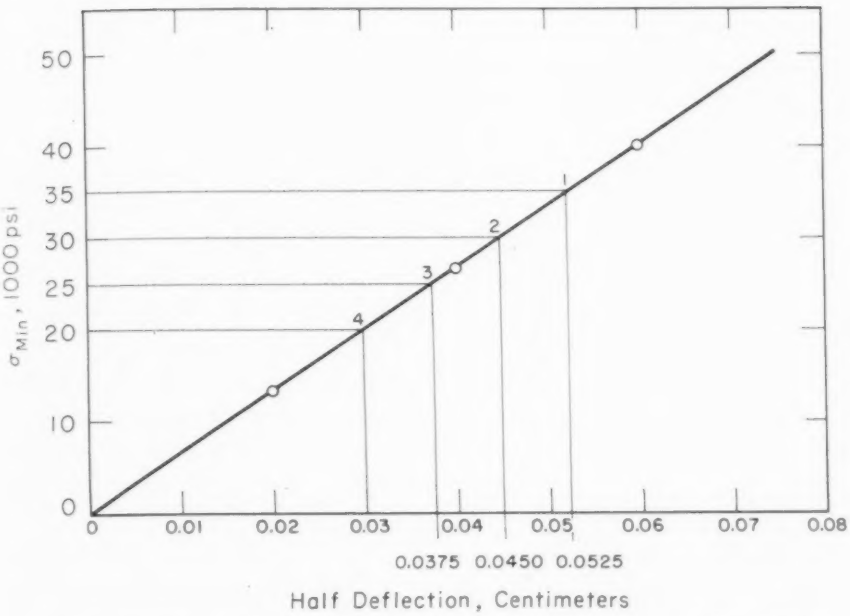


Fig. 2—Stress in the Top Fiber at the Minimum Section as a Function of Minimum Section Deflection.

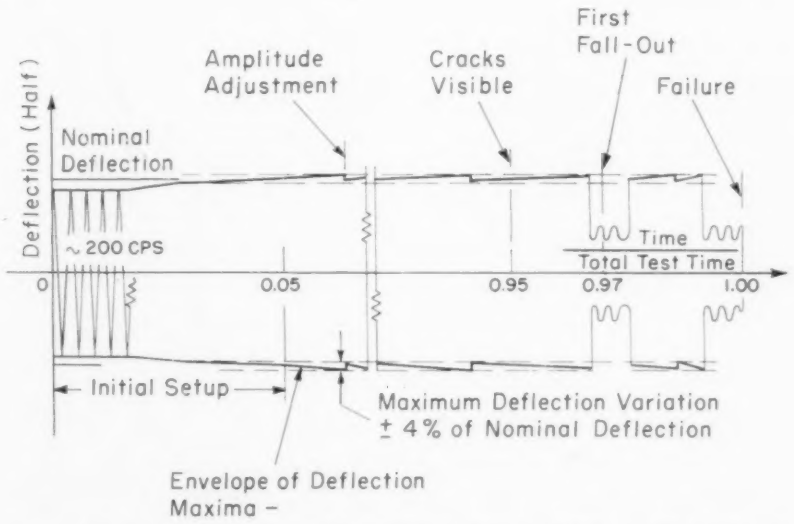


Fig. 3—Deflection of the Minimum Section vs Time During a Typical Test.

which proved to be by far the most feasible; for small cracks it yields a very good approximation of the arc length of the crack.

Such a definition of failure is identical at all stress levels if the resonance bandwidth (the range of frequencies within which the Rayflex frequency and the chuck-specimen frequency will not beat) is also the same at all stress levels; by utilizing adjustments on the Rayflex control unit, the resonance bandwidth was maintained the same at all stress levels.

Fig. 3 illustrates schematically how deflection at the minimum section varied with time during a typical test. The abscissa indicates the fractional part of the test that has elapsed. In general, the set-up time was less than 5% of the testing time. The resonance fall-outs were actually as distinct as those noted in the figure, which accounts to a considerable extent for the definition of failure that was chosen.

Temperature Control—When testing specimens at the higher stress levels, it was found that they could become quite warm, increasing in temperature to perhaps 150 to 175°F. To define the conditions of testing more accurately, and to keep conditions of testing as nearly identical as possible at all stress levels, cool air, which had been passed through a solids filter, was blown on specimens tested at the two highest levels of stress. As a result, all specimens felt reasonably cool during testing and could hardly have become heated to temperatures much above room temperature.

Crack Growth Measurement—After the specimens had failed and were found to contain cracks from 2 to 5 mm in projected length, further testing was carried out to measure the increase in crack length with additional cycles of stress. In making these measurements, test conditions providing an unchanging stress system at the tip of the advancing crack would have been preferred. Establishing those conditions, however, presented a difficult problem. As a substitute, therefore, a constant deflection at the minimum section was imposed on all specimens. The half-value of this deflection was 0.0375 cm, corresponding to a stress of 25,000 psi at the surface of the minimum section in the absence of any crack. While in an absolute sense such crack growth conditions are not well defined, growth at constant deflection is regarded as satisfactory for examining the relative crack growth behavior in the differently prestrained specimens.

Experimental Results

The results of the fatigue tests are presented graphically as the customary S-N curves in Fig. 4. Since the scale on the abscissa in Fig. 4 is logarithmic, the difference in the number of cycles between the two curves at constant stress appears, at first glance, to be larger at higher stress levels. Actually, the difference is smaller at higher stresses as a careful study reveals. A visual examination of the specimens tested in establishing the two curves showed that most cracks in the specimens prestrained by twisting and untwisting followed polishing scratches in the surface. In specimens prestrained by unidirectional twisting, cracks were found to be oriented at 76 to 80 degrees to the specimen axis and appeared to be independent of the polishing scratches. In addition, the number of cracks in the twisted and untwisted specimens averaged about 4, while in the specimens twisted unidirectionally 1 or perhaps 2 cracks formed on the average.

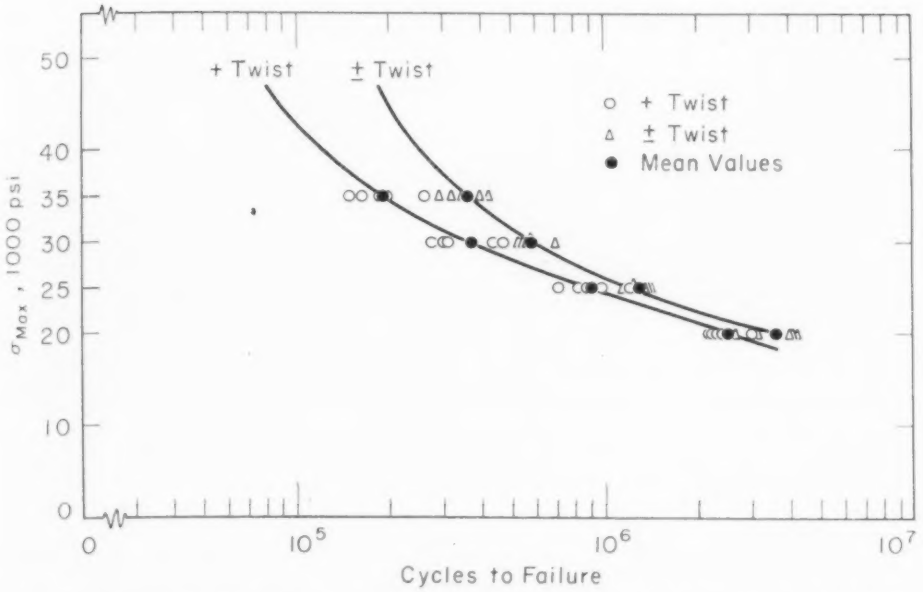


Fig. 4—Maximum Stress at the Top Fiber of the Minimum Section vs the Number of Cycles to Failure.

Photographs of completely fractured specimens prestrained in each of the two different ways are presented in Fig. 5. The fracture surfaces of the two specimens are strikingly different. In that on the right, which had been prestrained by twisting and untwisting, a crack started at the top and grew across the specimen, essentially perpendicular to the axis, with a straight front. In the specimen on the left, which had been prestrained by twisting in one direction only, a crack also grew inward from the surface into material where the twisting was less severe. However, at a distance of about 0.07 in. from the centerline, crack penetration ceased while the crack continued to grow around an intact core and generate a helical fracture surface. The core in this specimen, like the unfractured portion of the other specimen, was finally broken by hand after the test had been carried as far as the machine would permit. Measurements with a toolmaker's microscope with a magnification of 7 and ½ times showed that the average angle between the specimen axis and the helical fracture trace in the surface of the specimen was 77.5 degrees.

Fig. 6 charts crack growth from failure onward for three specimens from each of the differently prestrained sets. The slope of the growth curve for the twisted specimens is almost 3 (actually 2.88) times greater than the slope for twisted and untwisted specimens.

Discussion of Results

It is clear from Fig. 4 that specimens prestrained by twisting in only one direction had shorter lives than those that had been twisted and untwisted. That specimens twisted unidirectionally should have

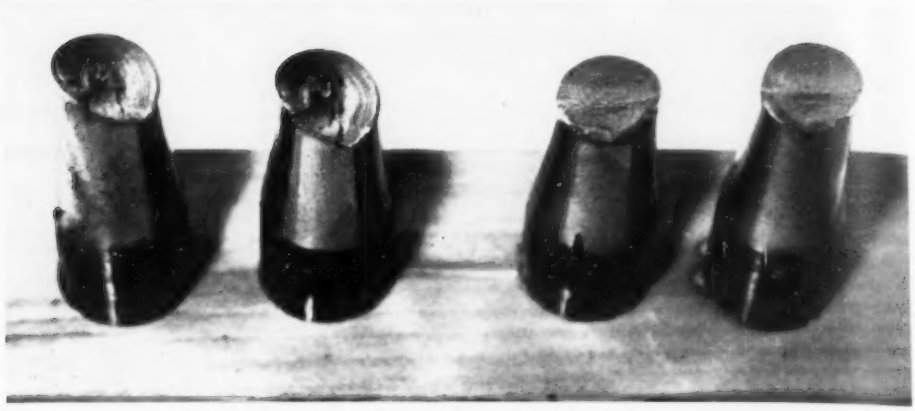


Fig. 5—Fracture Surfaces. Specimen on the right prestrained by forward and reverse torsion; that on the left by unidirectional torsion. Fracture in both cases started at the point most distant from the reader. Approximately ×1.5

shorter life is simply explained with the concept of oriented microcracks. In these specimens of shorter life, cracks at the surface where the stress was highest were directed very nearly at right angles to the stress axis and so hastened the onset of failure over surfaces defined by the orientation of the crack structure. At the highest stress, the average life of specimens that had been prestrained by unidirectional twisting was little more than 50% of the life of those that had been twisted and untwisted.

The appearance of the two fractures in Fig. 5 is also consistent with the explanation based upon oriented microcracks. The angle ϕ which the crack structure is considered to make with the axis of the specimen at the specimen surface after a shear strain of 5 at the surface is

$$\phi = \tan^{-1}\gamma = \tan^{-1}5 = 78.7°$$

and agrees very well with the measured angle between the fracture trace and specimen axis of 77.5 degrees.

As noted above, previous work on copper showed that a shear strain of approximately 2 was required before the helical tensile fracture was encountered. The intact core in the specimen at the left in Fig. 5, into which the helical fracture surface did not penetrate and that was finally broken by hand, measured approximately 0.07 in. in radius. Accordingly, the shear strain at the edge of the core for a surface shear strain of 5 and a specimen radius of 0.187 in. was

$$\gamma_{core} = \frac{0.07}{0.187} \times 5 = 1.9$$

Thus the helical fracture in fatigue similarly has occurred only in material previously twisted to a shear strain greater than about 2.

The most sensitive indication of the presence of a highly oriented microcrack structure is found in the rate of crack growth. In

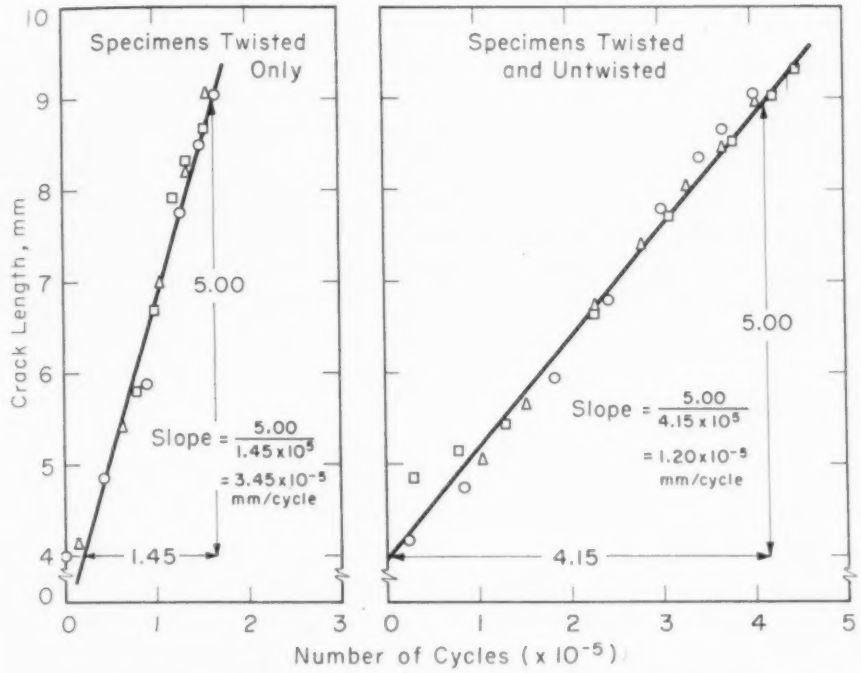


Fig. 6—Rate of Crack Growth in Specimens Twisted Only, Compared to That in Twisted and Untwisted Specimens. Constant deflection during growth of half-value, 0.0375 cm.

specimens that are simply twisted, the microcracks, because of their orientation, should contribute directly to the growth of the fatigue crack; while in those that are twisted and then completely untwisted, the cracks are still aligned parallel to the specimen axis and should have little effect on the propagation of a fatigue crack. As Fig. 6 shows, a crack advanced about 3 times as fast in the former specimens.

The data assembled in Fig. 4 have prompted some speculation about when damage begins during the life of a fatigue test specimen. All evidence that has been accumulated supports the idea that at the surface of each fatigue specimen prestrained by twisting to a shear strain of 5, there is an array of extremely small flaws, crack-like in nature and oriented nearly at right angles to the specimen axis. Since the microcracks in these specimens were almost perpendicular to the maximum tensile stress, they might be expected to reduce the number of cycles to failure considerably. Such microcracks were also present in specimens prestrained by twisting and untwisting through a shear strain of 2.5, but then they were aligned parallel to the specimen axis. The latter specimens, as Fig. 4 shows, withstood more cycling at each stress level. It is suggested, therefore, that the difference in life, or number of cycles, between the two sets of specimens at all stress levels is, to some extent, a measure of

the number of cycles required to generate cracks perpendicular to the axis, comparable to the microcracks, in the twisted and untwisted specimens of longer life. Expressed as a percentage of the average total life, this amounts to about 47 percent at the highest stress level and about 30% at the three lower levels. Dolan (6) has referred to work of Craig and Love in which minute cracks were detected by electron microscopy within as little as 0.1% of the normal fatigue life. Therefore, as an additional suggestion prompted by that work, if approximately 30% of expected life is expended growing cracks comparable to microcracks, it would certainly seem that with appropriate examination microcracks should be visible under the electron microscope.

Summary and Conclusions

The work reported above has shown that copper of commercial purity can be highly anisotropic with respect to its mechanical behavior under fatigue loading. Such behavior is considered to result from an extremely fine-scale, fibrous crack structure aligned parallel to the axis of the bar from which fatigue specimens were taken.

The anisotropy was established with bending-beam type tests on two sets of specimens after prestraining and work hardening by approximately the same amount; one set, however, was twisted to produce a shear strain of 5 at the surface of the minimum section of the fatigue specimen, while the other was twisted only to a shear strain of 2.5 and then completely untwisted. From tests at four stress levels, it was found that specimens twisted in only one direction (a) failed after fewer cycles of stress, (b) developed a helical, fibrous-appearing fracture rather than a fracture normal to the specimen axis, and (c) exhibited much more rapid crack propagation than the specimens that had been twisted and untwisted. A simple explanation is found by considering that the unidirectional twisting had reoriented the crack structure in a helical pattern nearly perpendicular to both the specimen axis and maximum tensile stress, and thus had facilitated the development of fatigue cracks and their rapid growth. In specimens prestrained by twisting and untwisting, the initial orientation of the crack structure parallel to the specimen axis was unaltered and it could not be expected, therefore, to make any direct contribution to the onset of failure. It follows from these observations that, in general, anisotropy in the fatigue properties of wrought metal may be at least partly caused by such a crack structure.

It is suggested that the difference in life at constant stress level represents the number of cycles before permanent damage from the generation of cracks comparable to microcracks has occurred in the twisted and untwisted specimens. As a consequence of this sugges-

tion, the formation of cracks equivalent to microcracks takes place within approximately the first 30% of the total number of cycles predicted by the S-N curve.

Acknowledgments

The work reported in this paper was conducted as part of a research program sponsored by the Office of Naval Research. The contributions of Professor E. R. Marshall, Professor W. M. Murray, Mr. David Norton, and Mr. Robert McMath are gratefully acknowledged.

References

1. W. A. Backofen and B. B. Hundy, "Mechanical Anisotropy in Some Ductile Metals," *Journal*, Institute of Metals, Vol. 81, 1953, p. 443.
2. W. A. Backofen, A. J. Shaler, and B. B. Hundy, "Mechanical Anisotropy in Copper," TRANSACTIONS, American Society for Metals, Vol. 46, 1954, p. 655.
3. J. T. Ransom, "The Effect of Inclusions on the Fatigue Strength of SAE 4340 Steels," TRANSACTIONS, American Society for Metals, Vol. 46, 1954, p. 1254.
4. R. Jacquesson and P. Laurent, "Les Renseignements Fournis par des Essais de Fatigue sur L'Etat Crystallin des Toles," *Revue de métallurgie*, Vol. 46, 1949, p. 89.
5. F. A. McClintock, Discussion, *Journal*, Applied Mechanics, Vol. 22, March 1955, p. 152.
6. T. J. Dolan, FATIGUE, Symposium, American Society for Metals, 1954, p. 13.

THE INFLUENCE OF VIBRATION ON THE SOLIDIFICATION OF AN ALUMINUM ALLOY

By R. S. Richards and W. Rostoker

Abstract

Vibration imposed during the solidification of an aluminum alloy has been shown to produce grain refinement, pipe suppression, suppression of columnar grain growth, and elimination of dendritic grain geometries. The behavior trends of various vibration parameters has been studied. Effects of melt superheat, solidification time, and rigidly coupled vs. impacting vibration are reported. Observations on chemical segregation, macro- and micro-voids, and hot tearing are made. It was shown that certain crystallization products coarsened rather than refined. A hypothesis to account for both effects is presented. (ASM-SLA Classification: C5, N12, Al)

DURING the past thirty years or more, the literature has contained references to the subject of the solidification characteristics of metals when acted upon by a vibratory motion. A critical review and extensive list of such references has appeared in a recent paper by Hiedemann (1).[1] The evidence has been quite positive that vibration can induce refinement of the as-cast grain size. The information on other effects is less well documented.

The results of preliminary experiments on this subject were reported by Berger and Rostoker (2). In this work, a series of aluminum-copper alloys were solidified under the influence of the rapping action of a pneumatic vibrator. Such a rapping device produces a wide spectrum of frequencies which is relatively fixed for any given system, but the total impacting energy can be varied through the line air pressure. With this relatively crude arrangement, a number of interesting effects were revealed.

Very pronounced grain refinement can be produced by vibrating a volume of metal during its solidification history, the degree being more marked at lower alloy contents. Slowly solidified ingots showed more grain refinement than chill cast ingots. Grain refinement de-

[1]The figures appearing in parentheses pertain to the references appended to this paper.

The work herein reported represents a portion of the thesis submitted by R. S. Richards to the Illinois Institute of Technology for the degree of Master of Science.

Investigation performed under contract No. DA-11-022-ORD-1307 for Frankford Arsenal.

A paper presented before the Thirty-Seventh Annual Convention of the Society, held in Philadelphia, October 17–21, 1955. Of the authors, R. S. Richards is metallurgist, Titanium Metals Corp., Henderson, Nevada, and W. Rostoker is supervisor, Physical Metallurgy Section, Metals Research Department, Armour Research Foundation of Illinois Institute of Technology, Chicago. Manuscript received February 16, 1955.

pended on impacting energy to a limit, beyond which no further benefit was derived. In fact, at the higher impacting energies, frequent hot tears were generated.

The application of vibration during solidification resulted in a pronounced suppression of columnar grain growth. In the equiaxed grain aggregates, there was a remarkable disappearance of dendritic growth patterns. While primary solid solution grains refined readily, primary intermediate phases and nonmetallic crystallization products showed little tendency to do so and in fact, often showed a definite coarsening of needles and plates.

This work has been continued to analyze more closely the effects noted. In particular, the nature of the vibration used was the subject of more detailed scrutiny. In order to accomplish this, equipment was used which permitted better control of pertinent parameters.

Material, Equipment, and Procedures

A single 2500-pound heat of an alloy approximately equivalent to Alcoa-195 was acquired. The analysis is given as follows:

Cu	4.35%	Zn	0.41%
Si	1.28	Ti	0.05
Fe	0.50	Ni	0.03
Mn	0.46		

Melting was performed in 100 KW, 3 KC induction melting furnaces using clay bonded graphite crucibles. Where necessary, heats of about 100 pounds were melted so that one 50-pound ingot could be cast with vibration and one consecutively cast without vibration. Except in earlier experiments, the heats were degassed with chlorine, the efficiency of hydrogen elimination being judged by a high vacuum solidification test.

The ingot molds were of welded sheet metal construction. Thus, the mass of the mold was small enough to have little chilling action on the solidifying metal. For the majority of the work, ingots of approximate dimensions 6 ×6 ×12 inch were cast. In the special experiments where vibration frequency was varied, the capacity of the vibration generators limited the ingots to about 10 pounds of aluminum alloy in the form of cylinders 4 inch diameter by 6 inch high.

Except in the above mentioned variable frequency experiments, vibration was generated by a commercial electro-magnetic type of unit[2] such as is used in barrel packing or investment mold production. These vibrator units are essentially electro-magnets operating on alternating current (60 c.p.s.). The solenoid and its core pull a steel table down against the opposition of heavy springs. The alternating current sets the table in continuous vibration. The

[2]Manufactured by the Syntron Company, Homer City, Pa.

amplitude of the vibration can be varied somewhat by the current control on the solenoid. The mold and its contents were rigidly clamped to the vibrator table. This served to introduce a much narrower spectrum of frequencies than was possible with the rapping device used in earlier experiments. Calibration of peak-to-peak displacements delivered by the vibrator showed that the machine was load sensitive and that with the approximately 60 lbs. load represented by the ingot and mold, the maximum deliverable displacement was of the order of 0.020 inch.

The basic table motion is sinusoidal, so that the instantaneous displacement $d = D \sin 2\pi ft$ where D is the peak displacement, f is the frequency and t is time. The total vertical traverse is 2D. Velocity is the first time derivative of displacement: $v = 2\pi fD \cos 2\pi ft$; the peak velocity is $2\pi fD$. Acceleration, the first time derivative of velocity, is: $a = 4\pi^2 f^2 D \sin 2\pi ft$ and the peak acceleration is simply $4\pi^2 f^2 D$. A power input can be computed for a rigidly coupled load in terms of the product of the peak velocity and the mass of the mold plus ingot. In all of these factors, there are only two independent parameters, frequency and peak-to-peak displacement. But since the mechanism by which vibration affects solidification was not known, it was appropriate that each of these vibration parameters be correlated with ingot structure, particularly grain size.

For macro-structure examination, a vertical slice from the center portion of each ingot was cut and machined to a good surface finish for etching. Grain sizes were determined by lineal count on a photomacrograph. Two types of porosity estimates were used. Total porosity was gained from density measurements on cylinders machined from identical locations within the ingot. This sort of measurement was very time consuming, and because the magnitude of porosity was small, the copper content of each cylinder had to be analyzed to apply a correction to the density measurement. A second method, estimated the volume of voids connected to the surface of the half-inch-thick machined slab. The connecting porosity was filled by impregnation with glycerine. Weight measurements before and after impregnation permitted calculation of the volume of interconnecting voids.

Influence of Vibration Parameters on Grain Size

In a preliminary series of experiments, 50-pound ingots poured at 1450°F were solidified over the range of deliverable vibration amplitudes. The correlation with resulting grain size is shown in Fig. 1. These results show that vibration "intensity" can exert a profound influence on grain refinement and in limiting instances can provide grain diameter reductions of as much as 10:1.

Although the Syntron vibrator was most practical for the

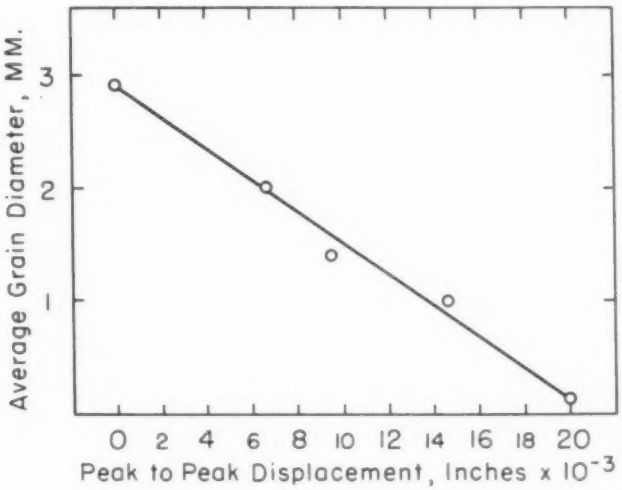
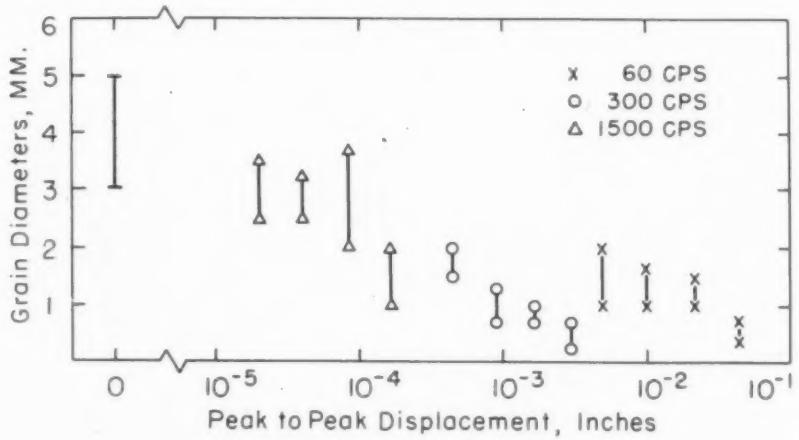


Fig. 1—Correlation of Grain Size with Vibration Amplitude (60 c.p.s.).



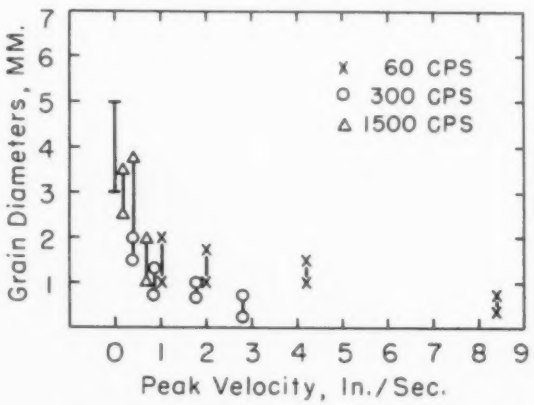


Fig. 2—Correlation of Grain Size with Vibration Frequency, Amplitude and Peak Velocity.

major portion of this program, it was necessary to have the use of a more flexible piece of equipment to provide a controlled variable

frequency vibration. For this purpose, the services of an MB C5H—650-pound force output, electromechanical vibration exciter[3] were acquired. This machine is capable of delivering frequencies from 5 to 2200 c.p.s. with accelerations to a 10-pound ingot of up to 15 G.

A series of 10-pound ingots were poured at 1400°F and solidified under five levels of acceleration at each of three frequencies, 60, 300,

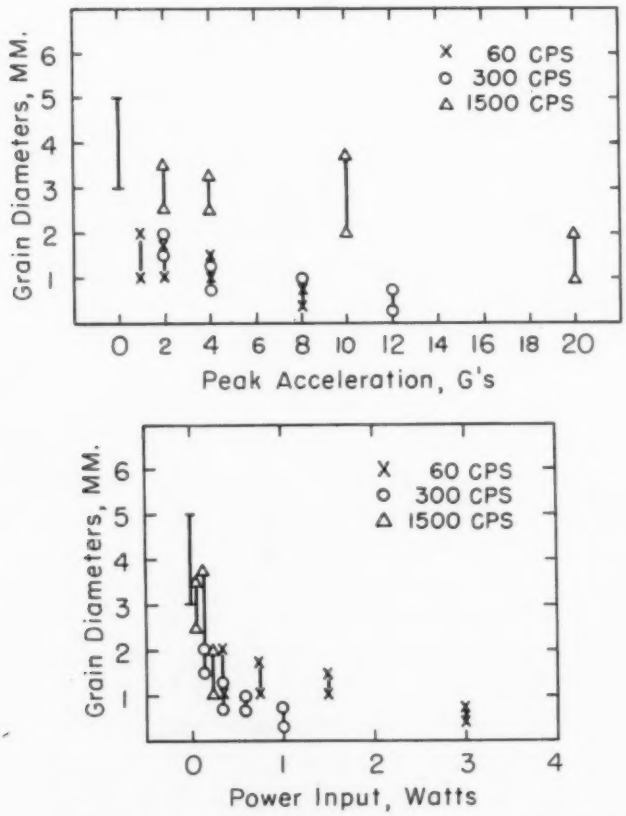


Fig. 3—Correlation of Grain Size with Vibration Frequency, Peak Acceleration and Power Input.

and 1500 c.p.s., respectively. The results of grain size measurements and their correlation with various vibration parameters are summarized graphically in Figs. 2 and 3. Because grain sizes in each ingot often varied considerably, the results are given as bands. All four factors, peak-to-peak displacement, peak velocity, peak acceleration, and power input, correlate with grain size. Grain size versus displacement yields a simple and frequency-independent correlation, and since the other parameters are only derivatives, displacement is regarded as the fundamental property. The independence from frequency is an important discovery, since the large

[3]Manufactured by the MB Manufacturing Company, New Haven, Conn.

majority of papers on this subject infer, if not actually state, that high frequencies are most effective.

There are practical reasons for selecting lower frequencies of vibration. The accelerations produced exert, on one half of the cycle, a force tending to separate droplets of metal from the liquid body. Because of the nature of the acceleration formula, at the displacements necessary to yield appreciable grain refinement, the accelerations associated with high frequencies are too high and a considerable amount of metal is sprayed out of the mold. The advantage of low frequencies over high frequencies is fortunate, since machinery to deliver the requisite displacements to large volumes of metal and heavy molds is considerably simpler in design and construction.

Rigidly Coupled versus Impacting Vibration

A direct comparison was made between the effects of vibration under conditions of rigid coupling (mold fixed to the table) and under impacting (mold resting on the table but uncoupled). Two ingots were poured at 1530°F and solidified one under each of the two types of vibration (at a setting for 3.5G acceleration with rigid coupling). In the case of the rigidly coupled ingot, the average grain size was 0.2 mm diameter, whereas in the impact ingot the average grain size was about 1 mm. So it would seem that both types of vibration can have effect but that the rigidly coupled vibration is the more efficient.

Grain Size versus Melt Superheat

With aluminum alloys, higher pouring temperatures yield generally larger as-cast grain sizes. On the other hand, high pouring temperatures are sometimes needed to insure complete filling of mold cavity. A series of experiments were conducted to see if by the use of vibration, the grain coarsening tendencies of superheating could be counteracted.

Hundred pound melts were made for these tests so that a 50-pound vibrated and an identical unvibrated ingot could be poured one after the other from the same melt. Pouring temperatures ranged from 1225 to 1750°F. The vibrator was set to deliver 3.5G acceleration. The results of grain size measurements on vertical slices taken from each ingot are summarized in Fig. 4. It may be seen that whereas the unvibrated ingots showed progressively increasing grain size with increasing pouring temperature, with the use of vibration, this tendency is completely eradicated.

One further point must be remarked upon. The ingot poured from 1750°F and solidified without vibration showed extremely coarse, dendritic grains. The companion ingot solidified under the

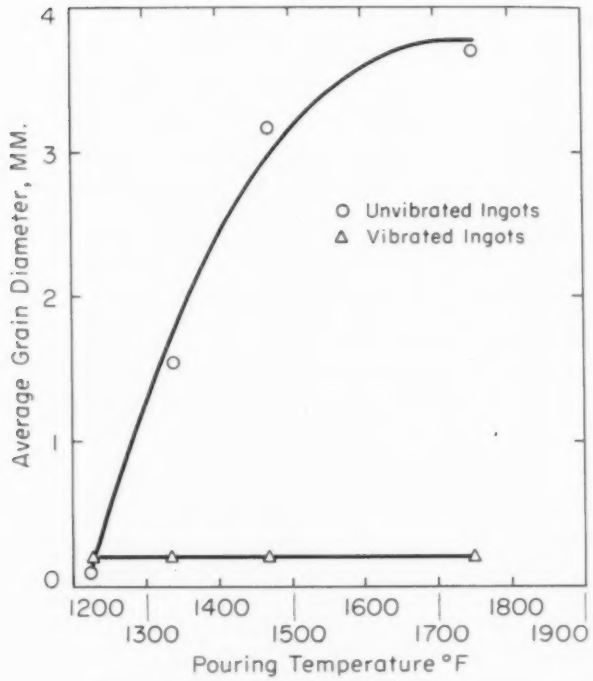


Fig. 4—Correlation of Grain Size of Vibrated (60 c.p.s., 3.5G Acceleration) and Unvibrated Ingots with Pouring Temperature.

influence of vibration not only had a very fine grain size, but also the dendritic configurations were completely absent. It is a general observation that vibrated ingots showed less tendency toward dendritic structures under either macro- or micro-examination.

The Effect of Discontinued Vibration

Three 50-pound ingots were poured from 1500°F. Vibration acceleration of 3.5G was imposed on one ingot during the period of cooling to 1320°F (at which temperature the metal was still all liquid) and then discontinued. A second ingot was vibrated during the whole period of solidification. A third ingot was permitted to solidify under quiescent conditions entirely. The first and third ingots were identical, indicating that vibration of the liquid itself has no influence on its subsequent solidification characteristics. It would appear that the vibration exercises its effect only during the "mushy" stage.

Grain Size vs Solidification Time

The freezing time of the 50-pound ingots in the sheet metal molds was of the order of 15 minutes. By inserting cooling coils at the bottom of the "can" mold, the freezing time could be shortened to less than five minutes. Extremely slow cooling rates of the order of 2 hours were achieved by insulating the mold walls with one inch

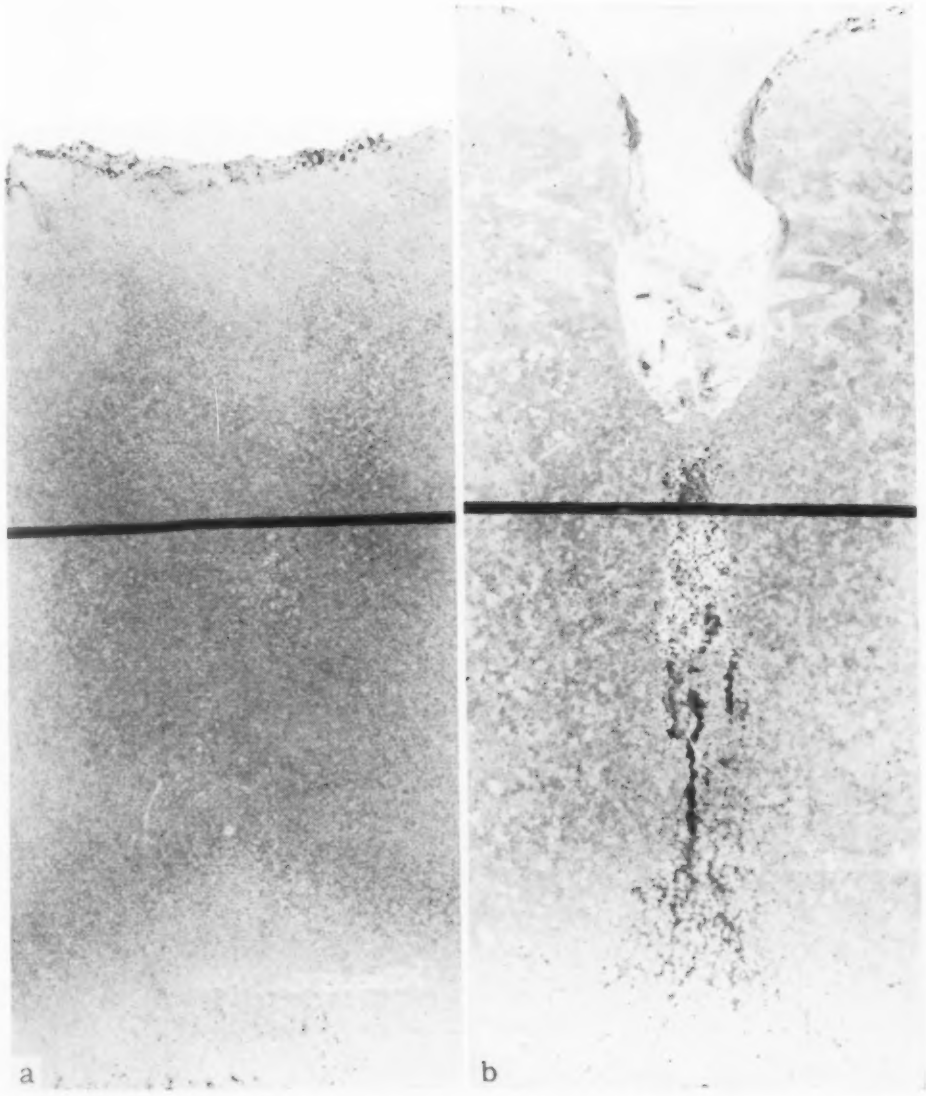


Fig. 5—Comparison of Depth of Pipe in Vibrated (60 c.p.s., 3.5G Acceleration) and Unvibrated Ingots.

of asbestos fiber and paper. This slow cooling rate simulates the conditions prevailing in the center of very large sections. Using the various cooling rates, it was found that unvibrated ingots developed a wide range of grain sizes from two centimeters for the insulated molds to two tenths of a millimeter for the highest cooling rates. Under these various cooling rate conditions, vibrated ingots (3.5G acceleration) developed grain sizes of 0.2–0.7 mm diameter.

The general conclusion is that vibration counteracts normal grain coarsening tendencies, but that conditions such as chilling, which naturally reduce the grain size of the unvibrated ingots, reduce the range over which vibration can contribute improvement.

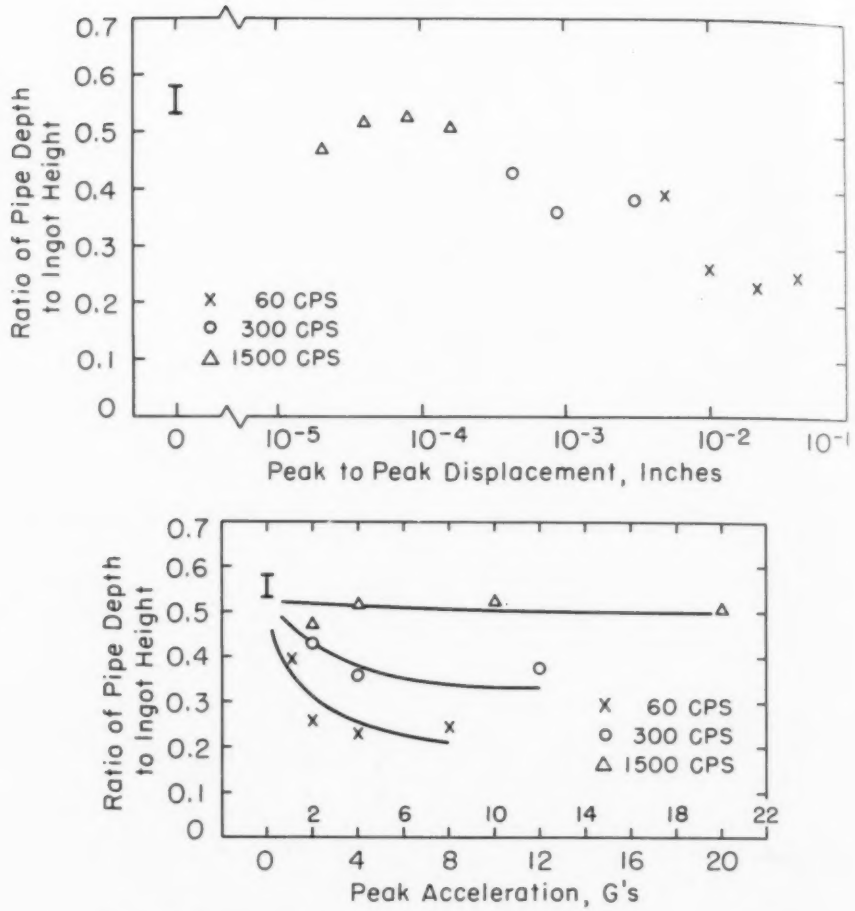


Fig. 6—Correlation of Pipe Formation with Vibration Frequency, Amplitude and Peak Acceleration.

Influence of Vibration on Ingot Soundness

One can describe soundness in terms of gross external defects such as "pipe," internal macro-shrinkage defects, hot tearing, micro-shrinkage, and gas porosity. The first three can be recognized visually; the latter two can at best be estimated in terms of density measurements.

The series of 50-pound ingots poured at 1450°F with varying degrees of vibration intensity (60 c.p.s.) apart from grain size trends showed positive evidence of elimination of "pipe" and other macro-shrinkage defects. In fact, at a displacement level of 0.018 inch (3.5 G), pipe was completely eliminated. A comparison of vibrated and unvibrated ingots is shown in Fig. 5. A general decrease in macro-shrinkage defects can easily be observed.

The observations on pipe formation on the 10-pound ingots solidified under various frequencies of vibration are summarized in Fig. 6. Clearly, pipe suppression as grain refinement is basically

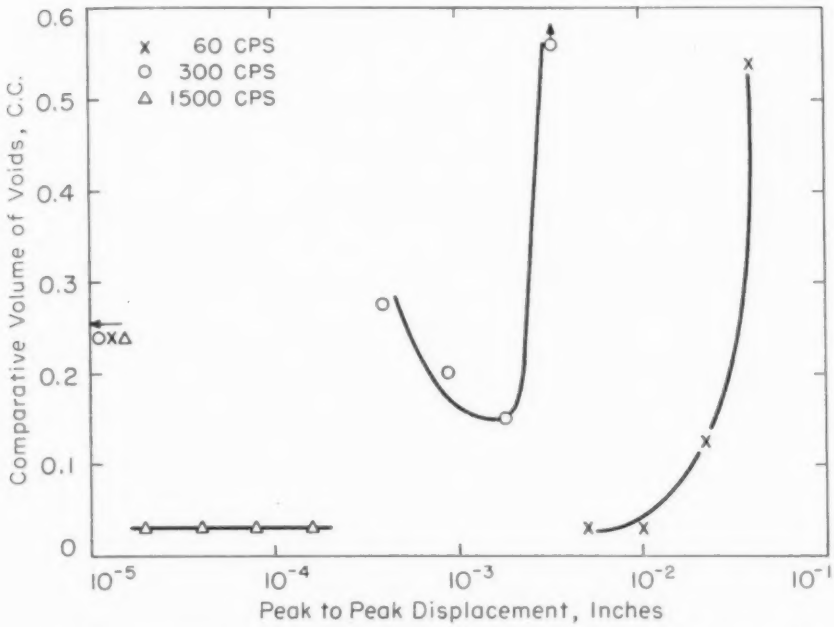


Fig. 7—Correlation of Void Volume with Vibration Frequency and Amplitude.

related to peak-to-peak displacement, but when judged in terms of acceleration, is definitely frequency dependent. Again practical considerations of producing requisite displacements dictate the use of lower vibration frequencies.

It is suggested that pipe elimination results from the action of vibration during the "mushy" stage of solidification. During this period, the "mush" is composed of an aggregate of solid grains surrounded by a liquid network. The vibration acts to segregate liquid from solid by packing the solid down and displacing the liquid up. In this way, unidirectional solidification from the bottom is simulated and pipe formation is suppressed.

A number of the 10-pound ingots solidified under various frequencies of vibration showed considerable hot tearing. There does not seem to be any clear correlation with vibration parameters. At 60 c.p.s., the ingot given vibration displacement of 0.044 inch showed hot tearing. At 300 c.p.s., the ingots given vibration displacements of greater than 0.0009 inch showed hot tearing. None of the ingots vibrated at 1500 c.p.s. showed hot tearing.

Estimations of the volume of micro-voids (of shrinkage or gas origin) were made in two separate sets of experiments. From a 50-pound ingot series poured at various temperatures, cylinders were machined from the central portions for density measurements. Each of the heats was degassed with chlorine prior to pouring. Density measurements were corrected to a common copper content[4] and the

[4]Measured density + (4.35 − %Cu)(0.022 gms/cc) = equivalent density at 4.35%Cu.

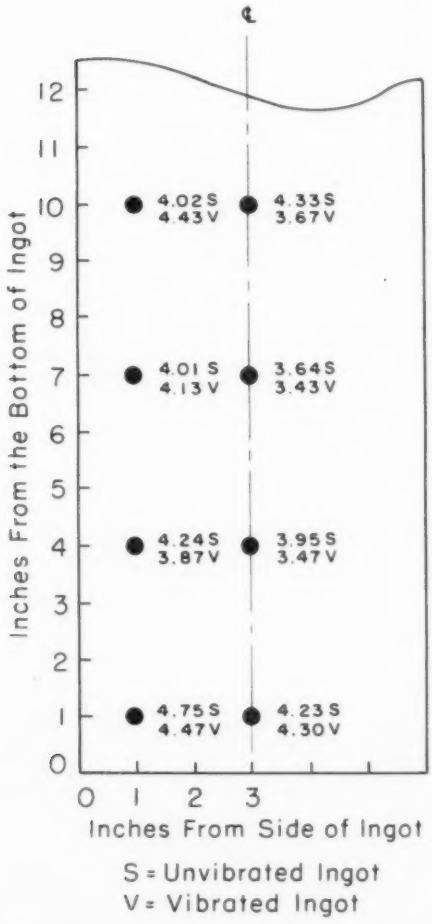


Fig. 8—Comparison of Copper Segregation in Vibrated (60 c.p.s., 3.5G Acceleration) and Unvibrated Ingots Poured at 1200°F.

averaged values of porosity from four positions are summarized in Table I.

Table I
Average Porosities of Vibrated and Unvibrated Ingots

Pouring Temperature, °F		% Relative Porosity
1500	vibrated	0.99
	unvibrated	0.72
1415	vibrated	0.95
	unvibrated	1.09
1320	vibrated	0.08
	unvibrated	0.53
1225	vibrated	0.34
	unvibrated	0.66

There does not seem to be any positive trend of superiority or inferiority in void content as a result of imposing vibration during solidification.

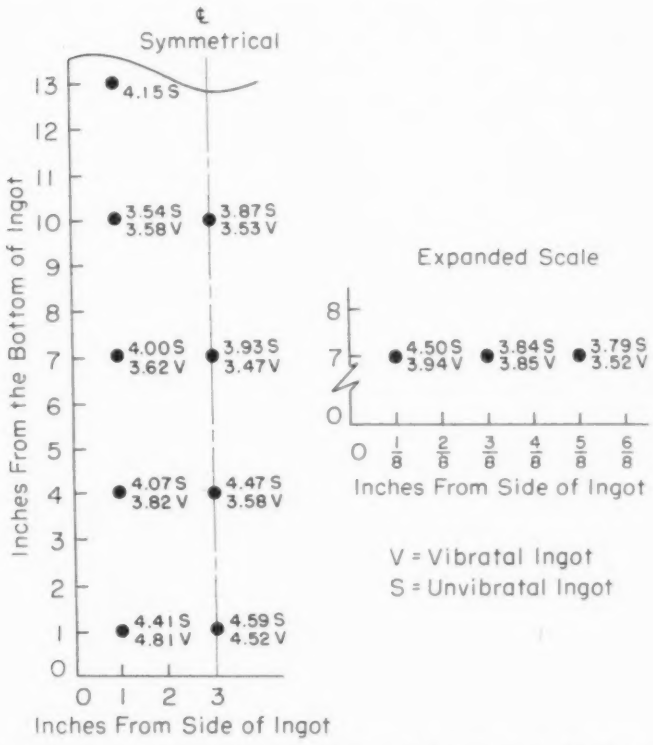


Fig. 9—Comparison of Copper Segregation in Vibrated (60 c.p.s., 3.5G Acceleration) and Unvibrated Ingots Poured at 1750°F.

In a second set of experiments, the central vertical slices from the 10-pound variable frequency experiments were machined and polished to a surface finish suitable for macro-examination. The two surfaces were then vacuum impregnated with glycerine and the surface excess cleaned off. By weight gain measurements, an estimate could be made of void volume exposed at the surfaces. This method had the disadvantage of not giving an absolute value of void volume, but as a comparative figure it was preferable because it was able to make use of a large sample. The results are plotted in Fig. 7. Both 300 and 60 c.p.s. ingots showed the same effect of a sudden upsurge in pore volume above a given value of vibration displacement.

Influence of Vibration on Chemical Segregation

Two pairs of ingots cast in the "superheat" experiments were analyzed for copper distribution. The two pairs represent pouring temperatures of 1200 and 1750°F, respectively. Drillings were taken at the various positions on the central plane of the ingots as shown in Figs. 8 and 9. An expanded scale is also utilized in Fig. 8 to show additional analyses taken near the surface of the ingots. These analyses indicate that the vibrated ingots exhibit somewhat more inverse segregation than do the unvibrated ingots.

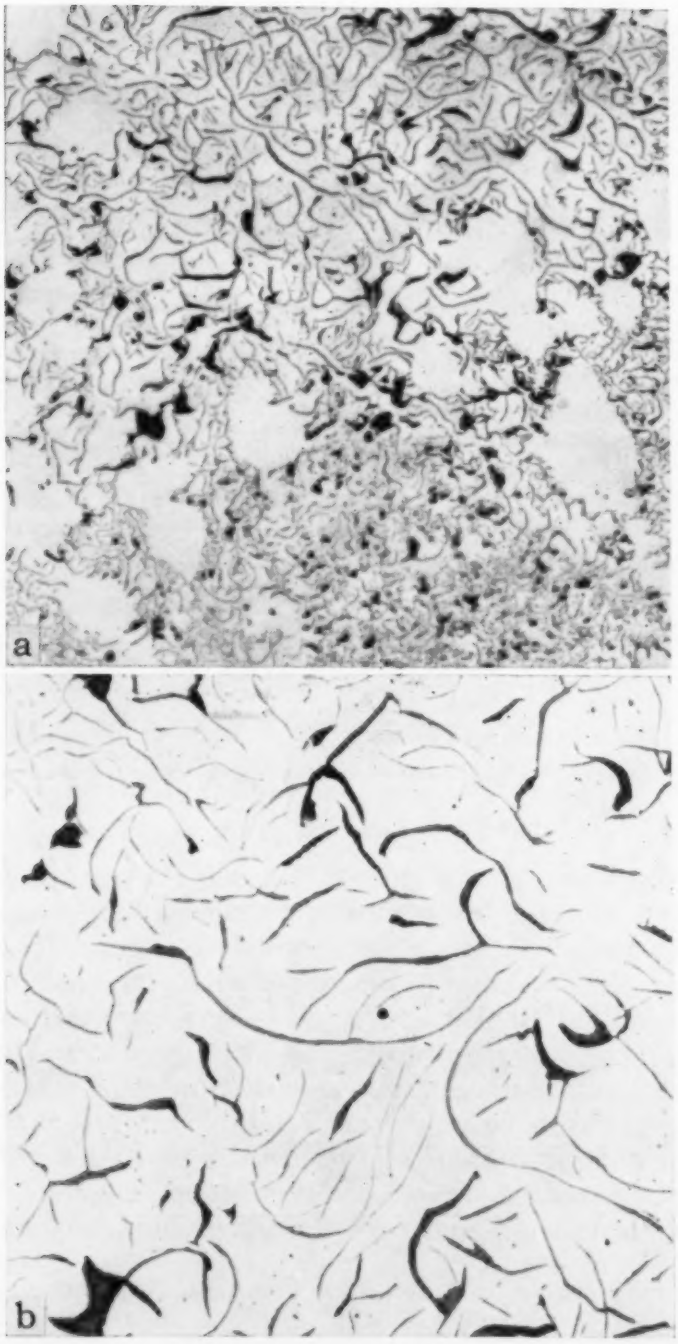


Fig. 10—Comparison of Graphite Flake Size in Grey Iron (a) Unvibrated, (b) Vibrated.

Discussion of the Mechanism of Grain Refinement by Vibration

With the results herein reported and those of ref. (2), there is ample and sustained evidence that the as-cast size of crystallites of terminal solid solutions can be substantially reduced by vibration.

However, not all products of crystallization are so affected. In the previous paper (2) it was shown that certain primary solids, notably Si plates and $FeAl_3$ needles, actually were coarsened by the action of vibration. A further example of this opposite behavior is the graphite flake size in cast iron. Two ingots of grey iron poured from 2625°F, one vibrated, the other not, gave the microstructures in Fig. 10. A very pronounced coarsening of the graphite flake size can be seen. It should also be remarked that the dendrite size of the primary austenite was, in contrast, refined.

The theory has been advanced (3) that grain refinement derives from fragmentation of primary crystallites, providing an artificial source of more nuclei. This concept, of course, cannot be reconciled with coarsening effects, especially when the crystallization products coarsened are significantly less ductile than those refined.

There seems to be further evidence which contradicts this theory. Van Hook and Frulla (4) have shown that sugar solutions require a supersaturation of about 1.6 before homogeneous nucleation occurs. Since the growth rate in their solutions even at very low supersaturations was fast, it follows that no nuclei larger than the critical size for stable growth were present. These authors noted that with supersaturations as low as 1.02, immediate nucleation and growth to visible size was achieved by application of vibration to the solution. That these solutions contained no nuclei larger than actual size was proven by the fact that the solutions were "practically permanent," that is, no nucleation was visible over long periods of time if the solutions were not subjected to vibration.

It does seem, therefore, that vibration affects the rate of formation of critical stable nuclei. The fragmentation hypothesis should give the wrong behavior trend in that critical stable nuclei spontaneously formed would be fragmented into sizes which were unstable and which would tend to disappear.

Now suppose it is hypothesized that vibration increases the nucleation rate. Since the specific volume of the solid is less than of the liquid, the pressure wave of vibration would tend to reduce the size of the critical stable nucleus. By the same token, the rarefaction wave would increase the size. Since as far as is known the pressure and rarefaction cycles are identical, the only way a net gain or loss of total number of stable nuclei could be effected is if the rate of embryo formation has a peculiar dependence on the embryo size as exemplified in Fig. 11. Note in case I, the average of $\dot{n}(r_{CP})$ and $\dot{n}(r_{CR})$ is greater than $\dot{n}(r_C)$. Accordingly, the total number of grains produced in finite time is increased and a grain refinement would be observed. In case II, $\frac{\dot{n}(r_{CP})+\dot{n}(r_{CR})}{2} < \dot{n}(r_C)$ and the net rate of nuclei formation is reduced, resulting in coarser products of crystal-

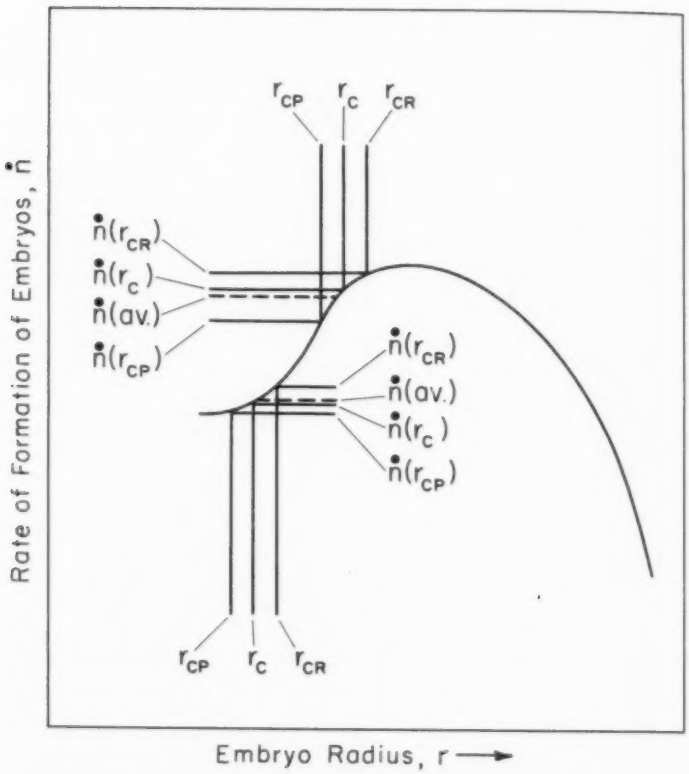


Fig. 11—Hypothetical Relationship Between Rate of Embryo Formation and the Size of the Embryo.

lization. This sort of embryo formation rate relationship is actually realized from the simple equation for the formation of a new phase: $\dot{n} = C \exp. -\Delta G/kT$ where ΔG is the work of formation per unit volume of the new phase and is equal to $4\pi\sigma\left(r^2 - \frac{2r^3}{3rc}\right) - \sigma =$ interfacial tension; $r =$ radius of embryo of new phase; $r_C =$ critical stable embryo.

It will be noted that the integrated time during which the melt experiences pressure and then rarefaction is independent of frequency, and accordingly the modified rate of embryo formation should also be independent of frequency. It will be recalled that this was actually found to be the case.

Summary

The application of vibration during the solidification of an aluminum alloy has been shown to induce a number of important modifications to the as-cast structure. Chief among these are a pronounced refinement of grain size and an impressive reduction in the depth of pipe. As reported in an earlier publication on the work, suppression of columnar grain growth and dendritic grain

geometries are also encountered. These effects appear to be fundamental to the solidification process and therefore should be reproducible on any alloy which is predominantly of the solid solution type.

All of the effects noted are enhanced by increasing vibration intensity whether expressed in terms of peak-to-peak amplitude, maximum velocity, maximum acceleration, or power input. When grain refinement is correlated with peak-to-peak displacement there is no dependence on frequency within the range 60–1500 c.p.s. The practical upper limit to vibration intensities is set by the occurrence of hot tearing and ejection of metal from the mold during solidification. In addition, above a certain level of vibration intensity the increase in grain refinement is relatively small. For the particular aluminum alloy studied a peak-to-peak displacement of about 0.020 inch at 60 c.p.s. gave optimum advantageous effects with no deleterious hot tearing or excessive metal ejection. The degree of grain refinement achieved by 60 c.p.s. vibration is at least as considerable as claimed in any published work with ultrasonic frequencies. The trend of peak-to-peak displacement vs pipe suppression would indicate that it would be impractical to try to achieve pipe elimination with ultrasonic frequencies. From the viewpoint of equipment necessary, every advantage lies in the use of low frequency vibration machinery.

For the particular type of vibration used, at a given power input, castings coupled rigidly to the machine were more effectively grain refined than identical castings resting in their mold unattached to the vibrator table (i.e. impact vibration).

Vibration has influence on the cast structure only when applied during the solidification period. It does not condition the liquid in any sense. Grain coarsening induced by high pouring temperatures and slow solidification rates can be completely counteracted by application of vibration during solidification.

Vibration does not seem to have a pronounced effect on micro porosity except at higher levels of vibration intensity, at which a sharp increase in void volume occurs. Vibration does appear to reduce the occurrence of large shrinkage defects. There is no significant dependence of chemical segregation on vibration.

The fragmentation theory of grain refinement by vibration does not seem compatible with the experience that under certain circumstances a pronounced coarsening of brittle solidification products can occur. An alternative hypothesis is suggested in terms of the pressure dependence of thermodynamic relations for nucleation.

Acknowledgment

Sponsorship of this work by Frankford Arsenal, Philadelphia,

Pa., and permission to publish are gratefully acknowledged. In particular, the advice and discussion contributed by Mr. H. Rosenthal of the Pitman-Dunn Laboratories, Frankford Arsenal, has been of great value to the progress of this work. Mr. A. Murphy conducted the experiments with the variable frequency machine.

References

1. E. A. Hiedemann, "Metallurgical Effects of Ultrasonic Waves," *Journal*, Acoustical Society of America, Vol. 26, 1954, p. 831.
2. M. J. Berger and W. Rostoker, "Effects of Vibration During Solidification of Castings," *Foundry*, July 1953, p. 100, p. 260.
3. G. Schmid and A. Roll, "The Importance of Frequency and Intensity of Vibration on Grain Refinement," *Zeitschrift fur Electrochemie*, Vol. 45, 1939, p. 769.
4. A. Van Hook and F. Frulla, "Nucleation in Sucrose Solutions," *Industrial and Engineering Chemistry*, Vol. 44, 1952, p. 1305.

DISCUSSION

Written Discussion: By A. H. Freedman and J. F. Wallace, research assistant and associate professor of Metallurgical Engineering, Case Institute of Technology, Cleveland.

This paper on the influence of vibration on a solidifying metal describes a well directed investigation in a very important field in which only a small amount of information is available. It is particularly notable that the authors found, in agreement with Schmid and Roll,[5] that grain refinement could be more easily obtained at lower frequencies, in contrast to the usually accepted theory that higher frequencies would have more effect.

Since it is hoped that some beneficial alterations in the mode of solidification of molten metals can be obtained by the application of vibration, it is regretted that no comparative mechanical properties for the vibrated and unvibrated alloys are shown. Do the authors now have any mechanical property data that they would care to present? It is noted that at the peak-to-peak displacement which yielded maximum grain refinement, considerable porosity was obtained in the vibrated metal. This increased porosity may be the result of a fine dispersement of the shrinkage pipe throughout the ingot with a resulting deleterious influence on mechanical properties.

The increase in inverse segregation reported is also very interesting. It is suggested that this effect is associated with the more extensive flow of higher copper liquid metal through the solid aluminum particles toward the voids caused by solidification contraction on the outside of the ingot as final solidification occurs. Substitution of the fine grain structure for the labyrinth of columnar dendrites probably facilitates this flow of high-copper molten metal.

The hypothesis that vibration influences the nucleation rate appears to be in conformance with the experimental evidence. The reasons for the increase in the rate of nucleation of solid solutions and the decrease in the rate for graphite, silicon needles, etc., however, are not immediately evident. It does appear that vibrating increases the nucleation rate of metals, which solidify in a dendritic manner, and decreases the rate for metals such as intermetallic compounds and eutectics which

[5] G. Schmid, A. Roll, "The Importance of Frequency and Intensity of Vibration on Grain Refinement," Zeitschrift für Electrochemie, Vol. 45, 1939, p. 769.

do not solidify as dendrites. Possibly additional information on the mode of nucleation of these materials would provide an insight into this problem.

Written Discussion: By P. R. Sperry, research metallurgist, Kaiser Aluminum and Chemical Corporation, Department of Metallurgical Research, Spokane, Washington.

To explain the elimination of pipe by the application of vibration during solidification of a casting, the authors postulate a settling of the solid crystals in the liquid matrix during the "mushy" stage. In view of the fact that these primary aluminum solid crystals are impoverished in alloying elements and the liquid is correspondingly enriched, one would expect to find segregation from top to bottom with the top being enriched in alloying element. This phenomenon would lend support to the proposed explanation of pipe elimination. However, it is conceivable that other effects such as segregation in the liquid could mask the settling effect.

The observations concerning the influence of vibrations on microstructure are quite interesting. The tendency toward elimination of dendritic structure of primary crystals is not easily explained, but, knowing that this occurs, it is not surprising that coarse secondary phases were encountered. Normally during solidification of complex aluminum alloys, the precipitation of the primary crystals is followed by a series of binary and possibly more complex eutectic crystallizations. These eutectics form over a temperature range and give rise to the "divorced" type of structure in which the intermetallic phase is not intimately connected with the secondary aluminum. The latter deposits upon the primary dendrites. The divorced eutectics form from the alloy enriched liquid in the dendrite interstices and the intermetallic phases can develop rather coarse structures, depending upon the volume of liquid from which they grow and the temperature range over which they solidify. Frequently these coarse intermetallic phases are mistaken for primaries but they are distinguished by being located in the dendrite interstices. If the dendrites were to be replaced by spheroidal shaped primary grains, as appeared to be the case when vibration was applied, it would seem that the reservoirs of alloy enriched liquid would be larger and would therefore promote coarser secondary phases. Without the benefit of photomicrographs, I cannot be certain that this explanation is correct but it certainly seems reasonable.

Authors' Reply

The authors have conducted a comparison of the tensile properties of test pieces machined from various positions in 50-pound ingots solidified with and without vibration and using various pouring temperatures. In order to minimize macro- and micro-voids, the ingot molds were tapered and water-cooled at the base and the melt was well de-gassed prior to pouring. The vibrated and comparative unvibrated ingots were cast from the same melt in every instance. Applied vibration was of the 60 cps type at 5 G acceleration. Standard 0.505 in diameter test specimens were machined from slices taken from various horizontal planes in the ingots. The slices were solution treated and aged before machining.

The tensile strength data are summarized in bands in Fig. 12. Overall average tensile ductilities are compared in Fig. 13. The conclusions seem to be that there is no systematic effect on tensile strength but that there is a systematic superiority in tensile ductility evidenced by the vibrated ingots.

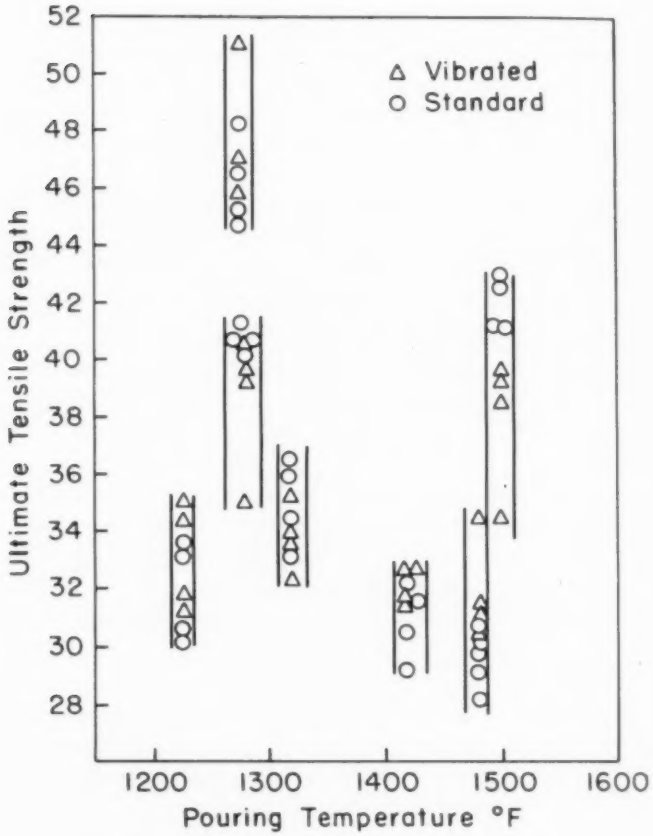


Fig. 12—Summary of Tensile Strength Data.

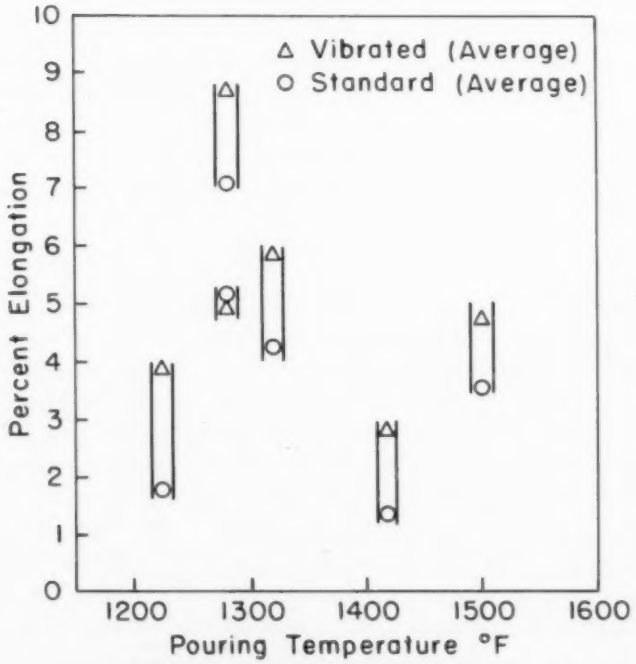


Fig. 13—Comparison of Overall Average Tensile Ductilities.

There is not a good correlation between pipe suppression and the anomalous increase in void volume (Fig. 7). At a peak-to-peak amplitude of 10^{-2} inches, the pipe suppression is as great as at an amplitude of 7×10^{-2} inches but the microporosity is markedly less even than that of the unvibrated ingot.

The authors are not convinced that the segregation pattern in the vibrated ingots are so markedly different from the unvibrated ingots as to warrant a special explanation. The authors would join Messrs. Freedman and Wallace in the opinion that a fundamental study of the mechanism by which vibration influences the cast structure would be a fruitful ground for study.

Mr. Sperry's corrollary to the "settling" hypothesis that there should also be a vertical segregation of alloying elements seems reasonable although one cannot easily anticipate the magnitude of such an effect. The ingots studied in this program were probably too short to test this hypothesis. These short ingots did show some vertical segregation of copper (Figs. 8 and 9) but the trend is opposite to what one would expect from the hypothesis.

Mr. Sperry's rationalization of eutectic coarsening is acceptable but the problem is still unresolved as to why intermetallic phases, when they are the primary crystallization products, show coarsening under vibration. Reference is made to microstructures of an Al-6% Fe alloy shown in an earlier paper (2). In this instance the $FeAl_3$ phase is the primary crystallization product and vibration definitely causes coarsening of the needles.

THE INTERMETALLIC PHASES IN 2024 ALUMINUM ALLOY

By Philip R. Sperry

Abstract

Aluminum alloy 2024 in the cast and wrought conditions was studied metallographically in order to positively identify the phases and to determine their mode of occurrence. Particular attention was given to the phases due to iron and manganese. The seven constituents found were $CuAl_2$, Al_2CuMg, Mg_2Si, Al_7Cu_2Fe, $MnAl_6$, $FeAl_3$, and αAl $(Mn, Fe)Si$. The latter three reacted with the liquid during solidification or with the aluminum solid solution during subsequent heating to form Al_7Cu_2Fe. The order of solidification for each of the phases was established and the relationship between 2024 and the Al-Cu-Fe-Mn and the Al-Cu-Mg-Si alloy systems was discussed. In the wrought condition the principal constituents were Al_2CuMg, $\alpha Al(Mn, Fe)Si$, Al_7Cu_2Fe, and Mg_2Si, with $CuAl_2$ occurring in relatively minor amounts (neglecting age hardening precipitates).

Introduction

IN spite of the numerous general descriptions of the metallography of aluminum base alloys containing copper and magnesium (Duralumin type), details concerning the identity of certain constituent phases and the mode of formation of these and other constituents are lacking. Alloy 2024 (formerly 24S), containing nominally 4.5% copper and 1.5% magnesium, is foremost among these alloys in strength properties. It was considered that a more complete exposition of the metallography of this important alloy would be of value to producers and users alike.

Among the noteworthy contributions to the metallography of Duralumin type alloys are those of Töllner (1),[1] Keller and Bossert (2), Mondolfo (3), and Phragmén (4). Agreement exists concerning the presence of the phases $CuAl_2$, Al_2CuMg, and Mg_2Si in alloy 2024 but the phases due to the presence of iron and manganese need clarification. The present work is an attempt to identify the phases containing iron and manganese and to present additional data on the mode of formation and stability of all the constituents.

Description of Phases

In cast or wrought 2024 aluminum alloy seven phases other

[1]The figures appearing in parentheses pertain to the references appended to this paper.

The author, Philip R. Sperry, is research metallurgist, Kaiser Aluminum and Chemical Corporation, Department of Metallurgical Research, Spokane, Washington. Manuscript received August 15, 1955.

than the aluminum solid solution were identified. These were $CuAl_2$, Al_2CuMg, Mg_2Si, $MnAl_6$, $FeAl_3$, $\alpha Al(Mn,Fe)Si$, and Al_7Cu_2Fe. It is to be noted that there are four phases containing iron and manganese and that one of these—$FeAl_3$—has not received prior mention in connection with Duralumin alloys.

Some of the useful optical properties and the etching characteristics using a special phosphoric acid etchant are listed in the accompanying table. Phragmén gives a more complete listing of the

Table I
Metallographic Characteristics of Phases in 2024 Aluminum Alloy

Phases	Appearance before etching: Ordinary light	Appearance before etching: Crossed polarizers	Appearance after etching 1 min in 10% H_3PO_4 at 120°F (50°C)
$CuAl_2$	Pale pink, roughened by prolonged polishing.	Changes from orange to greenish blue. Some orientations show little change.	Outlined slightly, no change in color.
Al_2CuMg	Light gray, roughened and tarnished by prolonged polishing.	All orientations change from orange to greenish blue.	Darkened slightly to markedly, depending on polish. Always roughened.
Mg_2Si	Bright blue, roughened, tarnished or pitted by prolonged polishing.	Should not change but does because of roughening.	Usually retains color and shape but is sometimes dissolved out.
$MnAl_6$	Very light gray, usually not much in relief.	Distinct change from light to dark gray, very little color.	Not, or very slightly, outlined from aluminum, uncolored or sometimes light brown, especially near Cu-rich phases.
$FeAl_3$	Darker gray than any other phase in this table, polishes in relief easily.	Very slight change, usually not detectable except for contrast between twins on large particles.	Very dark brown or bluish gray, partly dissolved. Etches lighter when enveloped by Al_7Cu_2Fe.
$\alpha Al(Mn,Fe)Si$	Light gray, shows greatest tendency to polish in relief.	No change.	Light brown and smooth to dark brown and slightly roughened, sharply outlined.
Al_7Cu_2Fe	Very light gray, just slightly darker than $MnAl_6$ and $CuAl_2$.	Weak but definite change from light to dark gray.	Outlined but not colored, sharply outlined from other Mn-Fe phases.

effects of more commonly used etchants, especially as they apply to the Duralumin compositions. However, the 10% phosphoric acid etchant employed as described in the table was found most useful for distinguishing the different constituents. Some of the characteristics of each of the phases are reviewed below.

$CuAl_2$ (also called θ phase)—This constituent remains clear and white in all the common acid etchants except 25% nitric acid which darkens it.

Al_2CuMg (also called $Al_5Cu_2Mg_2$, $Al_{13}Cu_7Mg_8$, Al-Cu-Mg, αAl-Cu-Mg, and S phase)—Al_2CuMg tarnishes and roughens upon prolonged polishing with magnesia and water and this effect causes variations in appearance and etching characteristics which can be confusing. Sometimes it etches darkly and other times lightly in phosphoric acid and other reagents. It shows marked changes in

color in polarized light as does $CuAl_2$ but the two are not hard to distinguish by other means.

Mg_2Si—There is no difficulty in recognizing Mg_2Si because of its characteristic blue color. It is best to examine for this phase before etching because all acid etchants dissolve it very readily.

$MnAl_6$—The simple designation for the binary phase is used herein in order to avoid such complex designations as $(Al,Cu)_6(Mn,Fe,Cu)$ such as was used by Phragmén (4). There is a ternary phase in the aluminum-copper-iron system which is isomorphous with $MnAl_6$. This ternary phase was called $(Al,Cu)_6(Fe,Cu)$ by Phragmén (4) and αAlCuFe by Phillips (5). $MnAl_6$ shows strong birefringence but it differs from $CuAl_2$ and Al_2CuMg in that there is more gray and less color.

$FeAl_3$—This constituent is known to dissolve some manganese and possibly a small amount of copper. $FeAl_3$ shows very weak birefringence. Before etching it has a darker gray color than any of the other iron-manganese constituents[2] and it darkens more than the others when etched with the phosphoric acid etchant.

αAl(Mn,Fe)Si—This phase is basically a ternary phase, found in both the aluminum-iron-silicon and the aluminum-manganese-silicon systems. αAl(Mn,Fe)Si apparently has a wide range of composition according to analyses reported in the literature. The change in etching characteristics shown by this phase in the presence of copper indicates that it dissolves some of this element (4). Its colors, either before or after etching in phosphoric acid solution, are midway in tone between those of $FeAl_3$ and $MnAl_6$. αAl(Mn,Fe)Si shows no change in polarized light.

Al_7Cu_2Fe (also called Al_6Cu_2Fe, N phase, and βAlCuFe)—The extent to which the composition can vary is not known, and nothing has been done to determine if manganese or silicon are soluble in this constituent. Al_7Cu_2Fe produces a weak but observable birefringence. The phosphoric etchant distinguishes between Al_7Cu_2Fe and the other iron-manganese phases but it is not easy to discern it from $CuAl_2$.

Many difficulties were encountered in attempting to identify the iron-manganese phases by etching characteristics based on published identification tables. It was necessary to study the phases in a number of high purity alloys with fewer components and to supplement this identification by X-ray diffraction of constituents separated from 2024 or from the simpler alloys. The methods and results are briefly described below.

Individual intermetallic phases were concentrated by dissolving the aluminum solid solution matrix and collecting the residue

[2]The designation, "iron-manganese constituents" is used to include the four phases which contain at least one of these two elements in major proportions. These are $MnAl_6$, $FeAl_3$, αAl(Mn,Fe)Si, and Al_7Cu_2Fe.

which consisted essentially of constituents whose rate of solution or solubility in the reagent used was relatively low. The reagents and the methods of dissolving the matrix varied with the alloy and its condition. Success was had under some conditions with a solution of 10% hydrochloric acid and in other cases with a solution of 10 grams of iodine to 100 ml of methanol. A portion of each residue was examined microscopically to ascertain that it contained a substantial amount of the phase in question. The alloy compositions and conditions were chosen so that the phase to be identified was present in large amount and with coarse particle size. In general, only the iron-manganese constituents were capable of separation since all others were dissolved in the reagents used. When copper was present in the residue, it could be removed by washing with a 25% nitric acid solution. Further purification of the residue was effected by floating off aluminum and other light contaminants in a high density liquid, tetrabromoethane (2.96 g/cm^3).

One sample consisted of 2024 which had been remelted and resolidified at a very slow rate. This produced a large quantity of coarse constituent resembling $MnAl_6$. A Debye-Scherrer pattern was obtained which matched that of $MnAl_6$ which had been separated from 3003 alloy and also from a high purity aluminum-manganese alloy.

A second sample of the same alloy was resolidified at a moderately fast rate to produce a cast structure similar to that of commercial direct chill ingot. Isolation of the iron-manganese phases for a Debye-Scherrer powder sample demonstrated that the predominant phase was αAl(Mn,Fe)Si, similar to that in 3003 alloy.

The constituent, Al_7Cu_2Fe, was not separated directly from 2024 alloy, but from high purity alloys of aluminum, copper, and iron (6). After confirmation of the identity by X-ray diffraction, the metallographic characteristics of Al_7Cu_2Fe in the high purity alloys were closely compared with those of the phase in 2024. This comparison was made more valuable by having $FeAl_3$, αAlCuFe (isomorphous with $MnAl_6$), and $CuAl_2$ also present in the high purity alloy. It was satisfactorily established that Al_7Cu_2Fe was present in 2024.

The quantity of $FeAl_3$ appearing in 2024 was so small that it could not be identified by X-ray diffraction but there was no trouble in proving its presence by metallographic means, especially by comparison with high purity aluminum-copper-iron alloys.

The remaining phases, $CuAl_2$, Al_2CuMg, and Mg_2Si, have been so well established as phases normally occurring in 2024 that no further work was considered necessary.

The phase designated as Al-Cu-Fe-Mn, which Keiler and Bossert (2) report to be present in 2024, is uncertain as to its identity. Phragmén (4) pointed out that this phase was probably $MnAl_6$ con-

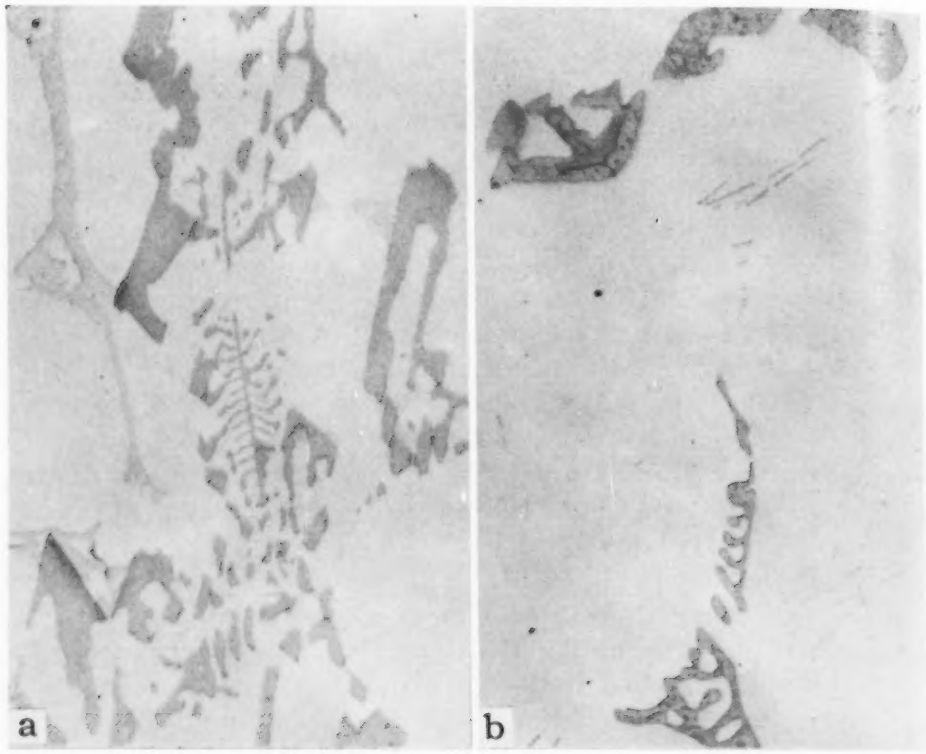


Fig. 1—High Purity Alloy, Al-4% Cu-0.5% Fe-0.6% Mn. (a) As-cast, shows $MnAl_6$ (medium gray) in script and parallelogram form, and $CuAl_2$ (light gray). (b) Heated at 930°F for 50 hours, water-quenched. $MnAl_6$ has almost completely transformed to Al_7Cu_2Fe and some other finely dispersed phase.

taining iron and copper. The Al-Cu-Fe-Mn phase was included in the well-known table of etching characteristics of Keller and Wilcox (9) and was said to be based upon a high purity alloy of aluminum with 4.0% copper, 0.5% iron, and 0.6% manganese. For the present investigation this alloy was duplicated. When the alloy was solidified at a moderate rate the constituents identified were $MnAl_6$, $FeAl_3$, Al_7Cu_2Fe, and $CuAl_2$. $MnAl_6$ was by far the most predominant of the phases containing iron and manganese. Fig. 1a shows this phase in two characteristic forms, script and parallelogram. When this casting was given a homogenization heat treatment at 930°F, most of the $MnAl_6$ transformed peritectically to Al_7Cu_2Fe as shown in Fig. 1b. All other phases tended to disappear, either by solution or by reaction to form Al_7Cu_2Fe. The latter phase exhibited a duplex structure, suggesting that there was another equilibrium phase present in minute proportions. A fine unidentified precipitate was also found within the aluminum dendrites. From these findings it appears that the phase which has been designated as Al-Cu-Fe-Mn could be basically either $MnAl_6$ or Al_7Cu_2Fe, depending upon the condition of the standard alloy used for its identification. It is suggested that the use of this ambiguous designation be abandoned in

favor of more explicit designations. It will be seen subsequently that in 2024 wrought products the predominant iron-manganese phases are actually αAl(Mn,Fe)Si and Al_7Cu_2Fe.

Conditions for Appearance of Phases

Because much of the microstructure of wrought alloys is inherited from the cast ingot, an analysis of cast microstructure proved to be informative. Most of the work is qualitative in nature but it offers a basis for further quantitative studies on this and similar alloys.

Initial observations concerned the significant effect of solidification rate on the iron-manganese constituents. An alloy of the following composition was allowed to solidify at various rates.

	Cu	Mg	Mn	Fe	Si
Weight %	4.88	1.69	0.55	0.29	0.15

A slow rate (about 6°F per minute from 1200 to 900°F) yielded $MnAl_6$ as the principal iron-manganese constituent. Fig. 2a shows a typical coarse particle. In spite of their large size, these particles were always located within dendrite interstices, indicating that they were eutectic in nature and not primary. Small quantities of $FeAl_3$ were also found but this phase was usually completely enveloped by Al_7Cu_2Fe. The $MnAl_6$ also showed evidence of reaction where it had remained in contact with liquid metal to form Al_7Cu_2Fe. Both of these features are illustrated in Fig. 2a. Al_7Cu_2Fe also occurred as long prismatic needles where it had formed eutectically, as shown in Fig. 2b. The remaining structure consisted of coarse divorced $CuAl_2$, Mg_2Si in script form, and a fine aggregate of Al_2CuMg and $CuAl_2$. There were only occasional particles of αAl(Mn,Fe)Si.

By increasing the solidification rate to about 50°F per minute the following changes were effected:

1. the quantity of $MnAl_6$ decreased,
2. the quantity of $FeAl_3$ increased,
3. αAl(Mn,Fe)Si appeared in polygonal form closely associated with $FeAl_3$ (Fig. 3a),
4. αAl(Mn,Fe)Si appeared in script-like form (Fig. 3b), and
5. the quantity of Al_7Cu_2Fe decreased.

The remaining fine structure was essentially the same except that Mg_2Si was encountered more frequently as fine particles within the aggregate containing Al_2CuMg and $CuAl_2$ rather than being in script form.

Further increase of solidification rate to about 100°F per minute resulted in almost complete suppression of $MnAl_6$, $FeAl_3$, and Al_7Cu_2Fe so that αAl(Mn,Fe)Si script was the only constituent to account for the iron and manganese.

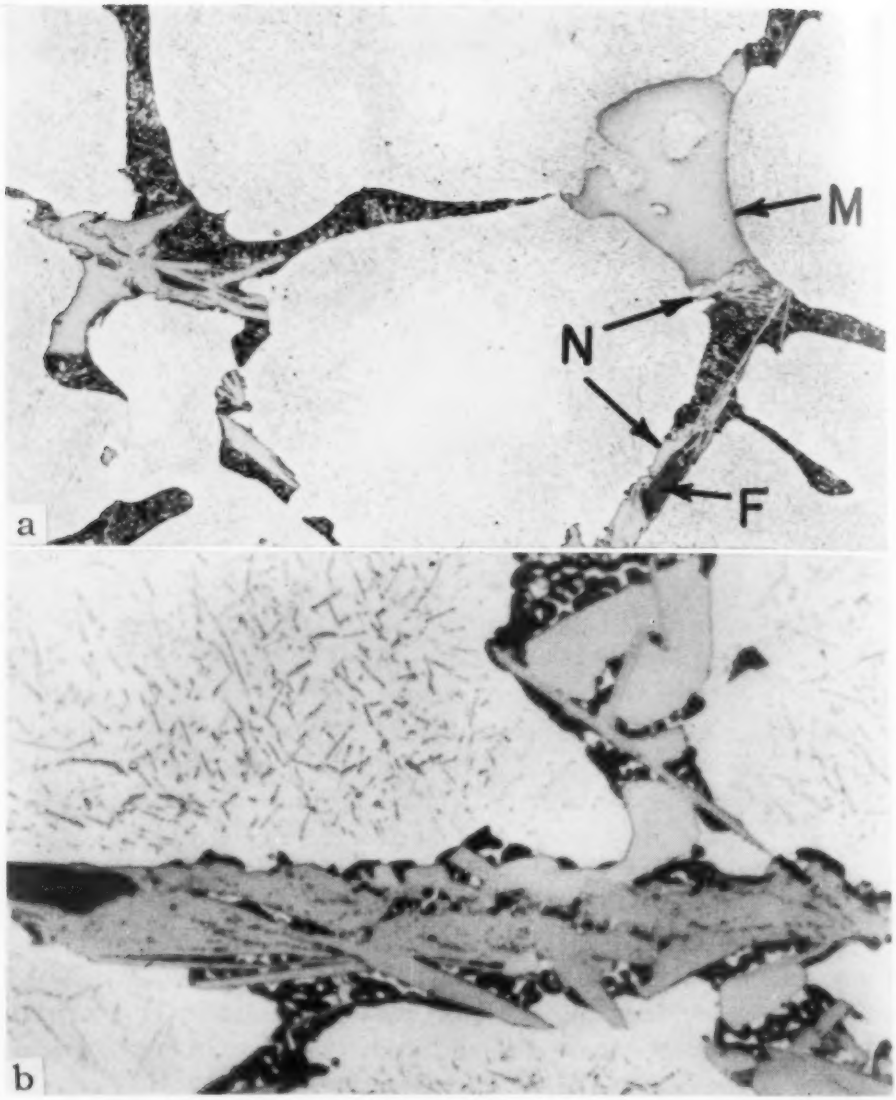


Fig. 2—2024 Alloy Solidified at 6°F Per Minute. (a) Shows coarse $MnAl_6$ (M) and $FeAl_3$ (F) both reacting to form Al_7Cu_2Fe (N). The fine eutectic contains Al_2CuMg (dark) and $CuAl_2$ (white). ×250 (b) showing the distinction between Al_7Cu_2Fe (very light gray) and $CuAl_2$ (white). H_3PO_4 etch. ×1000.

The predominant structure throughout an ingot is that of Fig. 3b, although areas containing $FeAl_3$ (Fig. 3a) and $MnAl_6$ (Fig. 3c) are found at intervals. Thus it is indicated that ingot solidification rates are in the order of magnitude of 50 to 100°F per minute within the solidification range for 2024 alloy, 1180 to 935°F.

The solidification process in 2024 alloy was further elucidated by allowing small melts to solidify at a controlled rate to various temperatures within the solidification range, followed by a rapid quench to transform the remaining liquid into a very fine structure. Thus, the liquid-to-solid reactions at various stages could be fol-

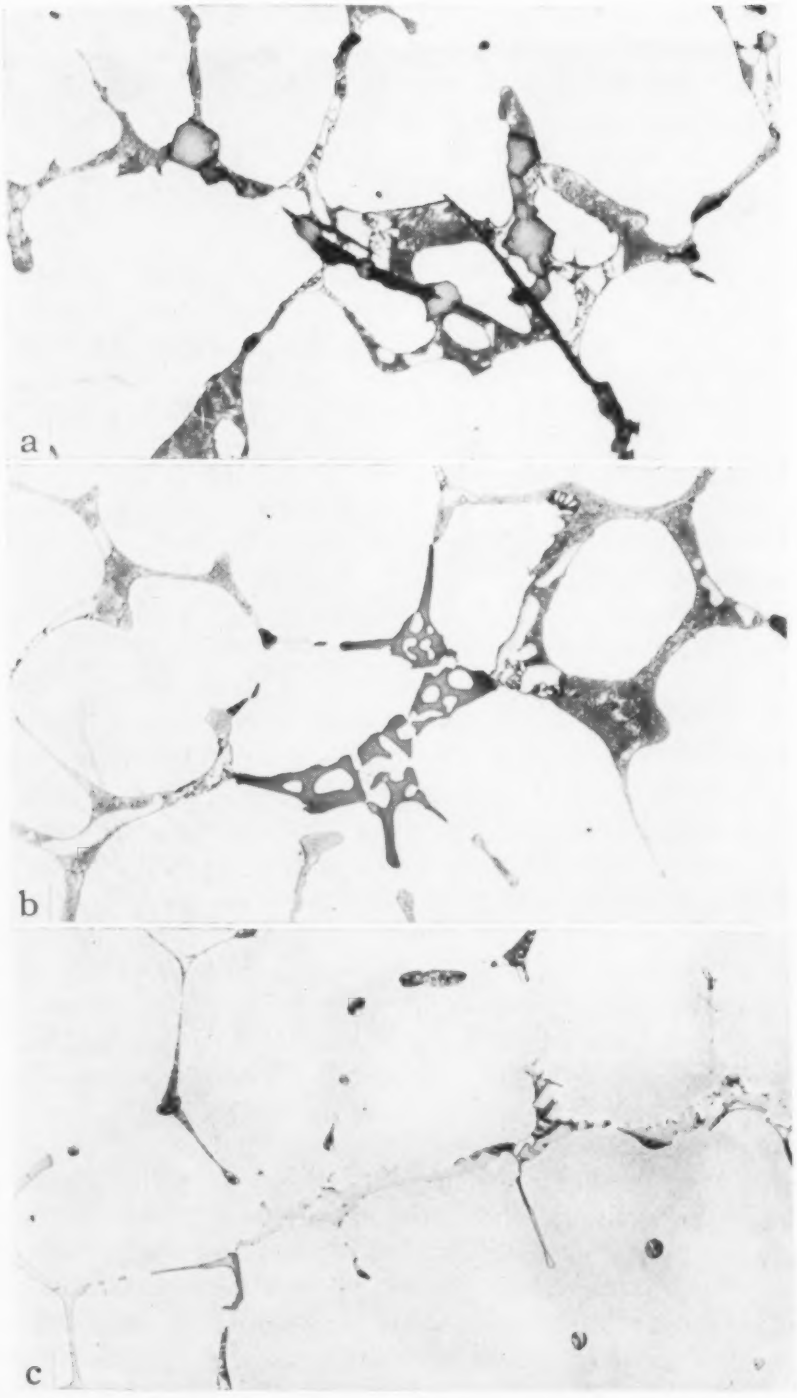


Fig. 3—Manner in Which Iron-Manganese Phases Appear in 2024 Cast Structures. (a) and (b) were solidified at 50°F per minute and quenched after solidification. (c) is from a D.C. ingot and coring is revealed by precipitation. (a) $FeAl_3$ blades (black) and αAl(Mn,Fe)Si polygons (gray with dark outlines); (b) αAl(Mn,Fe)Si script (medium gray, sharply outlined) which predominates in ingot structures; (c) $MnAl_6$ (light gray, not outlined). H_3PO_4 etch, ×250.

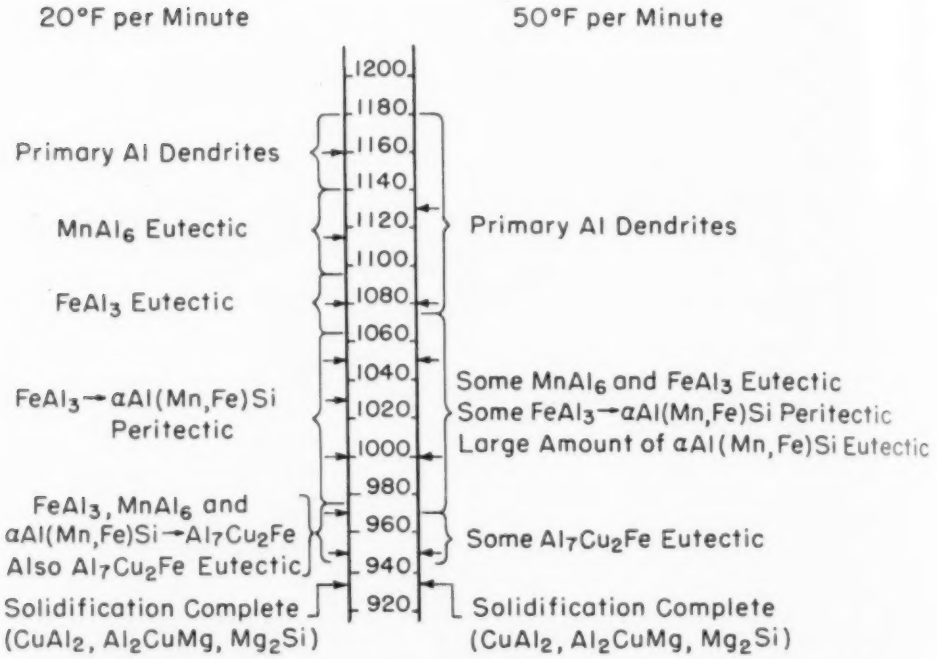


Fig. 4—Schematic Representation of Solidification of 2024 at Two Different Rates. Liquid-solid reactions below 950°F could not be followed so only the reaction products are given. All reactions should also include aluminum. Arrows indicate temperatures from which samples were quenched.

lowed. Fig. 4 shows schematically some typical results. The brackets represent the temperature range wherein the various reactions occurred. The reactions at the lower end of the solidification range were confined to such small temperature intervals that they could not be easily followed so they have been limited to a listing of the intermetallic phases involved. In some cases there seemed to be some overlapping with several reactions occurring within the same range. This may have been due to lack of adequate control of the cooling rate or to inhomogeneities of composition. The important differences due to cooling rate are quite obvious, however.

The effects of increased solidification rate appear to be to suppress the $MnAl_6$ eutectic reaction, to promote the formation of αAl(Mn,Fe)Si peritectic and eutectic, and to suppress the Al_7Cu_2Fe peritectic and eutectic reactions. It is not known whether these effects are due to supercooling alone or whether they are caused by changing composition relationships between solid and liquid.

The peritectic reaction by which αAl(Mn,Fe)Si forms from $FeAl_3$ produces an interesting and unusual structure. Fig. 3a shows that polygons of the new phase form at random along the $FeAl_3$ blades, sometimes producing strings of the αAl(Mn,Fe)Si crystals. These new crystals appear to grow with amazing rapidity, often consuming all the $FeAl_3$ with which they are in contact. This differs

markedly from the usual rimming by which peritectic reactions take place with the customary slow rates of formation.

The relationships among the three intermetallic phases which, with aluminum, make up the lowest melting eutectic structures can be inferred from the probable aluminum-copper-magnesium-silicon liquidus model. During solidification of an Al-Cu-Mg-Si alloy comparable with the composition of 2024, the order of solidification following precipitation of primary aluminum dendrites would be

1. Liquid→Al+Mg_2Si
2. Liquid→Al+$CuAl_2$+Mg_2Si
3. Liquid→Al+$CuAl_2$+Mg_2Si+Al_2CuMg

The temperature range over which the latter two reactions occur is less than 10°F. The binary and ternary eutectics solidify over a range of temperatures and, hence, would be the divorced type, ie, the intermetallic phases would be fairly coarse and separated from the eutectic aluminum which grows onto the primary aluminum dendrites. Such is the case in 2024. In 2024 the lowest melting eutectic appears to be the quaternary containing aluminum, $CuAl_2$, Mg_2Si, and Al_2CuMg but its solidification temperature, 935°F, is about 8°F lower than that for high purity Al-Cu-Mg-Si alloys as determined by Crowther (10). This is undoubtedly due to the influence of other elements in the commercial alloy. When the alloy is slowly solidified, very little Mg_2Si appears in the final eutectic, probably because the equilibrium proportion of Mg_2Si in this eutectic structure is very small. This lowest melting eutectic has been described elsewhere as the ternary forming aluminum, $CuAl_2$, and Al_2CuMg (3) but this eutectic cannot be obtained following solidification of Mg_2Si without circumventing the lowest melting composition yielding aluminum+$CuAl_2$+Al_2CuMg+Mg_2Si. Fig. 5a shows some of the fine Mg_2Si particles in the final eutectic as they appear after a brief reheating. The Al_2CuMg phase in this sample happened to etch lightly so that Mg_2Si could be distinguished from it.

The structure observed in laboratory produced cast samples of 2024 has been compared with numerous commercial ingot structures and no discrepancies have been found. Following the interpretation of the cast structure, the changes accompanying reheating of an ingot were studied on a commercially cast alloy of the following composition.

	Cu	Mg	Mn	Fe	Si
Weight %	4.90	1.40	0.70	0.30	0.15

Reheating of the cast structure to bring about homogeneity before hot working is common practice. This involves the solution of soluble constituents, removal of concentration gradients in the

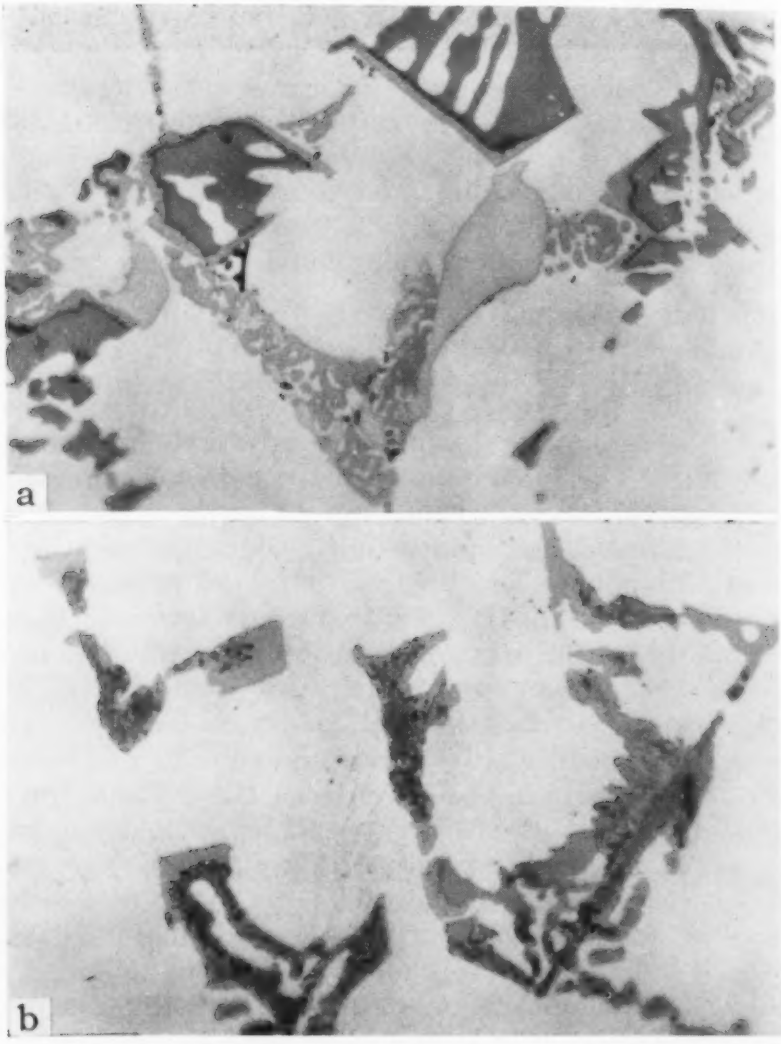


Fig. 5—Transformation of $MnAl_6$ (medium gray, not outlined) to Al_7Cu_2Fe (light gray, enveloping $MnAl_6$) and Fine Dark Etching Phase in 2024 Ingot Heated at 930°F and Water-Quenched. (a) 1 hour; (b) 16 hours. In the lower center of (a) some fine dark particles of Mg_2Si can be distinguished in the eutectic with $CuAl_2$ (white) and Al_2CuMg since the latter has etched lightly. Note the fine aggregate structure within the Al_7Cu_2Fe in (b). H_3PO_4 etch, ×500.

matrix, and the completion of suppressed peritectic reactions. The reactions occurring at the interfaces between aluminum solid solution and the phases, $FeAl_3$, $MnAl_6$, or αAl(Mn,Fe)Si, are of special interest since they indicate that these three phases are not stable and that Al_7Cu_2Fe is a stable phase. This is in agreement with Phragmén's predictions for 2024 (4) except that he made no mention of $FeAl_3$. The absence of αAl(Mn,Fe)Si in the slowly solidified cast structure (Fig. 2) suggests that this is not an equilibrium phase, but its low reaction rate during reheating indicates a high metastability.

Early and advanced stages in the transformation of $MnAl_6$ to Al_7Cu_2Fe are shown in Figs. 5a and 5b. It can be seen that initially

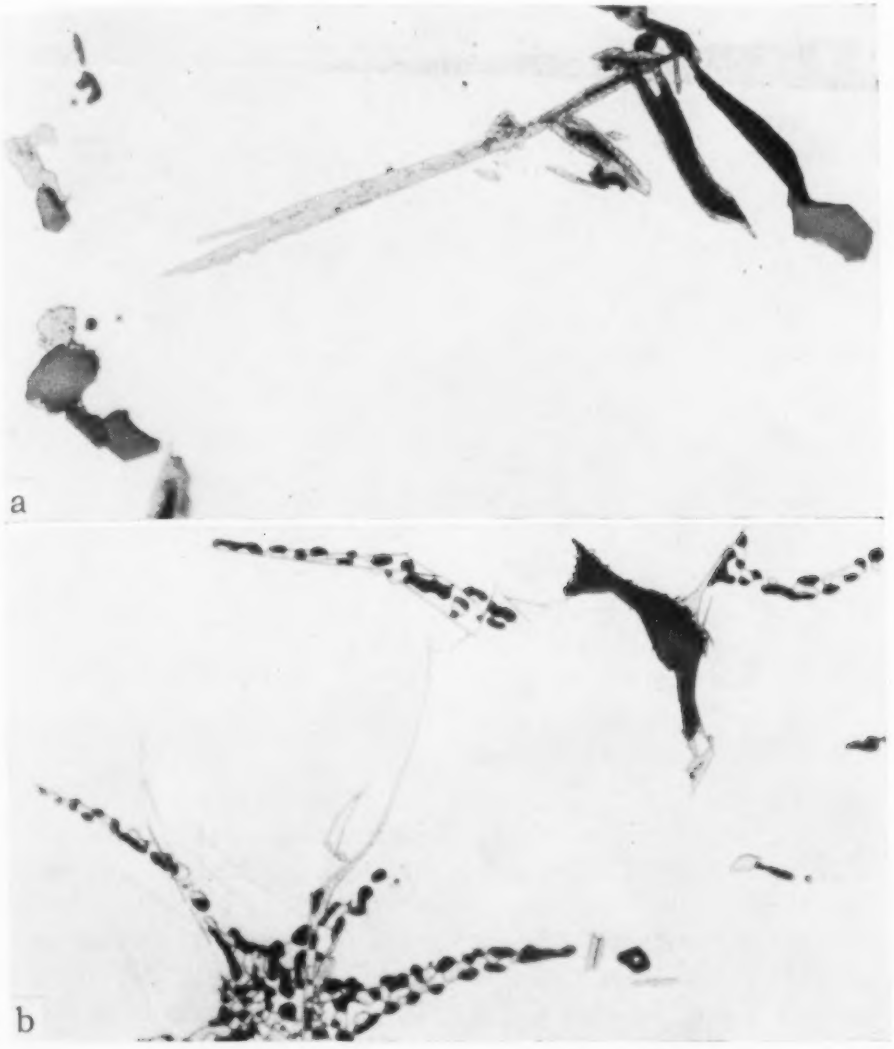


Fig. 6—Transition Structures in 2024 Ingot Heated at 930°F for 4 Hours, Water-Quenched. (a) $FeAl_3$ (dark gray) transforming to Al_7Cu_2Fe (light, enveloping $FeAl_3$) while αAl(Mn,Fe)Si polygons (medium gray) show little change. (b) Eutectic Al_7Cu_2Fe needles remaining undissolved while the $CuAl_2$ and Al_2CuMg are dissolving. H_3PO_4 etch, ×500.

the newly formed Al_7Cu_2Fe is smooth and uniform but at later stages it incorporates a fine dark etching phase to yield an aggregate structure. The resemblance between this and the reaction in the high purity Al-Cu-Fe-Mn alloy (Fig. 1b) is significant. Similar effects obtain for the transformation of $FeAl_3$ as Fig. 6a shows. It was not possible to identify the fine constituent distributed within the Al_7Cu_2Fe. Fig. 6b gives an indication of the low solubility of the Al_7Cu_2Fe phase. The phase which precipitated from the melt in eutectic form maintained its needlelike shape while the soluble constituents around it were dissolving and coalescing.

Seeman, et al (7,8) have described a precipitate in reheated

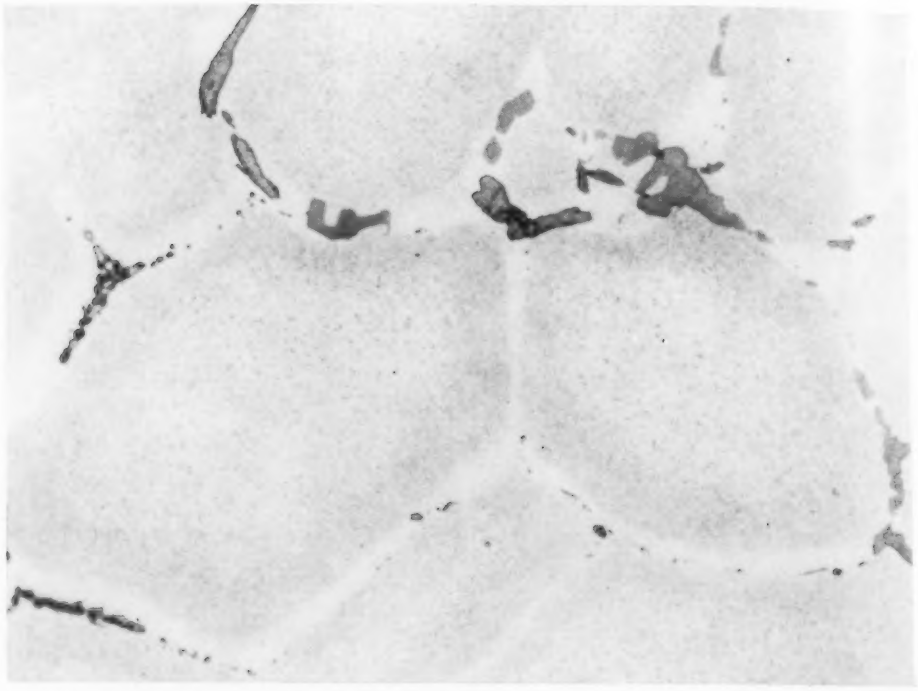


Fig. 7—2024 Ingot Heated at 930°F for 16 Hours, Water-Quenched. The dendritic precipitate pattern results from precipitation of some unidentified manganese-containing phase or phases. Etched with 1% HF for 5 seconds. ×250.

commercial ingots of Duralumin which was proved to be associated with the presence of manganese and was tentatively identified as $MnAl_6$. Fig. 7 shows a similar precipitate which appeared after heating a sample of 2024 ingot 16 hours at 930°F. In the present investigation the identity of the precipitate could not be established but it can be stated that $MnAl_6$ is not a stable phase and, hence, it is not a likely candidate. An explanation for a similar nonuniform precipitate distribution was given in connection with a study of 3003 aluminum alloy (11), a nonheat treatable alloy containing about 1.2% manganese. This explanation can be applied with little modification to 2024 alloy. It seems unnecessary to postulate an undercooling and suppression of a peritectic reaction with regard to the precipitate, as Seeman has done, although these phenomena undoubtedly occur and have other effects.

The working processes and further thermal treatments which 2024 alloy undergoes before reaching its final form and temper continue and sometimes accelerate the metallurgical changes which start with the reheating of the ingot. Therefore, the wrought structure is closely allied to the reheated ingot structure with respect to the intermetallic phases which are present.

In the wrought 2024 microstructures the principal phases are Al_2CuMg, Mg_2Si, $\alpha Al(Mn,Fe)Si$, and Al_7Cu_2Fe. If there are residual

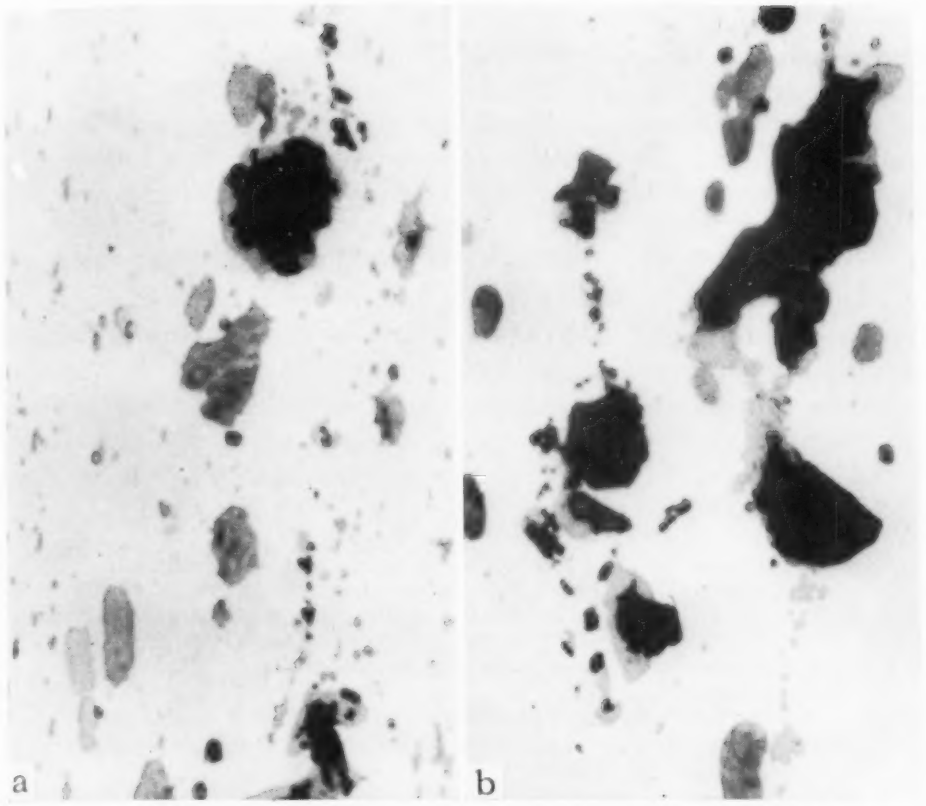


Fig. 8—Predominant Phases in 2024 Wrought Structures. (a) as extruded; (b) solution heat treated. αAl(Mn,Fe)Si (dark gray) is partially rimmed by Al_7Cu_2Fe (light gray). Al_2CuMg (medium gray, mottled) is the principal precipitate phase in (a) and is not completely dissolved in (b). H_3PO_4 etch, ×1000.

particles of $FeAl_3$ and $MnAl_6$ they are quite scarce and difficult to identify. $CuAl_2$ cannot be recognized in the fine precipitate in annealed or hot worked material and is found only occasionally as an undissolved constituent particle. Al_2CuMg predominates as the soluble phase. Figs. 8a and 8b show an extrusion before and after solution heat treating. In both photomicrographs dark etching αAl(Mn,Fe)Si rimmed with the light Al_7Cu_2Fe is evident. The Al_2CuMg constituent is medium gray and mottled and in Fig. 8b it has a more rounded shape as a result of the solution process. Mg_2Si cannot be distinguished after etching, but it is present as a random dispersion of fairly fine particles.

In view of the low solubility of the iron-manganese and Mg_2Si constituents, the matrix of alloy 2024 including the more soluble phases can be regarded as an alloy of aluminum, copper, and magnesium as an approximation. At the solution heat treating temperature the alloy matrix lies essentially in the two-phase field, $Al+Al_2CuMg$. Numerous observations show that this is true even when the ratio, Cu:Mg, based on the overall alloy composition, is

high. The copper content of the matrix is undoubtedly sensitive to the quantity of Al_7Cu_2Fe which has formed and the ratio of copper to magnesium in the matrix must actually be lower than the alloy composition indicates. The relative proportion of $\alpha Al(Mn,Fe)Si$ to Al_7Cu_2Fe in a 2024 microstructure serves as a rough index to the degree of homogenization which the alloy has undergone.

Acknowledgments

The author wishes to express his gratitude to Messrs. F. M. Krill, S. E. Maddigan and D. W. Smith for their encouragement in carrying out this project, to the numerous members of the staff of Kaiser Aluminum's Department of Metallurgical Research who cooperated in execution of the experimental work, and to Messrs. P. P. Zeigler and R. E. Knight for permission to publish the data.

References

1. Helmut Töllner, "Beitrag zur Gefugekenntnis der Aluminium-Legierungen der Gattung Al-Cu-Mg," *Aluminium-Archiv*, Vol. 34, 1940, 31 pages.
2. F. Keller and R. A. Bossert, "Revealing the Microstructure of 24S Alloy," *Metal Progress*, Vol. 41, January 1942, p. 63.
3. Lucio F. Mondolfo, *Metallography of Aluminum Alloys*, 1943, p. 249, published by John Wiley and Sons, Inc., New York.
4. Gösta Phragmén, "On the Phases Occurring in Alloys of Aluminium with Copper, Magnesium, Manganese, Iron, and Silicon," *Journal*, Institute of Metals, Vol. 77, 1950, p. 489.
5. H. W. L. Phillips, "The Constitution of Alloys of Aluminium, Copper, and Iron," *Journal*, Institute of Metals, Vol. 82, 1954, p. 197.
6. P. R. Sperry, Discussion of Reference 5, Ibid, p. 568.
7. M. Dudek, H. Mahl, and H. J. Seeman, "Ueber eine neuartige Gefugeerscheinung in manganhaltigen Aluminiumlegierungen auf Grund von licht- und elektronenmikroskopischen Untersuchungen," *Metall*, March 1948, p. 75.
8. H. J. Seeman and M. Dudek, "Zur Kenntnis des manganhaltigen Gefugebestandteils in technischen Aluminiumlegierungen," *Zeitschrift für Metallkunde*, Vol. 39, 1948, p. 319.
9. F. Keller and G. W. Wilcox, "Identification of Constituents of Aluminum Alloys," Aluminum Research Laboratories, Technical Paper No. 7, 1942, Aluminum Company of America.
10. J. Crowther, "Overheating Phenomena in Aluminium-Copper-Magnesium-Silicon Alloys of the Duralumin Type," *Journal*, Institute of Metals, Vol. 76, 1949–50, p. 201.
11. P. R. Sperry, "Metallographic Study of Equilibrium Relationships in 3S Aluminum Alloy," *Journal of Metals*, Vol. 7, 1955, p. 145.

GRAIN BOUNDARY CREEP IN ALUMINUM BICRYSTALS

By F. N. Rhines, W. E. Bond, and M. A. Kissel

Abstract

Grain boundary shearing in aluminum bicrystals at high temperature and low tensile stress is found to be spasmodic, beginning with an induction period. Its direction depends exclusively upon that of the maximum shear stress in the grain boundary, but its rate depends as well upon the orientation relationships of the conjugate crystals. The overall gliding rate is constant with the cube root of time, bears an Arrhenius relationship to the temperature and its logarithm is approximately proportional to the stress, over small ranges of stress. A mechanism for the process is proposed. (ASM-SLA Classification: Q3, Q2, Al)

THE gliding of metal crystals upon their mutual grain boundary was first reported, for the case of γ-iron, by Rosenhain and Humfrey (1),[1] who employed this observation in support of the amorphous cement hypothesis. Andrade (2), in his classic papers upon creep, ascribed to the grain boundary a capacity for viscous sliding, which he thought to be responsible, in part at least, for the uniform rate of secondary creep. Recently, there has been renewed and intensified interest in grain boundary gliding owing to the evident contribution of this mode of yielding to high temperature creep in structural alloys and to the fact that high temperature creep-rupture is commonly intergranular. A number of recent investigations (3 to 20) have dealt with this subject, but there remain many unanswered questions with regard to the nature of the process. It has been the purpose of the present research to obtain a more detailed and quantitative view of grain boundary gliding, with the hope of finding clues to its mechanism.

Experimental Procedure

Pure aluminum, (99.95%) was selected for these studies. An exhaustive spectrographic analysis,[2] after the fabrication of the

[1]The figures appearing in parentheses pertain to the references appended to this paper.

[2]Spectrographic analyses were kindly made for us at the Aluminum Company of America Research Laboratories, at New Kensington, Pennsylvania.

A paper presented before the Thirty-Seventh Annual Convention of the Society, held in Philadelphia, October 17–21, 1955. Of the authors, F. N. Rhines is Aluminum Company of America professor of light metals and member of the staff; W. E. Bond and M. A. Kissel are research assistants, Metals Research Laboratory, Carnegie Institute of Technology, Pittsburgh. Manuscript received May 12,1955.

metal into test specimens, indicated that the major impurity was copper, about 0.005%, followed by iron, chromium, silicon and magnesium, each about 0.001%, and sodium and calcium, each 0.0001%. No other impurity was found present in spectrographically detectable amount.

Apart from an exploratory survey, using polycrystalline aluminum, all of the studies were made upon bicrystals having flat grain boundaries accurately oriented at 45 degrees to the tension axis and perpendicular to the reference surface upon which all observations were made. These were in the form of bars, usually about 2½ inches long, by ⅜ inches wide and ⅝ inch thick, see Fig. 1. All but a very few were cut from coarse-grained rolled aluminum plate, which had



Fig. 1—A Typical Strain-Annealed Bicrystal, With Its Grain Boundary Aligned at 45 Degrees to the Tension Axis, Tucker etch, ×2 magnification.

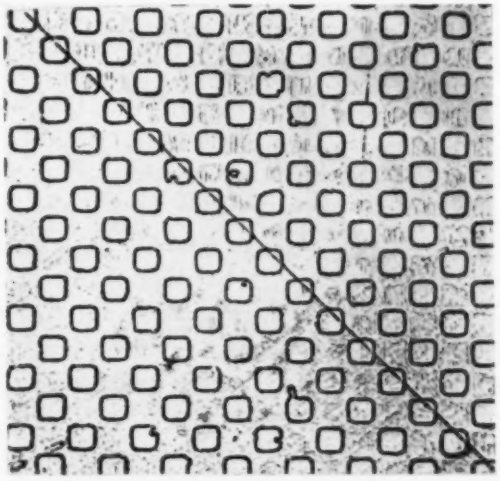


Fig. 2—Pattern of Reference Squares Superimposed Upon the Grain Boundary of an Aluminum Bicrystal, ×30 magnification.

been prepared by straining 1.7% in tension and annealing briefly in a salt bath adjusted at 659°C (1220°F). The few others were cut from cast bicrystals that had been made from the same metal by a conventional thermal gradient technique. Distorted metal was removed by alternate polishing and etching and a bright finished surface, with the grain boundary delineated as a fine line, was produced by electropolishing.

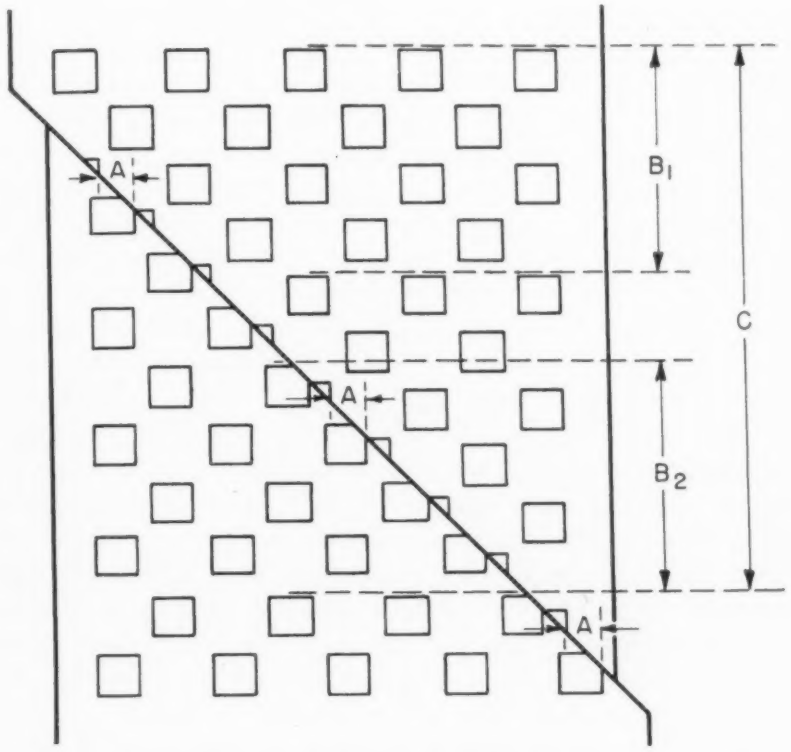


Fig. 3—Schematic Plan of Measurements Made Upon a Bicrystal During Creep at an Elevated Temperature; the Diagonal Line Represents the Grain Boundary Along Which Shearing is Taking Place.

A reference pattern was photoengraved upon one of the broad faces of each bar by a slight modification of a commercial cold-top process.[3] This involved coating the surface with a photosensitive material, exposure through a 133 line to the inch half tone screen, development to harden the exposed squares of the screen pattern, fixing to wash away the unexposed lines, re-electropolishing to "etch in" the lines and washing off the residual coating with a suitable solvent. The resulting pattern of squares protruding minutely from the surface, appears as in Fig. 2. As a result of electropolishing, there remained upon the surface a fairly heavy, although transparent, oxide film, which could be largely removed with a phosphoric acid solvent, but which was usually left as protection against further oxidation and tarnishing during subsequent testing at elevated temperatures. This film also served as a stress coat, which gave useful information.

The testing apparatus consisted of conventional dead-weight loaded creep machines with resistance furnaces, open to the atmosphere and provided with optical glass windows for observing the

[3]Either the cold-top process as supplied by the Mallinckrodt Chemical Works or an improved version that was made available through the courtesy of the American Newspapers Association Laboratories.

specimens. Temperatures were measured by means of thermocouples placed in near contact with the bicrystals at their grain boundaries. File-faced grips of light construction were used to hold the specimens. A specially designed long focusing telescope with both horizontal and vertical micrometer measuring scales was used for measuring the grain boundary displacement and elongation.

A plan of the measurements is shown schematically in Fig. 3. At a minimum of three points along the grain boundary the horizontal displacement (A) of bisected reference squares was measured and was averaged. Simultaneously, the elongation of each of the two crystals was measured parallel to the stress axis, along the lengths (B_1) and (B_2), which were initially 0.32 millimeters long. A total extension (C) was measured across the grain boundary between reference points 0.7 millimeters apart. In a few experiments, the vertical displacement along the grain boundary was measured also, using the same reference squares as for measurements (A) but measuring their displacement at right angles to the spans (A).

The conduct of the typical test consisted in placing the sample in the creep machine, adjusting the temperature, making an initial set of readings and then applying the load very gently. Another set of readings was made as soon after loading as possible; thereafter, readings were made at increasing time intervals until they were spaced 24 hours apart. About 100 such tests were run for times ranging up to an exceptional maximum of one year. The testing temperatures ranged from 200 to 650°C (390 to 1200°F) and the stresses from 10 to 1600 psi. Nearly half of the tests were terminated by transgranular rupture, the rest were stopped because the reference points had become obliterated by the fragmentation of the squares.

Considering the sensitivity of the measuring apparatus and the magnitude of the human error in locating the reference points from day to day, it is believed that the measurements of grain boundary displacement are significant within 0.005 millimeters. This sensitivity was of particular value in detecting irregularities in the progress of grain boundary gliding. Temperature readings were reliable within ± 5°C, stress measurements within 1%. The crystal orientation, determined by the Laue back-reflection method was dependable within about 1 degree of arc.

Experimental Results

When grain boundary creep is measured both parallel and transverse to the direction of loading of the bicrystal, entirely different results are obtained by the two measurements. Parallel to the stress direction, the metal, between gage points astride the grain boundary, extends in a regular manner, which is not to be distinguished from the elongation of the specimen as a whole, except

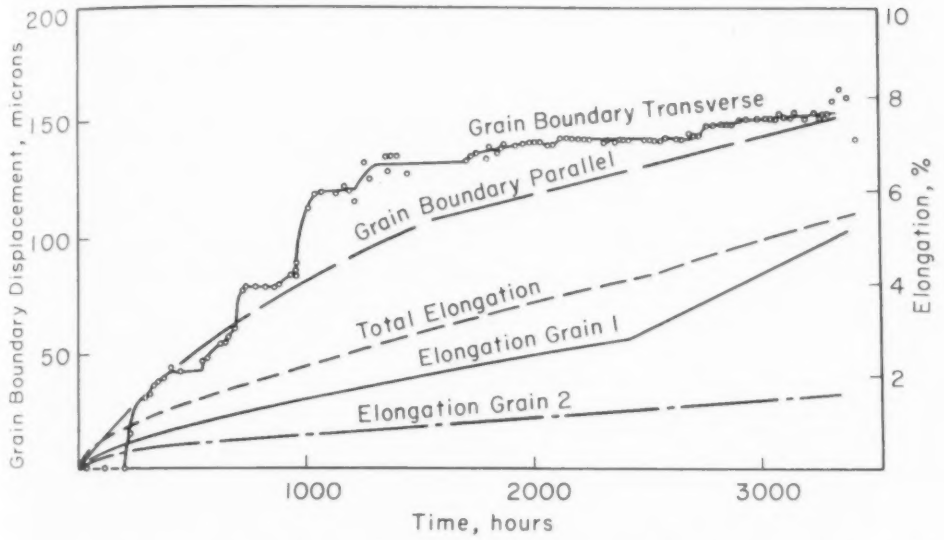


Fig. 4—Record of Grain Boundary Displacement and Longitudinal Extension in a Typical Bicrystal Tested at a Temperature of 300°C (570°F), Under a Stress of 100 psi. The heavy solid line, passing through plotted points, represents lateral displacement at the grain boundary, as measured over three spans, such as A in Fig. 2, and averaged. The long dash line represents displacement at the grain boundary, measured parallel to the stress axis at one point. Total elongation and the elongation in grains 1 and 2 are expressed in percent and have been measured along spans such as C, B_1 and B_2 in Fig. 2.

in its faster rate. That is, the extension, which is rapid at first, gradually decelerates until a steady progress of extension is established at a minimum rate, see the long dash curve in Fig. 4.

As observed transverse to the direction of loading, however, the onset of yielding is delayed until the termination of a more, or less, extended induction interval. Thereafter, an apparent shear begins at its maximum rate, soon declining in velocity until there is, once more, no perceptible yielding. Sometime later, shearing resumes at its original fast rate, again diminishes to zero and so on in a somewhat irregular sequence of surges, see the curve with plotted points, Fig. 4.

It is evident, at once, that the measurements made parallel to the applied stress do not report the lateral displacement of one grain with respect to the other, as they would if grain boundary displacement were a shear upon a single interface between the two grains. This can mean only that the lateral displacement of grains is occurring in a layer of metal of finite thickness. The layer is extending at a nearly constant rate in the stress direction, while yielding transversely in a sequence of surges. Although the uninterrupted rapid flow, parallel with the stress direction, is clearly of importance in accounting for the commonly observed increase in creep rate with a decrease in grain size, in polycrystalline aggregates, the subject of avowed interest in this paper is the lateral displacement of one grain with respect to its neighbor and it is apparent that this can be measured only transversely to the stress direction. Accordingly all

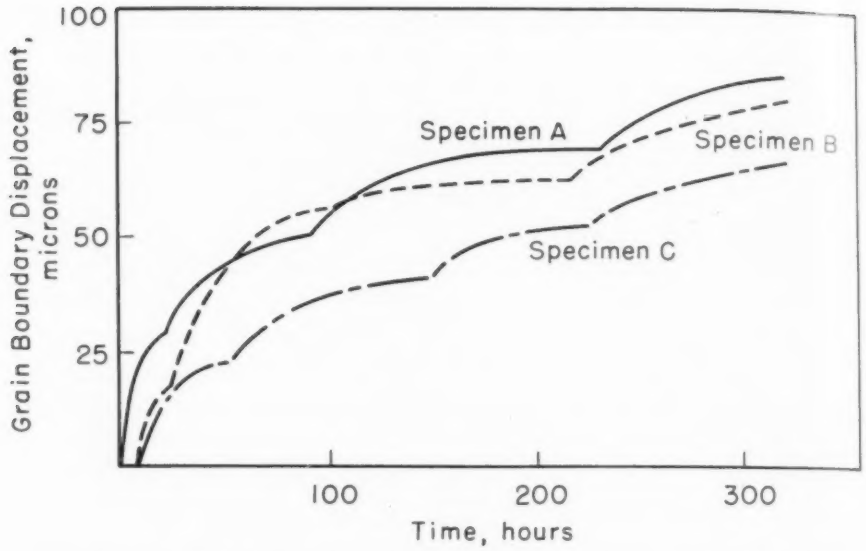


Fig. 5—Lateral Grain Boundary Displacement Versus Time for Three Identically Oriented Bicrystals cut from the same cast Bicrystal and identically tested at 300°C (570°F), Under a Stress of 400 psi. Data points, omitted to minimize confusion, exhibited slightly more scatter than those shown in Fig. 4.

of the results that follow relate to measurements such as span A in Fig. 3.

Induction Period

The duration of the induction period varies over a broad range, depending upon the crystallographic relationships, the temperature and the stress. Short induction periods, amounting to as little as a matter of minutes, are associated with large orientation differences between the conjugate crystals, high temperature and high stress. At the opposite extreme there are encountered periods as long as a month (in one case five months) preceding grain boundary gliding. The onset of movement at the end of the induction period is always abrupt and seems in no way related to any mechanical, or thermal, disturbance.

Spasmodic Motion

When the grain boundary is flat and regular, gliding begins simultaneously at all reference points and proceeds initially at much the same rate at all points. Later, and most evidently when the grain boundary is not flat, the surges of motion begin to appear at slightly different times at different reference points, and to have somewhat different magnitudes. With samples cut from the same pair of crystals and tested under identical conditions of stress and temperature, the surges are roughly of the same magnitude and duration, but are definitely not identical in either respect, Fig. 5. In contrast with this evidence of apparent sensitivity to subtile differences from point to point within the crystal, however, is the fact,

many times verified, that the progression of the surges is insensitive to external influences. During a rest period, neither a temperature excursion of several hundred degrees, nor a severe mechanical shock will initiate shearing prematurely. As an extreme example, one bicrystal, during the failure of a temperature controller, melted off at its upper grip, fell three feet from the furnace, was replaced in the testing apparatus and continued in the rest portion of its gliding cycle another fortnight before lateral motion was resumed.

Overall Rate of Gliding

If the lateral displacement at the grain boundary is plotted as a function of the cube root of the time, the resulting curve, although

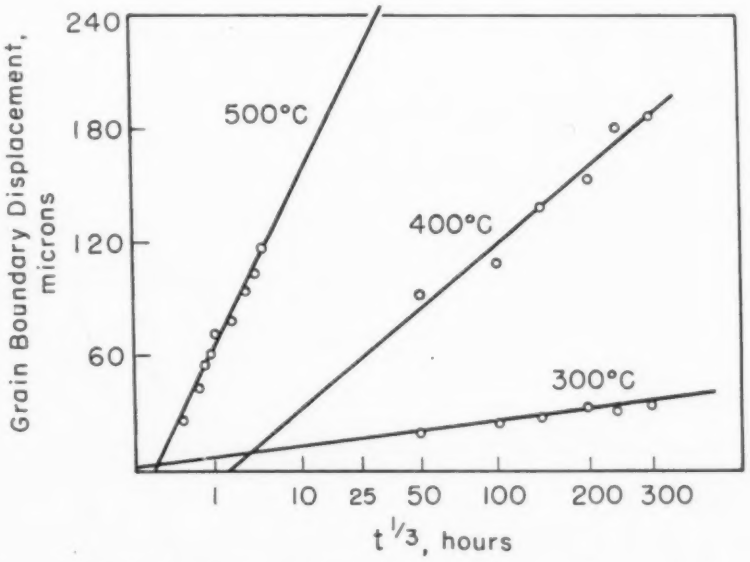


Fig. 6—Grain Boundary Displacement at Three Temperatures, Under a Stress of 100 psi, Averaged to Randomize the Crystal Orientation Effect, and Plotted as a Function of the Cube Root of the Time. Zero time represents the termination of the induction interval.

undulating, approximates a straight line. The slope of this line is sensitive to the prevailing temperature, stress and crystallographic orientation relationship. Since the orientation relationships were different in almost all of the bicrystals used, the effects of the temperature and the stress upon the gliding rate are best compared by averaging, to randomize the orientation effects. Thus, in Fig. 6, are presented three time-displacement plots made by averaging the results from all bicrystals tested at a stress of 100 psi and three temperatures (300, 400 and 500°C) regardless of their orientations. The results from 28 bicrystals are represented in the curve for 300°C (570°F), 18 in the curve for 400°C (750°F) and 6 in the curve for 500°C (930°F). This procedure tends also to smooth the undulations that arise from cyclic gliding. Although none of the three curves

presented in Fig. 6 passes through the origin, all cross the zero displacement axis within about one hour of zero time, the latter being defined as the end of the induction period.

Influence of Temperature

If the displacement in a given time is plotted, upon a logarithmic scale, as a function of the reciprocal of the absolute temperature, a linear plot results, Fig. 7. The points represented in this graph are

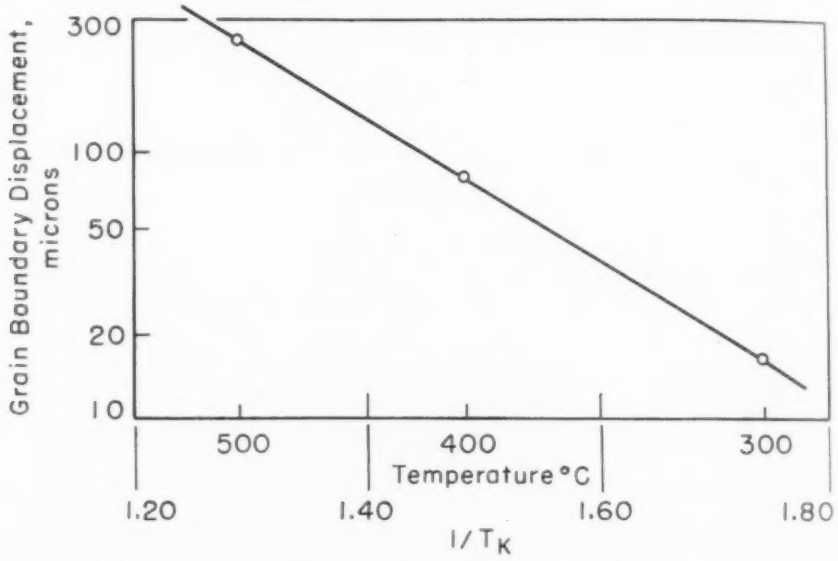


Fig. 7—Logarithm of the Average Grain Boundary Displacement in 50 Hours Under a Stress of 100 psi, Plotted as a Function of the Reciprocal of the Absolute Temperature.

taken (at a time of 50 hours) from the average displacement curves in Fig. 6. The resulting curve has the form that is typical of chemical-rate processes and its slope yields a "heat of activation" of 11000 ± 1000 calories per mole. Using measurements from this research, but a different mode of calculation, Dorn (21) has found a heat of activation approximating that of the self-diffusion of aluminum.

This relationship does not apply to the variation with temperature of the displacement in each surge; there the extent of gliding varies directly with the temperature, see Fig. 8. Curve A in this figure represents the total gliding accomplished during the first cycle in each of four samples of nearly identical orientation, tested at four temperatures. Curve B represents the average of the total gliding, in the first cycle, of all (52) samples tested at a stress of 100 psi.

It has been known, since the studies of Rosenhain and Humfrey (1), that grain boundary gliding does not occur at low temperature. As the temperature of testing is lowered, the effect disappears

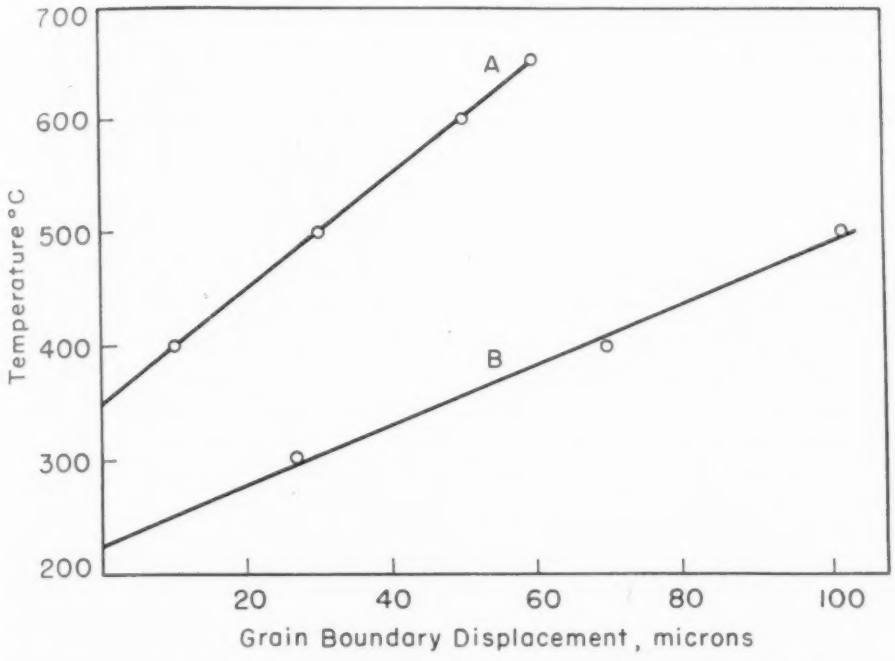


Fig. 8—Grain Boundary Displacement in the First Cycle of Gliding, Under a Stress of 100 psi Plotted as a Function of the Temperature; Curve A Was Obtained from a Series of Single Tests Made with Bicrystals With Similar Orientation Relationships, Curve B Employs Average Measurements from Bicrystals with Random Orientations.

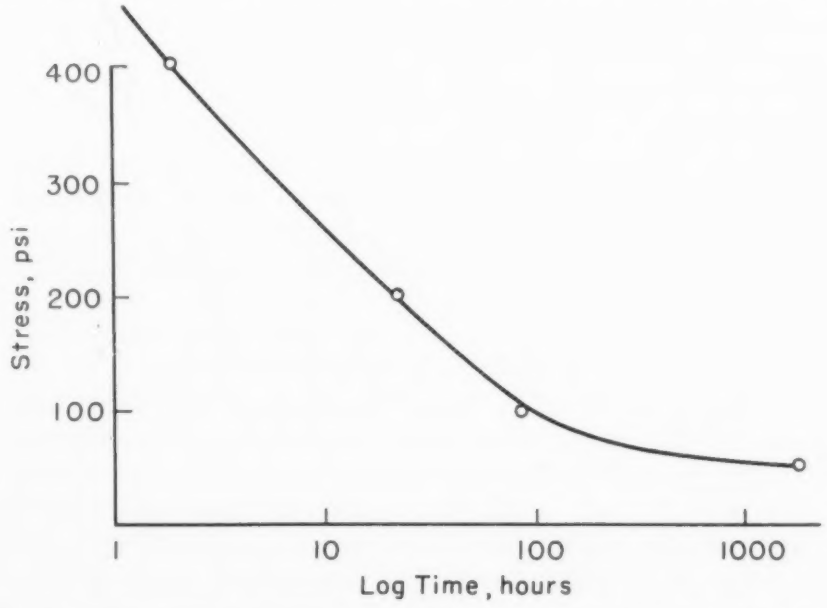


Fig. 9—Stress to Produce an Average Grain Boundary Displacement of 25 Microns, at a Temperature of 300°C (570°F), Plotted as a Function of the Logarithm of the Time.

by an increase in the length of the induction interval, until this time becomes greater than the time to rupture. Since the duration of the induction interval is sensitive also to the crystal orientation, the threshold temperature for gliding varies somewhat from one

grain boundary to the next. In a series of studies, conducted with a constant stress of 100 psi, no gliding was developed in any bicrystal tested at 200°C (390°F), while less than five percent of those tested at 300°C (570°F) failed to exhibit grain boundary displacement and this number decreased further as the temperature was raised.

Influence of Stress

The logarithm of the (average) time required to attain a displacement of 25 microns at a temperature of 300°C (570°F), is plotted as a function of the applied unit stress in Fig. 9. In order to randomize the influence of orientation, averages for all bicrystals tested under each set of conditions were again employed; in this instance there were available 2 bicrystals tested at 50 psi, 28 at 100 psi, 7 at 200 psi, and 14 at 400 psi. In the higher range, the stress is almost a linear function of the logarithm of the time for unit displacement, but this relationship is clearly not exact and fails altogether at low stresses. No satisfactory function of proportionality between the stress and the rate of gliding has yet been identified.

From a short series of tests conducted at various temperatures, (300 to 650°C) and at stresses down to 10 psi, it was concluded that there is an orientation sensitive threshold stress, corresponding to the threshold temperature, below which gliding does not occur. Again, the induction interval becomes very long. At 10 psi, no grain boundary shearing was observed in either of the samples tested, even at 650°C (1200°F), i.e., 10°C below the melting point of the aluminum.

At a unit stress of 1600 psi and above it was found impractical to conduct the kind of fine scale measurements used in this research. The grain boundary gliding so merges with the general distortion of the crystals themselves, that it can be perceived only qualitatively upon a coarse scale.

Influence of Orientation

The direction of grain boundary gliding appears to be altogether insensitive to the orientation of the conjugate crystals. Motion is always in the direction of the maximum shear stress resolved into the plane of the grain boundary and increases with the magnitude of the stress, as has been observed also by Chang and Grant (14). Where a grain boundary has complex shape, each increment of its area behaves according to its local orientation with respect to the stress axis, see Fig. 10.

For the case of a fixed grain boundary orientation, such as was employed in the present investigation, the relative orientation of the conjugate crystals exerts a profound influence upon the rate of gliding. The effect persists, apparently undiminished, moreover,

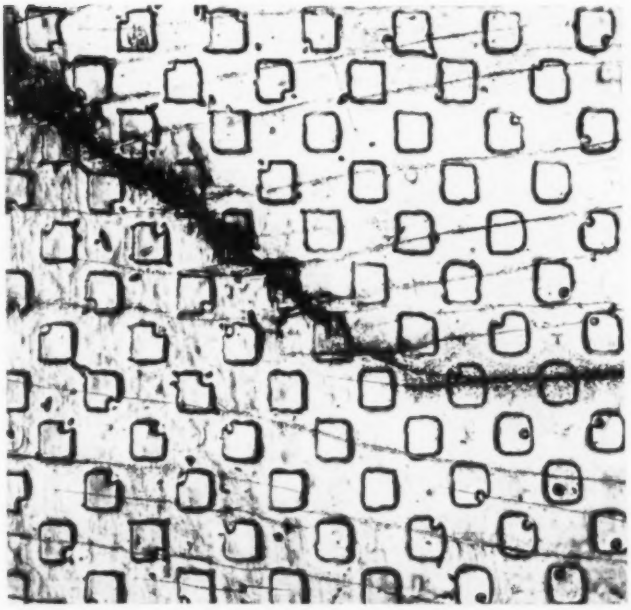


Fig. 10—Varying Displacement Along a Bent Grain Boundary in Coarse-Grained Aluminum. Tested at 384°C (720°F) Under a Stress of 120 psi, ×35 magnification.

through many cycles of motion and rest and despite considerable extension of the sample as a whole and obvious distortion of the metal in the region of the grain boundary.

Considering the evidence that gliding occurs within a layer of metal, rather than upon the grain boundary as an interface, it is not surprising that the assumption that the rate should vary with orientation difference, in the same manner as the grain boundary energy, should fail. This relationship was found to hold only to the extent that motion is slight when the angle of the boundary is small.

If, however, the overall rate of gliding is associated with the angular difference between the active slip systems in the conjugate crystals, a fairly satisfactory correlation is obtained. This was done through the use of stereographic projections, by identifying in each crystal its most favorably oriented slip plane and slip direction. The angle between the two slip directions was designated θ; that between the intersections made by the two slip planes in the grain boundary was designated ω. The sum of the θ and ω angles was found to vary almost linearly with the rate of gliding. These measurements are portrayed schematically in Fig. 11.

For making comparisons among bicrystals with grain boundaries at 45 degrees to the tension axis and tested at a given temperature and stress, it was found convenient to employ the empirical formula:

$$d = d_{(T,S)}(\theta+\omega)/65$$

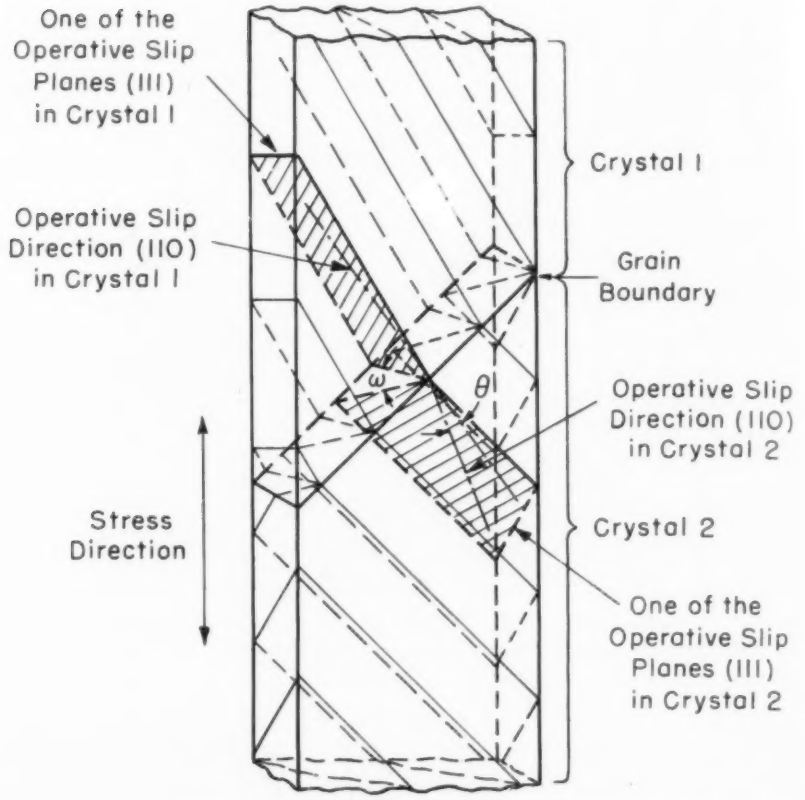


Fig. 11—Schematic Representation of a Bicrystal; the Angle θ is That Between the Active Slip Directions in the Two Crystals; ω is the Angle Between the Traces of the Two Active Slip Planes, Measured in the Plane of the Grain Boundary, Heavily Outlined.

where d is the displacement in unit time in a bicrystal having the angular relationships θ and ω, while $d_{(T,S)}$ is the observed average displacement (orientation randomized) for all bicrystals tested at temperature (T) under unit stress (S). Using this formula, the ratio of the predicted to the observed rate of gliding for all samples tested assumed a Gaussian distribution about unity with about half of the cases in the range 0.95 to 1.05. Occasional large deviations between the predicted and observed rates are to be expected, because it is sometimes possible for more than one slip system to be operative in one, or both, of the grains of the bicrystal, a condition which could not be dealt with by the method employed. Smaller deviations, outside the range of experimental error, may perhaps be the result of the occasional, or localized, operation of normally inactive slip systems. At least a dozen other relationships were tried without further success and that just described is, accordingly, considered the most acceptable.

Qualitatively, the step height in spasmodic gliding increases with the sum of the angles θ and ω. The length of the induction

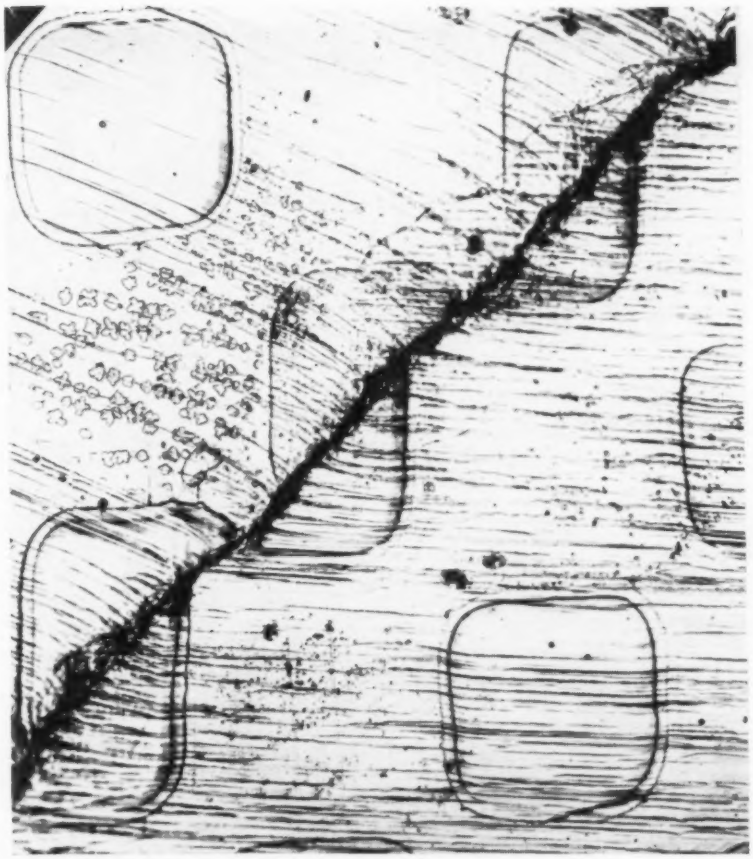


Fig. 12—Detail of Grain Boundary Displacement after 250 Hours at 300°C (570°F) Under a Stress of 100 psi; the Dark, Diagonal Trace is the Path of Shear and the Fine, Nearly Horizontal Lines are Stress Cracks in the Surface Film of Aluminum Oxide, ×200 magnification.

period, however, tends to vary inversely with $\theta+\omega$. The rest periods are so irregular in their duration that no more definite statement is justified than that, in a vague way, they seem also to vary inversely with θ and ω.

Structural Effects

At the lowest temperature and stress at which grain boundary gliding is observed, shearing appears superficially to occur upon a single interface, Fig. 12, although a careful examination of this photograph shows that stress cracks in the aluminum oxide film bend inward toward the grain boundary, indicating diagonal shearing within a zone of very real thickness.

With rising temperature, or stress, it becomes increasingly apparent that yielding along the grain boundary is distributed through a zone of substantial thickness, Fig. 13. Moreover, the motion continues upon the same path in cycle after cycle of yielding. Where a ledge is formed at the edges of the bicrystal, by the displacement of



Fig. 13—Detail of Grain Boundary Displacement in 936 Hours at 300°C (570°F), Under a Stress of 200 psi; the Translation Has Been 110 Microns, Approximately Equal to the Spacing Between Rows of Reference Squares, ×200 magnification.

one grain with respect to the other, it is not a sharply defined ledge, but is curved to produce an unbroken surface from one grain to the other, Fig. 14. Upon the surface of this ledge, Fig. 15, the oxide is fragmented and generally distributed, while the metal beneath remains glassy smooth, developing no markings of any kind. This is in contrast with the shapes of ledges that are produced by gross transcrystalline slip, Fig. 16. The latter have sharp edges and their surfaces have a stepped contour, retaining no visible remnants of the original oxide skin of the specimen. Obviously, slip occurs as a shear upon a limited number of interfaces, whereas gliding is distributed fairly evenly through a finite thickness of metal.

There appears qualitatively to be an inverse correlation between the thickness of the active zone and the rate of gliding at constant temperature and stress. Not only does the zone thicken as the gliding rate diminishes with time of testing, but it is much broader from the outset in those bicrystals which glide most slowly.

Further insight into the nature of the active zone is obtained from grain boundary displacement measurements that were made

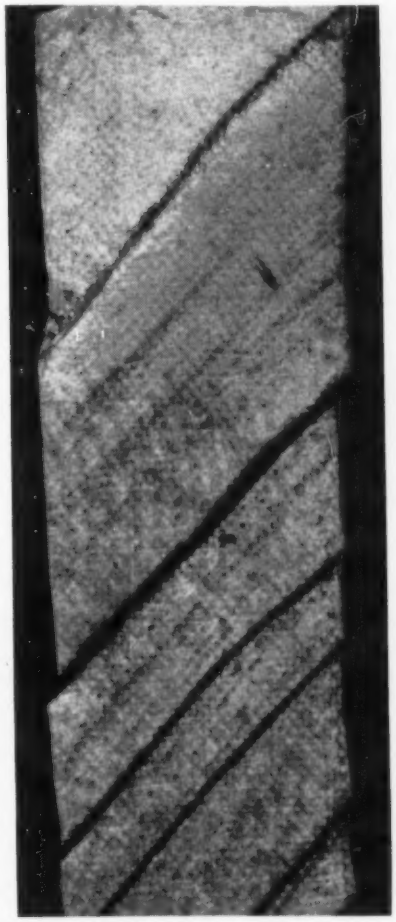


Fig. 14—Portion of a Bicrystal After 864 Hours at 400°C (750°F) Under a Stress of 100 psi; the Upper Diagonal Line is the Grain Boundary Upon Which Shear Occurred; Those Below are Traces of Gross Slip in a Direction That is Not Altogether Parallel With the Surface of Observation; Notice That the Ledge Formed by Grain Boundary Gliding is Curved, While that Formed by Slip is Sharp and Flat, ×5 magnification.

after the reference points had become engulfed in this zone, Fig. 17. Instead of progressing regularly, the reported displacement oscillates in an irregular manner, showing that the bit of metal upon which the reference point is located is rotating erratically this way and that. While this effect is apparent during periods of gliding, it is perhaps most noticeable during periods of rest, when, despite the activity of the reference points, no net shear is recorded. The precision of the measurements is such as to guarantee that this behavior is altogether real.

A comparison of Laue X-ray photograms taken in the grain boundary zone and at the ledge exposed by gliding, reveals much more sub-grain rotation in the active zone than in the body of the crystal, Fig. 18. Some of the Laue pictures showed that the sub-grains were rotated about an octahedral axis in the parent crystal;

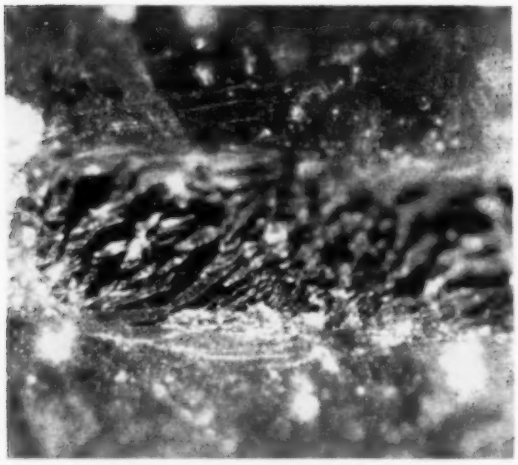


Fig. 15—Surface of a Ledge Produced by Grain Boundary Gliding; Light Areas are Fragments of the Original Oxide Skin; Dark Areas are Exposed Clean Metal Showing No Surface Detail; Fine Lines Above and Below the Ledge are Stress Cracks in the Oxide, ×50 magnification.

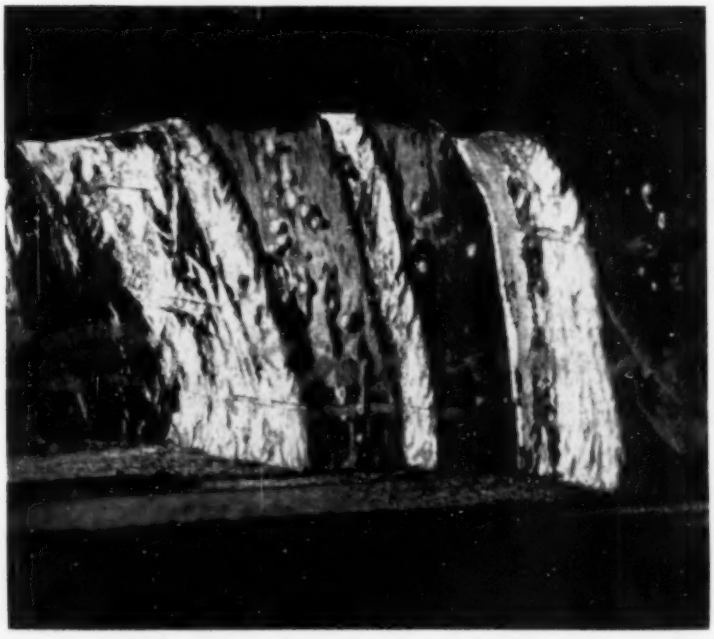


Fig. 16—Detail of One Side of a Crystal in Which Gross Slip had Occurred; Lighter Areas are Exposed Surfaces of Slip Bands; Steps on Each Surface May Represent Individual Slip Planes, ×15 magnification.

Gervais, Norton and Grant (22) report this type of rotation and also rotations about a [211] axis.

If, after creep testing, the bicrystal is deeply etched, electropolished and again etched to reveal the sub-grains, it is seen that there is a more or less sharply delineated band, along the grain boundary, in which the sub-grains display a somewhat less regular

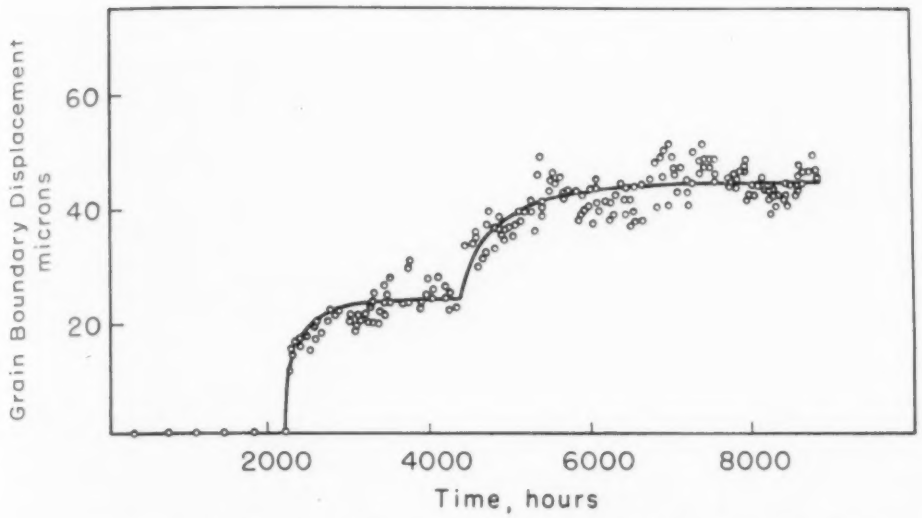


Fig. 17—Grain Boundary Displacement at 300°C (570°F) Under a Stress of 50 psi, Showing Scatter in Successive Readings that Results When the Reference Points Are Engulfed by the Active Zone Along the Grain Boundary.

pattern than elsewhere within the crystals, Fig. 19. Whether or not the sub-grain structure is brought out by deep etching, the active zone appears as a sloping terrace, joining the grains at different levels Gifkins (19) has reported a similar effect in Pb-Tl alloys. It will be observed also that the grain boundary remains sharp, possibly because the sub-grains, though having considerable divergence in their orientations, have a common axis of rotation that identifies them with their parent crystal. The boundary is here less straight than it was before creep testing. Although some local shifting of the grain boundary was often apparent after creep testing, it always remained within the initial path of active flow and never migrated to a new locality, (with gliding continuing upon a new path) as has been reported by Chang and Grant (9) in connection with studies upon polycrystalline aluminum.

Late in the creep test, rather similar structural changes become apparent within the bodies of the crystals. Surface rumpling, suggestive of that in the grain boundary zone, appears in ridges across the crystals, Fig. 20. These are probably the same as the markings identified as kink bands by McLean (17) and others. When the ridges are examined at higher magnification, Fig. 21, it is seen that the reference squares upon them are much more elongated in the direction of the applied stress, than are those in the valleys between.

Rupture

All of the bicrystals tested to failure broke transgranularly and usually as far from the grain boundary as circumstances would permit. Some time prior to rupture, it was always noticed that there

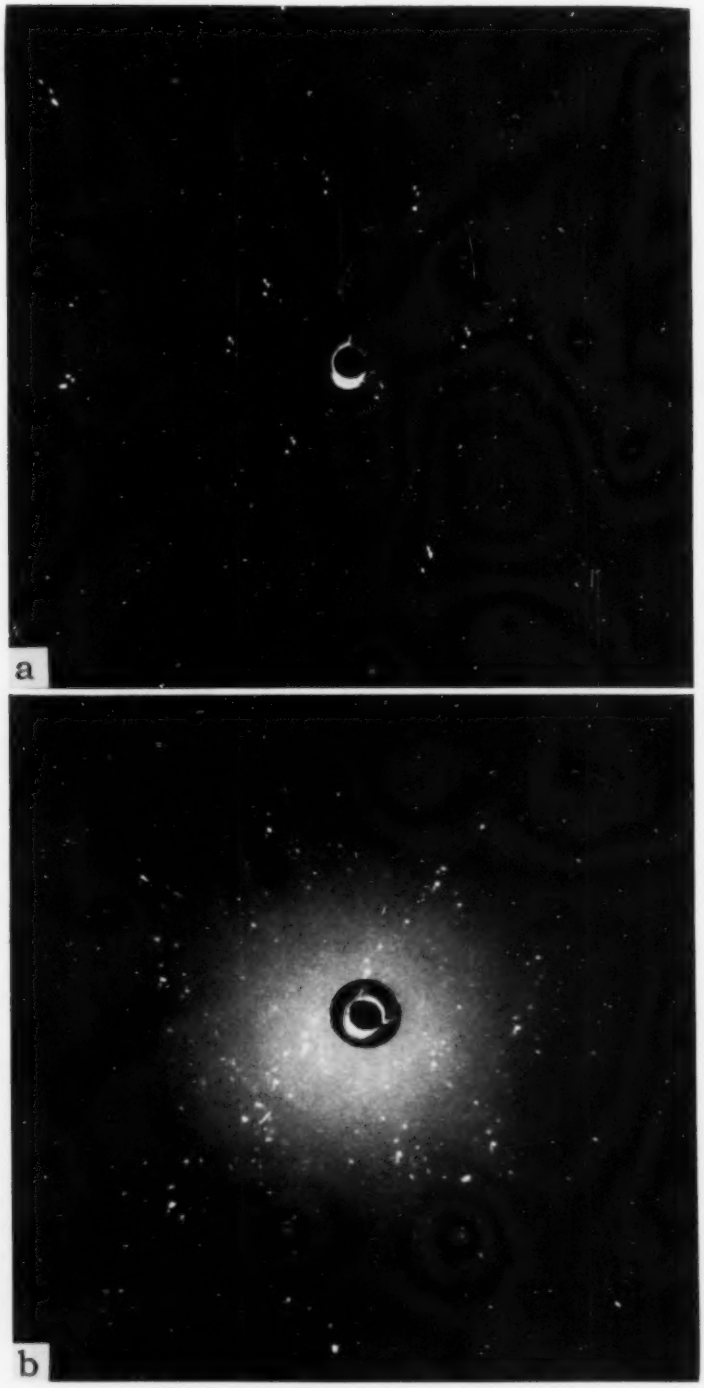


Fig. 18—Laue Photograms of Bicrystals after Creep Testing at 400°C (750°F) Under a Stress of 100 psi; (a) Representative of the Body of a Crystal, (b) Taken at the New Surface Exposed (as a curved ledge) by grain boundary gliding.

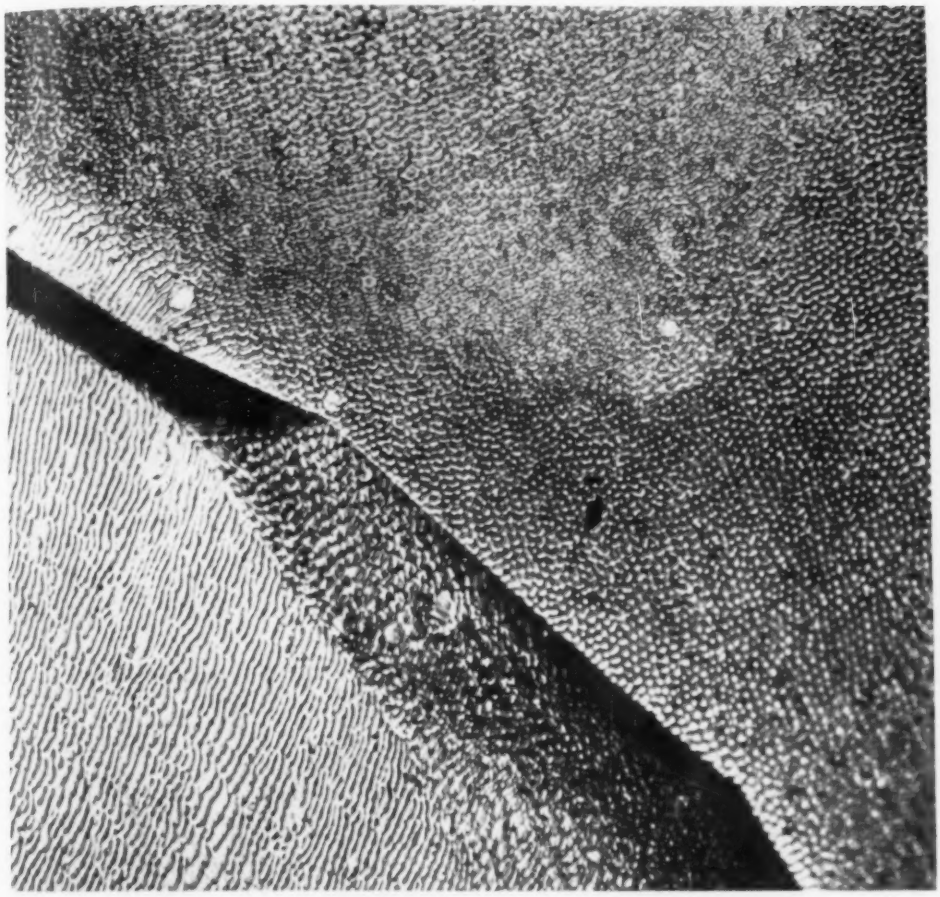


Fig. 19—Short Segment of Grain Boundary of a Sample Tested at 400°C (750°F), Under a Stress of 100 psi, Deeply Etched and Electropolished and Etched After Testing; Shows That the Sub-grain Structure Differs Somewhat in a Zone Along the Grain Boundary, ×400 magnification.

was an abrupt increase in the rate of extension of that grain which was destined to fail by necking and fracture, Fig. 4. It is noteworthy, first, that the increased rate was observable over a very short gage length adjacent to the grain boundary and often as much as an inch away from the fracture; second, that the new faster rate of extension was uniform to fracture; and third, that necking was not perceptible until long after the faster rate of extension had been established.

Some General Observations

It is to be noted that the grain boundary gliding, that has been described above, is always accompanied by a general creep extension of both crystals, this extension being at a constant rate, except during the first few minutes after loading and except for the rate increase prior to necking and rupture. No indication of the spasmodic shearing at the grain boundary is perceptible, either in the rates of extension of the individual grains, spans B_1 and B_2 of Fig. 3,

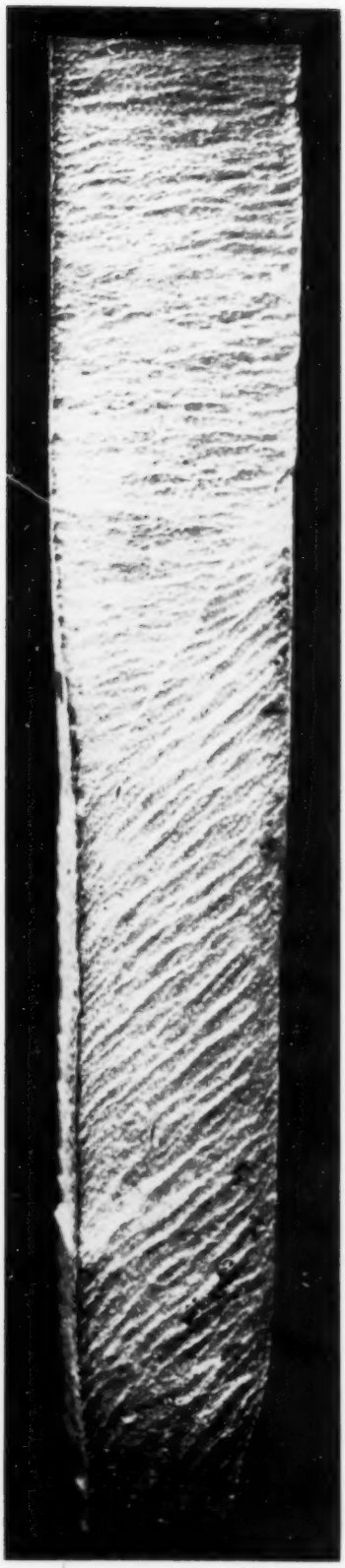


Fig. 20—Bicrystal That Has Failed By Transcrystalline Rupture After 19 Hours at 400°C (750°F), Under a Stress of 200 psi; Notice the Heavily Rumpled Surface that Has Developed During a Late Stage of Creep and Compare with Fig. 21, ×3.5 magnification.



Fig. 21—Same Sample as That Presented in Fig. 20, Showing Detail in the Surface of the Crystals Adjacent to the Grain Boundary; Notice in Particular that Individual Reference "Squares" Have Been Elongated in Greatly Differing Amount, Especially in the Crystal on the Right, ×100 magnification.

or in the rate of total extension, span C. Within the temperature range of active gliding the relative contribution of the grain boundary to the total extension appears almost constant; the ratio of the average total extension (which includes the grain boundary) to that of the individual grains at 300, 400 and 500°C (570, 750, and 930°F), respectively, was found to be: 1.65, 2.12 and 1.60. This much variation might well be the result of there being different mixtures of orientations among the cases averaged at each temperature.

A small number of tests, similar to those previously described, was made using cast instead of strain annealed bicrystals. There was no detectable qualitative difference in behavior, but quantitatively, both the general elongation of the individual crystals and gliding at the grain boundary proceeded at about one third the rate expected of strain annealed bicrystals of like $\theta+\omega$ value. The progress of grain boundary gliding in three identical bicrystal strips, cut from the same cast bicrystal has been shown in Fig. 5.

Discussion of Results

It is altogether clear from the experimental results that grain boundary gliding is not a sliding upon the grain boundary as an interface, but is rather an erratic lateral yielding within a zone of metal, of considerable thickness, adjacent to the grain boundary. It is apparent also that the creep extension of the metal, as a whole, must be in progress for gliding to occur.

Thus, gliding is seen, not as an independent flow process, but as an aspect of high temperature plastic yielding, that develops in those portions of the crystal which are adjacent to the boundary.

In 1926, Bailey (23) suggested that steady-state creep may be the result of a balance between work hardening and softening by annealing. This basic idea has been refined by Cottrell and Aytekin (24), among others, to describe a sequence of hardening by localized crystal bending and softening by polygonization, to account for the steady-state creep of the crystals themselves. As indicated in Figs. 20 and 21, such a process must be inhomogeneous and must result in localized rapid yielding from time to time, to produce an overall extension, mainly, as McLean has pointed out, through the medium of a complex of micro-slip in particles of the dimensions of the sub-grains. This concept of high temperature creep suggests to the authors the following explanation of the grain boundary gliding effect.

Mechanism of Grain Boundary Gliding

During the induction period it is presumed that slip, impinging upon the grain boundary, causes a localized bending of the crystals all across the face of the grain boundary. When sufficient energy has thus been stored, recovery occurs by a process such as polygonization. The metal in the recovered zone now forms a continuous layer of material that is softer than the enclosing metal and rapid yielding occurs, directed along the grain boundary, because this is the direction of minimum resistance to yielding.

Slip through the sub-grains will restore the mechanical state requisite to polygonization and the process will repeat in a sequence of slip-recovery operations, coordinated at first with respect to their timing, all across the grain boundary. Because the sub-grains can not remain identically oriented, however, the frequency of the slip-recovery cycle must differ slightly from point to point along the grain boundary, causing a growing interference with cooperative yielding, as the alternations in some regions become significantly out of phase with the alternations in other regions. Thus, grain boundary gliding is expected to decelerate and ultimately to stop.

In the rest interval that follows the sub-grains of the grain boundary zone may be expected to behave much like those else-

where within the crystals. They are subject to alternations of slip and recovery, but locally, contributing only to yielding in the direction of the applied stress. In the absence of coordinated lateral yielding, bending energy will again accumulate along the grain boundary and, presently, coordinated recovery and yielding, parallel to the grain boundary, will be resumed.

In support of this proposal, the following evidently consistent observations are recalled:

1. Gliding is spasmodic and begins only after an induction interval.
2. Extension in the stress direction continues throughout the cycles of gliding and rest.
3. The direction of gliding is responsive only to the direction of the maximum resolved shearing stress in the plane of the grain boundary.
4. The cumulative rate of gliding is greater and the induction interval shorter the larger the angle between slip systems in the conjugate crystals; i.e., the more rapidly is bending energy expected to accumulate at the grain boundary.
5. The logarithm of the average rate of gliding is a linear function of the reciprocal of the absolute temperature, as is true of creep extension within the crystals.
6. Gliding does not occur below the recovery temperature of the metal.
7. The onset of gliding is not induced by thermal or mechanical shock.
8. The sub-grains are rotated more in the grain boundary zone than elsewhere.
9. There is evidence of turbulent motion within the grain boundary zone, especially during the intervals of rest from gliding.
10. Gliding may occur at different times in different portions of the same grain boundary, especially where the boundary is not straight.

That the overall extent of grain boundary displacement should be a linear function of the cube root of the time, is not an especially evident consequence of the mechanism that has been proposed. It has been noted, during the research that, qualitatively, the breadth of the active zone of shearing varies directly with the gliding rate. Perhaps the decline in the gliding rate is a result of the dispersion of the cooperative yielding in an ever widening zone. If this is so, the cube root relationship must be related to the rate of broadening of the active zone, but no further development of this idea can be offered at this time. It is worthy of comment, however, that the

cube root relationship applies also to the transcient creep of polycrystalline metals and has yet to be adequately explained for this case.

The relationship between the stress and the overall rate of gliding is also similar to that between stress and creep in polycrystalline aggregates. A relationship of this kind is to be expected from the basic assumption of the proposed mechanism, namely, that the mechanism of gliding is the same, except for a higher degree of organization, as that of ordinary creep.

In a process of the evident complexity of the present one, it is perhaps not surprising that the "heat of activation" (11000 cal/mole) should not point to rate control by any single process. One of the complexities is that the amount of the displacement in a single surge of gliding varies directly with the temperature, whereas gliding, as a whole, follows the chemical rate law. If it is true that each surge of gliding is terminated by the progressive disorganization of cooperative yielding, this may require a rather definite number of repetitions of the slip-recovery cycles and the extent of shearing in one surge would then be controlled by the amount of slip that can take place before recovery occurs in each cycle. Whether this should or should not be a linear function of the temperature, can not be decided upon the basis of the existing knowledge of slip behavior.

Some Further Comments

In none of the tests conducted in the present studies was there encountered grain boundary migration of the kind described by Chang and Grant (9). Evidently migration is grain growth induced by the complex stresses set up in polycrystalline metals and is not an essential part of the gliding process.

That none of the bicrystals ruptured at, or near, the grain boundary seems to indicate that the grain boundary is not inherently weak. "Intergranular rupture" as it usually occurs in polycrystalline metals may, therefore, be due to some cause other than inherent weakness. If, as Grant has pointed out, gliding, occurring upon three intersecting grain boundaries, can produce a concentrated stress at the "triple point," sufficient to initiate rupture, it is not necessary that the grain boundary be weak. The shortest path of rupture from one triple point to the next will approximate the path of the grain boundary and, thus, give the illusion of grain boundary embrittlement.

Finally, it is interesting that a detailed examination of grain boundary gliding has failed to bring forth the evidence of viscous behavior that was postulated by Rosenhain and Humfrey, Andrade, and later by Ke. Neither of the major characteristics of viscous behavior, namely, constancy of the rate of yielding and propor-

tionality of the rate to the stress, is exhibited. To be sure, the component of extension parallel to the stress direction tends to assume a constant rate, but so also does the parallel component of yielding in the crystalline matter away from the boundary. Thus grain boundary gliding can not be held responsible for steady state creep.

Summary

As a product of creep studies conducted upon aluminum bicrystals, in the temperature range 200 to 650°C (390 to 1200°F) and the stress range 10 to 1600 psi, the following major characteristics of grain boundary gliding are reported:

1. Gliding upon the grain boundary is spasmodic and begins with an induction period;
2. The direction of gliding is determined by the direction of the maximum shear stress parallel with the grain boundary, and is independent of crystal orientation;
3. The velocity of gliding increases with the sum of the angular difference θ (between the operative slip directions in the conjugate crystals) and the angular difference ω (between the active slip planes as measured between their traces upon the grain boundary);
4. The displacement rate, averaged for all orientations, is constant with the cube root of the time;
5. The logarithm of the rate of gliding is a linear function of the reciprocal of the absolute temperature, the slope giving an activation energy of $11{,}000 \pm 1{,}000$ calories per mole;
6. Considering the detail of spasmodic gliding, the displacement in one cycle is a linear function of the temperature prevailing during the period of activity and the length of the rest period between cycles decreases with rising temperature;
7. For small stress ranges, the logarithm of the time for unit gliding is almost proportional to the stress, but no simple means has been found to relate the displacement and the stress over large ranges;
8. Gliding continues indefinitely in a sequence of cycles upon the same path, which becomes broader with time, and broadens the more rapidly the higher the temperature and the higher the stress;
9. The active zone along the grain boundary is composed of sub-grains that are rotated (about a [110] axis, among others) through rather larger angles than are the sub-grains of the body of the crystal, the direction of rotation reversing many times during a single cycle;
10. Rupture does not occur through the grain boundary in bicrystals, but is always transcrystalline;

11. Preceding necking and rupture, the crystal that is destined to fail, abruptly increases its rate of extension to a faster, but constant, rate that obtains throughout that crystal;

12. Cast aluminum bicrystals exhibit about one third the rate of extension and grain boundary gliding as do strain annealed bicrystals of the same analysis.

These observations are explained by the proposal of a mechanism of grain boundary gliding the essentials of which are: that plastic yielding, which proceeds in a unit of metal by an alternation of slip and recovery, becomes a temporarily self-sustaining and directed shear, when a number of such units yield and recover in unison in a physically continuous chain. The roles of the grain boundary are to provide a deformation barrier that initiates the process and to establish the direction of the chain.

Acknowledgments

The authors wish to express their appreciation to the National Advisory Committee for Aeronautics, for its generous support of this research over a period of four years. Special thanks are due to A. W. Cochardt and H. W. Paxton who were largely responsible for working out the experimental procedure. Among the laboratory and research assistants who contributed to the work at various times were: T. W. Eichelberger, R. C. Schell, L. T. Lloyd, A. Platt, J. Rydzak, F. Bourriaud, G. Hook, J. Hohman, C. Vogley, E. G. Haney, F. de Marco, E. Kalinowski, R. Rummel, A. Nemy and K. Semlak.

References

1. W. Rosenhain and J. C. W. Humfrey, "The Tenacity, Deformation and Fracture of Soft Steel at High Temperature," *Journal*, Iron and Steel Institute, Vol. 87, 1913, p. 219.
2. E. N. daC. Andrade, "The Flow of Metals Under Large Constant Stresses," *Proceedings*, Royal Society, London, Series A, Vol. 90, 1914, p. 329.
3. T. S. Ke, "Stress Relaxation Across Grain Boundaries in Metals," *Physical Review*, Vol. 71, 1947, p. 533, Vol. 72, p. 41.
4. R. King, R. W. Cahn and B. Chalmers, "Mechanical Behavior of Crystal Boundaries In Metals," *Nature*, Vol. 161, 1948, p. 682.
5. T. S. Ke, "A Grain Boundary Model and the Mechanism of Viscous Intercrystalline Slip," *Journal*, Applied Physics, Vol. 20, 1949, p. 274.
6. W. Betteridge and A. W. Franklin, "An Investigation of the Structural Changes Accompanying Creep in a Tin-Antimony Alloy," *Journal*, Institute of Metals, Vol. 80, 1950, p. 147.
7. I. S. Servi and N. J. Grant, "Structure Observations of Aluminum Deformed in Creep at Elevated Temperatures," *Transactions*, American Institute of Mining and Metallurgical Engineers, Vol. 191, 1951, p. 917.
8. F. N. Rhines and A. W. Cochardt, "Preview of the Behavior of Grain Boundaries in Creep of Aluminum Bicrystals," National Advisory Committee for Aeronautics, Technical Note 2746, July 1952.
9. H. C. Chang and N. J. Grant, "Observations of Creep of the Grain Boundary in High Purity Aluminum," *Transactions*, American Institute of Mining and Metallurgical Engineers, Vol. 194, 1952, p. 619.

10. W. A. Rachinger, "Relative Grain Translation in the Plastic Flow of Aluminum," *Journal*, Institute of Metals, Vol. 81, 1952, p. 33.
11. K. E. Puttick and R. King, "Boundary Slip in Bicrystals of Tin," *Journal*, Institute of Metals, Vol. 80, 1952, p. 537.
12. D. McLean, "Creep Process in Coarse-Grained Aluminum," *Journal*, Institute of Metals, Vol. 80, 1952, p. 507.
13. N. J. Grant, I. S. Servi and A. Chaudhuri, "Slip and Grain Boundary Sliding as Affected by Grain Size," *Transactions*, American Institute of Mining and Metallurgical Engineers, Vol. 197, 1953, p. 217.
14. H. C. Chang and N. J. Grant, "Grain Boundary Sliding and Migration and Intercrystalline Failure Under Creep Conditions," *Transactions*, American Institute of Mining and Metallurgical Engineers, Vol. 197, 1953, p. 305.
15. A. R. Chaudhuri, N. J. Grant and J. T. Norton, "Metallographic Observations of the Deformation of High Purity Magnesium in Creep at 500°F," *Transactions*, American Institute of Mining and Metallurgical Engineers, Vol. 197, 1953, p. 712.
16. H. C. Chang and N. J. Grant, "Inhomogeneity and Creep Deformation of Coarse Grained High Purity Aluminum," *Transactions*, American Institute of Mining and Metallurgical Engineers, Vol. 197, 1953, p. 1175.
17. D. McLean, "Grain Boundary Slip During Creep of Aluminum," *Journal*, Institute of Metals, Vol. 81, 1953, p. 293.
18. R. C. Gifkins, "The Influence of Thallium on the Creep of Lead," *Journal*, Institute of Metals, Vol. 81, 1953, p. 417.
19. R. C. Gifkins, "Structural Studies of the Creep of Lead," *Journal*, Institute of Metals, Vol. 82, 1953, p. 39.
20. C. S. Roberts, "Creep Behavior of Extruded Electrolytic Magnesium," *Transactions*, American Institute of Mining and Metallurgical Engineers, Vol. 197, 1953, p. 1121.
21. B. Fazan, O. D. Sherby and J. E. Dorn, "Some Observations on Grain Boundary Shearing During Creep," *Transactions*, American Institute of Mining and Metallurgical Engineers, Vol. 200, 1954, p. 919.
22. A. M. Gervais, J. T. Norton and N. J. Grant, "Kink Band Formation in High Purity Aluminum During Creep at High Temperatures," *Transactions*, American Institute of Mining and Metallurgical Engineers, Vol. 197, 1953, p. 1487.
23. G. E. Bailey, "Note on the Softening of Strain Hardened Metals and Its Relation to Creep," *Journal*, Institute of Metals, Vol. 35, 1928, p. 27.
24. A. H. Cottrell and V. Aytekin, "The Flow of Zinc under Constant Stress," *Journal*, Institute of Metals, Vol. 77, 1950, p. 389.

DISCUSSION

Written Discussion: By S. L. Couling and C. S. Roberts, Dow Chemical Company, Midland, Michigan.

One of the basic differences in the deformation mechanism proposed by the authors and that favored by Chang and Grant (Ref. 9) hinges on the role of grain boundary migration in the deformation process. The authors did not observe appreciable boundary migration in any of their specimens and infer that a complex stress system such as that found in a polycrystalline sample is necessary for it to be present. Weinberg,[3] however, has recently creep tested tricrystals of aluminum in pure shear and observed extensive shearing and boundary migration, thus supporting the mechanism of Chang and Grant. Is it not possible that the failure to observe migration in the present research is in some way attributable to the presence of the thick aluminum oxide layer on the bicrystals? A tightly adherent oxide coating might conceivably help to restrain shearing along the boundary and pre-

[3]F. Weinberg, "Grain Boundary Shear in Aluminum," ACTA METALLURGICA, Vol. 2, 1954, p. 889

vent migration of the boundary to a lower strain energy position. Wilms[4] has warned against the use of oxide coated aluminum specimens in plastic deformation studies because he observes that true deformation markings are masked and spurious ones obtained on straining such samples.

Written Discussion: By H. H. Bleakney, metallurgist, Mines Branch, Department of Mines and Technical Surveys, Ottawa, Canada.

The question of grain boundary motion has been a vexing one ever since the existence of grain boundaries was first recognized. Rosenhain's amorphous metal hypothesis appeared to be a happy solution and received wide acceptance. Then, when that hypothesis was just at the point of death, Ke produced his evidence of the viscous behavior of grain boundaries in metals;[5] and his arguments were so plausible that few rejected his thesis that it is not necessary for grain boundaries to be amorphous so long as they just behave as though they were.

As one who has consistently rejected the concept of viscous grain boundaries, and who has contributed some evidence[6] to support that objection, the writer of this discussion warmly welcomes this contribution by Messrs. Rhines, Bond and Kissel. In this paper they have provided the most direct evidence of the nature of grain boundary motion as yet produced. The thorough, patient, and careful work, everywhere manifest in their discussion, thoroughly justifies the conclusion that ". . . a detailed examination of grain boundary gliding has failed to bring forth the evidence of viscous behavior that was postulated by Rosenhain and Humphrey, Andrade, and later Ke."

In the light of this evidence, it seems scarcely possible for any student of the subject to assert the viscosity of grain boundaries as an established fact; and this discusser hopes that it will soon be recognized that grain boundaries do not behave as though they were amorphous.

Written Discussion: By N. J. Grant and A. R. Chaudhuri, Massachusetts Institute of Technology, Cambridge, Massachusetts.

The contents of this brief paper really do not do justice to the excellent work and extensive findings of the authors. The observations are very definitely an important contribution to the fast growing quantity of literature on deformation mechanisms at elevated temperatures.

It would appear, however, that caution should be exercised in the authors' interpretations of the creep deformation in general of polycrystalline materials, paying special attention to the process of grain boundary deformation, on the basis of observations confined to bicrystal test specimens. That there is little justification for such interpretations follows from a consideration of the observations given below.

1. In studies with polycrystalline aluminum, Chang and Grant[7,8] described the cyclic nature of the elongation of localized regions. These cycles were observed

---

[4]G. R. Wilms, "Note on the Use of Electropolishing in the Metallographic Study of Plastic Deformation," *Journal*, Institute of Metals, Vol. 76, 1950, p. 629.

[5]T. S. Ke, "Experimental Evidence of the Viscous Behaviour of Grain Boundaries in Metals," *The Physical Review*, Vol. 71, 1941, p. 533.

[6]H. H. Bleakney, "An Evaluation of the Recovery Theory of Creep" *Canadian Journal of Technology*, Vol. 33, 1955, p. 556.

[7]H. C. Chang and N. J. Grant, "Observations of the Creep of the Grain Boundary in High Purity Aluminum," *Transactions*, American Institute of Mining and Metallurgical Engineers, 1952, Vol. 194, p. 619.

[8]H. C. Chang and N. J. Grant, "Inhomogeneity in Creep Deformation of Coarse Grained High Purity Aluminum," *Transactions*, American Institute of Mining and Metallurgical Engineers, 1953, Vol. 197, p. 1175.

across small gage lengths both astride grain boundaries and in the grains forming the boundary. The measurements in both cases were made parallel to the stress axis. The nature and the extent of the cycles, i.e., the periods of alternating elongation and recovery were, of course, quite different in the two cases. Observations such as these taken in conjunction with the observations of Rhines et al., immediately suggest that the behavior of the grains is considerably modified through the presence of grain boundaries and triple points located throughout a polycrystalline specimen. These observations also tell us that the recovery process taking place along the grain boundary, as manifested by the periods of the cycles in which no elongation takes place, is dependent to a great extent on the recovery taking place in the grains. In short, the effects of the interaction between grains and grain boundaries in the resulting deformation cannot be minimized.

2. Grain boundary migration was not noted to be an important process by the authors. On the other hand, boundary migration was found to be extremely so in polycrystalline aluminum specimens[7,8]. This difference is dependent (a) on the much more severe and nonhomogeneous deformation which takes place along the grain boundaries; (b) on the presence of the triple points. These two factors provide the driving force for the grain boundaries to move to new unstrained positions. Such motion of grain boundaries is extremely important, along with other deformation and recovery mechanisms, in maintaining the condition of continuity of material at the grain boundaries. It has been shown[9] that parting at the grain boundaries, i.e., intercrystalline fracture, results when this condition is not fulfilled. Consequently, in a polycrystalline ductile material, such as aluminum, the ductility is certainly due to the extensive occurrence of such processes as grain boundary migration. Further, the observation of a lack of grain boundary migration in bicrystals made by Rhines and his co-workers is a special behavior rather than a general one.

3. It was suggested by the authors that there are proponents of the theory that grain boundaries slide upon the grain boundary surface. Although we do not believe that the extensive literature and photomicrographic evidence, coupled with X-ray studies, support such a rigorous viewpoint; on the other hand, no one has yet been able to define the thickness of the region in which grain boundary sliding takes place. The thickness of this region undoubtedly is dependent on temperature, strain rate, grain size, and orientation of the grain boundary and its adjacent grains. It is no more precise to use the expression "considerable thickness," since this does not define the situation any more rigorously than the undefined expression "grain boundary sliding."

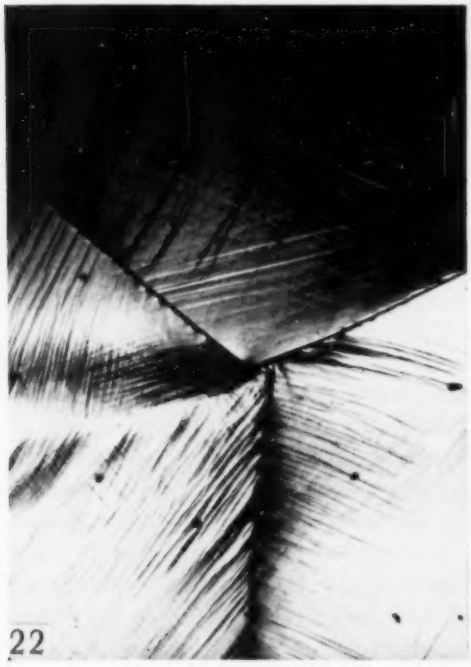
Of interest is the nature of grain boundary sliding shown in Fig. 22. Fig. 23 shows the same structure after repolishing to re-establish the position of the grain boundary. Here it will be noted that sliding has taken place along a grain boundary but involves a severely deformed region of indeterminate thickness. This specimen is an 80 Al—20 Zn alloy which was deformed at 500°F in a test which lasted only a matter of a few minutes.

4. Regarding the authors' proposed mechanism of deformation, relating to a zone adjacent to the boundary in which sliding takes place, there are a number of exceptions which are supported by observation over a long period of time by a

[9]H. C. Chang and N. J. Grant, "Mechanism of Intercrystalline Fracture," Submitted, American Institute of Mining and Metallurgical Engineers, 1955, to be published.

large number of investigators. Certainly the mechanism does not appear to apply to the behavior of polycrystalline materials. These items are:

a. There is no evidence that granular slip is evident as the first step in the process of achieving grain boundary sliding.



22



23

Fig. 22—An 80 Aluminum—20 Zinc High Purity Alloy, Tested at 500 °F, Rupture Life About 3 Minutes. ×75.
Fig. 23—Repolished View of Fig. 22. ×150.

b. We have also observed that grain boundary sliding can even take place immediately on loading of a specimen.

c. Subgrains are not noted along grain boundary areas until after grain boundary sliding has taken place.

d. Subgrain formation is readily and extensively noted after grain boundary sliding has taken place.

The authors suggest that the grain boundary will not slide until after polygonization has taken place. They suggest that the polygonization process, a recovery process, makes the region around the grain boundary "soft." To the contrary we contend that the polygonized areas are not as readily deformed as the unpolygonized areas along the grain boundaries. The completely annealed structure should yield more readily under stress since the entire grain is of essentially one orientation. After polygonization has occurred, the individual subgrains all show slightly different orientations, and as such should be more resistant to deformation. The work of Parker and Hazlett,[10] which showed that sub-boundaries have a strengthening effect, supports this argument.

Therefore, for grain boundary sliding to take place after polygonization, it would require that such deformation must wait until a more resistant grain boundary region is developed.

[10]E. R. Parker and T. H. Hazlett, "Principles of Solution Hardening," RELATION OF PROPERTIES TO MICROSTRUCTURE, 1953, p. 30. Published by The American Society for Metals, Cleveland.

Our observations indicated that grain boundary sliding is often in evidence before granular slip can be seen. Furthermore, if the phenomenon of sliding shown in Fig. 1 can take place in an extremely short time test at 500°F, it is difficult to see where there has been adequate time for recovery, following granular slip, to have taken place to permit the sliding observation.

Written Discussion: By D. McLean, Metallurgy Division, National Physical Laboratory, Teddington, England.

The activation energy of 11,000 cals/mol reported in this very interesting paper differs rather greatly from the value of 37,000 cals/mol found by Dorn et al[11,12] using polycrystalline aluminum. The difference may, however, be merely a result of different assumptions. The authors of this paper find that sliding $\alpha(\text{time})^{1/3}$. One can then assume that the effect of temperature may be expressed either as

$$\text{sliding } \alpha\ t^{1/3}e^{-\frac{Q}{RT}}$$

or

$$\text{sliding } \alpha\ (te^{-\frac{Q}{RT}})^{1/3}$$

If the former is assumed, a plot of displacement in 50 hours against 1/T (as in Fig. 7) gives $Q = 11{,}000$ cals/mol. If the latter is assumed, the same plot gives $Q = 3 \times 11{,}000 = 33{,}000$ cals/mol, which is quite close to the value reported by Dorn et al. The latter assumption was in effect made by Fazan, Sherby and Dorn[12] in deriving a value of 40,000 cals/mol from Rhine's previously published results. Such an assumption is moreover in keeping with the demonstration by Dorn and co-workers[11] that time and temperature are interchangeable in the way indicated by the second expression. It therefore seems that the difference between the activation energy now reported and the previous value may not be a real one.

Bragg has shown[13] that a material with finite minimum slip distance will not slip below a certain critical stress. His argument does not depend on the existence of planes of easy glide and therefore applies to grain boundaries, provided that a boundary cannot slide by vanishingly small amounts. The authors' observation that there is a threshold stress below which sliding does not occur suggests therefore that this is so.

Authors' Reply

The authors wish to thank Dr. McLean for his illuminating discussion of the evaluation of Q. While we had appreciated that the time variation in the rate of gliding is a complicating factor, we had overlooked the possibility of separating this factor in the manner suggested by Dr. McLean. The result adds weight to the mechanism proposed in the paper. It suggests a basic rate determination by a diffusion controlled process, such as recovery by polygonization, and it permits the isolation of the time effect as a purely geometric factor. We are disinclined, however, to accept the proposal that the threshold stress for grain boundary gliding is analogous to the critical stress for slip. The latter process is thought of as a shear upon a specific plane through the crystal, whereas grain boundary gliding is confined to no specific interface, and is, perhaps, better thought of as the periodic

[11]J. E. Dorn, N. P. L. Creep Conference, H. M. S. O. 1955.
[12]B. Fazan, O. D. Sherby and J. E. Dorn, *Journal of Metals*, Vol. 6, 1954, p. 919.
[13]L. W. Bragg, Symposium on Internal Stresses, Institute of Metals, 1947, p. 221.

organization into a direction parallel with the grain boundary of a portion of the plastic deformation that is in progress everywhere within the metal. Thus, the minimum stress is not that required to induce slip upon a plane but rather that required to sustain an alternation of slip and recovery within a special volume of metal.

The proposal by Grant and Chaudhuri, to the effect that grain boundary creep displays essentially different characteristics in bicrystals from those observed in polycrystalline metal provides a welcome opportunity to remove a potential source of misunderstanding. The essence of their proposal is that grain boundary migration, not found in bicrystals, is an essential feature of grain boundary creep in polycrystalline metal. There is, of course, no question that grain boundary gliding and grain boundary migration can and commonly do occur together in the high temperature creep of polycrystalline metals. Furthermore, it is sufficiently evident both that the strain resulting from grain boundary gliding can stimulate migration and that migration displaces the site of grain boundary gliding. This is not to say, however, that either process is dependent upon the other for its existence. The bicrystal studies stand as proof to the contrary; grain boundary creep can, and in bicrystals does, proceed and continue indefinitely upon the same path without the intervention of migration. It is elementary knowledge that grain boundary migration can be induced by a variety of stimuli including, for example, unbalanced interfacial tensions and "residual cold work." The fact that grain boundary creep and migration do interact in polycrystalline metals, thus partially obscuring the characteristics of both processes, is a major reason for turning to the bicrystal for clarification. In so doing it becomes apparent, for one thing, that the earlier conclusion of Grant and co-workers (derived from studies made upon polycrystalline metals) to the effect that the capacity of the grain boundary to support shear becomes exhausted, so that gliding can resume only at a new site, must be quite wrong.

While dealing with the subject of migration it is convenient to answer the inquiry of Couling and Roberts relative to the possible effect of the Al_2O_3 surface scale upon the incidence of grain boundary migration. That the absence of migration in the bicrystal studies is not to be associated with the presence of the oxide is indicated by a number of observations. Polycrystalline samples of the same material, which were given the same surface treatment as the bicrystals, did, in fact, exhibit migration. Also, some aluminum alloy bicrystals, tested subsequently, exhibited migration, but the initial grain boundaries in these were less regular than those in the high purity bicrystals. Finally, a study of the effect of thinning the oxide layer, by washing with a suitable solvent, produced no observable difference in the creep behavior.

Returning to the discussion of Grant and Chaudhuri, there remain further differences of opinion, some of which involve simple points of fact. In the realm of fact is the question whether the induction period occurs in polycrystalline aluminum. Our own observations, made during an orientation study that preceded the bicrystal measurements, revealed a delay in the beginning of grain boundary gliding in polycrystalline aluminum as well as in bicrystals. That this effect has, until now, gone unreported seems to be a matter of the absence of tests suitable for its detection. Unfortunately most of the prior grain boundary creep measurements have been made parallel to the applied stress; such measurements, as have been shown in the present paper, do not report the grain boundary shear and so could not detect the induction period. Puttick and King made their measurements on tin

bicrystals in a suitable direction, but imposed upon the metal such mechanical restraints that it could have had little if any opportunity to display the natural characteristics of grain boundary gliding. Lest a false impression has been given by emphasizing the occurrence of very long induction periods, however, the authors wish to point out that induction periods lasting less than a minute have been found when the $(\theta+\omega)$ angle was large and the stress and temperature high.

Another point of fact relates to the sequential precedence of transcrystalline plastic deformation (presumably by slip) over grain boundary gliding. It is true that convincing metallographic evidence of slip, prior to grain boundary gliding, is often difficult to obtain. The present authors contend, however, that a permanent extension of the specimen, without grain boundary yielding, is sufficient evidence that slip has occurred, even in the absence of visible slip traces. This kind of indication was always found and sometimes visible slip as well.

Concerning the different aspects of cyclic creep it may help to point out that three fairly distinct interrupted yielding processes have been reported. First is grain boundary gliding interrupted by grain boundary migration as reported by Grant and co-workers; second, spasmodic grain boundary gliding upon a fixed path, as reported in the present paper; and third, localized spasmodic motion over very short lengths within a crystal, as found by several observers including the discussors and the present authors. If it is appreciated that these are distinct processes and that they are all operative, frequently concurrently, in the same piece of metal, some confusion may be avoided.

The authors fail to see any distinction between the circumstances of the appearance of sub-grain rotation along the grain boundary, as described by these discussors and those described in the present paper. There is a clear difference, however, with regard to the resistance of the polygonized layer to subsequent deformation. Surely it cannot be doubted that the polygonized material will be less resistant to deformation than adjacent metal that has been cold-worked, but not quite enough to cause it to polygonize! The work of Parker and co-workers in no way argues against this assumption.

Messers. Grant and Chaudhuri appear to have answered their own question with regard to the meaning of the expression "considerable thickness" as it refers to the dimensions of the active zone where grain boundary gliding occurs. The thickness of the zone is "considerable" but, for reasons recited in part by the discussors, is not subject to precise definition.

The authors thank H. H. Bleakney for his emphasis upon a point with which we agree wholeheartedly.

INFLUENCE OF COLD WORK ON STRENGTH OF STEEL AT ELEVATED TEMPERATURES

By Paul Shahinian

Abstract

The effect of cold work on the high temperature properties of a quenched and tempered chromium-molybdenum steel was investigated by means of stress-rupture and relaxation tests. The material with several levels of cold reduction (0, 8, 15 and 39% of cross sectional area) was tested in stress-rupture at 700, 800, 900 and 1000°F in the stress range of 45,000 to 128,000 psi, and in relaxation at 900°F and 80,000 psi initial stress.

The rupture and creep strengths of the steel at 700°F were greatly enhanced by cold work, the improvement increasing with larger amounts of cold work. At 800 and 900°F the rupture and creep strengths were generally lowered by critical amounts of cold deformation (8 to 15%), while beyond the critical values increased strengths were obtained. An explanation for this behavior is given in terms of the Bauschinger effect. There was no apparent influence of prior deformation on rupture strength at 1000°F; however, creep strength decreased generally with increasing prior deformation. In relaxation at 900°F residual stress was lowered by an increase in cold work. (ASM-SLA Classification: Q3, Q4, Q24, AY)

Introduction

A KNOWLEDGE of the effect of metallurgical variables on the high temperature properties of metals is essential for the proper design of parts for service above room temperature. There is a particular need for information on the influence of cold deformation on the variation of strength with time of steel at elevated temperatures for the design of aircraft engine bolts. For example, the threads on some commercial bolts are formed by cold rolling, and it is not known whether this cold work is beneficial or deleterious. In addition to being of practical importance, the behavior of metals with prior cold work is of fundamental interest.

A number of investigations have been made, particularly on nonferrous metals and alloys (1–8),[1] of the effect of cold work on creep resistance at high temperatures. The results of these studies

[1]The figures appearing in parentheses pertain to the references appended to this paper.

A paper presented before the Thirty-Seventh Annual Convention of the Society, held in Philadelphia, October 17–21, 1955. The author, Paul Shahinian, is associated with the High Temperature Alloys Branch, Metallurgy Division, Naval Research Laboratory, Washington, D. C. Manuscript received April 11, 1955.

agree, in general, that prior cold work increases creep strength; however, the benefit from cold work is lost at temperatures where rapid recovery or recrystallization occur. In the case of Monel, there was found to be an optimum degree of cold work for improving the strength at each temperature; the optimum percentage of cold work was noted to decrease with increasing temperature (8). A similar effect has been observed with stainless steel (9). The improved creep resistance due to cold work of a high temperature alloy, low-carbon N-155, was attributed (10) to internal stresses in the crystal lattice. Very little information is available on the effect of prior deformation on the creep properties of carbon and low alloy steels. In a study (11) on a 0.40% carbon steel in the hot-rolled condition at 600–1000°F, previous cold work (6 and 12% elongation) was found to lower creep resistance. Although the latter results are not directly comparable with data on other materials, there is doubt as to the effect of cold work on the behavior of steel at elevated temperatures.

It was the object of this investigation to determine the influence of prior cold deformation on the high temperature strength of a chromium-molybdenum steel. Creep and rupture properties were evaluated by stress-rupture tests and, to a limited extent, the variation of strength with time was determined by stress relaxation tests.

Experimental Procedure

The investigation was conducted with a single bar of commercial steel of the following chemical composition: 0.38% C, 0.45% Mn, 1.57% Cr, 0.48% Mo, 0.70% Si, 0.008% P, 0.015% S. The material was received as hot-rolled ⅝-inch diameter rods and was heat treated prior to cold working. The treatment consisted of heating at 1800°F for 1 hour, oil quenching, and tempering at 1200°F for 2 hours. Several levels of cold reduction, 8, 15, and 39% of cross sectional area, were obtained by means of rolling. Bar sections of approximately 15 inches were rolled on six sides for all reductions except the case of the 39% reduction samples which were rolled on four sides. Reduction of area measurements were made on each specimen; the variation from the values indicated was no more than ±1%.

Room temperature tensile tests were made on the material with various degrees of cold work as well as without cold work. Standard 0.357-inch diameter specimens were used except for the 39% cold-worked material which permitted only a maximum specimen diameter of 0.250 inches.

Stress-rupture tests were conducted on the steel with 0, 8, 15, and 39% cold reduction at 700, 800, 900, and 1000°F in the stress range of 45,000 to 128,000 psi. The specimens employed were 0.250 inch diameter by 1.25 inch gage length and were machined from the

Table I
Room Temperature Tensile Properties

		Tensile Strength, psi	0.2% Yield Strength, psi	Elongation %	Reduction of Area, %
0%	Cold work	152,000	133,600	20	62
8%	Cold work	149,000	127,000	19	60
15%	Cold work	154,500	135,000	19	58
39%	Cold work	166,000	153,000	18	54

centers of the bars. Conventional single-lever constant-load stress-rupture machines were used. Temperatures were measured by a chromel-alumel thermocouple placed in contact with the center position of the specimen length; the temperatures were maintained to within ± 2°F. The temperature gradient did not exceed 2°F along the gage length of the specimen. The specimens were held at temperature for 1 hour prior to loading. Extension of the specimen was autographically recorded from the deflection of the loading lever, giving an elongation versus time curve; in addition, periodic readings were taken with a dial gage. Single tests were run, generally, for each condition of temperature, stress, and degree of cold work.

A series of specimens (stress-rupture type) with various degrees of cold work was tested in stress relaxation at 900°F. An initial stress of 80,000 psi was applied and the relaxation in stress was recorded for 500 hours. The tests were conducted in a machine normally used for constant strain rate tests. In operation the tensile load is applied rapidly by means of a motor-driven cam to the desired load level; the over-all strain is then held constant. A load cell placed in the grip system of the specimen permits the recording of the variation of load with time. The amount of elastic strain experienced by the loading members is small because of their large size. The strain in the specimen is constant except for possibly a minor change due to elastic recovery of the massive loading members. Comparison of relaxation curves obtained from this machine with those from a conventional relaxation machine showed no appreciable difference (12). After completion of the relaxation tests (500 hours), the specimens were tested in stress-rupture at 900°F and 80,000 psi.

Metallographic examinations and hardness measurements (discussed later) were made on the threaded and gage sections of some fractured specimens and on the material prior to testing. Vickers pyramid hardness measurements were obtained using a 5 kilogram load.

Results and Discussion

The room temperature tensile properties of the quenched and tempered steel with various degrees of cold reduction are listed in Table I. A reduction in tensile strength and in 0.2% yield strength was observed with the 8% cold-worked material. At the higher levels

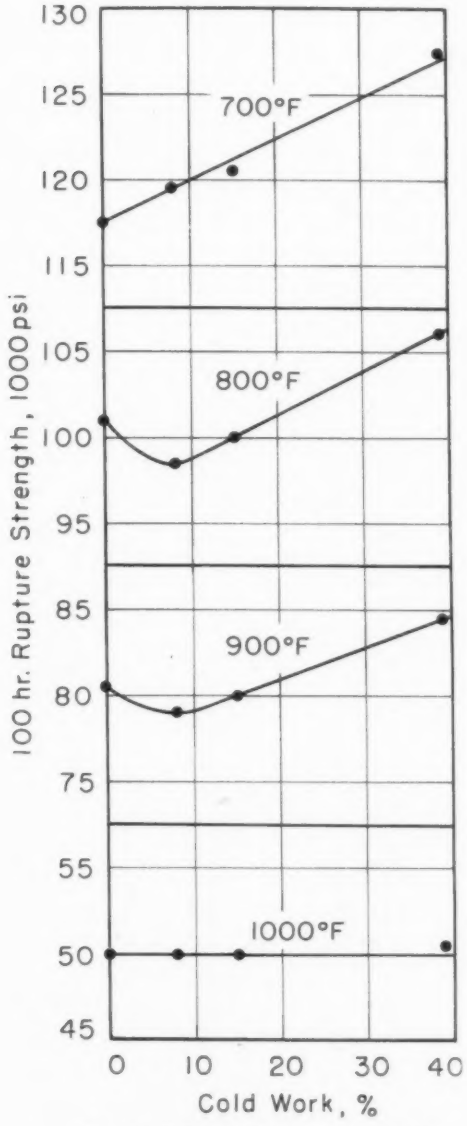


Fig. 1—Effect of Cold Work on 100-Hour Rupture Strength at 700, 800, 900 and 1000°F.

of cold work (15 and 39%), increases in tensile and yield strengths were obtained. Elongation and reduction of area values generally decreased with increasing cold work.

The effect of prior cold deformation on high temperature properties was evaluated in terms of rupture strength, creep strength and residual stress in the case of the relaxation tests. The stress to produce a minimum creep rate of 0.5 inch per inch per 1000 hours was used as a measure of creep strength. Time to rupture, minimum creep rate, total elongation, and reduction of area data, listed in Table II, were obtained from the stress-rupture tests.

Table II
Stress-Rupture Results

Code A—0% Cold-worked C—15% Cold-worked
B—8% Cold-worked D—39% Cold-worked

Temp. °F	Stress psi	Code	Rupture Time, Hours	Min. Creep Rate in./in. /1000 hr.	Elongation %	Reduction of Area %
700	128,000	DDO3	79.0	0.573	17	52
	125,000	A2	1.5	27.2	20	64
		B2	8.2	4.77	17	61
		C2	42.9	1.0	18	64
		D2	2756.	0.0266	19	52
	120,000	AO2	23.1	1.76	18	59
		BO2	80.4	0.636	21	60
		CO2	112.3	0.49	18	59
800	105,000	AO5	9.5	5.03	23	72
		BO5	6.4	8.05	21	70
		CO5	12.3	4.95	23	68
		DO5	166.	0.456	22	60
	100,000	A5	241.1	0.197	19	67
		B5	34.6	1.72	22	68
		C5	115.7	0.57	21	68
		D5	649.3	0.130	22	58
	95,000	A7	2906.	0.0262	19	56
		B7	608.6	0.0795	19	64
		C7	406.7	0.176	25	67
		D7	4270.	0.0228	23	58
900	85,000	A8	39.3	1.23	26	75
		B81	26.0	2.94	28	75
		C8	15.4	4.84	26	72
		D8	84.7	1.33	29	64
	80,000	A1	102.5	0.67	28	73
		B1	65.8	1.25	31	73
		C1	206.0	0.46	36	71
		D1	445.5	0.245	33	59
		AR*	50.3	0.927	18	68
		BR	58.5	1.18	20	71
		CR	74.0	0.90	21	67
		DR	281.0	0.317	27	59
	75,000	A6	419.2	0.133	29	67
		B6	342.0	0.246	31	67
		C6	347.0	0.262	36	68
		D6	732.6	0.128	24	52
	70,000	A9	1100.	0.0488	25	36
		B9	1120.8	0.0547	22	48
		C9	1352.0	0.0492	24	34
		D9	1193.4	0.065	25	46
1000	50,000	A4	104.7	0.528	13	22
		B4	101.5	0.513	17	22
		C4	97.9	0.835	25	32
		D4	108.4	1.01	32	46
	45,000	A3	182.4	0.197	10	12
		B3	192.0	0.247	13	15
		C3	176.0	0.328	14	15
		D3	188.3	0.354	27	33

*Specimens initially tested in relaxation at 900°F—80,000 psi.

Cold work affected the rupture strength for the steel differently depending on the temperature, Fig. 1. The 100-hour rupture strength at 700°F was greatly enhanced by prior cold work, the improvement increasing with larger amounts of cold work. At 800 and 900°F the

rupture strength was generally lowered by critical amounts of cold work (8 and 15%), while beyond the critical values increased strength was obtained. The lowest 100-hour rupture strength was exhibited by the 8% cold-worked material. The possible severity of this detrimental effect is shown by the reduction in rupture time to approximately 15% of its original value at 800°F and 100,000 psi, Table II. At 1000°F there was no apparent influence of cold work on rupture strength for tests of all durations as shown in Fig. 1. The

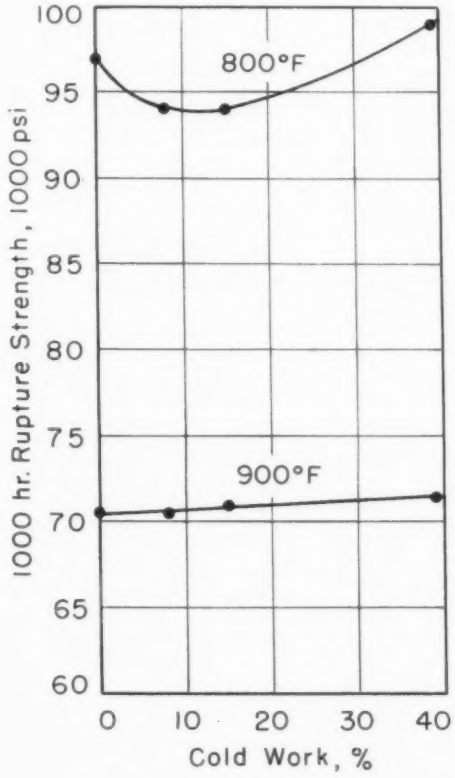


Fig. 2—Effect of Cold Work on 1000-Hour Rupture Strength at 800 and 900°F.

variation of the 1000-hour rupture strength due to prior deformation, presented in Fig. 2, was similar to that of the 100-hour rupture strength at 800°F; however, at 900°F a small increase in the 1000-hour strength with increasing cold work indicated a behavior differing from that of the shorter time strength. Apparently the longer test time at 900°F alleviated the influence of the cold deformation.

The effect of cold work on creep strength (stress for creep rate of 0.5 inch per inch per 1000 hours) was different at the various temperatures, Fig. 3. An improvement in creep strength with increasing cold work was obtained at 700°F. At 800 and 900°F the creep strength was lowered by 8 and 15% cold reduction; a reduc-

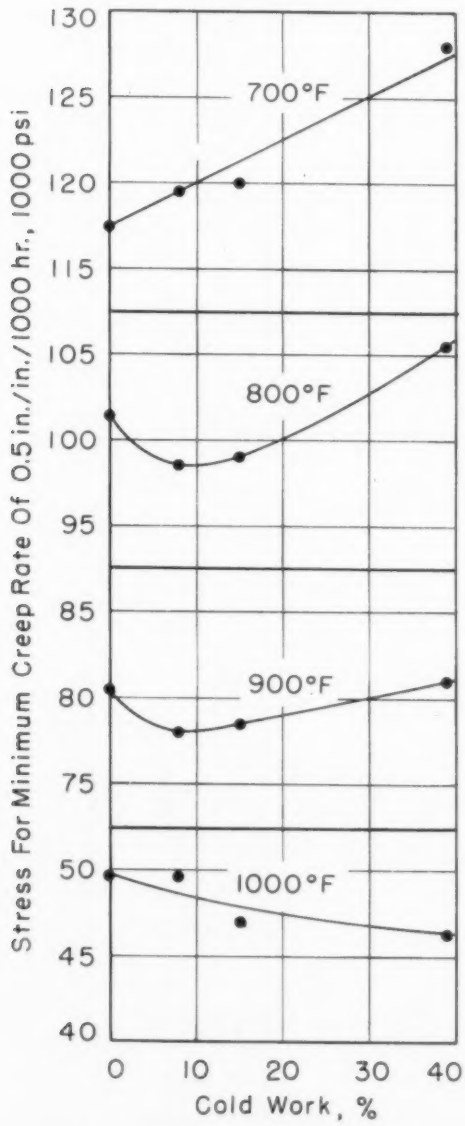


Fig. 3—Effect of Cold Work on Stress for Creep Rate of 0.5 in./in./1000 Hours at 700, 800, 900 and 1000°F.

tion of 39% raised the strength. A general decrease in creep strength with larger amounts of cold work was indicated at 1000°F.

The decrease in 100-hour rupture strength with increase in temperature, shown in Fig. 4, is essentially linear to 900°F; beyond this temperature the rate of weakening is greater. The loss of strength due to temperature appeared to be slightly greater for the 39% cold-worked material than for the less cold-worked material.

There was no apparent effect of cold work on elongation at fracture except at 1000°F where increasing prior deformation produced higher elongations, Fig. 5. The general level of elongation

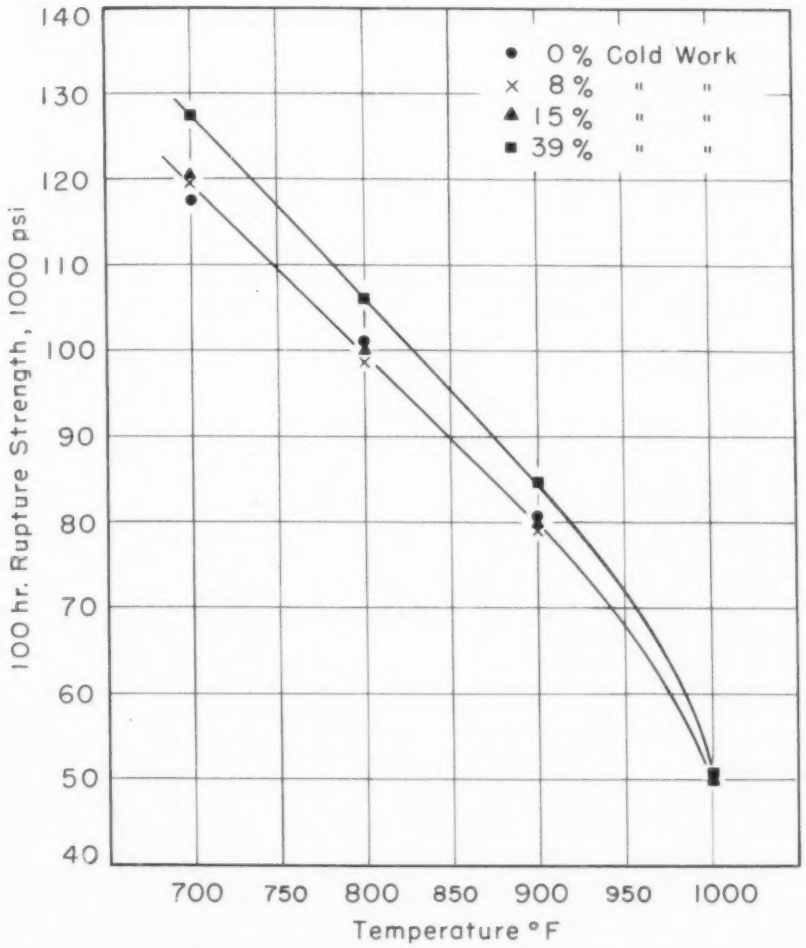


Fig. 4—Effect of Temperature on 100-Hour Rupture Strength.

values was raised with increase in temperature to 900°F; at 1000°F a downward trend was indicated. Variation of initial stress (or time of test) had no apparent effect on elongations at fracture at 700 and 800°F. However, at 900°F higher elongations were generally obtained at the two intermediate stress levels and at 1000°F smaller elongations were produced by the lower stresses.

No change in reduction of area due to cold work was observed at 700, 800, and 900°F except for the 39% reduced material which generally showed lower values. At 1000°F reduction of area increased with increase in deformation. There was no significant effect of stress at 700 and 800°F; however, at 900 and 1000°F reduction of area decreased with decreasing stress. The general level of reduction of area values was lower at 1000°F than at the other temperatures.

In stress relaxation tests, increased cold work produced greater relaxation at 900°F, Fig. 7. The decrease in residual stress (at 500 hours) with increase in deformation of the material loaded at 900°F

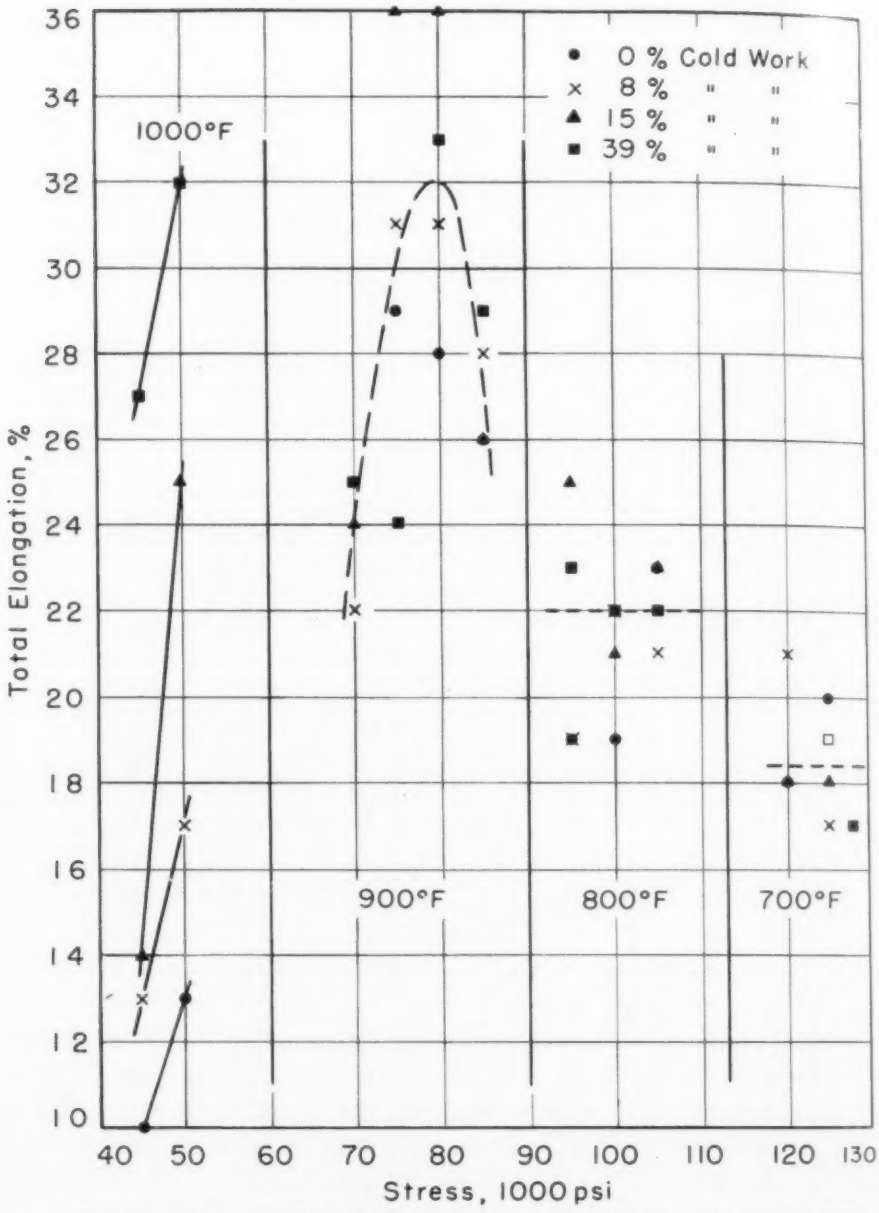


Fig. 5—Influence of Cold Work and Stress on Elongation at Fracture at 700, 800, 900 and 1000°F.

and 80,000 psi is presented in Fig. 8. A reduction of 8% lowered the residual stress by a proportionately larger amount than similar increments at higher levels of cold work. It should be noted that while 39% cold work showed no decrease in creep strength compared to the non-cold worked material (Fig. 3), a pronounced detrimental effect on relaxation strength was developed.

Stress-rupture tests at 900°F—80,000 psi of the specimens subjected to stress-relaxation for 500 hours revealed that prior relaxation lowered rupture time and increased minimum creep rate except

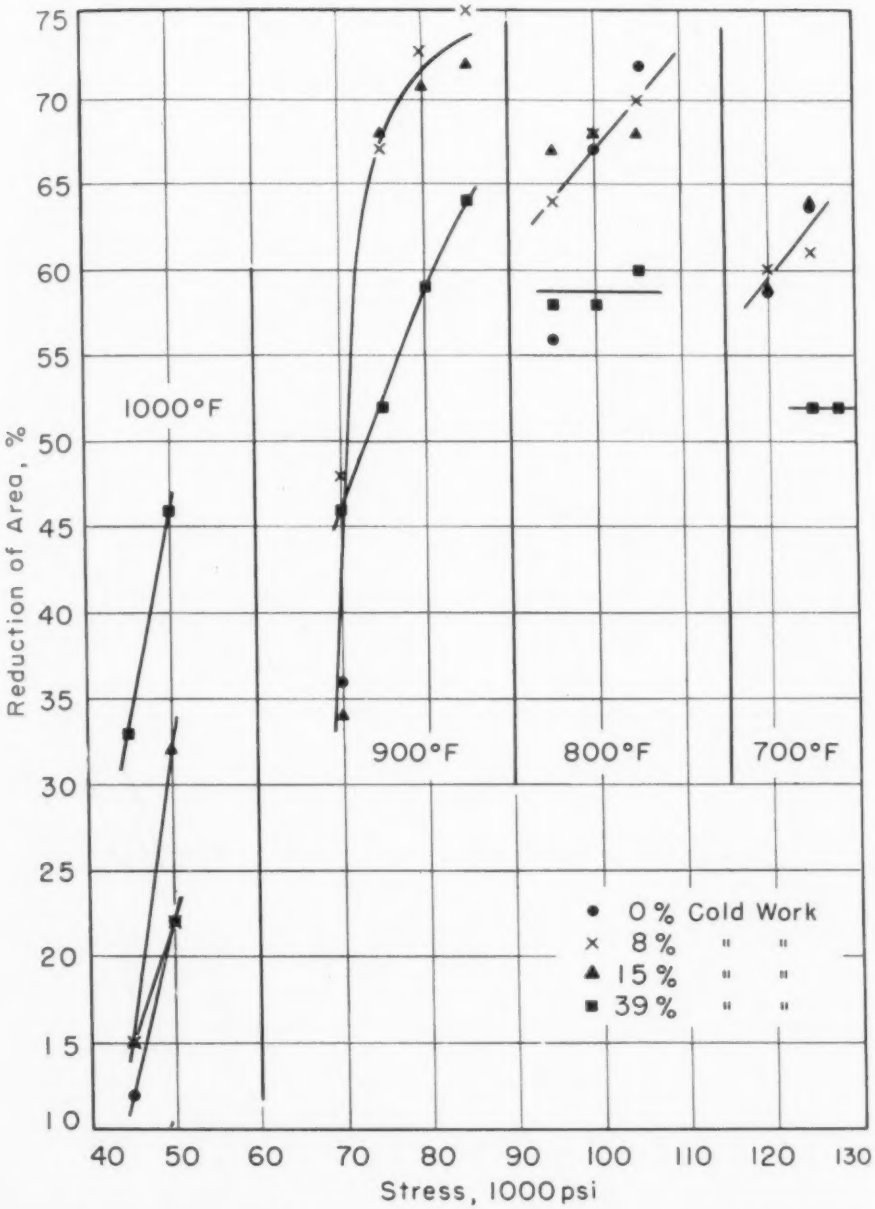


Fig. 6—Influence of Cold Work and Stress on Reduction of Area at 700, 800, 900 and 1000°F.

for the 8% cold-worked steel which was not materially affected, Fig. 9.

Hardness measurements of fractured stress-rupture specimens, presented in Fig. 10, indicate generally a slight increase in hardness after exposure to test temperatures. Hardness, measured on the threaded sections of specimens, before and after tests at 700, 800 and 900°F decreased for the 8% cold-worked material and increased for the materials with greater cold work. A general increase in hard-

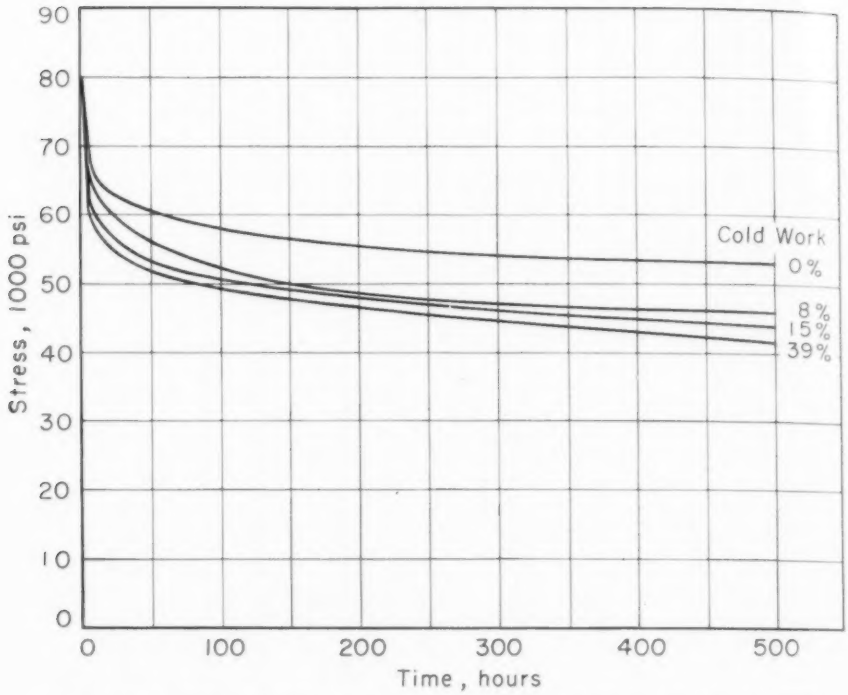


Fig. 7—Stress Relaxation Curves of Cold-Worked Cr-Mo Steel at 900°F—80,000 psi Initial Stress.

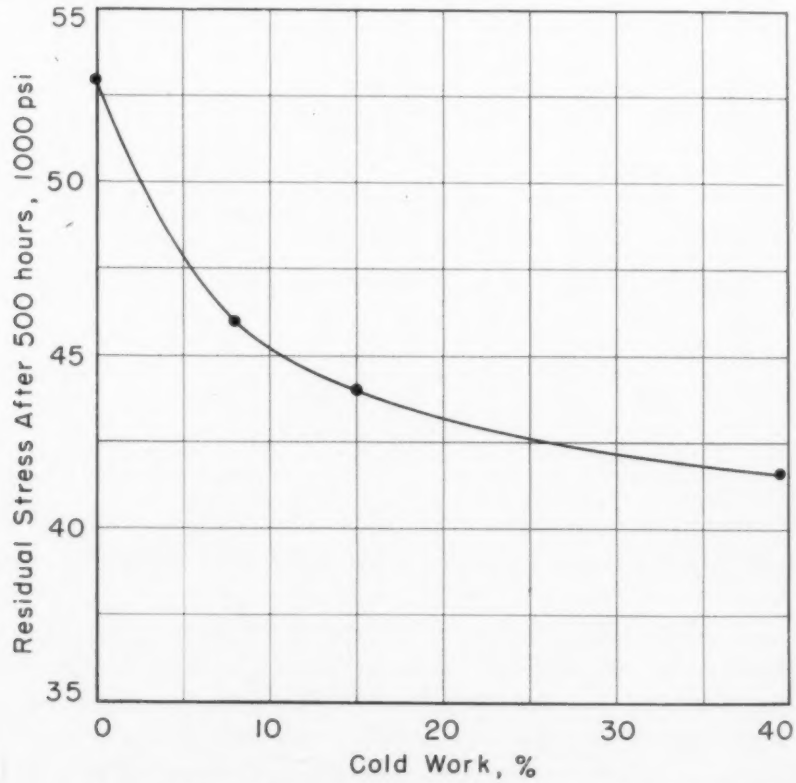


Fig. 8—Effect of Cold Work on Relaxation at 900°F and 80,000 psi Initial Stress.

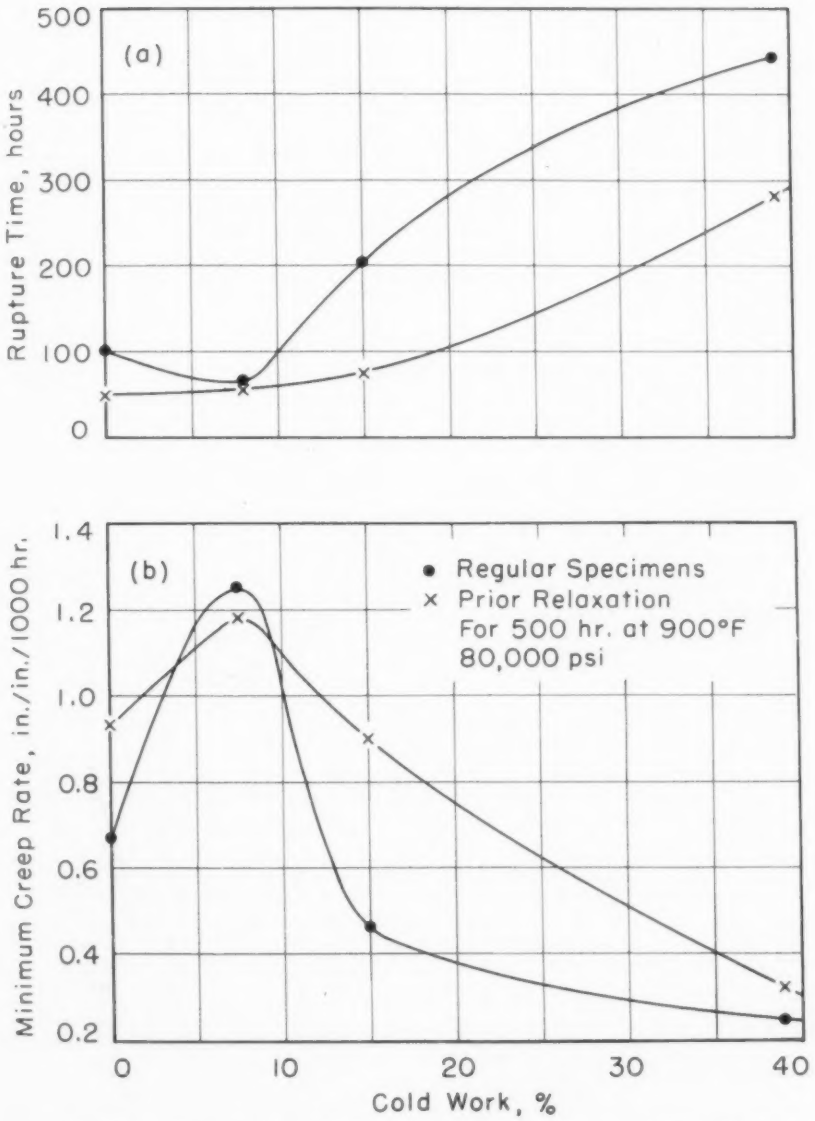


Fig. 9—Influence of Prior Relaxation on Rupture Time and Creep Rate at 900°F—80,000 psi.

ness with increasing prior cold work was observed in the gage sections after tests at these temperatures.

Fractured specimens which had been tested at stresses above 70,000 psi (900°F and below) displayed necking while those tested below this stress level showed intergranular fractures (without necking) except for a 39% cold-worked specimen under 50,000 psi which exhibited a slight neck. At 70,000 psi (900°F) either type of fracture occurred.

Metallographic examination of fractured specimens did not reveal any evidence of recrystallization. Coalescence of cementite was observed in specimens tested at the higher temperatures, par-

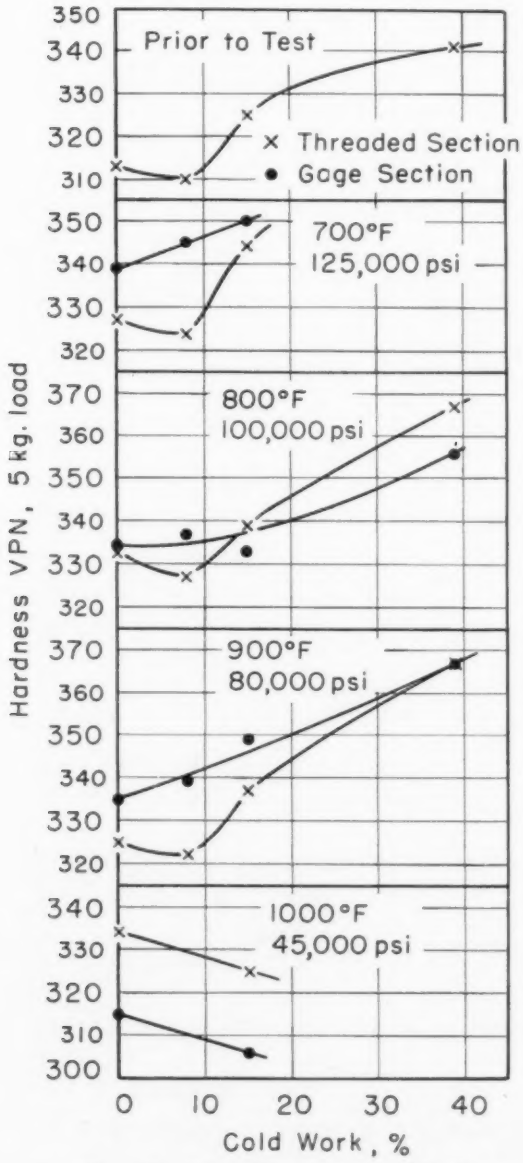


Fig. 10—Hardnesses of Stress-Rupture Specimens Prior to and After Tests.

ticularly in the highly cold-worked material. Intergranular oxidation was evident in the gage sections of specimens tested at 1000°F.

The lowering of rupture strength and creep resistance at 800 and 900°F by small amounts of prior cold deformation, is explainable on the basis of the Bauschinger effect. The Bauschinger effect (13) is concerned with the change in mechanical properties on reversing the direction of straining. Straining in either tension or compression raises the ability of the metal to withstand further stressing of the same kind and lowers its strength to stresses of the opposite kind. Work softening at room temperature, believed to be of this type,

was observed in this study, Table I. Since the final straining was in the same direction (tensile) with all the specimens, the differences noted may be related to differences in the initial stress state of the 8 and 15% cold-worked material compared to the 39% cold-worked material. According to Baldwin (14) the residual stress state resulting from nonpenetrating rolling (slight reductions) is different from that produced by penetrating (heavy) rolling. Light rolling produces a compressive stress at the rolled surface and a tensile stress in the interior whereas heavy rolling produces a tensile stress at the rolled surface and a compressive stress in the interior all acting in the rolling direction. Presumably the stress condition (with slight adjustments) remains after the machining of specimens. The decrease in room temperature yield strength of the material by 8% cold work may be attributed to the Bauschinger effect. This loss in strength due to a critical degree of deformation appears to carry to elevated temperatures, in this case to 900°F, and is evident in the creep and rupture strengths. This seems reasonable since it has been reported (15) that heating a 0.28% carbon steel at 750°F for 8 hours after prestraining did not eliminate the work softening effect. The absence of work softening effects in our tests at 700°F may be due to additional cold working of the material (5—6% elongation) upon application of the test load.

On the basis of hardness measurements, Fig. 10, softening by the 8% deformation persists even after prolonged holding at 900°F; however, straining appears to remove the softening. It should be noted that the hardness changes in the critical region were small. A similar behavior, work softening of a quenched and tempered steel, was reported by Polakowski (15) who presented the explanation that the steel in the quenched and tempered condition contains considerable internal stresses and consequently behaves like metals in which the internal stresses have been produced by cold work. It should therefore soften during cold working. However, the method of measuring this softness, indentation hardness with its complex mechanics, may be a factor in the behavior. Microstructure has been shown by Wilson (16) to influence this effect; a sorbitic structure showed the largest softening whereas a spheroidized structure displayed no softening. The work softening effect observed in this study is probably based on the macro-residual stresses and related micro-stresses induced by cold work.

The effect of cold work (39%) on relaxation strength and creep strength was found to be different at 900°F, the relaxation strength was lowered whereas the creep strength was slightly improved. This indicates that the steady-state creep, used as measure of creep strength, is not the controlling factor in relaxation. The first stage of creep is probably of more significance in estimation of relaxation behavior, although no evidence of this was apparent in this study.

Summary and Conclusions

The influence of cold work on creep, rupture and relaxation properties of a quenched and tempered chromium-molybdenum steel was investigated. The material with 0, 8, 15, and 39% cold reduction was tested in stress-rupture at 700, 800, 900 and 1000°F in the stress range of 45,000 to 128,000 psi. Relaxation tests were conducted at 900°F with an initial stress of 80,000 psi for 500 hours followed by stress-rupture tests of the relaxed specimens. Room temperature tensile properties of the unworked and worked steel were determined.

From the results of this study, the following conclusions may be drawn:

1. The effect of cold work on the creep and rupture properties of chromium-molybdenum steel varies depending on temperature and degree of deformation. Relaxation is affected in a different manner from creep.

2. Creep strength (stress to produce creep rate of 0.5 inch per inch per 1000 hours) and 100-hour rupture strength increase with increasing cold work at 700°F.

3. Creep strength and 100-hour rupture strength at 800 and 900°F are lowered by small amounts of cold work, 8 and 15%, but are improved by 39% cold work. The behavior is explainable on the basis of the Bauschinger effect. The effect of cold work at 900°F is less in long time tests (1000 hours).

4. At 1000°F there is no effect of cold work apparent on rupture strength; however, a decrease in creep strength is indicated with increasing cold work.

5. There is no apparent effect of cold deformation on elongation at fracture except at 1000°F where increasing prior deformation produces higher elongation values. Reduction of area is also unaffected at 700, 800 and 900°F except for the 39% reduced material which is generally lower. At 1000°F reduction of area increases with increase in deformation.

6. A decrease of residual stress in relaxation tests is obtained with increasing cold work at 900°F and 80,000 psi initial stress.

7. Room temperature tensile strength, 0.2% yield strength and hardness are lowered slightly by 8% cold work; with greater cold work (15 and 39%), increases are obtained.

Acknowledgment

The author wishes to express his appreciation to Dr. J. R. Lane for his interest and suggestions in this work. The testing was performed by J. T. Atwell and R. L. Saunders. The problem was suggested and supported by the U. S. Navy Bureau of Ships (E. Olcott).

References

1. H. L. Burhoff, A. I. Blank and S. E. Maddigan, "The Creep Characteristics of Some Copper Alloys at Elevated Temperatures," *Proceedings*, American Society for Testing Materials, Vol. 42, 1942, p. 668.
2. H. L. Burhoff and A. I. Blank, "Creep Characteristics of a Phosphorized Copper," *Transactions*, American Institute of Mining and Metallurgical Engineers, Vol. 161, 1945, p. 420.
3. A. D. Schwope, K. F. Smith and L. R. Jackson, "The Comparative Creep Properties of Several Types of Commercial Coppers," *Transactions*, American Institute of Mining and Metallurgical Engineers, Vol. 185, 1949, p. 409.
4. A. I. Blank and H. L. Burhoff, "Creep Characteristics of Phosphorized Copper (0.019 Per Cent P) at 300, 400, and 500°F," *Proceedings*, American Society for Testing Materials, Vol. 51, 1951, p. 981.
5. W. D. Jenkins and T. G. Digges, "Creep of Annealed and Cold-Drawn High Purity Copper," *Journal of Research*, National Bureau of Standards, Vol. 47, No. 4, Oct. 1951, p. 272.
6. N. D. Benson, J. McKeown and D. N. Mends, "The Creep and Softening Properties of Copper for Alternator Rotor Windings," *Journal*, Institute of Metals, Vol. 80, 1951–52, p. 131.
7. O. D. Sherby and J. E. Dorn, "The Effect of Cold Rolling on the Creep Properties of Several Aluminum Alloys," TRANSACTIONS, American Society for Metals, Vol. 43, 1951, p. 611.
8. N. J. Grant and A. G. Bucklin, "Creep-Rupture and Recrystallization of Monel From 700 to 1700°F," TRANSACTIONS, American Society for Metals, Vol. 45, 1953, p. 151.
9. H. R. Zschokke and K. H. Niehus, "Requirements of Steel for Gas Turbines," *Journal*, Iron and Steel Institute, Vol. 156, 1947, p. 271.
10. D. N. Frey and J. W. Freeman, "Fundamental Effects of Cold Working on the Creep Resistance of an Austenitic Alloy," *Transactions*, American Institute of Mining and Metallurgical Engineers, Vol. 191, 1951, p. 755.
11. C. L. Clark and A. E. White, "Creep Characteristics of Metals," TRANSACTIONS, American Society for Metals, Vol. 24, 1936, p. 831.
12. J. R. Lane and Paul Shahinian, "Stress Relaxation of Two Austenitic Alloys," Naval Research Laboratory Memorandum Report 430, Feb. 1955.
13. C. S. Barrett, "Structure of Metals," McGraw-Hill Book Co., Inc., 1952, p. 359.
14. W. M. Baldwin, Jr., "Macro-Residual Stresses in Metals Resulting from Plastic Deformation," COLD WORKING OF METALS, American Society for Metals, 1949, p. 31.
15. N. H. Polakowski, "Softening of Metals During Cold-Working," *Journal*, Iron and Steel Institute, Vol. 169, 1951, p. 337.
16. D. V. Wilson, Discussion of (15), *Journal*, Iron and Steel Institute, Vol. 172, 1952, p. 29.

DISCUSSION

Written Discussion: By John F. Ewing, The Babcock and Wilcox Company, Tubular Products Division, Beaver Falls, Pa.

The data presented in this paper regarding the relationship between cold work and the high temperature strength of the chromium-molybdenum alloys are of industrial significance. These alloys have found extensive industrial use as high strength structural components for process equipment capable of severe service at elevated temperatures and pressures.

It is frequently necessary to place certain fabricated components into service in the cold-worked condition due to the impossibility of heat treatment after cold fabrication because of section size or critical alignment requirements. The results and discussion of these experimental data have stressed the influence of cold work

on the 100 and 1000-hour creep-rupture strengths at several temperatures. Most industrial applications are concerned with long time service in excess of 10,000 hours. Since it might be advisable to consider cold work effects in the design of structural components for high temperature service the authors are asked for their comments regarding possible influences of cold work on the relatively long time strength properties (in excess of 10,000 hours) of the chromium-molybdenum alloys as a function of temperature. The rather pronounced decrease in the 1000-hour creep-rupture strength as the temperature is increased suggests structural instabilities from cold deformation that might easily reduce the long-time creep-rupture strengths, at least at the higher operating temperatures.

Written Discussion: By W. Lee Williams, metallurgist, U. S. Naval Engineering Experiment Station, Annapolis, Maryland.

This is an interesting paper, in that it extends our knowledge of the effects of cold work on elevated temperature properties to yet another material: this time, a high temperature bolting steel. The matter is of practical as well as academic interest. The cold straightening of bars from which bolt studs are made is a fairly common practice. In addition, more and more bolts are being roll threaded, and the effects of such operations on high temperature properties have been of some concern.

My main criticism of this paper is the ease with which one can be misled in making practical interpretations of the data. The following points in particular might be mentioned:

(a) The author determined the effect of cold work on creep rate on the basis of a minimum creep rate of 0.5 in./in./1000 hours (0.05% per hour). There is nothing wrong with this, but it should be pointed out that conclusions regarding the effect of cold work at such a high creep rate might not apply at much lower creep rates, say on the order of 0.0001% per hour or 0.00001% per hour. Yet the lower rates are the ones which would normally be used in the design of a high temperature bolt connection, at least if no relaxation data were available on which to base the design. Thus, I think the test program would have been of greater value if actual creep tests had been performed at practical creep rate levels.

(b) For a number of years, it has been common practice in our laboratory to make time-extension plots of our stress-rupture tests. We have found that minimum creep rate cannot be measured with any degree of accuracy unless the curve exhibits a distinct second stage. This is seldom the case, in our experience, if the rupture time is less than about 250 to 500 hours. At shorter rupture times, the first and second stages of creep are passed so quickly as to have little meaning and to defy precision measurements. It is noted from a comparison of Figs. 1 and 3 that the stress for a minimum creep rate of 0.5 in./in./1000 hours coincides almost exactly in most cases with the stress for 100 hours rupture. I would interpret this to mean that the creep rate measurements relied heavily on rupture tests of quite short duration. I wonder, therefore, how realistic are the relatively minor changes in creep rate which the author attributes to the cold work. I especially wonder if the declining creep rate curve plotted for the 1000°F tests is sufficiently reliable to warrant the author's conclusion No. 4.

(c) The author determined the effect of cold work on the 900°F stress relaxation resistance by starting his tests at an initial stress of 80,000 psi. This is an extremely high initial stress, amounting to the stress for 100-hour rupture life.

Ordinarily, stress relaxation tests are started at lower stresses corresponding to those expected to be used in actual bolting applications. If more realistic starting stresses are not used, one may get an erroneous impression of the holding power of bolts made of the material.

For example, Robinson[2] reported on the 900°F relaxation properties of a similar material, DM-45 steel (0.45%C, 1.26%Cr, 0.57%Mo), as follows:

Initial stress	38540 psi
Residual stress at 1000 hr.	15850 psi

(d) Had the author's stress relaxation tests been started at a lower initial stress, the creep of the material would have been at a lower rate. Thus, for the same reason as pointed out in (a) above, the effects of cold work might not have been so noticeable. Tests conducted in our own laboratory would tend to substantiate this. We made relaxation tests on full threaded bolt studs machined from a single bar of steel containing 0.33%C, 1.60%Cr and 0.50%Mo. Part of the bolts studs had cut threads. The others had cold-rolled threads. Results showed no deleterious effects of the thread rolling, as follows:

Table III

Test Temperature °F	Type of Threads	Initial Stress, psi	Final Stress, psi	Length of Test, hours
850	Machined	30,000	18,500	260
850	Rolled	30,000	19,600	167
950	Machined	30,000	14,200	208
950	Rolled	30,000	15,000	144

Author's Reply

The author appreciates the comments of Messers. Williams and Ewing.

Although it would have been of value if some tests had been run at lower creep rates as suggested by Mr. Williams, it was not the intent of this investigation to furnish design data, but rather to provide information on the influence of a metallurgical variable that could be used in connection with design data.

Comparing the effect of cold work on the basis of stress for a creep rate of 0.5 inch / inch/1000 hour does not mean, of course, that lower creep rates were not obtained. This rate which is an approximate mean value was selected so that a comparison of the effect of cold work at all four temperatures could be made on the same basis without extrapolation. In addition, this permitted a comparison of the variation of creep rate with the variation of rupture life in the same stress range.

The point raised by Mr. Williams that the effect of cold work at high creep rates might not apply at lower creep rates, is confirmed by the data in Table II. In this respect the behavior at 800°F was different from that at 900°F. At 900°F the increase in creep rate due to small amounts of cold work is evident at the high, but not at low creep rates. In the tests at 800°F, the increase in creep rate is present in the creep rate range of approximately 0.5%/hour to 0.0025%/hour and the magnitude of the change is not less at the lower creep rates. I see no reason, therefore, to expect the behavior to change in going to a creep rate level of 0.0001%/hour.

[2]E. L. Robinson, "High Temperature Bolting Materials," *Proceedings*, American Society for Testing Materials, Vol. 48, p. 214.

In regard to the reliability of creep rate measurements and the magnitude of the effect, the data, shown in Table II, are quite consistent and the changes in creep rates are large in comparison to inaccuracies of measurement that one might expect. The tests run at 800°F and 95,000 psi with rupture times in the range of 400 to 4270 hours show that 15% cold work raised the creep rate to 7 times that of the unworked material. At 1000°F, two series of tests show an increase in the creep rate of the highly cold-worked material to approximately twice that of the unworked material; and this change is consistent with elongation-at-fracture values. Conclusion No. 4 which is based on this appears justified.

The rather high initial stress for the relaxation tests was used in order to compare relaxation and creep in the same stress range. What the effect would be at lower stresses, I do not know. While the data presented by Mr. Williams are of practical significance in the evaluation of bolts with cut and cold-rolled threads, I wonder if they are comparable with our data since only the surface of the bolts were cold worked.

In regard to the discussion of Mr. Ewing, we do not have any information on the effect of cold work on the strength properties for times of 10,000 hours and longer. It, of course, would be rather dangerous to extrapolate the presented data because of the presence of cold work which promotes structural instabilities. The strengthening effect of cold work becomes less as service temperature is raised and also as time is increased. At the higher temperatures it has been observed on other materials that creep-rupture strengths, as a result of structural changes, are lowered to values below those of the unworked material. It is quite likely, as Mr. Ewing suggests, that long-time strengths of cold worked materials might be reduced sharply at temperatures lower than those indicated by shorter time tests. For the chromium-molybdenum steel used in this study, the temperature might be in the region of 900°F. Another type of deleterious effect, the lowering of creep-rupture strength by small amounts of cold rolling, might occur at even lower temperatures. The results of this study indicate that the effect would probably be evident in long-time strengths at 800°F; and it would not be surprising to find that it also occurs in very long-time tests at 700°F.

NOTCH DUCTILE HIGH STRENGTH NODULAR IRONS

By G. A. Sandoz, H. F. Bishop, W. S. Pellini

Abstract

Ferritized nodular iron may be reheated to intercritical temperatures (1400 to 1550° F depending on composition) to develop quasi-equilibrium mixtures of untransformed ferrite and austenite. Water quenching and 1200° F tempering of the partially austenitized material results in desirable combinations of high tensile strength and good notch ductility. Tensile strengths of 90,000 psi may be developed with notch ductility properties equivalent to the ferritized 60,000 psi grades. The quenched and tempered irons show greatly superior notch ductility compared to pearlitic grades of equal strength. (ASM-SLA Classification: Q23, CI)

Introduction

IT IS generally considered that the matrices of flake and nodular irons respond to heat treatment in the same manner as steels of equivalent alloy composition. Unfortunately, the presence of the graphite phase results in a high carbon saturation of the austenite during the usual austenitizing treatments, with the result that the transformations correspond to those of hypereutectoid steels. This simple picture must be modified somewhat in consideration of the fact that graphite rejection of existing flake or nodules may occur during slow cooling to eutectoid temperatures. If such rejection is accomplished, the transformations correspond to those expected of eutectoid steels.

By proper choice of cooling rates and of cooling delays at critical temperatures, it is possible to produce irons which vary from completely pearlitic to completely ferritic matrices. The ferritic malleable and nodular irons are characterized by relatively high ductility and low strength while the pearlitic grades are comparatively stronger but less ductile. Quenching treatments, such as applied in flame and induction hardening, develop very high hardness and strength, but at the expense of ductility.

In the case of alloy steels, high strength combined with high tensile and notch ductility is developed by quenching and tempering treatments, however, this combination is possible because the car-

A paper presented before the Thirty-Seventh Annual Convention of the Society, held in Philadelphia, October 17–21, 1955. The authors, G. A. Sandoz, H. F. Bishop and W. S. Pellini, are associated with the Metal Processing Branch, Metallurgy Division, Naval Research Laboratory, Washington, D. C. Manuscript received February 9, 1955.

bon content is controlled to certain maximum levels. It is well known that carbon in excess of approximately 0.40% is not desirable; accordingly, high strength engineering steels usually are kept at or below this carbon level.

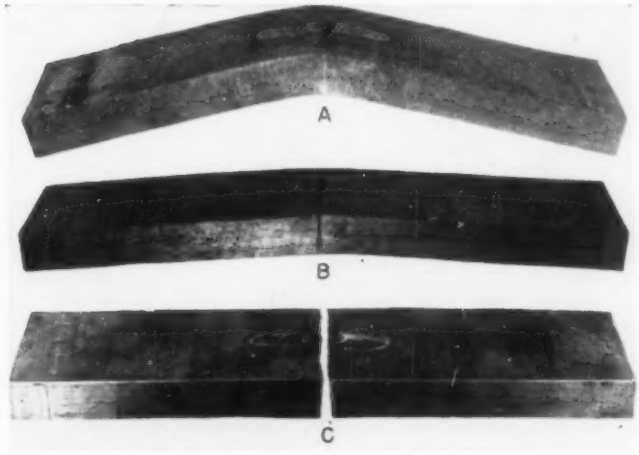
The problem of developing heat treatments which should result in ultra high strength nodular irons of good notch ductility is basically one of controlling the carbon content of the austenite to within desired limits by means of suitable austenitizing procedures. The desired carbon level presumably is the same as that which is ordinarily specified for the case of steels. This investigation was concerned initially with determining the feasibility of such an approach. The ultimate aim was the development of new classes of nodular irons featuring high strengths combined with good notch ductility.

Notch Ductility Considerations

It is generally recognized that notch ductility is an important consideration in the choice of engineering materials. In the presence of crack-like defects and of design notches, ferrous metals may fail in a brittle manner and without the prior deformation predicted by tensile ductility tests. Temperature is an important factor in the development of brittle fracture. It is well established, for example, that rolled mild steels of the tonnage plate variety develop brittle failures at temperatures of freezing and lower but not at summer temperatures (1,2).[1] Fig. 1 illustrates the general effect of temperature on the behavior of steels and nodular irons in sharp crack tests conducted by the authors (3,4). The Tc (critical temperature) point is established by a realistic test procedure which consists of determining the temperature below which deformation is not possible in the presence of a sharp crack defect, and the specimen fails in a brittle manner. The test specimens ($1'' \times 3\frac{1}{2}'' \times 14''$ plates) are of sufficient size to be considered representative of service parts. The sharp notch is developed by a bead of highly brittle, hard surfacing weld which cracks when a load is applied by the impact of a falling weight. Details of the "Drop-Weight Test" were provided in previous reports (1,2,3,4). The critical temperature, Tc, is best described by the term "nil ductility transition," i.e., the temperature of transition to essentially no ductility ($\%EL = 0$ in the presence of a sharp crack). In relation to the test the term used is drop-weight transition, or "D.W.T."

It is of interest to summarize the position of structural steels and nodular irons of various types with respect to tensile strength and notch ductility as measured by the drop-weight test, Fig. 2. The range of temperatures of the various "blocks" represent the D.W.T.

[1]The figures appearing in parentheses pertain to the references appended to this paper.



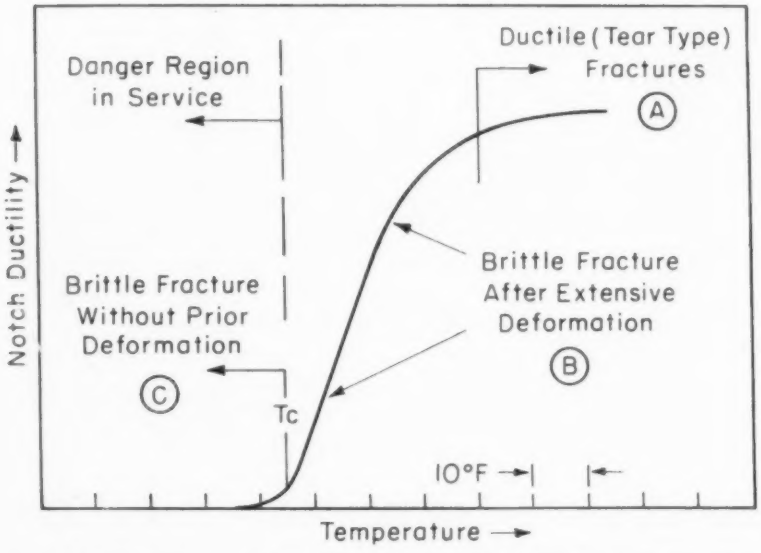


Fig. 1—Characteristic Behavior of Steels and Nodular Irons in Sharp Crack Tests. Within a narrow temperature interval the notch ductility of the metal falls to nil values.

temperatures obtained for tests of a large number of samples of the specified material. The drop-weight test predicts that brittle fracture at winter temperatures is possible for rolled mild steels containing notch defects. This is in agreement with actual service failure data. Cast steels are essentially equivalent to rolled steels in strength and notch ductility. The relative position of various nodular irons with respect to notch ductility and tensile properties is evident from the figure and does not require further discussion. Several desirable aims in the improvement of nodular irons may be deduced from these data, for example:

(a) Development of irons featuring tensile strengths equal to the pearlitic types but with notch ductility equal to ferritic grades.

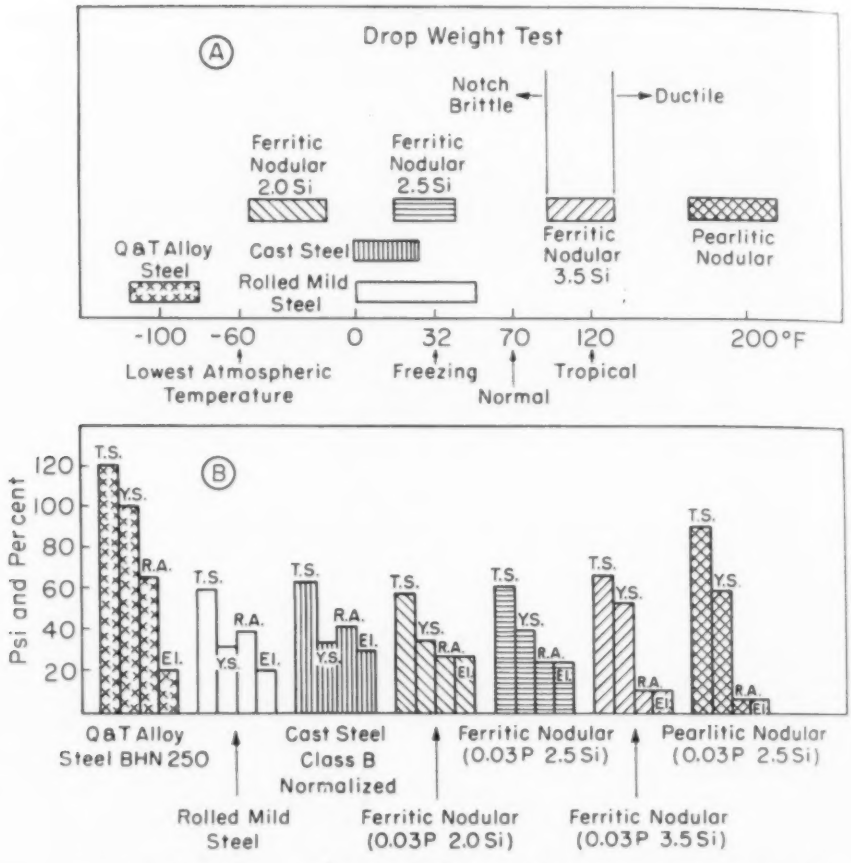


Fig. 2—Comparison of Steels and Various Nodular Irons with Respect to Tensile Properties and Notch Ductility as Measured by the Drop-weight Test.

(b) Development of alloyed nodular irons with strength and notch ductility approaching quenched and tempered steels.

Item (a) is considered to be achieved in the present investigation while item (b) is a subject of continued investigation.

Preliminary Studies

Heat treating procedures for developing nodular irons with tensile strengths in excess of 100,000 psi have been reported by Rehder (5). These methods involve quenching from high austenitizing temperatures, i.e., initiating quenching with the matrix structures composed of high carbon austenite and dispersed nodules of graphite. Irons quenched in this manner and tempered to a tensile strength of 100,000 psi exhibit a tensile elongation of about 10%. However, similar irons prepared at this Laboratory have proven to be brittle to very high temperatures (usually higher than 200°F) when subjected to the notch test. It was considered that quenching from within the critical temperature range might provide control

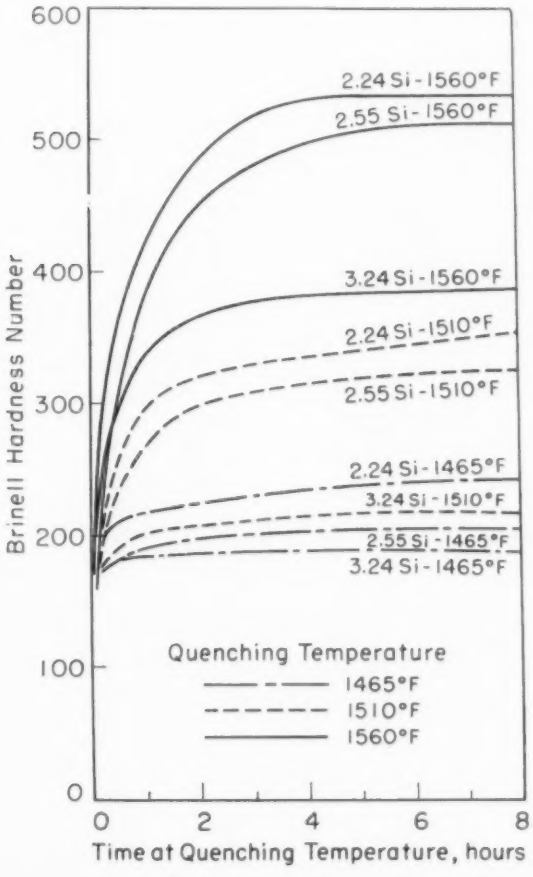


Fig. 3—Variation of "As quenched" Hardness with Austenitizing Time and Temperature for Irons of Various Silicon Contents.

over the carbon content of the austenite developed within a matrix of untransformed ferrite.

The critical temperature range of nodular iron is raised and broadened with increasing silicon content. However, the information in the literature as to the exact limits of the range is too sketchy to be directly applicable to the treatment of specific irons. In order to establish the required data, three ferritized irons of the same composition except for silicon level were selected for study, Table 1.

Table I
Ferritized Irons

Heat No.	C%	Si%	Mn%	P%
15	2.94	2.24	0.31	0.03
16	2.94	2.55	0.31	0.03
54	2.98	3.24	0.26	0.03

Samples (1-inch cubes) of these irons were heated for a series of times at temperatures which were expected to lie in or border the critical temperature range, and then quenched in water. Brinell hardness

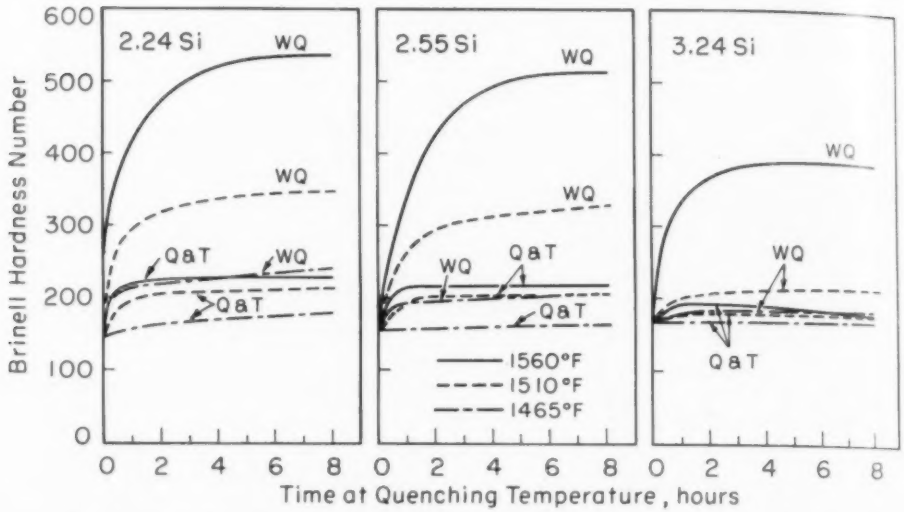


Fig. 4—Variation of Hardness with Austenitizing Time and Temperature for Irons of Various Silicon Contents, "As quenched" and After Tempering 1 Hour at 1200°F.

was determined for the as-quenched condition and after tempering 1 hour at 1200°F. Time at temperature was established by a thermocouple welded to the bottom of a small hole drilled to the center of one of the specimens.

The variation of as-quenched hardness with time, at temperatures of 1465, 1510 and 1560°F for the three silicon levels, are shown in Fig. 3; Fig. 4 presents the data for the individual irons and includes the hardness after tempering. It may be observed that after four hours at temperature there is little further rise in as-quenched hardness. This indicates that carbon saturation is essentially established during the 4-hour holding period. The saturation hardness level is increased rapidly with increasing temperature in the 100°F range selected (1465 to 1560°F) and with decreasing silicon for any given temperature.

Fig. 5 shows a typical example of the changes in microstructure with time, for the case of the 2.55% silicon iron heated at 1510°F. It is observed that in the early stages of austenitization the austenite forms first along the grain boundaries and certain preferred crystallographic planes.[2] With increasing time the austenitic areas (observed as martensite in the photomicrographs of quenched specimens) enlarge until a final saturation structure is approached. In the example of Fig. 5 the saturation structure was essentially established after 3 hours at temperature, as shown by the similarity of structures representing the 3 and 8-hour treatments.

The effect of silicon level on the maximum amount of austenite formed after 8 hours at 1465, 1510 and 1560°F may be observed in

[2]Extremely rapid rates of heating, as with flame or induction heating, result in different types of microstructures. These structures are adequately described in the literature (6).

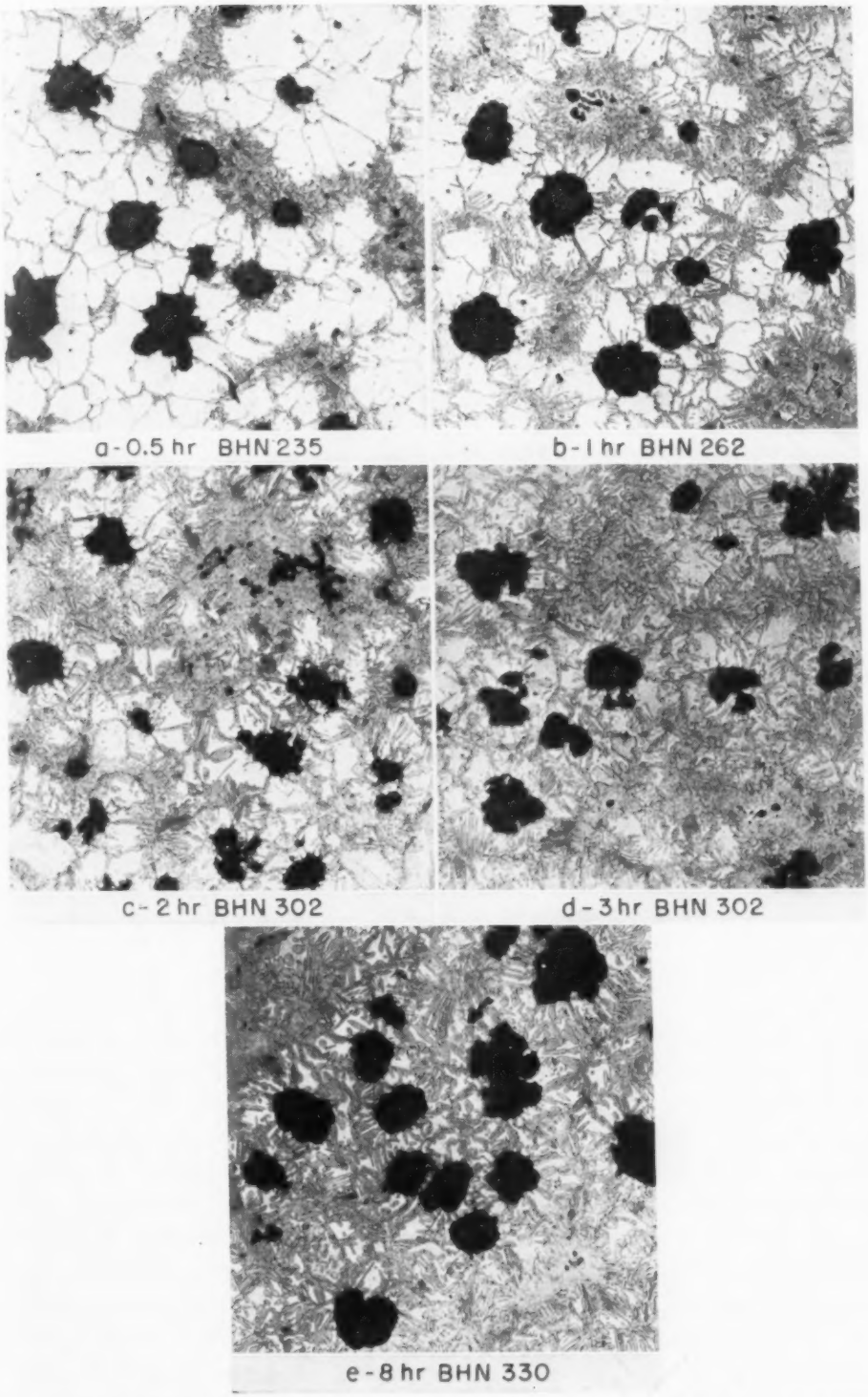


Fig. 5—Effect of Holding Time at 1510°F on the Microstructure and Hardness of a 2.55% Si Iron. Original magnification ×100 reduced ⅓ in reproduction.

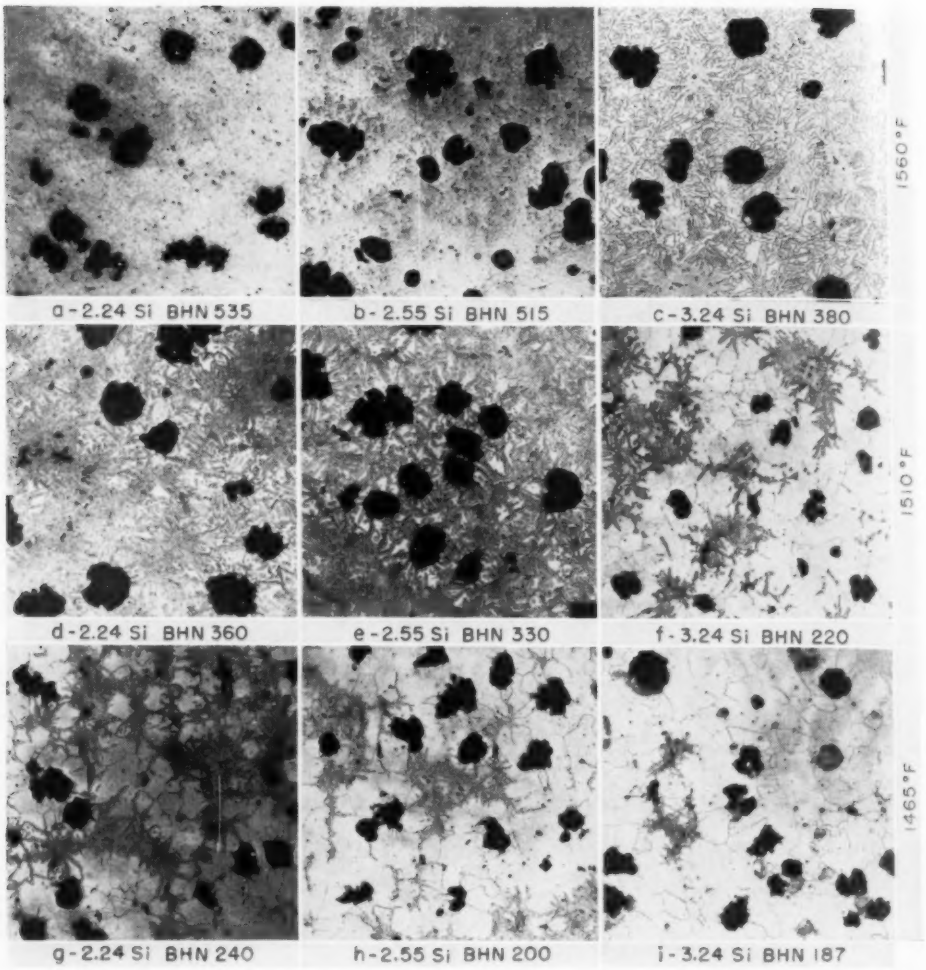


Fig. 6—Effect of Silicon Content on the Maximum Amount of Austenite (shown as martensite) Formed at Various Holding Temperatures. Original magnification ×100 reduced 57% in reproduction.

Fig. 6. These structures cover a hardness range from a maximum 535 BHN for the 2.24% silicon iron heated at 1560°F to a minimum of 187 BHN for the 3.24% silicon iron heated at 1465°F. These data illustrate that increasing the silicon content raises the critical temperature range so that higher temperatures are required to produce a given amount of austenite. The "as-quenched" hardness varies directly with the amount of austenite present at the quenching temperature. For example, essentially equivalent microstructure and hardness are produced with the 2.24% silicon iron quenched from 1465°F as with the 3.24% silicon iron quenched from 1510°F.

Heat treatment guides are provided in Figs. 7 and 8; Fig. 7 relates maximum "as-quenched" hardness and hardness after tempering at 1200°F for 1 hour, to the austenitizing temperatures. Fig. 8 provides similar information in relation to silicon contents.

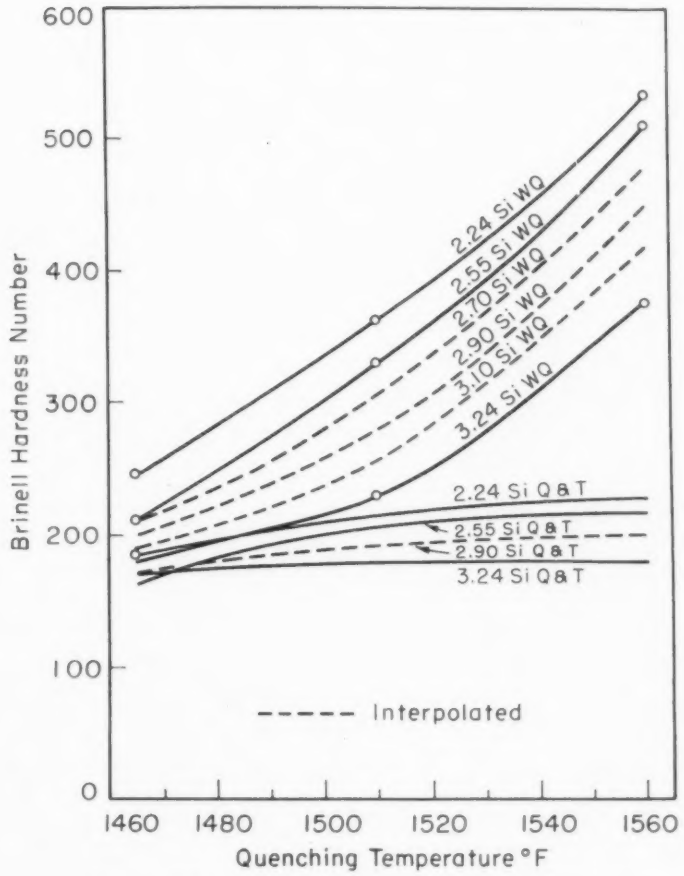


Fig. 7—Effects of Silicon Content and Austenitizing Temperature on the Saturation Hardness of Quenched and of Quenched and Tempered Nodular Irons.

Correlation of Tensile Properties with Notch Ductility

To investigate the combinations of tensile properties and notch ductility which could be obtained with nodular irons quenched from within the critical temperature range, three irons of the analyses shown in Table II were cast as 1″×3½″×14″ drop-weight test specimens.

Table II
Nodular Irons

Heat No.	C%	Si%	Mn%	P%	Cr%	Ni%
55	3.12	2.38	0.39	0.008	—	—
56	2.86	2.04	0.35	0.018	—	—
59	2.80	1.98	0.32	0.005	0.014	2.2

The irons were made in a 300-pound basic induction furnace from Armco iron melting stock. Nodulization was accomplished by the addition of 0.25% magnesium, as a ferrosilicon—magnesium alloy, to the ladle during tapping; 0.10% silicon as 50% ferrosilicon was

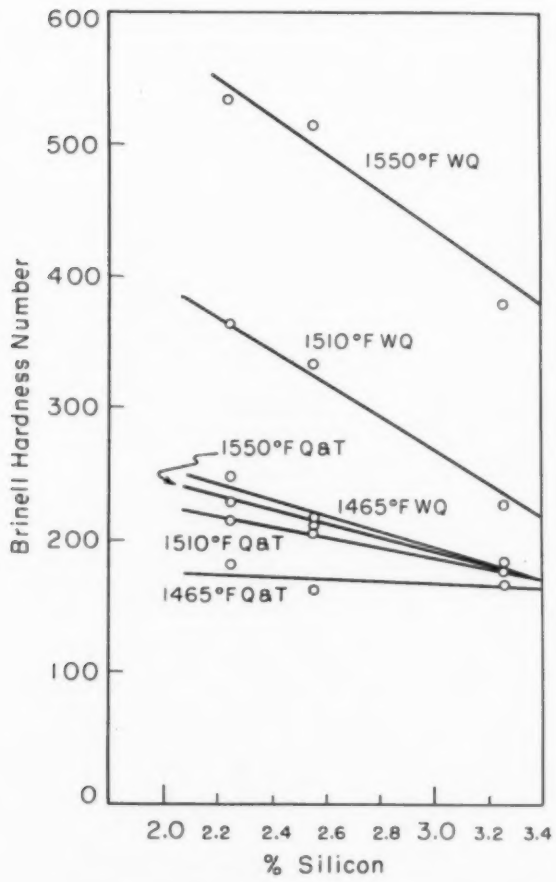


Fig. 8—Effect of Silicon Content on the Saturation Hardness Established for Three Quenching Temperatures.

added for secondary innoculation. The casting temperature was approximately 2500°F. Two of the irons, 55 and 56 were unalloyed and of similar composition except for silicon content; iron 59 was alloyed with 2.19% nickel. All of the irons were annealed to give an initial ferritized structure.

Specimens of iron 55 and 56 were heated to a range of temperatures between 1450 and 1550°F and specimens of iron 59 in the range of 1400–1500°F, spanning the critical temperature range for these materials. For convenience, the specimens were held at temperature for 15 hours prior to quenching in water, although, as described previously, approximately 4 hours would have sufficed to establish near-saturation conditions. Little distortion and no cracking resulted from water quenching because the untransformed ferrite served to accommodate the quenching stresses. Specimens quenched from above the critical temperature range did develop quench cracks. After quenching, all specimens were subsequently tempered for one hour at 1200°F. Drop-weight test transition tem-

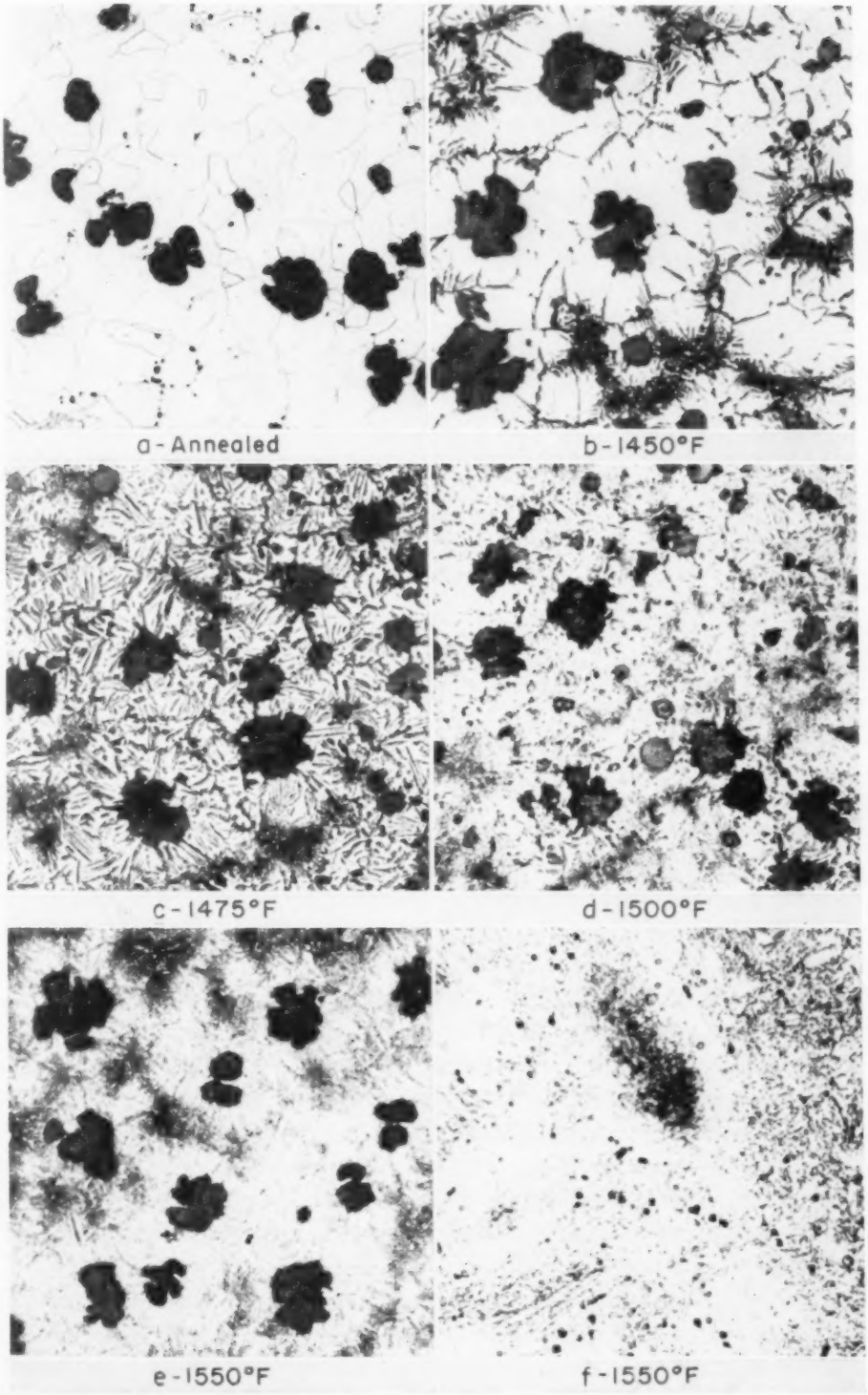


Fig. 9—Effect of Austenitization at Various Temperatures on the Microstructures of Quenched and Tempered Nodular Iron #55. Original Magnification a-e ×100; f ×1000 reduced ⅓ in reproduction.

peratures were determined for each composition and heat treatment. Tensile tests, hardness tests, and microstructural examinations were conducted with material removed from the center section of the broken drop-weight test specimens.

Typical microstructures of the heat treated materials are presented in Fig. 9, for iron 55. The microstructures differ from those shown previously in Figs. 5 and 6 in that the areas of carbon solution have been darkened as a result of tempering.

Fig. 10 summarizes the tensile, hardness, notch ductility, and combined carbon content data of the three irons as a function of

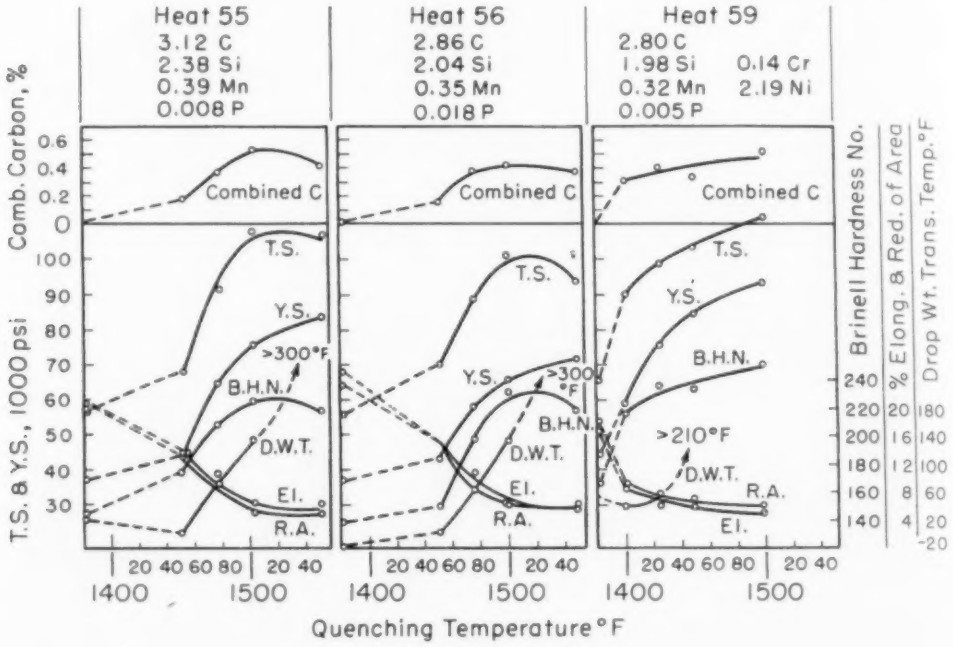


Fig. 10—Summary Data

quenching temperature. As the temperature of quenching is increased to 1500°F, the yield strength, tensile strength, hardness, and combined carbon contents increase, while the tensile ductility properties decrease. Quenching the un-alloyed irons, 55 and 56, from above 1500°F results in no further change in tensile ductility but causes a decrease in tensile strength, hardness, and combined carbon content following tempering; however, the yield strength continues to rise.

The decrease in hardness and tensile strength of material quenched from above 1500°F is attributed to the precipitation of graphite during tempering at 1200°F, as illustrated by the decrease in combined carbon and by the appearance of fine graphite particles throughout the microstructure, Fig. 9f. Precipitated graphite particles did not appear when lower quenching temperatures were used,

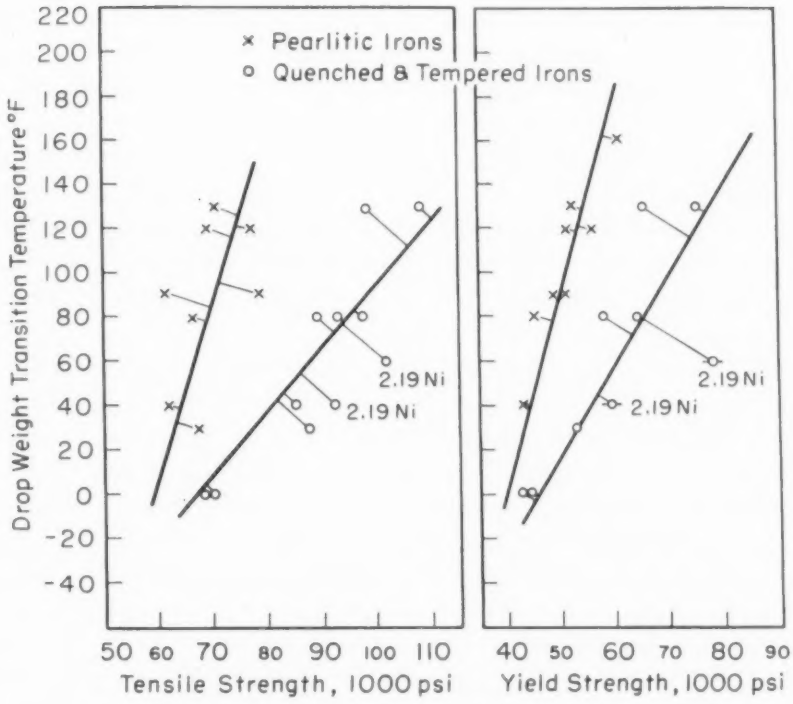


Fig. 11—Drop-Weight Test Transition Temperatures of Pearlitic and Quenched and Tempered Nodular Irons as a Function of Strength Properties.

probably because of lower carbon content of the resulting martensite pools. The appearance of graphite during tempering in the range of 1200°F in nodular irons quenched from above the critical temperature range has been observed by Rehder (5).

Occasional small patches of fine pearlite were observed at the center of the 1-inch thick drop-weight test specimens of irons 55 and 56. Such borderline hardenability was not exhibited by iron 59 containing 2.19% nickel. For unalloyed irons, these data should be considered applicable for plate sections which do not exceed 1 inch thickness and for bar sections which do not exceed approximately 2 inch thickness.

The drop-weight test transition temperatures of the three irons show that notch ductility is essentially the same as that of the ferritized irons when quenching temperatures are low. A steady rise in D.W.T. temperature, indicating gradual loss of notch ductility, occurs as quenching temperatures are increased to 1500°F for the unalloyed irons and 1450°F for the 2% nickel iron. Quenching from above these temperatures results in an abrupt rise in the D.W.T., indicating that the irons become highly notch brittle. In terms of microstructures, the embrittlement occurs at the point where the areas of carbon solution enlarge sufficiently to eliminate free ferrite.

With respect to tensile properties, the sharp loss in notch ductility occurs at about the 100,000 psi to 110,000 psi range.

The intermediate range of quenching temperatures offers the best combinations of tensile properties and notch ductility. The tensile strengths of the irons may be raised to approximately 90,000 psi with corresponding D.W.T. of approximately 60°F for the unalloyed irons and 40°F for the alloyed iron, i.e., essentially equal to rolled mild steel, of 60,000 psi tensile strength, Fig. 2. In comparison, pearlitic irons of 90,000 psi tensile strength level have D.W.T. temperatures of approximately +180°F.

Comparisons of the notch ductility of quenched and tempered nodular irons with irons strengthened by the presence of pearlite resulting from an arrested anneal or by increased silicon content are shown in Fig. 11. The figure presents the D.W.T. temperatures of a number of pearlitic and quenched and tempered irons as related to tensile and yield strengths. The convergence of the average lines indicates that the low strength level is attained only by achieving a common ferritized condition. It is noted that as tensile strength increases, the heat treated irons develop lower D.W.T. temperatures (better notch ductility) than the pearlitic irons and that this advantage increases with increasing strength. In general, an improvement of 50 to 100°F in the notch ductility transition is indicated. The heat treated irons also display superior notch ductility for a given yield strength level.

Summary and Conclusions

Conventional austenitization treatments of nodular irons develop high carbon austenites which preclude the obtaining of ductile material by quenching and tempering. This limitation is due to the inherent brittleness of the high carbon transformation products. The use of partial austenitization treatments, involving holding in intercritical temperature ranges, provides a means of controlling the carbon content of the austenite. The combinations of tensile properties and notch ductility which may be obtained by controlled partial austenitization, water quenching, and 1200°F tempering of various nodular irons were investigated.

The principal conclusions of this investigation are as follows:

(a) Ferritized nodular irons reheated to temperatures in the range of 1400 to 1550°F for periods of approximately four hours, develop quasi-equilibrium austenite—ferrite aggregate structures.

(b) The amount of austenite developed at quasi-equilibrium increases with increasing temperature in the intercritical range and with decreasing silicon at any given intercritical temperature. The austenitization changes are such as to permit practical control based on guide charts.

(c) The partially austenitized nodular irons may be quenched and tempered to develop tensile strengths in the order of 90,000 psi with notch ductility properties equivalent to the 60,000 psi ferritized material. The pearlitic nodular irons of 90,000 psi tensile strength show greatly inferior notch ductility in comparison to the quenched and tempered irons.

(d) Heat treatment to tensile strengths in excess of 100,000 psi results in an abrupt loss of notch ductility. The higher strength materials are inferior to the pearlitic 90,000 psi grades in this respect.

(e) The hardenability of unalloyed nodular irons is sufficient to develop the described properties in 1-inch plate sections and 2-inch rounds. At these limits, traces of pearlite are developed at the center of the sections. The limits may be raised by alloying to increase hardenability.

(f) The presence of untransformed ferrite permits water quenching without cracking or warping. In contrast, fully austenitized material is known to crack easily on water quenching.

Acknowledgments

This investigation is part of a broad program of studies relative to the notch ductility of cast materials, conducted at the request of Mr. George Sorkin, Code 343, Bureau of Ships.

References

1. W. S. Pellini, "Evaluation and Significance of Charpy Tests," American Society for Testing Materials, Publication #158, *Symposium on the Effect of Temperature on the Brittle Behavior of Metals*, 1954.
2. P. P. Puzak, M. E. Schuster and W. S. Pellini, "Crack Starter Tests of Ship Fracture and Project Steels," *Welding Journal*, October 1954.
3. W. S. Pellini, G. Sandoz and H. F. Bishop, "Notch Ductility of Nodular Iron," Transactions, American Society for Metals, Vol. 46, 1954, p. 418.
4. G. A. Sandoz, H. F. Bishop and W. S. Pellini, "Notch Ductility of Nodular Irons," *Foundry*, September 1954, p. 114.
5. J. E. Rehder, "Quench-Temper Treatment Improves Nodular Irons," *Iron Age*, January 17, 1952.
6. E. P. Rowady, W. J. Murphy and J. F. Libsch, "Hardening Characteristics of Induction Heated Ductile Iron," *Transactions*, American Foundrymen's Society, Vol. 61, 1953, p. 422.

DEFORMATION AND FRACTURE MECHANISMS OF POLYCRYSTALLINE MAGNESIUM AT LOW TEMPERATURES

By F. E. Hauser, P. R. Landon and J. E. Dorn

Abstract

The objective of this investigation was the determination of the deformation mechanisms in magnesium at low temperature by metallographic and X-ray techniques. Basal slip was found to be the main mechanism of deformation with duplex slip becoming more predominant as the temperature was decreased. Grain boundary shearing was found to be rare at the low temperature compared with that observed at room temperature. The appearance of twins and small angle boundaries was unchanged by lowering the test temperature. The fracture at low temperature was mainly intergranular with some complex transcrystalline modes. (ASM-SLA Classification: Q24, Q26, Mg)

Introduction

MANY extensive investigations have been directed toward uncovering the basic mechanisms of deformation and fracturing, in anticipation that such knowledge might prove useful in attempts to improve the properties of metals. In order to simplify analyses, most of such basic investigations have emphasized the elucidation of the behavior of metallic monocrystals under simple states of stress. And in view of the definitive correlations that have been uncovered between the structure and the mechanisms of deformation and fracturing of metallic monocrystals, the virtue of this approach is well established. The ultimate objective of all such investigations, however, is the complete rationalization of the complex behavior of polycrystalline aggregates. Several important investigations have been made in an effort to deduce the plastic behavior of polycrystalline aggregates from singular knowledge of the deformation mechanisms in metallic monocrystals. From his interesting experiments on the deformation of symmetrically disoriented bicrystals of Sn(1),[1] Chalmers found that the increase in the stress necessary to cause slip with increasing disorientation of the two grains of the bicrystal was exclusively ascribable to orientation differences; this suggested that the grain boundary per se had no

[1]The figures appearing in parentheses pertain to the references appended to this paper.

A paper presented before the Thirty-Seventh Annual Convention of the Society, held in Philadelphia, October 17–21, 1955. Of the authors, F. E. Hauser, P. R. Landon and J. E. Dorn are associated with the Department of Engineering, University of California, Berkeley, Cal. Manuscript received February 16, 1955.

effect on the plastic properties. The same assumption was introduced in Taylor's remarkable attempt to estimate the plastic properties of polycrystalline aggregates of aluminum from the known {111} <110> mechanics of slip in single crystals (2). In order to preserve continuity across grain boundaries Taylor assumed that each grain of the polycrystalline aggregate underwent similar macroscopic deformations. Consequently he deduced that, in general, at least five mechanisms of deformation would be operative in a single grain; the five operative mechanisms for any specific grain orientation were taken to be those of the total of twelve which required the least strain energy. Furthermore, Taylor assumed that the critical resolved shear stress law for slip was unmodified by the incidence of the assumed multiplex slip. In this way he found that the calculated stress-strain curve deduced from the behavior of monocrystals agreed well with an experimental stress-strain curve obtained from a randomly oriented polycrystalline aggregate.

Despite the success achieved by Taylor's challenging problem, much doubt yet persists as to whether it is possible to calculate the plastic properties of polycrystalline aggregates solely from a knowledge of the behavior of monocrystals or whether indeed other types of auxiliary data, not currently available, are yet required. These seeds of doubt arise because, as is well known, the stress necessary to induce plastic deformation increases with decreasing grain size whereas neither Chalmers' experiments nor Taylor's analyses reveal or consider the origin of this apparent anomaly. Furthermore, as has been shown by Barrett and Levenson (3), only about 50% of the grains are reoriented in the manner required by Taylor's analysis, suggesting that the well-known incidence of deformation banding might not constitute a disposable variable in a complete analysis of the problem. The occurrence of various types of low angle boundaries, accommodation kinks and grain boundary shearing during plastic deformation of polycrystalline aggregates undoubtedly complicates the problem of attempting to predict polycrystalline data exclusively from idealized simple single crystal behavior. Furthermore, as will be demonstrated in the text of this report, auxiliary mechanisms of deformation, not easily obtainable by single crystal studies, might also intrude upon deformation of polycrystalline aggregates.

The investigations recorded here were initiated in an attempt to uncover the various complex mechanisms of deformation that polycrystalline aggregates of metals might undertake. High purity magnesium was selected for study, not only because of the extensive interest in this light weight metal but particularly because the limited number of deformation mechanisms exhibited by single crystals of magnesium suggests that auxiliary factors should enter

prominently in the deformation of polycrystalline aggregates of magnesium. Detailed studies of the deformation and fracturing characteristics of large grained polycrystalline aggregates of magnesium at atmospheric temperature have already been presented in an earlier report (4). In the present report these studies have been extended to subatmospheric temperatures down to the boiling point of liquid nitrogen, 78°K. Special emphasis was placed on possible differences in the mechanisms of deformation and fracturing obtained with a decrease in test temperature.

Experimental Procedures

All specimens were prepared from the same stock of high purity magnesium[2] (99.97% Mg) extrusions used in the previously reported investigation (4). Specimens were machined from the original 0.75 inch wide 0.100 inch thick extrusions to provide tensile bars having a parallel 2-inch gage length and a width of 0.375 inch. The surface of each specimen was hand polished to remove the die markings following which each specimen was given a grain coarsening anneal for 3 hours at 575°C (1060°F) in dilute SO_2 atmosphere. This treatment yielded a mean grain diameter of about 1.0 mm, deemed large enough for easy metallographic observation.

After the annealing treatment each specimen was polished electrolytically in an ethyl alcohol solution containing 37.5% orthophosphoric acid using 1.5 volts and 20 ma per dm^2. Following the electrolytic polish, specimens were etched in an aqueous solution containing 10% citric acid.

In order to provide a simple method of detecting and analyzing grain boundary shearing several specimens were scribed with a ruling machine which provided a 0.02 inch square grid. The identification of the various crystallographic planes leading to deformation traces on the polished surface was accomplished by determining the orientations of a large number of grains using microbeam back reflection Laue techniques. A few specimens were prepared with "U" shaped notches in the gage section in order to localize fracturing in the region of several grains of known orientations.

The prepared specimens were pulled in a tensile testing machine at a constant strain rate of 1% per minute in the following media:

Liquid nitrogen	(78°K)
Dry ice-isopentane mixture	(195°K)
Ice-water mixture	(273°K)
Air	(298°K)

Metallographic Observations and Discussions

Slip. In the previous investigation it was shown that polycrystalline aggregates of magnesium slip exclusively by the {0001}

[2]Supplied by courtesy of The Dow Chemical Company.

$<2\bar{1}\bar{1}0>$ forms at atmospheric temperatures of about 298°K. Such basal slip was also found to be operative at 195°K and 78°K in the present investigation. In fact no significant differences were detected in either the spacing of the slip bands or in the extent of basal slip as a function of temperature over the range from 78°K to 298°K.

Whereas slip at 298°K was exclusively basal, there was extensive evidence of duplex slip at 78°K and 195°K. A typical example of such duplex slip is shown in Fig. 1. Since duplex slip of this kind cannot arise from basal slip alone, it is evident that a new slip mechanism becomes operative upon deformation of polycrystalline aggregates of magnesium at subatmospheric temperatures.

In an attempt to identify the operative slip mechanisms at 78°K, the orientations of 15 different grains that exhibited duplex slip were determined by means of the Laue microbeam back-reflection technique. In each of the 15 grains the predominant set of slip bands was identified as arising from slip on the basal plane {0001}. In 12 of the grains the second and minor set of slip bands was clearly identified as arising from slip on the prismatic planes of the form $\{1\bar{1}00\}$. In the remaining three grains that were analyzed, however, the traces of the second set of slip bands differed by a few degrees from the orientations suggested by prismatic slip. Although these slip bands might have arisen from slip on the $\{10\bar{1}2\}$, $\{10\bar{1}1\}$, $\{11\bar{2}2\}$ or the $\{1\bar{1}00\}$ planes respectively, their exact origin could not be definitely established.

Several factors suggest that basal slip is more pronounced than prismatic slip. While in most cases the traces of the basal slip were uniformly distributed throughout any one grain, the traces of the prismatic slip were visible only in parts of the grain such as near corners or reentrant angles. In addition, the occurrence of prismatic slip also seemed to be restricted to near cracks or other stress concentrators such as notches. Thus the appearance of duplex slip seems to be stimulated by complex local stress concentrations within the specimen.

Additional evidence as to the complex stress pattern near areas of duplex slip was obtained in an attempt to determine the critical resolved shear stress for prismatic slip. In the previous report (4) it was shown that the average critical resolved shear stress law for the onset of basal slip was obeyed within a broad scatter range by each individual grain in a polycrystalline aggregate. But in the present investigation the critical resolved shear stress for the occurrence of prismatic slip at the low temperatures was found to be completely random. Consequently the occurrence of duplex slip seems to be due to the localized inhomogeneous stressing caused by the various constraints imposed on a grain by its neighbors.



Fig. 1—Basal and Duplex Slip at 78°K. ×100.

As will be described more fully in a later paragraph of this report, grain boundary shearing was indeed rarely observed following deformation at 78°K, whereas it was quite prevalent upon deformation at atmospheric temperature. This suggests that the highly localized stresses, which are required to preserve continuity of deformation across the grain boundaries, are relieved at atmospheric temperatures by grain boundary shearing. But at lower temperatures, where grain boundary shearing is much less facile, the local

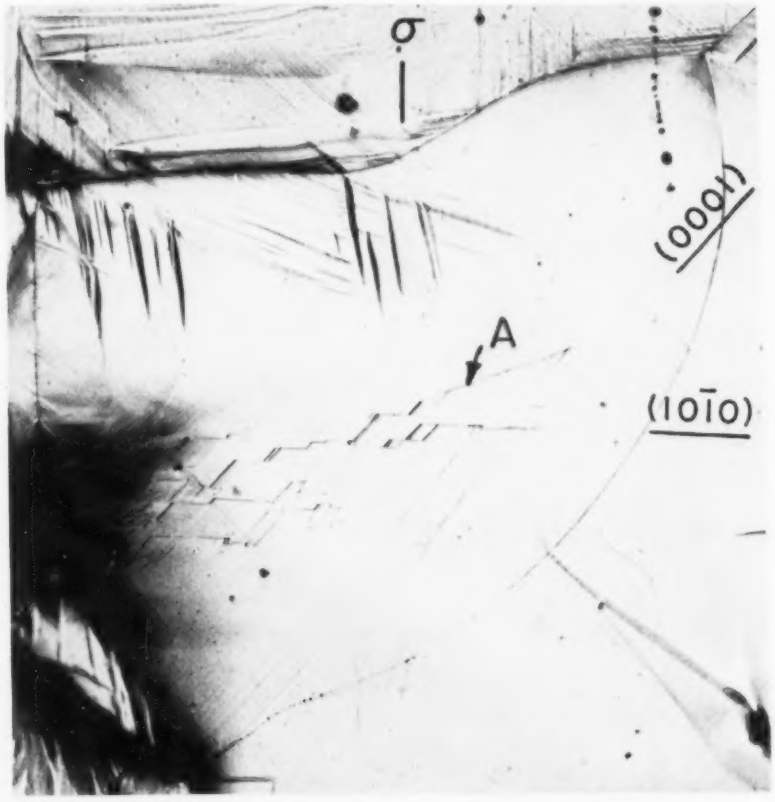


Fig. 2—Duplex Pencil Slip at 78°K. ×100.

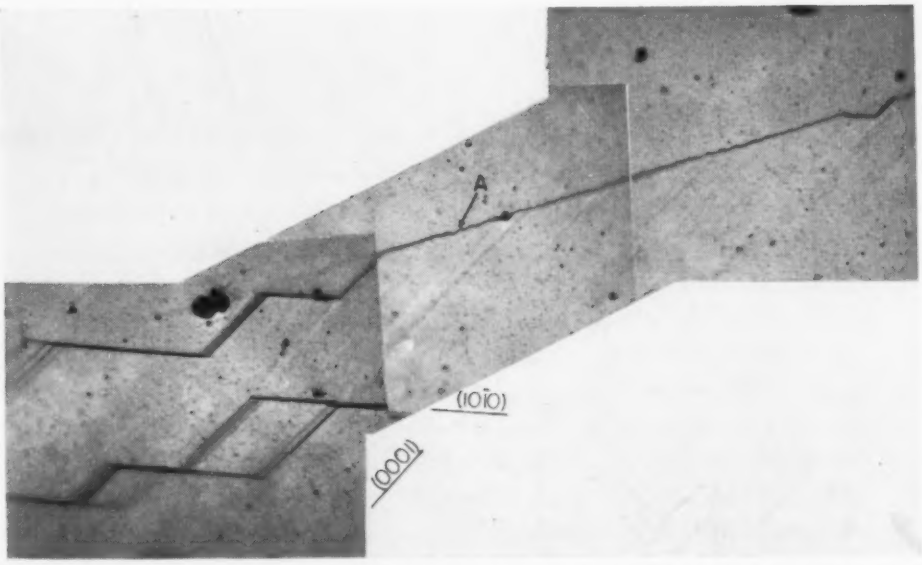


Fig. 3—Duplex Pencil Slip at 78°K. Detail of Fig. 2. ×500. Reduced 60% in Reproduction.

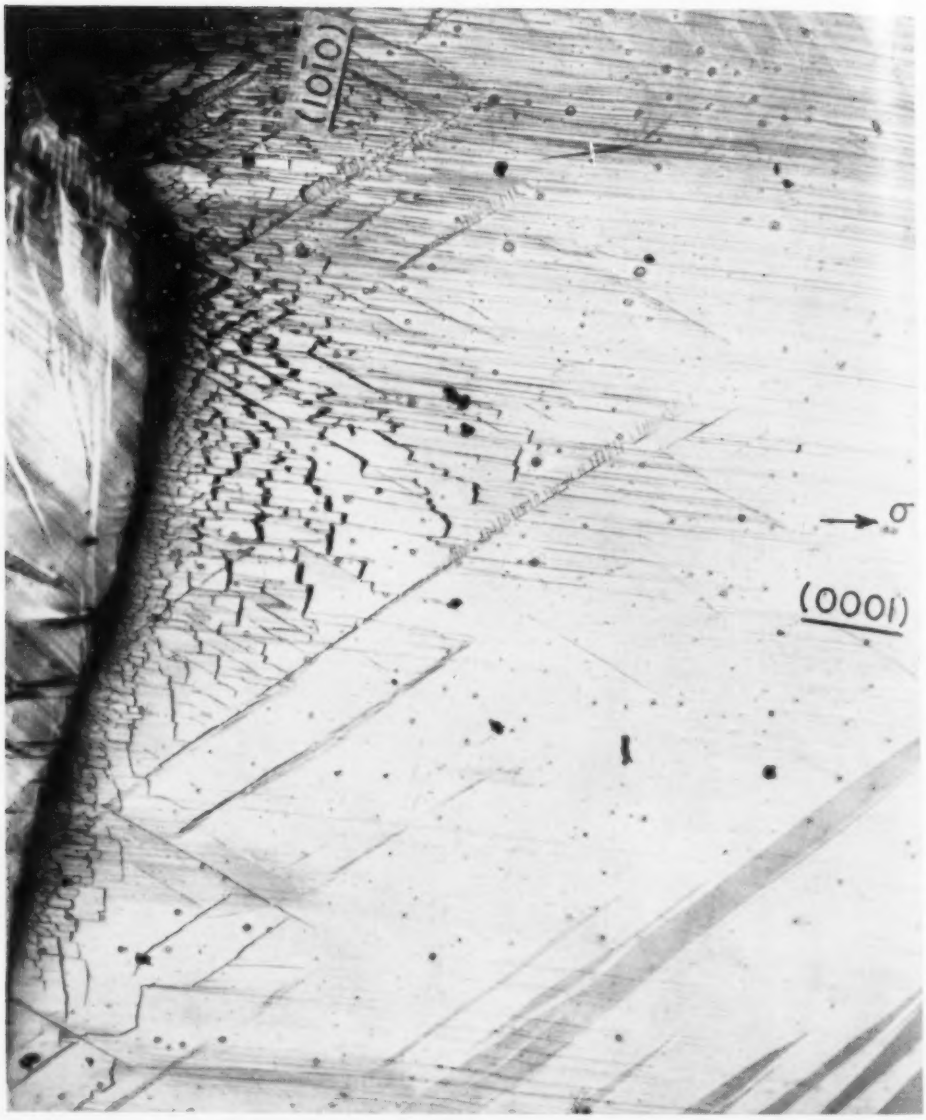


Fig. 4—Duplex Pencil Slip at 195°K. ×100. Reduced 20% in Reproduction.

stresses are not so relieved and therefore induce the auxiliary prismatic slip.

The metallographic appearance of the observed duplex slip took several forms. Fig. 1 illustrates independent duplex slip on two planes. The direction and amount of secondary slip is independent of the basal slip. Figs. 2 and 3 illustrate the appearance of duplex "pencil slip" (5), where slip occurs simultaneously on two planes in the same direction by nearly equal amounts. The small steps of each of the two slip systems is shown in what appears to be a third slip plane trace marked A in Fig. 2. Observations of the specimen at higher magnification, however, illustrate that the trace

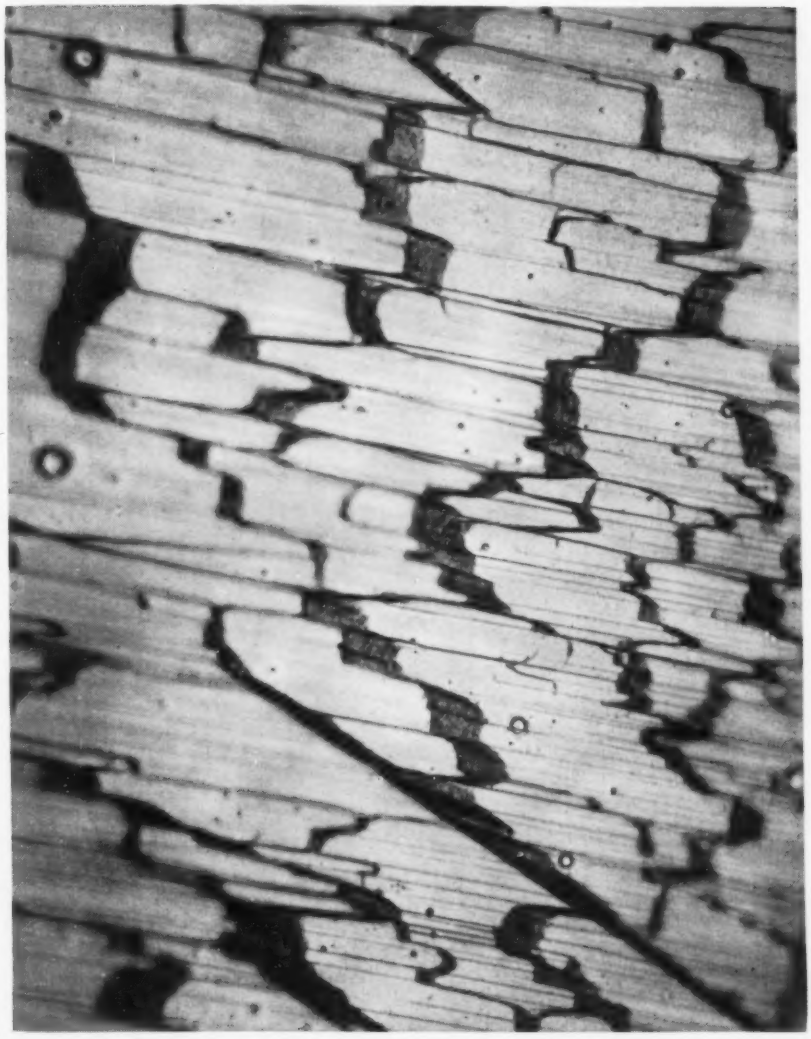


Fig. 5—Duplex Pencil Slip at 195°K. Detail of Fig. 4. ×500.

A is actually made up of short traces on basal and prism planes as shown in Fig. 3. Many similar apparently "noncrystallographic" slip traces were resolved as duplex pencil slip at high magnification. Another interesting example of duplex pencil slip is shown at various magnifications in Figs. 4,5 and 6, where the duplex slip took place at a reentrant angle of the grain boundary. At low magnification (Fig. 4) the slip traces have a crack like noncrystallographic appearance, but at higher magnifications (Figs. 5 and 6) the combination basal and prism slip mechanism becomes apparent. In Fig. 6 the relatively large pencil slip offset is illustrated by focusing on the upper and lower plane of polish respectively next to one of the cliff-like traces. Such large local strains are probably induced by the high local stresses due to the complicated constraints imposed by neighboring grains.

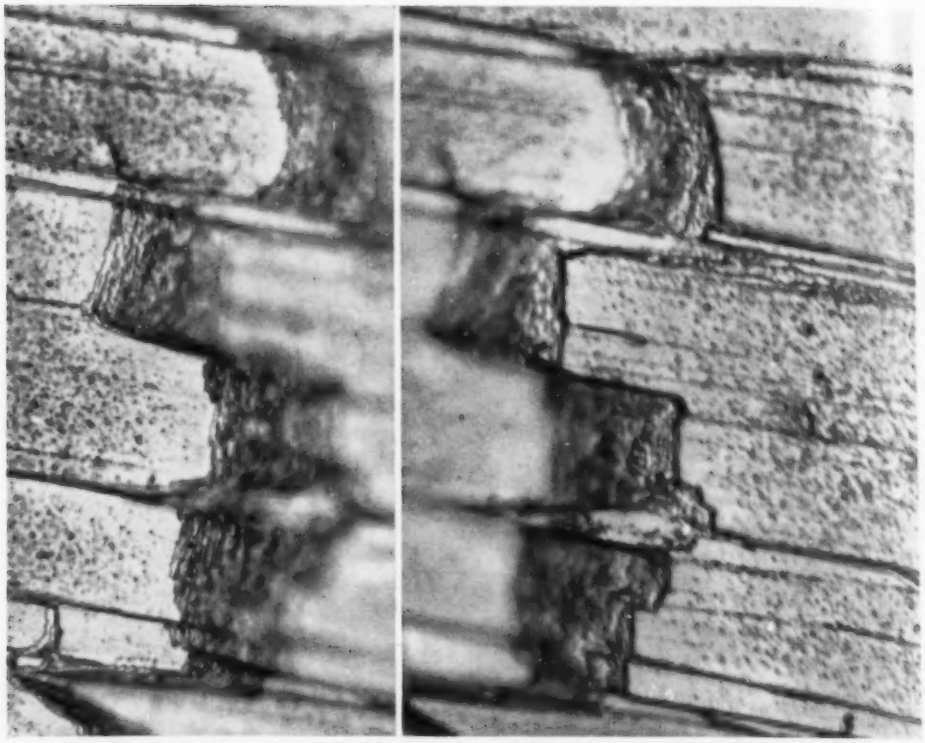


Fig. 6—Duplex Pencil Slip at 195°K. Detail of Fig. 4 and 5. ×2000. Reduced 30% in Reproduction.

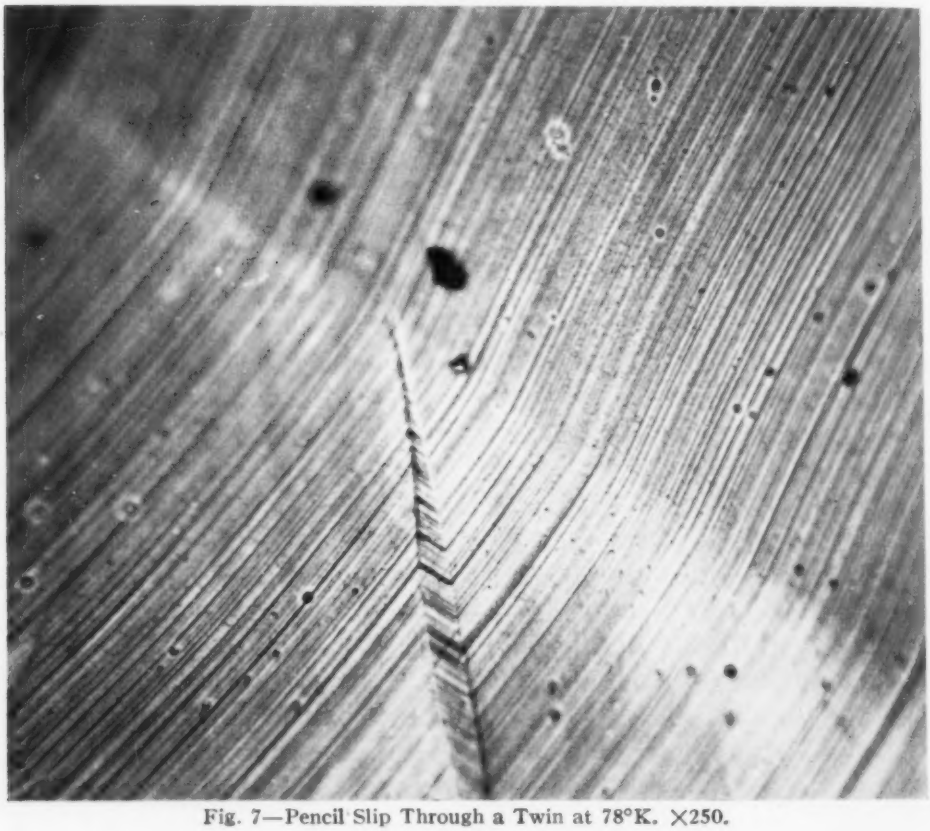


Fig. 7—Pencil Slip Through a Twin at 78°K. ×250.

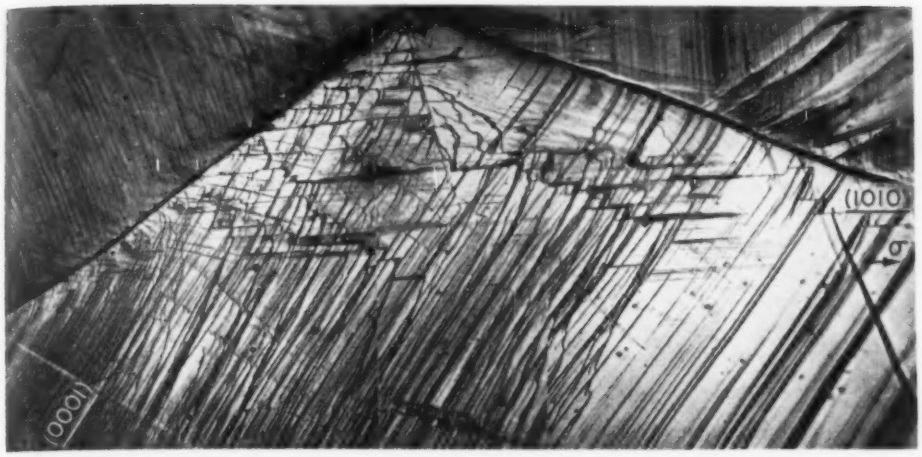


Fig. 8—Secondary Slip Mechanism Operating in Corner of Grain. Simple Duplex Slip, Pencil Slip and Apparent NonCrystallographic Slip at 78°K. ×250. Reduced 55% in reproduction.



Fig. 9—NonCrystallographic Small Angle Boundary at 78°K. ×100.

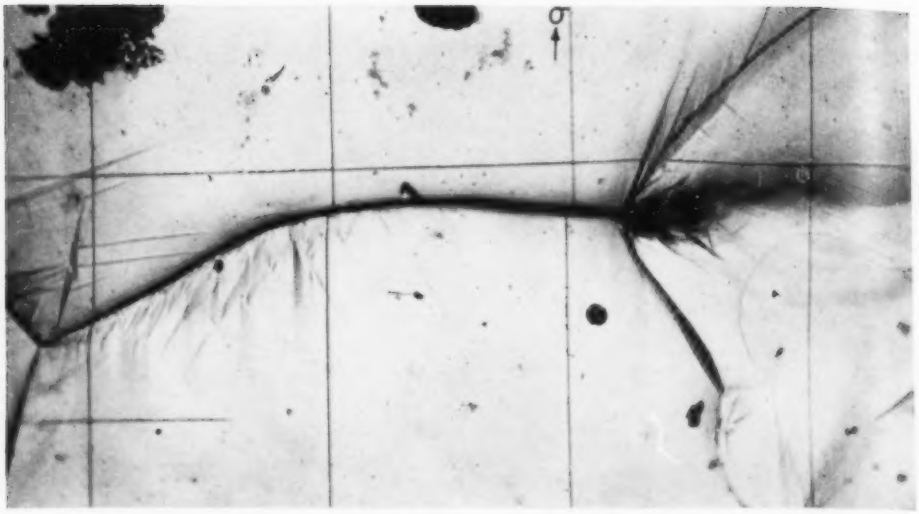


Fig. 10—Grain Boundary Shear at 78°K. ×100. Reduced 50% in reproduction.

The high incidence of pencil slip involving both the basal plane {0001} and the prismatic plane $\{1\bar{1}00\}$ strongly suggests that both planes slip along their common $<2\bar{1}\bar{1}0>$ direction.

In Fig. 7 is shown an interesting example of a more complex phenomenon than the more common type of pencil slip. Distinctly identical slip bands can be seen to traverse the original grain and its twin. A preliminary examination might suggest that these slip bands formed some time before twinning had occurred and were merely sheared over in the twin as a result of the twinning process. But the shear strain is much greater than that which occurs upon twinning of magnesium. Furthermore the slip bands follow the traces of the basal plane in both the original grain and in the twin. Consequently the concept that slip preceded twinning cannot be valid. This anomaly can be rationalized by assuming that twinning preceded slip and that slip took place simultaneously on the basal planes of both the twin and its parent grain. This is feasible because the basal planes of the twin and of the original grain intersect along a common $<2\bar{1}\bar{1}0>$ slip direction. In this way, pencil slip of this second type can take place in close-packed hexagonal systems. The visualization of how pencil slip of the second type might take place in terms of a dislocation model presents a challenging problem.

To summarize the appearance of slip at low temperatures Fig. 8 has been included. It illustrates all the different types of slip observed in magnesium at 78°K.

Twinning. As in the previous room temperature investigation, all twins obtained upon deformation at low temperatures formed along $\{10\bar{1}2\}$ planes. The number of twins and the general microscopic appearance of each twin was not altered by the lowering



Fig. 11—Intergranular Crack at 78°K. ×100. Reduced 25% in Reproduction.

of the test temperature; and the accommodation boundaries had the same sharp small angle ridge along $\{10\bar{1}0\}$ plane traces as was recorded in the previous report.

An interesting observation as to the rate of growth of twins was made during a test designed to reveal the onset of duplex slip at 78°K. A specimen was pulled at a rate of 0.01%/min. while under microscopic observation (×50) through a window in the Dewar flask containing the liquid nitrogen. It was noted the growth of twins in magnesium proceeded at what appeared to be a uniform rate on loading. This observation appears to be contrary to that of Thompson and Millard (6) on Cd who described the growth of twins as occurring by discontinuous jerks. Of course these small



Fig. 12—Spur of a Transgranular Crack at 78°K. ×100. Reduced 40% in Reproduction.

steps might occur at such a rapid rate as to give the impression of a continuous rate of growth at low power observation.

On unloading of magnesium specimens following a tensile test some twins gradually diminished in width, leaving only a fine trace behind. If slip had occurred within the twin the slip traces remained on the surface outlining the former twin boundary envelope (Center of Fig. 4). On reloading other twins seemed to grow in preference to the previously activated twins. This factor undoubtedly plays a role during fatigue testing of Mg.

Nóncrystallographic Small Angle Boundaries

The number and general appearance of the small angle boundaries formed during deformation appeared to be the same at the low temperatures as those previously studied at room temperature. This indicates that the mobility of dislocations even at 78°K is sufficient to permit the formation of vertical arrays of like dislocations into sharp small angle boundaries. It might be expected that due to the slow rate of diffusion at the low temperatures more small angle boundaries would have the rounded appearance of that shown in Fig. 7. But most boundaries had the appearance illustrated by Fig. 9, indicating a very sharp and precise vertical stacking of like dislocations.

In Fig. 9 an example is presented of a low angle boundary traversing a twin; the boundary exhibits a well-defined offset on the opposite sides of the twin which might be ascribable to differences in the rate of migration of the branches of the boundary on each side of the twin. Furthermore each of the offset low angle bound-



Fig. 13—Typical Final Fracture in Large Grain Specimen at 78°K. ×100. Reduced 40% in reproduction

aries in the grain exhibit fainter extensions into the twinned region.

Grain Boundary Shear. The phenomenon of grain boundary shearing which is usually associated with high temperature deformation, had been observed to be quite prevalent upon deformation of Mg at room temperature (4). At low temperatures, however, the occurrence of this deformation mechanism is quite rare; but Fig. 10 illustrates one of the few cases detected in magnesium at 78°K. This figure also shows the complex accommodation kinking at the triple point induced by grain boundary shearing. The high stress concentration and the high local strain at such triple points might lead to local cracking such as described in the next section.

Fracture. As at room temperature many cracks were visible throughout the tensile specimens at low temperature even before the final failure. The length of these preliminary part intergranular, part transgranular openings rarely exceeded one grain diameter. Fig. 11 shows a predominantly intergranular crack while Fig. 12 shows the spur of a transgranular crack. These cracks either cause high local strains in their vicinity or are the result of large strains due to stress concentrations. Because several spur cracks such as shown in Figs. 11 and 12 usually accompany these local separations, the point of origin of the rupture cannot easily be determined. Furthermore the high local deformation encountered in the region of local fracturing makes the crystallographic identification of possible shear or cleavage planes very difficult.

Fig. 13 was included in this report to illustrate the complexity of the final failure at 78°K. The fracture is partially intercrystalline and partially transcrystalline. Pieces of the opposite grain occasionally adhere to one side of the failure. One section of the failure seems to follow a prismatic trace. Although many and interesting details can be noted, it is difficult at present to draw definitive conclusions regarding the nature of fracturing from metallographic analysis alone.

Conclusions

1. Basal slip of the form $\{0001\}\langle 2\bar{1}\bar{1}0\rangle$ is the major deformation mechanism of polycrystalline magnesium from 298°K to 78°K.

2. Whereas grain boundary shearing is quite prevalent at 298°K its incidence is rare at 78°K.

3. But as the incidence of grain boundary shearing decreases with a decrease in the temperature for deformation, the incidence of prismatic slip of the form $\{1\bar{1}00\}\langle 2\bar{1}\bar{1}0\rangle$ increases.

4. These and other related observations suggest that highly localized stresses are relieved by grain boundary shearing at 298°K whereas they cause prismatic slip at lower temperatures where grain boundary shearing is rare.

5. Pencil slip occurs at the lower temperatures by the conjugate mechanisms on planes {0001} and {$1\bar{1}00$} along their common $<2\bar{1}\bar{1}0>$ direction.

6. Twinning takes place by shear parallel to the {$10\bar{1}2$} planes in the $<10\bar{1}1>$ direction over temperature range from 298°K to 78°K.

7. Fracturing occurred by intergranular and transcrystalline modes from 298°K to 78°K. The mechanism of transcrystalline fracture was not identifiable as cleavage along the {0001} planes.

ACKNOWLEDGMENTS

This investigation was sponsored by the Office of Ordnance Research. The authors wish to thank the OOR staff for their continued interest and support of this investigation.

References

1. B. Chalmers, "The Influence of the Difference of Orientation of Two Crystals on the Mechanical Effect of their Boundary," *Proceedings*, Royal Society, London, A, Vol. 162, 1937, p. 120.
2. G. I. Taylor, "Plastic Strain in Metals," *Journal*, Institute of Metals, Vol. 62, 1938, p. 307.
3. C. S. Barrett and L. H. Levenson, "The Structure of Aluminum after Compression," *Transactions*, American Institute of Mining and Metallurgical Engineers, Vol. 137, 1940, p. 112.
4. F. E. Hauser, C. D. Starr, L. S. Tietz and J. E. Dorn, "Deformation Mechanisms in Polycrystalline Aggregates of Magnesium," Institute of Engineering Research Report, University of California, Berkeley, Series No. 73, Issue No. 2, March 15, 1954; TRANSACTIONS, American Society for Metals, Vol. 47, 1955, p. 102.
5. G. I. Taylor and C. F. Elam, "The Distortion of Iron Crystals," *Proceedings*, Royal Society, A, Vol. 112, 1926, p. 337.
6. N. Thompson and D. J. Millard, "Twin Formation in Cadmium," *Philosophical Magazine*, Vol. 43, 1952, p. 422.

DISCUSSION

Written Discussion: By R. W. Guard, General Electric Research Laboratory, Schenectady, New York.

When a random polycrystalline metal is deformed, the stresses at any point in the interior will not be the same as the gross macroscopic stress. Would the authors explain how the resolved shear stresses for prismatic slip were calculated without knowing the complex stress pattern which surely exists at grain corners and boundaries? If it were possible to determine the actual stress in the region where prismatic slip systems were active, the calculations of critical stress for yielding on these systems might not show the random behavior observed by the authors. In this same regard, were any local strain measurements made except for grain boundary shearing?

In the case where nonbasal slip is observed there are two alternate explanations for its occurrence:

1. The resolved shear stress on the basal plane is so small that other slip systems operate first.
2. The conditions of strain prohibit basal slip by preventing the concomitant rotation.

In their observations did the authors observe whether prismatic slip occurred only at grain corners and boundaries or was also observed in the center of grains? Was there any tendency for nonbasal slip to occur only at large overall strains or was it also observed at small strains.

It does not seem necessary to postulate that dislocations have sufficient mobility at 78°K to move into small angle boundaries. The dislocations could be localized into walls by the sharp stress gradient at a grain corner such as Fig. 9. This explanation is more in agreement with the noncrystallographic nature of the boundary.

Authors' Reply

The authors wish to thank Mr. Guard for his discussion of this paper.

Resolved shear stresses for prismatic slip were calculated assuming a uniform stress field. This assumption had been shown to be approximately correct for determining the onset of basal slip in magnesium in a previous paper (4). Since the appearance of prismatic slip was highly localized and did not occur at a critical resolved average shear stress, the conclusions were that the stress pattern must be greatly distorted locally. Except for grain boundary shear measurements no local strain determinations were attempted.

In all cases basal slip was observed together with prismatic slip. Therefore the second explanation Mr. Guard offers for the occurrence of nonbasal slip namely, that the constraint of basal slip induces secondary slip seems to be the correct one. Prismatic slip was observed not only at grain boundaries but occasionally in small localized regions within the grains as revealed in Fig. 1. These regions of course could be near a grain boundary below the plane of polish.

The authors agree with Mr. Guard that sharp stress gradients could cause small angle boundaries without dislocation climb. Then the motion of these boundaries as documented in the previous report (4) is probably due to the gradual change in stress pattern on stressing.

DEFORMATION OF BERYLLIUM SINGLE CRYSTALS AT 25 TO 500°C

By H. T. Lee and R. M. Brick

Abstract

Compression tests at room temperature, 300°C, and 500°C have been conducted on single crystals of beryllium for various orientations.

Part I includes experimental observations of the study. Slip and twinning elements were determined from surface markings by microscopic examinations and by X-ray analyses. The operative slip planes at temperatures of 25, 300, and 500°C were established as (0001) and $\{10\bar{1}0\}$; the single twinning plane as $\{10\bar{1}2\}$. Cleavage planes were found to be either (0001) or $\{11\bar{2}0\}$. Deformation and kink bands were also observed. A peculiar type of macroscopic band was found present in several specimens with a particular orientation and an explanation accounting for its formation is given. Measurement of the displacement of cracks across slip bands has led to an evaluation of the local strains resulting from basal slip as a comparison to the average shear. A selection rule based on an extension of LeChatelier's principle is advanced for the choice of active twinning planes from the total ones available.

Part II consists of some crystallographic analyses regarding to twinning and slip. A mathematical relationship is given to describe the atomic movements in twinning of close-packed hexagonal metals. Factors of periodicity and crystallographic shear are also considered as affecting the selection of slip and twinning elements. (ASM-SLA Classification: Q24, M26, Be)

Part I—Experimental Observations of Beryllium Single Crystals under Compression

COMPLICATIONS involved in the production of beryllium single crystals (1–6)[1] of reasonable size and purity have thus far made it impossible to conduct an extensive study of the plastic behavior of this metal.

[1]The figures appearing in parentheses pertain to the references appended to this paper.

*This paper is taken from a dissertation submitted by H. T. Lee to the faculty of the Graduate School of the University of Pennsylvania in partial fulfillment of the requirements for the Ph.D. degree. The work has been carried out under Contract ONR-24908 with the office of Naval Research, U. S. Navy.

A paper presented before the Thirty-Seventh Annual Convention of the Society, held in Philadelphia, October 17–21, 1955. The authors, H. T. Lee and R. M. Brick, were associated with the School of Metallurgical Engineering, University of Pennsylvania, Philadelphia when this work was accomplished. R.M. Brick is presently Director of Metallurgy, Central Research and Engineering Division, Continental Can Co., Chicago. Manuscript received December 27, 1954.

In 1928, Mathewson and Phillips (7) established the slip and twinning planes of beryllium as (0001) and $(10\bar{1}2)$ respectively. The authors used polycrystalline specimens cut so as to expose two surfaces at right angles. No work on the plastic behavior of beryllium single crystals has been reported.

Preparation of Specimens

Two beryllium ingots 4 inches in diameter and approximately 6 inches in length were supplied by Dr. Kaufmann of M.I.T. These ingots were coarse-grained, with no more than six grains over the cross section. The material was over 99.8% pure.

Slices ¾ inch in thickness were first cut across the ingots by means of an abrasive wheel. After the individual orientations had been determined for the grains in a particular slice, compression pieces were cut from it with the aid of a high speed water sprayed glass cut-off wheel. A goniometer stage in front of the blade permitted the slice to be fed into the wheel at different angles. In this way, the desired orientations could be obtained without much difficulty. These pieces, about ½ inch cubes, were carefully hand ground to three sets of parallel surfaces. Due to the extreme brittleness of beryllium, even careful hand grinding almost invariably caused cracks to form along the sharp edges of the specimen. Corners were also very easily chipped. This was particularly true for specimens with basal plane inclined about 45 degrees to the compression surfaces. Cracks at the edges of the specimen were rounded off down to their base and grindings again proceeded on the relevant surfaces. When the grinding proved to be too vigorous for a particular case, the specimen was transferred to a finer grade of polishing paper. This tedious process was continued until a geometrically perfect specimen was obtained.

Specimens were polished on 240, 400, 600 papers, followed by a deep etching with Tucker's reagent to check the possible presence of grain boundaries on any of the six surfaces. After a repolishing of the specimens on 600 paper they were then annealed at 1000°C (1830°F) for 1 hour in vacuum. The annealing treatment eliminated surface twins and insured a comparable initial condition for all the testing specimens.

After annealing, all 6 surfaces of each specimen were given a final metallographic polish. The 4 vertical ones were prepared for subsequent microscopic examination and the two compression surfaces were polished to insure smoothness and minimize friction.

The dimensions of all specimens are given in Table I. Specimens numbered less than 100 were obtained from one ingot. Those numbered higher than 100 were obtained from a second ingot.

Table I
Testing Conditions of Specimens

Specimen Number	Temperature (°C)	θ(1)	λ(2)	%Red.	Initial Dimensions (in.) Thickness	Area
Be- 2	25	4	86, 87, 89	0	0.1138	0.2895 ×0.2875
Be- 4	25	1	89, 89, 89	Fract.	0.1751	0.3355 ×0.3358
Be- 5	25	1	89, 89, 89	Fract.	0.1431	0.3055 ×0.3048
Be- 1	300	2	88, 89, 90	Fract.	0.1718	0.3239 ×0.3231
Be- 2A	500	4	86, 87, 89	Fract.	0.1100	0.2865 ×0.2828
Be- 9	25	49.5	42, 64, 73	12.70	0.1650	0.3291 ×0.3212
Be- 11	25	50	40, 63, 73	3.62	0.1079	0.3104 ×0.3136
Be-109	25	38	53, 62, 66	2.37	0.1604	0.4051 ×0.4030
Be-113	25	57	35, 57, 74	2.35	0.1403	0.4152 ×0.4286
Be-141	25	43	47, 70, 71	3.60	0.2674	0.5020 ×0.5110
Be-153	25	38	52, 67, 77	6.10	0.1067	0.2943 ×0.2944
Be- 12	300	49	42, 62, 74	5.50	0.1180	0.3193 ×0.3180
Be-110	300	40	52, 64, 79	3.30	0.1299	0.3219 ×0.3220
Be-120	300	44	46, 65, 74	4.95	0.1931	0.5295 ×0.5290
Be-142	300	45	45, 69, 70	2.75	0.2831	0.4341 ×0.4342
Be-146	300	47	43, 68, 70	5.07	0.2851	0.3538 ×0.3515
Be-147	300	44	51, 55, 87	4.80	0.2206	0.4265 ×0.4247
Be-121	500	45	45, 64, 74	1.60	0.1908	0.5370 ×0.5391
Be-143	500	44	46, 70, 70	4.70	0.2390	0.4037 ×0.4108
Be-144	500	44	46, 68, 71	1.40	0.3053	0.4476 ×0.4717
Be-145	500	45	45, 68, 70	2.11	0.2753	0.4220 ×0.4312
Be-149	25	22	69, 73, 86	20.30	0.1677	0.3960 ×0.3945
Be-159	25	23	67, 72, 88	10.50	0.1570	0.2920 ×0.3131
Be- 14	300	18	74, 75, 88	1.20	0.1828	0.3720 ×0.3705
Be-148	500	24	68, 70, 88	1.08	0.1950	0.3966 ×0.3972
Be- 3	25	82	8, 60, 62	10.90	0.1503	0.2871 ×0.2867
Be- 6	25	83	6, 60, 60	3.86	0.1631	0.3419 ×0.3424
Be- 7	25	88	20, 40, 80	1.04	0.1541	0.2498 ×0.2505
Be- 22	300	88	10, 50, 70	1.80	0.0890	0.2845 ×0.2856
Be-151	300	7	5, 57, 63	2.66	0.1615	0.3188 ×0.3190
Be-150	500	88	4, 57, 63	2.74	0.2189	0.4241 ×0.4182
Be- 8	25	65	33, 50, 77	2.10	0.1342	0.2953 ×0.2988
Be-155	25	66	37, 38, 89	8.30	0.1085	0.3978 ×0.3966
Be-157	25	65	35, 41, 86	8.27	0.1016	0.3821 ×0.3850
Be-101	300	65	30, 48, 79	4.71	0.1485	0.3315 ×0.3320
Be-117	300	72	20, 59, 65	0.31	0.1598	0.3790 ×0.3770
Be-118	300	70	20, 61, 63	0.95	0.1770	0.3871 ×0.3888
Be-152	300	66	25, 60, 65	3.50	0.2392	0.3605 ×0.3644
Be-156	500	66.5	35, 40, 88	10.60	0.1190	0.2728 ×0.2605

(1) Angle between compression axis and pole of basal plane.
(2) Angles between compression axis and the three close packed directions in (0001).

Compression Procedure

The compression unit consisted of a cylindrical hardened steel plunger, an anvil and a container. One end of the plunger was machined to a half sphere to match the depression on a compression plate which was firmly bolted to the cross-head of a Southwark-Emery hydraulic machine. The other end was highly polished and faced parallelly the similarly polished surface of the anvil. Compressions were carried out in a series of steps with frequent lubrication. For the runs at temperatures above atmospheric, the compression unit was put in a nichrome wound furnace with a controller to maintain the desired temperature.

Tests were carried at three temperatures: 25, 300, and 500°C. At both room temp. and 300°C, Silicone DC 200 oil was used for

lubrication; and at 500°C Houghton's Mar-Temp salt was used. These served the double purpose of lubricating the compression surfaces and protecting the specimens from being exposed to air. The compression unit was first brought up to temperature and the specimen was then put in. Owing to the extremely small mass of a specimen as compared to that of the compression unit, temperature equilibrium was reached very rapidly.

Strain was measured by a microformer type extensometer attached across the stationary and movable posts of the testing machine. A lever combination connected to the plunger of the microformer enabled several different magnifications of the head movement. Throughout the test a constant rate of head movement of 0.002 inch per minute was maintained.

Both strain and load were recorded autographically. Prior to each test a blank run was made so that the deformation of the equipment might be evaluated.

Orientation of specimens was determined by the conventional Laue back-reflection method. To correlate the microscopic examination with the X-ray pattern, a special goniometer was constructed. Angular directions of the slip and twin traces as measured under microscope on each vertical surface were always plotted stereographically to the same reference plane of the original X-ray pattern.

Results and Discussion

Original orientations of the 39 specimens studied are shown in Fig. 1. The conventional method of orientation notation is adhered to; that is, the pole of the basal plane (0001) has been rotated to the center of the primitive circle, and the position of the compression axis of each specimen is represented by a cross in the basic triangle formed by the poles of three planes (0001), $(10\bar{1}0)$, and $(11\bar{2}0)$. The three triangles show the three groups of specimens compressed at 25, 300, and 500°C respectively.

A complete tabulated summary of the experimental conditions in these tests is given in Table I. The angles fixing the position of the compression axis are given as θ and λ, where θ is the angle between the compression axis and the pole of the basal plane, and λ the angles between the three poles of $\{11\bar{2}0\}$ planes and that of the compression surface.

Results of the investigation may be divided into the following groups according to the initial orientation of the specimens:

A. Orientations with Basal Plane Nearly Parallel to the Compression Surface

This group of specimens included Be-4, Be-5, Be-1, and Be-2, all possessing a θ value smaller than 5 degrees. The first two were com-

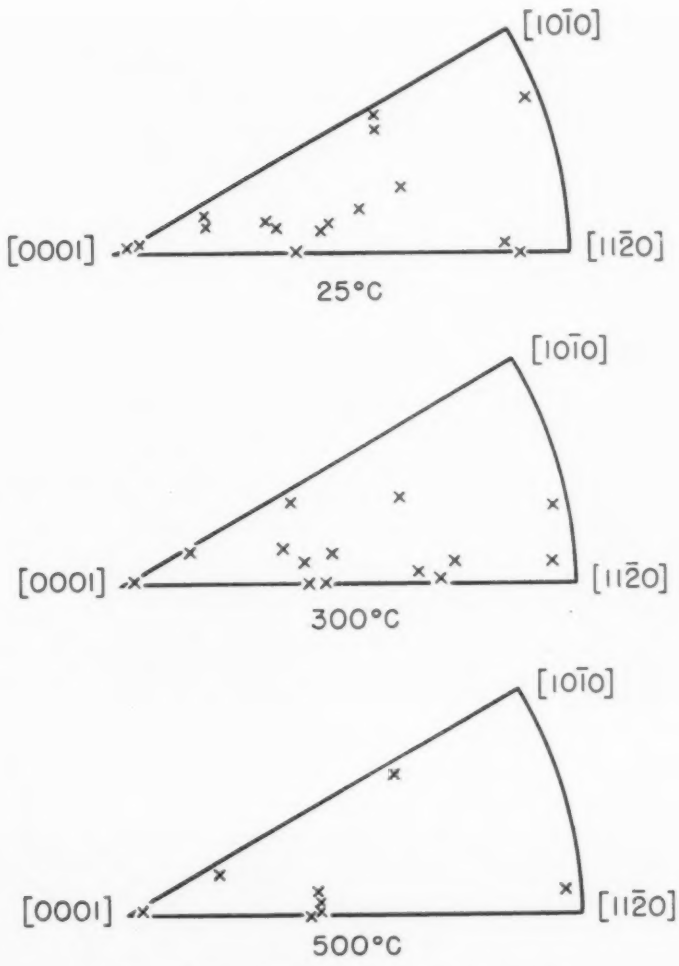


Fig. 1—Orientation of Specimens Prior to Test.

pressed at room temperature, and the last two, Be-1 and Be-2, were tested at 300 and 500°C respectively.

The room temperature specimens behaved almost completely elastically. Loading was accomplished in three steps: 2790 lbs., 23,600 lbs., and 26,500 lbs. Measurements after the first and second compressions did not reveal any change of dimensions from the original. No slip lines or twin traces were observed. The autographic curve was straight without any bend-point or change of slope prior to fracture. Fracture of the room temperature specimens occurred in such a way that the original specimens suddenly were pulverized into numerous fine particles. In both cases, fracture occurred at a stress of 285,000 psi.

Two of the small pieces were large enough to show that the main fracture had been along a plane 45 degrees to the compression surface. X-ray and microscopic examinations established that the basal plane and all three sets of {11$\bar{2}$0} planes also acted as cleavage

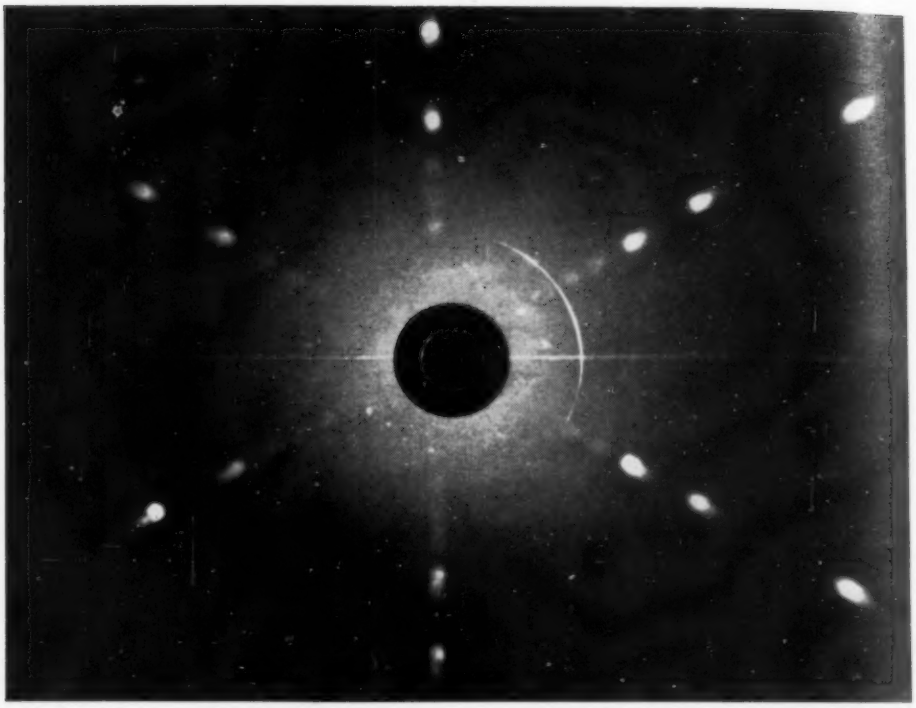


Fig. 2—Laue Pattern of Be-5 Before Compression.

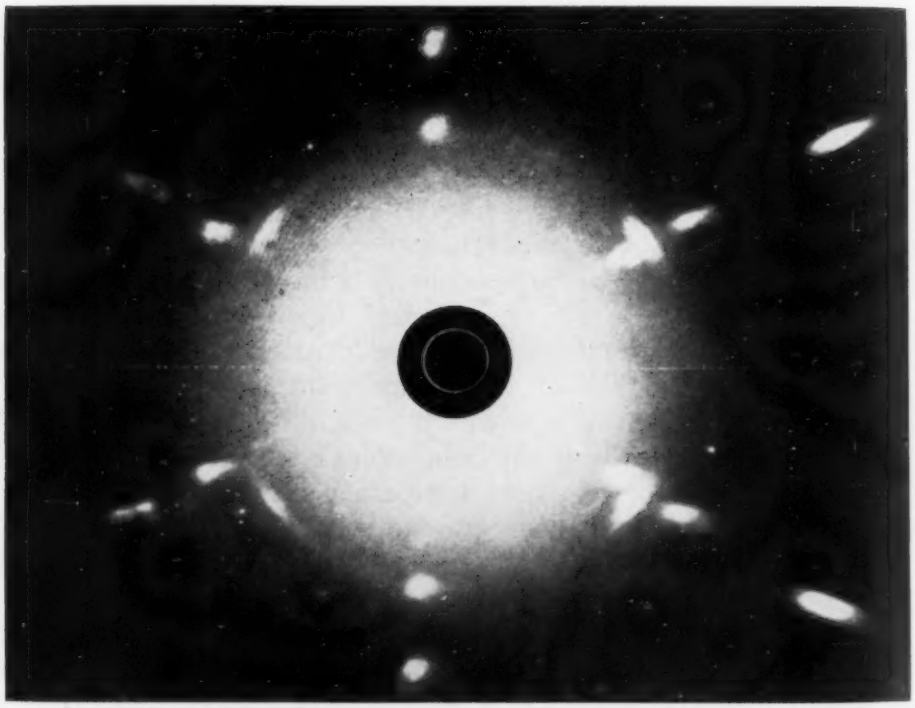


Fig. 3—Laue Pattern of Be-5 After Compression Taken Perpendicular to an (0001) Cleavage Face.

Table II
Fracture Data of Beryllium Compressed Perpendicularly to Basal Plane

Specimen Number	θ	Temperature	Fracture Stress (lbs./in.^{2})	Energy Prior to Fracture in-lbs./cu. in.
Be-4	1°	25°C	285,000	39,900
Be-5	1°	25°C	285,000	38,800
Be-1	2°	300°C	215,000	18,000
Be-2A	4°	500°C	227,000	29,900

planes. The orientation of the crystal apparently was in such an unfavorable position for either slip or twinning, that only elastic deformation was allowed. Gradually the elastic energy stored in the specimen built up until it reached the limit that could be sustained by the lattice, followed by fracture. The availability of four cleavage planes made it possible for the specimen to break into many fine pieces.

X-ray patterns (Figs. 2 and 3) show the difference between the original and the fractured states. One interesting aspect was that asterism only developed along two of the three $(11\bar{2}0)$ zones. No single rotation or bending axis could account for such an effect. A distortion like this could very well be introduced by the $\{11\bar{2}0\}$ cleavages. The broken concentric rings in Fig. 3 were identified as the $\{10\bar{1}4\}$ reflections from the small twins.

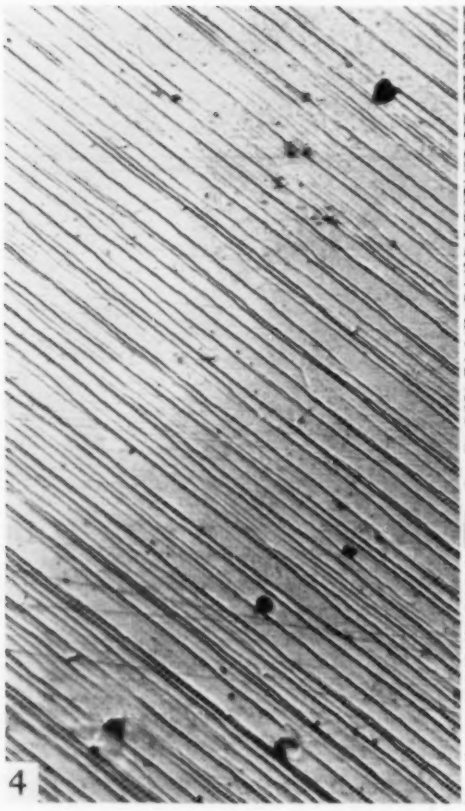
Specimens compressed at higher temperatures behaved similarly, except that the final breakages did not result in such small pieces. Also, at 500°C (930°F) the autographic curve indicated a levelling off just before fracture was reached.

The fracture stress and energy stored prior to fracture for Be-1 and Be-2 are also given in Table II. Increase in these values at 500°C (930°F) as compared to those at 300°C (570°F) may be ascribed to the increased strain and resultant hardening of Be at 500°C (930°F).

B. Orientations with Basal Plane at 45 Degrees

This group included 16 specimens with θ values ranging from 38 to 57 degrees, although the majority of them had the basal plane inclined to the compression surface only ± 2 from 45 degrees. Deformation of these specimens was predominantly by basal slip with one of the $<11\bar{2}0>$ axes as the direction of the glide.

The (0001) slip lines were straight when no deformation bands were present, and when they were away from inclusions. A typical state is represented by Fig. 4. At some locations in a later stage of deformation, the slip lines often formed as clusters which would produce an abrupt off-set at the free surface of the specimen and a basal fracture would thus be initiated. This situation is shown by Figs. 5 and 6.



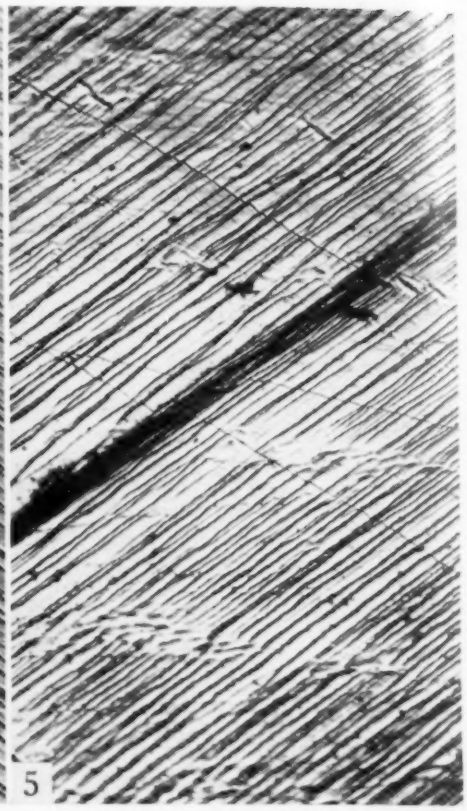


Fig. 4—Basal Slip Lines on Be-11 Strained at 25°C; (0001) 50 Degrees from Stress Axis. ×200.

Fig. 5—Cluster of Basal Slip Lines on Be-9, Strained at 25°C; (0001) 50 Degrees from Stress Axis. ×300.

When the slip lines approached a surface, Fig. 7, they were bent in such a way as to be as nearly perpendicular to the surface as possible. This often caused some tear-lines near the compression surface. Furthermore, owing to the extra energy required to break through a solid surface, the slip lines frequently stopped before they could penetrate through. The strain hardening near the surface due to lattice bending tended to make the density of slip lines decrease as they were approaching the end.

Deformation bands appeared in many of the specimens. The bands invariably were parallel to the plane of restriction, i.e., the compression surface.

Basal Slip, Room Temperature vs. High Temperature—An important difference seemed apparent between 500°C (930°F) specimens and those tested at room temperature and 300°C (570°F). Crystals compressed at the latter two temperatures did not reveal an appreciable change of slip line spacing, although the 300°C (570°F) specimens did infrequently show a tendency for branching of slip lines. However, the 500°C (930°F) specimens exhibited an obvious increase of slip line spacing as compared to both room temperature

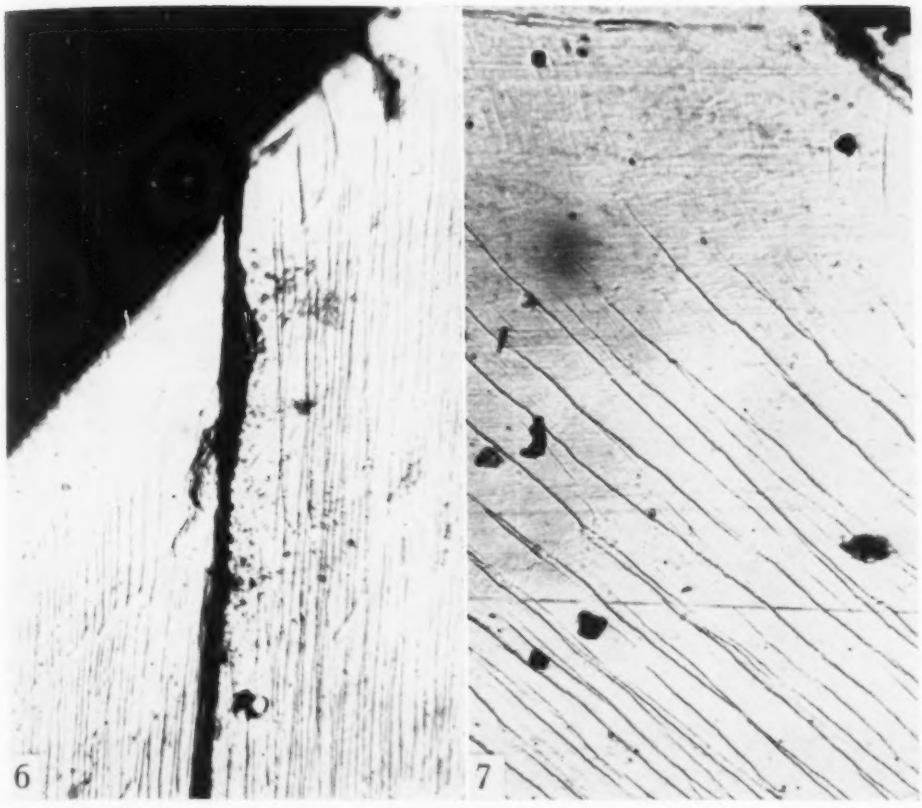


Fig. 6—Crack at Terminus of Cluster of Slip Lines of Be-9 at Side Surface. ×200.
Fig. 7—Basal Slip Lines on Be-11 at Compression Surface (Top). Crystal strained at 25°C. ×200.

and 300°C (570°F). A comparison of Fig. 4 and 9 clearly demonstrates this point. Both specimens, in this case, had nearly the same orientation and amount of reduction. Basal slip lines at 500°C (930°F) were also wavy and often branched in various directions to form an intricate network.

Evidence seemed to indicate that upon deformation at 500°C (930°F), the crystal became considerably more imperfect. Laue photograms, e.g., Fig. 10, showed differences of mosaic orientations often amounting to over 2 degrees. This was in contrast with the X-ray pattern obtained from specimens after being compressed at room temperature and 300°C (570°C) for a comparable amount of reduction, Fig. 11. This increased imperfectness seemed to appreciably strengthen the crystal at 500°C (930°F) and to account for the waviness and branching of the slip lines. The same change was also manifest in the autographic load-reduction curves obtained at different temperatures. While curves at both room temperature and 300°C (570°F) generally possessed a sharp bend-point, the 500°C (930°F) curves always had only a gradual bend and this occurred at a higher resolved shear stress.

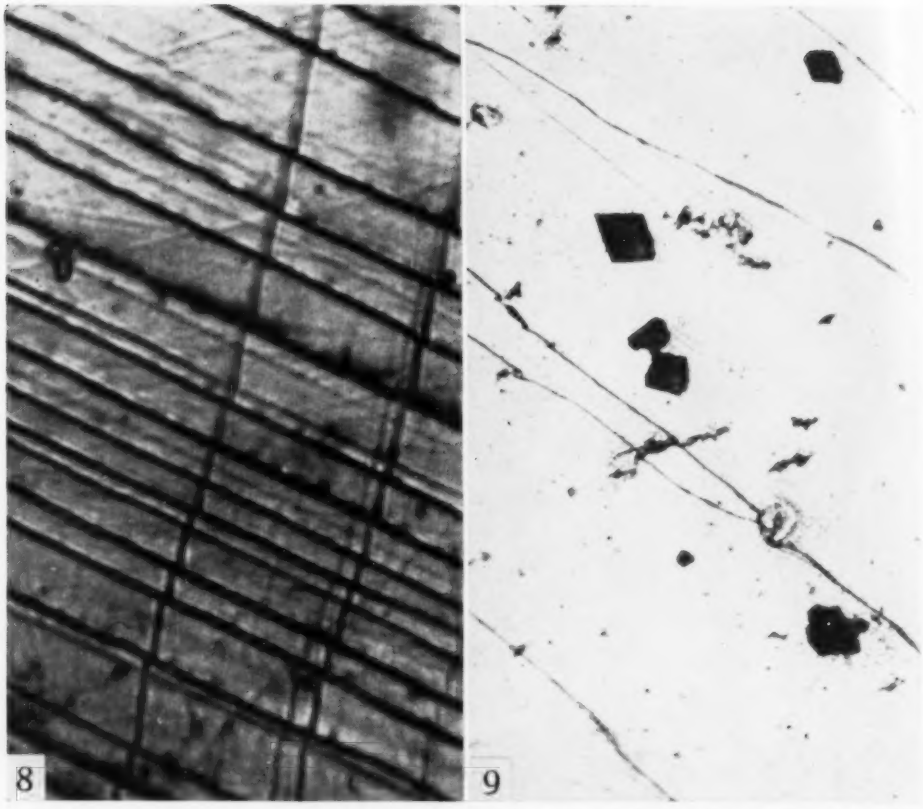


Fig. 8—Displacement of Scratches by Basal Slip in Crystal Be-9, Deformed at 25°C. ×2000.

Fig. 9—Slip Lines on Crystal Be-145 Deformed at 500°C. ×200.

Critical Resolved Shear Stress—By utilizing the bend-point of the autographic curves, an attempt was made to determine the critical resolved shear stress of beryllium at the three temperatures studied. Table III summarizes the results.

It is seen that within the limit of accuracy (a 2-degree difference of both θ and λ would throw the value off 10%) the critical resolved shear stress of beryllium at 300°C (570°F) as determined was practically the same as that at room temperature. Values at 500°C

Table III

Specimen	Temperature,°C	θ[1]	λ[2]	τ_0[3] psi	
Be- 9	25	49.5°	41.5°	4420	
Be- 8	25	65°	33°	4120	
Be- 11	25	50°	41°	4980	Ave. = 4600
Be-141	25	43°	47°	4180	
Be-153	25	38°	52°	5320	
Be-142	300	45°	45°	3910	
Be-147	300	44°	51°	4370	Ave. = 4060
Be-146	300	47°	43°	3910	
Be-143	500	44°	46°	6630	
Be-144	500	44°	46°	6220	Ave. = 6460
Be-145	500	45°	45°	6530	

(1) Angle between compression axis and basal plane.
(2) Angle between compression axis and active slip direction.
(3) Resolved shear stress at initial yielding of crystal.

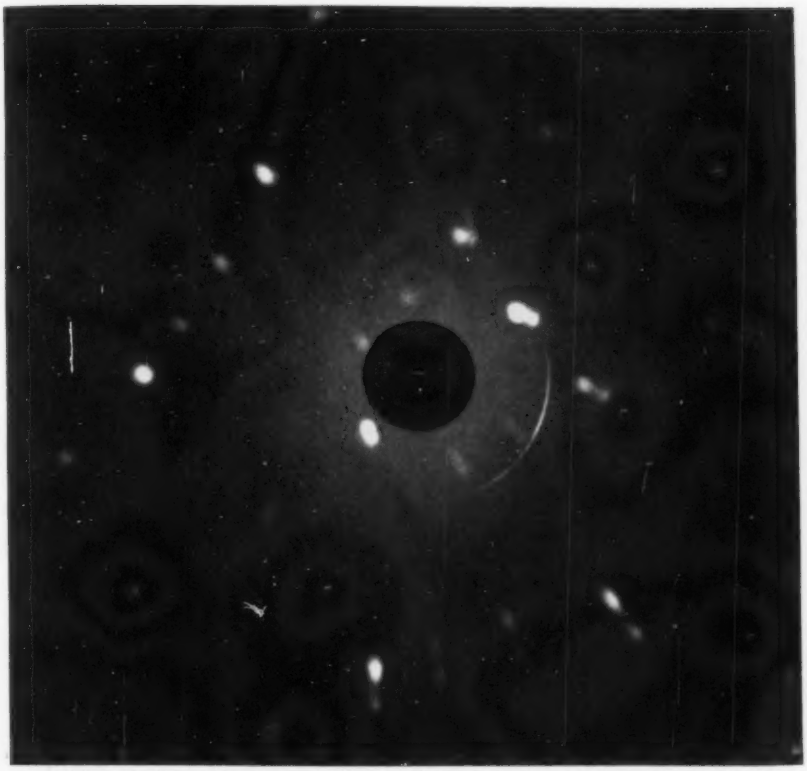


Fig. 10—Laue Photogram of Crystal Be-145 After Deformation at 500°C; Mosaic Structure Developed Upon Deformation.

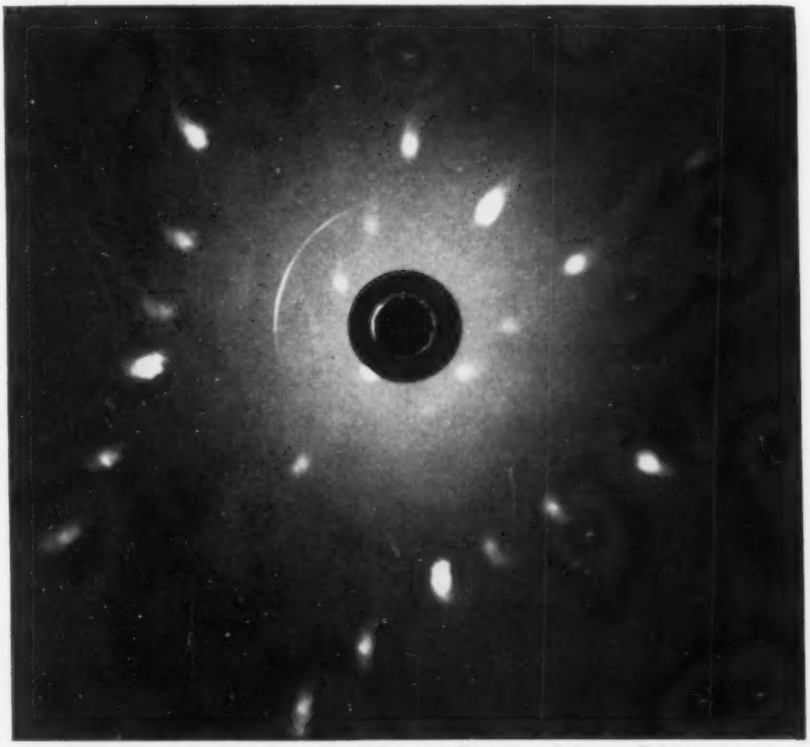


Fig. 11—Laue Photogram of Crystal Be-141, of Same Orientation and Equivalent Deformation as Above but Strained at 25°C.

(930°F) were considerably higher. This abnormal condition has been observed by Miller and Milligan (22) in single crystals of silver and aluminum, and was believed to be caused by the increase of thickness of oxide film with increasing temperature (23). It is quite probable that in the present case of beryllium, the presence of oxide film might also account partly for the increase of critical resolved shear stress at 500°C (930°F). However, it is believed that the rather drastic difference in slip behavior as shown in the last section would constitute a more important factor in contributing to such increase. In view of these two factors, it is doubtful that the values given in Table III for 500°C (930°F) could be regarded as the "true" critical resolved shear stress for beryllium, although the three specimens tested at this temperature appeared to be in a seemingly comparable state at the moment when the bend point occurred.

Rotation of Slip Plane—Owing to the restriction of the two compression surfaces, the lattice of the crystal was forced to gradually rotate in such a way that the slip plane would approach parallelism to the compression surface.

The familiar sine law takes either of the following forms:

$$\frac{l_1}{l_o}=\frac{\sin \lambda_o}{\sin \lambda_1} \text{ or } \frac{l_1}{l_o}=\frac{\sin \chi_o}{\sin \chi_1} \qquad \text{Equation 1}$$

where l_o and l_1 are the initial and final thicknesses, χ_o and χ_1 are the initial and final angles between the slip plane and compression axis and λ_o and λ_1 the equivalent angles between the slip direction and compression axis.

X-ray patterns of Be-9 before and after a 12.7% reduction gave experimental λ_1 and χ_1 as 50 and 49 degrees respectively. By using the above equations, the corresponding calculated values were 49°21′ and 48°2′. The agreement indicates that the geometrical dimensions of the specimens in the present studies were satisfactory.

Analyses of the asterism of the specimens after basal slip also established $<10\bar{1}0>$ as the rotational axis. This is the direction in the slip plane and perpendicular to the slip direction as had been observed by many workers on other close-packed hexagonal metals.

Overall versus Local Shear Strain—Both the autographic curves and micrometer measurements give only an overall reduction of thickness, which in turn yielded an average value of resolved shear strain along the slip plane.

The relationship between the crystallographic glide strain, a, the initial and the final orientations and the initial and final thicknesses of the specimen after a certain amount of reduction, is presented by the following equation, adapted from Schmid and Boas (21) to the present case of compression:

$$a=\frac{1}{\sin \chi_o}(\cos \lambda_o-\sqrt{d^2-\sin^2 \lambda_o})=\frac{1}{\sin \chi_o}(\cos \lambda_o-d \cos \lambda_1) \qquad \text{Equation 2}$$

Where χ_0 = angle between slip plane and compression axis before reduction.
λ_0, λ_1 = angle between slip direction and compression axis before and after reduction.

$d = \frac{l_1}{l_0}$, ratio of reduced thickness to the initial.

Applying this expression to Be-9 after a 12.7% reduction ($d = 0.873$, $\chi_0 = 40.5°$, $\lambda_0 = 41.5°$, $\lambda_1 = 49.5°$), the plastic shear strain was found to be 0.28.

An attempt was made to compare the local shear strains with this theoretical value. The scratches shown in Figs. 5 and 8 were used for this purpose. It is seen that an originally straight and continuous scratch was broken into steps after deformation. By measuring the displacements of the steps and the distance within which the displacements occurred, a value of shear strain can be calculated when other pertinent information was known. For specimen Be-9 and the particular plane of observation of Figs. 5 and 8, the crystallographic glide strain calculated within a long range is 0.27, which is practically the same as obtained theoretically from Equation 2. However, in more confined localities, the value varies from 0.14 to 0.96. The latter value, more than three times higher than the average, is obtained within the cluster shown in Fig. 5.

C. Orientations with Basal Plane at Approximately 25°

Four specimens, Be-149 (22°), Be-159 (23°), Be-14 (18°), and Be-148 (24°) were included in this group. The plastic behavior of these specimens may be described as intermediate between the two groups just discussed. No sharp bend point could be detected in the autographic load-reduction curves at any of the temperatures, although slip lines were observed in every case. At room temperature and 300°C (570°F) the lines were straight, while at 500°C (930°F) they were forked and wavy, and comparatively much more widely spaced.

Deformation of these specimens seemed to be confined to the regions near to the compression surface. In all cases, there was a diagonal macroscopic band present in the central portion of the specimen faces, see Fig. 12.

Formation of these bands seemed to indicate that the length of the glide direction played an important part during slip. The orientation of this group of specimens was such that a single basal plane ran from one specimen edge to another edge diagonally opposite to it, and the projection of the glide direction to the compression plane was approximately parallel to the other set of edges of the compression surface. As a consequence, there was a gradual difference of length of slip direction from one slip plane to the next. For example, plane A′ B′ C′ D′ in Fig. 12 obviously possesses a much shorter length of slip direction than the plane A B C D does. Slip would thus

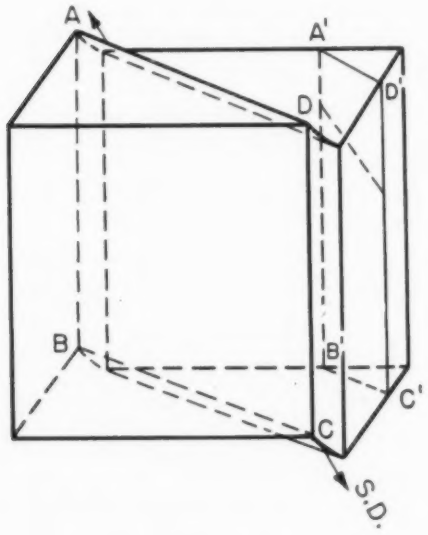


Fig. 12—Formation of the Centra Band, Schematic.

likely prefer those planes near the corners first and then shift gradually inward as the previous planes strain-hardened and ceased to operate further. The cumulative effect of the gradual transfer of slip planes in operation consequently resulted in the split of the two halves of the crystal and a band at the central portion was thus produced. This cumulative effect is believed also to account for the absence of bend-points in the autographic load-reduction curves. In view of the absence of a sharp boundary and also the absence of a sudden drop of load, the bands in the present case were not considered to be kink bands.

D. Orientations with Basal Plane Closely Parallel to the Compression Axis

The study of this orientation included six specimens whose θ values ranged from 82 to 88 degrees. Deformation of these specimens was predominantly by twinning. Two sets of branching and wavy slip lines were also abundant at all temperatures, particularly at 500°C (930°F). They were identified as $\{10\bar{1}0\}$ prismatic slip.

The $\{10\bar{1}0\}$ slip lines were in most cases so wavy as to make it difficult to get any consistent angular measurements, (see Fig. 18). Nevertheless, their general direction invariably came close to a $\{10\bar{1}0\}$ plane when plotted stereographically. In some areas the lines were fairly straight, Fig. 13, and measurements of angles from more than one face established their crystallographic habit with certainty. Quite frequently the $\{10\bar{1}0\}$ slip lines passed through the twins with a slight bend. This was because the basal plane of the twins, determined by the orientation relationship of twinning, was

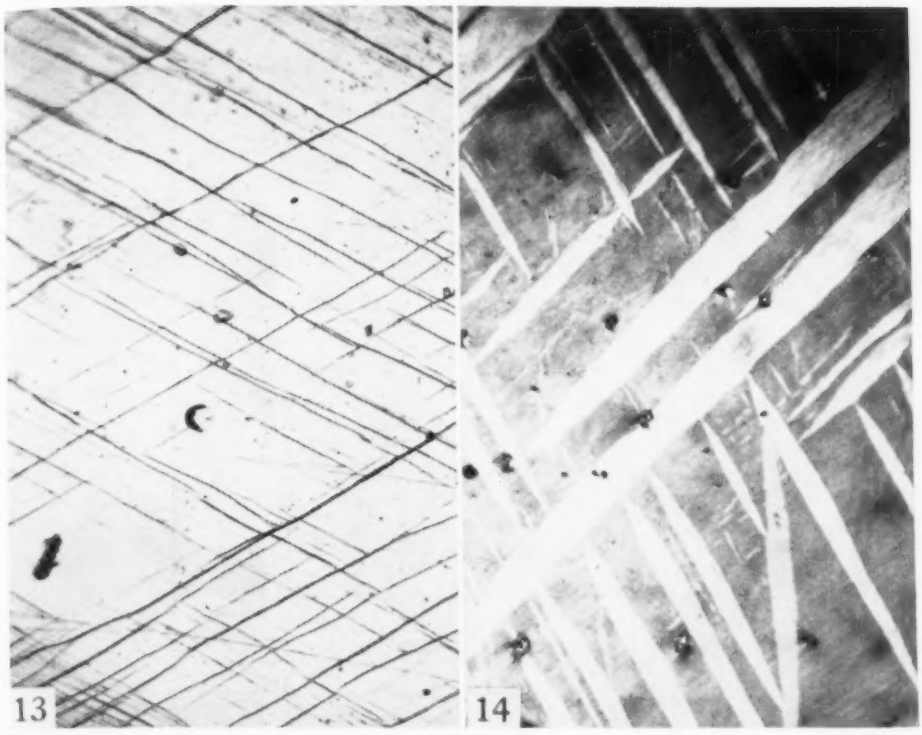


Fig. 13—(10$\bar{1}$0) Slip Lines in Crystal Be-151, Compressed Parallel to (0001) Plane at 300°C. ×200.

Fig. 14—A Zone of Be-6 Showing Only (10$\bar{1}$2) Twins. After compression parallel to (0001) plane at 25°C. ×100.

not more than 8 degrees from the corresponding {10$\bar{1}$0} planes of the matrix.

Twins were very abundant in this group of specimens. They appeared as minute diamond shaped islands, lenses, thin lamellae, or heavy bands running across the entire crystal, Fig. 14. Angular measurements have been made in every case, and no twinning plane other than {10$\bar{1}$2} was ever observed.

Load reduction curves of these specimens bore no sharp bendpoint at room temperature and 300°C (570°F). No distinct twinning clicks were heard. However, at 500°C (930°F) the curves showed abrupt drops, Fig. 15, and the twinning clicks were so loud as to be easily mistaken as fracturing. It is believed that the decrease of surface energy at this temperature permitted the twins to penetrate through to the specimen surface with comparatively greater ease. At room temperature and 300°C (570°F) the twins were frequently restricted within the body of the specimen, and distortion of the lattice was gradually built up at the ends of the twins. This would prevent an effective relaxation of load. While the number of twins at 500°C (930°F) did not show any increase—in fact, it appeared to be even less for the same reduction—the twins themselves always appeared as continuous heavy bands at this temperature. Owing to

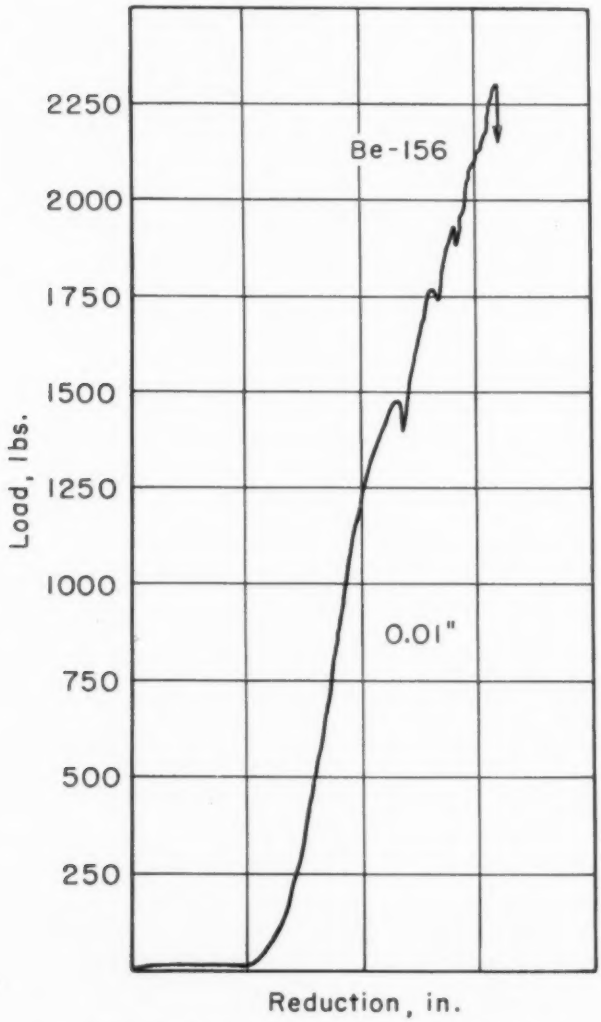


Fig. 15—Load—Deformation Graph for Crystal Be-156, Compressive Stress Axis 66 Degrees from (0001) Pole; Deformed at 500°C.

the large offset associated with them, these twins could be readily seen without resorting to the use of polarized light.

Aside from the microscopic measurements of the angular relationship of the twin bands, X-rays were also used to identify the crystallographic behavior of the twins. By assuming $\{10\bar{1}2\}$ as the twinning planes and $<\bar{1}011>$ the twinning direction, the six new positions of (0001) poles after twinning could be located stereographically as indicated. The X-ray beam was then directed in such a way that it was approximately perpendicular to one of the new (0001) planes, i.e., $(0001)_1$. The Laue pattern thus obtained disclosed a distinct 6-fold symmetry, indicating that the assumption was valid.

Selection of Twinning Planes—Compression tests of specimens where twinning had been the significant deformation process also

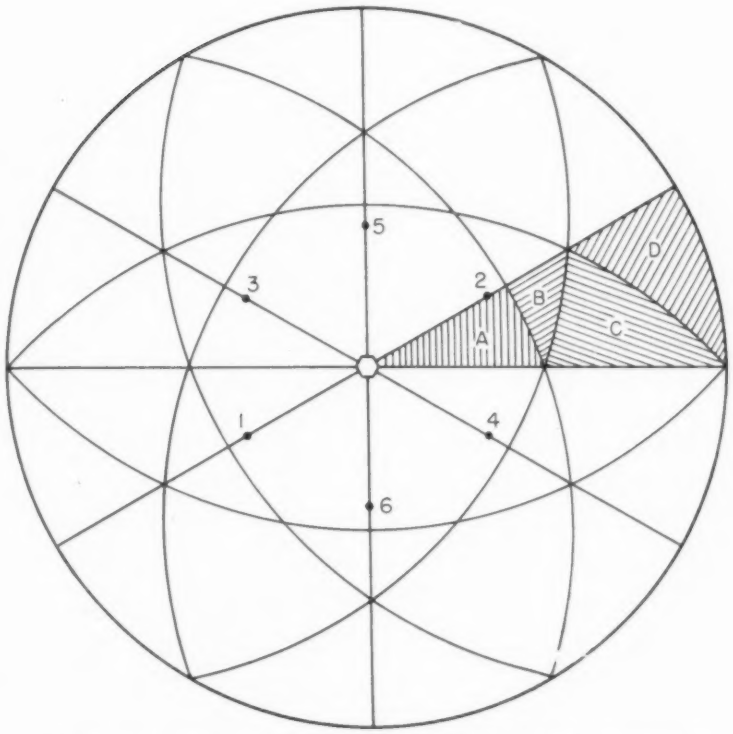


Fig. 16—Position of Compression Axis Governing Extension or Contraction of Crystal.
A—1, 2, 3, 4, 5, 6, Extension; B—3, 4, 5, 6, Extension; 1, 2, Contraction; C—5, 6, Extension; 1, 2, 3, 4, Contraction; D—1, 2, 3, 4, 5, 6, Contraction.

furnished some interesting observations relative to the selection of twinning planes. The basic problem is to determine which of the various twinning planes should be operative and what is the factor governing this selection.

Tentative answers to this question have been provided by a number of workers. Gough (25) in 1933 observed that twinning in zinc crystals took place on the two pairs of planes that did not contain the direction of slip. Andrade and Hutchings (26) in 1935 stated, for the twinning of mercury, "The operative planes are those for which the intersection with the glide plane makes an angle as near 90 degrees as is geometrically possible with the glide direction." Bakarian and Mathewson (27) modified this statement for magnesium as follows: "The operative pair of planes is the pair for which the intersections with the slip plane makes an angle as near 90 degrees as is geometrically possible with the projection of the compression axis in the same plane."

These statements describe a geometrical factor which governs the selection of twinning planes. All of the three rules require that the twinning planes should operate in pairs. Results of the present investigation found all the rules satisfactory.

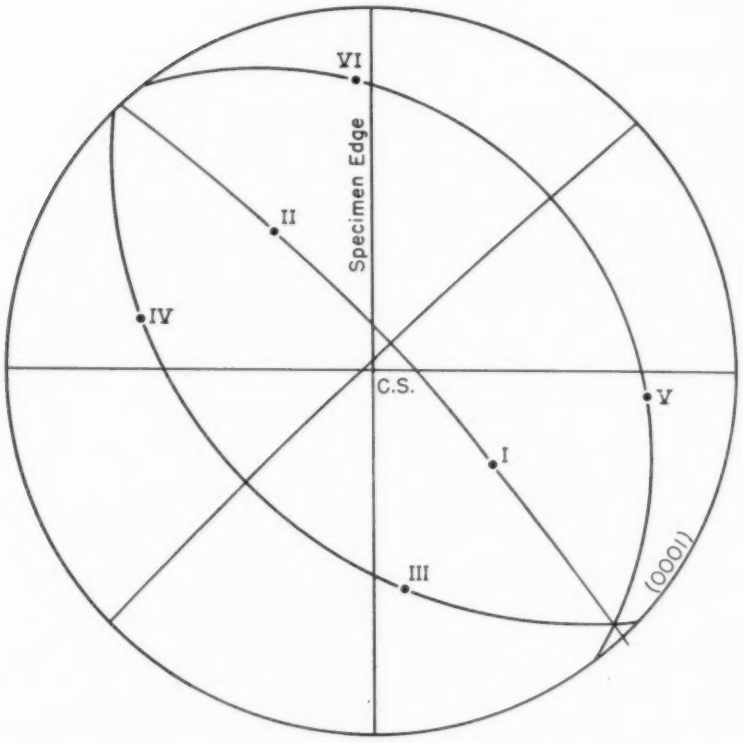


Fig. 17—Orientation of Be-7, Deformed at 25°C. I, II, III, IV, V, VI $\{10\bar{1}2\}$ Poles.

However, a more fundamental approach may be provided by simply extending the LeChatelier's principle to this particular problem of twinning, viz—that phenomenon will occur which most reduces the energy (elastic) of the system. Depending upon the orientation of the crystal in relation to the axis of loading, twinning on some of the $\{10\bar{1}2\}$ planes will lead to an extension of the specimen, while the others will lead to a reduction of specimen length. The diagram in Fig. 16 shows this relationship as adapted from Schmid (21) to the present case of beryllium. Location of the stress axis in one or another of the triangles A, B, C or D, determines which of the six $\{10\bar{1}2\}$ planes may lead to extension or contraction as noted in the caption. By following LeChatelier's principle, it is natural that in the case of compression, those planes which could lead to the reduction of specimen thickness should be the active ones and those which lead to an extension should not.

Quantitatively, when the orientation of the crystal is known, the amount of reduction of thickness of the specimen as any one of the six $\{10\bar{1}2\}$ planes functions can be calculated by the aid of the following equation (21):

$$\frac{1_o}{1_1} = \sqrt{1 + 2S \operatorname{Sin} \chi^* \cos \lambda^* S^2 \operatorname{Sin} \chi^*} \qquad \text{Equation 4}$$

Where, 1_o, 1_1 being the initial and final thicknesses;
χ^* = the angle between compression axis and the twinning plane;
λ^* = the angle between compression axis and the twinning direction.
and s, the twinning shear.

By comparing the calculated values of percent reduction for all six $\{10\bar{1}2\}$ planes, it is possible to find which of them offers the most effective contraction and consequently, the particular planes most likely to be active could be predicted.

This rule has been put to test for all the beryllium specimens with profuse twinning, and found to be satisfactory in every case. Space does not allow the inclusion of all the data. The result from Be-7 may serve to illustrate the observations.

The orientation of Be-7 (Fig. 17) was such that all six $\{10\bar{1}2\}$ planes would lead to contraction. However, the amount of reduction was different for different planes as shown in Table IV.

Table IV
Reduction of Thickness from Twinning on Each of the (10$\bar{1}$2) planes, Be-7

$\{10\bar{1}2\}$	χ^*	λ^*	l_1/l_0	% Reduction	$\cos\theta'\cos\lambda'$	$\frac{\cos\theta'\cos\lambda'}{\cos\theta\cos\lambda}$
I	44°	46°	0.916	8.4	0.173	5.28
II	40°	41°	0.916	8.4	0.187	5.70
III	27°	63°	0.962	3.8	0.493	15.00
IV	24°	61°	0.965	3.5	0.482	14.70
V	15°	76°	0.987	1.3	0.321	9.80
VI	12°	74°	0.987	1.3	0.321	9.80

(S = 0.186 for Be)

Planes I and II offered the greatest reduction, 8.4%; as compared to 3.8, 3.5 and 1.3% for the others. As a result, twinning should be expected to operate on these two planes in preference to the rest. Subsequent microscopic and stereographic analysis verified this expectation. At a reduction of 1.04%, twins were found only along these two planes. It is interesting to note, as the last two columns of Table IV indicate, that the ratio $\cos\theta'\cos\lambda'/\cos\theta\cos\lambda$ was by no means a deciding factor in the selection of twinning planes. Planes III and IV, though having a ratio as high as 15 in comparison with 5–6 of I and II, did not operate. In other words, the selection of twinning planes was not governed by the relative effectiveness for subsequent basal slip within the twins.

A quantitative study to determine how the amount of reduction introduced by each twinning plane would affect the thickness and degree of abundance of the twins has been inconclusive. There seemed no such dependence. Also, inconclusive results seemed to indicate there was no shift to new sets of twinning planes upon further deformation.

E. Orientations with θ Around 65°

This group consisted eight specimens with θ values ranging between 65 and 72 degrees. Their plastic behavior was somewhat similar to the group of specimens with the basal plane nearly perpendicular to the compression surface. The differences were, (a) for this

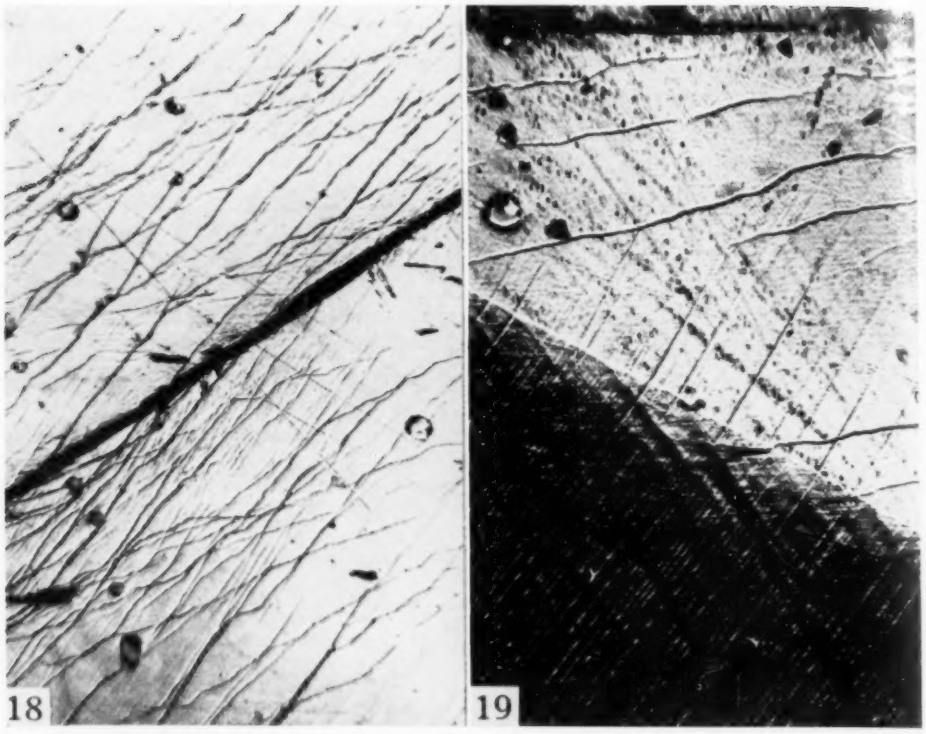


Fig. 18—(10$\bar{1}$0) Slip Lines in Crystal Be-152, Deformed at 300°C. ×100.

Fig. 19—Kink Band, Basal Slip Lines (Fine, Straight) and (10$\bar{1}$0) Slip Lines in Crysta Be-152, Deformed at 300°C. ×150.

group of specimens, basal slip was more prevalent, (b) {10$\bar{1}$2} twinning was less pronounced, as compared to the preceding group.

The presence of all the features in more or less equal prevalence made the appearance of the deformed surface very complex. Deformation was by no means homogeneous and no sharp bend points occurred with the load-reduction curves. The {10$\bar{1}$0} slip lines in these specimens remained wavy, especially near the specimen or twin surfaces and were complicated frequently by the formation of tear lines associated with the emergence of twins, Fig. 18. Basal slip was no longer confined merely to the regions near the compression surface.

Fig. 19 shows an interesting kink band where the sharp boundary is clearly seen. Basal slip lines changed direction and were symmetrically oriented across the boundary. A difference in density of slip lines is also apparent on the two sides, the less dense halve being the one adjacent to the compression surface. The specimen of this micrograph, Be-152, had a large thickness. Friction of the compression surface and the tendency for bending were increased. The kink band formed under this favorable circumstance.

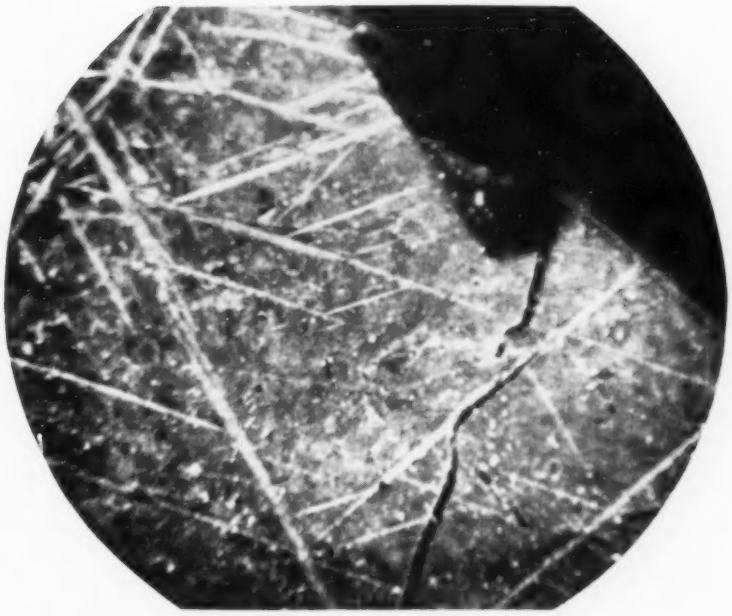


Fig. 20—Macrograph of Crystal Be-NT2, Deformed Until a Crack Formed. Note crack changing path to follow a twin boundary. ×10.

F. Cleavage and Brittleness of Beryllium

In all the groups of specimens considered above, cracks occasionally appeared. They were generally short in length and numbered not more than four or five in an entire specimen. Examination of the direction of the cracks disclosed they were either along the basal plane or $\{11\bar{2}0\}$ planes. Close examination of the fractures revealed that the basal cleavage was always flat while the $\{11\bar{2}0\}$ cleavages were curved.

The area surrounding a crack in another specimen is shown in Fig. 20. A Laue pattern obtained by directing the X-ray beam upon the crack showed the separation of spots, Fig. 21, and the line of separation followed the hyperbola of one of the $<11\bar{2}0>$ zones. It may also be pointed out that, as shown in Fig. 20, the cracks seemed to follow closely the twin boundaries as did the edges produced by chipping. This appears to be an indication that the $\{11\bar{2}0\}$ cleavages might be initiated by the presence of the weakness of twin surfaces. It should be noted that the twinning direction in $(10\bar{1}2)$, i.e. $[\bar{1}011]$, is also shared by $(1\bar{2}10)$, and the two planes, $(10\bar{1}2)$ and $(1\bar{2}10)$, are perpendicular to each other. Thus a twin along $(10\bar{1}2)$ would transmit its maximum strain on the plane $(1\bar{2}10)$, creating localities of high stress concentration.

The brittleness of beryllium has long been an interesting subject. Sloman (1) attributed it to the presence of oxide films. Gold (15) observed fine particles in the slip bands of beryllium when

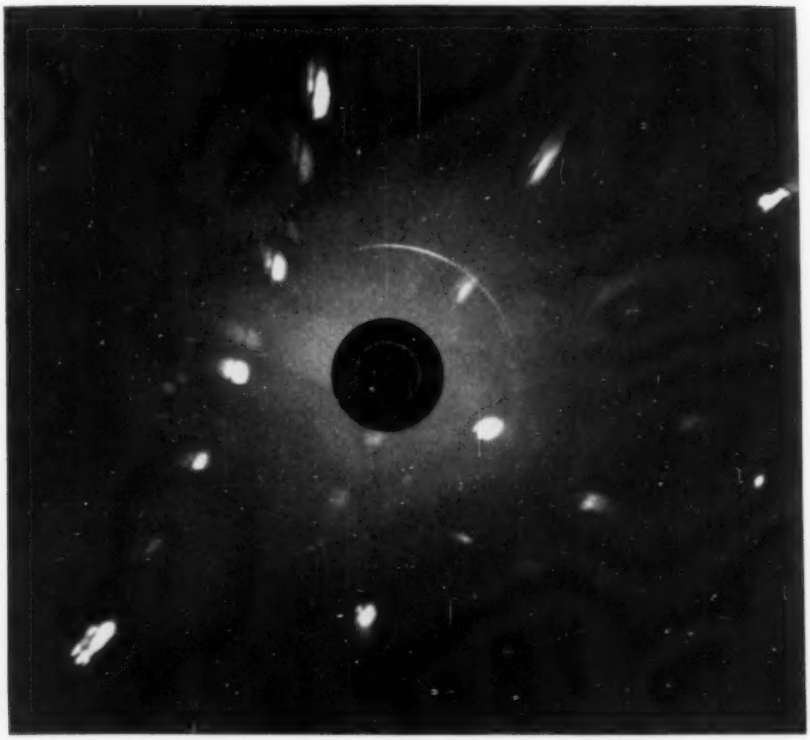


Fig. 21—Laue Taken with Beam Directed at Crack of Specimen in Fig. 20. Crack caused separation of spots and the line of separation of spots follows a $(11\bar{2}0)$ zone.

examining a cleaved surface of a single crystal. The nature of the particles was not identified but they were conceived to be the BeO phase as proposed by Sloman. The present investigation offers no affirmation or disproof of this concept. However, examinations of the compressed specimens and also specimens such as Be-NT2 (Fig. 21) appeared to afford some additional causes for the brittle behavior of beryllium. The availability of many cleavage planes, the aid to fracture offered by twinning and the inclusions all seem to be acting in concerted moves to contribute to the brittleness of beryllium.

Summary of Results of Experimental Work

1. Beryllium single crystals with a square cross section were studied under compression. The results indicate that slip on the basal plane and $\{10\bar{1}0\}$ planes in the original material, twinning on the $\{10\bar{1}2\}$ planes, slip on the basal plane of twinned regions, and cleavages along (0001) and $\{11\bar{2}0\}$ planes were the only mechanisms operating at room temperature, 300, and 500°C (570 and 930°F). The relative prevalence of these several mechanisms has been classified into five groups of orientation.

2. Secondary deformation features such as deformation bands

and kink bands were also observed when the strain was inhomogeneous. A peculiar type of band resulting from the change of length of slip direction from plane to plane was found in some specimens with particular orientations.

3. The critical resolved shear stress for basal slip of beryllium has been determined at 25, 300, and 500°C (77, 570, 930°F).

4. Basal slip lines generally were found to be straight at room temperature and 300°C (570°F). $\{10\bar{1}0\}$ slip lines always appeared wavy and forked at all temperatures.

5. By measuring the displacement of scratches, local shear strains have been calculated and compared to the average.

6. Stored elastic energy prior to fracture for several specimens which suffered little deformation before breakage has been calculated.

7. As an application of LeChatelier's principle, a selection rule governing the selection of $\{10\bar{1}2\}$ planes for twinning has been given. The rule was found to hold for beryllium crystals under compression.

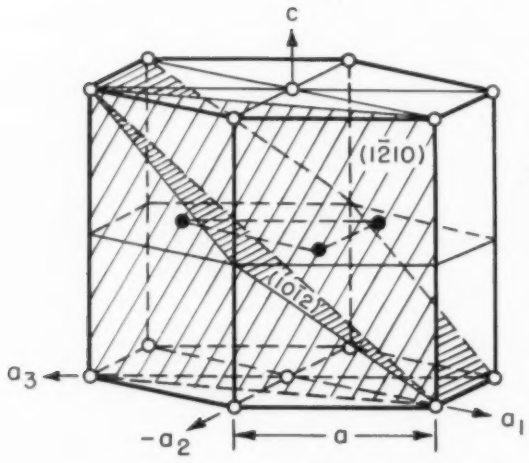
Part II—Analysis of Atomic Movements in Mechanical Twinning of Metals and Evolution of Factors Affecting Twinning

A. Twinning of HCP Metals

Twinning is generally described as a process of homogeneous shear, where all atoms involved translate in a common plane and a common direction. The displacement of a particular layer of atoms is proportional to its distance from the twinning plane. However, this simple picture is believed only exactly applicable to the cubic structures. As pointed out by Mathewson in 1928 (29), for hcp metals only one fourth of the atoms follow the restrictions of a homogeneous shear whereas the rest move irregularly.

1948 Barrett (30) deduced the movements of the atoms during twinning in HCP metals. Four possibilities were suggested. It was pointed out that the postulated atomic movements differed markedly from the ones in cubic structures. Barrett also suggested that the difference "seemed to account for the fact that hexagonal metals form obvious deformation twins while FCC metals do not."

In general, previous work has led to the conclusion that the mechanism of twinning of HCP metals is quite different from that of cubic structures. However, since twinning is a fundamental mechanism of plastic deformation, it is not too unreasonable to think that this mechanism should not change basically with change of the crystal lattice. Twinning systems of HCP metals have often been described by the use of two undistorted planes (21). This picture of two undistorted planes is derived from the assumption



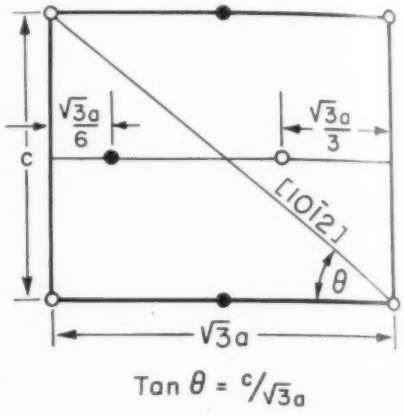


Fig. 22—(Left) A HCP Unit Cell.
Fig. 23—(Right) Projection of the Unit Cell on (1$\bar{2}$10).

of homogeneous shear. With this picture it is possible to calculate the amount of shear and the change of thickness of specimen as related to twinning. Work by Bakarian and Mathewson (27) on magnesium showed clearly that the calculations by the aid of Schmid's formulas derived from the assumption of homogeneous shear agreed very well with experimental results. Part I of the present investigation has also offered such agreement in the case of beryllium.

These thoughts lead to the suggestion that the twinning mechanism of HCP metals may very well be similar to a homogeneous shear even if it is not exactly so. If this is true, it may be said that the twinning mechanism of HCP metals is not too different from that of cubic metals.

For most HCP metals, twinning occurs on the {10$\bar{1}$2} planes. Fig. 22 shows a unit cell of HCP structure; the (10$\bar{1}$2) plane is shown as marked. In order to show correctly the atomic movements with respect to the twinning plane, the arrangement of the atoms in a (1$\bar{2}$10) plane which is perpendicular to the twinning plane and contains the twinning direction (shearing direction) has to be examined. Fig. 23 shows such a plane, the open and solid circles represent two different layers of atoms, a/2 apart. The (10$\bar{1}$2) plane is here shown perpendicular to the paper. The intersection of (10$\bar{1}$2) and (1$\bar{2}$10) is [$\bar{1}$011] which is the twinning direction.

Fig. 24 is a repetition of the unit cells as projected on the (1$\bar{2}$10) plane. Open and solid circles represent two layers of atoms in the matrix. Open and solid half circles represent atoms of the corresponding layers in the twin.

During the process of twinning, atoms represented by open circles move to the sites of open half circles, and solid circles move to

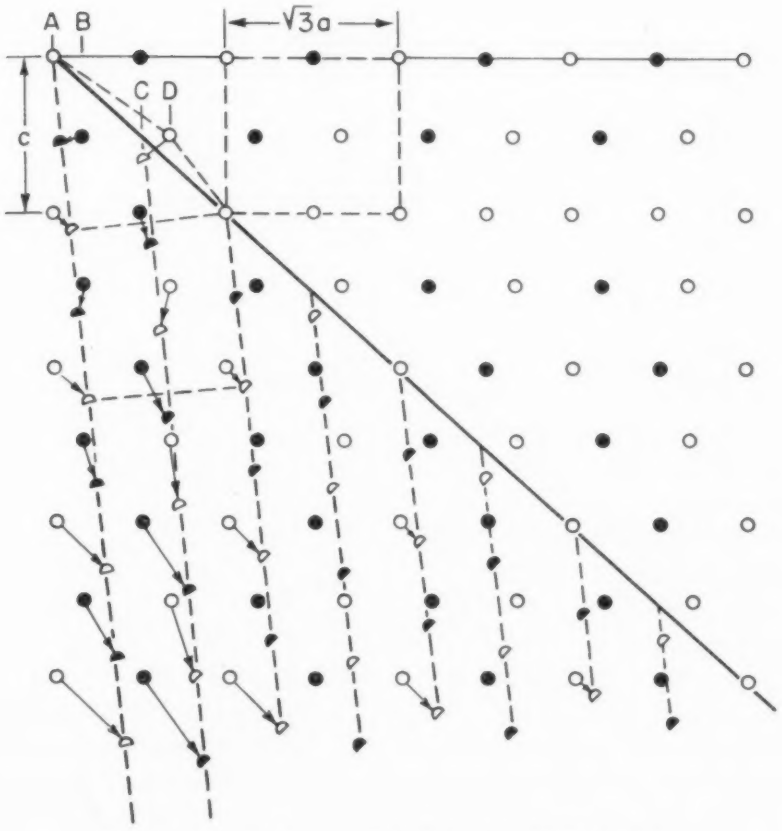
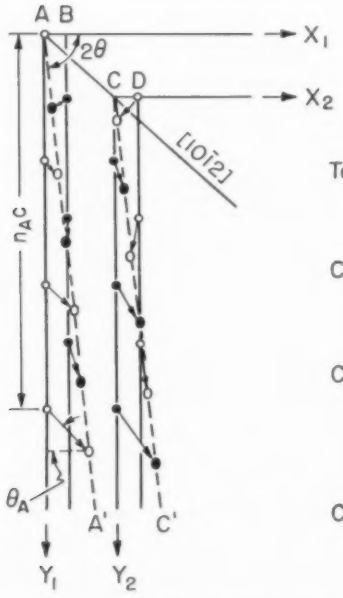


Fig. 24—Atomic Movements in Twinning of HCP Metals.

solid half circles. It will be noted, in doing so, the atoms in two original $\{10\bar{1}0\}$ planes of $\sqrt{3}a/6$ apart merge into a single plane of (0001) of the twin. The angle between the basal plane of the matrix and that of the twin is 2θ, where θ is the angle between (0001) and the twinning plane $(10\bar{1}2)$.

Examination of the atoms close to the twinning plane shows that their movements are truly complex. However, when planes farther away from the twin boundary are examined, it will be found the vectors of the atomic movements gradually rotate counter clockwise, towards parallelism of the $(10\bar{1}2)$ plane. The farther the atoms are from the twin boundary, the closer their movements approach to parallel to the twinning plane and direction.

It is possible to select a pair of axes and assign coordinates to positions of all atoms, before and after twinning, in terms of functions of the lattice parameters a and c. From the initial coordinates of an atom and the final coordinates of the same atom after twinning, the direction of the movement of this atom in the process of twinning, can easily be calculated.



$$\text{Tan}\,\theta_A = \frac{n_A \cdot \sqrt{3}\,a \cdot \text{Sin}\,2\theta - n_A c}{n_A \cdot \sqrt{3}a \cdot \text{Cos}\,2\theta} = \text{Tan}\,\theta$$

$$\text{Cot}\,\theta_B = \text{Cot}\,\theta \left\{ 1 - \frac{3 + (c/a)^2}{3(n_B+1)\,[3-(c/a)^2]} \right\}$$

$$\text{Cot}\,\theta_C = \text{Cot}\,\theta \cdot \frac{n_C + 2/3}{n_C + \frac{5a^2 - c^2}{2(3a^2 - c^2)}}$$

$$\text{Cot}\,\theta_D = \text{Cot}\,\theta \cdot \frac{n_D + \frac{a^2}{3a^2 - c^2}}{n_D - \frac{c^2}{3(3a^2 - c^2)}}$$

Fig. 25—Angular Direction of The Atomic Movements.

Take row A for example, in Fig. 25 with X_1 and Y_1 as the coordinates. The initial ordinates of the atoms in this row can be expressed by a simple function $n_A c$, where n_A is an integer representing the distance of a given atom from the origin in terms of interatomic distances along this row. The abcissa is zero. After twinning, these atoms assume new coordinates which may be represented as $(\frac{n}{2}\sqrt{3}a\cos 2\theta, \frac{n}{2}\sqrt{3}a\sin 2\theta)$ with respect to the same axes, where n is the number of atomic distances from the origin along the newly formed (0001) plane of the twin, i.e., AA′ in Fig. 25.

The direction of movements of the atoms in row A can, therefore, be formulated as:

$$\tan\theta_A = \frac{\frac{n}{2}\sqrt{3a}\sin 2\theta - n_A c}{n_A\sqrt{3a}\cos\theta} \qquad \text{Equation 5}$$

Notice that for row A, $n = 2n_A$. Equation (1) can thus be simplified to the form:

$$\tan\theta_A = \tan 2\theta - \frac{c}{\sqrt{3a}\cos 2\theta}$$

Since $$\tan\theta = \frac{c}{\sqrt{3a}}$$

$$\tan\theta_A = \tan\theta\left(\frac{2}{1-\tan^2\theta} - \frac{1}{\cos 2\theta}\right)$$

Simplifying further, $\tan\theta_A = \tan\theta$

This relation shows $\theta_A = \theta$; i.e., all the atoms in row A move parallel to the twinning plane and twinning direction when they are transferred from matrix to twin positions.

When the same procedure is followed for rows B,C, and D, it is found that the direction of movements of atoms in these three rows is not constant. Their movements can be shown as follows:

$$\mathrm{Cot}\theta_B = \mathrm{Cot}\theta \bullet \left\{1 - \frac{3+(c/a)^2}{3(n_B+1)\,[3-(c/a)^2]}\right\} \qquad \text{Equation 6}$$

$$\mathrm{Cot}\theta_C = \mathrm{Cot}\theta \bullet \frac{n_C+2/3}{n_C+\dfrac{(5a^2-C^2)}{2(3a^2-C^2)}} \qquad \text{Equation 7}$$

$$\mathrm{Cot}\theta_D = \mathrm{Cot}\theta \bullet \frac{n_D+a^2/(3a^2-C^2)}{n_D-C^2/3(3a^2-C^2)} \qquad \text{Equation 8}$$

In all cases, as n_B, n_C, or $n_D \rightarrow \infty$; θ_B, θ_C, $\theta_D \rightarrow \theta$. This shows that the further away the atoms are from the interface, the more nearly their movements approach parallelism to the twinning plane and direction. By plotting the cotangent of θ_B, θ_C, and θ_D against n_B, n_C, n_D correspondingly, for beryllium which has parameters a $=2.2871$Å, c$=3.5860$Å, it is found that as either of the three n-values reaches 100, the corresponding θ_B, θ_C, or θ_D will be all within 1 degree of θ.

In a HCP metal, a twin is generally much more than 100 atomic layers thick. For this reason, the twinning mechanism of a HCP metal, though not exactly a process of homogeneous shear, can rather safely be regarded as such in essence. Calculations based on this assumption, therefore, agree with experimental results. This analysis seems to bring the picture of twinning of HCP metals somewhat closer to that of the cubic structures.

The comparatively high strain of twin boundaries of HCP metals and the large number of atoms required to move approximately parallel to the twinning plane to offset the irregular movements of the atoms near the interface, all require the twins to be large in size in order to be stable enough to exist. This corresponds with the general observations of twinning in hexagonal metals.

It is not suggested here that the above derived process should be considered as the actual mechanism of twinning in HCP metals. Rather it merely serves as an explanation of the fact that for ordinary purposes, twinning of HCP metals can be treated as a homogeneous shearing process.

B. Factor of Periodicity

The foregoing analysis deals with only a particular crystal structure, where the twinning elements are experimentally determined. To further extend the analysis of the problem of twinning to other structures, a more general picture may be considered.

Fig. 26 shows strings of atoms put together in a two dimensional way. These arrangements of atoms can also be regarded as being the cross-sections of a certain crystal lattices.

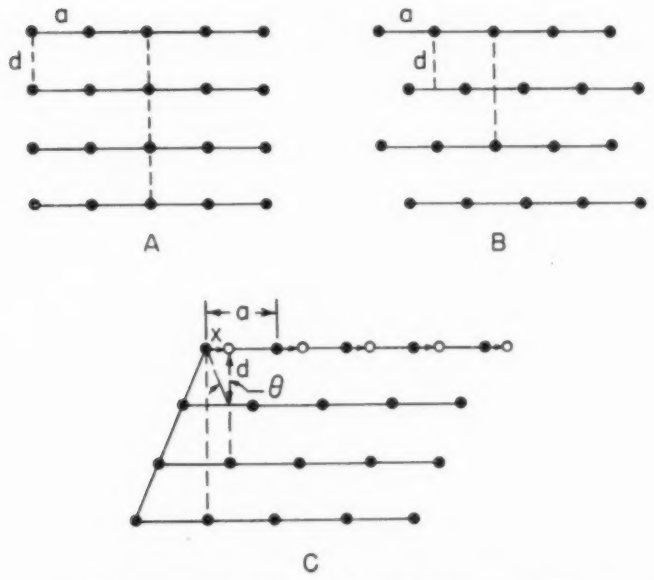


Fig. 26A—Periodicity—1 Crystal Shear—a/d; Slip
Fig. 26B—Periodicity—2 Crystal Shear—a/d; Slip
Fig. 26C—Periodicity—3 Crystal Shear—x/d. Twinning

It is immediately seen that there is no possibility of twinning in the first two cases, whereas the third arrangement does offer the possibility of twinning, as well as the possibility of slip. This situation can be described from several approaches. It could be said that the geometry in the first two cases does not allow twinning while in the third it does. In this way, one may call it a geometrical factor which governs whether slip or twinning should occur in a particular system. It could also be said that in the first two cases, part of the crystal is already a twin of the rest in that a mirror image is present. In the third case, however, parts of the crystal on two sides of the horizontal plane are not mirror images of each other. Therefore this plane offers the possibility of being used as a twinning plane. From this point of view, a similarity between slip and twinning is noticed. Both processes will offer in the end the symmetry of twins. The difference is, a slip plane has this property of symmetry all the time, before as well as after twinning; and a twinning plane has this property of symmetry only after being used as such.

A third way to describe it, is by examining the periodicity of the plane in consideration. By periodicity is meant the period through which the plane directly repeats itself. To assign a periodicity, one simply draws a line through an atom perpendicular to the plane in question to find out how often this line passes through another atom in a similar plane. In the first case, Fig. 26A, obviously

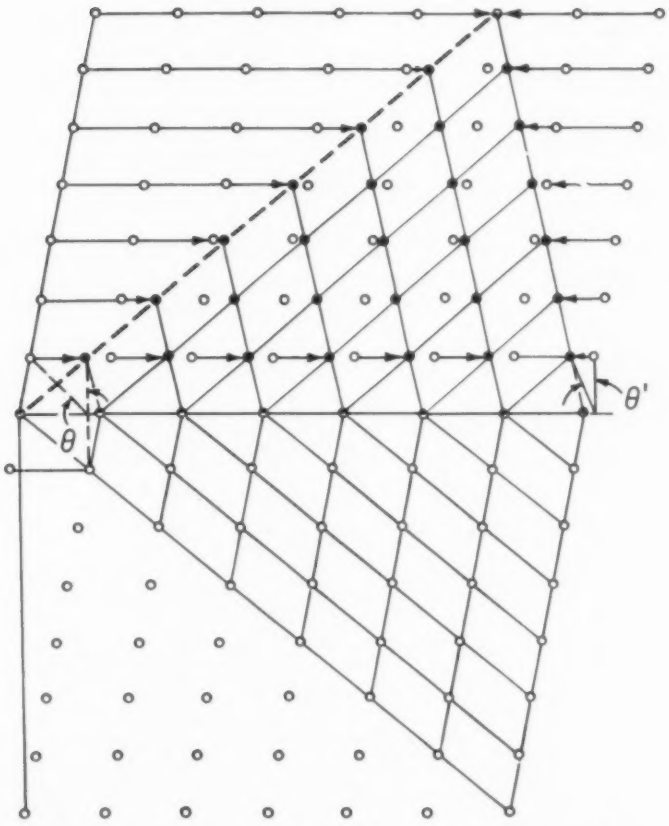


Fig. 27—A Hypothetical Case of Twinning of Periodicity 7.

the periodicity is 1; in the second case, 2; and the third case, 3. Only when the periodicity is 3 or larger can twinning occur. Otherwise, only slip is possible. In the light of the factor of periodicity, slip may be regarded as a special case of twinning where the periodicity is smaller than 3. Across a slip plane every layer of atoms constitutes a twin. Therefore, the two twins will be indistinguishable, or perfectly identical; since the atoms at the interface do not change their neighbors and no boundary could be detected. It is only when the periodicity reaches 3 or larger that a crystallographically distinguishable boundary can exist. Thus, twin of a periodicity of 1 is a slip; twin of a periodicity of 2 is also a slip; and twin of a periodicity of 3 or larger will be a true twin in its conventional sense. Very likely, the larger the periodicity of the twin, e.g., Fig. 27, the thicker the twin and the more stable the twin boundary will be.

Figs. 28 and 29, show two possible twinning systems for BCC metals. The twinning system (112) $[11\bar{1}]$, Fig. 28, possesses a periodicity of 3. For such a periodicity, three layers of atoms will be enough to create a twin of distinguishable boundaries, although

such a twin may properly be called a fault. On every third layer within the twin, the atoms move a whole interatomic distance or an integral multiple. A simple equation may describe such a condition as:

$$\tan\theta = \frac{ka}{pd} \qquad \text{Equation 9}$$

where p is periodicity, k is a constant representing the number of interatomic distances through which atoms of the pth layer trans-

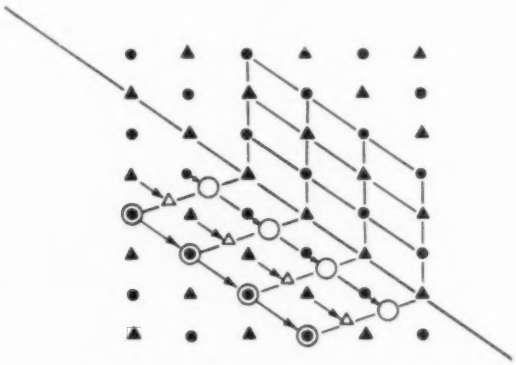


Fig. 28—BCC—{112} <111> Twinning System Plane of Projection—{110}; Periodicity —3; Crystal shear $\sqrt{2}/2$.

late, a is the interatomic distance in the plane, d is the interplanar spacing and $\tan\theta$ is the twinning shear. In this particular case, p equals 3 and k equals 1.

For this type of twinning, which is exactly represented as a process of homogeneous shear, p and k in this equation must be integers, and k is not always 1. It could be shown, when a particular shear direction is chosen, k and p may be related in such a manner as to give the following ratios:

$$k/p = 1/3,\ 2/4,\ 3/5,\ 4/6,\ 5/7,\ 6/8,\ 7/9, \text{ etc.} \qquad \text{Equation 10}$$

For all cases where $p > 5$, the shear direction may be reversed so as to give the smaller strain. Thus modified, the above series will then take the form:

$$k/p = 1/3,\ 2/4,\ 2/5,\ 2/6,\ 2/7,\ 2/8,\ 2/9, \text{ etc.} \qquad \text{Equation 11}$$

Fig. 27 is a hypothetical case illustrating twinning of a periodicity of 7. When the shear direction is chosen as shown in the left side of the drawing, the k/p must be 5/7, and the shear, 5a/7d. This will be the case of Equation 10. The reversed direction, shown in the right side of the drawing, will give a k/p of 2/7, and a twinning shear of only 2a/7d. This will be the case of Equation 11. Obviously

the latter direction should be chosen in calculating the twinning shear strain.

It will be noted that the ratios in Equation 11 are not all in their simplest forms. The denominators are maintained as the same integers as p's are. While the ratio of 2/4 may as well be written as ½, a periodicity of 2, nevertheless, will not produce a twin. Thus by maintaining the form 2/4 it will be clear the periodicity must be 4 in order to produce such a twin, which in its thinnest form has only two layers of atoms.

Generally speaking, the larger the periodicity the thicker will be the smallest possible twins. However, a closer examination will

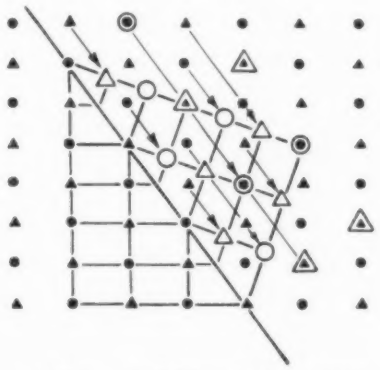


Fig. 29—BCC—{111} <112> Twinning System Plane of Projection —{110} Periodicity —3; Crystal shear $2\sqrt{2}$.

show Equation 11 may be broken into two parts. For all ratios where the denominators are odd, the denominators or periodicities will represent the number of atomic layers required to form a "unit twin." For all cases where the denominators are even, the denominators or periodicities represent the doubles of such layers.

Also, as seen from Equation 11, the larger the periodicity the smaller will be the twinning shear, provided a/d is constant. Thus, the thicker a "unit twin," the more easily it will be formed. For cubic metals the symmetry does not allow high periodicity systems. {112} or {111} twins are all of a periodicity of 3. Twins of such systems could occur in very few atomic layers and unless they are piled up in the right sequence for a very long range, the twins are likely to be so thin as to be hardly noticeable. It seems, as long as the twinning satisfies Equation 9, the same thing would prevail in all metals.

The $\{10\bar{1}2\}$ twinning of HCP metals can not satisfy Equation 9. In the first place, the $(10\bar{1}2)$ planes are not evenly spaced. In the second place, no definite value can be assigned for p in this case. It may be noticed from Fig. 24 that when a line is drawn perpendicu-

lar to the $(10\bar{1}2)$ plane through an atom no other atoms are met. The periodicity may be said to be infinity. A $(10\bar{1}2)$ twin, therefore, can not exist in only a few layers of atoms, according to Equation 9. Instead, the movements of the atoms can only be expressed as Equations 5,6,7, and 8, as previously described. The large periodicity, associated with a large number of layers of atoms necessary to form a twin and a small twinning shear, may be an explanation for the readiness of formation of large mechanical twins in HCP metals.

$\{10\bar{1}2\}$ twinning of beryllium has a shear of 0.186 based on the assumption of homogeneous shear. Substituting this shear in Equation 9, it is found the periodicity for $\{10\bar{1}2\}$ twinning of beryllium is equivalent to about 129. While this value by no means describes the exact nature of twinning of beryllium, the argument remains that twins thinner than this number of atomic layers are not likely to exist and twinning over several hundred layers of atoms can be treated as a homogeneous shear for purposes of making related calculations.

It should be noted that the above analysis is solely based on crystallographic aspects and no energy considerations entered. Creation of twin interfaces is associated with an increase of surface energy which must be overcome by the decrease of elastic strain energy by twinning. No computations of this nature have yet been successfully made.

C. Factor of Crystallographic Shear

In a crystal lattice, there are obviously many more than one type of plane which may possess a periodicity of 3 or larger. All of these planes have the possibility of serving as twinning elements. Yet, in reality, only a few of them are found to be the twinning planes. Therefore, a second factor affecting the selection of one particular system as favorable from among a number of possibilities, has to be introduced.

Theories of plastic flow propose various atomic movements to account for particular deformations. However, the net or gross displacements of the atoms to account for the deformation are generally quite simple. In either twinning or slip, when an atom is transferred from the initial to the end position, a crystallographic shear—the ratio of the displacement of an atom to its distance from either the twinning plane or the plane of slip—is accomplished. In Figures 26A and 26B, the atoms all move one whole interatomic distance during slip and the crystallographic shear is hence a/d. In Fig. 26C, the displacement is only a fraction of the interatomic distance and the crystallographic shear is x/d.

When the atomic displacement is large while the interplanar spacing is small, the crystallographic shear will be high and vice

versa. The smaller the crystallographic shear, the more easily will an atom move owing to the fact that the travel of the atom is relatively short and its bond to the neighboring layers is relatively weak. This is equivalent to the general statement that slip prefers to occur in a close packed plane and along a close-packed direction.

Examination of Fig. 28 will show the $\{112\}\ <11\bar{1}>$ system of BCC metals has a periodicity of 3, and the atomic movement for twinning along such a system demands a crystallographic shear of 0.707. However, the $\{112\}\ <11\bar{1}>$ is not the only system which could offer twinning in BCC metals. Fig. 29 shows another possibility where the twinning plane is $\{11\bar{1}\}$ and the direction $<112>$. The periodicity of this system $\{111\}\ <11\bar{2}>$, is also 3, but the crystallographic shear required for twinning along it is now 2.828. This value of shear is four times as large as that of the previous one. For this reason it should be expected that twinning of BCC metals would occur in the $\{112\}\ <11\bar{1}>$ system rather than in $\{111\}\ <11\bar{2}>$. The observed Neumann bands in α—Fe verify this point.

Summary

1. From purely a crystallographic basis, a mathematical formulation of the atomic movements in the twinning of hexagonal close packed metals has been proposed. This serves as a means to describe the transferring of atoms from matrix to the twinned positions. Orderliness to a certain extent could be assigned to the atomic movements.

2. The factor of planar periodicity has been introduced in an examination of the crystallography of slip and twinning in general, and based on this factor, a comparison of the two processes has been discussed.

3. An evaluation has been made of the factor of crystallographic shear as related to the selection of twinning and slip elements.

References

1. H. A. Sloman, "Researches on Beryllium," *Journal*, Institute of Metals, Vol. 49, 1932, p. 365.
2. P. W. Bridgman, "Compressibilities and Pressure Coefficients of Resistance of Elements, Compounds, and Alloys, Many of Them Anomalous," *Proceedings*, American Academy of Arts and Sciences, Vol. 68, March 1933, p. 27.
3. E. Grüneisen and H.-D. Erfling, "Thermokraft reiner Beryllium-kristalle und ihre Änderung im transversalen Magnetfeld," *Annalen der Physik*, Series 5, Vol 36, 1939, p. 357.
   H.-D. Erfling and E. Grüneisen, "Weitere Untersuchungen an Berylliumkristallen im transversalen und longitudinalen Magnetfeld," *Annalen der Physik*, Series 5, Vol. 41, 1942, p. 89.
   E. Grüneisen and H. Adenstedt, "Einfluss transversaler Magnetfelder auf Elektrizitäts- und Wärmeleitung reiner Metalle bei tiefer Temperatur," *Annalen der Physik*, Series 5, Vol. 31, 1938, p. 714.
4. E. A. Owen and T. L. Richards, "On the Thermal Expansion of Berryllium," *Philosophical Magazine*, Series 7, Vol. 22, 1936, p. 304.

5. A. R. Kaufmann and E. Gordon, "Vacuum Melting and Casting of Beryllium," *Metal Progress*, Vol. 52, September 1947, p. 387.
6. L. Gold, "An Apparatus for the Production of Large Metallic Crystals by Solidification at High Temperatures," *Review of Scientific Instruments*, Vol. 20, February 1949, p. 115.
7. C. H. Mathewson and A. J. Phillips, "Twinning in Beryllium, Magnesium, Zinc and Cadmium," *Technical Publication No. 53*, American Institute of Mining and Metallurgical Engineers, 1928.
This paper is the same as item no. 29 in this list.
8. E. J. Lewis, "Some Thermal and Electrical Properties of Beryllium," *Physical Review*, Series 2, Vol. 34, December 15, 1929, p. 1575.
9. G. F. Kosolapov and A. K. Trapeznikov, "On the Structure of Beryllium," *Zhurnal Eksperimentalnoy i Teoreticheskoy Fiziki*, Vol. 6, No. 10, 1936, p. 1163.
In Russian.
10. F. M. Jaeger and J. E. Zanstra, "The Allotropism of Beryllium," *Proceedings*, Koninklijke Akademie van Wetenschappen, Amsterdam, Vol. 36, 1933, p. 636.
11. L. Losana, "Studio sul Berillio. Nota I. Proprieta del Berillio ad Alto Grado di Purezza," *Alluminio*, Vol, 8, March-April 1939, p. 67.
12. M. C. Neuburger, "Gitterkonstante und Allotropie von Beryllium," *Zeitschrift für Kristallographie*, Vol. 92, 1935, p. 474.
13. E. A. Owen and L. Pickup, "The Lattice Constants of Beryllium," *Philosophical Magazine*, Series 7, Vol. 20, 1935, p. 1155.
14. E. A. Owen, L. Pickup and I. O. Roberts, "Lattice Constants of Five Elements Possessing Hexagonal Structure," *Zeitschrift für Kristallographie*, Vol. 91, 1935, p. 70.
15. L. Gold, "Growth and Perfection of Beryllium Crystals. I. Growth of Large Beryllium Crystals by Solidification," Atomic Energy Commission Declassified Document *AECD-2643*, Declassified July 20, 1949. 32 pp.
L. Gold, "Growth and Perfection of Beryllium Crystals. II. Studies of Crystal Perfection," Atomic Energy Commission Declassified Document *AECD-2645*, Declassified July 21, 1949. 18 pp.
16. M. C. Neuburger, "Präzisionsmessung der Gitterkonstanten von Beryllium. II.," *Zeitschrift für Kristallographie*, Vol. 85, 1933, p. 325.
17. G. I. Taylor and W. S. Farren, "The Distortion of Crystals of Aluminium under Compression.—Part I.," *Proceedings*, Royal Society of London, Series A, Vol. 111, 1926, p. 529.
18. F. L. Vogel, Jr. Master of Science Thesis, University of Pennsylvania.
19. F. R. Bichowsky and F. D. Rossini, *The Thermochemistry of the Chemical Substances*, 1936, Reinhold Publishing Corporation, New York.
20. E. Baur and R. Brunner, "Dampfdruckmessungen an hochsiedenden Metallen," *Helvetica Chimica Acta*, Vol. 17, 1934, p. 958.
21. E. Schmid and W. Boas, *Plasticity of Crystals with Special Reference to Metals*, 1950, F. A. Hughes & Co., Ltd., London.
22. R. F. Miller and W. E. Milligan, "Influence of Temperature on Elastic Limit of Single Crystals of Aluminum, Silver and Zinc," *Transactions*, American Institute of Mining and Metallurgical Engineers, Vol. 124, 1937, p. 229.
23. E. N. da C. Andrade and C. Henderson, "The Mechanical Behaviour of Single Crystals of Certain Face-Centred Cubic Metals," *Philosophical Transactions*, Royal Society of London, Series A, Vol. 244, 1951, p. 177.
24. E. Orowan, "A Type of Plastic Deformation New in Metals," *Nature*, Vol. 149, June 6, 1942, p. 643.
25. H. J. Gough, "Crystalline Structure in Relation to Failure of Metals—Especially by Fatigue," *Proceedings*, American Society for Testing Materials, Vol. 33, Part II, 1933, p. 3.
26. E. N. da C. Andrade and P. J. Hutchings, "The Mechanical Behaviour of Single Crystals of Mercury," *Proceedings*, Royal Society of London, Series A, Vol. 148, 1935, p. 120.
27. P. W. Bakarian and C. H. Mathewson, "Slip and Twinning in Magnesium Single Crystals at Elevated Temperatures," *Transactions*, American Institute of Mining and Metallurgical Engineers, Vol. 152, 1943, p. 226.

28. C. A. Zapffe and C. O. Worden, "Fractographic Study of an Ammonium Dihydrogen Phosphate Single Crystal," *Acta Crystallographica*, Vol. 2, 1949, p. 383.
29. C. H. Mathewson and A. J. Phillips, "Twinning in Beryllium, Magnesium, Zinc and Cadmium," *Proceedings*, Institute of Metals Division, American Institute of Mining and Metallurgical Engineers, 1928, p. 445.
30. C. S. Barrett, "The Crystallographic Mechanisms of Translation, Twinning and Banding," *Cold Working of Metals*, 1949, p. 65. American Society for Metals.
31. F. L. Vogel and R. M. Brick, "Deformation of Ferrite Single Crystals," *Journal of Metals*, Vol. 5, May 1953, p. 700.
32. R. P. Steijn and R. M. Brick, "Flow and Fracture of Single Crystals of High Purity Ferrite," *Transactions*, American Society for Metals, Vol. 46, 1954, p. 1406.
33. T. L. Wu and R. Smoluchowski, "A New Criterion for the Occurrence of Slip in Thin Single Crystals," *Physical Review*, Series 2, Vol. 78, May 15, 1950, p. 468.
34. L. W. McKeehan, "The Crystal Structure of Beryllium and of Beryllium Oxide," *Proceedings*, National Academy of Sciences, Vol. 8, September 1922, p. 270.
35. J. C. McLennan and C. D. Niven, "Electrical Conductivity at Low Temperatures," *Philosophical Magazine*, Series 7, Vol. 4, 1927, p. 386.

DISCUSSION

Written Discussion: By C. Elbaum, Department of Metallurgy, University of Toronto.

Frank and Thompson[2] have recently pointed out that the criterion used by the authors in determining whether, for a particular orientation of the crystal with respect to the axis of loading, any of the possible twinning systems will lead to a contraction or an extension of the specimen is incomplete. This criterion is applicable only in the case of total conversion of a crystal into its twin. In the case of thin twin laminae, the orientation diagram should be appropriately modified. Frank and Thompson treated the case of zinc in detail. For beryllium, the modification should be even more significant, because of the higher twinning shear (0.199 for beryllium as compared to 0.139 for zinc).

Detailed data, in agreement with the criterion used, are given for specimen Be-7. In this case, the orientation of the specimen is such that the proposed modification does not apply. However, some of the specimens among the group having an angle θ of about 65° might be within the regions of orientations for which the modification was proposed.

[2]F. C. Frank and N. Thompson, "On Deformation by Twinning," ACTA METALLURGICA, Vol. 3 January, 1955, p. 30.